

4. SITE 642: NORWEGIAN SEA¹

Shipboard Scientific Party²

HOLE 642A

Date occupied: 28 June 1985
Date departed: 28 June 1985
Time on hole: 11.0 hr
Position: 67°13.5'N, 2°55.7'E
Water depth (sea level; corrected m, echo-sounding): 1286
Water depth (rig floor; corrected m, echo-sounding): 1297
Bottom felt (rig floor; m, drill pipe measurement): 1292.7
Distance between rig floor and sea level (m): 11.1
Total depth (rig floor; m): 1303.5
Penetration (m): 10.8
Number of cores (including cores with no recovery): 1
Total length of cored section (m): 9.5
Total core recovered (m): 9.9
Core recovery (%): 100 %
Oldest sediment cored:
Depth sub-bottom (m): 10.8
Nature: glacial sandy mud
Age: late Pleistocene
Measured velocity (km/s): 1.49

HOLE 642B

Date occupied: 28 June 1985
Date departed: 29 June 1985
Time on hole: 30.0 hr
Position: 67°13.5'N, 2°55.7'E
Water depth (sea level; corrected m, echo-sounding): 1286
Water depth (rig floor; corrected m, echo-sounding): 1297

Bottom felt (rig floor; m, drill pipe measurement): 1292.7
Distance between rig floor and sea level (m): 11.1
Total depth (rig floor; m): 1513.8
Penetration (m): 221.1
Number of cores (including cores with no recovery): 25
Total length of cored section (m): 221.1
Total core recovered (m): 215.6
Core recovery (%): 97.5
Oldest sediment cored:
Depth sub-bottom (m): 221.1
Nature: olive-gray homogeneous diatomaceous ooze
Age: early Miocene
Measured velocity (km/s): 1.60

HOLE 642C

Date occupied: 29 June 1985
Date departed: 1 July 1985
Time on hole: 43.75 hr
Position: 67°13.2'N, 02°55.8'E
Water depth (sea level; corrected m, echo-sounding): 1277
Water depth (rig floor, corrected m, echo-sounding): 1288
Bottom felt (rig floor, m, drill pipe measurement): 1292.1
Distance between rig floor and sea level (m): 10.7
Total depth (rig floor, m): 1491.7
Penetration (m): 199.6
Number of cores (including cores with no recovery): 24
Total length of cored section (m): 199.6
Total core recovered (m): 192.8
Core recovery (%): 96.6
Oldest sediment cored:
Depth sub-bottom (m): 199.6
Nature: dark olive-gray bioturbated siliceous ooze; intercalated ash layers
Age: early Miocene
Measured velocity (km/s): 1.77

HOLE 642D

Date occupied: 1 July 1985
Date departed: 4 July 1985
Time on hole: 56.25 hr
Position: 67°13.2'N 02°55.8'E
Water depth (sea level; corrected m, echo-sounding): 1277
Water depth (rig floor; corrected m, echo-sounding): 1288
Bottom felt (rig floor; m, drill pipe measurement): 1292.1
Distance between rig floor and sea level (m): 10.7
Total depth (rig floor; m): 1622.0

¹ Eldholm, O., Thiede, J., Taylor, E., et al., 1987. *Proc., Init. Repts. (Pt. A), ODP*, 104.

² Olav Eldholm, (Co-Chief Scientist), University of Oslo, Oslo, Norway; Jørn Thiede (Co-Chief Scientist), Christian-Albrechts-Universität, Kiel, FRG; Elliott Taylor (Staff Scientist), ODP, Texas A&M University, College Station, TX; Colleen Barton, Stanford University, Stanford, CA; Kjell Bjørklund, University of Oslo, Oslo, Norway; Ulrich Bleil, Universität Bremen, Bremen, FRG; Paul Ciesielski, University of Florida, Gainesville, FL; Alain Desprairies, Université de Paris Sud, Orsay, France; Diane Donnally, Amoco Production Co., New Orleans, La.; Claude Froget, Faculté des Sciences de Luminy, Marseilles, France; Robert Goll, IKU/SINTEF, Trondheim, Norway; Rudiger Henrich, Christian-Albrechts-Universität, Kiel, FRG; Eystein Jansen, University of Bergen, Bergen, Norway; Larry Krissek, Ohio State University, Columbus, OH; Keith Kvenvolden, USGS, Menlo Park, CA; Anne LeHuray, Lamont-Doherty Geological Observatory, Palisades, NY; David Love, University of Waterloo, Ontario, Canada; Peter Lysne, Sandia National Laboratory, Albuquerque, NM; Thomas McDonald, Texas A&M University, College Station, TX; Peta Mudie, Geological Survey of Canada, Nova Scotia, Canada; Lisa Osterman, Smithsonian Institution, Washington, DC; Lindsay Parson, Institute of Oceanographic Sciences, Surrey, UK; Joseph Phillips, University of Texas, Austin, TX; Alan Pittenger, Texas A&M University, College Station, TX; Gunnbjørg Qvale, Norsk Hydro, Oslo, Norway; Günther Schönharting, University of Copenhagen, Copenhagen, Denmark; Lothar Viereck, Ruhr Universität, Bochum, FRG.

Penetration (m): 329.9
Number of cores (including cores with no recovery): 20
Total length of cored section (m): 140.0
Total core recovered (m): 117.0
Core recovery (%): 84.2 %
Oldest sediment cored:
 Depth sub-bottom (m): 328.5
 Nature: weathered, highly altered volcanoclastics
 Age: late Eocene
 Measured velocity (km/s): 1.86
Basement:
 Depth sub-bottom (m): 329.7
 Nature: basalt
 Measured velocity (km/s): 4.40

HOLE 642E

Date occupied: 4 July 1985
Date departed: 1 August 1985
Time on hole: 695.75 hr
Position: 67°13.2'N, 02°55.8'E
Water depth (sea level; corrected m, echo-sounding): 1277
Water depth (rig floor; corrected m, echo-sounding): 1288
Bottom felt (rig floor; m, drill pipe measurement): 1289
Distance between rig floor and sea level (m): 10.8 (July 4); 11.1 (Aug 1)
Total depth (rig floor; m): 2518.4
Penetration (m): 1229.4
Number of cores (including cores with no recovery): 107*
Total length of cored section (m): 906.8*
Total core recovered (m): 372.6
Core recovery (%): 41.1
Oldest sediment cored:
 Depth sub-bottom (m): 1211.0
 Nature: fine-grained volcanoclastic sediment, rich in quartz and mica
 Age: early Eocene
 Measured velocity (km/s): 3.70 (Core 104-642E-109R)
Basement:
 Depth sub-bottom (m): 1229.4
 Nature: fine-grained aphanitic dike of basaltic composition
 Measured velocity (km/s): 4.70
 *REMARKS: Although 110 cores were taken, Cores 104-642E-1W and -642E-2W are wash cores and Core 104-642E-49B is bit samples. They are treated only as samples and excluded in the core-recovery calculation.

SITE 642 SUMMARY

Introduction

ODP Site 642 is located at the outer Vøring Plateau, east of magnetic anomaly 24B and over the inner part of the wedge of the seaward-dipping reflector sequence. Coring at Site 642 recovered a volcanic sequence consisting of two main units below a cover of predominantly pelagic-hemipelagic Neogene and Quaternary sediments. A total of five holes were drilled at the site. These are:

642A. 1 APC core, 1.3–10.8 mbsf,
 642B. 25 APC cores, 0–221.1 mbsf,
 642C. 24 APC cores, 0–199.6 mbsf,
 642D. 18 XCB and 2 NCB cores, 189.9–329.9 mbsf, and
 642E. 107 R cores, 322.5–1229.4 mbsf.

The results of coring these holes, all of which are located within 450 m of each other, are summarized in a single lithostratigraphic column (Fig. 1).

Principal drilling results: The sedimentary section comprises four main lithologic units:

1. 0–60 m. Late Pliocene to Holocene. Interbedded dark, carbonate-poor glacial muds and light, carbonate-rich interglacial marine sandy muds.
2. 60–157 m. Middle Miocene to late Pliocene. The unit is divided into four subunits: (a) 60–83 m. Late Miocene/early Pliocene to late Pliocene. Nannofossil oozes with minor diatom-nannofossil oozes and muds, (b) 83–108 m. Late Miocene. Siliceous muds and siliceous oozes, (c) 108–146 m. Middle to late Miocene. Interbedded nannofossil oozes, marly nannofossil oozes, siliceous nannofossil oozes, siliceous muds, siliceous oozes, and (d) 146–157 m. Middle Miocene. Mixed siliceous-calcareous oozes with minor siliceous muds and nannofossil oozes.
3. 157–277 m. Early Miocene to middle Miocene. Siliceous muds and siliceous oozes.
4. 277–315 m. Eocene. Volcaniclastic and altered volcaniclastic muds, sandy muds and sands.

The high recovery and quality of the cores, the microfossil assemblages, and paleomagnetic record make the drilled sequence an excellent late Cenozoic reference section at high latitudes. In addition, about 50 discrete ash layers document adjacent North Atlantic (probably Icelandic) volcanism. The pelagic and hemipelagic Neogene and Quaternary sediments allow us to describe the depositional environment and the properties of surface and bottom-water masses during times of late Cenozoic glacial/interglacial climatic fluctuations (possibly lasting 4.5 m.y.), as well as during the “preglacial” timespan when the Norwegian Sea was filled with temperate to sub-polar water masses.

Seismic data, as well as physical properties measurements and their correlations, reveal a low seismic velocity, about 1.6 km/s, for the sedimentary section. The major intrasedimentary marker at the plateau appears to be of early or basal Miocene age, indicating that the seismic stratigraphy established by earlier studies may have to be reevaluated.

The entire volcanic section contains 137 volcanic flows, 59 volcanoclastic sediment layers, and seven units that may be dikes. The sequence can be divided into upper and lower series that are distinctive in the textural, mineralogical, chemical, and structural characteristics of the flows as well as in the compositions of interlayered volcanoclastic sediments. The entire series was deposited under terrestrial conditions. In the seismic record these series are separated by a band of low-frequency reflectors, the first of which is denoted “K.” The upper volcanic series composes the seaward-dipping reflector sequence at the outer Vøring Plateau.

315–1093 mbsf. Middle(?) / Early Eocene

The upper series consists of 120 tholeiitic basalt flows. Their composition suggests an affinity with the basalts of the North Atlantic Paleogene volcanic province. Two varieties of flows, fine- and medium-grained, which differ in quantitative mineral content, granularity, internal flow fabric, and average thickness have been observed. Interlayered volcanoclastic sediments, which make up about 4% of the series, are mostly basaltic-vitric in composition. Alteration in the upper sequence consists for the most part of smectite and celadonite infilling of vesicles.

1093–1229 mbsf. Early Eocene

The lower series is characterized by glassy, variolitic, and microcrystalline basaltic andesite flows. Interbedded volcanoclastic sedimentary rocks make up about 29% of the section, which also contains two dikes. The flows exhibit two magma types. One is derived by partial fusion of probable sediments or metasediments. The other appears to be formed from strong contamination of upper series tholeiites by the crustal melt. The volcanoclastic sediments include a 7-m-thick ignimbrite, the internal stratification of which indicates a proximal emplacement facies. The ignimbrite and other volcanoclastic units contain significant quantities of quartz and mica of conti-

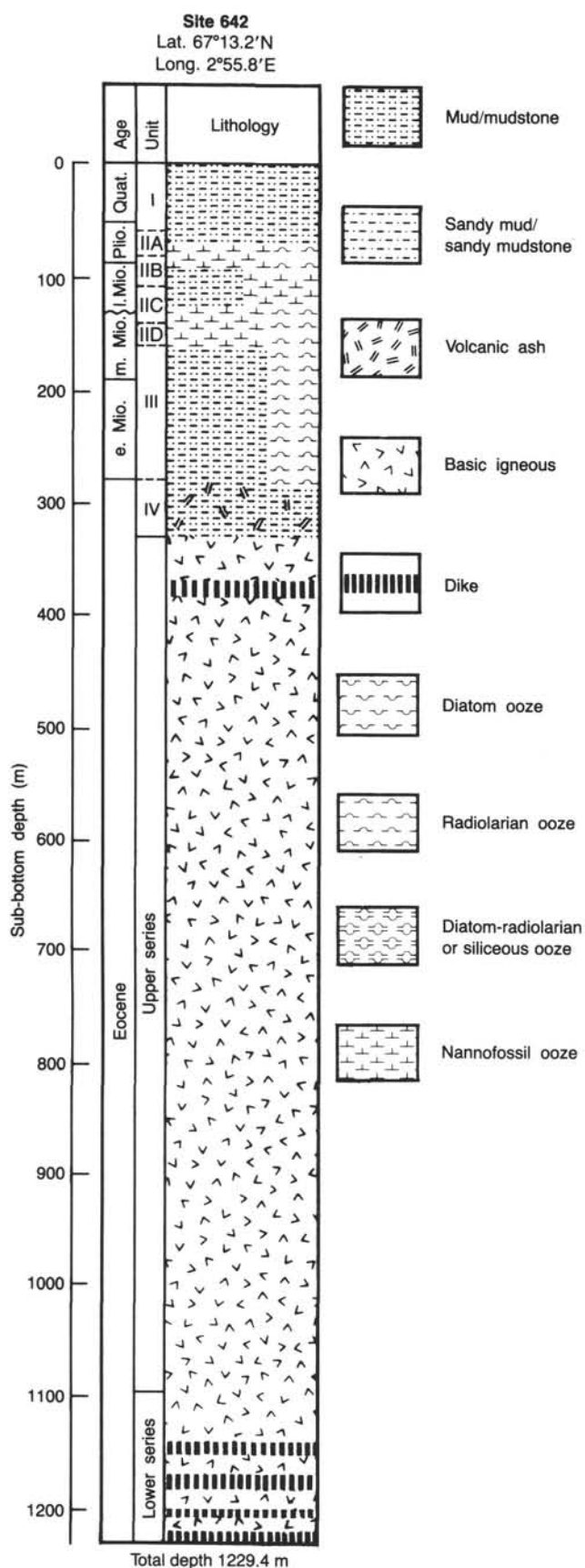


Figure 1. Summary lithostratigraphic column of ODP Leg 104, Site 642.

mental origin. Fragments of leucocratic gneiss and quartz-mica schist occur in at least two volcanoclastic units.

The boundary between the two series is believed to give rise to the onset of the band of low-frequency reflectors at the base of the dipping reflector sequence. Penetration of reflector K is also confirmed by the vertical seismic profile (VSP) experiment done on Leg 104. At the level of this reflector there are also typical changes in physical properties and magnetic character (predominantly reversed polarity throughout the volcanic section).

The drilling results indicate that current models for the evolution of the outer Vøring Plateau, including the mode of emplacement of the volcanic series, will have to be reconsidered.

Two standard Schlumberger logs were run in the intervals 0–208 and 320–1100 mbsf. The results were particularly useful in resolving the detailed flow structure. In terms of recovery, we are pleased to note that only a small number of flows were not detected during the shipboard core analysis.

SCIENTIFIC OBJECTIVES

The primary objective at Site 642 (Fig. 2) was to obtain cores and geophysical data that would provide constraints on the nature and evolution of the Vøring Marginal High and its depositional environment. Because similar features exist at many passive margins, an understanding of the geology of the outer Vøring Plateau might be used to elucidate events occurring during the late rifting/early seafloor spreading evolutionary stage of a passive continental margin.

A key feature of the marginal highs is the occurrence of zones of seaward-dipping reflector sequences. Probably the most thoroughly mapped unit of this kind lies below a moderately thick sediment section and a lower Eocene basalt flow at the outer Vøring Plateau. Several geological models have been put forward to explain the emplacement of these sequences. Within this framework, we aimed to obtain data about the structure, composition, and evolutionary history of the passive margin off Norway.

Specifically, we wanted to address:

1. The thickness, age, and composition of the early Eocene basalt, sampled during DSDP Leg 38, forming the lid of the dipping sequence;
2. The nature, age, physical properties, and mode of emplacement of the dipping reflector sequence proper;
3. The nature and age of the crust characterized by high-amplitude, low-frequency reflectors, underlying the dipping sequence (reflector K);
4. The volume and age of the sediments above the lower Eocene basalt, to study the vertical motion of the plateau through Cenozoic time.

The secondary objective at Site 642 was to have it serve as a key element in a short paleoenvironmental traverse, which consists of three sites (Fig. 2). The transect aimed at sampling the horizontal and vertical sedimentation gradients in the Neogene and Quaternary, and also partially during the Paleogene. The transect location also allows us to determine the paleoceanographic history of the Norwegian Current regime. From DSDP Leg 38 drilling, it is known that the pelagic sediment sequence at the Vøring Plateau is incomplete because of the existence of several major hiatuses. However, a more complete sedimentary record may be established by integrating the drilling information with the existing dense coverage of seismic reflection lines.

The selection of the location for Site 642 was controlled by the objectives requiring greater penetration depth. Although a relatively long Neogene and Quaternary section was expected, the Paleogene section was likely to be incomplete.

The major paleoenvironmental objectives were:

1. Nature and variability of the "glacial"-type Neogene and Quaternary sediment section;

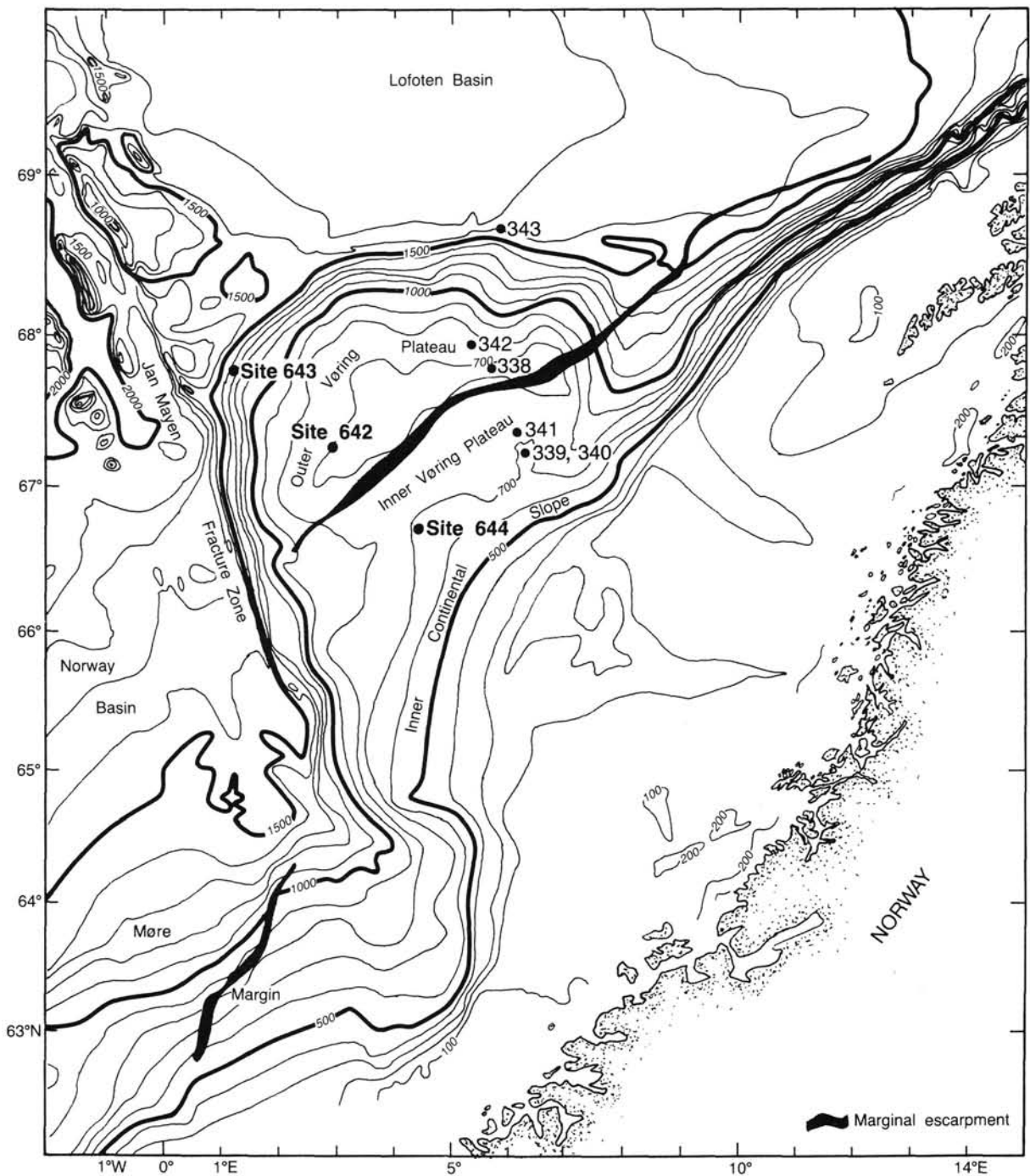


Figure 2. Bathymetry of the Norwegian margin, 62°–70° N (contour interval, 100 fm), and locations of the DSDP Leg 38 sites and of the three Leg 104 Sites 642, 643, and 644 (modified from Mutter et al., 1984).

2. Determination of the initiation of glacial paleoenvironments under the Norwegian Current;
3. Investigation of the “pre-glacial”-type Neogene sediment section;
4. Sampling of any Paleogene sediment section to determine its stratigraphy and depositional environment (especially its depth of deposition), including intrabasaltic sediment layers;
5. Investigations of the timing and nature of Norwegian-Greenland Sea volcanism during the Cenozoic.

OPERATIONS

Bremerhaven Port Call

Leg 104 had its official beginning when the first mooring line was put ashore in the North Harbor of Bremerhaven, Federal Republic of Germany, at 1530 hr, 19 June 1985.

Major ship work items for the port call included: overhaul of no. 3 main generator, installation of a new armature in propulsion motor 14A, installation by DRECO of new guide rollers on

the traveling block/heave compensator, and fueling with 503,000 gal. of diesel fuel. Sixty-four stands of used *GLOMAR Challenger* drill pipe were broken down into joints and inspected by AMF-Tuboscope. In all, 22 joints were downgraded by the inspection. The old pipe was stowed in the hold; new, internally zinc-coated, pipe was made up into stands to replace it. A representative of Rochester Corporation visited the rig to find and correct an electrical leak in logging cable no. 3 that was reported on Leg 102. The cable was tested thoroughly and no fault was found. ODP piston-coring equipment was off-loaded and taken to a local shipyard for shop modification of the rod connections. SEDCO and ODP freight, including the prototype Navidrill coring system, was loaded.

Tours, luncheons, and receptions were held involving numerous officials and dignitaries from educational institutions, industry, and government.

Bremerhaven to Site 642

The last line was cast off at Bremerhaven at 1852 hr, 24 June 1985. After clearing the harbor lock and the Weser Estuary, *JOIDES Resolution* proceeded northward across the uncharacteristically placid North Sea. The vessel averaged nearly 13 kt for the first 2 days of the northward journey. Winds gusting to 30 kt greeted the vessel on the third day as she approached the operating area, located in the Norwegian Sea about 240 mi west-southwest of the Lofoten Islands.

Hole 642A/B

The drill site was approached from the east along the track of MCS profile BGR-1, which was used as a seismic-stratigraphic reference. To improve seismic record quality, the vessel was slowed to 5 kt for the last 10 nmi of the approach. The track was maintained by the Decca navigation system, as satellite navigation (SATNAV) fixes were infrequent during that period. A positioning beacon was dropped on geographic coordinates at 2057 hr, 27 June. The profile was extended 10 nmi beyond the drop point. The towed seismic gear was then retrieved and the ship returned to the beacon.

As preparations for drilling and the pipe trip progressed, enough SATNAV fixes were received to verify that the initial position was about 1.3 nmi to the west-northwest of the desired site coordinates. Using offsets of the automatic stationkeeping (ASK) system, the vessel was carefully offset to the approximate desired location without interruption of the pipe trip. A new beacon was launched and position referencing was established on it before the hole was spudded.

The precision depth recorder (PDR) reading was interpreted for a water depth of 1297 m from the rig's dual elevator stool. Hole 642A was spudded at 1355 hr, 28 June, when the advanced piston corer (APC) system was actuated at a bit depth of 1294 m. The first core barrel arrived on deck completely filled with sediment, indicating that the bit had been positioned below the seafloor. Because the uppermost sediments were of considerable scientific interest and because of measurements for the reentry cone installation, it was imperative that a seafloor core be recovered. It was therefore necessary to raise the core bit a few meters higher to core the water/sediment interface. Because the core intervals overlapped and it is theoretically impossible to core the same section twice in the same hole, it was necessary to designate the new core as number one of Hole 642B. Thus, Hole 642A began and ended with a single core.

The second core attempt, "shot" from 1288 m, recovered 4.8 m of sediment from its 9.5-m stroke and established seafloor depth as 1292.7 m.

The absence of a full-stroke pressure bleedoff indication was noted from the beginning. It was soon realized that a modification of the bit sub for compatibility with the new Navidrill core

barrel (NCB) system was preventing the venting of fluid pressure. That shortcoming proved to be more an inconvenience than a problem as site operation continued.

APC coring continued with only minor mechanical difficulties and the "teething" problems of an inexperienced but highly motivated crew. Mud, glacial material, and nannofossil and diatom oozes were penetrated to 221.1 m below seafloor (mbsf). At this depth, no problem had been experienced in "punching" a full 9.5-m stroke into the stiff sediment, but the operational limit of 100,000-lb overpull on pullout was being approached. On the attempt to retract Core 104-642B-25H from the sediment, the pin connection of the liner seal sub at the top of the inner core barrel parted at 80,000-lb overpull.

A single attempt was then made to retrieve the inner barrel with a fishing spear. The core bit was "washed down" around the embedded core barrel for 6 m, and the spear was lowered to engage it. The initial attempt appeared to engage the "fish" but then lost it. Additional attempts were made with no change, and the spear was retrieved. On recovery, it was found that the plastic core liner, containing 8.5 m of core, had been plucked from the core barrel—leaving it behind.

Allowing further time for fishing the core barrel was judged to be counterproductive, so the hole was plugged by filling it with barite-weighted drilling mud. The bit was then pulled clear of the seafloor for the planned second APC penetration.

Hole 642C

The bit was then pulled back and APC coring continued from the depth reached by the first core. Objectives of operations at Hole 642C included the collection of core orientation and downhole temperature data. Core orientation with the Eastman multishot system appeared to be fully successful. Because of minor "bad luck" problems, only one successful temperature measurement for heat flow calculations had been obtained by the time penetration reached 199.4 mbsf. The self-contained "heat flow shoe" was deployed on the inner barrel that was to take the final APC core before the switch to the XCB system for further coring. After activation of the corer and the 8-min wait for temperature equilibration, the core barrel could not be withdrawn using 100,000 lb overpull. During attempts to free the barrel after drilling down around it, the pin of the upper piston rod was twisted off. The majority of the APC assembly and the temperature instrument were therefore left in the hole.

Hole 642D

The deeper objectives of the reentry exploratory hole remained, and it was again necessary to pull above the seafloor and respud. The rig was offset 10 m to the south to avoid possible contact with the steel at 200-m depth.

Hole 642D was spudded at 1600 hr, 2 July, and was drilled to drill string depth of 1482 m before the XCB "wash" barrel was pulled and continuous coring began. The XCB system performed nearly to perfection through the lower sediment section, which had not been cored in the earlier holes. Core recovery was over 92% for the first twelve cores.

Core 104-642D-14X recovered basalt in the core catcher from 1601 m (309 mbsf). That depth marked the beginning of "base-ment." The plan for the exploratory hole was to core with the XCB and NCB systems to about 50 m into the harder rocks, or further if necessary to find a firm footing for the second casing string. Five additional short XCB cores covered 20 m with only fair core recovery.

The lithology was weathered, rubbly basalt with clay and altered volcanoclastic strata—not good coring for any system. That was the setting given the NCB system for its debut. The first NCB coring, a 2.5-m attempt, produced 1.5 m of core. It contained predominantly softer lithologies and was badly jammed

into the steel liner. The corehead was damaged, but not destroyed. The second attempt penetrated 1 m at a slow rate. When the bit was raised off bottom, a momentary overpull and sudden release was noted. On recovery of the corer by wireline, we noted that the entire assembly was truncated about 31 cm above the former cutting head. About 50 cm of interesting core was recovered, however (for additional details, see the report on the NCB system by M. Storms, available from ODP Engineering and Drilling Operations).

At this stage in operations, we would gain little by spending time on fishing or re-drilling the exploratory hole. The hole was flushed with drilling mud to prepare it for logging, and the bit was pulled to 62 mbsf to expose maximum open hole for the logs.

The standard suite of two Schlumberger combination logs (sonic/induction/natural gamma and density/neutron/spectral gamma) was recorded. Unfortunately, bridges or ledges stopped the sondes and the lower 120 m of hole was not logged.

When logging operations were complete, the bit was run back to total depth and the hole was filled with 100 bbl of weighted mud. The drill string was then tripped for the reentry cone installation.

Hole 642E—Reentry Hole

Work commenced on deploying the reentry cone/conductor casing assembly just after midnight on 4 July. Approximately 15.5 hr was required for the operation. Deployment included dismantling (and reassembling) the guide horn assembly above the moon-pool doors, moving the reentry cone into position on the doors, making up four joints of 16-in. casing and landing it in the cone, assembling the lower BHA, latching the entire assembly together, and lowering it through the open moon-pool doors.

The assembly was then run on drill pipe to the seafloor, the top drive was deployed and Hole 462E was spudded at 2013 hr.

Jetting was found to be much more difficult with the large tri-cone drill bit and casing than it had been with the 11-7/16-in. core bit. That had been expected, to a degree, but the slow progress beyond about 35 mbsf had not been anticipated. Circulation rate and weight were both increased to the maximum to force the casing string into the sediment, but penetration slowed nearly to a standstill. As a last resort, nearly the entire BHA weight was applied while using the heave compensator, and an apparent “breakthrough” was made. After a few meters, the string was picked up. The weight of the casing/cone assembly was not regained until the “drilloff” point was reached indicating that a sag or bow was actually put into the drill string. Jetting continued until progress stopped completely with the casing shoe at 1340.1 m and the “mud skirt” of the reentry cone at 1288 m. That depth was about 4 m shallower than that measured by coring at Hole 642C (30 m north), but within a meter of PDR depth.

A “rotary” shifting tool was made up to an inner core barrel and run on the sandline to shift and release the DSDP paddle-type casing release sub. The inner barrel assembly should have passed the release sub without interference, and the plan was to run several meters past the internal sleeve of the release sub and then engage and shift it upward as the barrel was returned. Instead, the barrel stopped and became stuck with the shifting tool very close to the release sub. After the inner barrel was jarred loose and recovered, the shifting tool was attached directly to the smaller diameter sinker bars. It was then run past the release sub, but tended to stick at varying depths below it. The shifting tool was pulled through the release sub several times without indication of engagement. During these efforts, the pipe was “worked” to alternately apply and release weight on the release sub and to apply a small amount of torque. When

release was not achieved, the shifting tool was retrieved. Another attempt to “work” the pipe was made, with slightly more weight and torque applied. The drill pipe suddenly turned free, indicating release of the cone/casing at 0500 hr on 5 July.

A multishot survey was then run, confirming that there was a 2.5-in. bend in the pipe just above the seafloor and that the casing string was vertical. Because a bent bumper sub (located immediately above the release sub) was suspected, the bit was advanced with caution and slow rotation. The bumper sub passed through the latch sleeve of the running tool without difficulty, but cyclic torque and vibration soon indicated a bent BHA component. Drilling was terminated after about 5 m of new hole, and the drill string was tripped.

As suspected, the bumper sub was visibly bent. It was removed from service, along with the drill collar immediately above it (due to a possibly overstressed pin connection). The remaining BHA connections that had been located above the bumper sub were given a magnetic flux leakage inspection.

First Reentry—14-7/8-in. Core Bit

A 14-3/4-in. tri-cone drill bit had been deployed with the cone for drilling the hole for the surface casing. The unscheduled round-trip and reentry necessitated replacing it with an old-style 14-7/8-in. core bit, as the tri-cone bit had no central passage for the reentry sonar. The drilling/casing BHA was assembled and a routine pipe trip was made to reentry depth.

The logging line was then rigged for reentry and the Mesotech sonar tool was deployed. The cone/casing assembly had been released with the top of the cone (sonar reflectors) at about 1285.3 m. The bit, with sonar landed, was brought to 1282 m. The sonar range to seafloor at that point was 7.3 m, making drill pipe water depth 1289.3 m. It soon became apparent that the bit was positioned almost directly above the cone. The target presentation was highly cluttered (a problem previously reported on Leg 103) and the four reflectors were not readily discernible. An arbitrary ASK offset of 10 m to the north was then made to open the range enough to orient the target image and make gain adjustments to the sonar. As this was being done, a second target appeared about 10 m farther north. Its location and appearance left no doubt that it was the crater and cuttings left by the drilling of Hole 642D. The offset setting was removed and the pipe began to move directly back toward the reentry cone. It was just reaching the rim of the cone when the sonar stopped rotating, and scanning function was lost—possibly only seconds from a “stab” presentation.

The Mesotech tool could not be revived, so a wireline trip was made to replace it with the DSDP-vintage EDO sonar. Sonar scanning resumed after a 3.5-hr delay, with a normal reflector pattern presented. A 2-m offset and 17 min of scanning were required to bring the pipe into position for a reentry stab from 1288.3 m.

The sonar was retrieved and one stand of pipe was run to verify reentry. The top drive was then deployed and an inner core barrel was pumped into place at the bit. Drilling proceeded from 1345 m to 1499 m depth before the “wash” inner barrel was recovered. The multishot tool, run with the overshot on the sandline, indicated a hole deviation of only 1° off vertical.

Drilling then continued toward the intended coring point of 1614 m. The first hard-rock stratum was encountered at 1601 m, and progress slowed drastically at 1611 m. The wash barrel was recovered, and continuous coring began at that point.

Coring was intended to continue only until a suitable casing point could be found—preferably below any soft or unstable transitional sediments or highly altered igneous rock. A sequence of scoriaceous and soft altered basalts, volcanic ash, and altered pyroclastic sediments persisted until a “solid” basalt unit was encountered at 1655 m. The unit continued through the

interval of Core 104-642E-10R to 1672 m, where the 14-7/8-in. hole was terminated.

A wiper trip was then made, wherein the bit was pulled up past the 16-in. casing shoe and returned to the bottom of the hole. Only then was it realized that the hole was in fairly poor condition. Although some hole fill had been encountered on connections, that had been attributed to the poor cleaning action to be expected when drilling large-annulus holes with water as the drilling fluid. The wiper trip, however, found tight spots in the 1630–1640-m interval in both directions and about 19 m of hole fill. A “flush” of 60 barrels of high-viscosity drilling mud was then pumped and displaced to clean the hole and leave it full of seawater.

As a precaution, the casing string was redesigned while the drill string was being retrieved to shorten it by 10 m.

Second Reentry—Surface Casing

The 11-3/4-in. casing string was 369 m long and consisted of thirty joints of 54-lb/ft casing plus a special slip joint and a casing hanger joint. Total time for rigging and making up the casing string was 15 hr, including assembly of the “stinger” BHA. Drill pipe was then added to put the casing shoe at reentry depth.

After the sonar was rigged down, the casing was run to setting depth. Resistance was encountered at 1608–1616 m and 1621–1631 m. At about 1652 m, apparent hole fill was “felt” and pump circulation was used to advance the casing shoe beyond that point. The casing hanger landed and latched in at about the right depth, but the weight did not “come off” to permit rotation and release until the pipe had been lowered about 2.1 m farther. The weight of the second casing string apparently caused the conductor casing and reentry cone to settle by that amount. The surface casing was released at 1803 hr, 9 July, with the 11-3/4-in. casing shoe at 1660.5 m and the “mud skirt” of the reentry cone at 1290 m (1 m below seafloor as indicated by sonar).

The casing was then cemented into place as 115 bbl of 15-lb/gal seawater/cement slurry was mixed and displaced into the casing/hole annulus. When the latch-down top plug landed at the shoe, the “stinger” was unseated and the drill pipe was recovered for the installation of a coring BHA.

Third Reentry—C-4 Bit

A 9-7/8-in. RBI-Type C-4 core bit was selected, because the medium-length chisel inserts could be used to drill out the casing shoe and plug, as well as to core the hard basalt. The coring BHA was assembled and the pipe was run to reentry depth.

Even though the cement had been mixed with seawater to accelerate setting time, calculations indicated that about 24 hr would be required to ensure a good cement job at the low temperature of the shallow sediments. As the short round-trip time would necessitate some waiting, the opportunity was taken to perform a calibration check on the vertical reference unit of the ASK system. The EDO sonar was again deployed, and the reentry cone was used as a reference target as the vessel was taken through 180° of heading change. The 2.5-hr test confirmed that maximum heading-related positioning error was only about 7 m in 1300 m of water.

Reentry scanning then commenced and, as the cone was approached, it was necessary to lower the pipe to 1287 m to get the reflector pattern into proper range. A pipe-measurement error was suspected, as the new depth put the reflectors at about 1289 m (seafloor depth), whereas the 2 m of observed subsidence should have left them at about 1287 m. A successful reentry stab was made after about 25 min of scanning.

The trip then continued to 1623 m, the top drive was deployed, and an inner core barrel with a center bit was pumped

into place. An additional 1.5 hr of “wait-on-cement” time was then spent before drilling-out began. Only about 3 to 4 m of firm cement was found above the casing shoe. The float shoe and aluminum/rubber plug, which normally drill without undue difficulty, required 3 hr to dispose of. Considerable torque persisted for some time after the bit broke through the shoe. When the hole had been cleaned to total depth, about 12 m below the shoe, the center bit was retrieved. The center bit bore deep gouges that appeared to have been afflicted by the core trimming rows of bit inserts.

Coring of new hole commenced at 0045 hr, 11 July, with a 4-m core. Core recovery was a fair 1.9 m, but the diameter of the core was only 48 mm—a full 10 mm under normal gage. Because cores that far under gage had only been observed at the end of very long bit runs where three or four cones were quite loose from advanced bearing failure, another reason for small cores from this new bit was suspected. The prime candidate was a bent-in finger on the bit-throat core guide. A second (7.4-m) core was attempted to see if the basalt would wear away the steel finger. Only 1 m of core fragments and soft material was recovered, and bit failure was conceded.

Upon recovery of the drill string, the bit was indeed found to have undergone advanced bearing failure, with three cutter cones quite loose. The only plausible explanation appeared to be a manufacturing defect. The bit was returned to ODP headquarters in Texas for examination.

Fourth Reentry—F94CK Bit

A bit with similar cutting structure manufactured by Smith Tool Co. was selected to core the apparently interbedded basalt/sediment sequence. The down trip began after minimal turnaround time, and a silk-smooth reentry was made with just 8 min of scanning time. Total round-trip/reentry time was only 12.5 hr.

Coring proceeded with good results through alternating vesicular and massive basalts with a few thin sediment strata. Average penetration rate through 164 m was a quite respectable 3.6 m/hr. After an equally respectable rotating life of 45 hr, the bit was retired when decreasing core diameter signalled progressive bearing failure.

Fifth Reentry—C-57 Bit

Owing to the predominance of basaltic material, the next bit chosen was an RBI C-57 model, which featured conical cutting inserts. An additional stand of drill collars was put into the BHA to provide more weight for the hard-rock cutting structure.

The recently-repaired Mesotech sonar was deployed, and reentry operations began. A fairly good reentry cone target could be discerned from a distance of 10 m or more, but at close range the reflectors, cone and seafloor seemed to merge into an unrecognizable mass. The effect was attributed to excessive signal strength or gain settings in the sonar, as similar problems had been experienced. A “best guess” stab was made at the center of a very poor target after 36 min of scanning. Initial weight indications were favorable and the sonar was recovered to the rig floor before the Martin-Decker began to show suspicious signs that soon confirmed a misstab.

The Mesotech unit was replaced by the old EDO sonar for the new attempt. Scanning again failed to produce a good target, however. The reflector pattern was even worse, and repeated approach maneuvers failed to produce a range of less than 7 to 8 m to the reflectors. The bit was finally lowered to 1286 m and, after nearly 5 hr of scanning, a stab was made at the center of a rather amorphous target. Again the weight indication at the driller’s console looked good, and the sonar was pulled. When we ran a stand of pipe for verification of the reentry, however,

the string “took weight” and confirmed a second consecutive misstab.

By this time it was evident that the reflectors of the cone were at or below the seafloor and were covered with drill cuttings and/or seafloor sediment. At the suggestion of the Drilling Superintendent, the circulating head and kelly hose were rigged and both mud pumps were run at maximum rate to sluice off the rim of the cone and the reflectors. During this process, the bit was positioned at 1286 m and ASK offsets of 3 m were sequentially entered in all directions to sweep the pipe across the cone. As the Mesotech sonar had actually produced the better target presentation of the two runs, it was deployed for the third attempt. It failed to calibrate on the first in-pipe check at 250 m below the rig floor, however, and was pulled in favor of a second EDO tool (the first-string EDO had been badly damaged during the verification attempt). The washing tactic was a complete success, as a normal, distinct four-reflector pattern was acquired immediately. The ASK system was somewhat unresponsive owing to a lack of sufficient environmental forces, but a successful stab was made after 35 min.

The new bit also performed well and averaged about 3.2 m/hr through 73 m of basalt that was possibly somewhat harder than that higher in the hole. Then, after recovery of Core 104-642E-39R with only lumps in the core catcher, circulating pressure was too high on pumping down the next core barrel. That is usually an indication that the bit is partially plugged (throat or nozzles).

The inner core barrel was retrieved and a special bit deplugger was pumped down at high velocity in an attempt to dislodge any material that might be obstructing the bit throat. The deplugger was “spudded” with the wireline, but the abnormal pressure persisted. The heavy wall drilling joints (HWDJ) were laid out and the pipe trip continued after an inner barrel had been pumped down without the desired pressure decrease. A stop was made to wash off the reentry cone as on the previous reentry. (The practice became standard procedure for the remainder of operations at Hole 642E.)

On recovery, the throat of the bit was found to be completely plugged with pulverized basalt and claylike material. The bit showed no signs of wear or failure, but it had accumulated 23 rotating hours and was removed from service. It was replaced by an identical RBI C-57 bit.

Sixth Reentry—C-57 Bit

An easy (12-min) reentry was made with the EDO sonar. Six m of hole fill was found after the trip (fill was persistent for the remainder of operations, almost certainly because of cuttings falling back from the seafloor.)

After only 38 m had been cored, a zero-recovery inner barrel was retrieved and the subsequent barrel again showed excessive pressure on pump-down. The inner barrel was pulled and two wireline runs were made to use both the deplugger and shorter, chisel-shaped core breaker. Circulating pressure decreased, chalk indications on the core barrel were favorable, and another core was attempted. There was no recovery, however, and the plugged-bit indications were back. The pipe was tripped and the bit was found to be in the same condition as the previous one. Because of its like-new condition (despite 18-hr use) and because the bit supply was not unlimited, the same bit was cleaned out and reinstalled for continued coring.

Seventh Reentry—C-57 Bit

The minor problem with the Mesotech sonar had been rectified, and it received the reentry call. The reflector target pattern remained more difficult to resolve with this tool, despite minor modification to reduce incoming signal strength. The reentry stab was made after 40 min of scanning.

The cause of the plugged bits was, by this time, a topic of lively discussion. Formation conditions or contact with hole fill were suspected, as the RBI bits were manufactured to the same specifications as bits from previous vendors—except that it was noted that the jet nozzle size was larger than on the older generation bits. Inadequate hydraulics at the bit face were suspected by rig personnel for that reason. The C-57 bits also differed in that the detail of cutting insert shape was new to DSDP/ODP operations. As speculation continued, it was learned that the bit had again plugged after 38 m of coring.

As before, attempts to unplug the bit were unsuccessful and a round-trip was necessary. The same type of plug was again found in the throat. The bit was retired after 28 rotating hours, still in excellent condition. The rate of penetration had averaged over 3 m/hr with much of the coring done with a plugged throat—a situation of mixed reviews. The cause-of-plugging issue was not resolved, but there was sufficient cause to discontinue use of the RBI bits, at least temporarily.

Eighth Reentry—F99CK Bit

The amount of sediment and claylike alteration products in the material being cored had decreased to a very small amount, and an extra hard formation “button” F99CK bit (a survivor from the DSDP) was selected for the next run. Another stand of three drill collars was added to the BHA to provide the weight necessary for good performance of bits of that type.

The Mesotech tool had been modified further and was used again for the reentry. The pipe swung across the cone on the very first move of the search and a stab was made after 6 min on the basis of a marginal target presentation. Although the pattern had appeared to be centered, the rig floor reported an unfavorable weight indication. Considering the time involved for a wireline trip and conclusive verification, the bit was pulled back to scanning depth and scanning was reinitiated. A successful stab was made after an additional 7 min.

On two occasions there were pressure indications of bit plugging, but both followed cores with considerable recovery and both times the bit was cleared successfully with the core breaker. It is believed that pieces of core fell from the core catchers during retrieval of the core barrel and became lodged at the bit throat.

Performance of the hard-rock bit exceeded expectations, and an extraordinary run of 173.5 m in 41.8 hr ensued before reduced core diameter indicated bearing failure. Good heave compensation, porous vesicular basalt and the long, heavy BHA were all factors. Because of the bit’s great success, its “littermate” was chosen for the succeeding run.

Ninth Reentry—F99CK Bit

The round-trip and reentry were difficult owing to bad weather and were slowed by swells in excess of 3 m. The EDO sonar was used, as an uncluttered presentation was desired to minimize the effects of vessel motion. The target presentation was normal and the heave compensator was effective in keeping drill string motion to a minimum during the reentry operation. The environment made precise maneuvering with the ASK system difficult, however, and the scan took 53 min before the reentry was made.

The new bit accepted the challenge of its predecessor and actually drilled faster with increasing depth. One “dropped-core” obstruction was cleared with the core breaker. The end of an outstanding bit run was approaching when a sediment unit was encountered. There were no particular indications of bit failure, but 45.5 hr of rotating time had accrued. The new lithology contained altered volcaniclastic material, and the ROP had dropped sharply. The bit was therefore pulled “green” after a prodigious 211.8 m of basalt drilling with an average ROP of 4.7 m/hr.

Tenth Reentry—F94CK Bit

With time running out and the unknowns of reflector "K" lying ahead, a "drill anything" bit with intermediate-length chisel inserts (Smith F94CK cutters) was chosen.

The reentry was made with the Mesotech sonar. It was a difficult reentry, with the reflectors blending into the seafloor and forming a bright ring. It appeared that they were again partially covered with cuttings despite the "washing" operation on each out-trip. The stab was finally made into the center of a "pile" without discernible reflectors at the moment. The reentry was good, but 24 m of fill in the hole contributed to doubts that continued reentry operations would be feasible.

Coring continued through tuffs and basalts, some intensely altered. Most was fairly easy drilling, but an exceptionally hard basalt dike of about 15 m was penetrated. One bit obstruction was again cleared with the deplugger. Coring operations were finally terminated by time limitations and achievement of objectives at a total depth of 2518.4 m (1229.4 mbsf).

The hole was given an extra-thorough combination bentonite and polymer mud flush before the pipe was tripped for the logging BHA. The reentry cone was also given an extra thorough washing with the bit at 1287 m. A summary of coring operations at Site 642 is provided in Table 1.

Eleventh Reentry—Logging BHA

A short, open-ended logging BHA was assembled and run to reentry depth. Because of the poor presentation on the previous reentry, the EDO tool was run in the hope that anything would be an improvement. On commencement of scanning, it appeared that the washing tactic had once more been effective. A normal four-reflector pattern was detected but became indistinct as the drill string approached the cone. The reflectors fused with the seafloor on the 45° presentation and the 8° transducer seemed to "look over" the reflectors. In addition, the drill string was unresponsive to small ASK offsets—probably because of its light weight. The proper pattern was finally acquired after the pipe had been lowered almost to the seafloor, and the stab was made after 86 min of scanning.

On retrieval, the sonar tool was exchanged for logging equipment and the downhole measurements phase of operations began. The standard suite of two Schlumberger combination logs was recorded first. The logs were of good quality, but the tools would not pass an obstruction in the hole at 2388 m, 130 m off total depth. Sonic waveforms were recorded into the cased hole interval in an attempt to evaluate the cement job in the absence of cement-bond log equipment. Good bonding appeared to extend about 100 m above the shoe, with the cement top about 40 m above that.

The next downhole investigation attempt was with the LDGO borehole televiewer. Several problems related to the tool's light weight and stiff centralizers were experienced, costing considerable time. The tool eventually was deployed into the open hole but problems with the depth measuring system then resulted in loss of depth control and the experiment was terminated due to expiration of allotted time.

The vertical seismic profile (VSP) was the final in-hole measurement to be conducted. The 2.5-in. diameter clamped-geophone sonde was lowered into the borehole without difficulty and actually was worked past the obstruction that had stopped the larger logging tools. Owing to time limitations, however, the first and lowermost clamping station was made at 2400-m depth and no attempt was made to go deeper. The heave compensator was opened and the drill string was lowered to seat the large-diameter latch sleeve of the DSDP 16-in. casing running tool (located at the top of the BHA) in the base of the reentry cone. With 10,000 lb of BHA weight resting on the cone, the drill

string was immobilized to reduce noise for the duration of the experiment. A 1200-in³ air gun was suspended in the water from no. 3 crane and was used as a sound source for the seismometer. Several shots were recorded at each of 44 stations between 2400 m and 1740 m depth. Two failures of the geophone clamping arm safety shear pin occurred, one of which caused a 3-hr replacement delay and the second of which resulted in the termination of the experiment as time was running out.

As soon as the VSP experiment had been rigged down, the drill string was recovered. The ship departed immediately for Site 643 at 0000 hr, 2 August.

SEDIMENT LITHOLOGY

Lithologic Summary

Data and Methods

The sedimentary sequence drilled at Site 642 has been divided into four lithologic units: Unit I is a terrigenous-dominated unit of glacial/interglacial depositional cycles, Unit II contains a mixture of terrigenous/siliceous biogenic/calcareous biogenic deposits and has been split into four subunits, Unit III is a terrigenous/siliceous biogenic unit, and Unit IV is dominated by volcanic ash and altered volcanic ash. The lithologic divisions are summarized in Table 2 and Figure 3, while the smear-slide compositional data for these units are included in the barrel sheets and summarized in Figures 4 and 5. Shipboard carbonate-bomb analyses were conducted on samples used for physical properties tests; these results are shown in Figure 6 for Hole 642C. One-hundred-thirty-five samples were analyzed by X-ray diffraction (XRD) for bulk mineralogy, whereas oriented pastes of 35 samples were analyzed for clay mineralogy. The estimated mineral abundances are shown in Figure 7 for Holes 642C and D. Although the estimates of mineral abundances obtained from the XRD data are only relative and semiquantitative, a comparison of the carbonate contents estimated by XRD and measured by carbonate bomb (on splits of the same sample) reveals similar patterns for both analytical techniques (Figure 6). As a result, the XRD results provide useful semiquantitative estimates of bulk sediment composition. Volcanic ash is a minor to common component in most of the sedimentary sequence at Site 642, and the locations and characteristics of these discrete and disseminated volcanic ash layers are discussed in detail in the last portion of this lithologic summary. For this reason, the distribution of ashes is described only briefly in the discussion of individual lithologic units.

Lithologic Units

Unit I

Core 104-642A-1H; Section 104-642B-1H-1 to Sample 104-642B-8H-6, 132 cm (0–65.7 m sub-bottom); Section 104-642C-1H-1 to Sample 104-642C-8H-2, 108 cm (0–59.7 m sub-bottom). Age: late Pliocene to Recent.

Unit I consists predominantly of muds and sandy muds that display a repeated alternation of dark and light layers on two scales: a large scale (approximately 3 to 5 m thick) and a smaller scale (approximately 30 cm to 1 m thick). Although the exact colors present in the dark and light layers change downcore, these color alternations appear to be the most notable and consistent indicators of repeated complex cycles of sedimentation (Figs. 8 and 9). On the small scale, the most complete dark layers contain a basal dark-colored sandy mud, and grade upward into a very dark-colored sandy mud with a sharp base, a bioturbated top, and some Fe/Mn-enriched laminations near the top. These layers are then overlain by a light-colored, bioturbated

Table 1. Site 642 coring summary.

Core no. 104-	Date (1985)	Time (UTC)	Interval		Meters cored (m)	Meters recovered (m)	Percent recovery
			top (mbsf)	bottom (mbsf)			
Hole 642A							
1H	28 June	1430	1.3	10.8	9.5	9.9	104.2
Hole 642B							
1H	28	1520	0	4.8	4.8	4.8	98.9
2H	28	1626	4.8	14.3	9.5	8.7	91.2
3H	28	1755	14.3	20.7	6.4	6.2	96.9
4H	28	1906	20.7	29.4	8.7	9.1	104.3
5H	28	2040	29.4	38.9	9.5	10.3	107.9
6H	28	2142	38.9	47.4	8.5	8.4	98.8
7H	28	2217	47.4	56.9	9.5	9.9	104.3
8H	28	2328	56.9	66.4	9.5	9.8	102.8
9H	29	0045	66.4	75.9	9.5	9.9	103.9
10H	29	0145	75.9	85.4	9.5	9.9	103.7
11H	29	0255	85.4	94.9	9.5	9.9	104.4
12H	29	0342	94.9	104.2	9.3	9.3	100.1
13H	29	0440	104.2	114.0	9.8	9.8	99.7
14H	29	0540	114.0	123.5	9.5	1.8	18.4
15H	29	0715	123.5	128.1	4.6	4.5	98.0
16H	29	0850	128.1	138.0	9.9	9.9	99.9
17H	29	0945	138.0	147.8	9.8	9.7	98.8
18H	29	1044	147.8	157.7	9.9	9.6	97.1
19H	29	1134	157.7	167.4	9.7	9.5	98.0
20H	29	1220	167.4	177.1	9.7	9.8	101.0
21H	29	1305	177.1	186.7	9.6	9.5	99.4
22H	29	1346	186.7	196.0	9.3	9.4	101.4
23H	29	1420	196.0	205.6	9.6	9.7	100.7
24H	29	1525	205.6	213.1	7.5	7.4	98.9
25H	29	1750	213.1	221.1	8.0	8.1	100.8
Hole 642C							
1H	30	0010	0	3.4	3.4	3.4	100.3
2H	30	0445	3.4	13.2	9.8	10.0	101.9
3H	30	0537	13.2	23.1	9.9	9.9	100.0
4H	30	0634	23.1	32.9	9.8	9.9	101.0
5H	30	0732	32.9	41.4	8.5	8.6	101.5
6H	30	0836	41.4	50.9	9.5	9.2	96.9
7H	30	1005	50.9	57.1	6.2	6.3	102.3
8H	30	1105	57.1	60.7	3.6	3.9	109.4
9H	30	1205	60.7	63.5	2.8	2.8	100.0
10H	30	1254	63.5	73.0	9.5	9.5	100.0
11H	30	1400	73.0	82.5	9.5	9.8	103.2
12H	30	1445	82.5	92.0	9.5	9.6	101.2
13H	30	1540	92.0	101.5	9.5	3.7	38.5
14H	30	1645	101.5	111.0	9.5	9.9	103.7
15H	30	1810	111.0	120.5	9.5	9.5	100.0
16H	30	1858	120.5	130.0	9.5	9.4	99.2
17H	30	1943	130.0	139.5	9.5	8.7	91.7
18H	30	2035	139.5	149.0	9.5	8.7	91.6
19H	01 July	0118	149.0	158.5	9.5	10.1	106.6
20H	01	0231	158.5	168.0	9.5	9.8	102.8
21H	01	0425	168.0	177.5	9.5	9.6	101.1
22H	01	0540	177.5	184.3	6.8	7.0	103.4
23H	01	0908	184.3	192.4	8.1	8.1	99.4
24H	01	1046	192.4	199.6	7.2	7.5	103.8
Hole 642D							
1W	01	2050	0	189.9	189.9	5.4	2.8
2X	01	2200	189.9	199.6	9.7	9.9	101.8
3X	01	2257	199.6	209.2	9.6	7.9	81.9
4X	01	2350	209.2	218.9	9.7	9.7	99.5
5X	02	0100	218.9	228.5	9.6	9.7	101.5
6X	02	0203	228.5	238.2	9.7	7.8	80.1
7X	02	0309	238.2	247.8	9.6	9.8	101.9
8X	02	0401	247.8	257.5	9.7	9.6	99.2
9X	02	0455	257.5	267.1	9.6	9.8	102.3
10X	02	0602	267.1	276.8	9.7	9.8	100.7
11X	02	0654	276.8	286.5	9.7	3.3	33.5
12X	02	0756	286.5	296.2	9.7	9.8	101.0
13X	02	0850	296.2	305.8	9.6	6.9	72.3
14X	02	0957	305.8	315.4	9.6	3.4	35.2
15X	02	1100	315.4	315.9	0.5	0.7	138.0
16X	02	1225	315.9	317.4	1.5	0.6	38.0
17X	02	1351	317.4	321.6	4.2	2.2	51.6

Table 1 (continued).

Core no. 104-	Date (1985)	Time (UTC)	Interval		Meters cored (m)	Meters recovered (m)	Percent recovery
			top (mbsf)	bottom (mbsf)			
Hole 642D (Cont.)							
18X	02 July	1530	321.6	326.4	4.8	1.9	39.4
19N	02	1905	326.4	328.9	2.5	1.5	60.4
20N	02	2208	328.9	329.9	1.0	0.5	50.0
Hole 642E							
1W	06	1745	56.0	210.0	154.0	9.7	6.3
2W	06	2310	210.0	322.5	112.5	3.6	3.2
3R	07	0020	322.5	326.5	4.0	1.5	37.5
4R	07	0128	326.5	334.9	8.4	1.5	17.8
5R	07	0458	334.9	344.6	9.7	4.2	43.1
6R	07	0700	344.6	354.3	9.7	2.6	26.3
7R	07	0940	354.3	363.9	9.6	3.2	33.4
8R	07	1140	363.9	365.9	2.0	0.3	15.5
9R	07	1820	365.9	373.5	7.6	3.0	39.5
10R	08	0045	373.5	383.2	9.7	3.3	33.8
11R	11	0320	383.2	387.2	4.0	1.9	47.5
12R	11	0750	387.2	394.8	7.6	1.0	13.1
13R	12	0015	394.8	399.8	5.0	1.7	34.2
14R	12	0200	399.8	405.3	5.5	1.7	30.9
15R	12	0510	405.3	414.8	9.5	7.7	81.0
16R	12	0750	414.8	424.3	9.5	4.4	46.5
17R	12	1115	424.3	432.7	8.4	4.9	58.2
18R	12	1526	432.7	442.1	9.4	6.0	63.9
19R	12	1805	442.1	451.6	9.5	5.9	62.2
20R	12	2215	451.6	461.0	9.4	4.8	51.0
21R	13	0245	461.0	470.5	9.5	6.5	68.3
22R	13	0715	470.5	479.9	9.4	7.5	79.9
23R	13	0930	479.9	489.4	9.5	3.5	36.8
24R	13	1415	489.4	493.4	4.0	2.0	48.7
25R	13	1745	493.4	501.8	8.4	5.0	59.3
26R	13	2205	501.8	511.2	9.4	6.6	70.2
27R	14	0201	511.2	520.6	9.4	5.8	61.8
28R	14	0502	520.6	530.0	9.4	5.2	54.8
29R	14	0840	530.0	539.5	9.5	2.7	28.8
30R	14	1107	539.5	549.0	9.5	7.4	78.0
31R	14	1445	549.0	558.4	9.4	5.8	61.8
32R	16	0309	558.4	564.9	6.5	4.1	63.1
33R	16	0715	564.9	574.4	9.5	6.8	71.6
34R	16	1050	574.4	583.9	9.5	0.8	8.4
35R	16	1426	583.9	593.4	9.5	5.7	59.6
36R	16	1850	593.4	602.8	9.4	3.0	32.0
37R	16	2210	602.8	612.2	9.4	2.1	22.3
38R	17	0206	612.2	621.6	9.4	5.0	53.2
39R	17	0611	621.6	631.1	9.5	0.1	0.6
40R	18	0623	631.1	640.6	9.5	3.6	37.9
41R	18	1015	640.6	650.1	9.5	4.5	47.5
42R	18	1352	650.1	659.6	9.5	3.0	31.7
43R	18	1713	659.6	669.1	9.5	0.0	0.0
44R	19	0115	669.1	678.6	9.5	0.0	0.3
45R	19	2140	678.6	688.1	9.5	5.5	58.0
46R	20	0150	688.1	697.6	9.5	4.9	51.6
47R	20	0515	697.6	707.1	9.5	1.3	13.7
48R	20	0853	707.1	716.5	9.4	0.0	0.4
49R	20	1600	716.5	716.6	0.1	0.0	40.0
50R	21	0315	716.6	723.3	6.7	2.2	32.8
51R	21	0430	723.3	723.8	0.5	0.3	60.0
52R	21	0820	723.8	729.2	5.4	6.1	113.0
53R	21	1233	729.2	738.7	9.5	3.7	38.9
54R	21	1515	738.7	748.2	9.5	5.1	54.0
55R	21	1823	748.2	757.6	9.4	4.2	44.7
56R	21	2325	757.6	759.1	1.5	0.7	46.6
57R	22	0215	759.1	766.1	7.0	5.2	74.3
58R	22	0615	766.1	775.5	9.4	6.2	65.9
59R	22	1000	775.5	784.9	9.4	4.0	42.6
60R	22	1245	784.9	794.3	9.4	2.7	28.7
61R	22	1500	794.3	803.8	9.5	2.8	29.5
62R	22	2118	803.8	809.8	6.0	1.3	21.6
63R	23	0015	809.8	815.8	6.0	4.3	71.8
64R	23	0315	815.8	825.2	9.4	6.7	71.3
65R	23	0520	825.2	834.7	9.5	1.5	15.8
66R	23	0822	834.7	844.2	9.5	4.7	49.5
67R	23	1000	844.2	853.7	9.5	2.8	29.5
68R	23	1200	853.7	863.2	9.5	2.9	30.5
69R	23	1505	863.2	872.7	9.5	4.2	44.3
70R	23	1803	872.7	880.7	8.0	2.0	25.0

Table 1 (continued).

Core no. 104-	Date (1985)	Time (UTC)	Interval		Meters cored (m)	Meters recovered (m)	Percent recovery
			top (mbsf)	bottom (mbsf)			
Hole 642E (Cont.)							
71R	24 July	0215	880.7	890.1	9.4	5.3	56.4
72R	24	1833	890.1	896.3	6.2	2.4	38.7
73R	24	2145	896.3	902.4	6.1	5.2	85.2
74R	25	0201	902.4	911.9	9.5	7.5	79.0
75R	25	0500	911.9	921.4	9.5	2.7	28.4
76R	25	0730	921.4	930.9	9.5	2.5	26.3
77R	25	1025	930.9	940.4	9.5	3.9	41.0
78R	25	1345	940.4	949.9	9.5	2.9	30.5
79R	25	1835	949.9	959.3	9.4	2.7	28.8
80R	25	2124	959.3	968.3	9.0	3.1	34.4
81R	26	0105	968.3	977.8	9.5	3.0	31.6
82R	26	0510	977.8	987.3	9.5	1.0	10.5
83R	26	0700	987.3	996.8	9.5	2.2	23.1
84R	26	0940	996.8	1006.3	9.5	1.5	15.8
85R	26	1307	1006.3	1015.8	9.5	7.0	73.8
86R	26	1600	1015.8	1025.3	9.5	4.4	46.4
87R	26	1930	1025.3	1034.8	9.5	2.6	27.3
88R	26	2218	1034.8	1044.3	9.5	2.3	24.2
89R	27	0105	1044.3	1053.8	9.5	1.6	16.8
90R	27	0345	1053.8	1063.3	9.5	3.8	40.0
91R	27	0725	1063.3	1072.8	9.5	3.1	32.6
92R	27	0920	1072.8	1078.8	6.0	2.6	43.3
93R	27	1216	1078.8	1085.0	6.2	7.2	116.3
94R	27	1544	1085.0	1094.5	9.5	6.8	71.7
95R	27	2350	1094.5	1101.9	7.4	1.9	25.7
96R	28	1205	1101.9	1108.9	7.0	0.5	7.1
97R	28	1423	1108.9	1115.8	6.9	3.0	43.5
98R	28	1635	1115.8	1125.2	9.4	3.1	33.0
99R	28	1914	1125.2	1134.7	9.5	2.8	29.6
100R	28	2145	1134.7	1144.1	9.4	1.9	20.2
101R	29	0018	1144.1	1153.5	9.4	2.5	26.6
102R	29	0403	1153.5	1163.0	9.5	3.7	38.9
103R	29	0720	1163.0	1166.5	3.5	2.0	57.1
104R	29	1135	1166.5	1172.5	6.0	3.9	65.0
105R	29	1544	1172.5	1181.9	9.4	5.8	61.8
106R	29	2108	1181.9	1191.4	9.5	1.4	14.7
107R	30	0148	1191.4	1200.9	9.5	5.7	60.1
108R	30	0408	1200.9	1210.4	9.5	3.0	31.6
109R	30	0645	1210.4	1219.9	9.5	2.0	21.0
110R	30	0940	1219.9	1229.4	9.5	0.5	5.3

mud. The less-complete small-scale cycles show a simpler alternation of dark sandy muds and light-colored muds. The larger-scale cycles result from downcore changes in the relative abundances of dark and light layers, with the large-scale "dark" zones characterized by abundant and closely-spaced small-scale dark layers, while the large-scale "light" zones contain widely spaced and poorly developed small-scale dark layers (Figs. 8 and 9). The large-scale cycles are less easily identified downcore at Site 642, however, because the smaller-scale dark layers become more uniformly spaced and less intense below approximately 35 m sub-bottom. The major colors present in the lighter layers include gray (5Y 5/1), olive gray (5Y 5/2, 5Y 4/2), dark gray (5Y 4/1), grayish brown (2.5Y 5.2), dark grayish brown (2.5Y 4/2), and greenish gray (5GY 5/1). Of these, gray, olive gray, and dark gray are the most common. The major colors present in the darker layers include olive gray (5Y 4/2), dark olive gray (5Y 3/2), dark gray (5Y 4/1), and very dark gray (5Y 3/1), with dark gray and very dark gray most common. Bedding thicknesses range from less than 5 cm to greater than 50 cm for both light and dark layers; in a general sense, however, the lighter layers tend to be thicker than the adjacent darkest layers. Bioturbation is common throughout this unit.

The light and dark layers of Unit I exhibit general differences in dropstone abundance and carbonate content, but these differences are of limited magnitude and do not occur in all adjacent light/dark pairs. For example, dropstones of sand size and

larger (up to 1.5 cm in diameter) were identified in both light and dark layers during visual core description (Fig. 10). These dropstones occur both individually and in concentrated zones, with lithologies ranging from mudstone to crystalline rock fragments. Although dropstones were observed in both light and dark layers, the core description data indicate that the dropstones occur approximately three times more often in dark than in light layers (compare Figs. 8 and 9 with Fig. 10). Foraminifers, on the other hand, are more common in the light layers than in the dark ones. This trend is evident from the visual (not microscopic) identification of foraminifers at ten horizons in Unit I during visual core description; of those ten occurrences, nine are located in light-colored layers, suggesting a general pattern of enrichment in foraminifers within the light-colored layers.

This subtle pattern of compositional differences between light and dark layers is also apparent in smear-slide, carbonate bomb, and XRD data (Figs. 4 through 7). Only seven smear-slide samples from Unit I were classified as calcareous oozes or marly calcareous oozes; one of these was taken from a dark layer, while the other six were taken from light layers. Carbonate-bomb analyses indicate that samples from light layers contain up to 20% carbonate, with relative XRD abundances ranging up to 40% carbonate. As a result, all available data indicate that carbonates tend to be enriched in the lighter layers of Unit I. Additional preliminary shore-based carbonate analyses (obtained by thermal infrared spectroscopy) are summarized in Ta-

Table 2. Summary of lithologic units at Site 642.

Unit	Lithology	Interval (m sub-bottom)	Age	Average organic carbon content (%)	Occurrence, Sample 104-
I	Interbedded dark, carbonate-poor glacial muds and light, carbonate-rich interglacial sandy muds	0-65.7 (Hole 642B); 0-59.7 (Hole 642C)	late Pliocene- Holocene	0.39	642A-1H; 642B-1H to 642B-8H-6, 132 cm; 642C-1H to 642C-8H-2, 108 cm
IIA	Nannofossil oozes with minor diatom-nannofossil oozes and muds	65.7-90.4 (Hole 642B); 59.7-82.5 (Hole 642C)	late Miocene(?) - late Pliocene	0.83	642B-8H-6, 132 cm, to 642B-11H-4, 50 cm; 642C-8H-2, 108 cm, to 642C-11H-CC
IIB	Siliceous muds and siliceous oozes	90.4-107.2 (Hole 642B); 82.5-107.5 (Hole 642C)	late Miocene	Not available	642B-11H-4, 50 cm, to 642B-13H-2; 642C-12H-1 to 642C-14H-4.
IIC	Interbedded nannofossil oozes, marly nannofossil oozes, siliceous nannofossil oozes, siliceous muds, and siliceous oozes	107.2-138.0 (Hole 642B); 107.5-145.5 (Hole 642C)	middle Miocene- late Miocene	1.07	642B-13H-3 to 642B-16H-CC; 642C-14H-5 to 642C-18H-4.
IID	Mixed siliceous-calcareous oozes; minor siliceous muds and nannofossil oozes	138.0-158.4 (Hole 642B); 145.5-156.6 (Hole 642C)	middle Miocene	Not available	642B-17H-1 to 642B-19H-1, 72 cm; 642C-18H-5 to 642C-19H-6, 15 cm.
III	Siliceous muds and siliceous oozes	158.4-221.1 (Hole 642B); 156.5-199.6 (Hole 642C); 189.9-277.6 (Hole 642D)	early-middle Miocene	1.40	642B-19H-1, 72 cm, to 642B-25H; 642C-19H-6, 15 cm, to 642C-24H; 642D-2X to 642D-11X-1, 78 cm
IV	Volcaniclastic and altered volcaniclastic muds, sandy muds, and sands; some repeated coarsening-upward sequences	277.6-315.2 (Hole 642D)	Eocene	1.34	642D-11X-1, 78 cm, to 642D-14X-CC, 33 cm
V	Interbedded basalts and volcaniclastic sediments	315.2-1229.4 (Hole 642D and Hole 642E)	Eocene	Not available	642D-14X-CC, 33 cm, to 642D-15X; 642E-2R to 642E-110R.

ble 3 and are plotted in Figure 8. These analyses provide a preliminary carbonate curve for Unit I and indicate a pronounced change in carbonate accumulation across the Brunhes/Matuyama magnetic boundary. Below the Brunhes/Matuyama boundary, carbonate contents are very low, thereby complicating efforts to identify interglacials. The majority of smear-slide samples from Unit I, however, are classified as muds or sandy muds, with little compositional difference between the light and the dark layers. The muds have a compositional range of 10%-35% quartz, 0%-5% feldspar, 0%-5% detrital carbonate, 60%-85% clay minerals, and 0%-5% nannofossils and foraminifers, with an approximate average composition of 20% quartz, 1% feldspar, 1% detrital carbonate, and 77% clay. Trace and accessory phases in the muds include hornblende, pyrite, glauconite, and undifferentiated heavy minerals. The textural composition of the muds is approximately 1%-5% sand, 15%-40% silt, and 60%-80% clay (Fig. 5). The sandy muds have a compositional range of 35%-65% quartz, 0%-5% feldspar, 0%-2% detrital carbonate, and 30%-60% clay, and a textural composition of 10%-50% sand, 20%-30% silt, and 30%-60% clay.

Semiquantitative estimates of bulk mineralogy by XRD analyses (Fig. 7) indicate that clay mineral abundances remain low and uniform in both light and dark layers, but downcore fluctuations do occur in the quartz/calcite ratio and the clay mineralogy. As mentioned above, the light-colored layers appear to contain more calcite and a higher illite/chlorite ratio than the dark layers. A terrigenous origin for the clay mineral assemblage in this unit is indicated by its low smectite, high illite, and relatively high feldspar abundances.

Unit I contains very little volcanic ash, mostly as thin ash lenses and disseminated ash in Core 104-642C-7H. One well-developed ash layer was observed in Unit I, as described below in the discussion of distal tephra deposits.

Unit II

Sample 104-642B-8H-6, 132 cm, to Sample 104-642B-19H-1, 72 cm (65.7-158.4 m sub-bottom); Sample 104-642C-8H-2, 108 cm, to Sample 104-642C-19H-6, 15 cm (59.7-156.6 m sub-bottom). Age: middle Miocene to late Pliocene.

Unit II consists of four subunits, defined by varying importance of terrigenous, siliceous biogenic, and calcareous biogenic components. Semiquantitative XRD estimates of bulk mineralogy (Fig. 7) indicate that clay mineralogy content increases slightly downcore through Unit II, accompanied by a decrease in feldspar content. Within the clay mineral fraction, illite and chlorite contents decrease downcore, while smectite becomes more abundant; the detailed associations of lithology and clay type, however, indicate a predominantly detrital origin for the clay mineral assemblages throughout Unit II.

Subunit IIA. Sample 104-642B-8H-6, 132 cm, to Sample 104-642B-11H-4, 50 cm (65.7-90.4 m sub-bottom); Sample 104-642C-8H-2, 108 cm, to Section 104-642C-11H CC (59.7-82.5 m sub-bottom). Age: late Miocene/early Pliocene to late Pliocene.

This subunit predominantly consists of nannofossil ooze, but varying amounts of terrigenous and siliceous biogenic components are also present. As a result, nannofossil oozes, diatom-nannofossil oozes, and muds occur within this interval. The nannofossil oozes and muds generally contain 5%-20% siliceous material, reflecting its importance throughout this subunit (Fig. 4). Important colors in this subunit are olive gray (5Y 4/2), green gray (10Y 4/2), dark greenish gray (5GY 4/1), grayish green (5G 4/2), and dusky yellow-green (5GY 5/2).

This interval is moderately to heavily bioturbated, so that original bedding structures generally have been destroyed. Bioturbation features include several well-developed *Zoophycos* trace fossils, multiple faint simple burrows, and pyritized burrows.

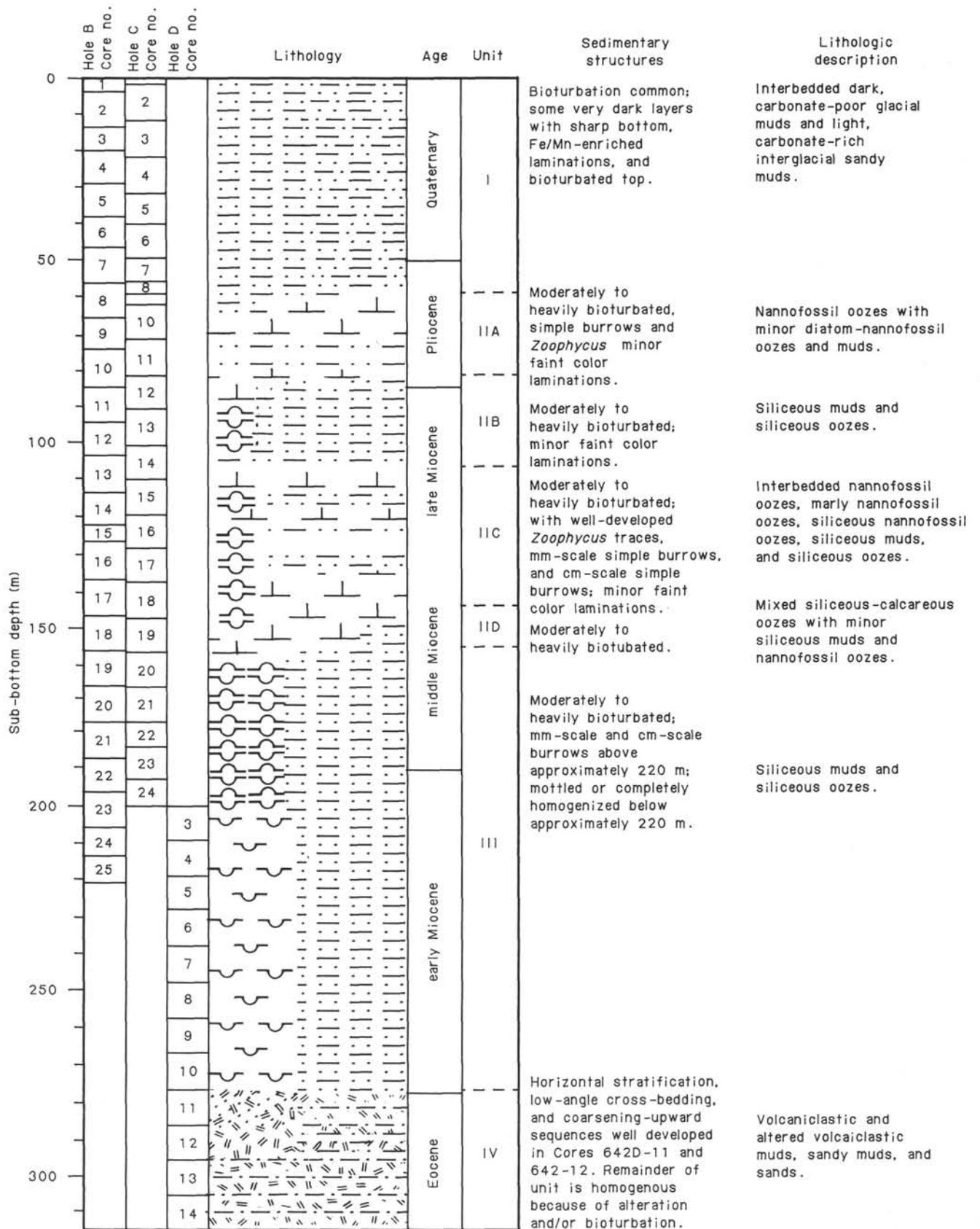


Figure 3. Graphic summary of lithologic units at Site 642. Bedding thicknesses presented are schematic.

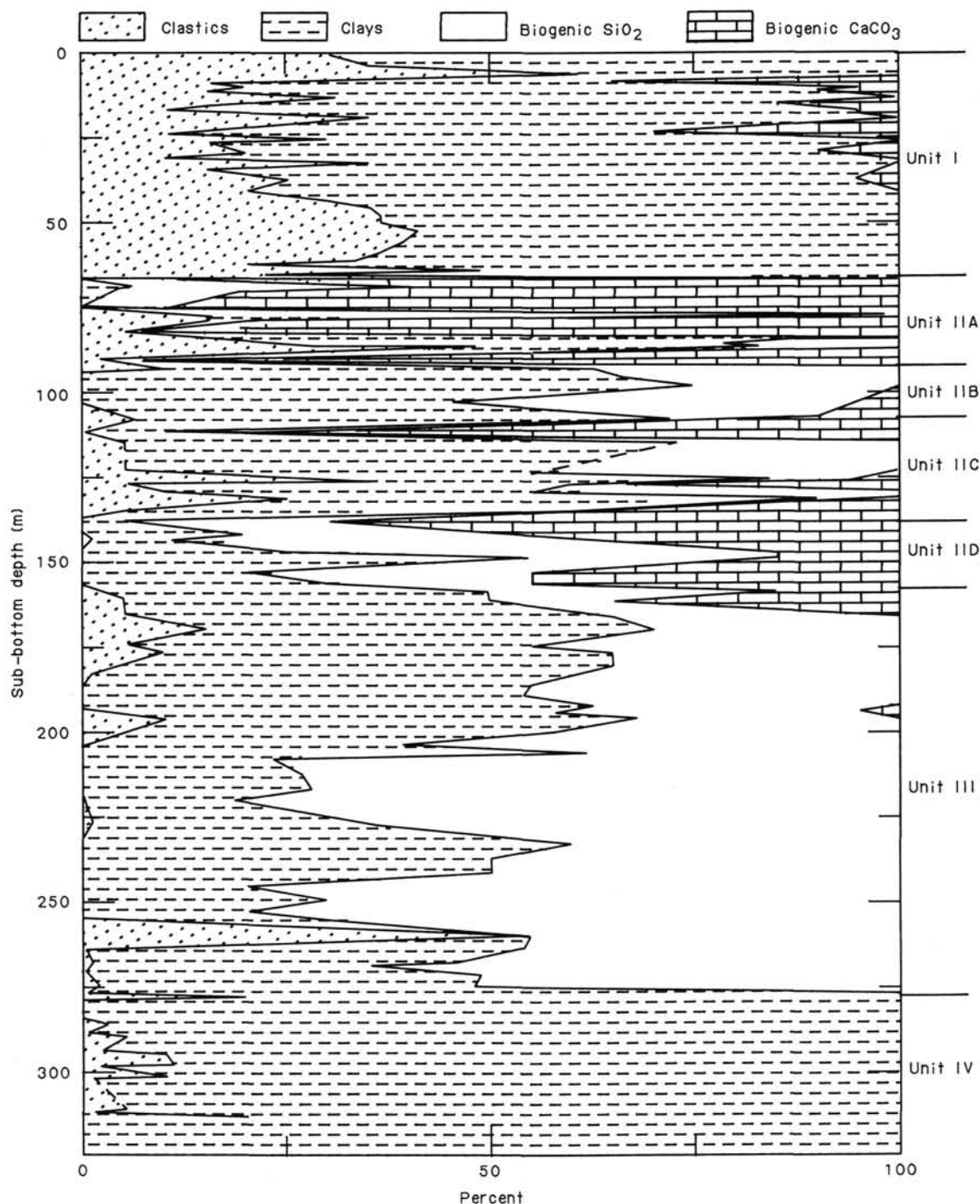


Figure 4. Summary of the composition of major lithologies at Holes 642B and 642D, from shipboard smear-slide data. Lithologic units at Hole 642C show similar characteristics.

The nannofossil oozes and diatom-nannofossil oozes contain 60%–90% nannofossils, 0%–10% diatoms, 0%–15% sponge spicules, and less than 5% terrigenous components (Fig. 4). The muds contain 20%–50% quartz, 50%–75% clay, trace amounts of other terrigenous components, and 5%–10% biogenic siliceous components, especially sponge spicules. Several of the quartz-rich muds contain appreciable sand-sized components (Fig. 5); the remainder of the samples from Subunit IIA form an association of muds and oozes with sand contents below 10%. Both carbonate-bomb and semiquantitative XRD analy-

ses of samples from Subunit IIA record a major increase in carbonate content relative to Unit I (Figs. 6 and 7). Relative peak intensities for quartz and feldspar decrease from those observed in Unit I, but the relative abundance of clay minerals appears to remain approximately constant. Volcanic ash is a minor component in Subunit IIA, consisting of one ash layer in Hole 642B and a disseminated ash in Hole 642C, as described in the discussion of distal tephra deposits (see below).

Subunit IIB. Sample 104-642B-11H-4, 50 cm, through Section 104-642B-13H-2 (90.4–107.2 m sub-bottom); Section 104-

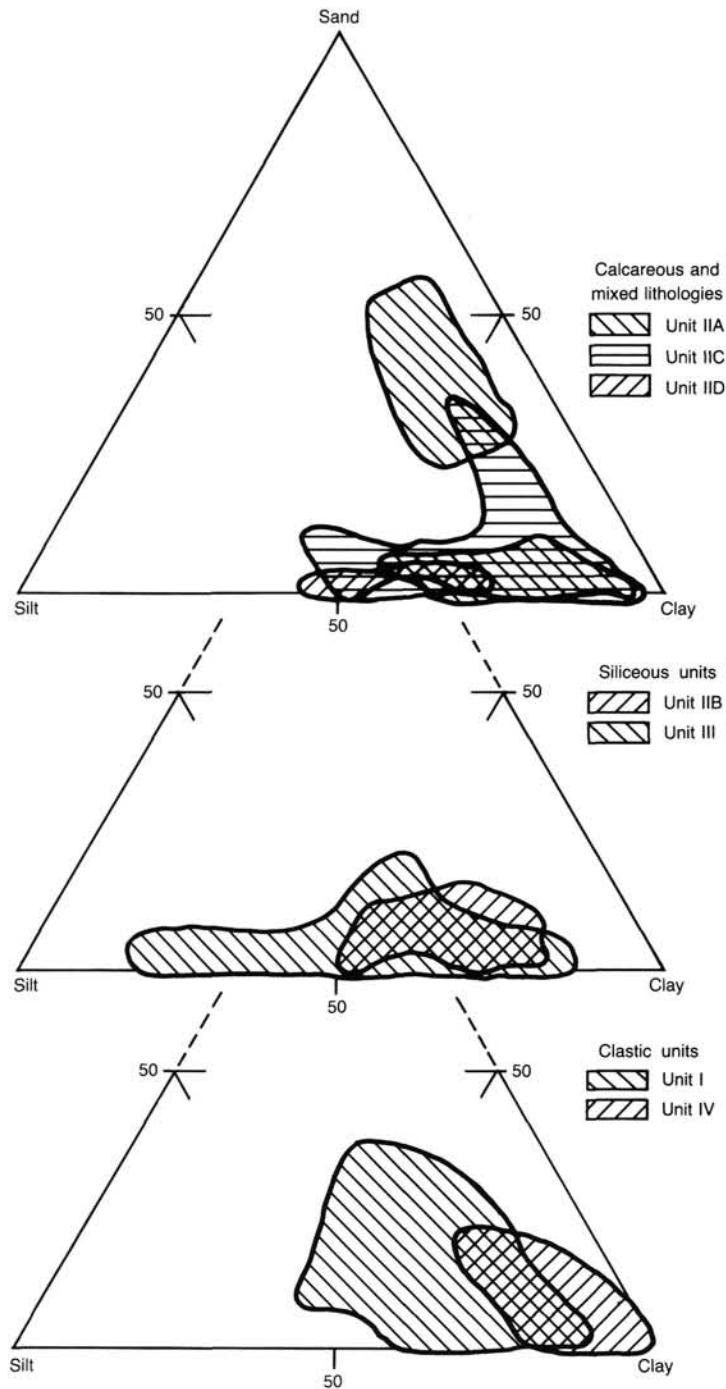


Figure 5. Summary of the textural composition of the major lithologic units at Site 642, from shipboard smear-slide data.

642C-12H-1 through Section 104-642C-14H-4 (82.5–107.5 m sub-bottom). Age: late Miocene.

This subunit consists almost entirely of siliceous muds and siliceous oozes, with one short interval of nannofossil ooze (Sample 104-642C-12H-6, 70 cm) and several minor volcanic ash and altered volcanic ash layers. Important colors in this subunit are dark gray (5Y 4/1), greenish gray (5GY 5/1), dark greenish gray (5GY 4/1), and grayish green (5G 4/2). This interval is moderately to heavily bioturbated, but only a few *Zoophycos* are identifiable as distinct trace fossils. The majority of the bioturbation is recorded as an indistinct mottling of the sediments.

The siliceous muds/oozes of Subunit IIB generally contain 3%–10% quartz, 30%–70% clay, 5%–30% volcanic glass, trace amounts of other terrigenous components, 2%–20% diatoms, 15%–30% sponge spicules, and 0%–5% radiolarians, with an average composition of approximately 5% quartz, 55% clay, 7% glass, 10% diatoms, and 22% sponge spicules (Fig. 4). Textural data for samples from Subunit IIB indicate the relatively intermediate grain sizes that are present; Subunit IIB materials are coarser than the pure carbonate oozes, but finer grained than some of the clastic deposits (Fig. 5). Carbonate-bomb and semiquantitative XRD analyses (Figs. 6 and 7) of samples from

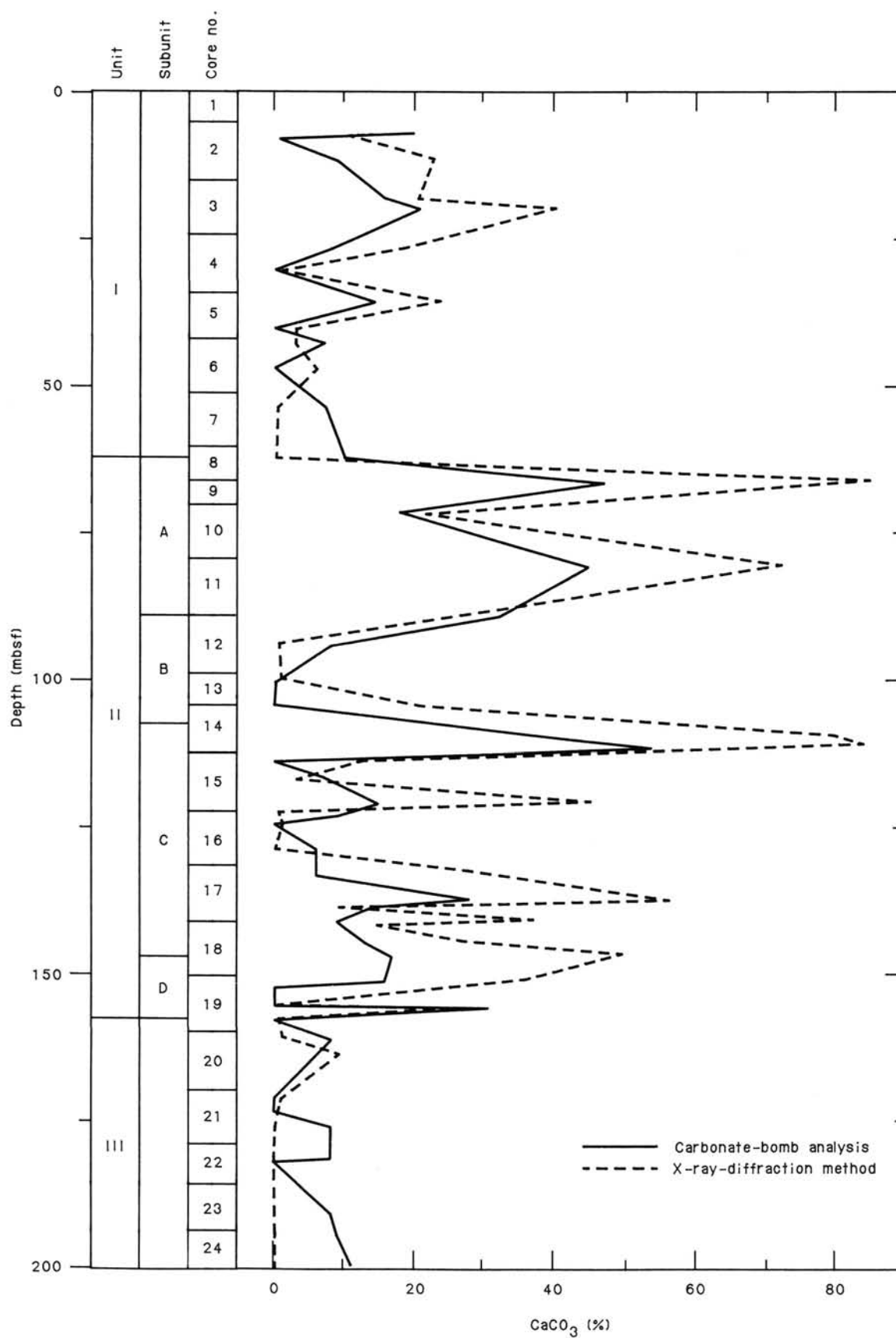


Figure 6. Carbonate content of samples from Hole 642C, measured by shipboard carbonate bomb and also estimated by semi-quantitative X-ray-diffraction (peak area ratio) techniques. Note similarity of patterns measured by the two techniques.

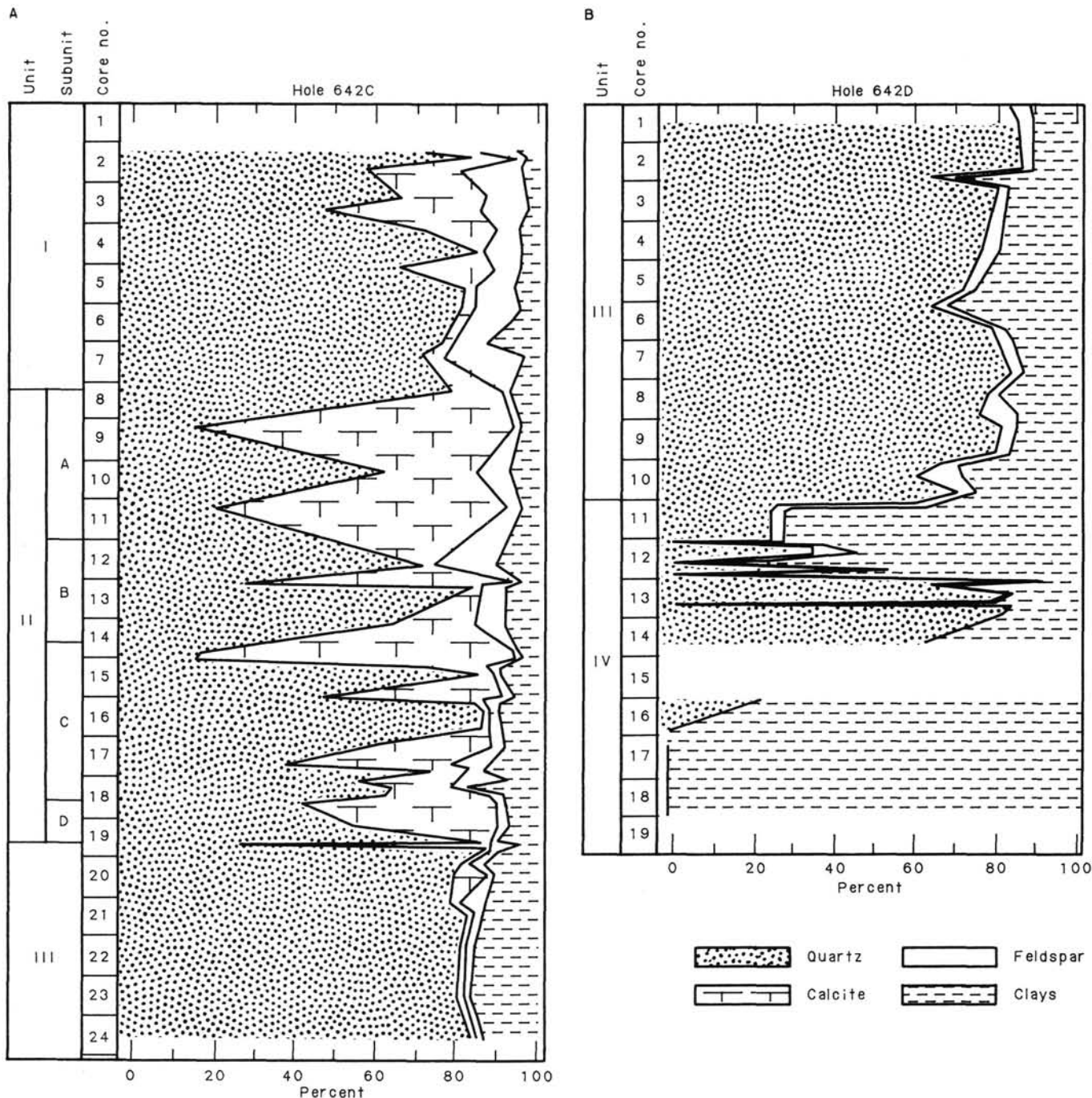


Figure 7. Semiquantitative estimates of the bulk mineralogy of the major lithologic units at Hole 642C (A) and Hole 642D (B), based on peak area ratios.

Subunit IIB indicate the major reduction or absence of carbonate and the continued importance of quartz, chlorite, illite, and kaolinite in these sediments. Smectites are also present. Volcanic ashes are a minor component in Subunit IIB, with one occurrence in Hole 642B and three occurrences in Hole 642C (see the discussion of distal tephra deposits, below).

Subunit IIC. Section 104-642B-13H-3 through Section 104-642B-16H-CC (107.2-138.0 m sub-bottom); Section 104-642C-14H-5 through Section 104-42C-18H-4 (107.5-145.5 m sub-bottom). Age: middle to late Miocene.

This subunit consists of interbedded nannofossil oozes, marly nannofossil oozes, siliceous nannofossil oozes, siliceous muds, and siliceous oozes, with a minor, but important, ash compo-

nent. The interbedded oozes and muds have individual unit thicknesses that range from approximately 2 m to greater than 10 m, but similar colors and extensive bioturbation reduce the visibility of boundaries between adjacent units. Subunit IIC consists of approximately 35% carbonate-rich and 65% opal-rich sediments in Hole 642B, while Subunit IIC in Hole 642C contains approximately 25% carbonate-rich and 75% opal-rich sediments. This compositional difference probably results from two factors: local variability in sediment component deposition, preservation, and reworking, and analytical uncertainty in visual core description and smear slide classification. Important colors in this subunit are dark gray (5Y 4/1), very dark gray (5Y 3/1), greenish gray (5GY 5/1), and dark green gray (5Y 4/1) for

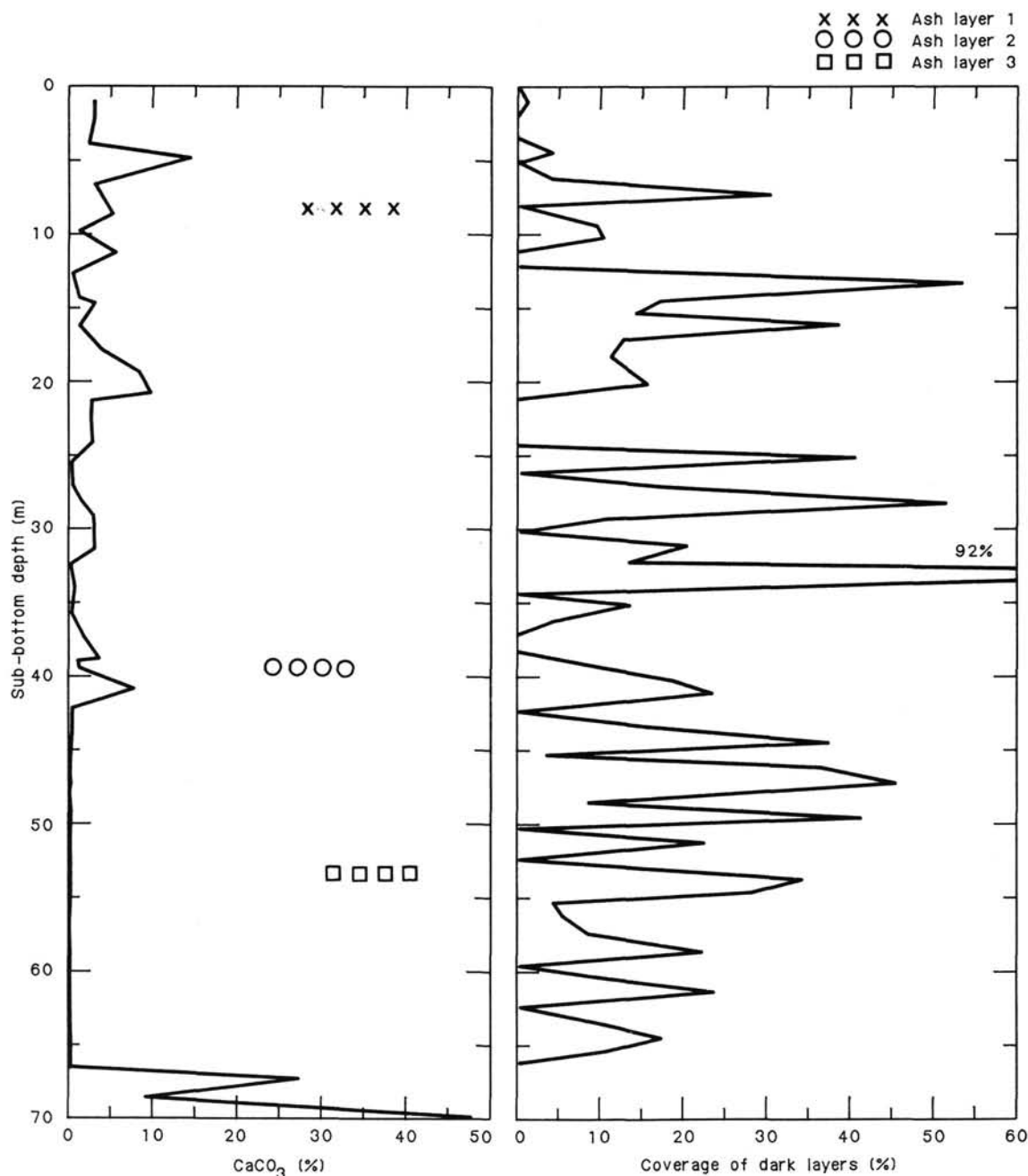


Figure 8. Preliminary summary of calcium carbonate contents in the upper 70 m sub-bottom at Site 642B (data from preliminary shore-based analyses), and percentage of core surface (per meter of core length) covered by dark layers in Unit I, plotted as a function of sub-bottom depth. Note inverse correlation of the two signals above 42 m sub-bottom, and absence of carbonate below 42 m.

the siliceous muds and oozes, and greenish gray (5GY 5/1) and olive gray (5Y 4/2) for the various nannofossil oozes.

Bioturbation effects in this subunit range from mild to intense, and include a variety of features. Discrete *Zoophycos* trace fossils are well developed throughout this interval, while other simple and complex burrows occur at scales ranging from approximately 1 mm to greater than 1 cm. Bioturbation is also recorded by mottling in a variety of colors.

Compositions of the siliceous oozes and muds range from 0%–5% quartz, 20%–75% clay, 1%–10% glass, 1%–30% diatoms, 10%–50% sponge spicules, and 0%–5% radiolarians, with an average composition of approximately 1% quartz, 50% clay, 4% glass, 15% diatoms, 23% sponge spicules, and 2% radiolar-

ians (Fig. 4). Compositions of the various nannofossil oozes and marly nannofossil oozes range from 5%–55% clay (average about 28%), 0%–5% glass (average about 1%), 30%–85% nannofossils (average about 54%), 0%–5% foraminifers (average about 1%), 0%–15% diatoms (average about 5%), and 5%–15% sponge spicules (average about 10%). Textural data reflect the variety of lithologies in Subunit IIC (Fig. 5), with grain sizes ranging from fine-grained calcareous oozes to coarse-grained siliceous muds. Carbonate-bomb and semiquantitative XRD data (Figs. 6 and 7) show the variable carbonate and quartz contents that also indicate this variety of lithologies. Volcanic ashes are a more important component in Subunit IIC than in the overlying sediments, as discussed more fully in the description of distal

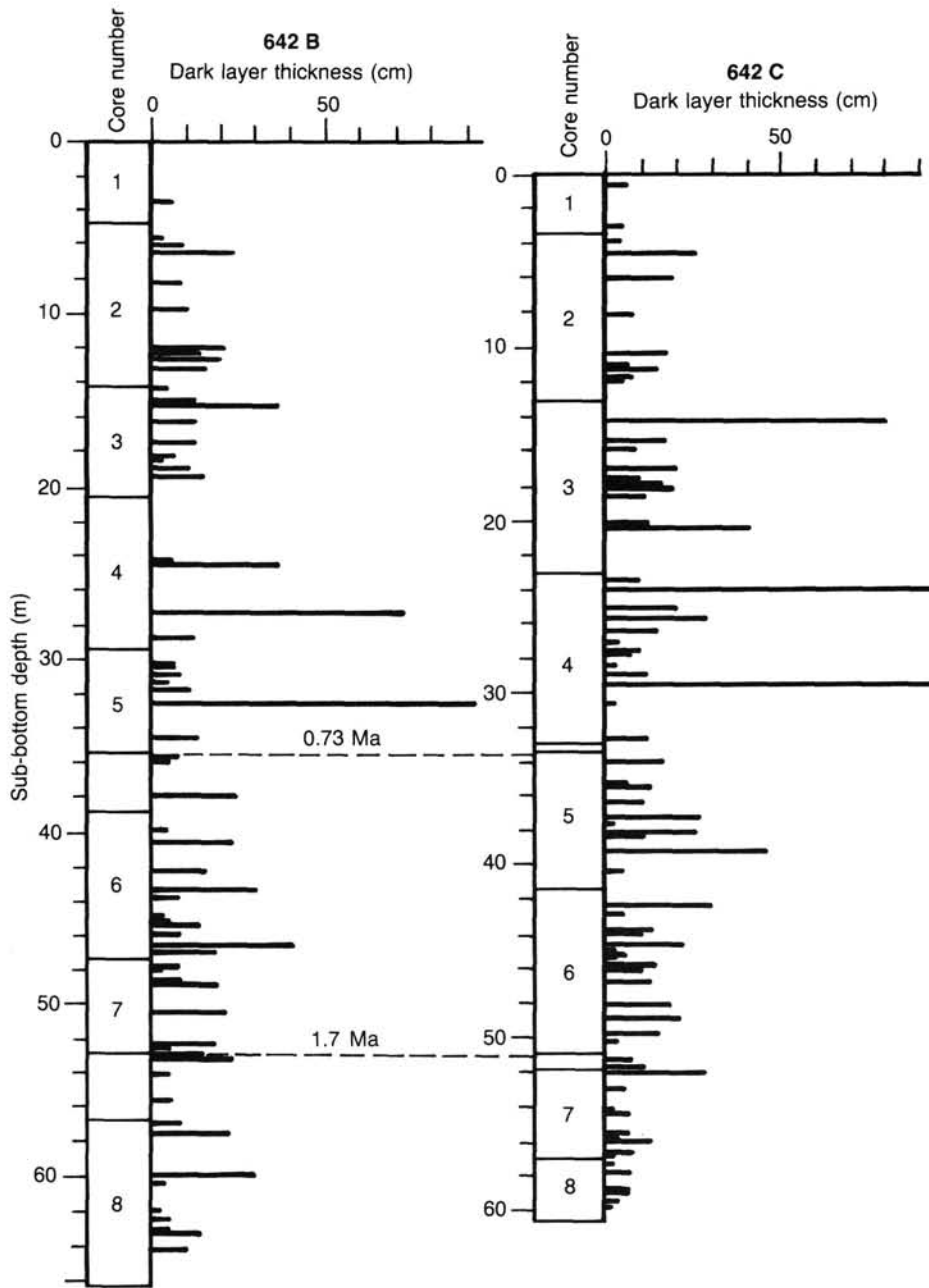


Figure 9. Thickness (cm) of individual dark layers in Unit I plotted as a function of sub-bottom depth for Holes 642B and 642C. These dark layers record periods of maximum glaciation; note correlation between the two records, as well as decrease in intensity and increase in frequency prior to approximately 0.73 m.y.

tephra deposits (see below). Nine discrete or disseminated ash layers have been identified in Subunit IIC in Hole 642B, while 20 discrete or disseminated ashes occur in this interval in Hole 642C.

Subunit IID. Section 104-642B-17H-1 to Section 104-642B-19H-1, 72 cm (138.0–158.4 m sub-bottom); Section 104-642C-18H-5 to Sample 104-642C-19H-6, 15 cm (145.5–156.6 m sub-bottom). Age: middle Miocene.

This subunit predominantly consists of mixed siliceous-calcareous oozes, with minor siliceous muds and nannofossil oozes in Hole 642B. The entire interval is uniform to slightly gradational in color and composition, so that individual layer thicknesses cannot be determined. In addition, moderate to intense bioturbation of this interval has destroyed essentially all primary bedding features. Important colors in this subunit are gray

(5Y 5/1), dark gray (5Y 4/1), olive gray (5Y 4/2), greenish gray (5GY 5/1), and dark greenish gray (5GY 4/1). The mixed siliceous-calcareous oozes in this interval have a compositional range of 5%–30% clay, 15%–55% nannofossils, 10%–40% diatoms, 0%–5% radiolarians, and 10%–25% sponge spicules, with average values of approximately 25% clay, 30% nannofossils, 25% diatoms, and 20% sponge spicules (Fig. 4). The minor lithologies, e.g., siliceous muds and nannofossil oozes, have compositions similar to those described for Subunit IIC. The relatively uniform lithology of Unit IID is also apparent in its grain-size data (Fig. 5), with the samples from this subunit occupying a relatively small field on the ternary diagram. Carbonate-bomb and semiquantitative XRD estimates (Figs. 6 and 7) also record the abundant carbonate present in most of this subunit. Vol-

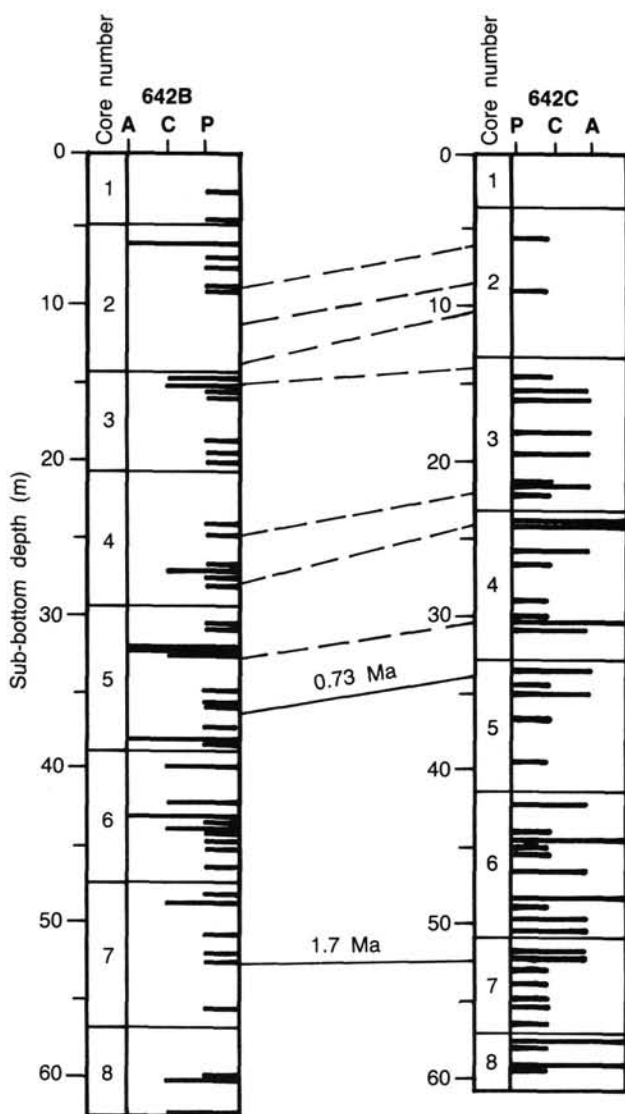


Figure 10. Macroscopic dropstone occurrences in Unit I, Holes 642B and 642C (P = present, C = common, A = abundant). Data from shipboard visual core descriptions. Solid lines are correlations based on magnetostratigraphic and biostratigraphic data; dashed lines are tentative correlations based on glacial/interglacial cycles.

canic ashes are a minor component in Subunit IID, as described in the discussion of distal tephra deposits (see below). Five ashes occur in this interval in Hole 642B, while only two occur in this interval in Hole 642C.

Unit III

Sample 104-642B-19H-1, 72 cm, through Core 104-642B-25H (158.4–221.1 m sub-bottom); Sample 104-642C-19H-6, 15 cm, through Core 104-642C-24H (156.5–199.6 m sub-bottom); Core 104-642D-2X through Sample 104-642D-11X-1, 78 cm (189.9–277.6 m sub-bottom). Age: early Miocene to middle Miocene.

This unit consists of siliceous muds and oozes throughout its length, with volcanic ashes providing the only minor lithology. In Hole 642B, the diatom content of Unit III increases down-core, with siliceous muds above Section 104-642B-21H-7, diatomaceous muds from Section 104-642B-21H-7 to Section 104-642B-24H-1, and diatom oozes from Section 104-642B-24H-2 through Core 104-642B-25H. This steady increase in diatom content with depth, however, is not apparent in Holes 642C and

Table 3. CaCO_3 contents in the glacial-interglacial cycles at Site 642B.

Core 104-642B-	Sub-bottom depth (m)	CaCO_3 Weight (%)
01H-01-74-78	0.76	2.60
01H-02-74-78	2.26	2.82
01H-03-74-78	3.76	2.34
01H-CC-14-18	4.66	14.18
02H-02-36-40	6.68	2.80
02H-03-36-40	4.96	8.18
02H-04-36-40	9.68	1.54
02H-05-36-40	11.18	5.30
02H-06-36-40	12.68	0.50
02H-CC-01-05	14.18	1.17
03H-01-36-40	14.68	2.81
03H-02-36-40	16.18	1.12
03H-03-36-40	17.68	3.69
03H-04-36-40	18.18	8.42
03H-CC-09-13	20.61	9.89
04H-01-35-39	21.07	2.56
04H-02-35-39	22.57	2.70
04H-03-35-39	24.07	2.58
04H-04-35-39	25.57	0.28
04H-05-35-39	27.07	0.34
04H-06-35-39	28.57	1.37
04H-CC-10-14	29.32	2.75
05H-01-74-78	30.16	2.91
05H-02-74-78	31.66	2.89
05H-03-74-78	32.76	0.28
05H-04-74-78	34.26	0.89
05H-05-74-78	35.76	0.28
05H-06-74-78	37.26	2.02
05H-07-74-78	38.76	3.60
05H-CC-15-19	38.87	1.04
06H-01-44-48	39.36	1.18
06H-02-44-48	40.86	7.76
06H-03-44-48	42.36	0.14
06H-04-44-48	43.86	0.12
06H-05-44-48	45.36	0.04
06H-06-44-48	46.86	0.03
06H-CC-18-22	47.28	0.01
07H-01-64-68	48.06	0.02
07H-02-64-68	49.56	0.05
07H-03-64-68	51.06	0.04
07H-04-64-68	52.56	0.04
07H-05-64-68	54.06	0.03
07H-06-64-68	55.56	0.02
07H-07-64-68	57.06	0.03
07H-CC-04-08	57.16	0.03
08H-01-64-68	57.56	0.35
08H-02-64-68	59.06	0.03
08H-03-64-68	60.56	0.03
08H-04-64-68	62.06	0.02
08H-05-64-68	63.56	0.03
08H-06-64-68	65.06	0.05
08H-CC-10-14	66.32	0.00
09H-01-52-56	66.94	26.82
09H-02-52-56	68.44	9.13
09H-03-52-56	69.94	48.21

642D. Important colors in this subunit are gray (5Y 5/1), dark gray (5Y 4/1), very dark gray (5Y 3/1), black (5Y 2.5/1), olive gray (5Y 4/2), dark olive gray (5Y 3/2), and very dark grayish brown (2.5Y 4/2).

Bioturbation is moderate to intense throughout Unit III, but gradationally changes character down-core. The upper part of Unit III, observable in Holes 642B and 642C, contains distinct burrows (on scales of both less than 2 mm and greater than 1 cm), indistinct mottling, and rare identifiable *Zoophycos* traces. Below approximately 220 m sub-bottom, however (observable only in Hole 642D), essentially all bioturbation is recorded as either an indistinct mottling or a complete homogenization of the sediment.

Compositions of the siliceous muds and oozes in Unit III show ranges of 0%–20% quartz, 0%–5% feldspar, 10%–80% clay, 0%–15% glass, 5%–50% diatoms, 0%–50% radiolarians,

5%–40% sponge spicules, and 0%–10% silicoflagellates. Average composition in this interval is approximately 3% quartz, 43% clay, 24% diatoms, 11% radiolarians, and 14% sponge spicules, with trace amounts of feldspar, glass, and silicoflagellates (Fig. 4). The range in abundance of silt-sized components (e.g., radiolarians, sponge spicules, and volcanic glass) also produces significant variability in the textural composition of this subunit (Fig. 5). Carbonate-bomb and semiquantitative XRD data (Figs. 6 and 7) indicate the absence of carbonate in Unit III.

The relative abundance of clay minerals increases downcore, and the clay mineral assemblage is dominated by smectite (an iron-rich beidellite phase). This composition suggests a volcanic origin for the smectite, as detrital altered ash and/or as volcanic ash altered *in situ*. Zones enriched in relatively unaltered volcanic ashes are common in Unit III, with 19 occurring in Hole 642B, 13 in Hole 642C, and 14 in Hole 642D. Differences in ash content between holes probably reflect differences in recovery, local variability in ash deposition, reworking by bottom currents, and dissemination by bioturbation. The locations and characteristics of these ashes are described in the discussion of distal tephra deposits (see below). A glauconite and phosphate-rich layer is located at 104-642D-8X-1, 85–86 cm.

Unit IV

Core 104-642D-11X-1, 78 cm, to Core 104-642D-14X, CC, 33 cm (277.6–315.2 m sub-bottom). Age: Eocene.

This unit contains volcanoclastic and altered volcanoclastic muds, sandy muds, and sands (Figs. 4 and 5). Dominant colors are dusky yellow-green (5GY 5/2) and light olive gray (5Y 6/2) for the sands, and greenish-gray (5GY 5/1), very dark gray (5Y 3/1), and black (5Y 2.5/1) for the muds. Individual beds range in thickness from 50 cm to approximately 5 m through most of this unit, but Sections 104-642D-12X-2, 642D-12X-5, and 642D-12X-6 contain a more complicated lithologic sequence. These three sections are characterized by repeated coarsening-upward beds, approximately 5 to 10 cm thick, separated by 20 to 40 cm-thick beds of a more vertically-uniform nature. The processes acting to develop this pattern are not completely obvious from visual examination, but this interval does appear to have experienced significant alteration.

Bioturbation is slight to intense in the more uniform lithologies, and is indicated only by indistinct mottling. Bioturbation effects are less apparent in the coarsening-upward beds.

A 10-cm-thick hardground forms the top of Unit IV, and contains some biogenic components, such as glauconitized echinoid spines, sponge spicules, and unidentifiable glauconitized debris (ash?). Some grains are surrounded by a thin fringe of birefringent phosphate. The matrix of the hardground is composed of colophane, including silty detrital quartz. The other components are concentrated in very thin layers, separated by dark irregular laminae of iron oxides, providing evidence of very slow sedimentation.

The composition of the remainder of Unit IV is dominated by volcanic ash (0%–90%), altered volcanic ash (0%–100%), and clays (0%–100%), with small amounts of quartz, limonite/goethite, and zeolites present. Glaucony is also present as an alteration product of volcanic glass through much of this interval; its abundance is generally low, but reaches as much as 100% in a few intervals. The ash-rich nature of this unit is emphasized in Figure 2. Semiquantitative XRD analyses (Fig. 7) of the coarsening-upward sequences in Unit IV indicate that the sandy muds contain approximately twice as much quartz as the interbedded muds do, and the sandy muds are also rich in glaucony. This glaucony displays all gradation between glauconite (*sensu stricto*) and mixed-layer illite-smectite species, with the smectite layers approaching nontronite in composition. The interbedded

muds also contain smectite, but of a beidellite composition. Both facies also contain the zeolites clinoptilolite, heulandite, and phillipsite. These occurrences suggest that the smectites, especially within the muds, developed by *in situ* alteration of volcanic ash. Below the interbedded muds and sandy muds, quartz content increases and illite reappears in the clay mineral fraction, suggesting an increase in terrigenous input. Diagenesis of volcanic ash has still occurred, however, as evidenced by samples containing only smectite and abundant, well-crystallized phillipsite.

Unit V

Section 104-642D-14X, CC, 33 cm, to Core 104-642D-15X; Core 104-642E-2R to Core 104-642E-110R (315.2–1229.4 m sub-bottom). Age: Eocene.

Unit V consists of irregularly interbedded basalts and volcanoclastic deposits, with variable lithologies, thicknesses, and degrees of alteration. A detailed discussion of the petrology and development of this unit is provided in the “Basement Lithology” section, this chapter.

Sedimentological Interpretation of the Depositional Environment

The sedimentary sequence overlying the uppermost basalts at Site 642 records three major shifts in depositional regimes, as recognized by the lithologic units described above. The oldest regime is characterized by a predominant input of pyroclastic material, which appears to have been reworked from a shallow marine environment and deposited in an undetermined depth of water at a relatively proximal site. This pattern is abruptly terminated by a major unconformity. The overlying regime is characterized by lower to middle Miocene siliceous-dominated facies, with relatively high organic carbon contents and moderate sedimentation and mass accumulation rates; these moderate accumulation rates may reflect the presence of multiple, short-ranging hiatuses, presently unidentified by shipboard stratigraphic control. As a result, this regime appears to have been established under relatively high productivity conditions, perhaps associated with a major concurrent oceanographic front. This regime gradually shifted from siliceous deposition in the early to middle Miocene to calcareous deposition in the late Miocene(?) to the late Pliocene, reflecting the development of less productive pelagic and hemipelagic environments. The possible rare occurrence of dropstones and the presence of low-diversity floras and faunas suggest the existence of cold water, subpolar environments during this time. The most recent regime is marked by the sudden onset of upper Pliocene and Pleistocene glacial and interglacial sedimentary cycles, with ice-rafting of coarse terrigenous grains as an important sedimentation process.

Unit IV

Unit IV consists of muds and sandy muds, with a major to predominant component of altered volcanic ash. Glaucony, which is abundant in most of this unit, is generally interpreted as a penecontemporaneous alteration product formed in shallow-water environments; as a result, the composition of Unit IV suggests that it was derived by the reworking of a primary, shallow-water deposit. The processes of reworking are recorded by repeated coarsening-upward beds, indicating that mass-flow mechanisms were active during deposition. Because such processes operate independently of water depth, these depositional structures do not uniquely identify the water depth of deposition; the relative thickness of this unit, however, suggests that it was deposited proximally to the pyroclastic source, perhaps at a distance not exceeding several tens of kilometers. As a result, Unit IV is interpreted to have been deposited in a shelf to proximal-slope environment.

The characteristics of Unit IV change from bottom to top, suggesting an evolution in the depositional conditions of this unit through time. The lower part of Unit IV consists almost entirely of homogeneous, structureless, zeolite and glaucony-rich dark muds, suggesting that deposition was predominantly of fine-grained material in a relatively quiet bottom-water environment. Under these conditions, chemical alteration effectively destroyed much of the primary depositional structure. The upper part of Unit IV, however, contains minor amounts of sand-sized quartz and feldspar, and exhibits well-developed horizontal stratification and low-angle cross-bedding. These characteristics suggest both a greater input of primary clastic material and an increase in the relative importance of depositional processes over processes of alteration. As a result, the frequency of mass-flow events at Site 642 probably increased during the deposition of Unit IV. In addition, the sources of material deposited at Site 642 also changed slightly, from fine-grained terrigenous and volcanoclastic sources early in the deposition of Unit IV to a mixture of volcanoclastic and coarser terrigenous sources later in its development. The top of Unit IV is a sandy, glauconite and phosphate-rich hardground, which is interpreted to have formed over an extended period of time, at a relatively elevated position, subject to very slow sedimentation rates and weak, but effective, currents. We propose that Unit IV was deposited in a quiet-water, shelf to proximal-slope environment, with frequent pyroclastic inputs (initially low energy, changing to frequent mass-flow events through time) as the only major depositional incursions.

A lithologically similar unit was drilled at Site 338 during DSDP Leg 38 (Talwani, Udintsev, et al., 1976) at a sub-bottom depth of 285 to 296 m. This interval (Unit 3A at Site 338) consists of a greenish-black, glauconitic, sandy mud, which is semi-indurated at its top. It has a sharp contact with the overlying, upper Eocene diatom ooze and muddy diatom ooze, and grades downcore into lower Eocene terrigenous gray muds, which are locally sandy, calcareous, or zeolitic. The glauconite replaces both microfossils and fecal pellets (White, 1978), similar to the process of origin observed at Site 642. Caston (1976) interpreted the localized development of glauconite as evidence of a significant variation in depositional environment at Site 338, and concludes that the glauconitic sands represent lower Eocene sediment partially reworked during a mid-Eocene hiatus. She suggested that this hiatus records high-energy/shallow water conditions at Site 338 through the middle Eocene, and that the transition to the overlying pelagic deposits resulted from either an abrupt subsidence of the Vøring Plateau or a final separation of the Greenland and Norwegian margins along the Jan Mayen Fracture Zone. Either event could change sediment dispersal or oceanic circulation patterns, thereby producing the observed change in sedimentation. The sequence of events recorded at Site 642 appears to be similar, with glauconite formation in a relatively shallow, high-energy environment, development of a major hiatus, and rapid transition to open-water deposits. Future mapping of the occurrence and age of similar glauconites and associated hiatuses may provide valuable insight into the paleogeographic evolution of the Vøring Plateau region from a terrigenous-dominated to a biogenous-dominated sedimentary province.

Unit III

The siliceous muds and oozes of Unit III lie above the major unconformity that caps Unit IV, and are early to middle Miocene in age. Although the sedimentation rate for Unit III is not particularly high, and also very tentative because of the lack of biostratigraphic control, its relatively high average organic carbon content, the marine nature of that organic carbon (see "Geochemistry" section, this chapter), and the abundance of si-

liceous components in this unit suggest that it records the occurrence of enhanced productivity at this time. In fact, other information suggests that the sediment accumulation rates may have been influenced by significant post-depositional alteration. Physical properties data indicate that water contents and porosities in Unit III are anomalously high for this sub-bottom depth, suggesting the presence of relatively high amounts of smectites within this interval. This interpretation is supported by the XRD data, which show smectite as the dominant clay mineral within Unit III. The occurrence of smectites may result from the diagenetic dissolution of biogenic silica, and the incorporation of that silica into associated clay minerals. This dissolution would tend to decrease the accumulation rates calculated for Unit III. The physical characteristics of the smectites would explain the increased water content in this interval, and might also cause a secondary expansion of the sediments during recovery. Such a secondary expansion would also decrease the accumulation rates calculated for Unit III. In addition, presently unidentified hiatuses may exist within the lower part of Unit III. Physical-properties data (see "Physical Properties" section, this chapter) suggest that one such hiatus may occur near 255 m subbottom. A glauconite and phosphate-rich layer located at 248.5 m sub-bottom may be interpreted as a thin hard ground that developed during such a hiatus. Such time gaps would also act to decrease the sedimentation rates.

In association with the high-productivity regime interpreted for Unit III, the preservation of biogenic carbonates decreases significantly. Intense carbonate dissolution at the sediment/water interface at this time may have resulted from the high organic carbon contents of the sediments. Although increased organic carbon and decreased carbonate contents are often interpreted as indicating low oxygen conditions in the overlying bottom waters during deposition, intense bioturbation rates have almost completely homogenized these sediments. In addition, a diverse and active bottom fauna is evident. These latter two observations suggest that bottom waters were not oxygen-deficient during the early to middle Miocene, leaving high-productivity conditions as the most plausible explanation of the characteristics of Unit III. Terrigenous clays and minor amounts of quartz and feldspar silt and sand are found throughout Unit III, although their abundances are generally low and variable. These fluctuations may reflect important variations at the terrigenous sources. Minor amounts of clay may also be attributed to altered volcanic components.

Data gathered during DSDP Leg 38 provide further support for the interpretations presented here. Miocene sediments from the Vøring Plateau consist almost entirely of siliceous oozes, with varying abundances of clay and calcareous nannoplankton (Caston, 1976). Unit 2B at Site 338 (Talwani, Udintsev, et al., 1976) is a middle Oligocene to middle Miocene diatom ooze with a minor component of calcareous diatom ooze, while Unit 2A at Site 338 is a middle to upper Miocene muddy diatom ooze. On the basis of lithologic descriptions and available age data from Site 642, Unit III at Site 642 appears to correlate with the upper part of Subunit 2B at Site 338, and may also correlate with all or the lower part of Unit 2A at Site 338. Caston (1976) interpreted the Miocene record of siliceous sedimentation as recording the progressive subsidence of the Vøring Plateau throughout this time, subject to the relatively high productivity regime proposed above. Nilsen and Kerr (1978) described the trace fossils in DSDP Leg 38 sediments, and noted the variety of discrete trace fossils and unidentifiable bioturbation features present throughout the sedimentary column in this region. Although they did not explicitly discuss trace fossil assemblages as indicators of bottom-water oxygenation, the compilation by Nilsen and Kerr (1978) provides further evidence that bottom waters in the Norwegian-Greenland Sea were sufficiently oxygenated to

support a diverse and active benthic fauna throughout the Miocene.

Unit II

During the middle Miocene to late Pliocene, the sediments of Unit II recorded a shift in deposition from predominantly siliceous to almost pure carbonate sediments. This shift begins with middle Miocene mixed nannofossil-siliceous oozes, continues with middle to upper Miocene interlayered nannofossil and siliceous oozes and muds, reverts to solely siliceous muds in the late Miocene, and concludes with the accumulation of essentially pure, pelagic nannofossil oozes in the upper Miocene(?) to upper Pliocene. The complex associations of these lithologies, with transitional zones several tens of centimeters thick, reflect the variability of transitional carbonate and siliceous facies and suggest that this area experienced significant environmental changes throughout this time. Short-duration hiatuses within this interval may also contribute to these sudden changes in lithologies. Despite this potential complication, the sequence of sediments present in Unit II provides an excellent opportunity to examine in detail the complexities of siliceous high-productivity systems, their paleoceanographic implications, and their mechanisms of development and collapse.

Terrigenous influence in Unit II is generally higher than in Unit III. A similar increase in terrigenous influence upsection was identified in Miocene sediments recovered from the Vøring Plateau during DSDP Leg 38 (Caston, 1976). Carbonate oozes in Unit II, however, contain less terrigenous material than the siliceous deposits in Unit II. At the same time, the importance of siliceous components decreases upsection, suggesting a gradual decrease in marine productivity. This long-term decrease is broken only by the short-term reestablishment of high-productivity conditions in the upper Miocene, as recorded in Unit IIB. The extremely high sedimentation rates, based on preliminary calculations and siliceous microfossil abundances in Unit IIB, support this interpretation. In addition, the degree of bioturbation shows a consistent change between siliceous and carbonate facies. The siliceous sediments of Unit II are extensively bioturbated, while the nannofossil oozes are often only moderately bioturbated. In many cases, in fact, the nannofossil oozes still contain faint laminations, which weakly preserve original bedding planes. Although changes in bioturbation intensity are often interpreted as reflecting changes in bottom-water oxygenation, the presence of trace fossils and mottling in both the carbonate and the siliceous facies of Unit II suggests that bottom-water oxygen levels were sufficient to support benthic faunas during both types of deposition. In this case, the bioturbation intensity may have been more strongly controlled by the rate and magnitude of organic material supply from the surface waters, as reflected by the higher organic carbon contents of the siliceous deposits. These data also support the interpretation of decreasing marine productivity from the base of Unit II to its top.

Although such observations of concurrent changes in productivity and terrigenous input might be explained by climatic variations of some type, such a proposal can only be presented as a working hypothesis at this time. A single dropstone may be present near the top of Unit II at Site 642B, and synchronous massive dropstone deposition has been inferred at Site 344 in the northern Norwegian-Greenland Sea (Warnke, 1982). These data suggest that at least some ice-rafting may have been occurring at this time, and support the earlier proposal of cold, sub-polar water masses at Site 642 during the deposition of Unit II. It must be stressed, however, that the occurrence of ice-rafted debris at Site 642 prior to the late Pliocene is presently unconfirmed, in marked contrast with the large volumes of ice-rafted material observed in the glacial/interglacial cycles of Unit I. As a result, the sediments of Unit II at Site 642 provide no conclu-

sive evidence of major, pre-upper Pliocene iceberg drift systems in the eastern sector of the Norwegian Sea.

The middle to upper Miocene sediments recovered from the Vøring Plateau during DSDP Leg 38 are intermediate in composition between lower Miocene diatom oozes and Pliocene muds and sandy muds (Caston, 1976). Terrigenous content gradually increases upsection, as does the abundance of illite (a terrigenous component) within the clay-sized fraction. At Site 338, this time is represented by Unit 2A, the middle-to-upper Miocene muddy diatom ooze described earlier, and the basal, carbonate-rich portion of Pliocene-Pleistocene Unit 1 (Talwani, Udintsev, et al., 1976). Attempts at lithologic correlations between the Site 642 and the Leg 38 results are complicated by three factors: the possible presence of a major middle to late Miocene hiatus at Site 642, the difficulty in separating Pliocene from Pliocene-Pleistocene deposits in the Leg 38 data (Caston, 1976), and the possible occurrence of a middle-to-late Miocene through Pliocene-Pleistocene hiatus at Site 338 (White, 1978). No major upper Miocene carbonates, equivalent to Unit IIC at Site 642, are obvious at Site 338. The nannofossil oozes of Unit IIA at Site 642, however, do have a possible lithologic equivalent in Cores 338-3, 4, and 5, even though those cores were included with the glacial/interglacial sequence (Unit I) by Talwani, Udintsev, et al. (1976). Such a correlation is preliminary at this time and will require detailed paleontologic data for further evaluation. If the proposed correlation is valid, then the observation of a gneiss pebble at Section 338-5-5 (Talwani, Udintsev, et al., 1976) has important implications for the onset of ice-rafting in the Norwegian-Greenland Sea. In particular, this pebble would correlate below Unit I at Site 642, indicating that minor ice-rafting began as an effective transport agent before the development of easily recognized glacial/interglacial sedimentary cycles (Unit I at Site 642). This correlation might also imply that a major west-to-east temperature gradient existed in the Norwegian-Greenland Sea during the late Miocene and the early Pliocene, and dominated its paleoceanography during that time; a relatively similar situation exists in its recent environments.

As discussed earlier, trace fossil and bioturbation data were compiled by Nilsen and Kerr (1978) from Miocene and Pliocene sections throughout the Norwegian-Greenland Sea. Those data indicate the presence of an abundant and diverse benthic fauna, and suggest that bottom waters were well-oxygenated throughout this interval, in agreement with the evidence from Site 642.

Unit I

Unit I is interpreted to be the record of upper Pliocene (less than 2.7 m.y. old) and Quaternary glacial/interglacial depositional cycles at Site 642. Because of the northern position of Site 642, the sedimentary fluctuations here are different from those developed at lower latitude marine locations (e.g., Roberts, Schnitker et al., 1984). They are, however, very similar to the "glacial" sediments recovered from the Vøring Plateau during DSDP Leg 38 (Talwani, Udintsev, et al., 1976), consisting of muds, sandy muds, and calcareous sandy muds, with ice-rafted components throughout the interval. Sedimentation rates for the Leg 38 cores average approximately 2 cm/1000 yr through the "glacial" sequence (Talwani, Udintsev, et al., 1976), in agreement with the overall sedimentation rate calculated for Unit I at Site 642. In both cases, relatively carbonate-rich, dropstone-poor, and lighter colored layers are interpreted as interglacial deposits. The combination of low carbonate content, relatively high dropstone abundance, and relatively dark color are characteristic features of glacial deposits.

Contrasts between glacial and interglacial deposits at Site 642 are best developed in the youngest cycles, which by our interpretation contain the Recent and the Eemian interglacials by inference from nearby piston cores (Ramm, unpublished data).

In these examples, interglacial sediments consist of brown to dark grayish brown foraminiferal muds, while the deglaciation event is represented by an Fe/Mn-rich, laminated sandy mud that is several centimeters thick. Glacial sediments in these cycles consist of both dark gray muds with scattered dropstones and very dark gray muds with only minor dropstones. The latter facies is interpreted to record times of maximum glaciation, with marked temporal variations between intervals of almost complete sea ice coverage of the Norwegian–Greenland Sea and intervals of extensive ice rafting.

The glacial/interglacial pattern changes significantly down-core, as the interglacials become less easily recognizable and the dark gray to black glacial horizons increase in thickness (Figs. 8 and 9). In addition, dropstone abundance in the dark glacial sediments increases downcore (Fig. 10). These changes are interpreted to record a significant change in the amplitudes of glacials and interglacials through time. A major sedimentary shift is recorded at a time prior to 0.73 Ma (compare Figs. 8 through 10), with longer periods of maximum glaciation (i.e., very dark layers) in the interval 0 to approximately 0.9 Ma, and a higher frequency of colder periods in the interval 0.9 to 2.8 Ma. A synchronous decrease is observed in the sedimentation and mass accumulation rates, with the highest rates developed during the period of most intense glacial maxima. The prominence of ice-rafted components in sediments deposited during maximum glaciations appears to decline from the oldest cycles to the youngest. This decrease may indicate that complete sea-ice coverage of the Norwegian–Greenland Sea has been more common during Recent glacial maxima than early Pleistocene glacial maxima. In addition, interglacial intervals in these early cycles appear to have been cooler and less productive than more recent interglacials, as indicated by the pronounced decrease in carbonate content during early Pleistocene glacials and interglacials (see Fig. 8).

Quaternary and Neogene Distal Air-fall Tephra Layers

Approximately 110 horizons of fresh tephra have been identified within lithologic Units I, II, and III at Site 642 (Table 4). Because Holes 642B and 642C cover approximately the same sedimentary section, these horizons represent about 50 different ash layers deposited on the Vøring Plateau during the Neogene and Quaternary. Massive, glauconite-rich, volcanoclastic layers of mass-flow origin (lithologic Unit IV) are located below a phosphate-rich hardground at about 280 m sub-bottom (104-642D-11X-01, 95–105 cm). These layers are of probable Eocene age, are more consolidated than the distal air-fall deposits, and are thoroughly altered to zeolite, smectite, and/or illite. Their volume and depositional mode indicate a source different than that of the tephra layers recovered from above the hardground. For this reason, the mass-flow deposits will not be discussed here.

The data presented are based on microscope studies of 70 smear slides, using the standard procedure for shipboard smear-slide description. Canada balsam (cb; refractive index $n = 1.537$) was used as the mounting medium. Shard sizes were measured on 45 slides. Shipboard XRF analyses were not available to confirm the petrographically determined range of chemical compositions of the fresh glass shards.

Data

Lithology

The identified tephra horizons occur in three lithologically distinctive forms. These forms and the number of observations in each form at Holes 642B through 642D are listed below:

	642B	642C	642D
Discrete ash layers	19	16	6
Disseminated ash layers and ash-enriched horizons in mud sequences	17	25	3
Pocket fillings, lenses	9	12	6
Total	45	53	15

Discrete layers of tephra are composed of unconsolidated, well-sorted, very fine sands and, less often, coarse silts. The layers are light gray to gray, and white in color. In some layers, pyrite coats up to 50% of individual shard surfaces. In a few cases (e.g., 104-642D-07H-06, 62–74 cm), up to 80% of the shard surface is coated by pyrite. In these cases, the ash layer is recognized as very dark gray to black pyrite sand that is occasionally cemented to form pyritized sandstone (104-642B-14H-05, 104–105 cm, and 104-642C-16H-02, 18–23 cm). Discrete layers often exhibit a sharp base and a gradational top. Some are graded (104-642C-15H-04, 85–95 cm, and 104-642C-19H-03, 67–78 cm), and others are color zoned (104-642B-13H-CC, 09–13 cm, 642B-16H-05, 104–109 cm, and 642B-16H-07, 99–101 cm). Layers range in thickness from less than 1 to 11 cm (Fig. 11), and average about 4 cm (4.2 ± 2.2 cm). The frequency distribution curve of layer thicknesses has a maximum at 3 cm and is skewed toward thicker layers. The tephra layers are exclusively vitric ashes and contain more than 95% fresh vitric shards. These layers are essentially free of lithics, but may contain a few percent of crystals (alkali feldspar, plagioclase, zircon, hornblende, apatite, quartz). The shards range in color from colorless to faintly brown and olive green to brown. With increasing coloration, their dominant shape changes from platy or cusped to tubular and to cuniformal. The average maximum size of the three largest shards is approximately 350 μm ($346 \pm 148 \mu\text{m}$) but may reach as large as 900 μm in the layer at 104-642B-13H-CC, 09–13 cm. The average median shard size is about 100 μm ($112 \pm 63 \mu\text{m}$), with the colorless shards having a slightly larger average than the colored shards (see below).

Disseminated ash layers vary in thickness from less than 1 cm to 10 cm, with a frequency maximum at 2 cm. These layers lack sharp bases, and are disseminated in horizons containing 15 to 50% (rarely up to 80%) ooze or fossiliferous mud. Enriched horizons most often occur as zones that overlie discrete or disseminated layers by as much as 100 cm, and are characterized by an ash content of 5 to 10% in mud or ooze; this value is markedly above the trace amounts of ash generally present in the remainder of the Quaternary and Neogene sediments cored.

Pocket fillings and ash lenses are most often distributed throughout horizons as much as 30 cm below or above discrete or disseminated tephra layers. They have a width of 1 cm or less, and are thought to be burrow fillings resulting from the strong bioturbation present throughout much of the core.

Chemical Composition

The composition of the tephra was estimated on the basis of color, shape and refractive index (RI) of shards. Increasing degrees of differentiation are correlated with:

1. Increasing vesicularity, resulting in the change of shard morphology from cuniformal to cusped and platy,
2. Decreasing coloration, and
3. Decreasing refractive index of the glass shards.

The criteria that were applied to distinguish between three compositionally different groups of tephra are listed below

Table 4. Tephra occurrences in Holes 642B, 642C and 642D.

Depth of top (m)	Core-section	Interval (cm)	Type of sediment ^a	Petrographic composition ^b	Remarks ^c
Hole 642B					
40.22	06-01	132-133	L	B	Biotite-enriched
53.80	07-05	40	E	A	
57.90	08-01	100-101	L		
63.16	08-05	26-27	L		
63.91	08-05	101-102	P		
64.19	08-06	129-130	L		
70.36	09-03	96-98	L	C	
70.38	09-03	98-106	E	C	Pyrite 35%
83.10	10-05	118-119	P	B	Pyrite 20%
87.63	11-02	73-74	P	A	
101.70	12-05	80-88	L	B	Pyrite 15%
113.79	13-CC	09-13	L	A	d _{max} 800 μm, pyr 50%
119.00	14-04 to 14-06			A and B	Abundant irregular lenses of ash in highly disturbed core
121.39	14-05	89-90	L	A	
122.67	14-06	67-68	P		
122.85	14-06	85-86	L	B	d _{max} 500 μm, HO, ZR, AP, KFSP
122.98	14-06	98-99	P		
123.03	14-07	03	P	B	HO, ZR, AP, KFSP
127.52	15-03	102-104	L	B	d _{max} 400 μm, pyr 17%
129.83	16-02	23-29	L	C	Pyrite 30%
130.70	16-02	110-113	D	C	Pyrite 15%
133.13	16-04	53-56	D		
133.72	16-04	112-114	D		
134.24	16-05	14-17	L	B	
135.14	16-05	104-109	L	B	
137.49	16-07	39-40			
137.99	16-07	99-101	L	A	
142.75	17-04	25-26	P		
144.54	17-05	54-57	L	A	
153.24	18-04	94-98	P		
159.95	19-02	75-79	L	B	d _{max} 400 μm
167.86	20-01	46-51	D	B	d _{max} 400 μm
174.50	20-05	110-114	L	A	
174.75	20-05	135-138	L	A	d _{max} 500 μm
179.92	21-02	132-140	E		
187.44	22-01	74	P		
188.08	22-01	138-143	D		
192.37	22-04	117-123	D		
194.74	22-06	54-64	D		
195.17	22-06	97-98	D		
195.22	22-06	102-105	D		
195.60	22-06	140-145	D		
196.43	23-01	43-44	D	B	
196.61	23-01	61-62	D		
196.78	23-01	78-79	D		
210.55	24-04	45	E		
Hole 642C					
8.78	02-04	88-98	D	B/C	10% very dark brown
36.82	05-03	92-94		B	Pyrite 20%
52.23	07-01	133-140	P	A	
53.20	07-02	58-150	E	B	
53.87	07-02	147-148	L		
61.29	09-01	59-60	D	B	
71.05	10-06	05-08	L	B	
77.20	11-03	120-122	D		
77.23	11-03	123-150	E		
77.50	11-04	00-67	E	A	
78.17	11-04	67-68	D		
84.30	12-02	30-32	D	A	
87.88	12-04	88-93	P		
92.50	13-01	50-55	P	B	
101.96	14-01	46-53	L		
113.32	15-02	82-87	L	A	
113.60	15-02	110-114	D	A	

Table 4 (continued).

Depth of top (m)	Core-section	Interval (cm)	Type of sediment ^a	Petrographic composition ^b	Remarks ^c
Hole 642C (Cont.)					
113.65	15-02	115-117	P	A	
116.27	15-04	77-85	E	B	
116.35	15-04	86-93	L	B	HO, ZR, AP, KFSP
118.91	15-06	41-44	L	B	
119.30	15-06	80-83	L	B	Pyrite 45%
121.01	16-01	51-53	D		
122.18	16-02	18-23	L	B	Pyrite 45%
122.33	16-02	33-36	P	B	
126.17	16-04	117-123	P		
127.67	16-05	117-124	P		
127.87	16-05	137-141	P		
127.91	16-05	141-144	L	B	Pyrite 55%
128.67	16-06	67-70	D		
129.13	16-06	113-114	D		
132.55	17-02	105-108	D	A	
134.06	17-03	106-109	D	A	
141.00	18-02	00-04	L	A	d _{max} 450 μm, ZR
142.52	18-03	02-03	D		
142.71	18-03	021-022	L	A	d _{max} 500 μm, CPX
143.42	18-03	92-98	E	C	Pyrite 20%
149.47	19-01	47-50	P	C	Pyrite 30%
152.67	19-03	67-78	L	B	
157.52	19-06	102-106	L	B	ZR
165.84	20-05	134-140	L	B	
166.98	20-06	98-100	E	B	
172.22	21-03	122-127	D	A	
172.53	21-04	03-05	D	A	
175.52	21-06	02-08	D	C	Pyrite 40%
177.65	22-01	15-18	E	B	
178.14	22-01	64-69	D	B	
186.20	23-02	40-41	L	B	
195.46	24-03	06-10	D	A	
195.87	24-03	47-48	E	A	
197.27	24-04	37-41	E		
197.38	24-04	48-55	L	B	
197.48	24-04	58-60	P		
197.57	24-04	67-69	P		
197.70	24-04	80-82	P		
Hole 642D					
199.50	02-CC	16-19	L	B	Pyrite 40%
199.55	02-CC	22-26	D		
230.05	06-02	05-06	P	A	
231.64	06-03	14-15			
231.71	06-03	21-22			
231.92	06-03	42-43			
241.00	07-02	130-136	L	C	Pyrite 35%
246.32	07-06	62-74	P	C	Pyrite 65%
249.00	08-01	120-121	P	C	Glauca 60%
252.50	08-04	20-25	L	B	
265.18	09-06	18-22	L	A	
267.16	10-01	06-08	D	B	
272.96	10-04	136-138	D	A	
277.58	11-01	78-87	L	B	HO, KFSP, CPX
277.68	11-01	88-94	L	B	HO, ZR, KFSP, PLAG

^a Type of sediment: L = discrete layer, D = disseminated layer, P = pocket filling, E = enriched mud.

^b Petrographic grouping:

A = shards are completely colorless with refractive indices smaller than Canada balsam (R.I. = 1.537);

B = shards are predominantly colorless, some are faintly brown to olive green in color; refractive indices range from predominantly smaller to higher than 1.54;

C = same range in color and refractive index as in B, but colored shards with R.I. higher than 1.54 dominant.

^c HO = hornblende, KFSP = alkali feldspar, CPX = pyroxenes, ZR = zircon, PLAG = plagioclase, AP = apatite, d_{max} = maximum grain size.

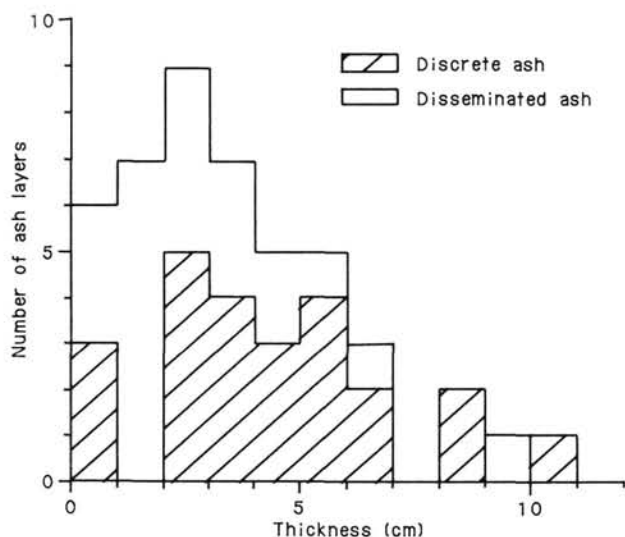


Figure 11. Frequency distribution of 46 distal air-fall tephra layer thicknesses in Holes 642C and 642D. Data are derived from visual core descriptions for both discrete and disseminated ash layers.

(magma terminology after Flower et al., 1982; SiO₂ content after Fisher and Schmincke, 1984):

Type	A	B	C
Refractive index	< cb*	± cb	≥ cb
Color	Colorless	Colorless (< cb) > faintly brown and olive green (> cb)	Faintly brown, olive-green and brown > colorless (n = cb)
Shape	Platy, cusate, tubular	Platy, cusate, tubular > very vesicular, cuniform	Cuniform and tubular > platy, cusate
SiO ₂ Content	> 60%	65%–55%	60%–50%
Magma type	Rhyolite	Icelandite	Tholeiitic andesite

*cb = Canada balsam.

The criteria listed show some compositional overlap between tephra layers of groups A and B, and of groups B and C, but the combined application of all criteria was sufficient for correlating identical units in Holes 642B and 642C (Table 5). Most of the shards were colorless, with their highest refractive index equal to that of Canada balsam. These characteristics indicate a SiO₂ content of about 60%, so that the tephra layers are dominantly of icelanditic to rhyolitic composition (Fig. 12).

Discussion

Tephra Correlation on the Vöring Plateau

The vitric tephra layers are well sorted, and are, therefore, interpreted to be of air-fall origin. These layers are common throughout the section, with an average frequency of about three layers per 1 m.y. (Fig. 13). In the Pliocene/Pleistocene-to-Recent sec-

Table 5. Tephrochronologic correlations, Site 642.

Hole 642B		Hole 642C	
Core	Interval (cm)	Core	Interval (cm)
06-01,	132-133	05-03,	92-94
07-05,	40	07-01,	133-140
09-03,	96-98	10-06,	05-08
10-05	120-122	12-02,	30-32
13-CC,	09-13	15-02,	82-87
		or	110-114
14-06,	85	15-04,	85-94
or	14-07,		
	03		
16-02,	110-113	16-02,	33-36
16-07,	99-101	17-02,	105-108
		or	17-03,
			106-109
17-04,	25-26	18-02,	0-04
17-05,	54-57	18-03,	21-22
20-05,	110-114	21-03,	122-127
20-05,	135-140	21-04,	03-05
21-02,	132-140	22-01,	15-18
		or	64-69

tion (above 90 m), they have a consistently low frequency of 1 to 3 layers/m.y. Cores 104-642B-16H and 104-642C-16H (128-138 and 120-130 m sub-bottom, respectively), however, have a high abundance of ash layers (Fig. 12). When plotted against a time scale developed from shipboard paleomagnetic and biostratigraphic data (Fig. 13), frequency maxima of tephra layers occur just before and just after a hiatus at 7.4 to 12.4 Ma suggested from biostratigraphic evidence. This may indicate an increase of explosive eruptions of highly differentiated magma in the source region of the ashes (see below) just prior to (possibly during) and after the time range marked by the hiatus. If we instead assume that a reduced sedimentation rate of 6 mm/1000 yr was maintained for the same interval, a more regular frequency pattern is apparent, with maxima of some 5 to 6 eruptions per 1 m.y. every 3 to 4 m.y. throughout all of the Miocene.

Ash layer thickness exhibits no regular stratigraphic variation. Several minor variations do occur, such as the lack of units thinner than or equal to 2 cm in the interval 90 to 160 m. This pattern, however, may be more a result of the wide range of parameters influencing layer preservation (e.g., bioturbation, drilling deformation, and bottom currents) than a primary feature. Vitric ashes of less differentiated composition, possibly tholeiitic andesite, seem to be restricted to a sub-bottom depth of more than 120 m, equivalent to ages older than about 7 Ma. A single exception to this observation occurs at 104-642C-02H-04, 88-98 cm.

The petrographic criteria and the median and maximum grain size data were used to correlate the tephra layers in Holes 642B and 642C as listed in Table 5 (cf. Fig. 12). In several instances, unique correlations cannot be proposed between the two cores. In those cases, however, two ash layers of similar composition in one core can then be identified as options for tentative correlation to the single ash layer in the other core. The most distinctive marker horizons are layers 104-642B-13H-CC, 09-13 cm; -642C-15H-04, 85-94 cm; -642D-11X-01, 78-87 cm; and 104-642D-11X-01, 88-94 cm. The first is characterized by a well-developed color zonation, as well as the largest median and maximum shard size (250 and 900 μm, respectively) of any of the Quaternary and Neogene ashes drilled. The two layers in Core 104-642D-11X-01 show some grading, but are especially characterized by the presence of euhedral amphibole, in addition to more common alkali feldspar, zircon, and apatite.

The tephra correlations indicate either a higher sedimentation rate in Core 104-642B-14H compared to the same interval in 104-642C-15H, an unconformity in 104-642C-15H, or both.

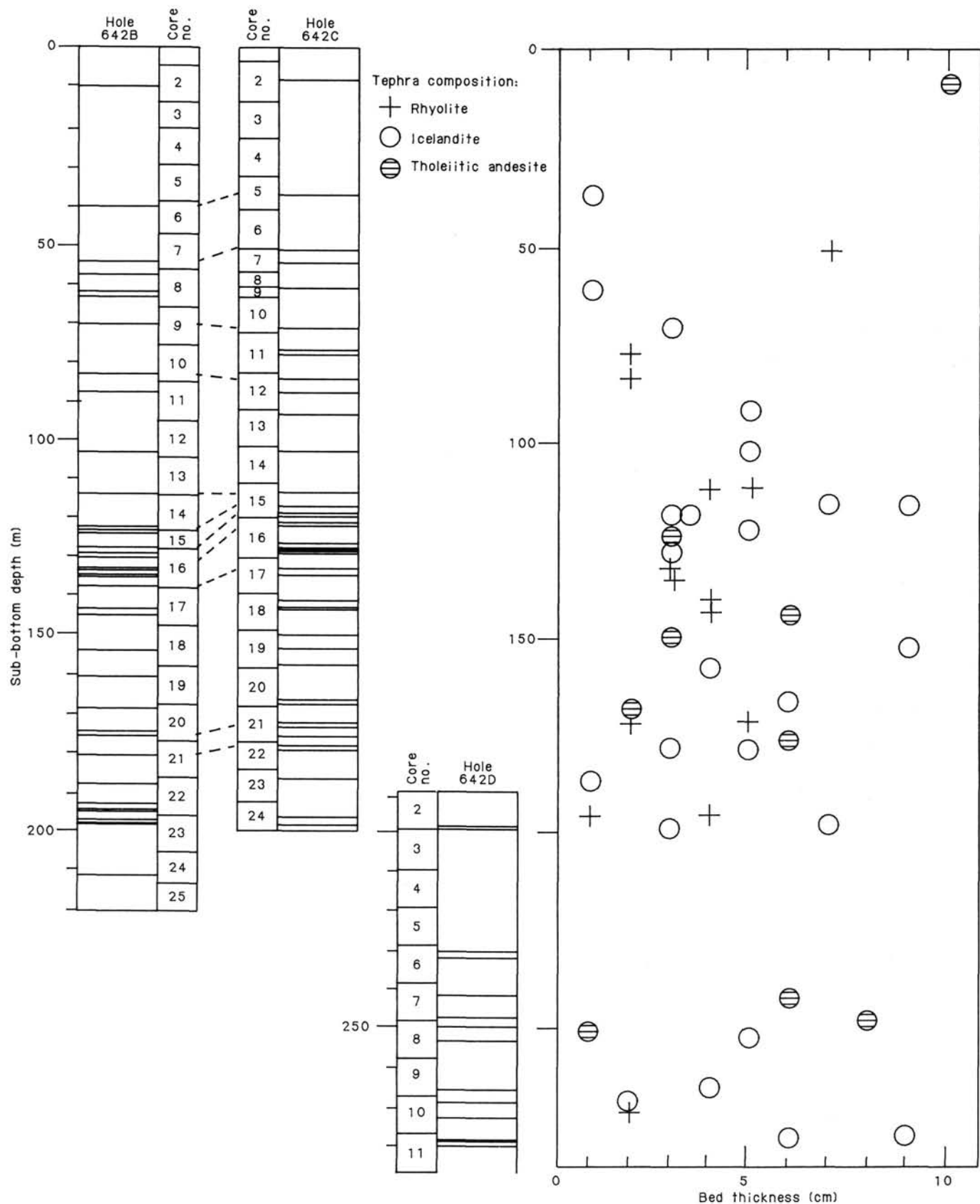


Figure 12. Distribution, geochemical composition, and thickness of distal air-fall tephra units at Site 642, plotted as a function of sub-bottom depth. Composition was determined petrographically (see text for explanation of techniques). Dashed lines are tentative correlations based on petrographic data.

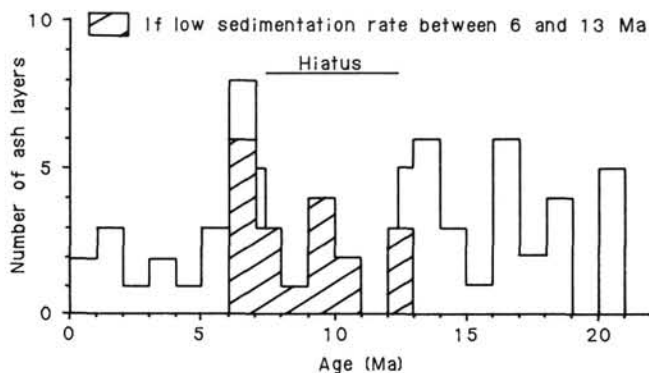


Figure 13. Frequency of distal air-fall tephra deposits recovered at Site 642 (measured as number of deposits per 10^6 -yr interval). Unfilled curve was calculated by removing time of hiatus (approximately 7.4 to 12.4 Ma). Cross-hatched pattern calculated by assuming slow but continuous sedimentation in the interval from 7.4 to 12.4 Ma.

A higher sedimentation rate is also indicated for the interval of Cores 104-642C-10H through -642C-5H in 642C (about 3 to 1 m.y.) compared to the stratigraphically identical interval of Cores 104-642B-9H to 104-642B-6H in Hole 642B.

A comparison of the Site 642 data with the section drilled on the Vøring Plateau at Site 338 during DSDP Leg 38 shows that two ash layers containing hornblende occur only 45 cm apart at a depth of about 194 m sub-bottom (Core 38-338-20-03, 55 cm and 100 cm). At Hole 642D, two closely spaced layers containing hornblende (104-642D-11X-01, 78–87 cm, and 104-642D-11X-01, 88–94 cm) occur at 278 m sub-bottom, directly overlying an 18-m-thick, fossil-baren, glaucony-rich, sandy, volcanoclastic sequence (278–296 m, Cores 104-642D-11X and 642D-12X). A petrographically identical, 19-m-thick sequence in Site 338 (Cores 38-338-30 and 338-31, 285 to 304 m) is separated from the two ash layers by some 91 m of nannofossil and diatomaceous ooze. This difference may indicate that 91 m of sediment is missing at Site 642 relative to Site 338. The biostratigraphic and paleomagnetic shipboard data give an early Miocene age of some 20 Ma for the two ash layers at Site 642, whereas the glaucony-rich volcanoclastic unit is most probably of Eocene age, as indicated by its stratigraphic position at Site 338. The 91 m missing at Site 642 would thus most probably be of Oligocene and late Eocene age, indicating differential uplift or erosion for parts of the Vøring Plateau during that time interval.

Tephra Sources to the Vøring Plateau

On the basis of petrographic data, all of the tephra layers identified at Site 642 are of moderate to highly differentiated chemical composition, and may belong to a common magmatic differentiation sequence (tholeiite—tholeiitic andesite—icelandite—rhyolite). The variation of glass shards present in each layer reflects some zonation of the magma chambers being tapped during each eruption. The presence of a common differentiation sequence suggests a common source region for all ash layers. The well-sorted vitric ashes have uniform thicknesses in the range of a few centimeters and a uniform median grain size of about $100 \mu\text{m}$. They are distal air-fall products of large Plinian-type eruptions. By comparing their grain-size characteristics with published data on distal fallout fan deposits (Fisher and Schmincke, 1984), and assuming the existence of a stable jet stream at this latitude in the Neogene, the source of the tephra can be tentatively identified to lie some hundred kilometers west of the Vøring Plateau. This approximate distance is also indicated by the dominance of ashes of differentiated (86%) over

more mafic (14%) compositions, the latter being generally less widely distributed. The large amounts of differentiated ash layers at Site 642 imply the existence of central volcanic complexes in the source region throughout the Neogene and Quaternary.

Iceland is the most likely eruptive source of all the tephra present in the Neogene and Quaternary section at Site 642. The same source has been suggested for ash layers drilled elsewhere on the Vøring Plateau (Talwani, Udintsev, et al., 1976), as well as elsewhere in the North Atlantic (Sylvester, 1978; Varet and Metrich, 1978; Kellogg, Duplessy, and Shackleton, 1978; Harrison, Knox, and Morton, 1979; Donn and Ninkovitch, 1980; Mangerud et al., 1984; Roberts, Schnitker et al., 1984). Central volcanic complexes that erupted differentiated magmas of a tholeiitic differentiation series are known from throughout the stratigraphic record of Iceland (Noe-Nygaard, 1974; Thorarinsson, 1981). Eruption magmas of the same composition are not known elsewhere in the North Atlantic region during Neogene time (Noe-Nygaard, 1974). In addition, rhyolitic ash from large, historically active Icelandic volcanoes, such as Hekla, is known to be transported for hundreds of kilometers downwind (Thorarinsson, 1967).

Tephra Correlation and Sources in the North Atlantic Region

The Neogene and Quaternary section recovered at Site 642 contains more than five times the number of ash layers identified in any other section of Miocene to Quaternary age drilled in the North Atlantic (Donn and Ninkovitch, 1980). Ash of Holocene age, however, including a widespread, 10,600-yr-old, rhyolitic marker horizon (Mangerud et al., 1984), was not recovered at Site 642. Ash layers of Pleistocene to Miocene age have previously been recovered in the North Atlantic on the Rockall Plateau (DSDP Leg 48, Sites 403–406 and Leg 81, Sites 552–554), on the Reykjanes Ridge (Leg 49, Sites 407–409), and on the Iceland–Faeroe Ridge, the Iceland Plateau, the Jan Mayen Ridge, the Vøring Plateau, and the Norway Basin (Leg 38, Sites 336–352). The lack of shipboard chemical analyses during Leg 104 prevents correlation of the ash layers identified at Site 642 with those drilled on the legs listed above. However, similar biostratigraphic positions and similar icelanditic to rhyolitic compositions of the tephra indicate some possible correlations.

One example of a probable correlation will be given here, but this proposal must be tested by on-shore geochemical and isotopic studies. A single pyritized, rhyolitic ash bed (2 cm thick) that occurs in Core 15 at DSDP Site 555 (168.6 m sub-bottom) has the same biostratigraphic age (middle Miocene) as two rhyolitic layers in Hole 104-642C (17H-02, 105–108 cm and 17H-03, 106–109 cm) correlated to the ash layer at 104-642B-16H-07, 99–101 cm).

On the basis of our shipboard studies, we conclude that the stratigraphic distribution of approximately 50 ash layers at Site 642 records a decrease in the rate of explosive eruptions—most likely on Iceland—from the Miocene to the Pliocene and Pleistocene (Fig. 13). This conclusion contrasts with the estimates of Donn and Ninkovitch (1980), who proposed an increase in explosive eruptions during this time.

BASEMENT LITHOLOGY

Introduction

At Site 642, early Miocene sediments overlie an unconformity of as yet undetermined duration. The glaucony-rich volcanoclastic sediments immediately below the unconformity have been described as Unit IV of the sedimentary sequence (“Sediment Lithology” section, this chapter). Unit IV has a thickness of about 38 m and overlies a pebble horizon that marks the top of a 914-m-thick sequence of volcanic rocks and dikes drilled in Hole 642E. Our data analysis aboard ship identified 121 lava

flows, 49 volcanoclastic sediment units, and 7 dikes at this site. Subsequent interpretation of geophysical logs revealed 16 further lava flows and 10 more sediment units. The sequence can be divided into an upper and a lower series that are different structurally, texturally, mineralogically, and chemically. The difference is also marked by changes in the composition of interlayered sediments. Whereas the lower series predominantly consists of peraluminous andesites with subordinate basalts, the upper series is tholeiitic in composition. Both series were apparently deposited under terrestrial conditions. The upper series constitutes the seaward-dipping reflector sequence recognized in geophysical profiles of the Vöring Plateau. The series are separated by a succession of pumiceous volcanoclastics and sandy quartz-siltstones. The physical contrast between these sediments and the overlying dense lava flows may produce the band of low-frequency reflectors seen on seismic profiles, one of which is the K reflector.

The complete lithologic sequence of Site 642 is summarized in Figure 1. An expanded lithostratigraphic column detailing the volcanic sequence and individual units is shown in Figure 14. Where recovery was incomplete, thicknesses of units (Table 6 and Fig. 14) have been deduced from the geophysical logs. Flows (*F*), sediments (*S*), and dikes (*D*) have been numbered sequentially from the top of the section and will be referred to with the appropriate letter designation followed by a number (e.g., F32). Units identified only from logging profiles have been labeled by adding a capital letter to the number of the previous lithological unit (e.g., F32A, S19B). The upper series is further subdivided into groups I, II, and III based primarily on stratigraphic variation in flow characteristics, as discussed below in the "Lithology and Petrography" of the upper series (Fig. 15).

Fifty-nine sediment units have been encountered in the volcanic section. The units here designated as S1, S2, and S3 have been described as Unit IV in the "Sediment Lithology" section, this chapter, and will therefore not be included in the following description. Sedimentary units are volcanoclastic in origin. They comprise about 7% of the 850-m-thick extrusive part of the basement section. The thickness of the sediments in the upper series increases up the section, from 0.5% in group III to greater than 5% in group I. They form 29% of the lower series (Fig. 16).

Correlation Between Holes 642D and 642E

Stratigraphic correlation between Holes 642D and 642E is based on the occurrence in both of a distinctive horizon containing pebbles of basaltic and metamorphic rocks. Underlying this level is a sequence of severely altered medium-grained basalt with interlayered sediments. The pebble horizon is dominated by fine-grained basalt with some calcite-cemented tuff and quartzfeldspathic biotite gneiss (104-642D-14X, CC, 33 cm, to 104-642D-16X-1, 24 cm, and as rubble in 104-642D-19N-1, 90-132 cm, and 104-642E-2W-03, 18 cm, to 104-642E-3R-01, 126 cm). The poor recovery prevented us from determining whether some of the fine-grained basaltic rubble is from a highly weathered *in-situ* basaltic flow. In Hole 642E, a basaltic lithic vitric tuff (S4) with locally abundant pumiceous shards is correlated with a lithologically identical section of red tuff in Hole 104-642D (104-642D-17X-01, 20-80 cm) in between drilling rubble (104-642D-16X-01, 24 cm, to 104-642D-19N-02, 25 cm). Unit S5, a red, altered lithic-vitric basaltic tuff, can also be recognized in Holes 642D and 642E. There is an apparent vertical offset of about 18 m between the holes (Fig. 14).

Hole 642D terminated in a moderately altered, medium-grained basalt that is not present in Hole 642E and is possibly a dike. We recovered 45 cm of sparsely plagioclase-phyric basalt in Section 104-642D-20N-01 after the drill bit shattered and ended drilling. A brief discussion of the resultant deformation of the basalt is included in "Pseudotachylite," this section.

Upper Series

Lithology and Petrography

The upper series is a 760-m-thick succession of 120 aphyric to moderately plagioclase-, olivine- and, rarely, clinopyroxene-phyric tholeiite lava flows. In the upper 100 m there are three fine-grained units with a total thickness of 15 m (2% of the upper series), which may be dikes (D1 to D3). A first-order lithologic differentiation between two major flow types may be made in terms of the grain-size characteristics of their subophitic matrix. These two types are termed "fine-grained" (Fig. 17) and "medium-grained" (Fig. 18), respectively. The section also contains "mixed" flows, which consist of intimately mixed fine- and medium-grained bands (Fig. 19).

Fine-grained flows have plagioclase laths less than 200- μ m long and clinopyroxene between 50 and 100 μ m. They are slightly plagioclase-phyric and are almost completely crystalline (Fig. 20). Euhedral tabular plagioclase phenocrysts (<5 mm) form 0%-1% of the rock, and euhedral to subhedral pseudomorphs after olivine phenocrysts (<2.5 mm) form 0%-1%. In the groundmass, plagioclase forms about 60%, clinopyroxene about 35%, olivine pseudomorphs about 3%-4%, Fe-oxide 2%-3%, and altered interstitial glass 2%.

Medium-grained flows have plagioclase about 300 μ m long and clinopyroxene 100 to 150 μ m. Compared to fine-grained flows, medium-grained flows are generally more phyric and less crystalline and contain altered glass in interstices and vesicles (Fig. 21). Euhedral tabular plagioclase phenocrysts form about 3% of the rock. The groundmass contains about 55% plagioclase, 30% clinopyroxene, 3% to 4% olivine, 3% Fe-oxide, and between 5% and 10% altered interstitial glass.

Plagioclase phenocrysts range from An₈₅ to An₄₀ and from An₇₀ to An₄₀ in the matrix. In fine-grained flows clinopyroxene is zoned, with cores of Wo₃₈ En₄₅ Fs₁₇ and rims of Wo₂₉ En₄₅ Fs₂₆. In medium-grained flows clinopyroxene is zoned, with cores of Wo₄₁ En₄₉ Fs₁₂ and rims of Wo₃₈ En₄₁ Fs₂₁. Subhedral to anhedral phenocrysts of clinopyroxene intergrown with plagioclase occur in trace amounts in about 25 flows. Further constraints on division of flows, including geophysical profiles, average thicknesses, and internal flow fabrics, are described for group I below. These lithological differences between flow types are not reflected chemically (see discussion on the significance of flow structure).

Alteration has been relatively minor, except in the uppermost 35 m where subaerial weathering has caused extensive alteration of all mineral phases. Fresh olivine has not been found in the upper series, having been altered to either iddingsite or smectite, the latter frequently coated with goethite/hematite. Plagioclase has suffered minor alteration to smectite between 600 and 700 mbsf and in some flow units below. Clinopyroxene is generally fresh. The alteration assemblages consist of smectite, calcite, celadonite, and, lower in the section, zeolite (analcite, heulandite). The alteration is discussed in more detail under "Alteration" in this section.

Interlayered volcanoclastic sediments make up about 2% of the recovered portion of the upper series. Interpretation of geophysical logs indicates a total thickness of 30 m, equivalent to about 4% of the upper series. The sediments are dominantly red-brown to dark brown lithic-vitric tuffs, with a median grain size of 0.1 to 0.3 mm. The arcuate morphology and yellowish to reddish brown color of the altered shards indicates a basaltic composition. The least altered shards consist of weakly anisotropic gel-palagonite, but most shards have been replaced to variable extents by smectite and iron hydroxides, with minor zeolite. Single units range in recovered thickness from 2 mm to 195 cm, and geophysical logs indicate a maximum thickness of 310 cm. Average thickness increases toward the top of the section. Sorting is excellent to moderate. Bedding is usually on a

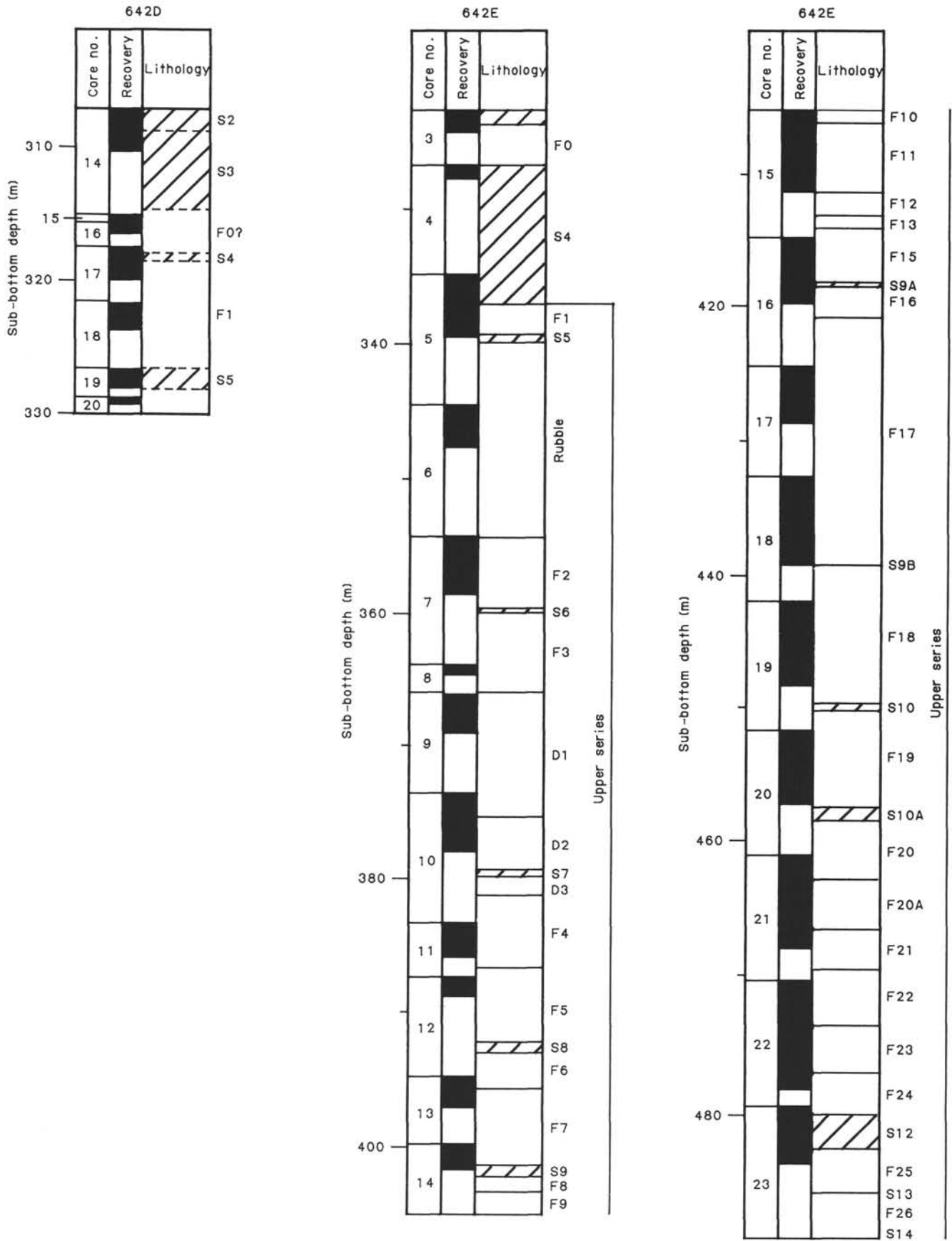


Figure 14. Lithostratigraphy and correlation between Holes 642D and 642E. Sediment units are shown with hatched pattern.

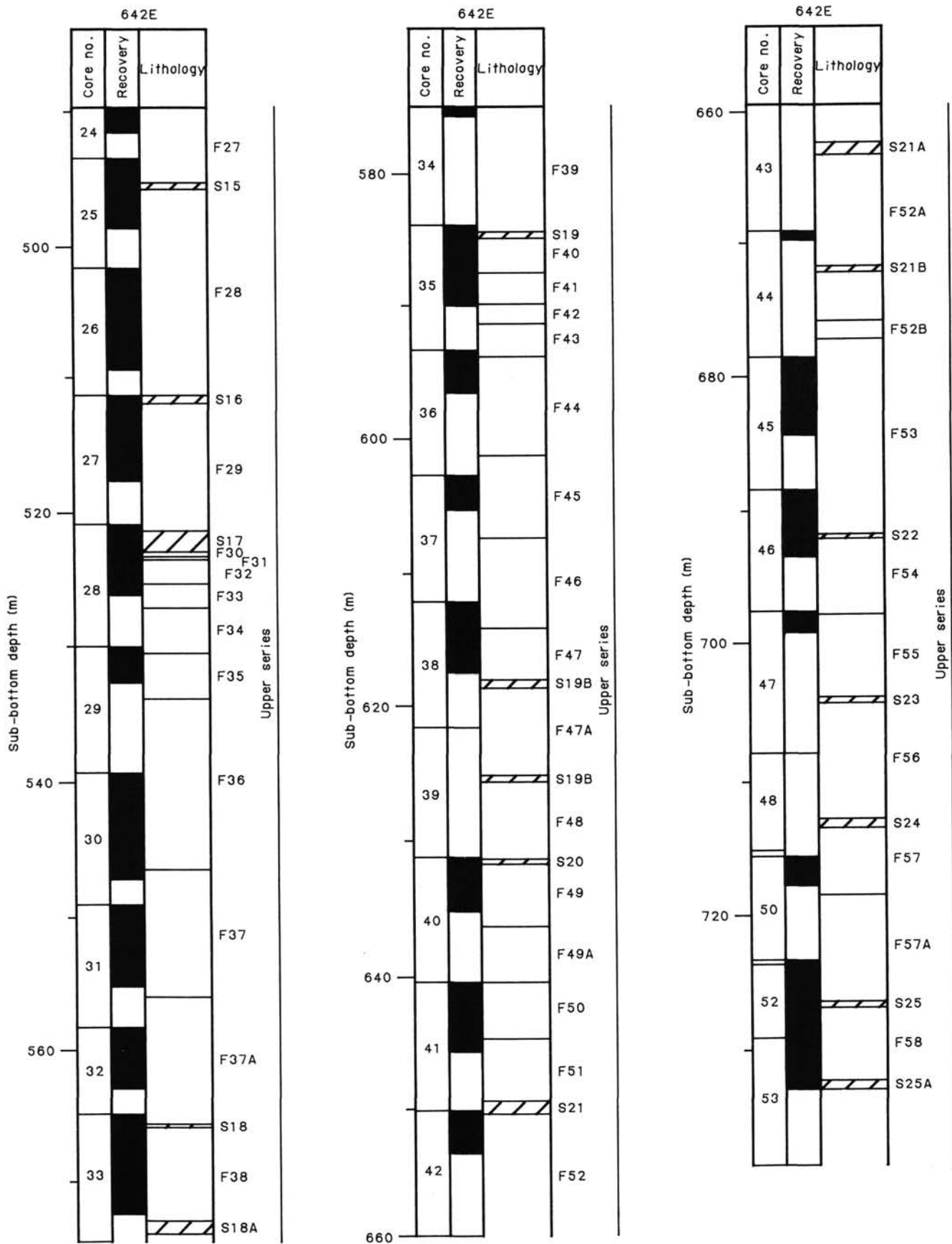


Figure 14 (continued).

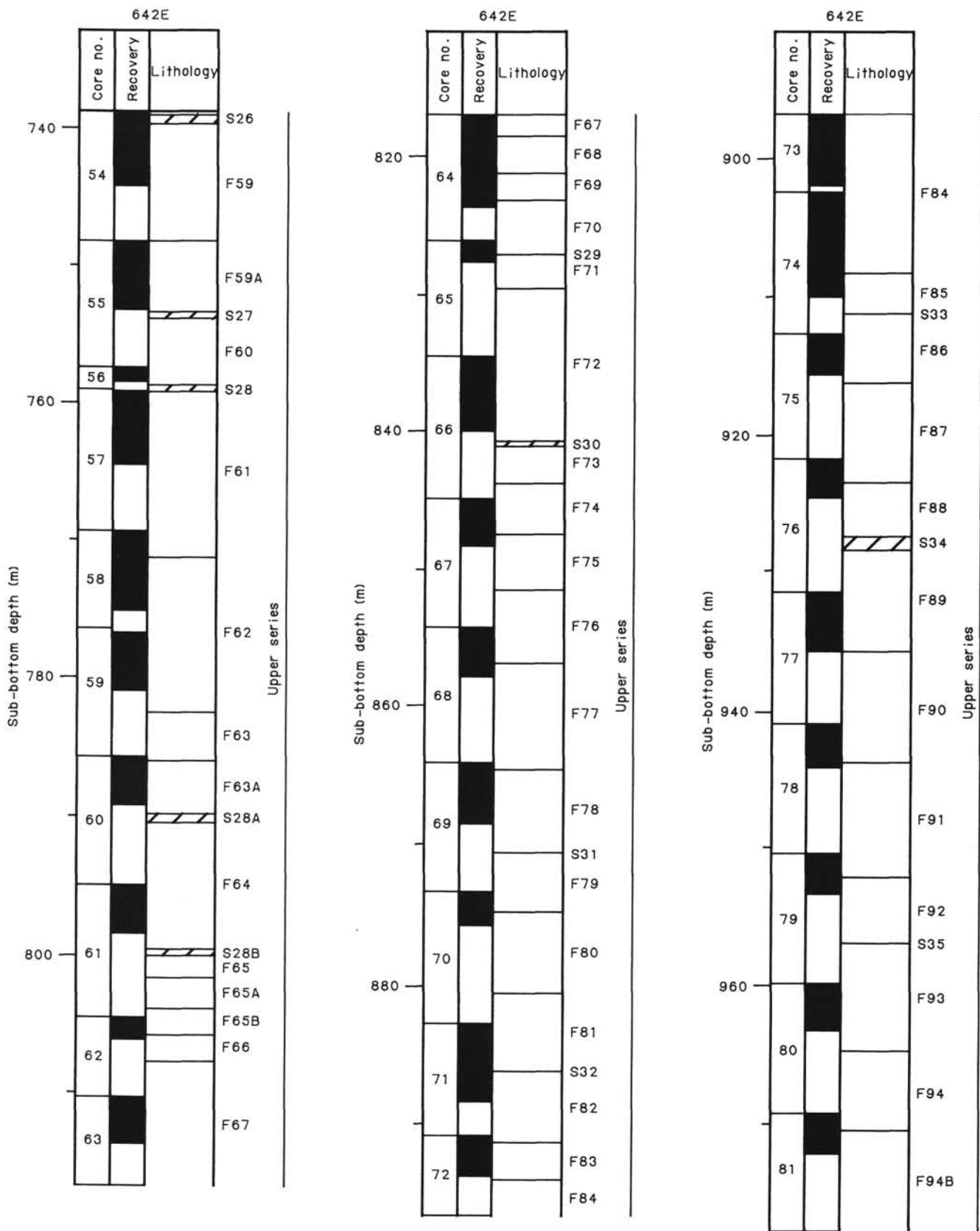


Figure 14 (continued).

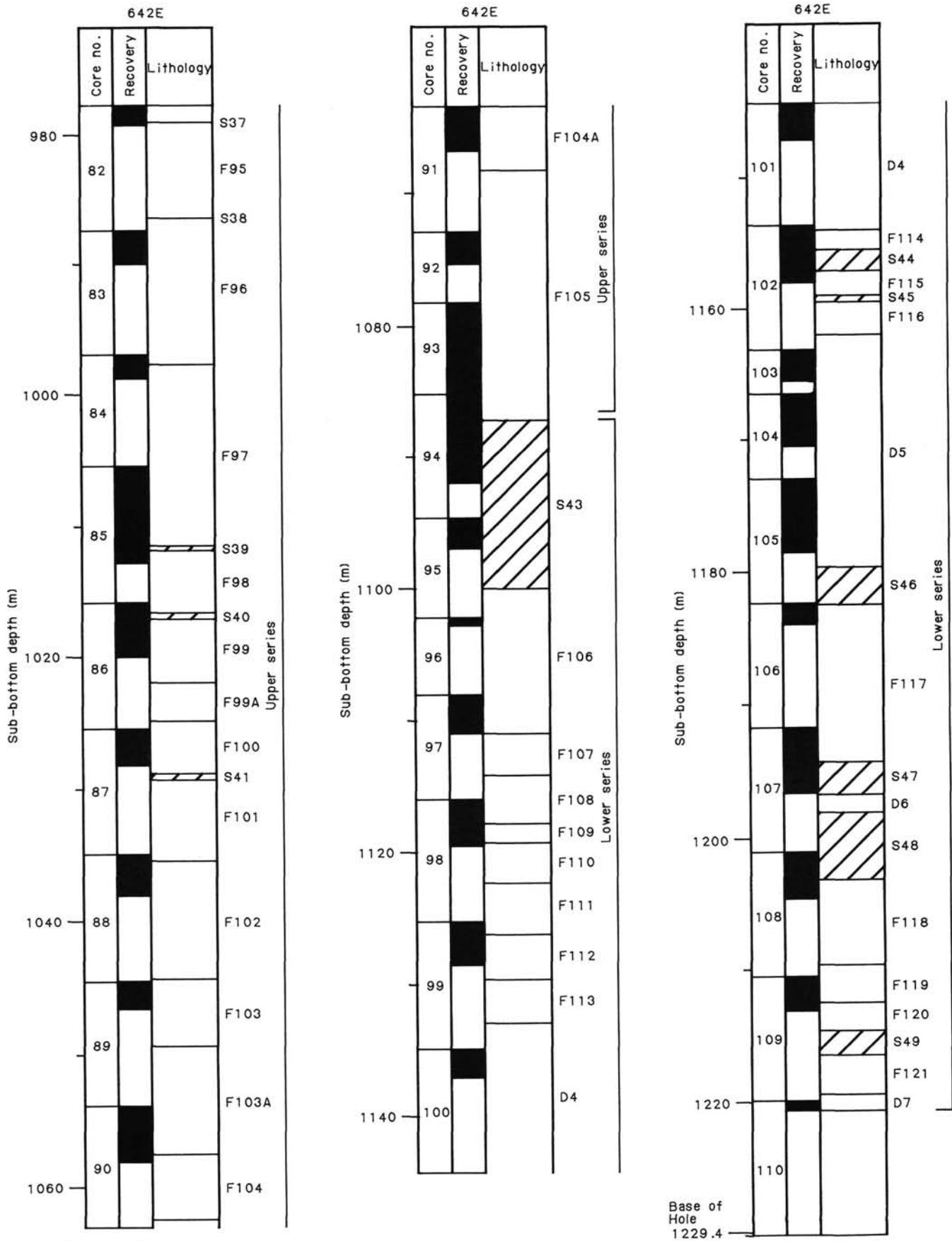


Figure 14 (continued).

Table 6. Core and depth intervals of lithologic units in Hole 642E.

Unit	Recovery Core-section, interval (cm)		Sub-bottom depth (mbsf)
	Top	Bottom	
conglomerate			
S 3	02W-3,018-03R-1,035		~ 320.0-323.5
Upper series Group I			
medium grained			
F 0	03-1,035-03-1,125		323.5-326.5
(Unrelated rubble at	04-1,000-04-1,031)		
S 4	04-1,031-05-2,046		326.5-336.9
(Unrelated rubble at	05-1,000-05-1,008)		
F 1	05-2,046-05-3,129		336.9-339.2
S 5	05-3,129-05-3,150		339.2-339.4
Unidentified drilling rubble	06-1,000-06-2,105		
F 2	07-1,005-07-2,111		354.3-359.5
S 6	07-2,111-07-2,123		359.5-360.0
F 3	07-2,123-09-1,022		360.0-366.0
fine grained			
D 1	09-1,022-10-1,004		366.0-375.4
D 2	10-1,004-10-1,137		375.4-379.2
F 3A	10-1,140-10-1,150		379.2-379.7
D 3	10-2,000-10-2,137		379.7-381.0
F 4	10-2,137-12-1,020		381.0-386.6
F 5	12-1,020-12-1,068		386.6-392.2
S 8	12-1,068-12-1,069		392.2-392.4
F 6	12-1,069-12-1,130		392.4-395.8
F 7	13-1,000-14-1,080		395.8-401.5
S 9	14-1,080-14-1,107		401.5-402.0
F 8	14-1,107-14-1,136		402.0-403.3
medium			
F 9	14-1,136-15-1,093		403.3-406.3
F 11	15-1,093-15-4,106		406.3-411.4
F 12	15-4,106-15-5,045		411.4-413.2
F 13	15-5,045-15-5,122		413.2-414.0
F 15	15-5,122-16-2,123		414.0-418.0
fine grained			
S 9A	Not recovered		418.0-418.3
F 16	16-2,123-16-3,100		418.3-420.7
F 17	16-3,100-18-4,150		420.7-439.2
S 9B	Not recovered		439.2-439.2
F 18	18-5,000-19-4,137		439.2-447.0
(Unrelated rubble at	19-1,000-19-1,022)		
S 10	19-4,137-19-5,020		447.0-450.1
F 19	19-5,020-20-4,104		450.1-457.4
(Unrelated rubble at	20-1,000-20-1,010)		
medium grained			
S 10A	Not recovered		457.4-458.2
F 20	20-4,104-20-4,120		458.2-463.0
(Unrelated rubble at	21-1,000-21-1,038)		
F 20A	21-1,038-21-3,048		463.0-466.2
F 21	21-3,048-21-5,061		466.2-468.9
F 22	21-5,061-22-3,086		468.0-473.2
F 23	22-3,086-22-6,020		473.2-477.1
S 11	22-6,020-22-6,021		477.1-477.1
F 24	22-6,021-23-1,073		477.1-480.5
fine grained			
S 12	23-1,073-23-2,125		480.5-482.7
F 25	23-2,127-23-3,126		482.7-485.8
medium grained			
S 13	23-3,126-23-3,127		485.8-486.3
F 26	23-3,127-24-1,027		486.3-489.6
fine grained			
S 14	24-1,027-24-1,030		489.6-489.6
F 27	24-1,030-25-3,076		489.6-495.2
S 15	25-3,076-25-3,079		495.2-495.8
F 28	25-3,079-27-2,035		495.8-511.0
S 16	27-2,035-2-2,064		511.0-511.5
F 29	27-2,064-28-3,117		511.5-521.2

Table 6 (continued).

Unit	Recovery Core-section, interval (cm)		Sub-bottom depth (mbsf)
	Top	Bottom	
Upper series Group I (cont.)			
medium grained			
S 17	28-3,117-28-3,140		521.2-522.7
F 30	28-3,140-28-4,016		522.7-523.3
F 31	28-4,016-28-4,053		523.3-524.2
F 32	28-4,053-28-4,110		524.2-525.0
F 33	28-4,110-28-5,042		525.0-526.9
F 34	29-1,000-29-1,103		526.9-530.2
F 35	29-1,103-29-2,150		530.2-533.7
fine grained			
F 36	30-1,000-30-6,135		533.7-546.3
S 17A	31-1,000-31-1,004		546.3-546.4
F 37	31-1,004-31-CC,22		546.4-556.0
(Unrelated rubble at	32-1,000-32-1,027)		
F 37A	32-1,027-33-1,136		556.0-565.6
S 18	33-1,136-33-1,138		565.6-565.7
F 38	33-1,138-33-5,134		565.7-572.6
S 18A	34-1,000-34-1,018		572.6-573.2
F 39	34-1,018-35-2,106		573.2-584.1
medium grained			
S 19	35-2,106-35-2,114		584.1-584.3
F 40	35-2,114-35-3,137		584.3-586.8
F 41	35-3,137-35-4,115		586.8-589.7
F 42	35-4,115-36-1,004		589.7-591.4
F 43	36-1,004-36-2,052		591.4-594.0
F 44	36-2,052-37-1,112		594.0-601.6
F 45	37-1,112-37-2,082		601.6-607.4
Group II			
fine grained			
S 19A	Not recovered		607.4-607.5
F 46	38-1,000-38-3,150		607.5-614.6
F 47	38-4,000-38-4,100		614.6-617.7
S 19B	Not recovered		617.7-618.5
F 47A	39-1,000-39-1,005		618.5-625.6
S 19C	Not recovered		625.6-625.9
F 48	40-1,000-40-2,040		625.9-631.6
S 20	40-2,040-40-2,046		631.6-631.7
F 49	40-2,046-40-3,134		631.7-636.6
F 49A	41-1,000-41-1,103		636.6-640.8
F 50	41-1,103-41-3,085		640.8-645.0
F 51	41-3,085-42-1,048		645.0-649.5
S 21	42-1,049-42-1,121		649.5-650.4
F 52	42-1,121-42-3,029		650.4-662.5
S 21A	Not recovered		662.5-663.4
F 52A	Not recovered		663.4-672.0
S 21B	Not recovered		672.0-672.2
F 52B	Not recovered		672.2-676.1
S 22	45-1,000-45-1,078		676.1-677.1
F 53	45-1,078-46-4,048		677.1-691.6
S 22A	47-1,000-47-1,002		691.6-691.7
F 54	47-1,002-47-1,136		691.7-697.6
F 55	47-1,137-47-1,149		697.6-703.9
S 23	47-1,136-137 & 149-150		703.9-704.0
F 56	48-1,000-50-2,032		704.0-712.9
S 24	50-2,032-50-2,040		712.9-713.4
F 57	50-2,040-51-1,035		713.4-717.4
F 57A	52-1,000-52-4,109		717.4-726.3
S 25	52-4,109-52-4,109		726.3-726.5
F 58	52-4,109-53-3,128		726.5-732.3
S 25A	Not recovered		732.3-732.5
F 58A	54-1,000-54-2,062		732.5-739.0
S 26	54-2,062-54-2,110		739.0-739.5
F 59	54-2,110-54-4,120		739.5-748.2
F 59A	55-1,000-55-2,085		748.2-753.3
S 27	55-2,085-55-2,088		753.3-753.4
F 60	55-2,088-57-1,128		753.4-758.7
S 28	57-1,128-57-1,130		758.7-758.8
F 61	57-1,130-58-5,090		758.8-771.3
F 62	59-1,000-59-4,030		771.3-782.1
F 63	60-1,000-60-2,133		782.1-785.4
F 63A	Not recovered		785.4-789.9
S 28A	Not recovered		789.9-790.0
F 64	61-1,000-61-2,128		790.0-798.5

Table 6 (continued).

Unit	Recovery Core-section, interval (cm)		Sub-bottom depth (mbsf)
	Top	Bottom	
Upper series Group III			
medium grained			
S 28B	Not recovered		798.5-798.6
F 65	61-2,128-61-2,132		798.6-801.5
F 65A	Not recovered		801.5-803.5
F 65B	62-1,000-62-1,017		803.5-805.5
fine grained			
F 66	62-1,017-62-1,135		805.5-807.5
F 67	63-1,000-64-4,103		807.5-818.0
F 68	64-4,103-64-5,010		818.0-820.8
F 69	64-5,010-65-1,000		820.8-822.7
F 70	65-1,000-65-1,064		822.7-826.6
S 29	65-1,064-65-1,064		826.6-826.6
F 71	65-1,064-65-1,112		826.6-829.2
F 72	65-1,112-66-4,067		829.2-840.5
medium grained			
S 30	67-1,000-67-1,005		840.5-840.6
F 73	67-1,005-67-1,081		840.6-844.0
F 74	67-1,081-68-1,006		844.0-847.9
fine grained			
F 75	68-1,006-68-1,100		847.9-851.0
medium grained			
F 76	68-1,100-68-2,060		851.0-856.6
F 77	68-2,060-68-2,150		856.6-864.1
F 78	69-1,000-69-2,120		864.1-870.6
fine grained			
S 31	69-2,120-69-2,125		870.6-870.7
F 79	69-2,125-70-1,088		870.7-874.3
F 80	70-1,088-70-2,099		874.3-880.3
F 81	71-1,000-71-2,056		880.3-886.2
S 32	71-2,056-71-2,058		886.2-886.2
F 82	71-2,058-72-1,071		886.2-891.2
F 83	72-1,071-72-2,124		891.2-894.0
F 84	73-1,000-74-6,072		894.0-908.2
F 85	74-6,072-75-1,038		908.2-911.2
S 33	75-1,038-75-1,045		911.2-911.2
F 86	75-1,045-75-2,150		911.2-918.2
medium grained			
F 87	76-1,000-76-2,075		918.2-923.5
F 88	76-2,075-77-1,013		923.5-927.6
fine grained			
S 34	77-1,013-77-1,047		927.6-928.1
F 89	77-1,047-77-3,150		928.1-935.9
F 90	78-1,003-78-3,018		935.9-944.0
mixed			
F 91	79-1,000-79-1,124		944.0-952.2
F 92	79-1,124-79-2,049		952.2-957.2
medium grained			
S 35	79-2,049-79-2,051		957.2-957.2
F 93	79-2,051-80-1,076		957.2-964.8
fine grained			
S 36	80-1,076-80-1,077		964.8-964.8
F 94	80-1,077-80-3,024		964.8-970.4
F 94A	80-3,024-81-2,125		970.4-974.5
F 94B	81-2,125-83-1,016		974.5-978.9

Table 6 (continued).

Unit	Recovery Core-section, interval (cm)		Sub-bottom depth (mbsf)
	Top	Bottom	
Upper series Group III (cont.)			
medium grained			
S 37	83-1,016-83-1,018		978.9-978.9
F 95	83-1,018-83-1,082		978.9-986.2
fine grained			
S 38	83-1,082-83-1,082		986.2-986.2
F 96	83-1,082-84-1,150		986.2-997.6
F 97	85-1,000-85-5,113		997.6-1011.3
medium grained			
S 39	85-5,113-85-5,134		1011.3-1011.6
F 98	85-6,000-86-2,085		1011.6-1016.4
mixed			
S 40	86-2,085-86-2,101		1016.4-1016.7
F 99	86-2,101-86-3,092		1016.7-1021.4
F 99A	86-3,092-86-4,051		1021.4-1024.5
F 100	87-1,000-87-1,100		1024.5-1028.7
fine grained			
S 41	87-1,100-87-1,108		1028.7-1028.8
F 101	87-1,108-88-1,099		1028.8-1035.0
F 102	88-1,099-88-2,096		1035.0-1044.1
F 103	89-1,000-89-2,042		1044.1-1049.1
F 103A	90-1,000-90-3,119		1049.1-1057.2
S 41A	90-3,119-90-3,119		1057.2-1057.2
F 104	90-3,119-90-3,125		1057.2-1062.0
F 104A	91-1,000-91-3,027		1062.0-1068.1
mixed grained			
S 42	91-3,027-91-3,030		1068.1-1068.1
F 105	92-1,000-94-3,117		1068.1-1086.8
Lower series			
S 43	94-3,117-95-2,036		1086.8-1100.0
F 106	95-2,036-97-1,115		1100.0-1111.0
F 107	97-1,115-97-2,038		1111.0-1114.0
F 108	97-2,038-98-1,096		1114.0-1117.5
F 109	98-1,096-98-2,097		1117.5-1119.0
F 110	98-2,097-99-1,010		1119.0-1122.0
F 111	99-1,010-99-1,101		1122.0-1126.0
F 112	99-1,101-100-1,010		1126.0-1129.5
F 113	100-1,010-100-2,018		1129.5-1132.7
D 4	100-2,018-101-2,141		1132.7-1153.5
F 114	102-1,000-102-1,042		1153.5-1155.0
S 44	102-1,042-102-1,123		1155.0-1156.8
F 115	102-1,123-102-2,057		1156.8-1158.5
S 45	102-2,057-102-2,062		1158.5-1158.9
F 116	102-2,062-102-2,117		1158.9-1161.5
D 5	102-2,117-105-4,063		1161.5-1179.5
S 46	105-4,063-105-5,038		1179.5-1182.3
F 117	106-1,000-107-1,102		1182.3-1194.0
S 47	107-1,102-107-2,067		1194.0-1196.6
D 6	107-2,067-107-2,140		1196.6-1198.0
S 48	107-2,140-108-2,047		1198.0-1203.0
F 118	108-2,047-108-2,150		1203.0-1209.5
F 119	109-1,000-109-1,043		1209.5-1212.0
F 120	109-1,043-109-1,060		1212.0-1214.2
S 49	109-1,060-109-1,132		1214.2-1216.0
F 121	109-1,132-109-2,112		1216.0-1219.0
D 7	110-1,000-110-1,055		1219.0-1229.4
(Total depth)			

Boundaries between 368 m and 1090 m redefined according to geophysical logging data (gamma ray, resistivity, density, and porosity — "Logging Results" section); Units F 10, F 14 and S 7 do not exist; F = flow, D = dike, S = volcanoclastic sediment; medium, fine, mixed = grain-size of matrix in flows of following sequence.

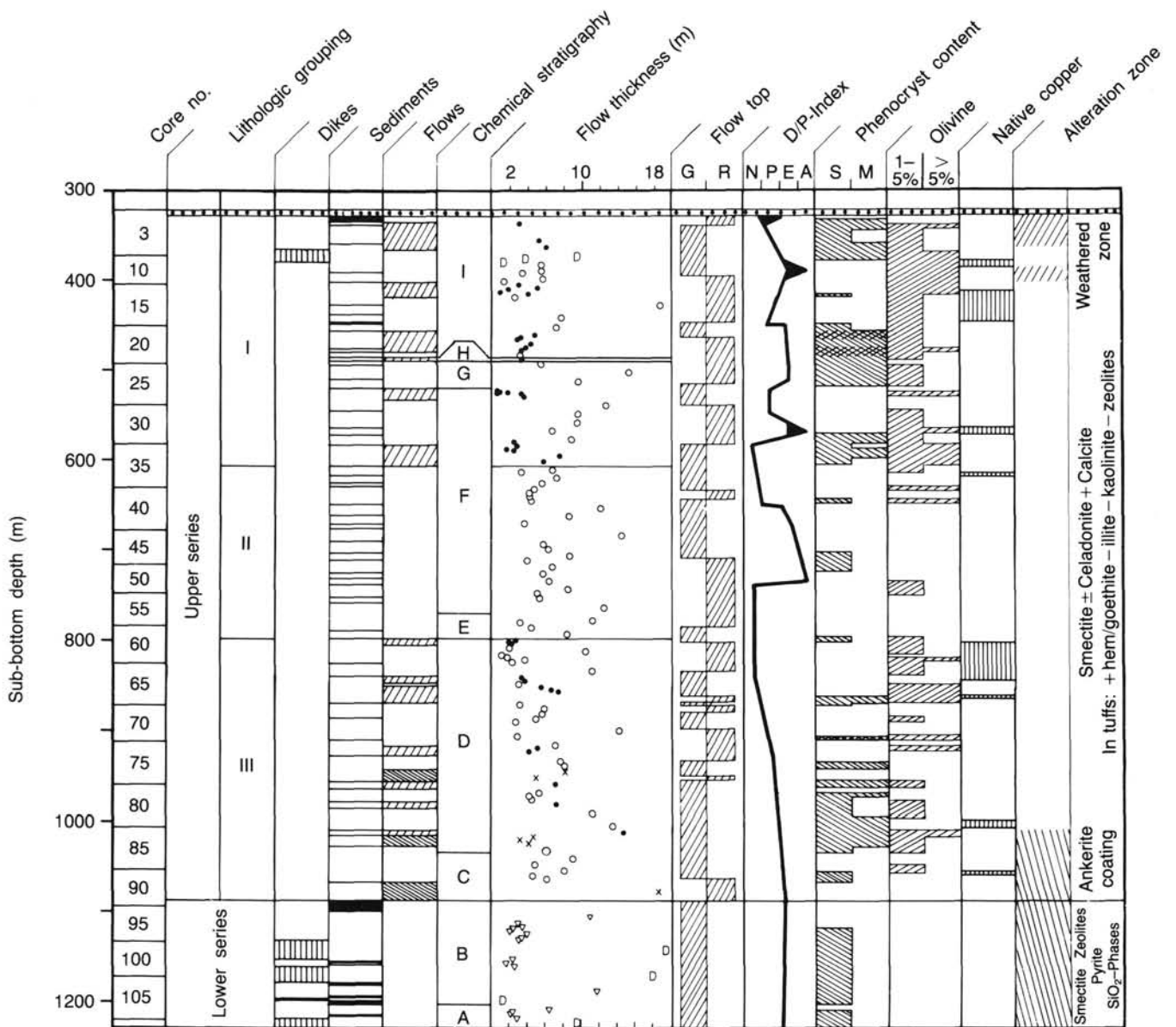


Figure 15. Lithostratigraphy, chemical stratigraphy, petrography, and alteration synthesis of the volcanic sequence, Site 642. Flows: no ornament = fine-grained flows, right-slant hatching = medium-grained flows, left-slant hatching = mixed flows. Flow thickness: open circles = fine-grained flows, filled circles = medium-grained flows, crosses = mixed flows, triangles = lower series flows, D = dikes. Flow top: G = gray, R = reddened. Dinoflagellate/palynomorph index: N = neritic, P = paralic, E = estuarine, A = subaerial. Phenocryst content: S = sparsely phytic, M = moderately phytic, cross-hatching = phytic. Alteration zones: no ornament = low-temperature mineral replacement, right-slant hatching = weathered zone, left-slant hatching = zeolitic and mineralized zone.

scale of centimeters, but some macroscopically massive beds occur.

The relative proportions of the fine- and medium-grained flows (Figs. 14 and 15) and the petrography of the volcanoclastic units (Fig. 16) permit a subdivision of the upper series into three groups. Group I consists of alternating sequences, 10 to 50 m thick, each sequence containing 3 to 6 fine- or medium-grained flows. Group II consists solely of fine-grained flows, and group III is made up of randomly alternating fine-grained, medium-grained, and mixed flows. Flow emplacement occurs in an oxidizing environment throughout. Reddened tops are one indication of subaerial weathering. Reddening is most intense in group I and comparatively weak in group III. Thin, quenched, glassy flow boundaries, less than 1 cm thick, occur in all three groups.

This type of boundary may indicate the presence of wet sediment or shallow water during emplacement, but is also known from terrestrial lavas on Hawaii and Iceland. There are no indications of marine emplacement of the lava flows. Variations in the extent of reddening probably reflect the duration of exposure between eruptions. The volcanoclastic units differ between the three groups in texture, thickness, content of vesicular shards, and content of terrigenous metasedimentary quartz and mica.

Group I (F1-F45, S4-S19, D1-D3; 328.6-607.4 mbsf)

Flows. Group I contains 11 alternating sequences of fine- and medium-grained flows. Sequences of fine-grained flows have an average thickness of 36 m (range: 22.3 to 50.4 m), and single flows average 8 m (range: 2.4 to 18.5 m). In contrast, sequences

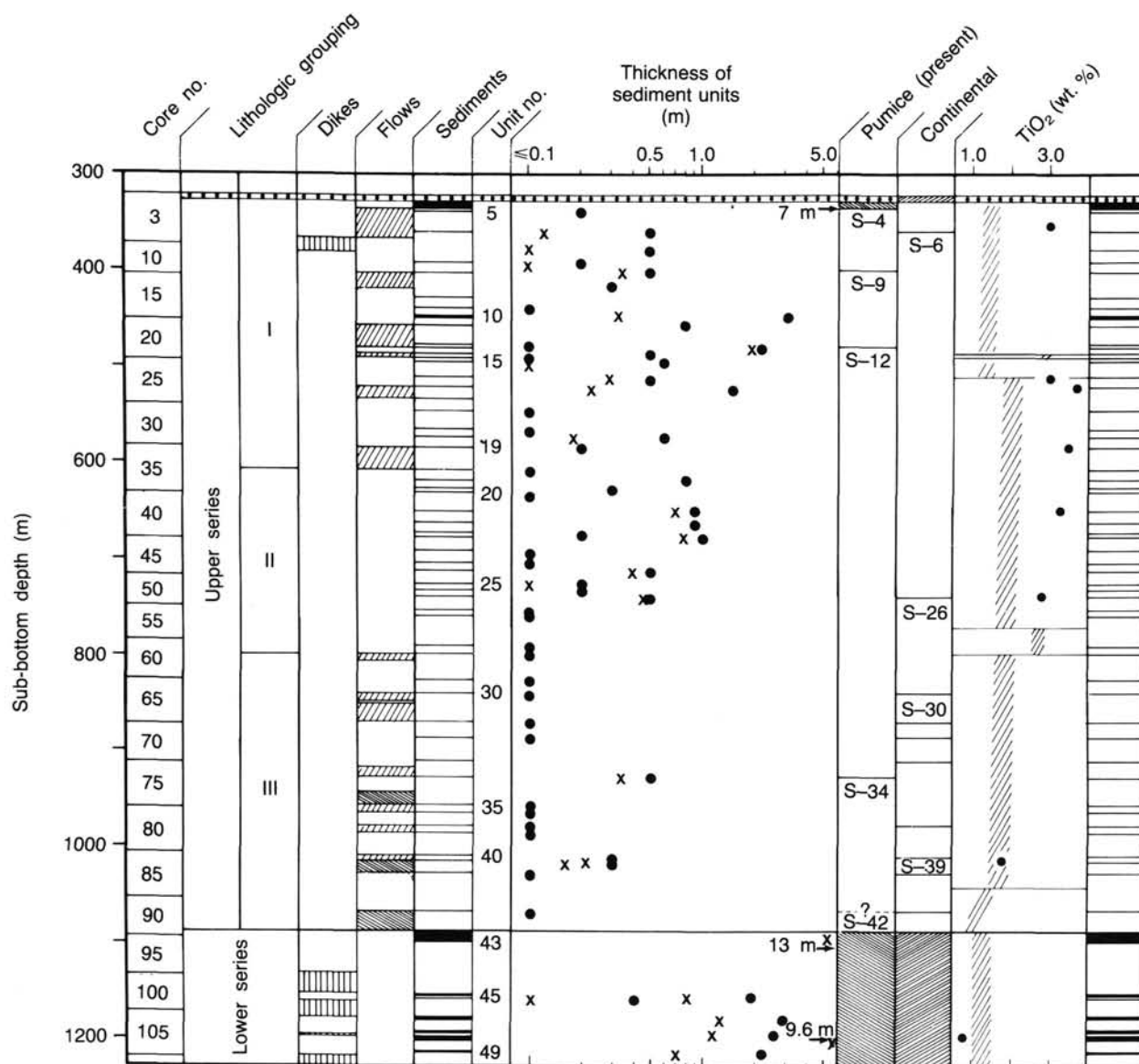


Figure 16. Lithostratigraphy, chemical stratigraphy, and petrography of sediments of the volcanic sequence, Site 642. Flows: no ornament = fine-grained flows, right-slant hatching = medium-grained flows, left-slant hatching = mixed flows. Thickness of sediment units: x's = recovered thickness, dots = estimated thickness. TiO_2 weight (%): hatching = flows, dots = sediments.

of medium-grained flows are thinner (average 17 m; range: 11.0 to 23.1 m) with an average flow thickness of 3.3 m (range: 0.6 to 7.6 m). Flows F25 and F26 do not conform to this pattern, each constituting a separate sequence. Only two thin sediment units occur between medium-grained flow units (S6 and S11), but sediments are common in fine-grained flow sequences (2 flows per sediment unit). Reddening of flow tops is common in fine-grained flows, but is virtually absent in medium-grained flows. Scarcity of interbedded sediment and absence of reddening indicate that medium-grained flow sequences were emplaced rapidly, and may be compound flow units representing one eruptive event. Extensive reddening and abundant interbedded sediment in fine-grained flow sequences suggest longer periods of quiescence.

Group I flows have an average phenocryst content of about 4% (plagioclase \gg olivine + rare clinopyroxene), with a range from 0% (F9) to more than 20% in F20 and F26. Boundaries between aphyric to sparsely phyrlic (F4 to F19, F30 to F38) and moderately phyrlic flow successions (F20 to F29) do not conform to sequence boundaries between fine- and medium-

grained flow sequences. Flows in group I have a higher average olivine content (5%-6%) than group II (2%) and group III (3%) (Fig. 15).

Sequence 1, comprising F1 through F3 and S4 through S6, consists of medium-grained, vesicular, moderately phyrlic flows. Sequence 1 flows are thoroughly altered. All primary mineral phases are replaced by kaolinite, goethite/hematite, and beidelite. The only comparable alteration in the remainder of the upper series is in F5 and F6. Flow F2 has a dark-gray flow top with a quenched variolitic matrix.

Sequence 2, comprising F4 through F8 and S8 through S9, is separated from sequence 1 by three dark-gray, fine-grained units, 1 to 2 m thick, which may be dikes (see "Dikes" below). Sequence 2 flows are dark gray to black, fine-grained, and generally aphyric, but are locally sparsely plagioclase- and/or olivine-phyric. F8 is fine- to medium-grained and appears to be transitional to the underlying predominantly medium-grained flows of sequence 3. F4 and F7 contain flow laminations defined by smectite-rich bands less than 1 mm wide ("Alteration," this sec-

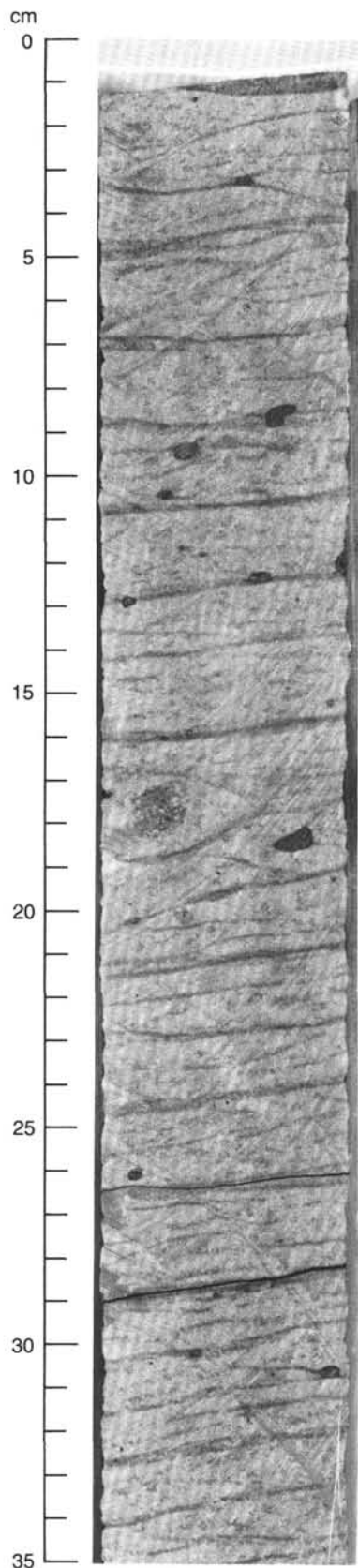


Figure 17. Photograph of Sample 104-642E-30R-4, 0-35 cm, laminar flow fabric in fine-grained tholeiitic basalt, flow F36. The laminations are disturbed by the cognate xenolith at 18 cm.

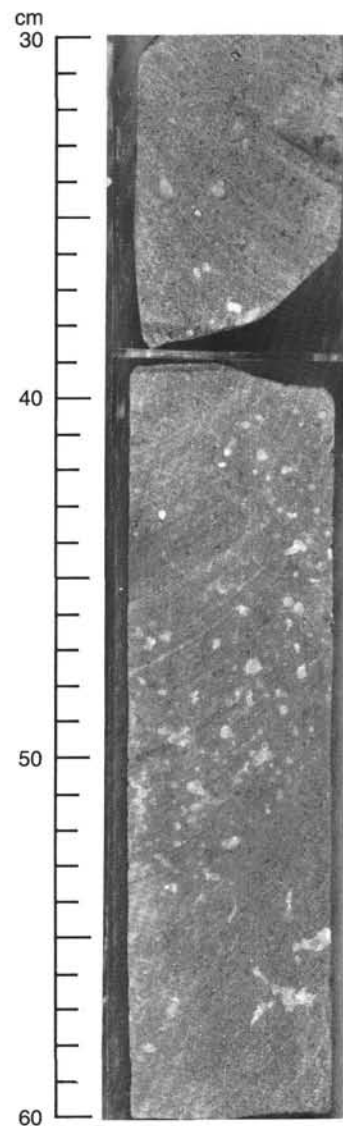


Figure 18. Photograph of Sample 104-642E-16R-1, 16-65 cm, medium-grained tholeiitic basalt flow F15.

tion). Like sequence 1 flows, F5 and F6 have been altered to soft crumbly material, and plagioclase has been altered to saponite and beidellite. The tops of F5 and F6 are black to dark gray (brown in thin section) and have a rapidly quenched variolitic texture. The microfossil/pollen assemblage of S8 indicates an estuarine to possibly terrestrial environment.

Sequence 3 flows (F9 to F15) are aphyric and medium-grained. The complex intermixture of fine-grained basalt within F15 may have resulted from the incorporation of an additional fine-grained flow. F15 has a reddened tachylitic top, but those above have dark gray or gray tops, suggesting an increase in rate of emplacement with time. The opposite trend is indicated in sequence 4, which includes the aphyric and sparsely phyric, fine-grained flows F16 to F19. Whereas F19 exhibits a dark gray, weakly quenched flow top, the reddening increases in intensity upward to F17. Microfossil data indicate a paralic environment for the deposition of unit S10 on top of F19 (see "Biostratigraphy" section, this chapter).

F20 through F29 are moderately phyric, with the dominant phenocryst phase, plagioclase, up to 4 mm in size. F20 and F21

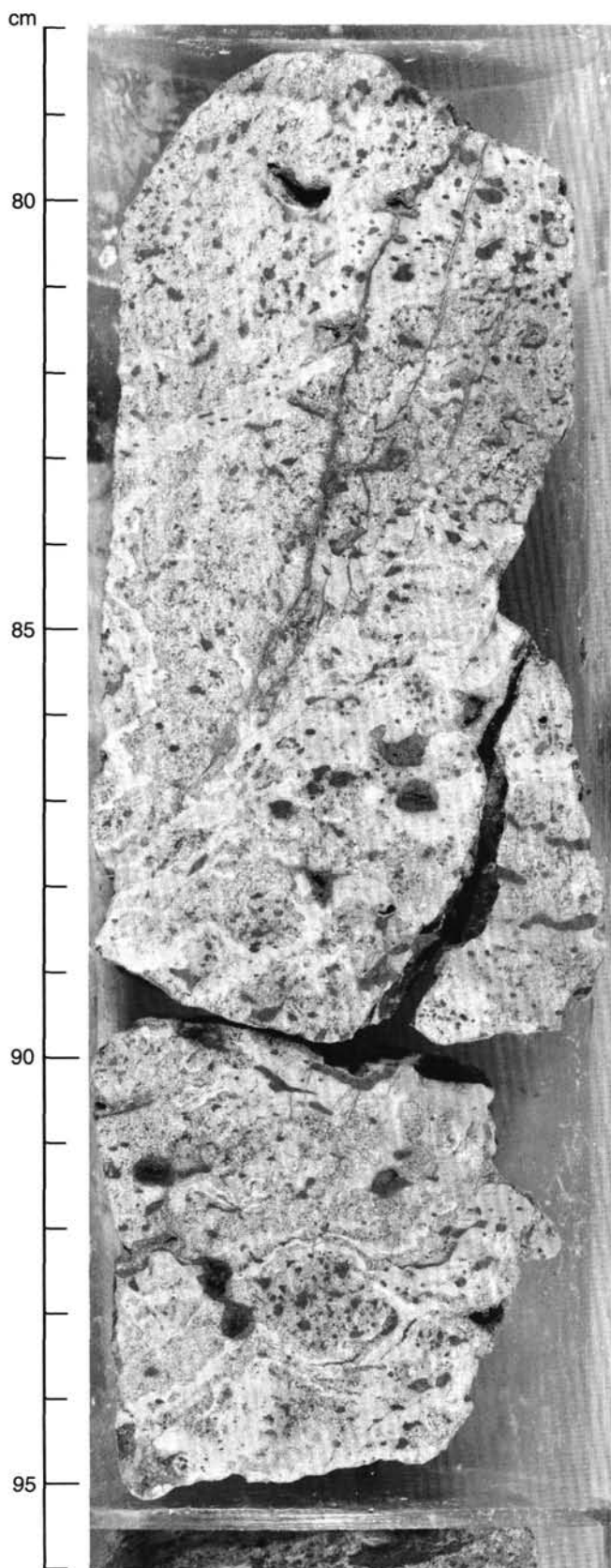


Figure 19. Photograph of Sample 104-642E-79R-1, 78–96 cm, mixed fine- and medium-grained tholeiitic basalt flow F91. Bands of fine-grained basalt are at 81–83 cm, 85–87 cm, and 90 cm.

are the most phyric of the upper series (>20% phenocrysts), and are also the most differentiated (see significance of flow structures, below). Within this interval, F20 through F24 comprise sequence 5, F25 and F26 are individually sequences 6 and 7, respectively, and F27 to F29 constitute sequence 8. F21 through F29 are devoid of quench textures, and tachylitic and reddened oxidized fragments occur in flow-top breccias, suggesting subaerial emplacement. Microfossil contents of S15 and S16 indicate estuarine conditions (see “Biostratigraphy” section).

Sequence 9 is composed of relatively thin, very dark gray, medium-grained flows F30 through F35. Their average thickness is less than 2 m, with thicker flows toward the base. The sequence is overlain by unit S17. All units appear to have been emplaced rapidly, as reddening of the flow tops is absent. The contact between the quenched top of F31 and the quenched base of F30 (104-642E-28R-04, 16 cm, 523.3 mbsf) was recovered (Fig. 22).

Flows F36 through F39 and volcaniclastic units S17A, S18, and S18B make up sequence 10. These fine-grained flows have gray or weakly reddened tops. With the exception of F39, the flows are aphyric. Terrestrial to freshwater environments are indicated for S18 and S18A by their microfossil assemblages.

Sequence 11 is a suite of six medium-grained moderately phyric flows (F40–F45) overlain by sediment unit S19. The two thickest flows occur at the base. Flow tops are reddish gray. F42 and F44 have quenched very dark gray flow bases. Paleontological evidence suggests a terrestrial setting for part of the sequence, but S19 contains three subaqueously deposited sediment cycles.

Volcaniclastic Sediments. Twenty-one volcaniclastic units are interlayered with the lavas of group I. Three of these (S9A, S9B, and S10A) were not recovered, but were detected by the response of the natural-gamma spectrometry tool run during downhole logging (see “Logging Results” section, this chapter). The volcaniclastic units have a total thickness of 22.5 m, or about 9% of the extrusive portion of group I. Apart from S4, units range in thickness from 2 mm to 3.1 m with an average of 0.6 m. Unit S4 is exceptional, being about 7 m thick, but this may be an artifact from core/wireline-log correlation, or it may be composite. However, it is coarser-grained than the overlying sediments and contains thick individual fining-upward sequences, suggesting it may be a genuinely thick unit. Units with thicknesses in excess of several tens of centimeters show sedimentary features such as upward-fining (S4, S16, and S19), internal erosional surfaces, and reworking of underlying sediment (S4, S5, S10, S12, S13, S16, and S19).

Vitric shards dominate over lithic clasts within the volcaniclastic units. Pumice, preferentially replaced by illite/kaolinite, is present in units S9 and S12 and forms a distinct bed 10 cm thick in S4 (104-642E-05R-01, 88–98 cm). Isolated unbroken accretionary lapilli are present in S10, indicating nearby subaerial explosive volcanism. TiO_2 contents of group I sediments are markedly higher than those of the lavas (Fig. 16), suggesting a different provenance.

Dikes. Dikes recovered in sequence 2 of group I are fine-grained, sparsely vesicular, sparsely olivine- and plagioclase-phyric tholeiite. No chilled margin was recovered at the top of D1. The base of D2 is a smectite-rich zone that may be a chilled margin against the highly deformed sediment unit S7. Both chilled margins were recovered from D3, the lower one dipping at 80° against F4. D3 has a macroscopic subhorizontal laminar streaking similar to that interpreted as a flow fabric in many fine-grained flows in the upper series. This, and the similarity in chemical composition of D1–D3 to adjacent flows (see “Flow Structure” below), suggests that they may also be flows. If so, the “chilled margins” may represent zones of tectonic deformation.

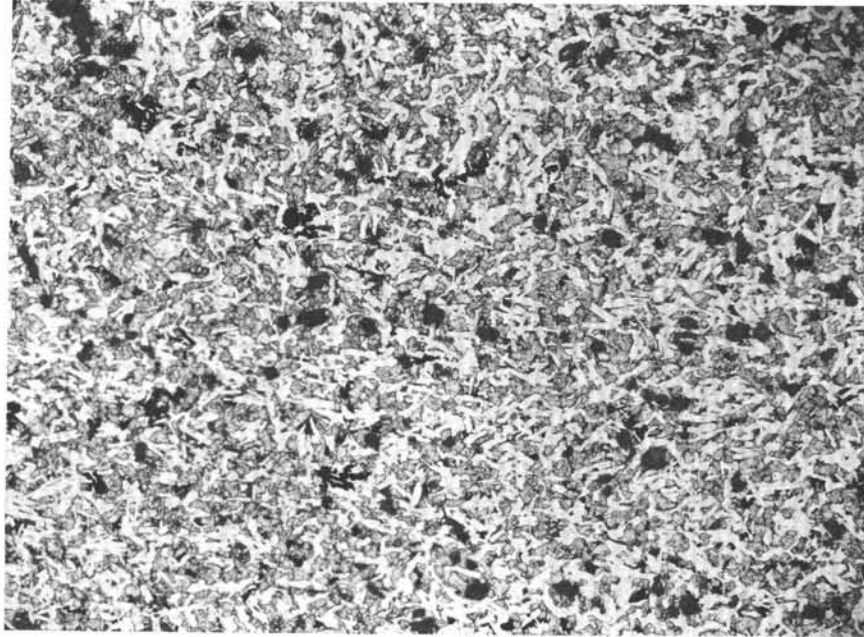


Figure 20. Sample 104-642E-30R-4, 31-33 cm, photomicrograph of aphyric, fine-grained flow F36. Plagioclase feldspar, augite (pale gray), iddingsitized olivine (dark gray), ilmenite (black) are visible. Width of field of view is 4 mm.



Figure 21. Sample 104-642E-36R-2, 114-116 cm, photomicrograph of medium-grained flow F44. Subophitic labradorite/augite, smectite is filling vesicles and replacing plagioclase. Width of field of view is 4 mm.

Group II (F46 to F64, S19A to S28A; 607.4 to 798.5 mbsf)

Flows. Group II consists solely of fine-grained flows. Unlike group I, group II flows are aphyric with a mean phenocryst content (plagioclase \gg olivine) of less than 0.5% and a maximum of about 1%. Trace amounts of clinopyroxene phenocrysts occur only in F57. The olivine content ranges between 1% and 5%, with the exception of F49 (13%) and F51 (8%).

The mean olivine content (2%) is the lowest of the three groups in the upper series. The mean flow thickness in group II is 6.8 m, with a range of 3.1 to 14.5 m. Intense reddening of flow tops occurs in F49 to F51 and F57 to F64, while F46 to F48 and F52 to F56 lack reddened tops. F47 has a quenched top and F48 has a quenched base.

Volcaniclastic Sediments. Ten volcaniclastic units were recovered in group II, but gamma-ray logs indicate the presence of

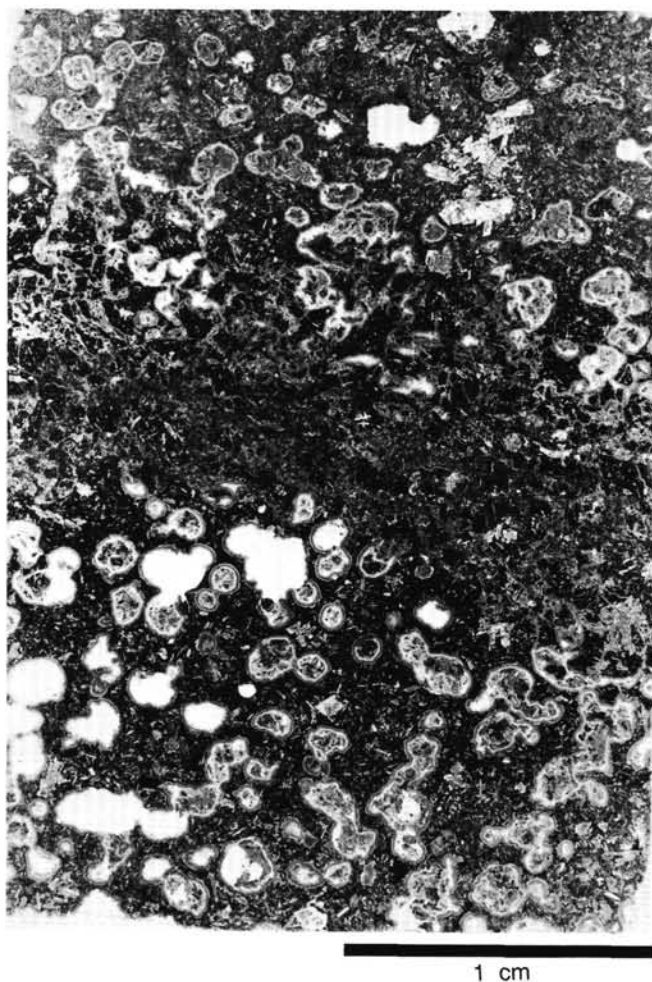


Figure 22. Sample 104-642E-28R-4, 16–18 cm. Photograph shows contact between base of flow F30 and top of flow F31. Collapsed vesicles and brecciated flow base correspond to flow F30.

another seven. The ratio of flow units to sediment units is therefore high (1.6). The recovered thicknesses range from less than 1 to 78 cm, with a mean of 21 cm. Thicknesses deduced from the gamma log range from less than 0.1 to 1.0 m, with an average of 0.36 m. The total thickness of sediments in group II is 6.2 m, equivalent to 3.4% of the interval. The volcanoclastic units are more uniform in lithology and color than the clastic units of group I, and are exclusively basaltic vitric tuffs with variable content of crystalline and quenched basaltic fragments. As with group I, TiO_2 contents are higher than those of the associated lavas, indicating a different provenance. Pumiceous shards are not present in any of the units recovered. Fining-upward sequences, between 7 and 17 cm thick, occur in units S21, S22, and S26. Unit S21 also contains reworked fragments of accretionary lapilli, products of subaerial explosive volcanism. Sediment unit S26 is the first unit below 360 mbsf that contains fragments of detrital quartz.

Group III (F65 to F105, S28B to S42; 798.5 to 1086.8 mbsf)

Flows. In group III, fine-grained and medium-grained flows alternate in an irregular pattern. Some mixed flows occur, characterized by millimeter- to tens-of-centimeters-wide contorted bands differing in grain size, crystallinity, and vesicularity. Medium-grained zones have higher contents of interstitial, originally glassy mesostasis than in groups I and II, and vesicles are

significantly more elongated. F86 exhibits a rare type of mixing where medium-grained droplets, 0.5 to 2.0 mm in diameter and rich in quenched glassy mesostasis, are set in a fine-grained matrix (104-642E-75R-02, 84–86 cm). Tops of flows are not intensely reddened, as they are in group I, but olivine microphe-nocrysts are iddingsitized. Flow tops are predominantly brecciated and purplish in color, and have quenched, variolitic mesostasis. F77, F83, F84, F93, F95, F96, F100, F102, F103, and F104 have quenched, variolitic or palagonitic tops, and F73, F81, F98, F99, and F100 have similar bases.

Volcanoclastic Sediments. Fourteen pyroclastic units have been recovered in group III. Gamma-ray logs indicate the possible existence of one more (S28B). These units range in recovered thickness from less than 1 to 20 cm (well logs indicate 0.5 m for S34), have an average thickness of about 10 cm, and an estimated total thickness of 1.5 m, with 0.58 m actually recovered. They make up about 0.5% of the total thickness of group III. The sediments are uniformly red-brown and contain more vesicular, tachylitic, or variolitic, lithic basaltic clasts compared with groups I and II. Most units seem to be hydroclastic sediments, genetically associated with the underlying flow. TiO_2 contents are generally similar to those of adjacent flows. Pumice is restricted to one 10-mm-wide layer in S34 (104-642E-77R-01, 13–21 cm), the thickest unit present in group III. Group III sediments are characterized by the common occurrence of terrigenous detritus. S30, S31, S32, S37, S39, and S41 contain variable amounts of detrital quartz, accompanied by light mica in S30 and S31, by augite in S30 and S41, and by aegirine-augite in S31.

Flow Structure

The study of the internal structures of the recovered flows making up the upper series reveals contrasts between the internal morphologies of the fine- and medium-grained flows. The thicker, fine-grained flows are characterized by a consistent and generally well-preserved zonal structure that contains planar fabrics developed during stratified laminar flow. In contrast, medium-grained flows are internally homogeneous and physically isotropic. A brief description and discussion of the internal fabrics of the two types of flows follows.

Fine-grained Flows

A section through an idealized fine-grained flow has been derived from the study of the best recovered examples (Fig. 23, left). Ten readily recognizable zones, developed to various degrees, occur throughout the fine-grained flows in a regular fashion.

Zone A: Upper Flow Top. The brecciated, scoriaceous to highly vesicular upper flow top varies from 0 to 3.1 m thick, and averages 0.74 m. Vesicles are 1 to 2.5 mm in diameter and are generally empty. Breccia clasts have a wide size range and include fine-grained glassy basalt fragments spalled from blocky flow tops. These clasts are locally intermixed with volcanoclastic material derived from overlying sediment units.

Zone B: Flow Top. This zone forms a highly vesicular, rapidly cooled, continuous upper margin to the flow. Vesicles are predominantly empty and less than 2.5 mm in diameter. Zone B ranges from 0 to 1.35 m in thickness and averages 1.1 m.

Zone C: Streamed Upper Vesicular Zone. The transition from zone B to zone C is marked by changes in the size, shape and filling of vesicles. Vesicles are locally greater than 5 mm in diameter. Commonly, coalescence of vesicles occurs and results in irregularities in vesicle shape. Vesicle elongation, entrainment, and collapse or partial collapse together constitute a texture referred to here as “streaming.” This texture has an overall subvertical orientation, but local inclined or chaotic streaming, reflecting laminar and turbulent flow of lava, respectively, also occurs. Toward the base of the zone, individual vesicles are

more uniform in size, and are invariably filled with dark green smectite. Zones of completely collapsed vesicles impart a discontinuous, dark green, and well-marked foliation.

Zone D: Upper Vesicular Zone. Zone D is moderately to sparsely vesicular, displaying only rounded or subrounded vesicles, and is gradational with zone C. Vesicles are almost all filled with dark green smectite, but up to 5% of vesicles contain calcite. There is no streaming or elongation of the vesicles. The number of vesicles decreases gradually with depth, although their average size remains constant.

Zone E: Upper Streaked Zone. The upper margin of zone E is identified by either a decrease in vesicularity to less than 5% or by the uppermost occurrence of a spaced, laminar, subhorizontal dark gray-green to black foliation. At the base of zone E, this fabric either disappears completely or gives way to a zone of highly disrupted and poorly developed streaking that may be randomly oriented. The thickness of zone E varies from 0.3 to 6.15 m and averages 1.8 m. Generally, the streaks are diffuse and discontinuous in the upper part of the zone, but become more closely spaced and coherent downward, imparting a well-developed, spaced fabric. Where best preserved, the fabric is defined by 1- to 2-cm-wide zones of fresh gray basalt separated by continuous, discrete, dark planar stripes between 1 and 2 mm wide. Although the fabric is commonly subhorizontal, dips of up to 50° occur. The average spacing between streaks is fairly constant, but some streaks bifurcate and curve, in extreme cases becoming chaotic. Rounded cognate xenoliths of highly vesicular basalt, 1 to 3 cm in diameter, are common throughout the central part of the flows in zones E, F, and G (Fig. 17). Streaks wrap around xenoliths to form "augen" structures. The fabric is locally disrupted on either side of xenoliths forming a pattern of short, irregular, and randomly orientated streaks. This probably marks localized turbulence within the laminar flow. The zone is sparsely vesicular or non-vesicular, and vesicles are filled with dark green smectite or by calcite rimmed by smectite.

Zone F: Central Streaked Zone. The central part of the streaked section is dominated by either weakly to randomly oriented discontinuous streaking or areas of massive basalt. The average recovered thickness of zone F is 0.98 m, although this zone is absent or was not recovered in almost half of the flows. The precise positions of the top and bottom of zone F are largely arbitrary, but the zone is identified where (a) streaks are more than 10 cm apart, (b) streaks are discontinuous or diffuse, (c) the fabric is randomly oriented, or (d) a significant proportion of subvertical discontinuous streaks occurs. Xenoliths are present throughout zone F; vesicles are rare or absent.

Zone G: Lower Streaked Zone. A zone of regularly oriented streaked fabric occurs toward the base of the flow, occupying much of the lower 25%. The zone has an average recovered thickness of 1.55 m. It differs from the upper streaked zone (E) by exhibiting a progressive decrease in spacing of streaks toward its base. The decreased spacing of the fabric is generally accompanied by a decrease in the definition of the streaks, which become more diffuse and less continuous. In the basal part of zone G, there may be an interval of massive basalt. Vesicularity is generally sparse to moderate, and vesicles are invariably filled with dark green smectite. In the lower part of the upper series, local flattening of the closely spaced streaks often results in subrectangular vesicles in zone G. Where the vesicles are not completely flattened, they display a sharp planar truncation against laminations. Even where vesicles are apparently undeformed, individual streaks commonly link, or propagate from vesicle margins.

Zone H: Lower Vesicular Zone. Beneath the lower streaked zone, the vesicularity of the flow increases from the sparsely or non-vesicular laminar zone (G) to a moderately vesicular to vesicular zone. This zone contains vesicles filled with dark green smectite. Vesicles vary in diameter from 0.2 to 1.0 cm, and some

coalesce. Rarely, vesicles are attenuated and ellipsoidal in shape, indicating flow movement. Zone H has an average recovered thickness of 0.29 m, and varies from 0 to 0.95 m.

Zone I: Basal Vesicular Zone. The lowest, highly vesicular section of the flow can be identified in over 90% of recovered flow bases. Zone I is relatively thin (averaging 0.13 m), and has empty, rounded vesicles, 0.5 to 2.0 mm in diameter.

Zone J: Basal Breccia. Only a few thin basal breccias were recovered, with an average thickness of approximately 0.2 m. In general, drilling disturbance has caused dissociated fragments from this zone to be incorporated into the upper surface of underlying volcanoclastic sediments, or to be intermixed with the brecciated top of the underlying flow.

Medium-grained Flows

In general, medium-grained flows are structurally homogeneous. Unlike fine-grained flows, there is little evidence of internal stratigraphy or flow fabric. Textural characteristics of medium-grained flows (Fig. 23, right) include (a) intense localized vesicle streaming without the full suite of gradational vesicularity observed in fine-grained flows, and (b) a narrow disturbed basal flow zone, locally cut by subvertical gas escape structures. These may be partly filled with smectite and/or sediment. Limited basal brecciation may occur within the most intensely vesicular zones. Vesicle diameters range from approximately 1 mm in the uppermost 0.2 to 0.5 m of the flow to around 6 mm in the central part. Diameters may locally exceed 1 cm. Vesicles are commonly filled with calcite rimmed with green smectite. Local non-vesicular zones may be cut by highly vesicular, internally brecciated areas.

Significance of Flow Structures

The internal structure of the fine-grained basaltic units includes intensely laminated sections that are interpreted as indicating differential flow. In the zonal structure described above, the composite streaked zone comprises two sections of approximately equal thickness that exhibit a fabric interpreted as resulting from laminar flow, separated by a central zone of disrupted or randomly oriented discontinuous streaks. These fabrics reflect zones of laminar flow surrounding a zone with little internal movement.

In detail, the laminar flow fabric is locally accompanied by a well-developed, subparallel alignment of plagioclase microlites in the groundmass. This fabric is rarely completely consistent in its orientation, and commonly exhibits aligned microlites in poorly defined domains. The domains are locally randomly oriented with respect to each other. This fabric also wraps microphenocrysts.

Geochemical data suggest that the distinction between the fine-grained and medium-grained flows is not the result of primary compositional differences. However, it is possible that the textural differences between the flows reflect differences in their volatile content, the medium-grained flows having higher primary volatile content. Such differences might also arise during eruption or flow of the lavas. It is possible that the coarser grained flows are proximal and volatile-rich, and form compound flows. Farther from the vent, the degassed magma formed thicker fine-grained flows. This model accounts for the lack of reddening on the tops of most individual coarser grained flow units, except for the uppermost flow unit in each compound flow.

Chemistry

The shipboard XRF was not working on Leg 104. Results of shore-based analyses performed at seven laboratories have been compiled for this preliminary discussion.

Major and trace element analyses are available for most of the 123 lava flows and dike units in the upper series. Rare-earth elements, Th, Ta, and Hf concentrations have been determined

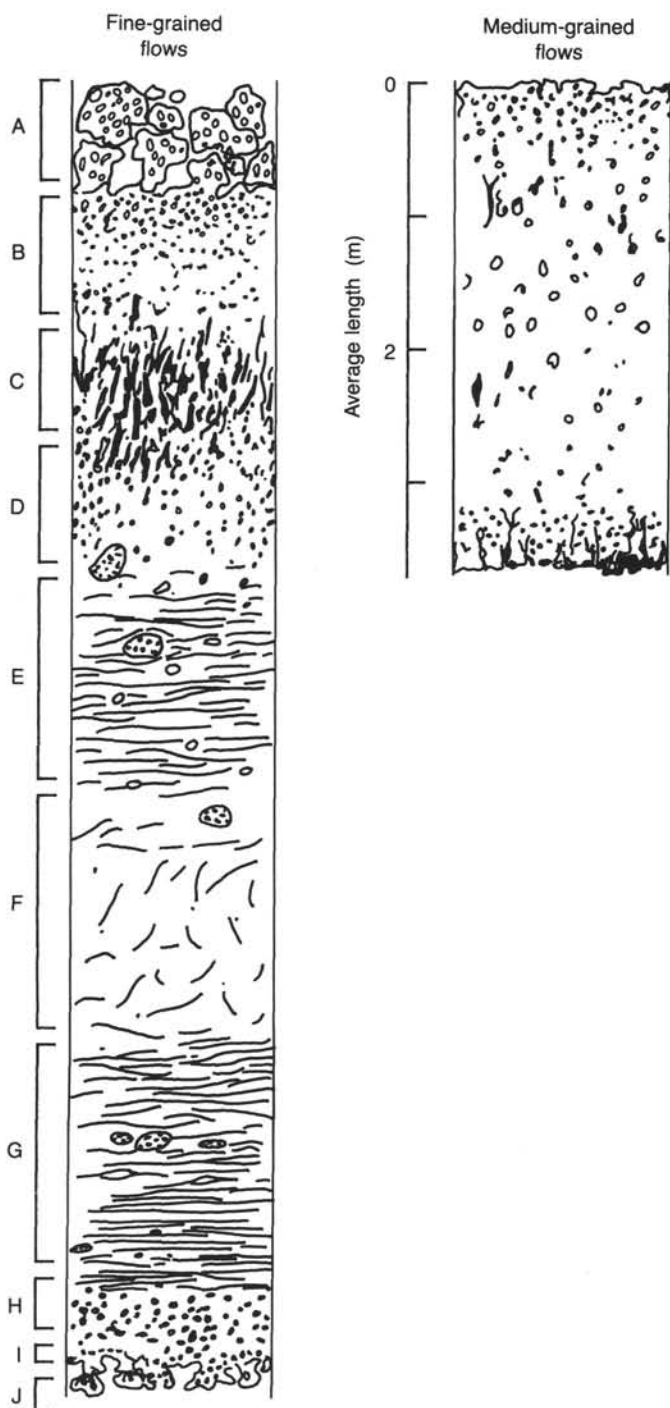


Figure 23. Schematic intraflow stratigraphy of (left) fine-grained and (right) medium-grained upper series flows. Zonation A to J shown in fine-grained flows is discussed in text.

for 57 units. Geochemical data indicate that alteration effects are relatively minor. Tables 8 through 10 give range and mean major, trace, and rare-earth-element abundances compiled from the 56 freshest flows, selected on criteria discussed in "Alteration," this section.

The upper series shows a clear chemical stratigraphy, with six chemical subdivisions (C to I, Table 7). Each subdivision is characterized by relatively uniform high field strength (HFS) and rare-earth-element contents, which reflect subdivision dif-

ferences in primary magma composition. Subdivisions C, G, and I have low HFS element contents (e.g., TiO_2 1.0% to 1.8%). Subdivisions D and F, which together constitute the majority of the upper series, have intermediate HFS contents, and subdivisions E and H have high HFS contents (e.g., TiO_2 2.6% to 2.9%). Boundaries between subdivisions are marked by pronounced changes in absolute contents of incompatible trace elements.

All upper series flows and dikes are uniformly basaltic, for the most part lacking significant variations in degree of differentiation. Mg, defined as $\% \text{MgO} / (\text{MgO} + 0.85\text{FeO} + 0.15\text{Fe}_2\text{O}_3)$, ranges from 54 to 67, with a mean of 58.5 ± 2.9 , similar to ocean floor basalt. MgO (6.60 to 8.68%, average 7.56%), Cr (100 to 394 ppm, average 225 ppm), and Ni (56 to 146 ppm, average 89 ppm) values indicate fractionation of about 5% to 10% olivine and 5% to 10% chromite, clinopyroxene, and plagioclase prior to eruption. F20, F21, F29, and F65 are more differentiated, with Cr as low as 38 ppm and Ni 53 ppm. Compatible elements show that the least differentiated, most primitive magmas were erupted at the base of the upper series, in subdivision C (F103 to F105, MgO 8.6% to 10.2%), and in subdivision I, between 400 and 500 mbsf (F9 to F19, MgO 7.8% to 8.7%).

Though their absolute contents of incompatible elements vary by a factor of almost 3, element abundances and $^{87}\text{Sr}/^{86}\text{Sr}$ and $^{143}\text{Nd}/^{144}\text{Nd}$ ratios indicate that upper series basalts have a mid-ocean ridge tholeiite character. Compared to North Atlantic mid-ocean ridge basalts (MORB), Leg 104 tholeiites are lower in SiO_2 by about 1.0% to 1.5%, Al_2O_3 by 1%, and CaO by 0.5% (Table 8). In contrast, the Leg 104 tholeiites are relatively Fe- and Ti-rich (FeO range 9.25% to 12.28%, mean 10.80%; TiO_2 range 1.11% to 2.73%, mean 1.75%), indicating an affinity with ferrobasalt and are slightly large ion lithophile (LIL) element enriched compared to N-type MORB (Fig. 24). La ranges from 2.69 to 11.4 ppm, with highest values in subdivision E (high-Ti flows) and lowest values in subdivision C (low-Ti flows). $(\text{La}/\text{Sm})_N$ and Zr/Nb ratios characterize the tholeiites as N-type MORB. They have convex-upward light rare-earth element (LREE) patterns (Fig. 25), with values between 7 and 30 times chondritic. The tholeiitic upper series flows therefore appear to be products of different degrees of partial melting of a uniform mantle source, less depleted than that of the average N-type MORB.

Initial $^{87}\text{Sr}/^{86}\text{Sr}$ ratios (Sr_i) of leached basalt range from 0.7031 to 0.7036, typically MORB-like in character. However, the highest values (0.7036) were found in flows with the highest Th contents (F7, F98). This selective enrichment in Th and Sr_i may indicate local contamination by continental crustal material.

Lower Series

Lithology and Petrography

The lower series extends from 1086.8 mbsf to the bottom of Hole 642E at 1229.4 mbsf. It consists of 43% flows (F106-F121), 21% volcanoclastic sediments (S43-S49), and 36% dikes (D4-D7) (Table 6). Rocks of the lower series are lithologically, petrographically, chemically, and consequently petrogenetically, distinct from the tholeiites of the upper series. They range from basaltic to peraluminous andesitic composition (Fig. 26). Dikes D5 and D6 are tholeiitic in composition and are more closely related to the upper series.

Recovery was only 34% in the lower series, and many of the defined flow unit boundaries may be significantly in error. Estimates of flow thicknesses are therefore highly suspect. For example, F109 was recovered in a single core, has typical internal structure (see discussion), and is about 1.5 m thick. F106 has a recorded thickness of 13.7 m, but recovery was very poor (only 7.1% in Core 104-642E-96R), and is probably a composite of sev-

Table 7. Subdivisions of the volcanic series based on chemical affinities.

Sub-division	Interval	Top 104-642E-	Bottom 104-642E-	Interval (mbsf)	Thickness (m)
I	F1-F25	5R-2, 46 cm	23R-3, 125 cm	337.0-485.8	148.8
H	F26	23R-3, 127 cm	24R-1, 27 cm	486.3-489.6	3.3
G	F27-F29	24R-1, 30 cm	28R-3, 117 cm	489.6-521.2	31.6
F	F30-F61	28R-3, 140 cm	58R-5, 90 cm	522.7-771.3	248.6
E	F62-F64	59R-1, 6 cm	61R-2, 128 cm	771.3-798.5	27.2
D	F65-F102	61R-2, 128 cm	88R-2, 96 cm	798.6-1044.1	245.5
C	F103-F105	89R-1, 0 cm	94R-3, 117 cm	1044.1-1086.8	42.7
B	F106-F117	97R-1, 115 cm	107R-1, 102 cm	1111.0-1194.0	83.0
A	F118-F121	108R-2, 47 cm	109R-2, 112 cm	1203.0-1219.0	16.0

Table 8. Basalt geochemical data, Site 642.^a

No. of samples	Upper series		Lower series					
			Type B		Type A		D5 & D6	
	56		8		8		3	
Type	Fresh		Least altered		All data		All data	
Compound	Range %	Mean %	Range %	Mean %	Range %	Mean %	Range %	Mean %
SiO ₂	47.90-50.10	48.17	58.60-61.90	59.87	47.02-55.50	51.09	48.90-51.80	50.03
TiO ₂	1.11-2.73	1.75	1.17-1.28	1.25	1.00-1.51	1.24	1.07-1.50	1.26
Al ₂ O ₃	13.12-17.04	14.74	14.20-15.69	14.90	14.87-17.60	16.33	13.28-18.20	14.93
FeO ^b	9.25-12.28	10.80	8.32-9.39	8.82	9.10-12.23	10.02	8.53-12.64	11.17
MnO	0.14-0.29	0.21	0.06-0.15	0.12	0.10-0.27	0.17	0.16-0.23	0.20
MgO	6.60-8.68	7.56	1.54-1.98	1.66	2.33-6.11	4.28	5.19-8.43	6.66
CaO	9.15-12.60	11.28	2.26-3.39	2.78	5.57-8.04	6.80	7.52-10.40	9.25
Na ₂ O	1.75-2.90	2.36	2.02-3.13	2.29	2.68-3.27	2.96	2.09-3.61	2.74
K ₂ O	0.06-0.24	0.13	1.03-1.75	1.38	0.86-2.16	1.49	0.11-0.34	0.22
P ₂ O ₅	0.10-0.27	0.16	0.09-0.28	0.17	0.11-0.19	0.17	0.09-0.13	0.11

^a Data not corrected for H₂O or CO₂.^b All Fe calculated as FeO.Data from: University of Newcastle upon Tyne, United Kingdom
Midland Earth Science Association, United Kingdom
Ruhr-University, Bochum, FRG

eral flows. On the basis of the most completely recovered flow units, a reasonable average thickness for lower series flows is 2 to 3 m.

Flows

Lower series flows can be divided into two distinct types based on petrographic criteria. F106 to F117 are characterized by dominantly perlitic glassy and variolitic mesostasis, whereas F118 to F121 have a microcrystalline matrix with intersertal texture. This distinction is supported by geochemical data (see lower series "Chemistry" below). The lower series is therefore divided in two (Fig. 15), subdivision B (F106 to F117) and subdivision A (F118 to F121).

An idealized typical flow from subdivision B consists of a glassy top, a variolitic middle and a glassy base, each with a thickness of about 0.4 to 1.0 m. The brownish to grayish-pink glass has been pervasively hydrated to perlite (Fig. 27) with a purple vitreous luster in hand specimens. Progressive alteration to smectite has occurred along fractures, causing the brecciated appearance of most perlitic flows. Close to flow bases and along internal fracture zones, brecciated and glassy fragments are, in general, extensively altered to smectite. Some vesicles and fractures in the glass are filled with smectite, chalcedony, agate, quartz, pyrite, and rarely, calcite. In some flows (e.g., F108 and F115), vesicles are elongated at an angle of 20°-40° from the horizontal. Geopetal vesicle fillings also occur, unfortunately in unoriented pieces.

Crystallinity and phenocryst content increase with depth in subdivision B lavas. Glassy flows (F106 to F109) contain rare pla-

gioclase microphenocrysts with slight zoning (An₇₄₋₈₄). F110 to F115 contain swallow-tailed plagioclase and swallow-tailed acicular pyroxenes, which are up to 0.5 mm long and have length/width ratios of 30. Skeletal, trellis-like crystals of oxides are abundant in the variolitic central zones of F110 to F115. These crystals reach lengths of 1 to 7 mm and length/width ratios are typically about 100. The phenocryst assemblage in these flows forms 1% to 2% of the rock and consists of hypersthene and calcic plagioclase (An₇₀₋₈₂). F116 and F117 contain 5% phenocrysts, with cordierite in addition to plagioclase and hypersthene. Plagioclase in F116 and F117 shows oscillatory zoning from An₇₀ to An₈₅. Skeletal oxides, swallow-tailed plagioclase (An₆₄), and pyroxene similar to those in F110 to F115 are also present. Subdivision B flows are commonly glomerophytic and individual plagioclases reach 3 mm in diameter. Crystals in most subdivision B flows have sub-parallel orientation.

Subdivision A flows (F118-F121) are microcrystalline and intersertal, with about 50% to 60% plagioclase and pyroxene in a quenched matrix. Large oxide needles and perlitic fractures are absent. Phenocryst aggregates of plagioclase and pyroxene are extensively replaced by smectite except in F120. F121 has well-developed segregation vesicles.

Volcaniclastic Sediments

Volcaniclastic sediments in the lower series are dissimilar to those in the upper series. Glass shards are tabular to cusped and are replaced by clinoptilolite, possibly indicating dacitic compositions. Terrigenous components, such as light and brown mica, quartz, and rare fragments of quartz-mica schist, occur

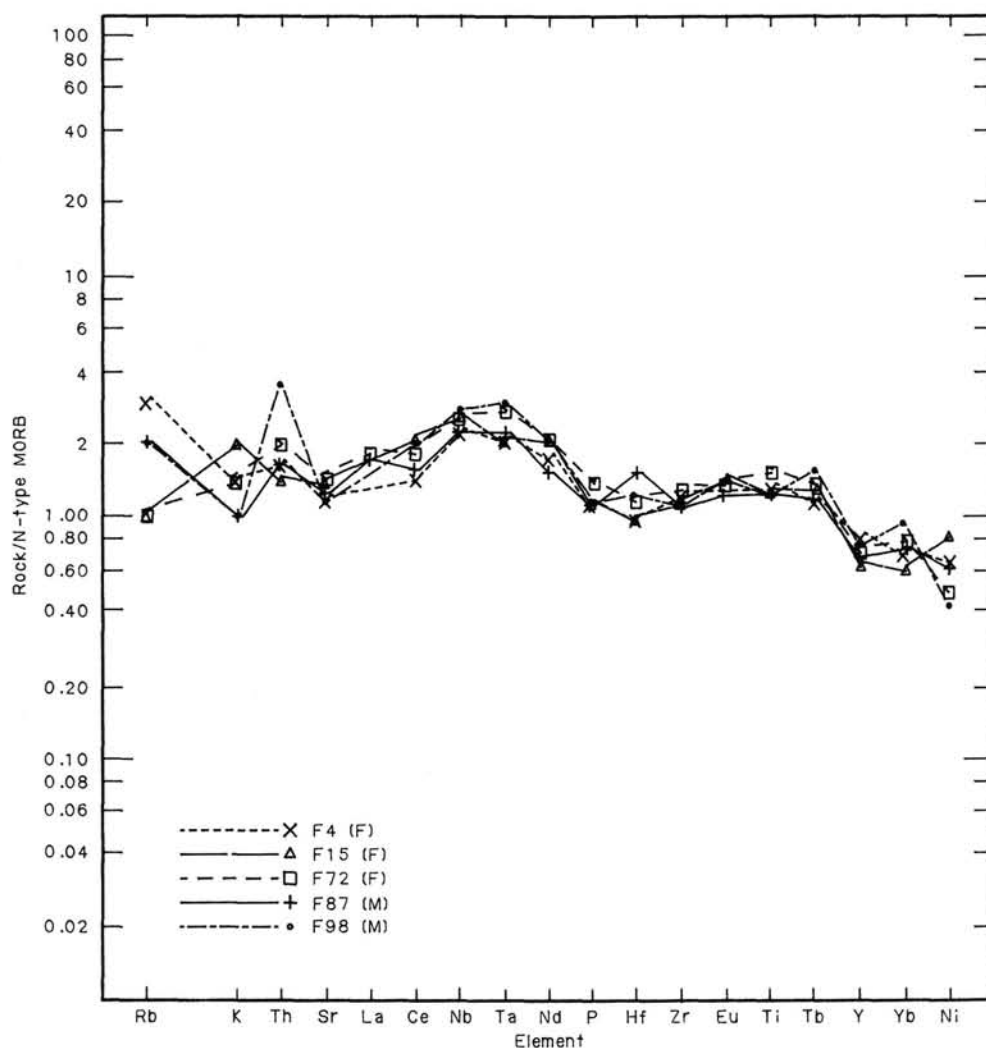


Figure 24. Representative mid-ocean ridge basalt (MORB)-normalized spidergrams of upper series flows. F = fine-grained, M = medium grained flows. Note the enrichment in flow F98.

throughout lower series sediments, forming about 10% of individual beds. The clastic units vary in recovered thickness from 0.05 to 5.55 m, with a mean thickness of 1.9 m. Thicknesses estimated from downhole logs range from 0.4 m (S45) to 13.2 m (S43), with a total thickness of 27.6 m and a mean of 3.9 m. The true thickness of S43 is in some doubt, as the depth of its base is not constrained by the geophysical logs. Volcaniclastic sediments form about 27% of the extrusive portion of the lower series.

The sediments are gray to grayish brown volcaniclastic mudstones. They are moderately to well sorted, with median grain diameters of about 0.1 to 0.5 mm. They are laminated or thinly bedded, and display slump structures, cross-bedding, and erosional features. Clinoptilolite, phillipsite, and carbonate are common cements. Idiomorphic replacement of shards (and, rarely, mica) by clinoptilolite is common.

The uppermost clastic unit (S43) is about 7 m thick and separates the upper and lower series. Its lower half consists of a succession of finely laminated mudstones, with well-developed slump folds. These mudstones contain compacted pumice fragments. The upper half consists of several fining-upward volcaniclastic mass flow units with interbedded zones rich in quartz and mica. Pumice fragments are uncollapsed. An erosion surface is present between the upper and lower parts of S43.

S47 and S48 belong to a single pyroclastic flow deposit cut by D6. It has an internal stratification similar to that in the proximal facies of subaqueously deposited ignimbrites (Figs. 28 and 29). A basal layer of fine-grained vitric tuff is overlain by a 1-m-thick lithic breccia with accidental, aphanitic to perlitic lapilli and blocks forming about 80% of the rock. The 6-m-thick central massive part contains accidental lithic and perlitic fragments which fine upward from 35 to 5 mm in diameter, whereas pumice lapilli increase upward both in diameter (from 1 to 20 mm) and abundance (from 1% to 10%). The upper 0.6 m of the massive poorly sorted part of the ignimbrite contains well sorted lapilli. The massive part of the ignimbrite is overlain by 2.6 m of light to medium gray, medium to well sorted, sand- to silt-sized, rhyodacitic tuff. Parallel laminations pass gradually upward into irregularly wavy and steeply inclined, discontinuous laminations. No undisputedly cognate crystals have yet been identified.

The large number of accidental clasts indicates extensive andesitic volcanism of lower series type prior to the ignimbrite-forming Plinian eruption. The well-sorted, silty-sandy tuffs also contain less than 1% or 2% quartz, mica, and reworked volcaniclastic sediments. Two rock fragments, less than 1 cm in diameter, are of particular interest. One appears to be a partly disintegrated (resorbed?) granite gneiss clast and the other a finer grained metamorphic siliceous rock.

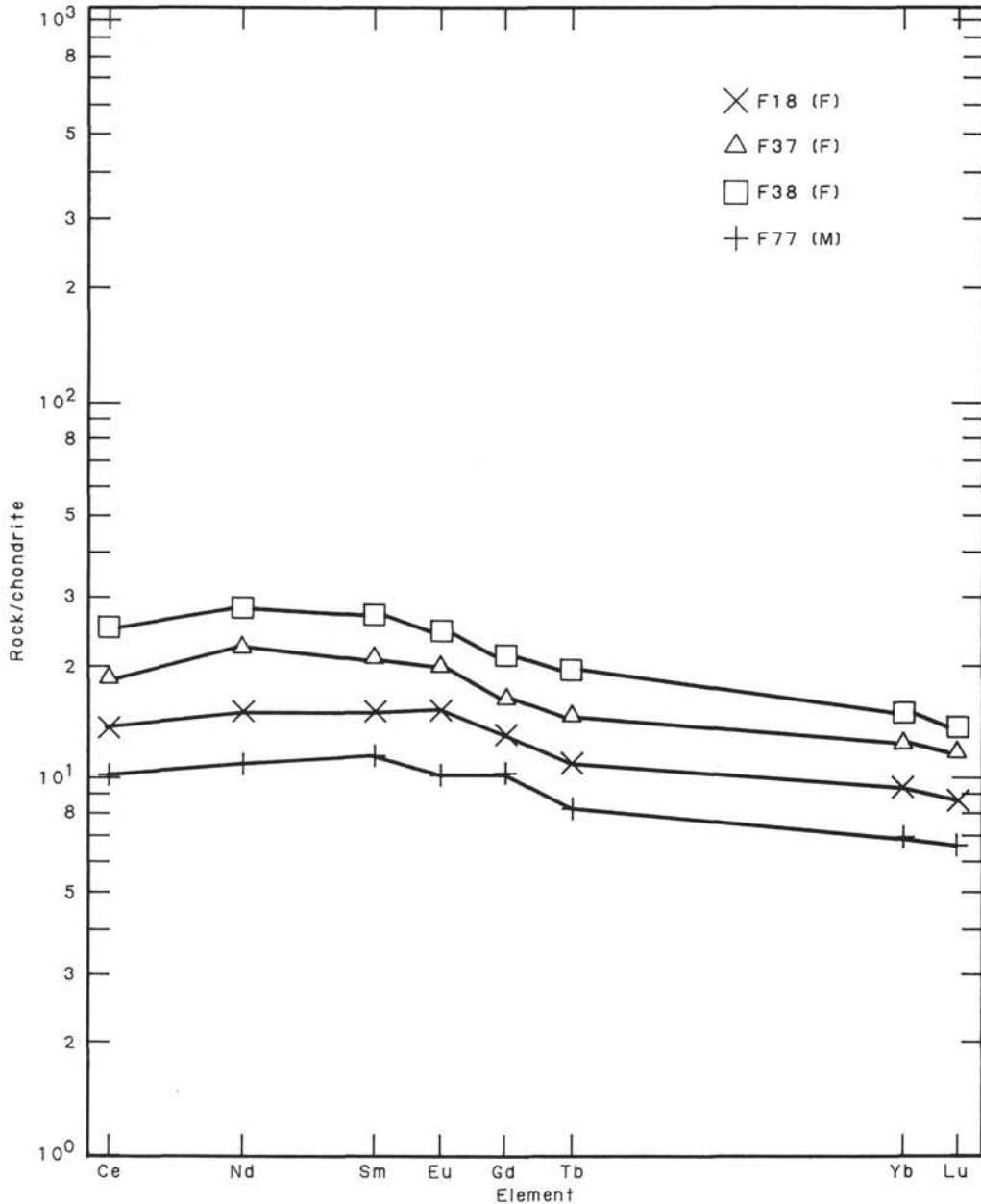


Figure 25. Representative chondrite-normalized light rare-earth element (LREE) plot of upper series flows. F = fine-grained, M = medium-grained flows.

Dikes

Four units were identified as dikes in the lower series. Of these, D4 and D7 have mineralogical and geochemical affinities to lower series flows. The evidence for the intrusive origin of D4 and D7 is ambiguous, and they are probably better interpreted as thick crystalline flows. Chilled margins to D4 and D7 were not observed. The status of D5 and D6 as dikes is not in doubt, as chilled margins were observed, and their mineralogy and geochemistry are distinctly different to the remainder of the lower series.

D4 is the uppermost "dike" in the lower series and is about 21 m thick. It "intrudes" flows of subdivision B, which it also resembles chemically (see "Chemistry" below). D4 is more crystalline than its bounding perlitic flows. It contains a microphenocryst assemblage that forms about 20% of the rock, consist-

ing of calcic plagioclase up to 0.8 mm in length, together with partly swallow-tailed pyroxene less than 1.3 mm long with a length/width ratio of 25, and oxides. In addition, glomerophytic aggregates of plagioclase, hypersthene, and cordierite form about 2% of the rock. The plagioclase phenocrysts are bytownitic and show marked oscillatory zoning. Many have an albite-rich rim (An_{40}). The phenocrysts and microphenocrysts are set in a variolitic matrix (exceeding 50%) and glassy mesostasis (20%). Saponite fills interstices, rare vesicles and replaces plagioclase. Pyrite is present in the groundmass.

D5 is aphyric, with a subophitic, intergranular to intersertal matrix of plagioclase (50%), clinopyroxene (40%), altered olivine (4%), oxides (2%), and altered glass (4%). In texture and grain size D5 closely resembles medium-grained upper series tholeiites. Saponite, pyrite, and rare zeolite are secondary mineral phases.

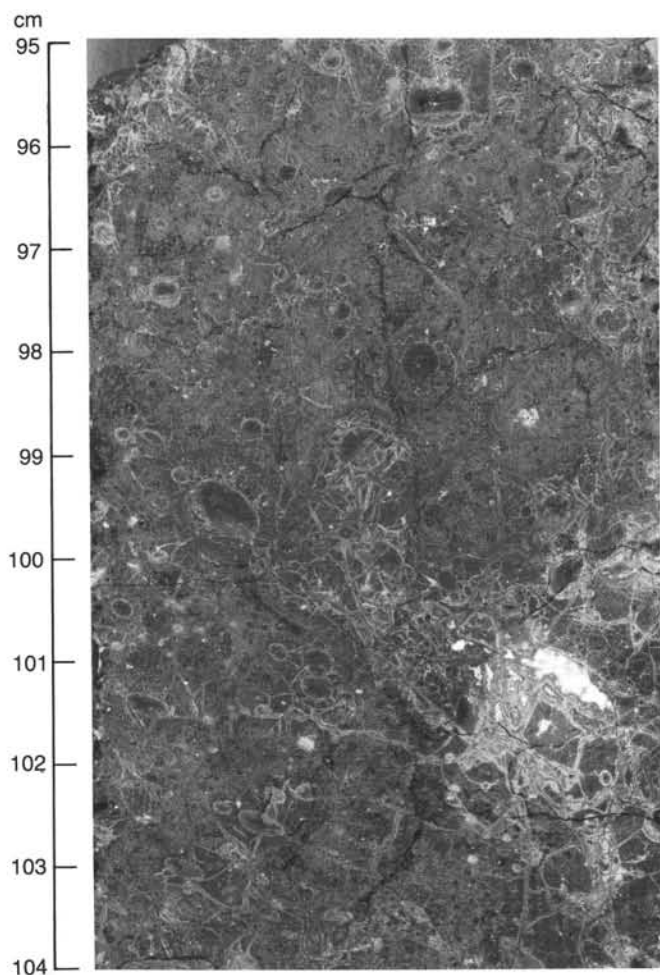


Figure 26. Photograph of Sample 104-642E-97R-1, 95-104 cm, peraluminous basaltic andesite, lower series flow F106. Smectite-filled perlitic fractures and vesicles in glassy groundmass are visible.

D6 is aphyric, hypocrySTALLINE, and sparsely vesicular, with an intersertal texture. Plagioclase constitutes 40% of the rock, and pyroxene, much of which is altered to smectite, forms about 30%. Olivine may have been present originally. Cryptocrystalline smectite replaces interstitial glass and fills vesicles. Pyrite is rare.

D7 is similar to D4 in being chemically similar to adjacent flows (F118 to F121). It is aphyric and hypocrySTALLINE, with a pilotaxitic, intersertal groundmass. Rare phenocrysts are present, consisting of resorbed anhedral pyroxene, less than 1 mm in diameter, and subhedral plagioclase. Plagioclase (45%), orthopyroxene (20%), and oxides (1-2%) occur as lathlike microphenocrysts, on average less than 250 μm in length. Late crystallizing poikilitic quartz (3%) commonly has graphic inclusions of glass and fills interstices. Saponite, pyrite, calcite, and rare, brown pleochroic mica are secondary phases.

Chemistry

Geochemical data indicate a two fold subdivision of the lower series into a basaltic group, subdivision A, and a group of peraluminous andesites, subdivision B (Table 7). D4 and D7 are chemically indistinguishable from their bounding flows and are included, for the following discussion, in subdivisions B and A, respectively. Subdivision A is Zr- and Nb-poor, whereas B is Zr- and Nb-rich (Table 9). SiO_2 has a narrow range in subdivision B, from 58.60% to 61.90%, markedly different from the more ba-

saltic subdivision A (SiO_2 47.02% to 55.50%). Other trace and rare-earth-element data (Tables 9 and 10) further emphasize the geochemical differences between the two magma types.

Lower series rocks (excluding D5 and D6) are strongly enriched in LIL elements and depleted in Sr, Eu, and high field strength (HFS) elements (Figs. 30 and 31). Subdivision A is less enriched in Nb, Th, and large ion lithophile (LIL) elements than is B by up to an order of magnitude, whereas HFS elements vary little between the two types. Sr_i values are high (exceeding 0.711) in subdivision B and somewhat lower in A, between 0.709 and 0.710.

We interpret these data as indicating that subdivision B magmas were derived by partial melting of continental crust, probably of sedimentary or metasedimentary origin. Magmas of subdivision A were probably derived by mixing of the crustal melt with N-type MORB magma, similar to that forming the upper series.

D5 and D6 have MORB-like signatures, but have enriched LIL-element contents indicating crustal contamination. This is supported by the Sr_i value for D5 of 0.705, intermediate between upper and lower series values.

Alteration

Environment

The common occurrence of reddened flow tops without pillow structures or thick glassy crusts indicates terrestrial and probably subaerial conditions throughout emplacement of the upper series. This interpretation is supported by the red color of interbedded sediments. The common occurrence of red, iddingsitized olivine in upper series flows also supports this view, although this occurrence has also been reported from ocean floor lavas. Thin, quenched, glassy to variolitic tops and bases of a number of flows possibly indicate emplacement onto wet sediments or into shallow water. The intensity of reddening, together with thickness of sediment, reflects the time interval between flow emplacement.

Sequences of medium-grained flows rarely contain interlayered sediments and few have reddened flow tops. They were emplaced rapidly and may be compound flow units proximal to the vent. Interlayering of fine-grained flows and sediments is common (flow/sediment ratio of less than 2). Sediment thickness increases above 740 mbsf, suggesting that the upper part of the upper series (326 to 740 mbsf) represents a greater time span than the lower part (740 to 1087 mbsf). The intensely weathered nature of the upper 70 m of the volcanic pile indicates that extrusion was followed by a long period of quiescence represented by the conglomerate horizon S3 (base of lithologic Unit IV).

Evidence for the environment of emplacement of the lower series is ambiguous. No pillows or hyaloclastites were observed, but there are no indications of oxidative weathering. Sedimentary structures (grading, slumping, cross-bedding, and fine lamination) in the interlayered sediment units, which constitute a large portion of the lower series, suggest subaqueous conditions throughout.

Mineralogy

Two types of alteration have affected the volcanics at Site 642. Throughout the pile there is a low-temperature suite of secondary minerals, which developed relatively early and is related to the environment of emplacement. Superimposed on this, there is a later, higher temperature overprint, which has affected the lower 50 m of the upper series and the entire lower series (Fig. 15).

In the upper series, the low-temperature suite consists of smectite (saponite > nontronite/beidellite) and minor calcite and celadonite. Zeolites (analcite and heulandite) occur near the

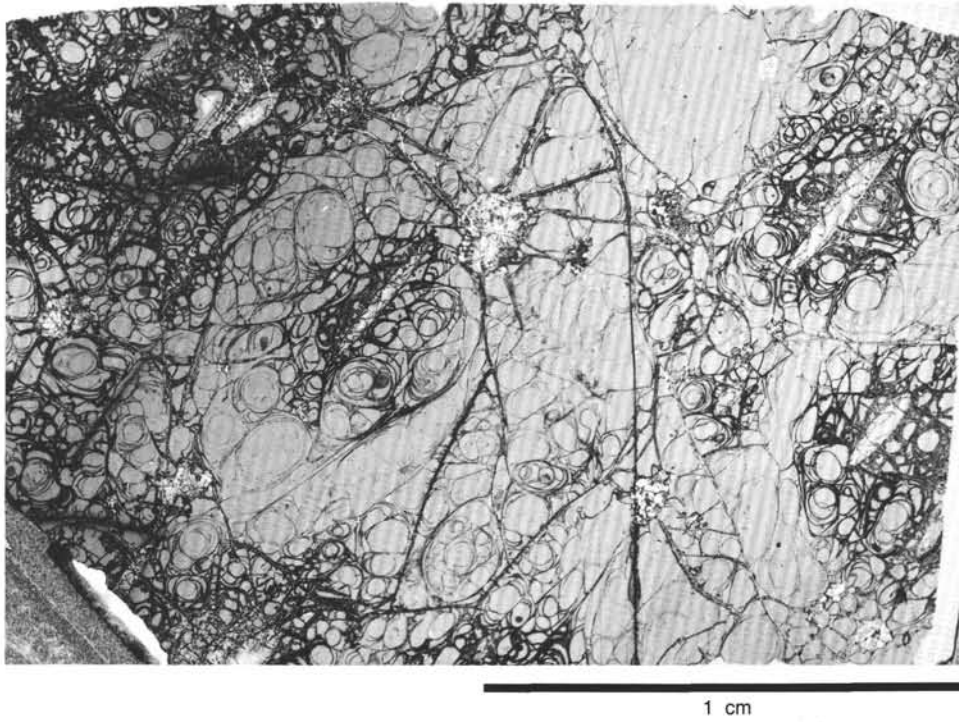


Figure 27. Sample 104-642E-98R-1, 62-64 cm, photomicrograph of perlitic texture in lower series flow F108.

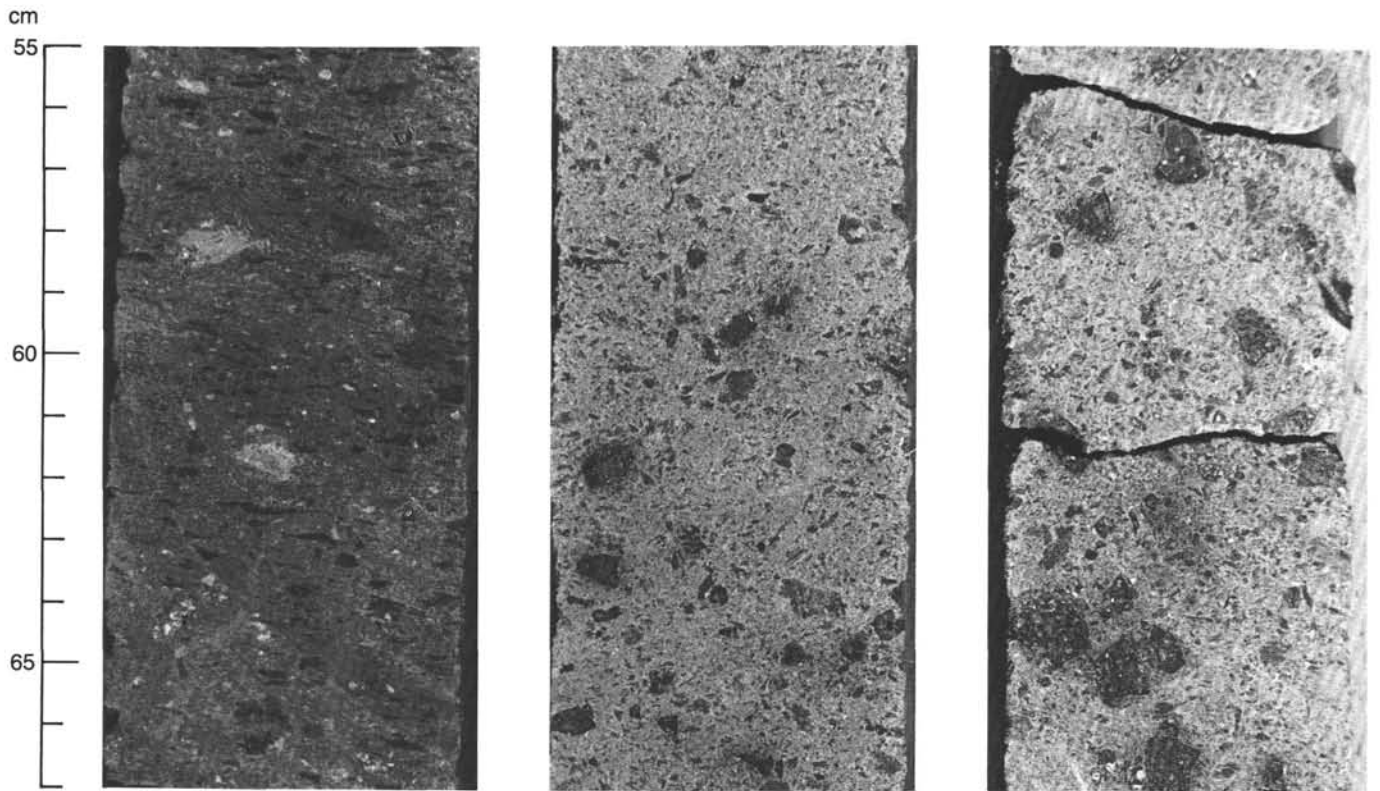


Figure 28. Core photographs of ignimbrite flow unit S48. Three sections represent (from right to left) the basal, middle, and upper portion of the central massive zone of the ignimbrite.



Figure 29. Ignimbrite flow unit S48. Thin-section photomicrograph of the central massive zone (104-642E-107R-4, 70-73 cm). Note ragged pumice (upper left) and angular perlitic xenoliths (upper right and lower middle).

base of the upper series. These phases fill vesicles, fractures, and interstices and replace some primary mineral phases. Apart from those in heavily weathered and brecciated zones, most groundmass and phenocryst minerals are relatively unaltered. An exception is olivine, which has either altered to iddingsite or Mg-smectite, commonly with an Fe-hydroxide coating. Pyroxene and plagioclase are generally fresh, except in vesicular zones at flow tops and in breccia fragments near flow-unit boundaries, where marginal replacement by smectite occurs. More intense replacement of plagioclase is present between 607 and 670 mbsf at the top of lithologic Unit II.

In most flow tops, particularly those of medium-grained flows, large vesicles are lined with dark brownish-green saponite. Elsewhere in the upper series, vesicles are completely filled with saponite, grading into green, pale green or light greenish-brown, less Mg-rich saponite and dioctahedral smectites (such as beidelite or nontronite). Celadonite is confined to the upper series, and is largely restricted to vesicles in the tops of reddened fine-grained flows and in quenched boundaries of medium-grained flows. A subtype of the fine-grained flows is distinguished by the common occurrence of intense blue-green celadonite (replacing smectite?) near flow tops. This is associated with blebs of native copper in vesicles and fracture fillings, and with a distinctive pinkish to pinkish gray alteration indicating that the mesostasis has a variolitic texture.

Some vesicles with diameters exceeding 1 cm in flow centers contain a central filling of calcite, some with zeolite. Subvertical fracture sets in the upper series are filled with saponite, some with calcite centers. F67 is unusual in containing several 2- to 4-mm-wide veins, one of which is lined with celadonite. This vein also contains native copper, an unidentified metallic mineral and calcite in the center. Vesicle and vein fillings suggest the paragenesis smectite → celadonite → calcite (with or without zeolite).

Smectite forms under nonoxidative conditions at low temperatures. Bass (1976), however, reported that celadonite is formed when basalts are exposed to oxygenated, cold seawater. The apparent zonation from Mg-smectites to celadonite may therefore indicate a shift from nonoxygenated to oxygenated waters. This change from Mg-rich to Fe-rich clays may be due to increasing water/rock ratios with time. Stakes and Scheidegger (1981) report a paragenesis similar to that observed in the upper series.

Table 9. Trace element data, Site 642.^a

	Upper series		Lower series					
	45		Type B 6		Type A 8		D5 & D6 3	
Type	Fresh		Least altered		All		All	
Element	Range (ppm)	Mean (ppm)	Range (ppm)	Mean (ppm)	Range (ppm)	Mean (ppm)	Range (ppm)	Mean (ppm)
V	287-511	370	117-165	147	170-300	241	362-595	473
Cr	100-394	225	58-136	84	89-261	159	127-268	200
Co	36-55	44	7-21	13	29-67	40	50-63	55
Ni	56-146	89	5-14	11	4-16	10	58-168	95
Cu	70-343	142	8-15	12	14-30	22	63-86	71
Zn	72-138	98	100-165	125	101-156	120	111-158	127
Rb	2-8	4	59-84	76	24-80	49	2-8	5
Sr	146-300	198	102-183	138	136-198	161	65-121	98
Y	18-34	27	28-82	48	31-47	41	32-41	36
Zr	62-169	100	251-297	276	126-223	153	67-97	77
Nb	3-11	5	16-20	19	6-14	9	1-4	3
Sc	28-48	36	26-31	29	44-58	50	48-65	57

^a Data not corrected for H₂O or CO₂.

^b Data from: University of Newcastle upon Tyne, United Kingdom
Midland Earth Science Association, United Kingdom
Ruhr-University, Bochum, FRG

Table 10. Rare-earth element and Ta, Th, and Hf concentrations, Site 642.

Element	Upper series		Lower series					
	46		Type B 7		Type A 4		D5 & D6 3	
Type	Fresh		Fresh-moderate alteration		All		All	
	Range %	Mean %	Range %	Mean %	Range %	Mean %	Range %	Mean %
La	2.69-11.4	5.90	23.0-53.6	38.6	16.1-30.7	21.0	4.10-11.5	6.84
Ce	8.35-22.6	16.31	61.1-129.0	87.6	38.2-75.8	51.4	8.23-14.7	11.1
Nd	7.01-17.8	12.46	26.7-56.4	39.1	17.7-36.1	25.0	6.70-9.82	8.42
Sm	2.45-5.23	3.93	5.66-11.1	7.97	4.45-7.67	5.66	2.44-3.93	3.22
Eu	0.70-1.73	1.42	0.92-1.72	1.24	1.26-1.62	1.44	0.89-1.35	1.05
Tb	0.53-1.10	0.83	0.78-1.62	1.18	0.98-2.38	1.76	0.75-1.14	0.95
Ho	0.69-1.75	1.10	1.43-5.18	2.62	1.40-2.38	1.86	1.40-1.74	1.05
Yb	1.64-4.23	2.69	3.30-5.24	4.34	3.04-5.69	4.41	3.93-5.41	4.59
Lu	0.22-0.56	0.39	0.46-0.83	0.64	0.50-0.74	0.63	0.57-0.80	0.65
Hf	1.46-3.55	2.67	5.70-9.36	7.26	3.33-7.90	4.86	1.81-3.56	2.51
Ta	0.17-0.58	0.40	1.16-1.66	1.34	0.53-1.04	0.78	0.17-0.25	0.22
Th	0.18-0.81	0.50	12.2-16.0	13.5	4.58-8.42	5.76	1.27-1.56	1.43

Data from: University of Newcastle upon Tyne, United Kingdom
 Midland Earth Science Association, United Kingdom
 Ruhr-University, Bochum, FRG

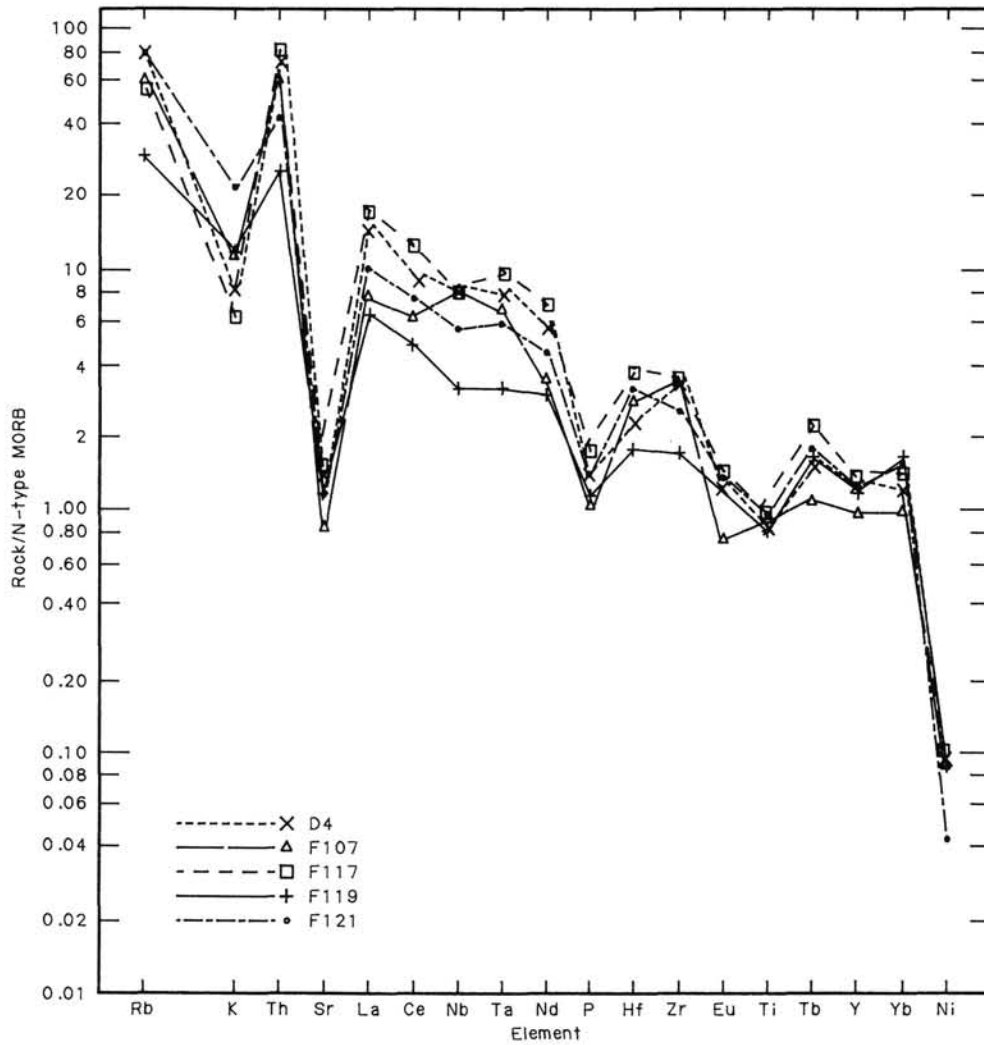


Figure 30. Representative MORB-normalized spidergrams of lower series flows.

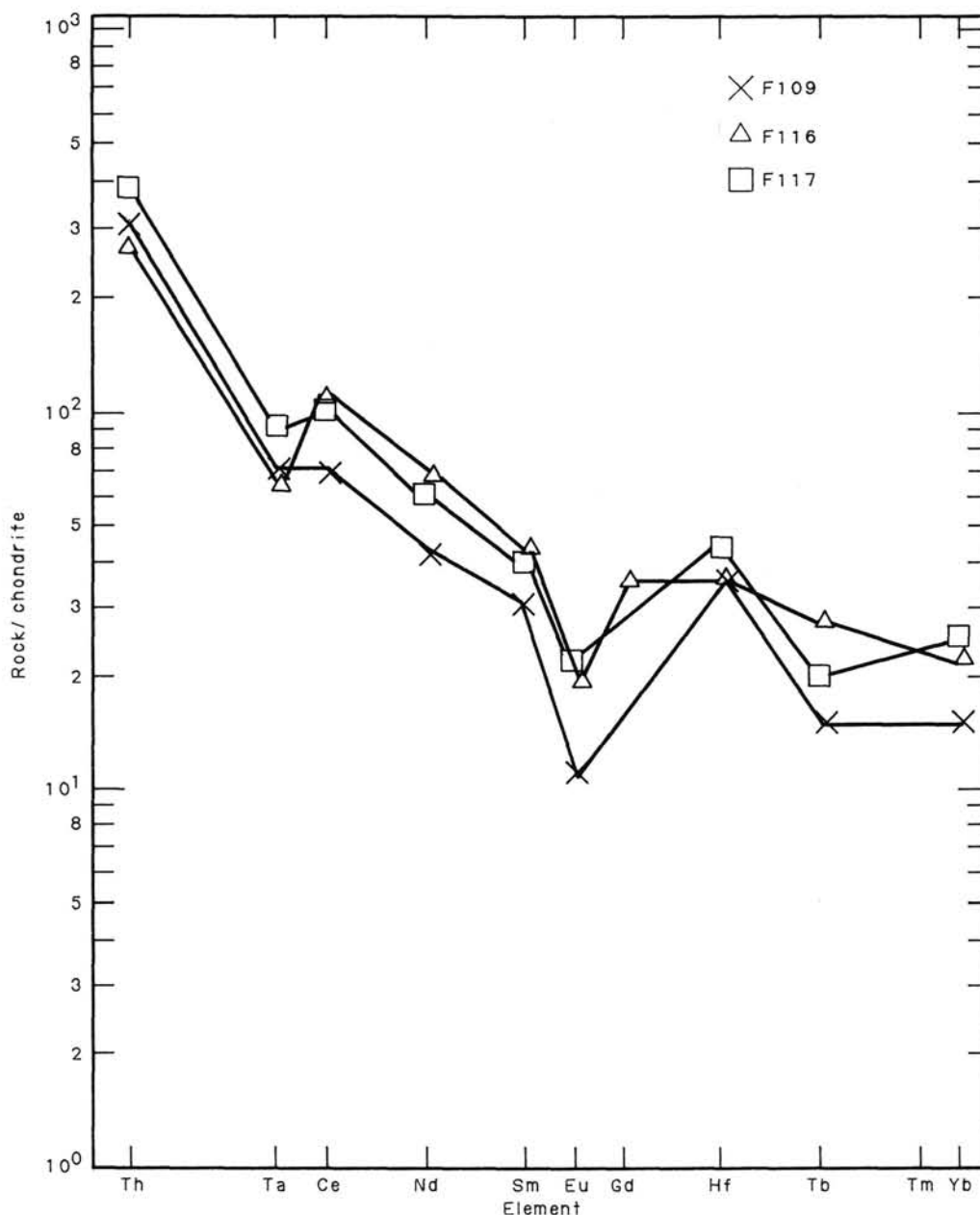


Figure 31. Representative chondrite-normalized spidergram of lower series flows.

They associate the presence of celadonite with circulating hydrothermal fluids, and late calcite infilling remaining voids marking a return to alkaline, nonoxidizing conditions.

Zeolites in the upper series are largely restricted to group III. Heulandite/clinoptilolite occurs in lithic fragments as well as in pore space in S30. Analcite and heulandite increase in abundance below 1000 mbsf.

A distinctive, late alteration assemblage first appears about 40 m above the base of the upper series, at the base of F102 (1044 mbsf). Below this point, yellow to orange-red discoloration increases downhole, impregnating the groundmass around vesicles, fractures, and glomerophytic clusters. Discoloration occurs in fronts surrounding flow pathways and is dependent upon the size of the conduit. Thus a filled vein in 104-642E-90R-01 is less than 0.2 mm wide and has a surrounding discolored zone 3 mm wide, whereas a vein over 1 mm wide in 104-642E-90R-03 has a 3-cm-wide orange-red halo. The orange-red

iron staining is locally accompanied by ankerite, by quartz in vesicles, and by the appearance of zeolites in volcanoclastic layers. One piece of basalt in 104-642E-90R-01 is distinctly bleached, possibly indicating higher alteration temperatures.

Sediment unit S43 not only marks the lithologic boundary between the upper and lower series, but also separates two types of alteration. Early, low-temperature alteration of the lower series has been overprinted by later, higher temperature effects that are variable but pervasive in effect. Whereas hydrated glass is present throughout, highly vesicular zones of F114, F115, and F116 are thoroughly leached. The leached zones are white, light gray, or light green (Fig. 32). Clots of plagioclase phenocrysts have been little affected by the bleaching event. Unbleached rock with no discoloration occurs within 20 cm of the most bleached areas. The bleached zones contain SiO₂ phases, calcite, ankerite, illite, pyrite, and zeolite groups in which clinoptilolite/heulandite dominate over phillipsite. The presence of

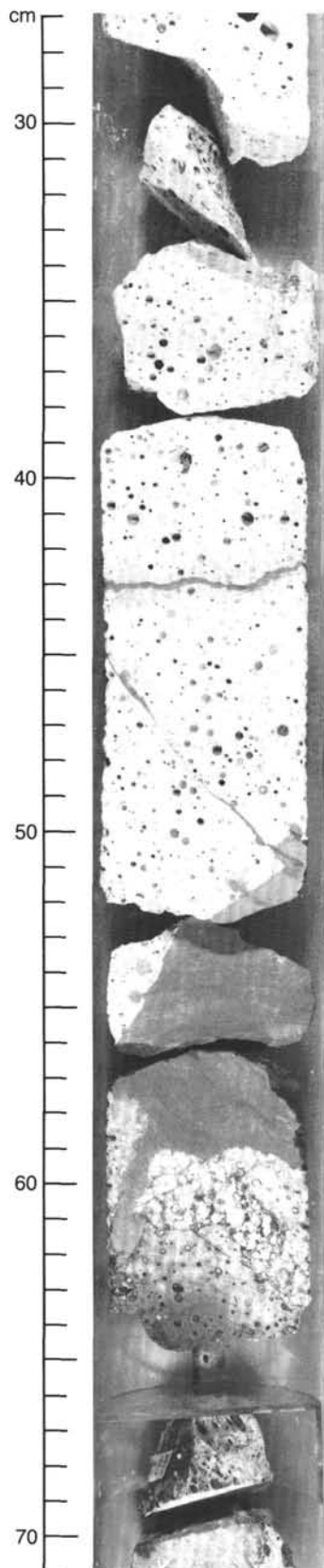


Figure 32. Photograph of Sample 104-642E-102R-2, 27-71 cm, leached zone of lower series flows F115 and F116. Vesicles are partially filled and lined with silica phase. The dense gray zone between 53 and 60 cm is volcaniclastic sediment S45.

clinoptilolite suggests fluid temperatures of 100° to 130°C. Vesicles have smectite rims and quartz cores, many including zones of opal and chalcedony (pale blue in hand specimen in Cores 104-642E-97R to 104-642E-107R). Most volcanoclastic sediments are silicified and commonly contain clinoptilolite. The hotter fluids therefore had high silica and alkali activities, and hence high pH. Clinoptilolite is most common in S45, which lies between the bleached flows F115 and F116, suggesting that the sediment layers acted as pathways for the high-temperature fluids.

Chemistry

Many of the upper series tholeiites are remarkably fresh, with even the most mobile elements (K, Rb) essentially unaffected by the low-temperature alteration phase. These "fresh" flows form about 50% of the analyzed samples, and are characterized by K_2O and Rb contents that increase from 0.06% to 0.23% and from 2 to 6 ppm, respectively, concomitant with increases in HFS element concentrations. Data from Bochum indicate that fresh flows have Fe^{3+}/Fe^{2+} ratios below 1, H_2O values below 1.5% and CO_2 below 0.25%. Fresh samples analyzed in the United Kingdom generally have loss-on-ignition (LOI) values below 0.9%. The chemical ranges and averages of upper series rocks given in Tables 8 through 10 are compiled from analyses having these characteristics.

Alteration of Leg 104 tholeiites has caused strong enrichment of K_2O , Rb, and Ba (often 5- to 10-fold), slight enrichment in Na_2O and MgO, and depletion in CaO. Na_2O values lie between 2.0% and 2.5% in fresh samples (Table 8), but reach 2.9% in altered samples. MgO values range from 7.0% to 7.9% in fresh samples, but reach 9.4% in alteration. CaO in unaltered samples ranges from 10.4% to 12.6%, whereas altered samples have CaO as low as 6.8%. With an increase in the degree of alteration, Fe^{3+}/Fe^{2+} increases, indicating oxidizing conditions. The high-temperature overprint has not caused significant chemical changes except within zones of discoloration, which are depleted in Si, Fe, and Mg and enriched in Mn, Ca, K, and H_2O .

Because of the unusual primary chemistry of lower series flows, alteration patterns are difficult to assess. However, two different alteration processes are apparent. One has caused K depletion, accompanied by Al, Ti, Ca, Na, and H_2O enrichment and loss of Si, Fe, and Mg. The other has caused K enrichment accompanied by a gain in Si and Al and depletion of Fe, Mn, Mg, and H_2O .

Pseudotachylite

The Navidrill bit failed at 329.9 mbsf while we were drilling Core 104-642D-20N. Basalt fragments recovered from the basal 8.0 cm of Core 104-642D-19N and the entire recovered section of 104-642D-20N (47 cm), have a complex series of fracture patterns and evidence of frictional melting (pseudotachylite). The only recovered material from the deeper core, 642D-20N, was 30 cm of basalt overlying 17 cm of slag-like material, which incorporated a short metallic section. The metal was identified as part of the collapsed drill bit. The extreme deformation of the basalt and the material produced during bit failure are discussed here in the context of the problems encountered during the use of the Navidrill at the base of Hole 642D, as presented in the ODP/SEDCO drilling report for Leg 104.

Core 104-642D-19N

The central, relatively unaffected, section of the two basalt fragments of Sample 104-642D-19N, 146-150 cm, consists of medium-grained, sparsely phyrlic, intersertal tholeiitic basalt, containing approximately 5% labradorite ($An_{55}-An_{60}$) phenocrysts in a groundmass of 50% labradorite (An_{55}), 23% clinopyroxene, 2% olivine, 3% oxide, and 22% tachylitic intersertal glass.

Sample Morphology and Structural Analysis

The lower face of the uppermost fragment (A, Fig. 33) is broken and can be approximately fitted to the upper broken face of piece B. The lower face of B is broken and marks the lower limit of recovery in Core 104-642D-19N. The two restored fragments together have a hyperboloid form. The long axis of the form is approximately 7 cm, and the basal radius is less than 2.4 cm.

Cataclastic features occur in zones in both hand specimen and thin section scale (Fig. 33). A thin rind of very dark-gray to black, aphanitic to glassy material, approximately 0.3 cm thick, forms the outermost upper margins of the fragments. This grades into an alternating series of gray and dark-gray aphanitic and fine-grained cataclastic material, which together total between 1.0 and 1.6 cm. The remainder of the sample, making up the central core, appears in hand-specimen scale to be relatively fresh, medium-grained gray basalt. In profile, this central core displays a series of symmetrical, nested, approximately hyperbolic fractures open to the base of the core with a maximum amplitude ranging from 3 to 7 cm (Fig. 33). Both the outermost rind of glassy material and the inner deformed zone conform to this symmetry.

The outermost deformed zone is poorly preserved and cannot be traced with certainty around the upper surface of the restored specimen. Internal fractures are in general asymptotic to the outer margins of the fragment. Fractures are filled with a uniform, dark aphanitic material and are thus readily traceable against the paler host basalt. In the two best preserved examples, the fracture tips are linked in the axial zone either by a small, single veinlike offset where the fracture-tip vertical offset (the amount by which they would miss) is <0.5 mm, or by a series of *en-echelon* tensional (?) fractures where the fracture-tip vertical offset is >0.5 mm. Figure 34 contains detailed line

drawings of these fracture-tip linkages. The two pieces of basalt themselves are separated by a surface of hyperbolic shape that may be a single fracture set.

Petrography

The area of deformation has been subdivided into a series of zones, in which A, B, and C represent relatively undeformed basalt, and P1 to P5 locate deformed zones (Fig. 35).

Zones A, B, and C are composed of medium-grained basalt, with grains averaging 0.3 mm in diameter. Grain shapes vary from granular anhedral clinopyroxenes, with radii around 0.2 mm, to prismatic laths of plagioclase approximately 0.5 mm in length.

The three areas of undeformed basalt identified in Figure 35 are separated or flanked by narrow zones, P1 to P5, of highly deformed basalt. Zones P1, P2, and P4 are similar and are described and discussed together. These three deformation zones contain porphyroclasts of plagioclase and clinopyroxene set in a black, tachylitic mesostasis (Fig. 36). The porphyroclasts range in size from 0.5 to 0.025 mm in diameter, locally constituting up to 60% of the vein fill, and averaging 40%. The clasts are approximately 55% plagioclase and 45% clinopyroxene. Pyroxene clasts are highly rounded, and few retain their original shape. The plagioclase laths and cleavage fragments are generally tabular or acicular, but may be well-rounded; even prismatic laths commonly have rounded corners. Zones P1, P2, and P4 are rectilinear and arcuate traces, but have ragged irregular margins.

These petrographic textures are identical to those identified in structurally high-level fault zones (Sibson, 1977), in which intense and localized frictional heating of rock along fractures and dislocations generates a melt-rock referred to as pseudotachylite. In the case of the sample from the base of 104-642D-19N, pseudotachylite may have formed during drilling.

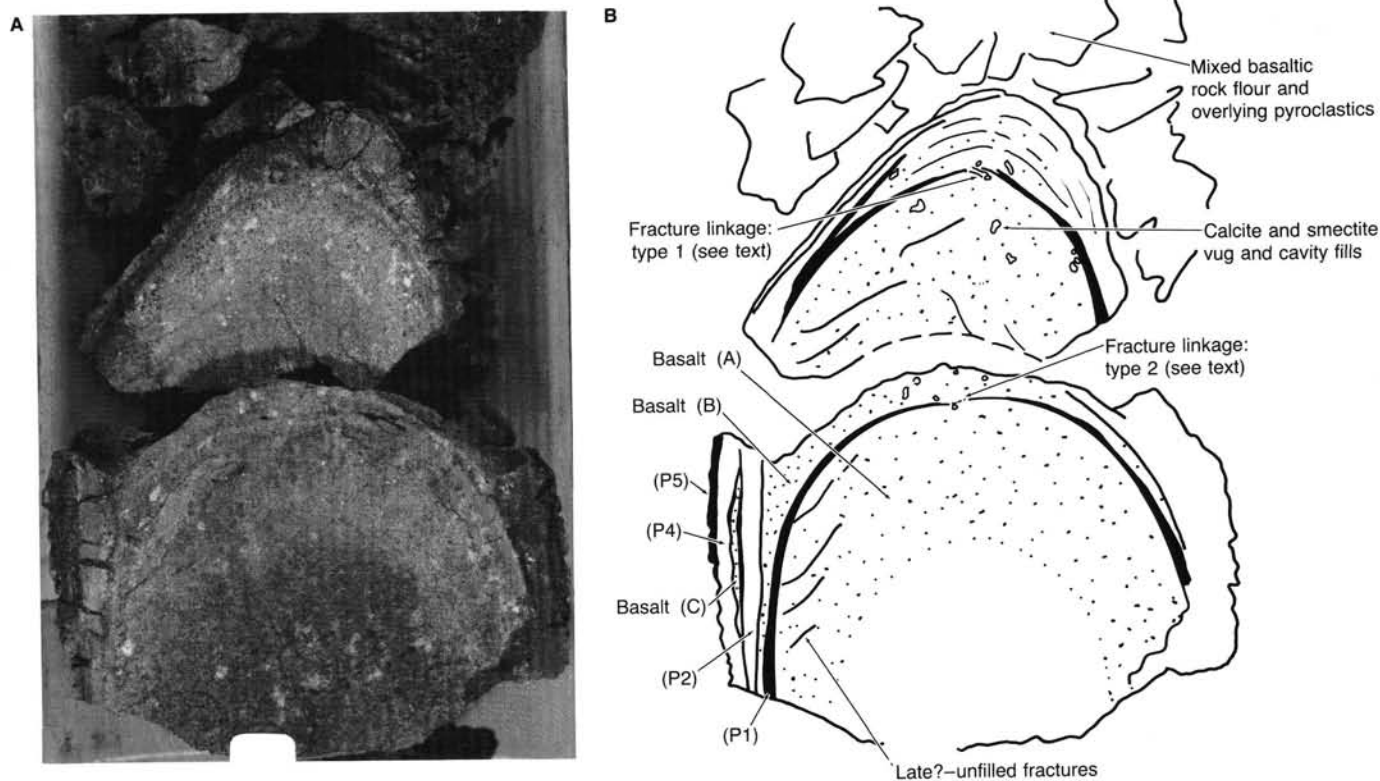


Figure 33. Close-up photograph of basal 10 cm recovered from Section 104-642D-19N-2 (A), with simplified line drawing of structure (B), Basalt fragments are at A and B. For discussion, see text.

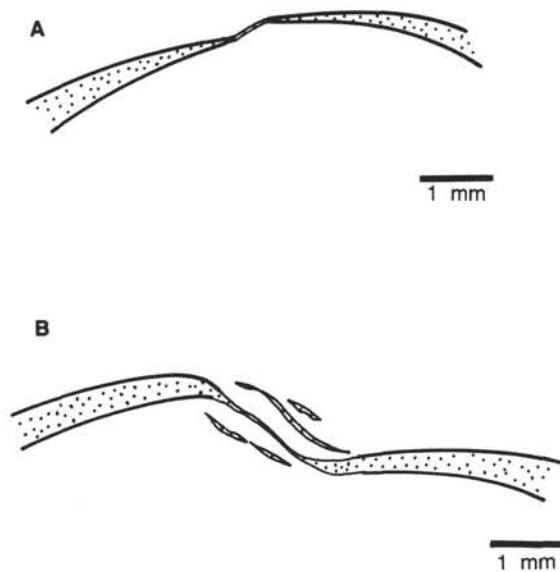


Figure 34. Styles of fracture-tip linkages. Type A, single strand; type B, multiple strand.

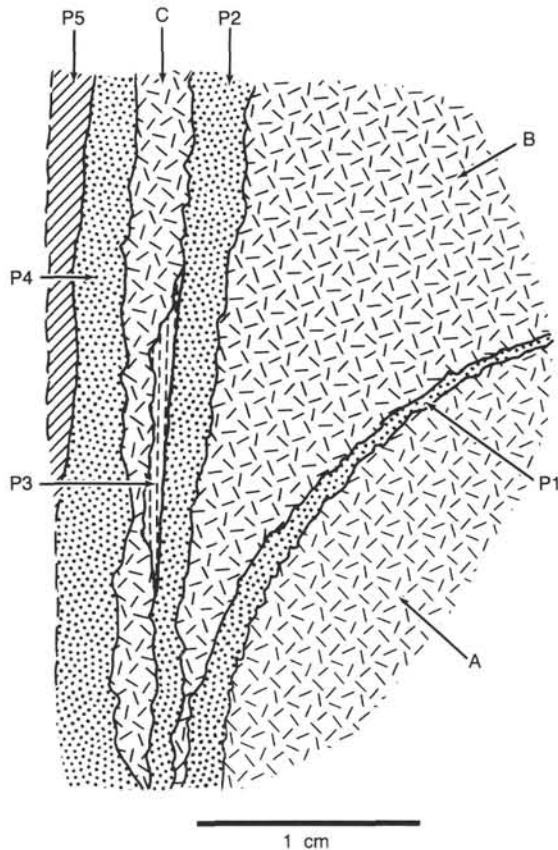


Figure 35. Schematic interpretation of thin sections prepared from Sample 104-642D-19N-2, 146-150 cm. Zones A, B, and C represent undeformed basalt; P1 through P5 are deformed zones discussed in text.

Between the outer edge of the pseudotachylite zone P2 and the outer sliver of basalt zone C, there is a narrow enclave of pseudotachylitic material (P3, Fig. 35) texturally different from the zones described above. It has a sharp rectilinear boundary with P2 and an irregular outer margin. Zone P3 has a delicate

alignment texture, in which acicular plagioclase porphyroclasts show a strong preferred orientation subparallel to the zone margin (Fig. 37). The plagioclase needles are accompanied by equant pyroxene grains set in a black isotropic matrix. This fabric is rare elsewhere in the sample. A preliminary electron microprobe study of the glassy matrix indicates a more siliceous, less calcic composition relative to that of average medium-grained flows.

The outermost zone of deformed material, P5 (Fig. 35), is composed of a dense, dark brown vitreous material, supporting porphyroclasts of subhedral to euhedral olivine as well as a number of other unidentified mineral clasts (Fig. 38). Zone P5 contains a distinctly vesicular zone in which unfilled vesicles are highly attenuated parallel to the sharp outer boundary of the pseudotachylite (Fig. 39). At the outermost preserved portion of zone P5, a clear quenched zone has fine frond-like or feathery textures. This material was melted, was rapidly chilled, and has resulted in a sideromelane-like material.

Scanning Electron Microscope Studies

The SEM investigation of these samples revealed the details of the pseudotachylite zones. Zone margins are highly irregular (Fig. 40B). Owing to different sample preparation techniques, the exact location of the specimen relative to the thin sections described above is uncertain, although it is likely that the field of view is comparable to one of the more irregular zone margins between A or B and P1 or P2. Figure 40B is an enlargement of the central section of Figure 40A and shows the vesicular nature of the material. The fine, flaky texture of the surface of the pseudotachylite seen in Figure 40B may be a fracturing fabric. The central, subspherical void is an enigma. Vesicles were not recognized in any of the thin sections of the pseudotachylite.

Discussion

The origin of meltphase deformation (P5) of basalt is problematic. Despite the problems experienced during the latter stage of drilling in 104-642D-19N, the natural "stick-slip" mechanism for the geological formation of pseudotachylite, i.e., brittle failure in zones of high shear stress, is difficult to apply here. Frictional melting may have occurred during a short interval of motion following the initial jamming of the basalt core inside the bit. Jamming followed loss of drilling water pressure and occurred immediately before detachment of the core from underlying basalt.

The observed pattern of fracturing is unknown in natural rock deformation studies. The three-dimensional stress trajectory distribution in the vicinity of a cylindrical drilling bit such as the Navidrill probably is highly complex, and the fracture patterns may reflect the stress regime within the drill bit. Deformation probably occurred more than once over a very short interval of time, because the cross-cutting boundary between zones P2 and P3 indicates multiphase generation of pseudotachylite. The junction between the outermost sideromelane-like material and the adjacent pseudotachylite suggests successive phases of deformation under different conditions, possibly determined by water availability. A narrow, but regular-sided, pseudotachylite vein branches outward from P4 and crosscuts the outermost quenched zone. The sporadic branching or generation of offshoots from zones of pseudotachylite generation is a well-documented phenomenon, but here it indicates a post-"quench" event forming additional pseudotachylite.

Core 104-642D-20N

Recovery from Core 104-642D-20N, between 326.4 and 329.9 mbsf, totaled only 47.5 cm, but consisted of the following materials: 0-24 cm, solid metal; 28.5-31.0 cm, fractured, gray, sparsely phyrlic tholeiitic basalt; and 31.0-47.5 cm, black, aphanitic, scoriaceous slag-material (Fig. 41). A report of the failure and subsequent "self-coring" by the Navidrill bit is included in



Figure 36. Photomicrograph of deformation zone P1 in Fig. 35. The pseudotachylite zone cuts the host plagioclase-phyric basalt, illustrating irregular margins to fracture and random orientation of porphyroclasts. Field of view = 5.0×3.0 mm in plane-polarized light.



Figure 37. Photomicrograph of deformation zone P3, flow-textured pseudotachylite. Plagioclase porphyroclasts show strong preferred orientation. Field of view = 5.0×3.0 mm in plane-polarized light. Sample 104-642D-19N-2, 146-150 cm.

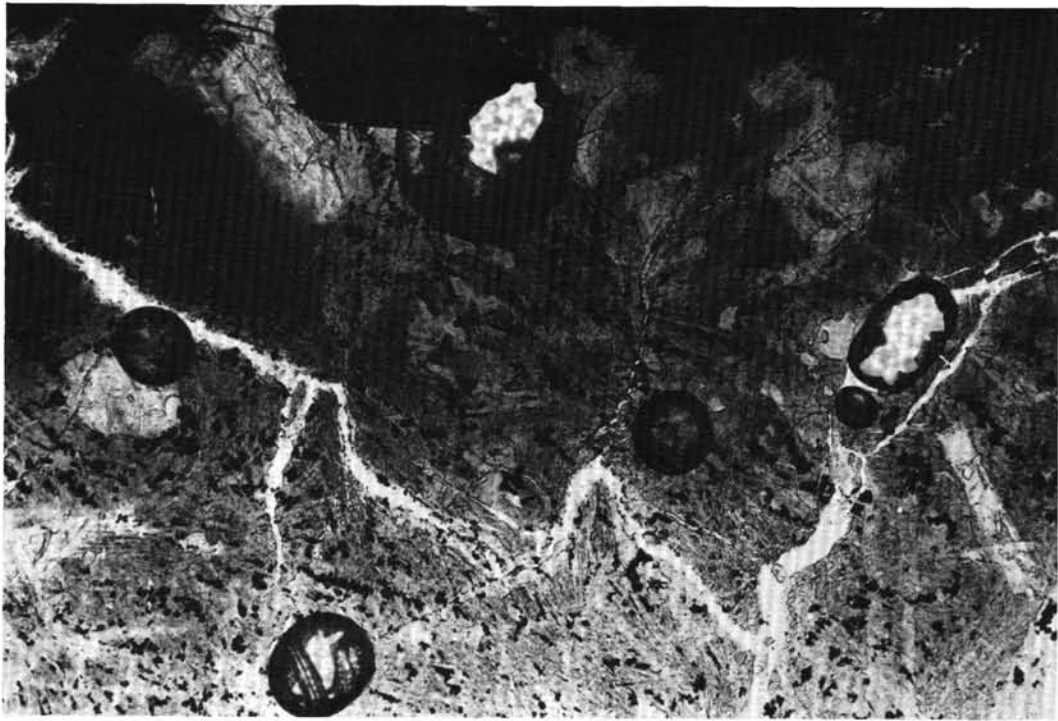


Figure 38. Photomicrograph of sideromelane in deformation zone P5. Cryptocrystalline quench texture, carrying small iron oxide grains, is evident. Slide cut by late brittle fractures. Field of view = 5.0×3.0 mm in plane-polarized light. Sample 104-642D-19N-2, 146–150 cm.

the SEDCO/ODP drilling report for ODP Leg 104, and is not referred to further. The petrographic characteristics and structural morphology of both the lowermost basalt recovered and the underlying slag is described and discussed below.

Petrographic Analysis

The basalt recovered from Core 104-642D-20N is considered to be of the same basaltic unit as that described above for the base of Core 104-642D-19N. However, the basalt is lighter colored and has a distinctly yellowish tinge in its lower part.

The most striking feature of the slag is that the vesicularity ranges from moderately vesicular (2%–10% vesicles) to highly vesicular (>20%). The vesicles are all open and generally sub-round. Irregular cavities, possibly resulting from the coalescence of two or more vesicles, are common.

The groundmass of the slag is composed of a dark tachylitic matrix, which under highest magnification can be seen to support fine microbreccia (Fig. 42). Abundant porphyroblasts of clinopyroxene and plagioclase are present throughout, composing up to 15% of the rock. They are either clearly fragmentary, having either fractured jagged grain margins or subangular, equant grains. Vesicles range from <5% to >60%. In the central part of the basal recovered material, the scoriaceous texture is so well developed that the sample has almost disintegrated.

Zonation, based on vesicle concentration, is regular and relates to a system of hyperboloids, probably reflecting a stress regime within the drill bit. The slag is subdivided into four zones based on vesicle concentration and fracture morphology (Fig. 41):

Zone A is sparsely vesicular, with the greatest concentration of cavities at the margins. The upper and lower surfaces of zone A are convex upward. The upper contact with the basalt is non-vesicular, black pseudotachylite, approximately 2 mm thick, and possibly the result of multiple periods of cataclastic deformation.

Zone B forms the outer section of the slag, tapering toward the base of the recovered pieces. It contains 2% to 10% uniformly small vesicles throughout, not exceeding 0.4 mm in diameter. Toward its base, between 40 and 45 cm, zone B becomes more fractured and has approximately subhorizontal, slightly concave-upward partings.

Zones C and D make up the core of the slag material. They are vesicular to highly vesicular and are subdivided into an upper zone C and lower zone D, separated by a zone of fractures, vesicle attenuation, and flattening. Zone C commonly contains subrounded vesicles up to 1 mm in diameter, and a few large cavities, up to 5 mm in diameter. Zone D is the most intensively vesicular, scoriaceous section of the slag and has some stretched vesicles at its margins with B and C. It is generally characterized by large open vesicles or vesicle clusters.

Discussion

The petrographic evidence for the origin of the pseudotachylitic material recovered from the base of Core 104-642D-20N is inconclusive. Gross morphological features of the rock such as vesicle development, entrainment, and coalescence—all features familiar in the generation of industrial slag during smelting ore—indicate melting during deformation. In contrast to the short-lived period of pseudotachylite formation envisaged for the cataclastic rock recovered in 104-642D-19N, however, the material recovered from 104-642D-20N was probably generated during prolonged frictional heating caused by the continuation of drilling following bit collapse.

Summary and Conclusions

In the volcanic section at Site 642 (327 to 1229 mbsf) we have identified 137 lava flows, 59 volcanoclastic sediment units, and seven units that may be dikes. The sequence is divided into an upper and a lower series that are texturally, structurally, mineral-

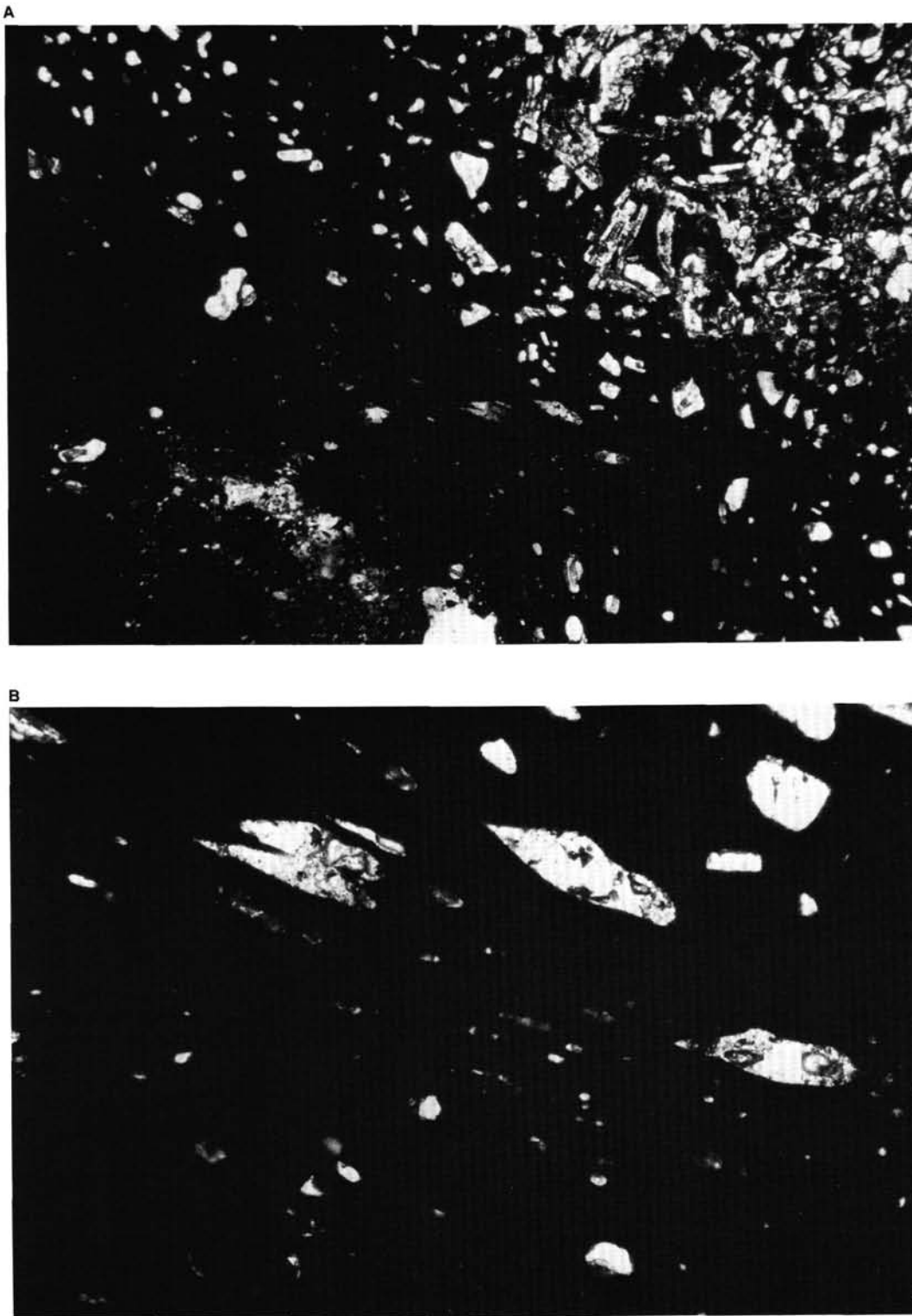


Figure 39. Photomicrograph of flow-textured pseudotachylite in deformation zone P4. (A) shows host basalt and junction with deformation zone. (B) is enlargement of central zone of (A). Field of view = 1.25×0.75 mm, in plane-polarized light. Sample 104-642D-19N-2, 146-150 cm.

ogically, and chemically distinct. The entire section was deposited in a terrestrial environment. The upper series is separated from the lower series by a 7-m-thick sequence of volcanoclastic and minor quartz- and mica-rich epiclastic sandy mudstones.

The upper series corresponds to the seaward-dipping seismic reflector sequence observed in reflection profiles through the

outer Vøring Plateau. This series is approximately 760 m thick (326 to 1087 mbsf) and consists of 120 aphyric to moderately plagioclase-, olivine- and, rarely, clinopyroxene-phyric lava flows with N-type MORB composition; $(La/Sm)_N$ falls between 0.54 and 0.97. The upper series volcanics have affinities to other Paleogene plateau basalts in the northeast Atlantic area, particu-

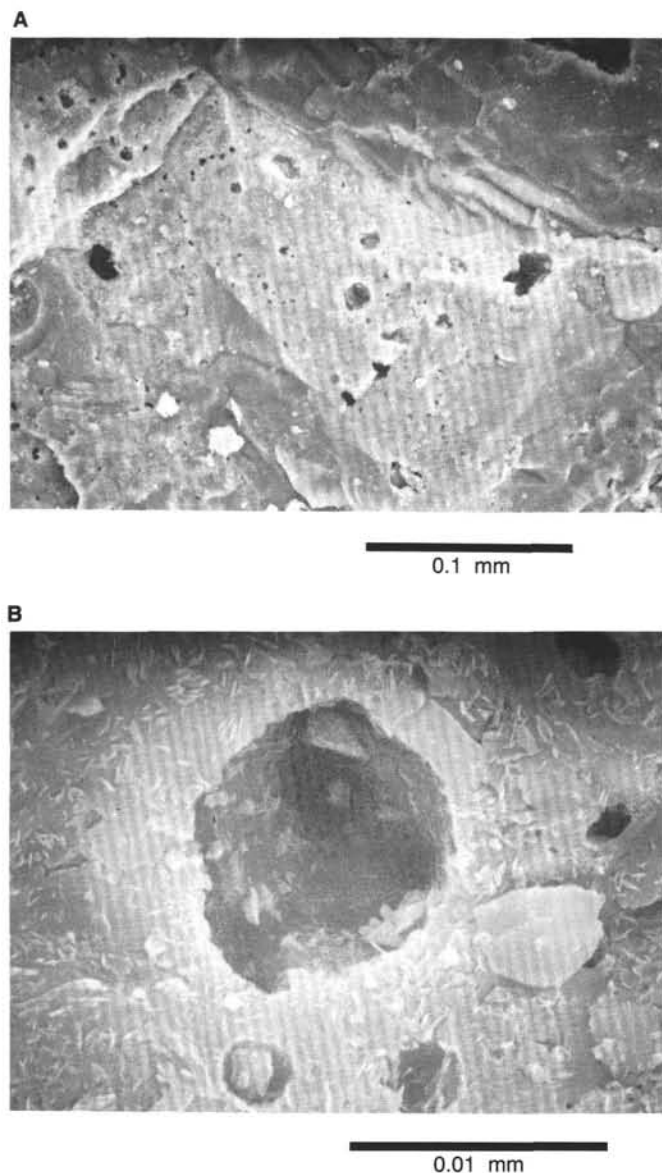


Figure 40. Scanning-electron micrographs of pseudotachylite-filled deformation zone P1. Photograph (A): Vein contacts with host crystalline basalt, magnification = $\times 345$. Photograph (B): Detail of (?) vesicular texture and "flaky" fracture surface, magnification = $\times 3080$. Sample 104-642D-19N-2, 146–150 cm.

larly those of East Greenland and the Faeroe Islands, and are also comparable with Mid-Atlantic Ridge basalts from the Reykjanes Ridge. The magmas were derived from a uniform, slightly depleted mantle source. Differences in absolute high field strength element contents resulted from different degrees of partial melting. The magmas have undergone uniform degrees of differentiation by fractionation of olivine, chromite, clinopyroxene, and plagioclase prior to eruption. Selective enrichment of Th occurs in a number of flows. This is accompanied by higher initial $^{87}\text{Sr}/^{86}\text{Sr}$ ratios and may indicate minor amounts of continental crustal contamination.

Both fine- and medium-grained flows occur in the upper series. These flows differ in granularity, crystallinity, internal flow fabric, physical properties, and average thickness but are indistinguishable chemically. The textural differences between fine- and medium-grained flows are believed to reflect variations in

distance from the vent, the medium-grained flows being proximal and the fine-grained flows being distal.

Fifty-three interlayered volcanoclastic sediments make up about 4% of the upper series and are dominantly basaltic vitric tuffs. Pumiceous lapilli are rare and occur mostly in the upper half of the series, where volcanoclastic units also tend to be thicker. The pyroclasts are derived from at least two different sources. Many are explosive or hydroclastic equivalents of the lavas they are interbedded with, but chemical analyses show that tuffs in groups I and II of the upper series represent products of explosive volcanism unrelated to the lavas at Site 642. These tuffs compositionally resemble ferrobasaltic magmas, similar to those of Iceland and the southern Mohns Ridge, derived from a LIL-element-enriched mantle source. Saponite is the most common alteration product in the upper series; minor celadonite, beidelite, nontronite, and calcite also occur as vesicle and vein fills. Olivine is completely replaced throughout the series, but clinopyroxene and plagioclase are generally fresh, with only minor replacement by saponite and, rarely, zeolite.

Approximately 140 m of the lower series was drilled below 1087 mbsf. Flows are glassy, variolitic, or microcrystalline. Two magma types are present, one derived by partial fusion of continental crust of probable sedimentary or metasedimentary origin, and the other resulting from heavy contamination of MORB tholeiites of upper series type by crustal melt. The former generated the peraluminous andesites in the upper part of the lower series, whereas the latter formed the more basaltic lower part of the lower series. Four units, possibly dikes, constitute about 35% of the lower series. Two of these (D4 and D7) are chemically comparable with their bounding flows, and are probably thick flow units of higher crystallinity. The other two dikes (D5 and D6) are tholeiitic, but of more depleted character than upper series basalts. Trace-element and isotope data indicate crustal contamination in these latter dikes.

Volcanoclastic sediments constitute about 29% of the lower series and contain significant quantities of quartz and mica of continental origin. A few fragments of leucocratic gneiss and quartz-mica schist occur in the lowest sediment unit cored (S49) and in a well-sorted tuff in the upper zone of an ignimbrite unit (S48). The xenolith assemblage of the ignimbrite is dominated by perlitic to microcrystalline fragments, which resemble lower series lavas. This may indicate extensive volcanism of lower series type in the vicinity of Site 642 prior to this explosive eruption.

The secondary mineral assemblage (Fe-saponite, opal, and chalcedony; quartz-filling vesicles, clinoptilolite replacing shards) indicates that the lower series has been hydrothermally altered by alkaline fluids with high Si activity at temperatures of about 100° to 130°C . This higher temperature alteration event also affected the lower 40 m of the upper series along smectite-ankerite filled veins.

BIOSTRATIGRAPHY

Introduction

Site 642 is the first of three sites to be drilled during Leg 104 of the *JOIDES Resolution* cruises. Five holes were drilled or cored (Holes 642A, 642B, 642C, 642D, and 642E) at this location on the outer Vøring Plateau. Described here are the micropaleontologic studies of the recovered sequence, which consists of Neogene and Quaternary hemipelagic sediments and an interbedded volcanoclastic sediment basalt.

Paleomagnetic-biostratigraphic correlations at Leg 73 sites and other sites (e.g., Leg 82, Sites 558 and 563) provide an important means of correlation for Norwegian Sea sediments. Although many of the Norwegian Sea calcareous and siliceous microfossil species are absent from these and other low- to middle-

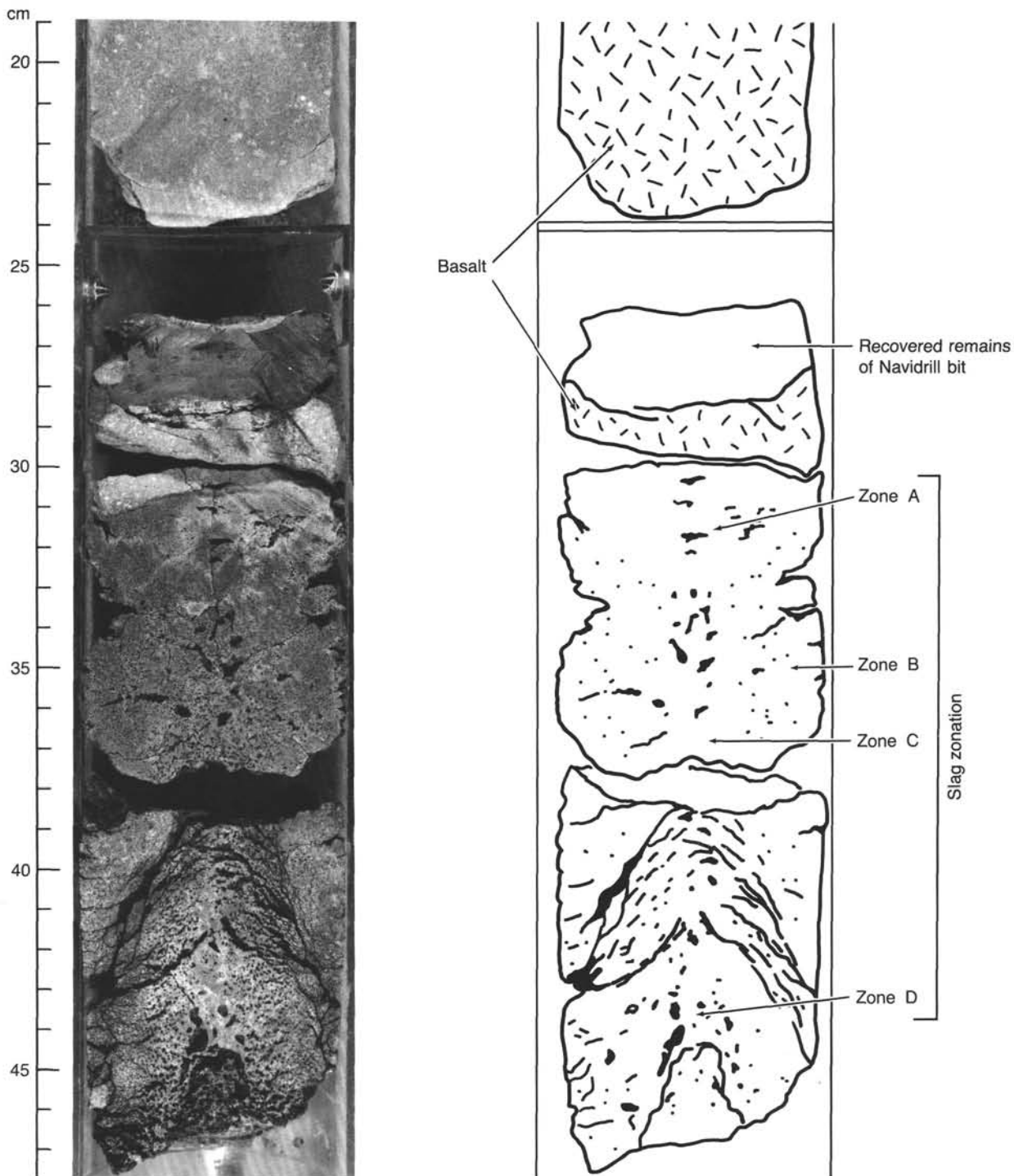


Figure 41. Close-up of the lowest recovery from Section 104-642D-20N-1. For description and discussion of core, see text.

latitude reference sites, biostratigraphic age estimates may be made by second-order correlation to sites where standard zonal species and Norwegian Sea species co-occur.

Difficulties with biostratigraphic age interpretations of the Norwegian Sea sediments have been the result of a combination of the following factors: (1) standard planktonic foraminiferal zones could not be directly applied, (2) few standard calcareous nannofossil markers are present, (3) standard low-latitude radiolarian zones are unrecognizable because of dominance of en-

demid species, (4) diatom zones could only be correlated to a small number of sections in the North Pacific or equatorial Pacific and were largely uncorrelated to paleomagnetic stratigraphy, (5) an applicable standard dinocyst-zonation was absent, and (6) carbonate microfossils were absent or poorly preserved.

Previous studies of Leg 38 holes from the Norwegian-Greenland Sea (Talwani, Udintsev, et al., 1976) found that "apart from the calcareous nannofossils and the silicoflagellates, standard zonal schemes could not be applied to this high-latitude re-

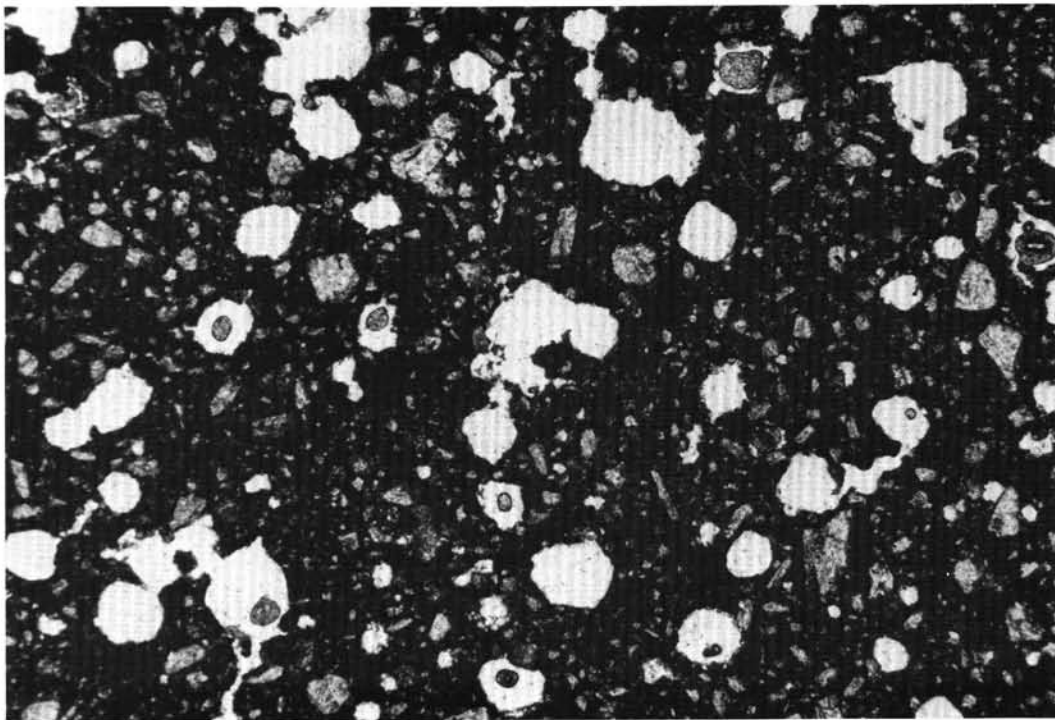


Figure 42. Photomicrograph of vesicular slag recovered from the base of Section 104-642D-20N-1. Fragments of clinopyroxene and plagioclase are set in a tachylitic matrix. Field of view = 5.0×3.0 mm, in plane-polarized light.

gion, and empirical local zonations were established for the different groups of fossils" (Schrader et al., 1976). The biostratigraphic interpretation of ODP Leg 104 sedimentary sequences must face some of the same problems encountered in Leg 38 studies. Unlike its predecessor leg in the Norwegian Sea, Leg 104 has recovered undisturbed HPC cores, which provide a late Miocene-Quaternary paleomagnetic record ("Paleomagnetism" section, this chapter). Pre-upper Miocene sediments of Site 642 cores have been demagnetized to reduce overprinting, but these records unfortunately do not appear to be adequate for biostratigraphic interpretation of polarity chrons and some sub-chrons. Utilizing the Site 642 paleomagnetic polarity record and new (post-Leg 38) diatom biostratigraphic data, we have employed the following strategy for developing an integrated biostratigraphic-magnetostratigraphic framework for all microfossil groups. Our procedure has been as follows:

1. Independently establish the biostratigraphic ranges of microfossil groups at Site 642.

2. Independently correlate Site 642 sediments with the standard paleomagnetic time scale utilizing only microfossil datums which have been correlated directly to magnetostratigraphy, dated by radiometric means, or, in a few cases, correlated indirectly with magnetostratigraphy. Most datums used to tie Site 642 to the paleomagnetic time scale are silicoflagellate or diatom events.

3. Use the biostratigraphic datums with direct or indirect paleomagnetic control to constrain interpretations of the paleomagnetic polarity reversal chronology established by shipboard paleomagnetists. Principal biostratigraphic datums used to interpret the polarity reversal sequence are given in the "Biostratigraphic Synthesis" (this section) along with their age. Datums are identified as being either directly or indirectly correlated with magnetostratigraphy and the literature source of the citation is given.

Diatom Stratigraphy

Methods

All core-catcher samples were examined for their diatom content from Holes 642B, 642C, and 642D. Because of time constraints, only selected tuff units were examined from Hole 642E. Two slides were prepared from each core-catcher sample, one from the untreated whole fraction and the other from the chemically treated $>45\text{-}\mu\text{m}$ fraction. To provide stratigraphic continuity in this discussion of the stratigraphy of Holes 642B through 642D, these holes are treated as a composite section. Zonal boundaries and datum levels are identified by hole and core number.

Results: Holes 642A, 642B, 642C, and 642D

Biostratigraphic Zones

Barren Interval Zone

Definition: The glacial lithologic Unit I, which is barren of diatoms in core-catcher samples.

Interval: $\sim 4.8\text{--}\sim 62$ m; top in Sample 104-642C-1H, CC, base between Samples 104-642C-8H, CC and 104-642C-9H, CC.

Age: Holocene to \sim the Matuyama-Gauss boundary.

Comments: Core catchers from this interval are barren of diatoms. Post-cruise examination of this interval is expected to result in the observation of some diatoms from within interglacial intervals which apparently were missed in the recovered core catchers.

Correlations: Ages assigned to this interval by other microfossil groups (see "Biostratigraphic Synthesis," this section) and the paleomagnetic record of Hole 642C suggest that this barren interval is correlative to the following diatom zones: the *Thalassiosira oestrupii* Zone, *Rhizosolenia barboi* Zone, and upper

Thalassiosira kryophila Zone of Schrader and Fenner (1976); the *Pseudoenotia doliolus* and *Nitzschia marina* Zones recognized from the Rockall Plateau by Baldauf (1984); and NNPD Zones 8–12.

Nitzschia jouseae Zone

Definition: Top. Last appearance datum (LAD) of *Nitzschia jouseae*, Baldauf (1984).

Base. LAD of *N. cylindrica*, this report.

Interval: ~62–79 m; top from between Sample 104-642C-8H, CC and 104-642C-9H, CC, base from between Sample 642B-9H, CC and 642C-11H, CC.

Age: ~4.3–2.6 Ma, early-middle Pliocene.

Correlations: Although the LAD of *Nitzschia jouseae* occurs directly below the glacial sequence, its last occurrence is judged to represent the approximate end of its range. Baldauf (1984) and Burckle and Trainer (1979) directly correlated its LAD to approximately one third of the way between the Kaena Event and the Gauss/Matuyama Epoch boundary (~2.6 Ma), similar to its relative position to the paleomagnetic record of Hole 642C.

Baldauf (1984) defines the base of this zone by the first appearance datum (FAD) of *Nitzschia jouseae*. The LAD of *N. cylindrica* is substituted here because of its more frequent occurrence. The later species has its LAD directly above the FAD of *N. jouseae* in Rockall Plateau sites; therefore, the zone as defined here is roughly equivalent with the *N. jouseae* Zone of Baldauf (1984). This zone is also correlative to within the *Thalassiosira kryophila* Zone of Schrader and Fenner (1976) based upon its position above the FAD of *Thalassiosira oestrupii* and below the LAD of *Thalassiosira convexa*. Based upon Baldauf's (1984) correlation of the *Nitzschia jouseae* Zone at the Rockall Plateau to North Pacific zones, this zone is equivalent to the *Denticulopsis seminae* var. *fossilis* Zone (NNPD8) and the *D. kamtschatica* Zone, Subzone C (NNPD7), both, Barron (1985b). No direct correlation of this interval at Site 642 to North Pacific zones is possible.

The age of the LAD of *Nitzschia cylindrica*, the base of the zone, was placed by Burckle (1978) above the Thevera Event of the Gilbert Epoch (~4.3 Ma). The paleomagnetic record of Hole 642C suggests a similar occurrence at this site.

Thalassiosira convexa Zone

Definition: Top. LAD of *Nitzschia cylindrica*, this report.

Base. FAD of *Thalassiosira convexa*, Burckle (1972).

Interval: ~79–112.5 m, top from between Samples 104-642B-9H, CC and 104-642C-11H, CC, base from between Samples 104-642B-13H, CC and 104-642C-14H, CC.

Age: ~6.2–4.3 Ma, late Miocene–early Pliocene.

Correlations: Burckle (1972) correlated the base of this zone directly to upper Chron C-3A-R2 and assigned an age ~6.2 Ma. These findings agree with Baldauf's (1984) conclusion that the FAD of *Thalassiosira convexa* is isochronous with its initial appearance in the equatorial Pacific (Burckle, 1972).

Since the LAD of *Nitzschia cylindrica* is approximately equivalent to the FAD of *N. jouseae* (see discussion of previous zone), the *Thalassiosira convexa* Zone is correlative with the *T. convexa* Zone as defined by Baldauf (1984) from Rockall Plateau sites. The FAD of *T. oestrupii*, between 85.4 and 82.5 m (5.1 Ma), is one of three datums used by Schrader and Fenner (1976) to define the base of their *T. kryophila* Zone; therefore, this level is tentatively correlated to the base of their Norwegian Sea zone. The boundary between the North Pacific *Denticulopsis hustedtii* Zone (NNPD6) and the *D. kamtschatica* Zone (NNPD7) cannot be recognized because of the absence of *D. kamtschatica*. Barron (1981) used the FAD of *Nitzschia rein-*

holdii as a substitute for this boundary in the middle latitude North Pacific. At Site 642 the FAD of *N. reinholdii* occurs between 95 and 92 m, thus the NNPD7/NNPD6 boundary is correlated to within the *Thalassiosira convexa* Zone of this site. The Subzone A/B boundary of the *Denticulopsis kamtschatica* Zone (NNPD7) by the FAD of *Thalassiosira oestrupii* (secondary marker); therefore, this boundary is correlative to the base of Schrader and Fenner's (1976) *T. kryophila* Zone as stated above.

Useful datums within this zone include the LAD of *Mesocena diodon* (82.5–75.9 m, 4.4 Ma), the FAD of *Thalassiosira oestrupii* (85.4–82.5 m, 5.1 Ma), the LAD of *Nitzschia miocenica* (92.0–85.4m, 5.55 Ma), and the FAD of *N. reinholdii* (95.0–92.0 m, 5.6 Ma).

Nitzschia porteri–*N. miocenica* Interval

Definition: Top. FAD of *Thalassiosira convexa* and *T. miocenica*, Burckle (1972).

Base. LAD of *Coscinodiscus yabei*, Burckle (1972).

Interval: ~112.5–~133 m, top from between Samples 104-642B-13H, CC and 104-642C-14H, CC and base between Sample 104-642C-16H, CC and Section 104-642C-17H-2.

Age: ~6.2–7.4 Ma, late Miocene.

Correlations: The *Nitzschia porteri* and the *N. miocenica* Zones of Burckle (1972, 1977) are combined here and designated as the *N. porteri*–*N. miocenica* Interval, following the practice of Baldauf (1984). This interval correlates with the upper portion of Subzone B of the *Denticulopsis hustedtii* Zone (NNPD6) of Barron (1980) and encompasses the lower *Coscinodiscus marginatus* Zone and a portion of the *Denticulopsis hustedtii* Zone of Schrader and Fenner (1976). The LAD of *D. hustedtii*, the base of their *Coscinodiscus marginatus* Zone, occurs between Samples 104-642B-15H, CC and 104-642B-14H, CC (128.1–123.5 m).

Denticulopsis hustedtii–*D. lauta* Zone

Definition: Top. The LAD of *D. dimorpha*.

Base. The evolutionary transition of *D. hyalina* to *D. hustedtii*.

Author: Koizumi (1973); emended by Barron (1980) and Barron and Keller (1983).

Interval: ~133–173 m; top between Sample 104-642C-16H, CC and Section 104-642C-17H-2 and base between Samples 104-642C-21H, CC and 104-642C-20H, CC.

Age: ~12.4–14.0 to 13.9 Ma.

Correlation: According to Barron (1980), the FAD of the *Coscinodiscus plicatus* group occurs in uppermost Subzone A of this zone. At Site 642 this datum occurs between Samples 104-642C-19H, CC and 104-642B-19H, CC (167.4–158.5 m). The FAD of *Denticulopsis praedimorpha*, which defines the Subzone A/B boundary, occurs slightly higher in the section, between Samples 104-642C-18H, CC and 104-642B-18H, CC (157.7–149 m).

An unconformity is suggested at approximately 133 m in Hole 642C and Hole 642B on the basis of the presence of five diatom datums within this interval, ranging in age from 11.2 to 8.7 Ma (see "Biostratigraphic Synthesis," this section).

The diatom assemblage below these levels is assigned to the lower Subzone C to Subzone B based upon the joint occurrence of *Coscinodiscus yabei*, the *C. plicatus* group, *Actinocyclus ingens*, *Denticulopsis hyalina*, *D. lauta*, and *D. praedimorpha*. None of these species is found above the inferred unconformity. Assemblages above and below the unconformity indicate that the missing section includes a portion of Subzone C and all of Subzone D of the *Denticulopsis hustedtii*–*D. lauta* Zone, as well as a portion of Subzone A of the *Denticulopsis hustedtii* Zone.

Denticulopsis lauta Zone (NNPD4)

Definition: Top. The evolutionary transition of *D. hyalina* to *D. lauta* s.s. (i.e., the first consistent dominance of *D. hustedtii* over *D. lauta*).

Base. The FAD of *D. lauta*.

Author: Koizumi (1973) and Barron (1980); amended by Barron and Keller (1983).

Interval: ~189–173 m, top between Samples 104-642C-21H, CC and 104-642C-20H, CC, base between Samples 104-642C-23H, CC and 104-642B-21H, CC.

Age: ~16.1–14.0 to 13.9 Ma, middle Miocene.

Correlations: This zone appears to be isochronous throughout all middle- to high-latitude regions of the Northern and Southern hemispheres (Barron, 1985a; Ciesielski, 1985). Barron (1981) indirectly correlated this zone to extend from within paleomagnetic Chron C-5A-N6 to lowermost Chron C-5B. The base of the *D. lauta* Zone closely approximates the early/middle Miocene boundary (Barron, 1980; Barron, 1981). The FAD of *D. hyalina*, between 184.3 and 177.5 m, defines the boundary between Subzones A and B (~15.0 Ma). Confident correlations with Schrader and Fenner's (1976) Norwegian Sea diatom zonation are not possible for reasons stated in the introduction. It appears that the *D. lauta* Zone probably extends from the upper portion of their *D. hyalina* Zone to within their upper *Rhizosolenia bulbosa* Zone.

Actinocyclus ingens Zone

Definition: Top. FAD of *Denticulopsis lauta*, Barron, 1980.

Base. FAD of *Actinocyclus ingens*, Barron, 1980.

Interval: ~189–207 m, top between Samples 104-642C-23H, CC and 104-642B-21H, CC, base between Samples 104-642D-3X, CC and 104-642C-23H, CC.

Age: ~16.8–16.1 Ma, late early Miocene.

Correlations: Barron's (1981) indirect correlation of this zone to paleomagnetic stratigraphy has the boundaries correlated to lowermost Chron C-5B and lower Chron C-5C-R2. Baldauf (1984) tentatively correlated the *Actinocyclus ingens* Zone to within the *Thalassiosira fraga* Zone of Schrader and Fenner (1976). Some of the nine datums used by Schrader and Fenner (1976) to define the top of their *T. fraga* Zone occur within the *Actinocyclus* Zone while others occur within the *T. spinosa* Zone of Site 642. Their use of multiple datums prevents direct correlation to Site 642; however, assemblage characteristics suggest that most or all of the *Actinocyclus ingens* Zone is correlative to their *Rhizosolenia bulbosa* Zone.

Thalassiosira fraga Zone

Definition: Top. FAD of *Actinocyclus ingens*.

Base. FAD of *Thalassiosira fraga*.

Author: Schrader and Fenner (1976); modified by Barron, 1985a.

Interval: ~207–263 m, top from between Samples 104-642D-3X, CC and 104-642C-23H, CC, base from between Samples 104-642D-9X, CC and 104-642D-8X, CC.

Age: ~19.9–16.8 Ma, early Miocene.

Correlations: Barron (1985a) recently proposed this zone on the basis of Schrader and Fenner's (1976) study of Norwegian Sea diatoms and examination of U.S. Geological Survey dredge material. He correlated these zones with the geologic time scale on the basis of the range of *T. fraga* in tropical Pacific sediments and concluded that the range of *T. fraga* exhibits little diachroneity between high and low latitudes. The FAD of *T. fraga* is assigned an age of ~19.9 Ma by secondary correlation of this datum to standard calcareous microfossil zonations (Barron, 1985b).

Utilizing the FAD of *T. fraga* as a basis of correlation with the Norwegian Sea zonation of Schrader and Fenner (1976), this

zone is estimated to encompass the following zones of these authors: the *T. fraga* Zone, *Nitzschia maleinterpretaria* Zone, *Coscinodiscus vigilans* Zone, *Rhizosolenia norvegica* Zone, *Synedra jouseae* Zone, and upper *Pseudodimerogramma elegans* Zone.

Thalassiosira spinosa Zone (NNPD2)

Definition: Top. FAD *Thalassiosira fraga*.

Base. FAD *T. spinosa*.

Author: Schrader and Fenner (1976), modified by Barron (1985a).

Interval: ~263–276.8 m, top between Samples 104-642D-9X, CC and 104-642D-8X, CC, base at 104-642D-10X, CC.

Age: ~21.5 (not the true base)–19.9 Ma.

Correlations: This is a tentative zone established by Barron (1985a), as no complete zonal sequence has been recovered from the North Pacific. The zone was established partially by comparison of Norwegian Sea sequences recorded by Schrader and Fenner (1976) with equatorial Pacific DSDP Site 71 and Bering Sea dredge samples. Barron (1985a, 1985b) correlated the base of the zone with approximately the Oligocene/Miocene boundary (~23 Ma). At Site 642, the base of the zone occurs in Sample 104-642D-10X, CC, directly above the volcanic ash of lithologic Unit IV. Based upon other components of the diatom assemblage and the accompanying silicoflagellate assemblage (see Silicoflagellate Section), the interval between ~263 and 276.8 m represents only the upper portion of the zone.

The portion of the *Thalassiosira spinosa* Zone represented at Site 642 appears to correlate to within the *Pseudodimerogramma elegans* Zone of Schrader and Fenner (1976). Barron (1985a) correlated the *T. spinosa* Zone with the N4 and lowermost N5 foraminiferal zones. This correlation agrees with silicoflagellate correlations to calcareous nannofossil zones (this section) and the interpreted paleomagnetic stratigraphy of Site 642.

Paleoenvironment

Early Miocene (276.8–~189 m, ~21.5–16.1 Ma). Sediments of the lower Miocene of Site 642 are characterized by a much higher biogenic opal content (mean = ~50%) than younger sediments and are indicative of high primary productivity in the Norwegian Sea at this time. The type of nutrient supply that permits this large primary production is possibly related to a higher degree of nutrient and organic run-off from the continent. Although this conclusion is highly conjectural, it would appear to be supported by the high organic content of the sediments, the occurrence of terrestrial organics, and common terrestrial palynomorphs.

Lower Miocene diatom assemblages contain a large proportion of species endemic to the Norwegian Sea (Schrader and Fenner, 1976); however, many cosmopolitan species (*Thalassiosira fraga*, *T. spinosa*, *Craspedodiscus coscinodiscus*, *Actinocyclus ingens*, and others) are also present. Many of these species have been noted in the Antarctic, Atlantic, Pacific, and Indian oceans. Some species have a definite affinity for the low to middle latitudes (e.g., *Craspedodiscus coscinodiscus*). These characteristics suggest the influx of relatively warm North Atlantic surface waters to the Norwegian Sea by the Norwegian Current or a similar predecessor. Lower Miocene diatom assemblages must have had relatively open communication with Atlantic waters to the south, unimpeded by shallow sill depths. The scarcity of neritic diatoms is used to infer relatively deep water conditions, whereas neritic diatoms are much more prevalent in Eocene–Oligocene assemblages from Leg 38 sites in this same region (Schrader and Fenner, 1976).

Middle Miocene (~189–133 m, ~16.1–12.4 Ma). The middle Miocene is marked by a major reduction in the sediment accumulation rates of biogenic opal (see "Sediment Lithology" section, this chapter) (between 170 and 150 m), which is accom-

panied by a related increase in carbonate deposition. The presence of common *Thalassionema* spp. within this interval of change indicates continued high fertility and supports the reduction in biogenic opal accumulation as being related to carbonate dilution rather than to decreased siliceous productivity. A possible model for this abrupt change in sedimentation might be a rapid deepening of the carbonate compensation depth (CCD) in the Norwegian Sea in response to an increased availability of carbonate related to a change in the global basin-to-basin fractionation of carbonate.

A major change also occurred in the biogenic sediment budget of the Southern Ocean during the middle Miocene as the Antarctic Convergence rapidly migrated northward (Ciesielski et al., 1982). This migration led to the rapid replacement of mixed calcareous/siliceous sediments by siliceous sediments, changing the Southern Ocean from a major zone of carbonate accumulation to a global silica sink. The increased availability of carbonate to the global ocean system may thus be manifested in the Norwegian Sea by an abrupt deepening of the CCD, which is no more abrupt than the temporally equivalent change in the Southern Ocean noted by Ciesielski et al. (1982) and Ciesielski and Weaver (1983).

This change is preceded by a massive influx of *Denticulopsis* spp. beginning at the base of the middle Miocene and continuing to the base of the proposed middle/late Miocene unconformity. The abundance of the genus *Denticulopsis* in this interval is similar in all mid- to high-latitude regions. Sea-surface temperatures appear to have been cooler than during the early Miocene; however, the occurrence of some species with low-latitude affinities suggests warmer conditions than during most of the late Miocene-Quaternary.

Late Miocene. Some samples within this interval contain calcareous nannofossils and planktonic foraminifers but are barren of diatoms and radiolarians. Complete silica recycling is a possible explanation for these occurrences. Such recycling occurs above the sill depths of some Antarctic basins (e.g., Bransfield Strait), leaving the seafloor barren of siliceous microfossils but with surface waters having high diatom productivity (Ciesielski, unpubl. pers. obs.).

Results: Hole 642E

Introduction

The basalt sequence of Hole 642E contains a number of tuff units which range in size from <1 cm to more than 1 m. Samples have been collected from all tuff units to examine for their possible diatom content. The present report cites the results of an examination of 16 tuff units; the remainder will be studied after completion of the cruise.

Summary

Six of the examined tuff units were barren of diatoms. Barren intervals include Samples 104-642E-7R-2, 117-119 cm, 104-642E-19R-4, 139-140 cm, 104-642E-23R-1, 128-130 cm, 104-642E-25R-3, 80-85 cm, 104-642E-28R-3, 126-128 cm, and 104-642E-39R, CC.

Five additional tuff units contain only very rare (a few per slide) whole diatoms or fragmented diatoms. Sample 104-642E-2R-3, 8-9 cm, contains only a few small diatom fragments of indeterminate age. A few very rare specimens of *Stephanopyxis* spp. were found in Sample 104-642E-19R-5, 3-5 cm, which are not age diagnostic.

Four additional samples contain sparse unidentifiable diatoms or diatoms with lengthy stratigraphic ranges. Sample 104-642E-21R-1, 21-23 cm, contains tuff which is interpreted as rubble from Section 104-642E-19R-4. This sample yielded only small fragments of undetermined taxonomic affinity. Only very rare

specimens of *Stephanopyxis* spp. were found in Sample 104-642E-27R-2, 45-60 cm. A rubble sample was examined from Sample 104-642E-31R-1, 1-3 cm, which is thought to be from Section 104-642E-30R-1. This sample contains a few specimens of the resistant long-ranging species *Coscinodiscus marginatus*, some sponge spicules, one radiolarian (*Larcoidea*), and a silicoflagellate (*Mesocena circulus*, middle to late Miocene), which because of its young age is probably a lab contaminant. Examination of Sample 104-642E-33R-1, 142-143 cm, yielded only one small diatom fragment.

Sample 104-642E-35R-2, 6-7 cm, contains a diverse and moderately well preserved assemblage of diatoms and silicoflagellates. From a brief examination of this sample, 16 species were noted. Silicoflagellates are indicative of an age of middle Eocene or younger (see "Silicoflagellates," this section). A middle Eocene to early Oligocene age is suggested by the occurrence of *Melosira architecturalis*, *Pterotheca aculeifera*, *Cestodiscus* aff. *muhiinae*, *Pseudostictodiscus picus*, *Rhizosolenia praearboi*, and *Coscinodiscus argus*.

A problem with interpreting the age of the assemblage in Sample 104-642E-35R-2, 6-7 cm, is the lack of a complete middle Eocene-Oligocene section for correlation purposes. The most complete diatom-bearing sequence that covers a portion of this interval is the upper Eocene-lower Miocene of DSDP Sites 511 and 513 in the Subantarctic. Studies of these sites by Gombos and Ciesielski (1983) reveal that the LAD of *Melosira architecturalis* is only slightly higher than the Eocene/Oligocene boundary, while *Pterotheca aculeifera* is absent. In a middle Eocene section from Site 512, the same authors found both of these species. In addition, all of the distinctive Oligocene species of these South Atlantic sites are absent from Core 104-642E-35R. Silicoflagellates from this sample are no older than middle Eocene (see "Silicoflagellates," this section). Altogether these scanty data might be used to support a middle Eocene age; however, it may be more confidently stated that Core 104-642E-35R is middle to late Eocene.

Sample 104-642E-42, 113-114 cm, has a sparse assemblage of siliceous microfossils including *Coscinodiscus* spp. (few), *C. marginatus* (rare), *Asteromphalus* sp. (rare), sponge spicules, and the silicoflagellate *Mesocena oamaruensis* (rare). *M. oamaruensis* is indicative of a middle Eocene-early Oligocene age. The genus *Asteromphalus* first occurred in the early Oligocene (Gombos, 1980), although it is mentioned as "possibly" within the late Eocene by Fenner in a personal communication to Gombos (1980). Gombos and Ciesielski (1983) found the genus to be absent from middle and upper Eocene sediments recovered by Leg 71; instead, they found the first occurrence to have been in the earliest Oligocene as previously reported by Gombos (1980). If the first occurrence of the genus *Asteromphalus* was indeed in the early Oligocene, such an age for this sample would be in conflict with the preliminary age assignment previously stated for Core 104-642E-35R. Given the uncertainty for the first occurrence of this genus, the ages for the assemblages of Cores 104-642E-42R and 104-642E-55R would appear more reliable.

Diatoms and silicoflagellates in Core 104-642E-55R exhibit the best preservation and greatest diversity of all examined tuff units. Diatoms are common and include specimens with delicate ornamentation. A brief survey of this sample noted 15 species of diatoms, five species of silicoflagellates, one ebridian, and one radiolarian. Most species are known from the middle Eocene to late Oligocene except *Stictodiscus picus*, which is restricted to the middle Eocene in DSDP Hole 390A on the Blake Plateau (Gombos, 1982). A fragment of the silicoflagellate *Dictyochoa quadria* was also noted. This species ranges through most of the upper Eocene (NP17-NP20, Martini and Müller, 1976). Based upon the ranges of these two species, a late middle to early late Eocene age would appear likely.

Paleoenvironment

No inferences are made about the depositional environment of tuff units barren of siliceous microfossils (Cores 104-642E-7R, 642E-19R-4, 642E-23R, 642E-25R, 642E-28R, and 642E-39R). A proper evaluation of the depositional environments of these units must await an examination for other microfossil groups (i.e., palynomorphs) and a thorough examination of their mineralogy, petrology, and sedimentology. The depositional environment of other tuff units, containing only fragments or rare diatoms (Cores 104-642E-2R, 642E-19R-5, 642E-21R, 642E-27R, and 642E-33R-1), is equally uncertain. These units may have been deposited in a marine environment or deposited in a sub-aerial environment that received eolian or aqueously transported marine diatoms.

A higher abundance of diatoms in Sample 104-642E-21R-1, 21–23 cm, suggests autochthonous deposition in an outer neritic to pelagic environment. A similar environment is likely for Sample 104-642E-42R-1, 113–114 cm. The presence of a well preserved *Asteromphalus* species further suggests little or no post-depositional reworking. Samples 104-642E-35R-2, 6–7 cm, and 104-642E-55R-2, 80–81 cm, contain a diverse assemblage of diatoms devoid of any apparent benthic species. Assemblages in these two cores would be expected to be indicative of depths no shallower than of an outer shelf.

Silicoflagellate Stratigraphy

Methods

All core-catcher samples within Leg 104 Holes 642A through 642E were examined for their silicoflagellate content within whole-fraction smear slides and sieved (>45 μm) fractions. Because of time constraints, only the occurrences of major stratigraphic indicator species were recorded.

To provide stratigraphic continuity in this discussion of the stratigraphy of Holes 642A through 642D, these holes are treated as a single composite section. Zonal boundaries and datum levels are identified by hole and core number. All samples referenced herein are core-catcher samples, hence samples are also identified by hole and core number only.

Results, Holes 642A, 642B, 642C, and 642D

Preservation Abundance and Diversity

Beneath the upper glacial sequence (~0 to 62 m) silicoflagellates are well preserved and vary in abundance from sparse to very abundant. Abundances are highest in the lower Miocene–lower Pliocene, decrease to sparse in the middle Pliocene and are apparently absent in the glacial upper Pliocene–Quaternary. Diversity is limited to a few species in the Pliocene; however, most Miocene cores contain a moderate diversity of species representing the genera *Distephanus*, *Mesocena*, *Corbisema*, and *Naviculopsis*. Below Core 104-642D-11X, silicoflagellates are once again absent to the base of the hole.

Biostratigraphic Zones

Distephanus boliviensis Zone

Definition: Top. LAD *D. boliviensis*, Ciesielski (1975).

Base. LAD *Mesocena diodon*, this report.

Interval: ~62.1–~78.2 m; top from between Samples 104-642C-9H, CC to 104-642C-8H, CC, base from between Samples 104-642C-11H, CC to 104-642B-9H, CC.

Age: early Pliocene; 4.4–3.1 Ma.

Comments: This zone combines the *D. boliviensis*, *Dictyocha pygmaea*-*Dictyocha pumila*, and *Distephanus pseudofibula* Zones of Ciesielski (1975).

Age and correlations: The last consistent common occurrence of the name species in the Southern Ocean is 3.1 Ma at the base of the Mammoth Event (Ciesielski, 1975). Its last occurrence at Site 642 is at the base of the glacial barren zone. Therefore, the top of the zone may be unrepresented. This conclusion is supported by both shipboard paleomagnetism and diatom biostratigraphy.

The base of the zone was correlated directly with paleomagnetism in numerous Southern Ocean piston cores. The LAD of *Mesocena diodon* occurs in the Sidufjall Event of the Gilbert Epoch at 4.4 Ma (Ciesielski, 1975, 1980, 1983, 1986; Osborn et al., 1983; Ledbetter and Ciesielski, 1986; and others).

Zonal markers are cosmopolitan species and have similar datum ages at all latitudes based on indirect correlations with magnetostratigraphy through other microfossil groups.

Mesocena diodon Zone

Definition: Top. LAD of *Mesocena diodon*.

Base. Last consistent occurrence of *M. circulus*, Busen and Wise (1977).

Interval: ~117.25 m–~78.2 m; top between Samples 104-642C-11H, CC and 104-642B-9H, CC, base between Samples 104-642C-15H, CC and 104-642B-13H, CC.

Age: late Miocene to early Pliocene; 6.4–4.4 Ma.

Comments: Ciesielski (1975) based the top of the *Mesocena diodon* Zone on the first common occurrence of *Distephanus pseudofibula*, whereas in this report the top is redefined as the LAD of *Mesocena diodon*.

Age and correlations: Direct correlation of the base of the zone with magnetostratigraphy places this boundary within Chron C-3A-N3 at ~6.4 Ma (Ciesielski, 1983; Shaw and Ciesielski, 1983) and closely approximates the upper Miocene carbon shift. The base of the zone is correlative with the lower *Coscinodiscus marginatus* Zone of the Norwegian Sea (Schrader and Fenner, 1976), upper *Nitzschia porteri*-*N. miocenica* Zone of the Rockall Plateau region (Baldauf, 1984), upper NNPD6-Subzone B of the North Pacific (Barron, 1985a), the upper *Denticulopsis hustedtii* Zone of the Southern Ocean (Shaw and Ciesielski, 1983), and occurs within N17 and NN11.

Mesocena circulus/*M. diodon* Zone

Definition: Top. Last consistent occurrence of *M. circulus*, Busen and Wise (1977).

Base. Lowest common occurrence of *Mesocena diodon* s.s., this report.

Interval: ~117.5 m–128.5 m; top between Samples 104-642C-15H, CC and 104-642B-13H, CC, base at Section 104-642C-17H-5.

Age: late Miocene; ~8.7–6.4 Ma, lower portion of zone absent at Site 642.

Correlations: The zone is correlative with the lower to middle *Denticulopsis hustedtii* Zone (NSD8) to upper *D. hustedtii*/*D. lauta* Zone (NSD7) of the Southern Ocean (Ciesielski, 1983; Shaw and Ciesielski, 1983; Ciesielski, 1986). Correlations with other diatom zones of the North Pacific, Rockall Region, and Norwegian Sea are given in the diatom section, this volume. At Southwest Pacific Site 594 the base of the zone as defined here occurs between the last *Denticulopsis praedimorpha*, below the last *D. lauta*; it is also coincident with the last *Cyrtocapsella japonica*. Ages for these and a number of other datums (Ciesielski, 1986) place the base of the zone in upper Chron C-5 to lowermost Chron C-4A (~9.0–8.7 Ma) and within the North Pacific diatom Zone NNPD6-Subzone A. These correlations require the base of the zone in Core 104-642B-15H (128.5 m) to be younger than ~9.0–8.7 Ma. Diatom zones at this level further constrain the age of the sediments in Core 642B-15H to younger than mid Chron C-4A, or < 8.5 Ma. This fact, and missing dia-

tom zones between Samples 104-642B-15H, CC and 104-642B-16H, CC (see diatom section), suggest that the boundary between this zone and the underlying *Mesocena circulus* Zone is a disconformity.

Mesocena circulus Zone

Definition: Top. First common (FC) occurrence of *Mesocena diodon*; Busen and Wise (1977).

Base. Lowest consistent occurrence of *M. circulus*; Ciesielski (1975).

Interval: ~113–130 m; top between Samples 104-642C-16H, CC and 104-642B-16H, CC, base between Samples 104-642B-19H, CC and 104-642C-19H, CC.

Age: ~8.7 to 13.9–13.8 Ma, middle Miocene–late Miocene.

Correlations: The base of this zone occurs in the Southern Ocean *Nitzschia denticuloides* Zone (NSD6) of the middle Miocene (Shaw and Ciesielski, 1983). In the Norwegian Sea, the FAD of *M. circulus* occurs between DSDP Samples 8-2, 58–59 cm, and 8-3, 2–3 cm, of Site 338 (Martini and Müller, 1976) and within Schrader and Fenner's (1976) *Nitzschia* sp. 8 Zone. At Site 642 this datum also occurs within the same diatom zone which is equivalent to NNPD5–Subzone A (Barron et al., 1985). The base of the zone is at approximately the same depth as the first *Coscinodiscus plicatus*, which according to Barron (1985b) is ~13.9 to 13.8 Ma. Thus, the base of this zone confirms an age for the Core 8 to Core 9 boundary in Site 338 of ~13.9 Ma. Based on the presence of the same zone in Core 7 of Site 338, it would appear that an unconformity exists in Site 338 between the base of the glacial sequence (~2.4 Ma) in Core 6 and Core 7–Core 8 (~13.9 Ma).

As was mentioned in the discussion of the previous zone, this zone has an unconformable boundary with the *M. circulus*/*M. diodon* Zone. On the basis of silicoflagellate evidence alone, an argument against the presence of this unconformity would require 5 million years (13.8 Ma—base of *M. circulus* Zone, 163 m to ~8.7 to 9.0 Ma—base of *M. circulus*/*M. diodon* Zone, 128.5 m) to be represented in a 34.5-m interval of Site 642.

No Zonal Designation Interval Zone

Definition: Top. Lowest consistent occurrence of *Mesocena circulus*, Ciesielski (1975).

Base. Last recognized occurrence of *Corbisema triacantha*.

Interval: ~163–~194.5 m; top between Samples 104-642B-19H, CC and 104-642C-19H, CC, base between Samples 104-642B-22H, CC and 104-642C-23H, CC.

Comments: Age diagnostic silicoflagellates are absent in this interval; therefore, no zonal designation is made. The base of the interval is defined by the last-noted *Corbisema triacantha*. Since *C. triacantha* is rare in the Norwegian Sea, its last observed occurrence in core catchers (104-642B-22H) is not likely its last true occurrence. This conclusion is supported by correlations with diatom zones at Site 642. Therefore, the last-noted *C. triacantha* should not be taken as correlative with the top of *C. triacantha* Zone (Martini and Müller 1976) at Site 338.

Age: Based upon correlations with Site 642 diatom datums, the zonal age is < ~16.0 Ma to 13.9–13.8 Ma.

Correlations: Correlations of diatoms between Sites 338 and 642 suggest most of this interval correlates with Martini's *C. triacantha* Zone and that shore-based studies should find *C. triacantha* close to the base of the *Mesocena circulus* Zone (this report). This interval correlates with the upper NNPD3 to lower NNPD5 diatom zones.

Corbisema triacantha Zone

Definition: Top. Last recognized occurrence of *Corbisema triacantha*.

Base. LAD *Naviculopsis quadratum* (syn. *N. rectangularis*), Martini (1971).

Interval: ~194.5–~233.5m; top between Samples 104-642B-22H, CC and 642C-23H, CC, base between Samples 104-643D-6X, CC and 104-642D-5X, CC.

Age: ~17.5 to < ~16.0 Ma. Early Miocene.

Correlations: Martini and Müller (1976) find the zone in Site 338, Cores 8–11. The base of the zone at that site occurs within the *Rhizosolenia bulbosa* Zone of Schrader and Fenner (1976).

Within Site 642, it is difficult to recognize the diatom zones of Schrader and Fenner (1976); however, the base of the zone appears to occur only slightly lower in the section. The base of the zone can be more accurately placed in the *Thalassiosira fraga* Zone (NNPD2), which is well defined at Site 642. Since the base of the zone is only ~10 m below the FAD of *Craspedodiscus coscinodiscus*, its absolute age must be only slightly older than the 17.3-Ma age of this datum as defined by its direct correlation with magnetostratigraphy (Barron, 1985a). Martini (1971) directly correlated the base of this zone to approximately the NN3/NN4 boundary. In a later study, Martini (1979) correlated the zonal base to approximately the NN3/NN2 boundary based on his examination of Site 407 from the western flank of the Reykjanes Ridge.

The base of this zone exhibits little diachroneity with respect to latitude and is a highly reliable stratigraphic datum at all latitudes in both hemispheres. For this reason, it is considered a primary datum at Site 642.

Naviculopsis navicula Zone

Definition: Top. LAD *Naviculopsis quadratum*, Martini, 1972.

Base. FAD *Naviculopsis navicula*, Martini, 1972.

Interval: ~233.5–~272 m; top between Samples 104-642D-6X, CC and 104-642D-5X, CC, base between Samples 104-642D-10X, CC and 104-642D-9X, CC.

Age: ~21.2–17.5 Ma. Early Miocene.

Correlations: Martini and Müller (1976) place the base of the zone between Core 17-4, 85–86 cm, and 18-1, 50–551 cm, in Site 338. This places the boundary in the lower *Synedra jouseae* Zone to the top of the *Pseudodimerogramma elegans* Zone of Schrader and Fenner (1976) at the same site. At Leg 104 Site 642, the base occurs in the *Pseudodimerogramma elegans* Zone of Schrader and Fenner (1976) and within the *Thalassiosira spinosa* Zone (NNPD1; range 23–19.5 Ma, Barron, 1985a). Martini (1972) correlated the base of the zone to within NN2. At Leg 49 Site 407, on the western flank of the Reykjanes Ridge, Martini (1979) directly correlated the zonal base with uppermost NN1, near the NN1/NN2 boundary. Based upon Martini's (1979) correlation with calcareous nannofossil stratigraphy and the direct calibration of the NN1/NN2 boundary to the geomagnetic reverse time scale (GRTS, Hsü et al., 1984), the FAD of *Naviculopsis navicula* has an age of ~21.2 Ma and correlates with Chron C-6A-N1.

Naviculopsis lauta Zone

Definition: Top. FAD *Naviculopsis navicula*, Martini (1972).

Base. FAD *Naviculopsis lauta*, Martini (1972).

Interval: ~272–>286.5 m; top between Samples 104-642D-10X, CC and 104-642D-9X, CC, base unrecognized because of the barren zone below Sample 104-642D-11X, CC.

Age: ~21.2–21.5 Ma. Early Miocene.

Correlation: Martini and Müller (1976) place the base of the zone between Core 19-2, 10–11 cm, and Core 19-5, 123–124 cm, at Site 338.

The absence of *Naviculopsis lauta* above the Site 642 barren zone suggests that this interval at Site 642 is above the true base of the zone. This conclusion is supported by the presence of *Corbisema triacantha* in Core 104-642D-11X. According to Mar-

tini and Müller (1976), this species only occurs above the base of the zone. Further resolution is provided by the LAD of *Naviculopsis biapiculata* in Core 104-642D-10X. This datum occurs in the upper *Naviculopsis lauta* Zone of Site 407 on the western flank of the Reykjanes Ridge, and is within upper NN1 (Martini, 1979). Based upon these correlations, basal Core 104-642D-11X should not be significantly older than the 21.2 Ma age for the top of the zone. Correlation of this core to upper NN1 suggests that this level is probably not older than Chron C-6A-N2.

Paleoenvironment

Very few paleoenvironmental conclusions can be drawn from the recorded silicoflagellate assemblage because of the lack of quantitative counts of species/genera.

The occurrence of small numbers of *Dictyochoa* species in three samples (104-642C-9H, CC, 642B-10H, CC, and 642B-14H, CC) is indicative of surface waters which are subpolar or warmer. In the Southern Ocean this genus is absent or rare in Antarctic surface water but rapidly increases in abundance between the Antarctic Convergence and the Subtropical Convergence (Ciesielski, 1975).

The significant last occurrence of pentagonal *Distephanus* spp. (e.g., *Distephanus quinganguellus*) occurred in the latest Miocene. Their last occurrence and high abundance in the late Miocene in the Norwegian Sea was of a similar age to the Antarctic, whereas in lower latitudes it consistently disappeared in the upper Pliocene cores. This would suggest that late Miocene surface water temperatures had already developed a significant thermal contrast with Atlantic waters to the south.

Results, Hole 642E

Stratigraphy

Only one long-ranging silicoflagellate species is consistently present in the tuff units interbedded with basalt flows. This species, *Distephanus speculum*, occurs rarely (1 to 2 specimens) in the following Hole 642E cores: 104-642E-5R, 642E-19R, 642E-21R, 642E-23R, 642E-27R, and 642E-35R. Two other species, *Distephanus crux* and *Mesocena apiculata*, occur in Core 104-642E-35R. The presence of the genus *Distephanus* indicates an age of middle Eocene or younger (Bukry, 1981). The species *Mesocena apiculata* has its first occurrence in the *Dictyochoa grandis* Zone (Shaw and Ciesielski, 1983) which is Lutetian in age (middle Eocene). Direct paleomagnetic correlations of the first occurrence of this species by Shaw and Ciesielski (1983) place this datum between magnetic chrons 18 and 19. Thus, the age of material studied from Hole 642E must be younger than ~42 Ma.

Paleoenvironment

With the exception of Core 104-642E-35X, the paleoenvironmental significance of silicoflagellates in other cores is discussed within the context of the diatom section because of the scarcity of silicoflagellates in sediments of Hole 642E. The tuff unit in Core 104-642E-35X contains a low abundance of silicoflagellates but which are numerous enough to probably preclude eolian transport from subaerially exposed sediments. This tuff unit appears to have been deposited in a subaqueous environment.

Radiolarian Stratigraphy

Introduction

Radiolarians in Site 642 sediments range in age from early Miocene to Holocene, and the lower Miocene section at this site contains the oldest radiolarian recovered on Leg 104. The biosiliceous section is 226 m thick, but the interval is far from complete. The radiolarian biostratigraphy indicates the presence of

five hiatuses of variable deviation, but the chronology of these erosive events is not yet clear. The lower four disconformity-bound intervals can be correlated to other biosiliceous intervals recovered at Sites 338, 341, and 643, but there is no section from the Norwegian Sea containing continuous deposition across the highest hiatus. Consequently, there is no local reference section for comparison, and the existence of this upper disconformity is based mainly on diatom data. The radiolarian data are somewhat equivocal on this point. There is no radiolarian evidence for other hiatuses above and below the biosiliceous interval that has been proposed on the basis of other microfossils.

Abundance and Preservation

The oldest radiolarian-bearing sediments at Site 642 directly overlie the disconformity-bound Eocene section in 104-642D-11X-2 (280 m). The top of Section 104-642A-1H-1 contains abundant, well-preserved specimens of the Holocene radiolarian fauna that have been described and illustrated by Bjørklund (1976). Radiolarians are not preserved in the underlying approximately 65 m of glacial marine sediments, which is consistent with the occurrence of these microfossils throughout much of the Norwegian Sea.

Radiolarian preservation improves markedly below the transition zone between glacial-marine and hemipelagic sediments, which occurs at the base of Samples 104-642B-8H, CC (66 m) and 104-642C-8H, CC (61 m). In general, radiolarians are common and display moderate to good preservation throughout the biosiliceous interval. The only exception is in sediment from Cores 104-642B-16H through 104-642B-19H and 104-642C-17H through 104-642C-19H (about 135–165 m, biozone NSR 8), where radiolarian diversity and preservation decline markedly.

The material recovered from Holes 642B through 642D has been assigned to radiolarian biozones NSR 1–12. The distribution of these biozones in each hole is shown in Figure 43. Zonal boundary correlation lines between these holes are not perfectly horizontal, despite their close proximity. The discordance is as much as 8.4 m (i.e., NSR 9/NSR 10). This phenomenon may have resulted from coring disturbance or it may be the natural result of sampling error. Similar disparity exists in the paleomagnetic records of these holes.

Five of the biozonal boundaries at Site 642 are located at unconformities. The sediments in biozone NSR 1 are probably coeval with the *Velicucullus oddgurneri* Biozone (upper Oligocene) of Leg 38, Samples 338-19 to 338-19-3 (Bjørklund, 1976). More detailed investigations are needed to confirm this correlation. If true, however, then approximately 50 m of sediment is missing in the hiatus between NSR 1 and NSR 2. The unconformity between NSR 2 and NSR 3 in Hole 642D is represented by about 30 m of sediment in Cores 104-643A-24X through 104-643A-27X. Biozone NSR 4 falls totally within an unconformity in Holes 642B and 642D, which is represented by about 55 m of sediment in Cores 104-643A-17X to 104-643A-22X. The unconformity at the boundary between NSR 7 and 8 is correlative with an unconformity in 104-643A-12H, which is represented by 30–50 m of sediment at Sites 338 and 341. The boundary between biozones NSR 8 and NSR 9 is associated with a shift in radiolarian faunas that is interpreted here as an unconformity in accordance with the diatom data. There are no coeval sediments from the Norwegian Sea.

Paleoenvironment

The isolation phase terminates in 104-642B-15H/642C-16H (base of the Biozone NSR 9, 130 m), which is marked by the absence of endemic species. They are gradually replaced by assemblages having components suggestive of transition and central provinces of modern plankton distributions. This subfauna persists to Core 104-642C-13H (101 m sub-bottom) but is absent in

Holes 642 Biozones	B	C	D
NSR 13 <i>Cycladophora davisiana</i>			
NSR 12 <i>Antarctissa whitei</i>	Section 8H-cc to 11H-5 (66.4 to 91.7 mbsf)	Section 8H-cc to 13H-1 (60.7 to 92.2 mbsf)	
NSR 11	Section 11H-5 to 12H-cc (91.7 to 104 mbsf)	Section 13H-1 to 14H-2 (92.2 to 103.5 mbsf)	
NSR 10	Section 12H-cc to 15H-2 (104 to 125.8 mbsf)	Section 14H-2 to 15H-5 (103.5 to 117.4 mbsf)	
NSR 9	Section 15H-2 to 16H-5 (125.8 to 134.2 mbsf)	Section 15H-5 to 16H-cc (117.4 to 130 mbsf)	
NSR 8 <i>Eucoronis fridjofnanseni</i>	Section 16H-5 to 19H-5 (134.2 to 164.4 mbsf)	Section 16H-cc to 20H-2 (130 to 160.5 mbsf)	
NSR 7 <i>Lithomelissa stigi</i>	Section 19H-5 to 22H-2 (164.4 to 188.7 mbsf)	Section 20H-2 to 23H-2 (160.5 to 186.3 mbsf)	
NSR 6 <i>Actinomma holtedahli</i>	Section 22H-2 to 23H-2 (188.7 to 198 mbsf)	Section 23H-2 to 24H-2 (186.3 to 194.4 mbsf)	Section 2H-1 to 2H-2 (190 to 190.5 mbsf)
NSR 5	Section 23H-2 to 24H-2 (198 to 207.6 mbsf)	Section 24H-2 to 24H-cc (194.4 to 199.6 mbsf)	Section 2H-5 to 2H-cc (196.8 to 199.6 mbsf)
NSR 4	—————		—————
NSR 3	Section 24H-2 to 25H-cc (207.6 to 221.1 mbsf)		Section 3H-1 to 4H-cc (199.6 to 218.9 mbsf)
NSR 2			Section 4H-cc to 10H-cc (218.9 to 276.8 mbsf)
NSR 1			Section 11H-1 to 11H-cc (276.8 to 286.5 mbsf)

Figure 43. Distribution and range of radiolarian biozones in Holes 642B, 642C, and 642D. NSR = Norwegian Sea radiolarian zone.

the overlying section. In Sample 104-642C-16H, CC, there is a limited occurrence of four species that are typical of tropical or subtropical oceans: *Anthocyrtidium zanquebaricum*, *Lamprocyclus maritimalis*, *Didymocyrtis antepenultimus*, and *Didymocyrtis mammiformis*. Temperate species gradually disappear in the uppermost radiolarian interval (Cores 104-642B-11H through 104-642C-8H, 60–95 m sub-bottom), indicating a sharp decline in surface water temperatures followed by the onset of glacial conditions.

Thus, Site 642 radiolarians document an asymmetrical temperature curve representing the injection of progressively more temperate waters into the Norwegian Sea (sediments from 277 to 95 m sub-bottom) followed by a relatively rapid retreat of these waters (in the interval 60–95 m sub-bottom). This smooth cycle is broken, however, by a pronounced isolation phase, documented at Site 642 between 130 to 158 m, when the Norwegian Sea must have reverted to conditions more characteristic of its Oligocene history.

The radiolarian faunas have many large fluctuations in composition. In some intervals, as for example, in the central part of biozone NSR 8, large spumellarians are the most dominating faunal elements. This can be a result of either dissolution or specific ecological conditions favoring the spumellarians. Diatoms are abundant in this zone, but are of a moderate preservation, indicating that dissolution can play a role in the general radiolarian faunal composition.

Calcareous Nannofossil Biostratigraphy

Introduction

Five holes were drilled at Site 642 in the Norwegian Sea. The sediments recovered yielded Quaternary through lower Miocene–upper Oligocene calcareous nannofossils. The smear slides studied, as a general rule, contained the low abundances and small diversity of coccoliths typical of low water temperatures. Many of the low-abundance slides studied contained insufficient information to provide accurate biostratigraphic zone determinations, especially when the zonal markers that do exist are rare. The species that are the standard low- to middle-latitude zone markers for the Neogene (discoasters, ceratoliths, and sphenoliths) are for all practical purposes missing from the Norwegian Sea because of dissolution, ecologic exclusion, and dilution owing to high glacial terrigenous input. The species that are found are mostly long-ranging species which are impractical to use for detailed biostratigraphic divisions.

Calcareous Nannofossil Zone Definitions

The standard nannofossil zonation of Martini (1971) was followed to some extent, but because of the absence of many marker species, various zones had to be combined into longer ranging zones. Thus, the biostratigraphic resolution of the nannofossils in the Norwegian Sea is poor. The nannofossil assemblages presented here are similar to those compiled in Leg 38 (Müller, 1976) with the exception of the interval containing *Cyclcoccolithus floridanus*, which is presented here.

The nannofossils found at Site 642 can be grouped into five assemblages based on first appearance datum (FAD) and last appearance datum (LAD) of the various marker species. Table 11 summarizes the calcareous nannofossil zonal boundary markers and the assemblages for each zone as well as the Martini standard zonation equivalent and corresponding age.

Emiliana huxleyi Zone (NN21)

Bottom: FAD *E. huxleyi*.
Age: late Quaternary.

Gephyrocapsa oceanica Zone (NN20)

Top: FAD *E. huxleyi*.
Bottom: LAD *Pseudoemiliana lacunosa*.
Age: middle Quaternary.

Interval with *P. lacunosa* (NN19–16)

Top: LAD *P. lacunosa*.
Bottom: LAD *Reticulofenestra pseudoumbilica*.
Age: late Pliocene to early Quaternary.

Interval with *R. pseudoumbilica* (NN15–7)

Top: LAD *R. pseudoumbilica*.
Bottom: LAD *C. floridanus*.
Age: middle Miocene to early Pliocene.

Interval with *C. floridanus* (NN6–1?)

Top: LAD *C. floridanus*.
Age: early Miocene to latest Oligocene or younger.

Methods

Samples from sediment bearing cores were prepared as smear slides and studied with the optical microscope. Selected upper Pleistocene samples were also prepared for scanning electron microscope (SEM) examination by treating them with ultrasonic and suspension settling techniques.

Results

Quaternary samples were recovered from ~34 m sub-bottom (104-642B-5H-4) followed by a barren to near-barren interval to ~57 m sub-bottom (104-642B-7H, CC). This interval fluctuated between glacial and interglacial deposition. Many interglacial sediments contained nannofossil ooze layers with abundant assemblages of *Gephyrocapsa* sp., *C. pelagicus*, and small *Reticulofenestra* sp. Also occurring but less abundant are *Coronocyclus nitescens*, *Cyclcoccolithus leptoporus*, *Dictyococcites* sp., *Discolithina* sp., and *Helicosphaera* sp. *E. huxleyi*, the marker for *E. huxleyi* Zone (NN21), was identified at a depth of ~4 m sub-bottom (104-642B-1H, CC) with the use of SEM. Neither *E. huxleyi* nor *P. lacunosa* was found at ~19 m sub-bottom (104-642B-2H, CC), indicating the *G. oceanica* Zone (NN20). Also occurring in this sample are reworked Cretaceous and some Paleocene nannofossils. The zonal marker for NN19–16, *P. lacunosa*, is first observed at a sub-bottom depth of ~20 m (104-642B-4H-1, 17 cm). The LAD of *R. pseudoumbilica*, the marker NN15–7, first occurs at a sub-bottom depth of 78 m (104-642B-10H-2, 96 cm).

At high latitudes, the calcareous nannofossil diversity is relatively low from the middle Miocene to early Pliocene (Backman, 1984). In the standard Martini zonation this interval is subdivided by the FAD and LAD of discoasters, ceratoliths, and sphenoliths, which are all essentially absent from Norwegian Sea sediments (Müller, 1976). The only discoaster present is the high-latitude form *D. intercalaris*, which is a long-ranging species with approximately the same range as *R. pseudoumbilica*. This zone commonly contains nannofossils, abundant but of low diversity. The assemblage consists mostly of *C. pelagicus*, small *Reticulofenestra*, and *R. pseudoumbilica*. Also occurring are *C. leptoporus*, *C. nitescens*, *Dictyococcites* sp., *D. intercalaris*, *D. aff. variabilis*, *Discolithina* sp., *Helicosphaera* sp., and *Sphenolithus moriformis*. At a sub-bottom depth of ~157.5 m (104-642B-18H, CC) is the LAD of *C. floridanus*. According to Backman (1984) and Bukry (1973) this corresponds to the top of NN6. Roth and Thierstein (1972) mention that the species has been recorded in the overlying *Discoaster kugleri* Subzone in some areas, and Miller et al. (1985) also show *C. floridanus*

Table 11. Calcareous nannofossil biostratigraphy, Leg 104, Site 642.

Depth to base	Nannofossil zonation	Zonal marker	Age	Species present
4 m? 642B-1H,CC	<i>Emiliana huxleyi</i> (NN21)	FAD <i>E. huxleyi</i>	Quaternary	<i>E. huxleyi</i> , <i>Gephyrocapsa</i> sp., <i>Coccolithus pelagicus</i> , small <i>Reticulofenestra</i> sp., <i>Coronocyclus nitescens</i> , <i>Cyclococcolithus leptoporus</i> , <i>Dictyococcites</i> sp., <i>Discolithina</i> sp., <i>Helicosphaera</i> sp.
20 m 642B-4H-1, 17 cm	<i>Gephyrocapsa oceanica</i> (NN20)	LAD <i>P. lacunosa</i>	Quaternary	Same as <i>E. huxleyi</i> Zone except no <i>E. huxleyi</i>
78 m 642B-10H-2, 960 cm	<i>Pseudoemiliana lacunosa</i> (NN19-16)	LAD <i>R. pseudoumbilica</i>	early Quaternary to late Pliocene	Same as <i>G. oceanica</i> Zone except add <i>P. lacunosa</i>
157.5 m 642C-11H,CC	<i>Reticulofenestra pseudoumbilica</i> (NN15-7)	LAD <i>C. floridanus</i>	early Pliocene to middle Miocene	<i>C. pelagicus</i> , small <i>Reticulofenestra</i> , <i>R. pseudoumbilica</i> , <i>C. leptoporus</i> , <i>C. nitescens</i> , <i>Dictyococcites</i> sp., <i>D. intercalaris</i> , <i>D. aff. variabilis</i> , <i>Discolithina</i> sp., <i>Helicosphaera</i> sp., <i>Sphenolithus moriformis</i>
> 157.5 642B-18H,CC	<i>Cyclococcolithus floridanus</i> (NN6-1?)		early Miocene	<i>C. floridanus</i> , <i>C. pelagicus</i> , <i>C. nitescens</i> , <i>Dictyococcites</i> sp., <i>D. deflandrei</i> , <i>D. intercalaris</i> , <i>Helicosphaera</i> sp., <i>R. pseudoumbilica</i> , <i>Reticulofenestra</i> sp., <i>S. moriformis</i> , <i>Coccolithus abisectus</i>

occurring in NN7. The LAD of *C. floridanus* found at Site 642 most likely concurs with the data of Backman (1984) and Bukry (1973) in representing the NN6/7 boundary owing to the fact that this LAD is found with the LAD of *Coccolithus abisectus*, which also represents the NN6/7 boundary (Backman, 1984). This boundary corresponds to the top of the interval with *C. floridanus* (NN6-1?). Also present in this zone are *C. pelagicus*, *C. nitescens*, *Dictyococcites* sp., *D. deflandrei*, *D. intercalaris*, *Helicosphaera* sp., *R. pseudoumbilica*, *Reticulofenestra* sp., and *S. moriformis*.

Below ~158.5 m sub-bottom (104-642C-19H, CC), Site 642 is mostly barren of calcareous nannofossils. At a sub-bottom depth of ~167 m (104-642B-19H, CC), ~213 m (104-642B-24H, CC), 293 m (104-642D-12X-5, 145-146 cm), and ~306 m (104-642D-14X-1, 5-6 cm) a few nannofossils were present but of too little diversity to be useful for zonal designators. At ~326 m sub-bottom (104-642E-4R-1, 1-2 cm) the same assemblage was found as at ~167 m sub-bottom and is still designated as belonging to the interval with *C. floridanus* (NN6-1?). This could represent downhole contamination. *H. ampliaperta*, the zonal marker for NN4, was found in Leg 38 sediments (Müller, 1976) but was not encountered at Site 642. The Oligocene nannofossil zonal markers found from Leg 38 sites, such as *Chiasmolithus altus*, *Zygrhabdolithus bijugatus*, and the acme of *C. abisectus*, were also not encountered at Site 642, suggesting the oldest nannofossils found at Site 642 are all younger than latest Oligocene.

Reworking and Preservation

Reworked specimens of older nannofossils are commonly present down to a sub-bottom depth of 47 m (104-642B-6H, CC). The reworking consists primarily of Cretaceous nannofossils, but Paleocene reworking was also found to a lesser extent. Reworking is present in the interglacial as well as the glacial sediments, but is much more pronounced in the glacial, commonly making up over 50% of the assemblage. Reworking is insignificant from about 47 m sub-bottom down to about 128 m sub-bottom (104-642B-15H, CC). From about 128 m sub-bottom to about 157.5 m sub-bottom (104-642B-18H, CC), Paleocene and

minor Cretaceous reworking is often encountered, but much less frequently than in the Quaternary intervals.

Preservation varies greatly throughout Site 642. The glacial sediments are characterized by poor preservation, while the interglacial intervals commonly contain well-preserved nannofossil oozes. The Pliocene section, as a general rule, contains moderately to poorly preserved nannofossils, while the upper-middle Miocene nannofossils are commonly moderately to well-preserved.

Diversity

The sediments at Site 642 as a general rule contain relatively few calcareous nannofossils and those that are present are of low diversity. There are, however, a few intervals with a relatively greater abundance of nannofossils. Low abundances suggest relatively low water temperatures, with the nannofossil-rich oozes possibly reflecting relatively warmer water influxes. Some interglacial sediments contain coccolith oozes with abundant, yet low diversity, nannofossils. The interval from ~104 m sub-bottom (104-642B-12H, CC) to ~158 m sub-bottom (104-642C-19H, CC) also contains some relatively nannofossil-rich zones. These upper-middle Miocene intervals show a slight increase in diversity. Both the Quaternary as well as the upper Miocene nannofossil-rich intervals contain many whole, intact coccospheres indicating low postdepositional disturbance from bioturbation. Such preservational conditions often are indicative of low bottom oxygen content.

Discoasters useful for biostratigraphic zonal determinations are absent at Site 642; however, a few long-ranging, colder water forms are found in the upper-middle Miocene section. The youngest discoaster observed, *D. intercalaris*, is present, but rare, at a sub-bottom depth of 104 m (104-642B-12H, CC) and is present consistently below that. *D. deflandrei* occurs at a sub-bottom depth of ~145 m (104-642B-18H, CC). Both of these are cold water species. Discoasters in general are among the most resistant to calcite solution, thus their scarcity at Site 642 must be mostly a function of paleoecologic exclusion rather than selective dissolution (Bukry, 1973). Thus, the unfavorably cold climate at Site 642 can account for the absence of all Pliocene dis-

coasters and for the occurrence of only a few rare species of middle-upper Miocene discoasters with cooler water affinities.

Planktonic Foraminifer Stratigraphy

Introduction

We analyzed the >63- μ m sieve fraction of core-catcher (CC) samples from the shipboard study and additional samples every second section. Results for Holes 642A, B, and C are presented in Tables 12 and 13. All of Holes 642D and 642E were barren in planktonic foraminifers with the exception of a few samples containing obvious downhole contamination. None of the marker species for the standard temperate and tropical zonation schemes (Blow, 1969; Kennett, 1973; Kennett and Srinivasan, 1981, 1983) are present. Thus the standard Neogene zonation is not applicable to this area. However, some *Neogloboquadrina* species used as zonal indicators in a preliminary zonation scheme for the high-latitude North Atlantic (Weaver, in press) are present. A tentative correlation with the evolving North Atlantic biozonation can be made. An informal local zonation mainly based on neogloboquadrinids is suggested in Figure 44. Some taxonomic problems are evident due to clear evolutionary trends within the *Neogloboquadrina* plexus. These will be addressed in future studies, which may alter the results presented here.

Results

The interval from the top of the section to 71.66 mbsf in Hole 642B (Sample 104-642B-9H-4, 74-78 cm) and 58.06 mbsf in Hole 642C (Sample 104-642C-7H-4, 77-81 cm) is strongly dominated by *Neogloboquadrina pachyderma* (sin.) in its encrusted form with very compact tests. Other species occur in variable amounts. Most common are *N. pachyderma* (dex.), *Globigerina bulloides*, *G. falconensis*, and *G. quinqueloba*. Sporadic occurrences of *Globigerinita glutinata* are also found. A similar zone was described from Leg 38 sites (Schrader et al., 1976), and has been found in DSDP sites in the North Atlantic, corresponding with N22 and upper parts of N21 (Berggren, 1972; Poore and Berggren, 1975; Poore, 1979; Huddleston, 1984; Weaver, in press).

Weaver and Clement (in press) indicate an age of 1.7 Ma for the FAD of encrusted *N. pachyderma*, whereas the data from this and the other Leg 104 sites may indicate a slightly older age of about 2-2.5 Ma for this event in the Norwegian Sea.

The LAD of *N. atlantica* (sin.) appears at 75.80 mbsf in Hole 642B (Sample 104-642B-9H, CC, 8-12 cm) and 60.55 mbsf in Hole 642C (Sample 104-642C-8H, CC, 14-18 cm). Berggren (1972) concluded that this event occurred at the Pliocene/Pleistocene boundary. New paleomagnetic constraints on this datum from Leg 94 in the high-latitude North Atlantic (Hooper and Weaver, in press; Weaver and Clement, in press) give an age of 2.3 Ma.

Relatively diverse faunas intermingled with barren samples continue down to 162.95 mbsf in Hole 642B (Sample 104-642B-19H-4, 74-78 cm) and to 158.50 mbsf in Hole 642C (Sample 104-642C-19H, CC, 46-49 cm). The amounts of planktonic foraminifers are highly variable from very rare to relatively abundant. *N. pachyderma* (sin. and dex.) forms a major element of the planktonic foraminiferal fauna together with *Globigerina bulloides* and *N. continuosa*. In some intervals *N. atlantica* is common.

The LAD of *N. continuosa* appears at 93.3 mbsf in Hole 642B (Sample 104-642B-11H, CC, 12-16 cm) and at 81.26 mbsf in Hole 642C (104-642C-11H-6, 74-78 cm). Kennett and Srinivasan (1983) indicate that this extinction occurred within the upper Miocene (N16/N17). Data from the North Atlantic indicate a younger age of about 4.5 Ma in the lower parts of the Gilbert Epoch (Weaver and Clement, in press).

Table 12. Planktonic foraminifers in Holes 642A and 642B.

Leg 104 Core/Sec/Int (in cm)	<i>N. pachyderma</i> (sin.)	<i>N. pachyderma</i> (dex.)	<i>N. atlantica</i> (sin.)	<i>N. atlantica</i> (dex.)	<i>N. acostaensis</i>	<i>N. continuosa</i>	<i>G. bulloides</i>	<i>G. falconensis</i>	<i>G. quinqueloba</i>	<i>G. glutinata</i>	<i>O. universa</i>	<i>N. duterrei</i>	Zones
642A													
1-5, 94-98	A	R					R	R					NSPF6
1-CC	A												
642B													
1-2, 74-78	A								R			R	NSPF6
1-CC, 14-18	A												
2-3, 36-40	A												
2-5, 36-40	A												
2-CC, 1-5	A												
3-2, 36-40	Barren												
3-4, 36-40	A	R					C			R			
4-1, 35-39	A						R						
4-3, 35-39	A												
4-5, 35-39	Barren												
4-CC, 10-14	A								R				
5-2, 74-78	A												
5-4, 74-78	A												
5-CC, 15-19	F												
6-2, 44-48	A	R											
6-6, 44-48	Barren												
7-1, 64-68	Barren												
7-3, 64-68	R												
7-5, 64-68	Barren												
7-7, 64-68	Barren												
8-1, 64-68	Barren												
8-3, 64-68	Barren												
8-5, 64-68	Barren												
8-CC, 10-14	Barren												
9-2, 52-56	Barren												
9-4, 52-56	C	R						C	R	C	R		NSPF5
9-6, 52-56	C	R		R				C	R	C			
9-CC, 8-12	C		R					C	R	R			
10-2, 52-56	C		C					R	R	R			
10-4, 52-56	F	R	F		R	R	F	C	C	C	R	R	
10-6, 52-56	C		R				R	C	R	R	R		NSPF4
10-CC, 15-19	R	R											
11-2, 46-50	Barren												
11-4, 46-50	F	C	R				R	C	C	R	C		
11-6, 46-50	F	R					R	F		C	C		
11-CC, 12-16	F		C	R			C	R	C	C	R		
12-2, 67-71	Barren												
12-4, 67-71	Barren												
12-6, 67-71	F	R	R				C	C	R	C	R		
13-1, 74-78	C	R	R	R	R		R	C	R	C		X	
13-3, 74-78	R							F	R	R	C		
13-5, 74-78	F	R	R	R				C	C	R	C		
13-CC, 14-16	R							R	R	R	R		
14-CC, 6-10	Barren												
15-2, 74-78	C	F		C	C	F	C						
15-CC, 7-11	C	F		F	C	F	F	R	C				NSPF3
16-2, 69-73	R			R	R	R	R						
16-4, 69-73	R									R			
16-6, 69-73										R			
16-CC, 8-12	C	R	R			C	C						
17-2, 71-75	F	F	R	C		F	C						
17-4, 71-75	Barren												
17-6, 71-75	C	R		R	R	C	R						
18-1, 72-76	R	C				C	F			C			
18-3, 72-76	C	C	R	R		C							
18-5, 82-86	C	C	R			F	C						
18-CC, 0-4	R	C	R	C	R	C	R						
19-2, 89-93	R	C	R	R	R	F							
19-4, 72-76	C	R			R	C							
Rest of hole barren.													

Note: A = abundant; F = frequent; C = common; R = rare; X = one or two specimens.

Table 13. Planktonic foraminifers in Hole 642C.

Leg 104 Core/Sec/Int (in cm)	<i>N. pachyderma</i> (sin.)	<i>N. pachyderma</i> (dex.)	<i>N. atlantica</i> (sin.)	<i>N. atlantica</i> (dex.)	<i>N. acostaensis</i>	<i>N. continuosa</i>	<i>G. bulloides</i>	<i>G. falconensis</i>	<i>G. quinqueloba</i>	<i>G. glutinata</i>	<i>O. universa</i>	<i>N. dutertrei</i>	Zones
1-2, 82-86	A												
1-CC, 7-11	F	R											
2-2, 28-32	A												
2-4, 28-32	C												
2-6, 28-32	C												
2-CC, 7-11	F												
3-2, 28-32	A												
3-4, 28-32	A												
3-6, 28-32	A												NSPF6
3-CC, 13-17	C												
4-2, 53-57	F												
4-4, 53-57	F												
4-6, 53-57	A	C											
4-CC, 1-5	R												
5-2, 67-71	F												
5-4, 67-71	R												
5-6, 67-71	R												
6-1, 67-71	Barren												
6-3, 67-71	Barren												
6-5, 67-71	Barren												
6-CC, 25-29	Barren												
7-2, 74-78	Barren												
7-4, 74-78	R												
8-1, 74-78	Barren												
8-CC, 14-18	R	C					C				R		NSPF4
9-2, 73-77	R	R					C	R	R				
10-1, 77-81	R												
10-3, 77-81	C	C					F	C		R			
10-5, 77-81	C	R					C	R	R	R			
10-CC, 9-13	F						C	C					
11-2, 74-76	F	R					C	C					
11-4, 74-76	C	R					C						
11-6, 74-78	C	F	R				C	F	R		R		
12-1, 73-77	C	R					C				R		
12-3, 73-77	R						C						
12-5, 73-77	Barren												
12-CC, 16-20	Barren												
13-2, 74-78	Barren												
14-1, 73-77	Barren												
14-3, 73-77	C	R	R				R			R			
14-5, 73-77	C	C					C	R	R				
14-CC, 24-26	F	R	R	R			C	F	R	R			
15-2, 74-78	Barren												
15-4, 74-78	Barren												
15-6, 74-78	R												NSPF3
16-2, 74-78	R	F	C				C	R					
16-4, 74-78	F		C	C			C	C					
16-6, 69-73	Barren												
17-1, 72-75	Barren												
17-3, 72-75	F	F	C	C	R		C	C					
17-6, 72-75	C	C	C				C	F					
18-1, 78-81	C	R	R	R	R		C	R					
18-3, 78-81							R						
18-5, 78-81	R	C	R	R			F						
18-CC, 10-13	C	C		R			F		R				
19-2, 68-71	R	R					C	R					
19-4, 68-71	R	C		R			F	F	R		R		
19-6, 68-71	C	C	R	R	R		F	C					
19-CC, 46-49	R	R		R			F	R					
Rest of hole barren.													

Note: A = abundant; F = frequent; C = common; R = rare.

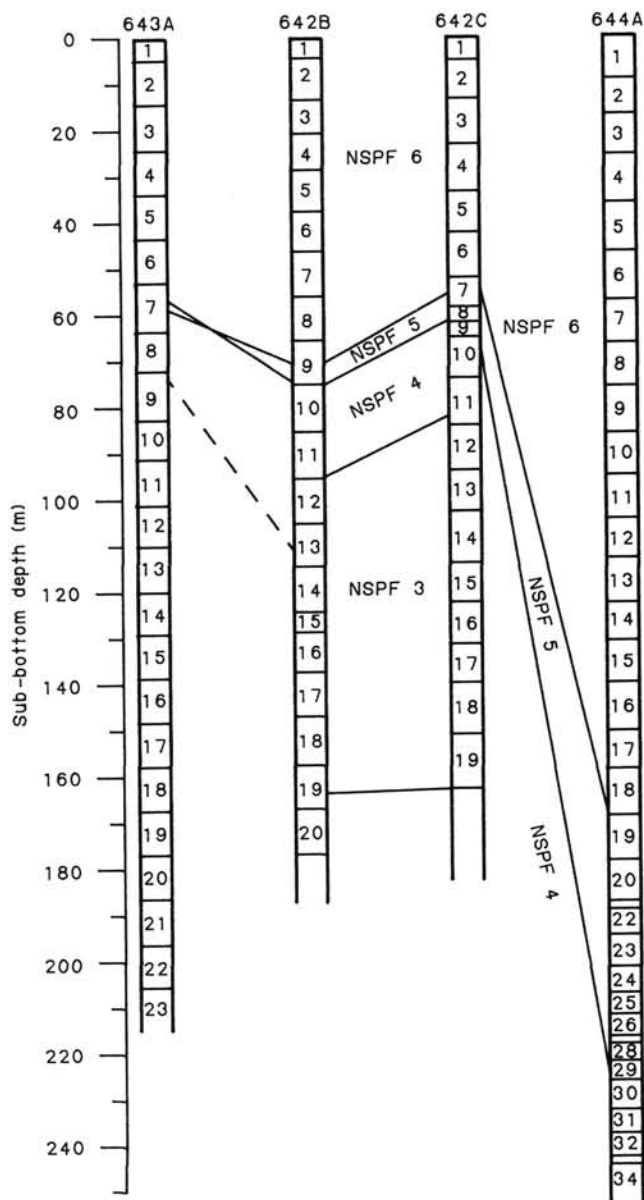


Figure 44. Informal local zonation based on neogloboquadrinids. For discussion, see the section on planktonic foraminifer stratification. NSPF = Norwegian Sea planktonic foraminifer zone.

Two changes in dominant coiling direction of *Neogloboquadrina* species have been recognized and may have regional significance as they also seem to appear in high-latitude records from the North Atlantic. Above 110.90 mbsf in Hole 642B (104-642B-13H-5, 73-78 cm) and at 108.35 mbsf in Hole 642C (104-642C-14H-5, 73-77 cm) sinistrally coiled *N. pachyderma* dominate strongly, whereas dextrally coiled specimens dominate or are much more common beneath. A similar change in coiling direction for this species in the North Atlantic was described and dated by Weaver (in press), Hooper and Weaver (in press), and Weaver and Clement (in press). A change in coiling direction for *N. atlantica*, from mixed dextrally and sinistrally coiled specimens below to dominant sinistrally coiled specimens above, appears at 124.76 mbsf in Hole 642B (104-642B-15H-2, 74-78 cm) and at 122.76 mbsf in Hole 642C (104-642C-16H-2, 74-78 cm).

cm). Berggren (1972) and Poore and Berggren (1975) have used this change to define the Miocene/Pliocene boundary in the North Atlantic. The data of Weaver and Clement (in press) tie this event to magnetostratigraphy which shows this to have occurred within the late Miocene at about 7.0 Ma.

Beneath 162.95 m in Hole 642B and 158.50 m in Hole 642C, the sediments are completely barren in planktonic foraminifers.

Preliminary Planktonic Foraminiferal Zones

Based on the assemblages of this study, a preliminary planktonic foraminiferal zonation can be established. The zones are local, and are only used as informal zones for correlation purposes within this volume.

Zone NSPF3

Base: FA of planktonic foraminifers.

Top: LAD *N. continuosa*.

Interval: 93.30–162.95 m in Hole 642B, 81.26–158.50 m in Hole 642C.

Age estimate: middle Miocene(?) to early Pliocene (ca. 4.5 Ma).

Zone NSPF4

Base: LAD *N. continuosa*.

Top: LAD *N. atlantica*.

Interval: 75.80–93.30 m in Hole 642B, 60.50–81.26 m in Hole 642C.

Age estimate: early Pliocene (ca. 4.5 Ma) to late Pliocene (ca. 2.3 Ma).

Zone NSPF5

Base: LAD *N. atlantica*.

Top: FAD *N. pachyderma* (sin.) encrusted.

Interval: 71.66–75.80 m in Hole 642B, 56.16–60.50 m in Hole 642C.

Age estimate: late Pliocene (ca. 2.3 Ma) to late Pliocene/early Pleistocene (1.7–2.0 Ma).

Zone NSPF6

Base: FAD *N. pachyderma* (sin.) encrusted.

Top: Top of sediment.

Interval: 0–71.66 m in Hole 642B, 0–60.5 m in Hole 642C.

Age: 0–1.7 Ma. Early to late Quaternary.

Preservation and Diversity

Planktonic foraminifers occur in variable amounts down to 158.5 mbsf (104-642C-19H, CC). Beneath this level no planktonic foraminifers were found except a very limited number of extremely etched specimens. This barren zone stretches from the middle Miocene to the lower parts of the lower Miocene. A number of barren samples were found also in the upper 158.5 m. Almost all of these contain either large amounts of detrital mineral grains or abundant volcanic glass particles. The preservation is very good to moderate down to 112.5 mbsf and good to moderate between 125.8 and 158.5 mbsf. No interval of particularly badly preserved planktonic foraminifers has been found in the upper parts of the section.

Down to 56.9 mbsf (104-642B-7H, CC) planktonic foraminifers dominate over benthic. Between this level and down to 114.0 mbsf (104-642B-13H, CC) the planktonic to benthic ratio is variable, with some samples having higher planktonic than benthic content, and others showing the opposite. Deeper than 128.1 mbsf (104-642-15H, CC), benthic foraminifers in most samples strongly dominate over planktonic ones.

The diversity of the planktonic assemblages is generally low with 1–6 species normally found within a sample. The highest diversity is found in samples within the upper parts of zone NSPF3 and in zone NSPF4.

Paleoenvironment

The assemblages of zone NSPF6 are polar to subpolar and reflect stadial to interstadial conditions associated with variations in inflow of North Atlantic Drift water in connection with glacial cycles. The environmental signals contained in the assemblages of the lower zones are more difficult to interpret owing to existence of assemblages that have no modern analogs.

The assemblages of the Zones 5 and 4 indicate subpolar environments. Both *G. bulloides*, *G. falconensis*, and *N. pachyderma* are subpolar species. The extinct species *N. atlantica* has also been interpreted as a subpolar species (Berggren, 1972; Poore and Berggren, 1975). None of the typical temperate species from the Pliocene have been recorded, thus further indicating a generally subpolar environment throughout the zone. *N. pachyderma* (sin.) dominate over *N. pachyderma* (dex.), which could indicate a rather cold environment. However, the climatic inferences that might be made from the coiling direction of *N. pachyderma* are not as straightforward in the Pliocene/Miocene as in the Pleistocene (Kennett and Srinivasan, 1981). In parts of the zones the diversity increases and *G. bulloides* strongly dominate over *N. pachyderma*. These parts indicate more favorable, probably warmer conditions near the early to middle Pliocene and a trend of cooling toward the late Pliocene.

The barren samples in the sediment section above 158.5 mbsf are most likely the result of episodes with increased non-biogenic sedimentation, mainly by pyroclastic ashfalls. Yet, the changing content of planktonic foraminifers and the variable planktonic-to-benthic ratio (Fig. 45) also leave open the possibility that periods with low productivity or high dissolution might have occurred.

The restricted assemblages of the lower parts of Zone NSPF3, together with lack of influence of temperate species, also indicate rather cold, subpolar conditions in this interval. The increased diversity and planktonic foraminiferal content upward in the zone might reflect improvements in living conditions. Still, the low planktonic-to-benthic ratio (Fig. 45) points to either low productivity or significant dissolution in the zone.

Below 158.5 mbsf the whole section is barren in calcareous foraminifers. The barren interval beneath NSPF3 indicates a significant lowering of the CCD from an extremely high position in the early to middle Miocene to a much deeper position in the late Miocene. This dramatic event is most likely linked with a major change in water circulation in the Norwegian Sea, possibly with a major inflow of Atlantic Surface Water. The preliminary age estimate for this event is middle Miocene. It is interesting to note that this age may correspond to the mid-Miocene 18-O enrichment and Antarctic ice-sheet buildup.

Benthic Foraminifer and Calcisphere Stratigraphy

Shipboard analysis of the benthic foraminifers in core-catcher samples from Holes 642A through 642D show that there is great variability in species between the individual holes (Table 14). In the samples from Hole 642E we found no foraminifers except for stray specimens that were clearly contamination from the overlying younger sediments. As Hole 642A consisted of only one sample, it will not be discussed further. In addition to the core-catcher samples some core samples were examined to improve the zonation.

Planktonic foraminifers dominate (83%–99% of the total foraminifers) the assemblage in the uppermost part of the sediment sequence cored (Samples 104-642B-1R-7, CC and 104-642C-1H-4, CC). There is a general decrease in frequency of planktonic species downcore (Fig. 45). Benthic foraminifers constitute more than 50% of the total assemblage in samples below approximately 60 m, except Samples 104-642B-6H, CC; 642B-8H, CC; 642B-11H-4; 642C-11H, CC; and 642C-12H, CC. In the arena-

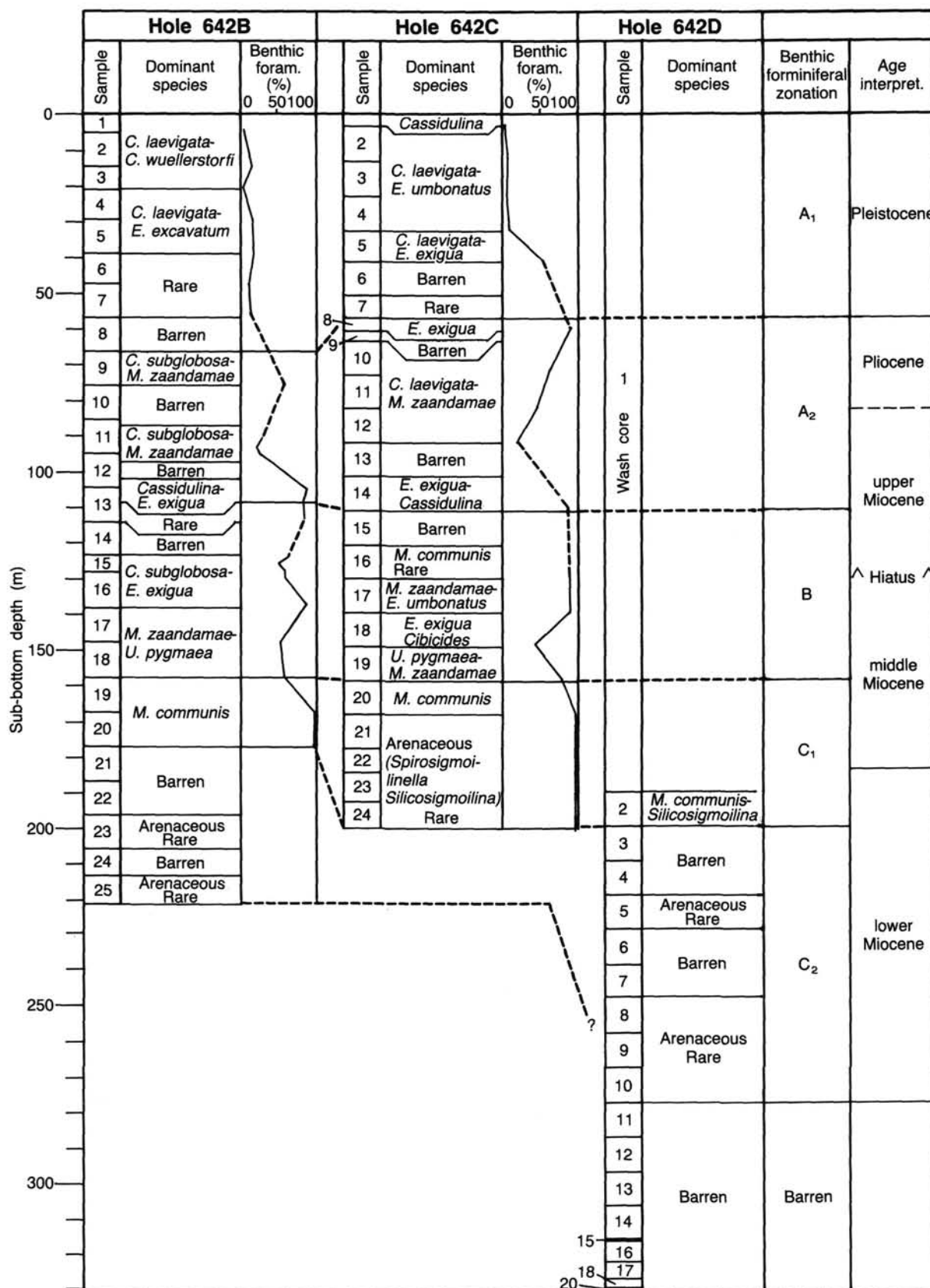


Figure 45. Core intervals in Holes 642B, 642C, and 642D. The characteristic species/species group and the frequency of benthic foraminifers (in % of total foraminifers) indicated for each core refer to the samples studied (mainly core-catcher samples). The benthic foraminiferal zonation is shown on the right side of the diagram. The age interpretations are based upon the other fossil groups.

Table 14. Distribution (in % total benthic foraminifers) of the most important species of benthic foraminifers in samples from Holes 642A through 642D.

Sample interval	<i>Cassidulina laevigata</i>	<i>C. reniforme</i>	<i>C. subglobosa</i>	<i>Eponides umbonatus</i>	<i>Melonis zaandamae</i>	<i>Cibicides</i> spp.	<i>C. wuellerstorfi</i>	<i>Bulimina marginata</i>	<i>Alabamina</i> spp.	<i>Vulvulineria</i> spp.	<i>Elphidium</i> spp.	<i>E. excavatum</i>	<i>Islandiella</i> spp.	<i>Epistominella exigua</i>	<i>Uvigerina pygmaea langeri</i>	<i>Silicosigmolina</i> spp.	<i>Pullenia bulloides</i>	<i>Martinottiella communis</i>	<i>Spirosigmolinella</i> spp.	Other species	% benthic forams	Abundance	Preservation	Other fossils				Reworking								
																								Siliceous fossils	Ostracodes	Bolboforma	Other									
642 A: 1 CC	69	5		17	3						x									6	13	A	G													
642 B: 1 CC	xx			x	x		xx	4	9	7	6		3							—	4	F	G										Transport from the shelf			
2 CC	35	7		6	8	x	4													16	15	F	G	Sp	x											
3 CC	51	5		3	3		28													10	3	F	P													
4 CC	32	3		4	4						x	49								12	15	F	M	Sp												
5 CC	xx	x		x	x			x			xx	x								17	17	F	M													
6 CC	x						x				x									11	11	R	M													
7 CC											x									xx	15	R	M													
8 CC																																				
9 CC	9	55		15																14	60	A	M	Sp, D												
10 CC																																				
11-1, 46-50 cm																																				
11-4, 46-50 cm	12	17		6	20															37	30	C	G	R, Sp	x									Fi, Bv		
11-6, 46-50 cm	x	x		x	x															x	23	F	M	R, Sp	x											
11 CC													xx							x	25	R	M													
12-3, 67-71 cm																																				
12-7, 17-21 cm																																				
12 CC																																				
13-1, 74-78 cm	38	21		6	3					3				x	11					8	91	C	M	R (O, Sp)	x									1 Fi, Sc		
13-3, 74-78 cm	3	14		4	x										72					2	89	C	G	R, Sp (O)	x									Ec		
13 CC						x	x							x							88	R	M	D, Sp, R												
14-1, 79-83 cm																																				
14 CC																																				
15-1, 74-78 cm				4	x					3				51	2					12	65	C	M	R, Sp, D	x										Ec	
15-3, 74-78 cm				x	8		x							62	2					9	50	A	M	R, Sp	x									Fi, Ec		
15 CC				25							x			69						5	60	A	G		x											
16-1, 69-73 cm				32	x	4	3							47						3	62	C	M	R, Sp (O)	x										Fi	
16-3, 69-73 cm																					11	60	A	G	R, Sp	x								Fi		
16 CC				4	5									83						x	90	C	M													
17 CC					10		8							x	12	29					7	53	F	M	D, R	x									Pt, Ec	
18 CC					x	xx			x					x	xx					xx	58	F	M	D, R	x										Ec, Bv	
19 CC																					100	R	P	D, R												
20 CC																					100	R	M	R (O, Sp)												
21 CC																																				
22 CC																																				
23 CC																																				
24 CC																																				
25 CC																																				

Note: Abbreviations: R = rare, F = few, C = common, A = abundant, P = poor, M = moderate, G = good, D = diatoms, R = radiolarians, Sp = sponge spicules, Ec = echinoderm spines, Sc = scolecodonts, Pt = pteropods, Bv = bivalves, Fi = fish remains (teeth, scales, bone fragments), W = wood fragments, X = scattered occurrence.

ceous zone C (Table 14), planktonic foraminifers are absent. The upper 158 m of Holes 642B and 642C contains a highly diverse calcareous assemblage, while only arenaceous foraminifers are found in the lower parts and in Hole 642D. Barren samples are numerous in all three holes.

Hole 642B

Samples from the upper 60 m contain relatively few benthic foraminifers. The uppermost 20 m of the sequence is dominated by *Cassidulina laevigata*, associated with *Cibicides wuellerstorfi*, *Bulimina marginata*, *Melonis zaandamae*, and *Eponides umbonatus* (Table 14). According to Belanger and Streeter (1980) and Streeter et al. (1982), *C. wuellerstorfi* does not inhabit the Norwegian Sea during full glacial periods. Sample 104-642B-3H, CC may therefore represent an interglacial. This is also confirmed by the sediment studies, which showed that this sample contained negligible amounts of ice-rafted debris. The samples from 20 to 40 m depth have considerable amounts of *Elphidium excavatum* and other elphidiids which most likely represent material transported from the shelf. Samples in which *Elphidium* spp. are abundant are barren of *C. wuellerstorfi*. Erosion and transportation of shelf material to deeper waters are likely to have taken place during glacial episodes, and Samples 104-642B-4H, CC and 104-642B-5H, CC probably represent glacial periods. As further support of this, the sediment studies have shown that these samples also contain a considerable amount of ice-rafted material.

Below 70 mbsf in Hole 642B the foraminiferal assemblages still contain *C. laevigata*, but the abundance of *Epistominella*

exigua gradually increases downcore. *E. exigua* is associated with *Cassidulina reniforme* and *M. zaandamae*. Samples 104-642B-17H, CC and 104-642B-18H, CC contain variable amounts of *Uvigerina* spp., mainly *Uvigerina pygmaea langeri*, but also including transitional forms to *U. pygmaea langensfeldensis* (Daniels and Spiegler, 1977), plus *Pullenia bulloides* and *Cibicides* spp.

In Sample 104-642B-19H, CC there is a change from a diverse calcareous to a poor arenaceous assemblage dominated by *Martinottiella communis* in the upper part of the zone and by *Spirosigmolinella* in the lower part.

Hole 642C

The uppermost three samples in this hole have faunas similar to the same interval in Hole 642B, but are generally richer in specimens. Between 25 and 60 mbsf the samples contain few benthic foraminifers. Below 60 mbsf the assemblages gradually become dominated by *E. exigua*, with a strong dominance of uvigerinids (especially *U. pygmaea langeri*), *P. bulloides* and *Cibicides* spp. in Samples 104-642C-17H, CC through 104-642C-19H, CC. At 160 m depth the calcareous fauna is replaced by a meager arenaceous assemblage.

Hole 642D

Samples from this hole are poor, or barren, and contain only arenaceous foraminifers (mainly *M. communis*, *Silicosigmolinella* sp., and *Spirosigmolinella* spp.). The lowermost portion of this hole is barren, except for one specimen of *Cribostrumoides* sp. in Sample 104-642D-17X, CC.

but the presence of different species has been noted in Table 14. The most abundant species occurring are *B. aculeata*, *B. laevis*, *B. clodiusi*, *B. metzmacheri*, and *B. ?spiralis*. Our specimens of *B. aculeata* possess long bifurcating spines and therefore differ from those described by Daniels and Spiegler (1974) from northwest Germany. However, Murray (1984) described similar specimens of calcispheres with bifurcating spines which he called *B. aculeata* (Murray, 1984, Plate 1, Figs. 1 and 2), after examining material from Daniels and Spiegler (1974). *Bolboforma* have been reported from northwest Germany (Daniels and Spiegler, 1974), the North Atlantic (Murray, 1984), and the Antarctic (Rögl and Hochuli, 1976), and appear to be useful stratigraphic markers. They range from the upper Oligocene to the upper Miocene (Daniels and Spiegler, 1974), and Murray (1984) has extended their range into the lowermost Pliocene. The species identified in our material have their main distribution in the middle and upper Miocene. However, one species, *B. spiralis*, described as upper Oligocene to lower Miocene (Daniels and Spiegler, 1974), was found in upper Miocene deposits on the Rockall Plateau (Murray, 1984). At present we doubt that the specimens found at this site belong to *B. spiralis*. This taxonomic problem has to be solved by later studies of more material and will be presented in Part B of Vol. 104.

Comparison to DSDP Leg 38

Six DSDP Sites, 338–342, were drilled on the Vøring Plateau during Leg 38 (Talwani, Udintsev, et al., 1976). Comparison of Site 642 to Leg 38 sites is difficult, first, because of the very incomplete sediment record recovered at the Leg 38 sites, and second, because of the general manner in which the foraminiferal results were presented. Nevertheless, there is good agreement in areas where there is stratigraphic overlap. The uppermost part of Site 642 is very similar to Sites 338, 341, and 342, which contain *C. laevigata* (= *I. teretis*) with *E. excavatum* (= *E. incertum* f. *clavatum*) from glacial periods and *C. wuellerstorfi* from interglacials. The major difference in the sites occurs in the middle and upper Miocene sequence because Leg 38 sites do not record the abundant calcareous assemblages observed in Site 642 Zone B, but this may be owing to lack of recovery at Leg 38 sites. Middle and lower Miocene benthic foraminifer assemblages at both Site 642 and Leg 38 sites are in agreement and show an arenaceous assemblage of *M. communis*, *Spirosigmölinella* and *Spirolocamina*. Sediments containing benthic foraminifers older than early Miocene were not recovered at Site 642.

Paleoenvironment

The calcareous foraminifers and the *Bolboforma* species found in Zones A and B indicate fully marine conditions. The one exception is the presence of the euryhaline species *E. excavatum* in the upper part of Hole 642B, which, as noted above, probably represents transported material. Most of the dominant benthic foraminifers are cosmopolitan species that are typical of deep water, including the Norwegian Sea (Belanger and Streeter, 1980; Sejrup et al., 1981). According to Thiede (1980), the Norwegian–Greenland Sea attained its present size, shape, and depth during the late Miocene. At present, we cannot explain the change from the *C. laevigata* assemblage of Zone A to the *E. exigua*/*M. zaandamae* assemblage of Zone B. Study of more closely spaced samples may solve this problem. The increasing frequency of *M. zaandamae* and *P. bulloides* and decrease of *E. exigua* downcore may reflect increasing bottom water temperatures, and probably decreasing water depths. *P. bulloides* and *M. zaandamae* are abundant in surface samples from the Norwegian continental shelf and upper slope (Qvale, 1985; Sejrup et al., 1981). In addition, the occurrence of *U. pygmaea langeri* also indicates shallower water depths. In the North Sea this species is common in deposits interpreted as outer littoral to epi-

bathyal (King, 1983). The change in the assemblage may also be caused by an environmental change not necessarily related to water depth. However, the decrease in frequency of planktonic foraminifers also indicates decreased oceanic influence. The absence of planktonic foraminifers might be due to an increased dissolution rate or a decrease in surface water productivity. The benthic foraminifers, however, despite some degree of fragmentation, seem not to be affected by dissolution. Most specimens are still transparent and glassy. The abundance of diatoms and *Bolboforma* does not reveal a decrease in surface productivity.

Some samples (104-642B-9H, CC; 642B-11H-4; 642B-15H-1; 642B-15H-3; 642C-8H, CC; and 642C-11H, CC) are characterized by containing very small specimens (dwarfs). In addition to *E. exigua*, which is normally smaller than 150 μm in diameter, small specimens of larger foraminifers are abundant. The occurrence of dwarfs may be the response to unfavorable environmental conditions.

The major change in the cored sequence, the switch from a diverse calcareous fauna to a poor arenaceous one, may have been caused by a major environmental change or may indicate a hiatus. Little is known about the ecology of *M. communis* (Zone C1). Species of the genus *Martinottiella* have been recorded from outer shelf to abyssal depths (Boltovskoy and Wright, 1976). Most of the arenaceous foraminifers observed at this site seem to be very tolerant of environmental changes. The lack of calcareous fossils may be the result of dissolution rather than absence owing to ecologic conditions at the time of deposition. Evidence for this dissolution is found from Sample 104-642D-12H, CC, where molds of dissolved foraminifer tests are possibly preserved as globular glauconite sand-sized grains.

At present, we are not able to fully explain the numerous barren intervals at this site. They may represent periods of low foraminifer production or extensive dissolution. Below 95-m depth at Site 642, the minerogenic sand fraction is mainly volcanic material. Heavy ashfall may kill benthic organisms either by burial, or by sealing off the substrate. Increased silica input from the ashfall may also lead to increased production of siliceous organisms which would lead to the increased decay of organic material, decreased pH, and the increased dissolution of calcareous material.

Palynology of Site 642

Dinocysts (dinoflagellate cysts), pollen, and spores were examined in core-catcher samples and volcanoclastic sediment units (Table 15) from Holes 642A through 642E, located on the Vøring Plateau, 67°13.2'N, 02°55.8'E, at about 1288-m water depth. Palynodebris (kerogen) types in the samples were also noted, but quantitative studies were not made. The methods used to process the palynological samples and to obtain numerical data are described in the "Explanatory Notes" chapter (this volume). The ratio of dinocysts to total pollen and spores (including reworked specimens) was plotted using the same method as Manum (1976) so that the results for ODP Leg 104 and DSDP Leg 38 would be directly comparable. This dinocyst ratio provides an index of the relative proportion of marine vs. terrigenous organic matter in the sediments, and it may provide approximate paleodepth estimates.

Figure 46 shows the ranges of the main dinocyst chronostratigraphic markers in Holes 642B, 642D, and 642E and the dinocyst ratio (D/P) for these samples. Table 16 lists the pollen and spore distributions and relative amounts of palynodebris. Only four samples from Hole 642C (Cores 104-642C-1H and 104-642C-22H through 104-642C-24H) were examined, which overlap with Hole 642B and have been included with data for Cores 104-642B-1H and 104-642B-21H through 104-642B-23H. Nine informal palynozones (PM) are tentatively delimited, based primarily on the stratigraphic ranges of well-known Neogene

Table 15. Samples examined for palynomorphs in Hole 642E.

Core, section and interval (cm) 104-642E-	Sub-bottom depth (m)	Volcaniclastic unit no.	Lithological characteristics (from shipboard petrology & microscopy)
2W-02, 70-72	320.22	S3	Gray sandy mud
2W-02, 120-124	320.74	S3	Gray sandy mud
2W-03, 8-9	321.09	S3	Gray mud above pebble horizon
4R-01, 0-4	326.50	S3	Muddy pebble horizon
5R-01, 20-22	335.10	S4	Dark red-brown, basaltic vitric tuff, Mn, Cu-rich
7R-02, 112-117	356.97	S6	Dark red-brown tuff, basaltic vitric feldspar and quartz grains well rounded
12R-01, 64-65	387.85	S8	Dark brown basaltic vitric tuff
12R-CC	395.80	?	Poorly sorted feldspar and quartz
19R-05, 3-5	450.10	S10	Dark red-brown tuff; subrounded feldspar and quartz grains; basaltic vitric, well sorted; few fresh shards
21R-01, 21-23	461.20	?S10	Probably rubble displaced from S10
23R-01, 114-115		S12	Well-sorted basaltic vitric tuff
25R-03, 80-85	498.95	S15	Red-brown, basaltic vitric bedded tuff; angular feldspar and quartz; fresh shards
27R-02, 45-60	514.80	S16, base	Gray-to-brown basaltic vitric tuff, partly well-sorted & graded; fresh shards; angular feldspar
31R-01, 0-2	549.50	?	Basaltic vitric tuff, probably displaced from top of flow Unit 36 at 539.5 m; poorly sorted feldspar-quartz
31R-01, 150	550.00	(Unit not logged)	Poorly sorted angular feldspar-quartz
33R-01, 140-144	566.34	S18	Red-brown basaltic vitric tuff
34R-01, 13-16	574.56	?S18	Red-brown basaltic vitric tuff, probably displaced from S18
35R-02, 6-7	586.97	S19	Top of red-brown basaltic vitric tuff with 3 graded beds; thin silt parting with common biosiliceous material
35R-02, 100-110	588.00	S19	Top of lowest graded bed in Unit S19
35R-02, 111-113	588.30	S19	Base of graded bed in Unit S19
42R-01, 56-57	650.67	S21	?Middle of upper bed in graded, well-sorted red-brown basaltic vitric tuff with some shards
42R-01, 75-76	650.86	S21	?Top of middle bed, Unit S21
42R-01, 94-95	651.05	S21	?Middle of middle bed, Unit 21
42R-01, 110-111	651.21	S21	?Base of middle bed, Unit S21
45R-01, 6-7	678.60	S22	Top of reworked dark red-brown basaltic vitric tuff
54R-02, 65-66	740.86	S26	Dark red-brown to dark-gray basaltic vitric tuff with graded beds; dark gray and well sorted from 65-66 cm
54R-02, 69-71	740.91		Red-brown tuff, fining up from 74-64 cm
54R-02, 78-80	741.00		Dark red-brown bed, sandy top 81-74 cm
54R-02, 87-88	741.08		Dark-brown silt below rounded clasts at 82-83
54R-02, 108-109	741.29		Brown silt below lapillistone and clasts from 104-108 cm
55R-02, 88-90	750.60	S27	Dark red-brown basaltic vitric tuff with uniform texture; abundant fresh shards
67R-01, 1-3	844.20	S30	Dark red-brown vitric-lithic tuff or sandy siltstone with vesicular clasts; nonvitric; no shards
77R-01, 14-16	931.06	S34	Dark brown vitric tuff with coarse silt matrix around vesicular clasts
85R-05, 125	1015.05	S39	Dark red-brown vitric lithic tuff, well sorted with graded beds
86R-02, 82	1019.62	S40	Dark red-gray brown vitric lapillistone tuff, well-sorted, grading upward from 93-85 cm; fresh shards
87R-01, 122	1026.52	S41	Dark brown-dark red-brown basaltic lithic vitric tuff, moderately well sorted, with deformation structures in coarse beds
94R-01, 20-24	1085.24	S44	Dark red-brown massive lithic vitric tuff with intervals of sorted graded beds, interspersed with homogeneous/bioturbated beds
94R-04, 20-24	1091.24		Bioturbated interval
95R-01, top	1094.50		
95R-03, base	1099.00		
96R-01, 24	1102.74		
98R-01, top	1115.80	?S46	?Basaltic vitric clast, probably displaced from higher unit
109R-01, 85	1211.25	?S47	Gray? vitric lithic tuff, fine grained with bioturbated intervals
110R-01, base	1229.40	Basalt	END OF HOLE

North Atlantic dinocysts (Williams, 1977; Harland, 1979; Edwards, 1984; Mudie, 1985) and on the ranges of diagnostic Paleogene species (Manum, 1976; Drugg and Stover, 1977; Williams, 1977; Costa and Downie, 1979; Elde, 1985; Brown and Downie, 1984). These dinocyst ages are supported by pollen and spore ages documented by Koreneva et al. (1976) for Leg 38 and by correlation with data from Neogene stratotypes (Suc and Zagwijn, 1983).

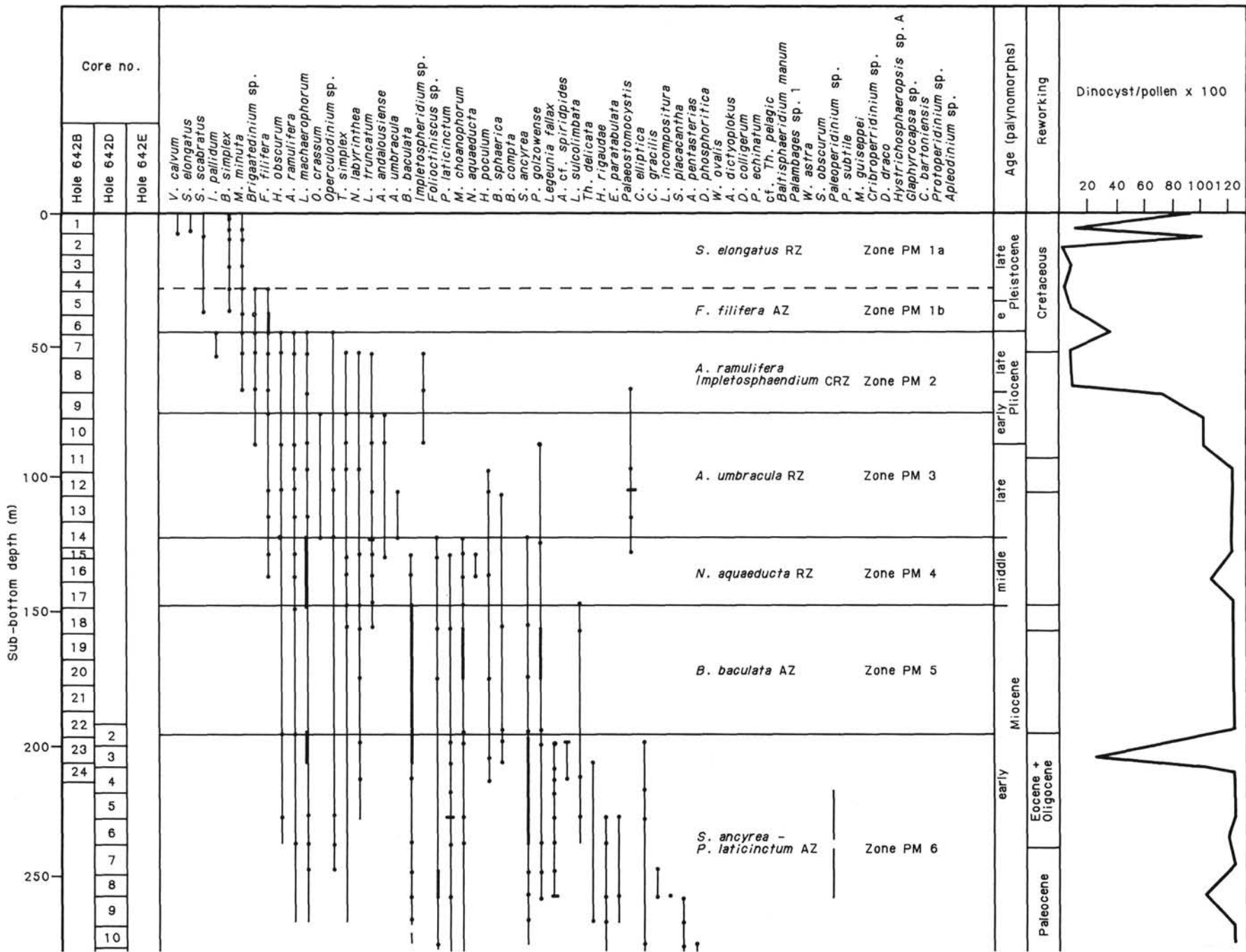
Problems regarding precise dating of the oldest sediments at Site 642 require that palynozones be described in descending order, starting at the top of the section where age designation is certain. Informal names are proposed for the palynomorph zones, based on either the most important range zone (RZ) or concurrent range zone (CRZ) taxa, or on species that have well-defined acme zones (AZ). It is important to note, however, that this zo-

nation is both tentative and informal because it is impossible to define precise palynostratigraphic zones from core-catcher samples alone. Onshore studies of samples from each section of cores from Holes 642B, 642C, and 642D are being made that will undoubtedly result in a more precise palynostratigraphy for ODP Site 642.

Zone PM1: (104-642B-1H-1, 0-2 cm, to 104-642B-6H, CC, 0-47.4 m)

Informal names: *Spiniferites elongatus* Range Zone (PM1a) and *Filispheera filifera* Acme Zone (PM1b).

Samples 104-642A-1H, CC; 642B-1H, CC to 642B-5H, CC; and 642C-1H, CC contained a small diversity of well-preserved Quaternary dinocyst, pollen, and spore taxa. Dinocyst assemblages at the top of the section are dominated by *Operculodi-*



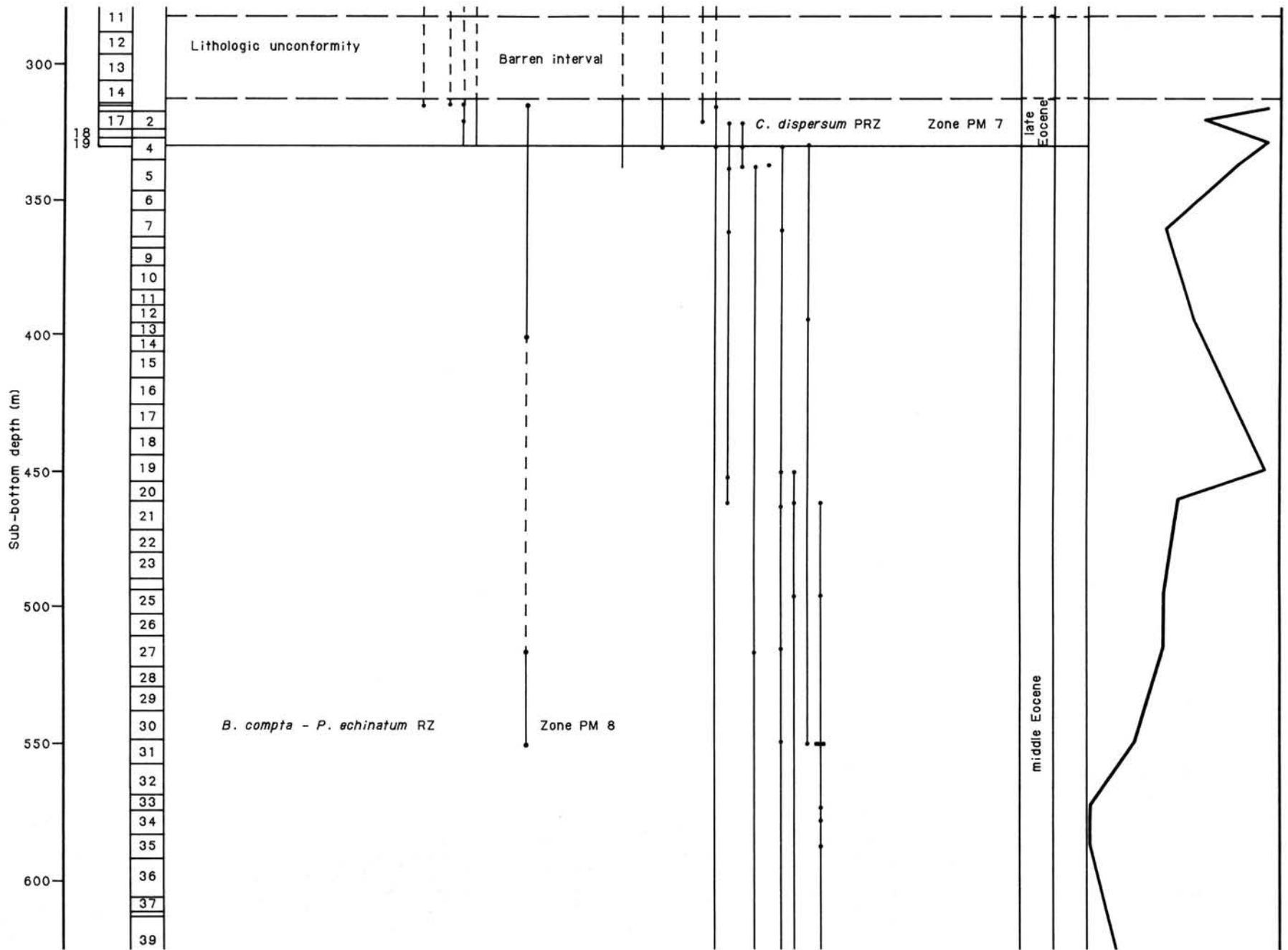
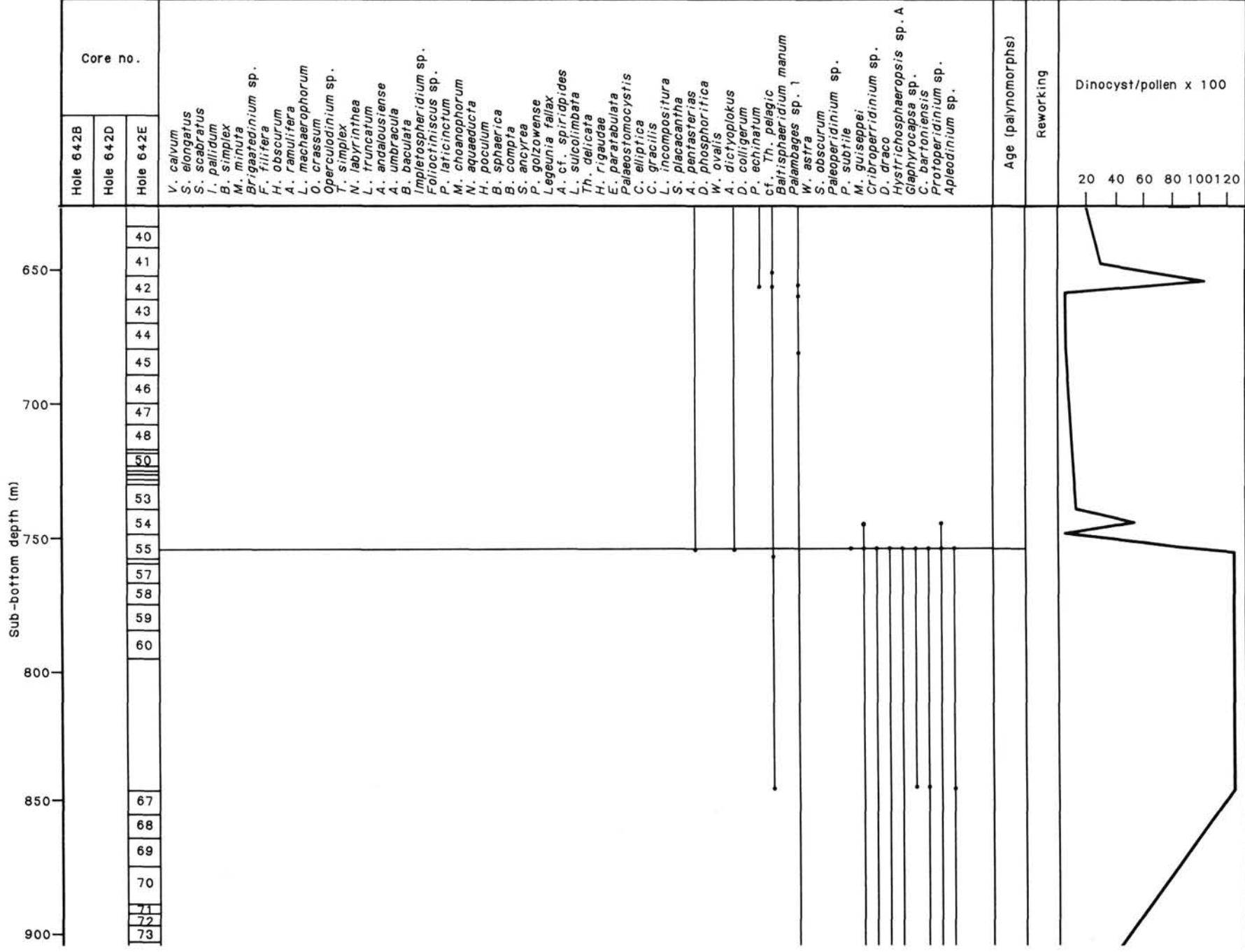
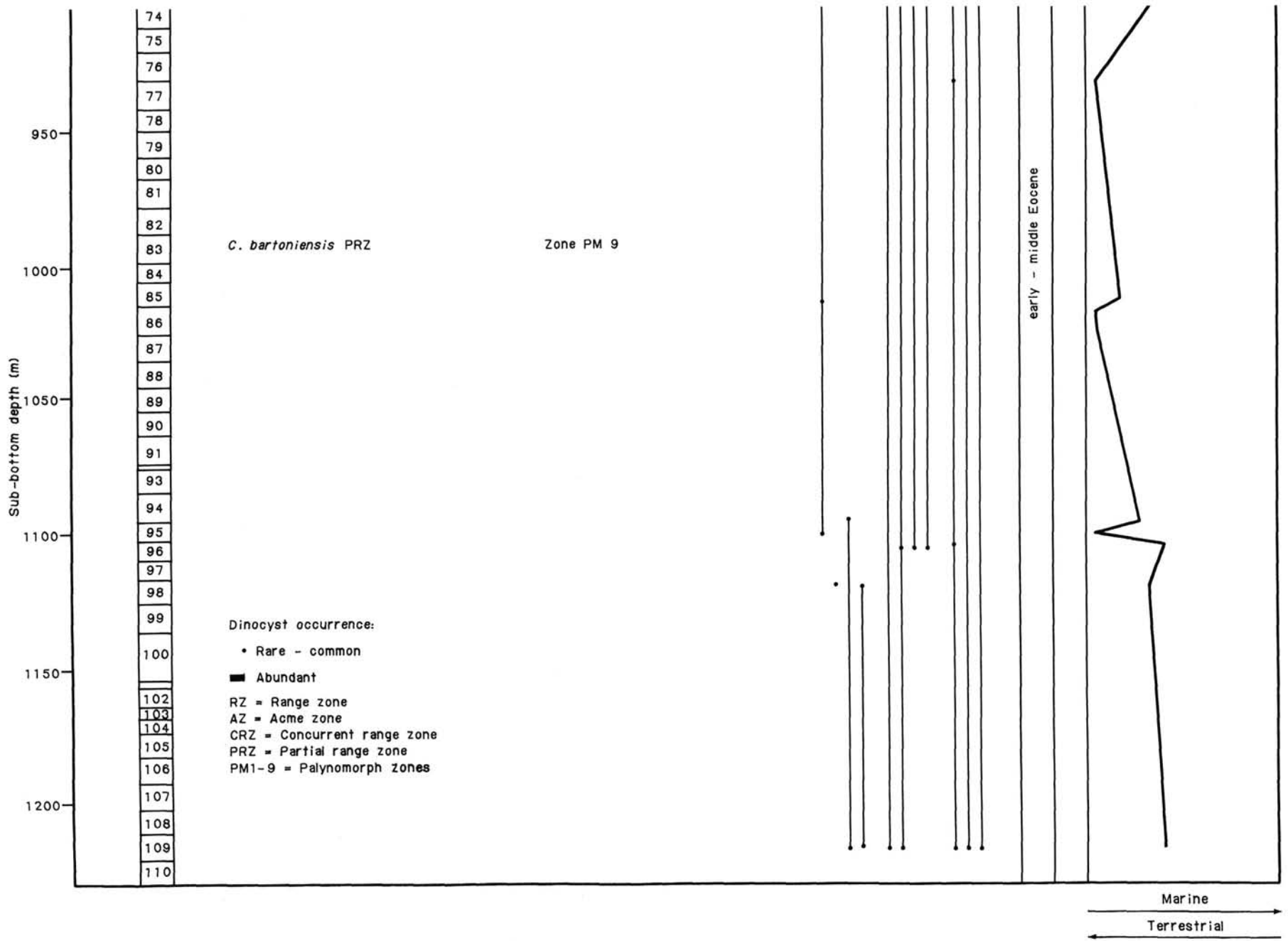


Figure 46. Dinocyst range chart and palynozones, Site 642.





SITE 642

Figure 46 (continued).

Table 16. Pollen and spore distribution and relative amounts of palynodebris, Holes 642B and 642C.

Hole	Core Section Sample	Preservation	<i>Pinus</i> cf. <i>P. sylvestris</i>	<i>Picea</i> cf. <i>P. mariana</i>	Gramineae	<i>Lycopodium reticulatum</i>	<i>Pinus</i> cf. <i>P. banksiana</i>	<i>Sphagnum</i>	<i>Carya</i>	<i>Fagus grandis</i>	<i>Alnus</i> cf. <i>A. viridus</i>	<i>Betula</i> sect. <i>Nanae</i>	<i>Osmunda regalis</i>	<i>Polypodium</i> cf. <i>P. reniforme</i>	<i>Pteridium</i> cf. <i>P. aquilinum</i>	<i>Castanea</i> sp.	<i>Gleichenia</i> sp.	<i>Betula</i> cf. <i>B. alba</i>	<i>Podocarpus</i> sp.	<i>Taxodium</i>	<i>Sequoia</i> sp. 1	<i>Juglans</i> sp.	<i>Tsuga</i> cf. <i>T. ignicula</i>	Ericales	<i>Selaginella</i>	
642B	1 CC	p	r	r		r																				
	2-1, 0-5	g	r		f	r																				
	2 CC	p	+																							
	3 CC	m	r	r																						
	4 CC	m	f	f			r	r	r	r																
	5 CC	m	f	f	r						r	r		f	r	r	r									
	6 CC	m	f	f					r					r	r			r								
	7 CC	m	a	a					f										r	r	c	r	r	+	r	
	8 CC	m	r	r																						
	9 CC	m	c	c		f	f		r							f				f	r					r
	10 CC	g	c	f	r											f					f					r
	11 CC	m	r	r												f								r		r
	12 CC	g	f	c												f								r		r
	13 CC	m	f	f					r																	
	14 CC	g	c	f				r								r										
	15 CC	g	a	c											r						c		r			
	16 CC	g	a	a																r		c				
	17 CC	g	a	a											r						c	r				
	18 CC	g	c	f																	c					
	19 CC	g	r	r																		r				
	20 CC	g	r	r																		r				
	21		No data																							
	22 CC	g	c	f																		r	r			
	23 CC	m	c	c																						
	24 CC	g	f	c																r	r					
25 CC	g	f	a																r	r	c					
642C	1 CC	m		c				f																		
	22 CC																									
	23 CC	g	c	a					r			r									c	f				
	24 CC	g	f	f																	f					

Note: Preservation: p = poor, g = good, m = moderate. Occurrence: r = rare, f = few, c = common, a = abundant, + = fragments.

nium centrocarpum (interglacial sediments) or *Multispinula minuta*, *Brigantedinium simplex*, *Bitectatodinium tepikiense*, and *Spiniferites* spp.; *Filisphaera filifera* becomes dominant in Samples 104-642B-5H, CC and 104-642B-6H, CC (29.4–38.9 mbsf). Quaternary sporomorph assemblages are dominated by *Pinus*, *Picea*, and *Sphagnum* species. Large numbers of reworked Cretaceous-Paleogene sporomorphs, dark-brown (thermally altered) wood fragments, and coaly (black, highly carbonized) particles are present in all samples except the surface carbonate ooze.

Comparison and Age

Zone PM1 is delimited primarily by the range of *B. simplex* (104-642B-1H-1, 0–2 cm, to 104-642B-5H, CC) and *Spiniferites scabratus* (104-642B-2H-1, 0–2 cm, to 104-642B-5H, CC). The base of the zone is marked by the LAD of *Achomospaera ramulifera*, *Hystrichosphaeropsis obscurum*, *Operculodinium* sp. of Jan du Chêne (1977) and *Lingulodinium machaerophorum*, all of which occur in Sample 104-642B-6H, CC (47.4 mbsf). The LAD of *A. ramulifera* is a well-known marker of the Pliocene-Pleistocene boundary in the North Atlantic (Williams, 1977; Mudie, 1986), and in DSDP Hole 611A on the southeastern Rekjanes Ridge, *H. obscurum* and *Operculodinium* sp. of Jan du Chêne both disappear at the top of the Olduvai magnetochron. Zone PM1 is therefore undoubtedly of Pleistocene age.

Zone PM1 is subdivided into Subzones PM1a (0–29.4 mbsf) and PM1b (29.4–47.4 mbsf) based primarily on the LAD of *F. filifera* in Sample 104-642B-4H, CC. At DSDP Sites 611 and 607 (Mudie, 1987), this datum corresponds to the Jaramillo magnetochron (0.94 Ma). Subzone PM1a is marked by the FAD of *Spiniferites elongatus*, *Votadinium calvum*, and *Protoperidinium faeroense* in Samples 104-642B-2H-1, 0–2 cm, and 104-642C-1H, CC. Subzone PM1a corresponds closely to the late Pleistocene dinocyst Zone IIIb at DSDP Site 611, and, in part, to dinocyst Zone IV at DSDP Site 400, Bay of Biscay (Harland, 1979).

Subzone PM1b is of early Pleistocene age and corresponds closely to Subzone IIIa at Site 611. At Site 642 and other sites on the Vøring Plateau, however, there is a sparsity of typical subarctic oceanic species, e.g., *Nematosphaeropsis labyrinthea* and *Impagidinium* spp., which presently occur in the eastern Norwegian Sea (Harland, 1983). Closely spaced samples, however, show that these species are present at sporadic (?interglacial) intervals in the Pleistocene sediments (Mudie, in prep.). The sporomorph genera *Tsuga* and *Osmunda* have their LAD in the early Pleistocene Subzone PM1b. These datums are in accord with the zonation of Williams and Bujak (1977) for eastern Canada, for Site 611 (Mudie, 1987) and for northwest European stratotypes (Suc and Zagwijn, 1983). Koreneva et al. (1976) give

Table 16 (continued).

Chenopodiaceae sp. Koreneva	Carpinus sp.	Larix	Fagus sp. Koreneva	Betula sp. Koreneva	Pteridium sp. Koreneva	Osmunda sp. Koreneva	Abies	Cedrus cf. C. perlatata	Botrychium sp.	Tricolporopollenites	Quercus	Alnipollenites sp.	Ulmus	Pterocarya	Tsuga sp. cf. Koreneva Pl 1	Cyathea sp. cf. Koreneva	Salix sp. (Tricolpites sp. 2. Koreneva)	Tricolpites sp. 1. Koreneva	? Proteacidites sp.	Polytrichum spores	Trilete spore 1	Lycopodium sp. Koreneva	Amorphogen	Woody/herbaceous	Coaly	DR sporomorphs																
	r f	f		r f r	r	r	r r r r r	r r r r	r	r	r r r r	r	r r f r	r r r	r		r r r	r r	r			r r c c	r c	c a c c	c c a c	c c c c	c f f f	a r	r f	c c	r r	c f	f r	r r	a a a c	c f f	r	a c	f c a	r	a	r
		c			f		r r	r		f					r			r		f		r		f	c	a																

older ages (Miocene-Pliocene) for the LAD of these genera at DSDP Sites 338 and 348, however, presumably owing to limited recovery and sampling of Pleistocene sediments.

Paleoenvironment

Palynomorphs in Zone PM1 are all characteristic of Pleistocene glacial-interglacial sediment cycles in the North Atlantic, and large fluctuations in D/P probably reflect variations in terrigenous sediment influx that accompany changes in sea level and the deposition of ice-rafted debris (Manum, 1976; Mudie and Asku, 1984; Asku and Mudie, 1985a; Mudie and Short, 1985; Harland 1984a, b). Dinocyst assemblage composition is similar to that found below modern subarctic-arctic surface waters in the North Atlantic and Baffin Bay (Harland, 1983; Mudie and Short, 1985). Sporomorph assemblages are also characteristic of marine sediments in modern subarctic to arctic regions (Mudie, 1982; Mudie and Short, 1985). The low numbers of Neogene pollen and spores indicate long-distance eolian transport from forest-tundra vegetation (Zone PM1a) and from boreal forest vegetation (Zone PM1b).

Zone PM2: (104-642B-6H, CC to 104-642B-9H, CC; 47.4-75.9 m)

Informal name: *Achomosphaera ramulifera*-*Impletosphaeridium* Range Zone.

Dinocyst assemblages in Zone PM2 of Hole 642B are dominated by *F. filifera*, *O. centrocarpum*, *Brigantidium* spp., and

Impletosphaeridium spp. Dinocyst species diversity is more than twice as high as in Zone PM1. Typical oceanic species, e.g., *N. labyrinthica* and *Impagidinium pallidum*, are sporadically present in addition to the oceanic-neritic species listed above. Neogene pollen and spores are still dominated by bisaccate pollen, *Pinus* and *Picea*, but species diversity is much higher than in Zone PM1. Scattered specimens of *Tsuga*, *Podocarpus*, and *Taxodium* are present, along with *Betula*, *Carpinus*, and rare *Juglans*. Neogene spores include *Pteridium*, *Lycopodium*, and *Selaginella*, in addition to *Sphagnum*. Abundant reworked (Mesozoic-Paleogene) bisaccate pollen and spores occur at the top of Zone PM2 (Samples 104-642B-6H, CC and 104-642B-7H, CC), followed by a rapid decrease downhole, and disappearance at the base of the zone (Sample 104-642B-9H, CC). Likewise, highly altered wood and black coaly fragments are abundant at the top of the zone, but only unaltered wood fibers/tracheids are present at the base.

Comparison and Age

The top of Zone PM2 is delimited by the LAD of *A. ramulifera*, *H. obscura*, *L. machaerophorum*, and *Operculodinium* sp. of Jan du Chêne (1977) in Sample 104-642B-6H, CC. Most of these species disappear at or near the Pliocene/Pleistocene boundary at the top of dinocyst Zone II at DSDP Site 400 (Harland, 1979). *I. pallidum* also has its LAD at the Zone PM2/1 boundary, which corresponds exactly to its LAD at Bering Sea DSDP Leg 19 sites (Bujak, 1984) and agrees well with its disappearance at the Reunion magnetic event (2.0 Ma) in CESAR Core 14

from the Central Arctic Ocean (Asku and Mudie, 1985b). *Tectatodinium simplex*, *N. labyrinthea*, *Labyrinthodinium truncatum*, and *Impletosphaeridium* spp. also disappear just below the Zone PM2/1 boundary in Sample 104-642B-7H, CC (56.9 mbsf). This LAD of *Impletosphaeridium* spp. agrees with the dinocyst zonation for DSDP Site 611, but at this lower latitude site, *T. simplex* and *L. truncatum* disappear earlier, at the dinocyst Zone I/II boundary, which corresponds to the middle of the Nunivak magnetic event (4.1 Ma). At Site 642, the LAD of *Palaeostomocystis* spp. and the FAD of *M. minuta* occur near the middle of Zone PM2, in Sample 104-642B-8H, CC (66.4 mbsf). At Site 611, the LAD of *Palaeostomocystis* spp. corresponds to the top of the Gauss magnetic event (2.48 Ma).

The base of Zone PM2 is marked by the LAD of *Achomosphaera andalousiense* and *Operculodinium crassum* in Sample 104-642B-9H, CC (75.9 mbsf). At Site 611, the LAD of *A. andalousiense* lies just below the base of dinocyst Zone II and it corresponds to the top of the Sidufjall magnetic event (4.41 Ma), whereas the LAD of *O. crassum* occurs at the base of the Gauss chron (3.4 Ma), marking the early/late Pliocene boundary. Thus Zone PM2 is of early-late Pliocene age, and by correlation with Site 611, the base of the zone has a maximum age of 4.41 Ma. General support for this age assignment is provided by the LAD of the pollen genera *Podocarpus*, *Taxodium*, and *Sequoia* in Zone PM2 (Sample 104-642B-7H, CC). In northwestern Europe (Leopold, 1969) and in eastern Canada (Williams and Bujak, 1977), these genera disappeared between the late Pliocene (Brunsumanian Stage, ca. 3 Ma) and the base of the Cromerian Stage (ca. 1.5 Ma).

Paleoenvironment

The increase in species diversity of the dinocyst assemblages in Zone PM2 is mainly owing to the presence of subtropical-temperate oceanic species, e.g., *N. labyrinthea*, *H. obscurum*. The presence of *L. machaerophorum* and *Palaeostomocystis* spp. may indicate lower than normal surface salinity (Williams, 1977; Harland, 1983; Mudie, 1986). The occurrence of the high latitude (Bering Sea-Arctic Ocean) taxa *I. pallidum* and *F. filifera* suggests a strong mixing of cold Arctic and warm Norwegian Current water. Pollen assemblages indicate a mixture of boreal and warm temperate forest vegetation onshore. The presence of *Taxodium* and *Sequoia* pollen suggests that climate was warm and moist in some regions, with summer and winter maxima of 24°C and 6°C, respectively (i.e., the present-day limits of *Taxodium*). The reduction of reworked sporomorphs in Zone PM2 coincides with the cessation of ice-rafted debris influx.

Zone PM3: (104-642B-9H, CC to 104-642B-14H, CC; 75.9–123.5 m)

Informal name: *Amiculosphaera umbracula* Range Zone.

Dinocysts and pollen are numerous and well preserved in this zone. Assemblages contain mostly the same species as Zone PM2, but dinocyst diversity is greater owing to the addition of several Miocene taxa. Dinocyst assemblages are dominated by *A. ramulifera*, *L. truncatum*, and *Palaeostomocystis* spp., which reached an acme in the lower part of the zone (Sample 104-642B-12H, CC, 104.2 mbsf). *L. machaerophorum* and *H. obscurum* are also common. In the upper part of the zone, there are sporadic occurrences of *Spiniferites splendidus* and a short-lived peak of *Impagidinium patulum* (Core 104-642B-10H, CC). In the lower part of the zone, *Amiculosphaera umbracula*, *Hystrichokolpoma* cf. *H. poculum* Harland (1979) and *Lejeunia* sp. 1 are present. Pollen and spore assemblages are dominated by *Picea*, *Pinus*, and *Pteridium* spp., with minor amounts of *Tsuga* or *Taxodium*, *Cedrus*, and *Podocarpus*. Small numbers of *Alnus*, *Betula*, and *Ericales* pollen are also present. Palynodebris in most samples includes about 30% amorphogen. Abundant reworked

Cretaceous-Paleogene bisaccates, spores, and coaly fragments are found in Samples 104-642B-10H, CC and 104-642B-12H, CC, but the other samples contain only small amounts of well-preserved wood fibers.

Comparison and Age

The top of Zone PM3 is marked by the LAD of *O. crassum* and *A. andalousiense* in Sample 104-642B-9H, CC. The ranges of *O. crassum*, *A. umbracula*, and *Lejeunia* sp. 1 are restricted to this zone in Hole 642B, and the base of PM3 is marked by the FAD of these species in Sample 104-642B-14H, CC. This boundary also marks the top of the *L. machaerophorum* acme in the underlying Zone PM4 and the LAD of *Melitosphaeridium choanophorum*, *Systematophora ancycra*, and *P. golzowense*. These three species disappeared in the early-late Miocene at DSDP Sites 553 and 551, Rockall Bank (Edwards, 1984), at Site 400, Bay of Biscay (Harland, 1979), and at the middle/upper Miocene stratotype near Gram, western Denmark (Piasecki, 1980). Dinocyst Zone PM3 can be correlated, in part, with dinocyst Zone 1b at DSDP Site 611, which is of late Miocene-early Pliocene age (10.1–4.41 Ma). The LAD of *O. crassum* at Site 611 corresponds to the top of Chron 7, which marks the base of the Messinian Stage (6.8 Ma), thereby providing some evidence that there is a hiatus between 7.4 and 12.4 Ma in the upper Miocene sediments of Hole 642B. If the interval containing the acme of *Palaeostomocystis* spp. (104-642B-11H, CC to 104-642B-13, CC, 94.9–114 mbsf) corresponds to the Pontian Stage, however, this correspondence provides evidence for a semi-isolated regional marine flora in the Norwegian Sea from ca. 8.8–6.8 Ma, which is the age of the Pontian Stage according to the most recent chronostratigraphic revision by Rögl and Steininger (1984).

Paleoenvironment

At present there is insufficient knowledge of Miocene-lower Pliocene dinocyst assemblages to make definite statements about the marine paleoenvironment in Zone PM3. By comparison with assemblages at DSDP Sites 611, 555, and 400, however, there is a low representation of typical temperate North Atlantic oceanic species. Conversely, in Zone PM3 there are large numbers of *Palaeostomocystis* species which dominate the brackish water, marginal marine sediments in the Pontian stratotype (Baltes, 1971). Pollen and spore assemblages in Zone PM3 mainly indicate a boreal-temperate climate similar to Zone PM2 but interspersed with some cooler (boreal) climatic intervals.

Zone PM4: (104-642B-14H, CC to 104-642B-17H, CC; 123.5–147.8 m)

Informal name: *Nematosphaeropsis aquaeducta* Range Zone.

Dinocysts and sporomorphs are abundant and well preserved throughout this palynozone. Dinocyst assemblages are dominated by *L. machaerophorum* and *L. truncatum*; *A. ramulifera*, *M. choanophorum*, and *Tectatodinium simplex* are common throughout, and *Nematosphaeropsis aquaeducta* is common in the middle of the zone. Bisaccate pollen (*Pinus*, *Picea*, *Abies*, and *Cedrus*) are dominant, *Taxodium* is common, and warm temperate hardwood species are frequent, e.g., *Quercus*, *Ulmus*, and *Pterocarya*. Fern spores are relatively rare. Palynodebris is mainly amorphogen (ca. 50%), with wood fragments common only in Sample 104-642B-17H, CC. Reworked palynomorphs are rare, with a few Paleogene dinocysts occurring in all samples.

Correlation and Age

The top of Zone PM4 is marked by the LAD of *M. choanophorum*, *S. ancycra*, *P. golzowense*, and *Foliactiniscus* spp.

in Sample 104-642B-14H, CC (123.5 mbsf). *Pentadinium laticinctum*, *Batiacasphaera sphaerica*, and *N. aquaeducta* also have their LAD just below the top of the zone, in Sample 104-642B-15H, CC (128.1 mbsf). The base of Zone PM4 is marked by the LAD of *Lophocysta sulcolimbata* in Sample 104-642B-17H, CC (147.8 mbsf), which also corresponds to the base of the *L. machaerophorum* acme and the top of the *B. baculata* acme. The assemblages in Zone PM4 correspond closely to those of the middle Miocene Zone B at DSDP Site 555 (Edwards, 1984), and, in part, to the upper-middle Miocene assemblages of Zone 1 at DSDP Site 400 (Harland, 1979) and at the Gram stratotype. In the type section, the LAD of *N. aquaeducta* corresponds to the base of the foraminiferal Zone N15. At DSDP Site 555, the boundaries of Zone B extend from the base of magnetochron 15 (ca. 15.5 Ma) to the top of Chron 12 (12.8 Ma). Hence, Zone PM4 appears to have a middle Miocene to very early late Miocene age.

Paleoenvironment

Dinocysts in Zone PM4 indicate a marine environment similar to Zone PM3 but with the acme of *L. machaerophorum* possibly indicating subtropical conditions. Pollen assemblages indicate a mixture of boreal and warm temperate or subtropical forest similar to Zone PM2, but the increase in thermophilous hardwood species and reduction in ferns suggest that the climate was periodically cooler and drier.

Zone PM5: (104-642B-17H, CC to 104-642C-23H, CC; 147.8–192.4 m)

Informal name: *Batiacasphaera baculata* Acme Zone.

Palynomorphs in this zone are common to abundant and both dinocysts and sporomorphs are well preserved. Dinocyst assemblages are dominated by *B. baculata*, *M. choanophorum*, and *P. golzowense*. Species diversity is relatively high, with *N. labyrinthea*, *H. poculum*, *Spiniferites ramosus*, *Tectatodinium pellitum*, and *S. ancyrea* commonly being present. Sporomorph assemblages are dominated by *Pinus*, *Picea*, and *Taxodium*; *Sequoia*, *Carya*, and *Juglans* are also common, and the Miocene *Tricolpites* sp. 1 of Koreneva et al. (1976) is present in all samples. Palynodebris is dominated by amorphogen (ca. 30%) at the top of the zone, but below Sample 104-642B-18H, CC (157.7 mbsf), only a few wood fibers are present. Reworked Paleogene dinocysts are common in Sample 104-642B-18H, CC and rare in other samples.

Correlation and Age

The top of Zone PM5 is marked by the LAD of *L. sulcolimbata* in Sample 104-642B-17H, CC, and the FAD of the upper middle Miocene guide species *L. truncatum* occurs just below this boundary, in Sample 104-642B-18H, CC (157.7 mbsf). The base of PM5 is marked by the LAD of *Lejeunia fallax*, *Samlandia chlamydomphora*, and *Cyclopsiella elliptica* at the base of Sample 104-642C-23H, CC (184.3 mbsf), which corresponds to the middle of Core 104-642B-22H (196 mbsf). The dinocyst assemblages in Zone PM5 can be correlated broadly with those in dinocyst Zones IIa–Ia of DSDP Leg 38, which range from upper Oligocene to middle Miocene age. Within this range, however, *B. baculata* is most common in the lower Miocene interval, and *L. sulcolimbata* has a restricted lower Miocene range. The siliceous endoskeletal dinoflagellates *Foliactiniscus atlanticus* and *F. folia* are also most common in sediments of early Miocene age at Site 338 (Perch-Nielsen, 1976). Therefore, an early Miocene age is tentatively assigned to Zone PM5.

Paleoenvironment

Little is known about the marine environment represented by the dinocysts in Zone PM5, although the presence of *N. labyrinthea* suggests temperate oceanic conditions. Pollen and spores in-

dicating a mixture of boreal and thermophilous hardwood forests on shore.

Zone PM6: (104-642C-23H, CC to 104-642D-10H, CC; 192.4–276.8 m)

Informal name: *Systematophora ancyrea*-*Pentadinium laticinctum* Acme Zone.

Palynomorphs in most parts of this zone are common and well preserved, but Samples 104-642D-2X, CC to 104-642D-4X, CC and 104-642D-10X, CC contain few palynomorphs that are only moderately well preserved. The interval from Samples 104-642D-11X, CC to 104-642D-14X, CC (285.5–315.4 mbsf) is barren except for one sample from Core 104-642D-13X (Manum, pers. comm., 1986). Dinocyst assemblages are dominated by *S. ancyrea*, *S. placacantha*, *P. laticinctum*, *L. machaerophorum*, and *L. fallax*. Pollen and spores in the upper part of this zone (104-642C-23H, CC to 104-642D-6X, CC) are dominated by *Picea* and other bisaccates (mostly *Pinus*). *Taxodium* is common from the top of the zone down to Sample 104-642D-4X, CC (218.9 mbsf); from this level to Core 104-642D-6X (238.2 mbsf), however, *Sequoia* becomes more common, along with a variable mixture of *Triporopollenites* and *Tricolpites* spp., *Betula*, and trilete fern spores, including rare *Gleicheniidites*. *Taxodium* and *Sequoia* are absent from the base of the zone (Samples 104-642D-6X, CC to 104-642D-10X, CC) where sporomorph assemblages are dominated by *Picea* and thermophilous hardwood species, e.g., *Quercus*, *Tilia*, and *Pterocarya*. Palynodebris is dominated by amorphogen; other samples in this zone contain only rare to common wood fibers/tracheids. Oligocene and Eocene dinocysts are common and are probably reworked.

Correlation and Age

The top of the zone is marked by the LAD of *C. elliptica*, *P. golzowense*, *L. fallax*, and *S. chlamydomphora* in Sample 104-642C-22H, CC. The base of the zone is marked by the FAD of *S. ancyrea* in Sample 104-642D-10X, CC. *Evittosphaerula paratabulata*, *Thalassiphora delicata*, *A. ramulifera*, *L. machaerophorum*, and *T. simplex* have their FAD in Sample 104-642D-9X, CC. Dinocyst assemblages in Zone PM6 cannot be correlated precisely with other dinocyst zones established for the North Atlantic, and more onshore work is needed to clarify the taxonomy of some species that resemble Oligocene taxa described for DSDP Leg 71 in the southwest Atlantic Ocean (Goodman and Ford, 1980). In general, however, the co-occurrence of *S. ancyrea*, *P. laticinctum* (= *Leptodinium* sp. II of Manum, 1976), *B. baculata*, *P. golzowense*, *Thalassiphora delicata*, and *Evittosphaerula paratabulata* (= Problematicum I of Manum 1976) corresponds to assemblages in dinocyst Zones III–IIb at DSDP Site 338, which are of middle-late Oligocene to early Miocene age. At DSDP Sites 403–406, *B. baculata*, (= *B. cf. B. compta*), *P. golzowense*, *T. delicata*, *M. choanophorum*, *N. labyrinthea*, *H. obscurum* (= *Hystrichosphaeropsis* sp. A) and *S. ancyrea* co-occur in mid Oligocene (Zone VI) to lower Miocene (Zone VIIb) sediments (Costa and Downie, 1979). The presence in Zone PM6 of taxa that characterize Eocene sediments at Site 338 (e.g., *Cyclopsiella* and *Phthanoperidinium*) is confusing because many of these taxa also occur in younger sediments in other North Atlantic regions (Manum, 1976). The FAD of *E. paratabulata* (Sample 104-642D-9X, CC), *H. obscurum* (Sample 104-642D-6X, CC) and *N. labyrinthea* (Sample 104-642D-5X, CC), however, appear to be good markers of the Oligocene/Miocene boundary in the North Atlantic (Williams, 1977; Manum, 1979). Zone PM6 is therefore provisionally assigned an early Miocene age.

Paleoenvironment

No interpretation of the dinocyst assemblages in Zone PM6 is possible at present, although the decline in amorphogen to-

ward the base of the zone suggests a trend toward shallower or less productive marine waters. Pollen and spores indicate a mixture of boreal and warm temperate forests onshore.

Zone PM7: (104-642D-15X, CC to 104-642E-4R-1, 0–4 cm; 315.9–326.5 m)

Informal name: *Chiropteridium dispersum* Partial Range Zone.

Palynomorphs in this zone are sparse (few to rare) except in Samples 104-642D-15X, CC; 104-642D-17X, CC; and 104-642E-4R-1, 0–4 cm; Sample 104-642D-16X, CC is barren. Preservation is moderate/good in the productive samples. Dinocyst assemblages are dominated by *S. placacantha*, *P. laticinctum*, and *Batiacasphaera* species. Pollen and spores are dominated by *Picea* and thermophilous hardwood species, including *Quercus*, *Tilia*, and *Pterocarya*, but thermophilous and subtropical conifers (*Sequoia*, *Taxodium*) are absent. The dinocyst index ranges from 0.75 to >1.0. Palynodebris is generally sparse: <20% amorphogen and a few wood fibers are present in most samples. A few reworked Paleocene–lower Eocene dinocysts are present.

Correlation and Age

The top of this zone is marked by the FAD of *Batiacasphaera baculata* and the LAD of *Batiacasphaera compta* in Sample 104-642D-15X, CC, and the base is marked by the FAD of *Chiropteridium dispersum*, *S. placacantha*, *P. laticinctum*, *M. choanophorum*, and *C. elliptica* in Samples 104-642D-19N, CC and 104-642E-4R-1, 0–4 cm. The range zone of *Wetzelia ovalis* (Samples 104-642E-4R-1, 20–22 cm, to 104-642D-17X, CC), also distinguishes this palynozone. As for Zone PM6, it is difficult to make a direct correlation with the dinocyst assemblages in the North Atlantic zones delimited by Manum (1976) and by Costa and Downie (1979) owing to taxonomic uncertainties and possible reworking of Paleocene–middle Eocene cysts. Furthermore, Elde (1985) has reexamined the middle–upper Eocene Zones V and IV of Manum (1976) and finds that they are both of late Eocene age, based on correlation with northwest European stratotypes and borehole data from the Norwegian Sea and eastern Canada. Using the zonations of Elde (1985) and the range chart of Williams (1977), Zone PM7 is tentatively assigned a late Eocene age based on the FAD of *C. dispersum*, *S. placacantha*, and *P. golzowense* (late Eocene) and the LAD of *W. ovalis* (Eocene–Oligocene). The siliceous endoskeletal dinocysts *Carduifolia gracilis* and *Actiniscus pentasterias* also have FAD in Eocene to Oligocene sediments at Site 338 (Perch-Nielsen, 1976). One sample (104-642D-13X-4, 81–84 cm), from the barren interval between Zones PM6 and PM7, also appears to be of Eocene age according to the onshore studies of Manum (pers. comm., 1986).

Paleoenvironment

There is a drastic reduction in dinocyst species diversity between Zone PM6 (15–21 spp.) and Zone PM7 (11 spp.). The reduction in diversity may be owing to the occurrence of volcanic activity as indicated by the lithofacies change below Core 104-642D-11X. It is also possible, however, that the decrease in dinocyst diversity and absence of subtropical conifers reflect the high-latitude Northern Hemisphere late Eocene–Oligocene cooling event reported by Norris (1982).

Zone PM8: (104-642E-4R-1, 0–4 cm, to 642E-55R-2, 88–90 cm; 326.5–750.6 m)

Informal name: *Batiacasphaera compta*–*Phthanoperidinium echinatum* Range Zone.

Dinocysts, pollen, and spores in this zone are rare to moderately common in Sample 104-642E-55R-2, 88–90 cm, and above

Sample 104-642E-31R-1, 150 cm, except in Samples 104-642E-12R, CC and 104-642E-31R, CC, which are barren of dinocysts. Preservation varies from good (pollen and spores) to moderate (dinocysts) except in Samples 104-642E-25R-3, 80–105 cm; 642E-33R-1, 140–144 cm; and 642E-42R-1, 94–95 cm, where specimens appear to be highly oxidized. Species diversity is small in both the dinocyst and sporomorph assemblages. Palynodebris consists mainly of small amounts of tracheids and phytoliths in the fine sediment fraction (<63 μm); scattered larger (>150 μm) wood particles, sclereids, and waxy structures (?anthers) were also found.

Correlation and Age

The top of Zone PM8 is marked by the LAD of *Phthanoperidinium echinatum* and *Baltisphaeridium nanum* in Sample 104-642E-4R-1, 20–22 cm, which occurs just below the LAD of *Deflandrea phosphoritica* and *Wetzelia ovalis* in Samples 104-642E-2R-3, 8–9 cm, and 104-642D-17X, CC. The base of the zone is presently defined by the FAD of *Aeosphaeridium dictyoplokus* in Sample 104-642E-55R-2, 88–90 cm. The small-diversity dinocyst assemblages cannot be correlated precisely with the zones of more diverse oceanic-neritic assemblages described for DSDP Leg 38 (Manum, 1976), Leg 48 (Costa and Downie, 1979) or Leg 81 (Brown and Downie, 1984). Most of the dinocyst species in Zone PM8, however, are well-known Eocene taxa, including *Diphyes colligerum*, *W. ovalis*, and *B. nanum*, which have their LAD in the middle Eocene (Manum, 1976; Drugg and Stover, 1977), and *D. phosphoritica*, *Aeosphaeridium dictyoplokus*, and *P. echinatum*, which have their LAD in upper Eocene–lower Oligocene sediments of the North Atlantic region (Elde, 1985). The age range of *Palambages* sp. 1 is presently uncertain, but this colonial alga resembles the *Palambages* species found in Maestrichtian–middle Eocene sediments of CESAR Core 6 from the central Arctic Ocean (Mudie, 1985).

Pollen and spores in Zone PM8 are dominated by temperate-subtropical angiosperm pollen taxa (*Aquilapollenites subtilis* and *Trudopollis* spp.) and trilete fern spores, including *Retitrisporites pseudoclavatus*, all of which characterize Eocene assemblages at DSDP Site 338 (Koreneva et al., 1976). Bisaccate pollen are relatively rare; the main species are *Pinus* sect. *Banksiana*, *Cedrus*, and *Dacrydium*, which are also the main conifers in the Eocene assemblages at Site 338.

Paleoenvironment

The small numbers and diversity of dinocysts and pollen in Zone PM8 are consistent with palynomorph assemblages in tuffaceous volcanoclastic deposits found in northern Greenland (Batten, 1982) and in CESAR Core 6, central Arctic Ocean (Mudie, 1985). It is also notable that there is no sign of thermal alteration in the palynoflora from the volcanoclastic beds in Hole 642E and CESAR Core 6, whereas the sporomorphs are highly altered in the thrust-fold beds of northern Greenland. Petrological and palynological data indicate that the volcanoclastic sediments in CESAR Core 6 were deposited in shallow marine water whereas the Greenland volcanics are subaerial. This observation may be pertinent to the interpretation of the paleoenvironments, thermal conditions, and weathering characteristics represented by the volcanoclastic units at Site 642. The environmental significance of between-sample variations in Zone PM8 is described in detail in the biostratigraphic synthesis for Site 642 (this section). In summary, fluctuations between neritic marine, fluvio-deltaic, and subaerial assemblages appear to be represented in the samples examined. Detailed studies are needed, however, to evaluate the extent to which these changes are a function of sediment sorting processes versus responses to fluctuations in relative sea level.

Zone PM9: (104-642-55R-2, 88–90 cm, to 104-642E-109R-1, 85 cm; 750.6–1218.8 m)

Informal name: *Cerebrocysta bartonensis* Range Zone.

Dinocysts and sporomorphs in this zone are common and well preserved in the volcanoclastic units of Cores 104-642E-55R, 642E-67R, 642E-96R, and 642E-109R, but they are rare and oxidized or fragmented in the units between Cores 104-642E-77R and 104-642E-95R. Dinocyst assemblages are dominated by *Cerebrocysta bartonensis* and cf. *Millioudodinium giuseppi* of Brown and Downie (1984). Also present are *Dracodinium draco*, *Polysphaeridium congregatum*, and *Th. pelagica*. Sporomorph assemblages are dominated by *Pistillipollenites*, *Normapolles*-type pollen, and trilete spores. *Taxodium* and bisaccate pollen are very rare. Palynodebris consists of a few wood fibers in the fine sediment fraction.

Correlation and Age

Dinocyst assemblages similar to those in Zone PM9 occur at the boundary of dinocyst Zones Ib and II of DSDP Leg 81, Hole 553A (Brown and Downie, 1984). The Zone II assemblages at that site were correlated tentatively with the lower sequence of Kap Dalton sediments in East Greenland and with dinocyst assemblages in the upper London clay, which has a late-early Eocene age. The LAD of *C. bartonensis*, however, suggests that Zone PM9 is correlative with the Barton Bed palynoflora, which is of late-middle Eocene age according to the time scale of Berggren, Kent, and Flynn (1985b). Pollen and spore assemblages in Zone PM9 are similar to the undifferentiated Eocene assemblages described for DSDP Site 338; however, the increase in relative abundance of *Normapolles*-type pollen suggests that Zone PM9 is slightly older than Zone 8. More detailed onshore studies of sporomorphs in the Eocene sediments of Site 338 must be carried out to improve the dating control for the dipping reflector sequence.

Paleoenvironment

Dinocyst assemblages in most samples from Zone PM9 appear to record a similar range of neritic to fluvio-deltaic conditions as in Zone PM8. The assemblages in Sample 104-642E-55R-02, 88–90 cm, however, are more diverse in species and the D/P ratio is 1.5, which suggests that this sample represents a more offshore, oceanic environment. Similar fluctuating inshore, estuarine, and outer-shelf environments are reported for dinocyst Zones II and Ib, which overlie the main basalt sequence at DSDP Site 553 and at Kap Dalton (Brown and Downie, 1984). Sporomorph assemblages do not indicate any major climatic change, although the decrease in arboreal pollen may denote more arid conditions.

Biostratigraphic Synthesis

Neogene Biostratigraphy

Introduction

In this section, we have integrated all the stratigraphic and paleoenvironmental conclusions. There is general agreement in the conclusions based on the different microfossil groups; however, there are some unsolved questions that will be discussed here. The microfossil group affinity of species mentioned in the text is indicated by symbols in parentheses (D = diatoms, S = silicoflagellates, R = radiolarians, N = calcareous nannofossils, F = foraminifers, and P = palynomorphs), if not otherwise identified in the text. Microfossil datums and zonal boundaries of all microfossil groups are defined by the stratigraphy of Holes 642B, 642C, and 642D (Fig. 47). Examination of correlative biostratigraphic datums as well as the sub-bottom depth of vol-

canic ash layers and lithologic unit boundaries in both Holes 642B and 642C suggests a variable mismatch of sub-bottom depths in these holes.

Biostratigraphy

Correlation of Biostratigraphic Zones. The biostratigraphic zones and/or assemblages of all microfossil groups studied in Holes 642B through 642D are presented in Figure 47. The biostratigraphic framework provided by the integrated microfossil biostratigraphy is as follows: (1) an absence of siliceous microfossils in lithologic Unit I (Matuyama and Brunhes Epochs), (2) generally large siliceous microfossil diversity and good stratigraphic resolution within the middle Miocene to middle Pliocene, (3) decreased siliceous microfossil biostratigraphic resolution in the lower Miocene, with an increase in endemic species, (4) a prevalence of radiolarian zones based on species endemic to the Norwegian Sea, although some species in the fauna permit correlation with Leg 81 on the Rockall Plateau, (5) long-ranging planktonic and benthic foraminifer zones and calcareous nannofossil zones from the middle of the middle Miocene through the Quaternary, (6) a lack of planktonic foraminifers and calcareous nannofossils within the lower Miocene to lower middle Miocene of lithologic Unit III, and (7) a nearly continuous record of palynomorph assemblages that yields ages consistent with other microfossil groups.

Quaternary Biostratigraphy (0–~1.6 Ma, 0–~50 m). Confirmation of the Gauss paleomagnetic Epoch immediately below the glacial lithologic Unit I confirms the paleomagnetic interpretations of the Brunhes Epoch, Matuyama Epoch, the Jaramillo Event, and the Olduvai Event. The LAD of *Achomphaera ramulifera* (P) in Sample 104-642B-6H, CC is a marker for the top of the Olduvai Event, closely agreeing with the normal polarity interval interpreted as the Olduvai Event. Assuming a constant sedimentation rate for the Olduvai Event, the base of the Quaternary should be at a depth of about 50 m. The FAD of *N. pachyderma* sin. encrusted type (F) is at 56.16 mbsf in Hole 642C, close to the proposed base of the Quaternary. The LAD of *Filisphaera filifera* (P), a marker for the Jaramillo Event, appears close to the normal polarity interval at ~41 mbsf, confirming its proper identification. A relatively complete Quaternary section is suggested by the presence of the NN21/NN20 boundary (0.27 Ma) between ~5 and 15 m. Further biostratigraphic resolution within the Quaternary is sparse because of the absence of siliceous microfossils in studied core-catcher samples.

Pliocene Biostratigraphy (~1.6–~5.2 Ma, ~50–82 m). Diatoms, palynomorphs, and silicoflagellates provide the best biostratigraphic resolution within the Pliocene. Radiolarians, foraminifers, and calcareous nannofossils are consistently present, somewhat diverse but mainly characterized by long-ranging or endemic species. All microfossil assemblages are apparently compatible with the biostratigraphic and paleomagnetic placement of boundaries of the Pliocene.

Biostratigraphic age control is lacking from the Pliocene/Quaternary boundary (~50 m) to the base of the glacial sequence of lithologic Unit I (~60 m in Hole 642B and ~65 m in Hole 642C). The apparent LAD of the diatom *Nitzschia jouseae* (2.6 Ma) closely approximates the upper boundary of the Gauss Epoch at 61 m. The LAD of *N. atlantica* (F) appears at 60.55 mbsf in Hole 642C, indicating an age of about 2.3 Ma. Further evidence for our identification of the Gauss Epoch is the LAD of *Palaeostomocystis* spp. (P, ~2.48 Ma) in Sample 104-642B-8H, CC. Several additional calcareous nannofossil, diatom, and silicoflagellate datums (datums 8–11) occur between 75.9 and 85.4 mbsf, with ages ranging from 3.56 to 5.1 Ma. In close agreement with these ages are the last occurrences of two palynomorphs in Sample 104-642B-9H, CC, *Operculo-*

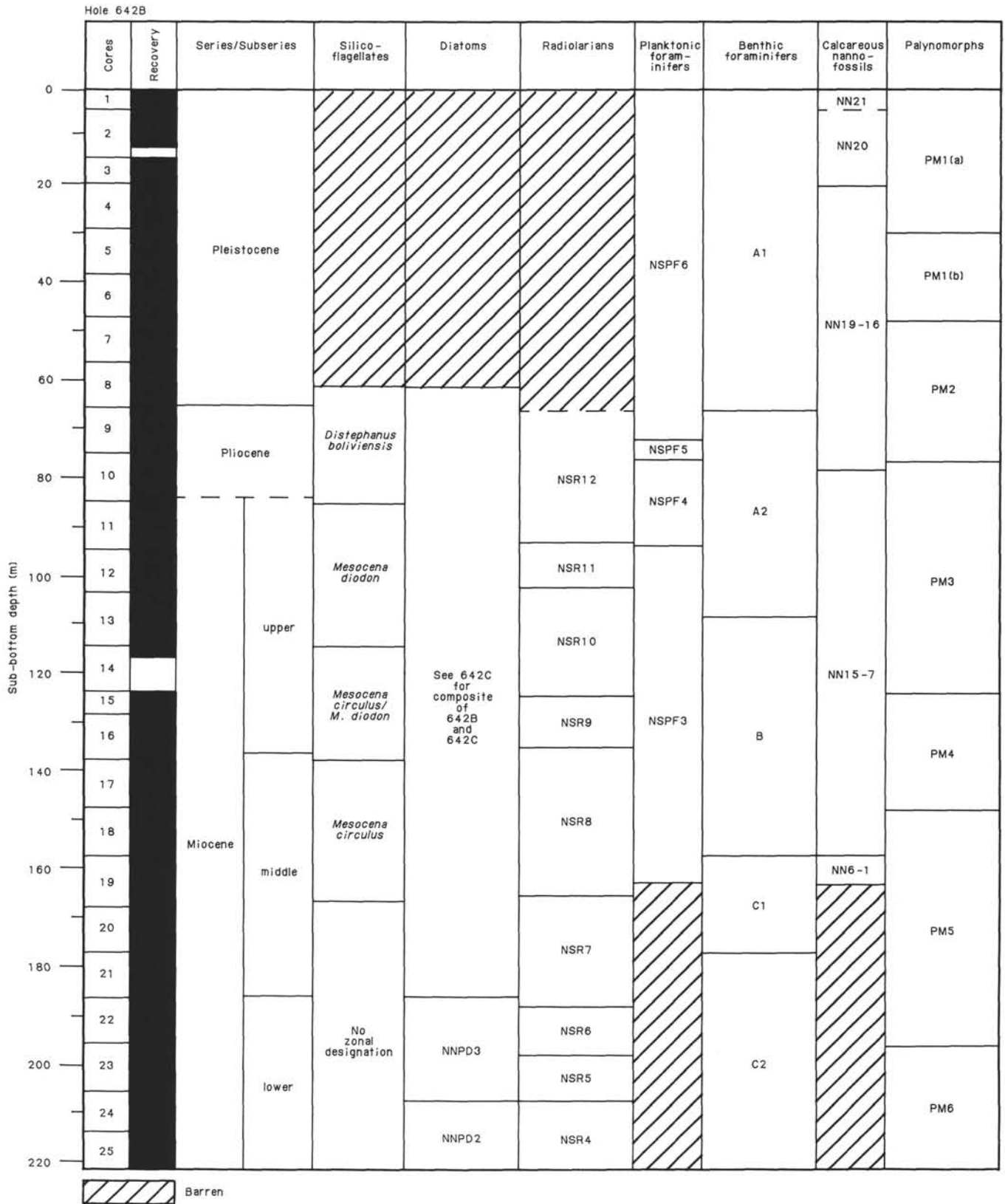


Figure 47. Site 642 biostratigraphy summary chart. NSR = Norwegian Sea radiolarian zone. NSPF = Norwegian Sea planktonic foraminifer zone.

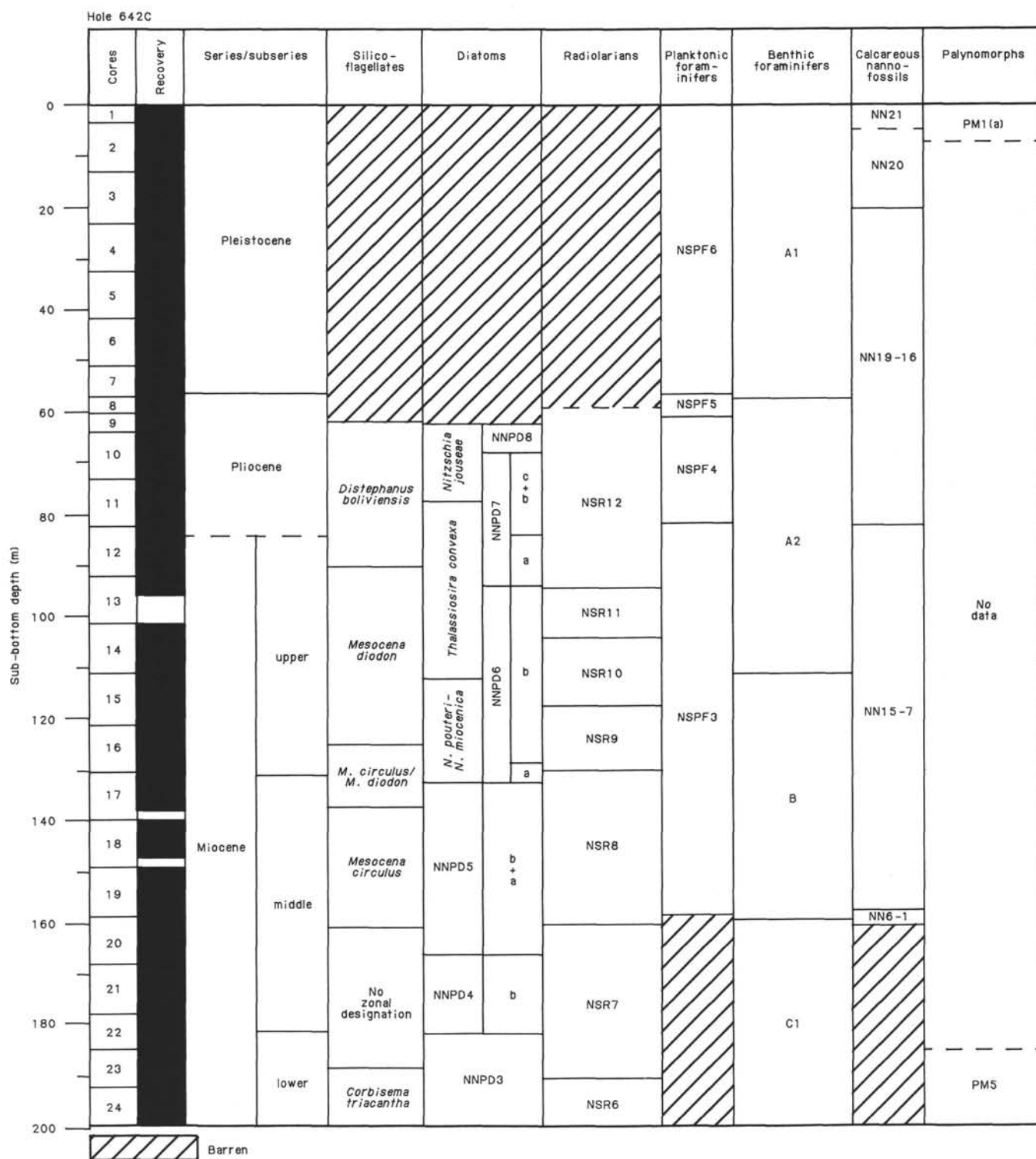


Figure 47 (continued).

dinium crassum (3.4 Ma) and *Achomosphaera andalousiense* (4.4 Ma). The FAD of *Thalassiosira oestruppi* (D, 5.1 Ma) and the LAD of *Nitzschia miocenica* (D, 5.55 Ma) bracket the Miocene/Pliocene boundary between 82.5 and 92 m; therefore, the change in paleomagnetic polarity at 79.8 m is interpreted as the Gilbert/Chron C-3A boundary.

Upper Miocene Biostratigraphy (~82-131 m in Hole 642C and ~82-136 m in Hole 642B). Upper Miocene sediments occur between ~82 and 131-136 mbsf. All microfossil groups are represented within this interval, with diatoms providing the best biostratigraphic resolution. Diatom and silicoflagellate datums (datums 12-15) are indicative of an age of 5.55 to 6.4 Ma be-

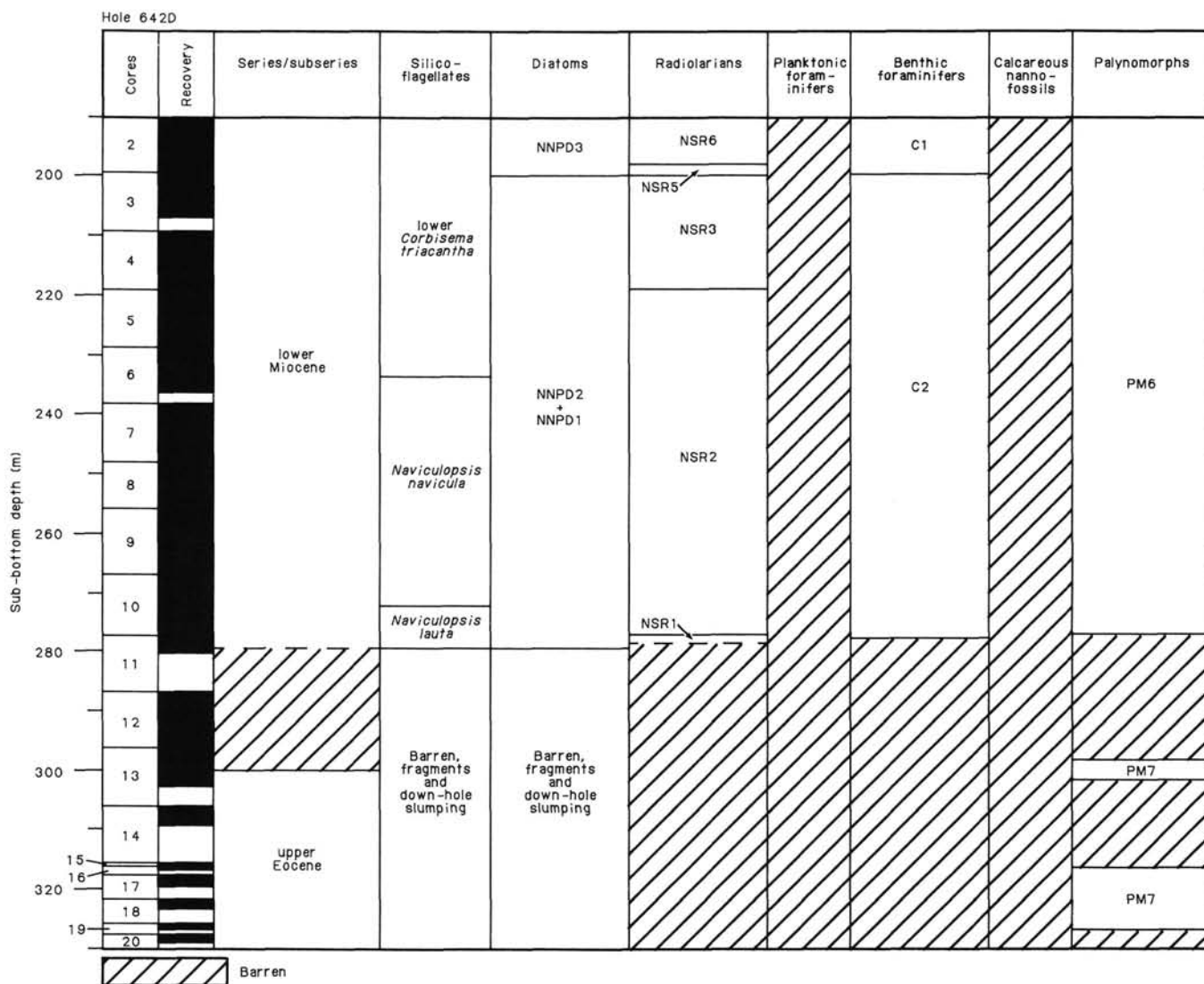


Figure 47 (continued).

tween 85.4 and 120.5 m. Based upon these ages and the accompanying assemblages, we interpret this interval as encompassing paleomagnetic Chron C-3A, which is correlative to the Messinian Stage. Diatom and silicoflagellate zones of this interval (Fig. 47) are firmly established to be late Miocene in age.

Between ~114 and 131 m, additional datums are lacking; however, this interval is correlative with the *Mesocena circulus/M. diodon* Zone (S), the *Nitzschia porteri-N. miocenica* Zone (D) of Baldauf (1984) and the North Pacific diatom *Denticulopsis hustedtii* Zone (NNPD6), Subzone B (Barron, 1980). The base of the aforementioned diatom zones correlates with the lower Chron C-4A (~8.7 Ma). Coinciding with the base of these diatom zones at ~128.5 m is the base of the *Mesocena circulus/M. diodon* Zone (S). The age for the base of this zone is approximately 8.7-9.0 Ma, based upon its relationship to other datums at Site 594, which have been correlated directly to paleomagnetic stratigraphy. Based upon diatoms and silicoflagellates, the 131-m (Core 104-642C-17H) level at Site 642 should therefore be no older than ~9.0 Ma.

Planktonic foraminifer assemblages are in agreement with a late Miocene age for sediment from 83-124.5 mbsf as this interval is no older than N17 (basal Chron C-4, 8.9 Ma). Calcareous

nannofossils offer little biostratigraphic resolution within this interval and they only provide an age of younger than late middle Miocene (NN7). Palynomorphs suggest a slightly older age of very early late Miocene, but dating control is poor for high latitude oceanic dinocyst assemblages in this time interval.

Based upon the results of all microfossil studies the interval between the Miocene/Pliocene boundary (~82 to ~131 m) appears to represent an uninterrupted record of between 5.2 Ma to <9.0 Ma.

Miocene Hiatuses. A large number of diatom and radiolarian first and last occurrences and a major change in palynomorph assemblages occur between 128 and 160 m in Holes 642B and 642C. Assemblage changes are most abrupt at approximately ~131 m sub-bottom in Hole 642C and ~136 m sub-bottom in Hole 642B, where there is also an adjacent zone of poor preservation of siliceous microfossils. Based upon the diatom assemblages above and below ~128 and 160 m sub-bottom, this 30-m interval must range in age from middle middle Miocene to late Miocene and represents 3 to 5 m.y.

At this time, the completeness of this interval cannot be resolved. Variations in sedimentation rate and preservation between Holes 642C and 642B will require further detailed biostrati-

graphic examination to determine if this interval is complete and had a much lower sedimentation rate than the adjacent sections or may have an unconformity of yet unknown duration.

Biostratigraphic resolution within the interval from the lower/middle Miocene boundary to the middle-middle Miocene is limited almost entirely to diatoms, radiolarians, and palynomorphs. Planktonic foraminifers are absent below the base of lithologic Unit II (~158 m). Calcareous nannofossils are present to only a slightly greater depth (~168 m), and they define the age at this depth as early to middle Miocene (NN1–NN6). Below ~168 mbsf, both planktonic foraminifers and calcareous nannofossils are absent. Silicoflagellates are present throughout the interval but are characterized by a low diversity of long-ranging species, which is typical of the middle Miocene at all latitudes.

Bracketing ages for this interval can be based upon two diatom zonal or subzonal boundaries that are well documented in numerous sections throughout the entire Pacific at virtually all latitudes, ranging from the mid- to high-latitude North Pacific to the sub-Antarctic. These are the base of the *Denticulopsis lauta* Zone (NNPD4), which has an age of approximately 16.1 Ma, and the Subzone A/B boundary of the *Denticulopsis hustedtii/D. lauta* Zone (NNPD6) with an age of 13.3 Ma. The first *Denticulopsis hyalina* (~15.0 Ma) occurs within the interval between 184.3 and 177.5 m. Other diatom datums (Datums 23 and 24) with an age of 14.0 to 13.8 Ma occur between 177.5 and 158.5 m.

Radiolarian biostratigraphy indicates the existence of four additional unconformities in Site 642 recovery, which were not apparent in other microfossil groups. Approximately 180–200 m of sediment coeval with these unconformities is present in the recovery at Sites 338, 341, and 643. These hiatuses indicate that sedimentation at Site 642 was periodically disrupted by intervals of erosion or nondeposition throughout the Neogene. The hiatuses in Hole 642D are located between Cores 104-642D-2X and 104-642D-3X, 104-642D-4X and 104-642D-5X, and 104-642D-10X and 104-642D-11X. The youngest of these unconformities is correlative with an unconformity in Core 104-642B-24H. The fourth unconformity is in Cores 104-642B-19H and 104-642C-20H, and this unconformity is also present in Core 104-643A-12H.

On the other hand, there is about 75 m of biosiliceous sediment above the unconformity in Cores 104-642B-16H and 104-642C-17H that was not recovered on Leg 38. These sediments have been assigned to three new provisional biozones, and only further study will permit additional biostratigraphic resolution of this important interval of the middle Miocene.

Palynomorph assemblages of this interval are at variance with the diatom age assignments. Correlations of these assemblages with type localities in the North Atlantic and Denmark give an age of early Miocene rather than early middle Miocene. Consistently older palynomorph ages below ~150 m cannot be explained at this time but add caution to rigid stratigraphic interpretations until more detailed shore-based work can be completed.

Lower Miocene Biostratigraphy (~16.1–~21.5 Ma, ~189.5–276.5 m). An early Miocene age is assigned to this interval based upon diatom, silicoflagellate, and palynomorph assemblages. This interval extends to the base of lithologic Unit III, directly overlying the volcanic units below 277.9 mbsf. Silicoflagellate biostratigraphy firmly places this interval in the lower Miocene. Recognized are the lower *Corbisema triacantha* Zone, *Naviculopsis navicula* Zone, and the upper *Naviculopsis lauta* Zone. These zones are defined on the basis of cosmopolitan species which have been recorded from all major ocean basins, ranging from the Ross Sea and margins of Antarctica into the Norwegian Sea. Previously, correlations of these zones with the standard calcareous nannofossil zonation at numerous localities

suggested that this interval is correlative to upper NN1 through NN4. The base of the *Naviculopsis navicula* Zone between Core 104-642D-10X, CC and Core 104-642D-9X (276.0–267.1 m) provides an important biostratigraphic age near the base of the Unit III sedimentary section. This boundary approximates the NN1/NN2 calcareous nannofossil boundary at Site 407 on the western flank of the Reykjanes Ridge south of Iceland. The relatively close proximity of Site 407 to Site 642 means that the *N. navicula* boundary probably exhibits little diachroneity at Site 642. If this conclusion is correct, approximate correlation of the base of this silicoflagellate zone with the NN1/NN2 boundary yields an age of ~21.2 Ma. Sample 104-642B-10H, CC (286 m) is only slightly older, correlative with NN1.

In this lower Miocene interval, three diatom zones are recognized: the *Actinocyclus ingens* Zone (NNPD3), the *Thalassiosira fraga* Zone (NNPD2), and the upper *Thalassiosira spinosa* Zone (NNPD1). Diatom datums defining the boundaries of these zones and additional datums within the zones range in age from 16.1 to 19.9 Ma. The last of the datums, the FAD of *Thalassiosira fraga* (19.9 Ma), occurs above (267.1–257.5 m) the 21.2-Ma FAD of *Naviculopsis navicula* (S).

Palynomorphs within this lower Miocene interval include lower Miocene assemblages (~148–238 m) and assemblages that contain several species with Oligocene to early Miocene age ranges (238–276.8 m). Reworked Eocene dinocysts occur in the interval between 238 and 276.5 mbsf (Samples 104-642D-6X, CC to 104-642D-10X, CC), which suggests that the lower part of the interval cannot be dated reliably by palynological data. Ages provided by diatoms and silicoflagellates appear to be reliable because they are based on cosmopolitan species whose ranges have been documented in numerous pelagic DSDP sites throughout the world. These siliceous microfossil assemblages are correlated with standard calcareous microfossil schemes and have been directly or indirectly correlated with the paleomagnetic time scale. At the present time, an early Miocene age is adopted for this interval.

Paleogene Biostratigraphy

Introduction

At Site 642, gray muds and strongly weathered volcanic sediments were cored in the lower part of Hole 642D (277.9–322.0 mbsf) and at the top of Hole 642E (321.0–326.8 mbsf). These sediments form the rhyolitic ash zone overlying the upper (tholeiitic) volcanic series at Site 642. Brownish volcanoclastic sediments were recovered at the base of Hole 642D (322.4–329.2 mbsf) and between the volcanic flow units in Hole 642E, at intervals from 321 to 1219 mbsf. Note that the sub-bottom depths in Table 17A and cited in this part of the section are the shipboard log depths and not the revised depths obtained from the geophysical logs. Most of the Paleogene biostratigraphic data are from the interbedded volcanoclastics in Hole 642E. All the core-catcher intervals of the rhyolitic ash zone and most of the volcanic intrabeds were sampled (Table 17A) and examined for all microfossil groups, including foraminifers, calcareous nannofossils, diatoms, silicoflagellates, radiolarians, and palynomorphs. No samples from Cores 104-642E-1W and 104-642E-2W are included here because they are contaminated by wash-down sediments. Initial biostratigraphic results are summarized in Table 17A and Figure 48.

Zonation of a composite biostratigraphy for Holes 642D and 642E has been attempted, although detailed sampling of lithofacies within the individual volcanoclastic units is required to resolve a possible difference of ca. 10 m.y. in minimum age assignments obtained for Core 104-642E-55R from siliceous microfossils (late middle Eocene–early Oligocene; NP17–20 of Martini and Müller, 1976) and from palynomorphs (Eocene to late-mid-

Table 17A. Summary of microfossil data from volcanoclastic units in Holes 642D and 642E and paleoenvironmental interpretations.

Core, sect. and interval (cm) 104-	Approximate sub-bottom depth (m)	Clastic unit no.	Microfossils								Paleoenvironment based on microfossils	Class		
			Organic				Siliceous			Calcareous		Microfossils	Petrology	
			Wood	Pollen/spores	Freshwater	Dinocysts	Diatoms	Silicoflagellate	Radiolarian	Foraminifers				Nannofossils
642D-11 CC -12 CC	286.50 296.20	S01	R R	B B	B B	B B	R _p B	B B	R _p B	B B	B F	?Paralic/littoral ?Shallow neritic	?W _m	W
642D-13 CC -14 CC	305.80 315.40	S02	R R	R R	B B	B F	F _p R _p	F _p B	R _p B	B B	B F	?Neritic Inner neritic	?W _m	W
642D-15 CC	315.90	S03	R	R	B	F	R _p	B	R _p	R _p	B	?Inner neritic	?W _m	W
642E-2-03, 8-9 -4-01, 0-4	321.09 326.50	S03	R	C	B	C	R _p C _p	B C _p	B C _p	B F _p	B R ⁺	Oceanic (S)/neritic (F/P)	W _m	W
642D-16 CC -17 CC -18 CC	317.40 321.60 326.40	S04	F C R	B C R	B B B	B C B	B C _p B	B B B	B B B	B R B	B R B	Paralic Neritic ?Paralic/littoral	W _m W _m W _m	W W ?
642E-5-01, 20-22	335.10	S04	C	R	B	F	R _p	B	B	B	B	Paralic/estuarine	W _m	?
642D-19 CC	328.90	S05	R	F	B	F	R _p	B	B	B	B	Inner neritic/paralic	W _m	W
642E-7-02, 112-117 117-119	356.97 356.99	S06	C	R	B	R	R _p B	B B	B B	B B	B B	Estuarine—marine delta	W _d	W
642E-12-01, 64-65 -12 CC	387.85 395.80	S08 ?	F B	F B	B B	F B	R _f B	B B	B B	B B	B B	Estuarine—marine delta ?Subaerial	W _d ?A	? ?
642E-19-04, 139-140 -19-05, 3-5	449.50 450.10	S10		ND			B R	B R	B B	B B	B B	Paralic	? W _m	W W
642E-21-01, 21-23	461.20	?S10	F	F	R	F	F _p	B	B	B	B	Estuarine→paralic	W _m	?
642E-23-01, 128-130 -23-01, 144-145	481.20 481.35	S12					B	B	B	B	B			W W
642E-25-03, 80-85	498.75	S15	F	R	R	R	B	B	B	B	B	Estuarine—marine delta	W	W
642E-27-02, 45-60	514.80	S16	C	F	R	R	R	R	B	B	B	Estuarine—marine delta	W	A
642E-28-03, 126-128	526.38	S17		ND			B	B	B	B	B		?	W
642E-31-01, 0-3 -31 CC	549.50 550	?top 30E ?top 30E	C	R	C	F	F	R?	R	B	B	Inner neritic→estuarine	W ?	? ?
642E-33-01, 140-144 -34-01, 6-7	566.34 574.56	S18 ?S18	F C	F R	F R	B B	R _f sponge	B B	B B	B B	B B	Subaerial→tidal plate Freshwater/subaerial	A A _f	A A?
642E-35-02, 6-7 -35-02, 100-110 -35-02, 111-113	586.97 588.00 588.30	S19	F	F	F	R	C	F	B	B	B	Neritic	W _m	W W W
642E-39 CC	631.10	—		ND			B	B	B	B	B	Insufficient data		?
642E-42-01, 56-57 -42-01, 75-76 -42-01, 94-95 -42-01, 110-111 -42-01, 113-114	650.67 650.86 651.05 651.21 651.24	S21	R R R	F F R	B B R	R B	B R _f R _f	B R _f B	B R _f B	B B B	B B B	Paralic Inner neritic Estuarine—intertidal	W _m W _m W/A	W W W W W
642E-45-01, 6-7	678.60	S22	R	R	C	B	B	B	B	B	B	Lagoonal	W _f	W
642E-54-02, 65-66 -54-02, 69-71 -54-02, 78-80 -54-02, 87-88 -54-02, 100-110 -54-02, 108-109	740.86 740.91 741.00 741.08 741.29	S26	F R B R B	R R B R R	R B B R _p R	R _p R	B B B B F	B B B B R _m	B B B B B	B B B B B	B B B B B	Lagoonal/intertidal Subaerial Erosion channel? Paralic→intertidal ?Paralic Neritic	W _f /A A ?W _f W _m /A W _m	W (A) W (A) W (A) W (A) W (A)
642E-55-02, 88-90	750.60	S27	R	F	B	C	C	F	R	B	B	Outer neritic	W _m	A
642E-67-01, 1-3	844.20	S30	R	R	B	F	F	B	B	B	B	Neritic	W _m	A
642E-77-01, 14-16	931.06	S34	R	R	B	R	R _p	B	B	B	B	?Paralic	?W _m	W
642E-85-05, 125 -86-02, ~82 -87-01, 122 -94-01, 20-24 -94-04, 20-24 -95-01, 75 -95-03, ~150 -96-01, 24	1015.05 1019.62 1026.52 ~1085.0 1091.24 1094.50 ~1099.00 1102.74	S39 S40 S41 S44												W W
-98-01, 0-2 -109-01, 85	1115.80 1218.15	S45? S46?	R C	R _p F	B B	R _p C	B B	B B	B B	? ?	? ?	?Paralic/intertidal Paralic/lagoonal	W _m W _m	

Note: Classes: W = subaqueous; A = subaerial; R⁺ = arenaceous benthics only; m = marine; f = freshwater; d = deltaic; B = barren; R = rare; F = few; C = common; ND = no data. Note that the depths shown here are those logged on shipboard for cores from Hole 642E; these depths are not the same as those calculated later from the geophysical logs.

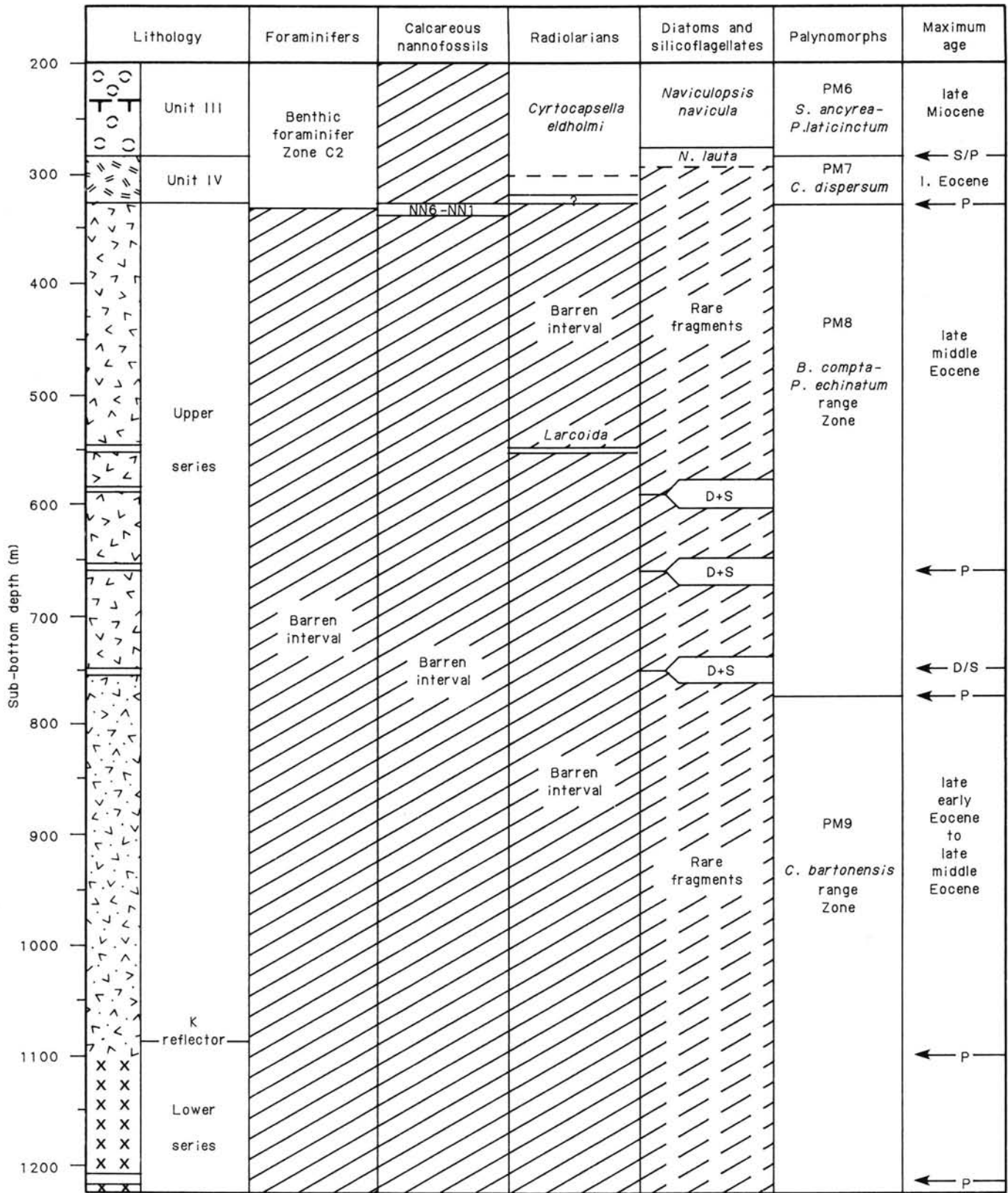


Figure 48. Summary of microfossil data from Holes 642D and 642E.

dle Eocene; NP12 to NP16–17). Inevitably, however, zonation of the Paleogene sediments presently must be based primarily on palynomorphs, for the following reasons:

1. The organic walled palynomorphs are the only fossils that are present throughout the stratigraphic section below 322 mbsf.

2. *In-situ* assemblages of palynomorphs are known to occur in all the clastic sedimentary environments that are possibly represented at Site 642, i.e., marine, deltaic, fluvial, and lacustrine aquatic environments and subaerial soils or tuffs, whereas the other microfossil groups have more limited ranges in marine deposits.

3. Dated palynological reference sections from analogous volcanoclastic sediments are available for several age ranges in the high-latitude northeast Atlantic region. These reference sections include middle–upper Miocene deposits in eastern Iceland (Mudie and Helgason, 1982); Eocene–lower Miocene marine and terrigenous sediments in Spitsbergen (Manum, 1962; Manum, unpubl. data), DSDP Sites 338–343 on the Vøring Plateau (Manum, 1976; Koreneva et al., 1976; Elde, 1985), DSDP Sites 403–406 (Costa and Downie, 1979) and Site 553A (Brown and Downie, 1984) on the Rockall Plateau, upper Paleocene (Sparnacian) to lower Eocene (Lutetian) deposits at Kap Dalton near Scoresby Sund, East Greenland (Soper and Costa, 1976; Soper et al., 1976), and upper Paleocene–lower Eocene deposits in the North Sea (Knox and Morton, 1983).

Although most of the volcanoclastics at these reference sections contain thin marine sequences, calcareous marine microfossils are rarely present and no biosiliceous stratigraphic markers have been reported. Correlation of Paleogene siliceous microfossil assemblages in the volcanoclastic sediments at Site 642 therefore can be made only with more distant sites, such as the Blake Plateau and Antarctic. Paleomagnetic data for the volcanic sequence and rhyolitic ash layer at Site 642 (see “Paleomagnetism” section) only record a long-reversed polarity interval that is tentatively placed in the Paleogene section of the global magnetochronology, but they do not provide definite dating control.

Biostratigraphic Zones and Correlation

Figure 48 shows the biostratigraphic zones and/or assemblages of all microfossil groups in the lower part of Hole 642D (Samples 104-642D-8X, CC to 104-642D-19N, CC; 250–328.9 mbsf) and in Hole 642E (321.09–1219 mbsf). General features of the biostratigraphy are summarized as follows:

1. Benthic foraminifers start to disappear from the sediment column in lithological Unit III near the top of the rhyolitic ash unit, in the interval from ca. 280 to 327 mbsf. Planktonic and benthic foraminifers and nannofossils disappear higher in the section, at the base of lithological Unit IIB, ca. 159 mbsf. Sparse benthic foraminifers are found at intervals in the ash zone. These assemblages apparently belong to arenaceous benthic foraminifer Zone C2 of Holes 642B, 642C, and 642D. The benthic assemblage is dominated by *Spirosigmoilina* sp. (*Miliammina* sp.) and *Silicosigmoilina* sp., which have an early–late Miocene age in DSDP Leg 38 sediments, but more work is needed to refine the taxonomy and correlation of these microfossils. In Sample 104-642D-17X, CC one specimen of a *Cribrorostomoides* sp. was found that may have an Oligocene–Miocene range, and a few reworked Eocene foraminifers were found. A few calcareous nannofossils were also found in Section 104-642E-4R-1, at the top of the pyroclastic sediment units in Hole 642E. This nannofossil assemblage includes the long-ranging (NN6-1) species *Cyclococcolithus floridanus* and *C. abisectus* that characterize the assemblages at the base of Unit III in Hole 642C, and they indicate an age of latest Oligocene to early Mio-

cene for sediments on top of the upper basalt flow series. No characteristic Oligocene nannofossil markers were found in the sample, however; hence it is not certain whether the nannofossils in Core 104-642E-4R are in place or have been washed down from a lower Miocene section.

2. Radiolarians are essentially absent from the sediment below Unit III, which is dated as late early Miocene. Radiolarians show a transition from abundant, well-preserved specimens in Core 104-642D-7X (ca. 250 mbsf) to few, poorly preserved specimens with smectite or glauconite infilling at the top of the rhyolitic ash unit (104-642D-11X, ca. 285 mbsf). This gradient suggests that the contact between the volcanoclastic and Miocene marine sediments is conformable. Several species of well-preserved radiolarians are present in a sample (104-642E-2X-1, 32–34 cm) of gray mud at the top of the basalt sequence. More study is needed to clarify the nature and age of this assemblage, which appears to be a melange of species from the middle–early Miocene biozones NSR1–8.

3. Diatoms and silicoflagellates were found in 11 of 16 samples from the pyroclastic beds in the upper tholeiitic basalt. Seven of these samples contained only small diatom fragments of indeterminate taxonomic affinity and/or age. A sample from 550 mbsf contained a few specimens of the resistant, long-ranging species *Coscinodiscus marginatus* and a silicoflagellate, *Mesocena circulus*, which normally occurs in the middle–upper Miocene. A sample from Core 104-642E-35R-2, 6–7 cm, 586.97 mbsf, contained a diverse assemblage of well-preserved diatoms and silicoflagellates. A middle Eocene age is suggested by the presence of *Melosira architecturalis*, *Pterotheca aculeifera*, *Cestodiscus* aff. *muhinae*, *Pseudostictodiscus picus*, *Rhizosolenia praebarboi*, *Coscinodiscus argus*, and silicoflagellates, which co-occur in this age interval at DSDP Sites 511 and 513 in the sub-Antarctic (see “Diatom Stratigraphy” and “Silicoflagellate Stratigraphy,” this section). However, this correlation is not exact and a wider age range of middle Eocene to early Oligocene is possible. Sample 104-642E-42R-07, 113–114 cm (651.24 mbsf), contains a sparse assemblage of diatoms and silicoflagellates, including *Mesocena oamaruensis*, which has a middle Eocene–early Oligocene age and *Asteromphalus* sp., which has a FAD in the early Oligocene in the sub-Antarctic (Gombos and Ciesielski, 1983). Diverse, well-preserved diatoms, silicoflagellates, and ebridians in Sample 104-642E-55R-02, 88–90 cm (750.66 mbsf), have middle Eocene–late Oligocene ages, except *Pseudostictodiscus picus*, which is restricted to the middle Eocene in DSDP Site 309A on the Blake Plateau, and the silicoflagellate sp., *Dityocha quadria*, which has a late Eocene age (NP17–20, Martini and Müller, 1976). Therefore, the siliceous microflora indicates a probable middle to early–late Eocene age for the base of the upper tholeiitic volcanic sequence at Site 642.

4. Palynomorphs are rare to common in almost all samples examined (Table 17A). Preservation is generally moderately good, although specimens in some samples have a thin-walled, oxidized appearance which seems to be related to their deposition in subaerial or estuarine tidal flat environments (see “Paleogene Paleoenvironments,” this section, and Fig. 49). Palynodebris content of most samples is low, and consists mainly of unaltered wood fibers and phytoliths. Spore color is light yellow, also indicating thermal immaturity. One exception to this general feature is found in the sample from the base of the volcanic sequence (104-642E-109-1, 85 cm; ca. 1219 mbsf). Pollen and spores in this sample are orange brown, indicating a TAI (thermal alteration index) value of 3+ on the Bayliss scale. This optical assessment of thermal maturity is further supported by Rock-Eval data (see Table 17B).

Three Paleogene palynozones are recognized and are described in detail in “Palynology of Site 642,” this section. Zone PM7 (*Chiropteridium dispersum* partial Range Zone) extends from

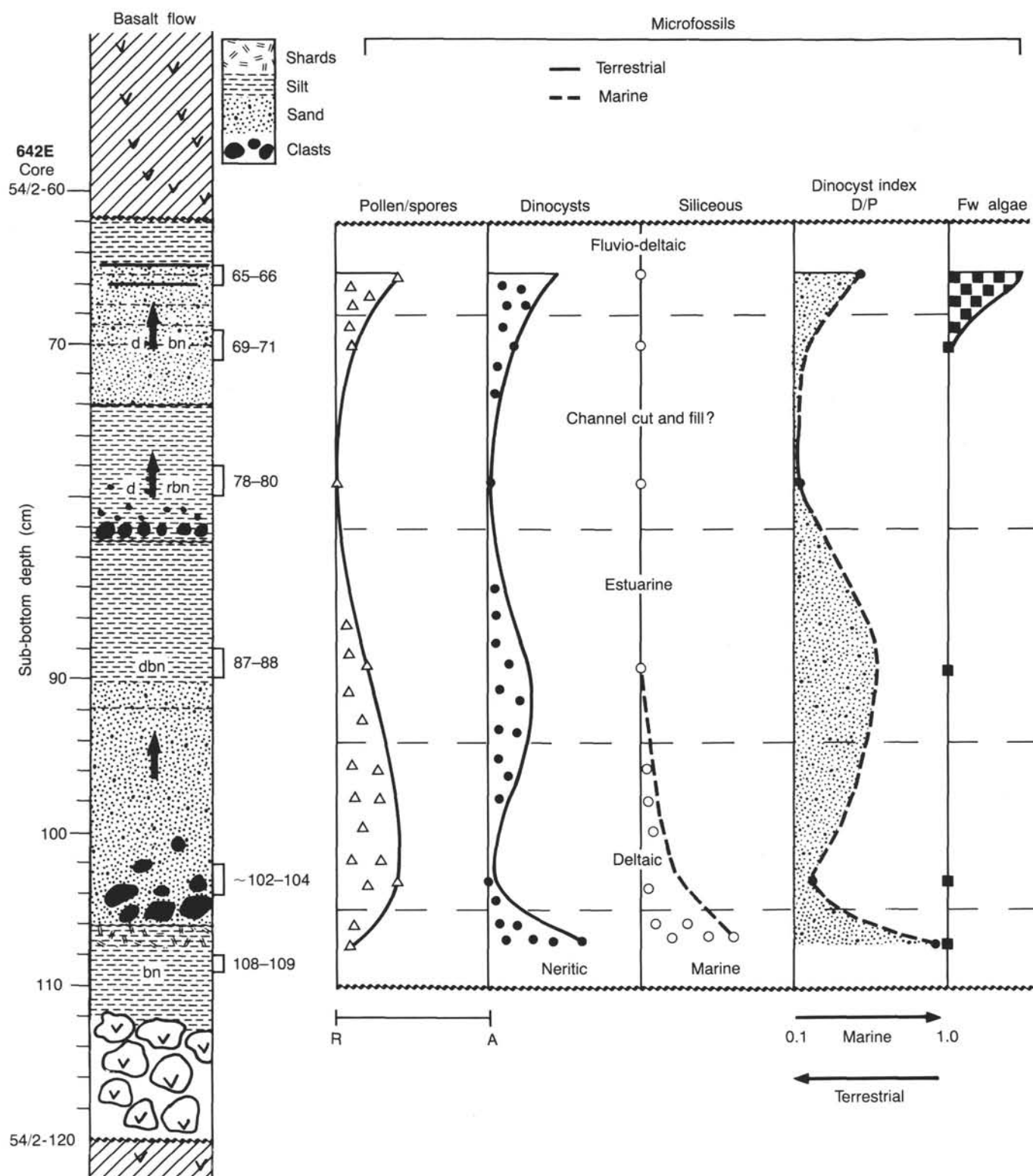


Figure 49. Relationship between lithology (semi-schematic) and microfossil frequency within a graded volcaniclastic unit. Rectangles mark samples. Microfossil frequency: R = rare, A = abundant; X = poor preservation; Py = pyrite; FW = freshwater; bn = brown, r = red, d = dark.

315.9 to 326 mbsf. Dinocyst assemblages are dominated by *S. placacantha*, *Pentadinium laticinctum*, and *Batiacasphaera* species. Pollen and spores are dominated by *Picea* and thermophilous hardwoods, including *Quercus*, *Tilia*, and *Pterocarya*. The dinocyst assemblages can be correlated, in part, with dinocyst

Zones V and IV of DSDP Site 338 (Manum, 1976); with dinocyst Zones IVa-IVb of DSDP Sites 403-406 (Costa and Downie, 1979); and with cyst Zone B of Site 338 (Elde, 1985). Cyst Zone B has been correlated with other sites in the Norwegian Sea and Europe (Elde, 1985) and with the standard nannofossil

Table 17B. Results of carbon and Rock-Eval analysis of samples from pyroclastic interbeds in Cores 104-642E-54R and 104-642E-109R, at depths of about 741 and 1211 mbsf, respectively.

Carbon Contents (%)		Core 104-642E-109	Core 104-642E-54
Total carbon (CHN)		1.13	0.01
Carbonate carbon (Coulometer)		0.02	0.02
Organic carbon (difference)		1.11	0

Rock-Eval										
Core 104-642E	T _{max}	S ₁	S ₂	S ₃	PI	S ₂ /S ₃	PC	TOC	HI	OI
109	429	0.08	0.40	0.20	0.17	2.0	0.04	1.18	33	16
109	426	0.08	0.36	0.18	0.18	2.0	0.03	1.17	30	15
54	429	0.00	0.01	0.11	—	0.09	0.10	0.00	0	0

Abbreviations: S₁ (mg HC/g rock) = volatile hydrocarbons; S₂ (mg HC/g rock) = kerogen-derived hydrocarbons; S₃ (mg CO₂/g rock) = organic CO₂ from kerogen; PI = (S₁ + S₂) = production index; S₂/S₃ = kerogen-type index; PC = petroleum potential. TOC = total organic carbon; HI (100 S₂/C_{org}) = Hydrogen Index, OI (100 S₃/C_{org}) = Oxygen Index; T_{max} = temperature (°C) of maximum hydrocarbon generation from kerogen.

Zones NP17 and 18 of Martini and Müller (1976), thereby providing a late-middle Eocene to early-late Eocene age (ca. 42–38 Ma) for the base of the rhyolitic ash zone. One sample from Core 104-642D-13X in the middle of this ash zone also contains dinocysts of Eocene age, according to the onshore studies of S. Manum (pers. comm., 1986).

Palynomorph Zone PM8 (*Batiacasphaera compta*-*Phthanoperidinium echinatum* Range Zone) extends from the top of the tholeiitic volcanic sequence (326.5 m) to 760.6 mbsf. Species diversity is low in both the dinocyst and sporomorph assemblages, but palynomorphs are moderately well preserved in most samples. The dinocyst assemblages are dominated by *B. compta*, *P. echinatum*, *Baltisphaeridium nanum*, and *Thalassiphora pelagica*. *Wetzeliella ovalis*, *Deflandrea phosphoritica*, and *Areosphaeridium dictyoplokus* have their LAD at the top of the zone. These assemblages can be correlated with cyst Zone A of Elde (1985), which corresponds to NP17 of Martini and Müller (1976) and has a late-middle Eocene age (ca. 42–44 Ma). Pollen and spores in Zone PM8 are dominated by temperate-subtropical angiosperm pollen, including *Aquilipollenites subtilis* and *Trudopollis* spp., trilete fern spores, e.g., *Retitrisporites pseudo-clavatus*, and rare gymnosperms, including *Pinus*, *Cedrus*, and *Dacrydium*. These assemblages characterize the Eocene basalts at DSDP Site 338 (Koreneva et al., 1976).

Palynozone PM9 (*Cerebrocysta bartonensis* Range Zone) contains dinocyst assemblages dominated by *C. bartonensis* and cf. *Millioudodinium guiseppi*, with scattered occurrences of *Dracodinium draco*, *Apteodinium* sp. of Brown and Downie (1984) and, toward the base, *Senegalinium* cf. *obscurem*, ?*Wetzeliella astra*, and *Paleoperidinium* sp. Similar assemblages occur in dinocyst Zones Ia to II in the intrabasaltic beds at DSDP Sites 403–407, 552, and 553A, and they have been correlated with assemblages in the upper intrabasaltic sediments of the Blossville Basalts at Kap Dalton. At the DSDP Leg 81 sites, these zones were dated by nannofossils as ranging from NP10 (ca. 55–58 Ma) to NP13 (ca. 52–53 Ma). The age of the lower volcanic series at Site 642 may therefore be as old as 58 Ma if the presence of *C. bartonensis* is owing to downhole contamination, or as young as 42 Ma if the lower Eocene palynomorphs are reworked. In general, however, the combined maximum ages obtained from diatoms (D), silicoflagellates (S), and palynomorphs (P) in the volcanic ash layer and basalt intrabeds show an agreement consistent enough to support a late-middle Eocene age assignment.

Neogene and Quaternary Paleoenvironments

Paleoenvironments of Surface Waters

Miocene. The planktonic microfossils indicate important paleoenvironmental changes during the Miocene. Thick-walled radiolarians indicating cold-water conditions or isolation are gradually replaced by more thin-walled temperate species. This signals an increasing water exchange with the North Atlantic, starting in the early Miocene. Pollen and spore assemblages indicate temperate to subtropical conditions during the early Miocene and fluctuations between boreal and warm temperate conditions in the middle Miocene.

A major environmental change that seems to have affected all microfossil groups is identified at about 160 m sub-bottom depth (Samples 104-642B-18H, CC and 104-642C-19H, CC) in the middle Miocene. The age may correlate to the global ¹⁸O-enrichment and Antarctic ice-volume increase (Shackleton and Kennett, 1975; Woodruff et al., 1981). This change marks the first appearances of planktonic foraminifers, which coincide with the boundary between sedimentary Units III and IID. Calcareous nannofossils appear slightly beneath this level, but occur abundantly only above. Zonal boundaries in dinoflagellates, silicoflagellates, diatoms, and radiolarians are located at about this level. The onset of carbonate deposition indicates a major decrease in CaCO₃ dissolution. In the radiolarian assemblages, however, there is a return to more thick-walled assemblages between 158 and 130 m (~13.5–~12.3 Ma), which could be interpreted as a decrease in temperatures and/or increased isolation of the Norwegian Sea. The carbonate deposition and presence of cosmopolitan species of planktonic foraminifers and calcareous nannofossils do not indicate isolation at this time. The planktonic foraminifer faunas display relatively low diversities in the middle Miocene. This may indicate a cool interval in parts of the middle Miocene, possibly correlating with the cold radiolarian assemblage. The diatom assemblages contain abundant productivity and upwelling indicators as well as cold-water species during the same period.

Relatively high-diversity calcareous nannofossil assemblages, indicative of relatively warm water, persisted through the middle and late Miocene. Planktonic foraminifers, radiolarians, and diatoms suggest that the Neogene was warmest during the late Miocene, probably continuing into the early Pliocene. Dinocyst and pollen data show the warmest period in the late-middle Miocene with increased influx of thermophilous pollen, and possibly a more temperate climate in the late Miocene. However, by comparison with North Atlantic records, the lower diversity and lack of temperate calcareous zonal markers in the late Miocene record from Site 642 strongly suggest a marked temperature gradient between the North Atlantic and the Norwegian Sea even during the relatively warm interval.

Pliocene. The low sedimentation rates in the Pliocene section and the relatively few samples representing this period available for shipboard studies limited the stratigraphic resolution of this interval. Despite these shortcomings, some important paleoenvironmental trends are present.

Some microfossil groups indicate a cooling trend from the early to the late Pliocene. Radiolarian assemblages indicate temperate water masses in the earliest Pliocene and a gradual decrease of temperate species up to the first major input of ice-rafted detritus (beneath the Matuyama/Gauss boundary). Planktonic foraminifers show relatively high diversity and a temperate subpolar assemblage with decreasing diversity and increased dominance of cold-water indicators toward the onset of major ice rafting. Preservation of silicoflagellates and diatoms is best in lower Pliocene sediments. Sample 104-642C-11H, CC contains exceptionally high abundances of silicoflagellates. The sig-

nificance of such blooms is not clearly understood at present. Large-amplitude fluctuations in carbonate content and variations in calcareous nannofossil content may indicate paleoceanographic and climatic changes of higher frequencies superimposed on this cooling trend. This may also be documented by mixed temperate- and high-latitude dinoflagellates and temperate and boreal pollen assemblages. Although the early Pliocene may have been relatively warm, the small diversities in calcareous nannofossils, planktonic foraminifers, and radiolarians still indicate a generally cool climate.

The onset of ice rafting and major glaciations had a great impact on all fossil groups. The faunas and floras of the late Pliocene from this boundary and up to the Pliocene/Quaternary boundary are markedly different from those below. The radiolarian assemblages show a marked decline in diversity. Diatoms and silicoflagellates disappear from the sediments. The diversity of planktonic foraminifers is reduced to a nearly monospecific polar assemblage with only minor abundances of subpolar species. Small diversity and low numbers of calcareous nannofossils also signal this cooling. Dinocyst assemblages show reduced diversity and the dinocyst-to-pollen ratio is greatly reduced. The abundance of reworked sporomorphs increased with the onset of large-scale ice rafting. These changes reflect a large-scale change in both the climate and surface-circulation regime of the Norwegian Sea. An onset of extended periods with extensive ice cover and southward deflections of the subpolar Atlantic inflow, probably into the North Atlantic, occurred. The correlation of this with the Gauss/Matuyama boundary is in accordance with the dating of similar events in the North Atlantic (Backman, 1979; Shackleton et al., 1984).

Quaternary. The Quaternary sediments encountered at Site 642 contain alternating assemblages of planktonic microfossils indicative of variations from polar to subpolar environments. This pattern is associated with variations in inflow of North Atlantic drift water in connection with glacial/interglacial cycles. The dinocyst assemblages characterize polar to subpolar surface waters. This cyclicity is also shown by large fluctuations in terrigenous, ice-rafted input. It is also reflected in the dinocyst/pollen ratio (D/P) (which reflects variations in terrigenous sediment influx) and in the calcareous nannofossils, whose abundance and composition alternate between nannofossil-rich interglacial sediments and nannofossil-poor, often highly reworked, glacial deposits. However, an important fossil-barren zone is identified around the base of the Quaternary, pointing to extended, cold glacial intervals below the Brunhes-Matuyama boundary.

Alternating polar-subpolar conditions are reflected in the pollen assemblages, which mainly contain long-distance transported forest-tundra and boreal elements. The siliceous microfossils are apparently missing from the Quaternary interval. These include the radiolarians (except for the sediment/surface layer, which has a high diversity of Holocene radiolarians), silicoflagellates, and diatoms. The low productivity of siliceous microfossils is most likely a result of prolonged periods of ice cover.

Paleoenvironments of Bottom Waters

Only two groups of benthic organisms are abundant throughout the Miocene to Quaternary sequence at Site 642, foraminifers and sponges. Ostracodes are found only rarely (one to five valves) in a few samples (Table 14), along with scattered scolecodonts, echinoderm spicules, and bivalves. Sponges are of little value to the paleoenvironmental interpretation because their taxonomy, ecology, and stratigraphic ranges are poorly known. Therefore, the paleoenvironmental interpretation of the bottom water is based on the benthic foraminiferal data.

Miocene (Benthic Foraminiferal Zones C, B, and Lower A2). The lower and lower-middle Miocene (BF Zones C1 and C2) are

represented by a small-diversity, sparse arenaceous fauna, and numerous barren samples. This assemblage may indicate severe carbonate dissolution or it may represent a shallow-water environment. There are also many terrestrially derived sediment components, including wood fragments, found in this section of the core. The evidence points to a relatively shallow, but definitely marine, depositional environment.

A major change in the bottom water occurred in the middle Miocene when there was a shift to a rich calcareous fauna (BF Zone B). This shift may have been caused by global oceanographic changes such as the establishment of the modern global deep-water circulation, a deepening of the CCD, and an intensified water exchange of the Norwegian-Greenland Sea with the North Atlantic. The upper-middle Miocene is characterized by *Uvigerina pygmaea langeri*, a species associated with the outer littoral-to-epibathyal environment in the North Sea area, along with *M. zaandamae* and *P. bulloides*, both of which are found associated with the upper slope water of the present Norwegian Sea, whereas the fauna of upper Miocene gradually changes to an *E. exigua/E. umbonatus* assemblage species typical of a deeper bathyal environment. In addition, there is a coeval increase in the number of planktonic foraminifers from the upper-middle to the upper Miocene. However, the good preservation of the benthics in the upper-middle Miocene does not suggest that dissolution is responsible for the lack of planktonic foraminifers in these sediments, but rather suggests a more restricted oceanic environment during the upper-middle Miocene. We interpret these data as reflecting a deepening of the sedimentary basin during the upper-middle Miocene. Nevertheless, the evidence may also reflect other environmental changes that are not necessarily directly tied to water depth, such as changes in the oxygen content or position of a water mass. These changes will be investigated with closer sampling in the postcruise studies.

The core interval from 130 to 110 m sub-bottom is characterized by the presence of several barren samples and one sample in Hole 642C containing only arenaceous species. The relationship between these sediments and the interval of very slow sedimentation (or hiatus) will also be investigated further.

Pliocene (Upper BF Zone A2). The benthic foraminifer assemblage of the Pliocene sediments at Site 642 is very similar to that of the present. Zone A is based on the presence of *C. laevigata*. Increased percentages of *M. zaandamae* and *C. subglobosa* in the lower Pliocene (a trend continuing from the upper Miocene) may indicate slightly higher bottom-water temperatures. The Pliocene sediments are also characterized by numerous barren intervals that may represent periods of extensive carbonate dissolution or dilution by terrigenous or siliceous sediment.

The uppermost Pliocene contains evidence for the initiation of Northern Hemisphere glaciation in the form of increased ice rafting. The benthic foraminifers become rare in this interval because of the increase of glacially derived sediments.

Quaternary (BF Zone A1). The samples from this interval are characterized by roughly the same species that occur in the Norwegian Sea today. Although only core-catcher samples have been studied in this interval, there is evidence for alternating glacial and interglacial sedimentation during the Quaternary. The presence of *C. wuellerstorfi* in Sample 104-642B-3H, CC indicates interglacials, whereas Samples 104-642B-4H, CC and 104-642B-5H, CC contain reworked shelf foraminifers (*E. excavatum*), indicating a glacial period.

Paleogene Paleoenvironments

Interpretation of the paleoenvironmental conditions represented by the microfossils in the volcanic intrabeds and overlying rhyolitic ash unit at Site 642 is presently constrained by (1) apparent absence of siliceous and calcareous microfossils and arenaceous benthic foraminifers from most of the samples exam-

ined; (2) probable isolation of the Norwegian Sea by the emergent Greenland–Scotland ridge during the interval from ca. 60–30 Ma (Schrader et al., 1976), which implies that the Paleogene marine microfossil assemblages would have a strong regional aspect; (3) evidence for fine-scale biofacies changes within individual volcanoclastic units (Fig. 49). The data shown in Figure 49 strongly suggest that several sample intervals, each ca. 1 cm thick, should be examined to reveal the range of biofacies present and to locate possible marine microfacies throughout the full time span of the volcanic sequence.

Within the constraints listed above, the following conclusions have been drawn regarding the Paleogene environment at Site 642.

1. Preliminary paleodepth data obtained from the lower Miocene benthic foraminifers suggest a trend toward a nearshore environment prior to the deposition of the rhyolitic ash unit at the base of Hole 642D. Similar paleodepth changes are reported by Manum (1976) for the early Miocene–Oligocene interval at DSDP Sites 336, 338, and 348. The dinocyst index also suggests a shallow marine to paralic or subaerial environment for the Eocene interval at DSDP Site 336. The D/P values for the volcanic intrabeds at Site 642 suggest generally shallow marine conditions for most of the section, but with several major marine incursions around 325, 450, 650, and 800 mbsf. Recognition of these incursions at Site 642 may reflect the fine scale of sampling permitted by the continuous coring for Leg 104, or it may reflect the slightly shallower location of Site 642 (1288 m) compared to Site 338 (1600 m). It is interesting, however, that the dinocyst index indicates relatively deeper marine conditions for the Eocene interval at Site 336. The interval is at a present water depth of <1000 m on the Iceland–Faeroe Ridge. This suggests that there may be significant regional differences between the paleodepth histories of the volcanic deposits in different regions of the Norwegian Sea.

2. Within the volcanoclastic units of Hole 642E, fluctuations are observed in the dinocyst index (Fig. 49), which correspond to changes in frequencies of (a) marine microfossils (biosiliceous diatoms, silicoflagellates and organic walled dinocysts), (b) pollen and terrigenous plant spores, and (c) freshwater algae (*Palambages* and/or *Pediastrum*).

An attempt has been made to delimit environmental facies using some known relationships between the ratios of recent dinocysts and pollen assemblages for marginal marine to oceanic deposits (Mudie, 1980, 1982; Miller et al., 1982; Hill et al., 1985), and with the following assumptions: (a) the presence of both siliceous- and organic-walled marine microfossils indicates a marine environment, and (b) subaerial environments are characterized by the absence of dinocysts and freshwater algae and by the presence of rare, oxidized pollen grains; wind-transported diatom fragments may be present or absent.

Four classes of marine environments can be recognized, as defined below:

1. Oceanic = upper continental slope (ca. 400 m) to pelagic (>1500 m), indicated by the presence of radiolarians (R) and/or calcareous nannofossils (N) in addition to diatoms and dinocysts. D/P is >1.0.
2. Neritic = upper slope (ca. 400 m) to inner shelf (ca. 50 m), indicated by the presence of both diatoms and dinocysts together with pollen. R and N are absent; D/P ranges from ca. 1.0 (outer shelf) to 0.7 (inner shelf).
3. Paralic = inner shelf (<50 m) to coastal bays, indicated by the presence of diatoms, dinocysts, relatively large amounts of pollen, and rare small wood fragments; D/P = ca. 0.5.

4. Estuarine = (i) fluvial marine delta—large amounts of coarse wood fragments, large spores and other plant remains, e.g., seeds and small amounts of freshwater algae are present; dinocysts are rare; D/P = ca. 0.7–0.5; (ii) intertidal mudflats—very low numbers of dinocysts, pollen, and wood fragments; palynomorphs are oxidized; D/P is <0.5; this environment is alternately subaqueous and subaerial, according to tidal range; (iii) lacustrine freshwater environments, recognized by the presence of large amounts of freshwater algae, pollen, and spores; dinocysts are absent; D/P < 0.1; and (iv) subaerial environments, including littoral beach deposits, characterized by rare oxidized pollen grains, absence of dinocysts, and freshwater algae; diatom fragments may be present or absent; D/P < 0.1.

Application of this classification to the microfossil assemblages in the series of graded beds in volcanoclastic unit S26 (740.86–741.08 mbsf) shows that different paleoenvironments are represented by the silt facies at the top of the graded beds (Fig. 49). These results suggest that the bedding represents minor transgressive-regressive facies within a shallow marine environment. A similar series of palynofacies records Pleistocene changes in relative sea level in the Beaufort Sea–Mackenzie Delta region (Hill et al., 1985).

Using the paleoenvironmental criteria listed above, the volcanoclastic units in Hole 642E were classified into subaqueous or subaerial environments (Table 17A). Comparison of this semiquantitative classification with independent assessments made from lithological and petrological criteria (see “Basement Lithology” section) shows that there is a large degree of agreement between the classifications. In general, then, it appears that the volcanoclastic beds at Site 642 were deposited in a relatively shallow (neritic) marine and in terrestrial environments that underwent minor changes in relative sea level of the order of less than 400 m. Similar paleoenvironmental reconstructions have been obtained for the Eocene volcanic sediments at DSDP Site 338 (Manum, 1976), DSDP sites on the Rockall Plateau (Costa and Downie, 1979; Brown and Downie, 1984), and at Kap Dalton (Soper et al., 1976).

PALEOMAGNETICS

Sediments

Available paleomagnetic results for the sediment series recovered from Holes 642A through 642D at Site 642 in the Norwegian Sea comprise:

1. Shipboard measurements, with the new pass-through cryogenic magnetometer, of the natural remanent magnetization (NRM) properties of virtually all core sections (Tables 18 and 19).

2. Shore-based NRM measurements and, for a major portion, complete AF analyses on a series of discrete samples taken at about 30-cm intervals in Holes 642A and 642B and at less closely spaced intervals in the other two holes.

Hole 642A

Only a single, 9.5-m core was retrieved from this hole. Results obtained all show normal NRM directions, indicating that these sediments were accumulated during the present geomagnetic Brunhes Epoch.

Hole 642B

In Hole 642B some 221 m of sediments was penetrated and, to a high percentage, recovered, in 25 cores. Paleomagnetic results were somewhat disappointing: for the lower half of the

Table 18. Paleomagnetic properties of Hole 642B sediments.

Sample interval (cm)	Sub-bottom depth (m)	J (NRM) (Gauss)	NRM		AF stable		Pol.	MDF (Oe)
			I	D	I	D		
1-1, 19-21	0.20	6.42 E-5	+74.5	145.5	+73.7	151.2	N	323
1-1, 49-51	0.50	1.05 E-5	+70.9	68.4	+77.9	135.4	N	170
1-1, 79-81	0.80	1.68 E-5	+78.7	148.0	+72.5	148.7	N	233
*1-1, 109-111	1.10	2.14 E-5	+77.7	104.1	+71.3	132.2		171
*1-1, 139-141	1.40	2.38 E-6	-24.6	327.6	-62.1	322.9		595
*1-2, 19-21	1.70	1.71 E-5	+50.7	125.1	+64.5	115.3		181
1-2, 49-51	2.00	8.25 E-6	+62.5	115.5	+69.6	114.9	N	116
1-2, 79-81	2.30	2.12 E-5	+47.4	122.4	+46.6	128.4	N	195
1-2, 109-111	2.60	6.18 E-6	+2.1	120.0	-40.1	135.1		277
1-3, 19-21	3.20	3.03 E-5	+74.3	146.7	+75.3	163.3	N	266
1-3, 49-51	3.50	4.05 E-5	+74.2	157.4	+69.1	153.0	N	225
1-3, 79-81	3.80	1.10 E-5	+70.1	275.5	+65.8	218.0	N	106
1-3, 109-111	4.10	4.63 E-5	+81.2	219.0	+81.6	208.3	N	255
*1-3, 141-143	4.42	2.13 E-5	+70.9	131.2	+71.4	144.6		155
2-1, 80-82	5.61	5.42 E-5	+83.3	135.3	+81.3	133.9	N	281
2-1, 109-111	5.90	3.09 E-5	+74.1	76.1	+73.6	95.0	N	180
2-1, 139-141	6.20	1.13 E-5	+82.5	192.9	+74.2	182.2	N	42
2-2, 20-22	6.51	9.34 E-6	+87.8	225.5	+76.6	229.2	N	97
*2-2, 50-52	6.81	7.15 E-6	+87.3	232.0	+78.7	32.6		48
*2-2, 80-82	7.11	1.69 E-5	+63.1	117.4	+68.8	114.8		220
*2-2, 110-112	7.41	1.56 E-5	+51.1	107.1	+43.9	113.5		132
*2-2, 140-142	7.71	2.81 E-6	+34.2	155.3	+43.3	187.4		161
*2-3, 10-12	7.91	1.51 E-5	+18.1	302.5	+5.0	263.9		97
*2-3, 44-46	8.25	2.00 E-5	+47.1	290.7	+41.1	276.1		177
2-3, 79-81	8.60	2.55 E-5	+59.6	339.5	+60.2	44.3	N	220
2-3, 110-112	8.91	2.29 E-5	+63.0	14.9	+59.5	8.3	N	121
2-3, 140-142	9.21	2.23 E-5	+69.2	52.8	+68.1	48.1	N	165
*2-4, 19-21	9.50	1.24 E-5	+70.2	45.8	+72.3	14.3		192
2-4, 50-52	9.81	1.59 E-5	+48.8	118.5	+48.3	122.1	N	221
2-4, 80-82	10.11	2.56 E-5	+44.8	101.6	+43.9	107.5	N	181
2-4, 110-112	10.41	1.22 E-5	+48.8	71.4	+70.7	95.0	N	77
*2-4, 140-142	10.71	1.51 E-5	+24.8	103.7	+21.6	97.7		206
2-5, 20-22	11.01	3.60 E-5	+50.3	110.7	+48.3	113.1	N	185
2-5, 50-52	11.31	2.66 E-5	+64.9	227.8	+57.4	225.3	N	227
2-5, 79-81	11.60	3.04 E-5	+65.4	199.3	+60.9	202.8	N	219
*2-5, 110-112	11.91	7.68 E-6	+76.3	212.8	+60.6	233.3		104
*2-6, 4-6	12.35	4.35 E-6	-7.1	233.1	+71.8	169.3		417
*2-6, 8-10	12.39	8.57 E-6	-22.5	86.5	-29.3	325.5		44
2-6, 31-33	12.62	6.10 E-6	+65.4	72.5	+60.5	68.3	N	128
2-6, 60-62	12.91	2.12 E-5	+63.4	86.0	+63.1	81.8	N	188
2-6, 92-94	13.23	2.41 E-6	+85.3	70.2	+78.9	310.5	N	333
3-1, 20-22	14.51	4.43 E-5	+58.4	105.8	+73.1	179.4	N	214
3-1, 50-52	14.81	3.26 E-5	+82.0	163.1	+78.1	162.7	N	214
3-1, 80-82	15.11	1.47 E-6	+65.3	114.8	+68.9	117.5	N	213
3-1, 110-112	15.41	2.18 E-5	+81.6	275.1	+79.4	262.7	N	262
3-1, 140-142	15.71	1.71 E-5	+78.6	245.4	+74.7	232.3	N	194
3-2, 20-22	16.01	7.28 E-5	+86.1	308.9	+85.1	278.2	N	450
3-2, 50-52	16.31	9.73 E-6	+63.4	178.7	+62.5	185.5	N	130
3-2, 79-81	16.60	2.05 E-5	+88.5	54.9	+87.4	38.5	N	224
3-2, 110-112	16.91	1.98 E-5	+83.7	262.0	+79.9	256.4	N	227
3-2, 140-142	17.21	3.06 E-5	+77.6	326.9	+75.9	311.0	N	262
3-3, 20-22	17.51	8.00 E-6	+79.9	328.2	+82.5	339.2	N	235
3-3, 50-52	17.81	4.34 E-5	+78.0	266.9	+76.5	264.2	N	281
3-3, 79-81	18.10	2.45 E-5	+85.8	349.7	+83.9	316.7	N	271
3-3, 109-111	18.40	2.88 E-6	+31.9	288.0	-60.3	290.3		425
3-4, 19-21	19.00	2.74 E-5	+72.5	48.5	+75.5	35.0	N	150
3-4, 49-51	19.30	6.89 E-5	+67.4	66.3	+69.0	62.0	N	234
3-4, 80-82	19.61	2.83 E-5	+58.2	101.4	+67.3	98.2	N	199
3-4, 109-111	19.90	5.07 E-5	+67.1	83.6	+67.5	84.0	N	226
4-2, 80-82	23.01	6.52 E-5	+80.4	18.7	+78.5	13.2	N	316
4-2, 110-112	23.31	2.28 E-5	+72.7	350.9	+71.3	351.5	N	288
4-2, 140-142	23.61	6.53 E-5	+84.0	62.7	+86.3	59.4	N	280
4-3, 20-22	23.91	6.43 E-5	+68.0	346.9	+68.0	347.0	N	305
4-3, 49-51	24.20	7.29 E-5	+52.3	0.7	+50.6	1.0	N	269
*4-3, 79-81	24.50	9.52 E-6	+65.9	319.2	+66.4	318.6		275
*4-3, 110-112	24.81	3.55 E-5	+29.2	358.0	+24.6	355.4		260
*4-3, 140-142	25.11	6.08 E-5	+38.9	344.6	+36.2	345.2		296
4-4, 19-21	25.40	8.11 E-5	+53.1	32.3	+51.7	31.9	N	313
4-4, 49-51	25.70	9.30 E-5	+48.8	3.3	+46.2	0.1	N	292
4-4, 79-81	26.00	8.14 E-5	+57.8	3.7	+55.8	1.9	N	319
4-4, 110-112	26.31	5.54 E-5	+56.0	351.4	+55.1	352.6	N	310
4-5, 19-21	26.90	5.80 E-6	+72.7	38.8	+71.9	38.3	N	237
4-5, 47-49	27.18	2.88 E-6	+65.0	18.6	+55.4	14.5	N	115
4-5, 79-81	27.50	3.13 E-6	+54.8	358.7	+78.6	353.2	N	153
*4-5, 110-112	27.81	3.33 E-5	+38.6	3.9	+37.6	1.9		269
*4-5, 140-142	28.11	1.60 E-5	+51.7	27.1	+48.1	19.9		264

Table 18 (continued).

Sample interval (cm)	Sub-bottom depth (m)	J (NRM) (Gauss)	NRM		AF stable		Pol.	MDF (Oe)
			I	D	I	D		
*4-6, 19-21	28.40	2.00 E-5	+68.9	322.3	+64.6	324.2		276
*4-6, 50-52	28.71	3.38 E-5	+16.4	325.5	+6.8	328.4		228
*4-6, 78-80	28.99	4.36 E-5	+46.5	355.4	+45.0	359.3		321
*4-6, 110-112	29.31	1.78 E-4	+22.2	313.8	-1.8	322.4		350
*5-1, 20-22	29.61	6.24 E-5	+74.0	145.7	+74.4	148.3		289
*5-1, 50-52	29.91	2.93 E-5	+70.6	96.2	+71.5	96.5		271
*5-1, 80-82	30.21	2.86 E-5	+81.0	162.4	+80.5	160.2		289
5-1, 110-112	30.51	3.20 E-5	+67.8	124.6	+68.0	131.3	N	255
5-1, 140-142	30.81	2.89 E-5	+75.5	158.5	+74.9	158.8	N	293
5-2, 20-22	31.11	3.66 E-5	+72.3	141.0	+72.4	152.0	N	261
5-2, 50-52	31.41	3.77 E-5	+78.3	113.0	+80.4	121.4	N	311
5-2, 80-82	31.71	2.72 E-5	+74.5	113.7	+75.1	117.6	N	294
5-3, 19-21	32.60	4.53 E-6	+80.7	186.5	+73.3	150.6	N	220
5-3, 50-52	32.91	4.90 E-6	+76.8	230.1	+79.5	207.2	N	310
5-3, 82-84	33.23	2.54 E-6	+68.9	287.2	+65.5	280.5	N	222
5-3, 110-112	33.51	1.24 E-5	+61.5	110.1	+51.0	133.5	N	108
*5-3, 139-141	33.80	2.31 E-5	+73.3	242.8	+71.3	234.5		238
*5-4, 20-22	34.11	3.90 E-5	+78.2	129.2	+75.6	136.2		216
*5-4, 50-52	34.41	8.61 E-6	+75.3	172.7	+66.9	189.8		115
*5-4, 80-82	34.71	1.07 E-5	+67.9	144.0	-38.2	170.2		90
*5-4, 110-112	35.01	4.22 E-5	+81.6	204.2	+79.3	159.4		241
5-5, 20-22	35.61	2.88 E-5	+80.4	160.1	+82.9	190.6	N	116
5-5, 50-52	35.91	6.68 E-5	+81.3	132.0	+76.9	141.7	N	212
5-5, 80-82	36.21	1.85 E-5	+50.3	115.6	+59.7	127.9	N	151
5-5, 110-112	36.51	1.82 E-6	+8.3	107.3	+58.1	134.1	N	50
5-5, 140-142	36.81	1.12 E-5	+74.0	296.7	+84.1	175.9	N	348
*5-6, 20-22	37.11	7.73 E-6	+81.0	336.9	+90.0	270.0		252
5-6, 49-51	37.40	2.58 E-5	-79.2	358.0	-76.3	330.8	R	208
5-6, 80-82	37.71	3.02 E-5	-67.4	322.0	-69.1	315.9	R	390
5-6, 110-112	38.01	3.36 E-5	-57.7	289.3	-60.8	290.8	R	321
5-6, 140-142	38.31	3.70 E-6	+8.6	11.5	-42.9	359.4	R	342
5-7, 19-21	38.60	1.31 E-5	+59.6	96.8	-40.5	155.1	R	46
5-7, 49-51	38.90	6.50 E-6	-16.7	75.9	-56.3	93.9	R	197
5-7, 80-82	39.21	1.62 E-5	+41.5	115.0	+59.8	132.0	N	99
*6-1, 20-22	39.11	7.42 E-6	+3.1	87.2	-26.2	79.8		61
6-1, 50-52	39.41	4.36 E-5	+84.3	162.2	+80.5	154.0	N	204
6-1, 80-82	39.71	3.23 E-5	+81.1	171.3	+78.7	168.9	N	263
6-1, 110-112	40.01	1.52 E-5	+75.9	76.7	+80.5	68.3	N	164
6-1, 140-142	40.31	5.16 E-5	-82.1	61.4	-82.1	233.6	R	315
6-2, 20-22	40.61	7.97 E-7	-73.7	168.3	-74.2	210.9	R	>500
6-2, 50-52	40.91	7.07 E-6	-82.7	347.9	-84.3	283.0	R	406
6-2, 80-82	41.21	2.37 E-6	-33.2	258.8	-66.5	249.5	R	>500
6-2, 110-112	41.51	9.95 E-6	+39.6	112.0	-66.1	165.6	R	67
6-2, 140-142	41.81	2.95 E-5	-60.5	138.1	-61.1	161.0	R	356
6-3, 20-22	42.11	2.21 E-5	+66.6	97.3	+65.9	96.3	N	243
6-3, 50-52	42.41	3.54 E-5	+83.7	110.3	+84.3	141.1	N	205
6-3, 80-82	42.71	17.3 E-5	-73.8	223.0	-78.1	237.6	R	474
6-3, 110-112	43.01	1.11 E-5	+35.8	260.9	-23.8	258.5	R	233
6-3, 140-142	43.31	7.85 E-7	-10.7	250.6	-64.3	253.9	R	>500
6-4, 20-22	43.61	8.59 E-6	+58.6	279.0	+43.1	274.5	N	178
6-4, 50-52	43.91	6.01 E-6	+75.3	324.8	+63.7	309.1	N	80
6-4, 80-82	44.21	1.38 E-5	-1.7	86.3	-58.4	93.0	R	247
6-4, 110-112	44.51	2.22 E-5	-81.8	58.8	-84.5	302.9	R	391
6-5, 20-22	45.11	1.21 E-5	+69.0	48.6	+59.2	53.7	N	265
6-5, 50-52	45.41	3.14 E-6	+57.0	96.2	+17.2	109.0	N	44
6-5, 80-82	45.71	9.44 E-6	-25.8	251.2	-61.1	249.6	R	>500
6-5, 110-112	46.01	6.49 E-6	+31.5	102.3	-71.1	151.9	R	242
6-5, 140-142	46.31	1.60 E-5	-51.8	297.1	-63.3	284.3	R	354
6-6, 20-22	46.61	8.22 E-7	-4.5	76.6	-76.3	111.8	R	363
*6-6, 50-52	46.91	1.09 E-5	+57.6	70.4	+34.7	7.9		35
*7-1, 109-111	48.50	6.34 E-6	+27.0	303.9	+18.8	295.7		298
7-1, 139-141	48.80	1.84 E-6	+38.7	289.3	-18.7	320.6	R	157
7-2, 8-10	48.99	3.21 E-5	-63.3	254.8	-67.3	254.7	R	320
7-2, 38-40	49.29	2.23 E-5	-70.1	280.3	-74.6	276.5	R	294
7-2, 68-70	49.59	4.00 E-6	-0.6	165.8	-51.8	213.2	R	289
7-2, 99-101	49.90	3.46 E-5	-74.9	230.8	-73.0	237.7	R	320
7-2, 139-141	50.30	2.70 E-5	-78.8	298.6	-75.6	273.9	R	335
7-3, 8-10	50.49	1.67 E-5	-71.0	273.7	-75.8	269.9	R	334
7-3, 38-40	50.79	3.38 E-5	-68.9	269.9	-76.3	264.5	R	326
7-3, 68-70	51.09	2.72 E-5	-63.3	268.0	-68.8	249.7	R	94
7-3, 99-101	51.40	1.67 E-5	-45.8	301.5	-56.3	291.3	R	370
7-3, 139-141	51.80	4.39 E-6	-10.8	266.2	-70.5	246.7	R	>500
7-4, 8-10	51.99	1.05 E-5	-52.3	278.1	-62.6	258.6	R	471
7-4, 38-40	52.29	6.43 E-7	+45.7	200.3	-57.7	222.6	R	383
7-4, 68-70	52.59	3.62 E-5	-79.6	219.9	-77.5	236.4	R	320
7-4, 99-101	52.90	2.81 E-6	-30.6	128.0	+58.1	52.0	N	198
7-5, 8-10	53.49	6.81 E-7	+39.6	109.6	+81.5	233.4	N	49

Table 18 (continued).

Sample interval (cm)	Sub-bottom depth (m)	J (NRM) (Gauss)	NRM		AF stable		Pol.	MDF (Oe)
			I	D	I	D		
7-5, 39-41	53.80	2.44 E-5	+82.1	91.2	+80.6	92.6	N	242
7-5, 68-70	54.09	3.85 E-5	+82.3	44.5	+83.0	85.0	N	309
7-5, 99-101	54.40	3.56 E-5	+73.6	55.6	+73.1	60.9	N	302
7-5, 139-141	54.80	1.06 E-5	+83.0	73.3	+83.1	70.8	N	149
7-6, 8-10	54.99	4.67 E-5	+73.0	43.5	+72.2	30.9	N	215
7-6, 39-41	55.30	7.16 E-6	-8.2	252.9	-41.4	250.7	R	305
7-6, 68-70	55.59	1.06 E-5	-45.0	263.9	-62.5	257.2	R	341
7-6, 99-101	55.90	1.01 E-6	-5.8	233.2	-62.0	232.4	R	>500
7-6, 139-141	56.30	2.87 E-6	-29.8	296.6	-64.1	255.9	R	>500
7-7, 8-10	56.49	9.20 E-6	-70.3	190.6	-70.6	204.0	R	472
7-7, 39-41	56.80	2.46 E-5	+31.9	100.9	+28.1	102.2	N	182
7-7, 68-70	57.09	7.24 E-7	-35.3	66.6	-62.0	62.9	R	318
*8-1, 39-41	57.30	1.87 E-5	+69.5	50.1	+67.4	45.9	R	170
8-1, 69-71	57.60	1.11 E-6	+75.1	145.1	+77.1	143.9	N	38
8-1, 99-101	57.90	5.46 E-6	+4.7	219.9	-58.2	215.1	R	>500
8-1, 129-131	58.20	7.53 E-7	-59.2	355.7	-74.7	337.0	R	>500
8-2, 9-11	58.50	6.72 E-6	-36.4	282.1	-60.1	278.6	R	486
8-2, 39-41	58.80	1.05 E-5	-22.9	291.4	-48.3	293.4	R	391
8-2, 69-71	59.10	1.73 E-5	-29.7	282.3	-52.2	286.4	R	435
8-2, 99-101	59.40	8.49 E-6	-37.2	283.0	-63.7	280.8	R	486
8-2, 129-131	59.70	2.08 E-5	-74.0	290.4	-73.7	291.9	R	381
8-3, 9-11	60.00	1.36 E-6	+63.5	344.4	+52.5	342.9	N	71
8-3, 43-45	60.34	1.56 E-5	-79.1	313.9	-79.6	310.8	R	395
8-3, 73-75	60.64	1.70 E-5	-62.2	88.4	-71.5	84.9	R	359
8-3, 99-101	60.90	1.57 E-6	-32.7	274.6	-65.5	272.9	R	>500
8-3, 129-131	61.20	9.24 E-6	-54.3	287.0	-61.5	294.9	R	384
8-4, 9-11	61.50	7.19 E-6	+71.1	25.5	-38.5	3.9	R	403
8-4, 39-41	61.80	6.56 E-6	-25.1	351.1	-61.1	322.7	R	>500
8-4, 69-71	62.10	1.43 E-5	-22.7	120.7	-64.8	335.2	R	75
8-4, 99-101	62.40	1.04 E-5	+64.2	126.7	-67.8	31.3	R	35
8-4, 129-131	62.70	8.64 E-6	-78.5	281.7	-64.9	286.3	R	333
8-5, 9-11	63.00	1.17 E-5	-36.4	0.0	-58.8	329.1	R	333
8-5, 39-41	63.30	2.75 E-5	-78.6	10.9	-75.4	332.4	R	291
8-5, 69-71	63.60	1.73 E-5	-50.0	73.6	-60.4	282.1	R	300
8-5, 99-101	63.90	4.92 E-6	-31.7	42.1	-60.5	293.3	R	477
8-5, 131-133	64.22	1.65 E-6	+53.2	271.8	-28.7	289.5	R	384
8-6, 9-11	64.50	1.44 E-6	-77.3	324.5	-77.5	318.7	R	709
8-6, 39-41	64.80	6.60 E-6	+52.8	110.2	+58.7	109.8	N	78
8-6, 69-71	65.10	2.84 E-5	+33.9	102.5	+48.3	96.4	N	107
8-6, 99-101	65.40	9.41 E-6	+49.5	96.3	+61.1	87.6	N	177
8-6, 129-131	65.70	4.09 E-6	+82.5	34.2	+80.0	9.0	N	134
8-7, 9-11	66.00	5.03 E-5	+32.4	152.3	+47.7	98.4	N	77
8-7, 39-41	66.30	1.80 E-5	+73.5	89.9	+69.2	87.8	N	142
9-1, 10-12	66.51	1.21 E-5	+22.4	91.5	+64.0	112.5	N	256
9-1, 40-42	66.81	3.14 E-5	+82.7	43.3	+83.0	61.2	N	275
9-1, 70-72	67.11	4.76 E-6	-76.6	145.6	-74.7	202.3	R	>500
9-1, 100-102	67.41	1.08 E-5	-65.8	202.3	-74.7	203.6	R	>500
9-1, 130-132	67.71	9.07 E-6	-30.7	236.5	-73.6	196.9	R	430
9-2, 10-12	68.01	1.02 E-5	-72.4	135.0	-65.4	191.1	R	457
9-2, 40-42	68.31	7.58 E-6	+3.2	172.5	+9.7	162.8	N	157
9-2, 70-72	68.61	2.09 E-5	+43.2	159.5	+29.8	157.4	N	329
*9-2, 100-102	68.91	4.48 E-6	+16.4	142.9	+8.9	168.5	R	298
*9-2, 130-132	69.21	1.08 E-5	+12.5	169.9	+7.5	164.6	R	342
9-3, 10-12	69.51	8.14 E-6	+73.2	99.8	+78.0	74.9	N	272
9-3, 46-48	69.87	5.53 E-6	+51.0	50.8	+49.6	50.7	N	75
9-3, 70-72	70.11	2.18 E-6	-3.6	260.2	-79.9	264.1	R	>500
9-3, 100-102	70.41	1.14 E-5	-59.8	160.3	-81.5	194.4	R	>500
9-4, 11-13	71.02	1.05 E-5	-58.3	145.4	-71.9	176.5	R	>500
9-4, 40-42	71.31	1.06 E-5	-54.9	162.3	-71.3	184.2	R	>500
9-4, 70-72	71.61	1.40 E-5	-74.8	123.8	-76.9	182.4	R	447
9-4, 102-104	71.93	1.54 E-5	-65.3	202.0	-73.4	199.6	R	483
9-4, 131-133	72.22	1.54 E-5	-55.1	161.1	-69.6	173.1	R	484
9-5, 11-13	72.52	1.30 E-5	-47.9	175.9	-67.4	187.0	R	483
9-5, 41-43	72.82	1.68 E-5	-61.0	177.0	-71.1	183.5	R	462
9-5, 71-73	73.12	1.77 E-5	-56.8	160.6	-69.0	167.3	R	422
9-5, 100-102	73.41	1.64 E-5	-62.2	154.1	-69.1	175.7	R	440
9-5, 131-133	73.72	3.55 E-5	-68.1	176.5	-72.3	177.5	R	314
9-6, 10-12	74.01	2.67 E-5	-69.2	194.8	-72.8	193.1	R	344
9-6, 39-41	74.30	2.46 E-5	-72.3	205.3	-76.0	199.8	R	405
9-6, 70-72	74.61	2.04 E-5	-65.9	172.8	-71.6	187.0	R	396
9-6, 99-101	74.90	1.29 E-5	-57.1	160.3	-69.3	159.5	R	438
9-6, 130-132	75.21	2.31 E-5	-77.1	141.0	-77.8	155.0	R	384
9-7, 9-11	75.50	1.86 E-5	-79.5	141.2	-81.0	158.7	R	428
9-7, 31-33	75.72	1.71 E-5	-62.2	206.4	-68.6	197.4	R	409
10-1, 8-10	75.99	8.68 E-6	+36.3	312.9	+54.9	304.0	R	277
9-7, 59-61	76.00	2.52 E-5	-68.3	179.7	-71.4	187.1	R	378
10-1, 69-71	76.60	1.04 E-5	+74.3	72.5	+74.7	90.0	N	105

Table 18 (continued).

Sample interval (cm)	Sub-bottom depth (m)	J (NRM) (Gauss)	NRM		AF stable		Pol.	MDF (Oe)
			I	D	I	D		
10-1, 100-102	76.91	2.72 E-6	+61.7	6.6	-67.7	269.9	R	61
10-1, 129-131	77.20	4.86 E-6	-74.7	243.3	-75.4	261.9	R	355
10-2, 10-12	77.51	6.01 E-7	+64.8	130.9	+71.0	125.0	N	41
10-2, 40-42	77.81	2.99 E-6	-79.7	216.9	-78.3	244.6	R	>650
10-2, 68-70	78.09	4.71 E-6	-76.0	55.9	-83.5	205.2	R	>500
10-2, 100-102	78.41	7.68 E-6	-77.6	212.3	-78.1	204.9	R	551
10-2, 130-132	78.71	8.95 E-6	-78.8	203.2	-80.0	232.6	R	534
10-3, 10-12	79.01	1.35 E-7	+52.9	124.2	-67.2	204.0	R	38
10-3, 40-42	79.31	7.48 E-8	+61.0	214.7	-58.2	204.0	R	47
10-3, 70-72	79.61	1.26 E-7	+72.2	19.5	-52.4	165.3	R	31
10-3, 99-101	79.90	2.57 E-7	+64.4	100.9	+64.0	88.5	N	73
10-3, 130-132	80.21	3.33 E-7	+70.7	71.4	+61.0	57.2	N	90
10-4, 10-12	80.51	1.30 E-6	+20.4	293.6	+73.8	36.8	N	30
10-4, 40-42	80.81	1.02 E-6	+20.4	272.1	+59.3	26.7	N	31
10-4, 70-72	81.11	5.00 E-7	+78.8	56.9	+71.0	59.6	N	46
10-4, 99-101	81.40	7.81 E-7	+76.6	57.3	+68.4	67.5	N	83
10-4, 125-127	81.66	7.75 E-7	+72.2	2.5	+74.6	83.1	N	37
10-5, 10-12	82.01	3.24 E-7	+77.2	135.0	-66.9	34.8	R	30
10-5, 40-42	82.31	8.19 E-7	-54.8	169.3	-75.2	205.1	R	624
10-5, 69-71	82.60	1.42 E-6	-66.8	266.0	-79.1	223.0	R	173
10-5, 98-100	82.89	2.51 E-7	+40.1	330.3	-82.7	300.0	R	31
10-5, 129-131	83.20	2.26 E-7	+16.7	318.3	-55.4	241.4	R	176
10-6, 9-11	83.50	4.73 E-7	+27.9	56.6	+64.7	79.2	N	152
10-6, 40-42	83.81	6.76 E-7	+76.7	355.5	+69.8	25.5	N	74
10-6, 70-72	84.11	7.47 E-7	+78.1	79.4	+74.3	57.7	N	46
10-6, 99-101	84.40	7.06 E-8	+46.7	217.6				
10-6, 129-131	84.70	6.14 E-8	+58.2	278.3				
10-7, 10-12	85.01	1.37 E-7	+72.4	18.3				
10-7, 40-42	85.31	2.68 E-7	+37.9	59.8	-62.1	169.3	R	33
11-1, 10-12	85.51	1.88 E-7	-1.0	41.2				
11-1, 40-42	85.81	2.77 E-8	+39.3	85.4				
11-1, 74-76	86.15	1.57 E-7	+71.8	19.8	-78.9	277.6	R	>500
11-1, 100-102	86.41	2.41 E-7	+39.3	192.4				
11-1, 130-132	86.71	3.81 E-6	-55.5	235.2				
11-2, 10-12	87.01	4.84 E-6	-50.2	162.4				
11-2, 40-42	87.31	2.49 E-7	-41.0	67.2				
11-2, 70-72	87.61	1.15 E-7	+29.3	356.4	-64.1	307.0	R	>300
11-2, 100-102	87.91	1.96 E-7	-20.1	190.3				
11-2, 130-132	88.21	1.50 E-7	-59.7	313.0				
11-3, 10-12	88.51	5.24 E-7	+66.6	164.6				
11-3, 40-42	88.81	2.14 E-7	+64.8	80.2				
11-3, 70-72	89.11	9.90 E-8	-44.3	103.0	-47.1	21.7	R	>500
11-3, 100-102	89.41	2.04 E-7	-38.6	144.0				
11-3, 130-132	89.71	3.54 E-7	-67.0	126.1				
11-4, 10-12	90.01	1.08 E-6	-65.7	187.3				
11-4, 40-42	90.31	2.35 E-6	-75.9	151.7				
11-4, 70-72	90.61	2.33 E-7	-32.0	140.9	-73.9	165.9	R	>500
11-4, 100-102	90.91	2.88 E-7	+56.1	102.7				
11-4, 130-132	91.21	5.92 E-8	+14.6	124.4				
11-5, 10-12	91.51	5.58 E-8	+0.9	91.7				
11-5, 40-42	91.81	1.56 E-7	+79.3	235.0				
11-5, 70-72	92.11	1.01 E-5	-73.6	158.6	-74.8	165.8	R	420
11-5, 100-102	92.41	7.42 E-7	-71.2	168.8				
11-5, 130-132	92.71	1.80 E-7	+53.9	281.6				
11-6, 10-12	93.01	4.10 E-7	+76.4	132.4				
11-6, 40-42	93.31	4.35 E-8	+50.3	80.5				
11-6, 70-72	93.61	4.38 E-7	-28.0	100.6	-80.6	134.6	R	>500
11-6, 100-102	93.91	1.39 E-6	-62.4	164.4				
11-6, 130-132	94.21	5.68 E-8	+49.4	60.3				
11-7, 10-12	94.51	1.99 E-7	+57.8	159.7				
11-7, 40-42	94.81	1.49 E-7	+46.8	154.2				
11-7, 63-65	95.04	1.98 E-7	-80.3	88.8	-86.4	125.3	R	>500
12-1, 25-27	95.16	1.43 E-7	+54.1	43.8				
12-1, 48-50	95.39	2.57 E-7	+68.5	31.1				
12-1, 70-72	95.61	2.56 E-7	+69.2	37.8	+68.8	65.4	N	45
12-1, 100-102	95.91	1.06 E-7	-3.6	8.3				
12-2, 25-27	96.66	6.58 E-7	-25.0	90.7				
12-2, 56-58	96.97	1.82 E-7	+82.3	44.0				
12-2, 70-72	97.11	3.60 E-7	+59.5	20.8	-70.1	65.0	R	50
12-2, 100-102	97.41	4.88 E-7	+85.2	306.6				
12-2, 130-132	97.71	9.28 E-7	+75.9	263.2				
12-3, 10-12	98.01	3.90 E-7	+86.2	296.4				
12-3, 36-38	98.27	4.11 E-7	+81.6	231.3				
12-3, 70-72	98.61	3.36 E-7	+82.1	0.4	+72.4	349.8	N	37
12-3, 100-102	98.91	1.33 E-6	+86.7	30.2				
12-3, 130-132	99.21	7.34 E-7	+80.4	162.8				
12-4, 10-12	99.51	1.41 E-6	+85.2	93.0				

Table 18 (continued).

Sample interval (cm)	Sub-bottom depth (m)	J (NRM) (Gauss)	NRM		AF stable		Pol.	MDF (Oe)
			I	D	I	D		
12-4, 43-45	99.84	7.95 E-7	+79.9	171.0				
12-4, 72-74	100.13	2.95 E-7	+69.2	267.9	+63.3	62.3	N	41
12-4, 102-104	100.43	3.12 E-7	+78.2	326.5				
12-5, 10-12	101.01	1.04 E-6	+79.2	321.4				
12-5, 43-45	101.34	5.28 E-7	+83.2	302.1				
12-5, 72-74	101.63	3.85 E-7	+79.6	58.4	+67.2	16.1	N	160
12-5, 102-104	101.93	3.98 E-7	+72.6	278.9				
12-5, 134-136	102.25	8.18 E-7	+85.6	299.7				
12-6, 10-12	102.51	8.38 E-7	+82.5	336.6				
12-6, 43-45	102.84	1.17 E-6	+81.8	255.3				
12-6, 72-74	103.13	1.05 E-6	+75.6	276.9	+71.4	277.6	N	175
12-6, 102-104	103.43	5.43 E-7	+76.9	272.7				
12-6, 134-136	103.75	3.34 E-7	+61.7	50.2				
12-7, 10-12	104.01	3.96 E-7	+71.9	29.0				
12-7, 24-26	104.15	3.44 E-7	+84.2	6.5	+68.1	251.5	N	41
13-1, 20-22	104.41	2.38 E-6	-72.5	80.7				
13-1, 50-52	104.71	9.77 E-7	+40.7	48.6				
*13-1, 80-82	105.01	1.35 E-6	+29.1	165.1	+52.4	107.3		32
13-1, 110-112	105.31	1.25 E-7	+67.3	358.4				
13-1, 144-146	105.65	2.08 E-7	+75.0	79.8				
13-2, 20-22	105.91	2.72 E-7	-16.8	336.2				
13-2, 50-52	106.21	3.81 E-7	+59.0	78.6				
13-2, 80-82	106.51	3.25 E-7	+66.2	65.2	+56.1	179.6	N	41
13-2, 110-112	106.81	9.34 E-7	+62.2	343.4				
13-2, 140-142	107.11	4.07 E-7	+75.2	65.5				
13-3, 20-22	107.41	4.06 E-7	+84.3	54.8				
13-3, 50-52	107.71	2.67 E-7	+73.5	46.4				
13-3, 80-82	108.01	6.17 E-7	+76.3	49.6	+73.2	56.6	N	79
13-3, 110-112	108.31	3.40 E-7	-50.2	208.9				
13-3, 140-142	108.61	1.87 E-7	+64.2	61.7				
13-4, 20-22	108.91	3.00 E-7	+75.2	356.5				
13-4, 50-52	109.21	7.48 E-7	+77.3	241.0				
13-4, 80-82	109.51	3.00 E-7	+80.7	41.0	+80.1	0.9	N	184
13-4, 110-112	109.81	2.64 E-7	+68.4	66.3				
13-5, 20-22	110.41	3.64 E-7	+65.2	43.9				
13-5, 55-57	110.76	2.53 E-7	+79.0	81.6				
13-5, 80-82	111.01	3.50 E-7	+74.8	45.0	+74.8	35.2	N	48
13-5, 110-112	111.31	1.71 E-7	+7.9	186.9				
13-5, 140-142	111.61	1.71 E-7	+33.7	161.7				
13-6, 18-20	111.89	2.31 E-7	+25.4	324.8				
13-6, 50-52	112.21	4.75 E-7	+45.9	327.2				
13-6, 80-82	112.51	2.80 E-7	+75.2	64.4	+70.3	70.2	N	154
13-6, 110-112	112.81	2.39 E-7	+84.4	53.5				
13-6, 140-142	113.11	2.96 E-7	+54.7	25.6				
13-7, 31-33	113.52	4.71 E-7	-81.7	120.6	-66.6	100.4	R	37
15-1, 42-44	123.93	9.13 E-8	+82.3	33.6	+66.6	110.4	N	33
15-1, 80-82	124.31	6.35 E-8	+52.6	97.3	+69.1	91.8	N	>200
15-1, 110-112	124.61	3.58 E-7	+56.2	39.9				
15-2, 18-20	125.19	4.11 E-7	+66.3	196.2				
15-2, 48-50	125.49	7.12 E-8	+43.6	65.8	-62.6	83.7	R	118
15-2, 109-111	126.10	8.13 E-8	+41.8	17.0				
15-3, 18-20	126.69	1.45 E-7	+65.2	73.0				
15-3, 80-82	127.31	1.04 E-7	+50.4	16.3	+59.6	8.7	N	92
16-1, 20-22	128.31	1.80 E-7	+1.1	22.2				
16-1, 50-52	128.61	4.68 E-8	+4.7	15.8				
16-1, 80-82	128.91	3.29 E-7	+82.0	346.5	-22.2	297.0	R	37
16-1, 110-112	129.21	1.79 E-7	+73.1	276.0				
16-1, 140-142	129.51	3.18 E-7	+74.1	204.5				
16-2, 20-22	129.81	2.41 E-6	+70.7	105.8				
16-2, 50-52	130.11	3.24 E-7	+73.8	272.1				
16-2, 80-82	130.41	1.66 E-7	+82.5	297.3	+77.7	215.2	N	203
16-2, 112-114	130.73	2.26 E-6	+78.8	225.0	+74.9	233.6	N	397
16-2, 140-142	131.01	8.75 E-7	+71.9	275.6				
16-3, 18-20	131.29	7.44 E-7	+76.4	314.7	+78.2	304.6	N	>500
16-4, 20-22	132.81	2.98 E-7	+56.7	31.4				
16-4, 50-52	133.11	2.62 E-6	+86.8	309.3				
16-4, 80-82	133.41	6.53 E-7	+42.0	324.2	+73.2	317.2	N	187
16-4, 108-110	133.69	1.15 E-6	+81.1	286.5				
16-4, 142-144	134.03	2.62 E-7	+76.6	344.0				
16-5, 19-21	134.30	8.67 E-7	+85.7	227.6				
16-5, 50-52	134.61	5.23 E-7	+86.7	142.4				
16-5, 80-82	134.91	2.46 E-7	+72.2	87.5	+76.7	75.4	N	162
16-5, 110-112	135.21	1.57 E-7	+82.4	267.6				
16-5, 141-143	135.52	1.47 E-7	+76.6	358.7				
16-6, 20-22	135.81	1.25 E-7	+74.6	342.6				
16-6, 49-51	136.10	5.27 E-7	+81.8	193.3				
16-6, 81-83	136.42	5.22 E-7	+76.9	98.6	+69.3	92.9	N	129

Table 18 (continued).

Sample interval (cm)	Sub-bottom depth (m)	J (NRM) (Gauss)	NRM		AF stable		Pol.	MDF (Oe)
			I	D	I	D		
16-6, 111-113	136.72	1.52 E-7	+ 83.4	162.5				
16-7, 19-21	137.30	1.23 E-7	+ 80.5	78.8				
16-7, 50-52	137.61	1.11 E-7	+ 65.8	1.9				
16-7, 80-82	137.91	1.70 E-7	+ 67.4	43.0	+ 60.8	44.6	N	40
16-7, 110-112	138.21	4.20 E-7	+ 79.0	21.5				
17-1, 50-52	138.51	3.38 E-7	+ 85.0	333.8				
17-1, 80-82	138.81	2.11 E-7	+ 73.8	74.5	+ 66.9	51.3	N	50
17-1, 110-112	139.11	6.51 E-7	+ 65.9	112.4	+ 61.7	109.4	N	234
17-1, 140-142	139.41	5.67 E-7	+ 73.6	160.6				
17-2, 20-22	139.71	3.21 E-7	+ 69.3	111.8				
17-2, 50-52	140.01	3.64 E-7	+ 84.7	31.0				
17-2, 80-82	140.31	4.72 E-7	+ 81.2	206.1	+ 61.5	230.3	N	44
17-2, 110-112	140.61	2.04 E-7	+ 78.9	64.1				
17-2, 140-142	140.91	2.74 E-7	+ 73.6	1.2				
17-3, 20-22	141.21	3.60 E-7	+ 42.4	349.6				
17-3, 50-52	141.51	1.65 E-7	+ 78.6	55.3				
17-3, 80-82	141.81	1.38 E-7	+ 75.6	343.2	+ 75.4	18.9	N	49
17-3, 110-112	142.11	1.68 E-7	+ 74.0	40.6				
17-4, 20-22	142.71	2.32 E-7	+ 76.3	64.0				
17-4, 50-52	143.01	8.82 E-8	+ 67.3	13.9				
17-4, 80-82	143.31	9.33 E-8	+ 69.9	157.7	+ 62.4	153.9	N	61
17-4, 110-112	143.61	8.27 E-8	+ 72.0	42.3				
17-4, 140-142	143.91	1.40 E-7	+ 70.4	23.8				
17-5, 20-22	144.21	1.52 E-7	+ 75.6	53.3				
17-5, 48-50	144.49	1.87 E-7	+ 72.2	38.5				
17-5, 80-82	144.81	1.87 E-7	+ 81.8	74.6	+ 75.5	114.0	N	50
17-5, 110-112	145.11	3.83 E-7	+ 72.7	82.3	+ 61.3	90.8	N	44
17-6, 20-22	145.71	1.97 E-7	+ 78.2	49.3				
17-6, 50-52	146.01	1.98 E-7	+ 71.5	43.1				
17-6, 80-82	146.31	2.27 E-7	+ 85.3	0.3	+ 76.9	95.0	N	43
17-6, 110-112	146.61	1.69 E-7	+ 80.0	350.5				
17-6, 140-142	146.91	3.15 E-7	+ 74.4	66.0				
17-1, 20-22	147.21	3.44 E-7	+ 79.2	51.2	+ 74.0	60.2	N	43
18-1, 20-22	148.01	9.78 E-8	+ 70.8	72.1				
18-1, 50-52	148.31	6.56 E-8	+ 62.3	31.3				
18-1, 80-82	148.61	1.45 E-7	+ 76.8	50.7	+ 75.8	43.8	N	60
18-1, 110-112	148.91	1.58 E-7	+ 60.5	29.1				
18-1, 140-142	149.21	1.42 E-7	+ 76.2	1.9				
18-2, 20-22	149.51	1.52 E-7	+ 77.6	39.6				
18-2, 50-52	149.81	1.44 E-7	+ 63.1	2.6				
18-2, 80-82	150.11	6.54 E-8	+ 78.5	22.8	+ 77.0	110.2	N	37
18-2, 110-112	150.41	1.05 E-7	+ 84.9	347.5				
18-2, 140-142	150.71	7.93 E-8	+ 63.3	28.3				
18-3, 20-22	151.01	1.14 E-7	+ 70.0	39.3				
18-3, 50-52	151.31	1.90 E-7	+ 72.4	56.6				
18-3, 80-82	151.61	1.10 E-6	+ 76.7	81.1	+ 73.3	87.4	N	102
18-3, 110-112	151.91	1.17 E-7	+ 83.5	48.0				
18-3, 140-142	152.21	4.92 E-6	+ 80.4	33.3	+ 83.3	30.5	N	261
18-4, 20-22	152.51	4.10 E-8	+ 67.4	79.0				
18-4, 50-52	152.81	9.58 E-8	+ 77.9	45.8				
18-4, 80-82	153.11	1.47 E-7	+ 75.6	72.0	+ 77.2	108.9	N	235
18-4, 110-112	153.41	1.17 E-7	+ 71.0	337.6				
18-4, 140-142	153.71	2.44 E-7	+ 80.5	121.7				
18-5, 20-22	154.01	1.02 E-7	- 64.7	79.6	+ 66.0	283.1	N	31
18-5, 50-52	154.31	7.13 E-8	+ 63.4	358.7				
18-5, 80-82	154.61	3.82 E-8	+ 79.6	145.9	+ 70.8	113.5	N	53
18-5, 110-112	154.91	2.48 E-7	+ 60.9	131.4	+ 73.5	133.0	N	146
18-6, 20-22	155.51	1.41 E-7	+ 68.1	52.9				
18-6, 50-52	155.81	1.13 E-7	+ 73.8	353.2				
18-6, 80-82	156.11	1.02 E-7	+ 69.4	125.2	+ 74.6	133.4	N	76
18-6, 110-112	156.41	4.39 E-8	+ 64.8	17.8				
18-6, 140-142	156.71	7.05 E-8	+ 48.3	347.9				
18-7, 20-22	157.01	5.52 E-8	+ 68.5	83.6	+ 71.3	77.5	N	59
19-1, 80-82	158.51	1.19 E-7	+ 84.1	281.1	+ 71.4	327.4	N	50
19-1, 110-112	158.81	9.84 E-8	+ 76.7	7.0				
19-1, 140-142	159.11	1.73 E-7	+ 48.0	34.7				
19-2, 20-22	159.41	1.52 E-7	+ 69.2	358.4				
19-2, 50-52	159.71	2.23 E-7	+ 72.6	74.6				
19-2, 86-88	160.07	2.24 E-7	+ 80.2	48.7	+ 70.2	108.8	N	48
19-2, 110-112	160.31	4.31 E-7	+ 75.5	46.3	+ 69.7	39.6	N	94
19-2, 140-142	160.61	2.83 E-7	+ 85.0	93.5				
19-3, 20-22	160.91	3.09 E-7	+ 77.2	58.8				
19-3, 50-52	161.21	2.86 E-7	+ 75.4	30.2				
19-3, 80-82	161.51	1.85 E-7	+ 87.8	89.8	+ 79.3	148.6	N	45
19-3, 110-112	161.81	1.77 E-7	+ 80.8	358.5				
19-3, 140-142	162.11	3.38 E-7	+ 85.4	51.3	+ 82.8	15.2	N	87
19-4, 20-22	162.41	2.18 E-7	+ 83.9	57.7				

Table 18 (continued).

Sample interval (cm)	Sub-bottom depth (m)	J (NRM) (Gauss)	NRM		AF stable		Pol.	MDF (Oe)
			I	D	I	D		
19-4, 50-52	162.71	2.41 E-7	+85.6	334.0				
19-4, 80-82	163.01	2.64 E-7	+81.1	311.9	+76.8	320.1	N	49
19-4, 110-112	163.31	2.40 E-7	+87.5	353.5				
19-5, 20-22	163.91	7.73 E-7	+80.4	11.2	+70.8	350.0	N	38
19-5, 50-52	164.21	2.92 E-7	+73.9	349.2				
*19-5, 80-82	164.51	2.10 E-7	+36.6	316.6	+65.6	55.8		31
19-5, 110-112	164.81	2.45 E-7	+73.9	29.8	+81.6	43.6	N	38
19-5, 140-142	165.11	1.19 E-6	-18.8	272.8	-52.1	340.5	R	50
19-6, 20-22	165.41	1.77 E-7	+75.0	38.4				
19-6, 50-52	165.71	2.05 E-7	+84.0	35.7				
19-6, 80-82	166.01	2.98 E-7	+78.0	214.4	+72.8	267.5	N	39
19-6, 110-112	166.31	3.00 E-7	+30.9	348.0				
19-6, 140-142	166.61	1.53 E-7	+49.4	356.4				
19-7, 20-22	166.91	3.80 E-7	-39.2	327.9	+73.7	269.5	N	37
20-1, 20-22	167.61	1.23 E-7	+58.6	311.4				
20-1, 50-52	167.91	4.00 E-6	+16.3	227.3	+67.8	217.1	N	49
20-1, 80-82	168.21	1.75 E-7	+65.2	84.2	+67.8	78.3	N	95
20-1, 110-112	168.51	1.40 E-7	+51.1	344.7				
20-1, 140-142	168.81	1.98 E-7	+27.8	311.8				
20-2, 20-22	169.11	5.50 E-7	+75.9	148.1	+61.1	156.6	N	62
20-2, 50-52	169.41	3.68 E-7	+88.4	106.1	+76.6	96.0	N	37
20-2, 80-82	169.71	1.60 E-7	+83.2	200.1	+82.0	208.4	N	49
20-2, 110-112	170.01	7.85 E-7	+80.6	229.9	+77.8	227.4	N	350
20-2, 140-142	170.31	2.93 E-7	+57.7	30.4				
20-3, 20-22	170.61	1.01 E-7	+67.0	11.9				
20-3, 50-52	170.91	9.93 E-8	+69.5	134.3				
20-3, 80-82	171.21	7.68 E-7	+61.0	155.5	+83.7	146.6	N	460
20-3, 110-112	171.51	1.95 E-7	+83.2	211.5				
20-3, 140-142	171.81	1.66 E-7	+74.9	70.7				
20-4, 20-22	172.11	6.10 E-7	+33.0	198.4	+84.7	251.7	N	66
20-4, 50-52	172.41	9.43 E-8	+63.1	38.2				
20-4, 80-82	172.71	1.27 E-7	+66.5	181.3	+73.8	228.6	N	213
20-4, 110-112	173.01	2.09 E-7	-66.1	28.4	+87.8	281.4	N	20
20-5, 20-22	173.61	1.27 E-7	+64.3	33.5				
20-5, 50-52	173.91	2.33 E-7	+79.9	74.4				
20-5, 80-82	174.21	2.80 E-7	+85.8	281.1	+75.2	256.8	N	94
20-5, 110-112	174.51	1.47 E-7	+71.4	0.9				
20-5, 140-142	174.81	1.23 E-7	+74.0	27.0				
20-6, 20-22	175.11	1.35 E-7	+79.7	347.5				
20-6, 50-52	175.41	3.05 E-7	+83.1	126.8	+82.3	149.6	N	88
20-6, 80-82	175.71	1.82 E-7	+85.6	343.1	+79.8	249.1	N	126
20-6, 110-112	176.01	2.33 E-7	+75.6	351.3				
20-6, 140-142	176.31	3.58 E-7	+80.2	46.2				
20-7, 20-22	176.61	1.32 E-6	+87.1	4.9	+86.4	236.2	N	350
20-7, 52-54	176.93	1.12 E-7	+79.3	134.5	+73.0	166.7	N	217
21-1, 80-82	177.91	1.12 E-7	+30.7	352.7	+81.4	163.9	N	39
21-1, 110-112	178.21	9.22 E-8	+78.4	26.2				
21-1, 140-142	178.51	7.56 E-8	+56.4	331.0				
21-2, 20-22	178.81	1.58 E-7	+47.3	347.0				
21-2, 50-52	179.11	7.45 E-8	+60.5	13.0	+67.4	170.8	N	343
21-2, 80-82	179.41	6.38 E-8	+74.2	209.5	+62.6	205.8	N	38
21-2, 110-112	179.71	9.82 E-8	+69.1	323.8				
21-3, 20-22	180.31	2.69 E-7	+67.7	352.3				
21-3, 50-52	180.61	1.64 E-6	+77.5	28.3	+73.9	52.1	N	155
21-3, 80-82	180.91	4.47 E-6	+71.1	100.3	+66.7	69.9	N	44
21-3, 110-112	181.21	1.34 E-6	+80.3	122.3	+74.8	171.0	N	40
21-4, 20-22	181.81	1.70 E-7	+77.1	9.6				
21-4, 50-52	182.11	1.75 E-7	-10.2	31.2	+73.8	112.3	N	246
21-4, 80-82	182.41	1.37 E-7	+60.7	77.2	+61.1	71.2	N	61
21-4, 110-112	182.71	2.15 E-7	+78.0	39.8				
21-4, 140-142	183.01	1.17 E-7	+62.6	101.6				
21-5, 20-22	183.31	1.71 E-7	+68.0	34.7				
21-5, 50-52	183.61	9.22 E-8	+64.9	16.3				
21-5, 80-82	183.91	1.19 E-7	+74.7	111.9	+73.5	84.0	N	45
21-5, 110-112	184.21	2.43 E-7	+78.8	48.8				
21-5, 140-142	184.51	4.73 E-7	+85.0	88.3	+81.7	81.4	N	79
21-6, 20-22	184.81	1.95 E-7	+83.3	31.7				
21-6, 80-82	185.41	1.71 E-7	+72.3	76.9	+72.3	84.9	N	122
21-6, 110-112	185.71	3.02 E-7	+81.7	83.5				
21-6, 140-142	186.01	2.19 E-6	+80.9	131.9	+80.1	120.3	N	350
21-7, 20-22	186.31	1.50 E-7	+84.3	30.2	+85.7	125.1	N	55
22-1, 20-22	186.91	1.47 E-7	+80.4	14.3				
22-1, 50-52	187.21	1.01 E-7	+58.7	9.2				
22-1, 80-82	187.51	3.13 E-7	+85.6	289.7	+78.6	6.6	N	145
22-1, 110-112	187.81	8.68 E-7	+78.1	122.9	+71.1	130.4	N	133
22-1, 140-142	188.11	7.73 E-7	+81.7	19.6				
22-2, 20-22	188.41	1.80 E-8	+70.1	117.9				

Table 18 (continued).

Sample interval (cm)	Sub-bottom depth (m)	J (NRM) (Gauss)	NRM		AF stable		Pol.	MDF (Oe)
			I	D	I	D		
22-2, 50-52	188.71	1.00 E-6	+88.7	349.2				
22-2, 80-82	189.01	8.02 E-7	+77.1	344.9	+75.9	343.6	N	217
22-2, 110-112	189.31	6.64 E-7	+77.8	24.6				
22-2, 140-142	189.61	1.36 E-7	+77.0	43.4				
22-3, 20-22	189.91	1.27 E-6	+87.5	46.8	+88.4	59.5	N	230
22-3, 50-52	190.21	2.20 E-7	+77.8	116.0				
22-3, 80-82	190.51	6.54 E-8	+75.5	143.9	+71.9	139.0	N	120
22-3, 110-112	190.81	2.67 E-6	+39.4	5.1	+70.6	333.8	N	190
22-3, 140-142	191.11	1.20 E-7	-5.6	33.4	+75.3	253.8	N	23
22-4, 20-22	191.41	9.52 E-8	+48.9	346.2	+66.1	319.8	N	51
22-4, 50-52	191.71	2.76 E-7	-20.8	210.9	-69.8	287.9	R	46
22-4, 80-82	192.01	5.62 E-8	+63.6	29.6	+65.0	10.6	N	48
22-4, 110-112	192.31	1.15 E-7	+77.4	253.4	+79.7	344.7	N	39
22-5, 20-22	192.91	7.16 E-8	+28.8	285.7	-79.2	34.5	R	21
22-5, 50-52	193.21	1.92 E-7	-76.5	203.8	-78.1	179.5	R	46
22-5, 80-82	193.51	1.08 E-7	-27.0	294.2	-66.3	276.3	R	87
22-5, 110-112	193.81	7.72 E-8	+73.7	213.3	+76.5	4.1	N	291
22-5, 140-142	194.11	4.38 E-8	+77.4	128.1	-58.7	186.8	R	20
22-6, 20-22	194.41	4.14 E-8	+60.1	2.0	-82.5	62.9	R	41
22-6, 50-52	194.71	6.62 E-8	+16.4	125.5	-4.5	130.6		67
22-6, 80-82	195.01	5.66 E-8	+60.5	127.3	+58.8	140.0	N	27
22-6, 110-112	195.31	1.57 E-7	+67.6	166.5	+61.2	180.8	N	40
22-6, 140-142	195.61	7.59 E-8	+68.6	55.1				
23-1, 11-13	196.12	7.00 E-7	-52.7	104.2	-55.6	96.6	R	42
23-1, 40-42	196.41	4.75 E-7	+78.1	73.0				
23-1, 70-72	196.71	1.80 E-7	+74.2	27.4	+68.5	11.4	N	49
23-1, 100-102	197.01	2.55 E-7	+80.0	35.0				
23-1, 130-132	197.31	2.04 E-7	+78.0	36.0				
23-2, 10-12	197.61	3.12 E-7	+70.8	93.1	+66.0	58.4	N	394
23-2, 40-42	197.91	1.44 E-7	+85.2	351.5				
23-2, 70-72	198.21	1.75 E-7	+68.1	69.0	70.6	5.0	N	41
23-2, 100-102	198.51	2.55 E-7	+60.3	164.1				
23-2, 130-132	198.81	1.59 E-7	+82.1	103.3				
23-3, 10-12	199.11	4.25 E-7	+41.4	315.0	+73.1	13.6	N	38
23-3, 40-42	199.41	1.34 E-7	+75.0	283.6				
23-3, 70-72	199.71	3.92 E-7	+35.8	23.0	+57.5	74.3	N	36
23-3, 100-102	200.01	4.92 E-7	-8.4	265.4	+58.2	351.4	N	38
23-3, 130-132	200.31	1.13 E-7	+78.8	27.4				
23-4, 9-11	200.60	1.90 E-7	+75.7	354.1				
23-4, 39-41	200.90	2.39 E-7	+78.0	53.8				
23-4, 69-71	201.20	2.34 E-7	+73.8	78.7	+74.7	81.7	N	172
23-4, 101-103	201.52	1.13 E-7	+71.3	10.2				
23-4, 130-132	201.81	1.24 E-7	+73.6	358.2				
23-5, 9-11	202.10	2.04 E-7	+71.8	28.2				
23-5, 39-41	202.40	1.08 E-7	+79.3	69.9				
23-5, 69-71	202.70	2.05 E-7	+87.8	135.9	+83.0	13.8	N	94
23-5, 101-103	203.02	1.32 E-7	+71.6	6.6				
23-5, 130-132	203.31	1.10 E-7	+72.4	49.0				
23-6, 9-11	203.60	1.28 E-7	+78.1	40.8				
23-6, 39-41	203.90	1.55 E-7	+79.0	340.7				
23-6, 69-71	204.20	1.32 E-7	+79.8	236.6	+85.9	54.5	N	49
23-6, 101-103	204.52	2.04 E-7	+82.3	43.7				
23-6, 132-134	204.83	1.62 E-7	+85.0	223.7				
23-7, 9-11	205.10	1.68 E-7	+76.8	336.0				
23-7, 39-41	205.40	5.74 E-7	+78.2	65.1	+74.8	47.4	N	114
24-1, 70-72	206.31	3.59 E-8	+81.3	126.6	+75.5	126.6	N	55
24-1, 99-101	206.60	4.68 E-8	+10.1	300.2				
24-1, 130-132	206.91	5.74 E-8	+45.5	97.5				
24-2, 10-12	207.21	8.03 E-8	+76.4	326.1				
24-2, 40-42	207.51	5.20 E-8	+67.9	269.6				
24-2, 70-72	207.81	3.66 E-8	+75.7	28.6	+66.2	353.5	N	>150
24-2, 99-101	208.10	2.01 E-8	+69.1	246.8				
24-2, 130-132	208.41	7.01 E-8	+68.6	344.5				
24-3, 10-12	208.71	1.31 E-7	+29.7	163.3	+76.3	246.2	N	118
24-3, 40-42	209.01	4.91 E-8	+57.6	20.5				
24-3, 70-72	209.31	6.48 E-9	+57.6	172.4	+57.6	172.4	N	>30
24-3, 99-101	209.60	2.36 E-8	+21.6	316.8				
24-4, 10-12	210.21	4.61 E-8	+57.4	14.2				
24-4, 40-42	210.51	5.10 E-8	+37.1	358.4				
24-4, 70-72	210.81	2.32 E-8	+71.7	178.1	-37.0	97.3	R	21
24-4, 99-101	211.10	3.44 E-8	+2.3	311.0				
24-4, 130-132	211.41	2.85 E-8	+47.4	312.4				
24-5, 10-12	211.71	6.43 E-8	+77.8	117.0				
24-5, 40-42	212.01	3.57 E-8	+33.0	304.8				
24-5, 70-72	212.31	4.97 E-8	+86.2	167.0	+72.8	34.9	N	29
24-5, 99-101	212.60	3.08 E-8	+8.8	340.4				
24-5, 130-132	212.91	7.87 E-8	+18.6	272.7				

Table 18 (continued).

Sample interval (cm)	Sub-bottom depth (m)	J (NRM) (Gauss)	NRM		AF stable		Pol.	MDF (Oe)
			I	D	I	D		
25-1, 40-42	213.51	3.97 E-8	+ 37.9	291.2				
25-1, 70-72	213.81	5.83 E-8	- 38.2	246.2	- 63.7	260.7	R	278
25-1, 100-102	214.11	2.40 E-8	+ 0.0	302.2				
25-1, 130-132	214.41	8.06 E-8	+ 76.6	343.8				
25-2, 10-12	214.71	2.55 E-8	- 26.4	311.8				
25-2, 40-42	215.01	3.41 E-8	+ 17.8	323.5				
25-2, 70-72	215.31	9.99 E-9	+ 56.7	258.9	- 63.9	223.4	R	>200
25-2, 100-192	215.61	5.76 E-8	- 18.6	308.5				
25-2, 130-132	215.91	4.27 E-8	+ 32.5	350.2				
25-3, 10-12	216.21	3.19 E-8	+ 1.9	322.5				
25-3, 40-42	216.51	3.12 E-8	+ 24.0	315.9				
25-3, 70-72	216.81	5.31 E-7	- 58.5	5.4	- 58.7	5.4	R	148
25-3, 100-102	217.11	3.25 E-8	+ 18.0	0.3				
25-3, 130-132	217.41	3.94 E-8	- 6.0	13.4	- 53.8	61.4	R	29
25-4, 10-12	217.71	1.02 E-7	+ 65.2	131.8	+ 75.2	161.3	N	205
25-4, 40-42	218.01	3.09 E-8	+ 22.7	356.7				
25-4, 70-72	218.31	1.95 E-8	+ 56.0	64.7	+ 65.6	21.9	N	91
25-4, 100-102	218.61	2.02 E-8	+ 66.0	332.7				
25-4, 130-132	218.91	2.28 E-8	+ 10.5	321.7				
25-5, 10-12	219.21	4.49 E-8	+ 28.6	293.2				
25-5, 40-42	219.51	1.85 E-8	+ 21.8	296.0				
25-5, 70-72	219.81	1.31 E-8	+ 37.4	23.1	+ 71.9	279.3	N	>150
25-5, 100-102	220.11	5.82 E-8	- 41.1	244.5	- 51.3	226.2	R	21
25-5, 130-132	220.41	1.84 E-7	+ 85.1	152.1				
25-6, 10-12	220.71	3.78 E-8	+ 52.0	254.2				
25-6, 40-42	221.01	4.15 E-8	+ 76.2	300.0	+ 80.0	76.3	N	122

* Disturbed core intervals; abbreviations: J = intensity, I = inclination, D = declination of natural remanent magnetization (NRM) and stable remanence after AF demagnetization, Pol = polarity, N = normal, R = reversed, MDF = median destructive field.

cores the data do not allow us to establish a plausible magnetostratigraphy.

The variation in stable magnetization, inclination, and NRM intensity with depth as obtained from shore-based work is shown in Figure 50. The respective data for some 650 discrete samples are listed in Table 18.

With but two exceptions, all NRM inclinations down to Section 104-642B-5H-5 consistently indicate a normal polarity corresponding to the present Brunhes field configuration. Although this conclusion is based on a rather fragmentary polarity record, the results summarized in Table 18 indicate the first clear horizon of negative inclinations in Section 104-642B-5H-6. The Brunhes/Matuyama geomagnetic boundary (0.73 Ma) was identified, therefore, at 37.11 mbsf. Higher in the core, the negative remanent directions obtained imply the presence of short reversed polarity intervals within the Brunhes Epoch.

Below Core 104-642B-5H, even the simple polarity sequence of the last four geomagnetic epochs spanning the period to about the uppermost Miocene was difficult to decipher. A preliminary tentative correlation of the rather peculiar downhole reversal pattern in the upper 100 m of the core with the geomagnetic polarity time scale is given in Table 20. The almost persistent positive inclinations of the sediment series recovered from the lower half of Hole 642B are interpreted as reflecting a major overprinting of the primary magnetization by subsequent secondary components. These components could be either of *in-situ* viscous origin resulting from the Brunhes field or else might have been acquired during the drilling process.

The downhole pattern in NRM intensity of the sediments recovered from Hole 642B shows various remarkable features. In the upper about 80 m (Core 104-642B-1H through about mid Core 104-642B-10H), remanent intensities of some 10^{-5} Gauss are typical, their variability being limited to roughly one order of magnitude at all levels. This high average value for marine sediments should mainly reflect the predominance of terrigenous components in these glacial/interglacial deposits. The base of

lithologic Unit I at 65.7 mbsf (Core 104-642B-8H-6, 132 cm), presently interpreted as marking the onset of the late Pliocene and Quaternary glacial/interglacial periods, reveals no conspicuous variations in magnetic properties. Instead, the sharp drop to, on average, some 10^{-7} Gauss in remanent intensity only occurs at around 79 mbsf (top of Section 104-642B-10H-3) about halfway between the lithologic boundaries Unit I/Unit II and Subunit IIA/Subunit IIB. This latter level of magnetization intensity, characteristic for most unconsolidated marine sediments, persists to the base of Hole 642B at about 221 mbsf. It is tempting to identify the earliest stage of late Neogene glaciation in the Norwegian Sea with the first occurrence of unusually high remanent intensities. In any case, this change toward higher intensities is most likely indicative of a significant environmental change toward an intensified influx of terrigenous materials. According to the interpretation of the paleomagnetic record (Fig. 52), this change in intensities almost coincides with the geomagnetic Gilbert/Epoch 5 boundary, indicating an age of about 5.3 Ma.

Hole 642C

Hole 642C penetrated a largely identical sediment series to that recovered from Hole 642B in a parallel APC operation. Their magnetic properties allowed establishment of a relatively complete magnetostratigraphy at least for the upper half of the cored interval. Several gaps in the paleomagnetic record here mainly result from more or less intensely disturbed sediment sections found at various levels.

The downhole variation in stable remanent inclination and NRM intensity of Hole 642C cores is shown in Figure 51. The respective data for discrete samples are listed in Table 19. The NRM intensity shows a very similar pattern to that observed in Hole 642B. A sharp decrease from an average high remanent magnetization of some 10^{-5} Gauss in Cores 104-642C-1H through 104-642C-10H to some 10^{-7} Gauss occurs within Section 104-642C-11H-4 (at about 79 mbsf, Fig. 51). As in Hole 642B, intensities

Table 19. Paleomagnetic properties of Hole 642C sediments.

Sample interval (cm)	Sub-bottom depth (m)	J (NRM) (Gauss)	NRM		AF stable		Pol.	MDF (Oe)
			I	D	I	D		
1-2, 79-81	2.30	3.24 E-6	+59.6	125.8	+57.0	135.0	N	136
1-2, 141-143	2.92	8.08 E-6	+81.0	197.3	+74.0	261.8	N	217
2-1, 41-43	3.82	3.22 E-5	+69.6	129.4	+71.5	133.4	N	257
2-1, 103-105	4.44	1.07 E-5	+60.0	68.8	+68.3	144.6	N	109
2-2, 48-50	5.39	1.40 E-5	+74.6	97.7	+73.2	103.7	N	154
2-2, 106-108	5.97	2.04 E-5	+72.9	82.9	+73.5	78.3	N	189
2-3, 48-50	6.89	3.48 E-5	+66.3	129.2	+71.4	137.9	N	236
2-3, 114-116	7.55	4.62 E-5	+75.7	142.3	+79.1	150.7	N	258
2-4, 48-50	8.39	1.46 E-5	+74.3	101.2	+76.8	113.5	N	210
2-4, 107-109	8.98	3.07 E-5	+66.7	107.0	+67.0	108.7	N	186
2-5, 44-46	9.85	6.93 E-5	+73.5	150.0	+75.3	151.7	N	241
2-5, 114-116	10.55	1.84 E-5	+72.5	133.9	+76.4	153.6	N	211
2-6, 20-22	11.11	3.69 E-5	+68.4	120.3	+71.1	122.2	N	299
2-6, 72-74	11.63	8.08 E-5	+64.7	129.0	+70.9	142.3	N	270
2-7, 28-30	12.69	3.16 E-5	+69.9	110.6	+75.3	117.0	N	149
3-1, 70-72	13.91	1.04 E-6	+62.3	139.5	+67.9	97.7	N	234
3-1, 133-135	14.54	1.04 E-5	+82.1	186.8	+77.7	220.6	N	310
3-2, 40-42	15.11	1.74 E-5	+87.3	2.5	+84.3	304.9	N	299
3-2, 117-119	15.88	1.40 E-5	+82.4	235.6	+81.4	247.7	N	555
3-3, 40-42	16.61	3.04 E-5	+79.6	226.7	+75.8	261.7	N	300
3-3, 117-119	17.38	2.65 E-5	+76.0	202.8	+73.9	231.5	N	234
3-4, 40-42	18.11	1.54 E-6	+67.7	134.1	+76.5	164.7	N	354
3-4, 117-119	18.88	1.44 E-5	+78.7	149.3	+75.4	262.9	N	244
3-5, 40-42	19.61	4.99 E-5	+78.6	218.2	+78.7	237.8	N	300
3-5, 117-119	20.38	9.69 E-6	+85.7	231.7	+81.5	242.6	N	324
3-6, 40-42	21.11	1.74 E-5	+9.1	194.7	+53.7	229.6	N	41
3-6, 117-119	21.88	5.34 E-5	-5.3	103.0	+65.7	180.3	N	46
3-7, 40-42	22.61	1.27 E-5	+70.5	188.3	+67.0	221.2	N	222
4-1, 63-65	23.74	2.87 E-6	+78.7	76.8	-54.5	180.6	N	50
4-1, 121-123	24.32	9.22 E-7	+4.6	301.5	+72.9	184.3	N	305
4-2, 64-66	25.25	3.18 E-5	+79.1	124.2	+82.4	116.8	N	276
4-2, 121-123	25.82	2.16 E-6	+65.2	37.6	-58.4	333.0	N	57
4-3, 49-51	26.60	5.04 E-5	+77.4	29.9	+75.8	20.7	N	292
4-3, 117-119	27.28	4.71 E-5	+72.6	4.2	+72.2	357.0	N	281
4-4, 45-47	28.06	7.74 E-5	+78.2	39.1	+78.8	39.6	N	259
4-4, 104-106	28.65	2.13 E-5	+79.5	62.1	+84.8	55.9	N	281
4-5, 33-35	29.44	4.23 E-6	+86.2	92.5	+81.5	38.6	N	167
4-5, 89-91	30.00	1.61 E-6	+73.1	81.4	+78.3	280.7	N	188
4-6, 34-36	30.95	2.47 E-5	+62.7	121.5	+79.7	90.8	N	141
4-6, 96-98	31.57	1.10 E-5	+80.7	100.3	+85.5	294.2	N	125
4-7, 31-33	32.42	3.91 E-5	+84.3	87.6	+85.5	67.3	N	213
5-1, 31-33	33.22	3.94 E-5	+74.8	188.5	+76.0	190.5	N	313
5-1, 100-102	33.91	3.24 E-6	-41.4	172.4	-22.4	166.9	R	259
5-2, 33-35	34.74	3.36 E-5	-58.1	167.0	-62.9	171.5	R	278
5-2, 102-104	35.43	1.25 E-5	-70.6	165.9	-75.8	175.1	R	294
5-3, 31-33	36.22	1.26 E-6	-25.3	80.6	-65.1	124.4	R	54
5-3, 100-102	36.91	5.96 E-5	-67.0	140.6	-71.7	144.9	R	279
5-4, 32-34	37.73	2.81 E-5	-68.8	155.0	-71.5	161.1	R	241
5-4, 100-102	38.41	4.25 E-7	-44.8	28.5	-66.6	66.2	R	48
5-5, 32-34	39.23	1.84 E-6	-55.3	89.4	-70.0	159.9	R	200
5-5, 100-102	39.91	1.22 E-5	+55.4	11.1	+65.0	351.2	N	381
5-6, 32-34	40.73	1.03 E-5	+68.5	144.4	+77.1	153.3	N	260
6-1, 42-44	41.83	3.45 E-5	+83.0	134.1	+83.2	142.8	N	264
6-1, 118-120	42.59	8.91 E-7	+67.5	75.5	+64.2	70.3	N	140
6-2, 44-46	43.35	2.19 E-5	-71.5	59.1	-77.3	21.3	R	374
6-2, 119-121	44.10	4.83 E-6	-36.4	19.7	-49.5	2.0	R	361
6-3, 42-44	44.83	9.60 E-7	+50.1	109.4	+11.6	100.2	N	74
6-3, 118-120	45.59	2.61 E-5	-75.9	341.3	-76.9	342.6	R	278
6-4, 42-44	46.33	1.42 E-5	-66.8	350.1	-69.8	354.6	R	355
6-4, 118-120	47.09	1.74 E-5	-64.7	19.4	-70.0	358.9	R	287
6-5, 43-45	47.84	2.00 E-5	-61.9	26.8	-66.9	7.6	R	352
6-5, 118-120	48.59	3.33 E-5	-71.3	8.7	-70.6	356.1	R	314
6-6, 41-43	49.32	5.41 E-6	-9.1	328.7	-73.1	332.2	R	596
6-6, 118-120	50.09	3.10 E-5	-70.1	353.5	-70.7	351.9	R	297
*7-1, 40-42	51.31	8.04 E-6	-27.0	140.6	-0.3	136.6	N	244
7-1, 109-111	52.00	3.58 E-7	+21.6	101.9	+42.5	2.3	N	81
7-2, 40-42	52.81	2.12 E-5	+87.9	41.6	+85.4	209.0	N	229
7-2, 112-114	53.53	1.26 E-5	+83.1	190.4	+83.8	186.6	N	193
7-3, 40-42	54.31	1.48 E-6	-33.7	35.2	-61.8	8.1	R	348
7-3, 112-114	55.03	2.46 E-6	-12.8	98.6	-70.4	35.9	R	79
7-4, 40-42	55.81	1.47 E-5	-67.9	65.3	-65.7	61.4	R	228
7-4, 112-114	56.53	2.37 E-5	-82.5	75.5	-83.5	49.0	R	283
8-1, 40-42	57.51	8.90 E-5	+60.1	147.9	+58.6	146.7	N	304
8-1, 110-112	58.21	5.14 E-6	+54.7	128.8	+67.6	31.6	N	286
8-2, 40-42	59.01	4.40 E-6	-70.9	188.7	-72.4	190.9	R	606
8-2, 110-112	59.71	9.14 E-6	-66.8	170.2	-75.6	170.0	R	331
8-3, 40-42	60.51	2.33 E-5	+81.3	230.8	+79.1	230.0	N	204
*9-1, 40-42	61.11	6.00 E-6	-65.5	132.7	-60.3	165.6	N	511
*9-1, 110-112	61.81	1.02 E-5	+78.0	254.2	+75.0	251.6	N	243
*10-1, 40-42	63.91	4.30 E-5	+85.3	104.7	+87.4	179.7	N	311
*10-1, 110-112	64.61	1.57 E-5	+77.8	167.0	+76.5	181.4	N	274

Table 19 (continued).

Sample interval (cm)	Sub-bottom depth (m)	J (NRM) (Gauss)	NRM		AF stable		Pol.	MDF (Oe)
			I	D	I	D		
10-6, 42-44	71.43	4.39 E-6	-54.8	228.9	-70.4	271.2	R	671
10-6, 110-112	72.11	1.23 E-5	-67.4	291.3	-71.0	302.6	R	515
10-7, 15-17	72.66	1.75 E-5	-82.1	236.1	-79.5	261.2	R	485
11-1, 40-42	73.41	3.34 E-5	-74.6	75.0	-76.6	58.3	R	316
11-1, 110-112	74.11	2.61 E-5	-74.7	92.5	-80.4	91.2	R	353
11-2, 40-42	74.91	1.63 E-5	-60.9	51.6	-70.1	45.8	R	396
11-2, 110-112	75.61	2.13 E-5	-75.3	93.3	-77.4	83.3	R	385
11-3, 40-42	76.41	2.14 E-5	-79.3	32.7	-77.5	45.2	R	354
11-3, 110-112	77.11	4.23 E-6	+25.5	100.0	-60.4	96.2	R	61
11-4, 40-42	77.91	3.85 E-6	-78.9	104.9	-81.8	42.8	R	226
11-4, 110-112	78.61	7.55 E-6	-79.8	78.9	-76.8	19.2	R	525
11-5, 40-42	79.41	1.83 E-7	-22.3	164.5	-72.4	14.2	R	>1000
11-5, 110-112	80.11	8.90 E-8	+75.6	329.2	+63.9	3.1	N	309
11-6, 40-42	80.91	2.41 E-7	+51.4	98.8	+72.6	107.5	N	418
11-6, 110-112	81.61	2.87 E-7	-16.8	64.8	+68.0	94.5	N	48
11-7, 40-42	82.41	4.64 E-7	+2.6	356.6	+58.4	69.0	N	42
12-1, 40-42	82.91	7.44 E-6	+49.1	135.3	+76.0	87.0	N	502
12-1, 110-112	83.61	1.49 E-6	+19.6	286.0	+67.8	320.9	N	31
12-2, 40-42	84.41	2.08 E-6	+73.1	177.9	+74.4	54.6	N	34
12-2, 110-112	85.11	3.13 E-8	+41.5	174.5	-82.2	132.5	R	>500
12-3, 40-42	85.91	4.52 E-8	-4.2	97.8	-79.2	173.0	R	>500
12-3, 110-112	86.61	1.72 E-7	+81.2	221.9	-72.6	202.8	R	33
12-4, 40-42	87.41	3.14 E-7	-44.4	111.8	-65.2	144.6	R	>500
12-4, 110-112	88.11	6.49 E-8	-3.9	152.3	-81.0	149.9	R	>500
12-5, 40-42	88.91	9.34 E-8	-26.6	210.6	-79.5	316.4	R	>500
12-5, 110-112	89.61	3.25 E-7	-26.8	147.6	-70.2	186.9	R	>800
12-6, 40-42	90.41	3.95 E-7	-21.5	81.3	-66.4	94.6	R	>500
12-6, 110-112	91.11	5.74 E-6	-66.7	174.5	-70.4	169.8	R	>500
13-1, 40-42	92.41	1.63 E-6	+22.8	138.8	-64.0	229.9	R	289
13-1, 110-112	93.11	2.96 E-7	+11.5	24.2	-49.0	142.5	R	296
13-2, 40-42	93.91	5.96 E-8	+46.3	78.1	-55.2	164.4	R	259
13-2, 110-112	94.61	1.63 E-7	+53.7	153.0	+67.9	121.5	N	433
13-3, 40-42	95.41	1.89 E-7	+47.7	13.5	+70.0	24.7	N	334
14-1, 40-42	101.91	3.39 E-7	+88.2	88.1	+84.9	16.4	N	284
14-1, 110-112	102.61	4.86 E-7	+86.7	60.0	+82.2	8.1	N	89
14-2, 40-42	103.41	6.63 E-7	+76.5	163.4	+84.7	228.9	N	219
14-2, 110-112	104.11	2.82 E-7	+79.9	353.1	+78.7	311.0	N	47
14-3, 40-42	104.91	2.54 E-7	-18.7	33.9	-65.0	58.6	R	>800
14-3, 110-112	105.61	2.84 E-7	+26.6	42.6	-61.8	8.4	R	479
14-4, 40-42	106.41	3.65 E-7	-86.3	12.3	-73.1	24.9	R	492
14-4, 110-112	107.11	3.28 E-6	+77.5	41.7	+82.8	343.2	N	274
14-5, 40-42	107.91	4.17 E-7	+73.5	63.2	+74.4	316.4	N	194
14-5, 110-112	108.61	2.12 E-7	+87.8	144.2	+81.6	238.4	N	189
14-6, 40-42	109.41	2.52 E-7	+80.1	93.5	+83.3	26.1	N	223
14-6, 110-112	110.11	7.69 E-7	+80.7	96.0	+83.6	91.5	N	334
14-7, 40-42	110.91	2.48 E-7	+77.6	33.1	+75.5	10.4	N	97
15-1, 110-112	112.11	6.99 E-8	+81.9	80.4	+81.2	59.6	N	>500
15-2, 39-41	112.90	4.70 E-8	+35.2	272.5	+71.8	286.9	N	>400
15-2, 100-102	113.51	3.15 E-7	+50.2	360.0	+66.1	359.6	N	490
15-3, 39-41	114.40	1.94 E-7	+57.7	343.2	+64.3	336.6	N	389
15-3, 110-112	115.11	1.93 E-7	+0.6	349.1	-80.1	77.8	R	209
15-4, 36-38	115.87	1.67 E-7	-76.0	104.5	-72.3	101.8	R	327
15-4, 106-108	116.57	4.72 E-8	-4.4	39.0	-47.4	349.3	R	275
15-5, 36-38	117.37	1.11 E-7	-7.5	40.7	-69.7	14.4	R	34
15-5, 108-110	118.09	2.20 E-7	-40.2	19.4	-72.9	30.0	R	112
15-6, 35-37	118.86	8.77 E-7	+50.2	338.1	+64.3	20.6	N	55
15-6, 110-112	119.61	9.97 E-7	-15.4	150.2	+63.8	23.7	N	31
15-7, 40-42	120.41	7.47 E-7	-22.3	25.1	-69.5	57.5	R	33
16-1, 40-42	120.91	9.86 E-7	+41.0	359.2	+79.8	45.4	N	31
*16-1, 110-112	121.61	4.20 E-7	+77.8	197.3	+77.3	191.5	N	52
16-2, 40-42	122.41	3.18 E-7	+58.6	346.1	+75.6	17.3	N	32
16-2, 110-112	123.11	1.58 E-7	+58.0	41.3	+76.1	104.7	N	52
16-3, 40-42	123.91	1.08 E-7	+86.1	44.4	+69.1	165.7	N	334
16-3, 110-112	124.61	2.03 E-7	+69.2	40.9	+64.8	29.2	N	30
16-4, 40-42	125.41	4.00 E-7	+73.8	14.0	+68.4	10.3	N	79
16-4, 110-112	126.11	2.24 E-7	+66.8	76.8	+71.0	89.7	N	50
16-5, 40-42	126.91	5.67 E-7	+42.8	334.6	+66.4	38.3	N	46
16-5, 110-112	127.61	8.99 E-7	+77.0	0.4	+82.9	10.4	N	277
16-6, 40-42	128.41	3.60 E-7	+78.7	17.9	+67.1	82.9	N	119
16-6, 110-112	129.11	2.74 E-6	+81.1	318.0	+80.3	106.5	N	557
17-1, 62-64	130.63	1.89 E-7	+68.2	127.9	+73.7	18.7	N	119
17-1, 122-124	131.23	2.29 E-8	-17.0	67.1	+68.9	307.5	N	>200
17-2, 27-29	131.78	1.13 E-7	+27.2	39.5	+58.3	31.1	N	23
17-2, 125-127	132.76	4.91 E-7	+69.6	360.0	-71.2	312.0	R	178
17-3, 36-38	133.37	3.87 E-6	-8.4	195.6	-55.0	267.0	R	38
17-3, 90-92	133.91	1.22 E-7	+16.8	133.0	+70.2	68.4	N	32
17-5, 33-35	136.34	1.25 E-7	+29.4	351.9	+64.3	37.0	N	98
17-5, 118-120	137.19	3.24 E-7	+4.4	207.4	+80.1	91.9	N	39
17-6, 26-28	137.77	8.65 E-8	+64.9	37.9	+60.7	34.9	N	107
17-6, 115-117	138.66	5.69 E-8	+27.2	25.6	+64.0	26.7	N	160
18-1, 60-62	140.11	6.31 E-8	+57.2	23.1	+65.3	33.0	N	128
18-1, 121-123	140.72	7.25 E-8	+49.8	23.5	+59.8	36.5	N	58

Table 19 (continued).

Sample interval (cm)	Sub-bottom depth (m)	J (NRM) (Gauss)	NRM		AF stable		Pol.	MDF (Oe)
			I	D	I	D		
18-2, 50-52	141.51	4.68 E-8	+79.5	320.9	+82.5	2.9	N	21
18-2, 100-102	142.01	4.95 E-8	+60.6	344.1	+65.6	305.4	N	43
18-3, 50-52	143.01	7.20 E-8	+28.7	24.2	+50.5	213.3	N	116
18-3, 100-102	143.51	9.23 E-7	+40.8	19.7	-68.0	25.4	R	190
18-4, 50-52	144.51	5.91 E-7	+76.6	336.2	+75.9	325.3	N	237
18-4, 100-102	145.01	8.42 E-8	+52.7	338.1	+61.3	343.8	N	142
18-5, 50-52	146.01	7.63 E-8	+65.5	51.1	+70.7	58.4	N	92
18-5, 100-102	146.51	5.35 E-8	+85.1	340.0	+82.2	70.1	N	59
18-6, 20-22	147.21	5.71 E-8	+77.9	315.5	+69.9	277.5	N	116
18-6, 71-73	147.72	1.49 E-7	+74.6	347.5	+82.2	39.6	N	78
19-1, 40-42	149.41	3.47 E-6	+75.4	13.3	+81.2	340.0	N	248
19-1, 100-102	150.01	1.27 E-7	-7.0	56.8	-27.8	78.5	R	536
19-2, 50-52	151.01	7.12 E-8	+58.8	20.1	+67.7	70.7	N	143
19-2, 110-112	151.61	5.67 E-8	+81.1	167.8	+83.4	58.5	N	47
19-3, 32-34	152.33	4.10 E-8	+48.0	90.5	-39.1	92.4	R	211
19-3, 92-94	152.93	3.57 E-8	+52.0	145.2	-49.6	68.5	R	21
19-4, 33-35	153.84	4.62 E-8	+51.9	23.5	-71.2	85.4	R	133
19-4, 92-94	154.43	5.07 E-8	+63.0	264.9	+60.1	279.7	N	118
19-5, 33-35	155.34	2.68 E-8	+60.3	341.3	+81.5	319.8	N	146
19-5, 95-97	155.96	3.68 E-8	+47.8	2.6	+66.0	23.4	N	164
19-6, 33-35	156.84	6.76 E-8	+57.3	68.9	+66.2	70.6	N	173
19-6, 95-97	157.46	2.58 E-7	+71.8	354.1	+76.4	2.0	N	308
19-7, 31-33	158.32	2.30 E-7	+79.3	315.5	+69.9	339.9	N	45
20-1, 45-47	158.96	2.97 E-7	+4.9	145.5	+55.5	193.3	N	274
20-1, 117-119	159.68	7.68 E-8	+62.2	353.5	+69.2	5.7	N	428
20-2, 45-47	160.46	1.69 E-7	+62.6	6.5	+63.2	9.2	N	180
20-2, 117-119	161.18	2.01 E-8	-4.2	52.6	-67.1	357.1	R	>500
20-3, 47-49	161.98	6.40 E-8	+33.9	19.4	+35.9	22.8	N	69
20-3, 101-103	162.52	1.20 E-7	+46.1	53.7	+61.2	40.8	N	83
20-4, 45-47	163.46	2.97 E-7	+46.5	35.6	+73.0	12.7	N	139
20-4, 101-103	164.02	1.66 E-7	+50.2	46.8	+65.9	33.3	N	149
20-5, 47-49	164.98	1.00 E-7	+58.3	78.2	+72.9	85.9	N	171
20-5, 101-103	165.52	1.18 E-7	+40.7	27.2	+69.1	7.2	N	205
20-6, 47-49	166.48	1.05 E-7	+67.2	39.3	+75.3	36.8	N	225
20-6, 101-103	167.02	3.40 E-7	+3.7	290.8	+67.2	19.5	N	335
20-7, 47-49	167.98	3.82 E-6	+64.3	54.5	+71.2	47.2	N	333
21-1, 42-44	168.43	1.69 E-7	+78.9	50.8	+72.9	73.3	N	173
21-1, 111-113	169.12	1.72 E-6	+74.8	60.2	+74.9	60.3	N	302
21-2, 42-44	169.93	1.63 E-7	+63.8	38.5	+71.6	59.9	N	175
21-2, 111-113	170.62	1.39 E-7	+68.2	62.5	+71.0	88.6	N	109
21-3, 42-44	171.43	2.94 E-7	+75.0	76.6	+77.4	59.6	N	219
21-3, 111-113	172.12	2.62 E-7	+85.8	121.3	+81.7	70.3	N	159
21-4, 42-44	172.93	8.31 E-8	+40.6	54.6	+63.3	57.2	N	40
21-4, 112-114	173.63	1.78 E-7	+71.2	43.1	+75.3	113.1	N	185
21-5, 43-45	174.44	4.96 E-7	+65.4	106.6	+70.8	104.7	N	397
21-5, 113-115	175.14	1.99 E-7	+70.8	78.7	+69.5	95.4	N	224
21-6, 43-45	175.94	6.07 E-8	+42.8	70.0	+39.9	79.6	N	82
21-6, 113-115	176.64	7.78 E-8	+69.0	142.9	+71.0	112.0	N	87
21-7, 43-45	177.44	4.99 E-8	+32.7	348.5	+64.6	343.3	N	25
22-1, 50-52	178.01	5.90 E-8	+44.6	343.1	+67.9	78.3	N	94
22-1, 110-112	178.61	1.47 E-7	+31.6	56.8	+68.0	86.1	N	128
22-2, 40-42	179.41	6.60 E-8	+61.6	338.0	+70.0	326.6	N	233
22-2, 110-112	180.11	1.01 E-7	+22.8	17.8	+54.7	18.5	N	61
22-3, 40-42	180.91	5.74 E-8	+27.5	64.6	+56.1	66.4	N	54
22-3, 110-112	181.61	6.76 E-8	+54.5	21.7	+68.8	350.3	N	195
22-4, 40-42	182.41	1.54 E-7	+31.4	339.9	+63.9	10.5	N	>500
22-4, 110-112	183.11	9.94 E-7	+70.7	65.9	+77.8	58.3	N	464
22-5, 40-42	183.91	1.07 E-7	+48.2	15.2	+59.8	34.2	N	334
*23-1, 92-94	185.23	5.67 E-7	+65.0	333.8	+69.5	345.8		167
*23-1, 133-135	185.64	1.12 E-7	+31.6	10.7	+26.8	29.8		49
*23-2, 28-30	186.09	5.60 E-7	+24.3	52.0	+13.4	55.9		320
*23-2, 103-105	186.84	1.61 E-7	+28.4	71.9	-69.7	320.3		32
23-3, 28-30	187.59	1.89 E-7	+72.1	42.5	+69.7	49.0	N	180
23-3, 103-105	188.34	2.34 E-7	+70.9	0.2	+75.3	336.2	N	186
*23-4, 41-43	189.22	5.09 E-7	+31.0	125.7	+37.0	126.3		75
23-4, 103-105	189.84	1.20 E-7	+87.2	163.8	+77.1	152.3	N	84
23-5, 36-38	190.67	1.07 E-7	+72.1	328.7	+69.8	338.8	N	81
23-5, 103-105	191.34	1.62 E-7	+75.3	338.6	+71.0	69.3	N	142
24-1, 51-53	192.92	1.91 E-8	+4.4	52.3	-64.8	101.9	R	188
24-1, 117-119	193.58	2.85 E-8	+58.7	36.2	+65.1	11.7	N	32
24-2, 51-53	194.42	3.15 E-8	+52.5	54.1	+69.1	43.3	N	57
24-2, 117-119	195.08	3.58 E-8	+48.4	24.1	-83.7	69.9	R	>400
24-3, 39-41	195.80	2.06 E-7	+72.4	105.3	+76.5	118.8	N	174
24-3, 117-119	196.58	9.03 E-8	+48.2	119.8	+74.8	133.0	N	145
24-4, 37-39	197.28	1.20 E-6	+47.5	42.5	+60.4	18.0	N	283
24-4, 100-102	197.91	2.17 E-7	+67.4	61.4	+70.3	50.6	N	352
24-5, 39-41	198.80	7.96 E-8	+74.6	47.5	+77.1	37.3	N	364
24-5, 104-106	199.45	1.09 E-7	+82.9	82.1	+72.5	101.9	N	141

* Disturbed core intervals; abbreviations: J = intensity, I = inclination, D = declination of natural remanent magnetization (NRM) and stable remanence after AF demagnetization, Pol = polarity, N = normal, R = reversed, MDF = median destructive field.

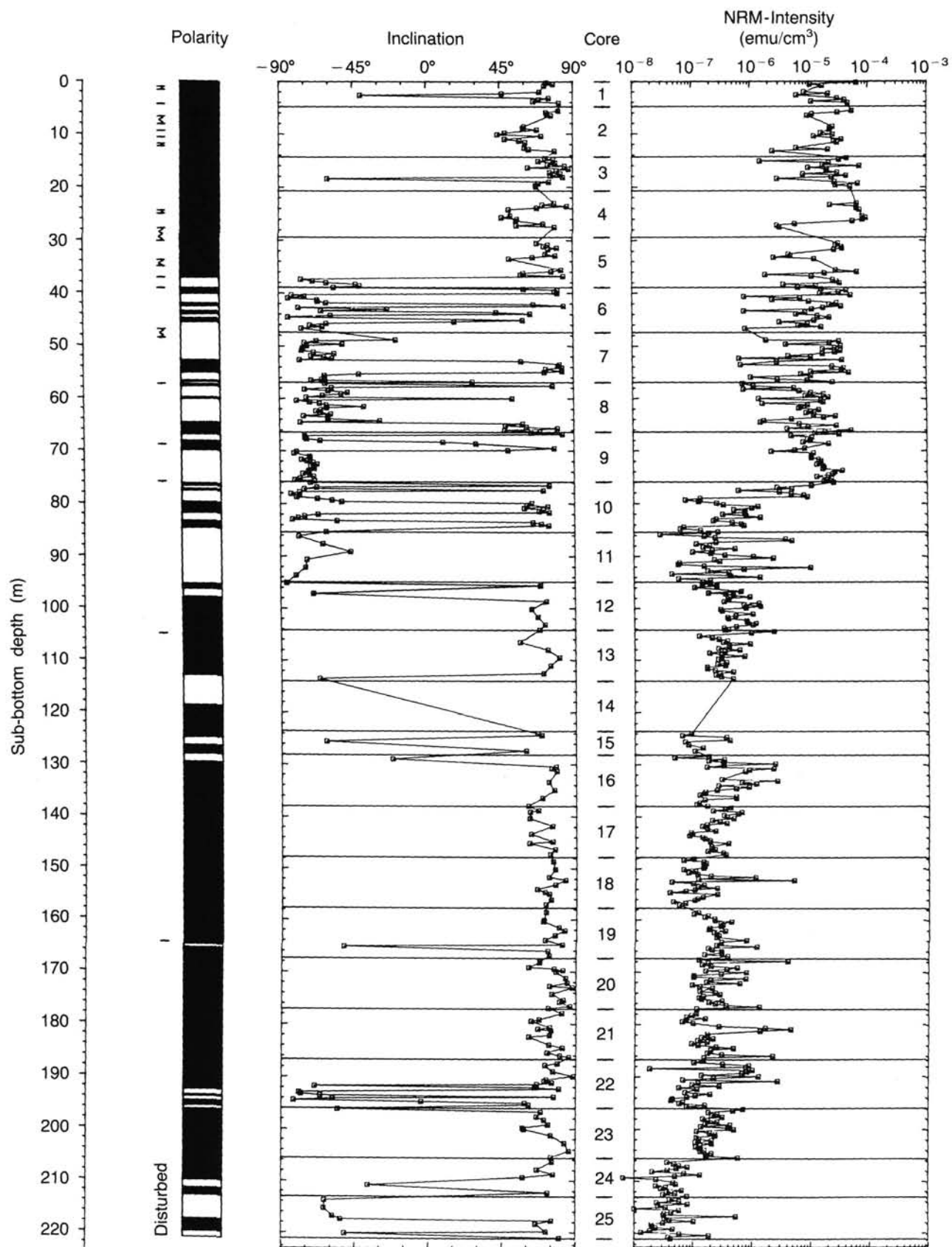


Figure 50. Stratigraphic sequence of the upper 220 m of Hole 642B showing the variations in inclination of the characteristic remanent magnetization and natural remanent magnetization (NRM) intensity. Horizontal lines indicate core boundaries. The paleomagnetic polarity log is based on stable inclinations, black being normal and white being reversed polarity. Disturbed intervals are indicated to the left of the polarity column.

Table 20. Magnetostratigraphic summary of Site 642.

Epoch	Event	Age (Ma)	Hole 642B boundaries		Hole 642C boundaries	
			Core-section-cm	Depth (mbsf)	Core-section-cm	Depth (mbsf)
Brunhes/Matuyama		0.73	5-5-141/5-6-50	37.11	5-1-32/5-1-101	33.57
	Jaramillo, top	0.91	6-2-141/6-3-21	41.96	5-5-33/5-5-101	39.57
	Jaramillo, base	0.98	6-5-51/6-5-81	45.56	6-1-119/6-2-45	42.97
	Olduvai, top	1.66	7-4-69/7-4-100	52.75	6-6-119/7-1-110	51.05
	Olduvai, base	1.88	7-6-9/7-6-40	55.15	7-2-113/7-3-41	53.92
Matuyama/Gauss		2.47	8-6-10/8-6-40	64.65	8-2-111/8-3-41	60.11
Gauss/Gilbert		3.40	9-3-47/9-3-71	69.99	—	—
Gilbert/Epoch 5		5.35	10-3-71/10-3-100	79.76	11-5-41/11-5-111	79.76
Epoch 5/Epoch 6		5.89	10-5-130/10-6-10	83.35	12-2-41/12-2-111	84.76
Epoch 6/Epoch 7		6.70	11-7-64/12-1-71	95.33	13-2-41/13-2-111	94.26
Epoch 7/Epoch 8		7.41	13-6-81/13-7-32	113.02	15-3-40/15-3-111	114.76

remain at this low level down to the base of the hole. The change in NRM intensity by almost two orders of magnitude is found at identical levels in both holes. From the magnetostratigraphic control in Hole 642C and its tentative interpretation given above as indicating the onset of the late Neogene glaciation in the Norwegian Sea, this event should have occurred at about 5.3 Ma (shortly after the Epoch 5/Gilbert transition).

A preliminary magnetostratigraphic summary of the Hole 642B and 642C sediments is given in Table 20. The Brunhes/Matuyama boundary (0.73 Ma) was recognized at about 33.57 mbsf (Section 104-642C-5H-1, Fig. 51). The two normal intervals within the Matuyama Epoch, the Jaramillo (0.91 to 0.98 Ma) and the Olduvai (1.66 to 1.88 Ma) Events, extend from 39.57 to 42.97 and from 51.05 to 53.92 mbsf, respectively. The base of the Olduvai Event provides a fairly precise horizon for the Pliocene/Pleistocene boundary in the Hole 642C sedimentary sequence.

The top of the interval representing the normal Gauss Epoch (2.47 Ma) is tentatively identified at 60.11 mbsf (Sections 104-642C-8H-2/3), since the fine structures and the base of this interval could not be quantified because of the poor and highly disturbed recovery in Cores 104-642C-9H and 642C-10H. For similar reasons, the series of four normal events in the reversed Gilbert Epoch are not documented in the paleomagnetic record. The Gilbert/Epoch 5 boundary is situated at 79.76 mbsf. Its position is known to be slightly lower than the Miocene/Pliocene boundary.

The base of the Epoch 5 (5.89 Ma) interval was identified in Section 104-642C-12H-2 (84.76 mbsf, Fig. 51). However, it was not possible to determine the reversed interval separating the two normals of Epoch 5. The inclination record of Cores 104-642C-12H through 104-642C-15H offers only a very limited resolution of the Epochs 6 and 7 reversal pattern. The Epoch 6/Epoch 7 boundary (6.70 Ma) is placed at 94.26 mbsf (Section 104-642C-13H-2). The Epoch 7/Epoch 8 boundary (base of marine magnetic anomaly 4, 7.41 Ma) at about 114.76 mbsf (Section 104-42C-15H-3) is the deepest polarity transition in Hole 642C that could be defined with a minimum of confidence. As in Hole 642B, sediments recovered from below 115 mbsf yield stable positive inclinations (Fig. 51). This pattern does not allow any plausible interpretation in terms of the Earth field polarity history but most likely results from spurious magnetization components that cannot be discriminated by AF technique.

Hole 642D

Hole 642D extends from about 190 to 329 mbsf and continues the previous APC Holes 642A, 642B, and 642C to greater depth. Fourteen cores were obtained using the extended-core-barrel (XCB) technique. The upper 12 cores have been analyzed with the pass-through cryogenic magnetometer for their natural remanent magnetization properties. In addition, shore-based NRM measure-

ments were performed for, on average, two discrete samples per section (Table 21). Neither data set provides an adequate basis for establishing a magnetostratigraphic record. There are indications that the problems encountered in the lower halves of Holes 642B and 642C prevail throughout Hole 642D and possibly cannot be solved by further demagnetization studies.

Summary

Preliminary paleomagnetic results presented in this report for the sediment series recovered from the four holes at Site 642 on the Vøring Plateau are based on shipboard natural remanent magnetization measurements performed with the new pass-through cryogenic magnetometer and, for the greater part, on shore-based AF studies.

In Hole 642A a single 9.5-m core contains the present Brunhes field configuration. The sediment series penetrated in Holes 642B and 642C provides a reasonably complete magnetostratigraphic record only to about 115 mbsf into geomagnetic Epoch 7 (Fig. 52). In this interval, the apparent sedimentation rate gradually decreases from about 46 (in Hole 642B) and 51 (in Hole 643C) m/m.y. in the Brunhes Epoch to about 5.0 m/m.y. in the Gilbert Epoch. Below the Pliocene/Miocene boundary to the base of Epoch 7, a progressively fragmentary and less-well-documented polarity reversal sequence is encountered. The magnetostratigraphic record for the late Miocene implies a continuous increase in sedimentation rates from about 9 to 29 m/m.y. during this period.

The downhole NRM intensity variation in the sediment columns shows a drastic decrease by almost two orders of magnitude at around 79 mbsf in both Holes 642B and 642C. This change most likely reflects a transition from predominantly biogenic to terrigenous accumulation regimes. The interpolated age of about 5.3 Ma for this horizon potentially marks the onset of the late Neogene glaciation cycles in the Norwegian Sea.

The Volcanic Sequence

The shipboard paleomagnetism on the volcanic sequence at Site 642 comprise measurements on the basalts as well as on intercalated volcanoclastic sediment sequences from Hole 642E.

The main purpose of the shipboard paleomagnetic study was to clarify the polarity pattern in the drilled igneous rocks and provide enough magnetic property information to enable the selection of paleomagnetic and rock-magnetic samples for shore-based studies. The investigations reported here, therefore, are of exploratory nature.

Hole 642D

The basalts encountered in Cores 104-642D-15X to 104-642D-19N in Hole 642D consisted of unoriented pebbles of a conglomerate unit as well as a strongly weathered volcanoclastic sediment and a basalt flow, which have been brecciated by drilling.

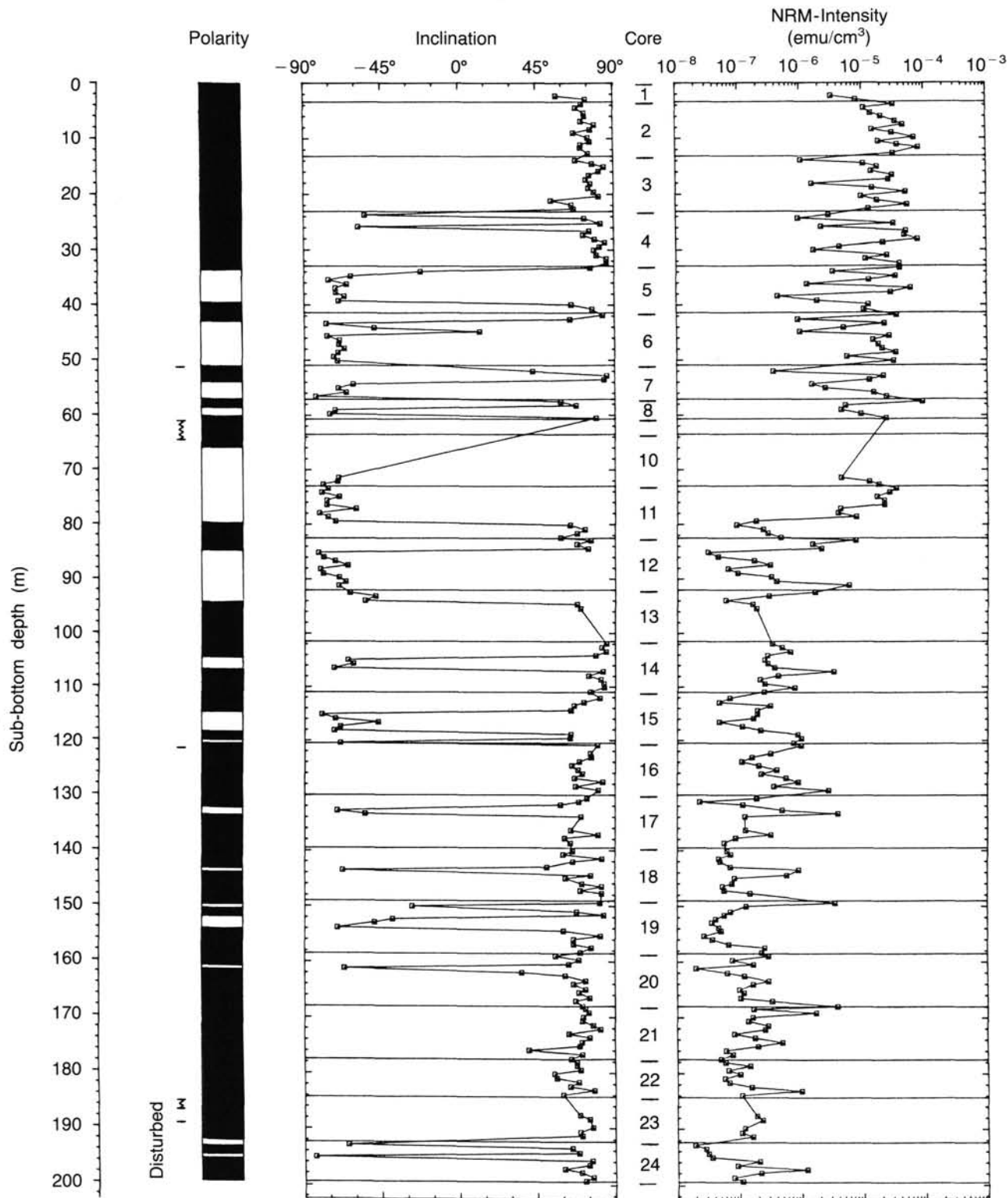


Figure 51. Stratigraphic sequence of the upper 200 m of Hole 642C showing the variations in inclination of the characteristic remanent magnetization and natural remanent magnetization (NRM) intensity. Horizontal lines indicate core boundaries. The paleomagnetic polarity log is based on stable inclinations, black being normal and white being reversed polarity. Disturbed intervals are indicated to the left of the polarity column.

In Section 104-642D-20N-1, a basaltic dike in part was melted during drilling operations (see "Basement Lithology" section) and thereby became completely remagnetized. For the reasons above no attempt was made to sample hard rocks from Hole 642D for paleomagnetic studies.

Hole 642E

Shipboard studies range from Section 104-642E-2W-2, where the first oriented igneous rocks were recovered, to Section 104-642E-110R-1, covering a sub-bottom depth interval from 320 to

Table 21. Paleomagnetic properties of Hole 642D sediments.

Sample interval (cm)	Sub-bottom depth (m)	J (NRM) (Gauss)	NRM	
			I	D
2-1, 40-42	190.31	3.90 E-7	-42.3	319.4
2-1, 110-112	191.01	5.49 E-8	+15.8	14.3
2-2, 40-42	191.81	2.20 E-8	-19.0	88.9
2-2, 110-112	192.51	2.70 E-8	+16.2	6.1
2-3, 40-41	193.31	4.48 E-8	+14.7	16.8
2-3, 110-112	194.01	1.15 E-8	+4.3	46.8
2-4, 40-42	194.81	2.78 E-8	+5.5	28.9
2-4, 110-112	195.51	4.04 E-8	+31.4	37.2
2-5, 40-42	196.31	1.23 E-7	+27.9	62.2
2-5, 110-112	197.01	7.57 E-8	+40.5	2.8
2-6, 40-42	197.81	7.18 E-8	+44.1	21.2
2-6, 110-112	198.51	1.04 E-7	+48.9	64.5
3-1, 40-42	200.01	6.69 E-8	+48.6	66.4
3-1, 110-112	200.71	5.11 E-8	+70.1	60.4
3-2, 40-42	201.51	5.48 E-8	+21.7	4.0
3-2, 110-112	202.21	7.23 E-8	+44.5	52.8
3-3, 40-42	203.01	1.73 E-7	+73.0	88.3
3-3, 110-112	203.71	3.19 E-8	+32.0	33.0
3-4, 40-42	204.51	1.32 E-7	+47.8	117.5
3-4, 110-112	205.21	5.28 E-7	+80.6	348.0
3-5, 40-42	206.01	3.97 E-8	+4.1	14.1
3-5, 110-112	206.71	1.13 E-8	+36.7	7.0
4-1, 40-42	209.61	5.82 E-8	+29.3	0.3
4-1, 110-112	210.31	2.66 E-8	-35.1	49.7
4-2, 40-42	211.11	8.05 E-8	-3.4	55.6
4-2, 110-112	211.81	3.32 E-8	+25.7	8.6
4-3, 40-42	212.61	7.76 E-7	+23.5	138.4
4-3, 110-112	213.31	1.52 E-8	+13.1	70.2
4-4, 40-42	214.11	6.44 E-8	-38.1	59.1
4-4, 110-112	214.81	6.25 E-8	-62.5	305.3
4-5, 40-42	215.61	3.10 E-8	+17.3	24.0
4-5, 110-112	216.31	4.60 E-8	+2.0	321.1
4-6, 40-42	217.11	3.81 E-8	-24.4	5.5
4-6, 110-112	217.81	4.13 E-8	-40.9	23.1
5-4, 39-41	223.80	4.13 E-8	-44.4	16.6
5-4, 109-111	224.50	6.72 E-8	+68.1	15.3
5-6, 39-41	226.80	3.82 E-8	-27.0	185.9
5-6, 109-111	227.50	3.46 E-8	-45.7	329.4
5-7, 39-41	228.30	2.23 E-8	-51.0	340.7
6-1, 40-42	228.91	8.30 E-8	+78.1	335.3
6-1, 130-132	229.81	1.16 E-8	+50.2	51.7
6-2, 40-42	230.41	7.27 E-9	-9.0	57.6
6-2, 110-112	231.11	3.13 E-8	+30.0	26.2
6-3, 40-42	231.91	8.96 E-8	+73.4	7.4
6-3, 110-112	232.61	5.37 E-8	+70.9	8.9
6-4, 40-42	233.41	3.75 E-8	-24.2	249.7
6-4, 110-112	234.11	1.44 E-7	-7.4	77.7
6-5, 40-42	234.91	1.04 E-7	-15.2	32.3
7-1, 40-42	238.61	4.96 E-8	+57.8	279.6
7-1, 110-112	239.31	9.42 E-8	+79.2	9.9
7-2, 40-42	240.11	1.68 E-7	+3.6	152.8
7-2, 110-112	240.81	3.74 E-7	+79.7	345.8
7-3, 40-42	241.61	1.46 E-7	+34.3	337.8
7-3, 110-112	242.31	4.40 E-8	+57.9	33.0
7-4, 40-42	243.11	1.42 E-6	+2.4	263.4
7-4, 110-112	243.81	1.60 E-7	+71.2	342.4
7-5, 40-42	244.61	2.54 E-8	+39.3	345.4
7-5, 110-112	245.31	4.02 E-8	+62.0	333.5
7-6, 40-42	246.11	3.33 E-8	+3.8	343.4
7-6, 110-112	246.81	2.53 E-8	+24.9	101.3
7-7, 40-42	247.61	6.13 E-8	+73.8	357.2
8-1, 40-42	248.21	3.99 E-8	+64.0	339.1
8-1, 110-112	248.91	1.51 E-7	+75.2	335.6
8-2, 40-42	249.71	1.80 E-7	+77.9	359.0
8-2, 110-112	250.41	6.24 E-8	+77.2	104.1
8-3, 40-42	251.21	1.90 E-7	+13.8	353.2

Table 21 (continued).

Sample interval (cm)	Sub-bottom depth (m)	J (NRM) (Gauss)	NRM	
			I	D
8-3, 110-112	251.91	1.87 E-7	+64.8	204.3
8-4, 40-42	252.71	5.70 E-8	+75.9	327.7
8-4, 110-112	253.41	8.13 E-9	+67.1	194.4
8-5, 40-42	254.21	5.47 E-8	+57.7	359.6
8-5, 110-112	254.91	4.29 E-8	+32.9	343.6
8-6, 40-42	255.71	4.29 E-8	+38.7	343.2
8-6, 110-112	256.41	1.24 E-7	+54.6	295.1
9-1, 50-52	258.01	2.61 E-8	+64.4	27.5
9-1, 101-103	258.52	1.60 E-7	-54.3	344.6
9-2, 50-52	259.51	3.58 E-8	+48.3	319.2
9-2, 101-103	260.02	1.37 E-7	+80.1	305.3
9-3, 50-52	261.01	6.10 E-8	+65.3	135.5
9-3, 101-103	261.52	8.34 E-7	+71.1	133.7
9-4, 50-52	262.51	2.92 E-8	+18.8	254.5
9-4, 101-103	263.02	7.43 E-8	+78.0	320.3
9-5, 50-52	264.01	1.38 E-8	-47.6	272.7
9-5, 101-103	264.52	1.29 E-7	+17.1	26.2
9-6, 50-52	265.51	5.50 E-8	+15.3	353.6
9-6, 101-103	266.02	2.43 E-7	-54.0	276.2
10-1, 43-45	267.54	3.28 E-8	+42.3	319.8
10-1, 119-121	268.30	1.84 E-8	+6.8	304.7
10-2, 45-47	269.06	6.22 E-9	+45.6	285.1
10-2, 123-125	269.84	4.16 E-8	-53.3	276.0
10-3, 45-47	270.56	7.69 E-8	+37.1	88.1
10-3, 125-127	271.36	3.21 E-8	+12.4	315.1
10-4, 42-44	272.03	3.00 E-8	-3.9	316.9
10-4, 125-127	272.86	7.15 E-8	+80.2	299.4
10-5, 42-44	273.53	4.80 E-8	+46.9	292.3
10-5, 123-125	274.34	5.61 E-8	+81.9	279.3
10-6, 48-50	275.09	3.92 E-7	-10.4	8.8
10-6, 127-129	275.88	5.21 E-8	-5.1	305.7
11-1, 33-35	277.14	1.39 E-7	+52.5	255.5
11-1, 75-77	277.56	3.69 E-7	+71.1	10.2
11-1, 108-110	277.89	3.80 E-5	+83.7	52.5
11-2, 33-35	278.64	3.61 E-5	-86.7	305.0
11-2, 109-111	279.40	5.47 E-7	-12.5	330.3
12-1, 39-41	286.90	2.80 E-5	+77.2	66.0
12-1, 110-112	287.61	1.77 E-5	+75.4	70.9
12-2, 39-41	288.40	2.60 E-5	+76.4	30.1
12-2, 110-112	289.11	7.51 E-6	+74.3	27.3
12-3, 39-41	289.90	6.63 E-6	+75.5	69.3
12-3, 110-112	290.61	2.28 E-6	+81.2	289.7
12-4, 39-41	291.40	9.34 E-7	+65.8	225.1
12-4, 110-112	292.11	1.51 E-6	+84.8	116.1
12-5, 39-41	292.90	1.49 E-6	+82.3	115.1
12-5, 110-112	293.61	6.63 E-7	+47.3	230.4
12-6, 32-34	294.33	9.15 E-7	+76.0	72.4
12-6, 118-120	295.19	2.69 E-7	-62.3	322.0
13-1, 30-32	296.51	1.17 E-6	+70.0	61.8
13-1, 90-92	297.11	4.92 E-7	+71.2	101.9
13-2, 30-32	298.01	1.65 E-7	+63.1	157.3
13-2, 90-92	298.61	7.45 E-7	+78.2	88.6
13-3, 30-32	299.51	4.56 E-7	+87.3	195.6
13-3, 90-92	300.11	7.19 E-7	+70.2	59.3
13-4, 30-32	301.01	6.29 E-7	+83.5	13.8
13-4, 90-92	301.61	1.67 E-6	+45.4	34.8
13-5, 35-37	302.56	8.92 E-6	-77.8	176.6
14-1, 35-37	306.16	5.15 E-5	+63.8	14.8
14-1, 103-105	306.84	1.94 E-5	+69.3	43.1
14-2, 33-35	307.64	3.38 E-5	+71.4	126.9
14-2, 103-105	308.34	5.03 E-6	-35.4	209.2
15-1, 19-21	315.60	5.31 E-5	+39.8	105.9

J = intensity, I = inclination, D = declination of natural remanent magnetization (NRM) and stable remanence after AF demagnetization.

1229.4 m. The paleomagnetic investigations are almost exclusively based on shipboard samples that were measured for density and velocity in the physical properties laboratory and then transferred to the paleomagnetism laboratory. After completion of magnetic measurements, samples were returned to the working half of the core. An average of one sample per section was

taken, totaling 307 7-cm³ cube samples. The cubes were oriented with respect to the vertical direction only, as no azimuthal orientation of the Hole 642E cores was accomplished.

The sample set of 307 cube samples consists of 282 from basaltic flows, 11 from basaltic dikes, and 14 from volcanoclastic layers. All samples were demagnetized in 50-Oe AF fields, and

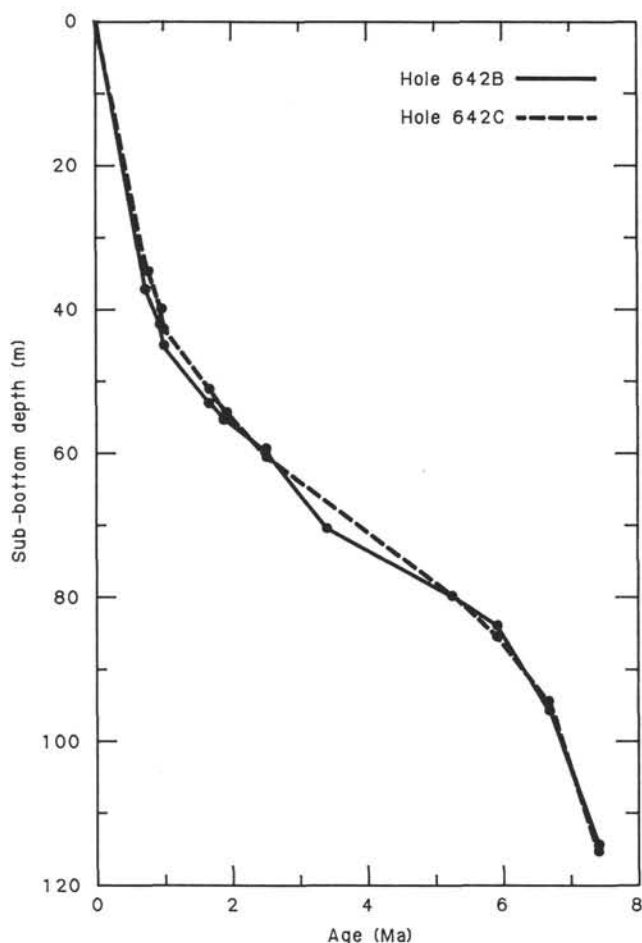


Figure 52. Apparent sediment accumulation at Site 642 derived from the correlation of the downhole pattern in remanent magnetization polarity with the geomagnetic polarity time scale of Berggren et al. (1985a).

the results of natural remanent magnetization (NRM), inclination, declination, and intensity in 0- and 50-Oe demagnetized states are listed in Table 22 together with initial susceptibility values.

A total of 89 samples were AF-cleaned in fields up to 1000 Oe to verify the primary polarity of samples, to arrive at stable inclination values, and to test for multicomponent magnetizations in the samples. In Table 23 these samples are listed together with the maximum AF-field applied and stable inclination and declination values.

In cases where a steepening of reverse inclination angles was observed during stepwise cleaning operation, followed by shallower angles at higher fields, the steepest angle has been listed. In those cases vector analyses performed after the cruise will help to define inclination values for the different magnetization components. N or R notations were used when no angle was obvious. When the polarity was in doubt, no character was noted.

The natural remanent magnetization of the samples investigated after cleaning them in 50-Oe fields (or up to 1000-Oe fields in a few cases) revealed a reverse polarity for the vast majority of samples throughout the drilled section, with the exception of three zones which are discussed below.

One of these zones, within a flow of reverse polarity (Section 104-642E-21R-3, 464.5 mbsf), may be related to remagnetization. Reddish/dark gray discoloration at that location of the flow may suggest the possibility of a nearby dike not penetrated

by drilling. Alternatively, rotation of a block of lava, which thereafter was integrated in the following flow of a multiple-flow system, cannot be excluded.

Of the remaining two zones of normal polarity, the upper one is represented so far by only four samples of a single core piece containing a thinly bedded tuff (Section 104-642-5R-3, 340 mbsf). The basaltic flow above this level is reversely magnetized and the two uppermost tuff samples show normal directions only after AF cleaning in fields of 50 and 100 Oe, respectively. Below the tuff, within Core 104-642E-6R, only pebbles and rock fragments from higher in the section were recovered together with mud. The possibility cannot be excluded, however, that this core piece was wrongly oriented before marking. In that case, the change in inclination during AF makes better sense and can be understood as the cleaning of a soft, viscous, normal component of Brunhes age. For this preliminary analysis we disregard the possibility of a limited normal event recorded in the tuff. Further analysis of the demagnetization characteristics on additional samples is needed to support this interpretation.

The lowermost zone of potentially normal polarity occurs in the interval between 1109 and 1182 mbsf. In this interval highly altered ash/tuffs and redeposited hyaloclastites alternate with extremely weakly magnetized flows of distinctly different petrology compared to the flows above this zone. Both flows and sediments display multicomponent magnetizations that partly may be related to alteration of these rocks. To obscure relationships further, a strongly magnetized dike may be the cause of thermal and/or chemical remagnetization of reverse polarity. Although the thickness of the dike is not known (it was penetrated by drilling between 1160 and 1180 mbsf), evidence from grain-size distribution as well as from magnetic characteristics indicates a thickness of a few meters. A dike this size may be a sufficient heat source to activate water within adjacent sediments and to cause alteration and consequent remagnetization. It is known from highly altered basalts, for example in eastern Iceland (Schoenharting and Ghisler, 1982), that remagnetization can affect different portions of flows in highly variable ways and that it can completely mask primary polarities. Obviously, such speculations have to be supported by detailed magnetic and petrological shore-based studies, and we have to leave the question open if indeed a normal polarity zone is present in this interval.

A main objective of the onshore studies is to clarify the complete polarity record and to provide a record of stable inclination values, as this may help in correlating the Vøring Plateau volcanics with those of east Greenland and the Faeroes as well as those from Rockall Plateau (Roberts, Schnitker et al., 1984). All of these volcanics are of predominantly reverse polarity (Abrahamsen et al., 1984; Larsen and Watt, 1985).

A number of samples, particularly from the interior of massive flow units, have high but unstable normal remanence components which almost completely disappear at 50-Oe cleaning fields. Usually these samples are also distinguished by their high magnetic susceptibility values. The normal, magnetically soft component can probably be explained by viscous magnetization acquired in the present normal magnetic epoch and/or by magnetization acquired during drilling. In some cases, as mentioned above, a possible normal component of high stability may also be present. A thorough analysis of this multicomponent magnetization must be performed before speculations on the origin of this component can be suggested (e.g., tectonic and/or low-temperature alteration effects). This analysis may also reveal declination relationships between the different magnetization components and, assuming one of the normal components gives average direction in the present (Brunhes) magnetic epoch, declinations for the reverse direction may be calculated.

Table 22. Paleomagnetic measurements of Hole 642E. Inclination and declination values in degrees, intensity (Int.) values in 10^{-4} emu/cm³, and susceptibility values (X) are in G/Oe.

Core/ sect.	Interval	Sub-bottom depth (m)	NRM			AF (50 Oe)			X ($\times 10^{-3}$)
			Decl.	(10 ⁻⁴ emu/cm ³)		Decl.	(10 ⁻⁴ emu/cm ³)		
				Incl.	Int.		Incl.	Int.	
104-642E-									
2W-2	58-60	210.59	100	-41	12.9	99	-46	13.7	46.9
4R-1	69-71	327.20	332	44	4.2	323	28	3.4	4.2
5R-1	45-47	335.36	319	79	3.6	310	82	3.1	1.9
5R-1	90-92	335.81	279	75	0.8	312	44	0.5	0.4
5R-3	63-65	338.45	243	-62	13.4	247	-70	13.2	2.1
5R-3	128-130	339.19	163	-2	1.8	167	36	1.9	2.1
5R-3	134-136	339.25	189	-29	2.0	201	0	1.2	1.7
5R-3	138-140	339.29	165	26	6.4	161	37	6.7	2.4
5R-3	146-148	339.37	162	32	3.5	162	36	3.0	0.5
7R-1	38-40	354.69	327	-62	120.5	—	no data	—	5.3
10R-1	104-106	374.55	60	-64	11.3	51	-72	10.2	6.4
10R-2	28-30	375.29	125	-40	8.6	128	-50	8.4	6.6
11R-2	54-56	384.25	250	-8	36.2	—	no data	—	14.2
12R-1	14-16	387.35	248	-64	24.0	247	-65	24.8	19.5
13R-1	95-97	395.76	258	21	35.6	261	-5	22.6	16.2
14R-1	38-40	400.19	160	36	30.4	154	1	14.5	15.8
14R-1	130-132	401.11	125	-53	5.0	125	-52	3.8	15.3
15R-2	15-17	406.96	13	-54	43.1	17	-56	46.2	18.0
15R-2	75-77	407.56	245	-57	72.0	245	-56	71.4	26.3
15R-2	136-138	408.17	81	-57	61.8	71	-58	59.8	5.4
15R-3	65-67	408.96	243	-54	56.8	245	-57	49.0	23.3
15R-4	100-102	410.81	17	-66	66.6	18	-64	67.2	28.0
15R-5	128-130	412.59	321	-69	26.1	322	-70	26.2	2.4
16R-1	33-35	415.14	201	-55	40.9	199	-57	38.6	22.3
16R-2	24-26	416.55	279	-52	44.5	285	-53	43.9	23.1
16R-3	91-93	418.72	136	-59	40.5	142	-64	35.8	15.2
17R-1	106-108	425.37	330	-69	32.4	328	-70	32.5	2.2
17R-2	107-109	426.88	137	-70	74.8	138	-74	75.3	—
17R-3	70-72	428.01	14	-70	22.7	13	-72	23.4	4.3
18R-1	40-42	433.11	297	-63	18.2	292	-66	21.6	11.4
18R-2	27-29	434.48	36	-76	21.8	25	-71	23.6	11.1
18R-3	72-74	436.43	10	-69	17.1	2	-71	21.5	12.2
18R-4	37-39	437.58	161	-55	30.8	151	-67	39.3	21.6
18R-5	55-57	439.26	250	-72	20.4	264	-73	20.4	3.1
19R-1	42-44	442.53	268	-71	19.2	263	-72	19.2	7.0
19R-2	102-104	444.63	3	-70	12.8	357	-72	12.9	7.0
19R-4	9-11	446.60	0	-76	16.2	357	-74	16.1	5.5
19R-5	43-45	448.44	266	16	70.8	267	13	69.3	53.7
20R-1	28-30	451.89	101	-55	76.5	101	-58	67.9	46.4
20R-2	85-87	453.96	352	-57	47.0	348	-64	40.6	31.3
20R-3	64-66	455.25	140	-74	41.5	157	-70	42.3	54.9
20R-4	35-37	456.46	325	-63	20.4	333	-67	17.6	37.4
21R-1	20-22	461.21	38	86	12.3	33	88	10.3	25.7
21R-2	88-90	463.39	96	-73	53.1	97	-75	53.5	21.9
21R-3	50-52	464.51	292	62	58.2	387	64	45.4	93.5
21R-3	106-108	465.07	156	64	27.4	155	67	29.1	24.6
21R-4	50-52	466.01	342	41	14.1	25	-58	6.8	24.5
21R-5	109-111	468.1	326	-74	32.9	308	-75	34.2	31.7
22R-1	30-32	470.81	44	-48	24.4	46	-60	26.4	20.9
22R-2	8-10	472.09	53	-60	19.5	58	-65	21.9	25.2
22R-3	43-45	473.94	151	-12	30.7	154	-12	28.1	21.1
22R-5	79-81	477.3	145	-70	76.3	146	-69	76.5	23.2
22R-6	77-79	478.78	235	-61	64.6	237	-61	63.9	9.6
23R-1	106-108	480.97	250	-58	9.6	248	-57	9.5	15.0
23R-3	44-46	484.35	283	-69	28.5	282	-74	27.6	23.0
24R-1	79-81	490.20	299	-7	106.6	298	-14	82.5	57.9
24R-2	56-58	491.47	133	-19	15.1	130	-24	22.3	13.4
25R-1	35-37	493.76	20	-27	19.0	20	-27	18.4	10.7
25R-2	89-91	495.80	352	11	10.6	356	-31	9.3	21.7
25R-3	62-64	497.03	273	-19	51.6	271	-24	49.4	23.9
25R-4	85-87	498.76	262	-40	16.5	258	-44	16.4	63.4
26R-1	80-82	502.61	2	25	8.0	4	-32	8.0	53.4
26R-2	72-74	504.03	130	22	6.6	126	-41	6.5	62.3
26R-3	7-9	504.88	171	-44	9.2	171	-47	8.8	31.4
26R-5	91-93	507.22	23	78	2.1	65	61	0.8	92.2
27R-1	7-9	511.28	145	-35	16.3	148	-46	17.7	35.6
27R-2	70-72	513.41	223	-33	15.2	222	-33	15.3	15.4
27R-3	118-120	515.39	141	-80	254.7	140	-80	225.9	87.4
27R-4	67-69	516.38	86	-74	105.3	88	-74	105.8	46.6
27R-5	11-13	517.32	232	23	8.5	209	-71	23.5	32.2
28R-1	26-28	520.87	225	-44	41.8	239	-73	75.2	33.3
28R-4	38-40	565.99	338	-63	107.3	336	-64	108.2	17.3
28R-5	5-7	567.16	232	-55	141.8	231	-57	142.1	24.1

Table 22 (continued).

Core/ sect.	Interval	Sub-bottom depth (m)	NRM			AF (50 Oe)			X ($\times 10^{-3}$)
			Decl.	Incl.	Int.	Decl.	Incl.	Int.	
104-642E-									
29R-1	108-110	531.09	87	-54	79.4	88	-54	80.6	30.1
29R-2	83-85	532.34	50	-54	53.4	50	-57	52.8	29.3
30R-1	51-53	540.02	293	-75	132.0	288	-75	132.5	31.6
30R-3	89-91	543.40	161	77	33.1	56	-72	7.4	15.9
30R-4	62-64	544.63	185	76	77.3	176	-40	6.4	20.5
30R-6	85-87	547.86	285	-71	240.8	285	-71	239.5	36.4
31R-1	91-93	549.92	157	-65	152.4	158	-66	153.1	32.7
31R-2	39-41	550.90	34	-67	45.7	46	-71	47.3	60.9
31R-3	122-124	553.23	128	-66	56.9	129	-67	57.9	20.2
31R-4	103-105	554.54	115	-62	59.8	115	-63	61.6	18.7
32R-1	87-89	559.28	179	-62	52.1	177	-63	56.2	17.8
32R-2	59-61	560.50	74	-70	111.4	74	-70	111.8	27.6
32R-3	95-97	562.36	2	-66	158.2	4	-67	158.2	34.1
33R-1	93-95	565.84	195	-59	115.7	194	-60	117.1	32.1
33R-2	55-57	566.96	244	-66	104.9	244	-66	105.1	7.1
33R-2	95-97	567.36	348	-70	66.9	348	-70	66.5	5.9
33R-3	143-145	569.34	63	-67	50.4	62	-67	50.6	15.0
33R-4	72-74	570.13	62	-68	45.6	62	-68	45.9	18.4
33R-5	29-31	571.2	11	-69	50.7	12	-69	51.3	24.8
33R-5	123-125	572.14	121	-64	39.4	121	-65	39.4	11.4
34R-1	4-6	574.45	204	-54	35.7	203	-54	36.2	18.8
34R-1	78-80	575.19	287	-48	48.3	287	-52	51.4	28.8
35R-1	71-73	584.62	312	-52	43.5	310	-52	47.3	27.3
35R-2	42-44	585.83	360	-48	35.3	9	-53	38.7	28.2
35R-2	127-129	586.68	69	-59	26.1	69	-59	26.2	6.6
35R-3	63-65	587.54	63	-59	47.5	64	-59	47.8	23.0
35R-4	95-97	589.36	263	-67	47.8	262	-69	49.4	33.9
36R-1	28-30	593.69	241	-84	84.4	242	-83	85.2	15.5
36R-2	38-40	595.29	303	-78	35.7	303	-78	35.8	13.6
36R-3	17-19	596.58	209	-79	50.7	209	-80	51.9	26.3
37R-1	20-22	603.01	289	-79	44.4	282	-79	44.8	25.4
37R-2	67-69	604.98	32	-58	47.7	30	-59	45.3	21.6
38R-1	56-58	612.77	293	-69	32.1	292	-68	31.9	13.4
38R-2	115-117	614.86	100	-69	42.1	101	-70	41.3	15.2
38R-3	68-70	615.89	111	-75	103.7	109	-74	105.8	35.3
38R-4	76-78	617.47	11	-76	124.6	12	-77	124.8	19.9
40R-1	85-87	631.96	245	-76	11.8	226	-75	12.9	13.0
40R-2	71-73	633.32	227	-70	21.4	229	-70	22.0	11.8
40R-3	45-47	634.56	234	-75	8.9	237	-76	8.8	5.6
41R-1	52-54	641.13	198	-61	23.3	172	-74	30.2	28.6
41R-1	116-118	641.77	226	-74	47.0	226	-74	47.6	16.9
41R-2	69-71	642.80	7	-86	19.7	105	-82	22.5	30.9
41R-3	9-11	643.70	73	-81	55.2	67	-80	53.7	29.8
41R-3	131-133	644.92	269	-58	9.0	270	-74	13.7	78.8
41R-4	58-60	645.69	183	-62	19.9	190	-73	23.8	20.1
42R-1	34-36	650.45	53	-75	13.2	84	-85	10.4	32.9
42R-1	56-58	650.67	197	-40	4.8	191	-44	5.1	128.7
42R-2	74-76	652.35	245	-71	61.2	245	-70	62.1	35.9
42R-3	8-10	653.19	77	-72	55.0	78	-71	54.5	28.7
45R-1	108-110	679.69	193	-42	70.6	187	-39	48.7	26.8
45R-2	75-77	680.86	232	-60	36.2	224	-65	36.3	28.2
45R-3	73-75	682.34	318	-60	35.3	304	-67	38.2	30.7
45R-4	118-120	684.29	267	76	57.6	313	-19	46.3	24.2
45R-5	15-17	684.76	130	79	40.6	195	-45	5.5	22.5
46R-1	63-65	688.74	86	87	66.9	31	-9	3.1	21.8
46R-2	136-138	690.97	206	77	57.1	212	4	4.5	25.8
46R-3	129-131	692.40	19	19	9.9	32	-54	9.4	84.1
46R-4	23-25	692.84	35	-68	32.1	35	-69	33.4	27.7
47R-1	58-60	698.19	257	-58	44.1	236	-66	17.3	26.3
47R-1	106-108	698.67	333	-64	11.5	325	-70	12.9	14.5
50R-1	80-82	717.41	359	-65	38.4	0	-73	44.7	22.4
50R-2	8-10	718.19	—	—	11.6	—	—	11.4	3.4
51R-1	7-9	723.38	72	-80	46.1	88	-80	50.1	25.3
52R-1	76-78	724.57	322	-78	67.5	324	-79	71.0	26.1
52R-2	10-12	725.41	302	-77	86.8	301	-79	87.9	28.0
52R-3	103-105	727.84	38	84	114.3	10	-9	5.5	30.2
52R-4	100-102	729.31	192	-68	230.4	193	-70	214.8	82.0
52R-5	37-39	730.18	232	-51	62.8	232	-54	61.4	39.9
53R-1	24-26	729.45	263	-63	42.2	267	-71	46.1	41.7
53R-1	119-121	730.40	113	-80	55.9	97	-80	64.6	54.2
53R-2	104-106	731.75	83	-75	51.3	84	-78	57.6	22.4
54R-1	17-19	738.88	226	-62	19.8	229	-73	25.5	16.8
54R-2	42-44	740.62	237	-69	8.1	231	-72	9.1	15.6

Table 22 (continued).

Core/ sect.	Interval	Sub-bottom depth (m)	NRM			AF (50 Oe)			X ($\times 10^{-3}$)
			Decl.	Incl.	Int.	Decl.	Incl.	Int.	
104-642E-									
54R-3	108-110	742.79	228	-63	37.2	220	-73	50.4	16.0
54R-4	17-19	743.38	162	-55	27.9	145	-70	49.4	12.8
55R-1	94-96	749.15	309	-30	17.5	315	-68	41.0	16.8
55R-2	25-27	749.96	227	-33	20.6	223	-68	26.2	10.3
55R-3	101-103	752.22	16	-54	6.7	6	-70	16.6	23.8
56R-1	68-70	758.29	286	-65	21.8	262	-68	26.9	43.0
57R-1	28-30	759.39	246	-83	34.8	194	-73	36.0	31.9
57R-2	56-58	761.17	210	-68	151.9	208	-69	153.8	31.4
57R-3	109-111	763.20	233	-49	36.0	235	-57	41.3	12.5
57R-4	69-71	764.30	352	0	16.8	328	4	3.9	91.5
58R-1	37-39	766.50	257	-36	22.5	248	-49	27.8	70.1
58R-2	103-105	768.64	19	-17	27.1	40	-43	13.5	47.0
58R-3	82-84	769.93	273	-31	8.8	226	-43	15.4	47.7
58R-4	85-87	771.46	130	59	3.4	282	-33	2.8	35.3
58R-4	135-137	771.96	35	50	2.7	12	16	2.3	110.0
58R-5	14-16	772.25	87	52	24.9	75	-19	13.6	43.9
58R-5	96-98	773.07	52	-53	39.9	55	-53	41.3	35.0
59R-1	103-105	776.54	184	-11	13.9	181	-14	13.7	17.2
59R-2	70-72	777.71	122	-39	13.0	119	-61	18.9	35.7
59R-3	135-137	778.36	39	-79	11.4	43	-72	15.9	33.3
60R-1	21-23	785.12	314	-68	24.9	315	-69	25.7	21.5
60R-1	102-104	785.93	209	-58	42.9	208	-63	48.0	64.1
60R-2	110-112	787.51	155	73	21.6	117	-38	8.2	43.0
61R-1	69-71	795.00	288	64	38.6	298	-36	13.9	48.1
61R-1	137-139	795.68	125	21	8.6	216	-58	8.6	43.2
61R-2	121-123	797.02	80	-69	8.4	82	-73	13.4	9.0
62R-1	4-6	803.85	100	-76	35.1	101	-77	37.7	18.1
62R-1	115-117	804.96	341	-72	42.2	342	-77	47.5	25.9
63R-1	15-17	809.96	90	-70	88.8	90	-72	93.8	51.9
63R-2	103-105	812.34	328	-74	28.1	345	-80	53.3	28.2
63R-3	26-28	814.57	182	-74	38.7	191	-79	45.9	21.2
63R-4	4-6	815.85	172	-65	26.9	167	-77	46.8	19.6
64R-1	59-61	816.40	176	83	69.9	167	-17	2.6	20.3
64R-2	47-49	817.78	288	-79	55.9	289	-81	61.7	20.0
64R-3	124-126	820.05	150	80	88.5	160	78	36.9	29.0
64R-4	119-121	821.50	232	-83	89.3	231	-83	92.1	22.9
64R-5	83-85	822.64	326	-82	113.3	327	-82	115.5	23.4
65R-1	27-29	825.48	310	-81	2.5	305	-82	2.2	2.8
66R-1	10-12	834.82	13	-73	94.1	12	-73	95.5	22.8
66R-2	19-21	836.40	206	-61	44.6	211	-68	49.2	24.5
66R-3	77-79	838.48	333	-60	19.9	340	-70	32.2	32.3
66R-4	47-49	839.68	322	-58	35.9	321	-67	43.9	30.0
67R-1	122-124	845.43	45	-73	183.9	47	-73	186.2	29.7
67R-2	52-54	826.23	324	-72	96.8	324	-72	100.3	28.0
67R-2	123-125	846.94	169	-71	201.3	169	-71	202.6	25.4
68R-1	38-40	854.09	173	-74	88.8	170	-77	101.0	50.7
68R-1	121-123	854.92	69	-82	48.9	70	-83	49.4	20.2
68R-2	130-132	856.51	294	-66	47.0	294	-68	50.2	20.1
69R-1	18-20	863.39	15	-65	74.2	15	-65	74.8	10.8
69R-1	87-89	864.08	344	-71	76.9	344	-71	77.1	20.2
69R-2	47-49	865.18	326	-71	44.2	326	-72	45.3	28.8
69R-3	108-110	867.29	203	-28	20.7	208	-59	31.4	23.7
70R-1	80-82	873.51	142	-56	47.2	142	-61	47.8	30.5
70R-2	35-37	874.56	161	-59	23.8	158	-68	27.4	23.2
71R-2	10-12	882.31	44	-30	24.0	30	-58	29.1	46.4
71R-3	125-127	884.96	74	-84	42.8	76	-85	46.1	18.5
71R-4	82-84	886.03	89	-72	209.6	84	-75	197.3	38.7
72R-1	112-114	891.23	159	-53	85.5	159	-55	86.0	44.2
72R-2	89-91	892.50	202	-21	41.3	201	-45	49.5	40.0
73R-1	23-25	896.54	275	-55	172.3	276	-56	171.8	25.4
73R-2	103-105	898.84	317	-29	60.2	318	-41	71.0	40.4
73R-3	81-83	900.12	112	-32	42.7	109	-41	46.5	98.0
73R-3	94-96	900.25	104	-28	59.3	104	-36	61.7	122.1
73R-4	135-137	902.16	299	-25	67.9	301	-42	81.9	38.7
74R-2	109-111	905.00	190	81	189.4	98	46	11.5	47.7
74R-4	24-26	907.15	96	84	65.1	65	-17	9.2	54.2
74R-6	50-52	910.41	45	-45	221.5	46	-44	216.9	57.6
75R-1	55-57	912.46	29	-26	37.7	26	-30	40.5	37.8
75R-2	51-53	913.92	108	-21	4.5	135	-86	20.2	102.8
75R-2	117-119	914.58	158	-69	19.4	189	-82	24.2	49.2
76R-1	75-77	922.16	131	-39	110.9	131	-43	115.2	83.9
76R-2	108-110	923.99	306	-6	7.3	309	-54	7.7	38.5
77R-1	59-61	931.50	309	-47	157.7	313	-53	165.1	115.4
77R-2	71-73	933.12	268	-53	52.5	272	-60	62.6	54.6
77R-3	145-147	935.36	183	-24	30.7	184	-54	37.7	45.2

Table 22 (continued).

Core/ sect.	Interval	Sub-bottom depth (m)	NRM			AF (50 Oe)			X ($\times 10^{-3}$)
			Decl.	(10^{-4}emu/cm^3)		Decl.	(10^{-4}emu/cm^3)		
				Incl.	Int.		Incl.	Int.	
104-642E-									
78R-1	103-105	941.44	185	-58	36.9	185	-57	38.7	49.9
78R-2	79-81	942.70	163	-59	37.5	162	-63	41.7	21.9
78R-3	13-15	943.54	124	51	17.8	146	-44	7.9	31.7
79R-1	92-94	950.83	137	-67	41.3	132	-68	43.2	22.2
79R-1	125-127	951.16	205	-63	49.9	207	-62	50.2	7.0
79R-2	78-80	952.19	75	-47	37.7	74	-50	38.7	21.9
79R-3	4-6	952.95	348	-81	18.5	340	-86	19.4	22.2
80R-1	23-25	959.54	175	40	8.7	166	-68	16.3	34.5
80R-2	59-61	961.40	234	-47	47.0	232	-50	50.0	27.6
81R-1	61-63	968.92	26	73	31.7	18	32	2.6	89.9
81R-2	119-121	971.00	305	-84	32.9	216	-83	39.3	36.2
82R-1	26-28	978.07	291	-64	0.7	268	-82	3.3	14.1
82R-2	67-69	979.98	160	71	5.5	234	-76	5.5	30.8
83R-1	62-64	987.93	62	-62	90.4	61	-61	90.6	17.2
83R-2	87-89	989.68	320	-37	102.7	320	-39	101.0	46.0
84R-1	37-39	997.18	283	-52	35.9	279	-56	41.2	37.8
85R-1	74-76	1007.05	96	-42	22.8	97	-42	22.8	20.6
85R-3	19-21	1009.50	120	-20	25.2	113	-38	29.6	16.8
85R-4	98-100	1011.79	178	76	60.0	157	15	5.7	23.7
85R-5	18-20	1012.49	319	-34	0.8	321	-41	0.8	2.6
85R-5	118-120	1013.49	140	-41	38.6	139	-43	39.9	31.2
85R-6	42-44	1014.2	355	-2	14.6	358	-32	15.3	52.0
86R-1	64-66	1016.45	52	-73	23.0	49	-76	26.7	30.5
86R-2	50-52	1017.82	241	-62	9.6	242	-72	11.6	21.9
86R-2	137-139	1018.68	325	-60	4.2	4	-71	9.3	48.0
86R-3	74-76	1019.55	47	-68	21.2	46	-70	22.8	22.8
87R-1	54-56	1025.85	166	-58	10.5	162	-66	13.2	21.9
87R-1	125-127	1026.56	38	-53	6.1	39	-58	6.7	13.0
87R-2	54-56	1027.35	315	-69	13.6	317	-71	17.4	33.1
88R-1	71-73	1035.52	290	-48	171.8	289	-49	170.7	31.3
88R-2	31-33	1036.62	31	-51	74.7	34	-56	78.0	33.5
89R-1	50-52	1044.81	268	-56	112.3	268	-56	113.3	25.7
89R-2	9-11	1045.90	19	-63	62.9	18	-63	62.7	12.5
90R-1	83-85	1054.64	94	-83	8.1	108	-85	8.7	7.9
90R-2	80-82	1056.11	172	-2	0.9	116	-85	4.3	8.2
90R-3	72-74	1057.53	357	85	4.1	277	-75	2.2	11.4
91R-1	62-64	1063.93	254	-25	53.5	254	-36	60.7	40.4
91R-2	40-42	1065.21	93	-63	37.0	91	-68	40.8	24.7
91R-3	11-13	1066.42	99	-61	14.7	93	-68	17.3	17.7
92R-1	24-26	1073.05	169	-68	10.5	167	-69	10.7	6.0
92R-2	131-133	1075.62	337	-64	14.6	336	-65	14.9	6.1
93R-1	109-111	1079.90	76	-17	4.6	62	-59	7.2	15.5
93R-3	15-17	1081.96	77	4	4.1	57	-56	6.4	10.8
93R-4	109-111	1084.48	283	-55	21.8	287	-63	27.1	11.1
93R-6	26-28	1086.57	78	-63	31.7	73	-67	35.8	13.8
94R-2	35-37	1086.86	191	-64	37.7	191	-66	39.4	12.0
94R-3	103-105	1089.04	253	-66	17.9	256	-68	18.6	14.2
94R-3	129-131	1089.30	194	65	36.9	187	61	28.8	119.1
94R-5	31-35	1091.30	195	53	3.5	196	44	2.2	8.1
95R-1	51-53	1095.02	252	-38	0.01	240	-29	0.01	3.0
95R-2	39-41	1096.04	162	77	0.2	168	79	0.2	1.6
97R-1	101-103	1109.92	64	-13	0.02	92	21	0.01	0.5
97R-2	110-112	1111.51	235	76	0.04	319	76	0.03	0.4
98R-1	106-108	1116.87	139	21	0.01	214	-16	<0.01	0.3
98R-3	14-16	1118.95	88	76	0.08	69	74	0.08	0.7
99R-2	20-22	1125.41	40	-67	0.03	48	-69	0.03	0.3
99R-3	13-15	1128.34	257	-80	2.84	257	-80	2.93	1.4
100R-1	79-81	1135.50	189	-73	0.06	147	-72	0.05	0.2
100R-2	47-49	1136.68	15	86	1.00	61	83	0.75	0.6
101R-1	41-43	1144.52	230	86	0.19	225	85	0.16	0.4
101R-1	104-106	1146.65	294	-78	0.10	288	-79	0.10	0.4
102R-1	105-107	1154.55	333	22	0.01	333	-7	0.01	0.1
102R-2	26-28	1155.27	249	61	<0.01	212	67	<0.01	<0.1
102R-3	45-47	1156.96	75	82	128.7	66	33	10.6	42.9
103R-1	7-9	1163.08	73	69	130.3	69	-14	28.5	40.5
103R-2	66-68	1165.17	227	85	72.2	239	73	11.3	46.9
104R-1	24-26	1166.75	135	75	54.5	117	44	3.6	62.5
104R-3	34-36	1169.85	154	71	180.5	124	-17	20.4	45.2
105R-1	78-80	1173.29	234	80	165.0	266	-30	22.8	43.9
105R-2	105-107	1175.06	2	84	86.2	353	-31	7.8	48.2
105R-4	22-24	1177.23	184	78	189.9	179	59	24.8	51.6
105R-4	136-138	1178.37	138	-05	<0.01	131	-39	<0.01	0.2
106R-1	50-52	1182.41	300	82	0.15	291	82	0.12	0.5
107R-1	58-60	1191.99	351	70	<0.01	197	65	<0.01	0.3
107R-2	12-14	1193.03	76	41	0.01	69	12	0.01	0.2

Table 22 (continued).

Core/ sect.	Interval	Sub-bottom depth (m)	NRM			AF (50 Oe)			X ($\times 10^{-3}$)
			Decl.	(10 ⁻⁴ emu/cm ³)		Decl.	(10 ⁻⁴ emu/cm ³)		
				Incl.	Int.		Incl.	Int.	
104-642E-									
107R-3	106-108	1195.47	222	-27	<0.01	216	-42	<0.01	<0.1
107R-4	49-51	1196.40	0	-22	<0.01	74	-22	<0.01	0.2
108R-1	116-118	1202.07	127	83	<0.01	207	86	<0.01	0.4
108R-2	95-97	1203.36	100	68	<0.01	112	55	<0.01	0.4
109R-1	69-71	1211.60	162	51	0.01	261	69	<0.01	0.1
109R-2	61-63	1213.02	318	-77	1.1	316	-78	1.1	0.4
110R-1	48-50	1220.39	266	-84	0.2	270	-84	0.2	0.4

A small number of samples exhibit shallow inclinations of fairly high stability. These samples mostly stem from the brecciated top zones of flows, and it is suggested here that they are parts of blocks that rotated during emplacement of the flow or of that of the next flow unit.

In spite of the preliminary stage of analysis and interpretation of the inclination record (see for comparison Table 23 for AF-cleaned directions of selected samples), we note a few down-hole features which may reflect magnetic field behavior during emplacement, post emplacement effects of tectonic rotations, and/or overprinting by secondary components. Correlations of magnetic features with petrological units can assist in distinguishing geomagnetic field variations during emplacement of the dipping basalts from later effects. For example, a marked change in NRM intensity and inclination values takes place above and below the interval from 490 to about 514 mbsf.

Other zones of apparent low inclination values are found from 684 to 692 mbsf and from 763 to 777 mbsf. The samples taken from these zones are from the interior of massive, thick basalt flows and display multicomponent remanence behavior during demagnetization. An example of a stable and a comparatively unstable behavior of two samples is given in Figure 53, one from the fine-grained lower margin of a thin flow (Section 104-642E-67R-2) and the other from the massive interior of a flow (Section 104-642E-69R-3). From this figure it is obvious that AF demagnetization to at least a few hundred Oe is required to determine stable inclination values. Similar results have been reported from basalts elsewhere in the North Atlantic area, for example, the upper portion of the plateau basalts in eastern Iceland (Bleil et al., 1982) and the upper and middle basalts of the Faeroes (Abrahamsen et al., 1984).

By far the greatest change in magnetic characteristics, however, occurs at the already mentioned boundary of less altered, mostly massive basaltic flows and the much more altered sediment/glassy flow sequence at 1109 mbsf. Below 1100 mbsf, intensities of both natural remanent magnetization and of susceptibility are lower by about two orders of magnitude compared to the rocks above this boundary (if we disregard the dike unit that was encountered at about 1160 mbsf and which compositionally resembles the upper zone). The low remanence values of generally less than 0.2×10^{-4} emu/cm³ are not restricted to the sediments in the lower part of the hole but are typical for the flows as well. At this stage we are uncertain of the origin of the low remanence values. They may be caused by alteration or by primary magnetic properties or a combination of both.

The described changes across the boundary at about 1109 mbsf may also be indicative of a hiatus between the emplacement of the lower and the upper parts of the drilled igneous section.

Summary

The magnetic polarity of the 907-m drilled igneous and sedimentary sequence is predominantly reverse, with the possible

exception of two minor zones at about 340 to 350 mbsf and 1109 to 1182 mbsf, respectively. Remanence intensity, susceptibility, and inclination, as well as demagnetization behavior of the samples from the top of the igneous sequence to about 1109 mbsf, resemble those for other basalt areas in the North Atlantic area where basalts are only mildly altered and particularly where samples from the interior of massive flows display multicomponent remanence behavior.

Below 1109 mbsf, however, alteration and primary magnetic properties are distinctly different from the sequence above. Within the lower section secondary components are much more stable, and remanence and susceptibility values are reduced by two orders of magnitude. This major magnetic disparity indicates a major gap in the volcanic development in the area of Site 642.

Comparison and correlation with the other areas in the North Atlantic basalt province (the Faeroes, east Greenland, and Rockall Plateau) will have to await results from detailed shore-based magnetic studies, especially in light of the predominantly reverse magnetization in Hole 642E.

GEOCHEMISTRY

Organic

At Site 642, organic geochemical studies included measurement of methane, determination of organic and inorganic carbon, and characterization of the organic matter by Rock-Eval pyrolysis. In addition, while waiting for this site to be completed, a survey was conducted of potential organic geochemical contaminants used during the core-recovery procedure. The results of this survey can be found in Kvenvolden and McDonald (1986).

Methane

Twenty sediment samples (5-cm length of full round core) were collected between sub-bottom depths of 2.9 and 326.4 m in fine-grained sediment which ranged in age from Quaternary to early Miocene. Only methane in very small concentrations—ranging from 1.7 to 23.0 ppm (vol. of methane/vol. of gas)—was detected in these samples (Table 24). Concentrations of methane were highest in the middle Miocene sediments and decreased with depth (Fig. 54). At 326.4 m (the deepest sample analyzed) methane could not be detected. The low concentrations of methane at this site are likely the result of early diagenetic processes.

Carbon

Sampling strategy at this site called for the collection of sediment for headspace gas analyses adjacent to the samples recovered for the determination of the chemistry of interstitial water (IW). Before the IW sediment sample was squeezed to obtain pore fluids, a subsample of sediment (about 5 cm³) was removed and dried. From this sample, values were obtained for carbon-

Table 23. Hole 642E. Stable inclination, declination, and maximum demagnetizing field applied to samples that were demagnetized in fields above 50 Oe.

Core/section interval (cm)	Inclination (degrees)	Declination (degrees)	AF (Oe)
104-642E-			
2W-3, 58-60	R	94	500
4R-1, 69-71	R		500
5R-1, 45-47	R		100
5R-1, 90-92	R		400
5R-3, 63-65	-74	247	300
5R-3, 128-130	N		300
5R-3, 134-136	N		300
5R-3, 138-140	N		500
5R-3, 146-148	N		500
10R-2, 28-30	-68	146	500
11R-2, 54-56	R		500
12R-1, 14-16	-67	255	650
13R-1, 95-97	-44	225	300
14R-1, 38-40	R		300
15R-2, 75-77	-58	248	1000
15R-2, 136-138	-56	77	400
15R-5, 128-130	-70	321	600
16R-1, 33-35	-56	204	900
16R-2, 24-26	-55	284	600
17R-1, 106-108	-72	328	1000
18R-1, 40-42	-68	292	900
19R-1, 42-44	-72	260	600
20R-1, 28-30	-66	100	1000
21R-3, 50-52	72	308	700
21R-3, 106-108	75	156	900
21R-5, 109-111	-68	273	500
22R-3, 43-45	-13	155	300
23R-1, 106-108	-60	245	300
25R-2, 89-91	-32	19	700
25R-3, 62-64	-29	273	900
26R-1, 80-82	-50	2	600
26R-3, 3-7	-60	190	800
27R-2, 70-72	-33	222	900
27R-5, 11-13	-78	237	700
28R-1, 26-28	-78	260	500
29R-1, 108-110	-55	87	1000
30R-4, 62-64	-78	150	300
31R-4, 103-105	-65	115	1000
32R-3, 95-97	-68	4	900
33R-1, 94-95	-61	196	900
33R-2, 55-57	-66	245	400
34R-1, 4-6	-58	206	1000
34R-1, 78-80	-53	286	1000
37R-2, 67-69	-61	28	900
41R-2, 69-71	-84	121	1000
42R-1, 34-36	-85	110	300
42R-1, 56-58	-77	200	1000
45R-1, 6-8	-70	168	600
45R-1, 108-111	-35	180	1000
46R-2, 136-138	-63	225	600
46R-3, 129-131	-71	32	1000
47R-1, 106-108	-74	323	1000
50R-1, 80-82	-78	359	900
52R-3, 103-105	-73	10	850
52R-5, 37-39	-58	233	1000
53R-1, 119-112	-80	98	700
54R-2, 42-44	-74	224	850
55R-1, 94-96	-71	315	1000
57R-1, 28-30	-73	185	300
58R-2, 103-105	-52	53	600
58R-4, 135-137	-47	323	400
58R-4, 85-87	-47	296	150
59R-1, 103-105	-17	182	400
60R-2, 110-112	-70	95	500
66R-2, 19-21	-73	216	900
67R-2, 123-125	-72	169	950
69R-3, 108-110	-68	214	800
73R-3, 94-96	-54	98	600
74R-2, 109-111	-45	70	850
85R-5, 18-20	-65	189	1000
93R-3, 15-17	-63	47	250
93R-6, 26-28	-68	71	300

Table 23 (continued).

Core/section interval (cm)	Inclination (degrees)	Declination (degrees)	AF (Oe)
104-642E-			
94R-4, 129-131	-33	179	850
94R-5, 31-35	-45	210	300
95R-2, 39-41	R		400
97R-1, 101-103			300
97R-2, 110-112	N		500
98R-1, 106-108	R		200
98R-3, 14-16	75	67	1000
99R-2, 20-22	-79	16	600
100R-2, 47-49	66	76	500
101R-1, 41-43	-52	177	1000
102R-3, 45-47	-51	2	500
103R-2, 66-68	R		500
104R-1, 24-26	-71	41	900
105R-4, 136-138	-60	128	700
106R-1, 50-52	83	290	350
107R-2, 12-14	-51	55	500
109R-1, 69-71	-65	146	500

Note: Inclination and declination values are preliminary only, partly due to incomplete demagnetization and partly to multicomponent magnetization where detailed analysis is required.

ate carbon by means of the carbonate bomb and by the Carbonate Carbon apparatus (coulometry). Acidified samples from the carbonate bomb were washed and organic carbon was measured with the Elemental Analyzer. Separate portions of non-acidified samples were analyzed by coulometry and Rock-Eval pyrolysis.

Values of carbonate carbon from the carbonate bomb and from coulometry were remarkably similar except that the coulometer was more sensitive. Table 24 shows the percentages of carbonate carbon as determined by coulometry. In general the carbonate content of these sediments is very low (0% and <0.12%) in the Pliocene and lower Miocene sediments. Highest values of carbonate carbon occur in middle and upper Miocene sediments with three values averaging 1.85%.

Values for organic carbon (Table 24) represent replicates and are believed to be good estimates of the organic carbon content of these sediments. Percentages of organic carbon increase steadily with depth (Fig. 54) from the Quaternary through middle Miocene (0.34% to 1.84%) and then decrease to lower values in the lower Miocene (average about 1.21%). The trend of the organic carbon values with depth more or less parallels the trend of the methane concentrations (Fig. 54). This parallelism supports the idea that the small concentrations of methane are mainly derived from the decomposition of organic matter.

Organic Matter Characteristics

The procedure of Rock-Eval pyrolysis provides a preliminary survey of the source and maturity of organic matter in sediments, but in general the results (Table 25) are not particularly satisfying although trends are present from which tentative interpretations can be made by following Tissot and Welte (1984). Values of total organic carbon (TOC) obtained from the Rock-Eval II Plus TOC instrument did not agree with organic carbon values obtained by elemental analysis. Therefore, the latter values were used to calculate the hydrogen and oxygen indices (HI and OI) from Rock-Eval S_1 , S_2 , and S_3 parameters (Table 25). Both HI and OI values vary widely, and OI values are particularly large, suggesting that the organic matter is oxygen rich and very immature.

T_{max} is the temperature at which maximum generation of hydrocarbons from kerogen occurs in the pyrolysis procedure. T_{max} values correlate with organic matter maturation; $T_{max} < 435^\circ\text{C}$

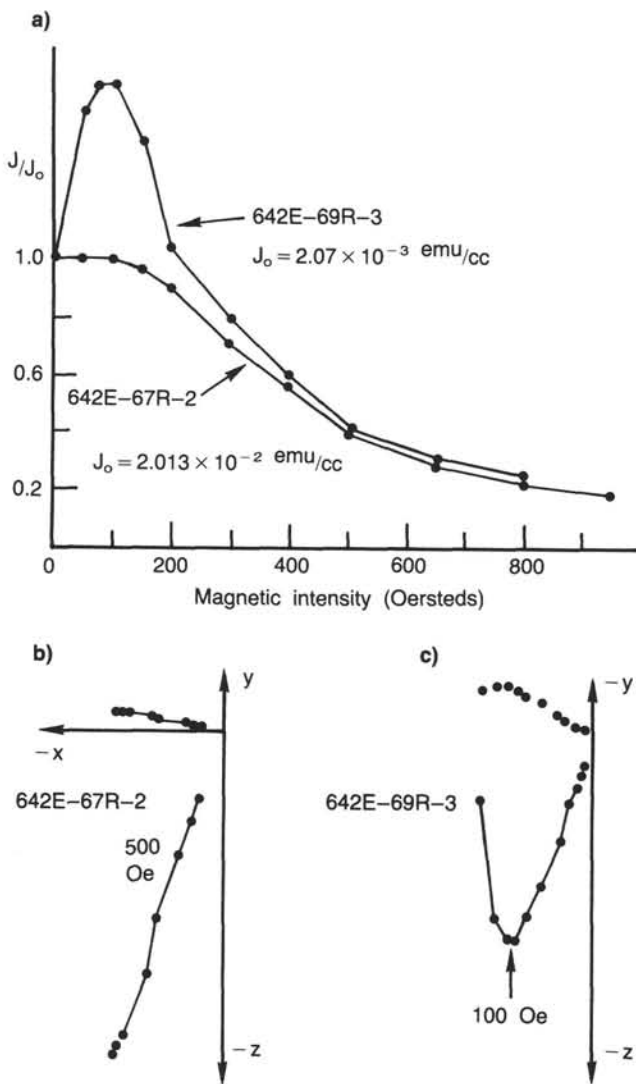


Figure 53. AF-demagnetization plots of samples from two different basaltic flows from Sections 642E-67R-2 and 642E-69R-3. Plot a): Intensity of remanent magnetization, J , divided by NRM, J_0 . Plots b) and c): X-, Y-, and Z-components of remanent magnetization (arbitrary units).

signals immaturity, whereas $T_{max} > 470^\circ\text{C}$ indicates postmaturity. Thus, T_{max} values of 400° to 431°C of most Miocene sediments also support the idea that this organic matter is immature. Such immaturity is to be expected in these shallow marine sediments. Average T_{max} values of 555°C for the Quaternary and Pliocene sediments suggest the presence of postmature, reworked organic matter. Based on considerations of HI and OI, it is concluded that the kerogen in the upper Miocene through Quaternary sediments is mainly type III (dominantly terrestrial in origin), whereas the kerogen in the middle and lower Miocene sediments is generally a mixture of type II and III with type II kerogen being mainly of marine origin.

Inorganic

The chemistry of interstitial water at Site 642 was routinely monitored in Quaternary to lower Miocene sediments overlying basalt. The parameters measured included pH, alkalinity, chloride, sulfate, calcium, and magnesium. In addition to these pa-

rameters, inorganic carbon was determined; results for this component are reported with the organic geochemistry data.

The results are shown in Table 26, where depths are measured from the seafloor. Alkalinity ranged from 3.29 milliequivalents per liter (meq/L) at 2.9 mbsf to 1.86 meq/L at 299.1 mbsf. A weak maximum of 10.12 meq/L occurred at 53.3 mbsf (Fig. 55). Maximum alkalinity values were commonly observed in the upper 100 m of sediment in cores taken during Leg 38 (Gieskes, Lawrence, and Galleisky, 1978). This maximum value generally corresponds to the zone where sulfate reduction takes place (Emerson et al., 1981). Values of pH ranged from 7.82 at 2.9 m to a maximum of 8.24 at 53.3 mbsf and then decreased slightly and irregularly with depth. Deflections in the alkalinity depth profile may have been caused by the reactions of pore waters with the surrounding sediments. Salinity decreased slightly with depth, ranging from 37.5 parts per thousand (ppt) at 2.9 mbsf to 34.2 ppt at 245.6 mbsf. This change suggests that chemical species are being bound to the sediment (Gieskes, 1981). The chloride concentration was irregular, showing a general decrease with depth.

Calcium and magnesium exhibited the greatest differences in concentrations of the inorganic chemical species monitored. Calcium increased from 10.88 millimole/liter (mmol/L) at 2.9 mbsf to 50.50 mmol/L at 299.1 mbsf. Magnesium showed the opposite trend in decreasing from 50.81 mmol/L at 2.9 mbsf to 14.68 mmol/L at 299.1 mbsf (Fig. 55). These opposing trends of calcium and magnesium concentrations were seen at all sites drilled on Leg 38 (Gieskes, Lawrence, and Galleisky, 1978). The relationships between calcium and magnesium profiles have been explained by Gieskes (1981) to result from the alteration of volcanic ash in the sediment column and the alteration of the underlying basalts.

Sulfate values decreased significantly in the upper 137 m of the sediment column, where concentrations ranged from 26.1 mmol/L at 5.7 mbsf to 8.6 mmol/L at 137.0 mbsf. Below this latter depth sulfate increased to a maximum value of 19.9 mmol/L at 192.6 m, then decreased to 12.5 mmol/L at 299.1 m. This type of profile may exemplify a non-steady state condition (Gieskes, Lawrence, and Galleisky, 1978). Overall the inorganic geochemical results at Site 642 suggest that substantial postburial, diagenetic changes have taken place in these sediments.

PHYSICAL PROPERTIES

Sedimentary Section

Coring during Leg 104 on the outer Vøring Plateau sampled an upper 320-m-thick sedimentary sequence ranging from Recent to Eocene in age. Routine physical properties measured on sediments from this sequence include water content (expressed as weight of water relative to the total dry weight), porosity, bulk density, vane shear strength, thermal conductivity, and compressional wave velocity (see "Explanatory Notes" chapter, this volume).

DSDP Leg 38 coring on the outer Vøring Plateau provided the first opportunity to study sediments from below several meters sub-bottom for analysis of physical properties. Although these cores provided a first glimpse at physical properties for sediments from deeper in the section, interpretations were limited due to incomplete recovery and disturbance induced from rotary drilling. Sediments recovered at DSDP Sites 338 and 342 consisted of Pleistocene through Miocene sediments, extending into Eocene sediments at Site 338 (Talwani, Udintsev, et al., 1976). These sediments were described as muds, sandy muds, and oozes having bulk densities ranging from 1.25 to 2.23 g/cm³. Vane shear measurements showed an increment up to approximately 13 kPa at 8 m sub-bottom. Peak strengths of 11 kPa at

Table 24. Organic geochemistry for Site 642, Leg 104.

Hole	Core number	Section number	Sub-bottom depth (m)	Age	Methane (ppm)	C _{carb} (%)	C _{org} (%)
B	1H	2	2.9	Quat	2.7	—	—
A	1H	3	5.7	Quat	11.0	—	—
B	2H	5	12.2	Quat	2.3	—	—
B	4H	4	26.6	Quat	1.7	0.85	0.34
B	5H	4	35.3	Quat	3.3	—	—
B	7H	4	53.3	Plio	4.5	0	0.44
B	8H	4	62.8	Plio	4.9	—	—
B	10H	4	81.8	Plio	9.2	0	0.83
B	11H	4	91.3	l. Mio	8.5	—	—
B	13H	4	110.1	l. Mio	6.1	1.97	0.66
B	16H	6	137.1	l. Mio	11.9	1.66	1.43
B	19H	4	163.6	m. Mio	15.3	1.91	1.50
C	22H	3	181.9	m. Mio	14.5	0.16	1.74
B	22H	4	192.6	m. Mio	23.0	<0.10	1.84
D	4X	5	216.6	e. Mio	21.7	0	1.17
B	25H	4	219.0	e. Mio	12.9	0	1.25
D	7X	5	245.6	e. Mio	10.8	<0.10	0.98
D	10X	5	274.5	e. Mio	5.8	<0.10	1.31
D	13X	2	299.1	e. Mio	1.4	<0.10	1.34
D	18X	2	326.4	e. Mio	nd	—	—

— = not determined; nd = not detected; C_{carb} = carbonate carbon; C_{org} = organic carbon.

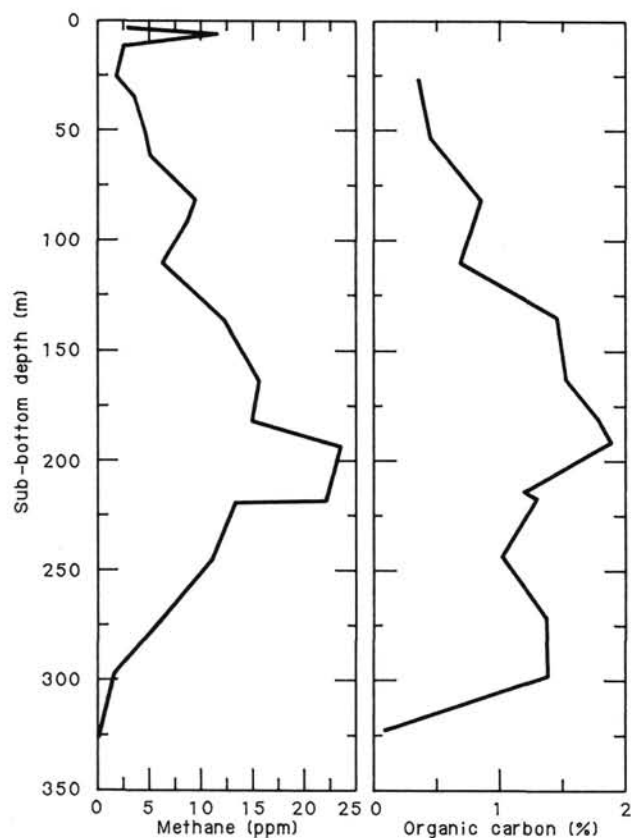


Figure 54. Variation of methane and organic carbon with sub-bottom depth at Site 642, Leg 104.

depths of 20 mbsf strongly suggested drilling-induced disturbance. Velocities were measured only on sediments of the uppermost section and on indurated material from deep in the hole because most material was either so gassy or so disturbed that excessive attenuation of the acoustic signal resulted.

Fairly undisturbed cores, obtained primarily by hydraulic piston core (HPC) operations, were used for shipboard analysis of physical properties on ODP Leg 104. Double HPC coring

(Holes 642B and 642C) provided an opportunity to check results of physical-properties measurements in the less-disturbed HPC material versus those of earlier studies. Results for Holes 642A, 642B, 642C, and 642D are discussed herein as a continuous sequence. Table 27 is a summary listing of Site 642 physical-properties measurements.

Index Properties

The distribution of index properties, such as bulk density, water content, and porosity, are plotted relative to sub-bottom depth in Figure 56. The vertical distribution of these properties is closely related to the lithologies recovered. The contrast between physical properties of lithologic Units I and II, at 67 mbsf, is quite distinguishable. A sharp contact indicated by decreasing bulk density and increasing water content and porosity marks this lithologic boundary. Additionally, the variability of the index properties decreases abruptly from the upper lithologic Unit I to those below. Sediments of lithologic Units II and III exhibit only subtle differences in their physical properties, with Unit III having the highest porosities and water contents of the entire sedimentary sequence. The lowermost sedimentary contact between Units III and IV is reflected in the physical properties by a decrease in water content of 80% and a 30% drop in porosity.

Lithologic Unit I, representing alternating glacial and interglacial sequences of the Quaternary (see "Sediment Lithology" section), is characterized by bulk densities ranging between 1.53 and 2.02 g/cm³. This unit extends from the mud line to 67 mbsf where it contacts the underlying nanofossil muds of lithologic Subunit IIA. Porosities in the upper 67 m of the sediment column vary between 40% and 70%. Water contents, following porosity trends, fluctuate between 25% and 87% in the same interval. The profiles illustrated in Figure 56 show that index properties vary systematically in the upper 67 m, corresponding to either glacial or interglacial facies. The average porosity of interglacial/glacial facies is 61%, corresponding to a bulk density of 1.74 g/cm³. However, very dark-gray to black layers of sandy mud form what is interpreted to be a deposit associated with glacial maxima. During the time of maximum ice coverage, anoxic conditions persisted, allowing these very dark layers to form. The index properties of these portions of the glacial facies, typically poorer in biogenic material and subsequently enriched in terrigenous material, have an average porosity of 43% and bulk density of 1.93 g/cm³. Despite the systematic variation of these facies, a general downhole decrease of water content and porosity suggests a response of these sediments to burial depth.

The contact at 67 mbsf represents a primary interface in the physical properties as well as lithology at Site 642. Bulk densities drop from the higher values of Unit I to a nearly constant value of 1.49 g/cm³ in lithologic Subunit IIA, a nanofossil mud. Water contents in Subunit IIA average 95% and porosities vary between 70% and 83%. The variability of bulk density decreases noticeably in this section of the core in which a more homogeneous sedimentary structure is observed.

Lithologic Subunit IIB extends from 83 to approximately 104 mbsf. This subunit consists of a siliceous mud, characterized by a small shift of index properties. The average measured bulk density for this unit is 1.47 g/cm³, porosity 74%, and water content 100%.

Subunit IIC extends from 104 to 151 mbsf. The siliceous nanofossil ooze of lithologic Subunit IIC exhibits more variability of index properties as compared to the previous lithologic subunits of Unit II. The shifts in bulk density, ranging between 1.40 and 1.61 g/cm³, reflect a compositional influence of the biogenic fraction. The higher water contents and porosities in this subunit correspond to those intervals enriched in the siliceous fraction. Porosities range from 63% to 81% with an aver-

Table 25. Rock-Eval data for Site 642, Leg 104.

Hole	Core no.	Section no.	Sub-bottom depth (m)	Age	%C _{org}	S ₁	S ₂	S ₃	PI	S ₂ /S ₃	HI	OI	T _{max}	Kerogen type
B	4H	4	26.6	Quat	0.34	0.02	0.09	1.29	0.20	0.06	27	379	483	III
B	7H	4	53.3	Plio	0.44	0.07	1.26	0.21	0.05	6.0	286	48	584	II-III
B	10H	4	81.8	Plio	0.83	0.75	1.25	2.41	0.37	0.51	151	290	597	III
B	13H	4	110.1	l. Mio	0.66	0.20	0.27	2.93	0.43	0.09	41	444	410	III
B	16H	6	137.0	l. Mio	1.48	0.40	0.85	4.00	0.32	0.21	59	280	400	III
B	19H	4	163.6	m. Mio	1.50	0.32	1.11	4.14	0.23	0.26	74	276	406	III
C	22H	3	181.9	m. Mio	1.74	0.64	2.76	2.54	0.19	1.08	158	146	401	II-III
B	22H	4	192.6	m. Mio	1.84	0.00	0.17	2.35	0.00	0.01	9	128	476	III
D	4X	5	216.6	e. Mio	1.17	0.65	4.08	2.39	0.14	1.70	349	204	406	II-III
B	25H	4	219.0	e. Mio	1.25	0.49	3.10	1.60	0.14	1.92	248	128	404	II-III
D	7X	5	245.6	e. Mio	0.98	0.50	3.13	2.45	0.14	1.27	320	250	431	II-III
D	10X	5	274.5	e. Mio	1.31	0.43	2.33	3.43	0.16	0.67	178	262	407	II-III
D	13X	2	299.1	e. Mio	1.34	0.10	1.42	3.35	0.07	0.42	106	250	429	III

S₁ (mg HC/g rock) = volatile hydrocarbons; S₂ (mg HC/g rock) = kerogen-derived hydrocarbons; S₃ (mg CO₂/g rock) = organic CO₂ from kerogen; PI (S₁ + S₂) = productivity index; S₂/S₃ = kerogen-type index; HI (100 S₂/C_{org}) = hydrogen index; OI (100 S₃/C_{org}) = oxygen index; T_{max} = temperature (°C) of maximum hydrocarbon generation from kerogen; kerogen type: II - marine, oil/gas prone; III - terrestrial, gas prone.

Table 26. Interstitial water chemistry for Site 642, Leg 104.

Hole	Core number	Section number	Sub-bottom depth (m)	Salinity (ppt)	Chloride (mmol/L)	pH	Alkalinity (meq/L)	Sulfate (mmol/L)	Magnesium (mmol/L)	Calcium (mmol/L)
B	1H	2	2.9	37.5	562	7.82	3.29	20.7	50.81	10.88
A	1H	3	5.7	35.1	557	7.82	2.45	26.1	50.41	10.81
B	4H	4	26.6	35.9	571	7.75	5.67	13.1	45.77	11.16
B	7H	4	53.3	34.2	563	8.24	10.12	11.7	**	**
B	10H	4	81.8	33.9	575	7.90	7.48	10.6	32.97	18.33
B	13H	4	110.1	35.1	566	7.44	5.49	9.1	30.46	23.06
B	16H	6	137.0	34.2	576	7.34	5.84	8.5	25.21	28.71
B	19H	4	163.6	34.2	572	7.25	6.22	16.3	22.06	34.47
C	22H	3	181.9	36.4	568	7.45	5.18	13.7	19.93	37.79
B	22H	4	192.6	35.0	577	7.33	5.63	19.9	20.21	38.31
D	4X	5	216.6	34.3	562	7.31	3.08	13.8	19.42	41.00
B	25H	4	219.0	34.5	565	7.20	4.58	13.5	18.01	41.15
D	7X	5	245.6	34.2	567	7.43	3.04	9.5	18.01	44.08
D	10X	5	274.5	34.5	567	7.15	2.27	12.8	**	**
D	13X	2	299.1	34.4	556	7.63	1.86	12.5	14.68	50.50

** Insufficient sample for analysis.

age value of 73%. The interval from 105 to 120 mbsf shows typical trends of sediment response to overburden. A discontinuity of this trend, however, is apparent at 120 mbsf where densities decrease while porosities and water contents increase. This marker correlates with a possible 5-m.y. hiatus documented within lithological Subunit IIC. Below this depth a reverse trend to normally consolidated sediments is developed, with increasing porosities and water contents. The causes for this opposite trait may be related to the amounts of incorporated silica and different clay minerals, compounded by rebound resulting from removing the core from *in-situ* confining stresses.

A short interval between 151 and 155 mbsf corresponds to lithologic Subunit IID. The primary lithological difference between Subunits IIC and IID is the decrease of nannofossils in sediments from the latter. The calcareous siliceous mud has a more coherent set of index properties, with an average bulk density of 1.49 g/cm³, porosity of 74% and water content equal to 96%.

Lithologic Unit II represents a set of virtually constant index properties. In contrast, Unit III is clearly distinguished by a well-developed downhole trend of increasing water content and porosity, and decreasing bulk density. Again, as in Subunit IIC, this trend may be related either to a systematic compositional shift downhole, and/or to mechanical rebound, with increasing elasticity of the lowermost sediments. Water contents increase from 95% at 164 mbsf to a high of 155% at 220 mbsf. Porosities vary within this unit from 74% to 80% and bulk densities

between 1.28 and 1.54 g/cm³. A contrasting, and normal, trend of decreasing water content and increasing density is developed in the lower 40 m of this unit. Although no lithologic contact is described around 255 mbsf, the shift in index properties suggests that a hiatus in net accumulation may exist at this point in the sedimentary record. Very low accumulation rates within this interval (see "Sediment Lithology" section) also point to a possible episode of erosion.

The index properties of lithologic Unit IV represent a strong contrast with all of the above units. Within this lithologic unit oceanic sedimentary sources give way to a volcanogenic origin. Ashes, pyroclastic flows, and basaltic rubble bear dramatically different index properties, with bulk densities ranging from 1.55 g/cm³ in an ash-enriched mud to 2.64 g/cm³ in a weathered basalt. Porosities and water contents follow suit, varying between 50%-72% and 76%-116%, respectively.

Undrained Shear Strength

Undrained, vane shear-strength measurements were plotted on an X-Y recorder to obtain peak torque values during rotation. Examples of the shear-test record are illustrated in Figure 57. Figure 58 displays the shear-strength profile at Site 642. A monotonic increase of shear strength is seen from the mud line to approximately 90 mbsf. Values of 6.78 kPa at the mud line increase to 142 kPa at 91 mbsf. Shear strength becomes more variable below this latter depth, yet continues to increase to a maximum of 203 kPa at 174 mbsf. The sediments from lower in the

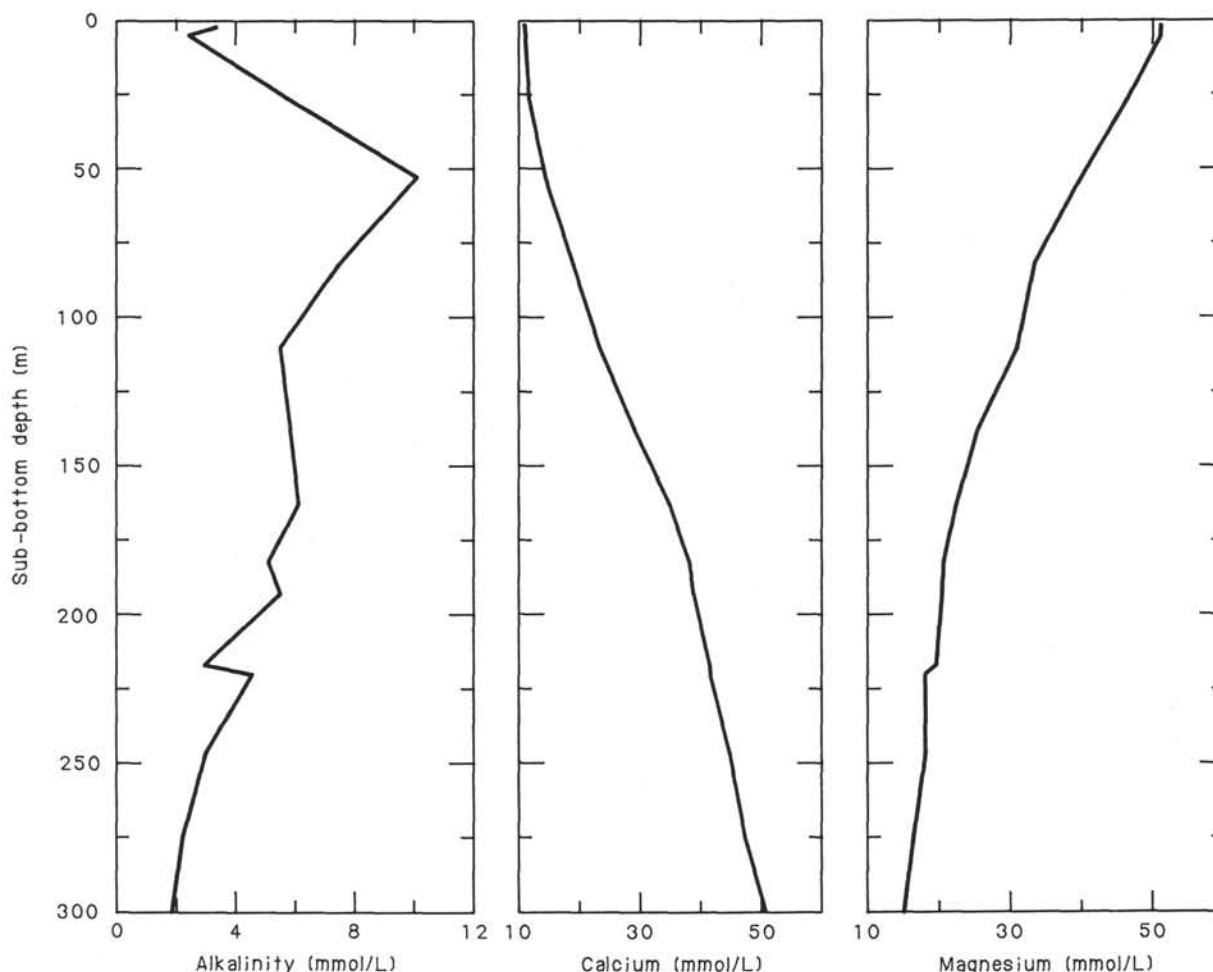


Figure 55. Variation of magnetism, calcium, and alkalinity with sub-bottom depth at Site 642, Leg 104. Units: meq/L = milliequivalents per liter; mmol/L = millimoles/liter.

section were disturbed by HPC fracturing during punch in or fractured during the strength test. Most vane shear values below 180 mbsf are therefore suspect.

Shear-strength trends within lithologic Unit I show a gradient increase from approximately 1.3 kPa/m between 0 and 36 mbsf to 2.0 kPa/m below this interval. The contact with lithologic Unit II marks an interval of variable shear strength, ranging between 29 and 109 kPa in Subunit IIA. This is most likely an artifact of the changes in calcium carbonate content, ranging from 0% to 49% dry weight, and related coring disturbance. The bulk of lithologic Subunits IIB, IIC, and IID have fluctuating shear strengths between 43 and 200 kPa with a general downhole gradient near 1 kPa/m.

Lithologic Unit III, characterized by its siliceous component, has an increase in shear strength similar to the three previous subunits. The maximum measured value of shear strength at Site 642, 203 kPa, was obtained in this unit at 174 mbsf. Below 185 mbsf, shear-strength values decrease and are much more erratic. The decrease of shear strength may be associated with a number of factors including downhole increases of siliceous components and/or smectites, and coring disturbance.

A comparison of the state of consolidation for sediments from Site 642 with the range defined for marine sediments (Skempton, 1970) is also shown in Figure 58. Skempton's definition of normally consolidated sediments ranges from 0.2 to 0.7 of the computed effective overburden stress. The effective overburden stress at Site 642 was calculated using an average bulk density

for each lithologic unit, and assuming hydrostatic conditions. Most of the vane shear-strength measurements show sediments from Units I and II are normally consolidated. Sediments of Unit III have shear strengths that fall below the lower limit of normally consolidated sediment, indicating an underconsolidated state for these diatomaceous sediments.

Compressional-Wave Velocity and Acoustic Impedance

Measurements made on sediments from the upper 67 m exhibit velocities fluctuating between 1490 and 2000 m/s (Fig. 59). Velocities decrease below lithologic Unit I and are more erratic. A slow increase in velocity occurs throughout Units II and III, ranging from lows in the 1400-m/s range to 1780 m/s. An Fe/Mg-enriched sediment layer at 95 mbsf has a distinctly higher velocity of 2225 m/s. The base of lithologic Unit III, marked by a transition from siliceous mud to volcanoclastics, represents a clear shift in velocities. Unit IV velocities range from 1400 m/s in a loose, soft mud (ash) to 4402 m/s in a fairly fresh basalt sample. Within this unit velocities average 2000 m/s. Low velocities, less than 1500 m/s, are probably artifacts of unsaturated sediments and/or saturated sediments with high attenuations.

Also shown in Figure 59 is the profile of acoustic impedance. The extremes of both velocities and bulk densities in the Quaternary glacial/interglacial sequence provide ample sources of near-surface reflectors. Below lithologic Unit I, the Fe/Mn enriched layer at 91 mbsf shows a contrast with surrounding nannofossil/siliceous mud, and may give rise to another reflector on seismic

Table 27. Summary of physical-properties data for sediments from ODP Site 642.

Hole	Core	Sec	Top (cm)	Bot (cm)	Depth (mbsf)	Bulk density (g/cm ³)	Porosity (%)	Water content (%)	Velocity (m/s)	Van shear strength (kPa)
A	1	2	71	74	3.51	1.66	64.4	63	1459	6.78
A	1	4	41	44	6.24	1.67	63.8	61	1487	6.78
A	1	5	142	145	8.72	1.91	47.9	33	1494	11.02
B	1	2	75	78	2.25	1.53	70.2	84	1569	4.52
B	1	3	67	70	3.67	1.88	49.3	35	1645	4.80
B	1	3	103	106	4.03	1.62	66.0	68	1641	6.55
B	2	2	14	17	6.44	1.84	53.2	41	1659	10.45
B	2	5	131	134	7.61	1.71	61.4	56	1590	5.08
B	3	2	63	66	14.98	1.71	60.7	55	1389	23.73
B	3	3	15	18	17.45	2.02	42.2	27	1835	21.47
B	3	4	57	60	19.37	1.62	66.8	69	1783	29.38
B	4	2	128	131	23.48	1.61	66.0	69	1512	8.76
B	4	5	51	54	27.21	1.98	44.9	30	1677	24.29
B	4	5	100	103	27.70	1.74	65.5	60	1524	11.13
B	5	2	29	32	31.19	1.74	60.5	53	1542	24.41
B	5	3	79	82	33.19	1.93	46.1	32	1665	32.66
B	5	5	68	71	36.08	1.76	59.1	51	1556	33.22
B	6	2	27	30	40.67	1.96	47.6	32	1300	58.76
B	6	3	93	96	42.83	1.75	59.7	52	1200	42.04
B	6	5	29	32	44.90	1.79	58.0	48	1350	58.34
B	7	2	96	99	49.86	1.73	61.0	54	1535	56.50
B	7	4	47	50	52.37	1.96	45.6	31	1664	64.18
B	7	6	57	60	55.47	1.74	62.3	56	1703	78.87
B	8	2	75	78	59.15	1.64	65.8	67	1512	76.84
B	8	4	36	39	61.76	1.73	61.1	54	1535	76.84
B	8	5	33	36	63.23	1.99	39.8	25	1715	85.65
B	8	7	15	18	66.05	1.60	67.4	72	1540	91.25
B	9	1	20	23	66.70	1.72	58.3	51	1547	84.19
B	9	1	66	69	67.16	1.42	77.1	116	1463	99.72
B	9	3	40	43	69.90	1.51	71.9	88	1589	99.66
B	9	4	81	84	71.81	1.51	73.5	93	1571	106.22
B	10	2	73	76	79.63	1.49	74.7	99		106.22
B	10	4	55	58	82.45	1.50	69.8	86	1603	109.38
B	11	4	83	86	91.33	1.43	75.9	110	2225	142.15
B	11	5	51	54	93.51	1.43	75.8	109	1236	104.86
B	12	3	44	47	100.34	1.52	73.2	91		61.02
B	12	6	51	54	104.91	1.47	74.2	100	1783	138.99
B	13	2	76	79	108.46	1.53	72.6	89	1590	120.68
B	13	5	76	79	112.96	1.58	68.7	76	1550	135.60
B	15	2	66	69	127.66		63.4			59.89
B	15	CC	3	6	129.83	1.52	81.5	112		90.40
B	16	1	92	95	131.02			78		72.32
B	16	3	22	25	133.32	1.51	74.7	96		140.69
B	17	2	84	87	140.34	1.44	75.9	108		90.40
B	17	6	86	89	146.36	1.53	74.8	94		169.50
B	18	5	71	74	154.51	1.47	73.8	98		200.01
B	19	5	43	46	164.13	1.50	73.8	95		159.33
B	19	6	85	88	165.20	1.47	73.8	99		152.55
B	20	5	90	93	174.30	1.45	76.2	109		203.40
B	20	7	47	51	176.87	1.42	79.1	122		159.33
B	21	2	67	70	179.27	1.41	78.4	122		178.54
B	21	5	118	121	184.28	1.42	75.9	111		186.45
B	22	2	84	87	189.04	1.39	78.3	125		133.34
B	22	7	21	25	195.91	1.54	80.1	106		118.65
B	23	4	97	100	201.47	1.40	75.7	114		160.46
B	23	7	25	28	205.17	1.33	78.3	136	1373	104.52
B	24	2	60	63	207.70	1.34	79.4	140	1329	
B	24	4	47	50	210.57	1.36	76.9	125	1537	
B	25	3	20	23	216.30	1.30	80.5	154	1590	
B	25	5	45	48	219.55	1.28	79.6	155	1598	
C	2	2	110	113	6.00	1.65	66.5	67	1504	15.48
C	2	2	130	133	6.20	1.92	49.1	35	1654	11.47
C	2	5	50	53	9.90	1.54	72.6	87	1491	20.90
C	3	3	99	102	17.19	1.78	57.5	48	1574	10.17
C	3	5	70	73	19.90	1.64	67.4	70	1548	30.96
C	4	2	71	74	25.31	1.75	60.8	53	1551	26.21
C	4	5	102	105	30.12	1.95	46.0	31	1663	33.56
C	5	2	110	113	35.50	1.84	55.7	44	1644	31.41
C	5	5	72	75	39.62	1.78	60.5	52	1573	50.28
C	6	2	50	53	42.95	1.78	60.1	51	1603	55.93
C	6	5	47	50	47.87	1.71	63.1	58	1535	79.10
C	7	3	67	70	54.57	1.72	63.0	57	1539	83.05
C	8	2	118	121	59.78	1.73	68.2	64		117.52
C	9	2	50	53	62.70	1.47	83.1	127		25.99
C	10	2	84	87	65.84	1.48	76.0	103		36.16
C	11	2	91	94	75.41	1.51	71.9	90	1298	63.28
C	12	1	60	63	83.10	1.53	71.6	86	1239	89.27

Table 27 (continued).

Hole	Core	Sec	Top (cm)	Bot (cm)	Depth (mbsf)	Bulk density (g/cm ³)	Porosity (%)	Water content (%)	Velocity (m/s)	Van shear strength (kPa)
C	12	5	40	43	88.90	1.48	73.6	97	1495	114.13
C	13	2	49	51	93.99	1.45	75.6	106	1267	136.73
C	14	2	43	47	103.43	1.46	75.4	105	1449	111.87
C	14	7	17	20	110.67	1.61	67.7	72	1392	108.48
C	15	1	63	65	111.63	1.57	67.9	76	1226	43.33
C	15	4	40	43	115.90	1.40	78.9	124	1339	110.74
C	16	2	49	52	122.49	1.52	73.1	91	1486	142.38
C	16	6	30	33	128.30	1.55	73.5	88	1456	153.68
C	17	5	130	133	136.12	1.45	75.2	105	1444	136.05
C	18	2	68	71	140.33	1.45	76.6	109	1339	156.17
C	18	4	75	78	144.75	1.48	74.8	100	1340	156.05
C	19	2	84	87	151.34	1.48	74.0	97	1252	127.12
C	19	5	102	105	154.67	1.51	73.3	93	1478	152.55
C	20	2	51	54	160.51	1.47	76.3	106	1480	
C	20	4	47	50	163.14	1.42	79.2	121	1331	
C	21	2	70	73	170.20	1.41	76.5	115	1515	
C	21	4	45	48	172.95	1.42	78.1	119	1518	
C	21	6	50	53	174.50	1.36	78.1	130		
C	22	3	65	68	181.15	1.37	78.8	130	1550	
C	23	5	38	40	190.68	1.36	79.7	135	1723	
C	24	2	53	56	194.43	1.35	77.8	131	1767	
C	24	5	43	46	198.83	1.38	76.6	120	1683	
D	1	2	33	35		1.46	74.6	102	1356	35.03
D	1	4	20	23		1.44	78.0	114		74.58
D	2	5	77	80	196.67	1.37	78.3	128	1340	57.63
D	3	2	28	31	199.93	1.32	79.5	144	1503	61.02
D	4	5	15	18	215.35	1.29	80.5	156	1630	93.79
D	5	6	32	35	226.62	1.28	83.0	172	1838	41.81
D	6	1	109	112	229.59	1.26	81.6	172	2229	45.20
D	6	6	12	15	236.12	1.30	80.9	158		72.89
D	7	1	45	48	238.55	1.33	79.9	143	1356	106.61
D	7	7	16	19	247.26	1.35	91.2	192	1442	65.54
D	8	4	47	50	252.77	1.33	80.3	145	2309	87.01
D	8	7	14	17	256.94	1.33	79.5	142		
D	9	2	74	77	259.74	1.34	78.8	138	1713	
D	9	7	9	12	266.59	1.37	80.2	136	1738	
D	10	2	17	19	268.77	1.32	78.6	141	1764	
D	10	4	20	23	270.45	1.37	78.4	130	1718	
D	10	7	23	26	276.33	1.37	77.9	126	1767	
D	11	2	98	100	279.28	1.90	49.9	36	2504	
D	11	2	113	116	279.43	1.80	61.3	52	1849	
D	12	2	25	28	288.15	1.62	66.8	70	1965	
D	12	4	80	83	291.70	1.58	70.9	80	1835	
D	12	6	27	30	294.17	1.66	64.2	63	1855	
D	12	6	127	130	295.17	1.62	69.5	74	1945	
D	13	2	122	125	297.57	1.55	71.9	85	1737	
D	13	5	47	50	302.67	1.68	62.0	58	1692	
D	14	3	60	63	309.28	1.63	68.1	71	1855	
D	16	1	6	8	315.96	2.64			4402	
D	17	1	57	59	317.97	1.75	81.9	86	1400	
D	18	1	27	30	321.87	1.80	61.2	52		
D	19	2	7	10	327.97	1.91	59.9	46		
D	19	2	87	90	328.00	1.81			2811	
D	19	2	121	125	328.90	1.86				

profiles. Undoubtedly the strongest reflector within the drilled sequence corresponds to the contact between basalt and overlying volcanics (see "Seismic Correlation" section). An impedance contrast of nearly $10^4 \text{ Mg} \times \text{m}^{-2} \times \text{s}^{-1}$ at 315 mbsf, offscale in Figure 59, is well constrained in the seismic record. Other contacts having distinct acoustic impedances are found at 67 mbsf (base of lithologic Unit I), 230, 255, and 277 mbsf. Tentative correlations with the seismic record are discussed in "Seismic Correlation" section.

Thermal Conductivity

Thermal conductivities measured at Site 642 are illustrated in Figure 56, along with index properties. The conductivities measured vary between 2 and $4 \times 10^{-3} \text{ cal} \times \text{°C}^{-1} \times \text{cm}^{-1} \times \text{s}^{-1}$ to 67 mbsf and show a well-defined gradient of decreasing conductivity from approximately 2.3 to $1.9 \times 10^{-3} \text{ cal} \times \text{°C}^{-1} \times \text{cm}^{-1} \times \text{s}^{-1}$ in lithologic Units II and III. Lithologic Unit IV

exhibits a slight increase relative to overlying sediments, reaching a high of $2.49 \times 10^{-3} \text{ cal} \times \text{°C}^{-1} \times \text{cm}^{-1} \times \text{s}^{-1}$ at 308 mbsf. Thermal conductivities were not measured in the indurated material underlying Unit IV.

The character of the thermal conductivity profile mimics that of water content. This relationship, well documented in previous research, confirms the trend seen in other index properties. The variation of sediment lithology in lithologic Unit I leads to a wide range of thermal conductivity in this same unit. Lithologic Subunit IIA has a nearly constant thermal conductivity of $2.4 \times 10^{-3} \text{ cal} \times \text{°C}^{-1} \times \text{cm}^{-1} \times \text{s}^{-1}$. A slight decrease marks lithologic Subunit IIB. In contrast, there is a quick increase in thermal conductivities in Subunit IIC. Subunit IIC has a high conductivity of $2.63 \times 10^{-3} \text{ cal} \times \text{°C}^{-1} \times \text{cm}^{-1} \times \text{s}^{-1}$ at 112 mbsf decreasing steadily into Unit III until reaching a low of $1.78 \times 10^{-3} \text{ cal} \times \text{°C}^{-1} \times \text{cm}^{-1} \times \text{s}^{-1}$ at 226 mbsf. The sediments from below 255 mbsf exhibit a gradual increase

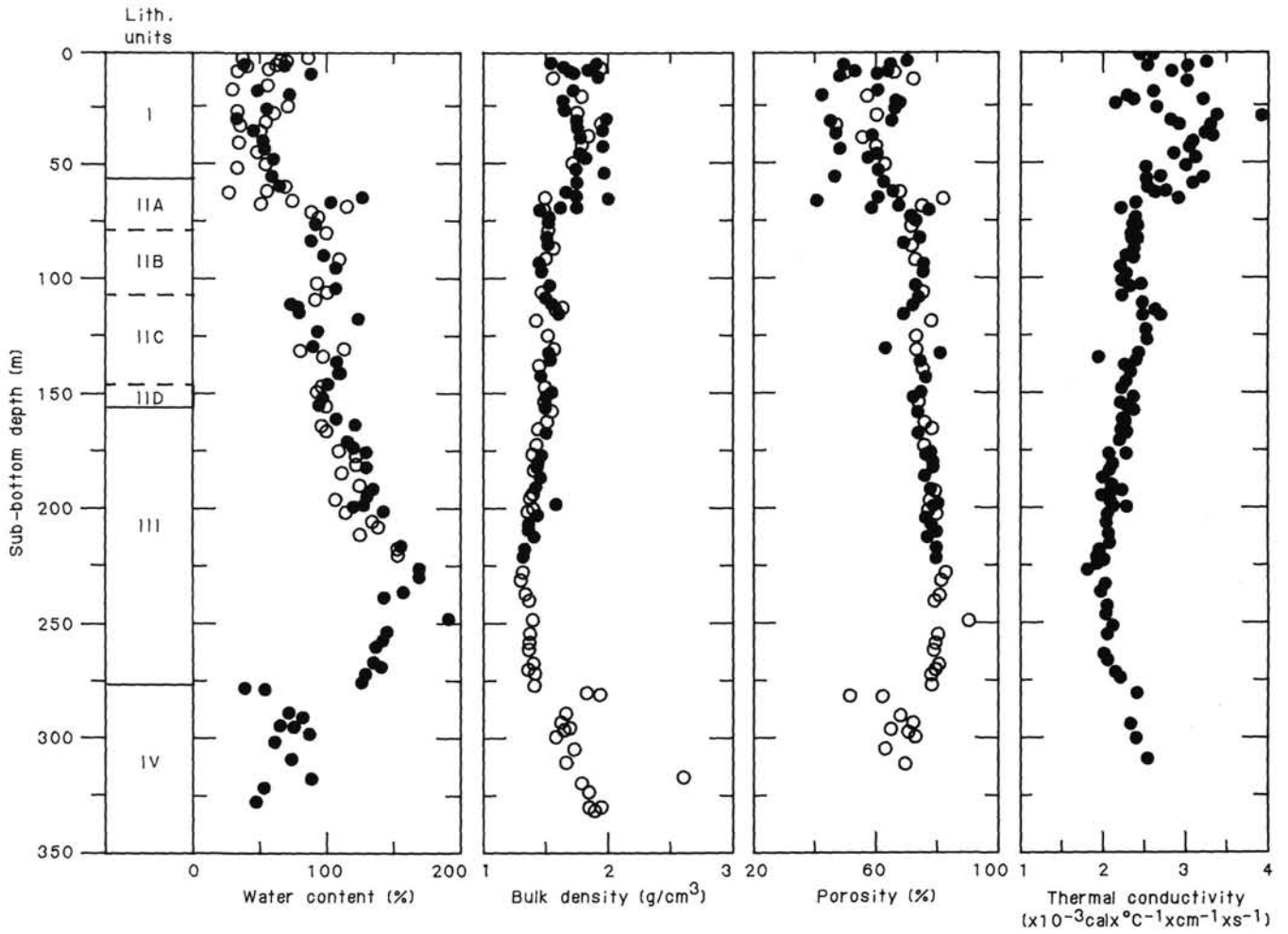


Figure 56. Water content, bulk density, porosity, and thermal conductivity profiles for Site 642 sediments.

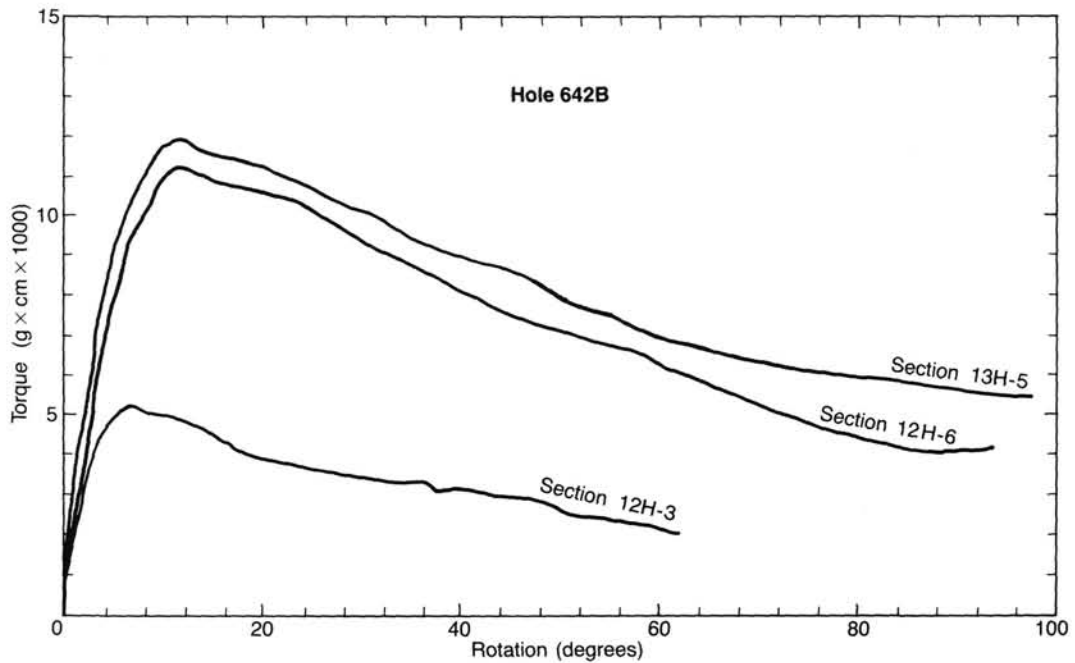


Figure 57. Typical torque vs. rotation plots of Site 642 sediments obtained from vane shear-strength measurements.

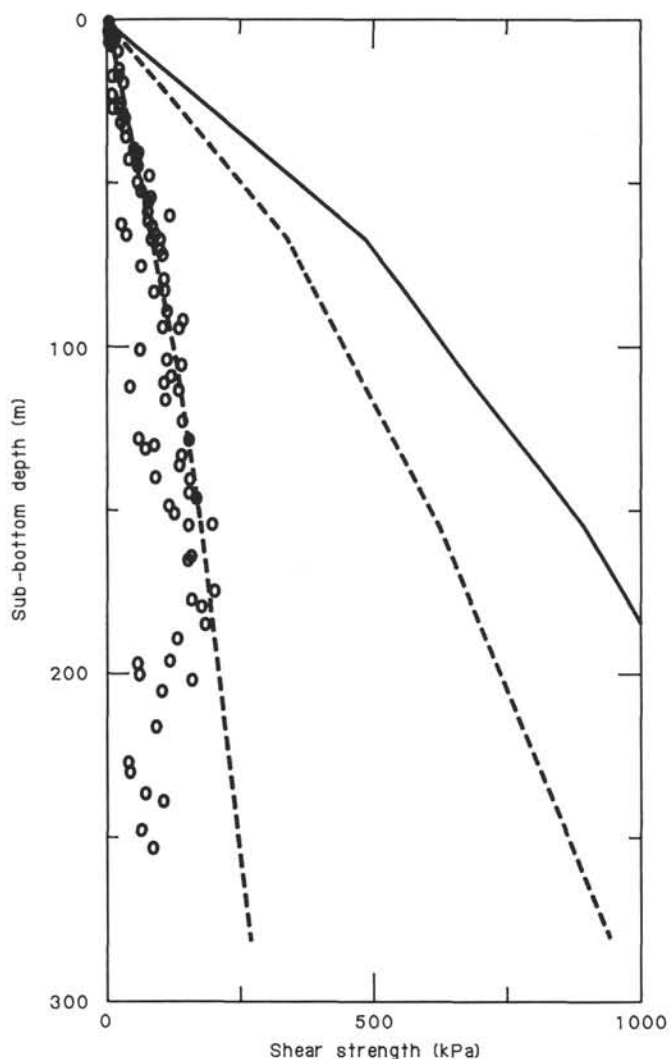


Figure 58. Shear strength (0) and computed effective overburden stress (solid line) profiles for Site 642 sediments. The area between the dashed lines corresponds to the range of estimated normal consolidation for marine sediments (Skempton, 1970).

in thermal conductivity extending into Unit IV for a maximum measured value of $2.52 \times 10^{-3} \text{ cal} \times \text{°C}^{-1} \times \text{cm}^{-1} \times \text{s}^{-1}$ at the base of the sedimentary section.

Heat-flow estimates were computed at Site 642 using information from both thermal conductivities and one downhole temperature measurement obtained at 50 mbsf and from resistivities measured during logging. Using the information from the temperature probe, namely the lowest values corresponding to the mud line and the decayed temperature after HPC punch-in, a gradient of approximately 0.08°C/m was calculated. Although this information is preliminary, the gradient corresponds closely to that deduced from logging (see "Logging Results" section).

Summary

The profiles illustrated in Figures 56, 58, and 59 clearly indicate a direct correlation between sediment type and the bulk and mechanical properties of sediments from ODP Site 642. The contrast between glacially influenced Pliocene-Pleistocene sediments and the more homogeneous and bioturbated Miocene sediments accounts for changes in both variability of different physical properties and their gradients.

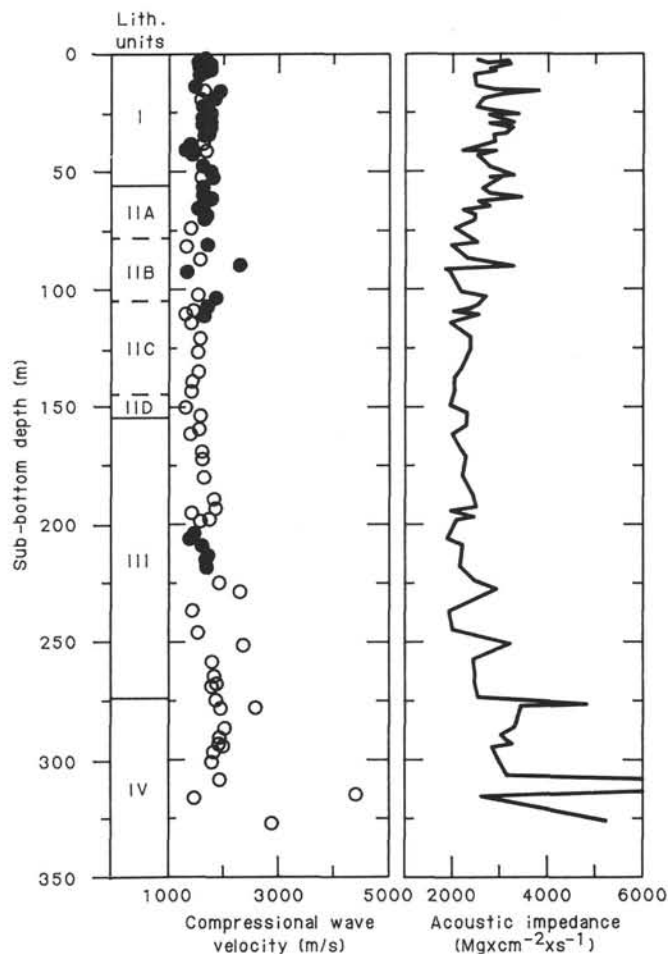


Figure 59. Profiles of acoustic impedance and compressional wave velocity for the sedimentary section at Site 642.

A review of physical properties for the upper 100 m of sediments shows the contrasting properties between dark glacial layers and other sediments of glacial/interglacial events. Similarly, the difference between the Quaternary-Pliocene sediments and underlying Miocene section is also apparent. Bulk densities measured on both discrete samples and the GRAPE record reflect the interbedded, dark-layer glacial events as high values, usually ranging between 1.8 to 2.1 g/cm^3 . The continuous GRAPE record thus provides an excellent pictorial of these events (Fig. 60). Similar responses are seen in the other index properties, as well as in thermal conductivities. Sediments from these glacial events have an average bulk density of 1.93 g/cm^3 and water content of 40%. Conversely, the remainder of the glacial/interglacials are typified by a bulk density of 1.74 g/cm^3 and a water content of 63%. The primary difference between these two sedimentary types consists of an increase of incorporated calcareous material during interglacials and an increase of coarser grained clastics during other periods within the glacials.

The increase of diatoms in sediments during the Miocene accounts for the dramatic shift in physical properties with depth. Hamilton (1976) documented the relatively slow change in porosity and bulk density with depth that distinguishes diatomaceous oozes from other sediment types. The abnormal decrease in bulk density and increase in porosity with depth within Unit III, however, points to an overriding effect of changing sediment composition compared to the expected mechanical response from overburden. A compositional source for the reverse downhole trend of index properties is the amount of disseminated ash and

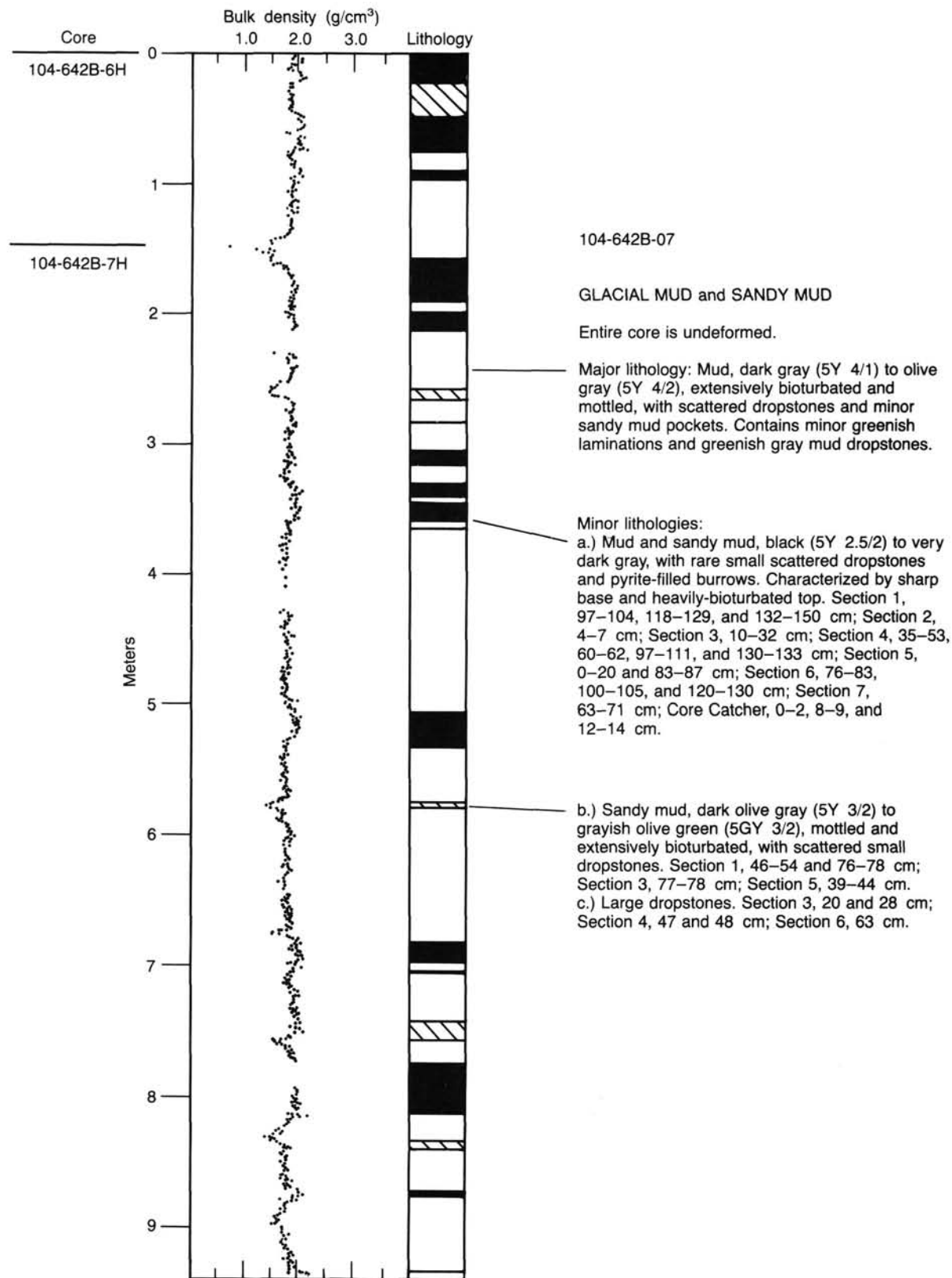


Figure 60. Continuous GRAPE records of glacial and interglacial sediments cored at Site 642. Values of bulk density in excess of 1.7 g/cm³ represent dark gray to black sandy muds probably deposited during glacial maxima.

smectite in the lower section. Lithologic descriptions of the lower Miocene section show increasingly greater quantities of ash as one approaches lithologic Unit IV (see "Sediment Lithology" section). The hydrophilic nature of smectites could account for both a greater amount of bound water and greater rebound characteristics resulting in anomalously low bulk densities.

The undrained shear-strength profile of the upper 100 m does not show the fluctuations of index properties profiles in response to the glacial and interglacial events (Figs. 56 and 59). The variability of index properties and lithology within the Quaternary sediments is dramatic; however, those factors producing changes in index properties apparently do not govern shear strength. A possible explanation for this may rest in the amount of sand found within the dark, glacial layers. Sand, although quite capable of forming a relatively dense layer, will often decrease the shear strength of a sandy clay matrix. The combined effect of density increase, burial, and possibly organic carbon in these dark, sandy layers can result in a monotonic increase of shear strength even when index properties fluctuate.

The hemipelagic sediments of Units I and II exhibit a normally consolidated history, reacting to the increasing weight of overlying sediments (Fig. 58). Sediments from Unit III are clearly underconsolidated using the criteria discussed by Skempton (1970). Bryant et al. (1981) described shear strengths of different marine sediments and indicated that shear strengths in diatomaceous oozes seldom exceeded 150 kPa. Owing to this distinct behavior, the Skempton criteria may need to be revised for sediments of contrasting composition. Despite their different behavior, the sediments from Unit III are still considered underconsolidated, perhaps as a result of diagenetic processes acting in the smectite and ash fractions.

The lower Miocene-Eocene unconformity at 280 mbsf marks the transition from nearly 200 m of a relatively homogeneous sequence to sediments of the early Norwegian Sea. Glauconitic sands, ashes, and weathered sediments cap a basalt flow found at 315 mbsf. The physical properties across this interval show penetration into less-weathered material, with higher densities, velocities, acoustic impedance, and thermal conductivities.

Volcanic Section

Coring at ODP Hole 642E penetrated over 900 m of two series of volcanic rocks, of which the upper series forms the dipping reflectors observed on seismic records across the outer Vøring Plateau. Physical properties analyzed on samples from this sequence consisted of 2-min. GRAPE (bulk density) and compressional-wave velocity. Results of these analyses are listed in Table 28.

Bulk Density

The volcanic section penetrated at Site 642 can be divided into two distinct intervals, above and below 1089 mbsf, on the basis of density (Fig. 61). Above 1089 mbsf, bulk density tends to vary widely over short intervals. Values range from 1.76 to 3.08 g/cm³; however, an average value of 2.66 g/cm³ is nearly constant throughout the upper interval. Below 1089 mbsf there is an abrupt decrease in average density to 2.44 g/cm³ and a somewhat narrower range of values, 2.02 to 2.94 g/cm³.

Compressional-Wave Velocity

Compressional-wave velocity is a clearly defined function of density in the hard rock section at Site 642 (Fig. 62). Changes in velocity closely track, and are roughly proportional to, density variations (Fig. 61). A distinct shift in average vertical velocity occurs at 1089 mbsf, decreasing from 4685 m/s above this depth to 4118 m/s below. These average velocities are higher than those estimated from VSP and multichannel seismic analyses

and are probably an artifact of preferred recovery and sampling of structurally intact rock.

Velocities in the two horizontal directions (Vel B and Vel C, Table 28) are generally comparable to vertical velocity (Vel A). Calculated velocity anisotropies (see "Explanatory Notes") of up to 30% were obtained in different lithologies; however, most lithologies exhibit anisotropies ranging between -10% to 10%. As opposed to typical anisotropies measured in sediments, the material at Hole 642E had both positive and negative values for velocity anisotropy (Fig. 63). No correlation was found between the number or the magnitude of anisotropies with changes in depth, bulk density, or velocity. A preliminary review of these measurements reveals the largest anisotropies are associated with fine-grained, vesicular, or streaky basalt.

Acoustic Impedance

The acoustic impedance curve (Fig. 61, computed from bulk density and Vel A, Table 28) reflects the changes in both density and velocity. The amount of impedance contrast varies widely throughout the hard-rock section with the larger contrasts occurring below the interval around 1089 mbsf. These strong acoustic impedance contrasts are probably associated with the high-amplitude seismic reflectors near the base of the dipping reflector sequence (see "Seismic Correlation" section). The largest impedance contrast is at 1089 mbsf, where abrupt shifts in average density and velocity occur (Fig. 61). This event, perhaps enhanced by the second large contrast around 1170 mbsf, is believed to correspond to seismic reflector K. Other large impedance contrasts also occur at 450 and 680 mbsf, corresponding to contacts between volcanic tuffs and fine-grained basalt.

The average impedance in the hard-rock section (12631 Mg × m⁻² × s⁻¹) is much higher than in the overlying sedimentary section, which averages 2622 Mg × m⁻² × s⁻¹, and accounts for the high-amplitude reflector near the base of the sediments.

Relationship of Physical Properties to Lithologic Units

The highest values of density and velocity are associated most often with fine-grained, streaky, aphyric basalt. The lowest values occur in brown tuffs and scoria.

Compressional-wave velocities in some intervals of the section suggest repeated sequences of increasing velocity with depth. These sequences extend across several flows. Detailed future analyses may establish a correlation between these patterns and flow boundaries or flow-sequence boundaries. Gebhard and Carlson (1983) found that compressional-wave velocity in basalt from the Rio Grande Rise (Site 516F, DSDP Leg 72) increases with depth below the flow surface due to a progressive decrease in the degree of alteration. A correlation between sequences of increasing velocity with depth and flow boundaries would suggest a similar cause in the Site 642 basalt. Chemical alteration does occur in some intervals of the Site 642 basalt ("Basement Lithology" section). A correlation between velocity sequences and sequences of basalt flows may reflect compositional/alteration changes between and within flows.

LOGGING RESULTS

Background

The geophysical logs run at Site 642 were selected to augment laboratory measurements, to support other experiments planned at the site and to provide engineering data. Two holes were logged at this site; two suites of logs were recorded in Hole 642D which penetrated the upper sedimentary section, and three runs were made in Hole 642E which traversed the upper volcanic series.

The compensated neutron porosity tool was used because it samples a larger formation volume than that possible from cor-

Table 28. Summary of physical-properties data obtained from the volcanic sequence at ODP Hole 642E.

Depth (mbsf)	Core	Section	Bulk density (g/cm ³)	Vel A	Vel B	Vel C	Acoustic impedance (Mg × m ⁻² × s ⁻¹)	Average velocity	Anisotropy
355.27	7	1	2.06		3312				
356.43	7	2	2.09		3072				
367.05	9	1	2.87		5492				
374.50	10	1		5717	5603	5651		5657	1.590949
374.54	10	1	2.89			4960			
375.25	10	2	2.86			5160			
377.40	10	3		5104	5104	5131		5113	-0.264033
385.25	11	2	3.08			8721			
389.29	12	1	1.97			2552			
395.74	13	1	2.82	4420	4472	4863	12464.40	4595	-5.398037
400.17	14	1	2.74			4853			
401.09	14	1	2.51			3988			
406.94	15	2	2.69			4746			
407.54	15	2	2.43			4388			
408.15	15	2	2.84			4625			
408.95	15	3	2.81	4779	4695	4655	13429.99	4709	2.208224
410.80	15	4	2.42			4668			
412.56	15	5	2.73	4764	4806	4323	13005.72	4631	4.307925
415.12	16	1	2.79			4655			
416.54	16	2	2.65	3996	4439	4351	10589.40	4262	-3.361802
418.71	16	3	2.75	4781	5046	4230	13147.75	4995	-3.213482
425.36	17	1	2.75	4293	5010	5000	13455.75	4967	-2.254580
426.87	17	2	2.82	5144	5028	4687	14506.08	4953	5.784373
428.00	17	3	2.90	5880	5865	5330	17052.00	5691	4.963397
433.10	18	1	2.93	6068	5264	5425	17779.24	5585	12.952796
437.57	18	4	2.95	6043	5967	6159	17826.85	8056	-0.330233
439.25	18	5	2.80	5255	5255	4820	14714.00	5110	4.256360
442.52	19	1	2.87	5107			14657.09		
446.69	19	4	2.87	5431			15586.97		
448.44	19	5	2.12	2225			4717.00		
451.89	20	1	2.49	3508	3616	3506	8734.92	3543	-1.495767
453.94	20	2	2.57	3962	4122		10182.34		
455.24	20	3	2.65	3725			9871.25		
461.20	21	1	2.09	1542	2029		3222.78		
463.38	21	2	2.71	3772			10222.12		
464.50	21	3	2.50	3932	4313	4315	9630.00	4187	-9.157844
465.06	21	3	2.50	4779			11947.50		
466.08	21	4	2.66	4472	4525		11895.52		
468.09	21	5	2.62	4301	4520		11268.62		
470.00	22	1	2.72	4530			12321.60		
472.08	22	2	2.69	4433			11924.77		
473.93	22	3	2.77	5331			14799.87		
477.29	22	5	2.84	5267	5573	5089	14958.28	5309	-1.205349
478.77	22	6	2.65	4295	3319	4431	11381.75	4015	10.460772
480.96	23	1	1.91	1901	3465	3518	3630.91	2961	-53.708915
483.34	23	3	2.53	4069	4071	3722	10294.57	3954	4.362671
490.26	24	1	2.37	3416	4759	4825	8095.92	4333	-31.753846
491.46	24	2	2.77	4613	4759	3722	12778.01	4364	8.534443
497.04	25	3	2.80	4518	3964	4542	12650.40	4341	6.104115
498.26	25	4	2.44	2902	2835	2867	7080.88	2868	1.778243
502.60	26	1	2.86	5471	4667	4826	15647.06	4988	14.524860
504.86	26	3	2.62	4282	4225	4461	11129.76	4311	-2.203495
508.71	26	5	2.93	5776	5979	6052	16923.68	5935	-4.034930
513.10	27	2	2.42	3852			9321.84		
513.87	27	3	2.51	3873	3429		9721.23		
517.31	28	5	2.72	4129	5209	4533	11230.88	4623	-16.047870
525.48	28	4	2.30	2156			4958.80		
525.79	28	5	2.71	4225	3654	3863	11449.75	3914	11.918753
531.08	29	1	2.22	3596	3596	3634	7983.12	3608	-0.526510
532.33	29	2	2.73	4390	4659	4318	11984.70	4455	-2.210668
540.01	30	1	2.78	5075	5091	5001	14108.50	5055	0.573614
543.39	30	3	2.87	5698	5833	4820	16353.26	5450	6.816097
544.62	30	4	2.90	5657	5671	5581	16405.30	5636	0.550003
547.75	30	6	2.55	3982	4123	4000	10154.10	4035	-1.970260
549.90	31	1	2.60	3619	3959	3294	9403.40	3624	-0.206954
554.45	31	4	2.79	4228	4822	5195	11796.12	4748	-16.437346
560.47	32	2	2.93	5280	4982	5369	15470.40	5210	2.005630
562.35	32	3	2.95	5670	5684	4643	16726.50	5332	9.498656
565.84	32	1	2.94	5429	5507	5355	15961.26	5430	-0.036830
565.84	33	1	2.88	5714	5646	5592	16456.32	5650	1.681218
566.94	33	2	2.81	4761	4591	4955	13378.41	4769	-0.251625
567.32	33	2	2.59	4822	4756	5106	12486.98	4894	-2.226914
569.33	33	3	2.78	5338	5227	4852	14839.64	5139	5.808523
570.12	33	4	2.85	5501	5338	5473	15677.85	5437	1.756376
571.19	33	5	2.88	5634	5541	5450	16225.92	5541	2.499248
572.13	33	5	2.79	4917	5165	4991	13718.43	5024	-3.204405

Table 28 (continued).

Depth (mbsf)	Core	Section	Bulk density (g/cm ³)	Vel A	Vel B	Vel C	Acoustic impedance (Mg × m ⁻² × s ⁻¹)	Average velocity	Anisotropy
574.44	34	1	2.11	3110	3174	2992	6562.10	3092	0.873221
575.18	34	1	2.75	4701	4886	4822	12927.75	4803	-3.185509
595.82	35	2	2.82	5199	5175	4908	14661.18	5094	3.091873
586.67	35	2	2.40	4182	4148	3963	10036.80	4097	3.087123
587.53	35	3	2.72	5402	5404	5326	14693.44	5377	0.688073
589.32	35	4	2.69	4317	4594	4509	11612.73	4473	-5.242176
593.67	36	1	2.08	4433	4400	5006	9220.64	4613	-5.853024
603.00	37	1	2.73	5697	5671	5669	15552.81	5679	0.475436
612.80	38	1		5744	5702	5347		5597	3.921277
615.90	38	3	2.80	5547	5672	5053	15531.60	5424	3.401549
617.50	39	4	2.59	4193	4276	4378	10859.87	4282	-3.129135
631.90	40	1	2.79	5297	5187	5220	14778.63	5234	1.786169
633.30	40	2	2.67	4517	4373	4486	12060.39	4458	1.962470
634.50	40	3	2.55	4718	4432	4552	12030.90	4567	4.948183
641.10	41	1	2.74	5236	5239	5066	14346.64	5180	1.611865
641.80	41	1	2.41	3643	3470	3386	8779.63	3499	6.143442
642.80	41	2	2.46	3875	3968	3936	9532.50	3926	-1.961117
643.70	41	3	2.71	4678	5054	4783	12677.38	4838	-4.970720
644.90	41	3	2.63	4388	4371	4032	11540.44	4263	4.374169
650.65	42	1	2.14	2413	2283	2468	5163.82	2388	1.570352
652.34	42	2	2.77	5039	5013	4174	13958.03	4742	9.394770
653.16	42	3	2.73	5094	4626	3671	13906.62	4463	21.182137
679.63	45	1	1.91	2296	2320	2356	4385.36	2324	-1.807229
680.85	45	2	2.51	5653	5775	5229	14189.03	5552	2.719577
682.32	45	3	2.67	6059	5870	5359	16177.53	5762	7.713443
684.24	45	5	2.91	6497	5809	5880	18906.27	6062	10.763774
688.73	46	1	2.92	6330	6053	6389	18483.60	6257	1.741956
690.96	46	2	2.95	5680	6256	5654	16756.00	5863	-4.690165
692.39	46	3	2.78	4133	4552	4921	11489.74	4535	-13.306629
692.83	46	4	2.54	3842	3369	3497	9758.68	3569	11.458722
697.68	47	1	2.57	4549	4568	4617	11690.93	4578	-0.950197
698.66	47	1	2.65	4604	4029	4379	12200.60	4337	9.222256
717.40	50	1	2.87	5235	5305	5077	15024.45	5205	0.845233
718.18	50	2	2.45	3786	3677	3710	9275.70	3724	2.483666
718.59	50	2	2.57	4031	3662	3767	10359.67	3820	8.285340
723.39	51	1	2.75	4589	4558	4539	12619.75	4562	0.887769
729.44	53	1	2.43	3946	4019	3420	9588.78	3795	5.968379
730.39	53	1	2.54	4319	4318	4026	10970.26	4221	3.482587
731.74	53	2	2.76	5305	5276	5321	14641.80	5300	0.122626
738.87	54	1	2.87	5976	6022	5430	17151.12	5809	4.303420
740.62	54	2	2.51	4234	4155	3994	10627.34	4127	3.864169
740.93	54	2	2.36	3255	3145	2731	7881.80	3043	10.415070
742.78	54	3	2.88	5588	5503	5599	16093.44	5563	0.665069
743.37	54	4	2.77	5720	5794	5439	15844.40	5651	1.831534
758.28	56	1	2.54	4244	3930	4259	10779.76	4144	3.607335
759.38	57	1	2.60	4439	4135	3937	11541.40	4170	9.663496
761.16	57	2	2.45	3667	3617	3709	8984.15	3664	0.109160
763.19	57	3	2.54	3801	3777	3633	9654.54	3737	2.568906
764.29	57	4	2.77	5044	4497	4965	13971.88	4835	6.473184
766.47	58	1	2.74	5057	4937	4763	13856.18	4889	5.154428
768.63	58	2	2.69	4975	4937	4783	13382.75	4898	2.347737
769.92	59	3	2.77	5163	4949	5257	14301.51	5123	1.171189
771.45	58	4	2.78	5574	5639	5627	15495.72	5613	-1.051069
771.95	58	4	2.78	5172	5164	5261	14378.16	5199	-0.778996
772.24	58	5	2.86	5602	5607	5636	16021.72	5615	-0.347284
773.06	58	5	2.68	4851	4792	4483	13000.68	4708	4.534192
776.53	59	1	2.50	3854	3780	3739	9635.00	3791	2.492746
777.70	59	2	2.74	5099	5036	5048	13971.26	5061	1.126260
779.85	59	3	2.82	5535	5548	5559	15608.70	5547	-0.333494
785.11	60	1	2.26	5010	4847	4841	11322.60	4899	3.388216
785.92	60	1	2.56	3935	3922	3933	10073.60	3930	0.190840
787.52	60	2	2.87	5614	5634	5523	16112.18	5590	0.635025
794.99	61	1	2.64	4052	4103	4152	10697.28	4102	-1.840416
795.67	61	1	2.57	4111	4236	4220	10565.27	4189	-2.793029
797.01	61	2	2.58	3974	4103	3992	10252.92	4023	-1.825995
803.84	62	1	1.76	3961	4132	3752	6971.36	3948	0.481216
804.95	62	1	2.72	3980	4313	4177	10825.60	4156	-6.375301
809.95	63	1	2.54	3721	3375	3419	9451.34	3505	9.243937
812.33	63	2	2.82	3829	5577	5647	10797.78	5017	-35.534445
813.06	63	3	2.92	5049	5728	5678	14743.08	5485	-11.923428
814.34	63	4	2.94	5942	5826	5379	17469.48	5715	5.939815
816.39	64	1	2.81	6263	6317	6253	17599.03	6277	-0.350449
817.77	64	2	2.94	5960	6395	6161	17522.40	6172	-5.152301
820.04	64	3	2.78	5991	6161	5189	16654.99	5780	5.466813
820.49	64	4	2.46	4147	4155	4071	10201.62	4124	0.824376
822.63	64	5	2.37	3748	3705	3603	8882.76	3685	2.550651
825.47	65	1	2.54	6032	4268	4387	15321.28	4895	34.816504

Table 28 (continued).

Depth (mbsf)	Core	Section	Bulk density (g/cm ³)	Vel A	Vel B	Vel C	Acoustic impedance (Mg × m ⁻² × s ⁻¹)	Average velocity	Anisotropy
834.80	66	1	2.68	4123	4029	4105	11049.64	4085	1.370645
836.39	66	2	2.71	5229	5292	4383	14170.59	4968	7.880435
838.47	66	3	2.80	5044	5052	4842	14123.20	4979	1.948052
839.67	66	4	2.76	5409	5476	4040	15037.02	4975	13.085427
845.42	67	1	2.31	3784	3888	3755	8741.04	3809	-0.984510
846.22	67	2	2.75	4509	4604	4478	12399.75	4530	-0.706350
846.93	67	2	2.67	4658	4704	4644	12436.86	4668	-0.342710
854.08	68	1	2.59	3865	4025	3913	10010.35	3934	-2.643395
854.91	68	1	2.63	4199	4205	4077	11043.37	4160	1.394119
856.50	68	2	2.57	4442	4697	4603	11415.94	4580	-4.540824
863.38	69	1	2.68	4565	4656	4632	12234.20	4617	-1.710821
864.07	69	1	2.85	5451	5466	5270	15535.35	5395	1.538271
865.17	69	2	2.78	4868	4942	5162	13533.04	4990	-3.686882
867.28	69	3	2.89	5708	6849	5746	16496.12	6101	-9.6623250
873.50	70	1	2.42	3272	3479	3466	7918.24	3405	-5.887247
874.55	70	2	2.74	4831	4856	4831	13236.94	4839	-0.258300
882.30	71	2	2.64	3879	4456	4240	10240.56	4191	-11.188867
884.95	71	3	2.85	5532	5527	5264	15766.20	5441	2.508730
886.02	71	4	2.83	5444	5278	5371	15406.52	5364	2.22767
891.21	72	1	2.06	3015	2839	2635	6210.90	2829	9.824479
892.49	72	2	2.55	3742	4216	3275	9542.10	3744	-0.093475
896.53	73	1	2.65	4140	4383	4156	10971.00	4226	-3.064122
898.83	73	2	2.92	5672	5736	5216	16562.24	5541	3.537055
900.11	73	3	2.83	5322	5392	5195	15061.26	5303	0.537432
900.24	73	3	2.91	5501	5511	4350	16007.91	5120	11.141127
902.05	73	4	2.90	5966	5948	5986	17301.40	5966	-0.016760
904.99	74	2	2.89	5796	6129	5917	16750.44	5947	-3.816837
907.14	74	4	2.89	5954	6012	5880	17207.06	5948	0.134484
910.40	74	6	2.79	5184	5005	5305	14463.36	5164	0.561508
912.45	75	1	2.54	4090	4065	4332	10388.60	4162	-2.606711
913.92	75	2	2.47	3955	3994	3940	9766.85	3963	-0.302801
914.57	75	2	2.74	4694	4868	4719	12861.56	4760	-2.090190
922.15	76	1	2.51	4196	4365	4301	10531.96	4287	-3.195459
923.98	76	2	2.61	4296	4371	4234	11212.56	4300	-0.151151
931.49	77	1	2.61	3691	3975	3804	9633.51	3823	-5.191805
933.11	77	2	2.65	4119	4247	4148	10915.35	4171	-1.881892
935.35	77	3	2.84	5393	5421	5200	15316.12	5338	1.545523
941.43	78	1	2.53	3191	3537	3936	8073.23	3554	-15.346024
942.69	78	2	2.75	4893	4510	4270	13445.75	4557	11.036349
950.82	79	1	2.61	4184	4432	3594	10920.24	4070	4.201474
951.15	79	1	2.31	3664	4075	3998	8463.84	3912	-9.521172
952.18	79	2	2.56	4086	3907	4043	10460.16	4012	2.766700
959.53	80	1	2.79	5609	5713	5553	15649.11	5625	-0.426667
961.39	80	2	2.48	3888	3978	3843	9642.24	3903	-0.576480
968.91	81	1	2.84	5558	5458	5768	15784.72	5594	-0.983079
970.99	81	2	2.76	5518	5580	5328	15229.68	5475	1.168879
978.06	82	1	2.70	4621	4517	4564	12476.70	4567	1.762516
978.47	82	1	2.70	4875	4276	4722	13162.50	4624	8.130902
987.92	83	1	2.47	3541	3969	3711	8746.27	3740	-7.993940
989.67	83	2	2.75	4683	4975	4401	12878.25	4686	-0.106693
997.20	84	1	2.77	5192	5219	5245	14381.84	5218	-0.766479
1007.10	85	1	2.87	5903	5786	5847	16941.61	5845	1.479813
1009.50	85	3	2.92	5960	5960	5929	17403.20	5949	0.260519
1011.80	85	4	2.91	5900	6050	5887	17169.00	5945	-1.152100
1012.50	85	5	2.82	5259	5305	5378	14830.38	5314	-1.552503
1013.50	85	5	2.33	2337	3322	3214	5445.21	2957	-31.477516
1014.20	85	6	2.62	3802	4110	3965	9961.24	3959	-5.948472
1016.50	86	1	2.83	5363	5483	5303	15177.29	5383	-0.557310
1017.80	86	2	2.58	3829	4327	4143	9878.82	4099	-9.903244
1018.70	86	2	2.73	3757	4353	4298	10256.61	4136	-13.745164
1019.60	86	3	2.57	3544	3721	3677	9108.08	3647	-4.249880
1025.80	87	1	2.52	4324	4384	4380	10896.48	4362	-1.329462
1026.60	87	1	2.47	4223	4147	4297	10430.81	4222	0.023684
1027.40	87	2	2.83	5351	5304	5312	15143.33	5322	0.807916
1035.50	88	1	2.60	4029	3709	3895	10475.40	3877	5.854036
1036.60	88	2	2.91	4970	4471	4742	14462.70	4727	7.688782
1044.80	89	1	2.48	3753	3746	3519	9307.44	3672	3.280995
1045.89	89	2	2.60	3949	3976	4087	10267.40	4004	-2.060440
1054.63	90	1	2.76	5003	4990	4912	13808.28	4968	1.046629
1055.30	90	2	2.93	6078	6062	5984	17808.54	6041	0.910395
1057.72	90	3	2.87	6062	5804	5788	17397.94	5884	4.520222
1063.92	91	1	2.35	2705	2365	3171	6356.75	2747	-2.293411
1065.20	91	2	2.71	4675	4803	4955	12669.25	4811	-4.240283
1066.41	91	3	2.75	4675	4803	4955	12856.25	4811	-4.240283
1073.10	92	1	2.43	5313	5313	4717	12910.59	5114	5.826761
1075.60	92	2	2.82	5704	5675	5468	16085.28	5615	2.359471
1079.90	93	1	2.77	5321	5283	5051	14739.17	5218	2.951134

Table 28 (continued).

Depth (mbsf)	Core	Section	Bulk density (g/cm ³)	Vel A	Vel B	Vel C	Acoustic impedance (Mg × m ⁻² × s ⁻¹)	Average velocity	Anisotropy
1082.00	93	3	2.90	6364	6413	6299	18455.60	6358	0.125813
1084.50	93	4	2.93	6271	6483	6304	18374.03	6352	-1.928324
1085.10	93	6	2.94	6364	6498	6356	18710.16	6406	-0.983453
1086.90	94	2	2.92	6492	6561	6391	18956.64	6481	0.246863
1089.00	94	3	2.43	3645	3639	3529	8857.35	3604	1.692407
1089.30	94	3	2.47	2335	2630	2655	5767.45	2540	-12.106299
1091.30	94	5	2.25	2145	2291	2307	4826.25	2247	-6.851550
1102.40	95	1	2.15	2066	2226	2404	4441.90	2232	-11.155914
1103.90	95	2	2.15	2565	2721	2620	5514.75	2635	-4.003289
1109.90	97	1	2.34	3863	3895	2936	9039.42	3564	12.553768
1111.50	97	2	2.17	2936	3281	2955	6371.12	3057	-5.952900
1116.90	98	1	2.18	3217	3323	3114	7013.08	3218	-0.046613
1119.00	98	3	2.47	5479	5471	4996	13533.13	5282	5.594472
1126.90	99	2	2.20	3457	3351	3278	7605.40	3362	4.238548
1128.40	99	3	2.35	3845	3846	3874	9035.75	3855	-0.389105
1135.50	100	1	2.12	3006	2898	2849	6372.72	2917	4.541300
1136.70	100	2	2.51	4078	5172	4862	10235.78	4704	-19.961735
1144.50	101	1	2.49	4924	4875	4607	12260.76	4802	3.810912
1146.60	101	2	2.48	4240	4479	4419	10515.20	4379	-4.772416
1154.60	102	1	2.36	3152	3376	3130	7438.72	3219	-3.137296
1155.30	102	2	2.04	3440	3260	3407	7017.60	3369	3.161175
1156.90	102	3	2.83	5683	5365	5593	16082.89	5547	3.677664
1163.10	103	1	2.92	5942	5916	6030	17350.64	5929	0.320441
1165.20	103	2	2.86	5972	5833	5137	17079.92	5647	8.623539
1166.80	104	1	2.90	6128	6253	6108	17771.20	6163	-0.851858
1169.80	104	3	2.94	6389	6365	6401	18783.66	6385	0.093970
1173.30	105	1	2.93	6423	6413	6293	18819.39	6376	1.097810
1175.10	105	2	2.88	5880	5880	5804	16934.40	5854	0.649055
1177.20	105	4	2.94	6220	6277	6292	18286.80	6263	-1.029858
1178.40	105	4	2.37	3530	3647	3581	8366.10	3586	-2.342443
1182.40	106	1	2.26	3960	4399	3997	8949.60	4112	-5.544747
1191.40	107	1	2.20	2783	2933	2489	6122.60	2735	2.632541
1193.02	107	2	2.46	3557	3976	4077	8750.22	3870	-12.131783
1195.46	107	3	2.18	3323	3666	3590	7244.14	3526	-8.649211
1196.39	107	4	2.02	2794	3167	2765	5643.88	2908	-5.913362
1201.26	108	1	2.37	3185	3707	3735	7548.45	3542	-15.131269
1202.40	108	2	2.29	3389	3670	3270	7760.81	3443	-2.352599
1211.09	109	1	2.45	3472	4050	3520	8506.40	3680	-8.503894
1212.51	109	2	2.46	3737	3910	3895	9193.02	3847	-4.301681
1220.36	110	1	2.48	4541	4622	4798	11261.68	4653	-3.631545

Note: Vel A: compressional wave velocity measured parallel to the core (m/s); Vel B and Vel C: compressional wave velocity measured in mutually perpendicular directions and perpendicular to core penetration (m/s); average velocity from Vel A, B, C (m/s); Anisotropy: vertical compressional wave anisotropy (%).

ing and it perhaps gives better porosity values because porosity changes caused by the coring operation are eliminated. The lithodensity tool was run for similar reasons. A spectral resolution of the natural radiation from the potassium, uranium, and thorium decay series was recorded with the natural gamma-ray spectroscopy tool (NGT) and the data aided in the identification of clay zones. The natural radiation log provided depth markers used to tie the logging runs together. Together the radiation tools gave an indication of the location of some of the ash layers encountered in the sedimentary section of Hole 642D, and were very successful at locating the depth of sedimentary layers in the volcanic section of Hole 642E. The dual induction tool measured the formation resistivity, which provided a check on the porosity log by interrogating the formation for large-scale inhomogeneities well removed (5 m) from the borehole. Another focused electric tool measured resistivities near the borehole. The long spacing sonic (LSS) tool was run to measure the sonic velocity of the sediments and volcanics in support of the vertical seismic profiling experiment. Unfortunately, in the upper sedimentary section, this log was largely unsuccessful because of the very low velocity characteristics of the formation. The sonic logging run in the lower hard-rock section, however, provided an excellent velocity profile of the basalt flows. The caliper tool was run to record borehole diameter. The acoustic borehole televiewer was run in Hole 642E.

All depths referenced were measured by the movement of the logging cable. All data recorded in Holes 642D and 642E are presented as figures at the end of this chapter. Logs can be obtained at a scale of 1:500 from the Lamont-Doherty Geological Observatory, Borehole Research Group, Palisades, New York, 10964.

Hole 642D

Sedimentary Section

Two logging suites were run in Hole 642D of the ODP Leg 104 program. The tools run in each suite and the quality of the resulting logs are summarized below.

Run no.	Log name	Sub-bottom depth interval (m)	Quality
1	Long-spaced sonic	30.9–207.9	Poor
1	Dual induction	33.0–198.0	Good
1	Natural gamma ray	30.9–207.9	Good
1	Caliper	30.9–207.9	Failed
2	Natural gamma-ray spectrometry	33.0–208.0	Good
2	Lithodensity	33.0–208.0	Good
2	Compensated neutron	40.0–203.0	Good

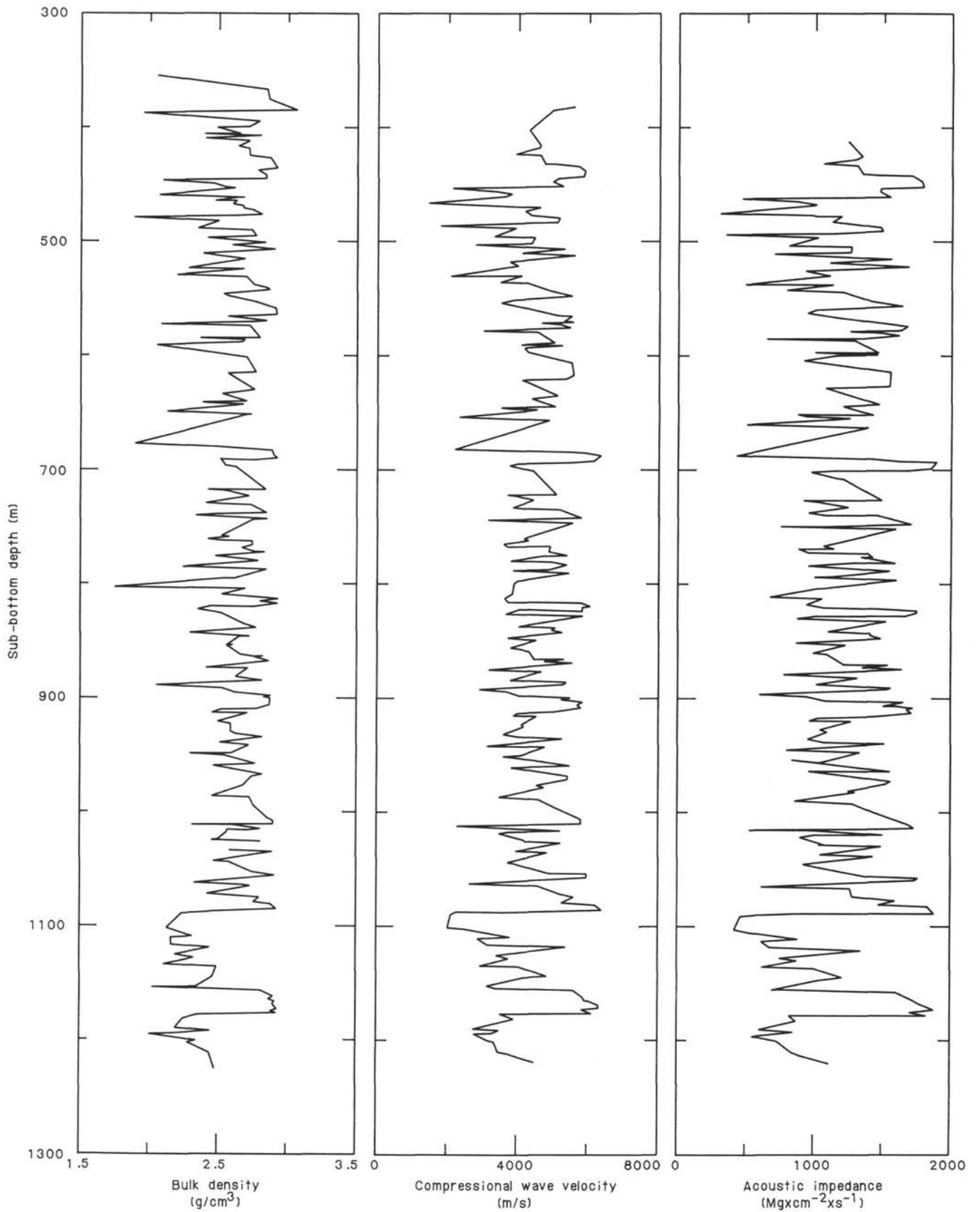


Figure 61. Profiles of bulk density, compressional wave velocity, and acoustic impedance from the volcanic sequence cored at Hole 642E.

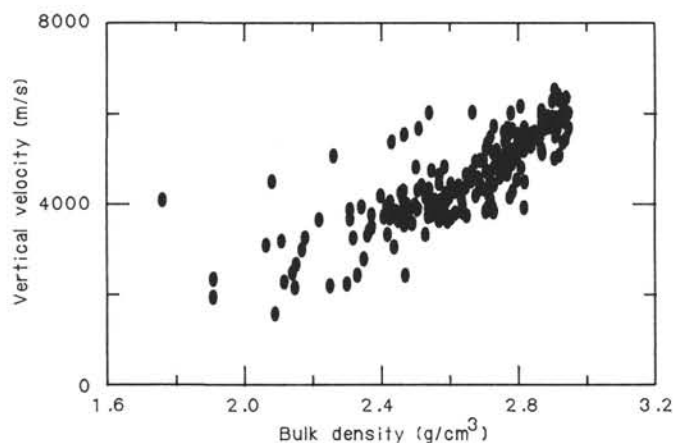


Figure 62. Compressional wave velocity–bulk density crossplots obtained from shipboard-laboratory measurements of the volcanic sequence at ODP Site 642.

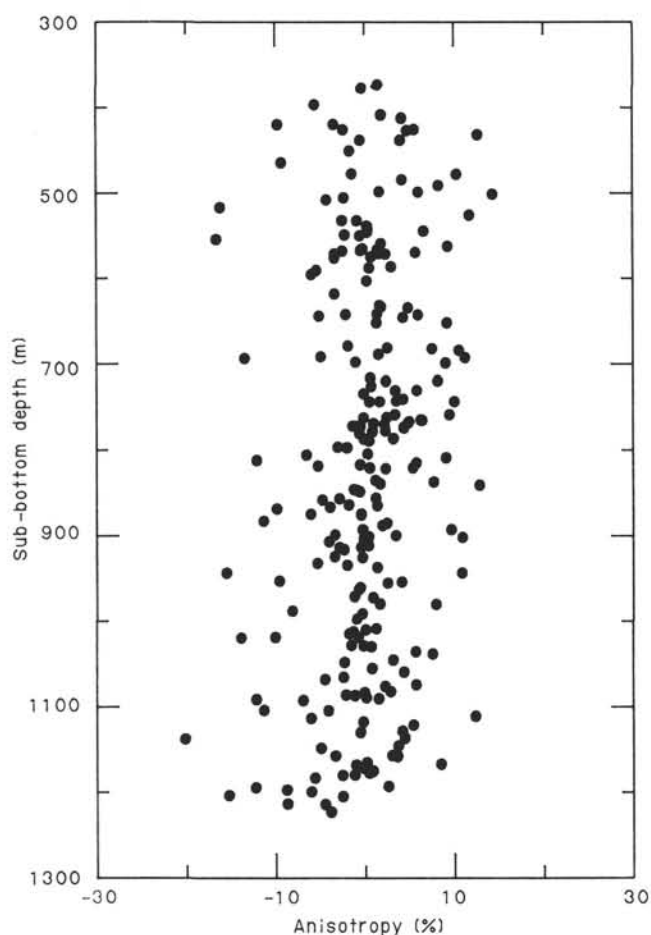


Figure 63. Vertical anisotropy profile of samples from the volcanic sequence recovered at Hole 642E.

Interpretation

Dual Induction Log

The electrical resistivities measured by the Schlumberger deep (ILD) and medium (ILM) induction tools were essentially the same. While the Schlumberger spherically focused electric tool

tracked the induction tools, its measured resistivities were consistently about 0.1 ohm-m lower (see Hole 642D log at end of this chapter). This effect is a manifestation of conductive fluids in the borehole and its consequences on the log interpretation are negligible. In particular, both the ILD and ILM induction tools are measuring the true formation resistivities in Hole 642D.

The formation resistivity measured in Hole 642D is nearly a featureless function of depth, the only exception being the 0.5 ohm-m change across the contact between sandy mud to siliceous mud sediments at approximately 63 mbsf. The electric tools did not provide a mark when they passed through the numerous ash layers encountered in Hole 642D.

When the electrical resistivity is combined with suitable electrical constitutive relations, it can provide an estimate of porosity. Unfortunately, such a relation is unavailable for the present lithology; however, available data may be used to formulate such an expression, which should be useful in future logging efforts where porosity information is not available from neutron logs.

The form of an electrical model for porosity was first put forth by Archie (1942):

$$R_f = R_w \phi^{-m} \quad (1)$$

where R_f is the formation resistivity, R_w is the resistivity of the pore fluids (taken here to be sea water), ϕ is the porosity and m is a constant for a given formation fabric and often has a value near two. In the following, m is evaluated for the sediments encountered in Hole 642D.

The formation water resistivity is a function of its ionic content and its temperature. For this calculation, the temperature variation in the hole is neglected since its effect on m is small. The ionic content of the water was taken to be 30,000 ppm (approximately seawater), temperature = 10°C, and $R_w = 0.295$ ohm-meter. Porosities in the hole were obtained from the neutron porosity logs. From these inputs, one finds:

Depth (mbsf)	m of Archie's Eqn.
33–64.4	2.3
64.4–198	2.2

The reader is forewarned that these numbers are approximate; however, in the absence of better porosity information, they will provide porosity estimates in formations similar to those encountered in Hole 642D.

The resistivity data also can be used to provide an estimate of the temperature gradient in Hole 642D. Essential to this estimate are three important assumptions: (1) Archie's rule is valid, at least in its form given above in equation 1; (2) the porosity is constant in the interval 65 to 198 mbsf (see discussion of the neutron porosity log in the following sub-section); and (3) the hole is close to temperature equilibrium. Of the three assumptions, (3) is by far the most uncertain since the logging took place only about 10 hr after circulation in the hole was stopped. Under these conditions, one finds:

$$\frac{R_f(65)}{R_f(198)} = \frac{R_w(65)}{R_w(198)} = 1.33.$$

Then, from published values for the temperature variation of the resistivity (Dresser Atlas, Inc., 1982) the temperature gradient in Hole 642D is found to be about 85°C/km. This gradient is higher than what one might expect for regions without hydrothermal activity. The perturbation is probably caused by non-equilibrium conditions. However, the gradient is in accord with other data in the area and with those computed from downhole temperature measurement in Hole 642C (see "Physical Properties" section, this chapter).

Compensated Neutron Log

The neutron porosity log run in Hole 642D shows fine structure resulting from changes in the sedimentary materials or depositional environment (e.g., interbedded sediments) (see Hole 642D log at end of this chapter). For the present, no attempt has been made to evaluate the cause of this structure. We note that obvious formation contacts, such as those occurring at ash/sediment boundaries, produced some perturbation to the log. The gross porosities obtained may be summarized as:

Depth (mbsf)	Porosity (%)
33–64	55 ± 5 (fine structure)
64–208	63 ± 5 (fine structure)

It must be noted that these porosities are based on the assumption that all of the observed water is contained in the pore structure whereas some of this water is bound to formation particles. The ratio of free to bound water is presently unknown.

Lithodensity Log

Like the porosity log, the density log exhibits fine structure (Hole 642D log, end of chapter). This structure is about ± 0.1 g/cm³ at the top of the hole, and it increases to about ± 0.2 g/cm³ toward the bottom. In some cases there is a good inverse correlation between the density and porosity logs, i.e., porosity increases result in density decreases. In other cases, a relationship is not apparent. The fine structure is within the measurement capability of the tool; its cause is presently unknown.

A summary of the gross density measurements made in Hole 642D is as follows:

Depth (mbsf)	Density (g/cm ³)
40–64	1.80 – 0.15 (<i>d</i> -40)
64–124	1.42
124–208	1.25

In the table above, *d* is the depth to the density log (mbsf). The reader is referred to the density log for more detailed information.

Sonic Log

The results of the LSS logging run from the far receiver pair in Hole 642D are shown in the log at the end of this chapter. Data quality is low over this 177-m interval. Transit-time measurements for the 8–10 ft (2.43–2.05 m) and 10–12 ft (3.05–3.66 m) source/receiver spacings recorded from depth 30.9 to 207.9 mbsf are summarized as follows:

Depth (mbsf)	Velocity (m/s)	
	Near receiver	Far receiver
0.9–60.4	1560	1560
60.4–65.9	1650–1400	1690
65.9–78.4	1400	1790
78.4–89.8	—	—
89.9–94.4	1650	1650
94.4–101.9	—	—
101.9–106.9	1510	—
106.9–139.9	1510	1840
139.9–154.9	1510	1510
154.9–207.9	1510	1850

Note that transit-time measurements are calculated from first arrivals at the geophone and the calculations assume both receivers are recording travel paths through the same material. The acoustic velocity of seawater is 1510 m/s. Unreadable signals were recorded in the dashed intervals of the table above owing to cycle skipping of the automatic first-pick scheme used in

the field data processing. Shore-based processing of the full waveforms recorded by the LSS tool may produce reliable data in these intervals.

Tool geometry, lithology, and wellbore conditions in Hole 642D determined the quality of the sonic logging data. The greater source-receiver separation of the long-space pair was generally better at recording accurate traveltimes for the soft formation logged; however, even this geometry was perturbed by the relatively small depth of penetration of the acoustic pulse. The upper-section formation velocity (measured between 64 and 78 mbsf) is 1790 m/s and the lower section (measured between depths 108 to 208 mbsf) is 1850 m/s. The apparent increase in velocity from 1790 to 1850 m/s may correspond to the lithologic change at approximately 63 mbsf from sandy mud to siliceous mud (see section on comparison with other data—Hole 642D).

Without corroboration, velocities obtained in this log are of dubious value. Velocity variations cannot be used to map horizons because the spatial resolution of the sonic tool (i.e., the source-detector spacing) is greater than zone thicknesses of typical sedimentary layers.

Natural Gamma Log

The natural gamma content of the sedimentary section in Hole 642D was recorded between 30.9 and 207.9 mbsf. The depth profile of the recorded NGR is shown in the Hole 642D log at the end of this chapter. The natural gamma content generally decreases with depth. The natural gamma depth profile is summarized as follows:

Depth (mbsf)	Natural gamma content (GAPI)
30.9–62.9	60–80
62.9–75.9	35–45
77.9–82.9	gradual increase from 40 to 75
82.9–86.9	50–70
86.9–172.9	40–55
172.9–197.9	gradual decrease from 55 to 20
197.9–207.9	50–58

The natural gamma count method employed in Hole 642D is most sensitive to the abundant clay minerals in the sedimentary section. The decrease in gamma count at depth 62.9 mbsf correlates with a lithologic change from the sandy mud of lithologic Unit I to a more siliceous mud of Unit II. The abundant ash horizons in the logged section also show some response to the gamma log. Preliminary correlation of the ash zones with the natural gamma log indicate that ash layers thicker than 5 cm generally cause a positive deflection of the GR curve. A relatively thick (11-cm) ash layer at depth 157 mbsf, however, appears to produce a negative deflection. See log at the end of this chapter.

Natural Gamma-Ray Spectrometry Log

The log at the end of this chapter shows the results of the Schlumberger NGT logging run. Curve SGR is the total computed gamma count of thorium, uranium, and potassium, and curve CGR gives the computed total gamma-ray count minus the uranium component. The end-of-chapter log gives a breakdown of the individual thorium, uranium, and potassium depth profiles. Each gamma-ray spectral component generally decreased with depth and there is consistency among the three components. The following list summarizes the NGT logging run:

Depth (mbsf)	CGR (GAPI)	SGR (GAPI)
33–63	60–75	75–85
63	sharp decrease to 40	55
63–187	gradual decrease 40–15	55–30

The CGR and SGR track the natural gamma profile (log at end of this chapter) very well. The thorium and potassium counts are most sensitive to the clay content of the sediment in the logged interval. The abrupt decrease in recorded counts for all three components at 63 mbsf correlates with the change from sandy mud to siliceous mud determined from core analysis. Preliminary correlation of the depth and thickness of ash horizons with the spectral gamma data and natural gamma data indicates the depths determined for ash layers by core measurements are consistent with positive deflections of these logs.

Caliper Log

A three-arm caliper tool was run along with the dual induction and sonic logging run. The results are displayed in the log at the end of this chapter. The caliper arms did not function owing to rock chips wedged in the extension mechanism of the tool, and the data are therefore inaccurate. For reference the drill-bit diameter used in Hole 642D was 11 3/8 in. (0.289 m).

Comparison with Other Data

The density log provided the best information regarding lithologic variations with depth. Plotted with each figure are log-based depths of the three main lithostratigraphic units and the four subdivisions of Unit II. These units and subdivisions came from sedimentological core analysis. The log depths are based primarily on density and spectral gamma logs. The log depths for lithologic contacts agree with those defined from core analysis usually to within 2 or 3 m, with occasional variations to 6 m. No systematic depth offset is seen.

The logging runs traversed only 30 m of the Unit I glacial and interglacial sediments. *In situ* densities and porosities recorded are thus within a more limited range of values than those recorded by physical properties measurements (see "Physical Properties" section). The far-receiver pair of the sonic log did respond to a portion of Unit I where it measured a compressional velocity of 1690 m/s. This value is within the range of laboratory measurements.

Subdivision into lithologic Subunits IIA and IIB was not well marked by density or porosity log traces. The tentative pick for this horizon at 78 mbsf corresponds to less variability in these logs. A similar change in variability of porosity and bulk density was noted in shipboard analysis of sediments from these two subunits. Log densities in the interval of Subunits IIA and IIB are close to lab measurements of density whereas porosities are 10%–15% lower. The far-receiver-pair sonic log recorded compressional velocities of 1790 m/s to a depth of 79 mbsf, where an interval of unreliable data began. A velocity of 1790 m/s for Subunit IIA is in accord with shipboard physical-properties measurements.

An abrupt change in density at 110 mbsf marks the top of Subunit IIC, 6 m lower than the depth determined from core descriptions. Densities recorded *in situ* are 10%–20% lower than lab measurements for this unit. In general, density increases with depth; however, in the interval 120–135 mbsf a reverse trend is observed in the density profile that was also noted in shipboard physical-properties measurements. The porosity log, however, shows a subtle decrease rather than an increase over this interval. The far-receiver-pair sonic log begins to provide compressional velocity data at 1840 m/s at a depth of 107 mbsf, a depth that marks the top of Subunit IIC based on core and density logs.

Subunit IID shows as a 4-m interval of increased density relative to over and underlying units. The sonic log far-receiver-pair data have a sharp jump to higher velocities over the interval 153–160 mbsf. More consistent and slightly lower density and porosity values were recorded *in situ* than by lab measurements made in Subunit IID.

Thirty meters of Unit III was logged in Hole 642D. Again, density and porosity values were 10% lower *in situ* than in lab measurements. The sonic velocity recorded by the far-receiver pair gives a consistent compressional velocity at 1850 m/s, a value slightly higher than laboratory measurements.

In summary, *in-situ* measurements of density and porosity tend to be lower than those measurements made through physical properties analysis. Porosities were usually 10% lower while density values were low to comparable with the exception of Subunit IIC where they show a similar decreasing trend but are 10%–20% lower. The values of the compressional velocities recorded during the sonic logging are within those measured in the lab; however, only one source-receiver pair gave measurements for about 80% of the logging effort. Without data from both source-receiver pairs, the sonic log provides only qualitative velocity information and some indication of the depth of the various lithologic units.

Conclusions

Hole 642D penetrated the sedimentary section on top of the volcanic sequences at the outer Vøring Plateau. The hole was terminated near the top of a basalt flow at 330 mbsf. Sloughing in the hole prevented logging below 203 mbsf. Sea conditions at the time of logging were good. The ship's heave was estimated to be 0.25 m (Skelly, 1985, pers. comm.), but it is thought to be higher by a factor of 2 or more.

Two Schlumberger logging suites constitute the effort on Hole 642D. The first run contained deep- and medium-induction tools, a spherically focused electric tool, a dual spaced sonic tool and a gross-gamma tool. The second run consisted of a gamma-gamma density tool, a neutron porosity tool and a spectrally resolving natural gamma tool.

The results of the effort show the following:

1. Good porosity and density profiles were obtained over the logged interval.
2. Correlation of the electric logs with porosity logs enabled a calculation of Archie's cementation factor, $m = 2.2$ – 2.3 . This factor allows an estimate of porosity in sedimentary formations with large porosities.
3. A temperature-gradient estimate obtained from the electric log is $85^{\circ}\text{C}/\text{km}$ (see discussion in the text).
4. The sonic log data were erratic and should be used only as a qualitative estimate of the low formation velocities in the sedimentary section logged unless further corroboration is possible.
5. Correlation between natural gamma radiation and ash flows was noted.

Hole 642E

Volcanic Section

Three logging suites were run in Hole 642E of the ODP Leg 104 program. The tools run in each suite and the quality of the resulting logs are summarized below.

Run no.	Log name	Depth (mbsf)	Quality
1	Long-spaced sonic	375–1085	Good
1	Dual induction	375–1101	Good
1	Spherically focused electric	375–1101	Good
1	Natural gamma ray	375–1089	Good
1	Caliper	375–1089	Good
2	Natural gamma-ray spectrometry	346–1085	Good
2	Lithodensity	346–1101	Good
2	Compensated neutron	346–1089	Suspect
3	Borehole televiewer	371–771	Incomplete data

(Note: The logs from run 1 appear to be 2 m lower than those of run 2.)

Interpretation

Dual-Induction/Spherically Focused Electric Logs

In contrast to the sedimentary zones logged in Hole 642D, the basalt flows of Hole 642E exhibit a distinct resistivity character (Hole 642E log, end of this chapter). This difference is to be expected and provides a means of locating flow boundaries. A pattern of successive cycles of increasing resistivity are readily observed in the data and correspond to similar trends in other logs. The low-resistivity top of a typical cycle ranges from 1.0 to 4.0 ohm-m and the high-resistivity base from 30 to 1000 ohm-m.

The deep (ILD) and medium (ILM) induction logs tracked within approximately 10%–20% of each other and, considering the inhomogeneous nature of the formations, this difference is reasonable. In contrast is the response of the spherically focused log. Resistivities measured by this device were consistently greater than those inductively measured. Usually the difference was 20% to 30%. Sometimes the difference was an order of magnitude and it occurred in regions of high natural gamma count and porosity, and low density and sonic velocity.

Recall that the induction tools measure formation resistivities a few meters removed from the borehole and the spherically focused tool interrogates close-in resistivities. Furthermore, note that the hole had been flushed with a freshwater mud prior to logging. A plausible explanation for the difference between induction and spherically focused resistivities is that resistive fluids invaded intra-flow zones which tend to be permeable. Should this explanation remain plausible after further analysis, permeabilities of intraflow zones may be estimated.

Lithodensity Log

Densities obtained from the Schlumberger Lithodensity Log (LDT) exhibit strong depth variation that is undoubtedly owing to individual basalt flows (Hole 642E log, end of this chapter). The data are of good quality and show a repeated cycle of low to high density with depth similar to the trends observed in resistivity, sonic, and porosity data. The density at the top of a typical cycle is in the range 2.1–2.4 g/cm³ and 2.7–2.9 g/cm³ at the bottom. These cycles repeat throughout the entire logged section and no overall trend is observed with depth. A preliminary correlation between log- and lab-based data indicates that the detailed correlations will be good.

Compensated Neutron Log

Porosities obtained from this log are highly variable (Hole 642E log, end of this chapter). They often exceed 50% and rarely ever fall below 10%. While the variability is probably caused by individual basalt flows, it is known from core data that some of the basalts are massive with near-zero porosity. Furthermore, porosities obtained from the gamma-density log are consistently 10 to 20 porosity units less than those from the neutron log. Thus, the neutron porosity log is suspect. The inconsistency may be due to an equipment failure. However, no problems were observed on tool check-out either before or after the log runs. Errors can be introduced if the formation contains elements which are strong absorbers of thermal neutrons. Specimens from a hole containing similar basalt flows (DSDP, Hole 504B) are presently being analyzed for the presence of such elements (Lysne, Anderson, and Moos, 1985) and similar work may be appropriate for the present hole. The neutron porosity log may be useful for picking zone boundaries.

Sonic Log

The results of the LSS logging run in Hole 642E are shown in the Hole 642E log, end of this chapter. The sonic data are generally of very good quality over the 715-m interval logged. At three depth locations of the upper section, interbedded material

with highly variable velocities produces unusable data. Note that transit-time measurements are calculated from first-arrivals at the geophone, and the calculations assume both receivers are recording travel paths through the same material. Where materials with highly contrasting velocities have layer thicknesses less than 0.61 m, data are averaged. Unreadable signals were recorded in the dashed intervals of the table below, owing to cycle skipping by the field-processing scheme. Future analysis of the individual full waveforms recorded by the LSS tool over these intervals will likely provide good data.

The data show a cyclic repetition of velocity structure. Transit-time measurements for the 8–10 ft (2.43–2.05 m) and 10–12 ft (3.05–3.66 m) source/receiver spacings correlate well over 95% of the logged section. Sonic velocities recorded from 371 to 1086 mbsf are summarized as follows:

Depth (mbsf)		Velocity (m/s)
371–386	Cyclic pattern velocity range	2900–5080
386–403		—
403–436	Cyclic pattern velocity range	3050–6096
436–442		—
442–475	Cyclic pattern velocity range	2900–5080
475–481		—
481–1086	Cyclic pattern velocity range	2900–6100

Typically a low velocity (approximately 2900 m/s) marks the top of a velocity cycle. There is an overall increase in velocity over this cycle to about 5080 m/s, often with four or five velocity inflections within the cycle (Hole 642E log, end of this chapter). These cycles repeat over the entire sequence logged and vary in interval depth between 4 and 12 m. The majority of cycles span the velocity range 3390–5540 m/s. The cyclic nature of the data concur with density, resistivity, and porosity logs. Thus, they provide both a tool to locate flow boundaries and a means to analyze the velocity structure of individual flows of the basalt sequences. (See section on correlation with other data.)

Natural Gamma Log

The natural gamma content of the volcanic section in Hole 642E was recorded between 375 and 1089 mbsf. The depth profile of the recorded NGR is shown in the Hole 642E log. The natural gamma logs are of very good quality, giving a continuous profile of variations in natural gamma count from a base value between 5 and 10 GAPI (Note: GAPI units are test pit calculated; Dresser Atlas, Inc., 1982). Fluctuations from this background level to 20 GAPI characterize the entire profile, with occasional counts as high as 35 GAPI. No overall trend with depth is seen in the data.

The natural gamma log is sensitive to the abundant clay minerals within the low-velocity zones (volcaniclastics, tuffs) that are interlayered between basalt flow sequences; hence, sharp increases in the natural gamma count mark the boundary between successive basalt flows (see Fig. 65 and section on correlation with other data). Preliminary correlation of the sedimentary horizons determined from core descriptions with the deflections in natural gamma count is very good and indicates that this log will provide valuable information on possible sedimentary zones not recovered in core.

Natural Gamma-Ray Spectrometry Log

The Hole 642E log at the end of this chapter shows the results of the Schlumberger NGT logging run. The SGR curve is the total spectral gamma count of thorium, uranium, and potassium and curve CGR gives the computed total gamma-ray count minus the uranium component. Also shown is a breakdown of the individual potassium, uranium, and thorium (KUT) depth profiles. The CGR and SGR track the natural

gamma profile very well. Each gamma-ray spectral component shows the individual response to the high clay content of the sedimentary horizons encountered over the logged interval. The natural gamma count has the highest response to the potassium content with uranium providing the next-greatest contribution. Thorium was detected in minor amounts.

Initial correlation of the NGT spectrometry log with core description indicates that NGT spectrometry will provide log-based depth markers for basalt flow boundaries. In addition, when chemical analyses of the sedimentary layers become available it may be possible to recover some compositional information from the KUT breakdown where sedimentary layers were not recovered from core.

Caliper Log

A three-arm caliper tool was run along with the dual-induction and sonic logging run. The results are displayed in the Hole 642E log, end of this chapter. Good-quality caliper data were obtained for the logged interval. Borehole diameter varies from 0.33 to 0.36 m over most of the section. Good borehole conditions are indicated by the relatively smooth profile. The following table summarizes the caliper log data:

Depth (mbsf)	Diameter (m)
371-687	0.32-0.36
687-704	0.27-0.32
704-1086	0.32-0.33

Acoustic Borehole Televier

A televier run was included in the logging suite for Hole 642E to map lithologic boundaries, to determine the distribution and orientation of fractures, and to detect stress-induced hole deformation (breakouts). For a multitude of reasons, televier data obtained in Hole 642E are incomplete. Televier logging at normal logging speeds was possible over only a small depth interval. Because of a failure of the depth-encoding system, the logging depth was approximated from a cable marker.

The first televier experiment in Hole 642E was performed at about 800 mbsf. It was conducted while the cable winch was locked and the drill pipe was made fast to the reentry cone, not to the ship. This experiment was intended to provide a detailed televier log over a limited interval. Stick-slip conditions caused by the ship's heave resulted in a repetition of televier scan lines, substantially reducing the image quality at this logging rate (0.025 m/s). Approximately 25 m of televier data was collected at this normal logging speed. Reconstruction of the digitized televier data does not indicate the presence of through-going fractures or lithologic changes over this interval. A test of the heave response of the sonde was conducted by keeping the winch stationary in the borehole. It has been determined that ship's heave greater than 0.2 m is required to induce motion into the sonde. Similar data taken for a cable speed of 0.3 m/s do not show evidence of ship's heave. It is apparent from this experiment that increasing the logging speed, although decreasing the resolution of the televier image, will reduce the effects of ship's movement on the data. At the time of logging, the *Resolution* was not equipped with a heave-compensating mechanism for logging tools.

In the second televier experiment, the tool was moved up-hole at about 1290 m/hr, or about 12 times the normal logging speed. Even so, the spatial resolution of the tool exceeds that of other logs run in Hole 642E. Below the casing, the televier data contain caliper and amplitude information in the form of a helix with a pitch of about 12 cm. These data have been analyzed for information on hole shape and for evidence of breakouts. Traveltime of the acoustic pulse and amplitude of the re-

flected energy, available through the digitization of the analog field data, show no evidence of wellbore breakouts.

Comparison with Other Data

The sensitivity of many of the logs to variations of lithology permits a log-based analysis of the depth of such horizons in Hole 642E. We completed a geophysical log-based analysis of the depths of the markers between basalt flows that have been described in petrographic core descriptions (see "Basement Lithology" section, this chapter). The log-based depth horizons have been correlated with core data and the combined interpretation of these depths appears in Figure 14. The log depths are a combined analysis of the sonic velocity, porosity, density, induction, and natural gamma logs. The natural gamma and porosity logs were used to determine the possible location of sedimentary or breccia layers that occur at the top of basalt flows throughout the section. These layers show a relatively high average porosity with respect to the basalts and a potassium content greater than 0.01 ppm. The velocity, density, porosity, and resistivity logs were used together to map the flow boundaries. Figure 64 shows the correlation among these four logs and the typical flow cycles viewed from geophysical logging.

The characteristic flow cycle of a basalt sequence begins with a sedimentary layer overlying a basalt section with a vesicular or brecciated top that increases in velocity, resistivity, and density and decreases in porosity with depth (Fig. 64) as the basalt becomes more massive. Discrimination of sedimentary layers as opposed to highly vesicular or brecciated zones at the top of a flow is difficult; the log response to these two conditions is very similar. A comparison between a sedimentary layer at 739 mbsf (core description unit S-26) and a brecciated zone at 892 mbsf show identical values of porosity and potassium content.

In this initial study, two types of geophysically determined structures for the basalts were discerned. Both types, shown in Figures 64 and 65, have an overlying low-velocity layer with velocities between 2900 and 3200 m/s, high porosities, resistivities of about 3 ohm-m and densities between 2.1 and 2.4 g/cm³. One basalt cycle type (Fig. 64) shows an overall increase in velocity with depth: a minimum velocity of approximately 3800 m/s and a maximum of 5080 m/s with four or five velocity inflections of ± 250 m/s within the cycle. The resistivity is lowest at the top of the basalt flow cycle at 3 ohm-m and greatest at the cycle bottom at 10 ohm-m. The within-cycle inflections are again observed in the resistivity logs. The densities of the basalt cycle follow the same course with upper flow densities of 2.45 g/cm³ and bottom flow densities of 2.7-2.8 g/cm³. Within-flow fluctuations in density are on the order of 0.25 g/cm³. In this flow type, porosity variations are negatively correlated with the other logs. Owing to the suspect nature of the neutron-porosity log, it can be used only as a qualitative measure of porosity. There are inflections of ± 3 porosity units within the cycle.

A second flow type (Fig. 65) was observed with a velocity gradient below the low-velocity layer that consists of increasing velocity from 2770 m/s to a maximum of 6096 m/s at about mid-flow cycle. This higher velocity interval is maintained until the end of the cycle. The resistivity increases from 2 to 40 ohm-m over the same depth interval. Porosity values again negatively correlate with the other logs. Densities increase from about 2.3 to 2.95 g/cm³ at the lower part of the flow corresponding to the higher velocity sections. Only minor inflections in the geophysical records are observed within this flow type. This second type of flow was observed to be thicker, on the order of 12 m, whereas the first flow type is usually 4 m thick.

The distinction between these two types of basalt flows correlates with both physical-properties measurements and core descriptions. Flow type 1 above corresponds to the medium-grained

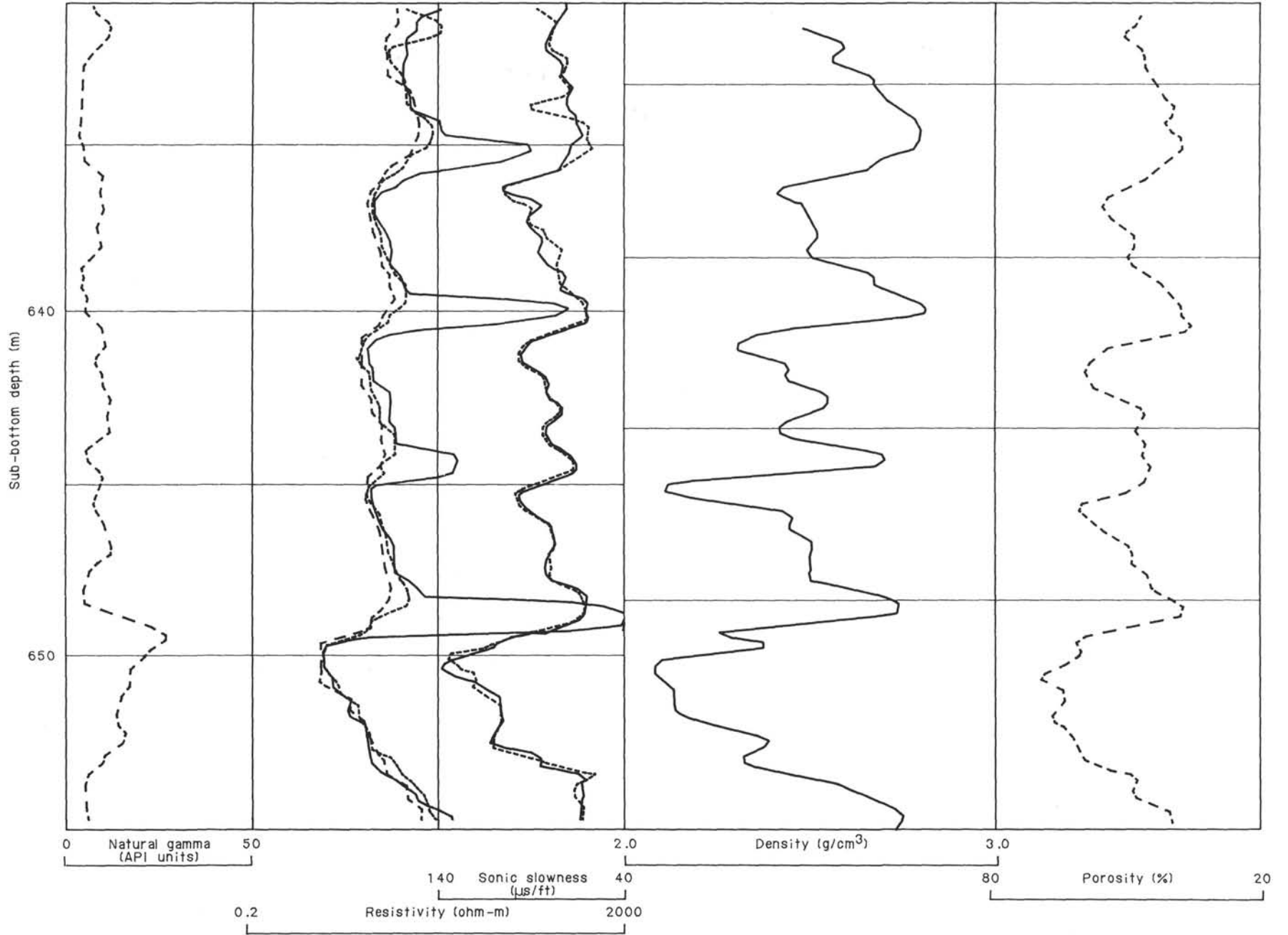


Figure 64. Geophysical view of cyclic nature of basalt flows (type 1) over the depth interval 631–655 mbsf, Hole 642E.

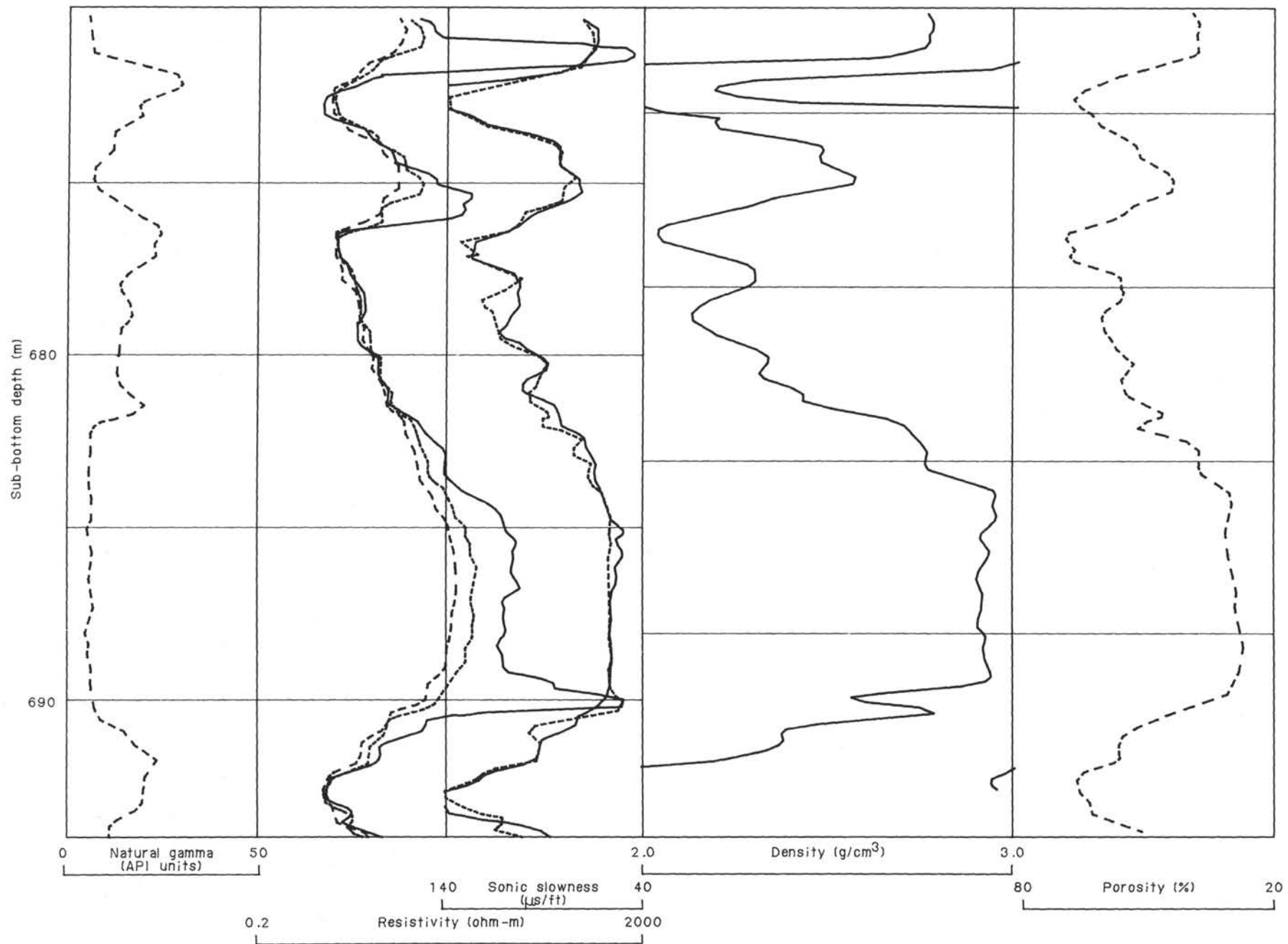


Figure 65. Geophysical view of type 2 basalt flow over the depth interval 675-691 mbsf, Hole 642E.

basalt flows having low velocities and densities. Type 2 flows are fine grained and have relatively higher velocities and densities (see "Physical Properties" section). The range of velocity and density values recorded by physical-properties measurements is in accord with *in-situ* measurements.

So far, 137 flows have been delineated from this combined interpretation of the geophysical logs and the core descriptions. Core recovery was approximately 40% through the basalt sequence drilled at Hole 642E and a 9.5-m core barrel was used in this interval. Thus, logs likely increase the accuracy of the depth information available in core recovery.

All of the sedimentary units described by petrographic core analysis that were encountered in logging suites (S-07 through S-41) could be depth-located through the log analysis. Because the gamma log responds to the clay mineral content of the sediments, it may provide a measure of the thickness of the sedimentary units.

The repetitive cycle of sediments and/or high-porosity zones overlying basalt flows continues from 371 to 1089 mbsf where an abrupt decrease in density from 2.9 to 1.5 g/cm³ is encountered. At 1095 mbsf density again decreases from 2.3 to 1.1 g/cm³. This boundary concurs with the thick sedimentary bed at the top of the lower volcanic series.

Conclusions

In addition to upper sedimentary layers, Hole 642E penetrated 906.9 m of basalt series. The hole was terminated at 1229.4 mbsf, 137 m deeper than a thick sedimentary layer at 1092 mbsf. Sea conditions at the time of logging were fair. The ship's heave was estimated to be 0.5 m.

Three logging suites constitute the logging effort on Hole 642E. The first run contained deep- and medium-induction tools, a spherically focused electric tool, a dual-spaced sonic tool, and a gross-gamma tool. The second run consisted of a gamma-gamma density tool, a neutron porosity tool, and a spectrally resolving natural gamma tool. The third run contained a borehole televiewer.

The preliminary results of the logging effort are:

1. Good-quality resistivity, velocity, natural gamma and density profiles.
2. Correlation between logs and core descriptions indicates that the logs provide important information on the location of basalt-flow boundaries and the location and possible thickness of the interlayered sedimentary rocks.
3. For the first time, a correlation has been made between ship's heave and sonde motion at depth.

VERTICAL SEISMIC PROFILE EXPERIMENT

Introduction

A vertical seismic profile (VSP) experiment was conducted to determine the detailed velocity-depth structure and reflection seismogram for the seaward-dipping reflector sequence at Site 642 (Fig. 66). VSP measurements provide such seismic information not only for the interfaces penetrated by the borehole but they can also be used to predict the nature and depth of reflection interfaces below the borehole (Gal'perin, 1974). Figure 67 shows a generalized, schematic representation of the ray paths and diverging wavetrain pattern for direct and reflected arrivals in a VSP experiment (Mons and Barbour, 1981).

Objectives

The primary objectives of the VSP experiment at Site 642 on the Vøring Plateau margin were to (1) determine the feasibility of conducting VSP experiments aboard the *JOIDES Resolution*; (2) verify that the target horizon, reflector "K" near the

base of the seaward-dipping reflector sequence at about 2.53 s, two-way traveltimes multichannel seismic profile BFB-1 (Fig. 68), was actually penetrated by the drill bit; (3) determine the detailed velocity-depth profile and vertical reflection seismogram of the seaward-dipping reflector sequence and the underlying sub-"K" reflectors; (4) precisely relate the seismic profile to the borehole lithology and other logging information and thereby determine the physical origin of the dipping reflectors; and (5) correlate the VSP reflection seismogram with the regional surface multichannel seismic (MCS) lines which located Site 642 (Hinz, 1981; Mutter et al., 1982). Virtually all of the objectives were accomplished to some extent during the cruise. However, objectives (4) and (5) will require more extensive computer studies ashore before they can be fully realized.

Method

The sound source for the Site 642 experiment was a large volume (1250 in.³, 20.5 L), high-pressure (2000 psi, 133 bars) air gun (Bolt Model 1500C) suspended from a buoy at 30 ft (9.15 m) water depth (Fig. 69). The buoy was tethered from the drill ship's aft port crane about 80 ft (24.4 m) abeam. The seismic signals were recorded on a prototype, three-component, radial geophone array seismometer developed by Phillips Petroleum Co. (patent pending). Its three 8-Hz geophones (Mark Products L28) were mounted in a 120° azimuthal configuration and inclined 35.3° (Fig. 70). Two seismometer units were available for this experiment. The air gun's acoustic signals were also received by a calibrated hydrophone (Benthos Model 48h) mounted at a fixed height above the seafloor on the drill ship's tautline mooring cable. This provided a stable reference that would allow real-time summing of multiple shots at each recording level in the event of severe air-gun motion during high seas.

The air-gun-generated signals received by the borehole seismometer were preamplified downhole, transmitted up the logging cable, and digitally recorded aboard the drill ship, along with the hydrophone signals, by a Masscomp minicomputer and A/D converter (Fig. 71). Timing information was logged with millisecond accuracy. The shot number and geophone depth for each shot were digitally recorded. The seismogram waveforms were displayed in real time on a four-channel oscilloscope and plotted after each shot using a graphics printer.

A special effort was made to reduce the downhole seismic noise caused by drill pipe and logging cable slamming against the borehole wall. This was done by locking the bottom of the pipe string in the seafloor reentry cone with a casing landing/running tool assembly (Fig. 69). With the pipe immobilized, the special high-capacity, precision heave compensator in the drill ship derrick was able to isolate the ship's motion from the downhole pipe string and logging cable.

Data Acquisition and Processing

For the acquisition and real-time processing of vertical seismic reflection data, we modified the HIGHRES/PROCESS computer software system normally used to collect underway seismic profiles aboard the *JOIDES Resolution*. This system, originally developed for ODP by scientists at the University of Texas Institute for Geophysics (UTIG), is capable of acquiring, processing and displaying single channel seismic data in real time. The modification of HIGHRES/PROCESS included (1) adding three more data channels to allow three-component seismometer and hydrophone recording, (2) developing new modules which take advantage of the unconventional geometry of the radial geophone configuration in the Phillips Petroleum Co. tool, and (3) providing a real-time estimate of the signal-to-noise ratio improvement as successive air-gun shots were summed at each clamping depth. The software changes also provided for the last trace for the composite of all traces summed at each depth to be

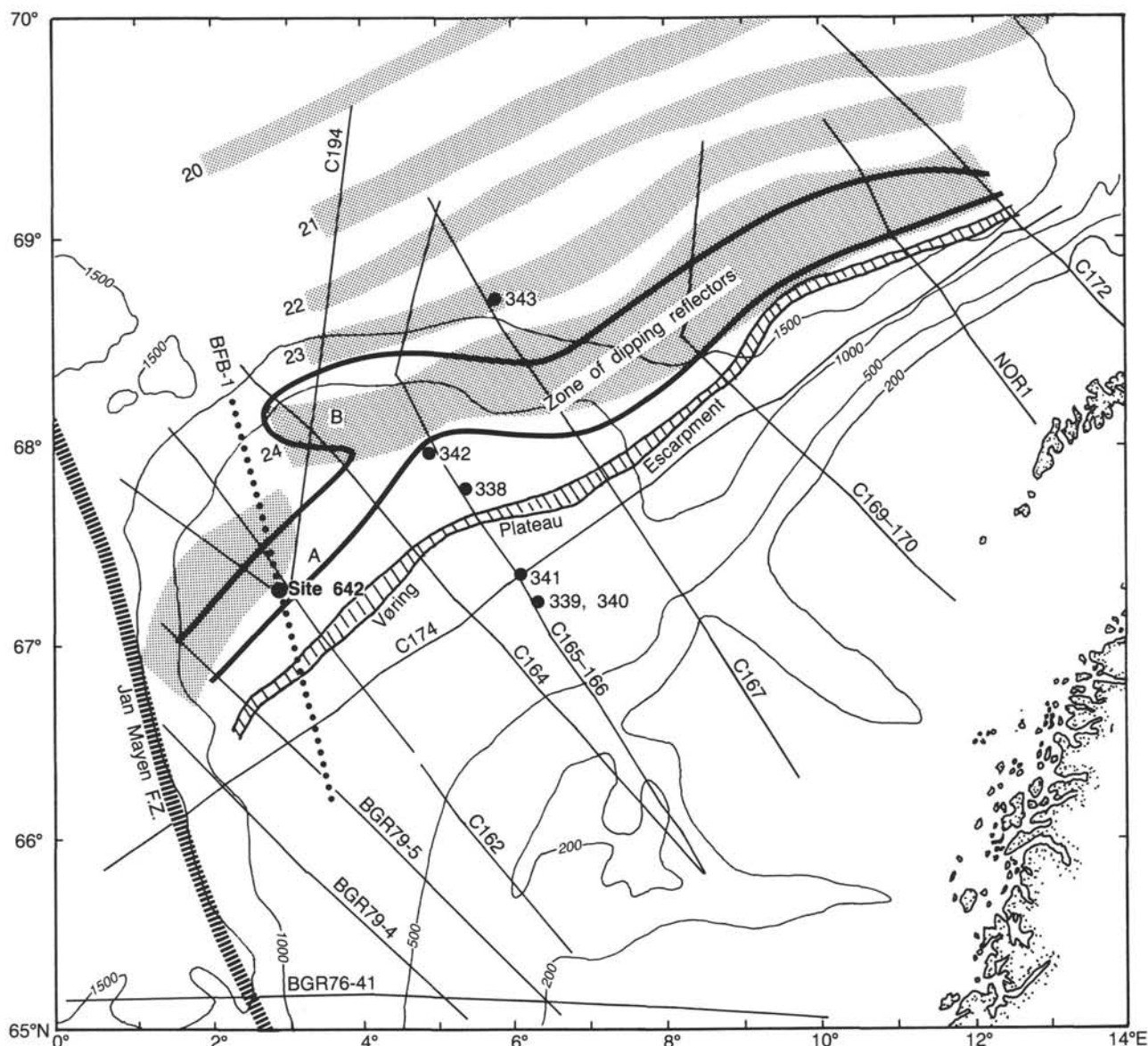


Figure 66. Location chart showing ODP Site 642 multichannel seismic (MCS) profile BFB-1 and the magnetic anomaly patterns with respect to the dipping reflector sequences off Norway (from Mutter et al., 1982). Depths are shown in fathoms.

written to disk memory in real time. This improvement allowed us to plot a preliminary stack of the seismograms recorded at each depth interval immediately after the experiment.

Note that the unconventional geophone arrangement of the Phillips Petroleum Co. tool is geometrically equivalent to simply rotating the orthogonal coordinates of a cube so that its opposite corners are aligned along vertical and horizontal axes (Fig. 72). This is a particularly useful experimental configuration in that the vertical component can be easily derived by summing the three inclined components and normalizing. It is also more robust for estimating the vertical component in the event of hardware malfunction or noise on one or two of the three components. In a conventional x, y, z orthogonal system, if the vertical component (z) is lost, the experiment may be doomed to failure. Therefore our acquisition software was designed to first sum the three geophone channels to derive the vertical component, and then add this vertical component into the running mix of previous shots at that depth.

Using this approach we were able to see notable improvements in the signal-to-noise ratio with successive shots. How-

ever, room for improvement of the real-time VSP acquisition system remains. The logical next step would be to take advantage of the Masscomp's video screen graphics capabilities to display not simply the running mix of traces but also each of the three-component raw traces from each shot. This improvement would have allowed us to identify and eliminate sources of noise which degraded the data quality of geophone channel 3 during recording in the upper part of the borehole. Other improvements should permit automatic encoding of the seismometer depths and shipboard amplifier gains into the SEG Y trace headers in real time.

Experimental Procedure

After locking the drill pipe into the reentry cone and engaging the heave compensator, the experiment proceeded as follows: the seismometer was first deployed to the bottom of the borehole (50 m/min lowering rate) and clamped to the borehole sidewall. The logging cable was slacked about 5 m. The air gun was then fired several times at a 20-s repetition rate. Approximately 8-15 useful shots were recorded at each seismometer

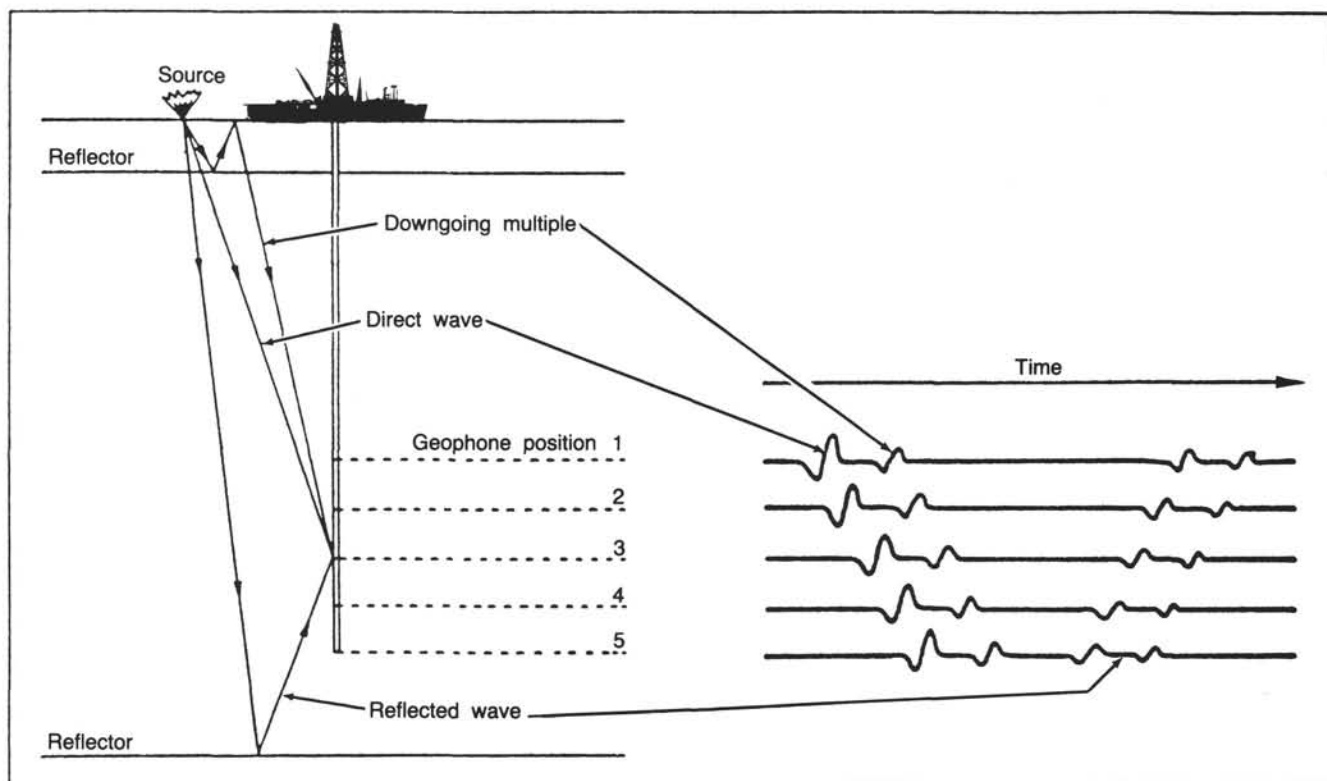


Figure 67. Schematic representation of acoustic ray paths and wave train arrivals for vertical seismic profile experiment (modified after Mons and Babour, 1983).

clamping depth position. The multiple shot recordings at each geophone position were summed, normalized, and displayed in real time on the graphics printer to provide a continuous estimate of the seismic signal-to-noise ratio. After an adequate number of shots were fired, the seismometer was unclamped and raised 15 m up the borehole and the procedure was repeated. During the unclamped period, the air guns were not fired, to conserve the high-pressure air supply available from the drill ship's compressor system. Only one of the ship's two compressors was available for this experiment.

Results

The VSP experiment started at 0100 UTC, 1 August 1985, at 2400 m depth below the drill floor, or 1111 mbsf. The water depth was 1289 m. The bottom of the borehole, at 1229 m below seafloor (mbsf), could not be reached owing to drill-mud backfilling by the reentry cone washdown just before the logging operations. During the experiment's 15-hr period, seas were moderate with 2- to 3-ft waves and a 4- to 5-ft swell. A total of 44 seismometer clamp positions were occupied, utilizing about 9 hr of total recording time. After the initial start-up to set gain levels, less than 10 min was required at each depth position. Approximately 3 hr of recording time was lost owing to the breakage of the clamping arm on seismometer unit no. 2 at 1036 mbsf. This unit was quickly replaced by modifying and deploying seismometer unit no. 1. These units were identical except for their preamplifiers' gains ($\times 50$ and $\times 100$, respectively). A subsequent clamping arm failure on unit no. 1 terminated the VSP experiment at 1621 UTC at 451 mbsf depth. Approximately 3 hr was required to deploy and recover the seismometers.

Figure 73 shows raw, true-amplitude seismograms for each of the three components for a selected air-gun shot. Aside from occasional cable-slammings noise bursts (arrow), only very low-level digitizing noise is seen. Note the close similarity of the

waveforms. This similarity is to be expected for normal incidence plane waves on a radial geophone configuration. In general, geophone 1, which was oriented in the plane of the clamping arm, was the most noise-free. Geophones 2 and 3 appeared to be more prone to tool resonance-type noise when the tool was not securely clamped to the borehole side walls.

Careful inspection of the true-amplitude seismograms in Figure 74 shows that a very high signal-to-noise (S/N) ratio can be achieved by the summing of multiple shots at each depth and by the use of the large air-gun source and the drill-pipe immobilization scheme described above. The S/N ratio estimated from the first break of the downgoing direct waves relative to the background noise is greater than +40 dB.

Figure 75 shows a depth-time plot stack for the seismograms collected within the upper basalt series dipping reflector sequence at Site 642 over the depth interval 1111–451 mbsf. The data are for the single component of the seismometer's radial geophone array that was in the plane of the clamping arm (geophone 1). The data have been edited to eliminate those data traces showing excessive pipe/cable slamming and tool resonance noise. Only a 5- to 50-Hz band-pass filter has been applied. No deconvolution or spherical divergence corrections have been made. Each trace represents the normalized sum of several traces and has been amplitude-scaled using a time linear gain function. The direct downgoing waves are the strong first arrivals sloping downward at the left of Figure 76 and the water bottom multiple at about 3-s traveltime. Note that the direct arrival times decrease with decreasing seismometer depth position. The reflected waves are best seen by holding the page on edge and viewing the seismogram stack from a low angle. The divergent wave-train pattern results from the decreasing range to the source for direct waves and increasing range from the reflecting interfaces as the seismometer is raised to shallower depths as shown in Figure 67. Note that the wave trains of the reflected arrivals intersect the

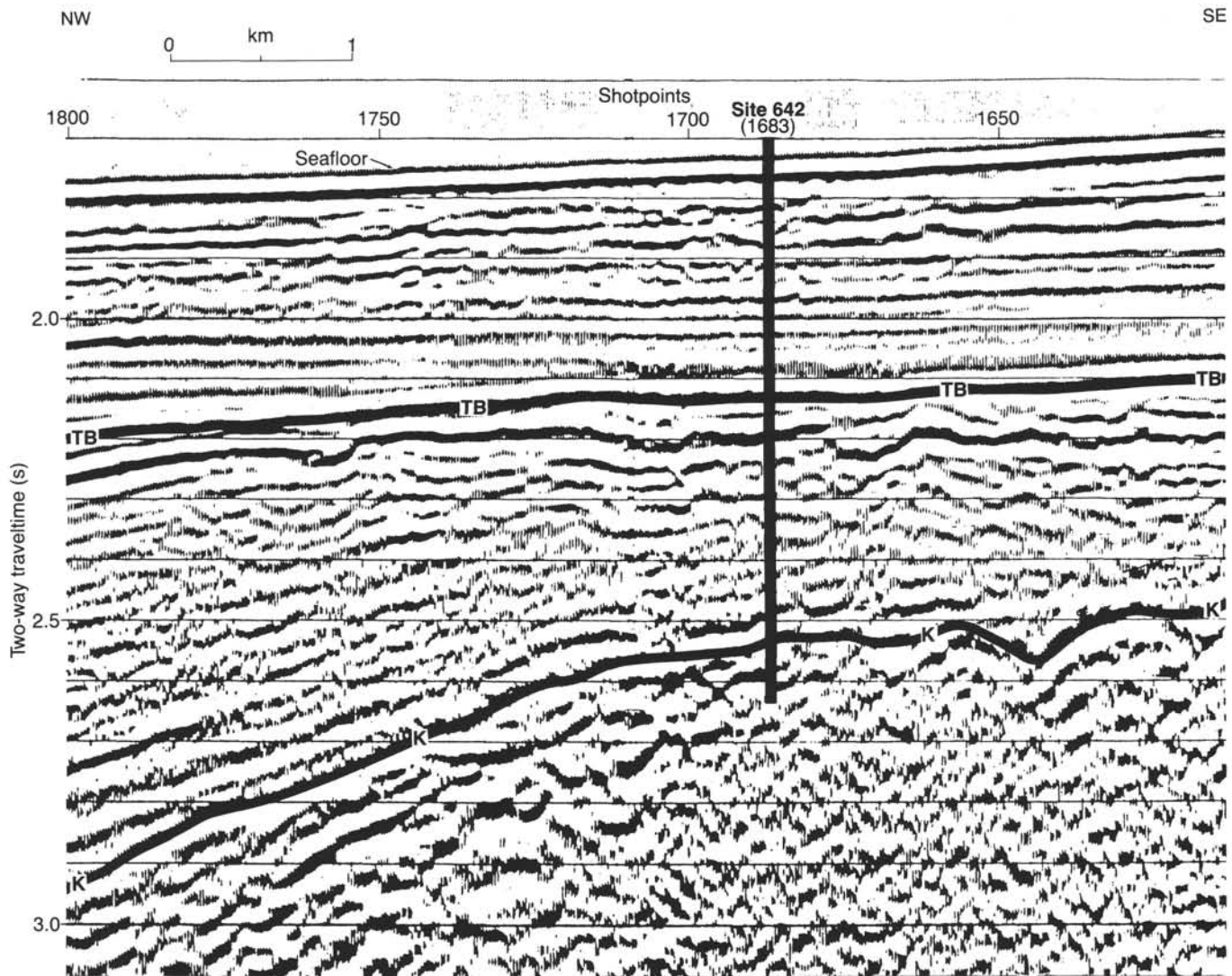


Figure 68. MCS profile line BFB-1 showing Site 642 location. Note estimated borehole penetration to approximately 2.63-s two-way traveltime. Deepest seismometer clamping position was at 1111 m total depth below seafloor where a direct wave, two-way travel-time (TWT) of 2.56 s was observed. The two-way traveltime to the borehole total depth (1229 mbsf) would be 2.63 s, assuming a 3.5-km/s interval velocity. TB = top of basaltic basement. K = base of seaward dipping reflector sequence.

direct, downgoing wave train at the exact depth of the respective reflecting interfaces and that the slopes of the downgoing and upgoing wave trains are equal but of opposite sign.

Discussion

A preliminary interpretation of the velocity-depth structure can be made by computing the difference in the first-break arrival times of the direct downgoing waves shown in Figure 75 for various depth intervals in the borehole (Mons and Barbour, 1981). This has been done to estimate a velocity of 3.728 km/s over the depth interval 451–1111 mbsf, for the lithologic unit identified as the upper basalt series. Interval velocities estimated for the subgroups I–III within the upper basalt series are shown in Table 29.

The laboratory measurement of sound velocity on the upper basalt series core samples yielded an average formation velocity of about 4.685 km/s (“Physical Properties” section). This difference from the 3.771 km/s VSP velocity might be expected be-

cause the laboratory measurements are biased toward measuring only the hard, higher-velocity samples that are usually recovered in the coring operations. The interbedded, lower-velocity, soft volcanics and scoriaceous basalts are not as well recovered. The VSP velocity determination method samples all the rock materials over the depth interval measured.

Comparison of the VSP velocities with interval velocities computed by integrating the sonic well-logging velocities (“Logging Results” section) should show better agreement in that all the lithologic units in the borehole transmit the sonic pulse and are measured. Detailed comparison of sonic as well as other logging results will be an important part of future shore-based VSP analysis work. Synthetic seismogram modeling based on the logging measurements of velocity and density should be particularly useful.

Detailed interpretation of the reflected wave field in VSP experiments requires the careful separation of the upgoing and downgoing waves using velocity filtering (Seeman and Horo-

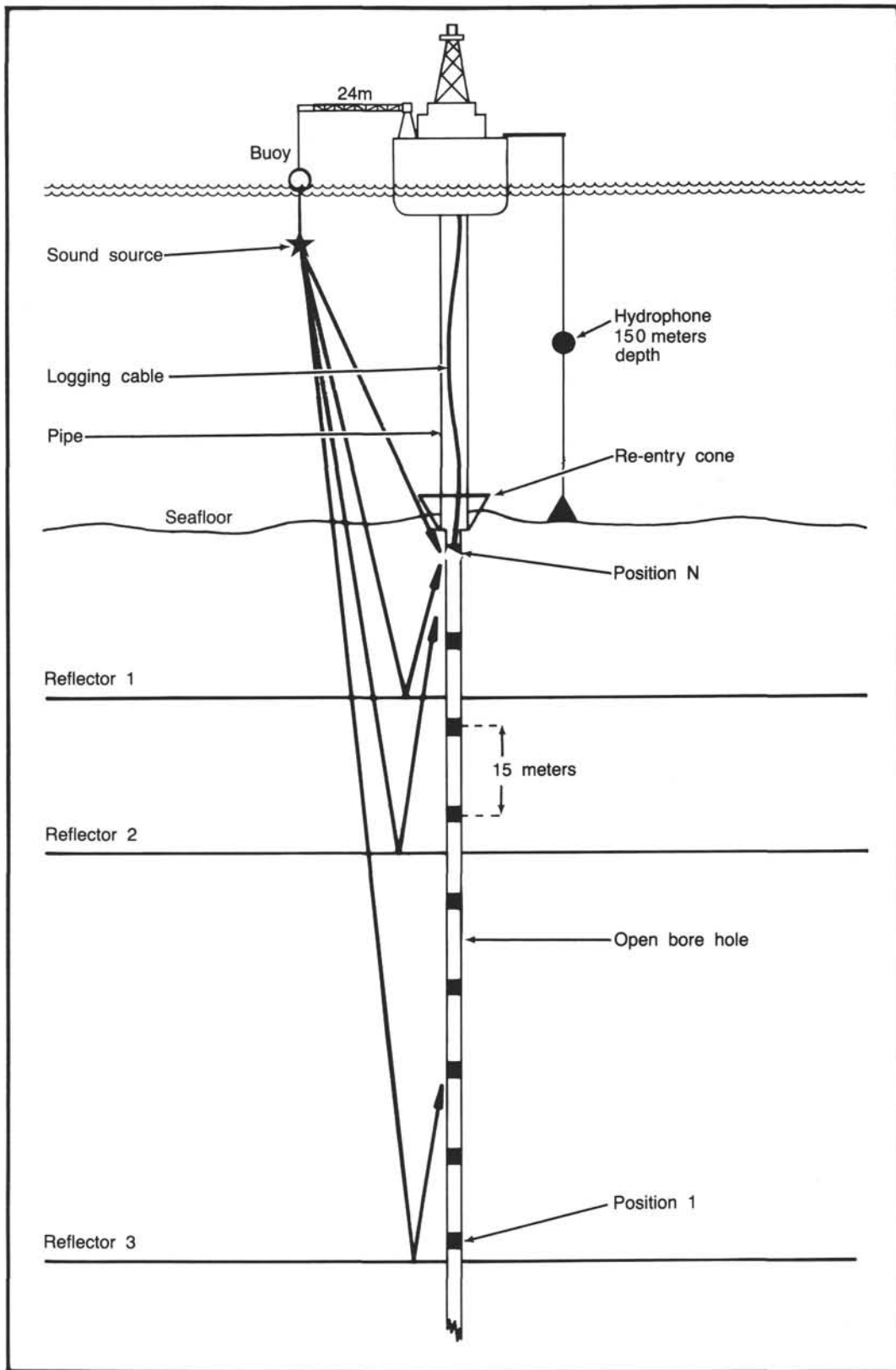


Figure 69. Vertical seismic profile experiment (VSP) configuration at Site 642. Downgoing direct and upgoing reflected ray paths are shown for multiple seismometer depth positions.

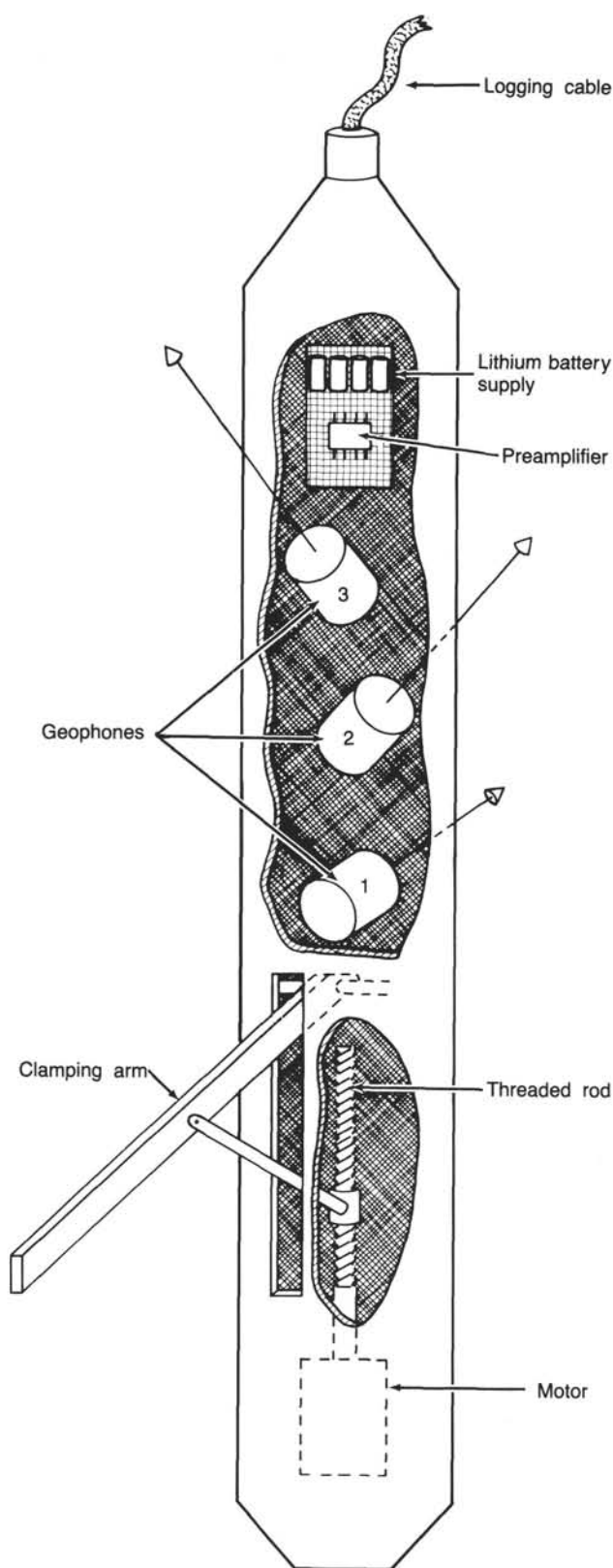


Figure 70. Schematic drawing of the Phillips Petroleum Co.-designed three-component borehole seismometer utilized for the VSP experiment at ODP Site 642. The approximate tool dimensions are 66-in. length, 3.5-in. diameter, 50-lb. weight.

wicz, 1983) and deconvolution of the reflected waves using the downgoing, direct wave to derive the source wavelet operator (Lee and Balch, 1983). Iterative modeling techniques can then be employed to develop synthetic seismograms from the physical-properties/logging information that can be compared to the observed VSP reflected wave field (Grivelet, 1985). The resulting VSP seismogram can also be compared to the surface ship multichannel seismic reflection (MCS) profiles that established the regional seismic structure of the drill site (Poster, 1983). At present this detailed analysis work must await more extensive computer data processing ashore. However, certain qualitative inferences can be made about the reflected, upgoing wave field from the shipboard-observed data by simply time-shifting each seismogram shown in Figure 75 by its first break time. This shifting results in a two-way traveltime plot as shown in Figure 76. More importantly, this time-shifting serves to align the reflected wave trains vertically along the two-way traveltime isochrons. Visual alignment of the reflected wave trains is markedly enhanced. This alignment is best seen by holding Figure 76 on edge and viewing it from the bottom. Note that downward seismometer motions are shaded in Figure 76, whereas the black reflection horizons shown in the BFB-1 surface ship MCS profile represent negative acoustic compression on the hydrophone sensors.

Careful inspection of Figure 76 in the manner described above shows several weak events at 2.32, 2.40, 2.50, and 2.55 s (TWT). They are labeled G_1 , G_2 , G_3 , and S_1 , respectively. These events intersect the observed downgoing direct wave at 676, 826, 1021, and 1096 mbsf, respectively. Significantly, these events appear to coincide with moderately strong and continuous reflection horizons seen in the BFB-1 surface ship MCS profile within the dipping reflector sequence at nearly the same traveltimes, 2.29, 2.38, 2.49, and 2.53 s (TWT), respectively. However, confirmation of these correlations must await sources deconvolution of the VSP data to make them more compatible with the MCS data (Fig. 77). The VSP reflection depths also coincide with sharp acoustic impedance contrasts as indicated by the physical-properties measurement of the core samples ("Physical Properties" section) at 680, 840, 1014, and 1089 mbsf, respectively. Reflector S_1 also correlates with an 8-m-thick volcanoclastic sediment layer at 1093 mbsf and with the reflector "K" horizon seen in the BFB-1 seismic profile.

In addition to these weak reflections that can be directly observed to intersect the downgoing wave above the bottom of the borehole recordings, two other reflectors which emanate from just below the deepest recording depth (1111 mbsf) can also be projected to intersect a downgoing wave in the borehole. These events are labeled D_1 and D_2 in Figure 76. They show arrival times of 2.58 and 2.63 s and would appear to intersect the downgoing wave at 1164 mbsf and near the borehole bottom at 1229 mbsf, respectively. The strong D_1 reflection closely coincides with a very strong continuous reflection horizon also seen in the BFB-1 seismic profile (Fig. 77) at 2.59 s. Also, reflector D_1 correlates well with the laboratory-measured very high acoustic impedance zone between 1155 and 1177 mbsf. This zone also contains dike D5, the thickest of the only two unequivocal dike units cored at Site 642. Its estimated thickness is about 18 m. Several well-crystallized thick basalt flows are found at the bottom of the borehole. The laboratory physical-properties measurements show the bottom 50 m of the hole to be a low-acoustic-impedance zone. However, the bottommost measurement at 1220 mbsf indicated a sharp impedance increase.

Two other strong reflections are shown in Figure 76 at 2.72 and 2.85 s (TWT) which emanate from below the borehole bottom. These are labeled D_3 and D_4 , respectively. Although D_3 correlates well with a weak discontinuous reflection horizon at

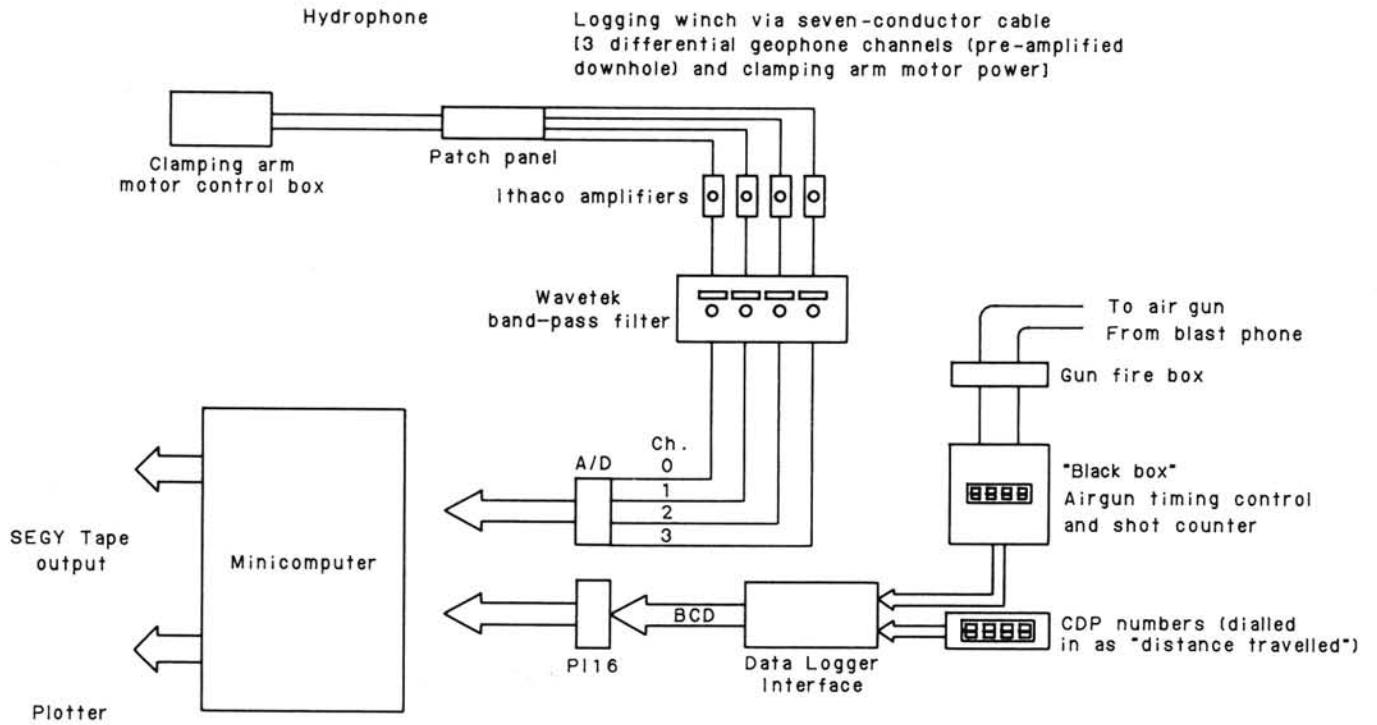
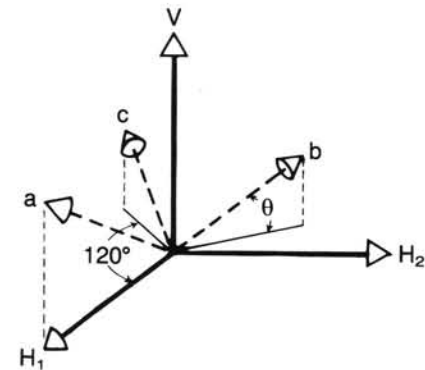


Figure 71. Equipment block diagram for the VSP experiment. The interconnection of the air gun, hydrophone, and shipboard data acquisition equipment used is shown schematically.



$$\begin{bmatrix} H_1 \\ H_2 \\ V \end{bmatrix} = \begin{bmatrix} \cos \theta & -\frac{1}{2} \cos \theta & -\frac{1}{2} \cos \theta \\ 0 & \frac{\sqrt{3}}{2} \cos \theta & -\frac{\sqrt{3}}{2} \cos \theta \\ \sin \theta & \sin \theta & \sin \theta \end{bmatrix} \begin{bmatrix} a \\ b \\ c \end{bmatrix}$$

H_1 = plane of clamping arm

$$\theta = \text{angle of elevation} = \tan^{-1} \left[\frac{\sqrt{2}}{2} \right] = 35.3^\circ$$

a,b,c = recording configuration (a = channel 1)

Figure 72. Matrix transformation to conventional H1, H2, V coordinate system from radial array geophone recording coordinate system.

2.73 s (TWT) as seen in the BFB-1 profile (Fig. 77), it is somewhat later than the strong reflection horizon seen at 2.68 s (TWT) in the BFB-1 profile. No reflection horizons are seen below 2.70 s to correlate with the VSP reflector D_4 .

Conclusion

Vertical seismic profiling is clearly feasible aboard the drill ship *JOIDES Resolution*. High-energy air-gun sources and drill-pipe immobilization techniques were used with multiple-shot summing to achieve adequate signal-to-noise ratio to receive seismic reflection information not only from interfaces penetrated by the drill but also from interfaces below the borehole's total depth. Ultimately, VSP information could prove a boon to the geophysicist for imaging and interpreting the detailed seismic structure of a drill site. At Site 642 we were able to determine the traveltime to the borehole's total depth and to verify that the target horizon, reflector "K," was reached (see Fig. 77). In addition, we correlated major reflection events within the borehole with the core lithology information and the surface seismic profile BFB-1, which located the drill site, and made some preliminary estimates of sub-borehole reflectors.

With a modest enhancement of shipboard computer data-processing capability, quasi-real time, precise VSP information about the rock structure ahead of the drill bit could also provide an invaluable aid for guiding the drilling operations themselves. VSP information could enable us to predict whether a reflecting target has been reached by the bit or estimate how much deeper it may be. To acquire this predictive capability, a post-experiment shipboard computer data-processing system should be developed that includes velocity filtering for wave-field separation, deconvolution, and synthetic seismogram modeling for quantitative analysis of the upgoing reflected wave field.

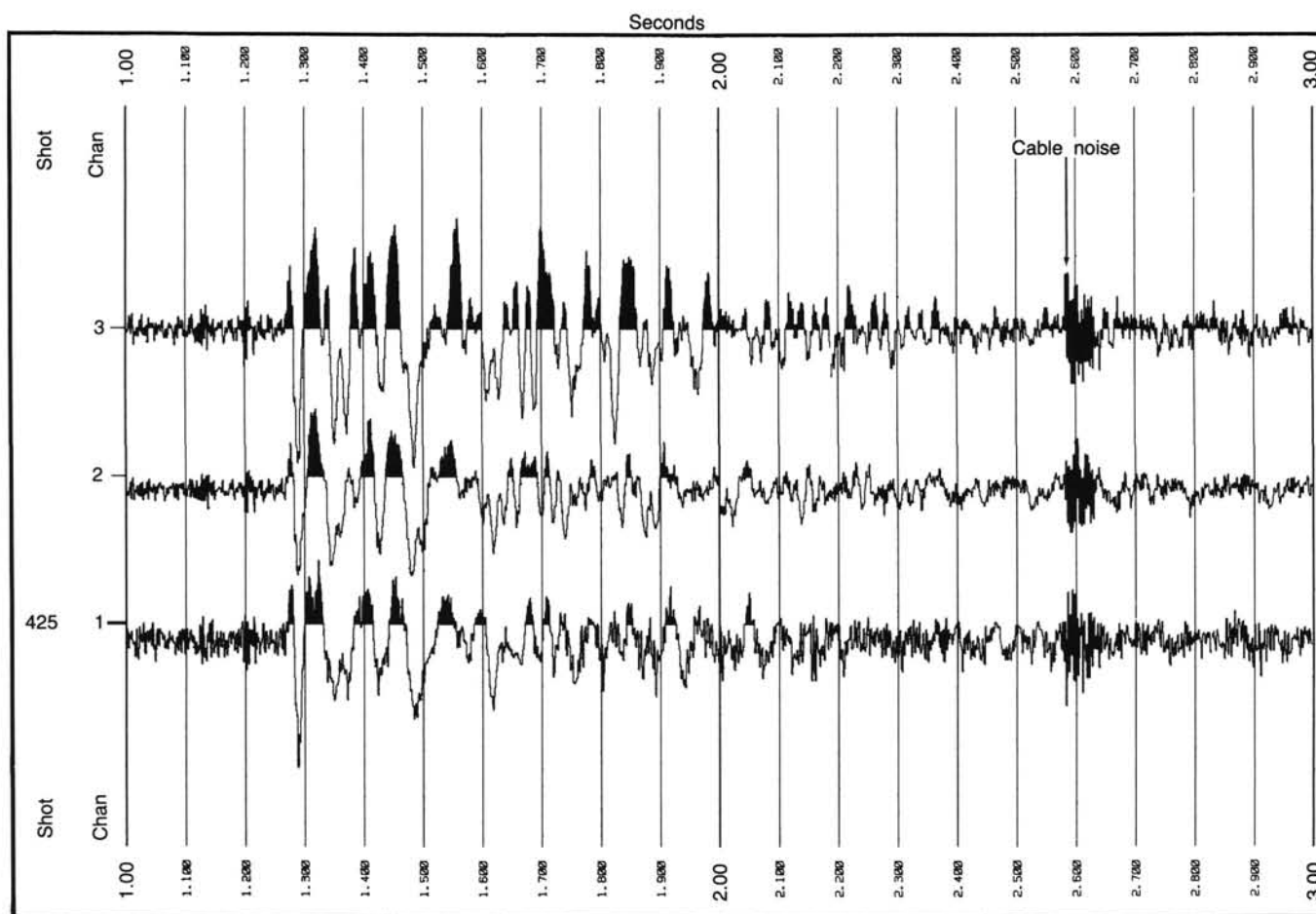


Figure 73. True-amplitude, raw-data seismogram for each of the three components of the radial geophone array configuration for air-gun shot No. 425 at 1096 mbsf.

Acknowledgments

We thank Glen Foss, ODP Operations Superintendent for Leg 104, for his technical advice in designing and carrying out this experiment. Burney Hamlin, Matt Mefferd, and Don Sims were most helpful in deploying the air gun and hydrophone equipment required for the experiment. Dan Larson helped in setting up the underway geophysics laboratory for this experiment. Mike Reitmeyer aided in the preparation of the seismometer tools for deployment. The cooperation and help of the *JOIDES Resolution* rig floor crew and winch and crane operators in deploying the seismometers were most appreciated. Peter Lysne and Colleen Barton contributed many useful discussions and much needed support during the course of the cruise. Also, Forrest Howard of Baker Packers, Houston, originated the drill-pipe immobilization idea for reducing pipe slamming noise and provided a downhole tool for this purpose. Ian McMillan of GECO Inc., Houston, kindly loaned the large-volume air-gun chamber for the experiment. Paul Stoffa, Mark Wieder-spahn, Ali Tafalyli, and Ken Griffiths of UTIG are acknowledged for their expertise and cooperation in developing the HIGHRES/PROCESS computer data acquisition system used in this experiment. Their help was essential.

SITE 642 SEISMIC CORRELATION

Introduction

Acoustically and geologically the area in the vicinity of Site 642 at the outer Vøring Plateau is composed of three main sequences: an upper sedimentary series, overlying a volcanic sequence of seaward-dipping beds, resting on a basal section. The

upper two sequences are separated by a prominent marker reflector, EE, that has been correlated with the top of the early Eocene basalts sampled during DSDP Leg 38 (Talwani, Udintsev, et al., 1976). The top of the basal section is defined by a seismic marker, K. This general division has subsequently been verified by a large number of multichannel seismic profiles as well as the Site 642 drilling results. Hence, we discuss the sequences separately.

The following description is based on multichannel seismic profile BGR-1 (same as BFB-1) on which Site 642 was chosen at shotpoint 1683. However, several other profiles located in the immediate vicinity of the drill site (BGR 76-38, N29, NH-1, B12-81, 162) yield the same seismic pattern with only small differences in the depth to the various reflecting interfaces (Norwegian Sea Working Group, 1984).

The approach to Site 642 was made along line BGR-1. Approximately 10 mi on either side of the site, the ship's speed was slowed down to about 5 kt (Fig. 78), and analog and digital single-channel profiles were recorded. The records do not show much detail, but reflector EE and an interface, A, lying above are easily recognized (Figs. 79 and 80).

The Sedimentary Sequence

In the vicinity of Site 642 the early Eocene basalt surface, EE, and an intrasedimentary reflector, A, just above EE, are the most prominent horizons in the seismic record. Both reflectors can be followed over the entire outer Vøring Plateau. In addi-

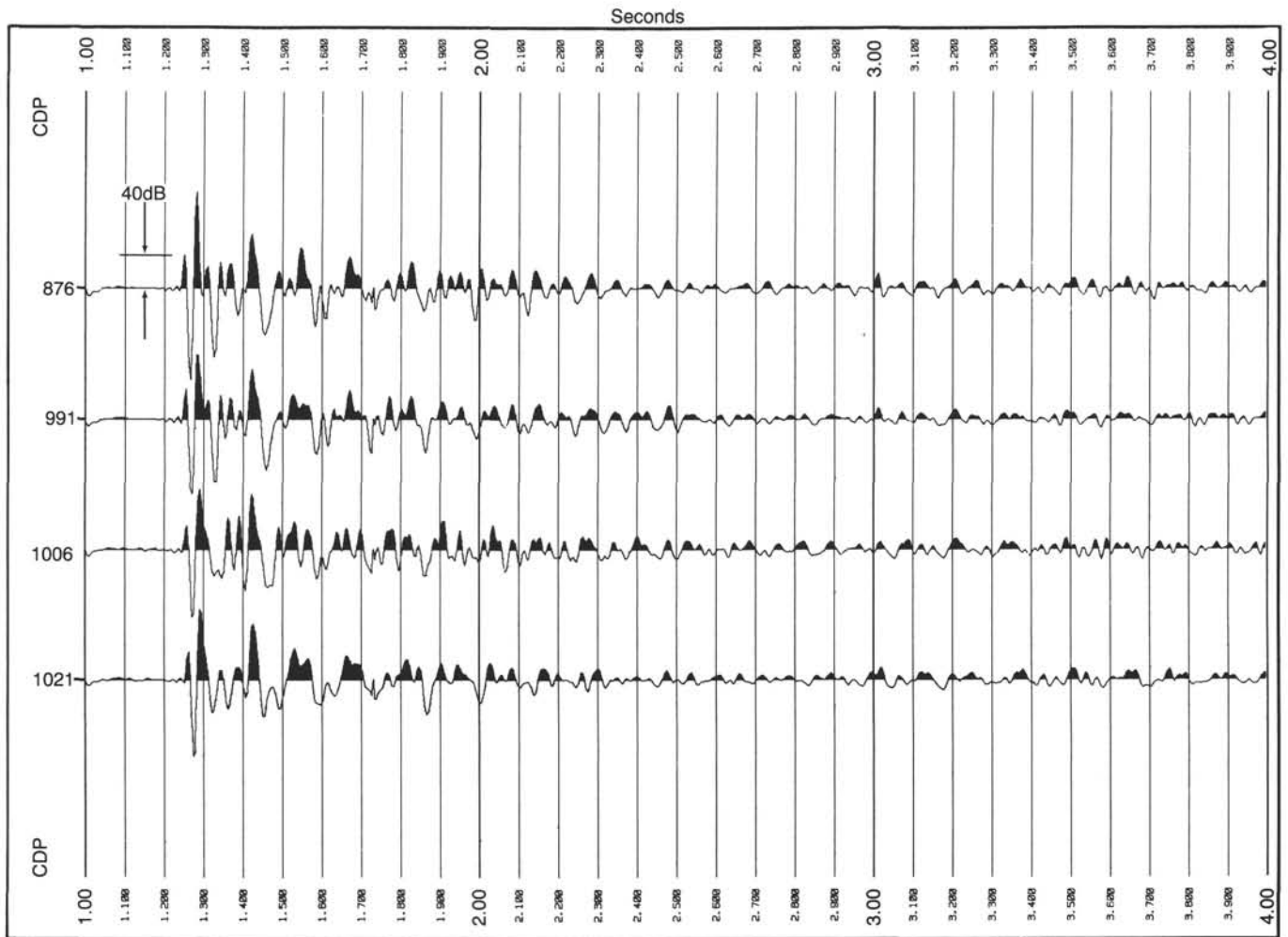


Figure 74. True-amplitude seismograms for geophone no. 1 (clamping arm plane) at sequential seismometer depth positions. Multiple shots have been summed and normalized for each depth. A 5- to 50-Hz band-pass filter has been applied. The signal-to-noise ratio of the initial air gun's direct, downgoing wave relative to the background noise prior to the first break is estimated to be greater than +40 dB.

tion, we have identified two less-distinct horizons above reflector A (Figs. 81 and 82). Reflector A has also been designated "O" by Hinz et al. (1984), a notation that was used by the Norwegian Sea Working Group (1984, unpublished) and in the Leg 104 prospectus (Eldholm et al., 1985). Here, we use the standard reflector nomenclature of Jørgensen and Navrestad (1981) for the shelf and upper slope, later extended to the outer Vøring Plateau by Skogseid (1983). See Figure 12, "Evolution of the Norwegian Continental Margin" chapter, in this volume.

Site 642 confirms that reflector EE originates from the top of the volcanic sequence. It is evident from the physical-property measurements ("Physical Properties" section) that EE owes its prominence to significant increases in both velocity and density at the sediment/volcanic transition.

Owing to its position with respect to EE, we correlate reflector A with an unconformity at 277.6 mbsf. Distinct increases in velocity and density across the unconformity give rise to a clear acoustic impedance contrast (Fig. 59, "Physical Properties" section, this chapter). The sediments above the unconformity are of early Miocene age, thus placing this contact near the assumed base of the Miocene. This result differs from DSDP Leg 38 drilling results at Site 338, which is 120 km to the northeast of Site 642. Caston (1976) placed the main seismic marker at Site 338 to correspond to the change in sediment competency and velocity near the mid-middle Oligocene level. Similarly,

Hinz et al. (1984) and Mutter (1984) identified the reflector as an unconformity of mid-Oligocene age. On the other hand, Skogseid (1983) correlated DSDP data with available information from the landward sedimentary basins, and suggested that the corresponding reflector in line NH-1 (Fig. 11, Chapter 1) was located at the basal Miocene level. Because parts of the pre-A sequence may be absent in areas of shallowing EE, the unconformity forming reflector A could also encompass reflector A' (mid-Oligocene) and earlier Eocene markers locally. Finally, we note that a reevaluation of the Site 338 unconformity, in view of the Site 642 results, suggests that parts of the Oligocene and upper Eocene section may be missing. Thus, the unconformity at Site 338 could indeed be analogous to that of Site 642. A consequence is that the Vøring Marginal High, as well as the Faeroe-Shetland marginal high (Gravdal, 1985), may not have been completely covered by sediments before the earliest Miocene time.

Analysis of sonobuoy profiles has yielded average velocities of 1.78 and 2.25 km/s for the sediments above and below A, respectively (Eldholm and Windisch, 1974). Shipboard analyses during Leg 104, based on the drilled depth to EE, yield a very low average sedimentary velocity, 1.57 km/s, for the entire drilled section. Owing to the small time difference between A and EE and the uncertainty in picking the onset of the low-frequency signals precisely, we have not found it meaningful to estimate a

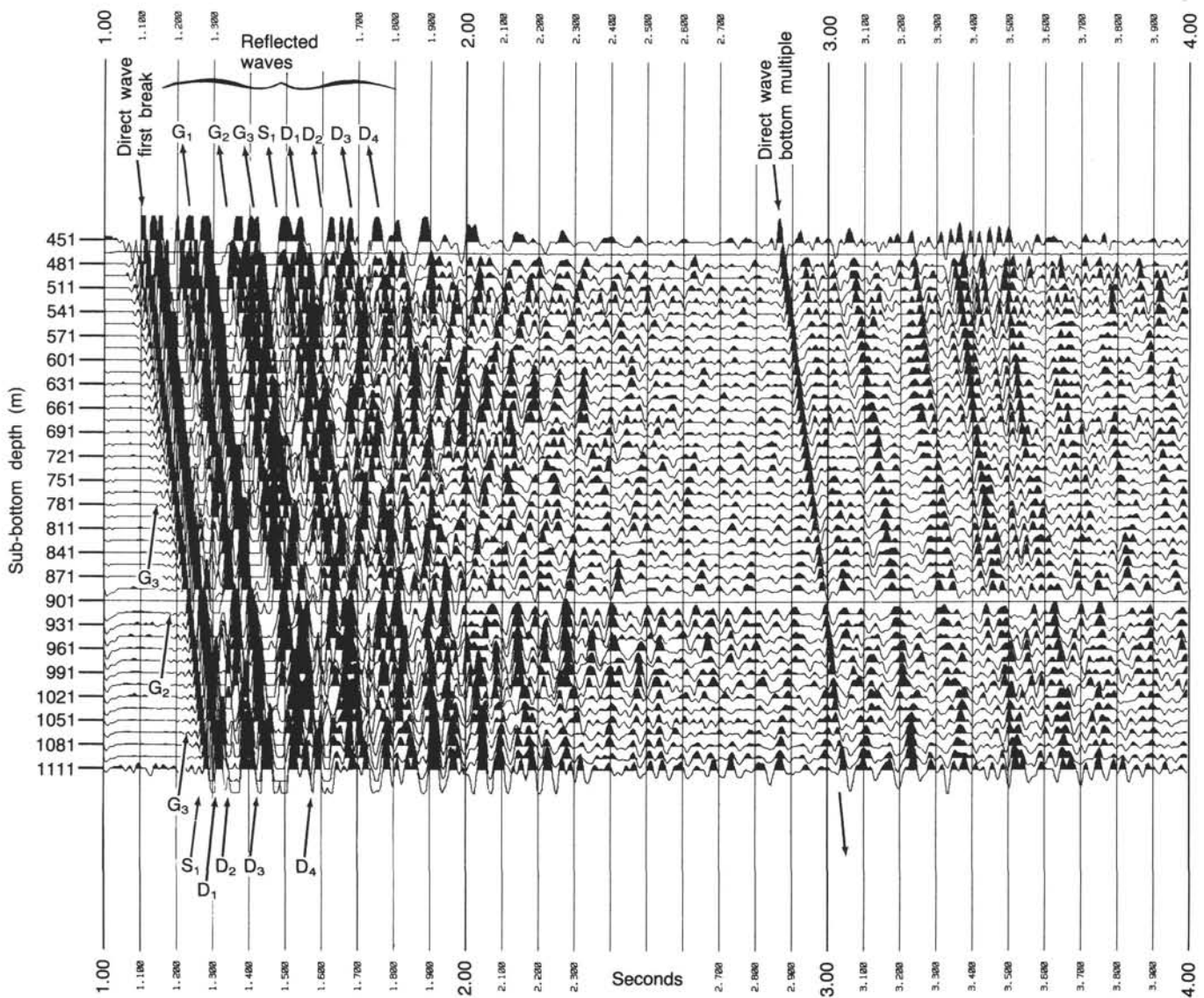


Figure 75. Preliminary stack of VSP seismograms collected at Site 642 for the depth interval 1111–451 mbsf. Multiple shots have been summed and normalized for geophone no. 1 data at each seismometer depth position. The seismometer depth interval is 15 m. A 5- to 50-Hz band-pass filter has been applied. The seismograms have been amplitude-scaled using a time linear gain function. Reflected waves are tentatively identified at the top of the figure: G1–G2 for upper basalt series subgroups I–II bases and tops, respectively. Reflectors G3 and S1 are within subgroup III; reflector S is at the base of subgroup III and corresponds to reflector “K” in the MCS line BFB-1. Reflectors D1–D4 may be related to dikes beneath the basalt layers.

separate interval velocity for the pre-Miocene sediments. Similarly, low compressional wave velocities are measured in the recovered cores (“Physical Properties” section, this chapter). Above reflector A velocities lie between 1.5 and 1.75 km/s, with the highest values occurring in the uppermost 100 m. In the pre-Miocene section the velocities increase somewhat, averaging 2.0 km/s. Although the sonic logging velocities obtained at Site 642 appear to be unreliable, low values are definitely indicated in the interval above 208 mbsf (see “Logging Results” section, this chapter).

In the Neogene section we observe an almost direct correlation of reflectors and acoustic impedance changes. In particular, two of the reflectors show good regional continuity and have been indicated in Figure 81.

The uppermost Neogene reflector is defined at a depth of 91 mbsf, where there is a local increase in the acoustic impedance (Fig. 59). At this level we also observe a pronounced change in sedimentation rates (“Biostratigraphy” section) as well as in

mass accumulation rates (“Sediment Lithology” section). The above changes closely correspond to the transition between lithological Subunits IIA and IIB at the Miocene/Pliocene boundary. We shall, therefore, refer to this marker as the basal Pliocene reflector designated O by Jørgensen and Navrestad (1981).

The lower Neogene reflector is observed at a depth of 196 mbsf, a level that is also recognized by a perturbation in the acoustic impedance curve (Fig. 59). Moreover, the level of the reflector again corresponds to increases in sedimentation and mass accumulation rates. The reflector lies within lithological Unit III at the early/middle Miocene transition. We designate the reflector as basal middle Miocene, O’.

The Volcanic Sequences

The seismic sequence below reflector EE is characterized by a sequence of dipping reflectors overlying a band of high-amplitude, low-frequency reflectors at the base of the dipping layers. The upper seismic sequence exhibits a series of seaward-dipping

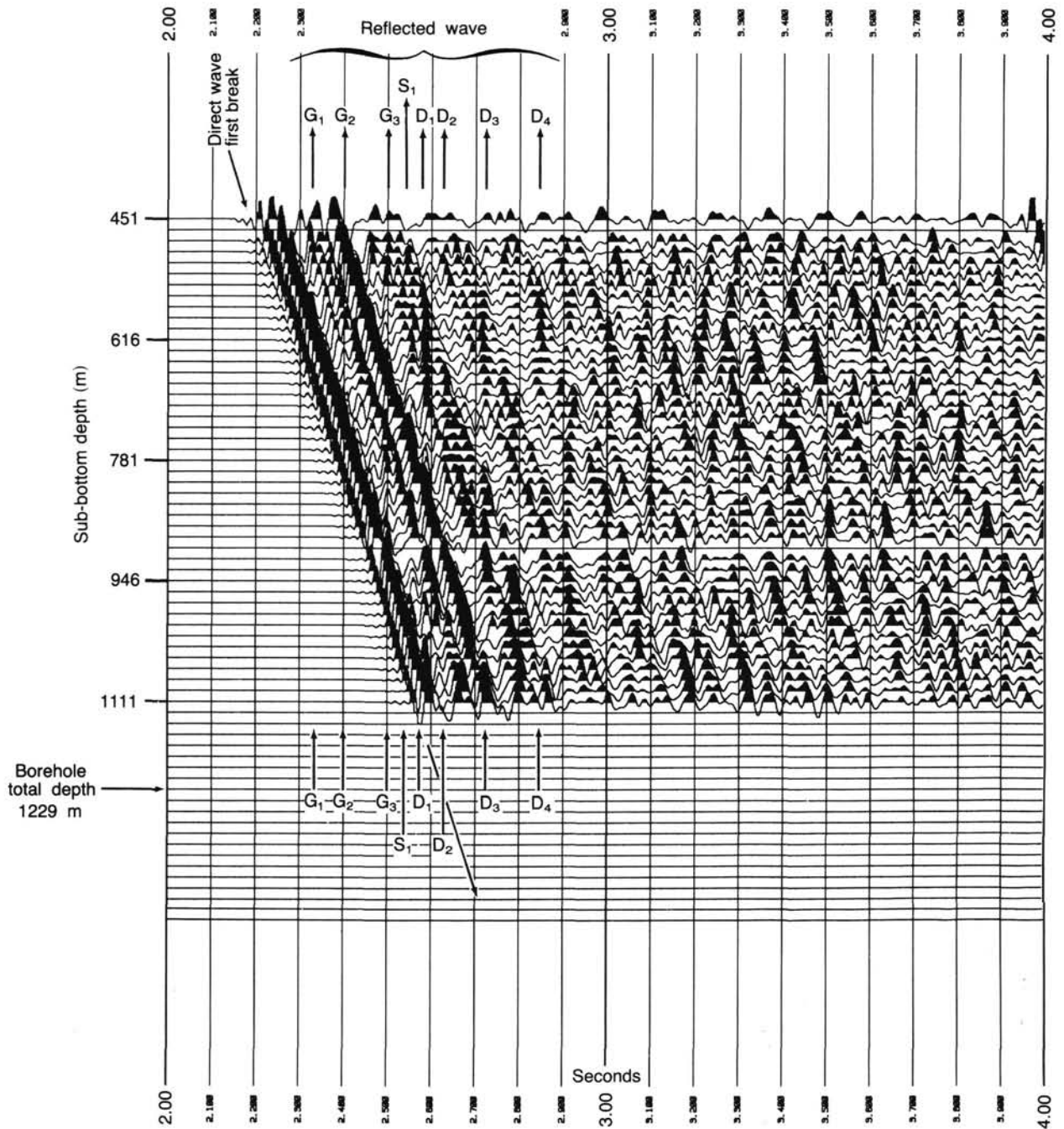


Figure 76. Same preliminary stack of VSP seismograms shown in Figure 75 except time shifted for first break time of downgoing direct wave.

Table 29. Preliminary borehole interval velocity estimates (downgoing waves).

Depth interval (mbsf)	Time interval (m/s)	Lithologic unit	Interval velocity (km/s)
451-1111	1100/1275	Upper basalt series	3.771
451-676	1100/1165	Subgroup I	3.462
676-841	1165/1205	Subgroup II	4.125
841-1111	1205/1275	Subgroup III	3.857

reflectors of poor to moderate continuity. The layers appear to flatten out at the top and in the landward part of the wedge. Acoustically, however, this unit is a direct continuation of the better developed layering observed in the main part of the dipping sequence to the west of Site 642.

The base reflectors consist of an upper strongly reflecting interface onlapping a regionally continuous marker identified as reflector K (see "Evolution of the Norwegian Continental Margin" chapter; Figs. 81 and 82). Just below K there are some additional low-frequency signals which may, in part, originate from reverberations and internal multiples. At the deeper levels the seismic record is largely acoustically unstructured (basement-like).

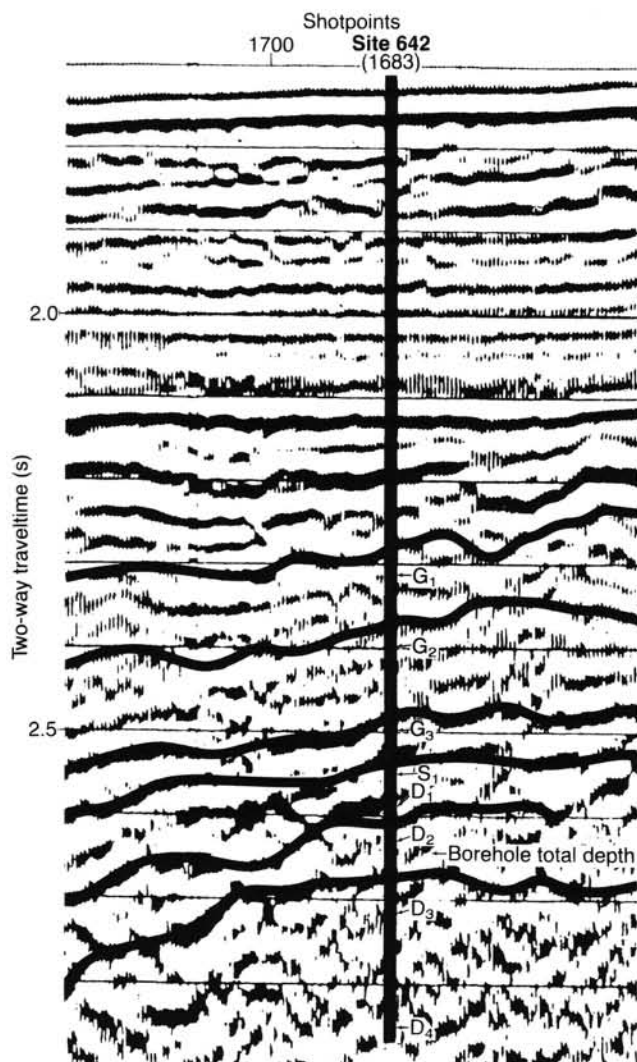


Figure 77. Detail of MCS profile line BFB-1 in Figure 68 showing tentative correlation of VSP reflection events with surface ship seismic reflection horizons. Total depth of drill penetration (T.D.) is shown.

In relating the seismic record to the drilled section, we believe the onset of the low-frequency band of reflectors originates at the top of the tuffaceous unit at about 1090 mbsf, which marks the change from the tholeiitic flows and volcanics above to a sequence of glassy-to-aphanitic flows and interbedded lithified volcanics below. At this level there is also a pronounced change in acoustic impedance (Fig. 61) yielding a reflection coefficient of about -0.30 . A reflection coefficient of such magnitude is expected to produce a prominent reflector in the seismic record. Below this boundary, the drilled section exhibits lower densities and velocities than above, although there is a gentle increase with depth and a local dike shows higher values (Fig. 61). From the interpretation of velocities and densities we expect to have reached the level of reflector K, as defined by Hinz et al. (1984), above the total depth. Thus, we conclude that reflector K lies just below the boundary between the two main volcanic units. This interpretation results in an interval velocity for the dipping sequence of about 4.1 km/s.

Within the dipping sequence there are no prominent reflectors having good continuity. The acoustic impedance log (Fig. 61) reflects a series of events apparently related to the cyclic pattern of homogeneous flows and interbedded volcanics. An exception is the event at about 680 mbsf, which is associated

with a reflector of moderate continuity at a depth of 2.29 s (Fig. 81). This reflector appears to correspond to the contact between volcanic tuffs and fine-grained basalt.

REFERENCES

- Abrahamsen, N., Schoenharting, G., and Heinesen, M., 1984. Paleomagnetism of the Vestmanna core and magnetic age and evolution of the Faeroe Islands. In Berthelsen, O., Noe-Nygaard, A., and Rasmussen, J. (Eds.), *The Deep Drilling Project 1980-1981 in the Faeroe Islands*: Ann. Soc. Sci. Faeroe., Suppl., 9:93-108.
- Aksu, A. E., and Mudie, P. J., 1985a. Late Quaternary stratigraphy and paleoecology of northwest Labrador Sea. *Mar. Micropaleontol.*, 9: 537-557.
- _____, 1985b. A 4-million year Arctic Ocean record dated by magnetostratigraphy and palynology. *Nature*, 318:280-283.
- Archie, G. E., 1942. The electrical resistivity log as an aid in determining source reservoir characteristics. *Pet. Technol.*, 5.
- Backman, J., 1979. Pliocene biostratigraphy of DSDP Sites 111 and 116 from the North Atlantic Ocean and the age of Northern Hemisphere glaciation. *Acta Univ. Stockholm Contrib. Geol.*, 32(3):115-137.
- _____, 1984. Cenozoic calcareous nannofossil biostratigraphy from the northeastern Atlantic Ocean-Deep Sea Drilling Project Leg 81. In Roberts, D. G., Schnitker, D., et al., *Init. Repts. DSDP*, 81: Washington (U.S. Govt. Printing Office), 403-428.
- Backman, J., and Shackleton, N. J., 1983. Quantitative biostratigraphy of Pliocene and early Pleistocene calcareous nannofossils from the Atlantic, Indian, and Pacific oceans. *Mar. Micropaleontol.*, 8:141-170.
- Baldauf, J. G., 1984. Cenozoic diatom biostratigraphy and paleoceanography of the Rockall Plateau region, North Atlantic, Deep Sea Drilling Project Leg 81. In Roberts, D. G., Schnitker, D., et al., *Init. Repts. DSDP*, 81: Washington (U.S. Govt. Printing Office), 439-478.
- Baltes, N., 1971. Pliocene dinoflagellata and acritarcha in Romania. In Farinacci, A. (Ed.), *Proc. Second Planktonic Conf.* (Rome 1970, Edizioni Tecnoscienza), 1:1-16.
- Barron, J. A., 1980. Lower Miocene to Quaternary diatom biostratigraphy of Leg 57, off northeastern Japan. In Langseth, M., Okada, H., et al., *Init. Repts. DSDP*, 56, 57, Pt. 2: Washington (U.S. Govt. Printing Office), 641-685.
- _____, 1981. Late Cenozoic diatom biostratigraphy and paleoceanography of the middle-latitude eastern North Pacific, DSDP Leg 63. In Yeats, R. S., Haq, B. U., et al., *Init. Repts. DSDP*, 63: Washington (U.S. Govt. Printing Office), 507-538.
- _____, 1985a. Miocene to Holocene planktic diatoms. In Saunders, J. B., Bolli, H. M. and Perch-Nielsen, K. (Eds.), *Plankton Stratigraphy*: Cambridge (Cambridge University Press), 763-809.
- _____, 1985b. Late Eocene diatom biostratigraphy of the equatorial Pacific Ocean, DSDP Leg 85. In Mayer, L., Theyer, F., et al., *Init. Repts. DSDP*, 85: Washington (U.S. Govt. Printing Office), 413-455.
- Barron, J. A., and Keller, G., 1983. Paleotemperature oscillations in the middle and late Miocene of the northeastern Pacific. *Micropaleontology*, 29:150-181.
- Barron, J. A., Keller, G., and Dunn, D. A., 1985. A multiple microfossil biochronology for the Miocene. *Geol. Soc. Am. Mem.*, 163:21-36.
- Bass, M. N., 1976. Secondary minerals in oceanic basalts with special reference to Leg 34, Deep Sea Drilling Project. In Yeats, R. S., Hart, S. R., et al., *Init. Repts. DSDP*, 34: Washington (U.S. Govt. Printing Office), 393-432.
- Batten, D. J., 1982. Palynology of the shales associated with the Kap Washington Group volcanics, central north Greenland. *Rapp. Grøn. Geol. Unders.*, 108:15-23.
- Belanger, P. E., and Streeter, S. S., 1980. Distribution and ecology of benthic foraminifera in the Norwegian-Greenland Sea. *Mar. Micropaleontol.*, 5:401-428.
- Berggren, W. A., 1972. Cenozoic biostratigraphy and paleobiogeography of the North Atlantic, In Laughton, A. S., Berggren, W. A., et al., *Init. Repts. DSDP*, 12: Washington (U.S. Govt. Printing Office), 965-1001.
- Berggren, W. A., and Van Couvering, J. A., 1974. The late Neogene. *Palaeogeogr., Palaeoclimat., Palaeoecol.*, 16:1-216.

- Berggren, W. A., Kent, D. V., Flynn, J. J., and Van Couvering, J. A., 1985a. Cenozoic geochronology. *Geol. Soc. Am. Bull.*, 96:1407-1418.
- Berggren, W. A., Kent, D. V., and Flynn, J. J., 1985b. Paleogene geochronology and chronostratigraphy. In Snelling, N. J. (Ed.), *Geochronology and the Geological Record*: Geol. Soc. Spec. Publ. (London).
- Bjørklund, K. R., 1976. Radiolaria from the Norwegian Sea, Leg 38 of the Deep Sea Drilling Project. In Talwani, M., Udintsev, G., et al., *Init. Repts. DSDP*, 38: Washington (U.S. Govt. Printing Office), 1101-1168.
- Bleil, U., Hall, J. M., Johnson, H. P., Levi, S., and Schoenharting, G., 1982. The natural magnetization of a 3-km section of Icelandic crust. *J. Geophys. Res.*, 87:6569-6589.
- Blow, W. H., 1969. Late middle Eocene to Recent planktonic foraminiferal biostratigraphy. In Brönnimann, P., and Renz, H. H. (Eds.), *Proc. First Int. Conf. Planktonic Microfossils (Geneva, 1967)*, 1: 199-421.
- Boltovskoy, E., and Wright, R., 1976. *Recent Foraminifera*: The Hague (Dr. W. Junk BV Publ.).
- Brown, S., and Downie, C., 1984. Dinoflagellate cyst biostratigraphy of late Paleocene and early Eocene sediments from Holes 552, 553A, and 555, DSDP Leg 81, (Rockall Plateau). In Roberts, D. G., Schnitker, D., et al., *Init. Repts. DSDP*, 81: Washington (U.S. Govt. Printing Office), 565-579.
- Bryant, W. R., Bennett, R. H., and Katherman, C. E., 1981. Shear strength, consolidation, porosity, and permeability of oceanic sediments. In Emiliani, C. (Ed.), *The Oceanic Lithosphere, The Sea* (Vol. 7): New York (Wiley), 1555-1616.
- Bujak, J.P., 1984. Cenozoic dinoflagellate cysts and acritarchs from the Bering Sea and northern North Pacific, DSDP Leg 91. *Micropaleontology*, 30:180-212.
- Bukry, E., 1973. Low-latitude coccolith biostratigraphic zonation. In Edgar, N. T., Saunders, J. B., *Init. Repts. DSDP*, 15: Washington (U.S. Govt. Printing Office), 685-703.
- _____, 1981. Synthesis of silicoflagellate stratigraphy for Maastrichtian to Quaternary marine sediment. *SEPM Spec. Publ.*, 32:433-444.
- Burckle, L. H., 1972. Late Cenozoic planktonic diatom zones from the eastern equatorial Pacific. *Nova Hedw., Beihft.*, 39:217-250.
- _____, 1977. Pliocene and Pleistocene diatom datum levels from the equatorial Pacific. *Quat. Res.*, 7:330-340.
- _____, 1978. Early Miocene to Pliocene diatom datum levels for the equatorial Pacific. In *Proc. Second Working Group Meeting, Biostratigraphic Datum-Planes of the Pacific Neogene, IGCP Project 114*: Republic of Indonesia Ministry of Mines and Energy, Directorate General of Mines, Geological Research and Development Center, Spec. Publ., 1:25-44.
- Burckle, L. H., and Opdyke, N. D., 1977. Late Neogene diatom correlations in the circum-Pacific. In *Proc. First Int. Cong. Pacific Neogene Stratigraphy (Tokyo, 1976)*: Tokyo (Kaiyo Shuppan, Ltd.), 255-284.
- Burckle, L. H., and Trainer, J., 1979. Middle and late Pliocene diatom datum levels from the central Pacific. *Micropaleontology*, 25:281-293.
- Burckle, L. H., Keigwin, L. D., and Opdyke, N. D., 1982. Middle and late Miocene stable isotope stratigraphy: Correlation to the paleomagnetic reversal record. *Micropaleontology*, 28:329-334.
- Busen, K. E., and Wise, S. W., Jr., 1977. Silicoflagellate stratigraphy, Deep Sea Drilling Project, Leg 36. In Barker, P. F., Dalziel, I. W. D., et al., *Init. Repts. DSDP*, 36: Washington (U.S. Govt. Printing Office), 697-743.
- Caston, V. N. D., 1976. Tertiary sediments of the Vøring Plateau, Norwegian Sea, recovered by Leg 38 of the Deep Sea Drilling Project. In Talwani, M., Udintsev, G., et al., *Init. Repts. DSDP*, 38: Washington (U.S. Govt. Printing Office), 761-782.
- Ciesielski, P. F., 1975. Biostratigraphy and paleoecology of Neogene and Oligocene silicoflagellates from cores recovered during Antarctic Leg 28, Deep Sea Drilling Project. In Hayes, D. E., Frakes, L. A., et al., *Init. Repts. DSDP*, 28: Washington (U.S. Govt. Printing Office), 625-691.
- _____, 1980. On the age of Neogene deposits at Site 329 (DSDP, Leg 36): Discussion. *Rev. Espan. Micropaleontol.*, 12:87-89.
- _____, 1983. The Neogene and Quaternary diatom biostratigraphy of sub-Antarctic sediments, Deep Sea Drilling Project Leg 71. In Ludwig, W. J., Krashennikov, V. A., et al., *Init. Repts. DSDP*, 71, Pt. 2: Washington (U.S. Govt. Printing Office), 635-665.
- _____, 1986. Middle Miocene to Quaternary diatom biostratigraphy of Deep Sea Drilling Project Site 594, Chatham Rise, southwest Pacific. In Kennett, J. P., von der Borch, C. C., et al., *Init. Repts. DSDP*, 90: Washington (U.S. Govt. Printing Office), 863-885.
- Ciesielski, P. F., Ledbetter, M. T., and Ellwood, B. B., 1982. The development of Antarctic glaciation and the Neogene paleoenvironment of the Maurice Ewing Bank. *Mar. Geol.*, 46:1-51.
- Ciesielski, P. F., and Weaver, F. M., 1983. Neogene and Quaternary paleoenvironmental history of Deep Sea Drilling Project Leg 71 sediments, southwest Atlantic Ocean. In Ludwig, W. J., Krashennikov, V. A., et al., *Init. Repts. DSDP*, 71: Washington (U.S. Govt. Printing Office), 461-477.
- Cita, M. B., and Blow, W. H., 1969. The biostratigraphy of the Langhian, Serravallian, and Tortonian stages in the type sections in Italy. *Riv. Ital. Paleont. Strat.*, 75:549-603.
- Costa, L. I., and Downie, C., 1979. Cenozoic dinocyst stratigraphy of Sites 403 to 406 (Rockall Plateau), IPOD, Leg 48. In Montadert, L., Roberts, D. G., et al., *Init. Repts. DSDP*, 48: Washington (U.S. Govt. Printing Office), 513-529.
- Daniels, C. H. von, and Spiegler, D., 1974. *Bolboforma* n. gen. (Protozoa?)-eine neue stratigraphisch wichtige Gattung aus dem Oligozän/Miozän Nordwestdeutschlands. *Paläontol. Z.*, 48:57-66.
- _____, 1977. *Uvigerina* (Foram.) im Neogen Nordwestdeutschlands (Das Nordwestdeutsche Tertiärbecken, Beitrag Nr. 23). *Geol. Jahrb.*, A, 40:1-59.
- Donn, W. L., and Ninkovitch, D., 1980. Rate of Cenozoic explosive volcanism in the North Atlantic Ocean inferred from deep sea cores. *J. Geophys. Res.*, 85, B10:5455-5460.
- Dresser Atlas, Inc., 1982. *Well Logging and Interpretation Technique*: Houston (Dresser Atlas Industries).
- Drugg, W. S., and Stover, L. E., 1977. Stratigraphic range charts for selected Cenozoic dinoflagellates. *Am. Assoc. Stratig. Palynol. Contrib. Ser.*, 4:73-91.
- Edwards, L. E., 1984. Miocene dinocysts from Deep Sea Drilling Project Leg 81, Rockall Plateau, eastern North Atlantic Ocean. In Roberts, D. G., Schnitker, D., et al., *Init. Repts. DSDP*, 81: Washington (U.S. Govt. Printing Office), 581-594.
- Eide, T., 1985. Dinoflagellatfloraen i øvre Eocen i DSDP 338, Vøring-platået [Cand. Scient. dissert.]. University of Oslo, Oslo.
- Eldholm, O., and Windisch, C. C., 1974. Sediment distribution in the Norwegian-Greenland Sea. *Geol. Soc. Am. Bull.*, 85:1661-1676.
- Eldholm, O., Thiede, J., and Taylor, E., 1985. Leg 104 Scientific Prospectus, ODP, Texas A&M University, College Station.
- Emerson, S., Jahnke, R., Bender, M., Froelich, P., Klinkhammer, G., Bowser, C., and Setlock, G., 1981. Early diagenesis in marine sediments from the eastern equatorial Pacific, Pt. 1: pore water nutrient and carbonate results. *Earth Planet. Sci. Lett.*, 49:57-80.
- Fisher, R. V., and Schmincke, H.-U., 1984. *Pyroclastic Rocks*: New York (Springer-Verlag).
- Flower, M. F. J., Pritchard, R. G., Brem, G., Cann, J. R., Delaney, J., Emmermann, R., Gibson, I. L., Oakley, P. J., Robinson, P. T., and Schmincke, H.-U., 1982. Chemical stratigraphy, Iceland Research Drilling Project, Reydarfjordur, eastern Iceland. *J. Geophys. Res.*, 87, B8:6489-6510.
- Gal'perin, E. I., 1974. *Vertical Seismic Profiling*: SEG Spec. Publ., 12.
- Gebhard, S. N., and Carlson, R. L., 1983. Compressional-wave velocities on basalts from the Rio Grande Rise. In Barker, P. F., Carlson, R. L., Johnson, D. A., et al., *Init. Repts. DSDP*, 72: Washington (U.S. Govt. Printing Office), 577-579.
- Gieskes, J., 1981. Deep sea drilling interstitial water studies: implications for chemical alterations of the oceanic crust, layers I and II. In *The Deep Sea Drilling Project: A Decade of Research*: SEPM Spec. Publ., 32:149-167.
- Gieskes, J. M., Lawrence, J. R., and Galleisky, G., 1978. Interstitial water studies, Leg 38. In Talwani, M., Udintsev, G. et al., *Init. Repts. DSDP*, Suppl. to Vols. 38, 39, 40, 41: Washington (U.S. Govt. Printing Office), 121-133.
- Gieskes, J., and Peretsman, G., 1986. *Water-chemistry procedures aboard JOIDES Resolution-some comments*: ODP Tech. Note, 5.
- Goll, R. M., and Bjørklund, K. R., 1980. The evolution of *Eucoronis friditjofnanseni*, n. sp., and its application to the Neogene biostratigraphy

- raphy of the Norwegian–Greenland Sea. *Micropaleontology*, 26: 356–371.
- Gombos, A. M., 1980. The early history of the diatom family Astero-lampraceae. *Bacillaria*, 3:227–272.
- , 1982. Early and middle Eocene diatom evolutionary events. *Bacillaria*, 5:225–242.
- Gombos, A. M., and Ciesielski, P. F., 1983. Late Eocene to early Miocene diatoms from the southwest Atlantic. In Ludwig, W. J., Krashennikov, V. A., et al., *Init. Repts. DSDP*, 71, Pt. 2: Washington (U.S. Govt. Printing Office), 583–634.
- Goodman, D. K., and Ford, L. N., Jr., 1980. Preliminary dinoflagellate biostratigraphy for the middle Eocene to lower Oligocene from the southwest Atlantic Ocean. In Ludwig, W. I., Krashennikov, V. A., et al., *Init. Repts. DSDP*, 71, Pt. 2: Washington, (U.S. Govt. Printing Office), 859–877.
- Gravdal, N., 1985. The Møre Basin [Cand. Scient. thesis]. University of Oslo, Oslo.
- Grivelet, P., 1985. Inversion of vertical seismic profiles by interactive modelling. *Geophysics*, 50:924–930.
- Hagevang, T., Eldholm, O., and Aalstad, I., 1982. Pre-23 magnetic anomalies between Jan Mayen and Greenland–Senja Fracture zones in the Norwegian Sea. *Mar. Geophys. Res.*, 5:345–364.
- Hamilton, E. L., 1976. Variations of density and porosity with depth in deep-sea sediments. *J. Sed. Pet.*, 46:280–300.
- Harland, R., 1979. Dinoflagellate biostratigraphy of Neogene and Quaternary sediments at Holes 400/400A in the Bay of Biscay (Deep Sea Drilling Project Leg 48). In Montadert, L., Roberts, D. G., et al., *Init. Repts. DSDP*, 48: Washington (U.S. Govt. Printing Office), 531–545.
- , 1983. Distribution maps of recent dinoflagellate cysts in bottom sediments from the North Atlantic Ocean and adjacent seas. *Palaeontology*, 26:321–387.
- , 1984a. Recent and late Quaternary dinoflagellate cysts from the area of the Greenland–Iceland–Faeroe–Scotland Ridge. *J. Micro-paleontol.*, 3:95–108.
- , 1984b. Quaternary dinoflagellate cysts from Hole 552A, Rockall Plateau, Deep Sea Drilling Project Leg 81. In Roberts, D. G., Schnitker, D., et al., *Init. Rept. DSDP*, 81: Washington (U.S. Govt. Printing Office), 541–546.
- Harland, W. B., Cox, A. V., Llewellyn, P. G., Pickton, C. A. G., Smith, A. G., and Walters, R., 1982. *A Geologic Time Scale*: Cambridge (Cambridge University Press).
- Harrison, R. K., Knox, R. W. O'B., and Morton, A. C., 1979. Petrography and mineralogy of volcanogenic sediments from DSDP Leg 48, southwest Rockall Plateau, Sites 403 and 404. In Montadert, L., Roberts, D. G., et al., *Init. Repts. DSDP*, 48: Washington (U.S. Govt. Printing Office), 771–783.
- Hill, K. J., LaBrecque, J. A., et al., 1984. Numerical ages of Cenozoic biostratigraphic datum levels: results of South Atlantic Leg 73 drilling. *Geol. Soc. Am. Bull.*, 95:863–876.
- Hill, R. R., Mudie, P. J., Moran, K., and Blasco, S. M., 1985. A sea-level curve for the Canadian Beaufort Shelf. *Canad. J. Earth Sci.*, 22:1383–1393.
- Hinz, K., 1981. A hypothesis on terrestrial catastrophes, wedges of very thick oceanward dipping layers beneath passive continental margins—their origin and paleoenvironmental significance. *Geol. Jahrb.*, 22: 2–28.
- Hinz, K., Dostman, H. J., and Hanisch, J., 1984. Structural elements of the Norwegian continental margin. *Geol. Jahrb.*, A75:193–211.
- Hooper, P. W. P., and Weaver, P. P. E., in press. Late Neogene species of the genus *Neoglobobadrina* Bandy, Fredrichs, and Vincent in the North Atlantic: a biostratigraphic, paleoceanographic, and phylogenetic review. *Mar. Micropaleontol.*
- Hsü, K. J., LaBrecque, J. A., et al., 1984. Numerical ages of Cenozoic biostratigraphic datum levels: results of South Atlantic Leg 73 drilling. *Geol. Soc. Am. Bull.*, 95:863–876.
- Huddleston, P. F., 1984. Planktonic foraminiferal biostratigraphy, Deep Sea Drilling Project Leg 81. In Roberts, R. G., and Schnitker, D., et al., *Init. Repts. DSDP*, 81: Washington (U.S. Govt. Printing Office), 429–438.
- Jan du Chêne, R., 1977. Étude palynologique du Miocène supérieur Andalou (Espagne). *Rev. Espan. Micropaleontol.*, 9:97–114.
- Jørgensen, R., and Navrestad, T., 1981. The geology of the Norwegian Shelf between 62°N and the Lofoten Islands. In Illing, L. V., and Hobson, G. D. (Eds.), *Petroleum Geology of the Continental Shelf of Northwest Europe*: London (Institute of Petroleum), 407–413.
- Kellogg, T. B., Duplessy, J. D., and Shackleton, N. J., 1978. Planktonic foraminiferal and isotopic stratigraphy and paleoclimatology of Norwegian Sea deep-sea cores. *Boreas*, 7:61–73.
- Kennett, J. P., 1973. Middle and Late Cenozoic planktonic foraminiferal biostratigraphy of the southwest Pacific—DSDP Leg 21. In Burns, R. E., Andrews, J. E., et al., *Init. Repts. DSDP*, 21: Washington (U.S. Govt. Printing Office), 575–640.
- Kennett, J. P., and Srinivasan, M. S., 1981. Surface ultrastructural variation in *Neoglobobadrina pachyderma* (Ehrenberg): phenotypic variation and phylogeny in the late Cenozoic. In Sliter, W. V. (Ed.), *Studies in Marine Micropaleontology: A Memorial Volume to Orville L. Bandy*: Cushman Found. Foram. Res. Spec. Publ., 19:134–162.
- , 1983. *Neogene Planktonic Foraminifera: A Phylogenetic Atlas*: Stroudsburg, PA (Hutchinson Ross).
- King, C., 1983. Cenozoic micropaleontological biostratigraphy of the North Sea. *Rept. Inst. Geol. Sci. London*, 82(7):1–40.
- Knox, R. W. O., and Morton, A. C., 1983. Stratigraphical distribution of early Paleogene pyroclastic deposits in the North Sea Basin. *Proc. Yorkshire Geol. Soc.*, 44:355–363.
- Koizumi, I., 1973. The late Cenozoic diatoms of Sites 183–193, Leg 19, Deep Sea Drilling Project. In Creager, J. S., Scholl, D. W., et al., *Init. Repts. DSDP*, 19: Washington (U.S. Govt. Printing Office), 805–855.
- , 1977. Diatom biostratigraphy in the North Pacific region. *Proc. First Congr. Pacific Neogene Stratigraphy*: Tokyo (Kaiyo Shuppan, Ltd.), 235–253.
- Koreneva, E. V., Zaklinskaya, E. D., Bratseva, G. M., and Kartashova, G. G., 1976. Palynology studies of Sites 336, 338, 346, and 348, DSDP Leg 38. In Talwani, M., Udintsev, G., et al., *Init. Repts. DSDP*, 38: Washington (U.S. Govt. Printing Office), 1169–1193.
- Kvenvolden, K. A., and McDonald, T. J., 1986. *Organic Geochemistry on the JOIDES Resolution—an assay*: ODP Tech. Note, 6.
- LaBrecque, J. L., Hsü, K. J., et al., 1983. DSDP Leg 73: Contributions to Paleogene stratigraphy in nomenclature, chronology and sedimentation rates. *Palaeogeogr., Palaeoclimat., Palaeoecol.*, 42:91–125.
- Larsen, L. M., and Watt, W. S., 1985. Episodic volcanism during breakup of the North Atlantic: evidence from the east Greenland Plateau basalts. *Earth Planet. Sci. Lett.*, 73:105–116.
- Ledbetter, M. T., and Ciesielski, P. F., 1986. Post-Miocene disconformities and paleoceanography in the Atlantic sector of the Southern Ocean. *Palaeogeogr., Palaeoclimatol., Palaeoecol.*, 52:185–214.
- Lee, M. W., and Balch, A. H., 1983. Computer processing of vertical seismic profile data. *Geophysics*, 48:272–287.
- Leopold, E. B., 1969. Late Cenozoic palynology. In Tschudy, R. H., and Scott, R. A. (Eds.), *Aspects of Palynology*: New York (Wiley), 377–438.
- Lysne, P., Anderson, R., and Moos, D., 1985. Sandia Laboratories Rept., Albuquerque, NM.
- Mangerud, J., Lie, S. E., Furnes, H., Kristiansen, I. L., and Lømo, L., 1984. A Younger Dryas ash bed in western Norway and its possible correlations with tephra in cores from the Norwegian Sea and the North Atlantic. *Quat. Res.*, 21:85–104.
- Manum, S. B., 1962. Studies in the Tertiary flora of Spitsbergen, with notes on the Tertiary floras of Ellesmere Island, Greenland and Iceland. *Nor. Polarinst. Skri.*, 125:1–127.
- , 1976. Dinocysts in Tertiary Norwegian–Greenland Sea sediments (Deep Sea Drilling Project Leg 38) with observations on palynomorphs and palynodebris in relation to environment. In Talwani, M., Udintsev, G., et al., *Init. Repts. DSDP*, 38: Washington (U.S. Govt. Printing Office), 897–919.
- , 1979. Two new Tertiary dinocyst genera from the Norwegian Sea: *Lophocysta* and *Evittosphaerula*. *Rev. Palaeobotan. and Palynol.*, 28:237–248.
- Martini, E., 1971. Standard Tertiary and Quaternary calcareous nannoplankton zonation: *Proc. Second Planktonic Conf.* (Rome, 1970), *Edizioni Tecnoscienza*, 2:739–785.
- , 1972. Silicoflagellate zones in the late Oligocene and early Miocene of Europe. *Senckenbergiana lethaea*, 53:119–122.

- _____, 1979. Calcareous nannoplankton and silicoflagellate biostratigraphy at Reykjanes Ridge, northeastern North Atlantic (DSDP Leg 49, Sites 407 and 409). In Luyendyk, B. P., Cann, J. R., et al., *Init. Repts. DSDP*, 49: Washington (U.S. Govt. Printing Office), 533-549.
- Martini, E., and Müller, C., 1976. Eocene to Pleistocene silicoflagellates from the Norwegian-Greenland Sea (DSDP Leg 38). In Talwani, M., Udintsev, G., et al., *Init. Repts. DSDP*, 38: Washington (U.S. Govt. Printing Office), 857-895.
- Miller, A. A. L., Mudie, P. J., and Scott, D. B., 1982. Holocene history of Bedford Basin, Nova Scotia: foraminifera, dinoflagellate, and pollen records. *Canad. J. Earth Sci.*, 19:2342-2367.
- Miller, K. G., Aubry, M. P., Khan, M. J., Melillo, A. J., Kent, D. V., and Berggren, W. A., 1985. Oligocene-Miocene bio-, magneto-, and isotopic stratigraphy of the western North Atlantic. *Geology*, 13: 257-261.
- Mons, R., and Babour, K., 1981. *Vertical Seismic Profiling*. Schlumberger Wireline Atlantic-Marketing Geophysics, vol. SMP-1108.
- Mudie, P. J., 1982. Palynology of late Quaternary marine sediments, eastern Canada. *Canad. J. Earth Sci.*, 19:729-747.
- _____, 1985. Palynology of the CESAR cores, Arctic Ocean. In Jackson, H. R., Mudie, P. J., and Blasco, S. M. (Eds.), *Init. Results of Geological Studies of CESAR, Canadian Expedition to Survey Alpha Ridge*: Geol. Surv. Canad. Rep., 84-22, 149-174.
- _____, 1987. Palynology and dinoflagellate biostratigraphy of DSDP Leg 94, Sites 607 and 611, North Atlantic Ocean. In Ruddiman, W. T., Kidd, R., et al., *Init. Repts. DSDP*, 94: Washington (U.S. Govt. Printing Office), 785-812.
- Mudie, P. J., and Aksu, A. E., 1984. Paleoclimate of Baffin Bay from 300,000-year record of foraminifera, dinoflagellates, and pollen. *Nature*, 312:630-634.
- Mudie, P. J., and Helgason, J., 1982. Palynological evidence for Miocene climatic cooling in eastern Iceland about 9.8 m.y. ago. *Nature*, 303:689-692.
- Mudie, P. J., and Short, S. K., 1985. Marine palynology of Baffin Bay. In Andrews, J. T. (Ed.), *Environments: eastern Canadian Arctic, Baffin Bay and West Greenland*: Boston (Allen and Unwin), 263-308.
- Müller, C., 1976. Tertiary and Quaternary calcareous nannoplankton in the Norwegian-Greenland Sea, DSDP Leg 38. In Talwani, M., Udintsev, G., et al., *Init. Repts. DSDP*, 38: Washington (U.S. Govt. Printing Office), 823-841.
- Murray, J. W., 1979. Cenozoic biostratigraphy and paleoecology of Sites 403 to 406 based on the foraminifera. In Montadert, L., Roberts, D. G., et al., *Init. Repts. DSDP*, 48: Washington (U.S. Govt. Printing Office), 415-430.
- _____, 1984. Biostratigraphic value of *Bolboforma*, Leg 81, Rockall Plateau. In Roberts, D. G., Schnitker, D., et al., *Init. Repts. DSDP*, 81: Washington (U.S. Govt. Printing Office), 535-539.
- Mutter, J. C., 1984. Cenozoic and late Mesozoic stratigraphy and subsidence history of the Norwegian Margin. *Geol. Soc. Am. Bull.*, 95: 1135-1149.
- Mutter, J. C., Talwani, M., and Stoffa, P. L., 1982. Origin of seaward dipping reflectors in oceanic crust off the Norwegian Margin by "subaerial seafloor spreading." *Geology*, 10:353-357.
- _____, 1984. Evidence for a thick oceanic crust adjacent to the Norwegian margin. *J. Geophys. Res.*, 89:483-502.
- Nilsen, T. H., and Kerr, D. R., 1978. Turbidites, redbeds, sedimentary structures, and trace fossils observed in DSDP Leg 38 cores and the sedimentary history of the Norwegian-Greenland Sea. In Talwani, M., Udintsev, G., et al., *Init. Repts. DSDP*, Suppl. to Vols. 38, 39, 40, and 41: Washington (U.S. Govt. Printing Office), 259-288.
- Noe-Nygaard, A., 1974. Cenozoic to Recent volcanism in and around the North Atlantic basin. In Nairn, A. E. M., and Stehli, F. G. (Eds.), *The Ocean Basins and Margins*, Vol. 2, North Atlantic: New York (Plenum), 391-443.
- Norris, G., 1982. Spore-pollen evidence for early Oligocene high-latitude cool climatic episode in northern Canada. *Nature*, 297:387-389.
- Osborn, N. I., Ciesielski, P. F., and Ledbetter, M. T., 1983. Disconformities and paleoceanography in the Southwest Indian Ocean during the last 5.4 million years. *Geol. Soc. Am. Bull.*, 94:1345-1358.
- Perch-Nielsen, R., 1976. Eocene to Pliocene archeomonads, ebridians, and endoskeletal dinoflagellates from the Norwegian Sea, DSDP Leg 38. In Talwani, M., Udintsev, G., et al., *Init. Repts. DSDP*, Suppl. to Vols. 38, 39, 40, and 41: Washington (U.S. Govt. Printing Office), 147-175.
- Piasecki, S., 1980. Dinoflagellate cyst stratigraphy of the Miocene Hode and Gram formations, Denmark. *Bull. Geol. Soc. Denmark*, 29:53-76.
- Poore, R. Z., 1979. Oligocene through Quaternary planktonic foraminiferal biostratigraphy of the North Atlantic: DSDP Leg 49. In Luyendyk, B. P., Cann, J. R., et al., *Init. Repts. DSDP*, 49: Washington (U.S. Govt. Printing Office), 447-517.
- Poore, R. Z., and Berggren, W. A., 1975. Late Cenozoic planktonic foraminiferal biostratigraphy and paleoclimatology of Hatton-Rockall Basin, DSDP Site 116. *J. Foram. Res.*, 5:270-293.
- Poore, R. Z., Tauxe, L., Percival, S. F., LaBrecque, J. L., Wright, R., Peterson, N., Smith, C. L., Tucker, P., and Hsü, K., 1983. Late Cretaceous-Cenozoic magnetostratigraphy and biostratigraphy correlations of the South Atlantic Ocean, DSDP Leg 73. *Palaeogeogr., Palaeoclimat., Palaeoecol.*, 42:127-149.
- Poster, D. K., 1983. Interpretation aspects of offshore VSP data [paper presented at the 15th Annual Offshore Technology Conference, Houston, TX].
- Qvale, G., 1985. Distribution of benthic foraminifera along the Norwegian continental margin [Dr. Scient. thesis]. University of Oslo, Oslo.
- Roberts, D. G., Backman, J., Morton, A. C., Murray, J. W., and Keene, J. B., 1984. Evolution of volcanic rifted margins: synthesis of Leg 81 results on the west margin of Rockall Plateau. In Roberts, D. G., Schnitker, D., et al., *Init. Repts. DSDP*, 81: Washington (U.S. Govt. Printing Office), 883-911.
- Roberts, D. G., Schnitker, D., et al., 1984. *Init. Repts. DSDP*, 81: Washington (U.S. Govt. Printing Office).
- Rögl, F., and Hochuli, P., 1976. The occurrence of *Bolboforma*, a probable algal cyst, in the Antarctic Miocene of DSDP Leg 35. In Hollister, C. D., Craddock, C., et al., *Init. Repts. DSDP*, 35: Washington (U.S. Govt. Printing Office), 713-719.
- Rögl, F., and Steininger, F. F., 1984. Neogene paratethys, Mediterranean and Indopacific seaways. In Brenchley, P. (Ed.), *Fossils and Climate*: New York (Wiley), 171-200.
- Roth, P. H., and Thierstein, H. R., 1972. Calcareous nannoplankton: Leg 14 of the Deep Sea Drilling Project. In Hayes, D. E., Pimm, A. C., et al., *Init. Repts. DSDP*, 14: Washington (U.S. Govt. Printing Office), 421-485.
- Ryan, W. B. F., Cita, M. B., Rawson, M., Dreyfus Rawson, M., Burckle, L. H., and Saito, T., 1974. A paleomagnetic assignment of Neogene stage boundaries and the development of isochronous datum planes between the Mediterranean, Pacific, and Indian oceans in order to investigate the response of the world ocean to the Mediterranean "salinity crisis." *Riv. Ital. Paleontol.*, 80:631-688.
- Schaftenaar, C. H., Moore, R. P., and Carlson, R. L., 1983. Summary of shipboard physical properties of mudstones, carbonates, and clastic sediments, Deep Sea Drilling Project, Leg 72. In Barker, P. F., Carlson, R. L., Johnson, D. A., et al., *Init. Repts. DSDP*, 72: Washington (U.S. Govt. Printing Office), 551-564.
- Schoenharth, G., and Ghisler, M., 1982. Zones of polarity reversal of stable remanent magnetization within some basaltic flows of the Iceland Research Drilling Project core. *J. Geophys. Res.*, 87:6591-6600.
- Schrader, H. J., Björklund, K. R., Manum, S., Martini, E., and Van Hinte, J., 1976. Cenozoic biostratigraphy, physical stratigraphy and paleoceanography in the Norwegian-Greenland Sea, DSDP Leg 38 paleontological synthesis. In Talwani, M., Udintsev, G., et al., *Init. Repts. DSDP*, 38: Washington (U.S. Govt. Printing Office), 1197-1211.
- Schrader, H. J., and Fenner, J., 1976. Norwegian Sea Cenozoic diatom biostratigraphy and taxonomy. In Talwani, M., Udintsev, G., et al., *Init. Repts. DSDP*, 38: Washington (U.S. Govt. Printing Office), 921-1099.
- Seeman, B., and Horowitz, L., 1983. Vertical seismic profiling: Separation of upgoing and downgoing acoustic waves in a stratified medium. *Geophysics*, 48:555-568.
- Sejrup, H.-P., Fjaeran, T., Hald, M., Beck, L., Hagen, J., Miljeteig, I., Morvik, I., and Norvik, O., 1981. Benthonic foraminifera in surface samples from the Norwegian continental margin between 62° and 65° N. *J. Foram. Res.*, 11:277-295.
- Shackleton, N. J., and Kennett, J. P., 1975. Paleotemperature history of the Cenozoic and the initiation of Antarctic glaciation: oxygen and

- carbon isotope analysis in DSDP Sites 277, 279 and 281. *In* Kennett, J. P., Houtz, R. E., et al., *Init. Repts. DSDP*, 29: Washington (U.S. Govt. Printing Office), 743-755.
- Shackleton, N. J., Backman, J., et al., 1984. Oxygen isotope calibration of the onset of ice-rafting and history of glaciation in the North Atlantic region. *Nature*, 307:620-623.
- Shaw, C. A., and Ciesielski, P. F., 1983. Silicoflagellate biostratigraphy of middle Eocene to Holocene sub-Antarctic sediments recovered by Deep Sea Drilling Project Leg 71. *In* Ludwig, W. J., Krashennikov, V. A., et al., *Init. Repts. DSDP*, 71: Washington (U.S. Govt. Printing Office), 687-737.
- Sibson, R. H., 1977. Fault rocks and mechanisms. *J. Geol. Soc. London*, 135:191-213.
- Skempton, A. W., 1970. The consolidation of clays by gravitational compaction. *J. Geol. Soc. London*, 125:373-411.
- Skogseid, J., 1983. A marine geophysical study of profiles between the Vøring Plateau margin and the Jan Mayen Ridge [Cand. Scient. thesis]. University of Oslo, Oslo.
- Soper, N. J., and Costa, L. I., 1976. Palynological evidence for the age of Tertiary basalts and post-basaltic sediments at Kap Dalton, central east Greenland. *Rapp. Groenl. Geol. Unders.*, 80:123-127.
- Soper, N. J., Downie, C., Higgins, A. C., and Costa, L. I., 1976. Biostratigraphic ages of Tertiary basalts on the east Greenland continental margin and their relationship to plate separation in the northeast Atlantic. *Earth Planet. Sci. Lett.*, 32:149-157.
- Stakes, D. S., and Scheidegger, K. G., 1981. Temporal variations in secondary minerals from Nazca Plate basalts, diabbases, and microgabros. *Geol. Soc. Am. Mem.*, 154:109-130.
- Streeter, S. S., Belanger, P. E., Kellogg, T. B., and Duplessy, J. C., 1982. Late Pleistocene oceanography of the Norwegian-Greenland Sea: benthic foraminiferal evidence. *Quat. Res.*, 18:72-90.
- Suc, J.-P., and Zagwijn, W. H., 1983. Plio-Pleistocene correlations between the northwestern Mediterranean region and northwestern Europe according to recent biostratigraphic and paleoclimatic data. *Boreas*, 12:153-166.
- Sylvester, A. G., 1978. Petrography of volcanic ashes in deep-sea cores near Jan-Mayen Island: Sites 338, 345-350, DSDP Leg 38. *In* Talwani, M., Udintsev, G., et al., *Init. Repts. DSDP*, Suppl. to Vols. 38, 39, 40, and 41: Washington (U.S. Govt. Printing Office), 101-109.
- Talwani, M., Udintsev, G., et al., 1976. Sites 338-343. *In* Talwani, M., Udintsev, G., et al., *Init. Repts. DSDP*, 38: Washington (U.S. Govt. Printing Office), 151-388.
- Tauxe, L., Monaghan, M., Drake, R., Curtis, G., and Staudigel, H., 1985. Paleomagnetism of Miocene East African Rift sediments and the calibration of the geomagnetic reversal time scale. *J. Geophys. Res.*, 90:4639-4646.
- Tauxe, L., Opdyke, N. D., Pasini, G., and Elmi, L., 1983. The age of the Plio/Pleistocene boundary at Vrica (southern Italy). *Nature*, 304:125-129.
- Tauxe, L., Tucker, P., Peterson, N., and LaBrecque, J., 1984a. The magnetostratigraphy of Leg 73 sediments. *Palaeogeogr., Palaeoclimat., Palaeoecol.*, 42:65-90.
- , 1984b. Magnetostratigraphy of Leg 73 sediments. *In* Hsü, K. J., LaBrecque, J. L., et al., *Init. Repts. DSDP*, 73: Washington (U.S. Govt. Printing Office), 609-621.
- Thiede, J., 1980. Paleo-oceanography, margin stratigraphy and paleo-physiography of the Tertiary North Atlantic and Norwegian-Greenland Seas. *Phil. Trans. R. Soc. London.*, A294:177-185.
- Thorarinsson, S., 1967. The eruption of Hekla 1947-48. I. The eruptions of Hekla in historical times. A tephrochronological study. *Vísindafélag Íslendinga*, Reykjavik:1-183.
- , 1981. Tephra studies and tephrochronology: A historical review with special reference to Iceland. *In* Self, S., and Sparks, R. S. J., (Eds.), *Tephra Studies*: Dordrecht (D. Reidel), 1-12.
- Tissot, B. P., and Welte, D. H., 1984. *Petroleum Formation and Occurrence* (2nd ed.): Berlin (Springer-Verlag).
- Varet, J., and Metrich, N., 1978. Ash layers interlayered with the sediments of Holes 407 and 408, IPOD Leg 49. *In* Luyendyk, B. P., Cann, J. R., et al., *Init. Repts. DSDP*, 49: Washington (U.S. Govt. Printing Office), 437-441.
- Warnke, D. A., 1982. Pre-middle Pliocene sediments of glacial and periglacial origin in the Norwegian-Greenland Seas: Results of DSDP Leg 38. *Earth Evol. Sci.*, 2:69-78.
- Weaver, P. P. E., 1987. Late Miocene to Recent planktonic foraminifers from the North Atlantic: Deep Sea Drilling Project Leg 94. *In* Kidd, R. B., Ruddiman, W. F., et al., *Init. Repts. DSDP*, 94: Washington (U.S. Govt. Printing Office), 703-727.
- Weaver, P. P. E., and Clement, B. M., 1987. Magnetobiostratigraphy of planktonic foraminiferal datums: DSDP Leg 94 North Atlantic. *In* Kidd, R. B., Ruddiman, W. F., et al., *Init. Repts. DSDP*, 94: Washington (U.S. Govt. Printing Office), 815-829.
- White, S. M., 1978. Sediments of the Norwegian-Greenland Sea, DSDP Leg 38. *In* Talwani, M., Udintsev, G., et al., *Init. Repts. DSDP*, Suppl. to Vols. 38, 39, 40, and 41: Washington (U.S. Govt. Printing Office), 193-258.
- Williams, G. L., 1977. Dinocysts: their classification, biostratigraphy and paleoecology. *In* Ramsey, A. T. S. (Ed.), *Oceanic Micropaleontology* (Vol. 2): London (Academic Press), 1231-1325.
- Williams, G. L., and Bujak, J. P., 1977. Cenozoic palynostratigraphy of off-shore eastern Canada. *Am. Assoc. Stratigr. Palynol., Contr. Ser.*, 5A:14-47.
- Woodruff, F., Savin, S. M., and Douglas, R. G., 1981. Miocene stable isotope record: a detailed deep Pacific Ocean study and its paleoclimatic implications. *Science*, 212:665-668.

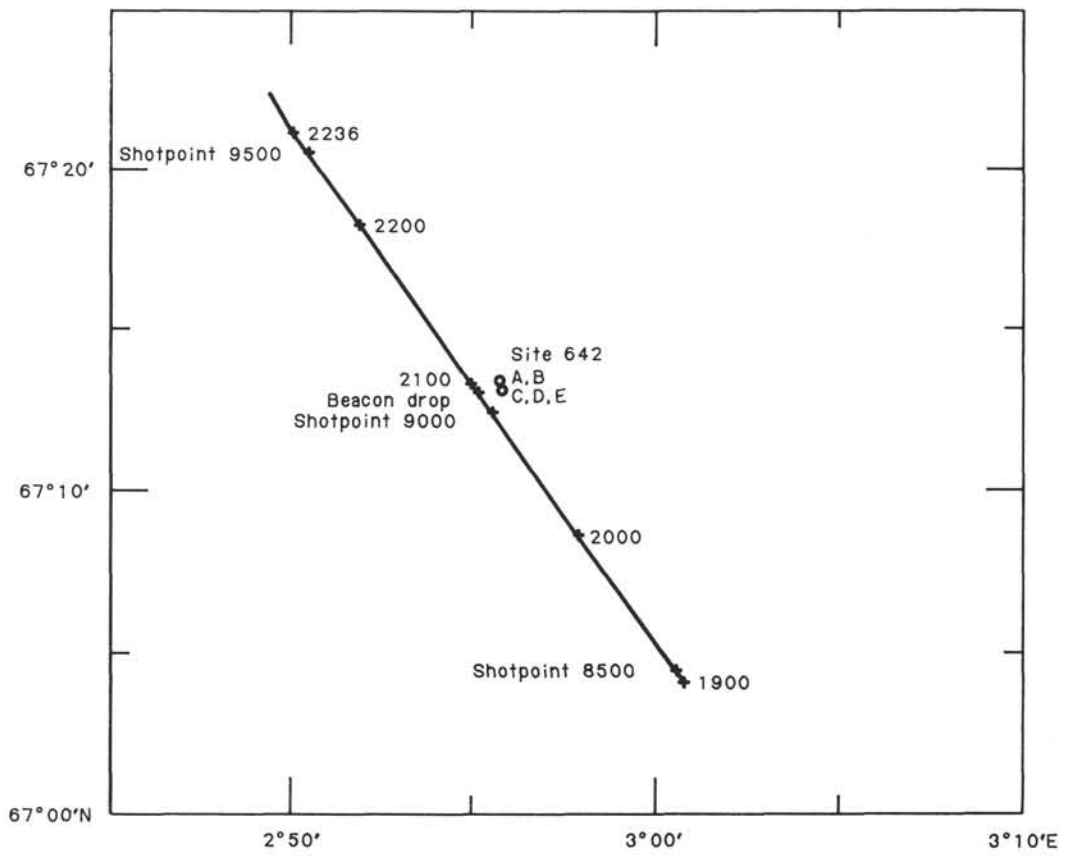


Figure 78. Site 642 survey line. Letters show locations of the five holes drilled. Shotpoint numbers and local time during the survey are shown.

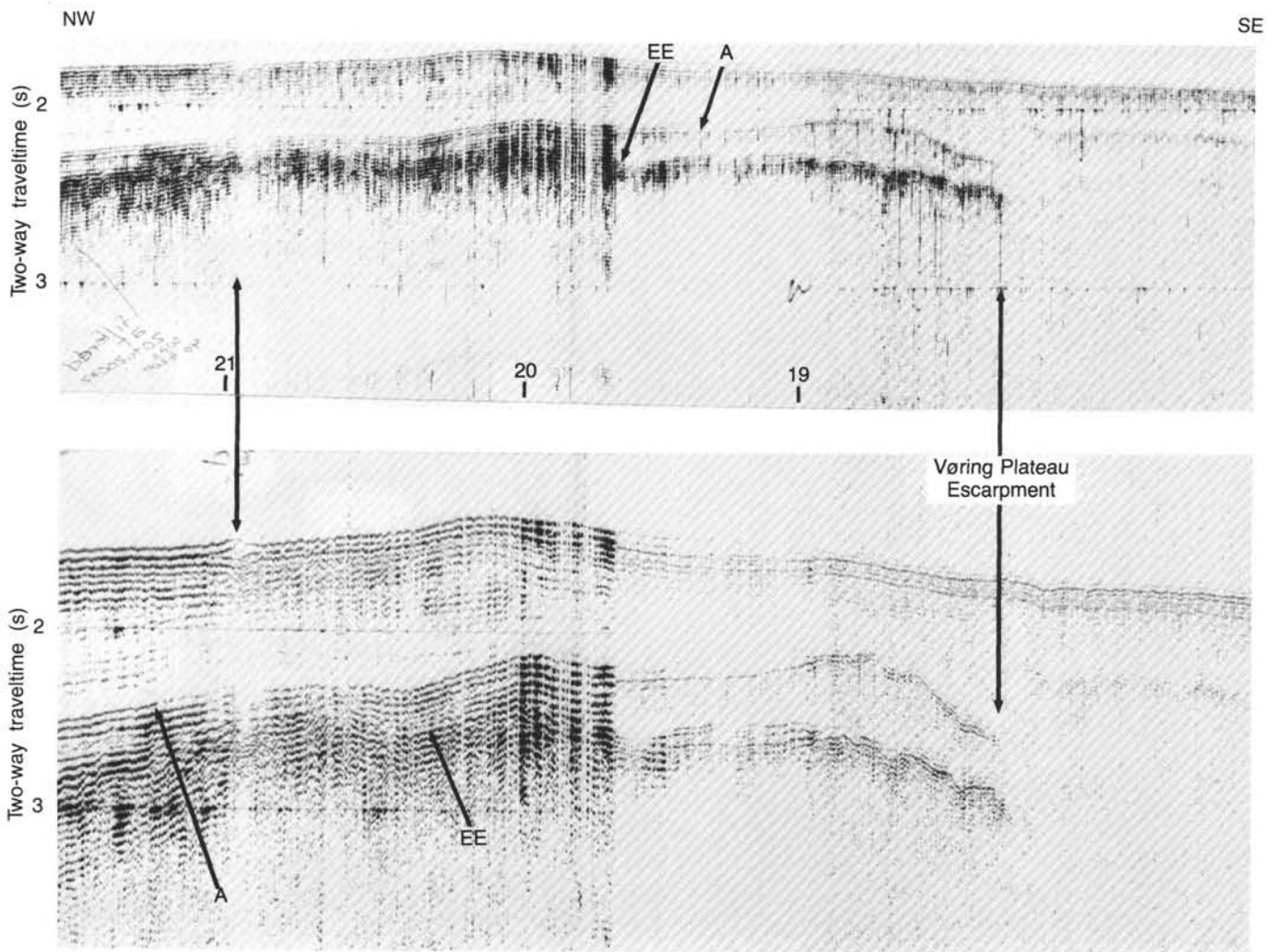


Figure 79. Analog seismic profiles recorded along survey line at Site 642 (Fig. 78). A 10-s sweep (top) and 5-s sweep (bottom) are used. Vertical arrows show features used to match the two profiles.

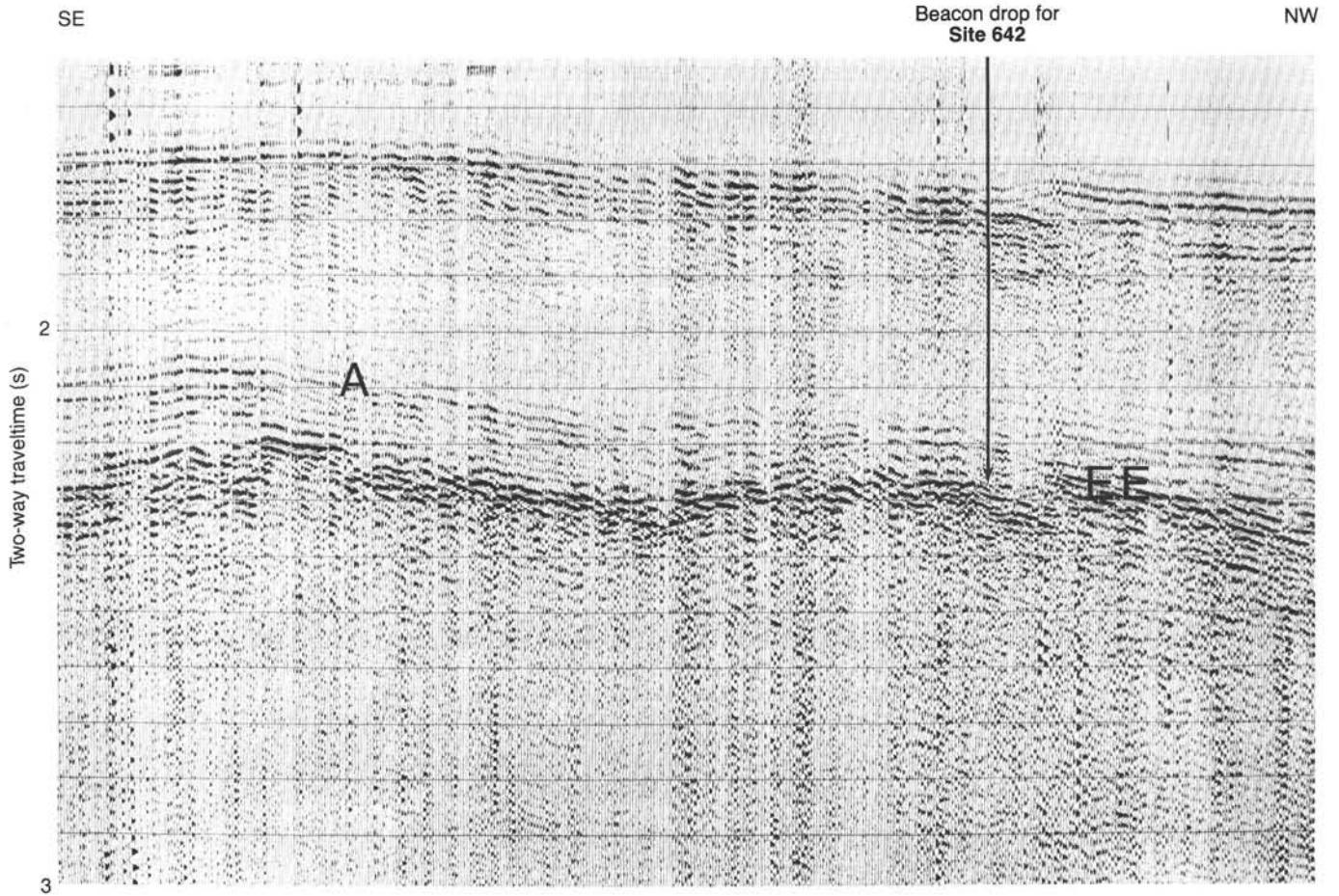


Figure 80. Digital shipboard single-channel seismic profile recorded along survey line (Fig. 78).

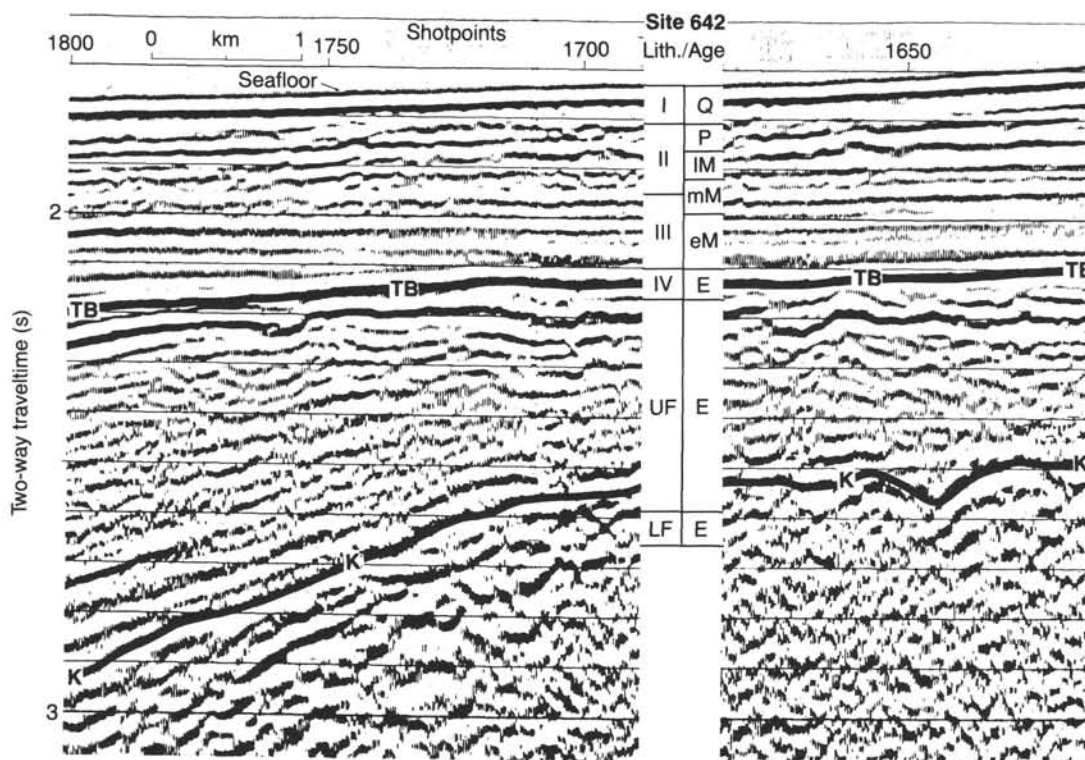


Figure 81. Multichannel profile BGR-1 in the vicinity of Site 642 (migrated time section). Lithology and ages from Site 642 are included. *O*: base of Pliocene, *O'*: base of middle Miocene, *A*: base of Miocene, *EE*: early Eocene.

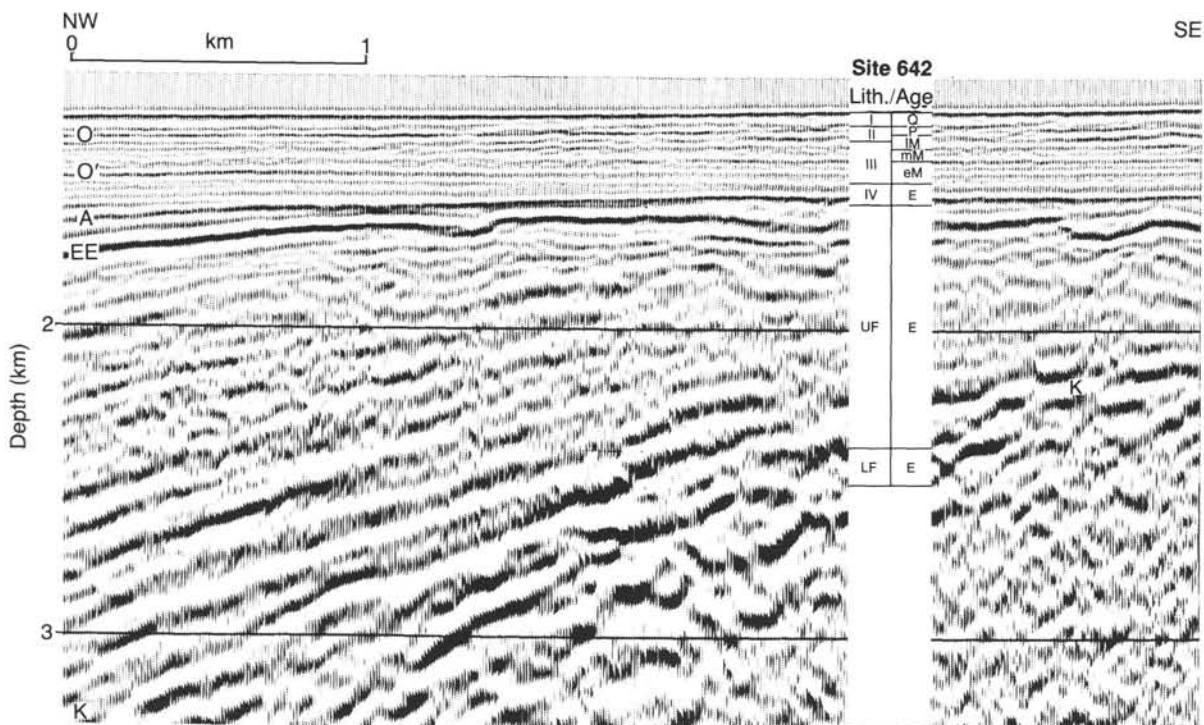
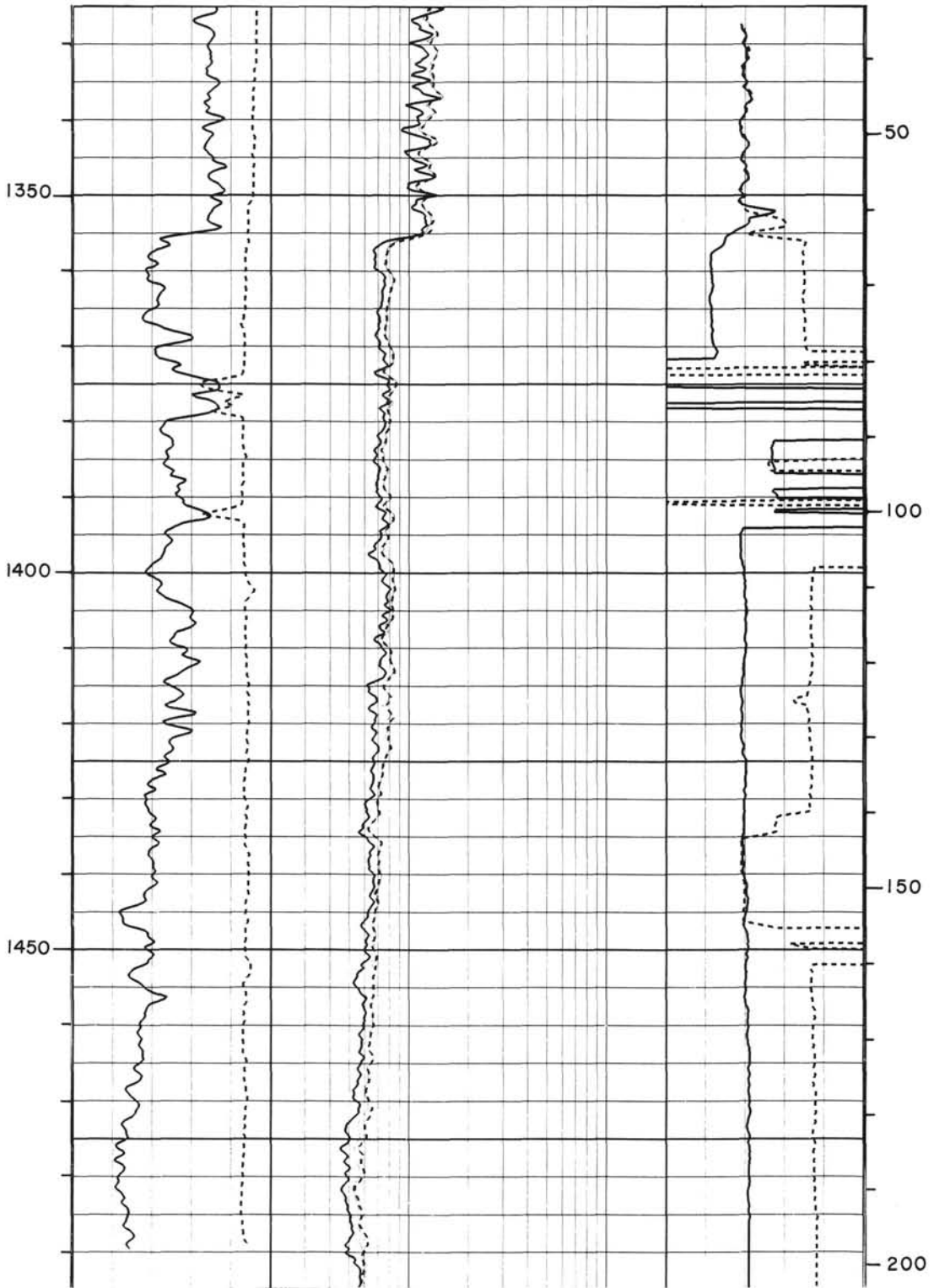


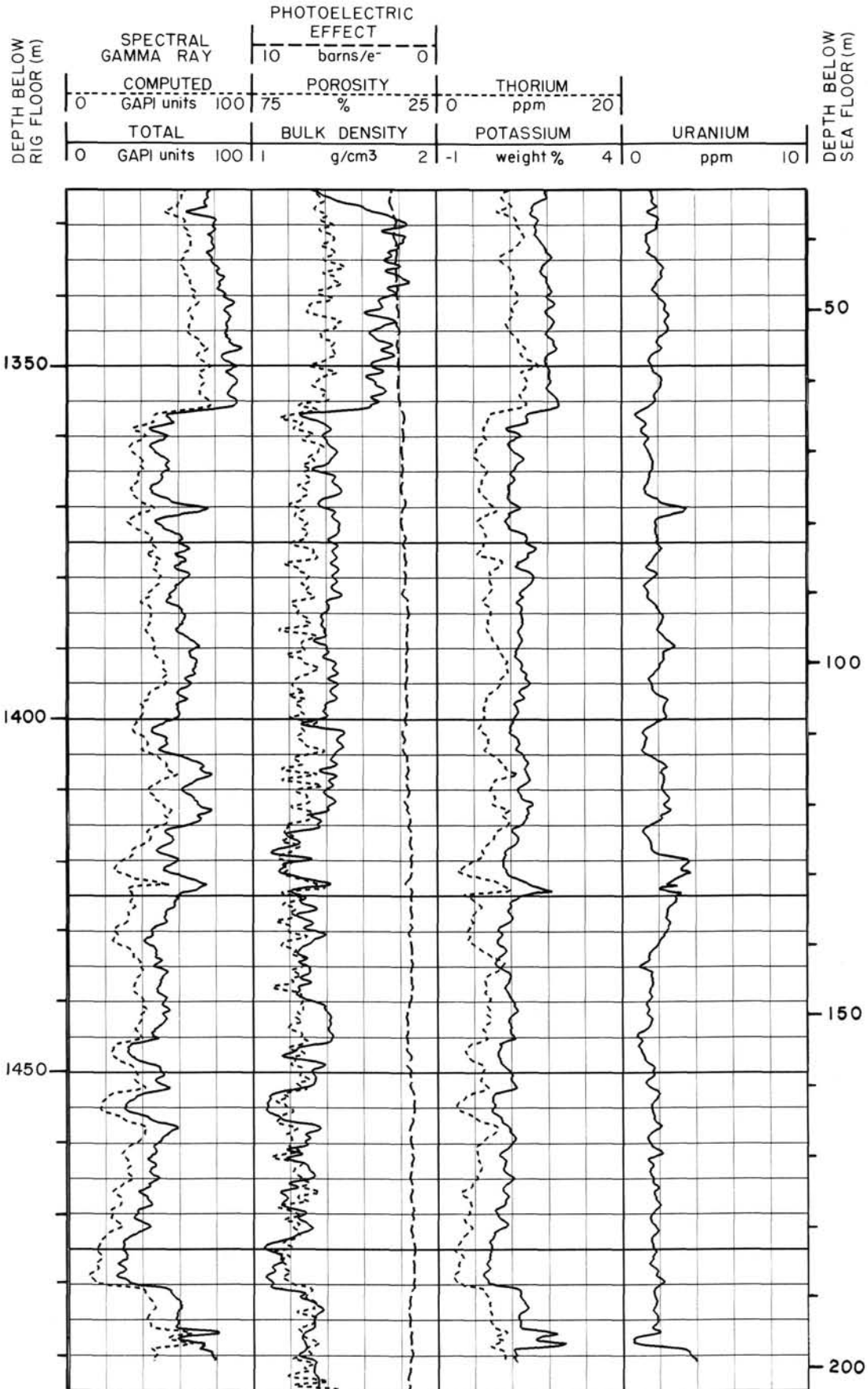
Figure 82. Multichannel profile BGR-1 in the vicinity of Site 642 (migrated depth section). Lithology from Site 642 included. *UF*: upper volcanic flow series; *LF*: lower volcanic series.

Summary log for Hole 642D.

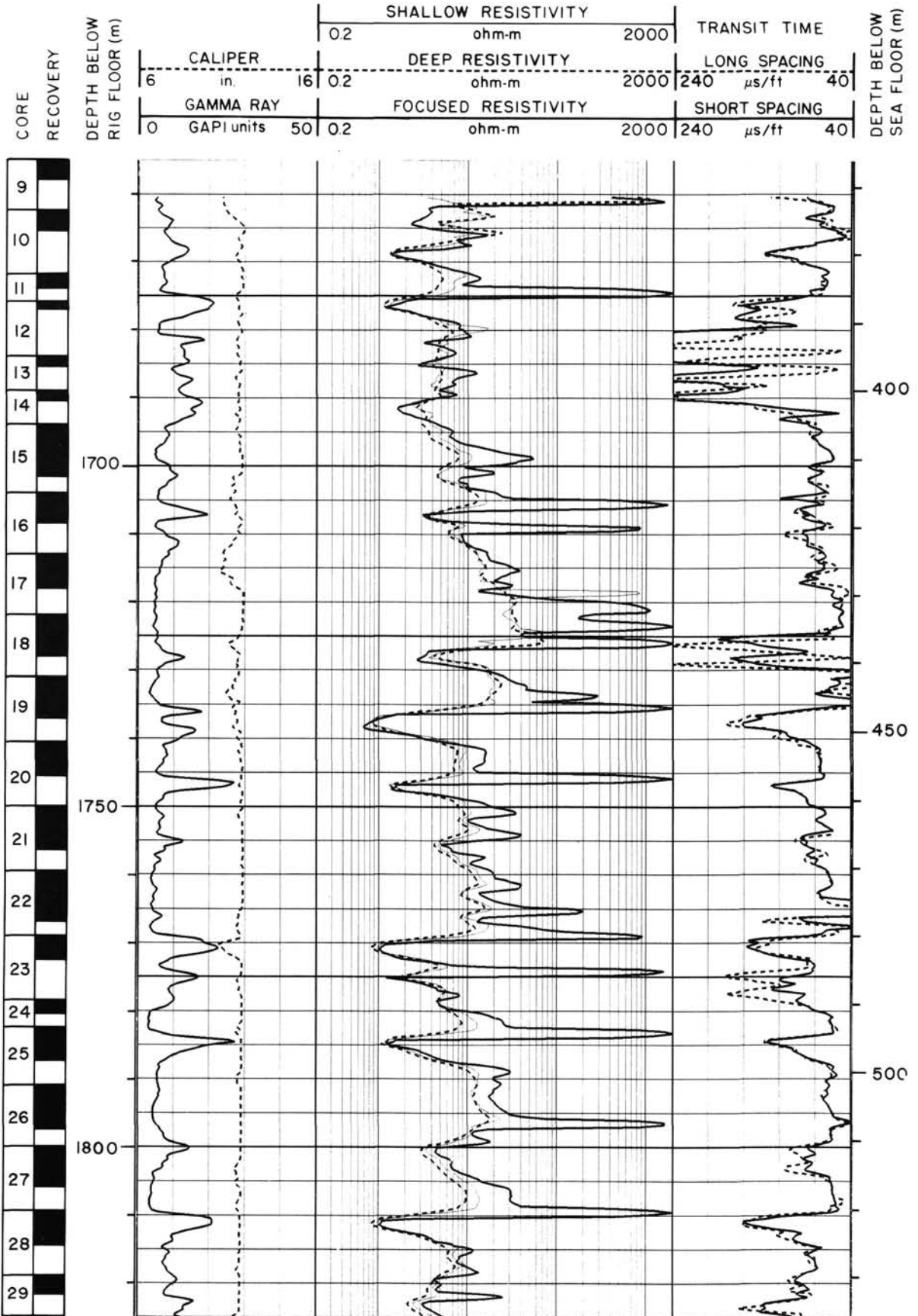
DEPTH BELOW RIG FLOOR (m)	CALIPER		SHALLOW RESISTIVITY		TRANSIT TIME		DEPTH BELOW SEA FLOOR (m)
	-2	8	0.2	20	240	140	
	in.		ohm-m		$\mu\text{s}/\text{ft}$		
DEPTH BELOW RIG FLOOR (m)	DEEP RESISTIVITY		FOCUSED RESISTIVITY		LONG SPACING		DEPTH BELOW SEA FLOOR (m)
	0	100	0.2	20	240	140	
	GAPI units		ohm-m		$\mu\text{s}/\text{ft}$		
GAMMA RAY		FOCUSED RESISTIVITY		SHORT SPACING			
0		0.2		20		240 $\mu\text{s}/\text{ft}$ 140	



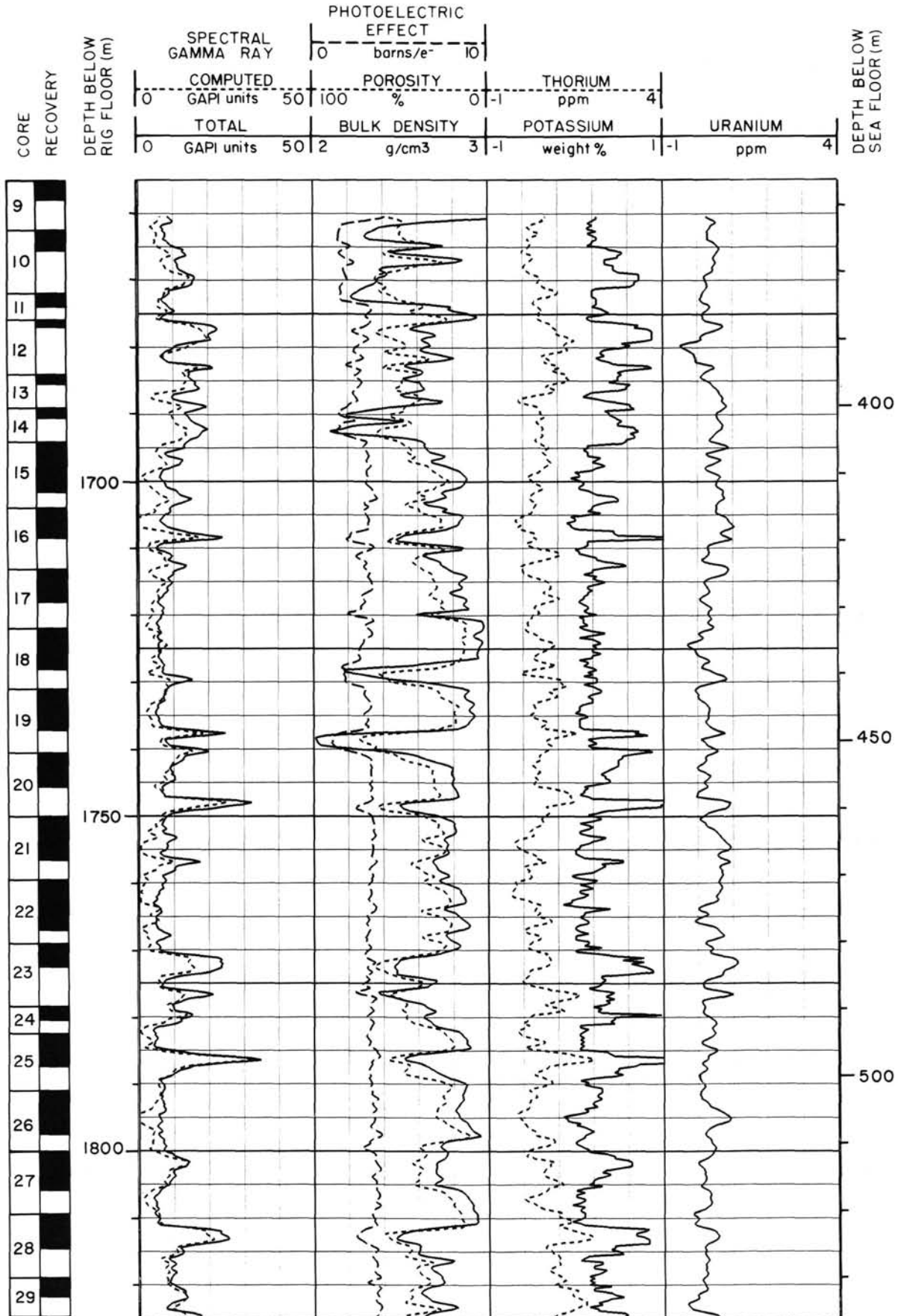
Summary log for Hole 642D (continued).



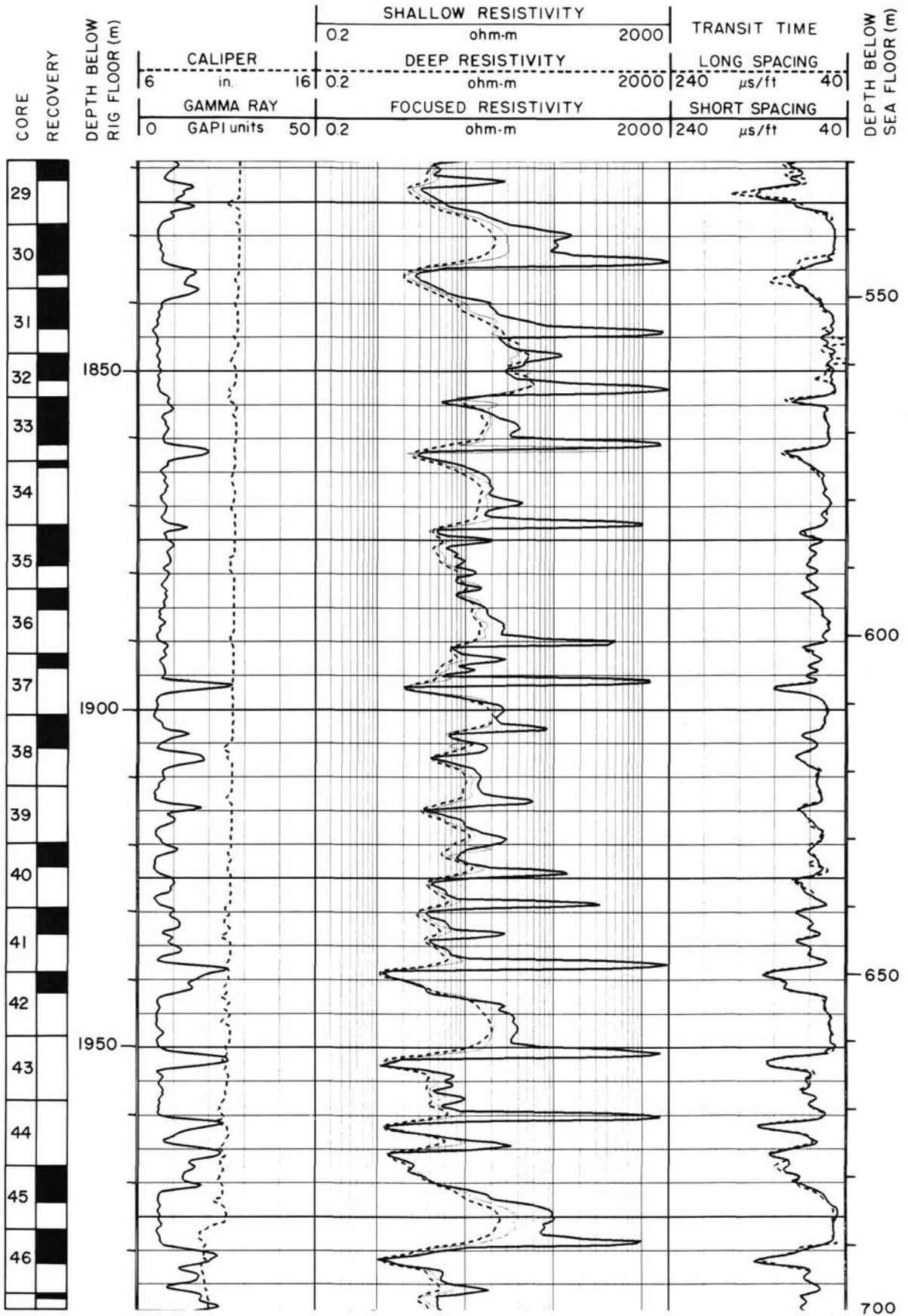
Summary log for Hole 642E.



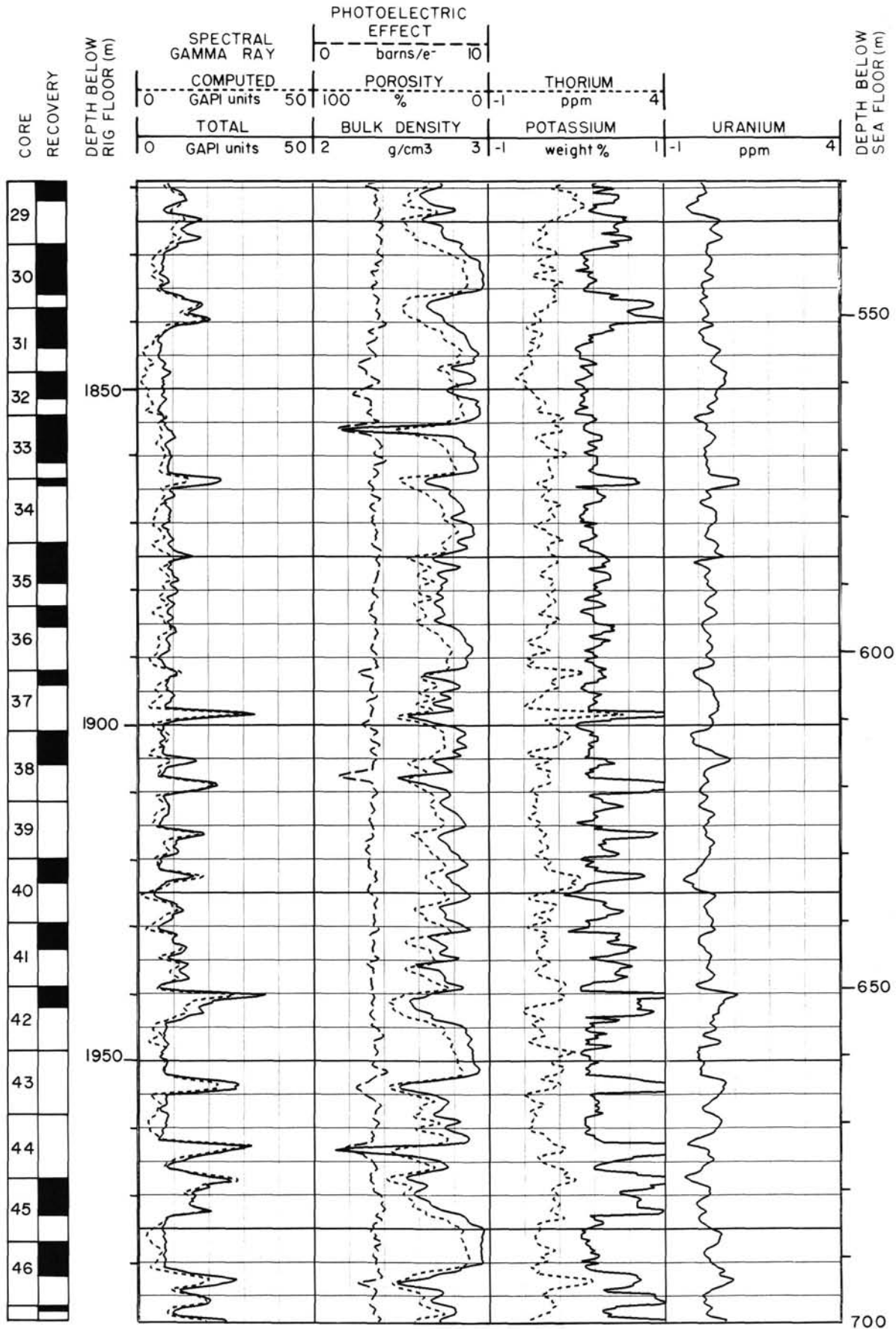
Summary log for Hole 642E (continued).



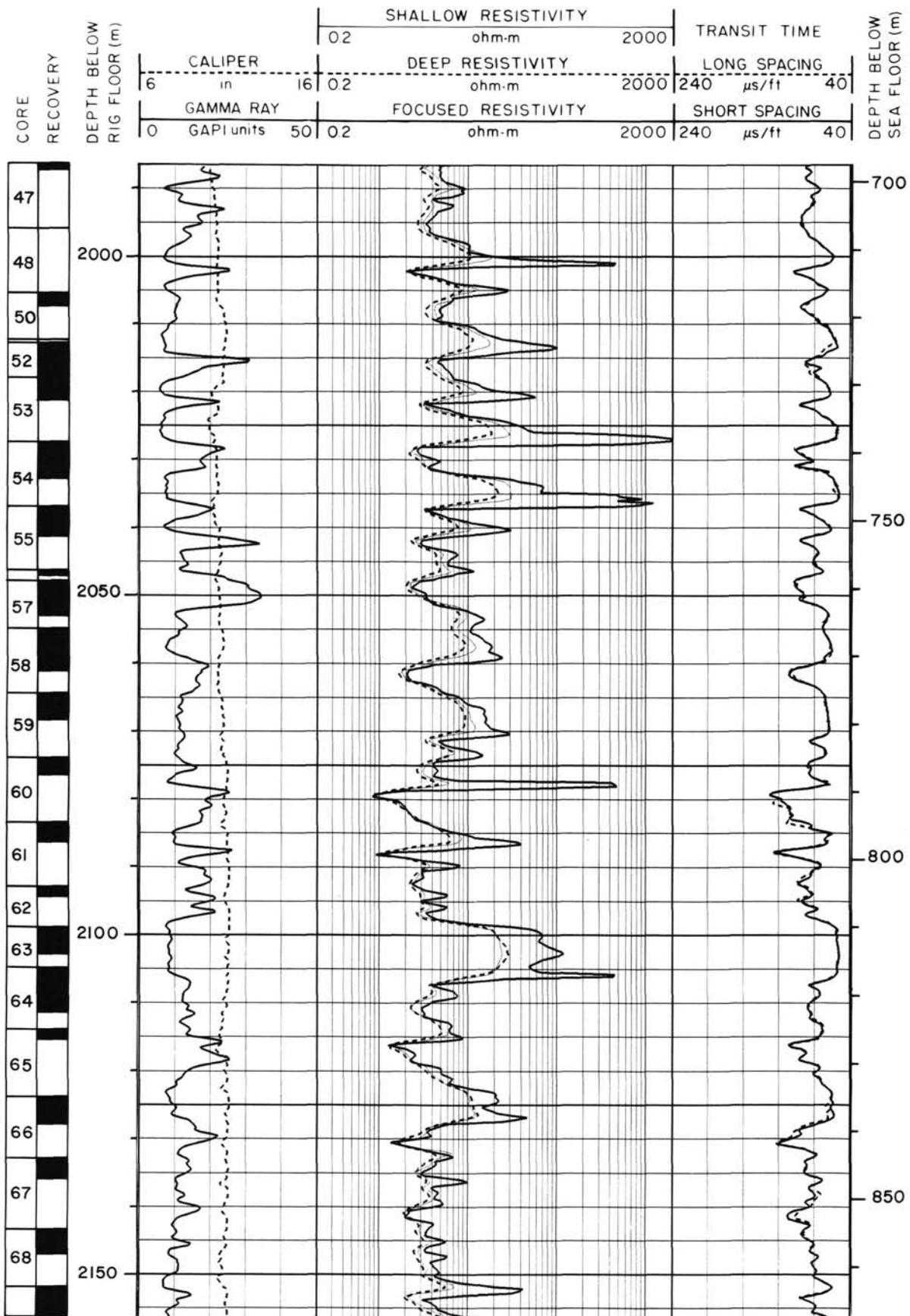
Summary log for Hole 642E (continued).



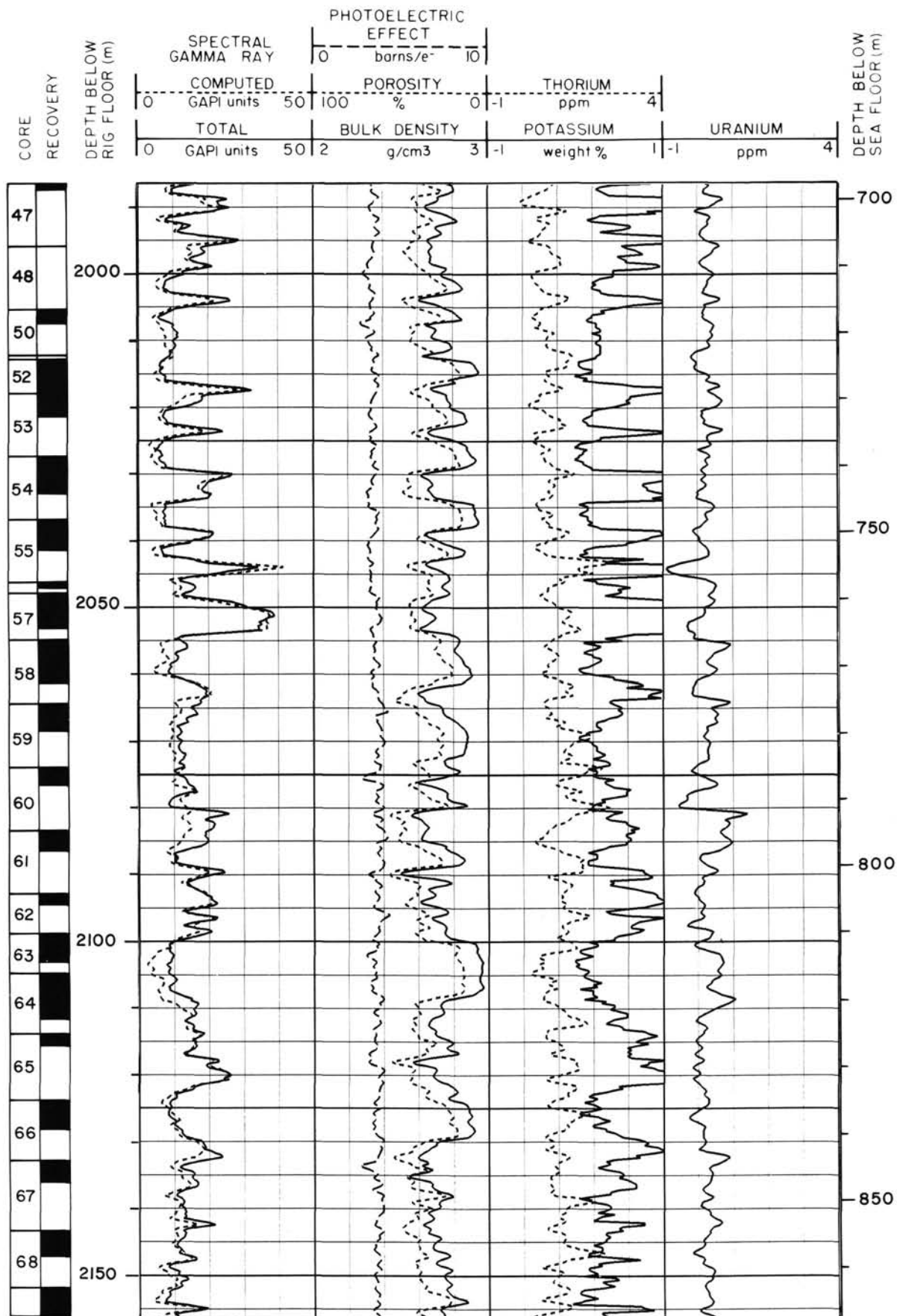
Summary log for Hole 642E (continued).



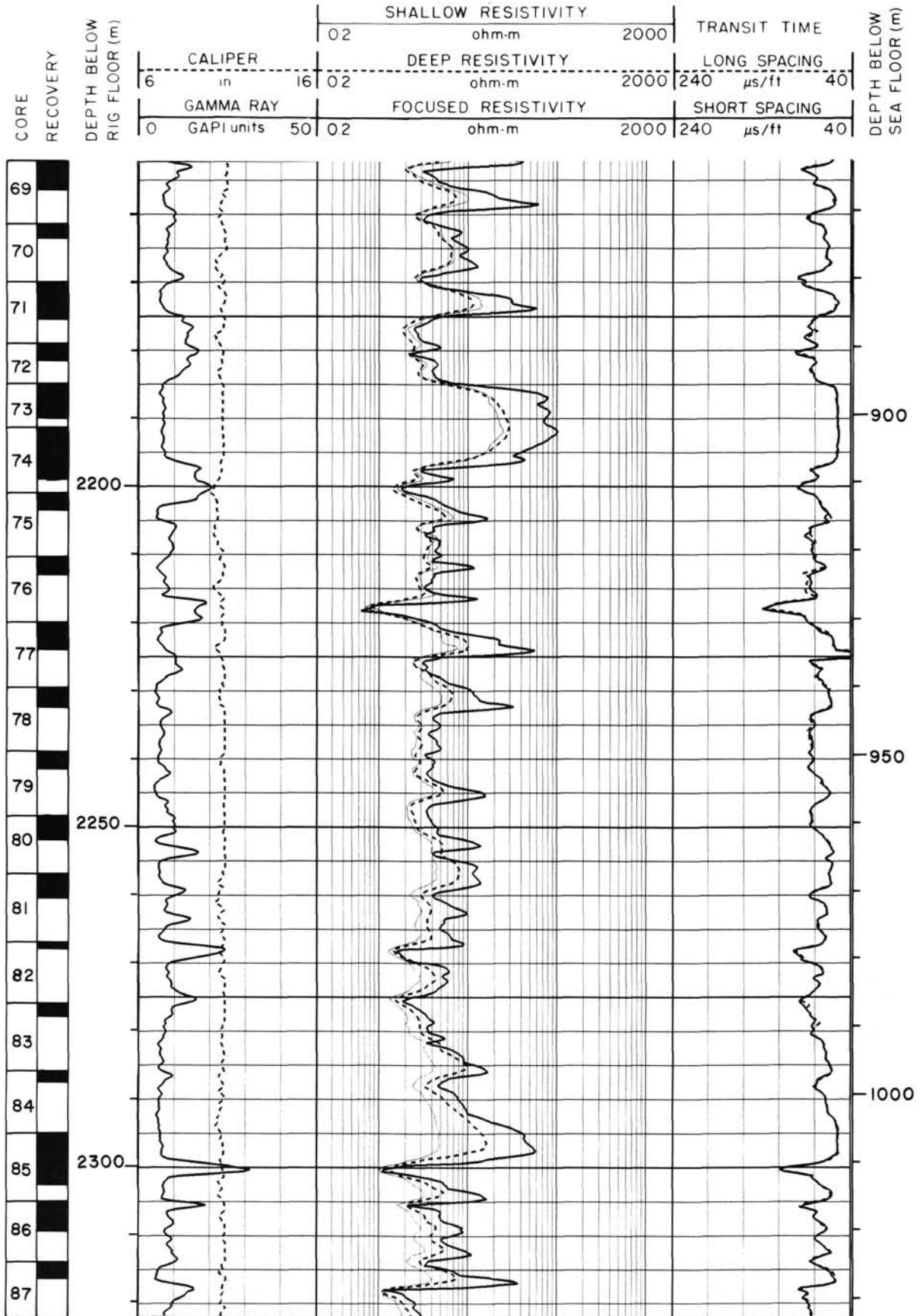
Summary log for Hole 642E (continued).



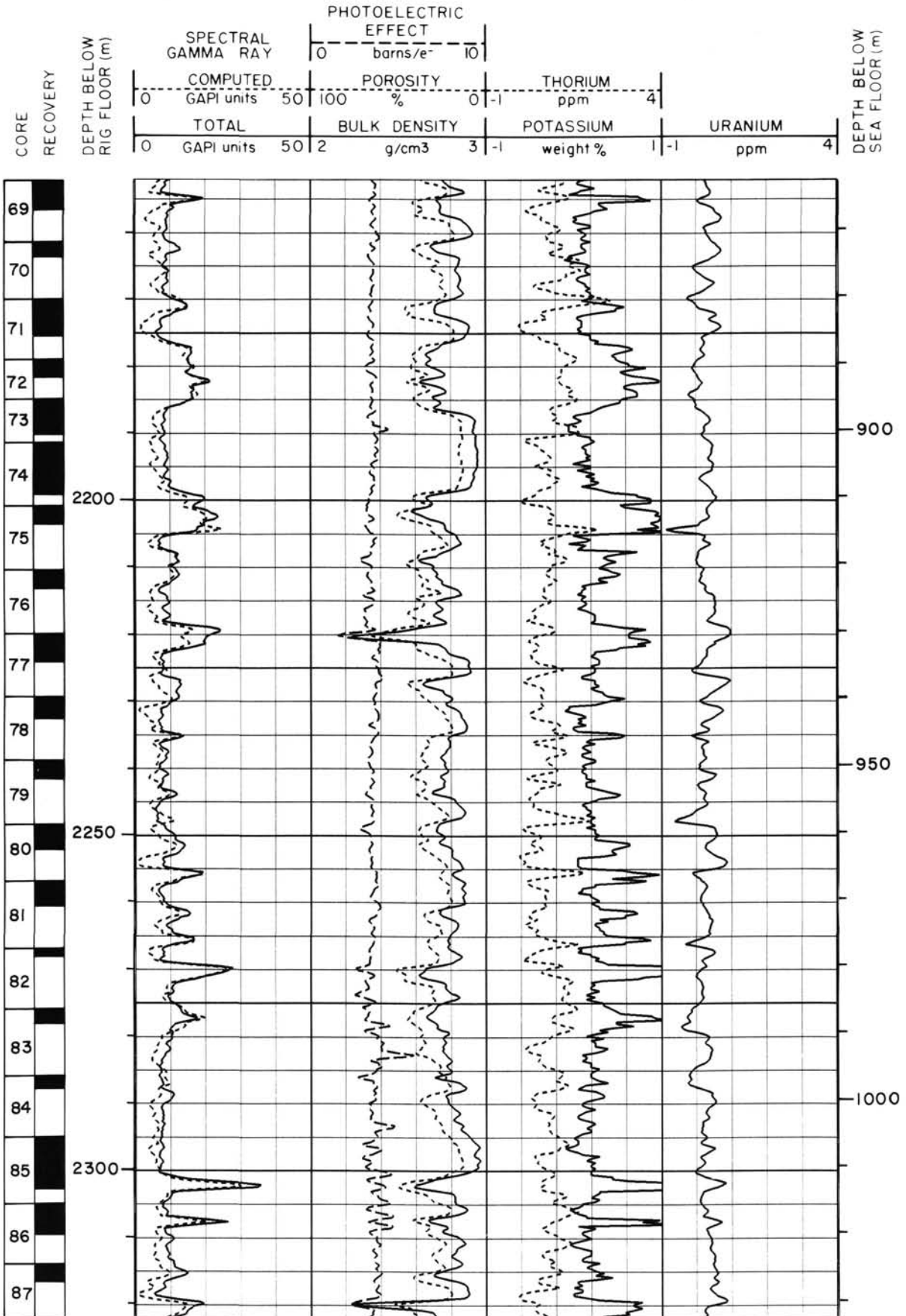
Summary log for Hole 642E (continued).



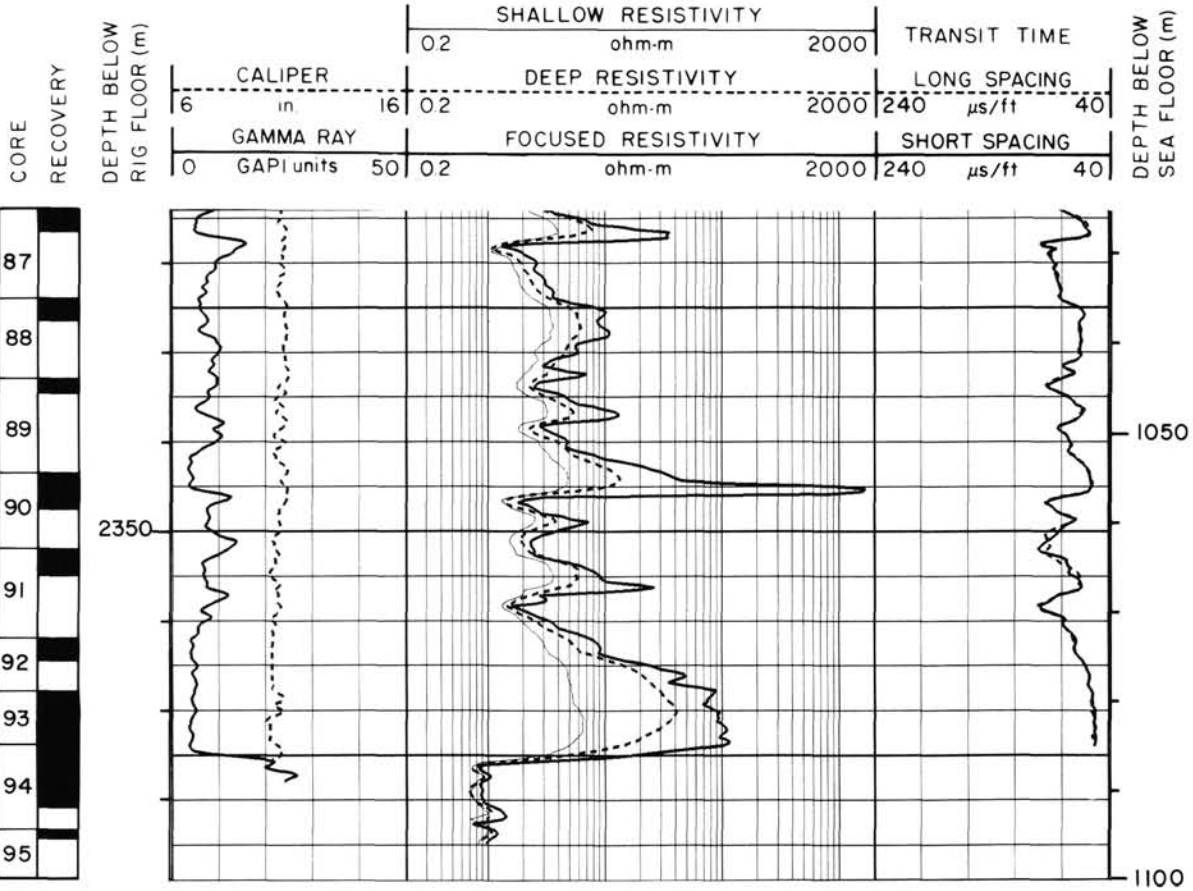
Summary log for Hole 642E (continued).



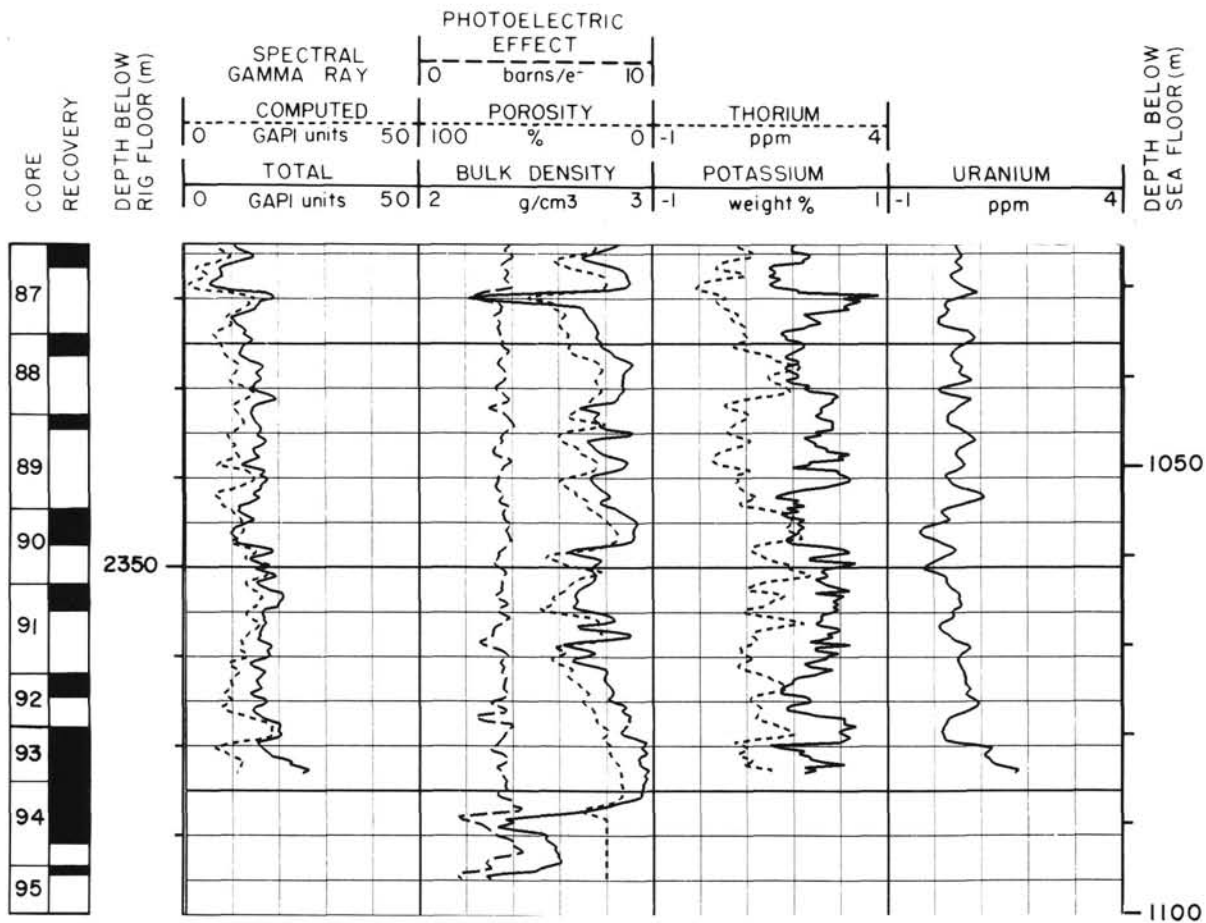
Summary log for Hole 642E (continued).

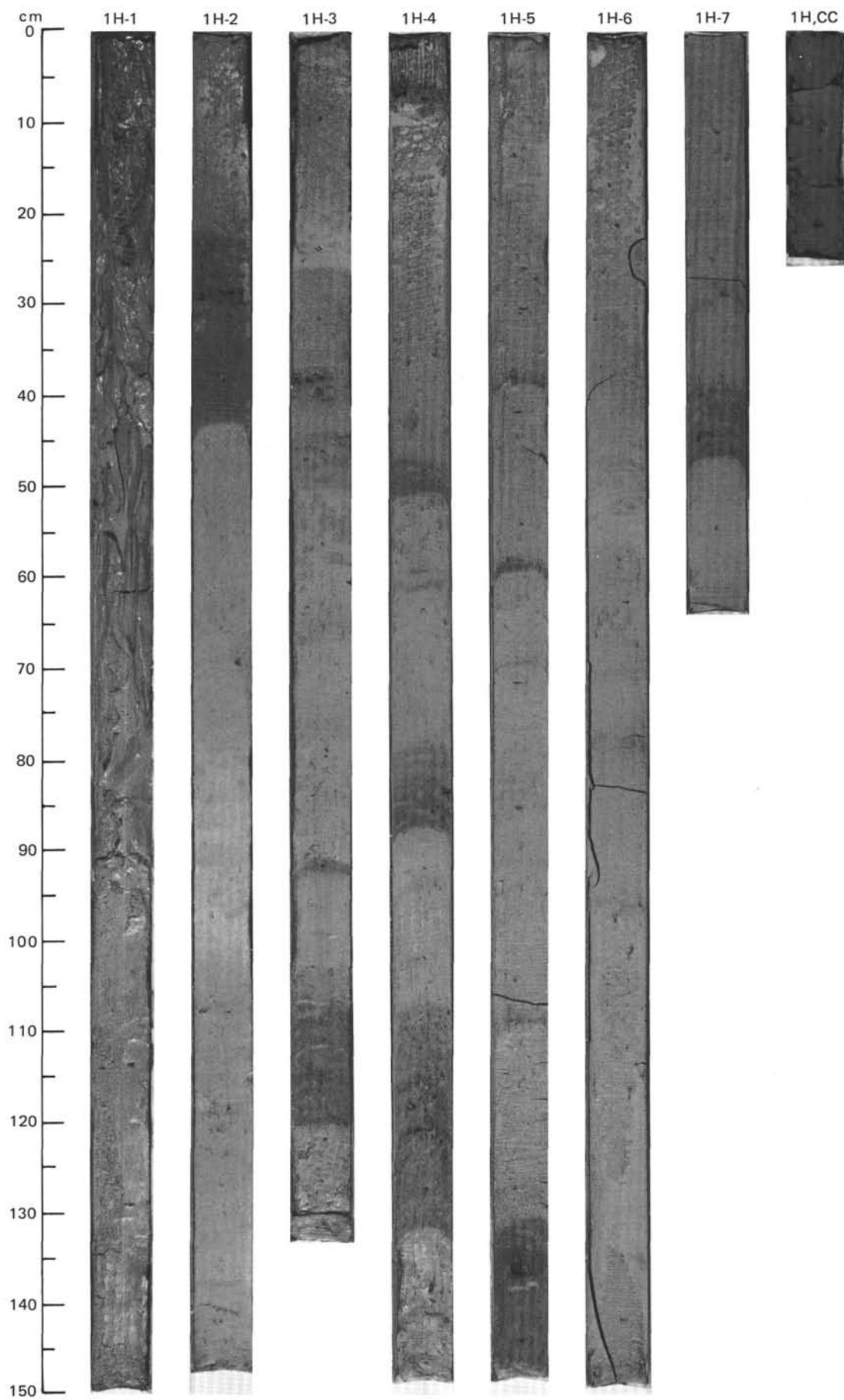


Summary log for Hole 642E (continued).

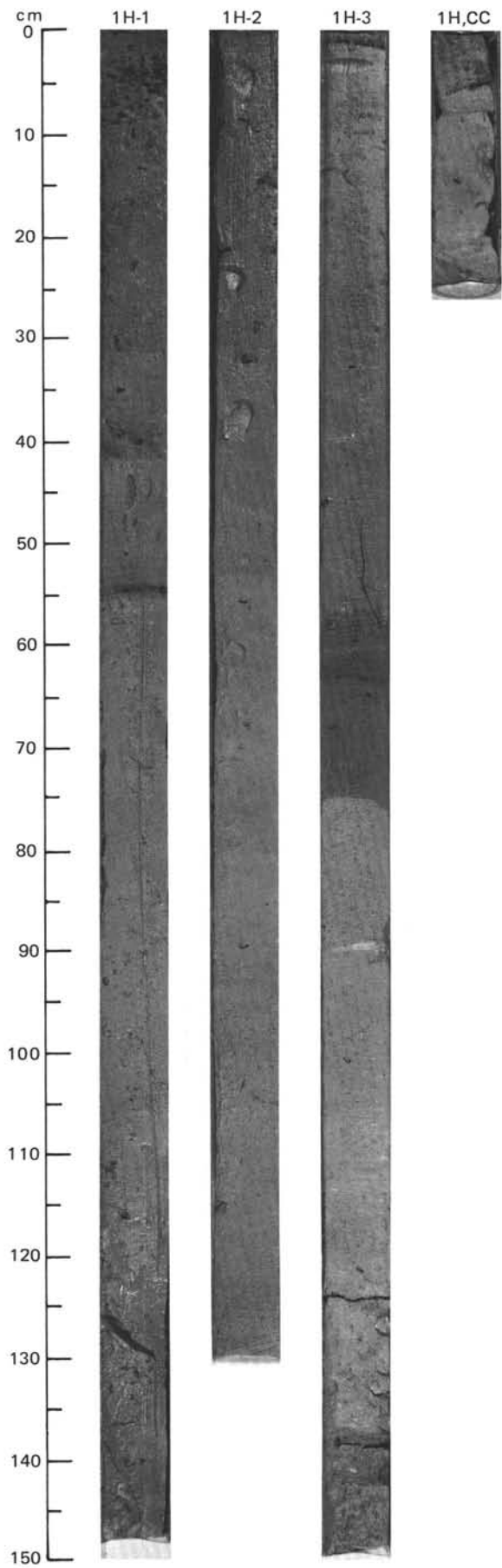


Summary log for Hole 642E (continued).

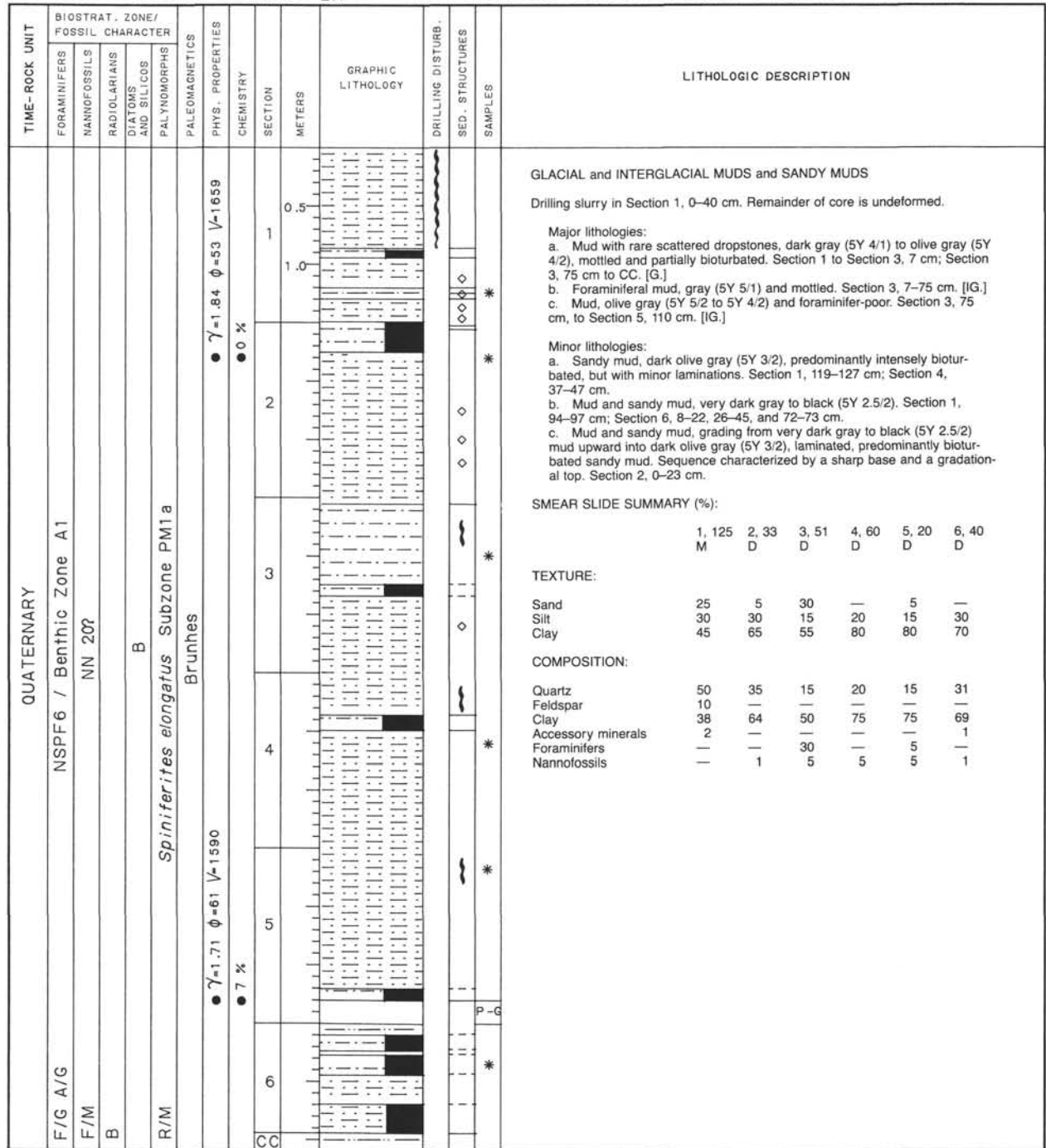


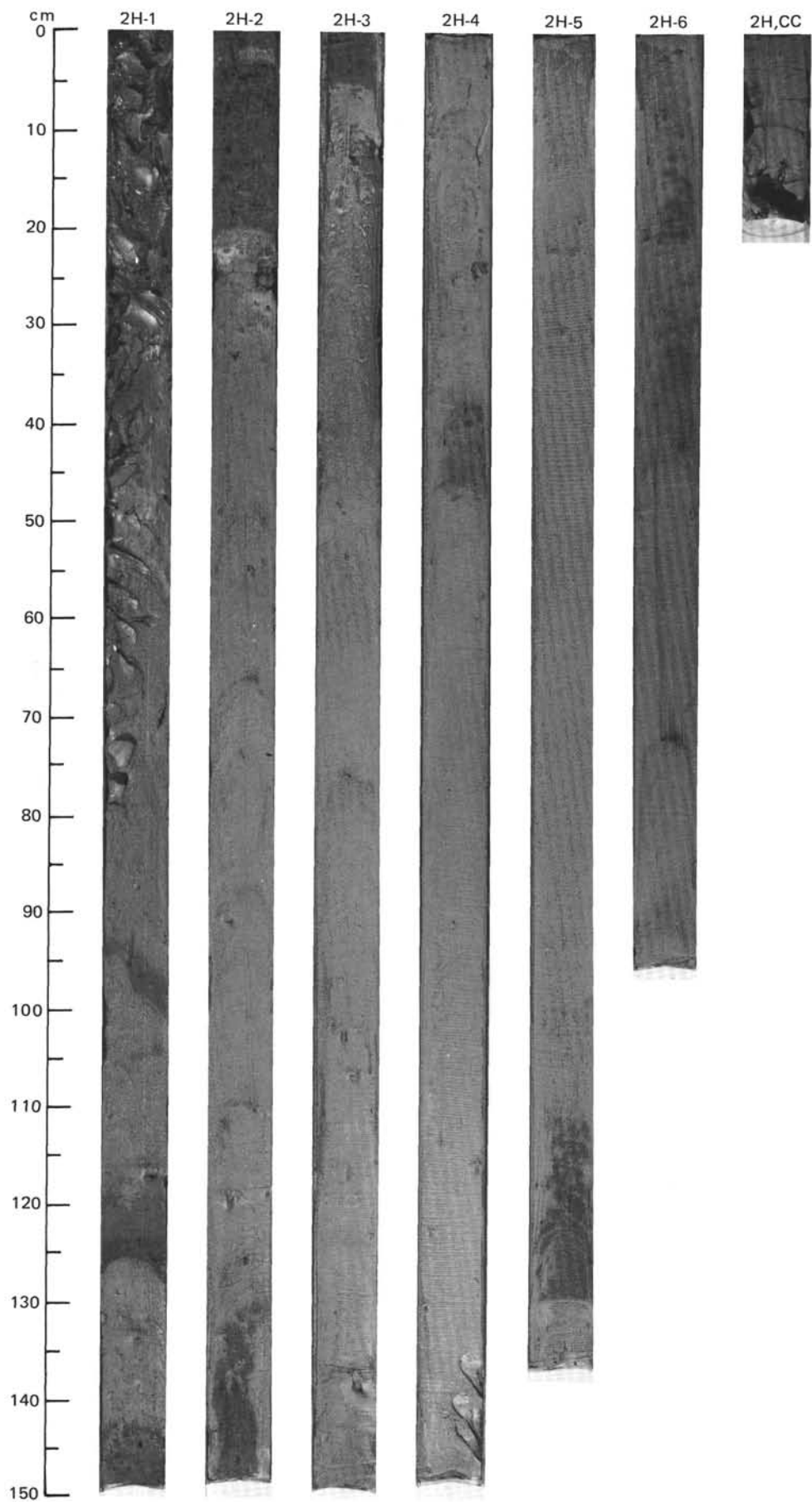


TIME-ROCK UNIT		BIOSTRAT. ZONE/ FOSSIL CHARACTER		PALEOMAGNETICS	PHYS. PROPERTIES	CHEMISTRY	SECTION	METERS	GRAPHIC LITHOLOGY	DRILLING DISTURB.	SED. STRUCTURES	SAMPLES	LITHOLOGIC DESCRIPTION																																																
FORAMINIFERS	NANNOFOSSILS	RADIOLARIANS AND SILICIDS	DIAATOMS AND SILICIDS																																																										
QUATERNARY																																																													
F/G A/G	NSPF6/Benthic Zone A1												<p>GLACIAL and INTERGLACIAL MUDS and SANDY MUDS</p> <p>Entire core is undeformed.</p> <p>Major lithologies:</p> <p>a. Foraminiferal mud with scattered clay lumps, brown (10YR 4/3) to dark grayish brown (2.5Y 5/2). Section 1, 0-55 cm; Section 3, 75 cm to CC. [IG.]</p> <p>b. Mud and sandy mud, dark gray (5Y 4/1) to olive gray (5Y 4/2), with minor scattered mud dropstones. Mottled throughout interval. Section 1, 90 cm to CC.</p> <p>Minor lithologies:</p> <p>a. Sandy mud with Fe/Mn-rich laminations, dark brown to dark yellowish brown (10YR 3/3.5). Section 1, 54-55 cm.</p> <p>b. Mud, very dark gray to black (5Y 2.5/2). Section 3, 63-74 cm.</p> <p>c. Foraminiferal mud, grayish brown (2.5Y 5/2). Current deposit or turbidite. Section 3, 138-144 cm.</p> <p>SMEAR SLIDE SUMMARY (%):</p> <table border="1"> <tr> <td></td> <td>1, 54</td> <td>2, 68</td> <td>3, 33</td> </tr> <tr> <td></td> <td>M</td> <td>D</td> <td>D</td> </tr> </table> <p>TEXTURE:</p> <table border="1"> <tr> <td>Sand</td> <td>2</td> <td>1</td> <td>10</td> </tr> <tr> <td>Silt</td> <td>32</td> <td>39</td> <td>30</td> </tr> <tr> <td>Clay</td> <td>66</td> <td>60</td> <td>60</td> </tr> </table> <p>COMPOSITION:</p> <table border="1"> <tr> <td>Quartz</td> <td>30</td> <td>30</td> <td>35</td> </tr> <tr> <td>Feldspar</td> <td>—</td> <td>2</td> <td>1</td> </tr> <tr> <td>Clay</td> <td>70</td> <td>64</td> <td>60</td> </tr> <tr> <td>Calcite/dolomite</td> <td>—</td> <td>2</td> <td>2</td> </tr> <tr> <td>Accessory minerals</td> <td>—</td> <td>1</td> <td>1</td> </tr> <tr> <td>Goethite</td> <td>Tr</td> <td>—</td> <td>—</td> </tr> <tr> <td>Foraminifers</td> <td>—</td> <td>1</td> <td>1</td> </tr> </table>		1, 54	2, 68	3, 33		M	D	D	Sand	2	1	10	Silt	32	39	30	Clay	66	60	60	Quartz	30	30	35	Feldspar	—	2	1	Clay	70	64	60	Calcite/dolomite	—	2	2	Accessory minerals	—	1	1	Goethite	Tr	—	—	Foraminifers	—	1	1
	1, 54	2, 68	3, 33																																																										
	M	D	D																																																										
Sand	2	1	10																																																										
Silt	32	39	30																																																										
Clay	66	60	60																																																										
Quartz	30	30	35																																																										
Feldspar	—	2	1																																																										
Clay	70	64	60																																																										
Calcite/dolomite	—	2	2																																																										
Accessory minerals	—	1	1																																																										
Goethite	Tr	—	—																																																										
Foraminifers	—	1	1																																																										
F/P	NN 21?																																																												
	NSR 13																																																												
	B																																																												
F/G	<i>Spiniferites elongatus</i> Subzone PM1a																																																												
	Brunhes																																																												
	$\gamma = 1.05$ $\phi = 08$ $V = 1041$ ● $\gamma = 1.89$ $\phi = 49$ $V = 1645$ ● $\gamma = 1.53$ $\phi = 70$ $V = 1569$																																																												
				16 % ●	0 % ●	16 % ●																																																							
							1																																																						
							2																																																						
							3																																																						
							CC																																																						

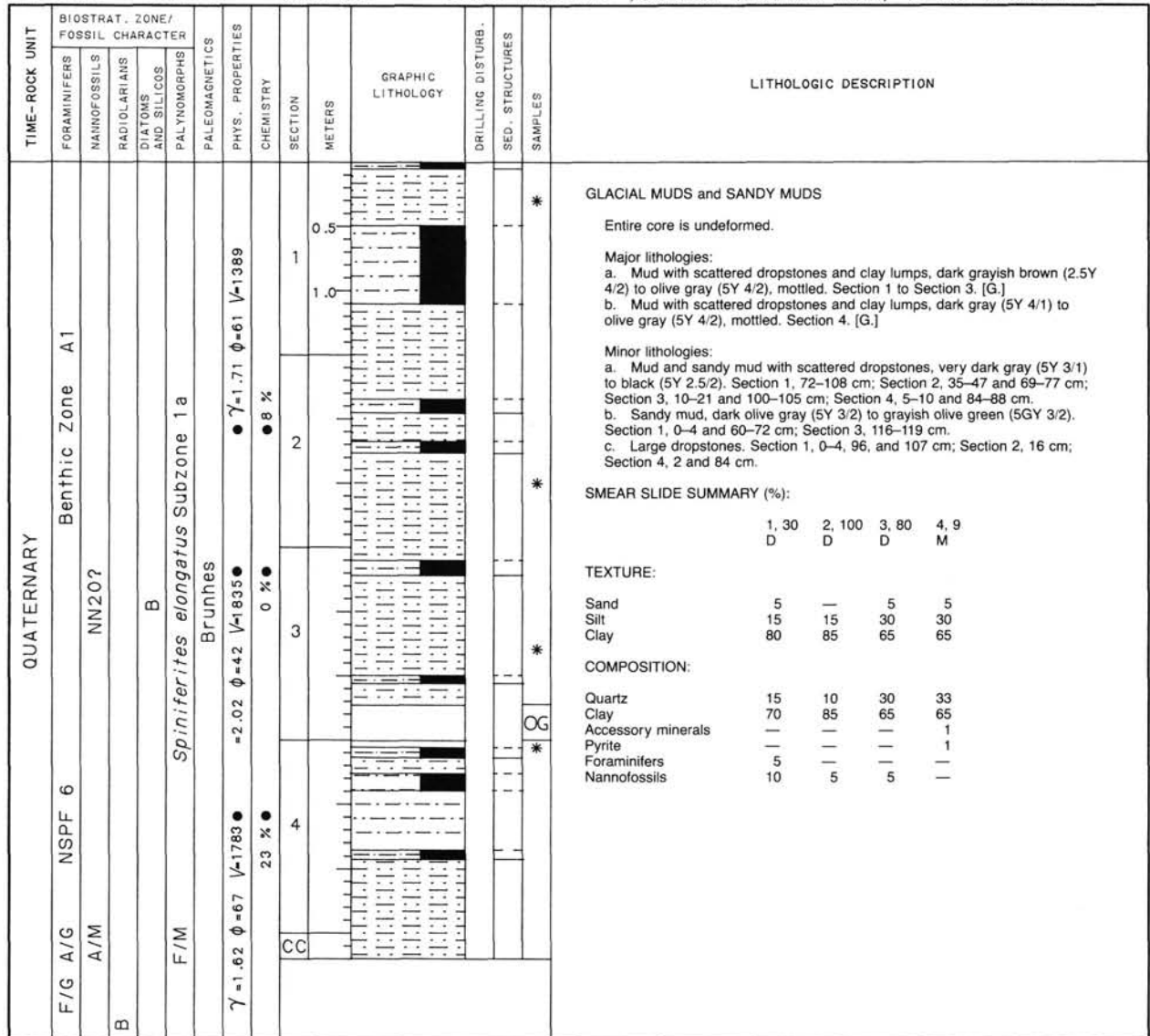


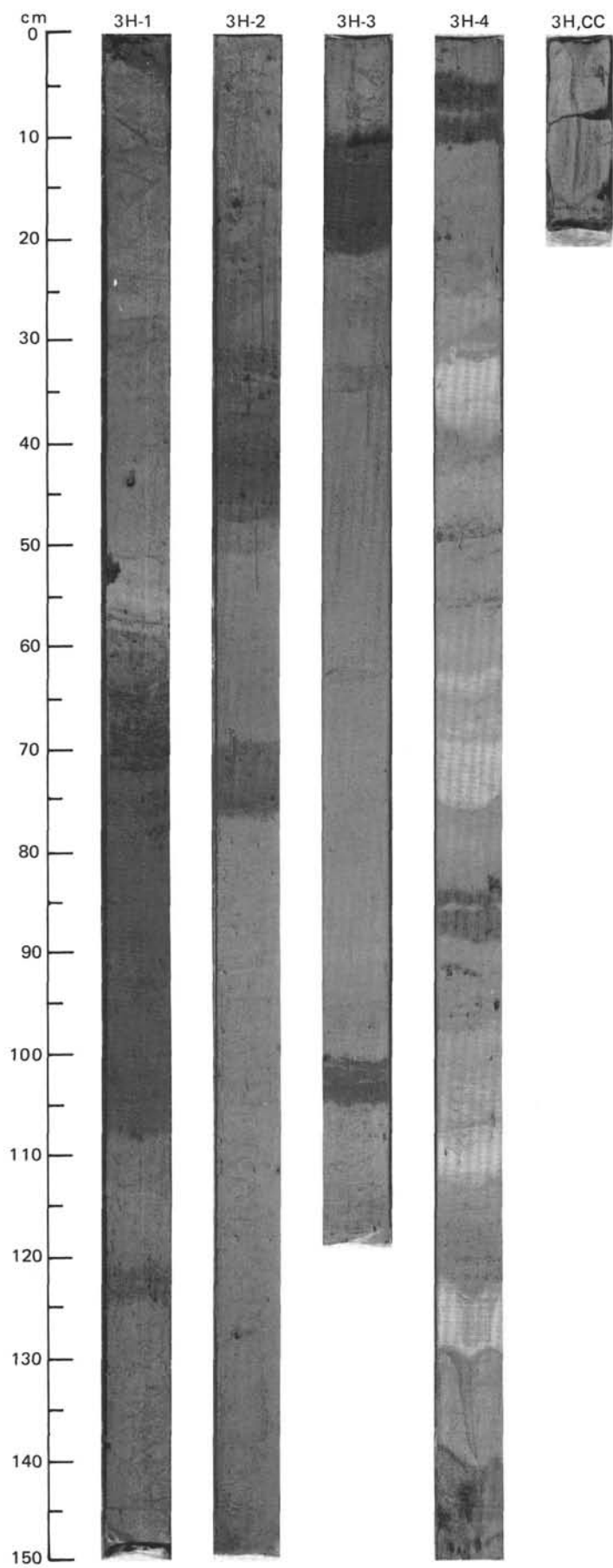
SITE 642 HOLE B CORE 2H CORED INTERVAL 1290.80-1300.30 mbsl; 4.80-14.30 mbsf

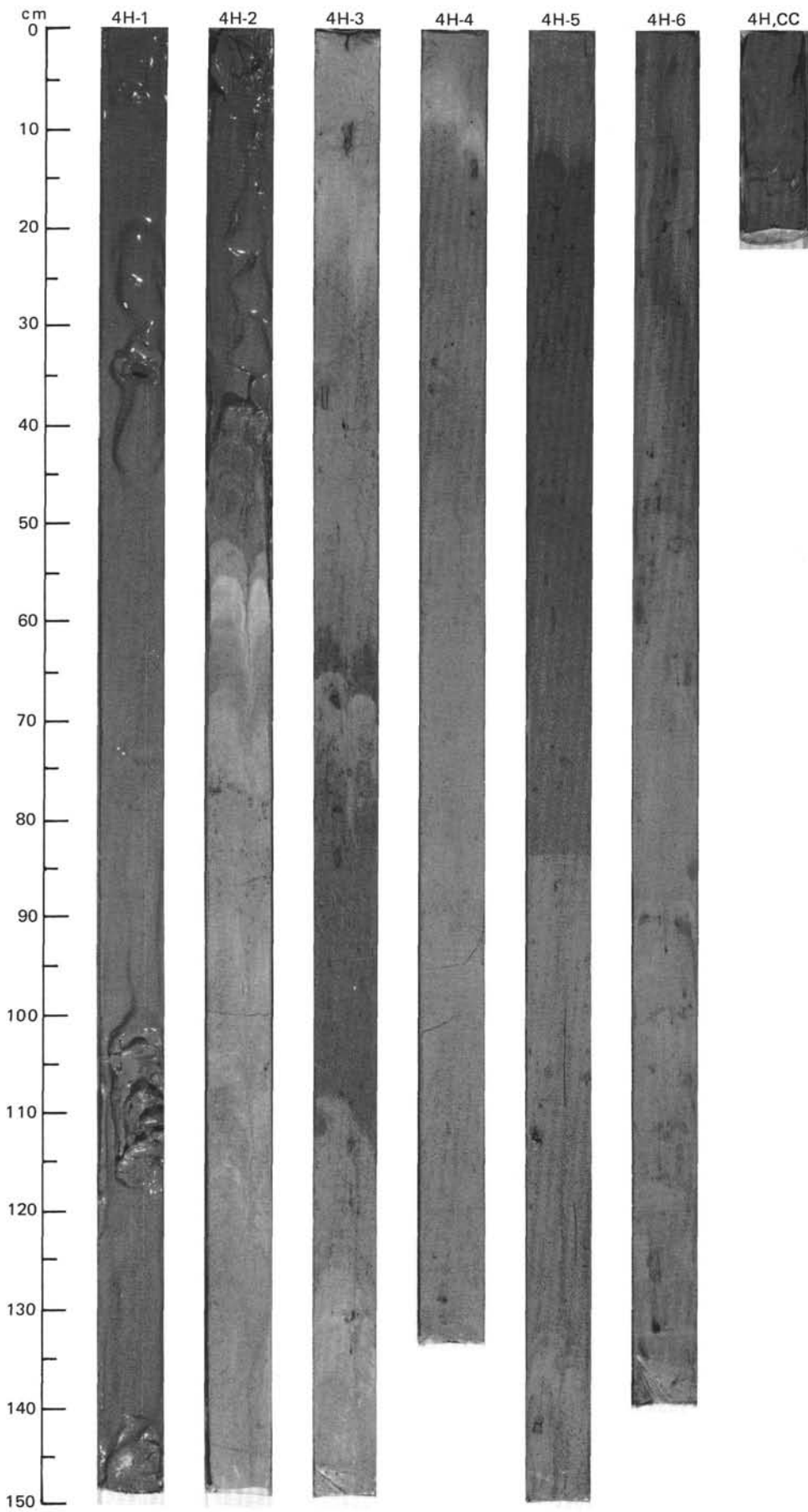




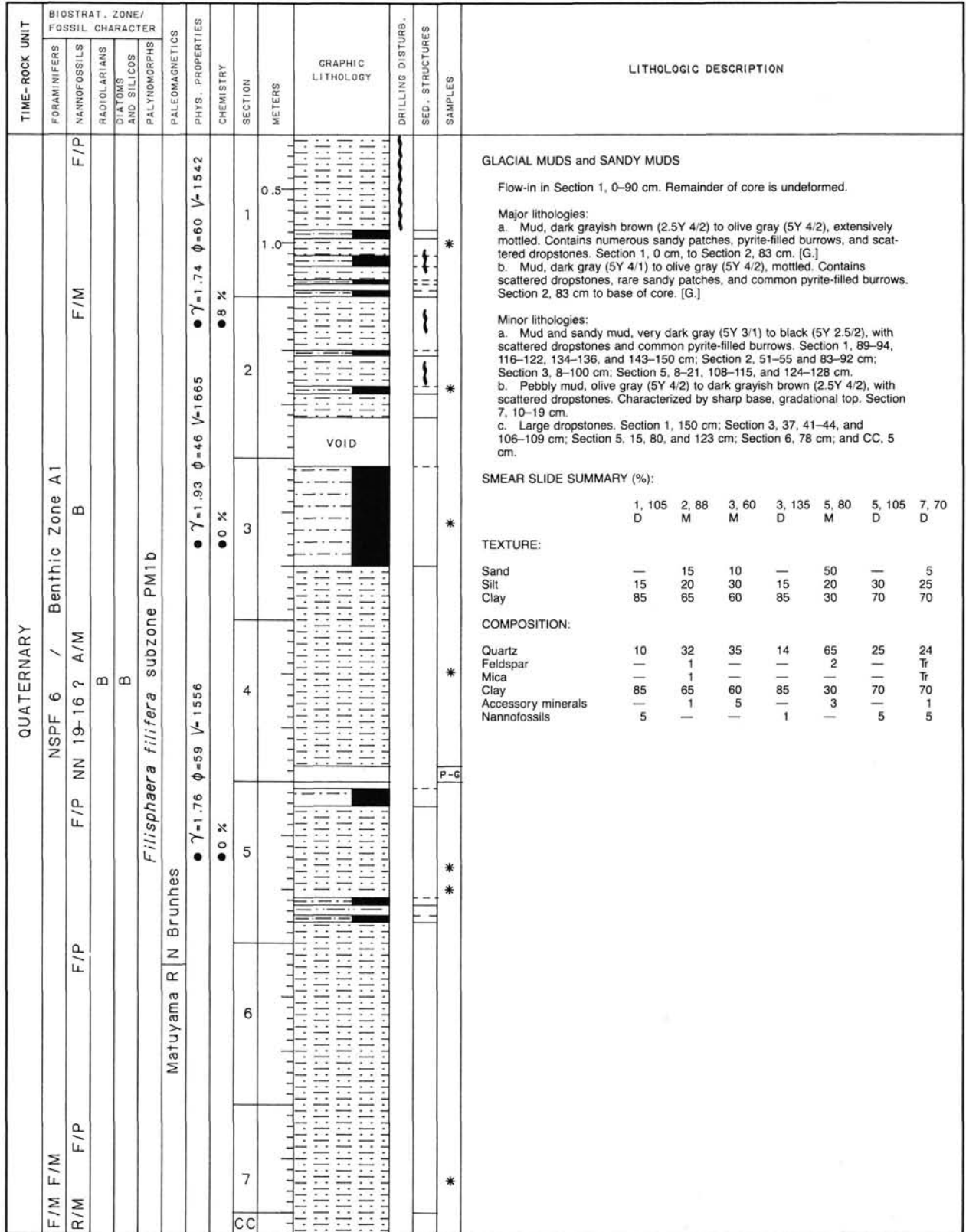
SITE 642 HOLE B CORE 3H CORED INTERVAL 1300.30-1306.70 mbsf; 14.30-20.70 mbsf

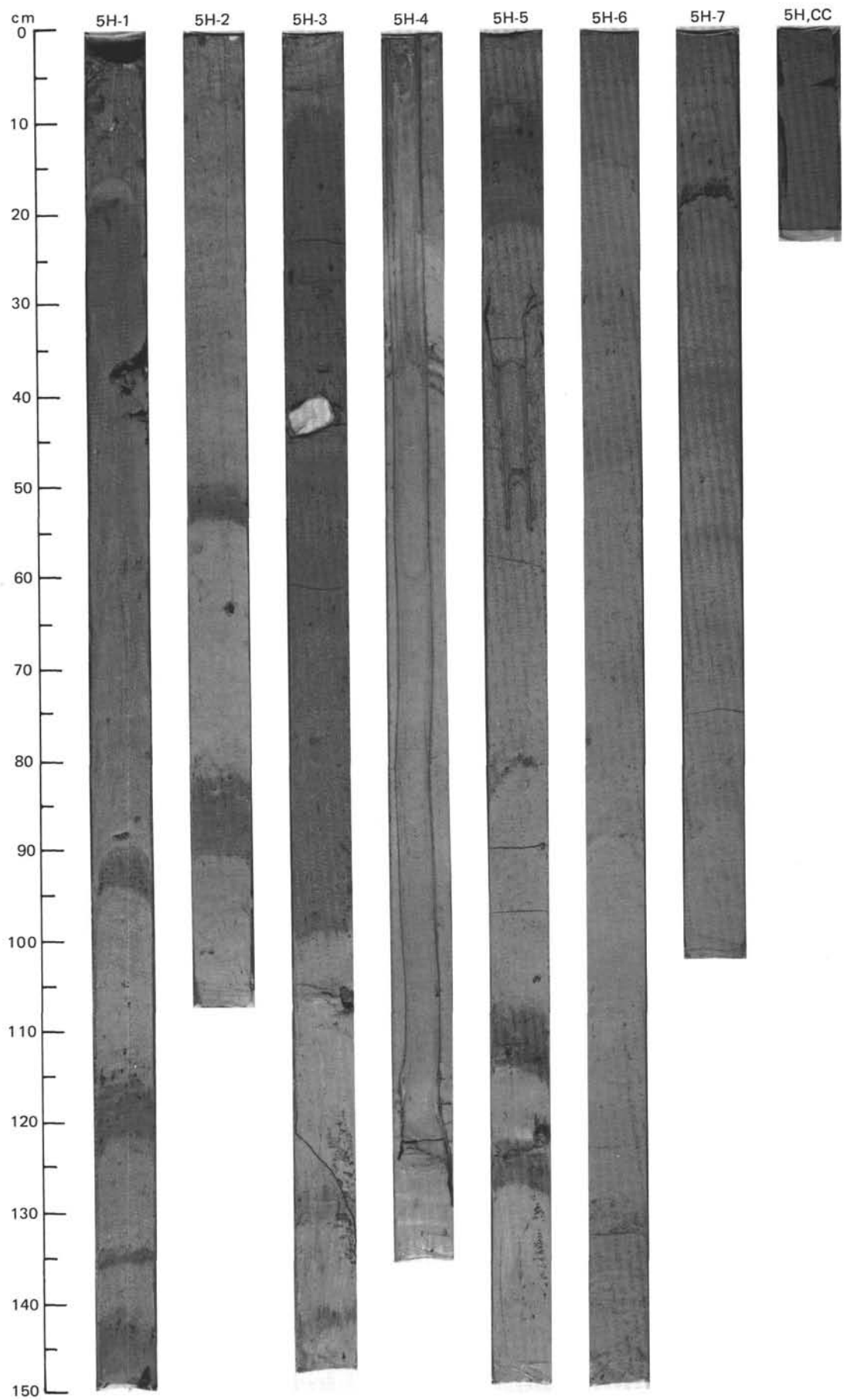


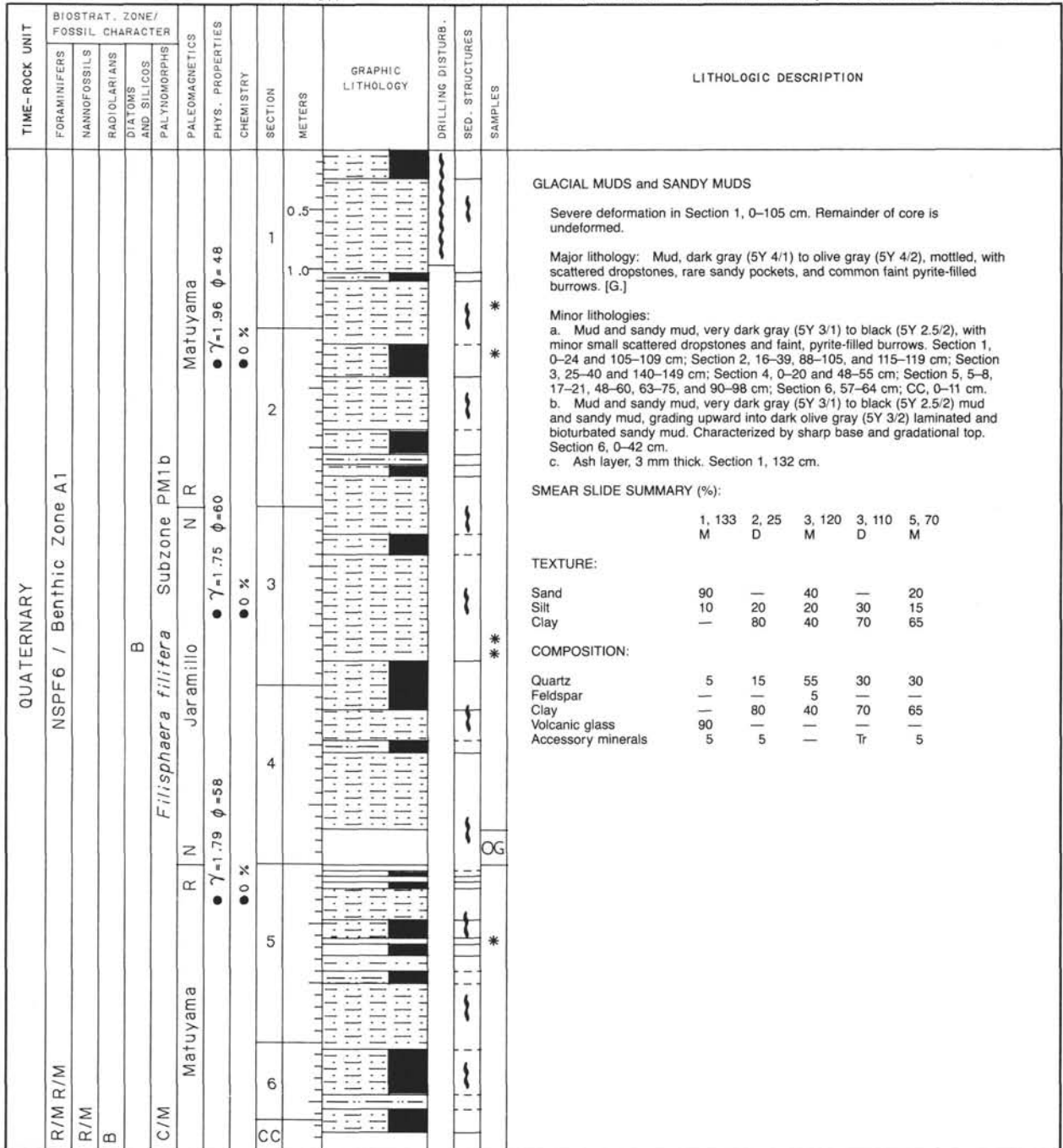


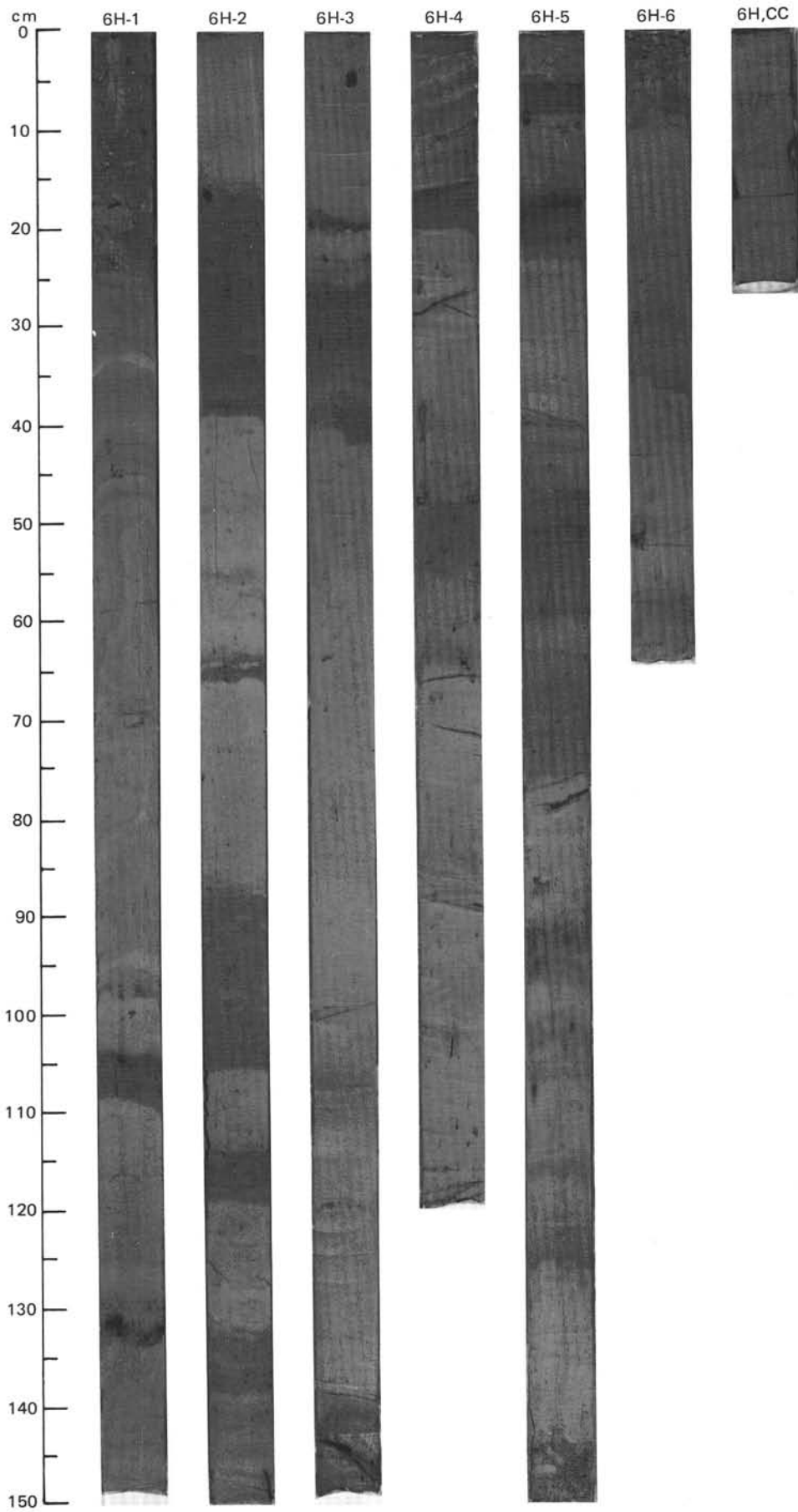


SITE 642 HOLE B CORE 5H CORED INTERVAL 1315.40-1324.90 mbsl; 29.40-38.90 mbsf

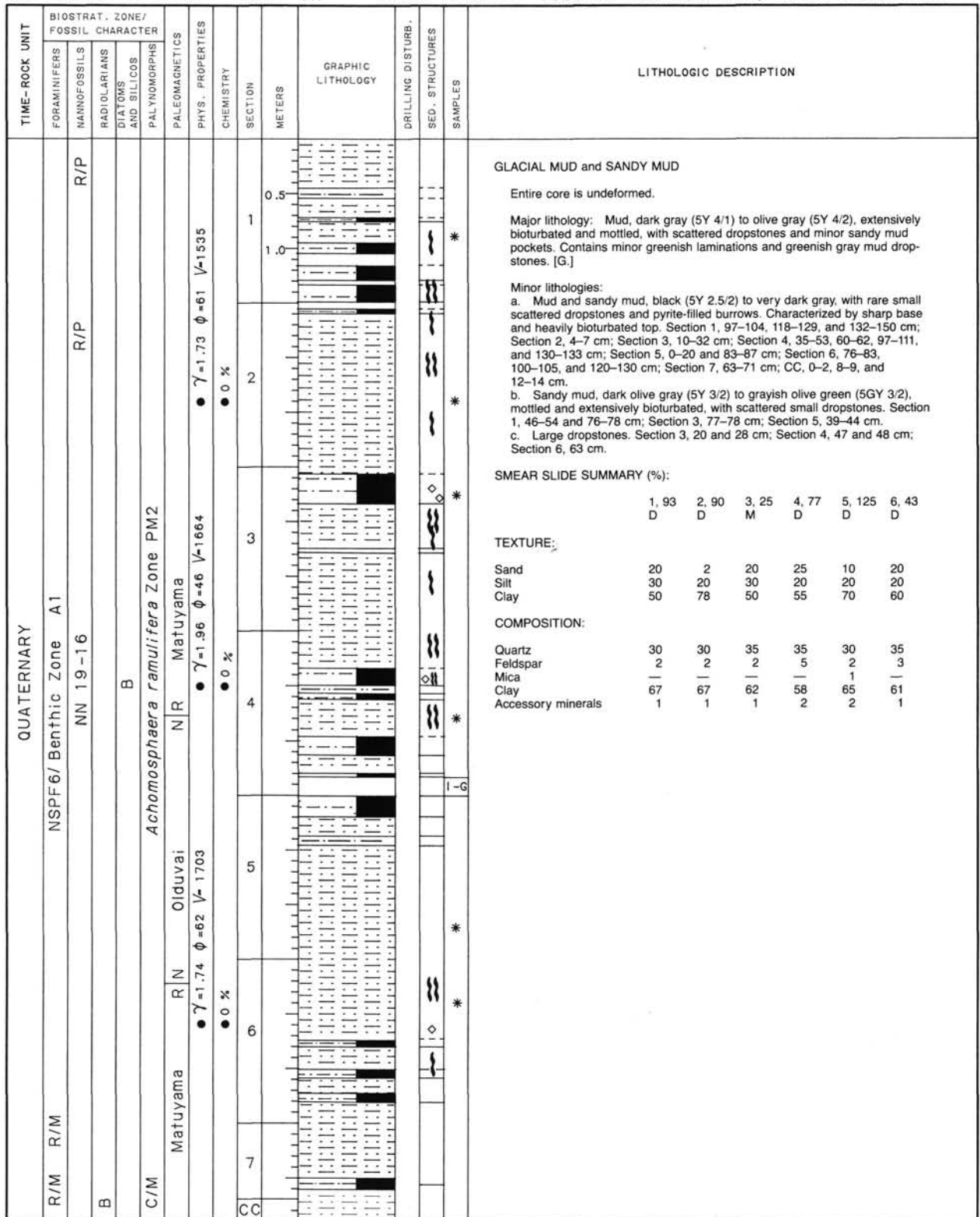


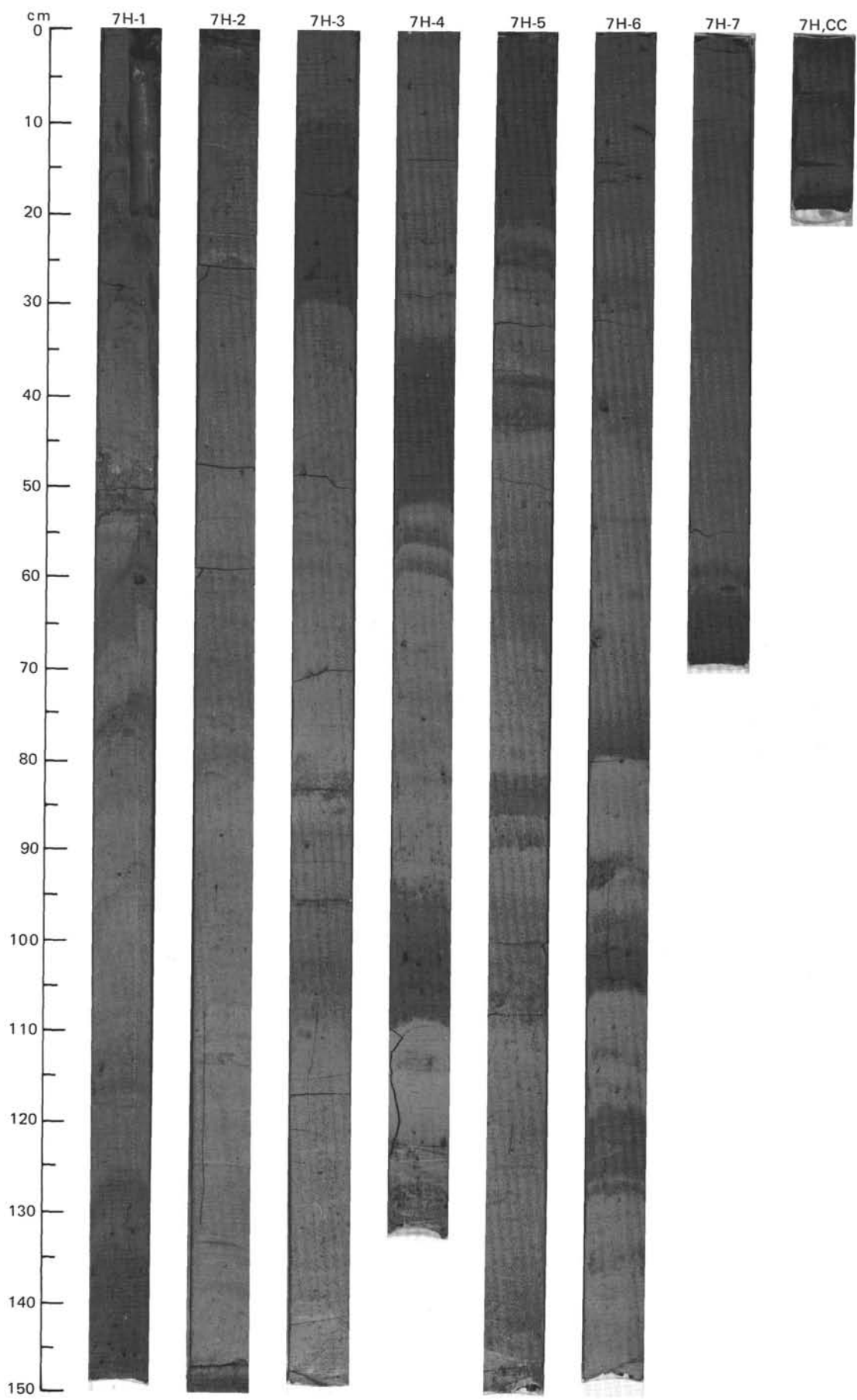


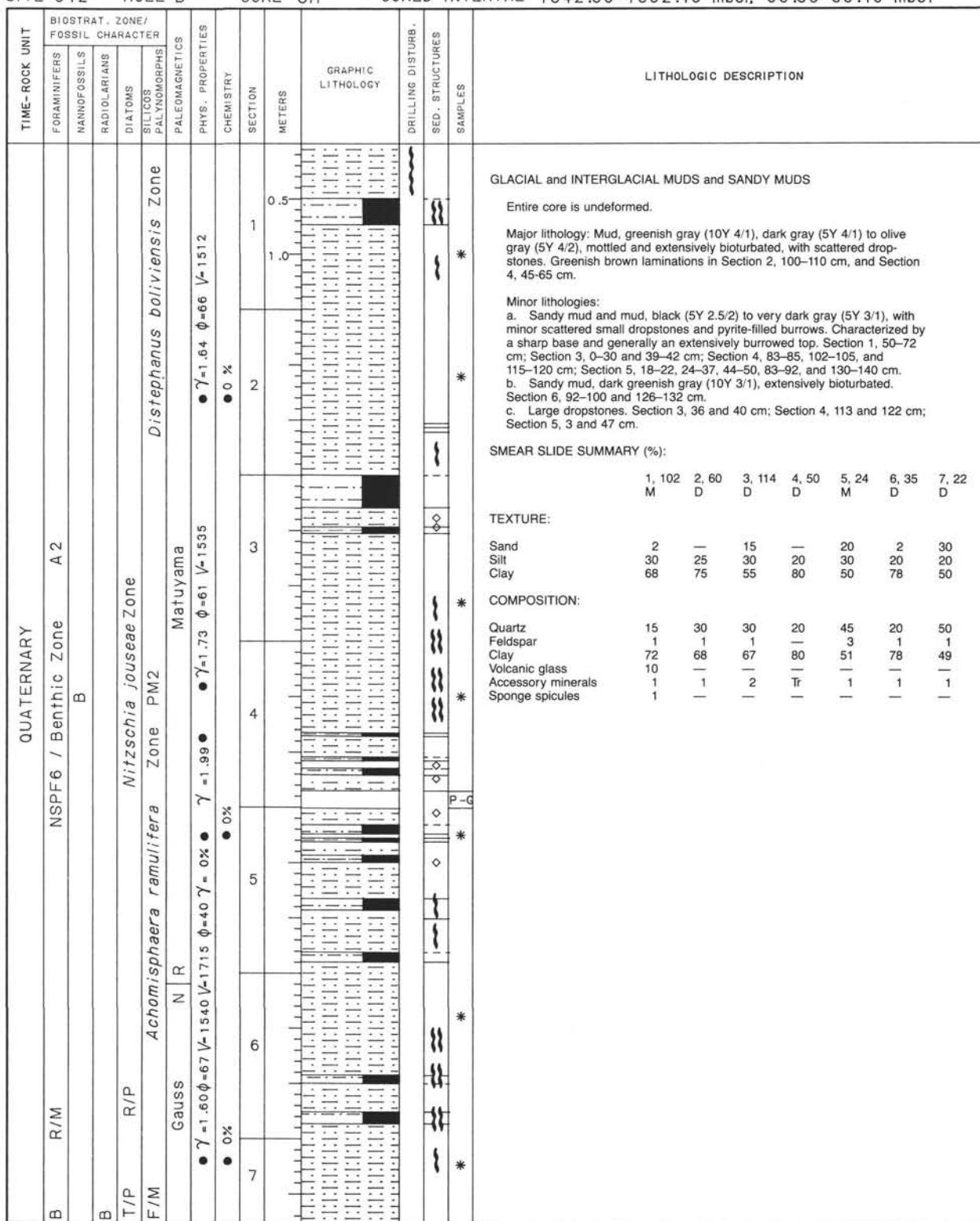


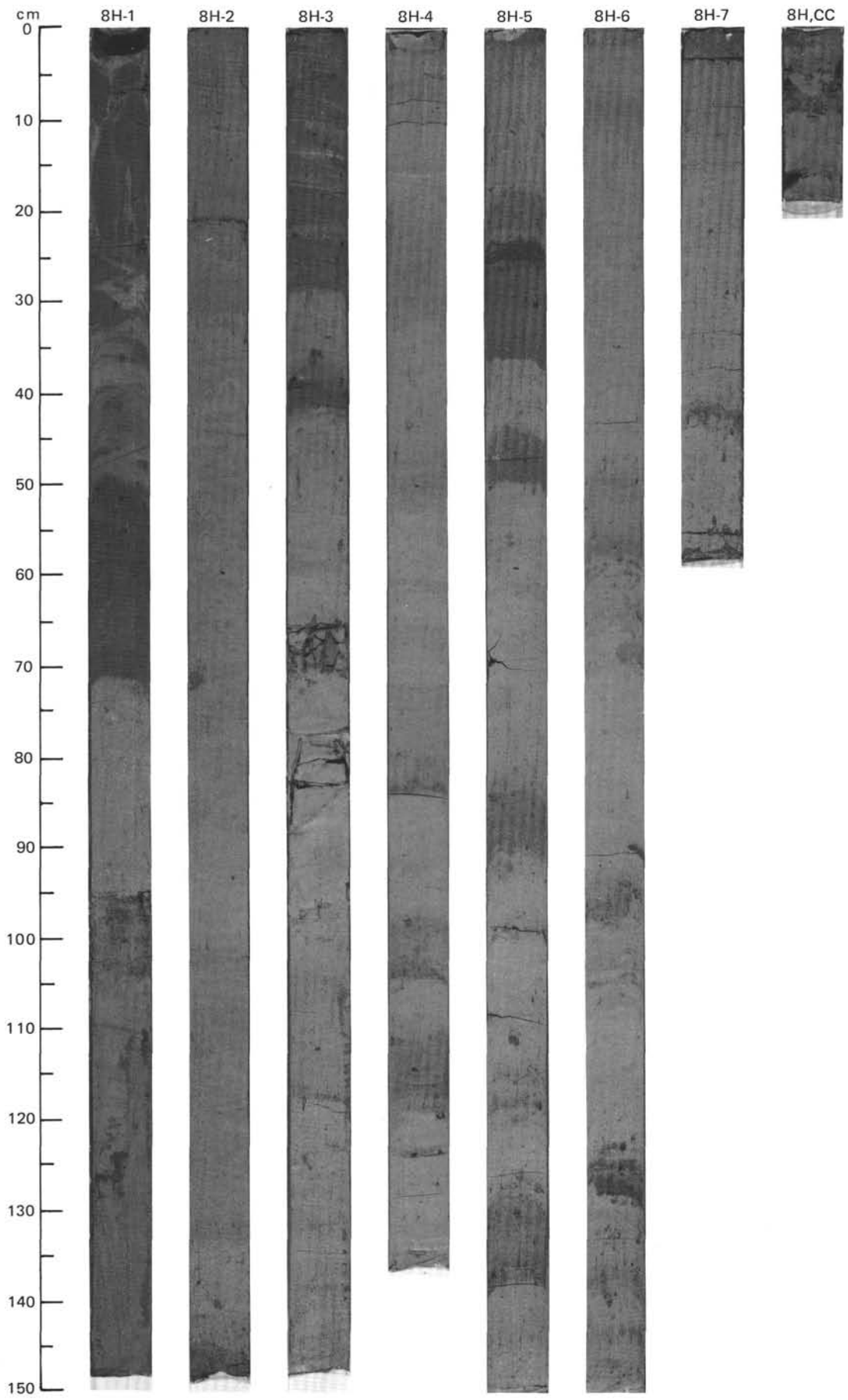


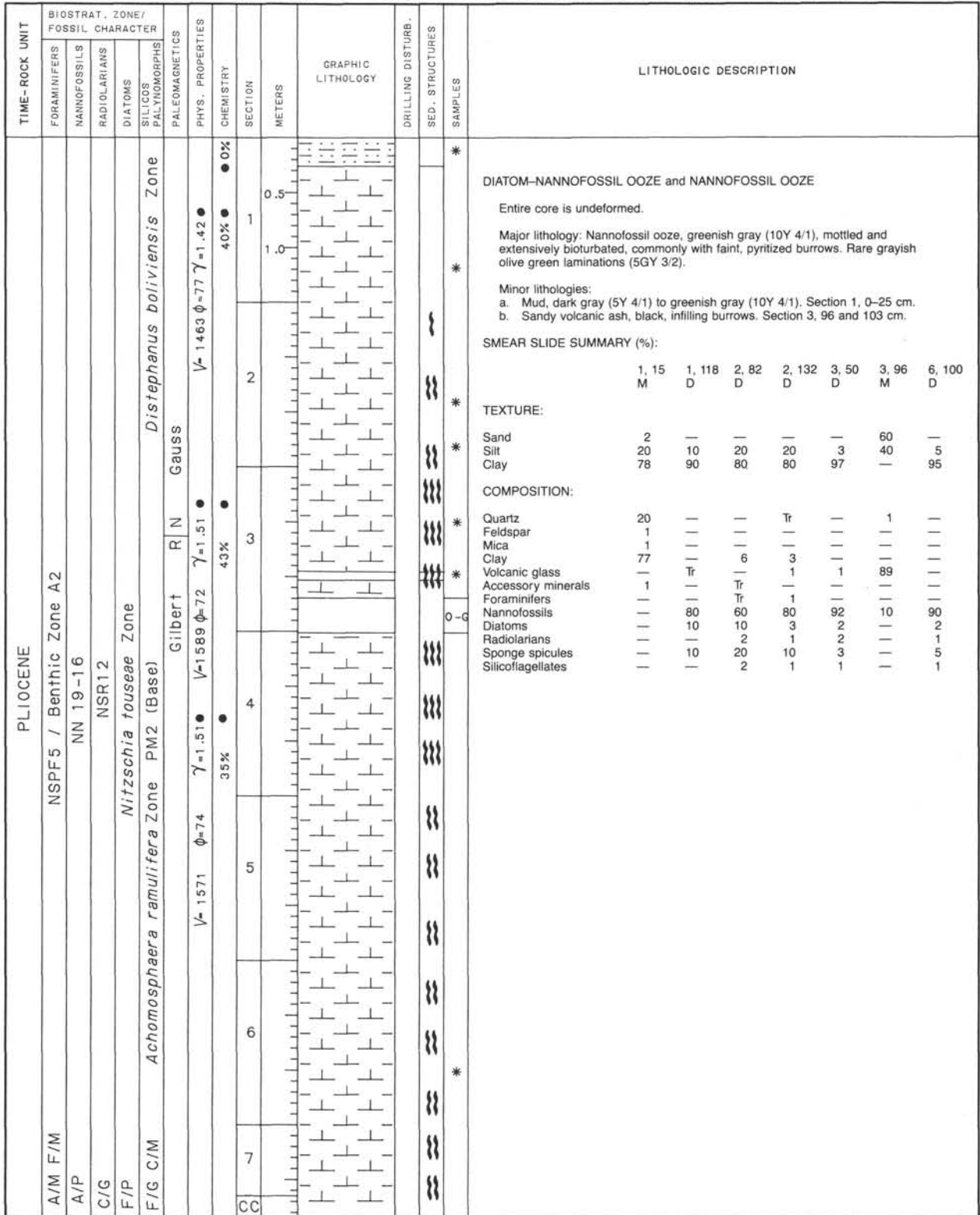
SITE 642 HOLE B CORE 7H CORED INTERVAL 1333.40-1342.90 mbsl; 47.40-56.90 mbsf

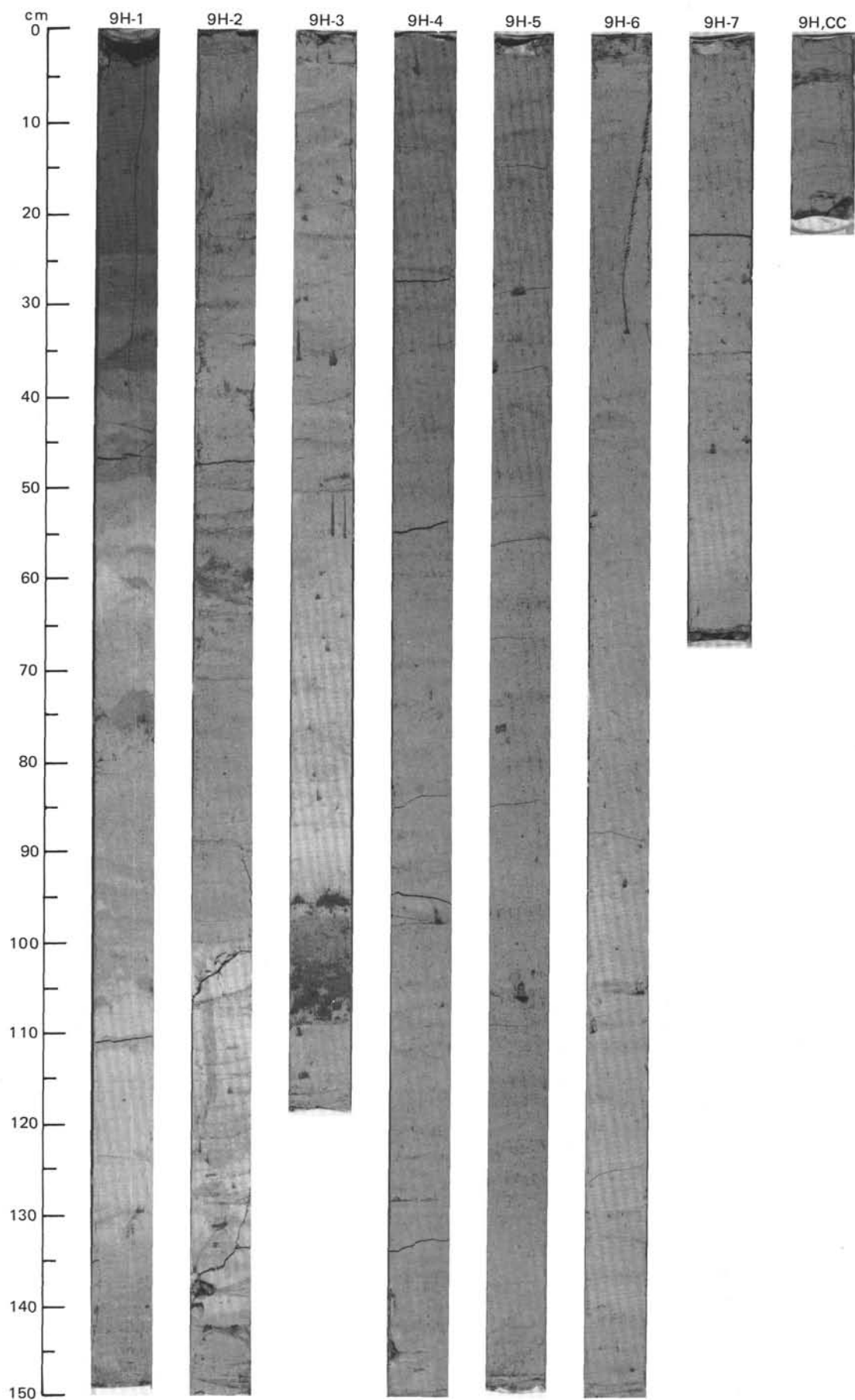






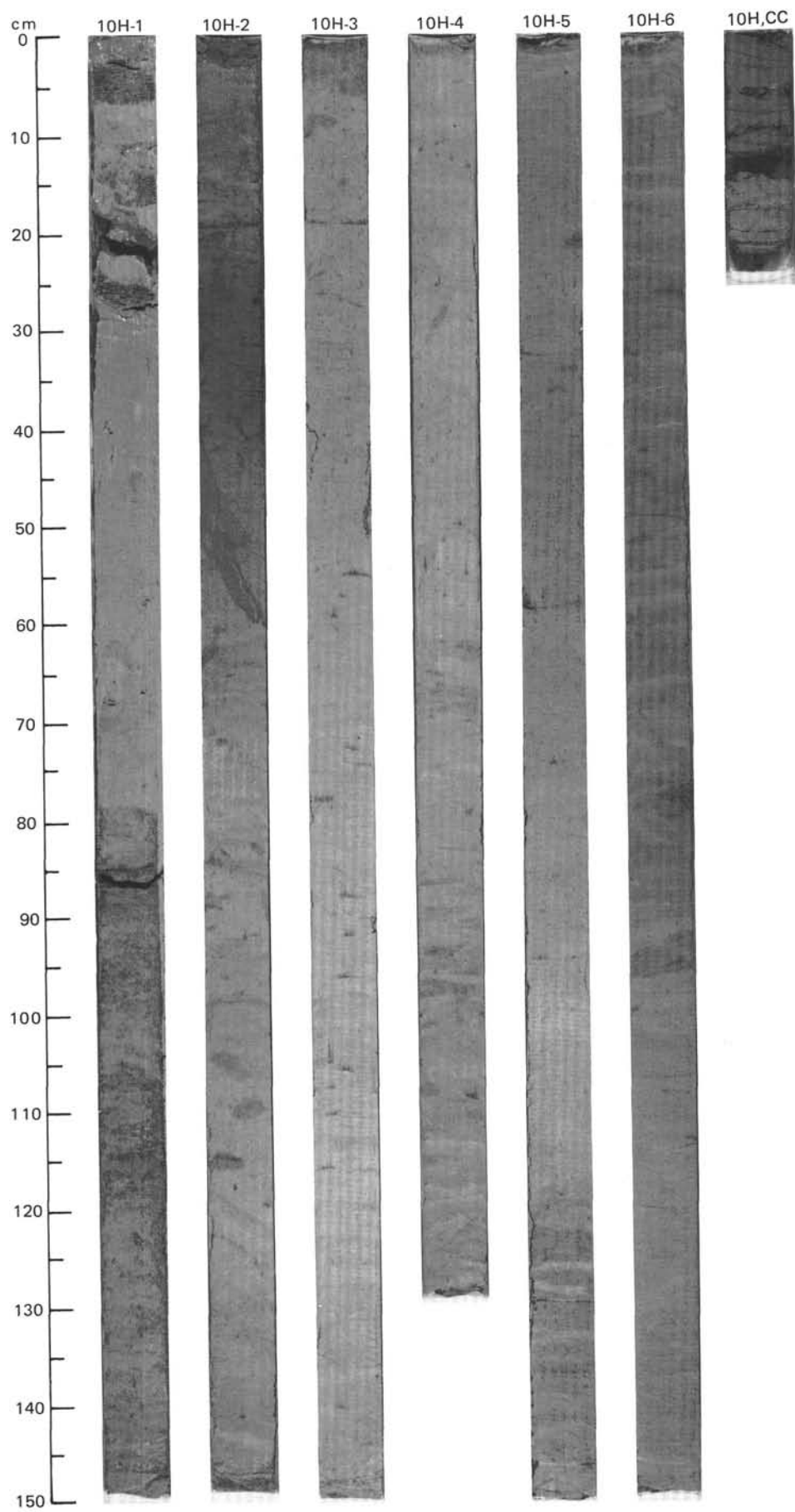






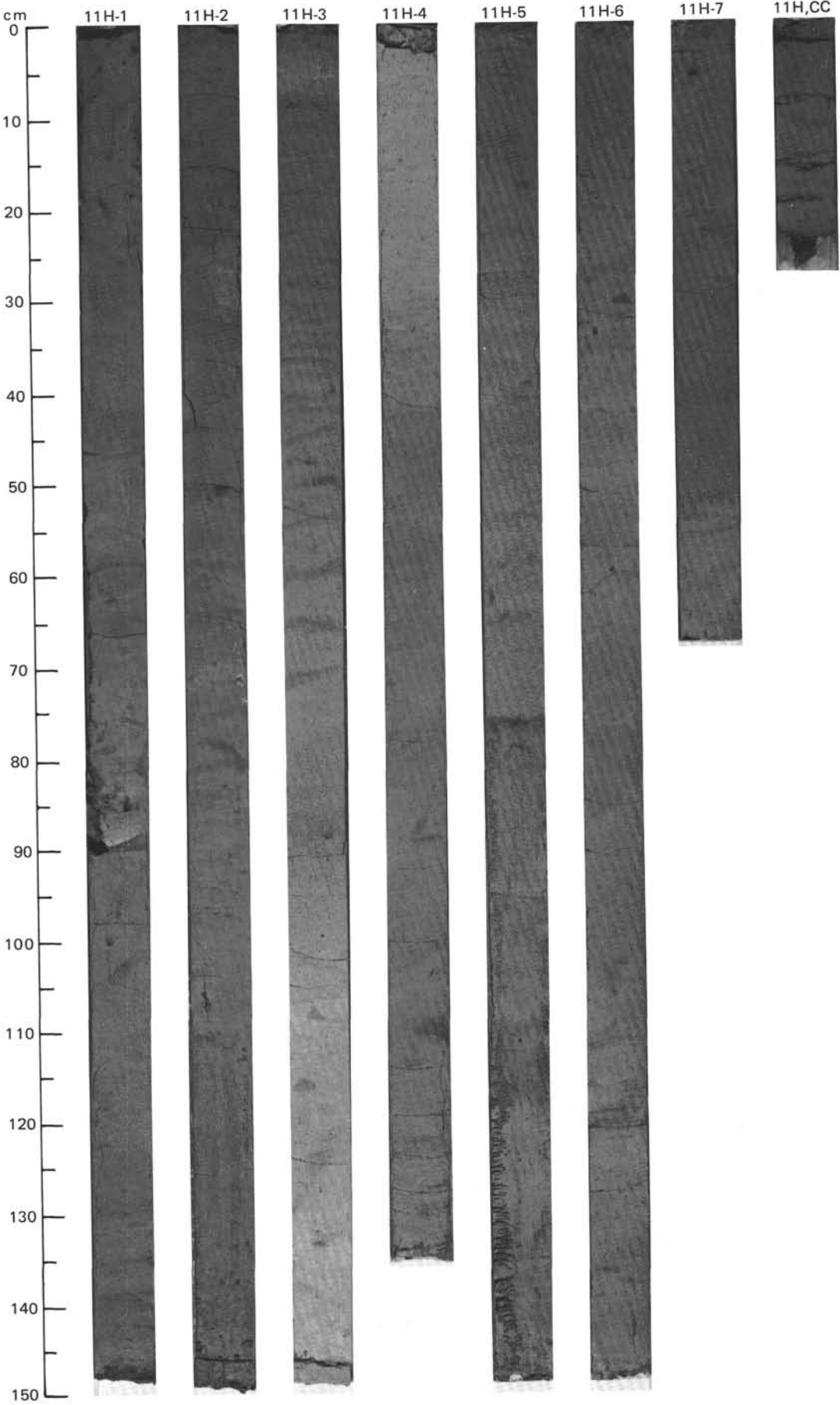
SITE 642 HOLE B CORE 10H CORED INTERVAL 1361.9-1371.4 mbsl; 75.90-85.40 mbsf

TIME-ROCK UNIT		BIOSTRAT. ZONE/ FOSSIL CHARACTER				PHYS. PROPERTIES	CHEMISTRY	SECTION	METERS	GRAPHIC LITHOLOGY	DRILLING DISTURB.	SED. STRUCTURES	SAMPLES	LITHOLOGIC DESCRIPTION													
FORAMINIFERS	NANNOFOSSILS	RADIOLARIANS	DIATOMS	SILICOS PALYOMORPHS																							
PLIOCENE																											
B B	NSPF4 / Benthic Zone A2				Epoch 5	● $\gamma = 1.49$ $\phi = 75$ ● 29 %	1	0.5 1.0					NANNOFOSSIL OOZE and MUD														
F/P	NN 15-7																										
C/G	NSR12				Epoch 5	● $\gamma = 1.50$ $\phi = 70$ $V = 1603$ ● 33 %	2						Entire core is undeformed. Major lithology: Nannofossil ooze, dusky yellow green (5GY 5/2) to gray (5Y 5/1), and mud, dark greenish gray (5GY 4/1), alternating in gradational beds 100-450 cm thick. Strongly bioturbated throughout, with small, faint burrows, well-developed <i>Zoophycos</i> , and pyritized burrows. Minor lithology: Volcanic ash, thin layer. Section 5, 120-122 cm.														
C/M	<i>Denticulopsis kantschatkii</i> Zone, subzone A <i>Cosinodiscus marginatus</i> Zone																										
F/G	C/G <i>Amiculosphaera umbracula</i> Zone PM3 <i>Distephanus boliviensis</i> Zone				Epoch 5		3						SMEAR SLIDE SUMMARY (%):														
R	R N																										
<table border="0" style="width: 100%;"> <tr> <td></td> <td style="text-align: center;">1, 88</td> <td style="text-align: center;">2, 79</td> <td style="text-align: center;">4, 80</td> <td style="text-align: center;">5, 122</td> <td style="text-align: center;">5, 140</td> <td style="text-align: center;">CC, 10</td> </tr> <tr> <td></td> <td style="text-align: center;">M</td> <td style="text-align: center;">D</td> <td style="text-align: center;">D</td> <td style="text-align: center;">M</td> <td style="text-align: center;">D</td> <td style="text-align: center;">D</td> </tr> </table>															1, 88	2, 79	4, 80	5, 122	5, 140	CC, 10		M	D	D	M	D	D
	1, 88	2, 79	4, 80	5, 122	5, 140	CC, 10																					
	M	D	D	M	D	D																					
TEXTURE:																											
Sand	—	10	—	50	3	25																					
Silt	20	13	10	30	20	25																					
Clay	80	77	90	80	77	50																					
COMPOSITION:																											
Quartz	15	10	5	2	20	15																					
Clay	77	7	2	—	67	50																					
Volcanic glass	Tr	—	—	70	—	10																					
Accessory minerals	1	—	—	—	1	3																					
Pyrite	—	5	—	20	—	—																					
Foraminifers	—	1	1	—	—	1																					
Nannofossils	2	80	85	—	—	1																					
Diatoms	—	1	3	1	1	3																					
Radiolarians	—	—	1	1	1	1																					
Sponge spicules	5	3	3	5	10	15																					
Silicoflagellates	—	—	—	—	—	1																					

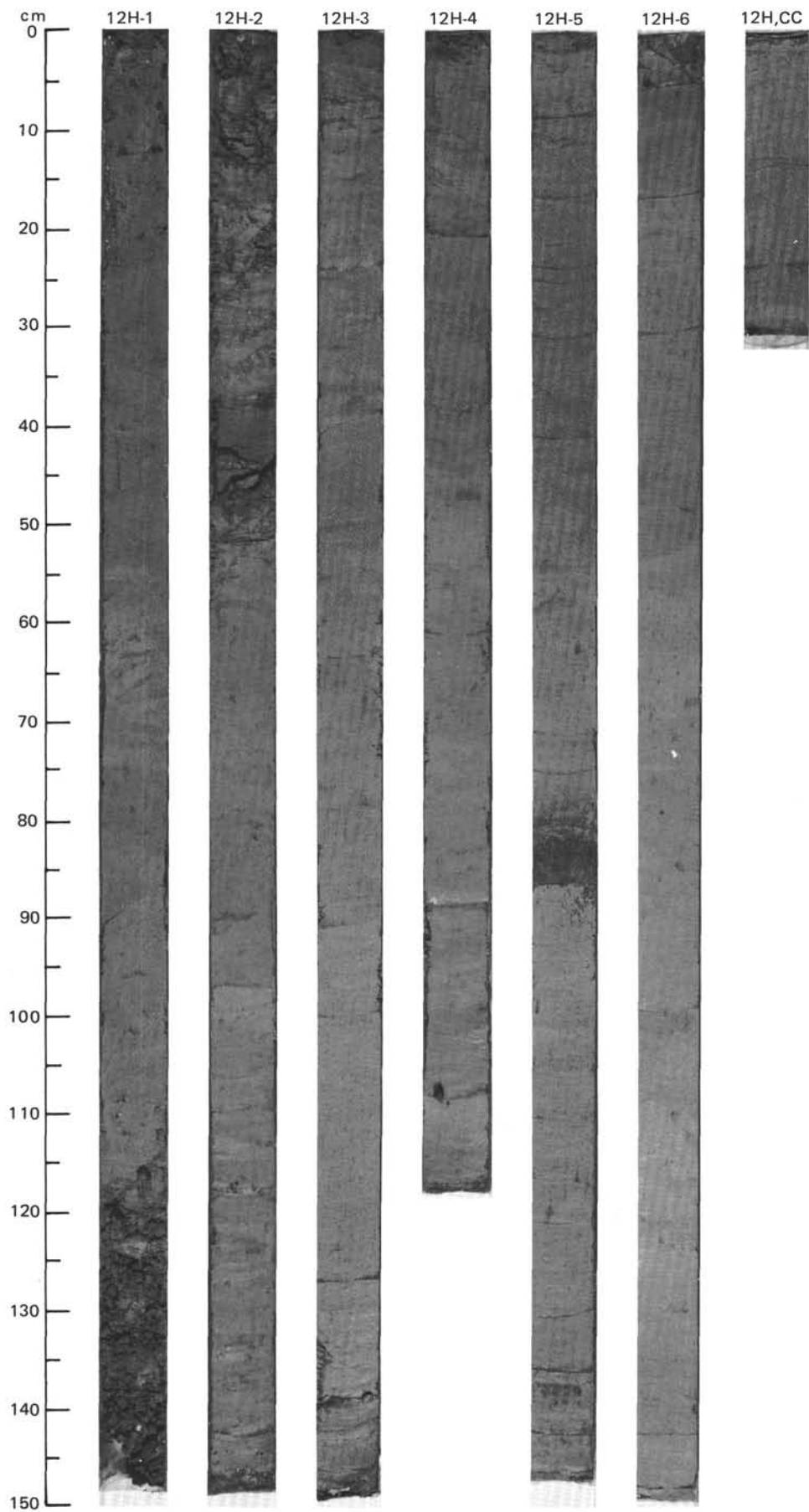


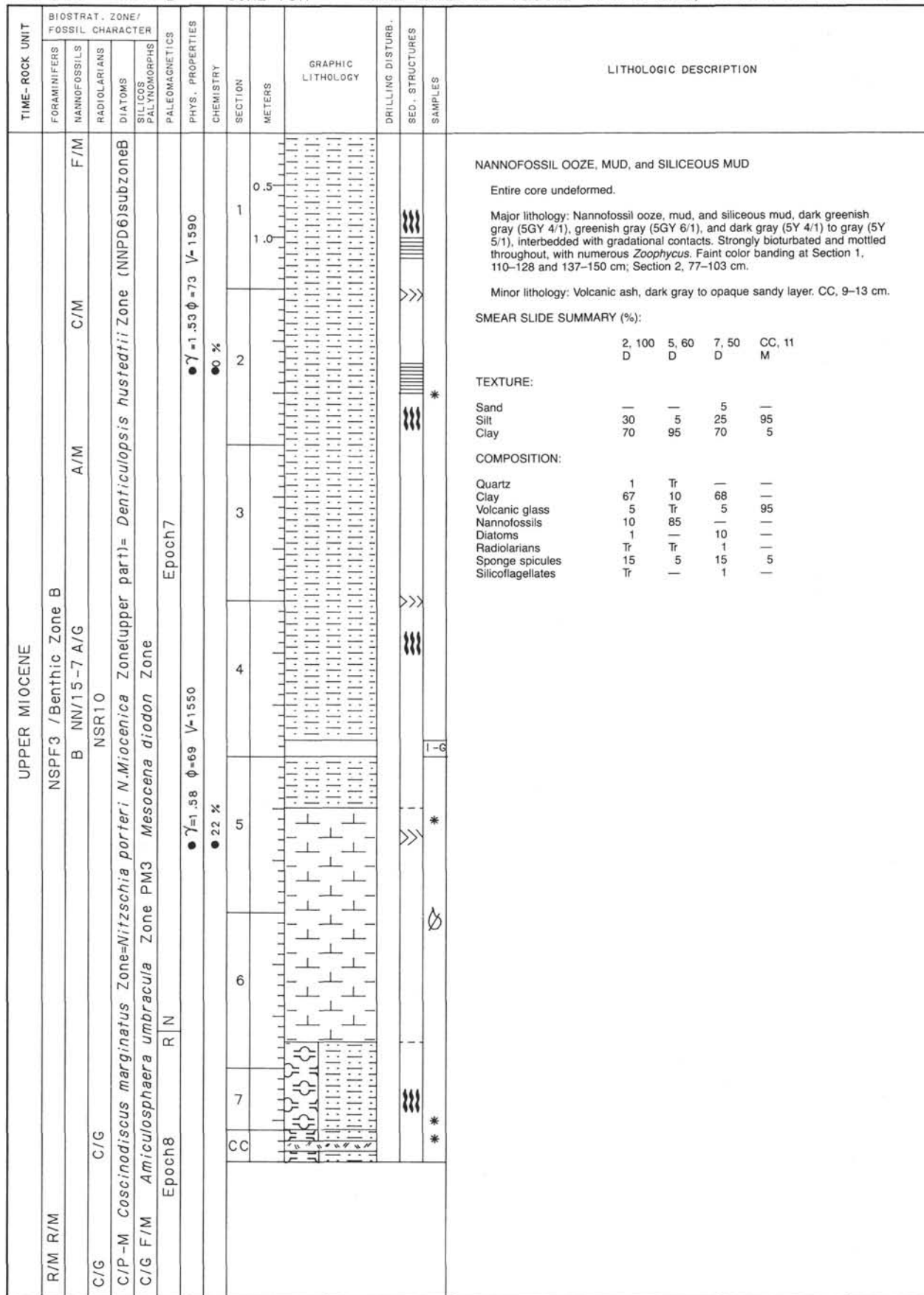
SITE 642 HOLE B CORE 11H CORED INTERVAL 1371.4-1380.9 mbsf; 85.40-94.90 mbsf

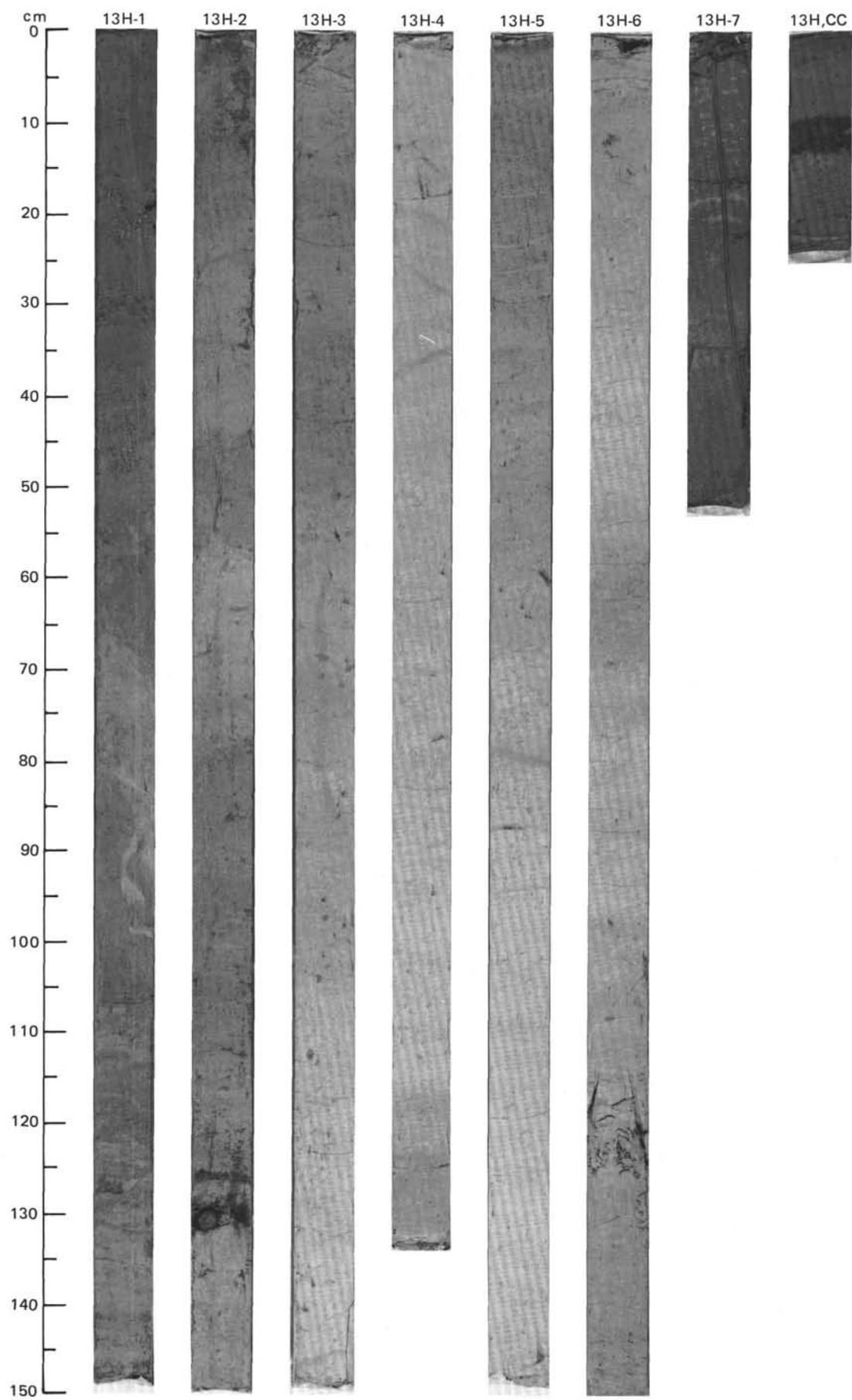
TIME-ROCK UNIT		BIOSTRAT. ZONE/ FOSSIL CHARACTER	SECTION	METERS	GRAPHIC LITHOLOGY	DRILLING DISTURB.	SED. STRUCTURES	SAMPLES	LITHOLOGIC DESCRIPTION																																																																																										
R/M B	F/M	C/G																																																																																																	
UPPER MIOCENE																																																																																																			
	NSPF3 / Benthic Zone A2																																																																																																		
	NN 15-7																																																																																																		
	NSR12																																																																																																		
	NSR11																																																																																																		
	C/P <i>Coscinodiscus marginatus</i> Zone = <i>Thalassiosira convexa</i> Zone = upper <i>Denticulopsis hustedii</i> Zone (NNPD6)Subzone B																																																																																																		
	F/M C/M <i>Amiculospaera umbracula</i> Zone PM3 <i>Mesocena diodon</i> Zone																																																																																																		
	Epoch / 6																																																																																																		
	● $\gamma=1.43$ $\phi=76$ ● $\gamma=1.43$ $\phi=76$																																																																																																		
	● 0 %																																																																																																		
	● 0 %																																																																																																		
			1	0.5				*	<p>SANDY MUD, NANNOFOSSIL OOZE, and SILICEOUS MUD</p> <p>Entire core is undeformed.</p> <p>Major lithology: Nannofossil ooze, dusky yellow green (5GY 5/2), and sandy mud and siliceous mud, dark greenish gray (5GY 4/1) to dark olive gray (5Y 3/2), alternating in gradational beds 150-300 cm thick. Strongly bioturbated throughout, with faint pyritized burrows common. Zoophycos well developed in Section 3.</p> <p>Minor lithologies:</p> <p>a. Faint banding in blue green. Section 2, 28-30 cm; Section 6, 0-70 cm.</p> <p>b. Mud, dark greenish gray (5G 4/1). Section 5, 76-77 cm. Possibly altered basaltic ash.</p> <p>c. Fresh volcanic glass. Section 2, 70-72 cm.</p> <p>SMEAR SLIDE SUMMARY (%):</p> <table border="1"> <tr> <td></td> <td>1, 60</td> <td>2, 70</td> <td>3, 100</td> <td>5, 112</td> <td>6, 60</td> </tr> <tr> <td></td> <td>D</td> <td>M</td> <td>D</td> <td>D</td> <td>D</td> </tr> </table> <p>TEXTURE:</p> <table border="1"> <tr> <td>Sand</td> <td>50</td> <td>85</td> <td>5</td> <td>10</td> <td>—</td> </tr> <tr> <td>Silt</td> <td>15</td> <td>5</td> <td>10</td> <td>30</td> <td>30</td> </tr> <tr> <td>Clay</td> <td>35</td> <td>10</td> <td>85</td> <td>60</td> <td>70</td> </tr> </table> <p>COMPOSITION:</p> <table border="1"> <tr> <td>Quartz</td> <td>35</td> <td>—</td> <td>2</td> <td>—</td> <td>—</td> </tr> <tr> <td>Feldspar</td> <td>1</td> <td>—</td> <td>—</td> <td>—</td> <td>—</td> </tr> <tr> <td>Clay</td> <td>35</td> <td>10</td> <td>5</td> <td>53</td> <td>63</td> </tr> <tr> <td>Volcanic glass</td> <td>10</td> <td>73</td> <td>—</td> <td>10</td> <td>—</td> </tr> <tr> <td>Accessory minerals</td> <td>2</td> <td>—</td> <td>—</td> <td>—</td> <td>—</td> </tr> <tr> <td>Nannofossils</td> <td>—</td> <td>—</td> <td>85</td> <td>—</td> <td>—</td> </tr> <tr> <td>Diatoms</td> <td>1</td> <td>1</td> <td>1</td> <td>10</td> <td>10</td> </tr> <tr> <td>Radiolarians</td> <td>—</td> <td>Tr</td> <td>—</td> <td>1</td> <td>1</td> </tr> <tr> <td>Sponge spicules</td> <td>15</td> <td>15</td> <td>5</td> <td>25</td> <td>25</td> </tr> <tr> <td>Silicoflagellates</td> <td>1</td> <td>1</td> <td>1</td> <td>1</td> <td>1</td> </tr> </table>		1, 60	2, 70	3, 100	5, 112	6, 60		D	M	D	D	D	Sand	50	85	5	10	—	Silt	15	5	10	30	30	Clay	35	10	85	60	70	Quartz	35	—	2	—	—	Feldspar	1	—	—	—	—	Clay	35	10	5	53	63	Volcanic glass	10	73	—	10	—	Accessory minerals	2	—	—	—	—	Nannofossils	—	—	85	—	—	Diatoms	1	1	1	10	10	Radiolarians	—	Tr	—	1	1	Sponge spicules	15	15	5	25	25	Silicoflagellates	1	1	1	1	1
	1, 60	2, 70	3, 100	5, 112	6, 60																																																																																														
	D	M	D	D	D																																																																																														
Sand	50	85	5	10	—																																																																																														
Silt	15	5	10	30	30																																																																																														
Clay	35	10	85	60	70																																																																																														
Quartz	35	—	2	—	—																																																																																														
Feldspar	1	—	—	—	—																																																																																														
Clay	35	10	5	53	63																																																																																														
Volcanic glass	10	73	—	10	—																																																																																														
Accessory minerals	2	—	—	—	—																																																																																														
Nannofossils	—	—	85	—	—																																																																																														
Diatoms	1	1	1	10	10																																																																																														
Radiolarians	—	Tr	—	1	1																																																																																														
Sponge spicules	15	15	5	25	25																																																																																														
Silicoflagellates	1	1	1	1	1																																																																																														
			2	1.0				*																																																																																											
			3					*																																																																																											
			4					*																																																																																											
			5					*																																																																																											
			6					*																																																																																											
			7					*																																																																																											
			CC																																																																																																



TIME-ROCK UNIT		BIOSTRAT. ZONE/ FOSSIL CHARACTER	PHYS. PROPERTIES	CHEMISTRY	SECTION	METERS	GRAPHIC LITHOLOGY	DRILLING DISTURB.	SED. STRUCTURES	SAMPLES	LITHOLOGIC DESCRIPTION																																																																											
FORAMINIFERS	NANNOFOSSILS																																																																																					
UPPER MIOCENE																																																																																						
B B	NSPF3 / Benthic Zone A2				1	0.5					<p>SILICEOUS MUD</p> <p>Moderate deformation at Section 1, 120 cm, to Section 2, 50 cm. The rest of the core is undeformed.</p> <p>Major lithology: Siliceous mud, dark greenish gray (5GY 4/1) to dark gray (5Y 4/1), strongly bioturbated. Pyrite impregnations common along burrows.</p> <p>Minor lithologies: a. Sand, patchy, Section 5, 135-145 cm; Section 6, 130-150 cm. b. Ash, dark gray (5Y 4/1). Section 5, 80-90 cm.</p> <p>SMEAR SLIDE SUMMARY (%):</p> <table border="1"> <thead> <tr> <th></th> <th>1, 80 D</th> <th>3, 60 D</th> <th>5, 84 M</th> <th>6, 80 D</th> </tr> </thead> <tbody> <tr> <td>TEXTURE:</td> <td></td> <td></td> <td></td> <td></td> </tr> <tr> <td>Sand</td> <td>—</td> <td>2</td> <td>65</td> <td>—</td> </tr> <tr> <td>Silt</td> <td>30</td> <td>18</td> <td>5</td> <td>50</td> </tr> <tr> <td>Clay</td> <td>70</td> <td>80</td> <td>20</td> <td>50</td> </tr> </tbody> </table> <p>COMPOSITION:</p> <table border="1"> <thead> <tr> <th></th> <th>1, 80 D</th> <th>3, 60 D</th> <th>5, 84 M</th> <th>6, 80 D</th> </tr> </thead> <tbody> <tr> <td>Quartz</td> <td>—</td> <td>1</td> <td>—</td> <td>—</td> </tr> <tr> <td>Mica</td> <td>—</td> <td>Tr</td> <td>—</td> <td>—</td> </tr> <tr> <td>Clay</td> <td>66</td> <td>75</td> <td>20</td> <td>45</td> </tr> <tr> <td>Volcanic glass</td> <td>—</td> <td>2</td> <td>64</td> <td>—</td> </tr> <tr> <td>Nannofossils</td> <td>—</td> <td>—</td> <td>—</td> <td>5</td> </tr> <tr> <td>Diatoms</td> <td>5</td> <td>1</td> <td>5</td> <td>10</td> </tr> <tr> <td>Radiolarians</td> <td>2</td> <td>1</td> <td>1</td> <td>Tr</td> </tr> <tr> <td>Sponge spicules</td> <td>25</td> <td>20</td> <td>10</td> <td>35</td> </tr> <tr> <td>Siicoflagellates</td> <td>2</td> <td>—</td> <td>Tr</td> <td>5</td> </tr> </tbody> </table>		1, 80 D	3, 60 D	5, 84 M	6, 80 D	TEXTURE:					Sand	—	2	65	—	Silt	30	18	5	50	Clay	70	80	20	50		1, 80 D	3, 60 D	5, 84 M	6, 80 D	Quartz	—	1	—	—	Mica	—	Tr	—	—	Clay	66	75	20	45	Volcanic glass	—	2	64	—	Nannofossils	—	—	—	5	Diatoms	5	1	5	10	Radiolarians	2	1	1	Tr	Sponge spicules	25	20	10	35	Siicoflagellates	2	—	Tr	5
	1, 80 D	3, 60 D	5, 84 M	6, 80 D																																																																																		
TEXTURE:																																																																																						
Sand	—	2	65	—																																																																																		
Silt	30	18	5	50																																																																																		
Clay	70	80	20	50																																																																																		
	1, 80 D	3, 60 D	5, 84 M	6, 80 D																																																																																		
Quartz	—	1	—	—																																																																																		
Mica	—	Tr	—	—																																																																																		
Clay	66	75	20	45																																																																																		
Volcanic glass	—	2	64	—																																																																																		
Nannofossils	—	—	—	5																																																																																		
Diatoms	5	1	5	10																																																																																		
Radiolarians	2	1	1	Tr																																																																																		
Sponge spicules	25	20	10	35																																																																																		
Siicoflagellates	2	—	Tr	5																																																																																		
F/M	NN 15-7				1.0																																																																																	
C/G	NSR11				2																																																																																	
C/M	<i>Coscinodiscus marginatus</i> Zone = <i>Thalassiosira convexa</i> Zone = <i>Denticulopsis hustedtii</i> Zone (NNPD6), subzone B				3																																																																																	
F/G C/G	<i>Amiculospaera umbracula</i> Zone PM3 <i>Mesocena diodon</i> Zone				4																																																																																	
	Epoch 7				5																																																																																	
					6																																																																																	
					CC																																																																																	

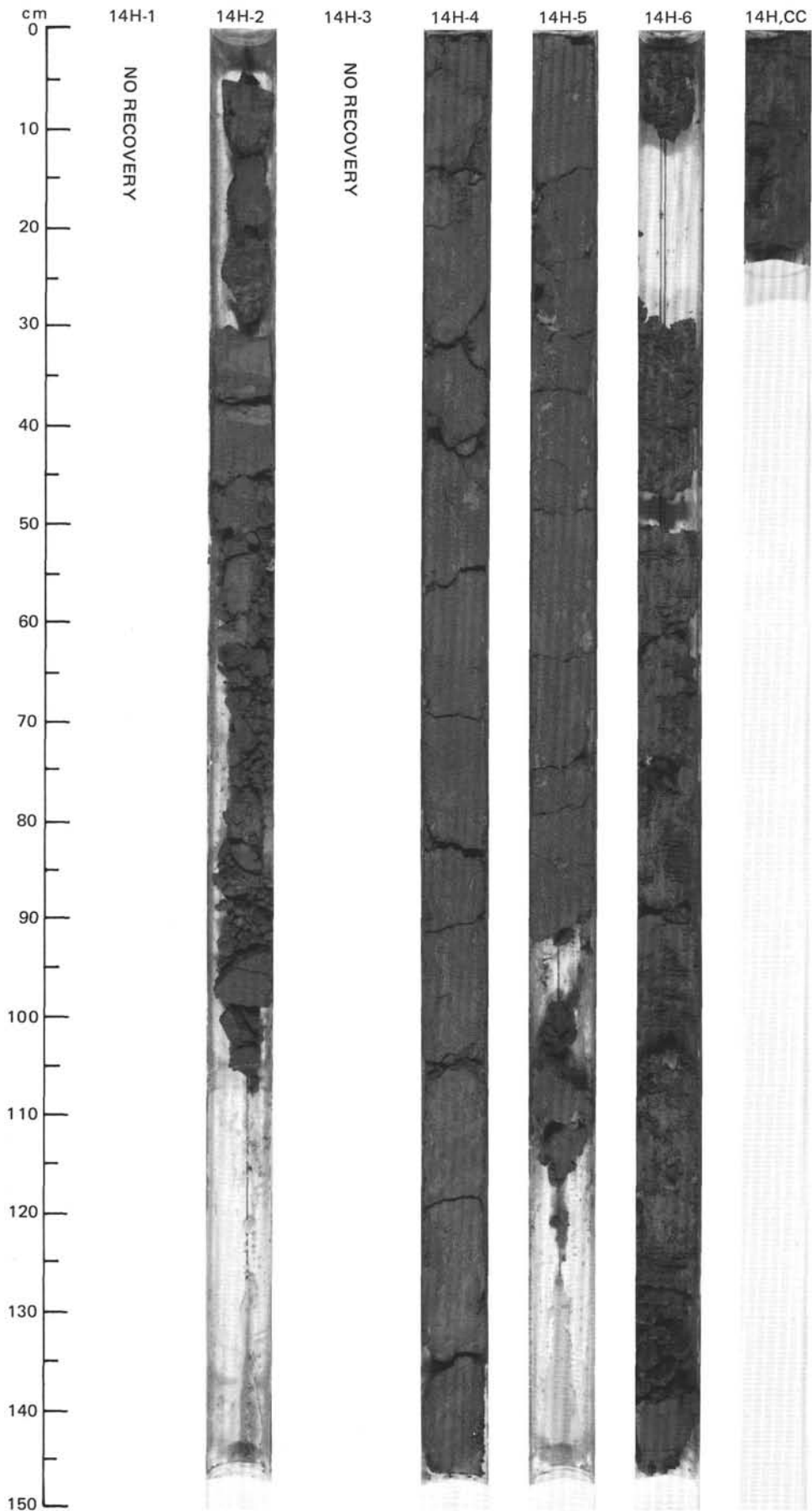




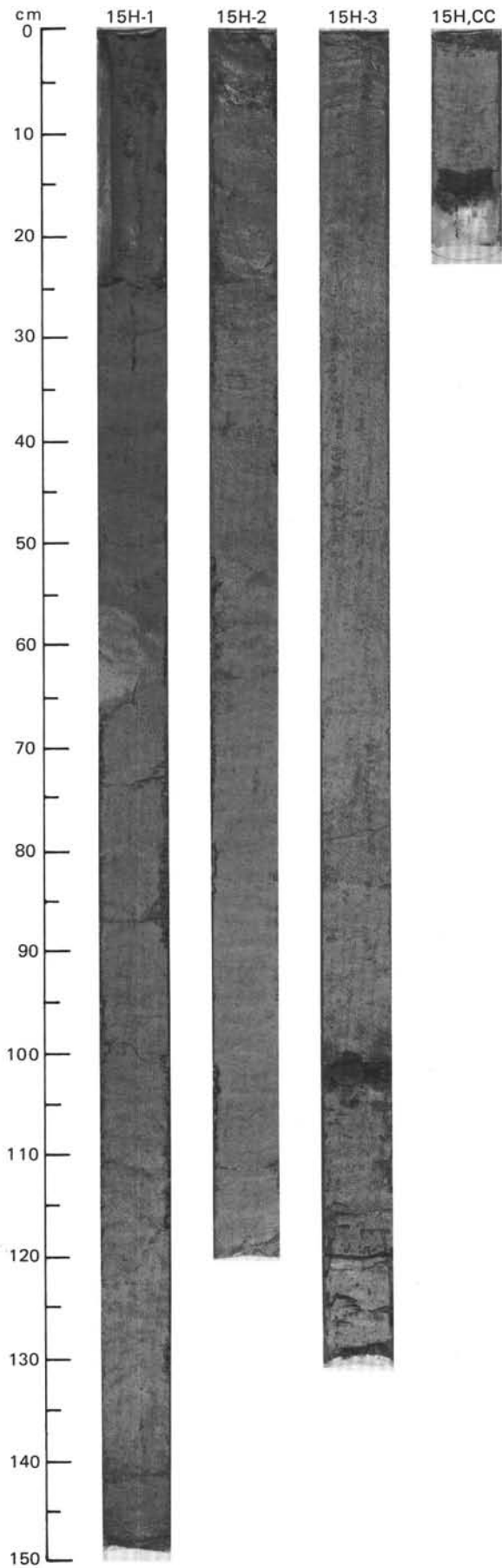


SITE 642 HOLE B CORE 14H CORED INTERVAL 1400.0-1409.5 mbsl; 114.00-123.50 mbsf

TIME-ROCK UNIT		FORAMINIFERS	NANNOFOSSILS	RADIOLARIANS	DIATOMS	SILICOS PALYMONORPHS	PALEOMAGNETICS	PHYS. PROPERTIES	CHEMISTRY	SECTION	METERS	GRAPHIC LITHOLOGY	DRILLING DISTURB.	SEC. STRUCTURES	SAMPLES	LITHOLOGIC DESCRIPTION																																																
BIOSTRAT. ZONE/ FOSSIL CHARACTER																																																																
UPPER MIOCENE																																																																
BB	NSPF3 / Benthic Zone B																																																															
F/M	NSR10																																																															
C/M	F/M																																																															
C/G	C/G																																																															
Coscinodiscus marginatus Zone= Nitzschia porteri -N.miocenica Zone= Dentikulopsis hustedii Zone (NNPD6), subzone B																																																																
Amiculospaera umbracula Zone PM3 Mesocena circulus/mesocena diodon Zone																																																																
											0.5	VOID				<p>SILICEOUS MUD</p> <p>Entire core is moderately disturbed.</p> <p>Major lithology: Siliceous mud, dark greenish gray (5GY 4/1), bioturbated and mottled.</p> <p>Minor lithologies:</p> <p>a. Sand, dark greenish gray (5GY 4/1), occurs in small pockets throughout the core.</p> <p>b. Volcanic ash, occurs as lenses. Section 1, 85 and 103 cm.</p> <p>SMEAR SLIDE SUMMARY (%):</p> <table border="1"> <tr> <td></td> <td>4, 80</td> <td>5, 103</td> <td>CC, 14</td> </tr> <tr> <td></td> <td>D</td> <td>M</td> <td>D</td> </tr> </table> <p>TEXTURE:</p> <table border="1"> <tr> <td>Sand</td> <td>85</td> <td>80</td> <td>5</td> </tr> <tr> <td>Silt</td> <td>15</td> <td>15</td> <td>45</td> </tr> <tr> <td>Clay</td> <td>—</td> <td>5</td> <td>50</td> </tr> </table> <p>COMPOSITION:</p> <table border="1"> <tr> <td>Quartz</td> <td>2</td> <td>1</td> <td>3</td> </tr> <tr> <td>Clay</td> <td>5</td> <td>1</td> <td>50</td> </tr> <tr> <td>Volcanic glass</td> <td>78</td> <td>60</td> <td>—</td> </tr> <tr> <td>Accessory minerals</td> <td>5</td> <td>38</td> <td>2</td> </tr> <tr> <td>Diatoms</td> <td>Tr</td> <td>Tr</td> <td>25</td> </tr> <tr> <td>Sponge spicules</td> <td>10</td> <td>Tr</td> <td>15</td> </tr> <tr> <td>Silicoflagellates</td> <td></td> <td></td> <td>5</td> </tr> </table>		4, 80	5, 103	CC, 14		D	M	D	Sand	85	80	5	Silt	15	15	45	Clay	—	5	50	Quartz	2	1	3	Clay	5	1	50	Volcanic glass	78	60	—	Accessory minerals	5	38	2	Diatoms	Tr	Tr	25	Sponge spicules	10	Tr	15	Silicoflagellates			5
	4, 80	5, 103	CC, 14																																																													
	D	M	D																																																													
Sand	85	80	5																																																													
Silt	15	15	45																																																													
Clay	—	5	50																																																													
Quartz	2	1	3																																																													
Clay	5	1	50																																																													
Volcanic glass	78	60	—																																																													
Accessory minerals	5	38	2																																																													
Diatoms	Tr	Tr	25																																																													
Sponge spicules	10	Tr	15																																																													
Silicoflagellates			5																																																													
										1.0																																																						
										2																																																						
										3	VOID																																																					
										4					*																																																	
										5					*																																																	
										6	VOID																																																					
										CC	VOID				*																																																	

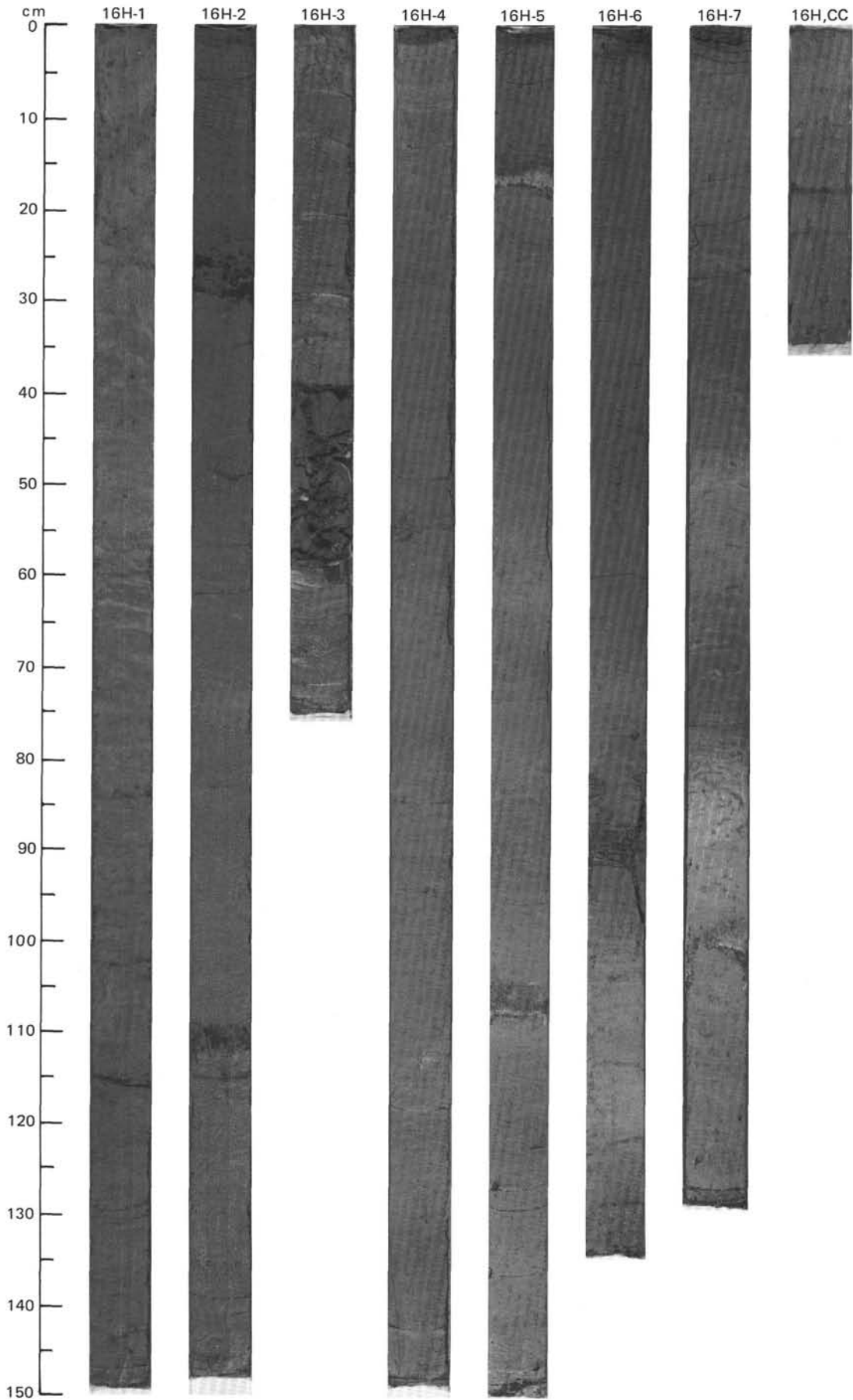


TIME-ROCK UNIT		BIOSTRAT. ZONE/ FOSSIL CHARACTER				SECTION	METERS	GRAPHIC LITHOLOGY	DRILLING DISTURB.	SED. STRUCTURES	SAMPLES	LITHOLOGIC DESCRIPTION																																																								
FORAMINIFERS	NANNOFOSSILS	RADIOLARIANS	DIATOMS	SILICOS PALEOMORPHS	PALEOMAGNETICS								PHYS. PROPERTIES	CHEMISTRY																																																						
UPPER MIOCENE																																																																				
A/G C/G	NSPF3 / Benthic Zone B																																																																			
C/P	NN 15-7				C/M																																																															
F/M					F/M																																																															
C/M <i>Coccinodiscus marginatus</i> Zone= <i>Nitzschia porteri</i> - <i>N.miocenica</i> Zone= <i>Denticulopsis hustedii</i> Zone (NNPD6).subzone B <i>Nematosphaeropsis aquaeducta</i> Zone PM4 <i>Mesocena circulus</i> / <i>M. diodon</i> Zone																																																																				
<ul style="list-style-type: none"> ● $\phi=63$ ● $\gamma=1.52$ $\phi=82$ ● 15 % ● 0 % 																																																																				
						1	0.5 1.0					<p>MUD and MARLY NANNOFOSSIL OOZE</p> <p>Entire core is undisturbed.</p> <p>Major lithology: Mud and marly nannofossil ooze, dark greenish gray (5GY 4/1) to greenish gray (5GY 5/1), interbedded with gradational and indistinct boundaries. Heavily bioturbated and mottled throughout.</p> <p>Minor lithology: Volcanic ash. Section 3, 102-104 cm.</p> <p>SMEAR SLIDE SUMMARY (%):</p> <table border="1"> <tr> <td></td> <td>1, 100</td> <td>3, 60</td> <td>3, 103</td> </tr> <tr> <td></td> <td>D</td> <td>D</td> <td>M</td> </tr> </table> <p>TEXTURE:</p> <table border="1"> <tr> <td>Sand</td> <td>35</td> <td>10</td> <td>70</td> </tr> <tr> <td>Silt</td> <td>15</td> <td>10</td> <td>10</td> </tr> <tr> <td>Clay</td> <td>50</td> <td>80</td> <td>20</td> </tr> </table> <p>COMPOSITION:</p> <table border="1"> <tr> <td>Quartz</td> <td>5</td> <td>—</td> <td>1</td> </tr> <tr> <td>Clay</td> <td>49</td> <td>54</td> <td>20</td> </tr> <tr> <td>Volcanic glass</td> <td>30</td> <td>5</td> <td>67</td> </tr> <tr> <td>Foraminifers</td> <td>1</td> <td>5</td> <td>—</td> </tr> <tr> <td>Nannofossils</td> <td>5</td> <td>30</td> <td>1</td> </tr> <tr> <td>Diatoms</td> <td>Tr</td> <td>1</td> <td>1</td> </tr> <tr> <td>Radiolarians</td> <td>Tr</td> <td>—</td> <td>Tr</td> </tr> <tr> <td>Sponge spicules</td> <td>10</td> <td>5</td> <td>10</td> </tr> <tr> <td>Silicoflagellates</td> <td>—</td> <td>—</td> <td>Tr</td> </tr> </table>		1, 100	3, 60	3, 103		D	D	M	Sand	35	10	70	Silt	15	10	10	Clay	50	80	20	Quartz	5	—	1	Clay	49	54	20	Volcanic glass	30	5	67	Foraminifers	1	5	—	Nannofossils	5	30	1	Diatoms	Tr	1	1	Radiolarians	Tr	—	Tr	Sponge spicules	10	5	10	Silicoflagellates	—	—	Tr
	1, 100	3, 60	3, 103																																																																	
	D	D	M																																																																	
Sand	35	10	70																																																																	
Silt	15	10	10																																																																	
Clay	50	80	20																																																																	
Quartz	5	—	1																																																																	
Clay	49	54	20																																																																	
Volcanic glass	30	5	67																																																																	
Foraminifers	1	5	—																																																																	
Nannofossils	5	30	1																																																																	
Diatoms	Tr	1	1																																																																	
Radiolarians	Tr	—	Tr																																																																	
Sponge spicules	10	5	10																																																																	
Silicoflagellates	—	—	Tr																																																																	
						2																																																														
						3																																																														
						CC																																																														

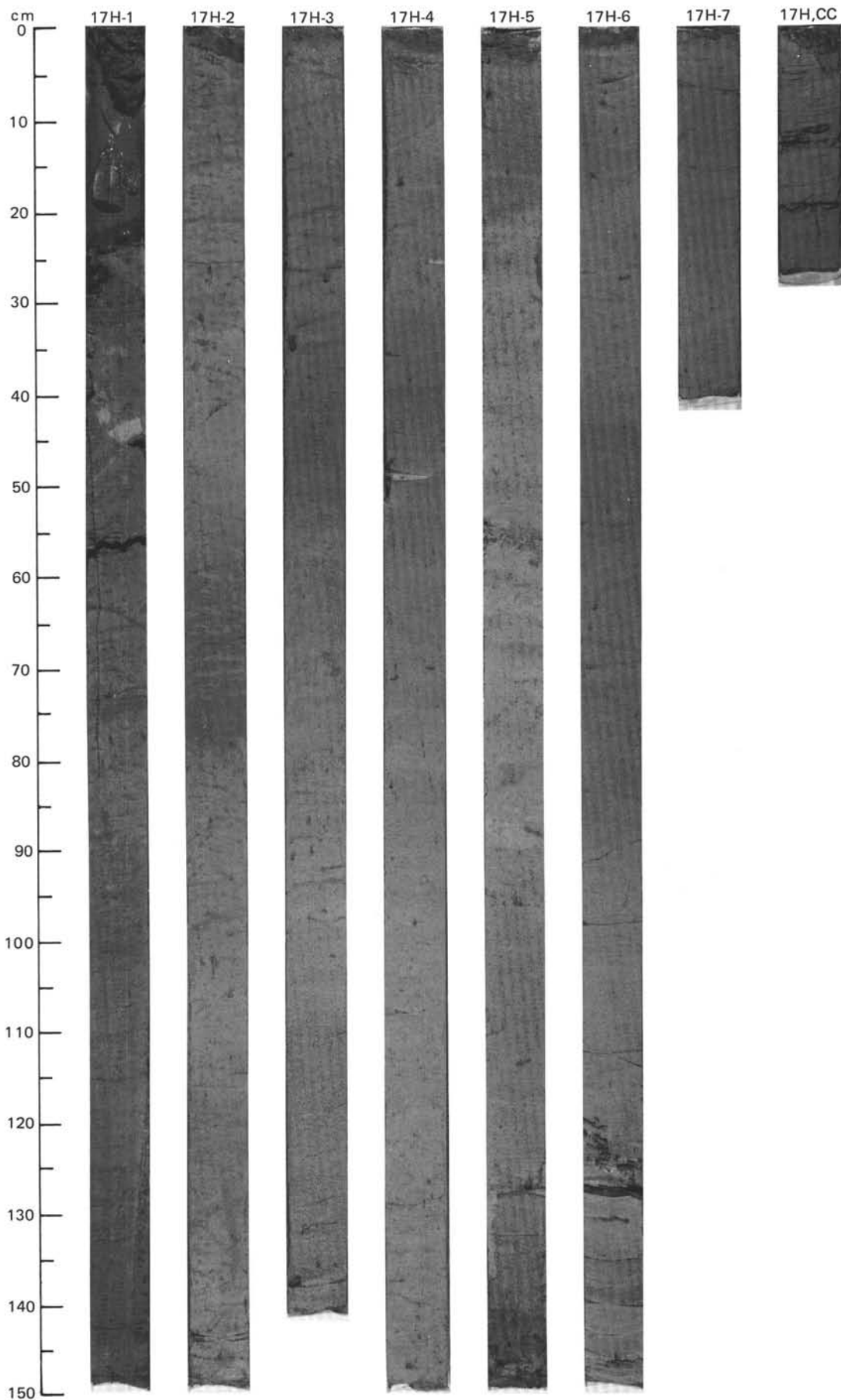


SITE 642 HOLE B CORE 16H CORED INTERVAL 1414.1-1424.0 mbsl; 128.10-138.00 mbsf

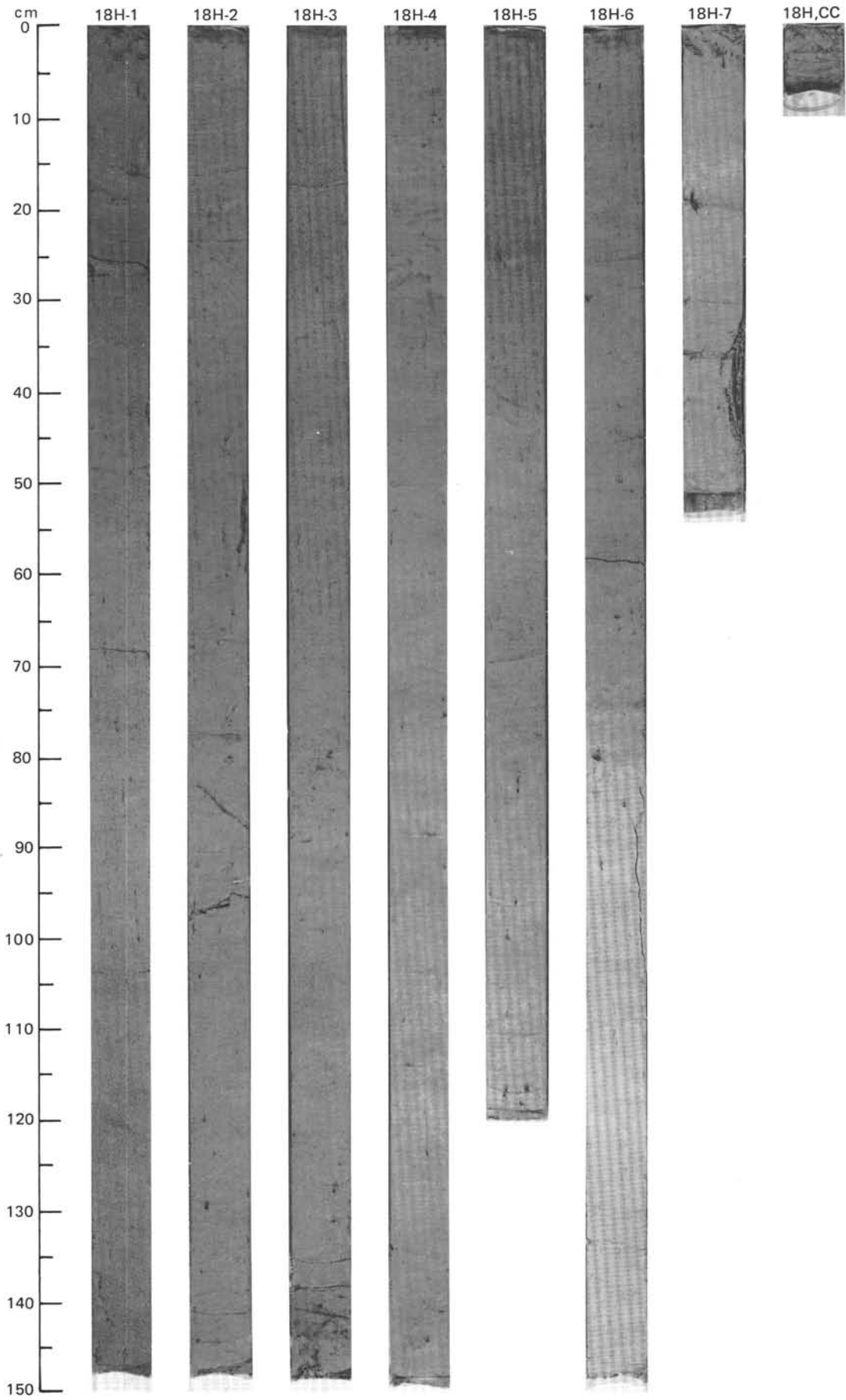
TIME-ROCK UNIT			FORAMINIFERS	MANNOFOSFILLS	RADIOLARIANS	DIATOMS	SILICOS PALYNO MORPHS	PALEOMAGNETICS	PHYS. PROPERTIES	CHEMISTRY	SECTION	METERS	GRAPHIC LITHOLOGY	DRILLING DISTURB.	SED. STRUCTURES	SAMPLES	LITHOLOGIC DESCRIPTION																																																																																																																																																																																																								
BIOSTRAT. ZONE/ FOSSIL CHARACTER																																																																																																																																																																																																																									
UPPER MIOCENE			NSPF3 /Benthic Zone B			B																																																																																																																																																																																																																			
C/M	R/M	A/G	A/P	C/P	NSR9																																																																																																																																																																																																																				
L/P	C/M	F/M	NSR8	15-7																																																																																																																																																																																																																					
C/M	Denticulopsis hustedtii-D.lauta Zone (NNPD5), subzone B																																																																																																																																																																																																																								
F/G	A/G	Nematosphaeropsis aqueducta Zone PM4 Mesocena circulus Zone																																																																																																																																																																																																																							
			● $\gamma = 1.51$ $\phi = 75$																																																																																																																																																																																																																						
			● 0 %																																																																																																																																																																																																																						
C	C	1	0.5	1.0	2	3	4	5	6	7	1-6																																																																																																																																																																																																														
<p>MUD, SILICEOUS MUD, MARLY NANNOFOSSIL OOZE, and NANNOFOSSIL OOZE</p> <p>Entire core is undisturbed.</p> <p>Major lithology: Mud, siliceous mud, marly nannofossil ooze, and nannofossil ooze, dark gray (5Y 4/1) to very dark gray (5Y 3/1), interbedded with gradational and indistinct boundaries. Heavily bioturbated and mottled throughout. Faint grayish-green (5G 4/2) laminations at Section 5, 28-30 and 60-62 cm, and Section 7, 37-41 cm.</p> <p>Minor lithology: Volcanic ash, white to gray (2.5Y 8/0), sandy, with sharp bases and gradational tops. Section 2, 23-29 and 110-113 cm; Section 5, 14-17 and 104-109 cm; Section 7, 99-101 cm.</p> <p>SMEAR SLIDE SUMMARY (%):</p> <table border="1"> <thead> <tr> <th></th> <th>1, 80</th> <th>2, 27</th> <th>3, 20</th> <th>5, 80</th> <th>5, 105</th> <th>7, 40</th> <th>7, 86</th> </tr> <tr> <th></th> <th>D</th> <th>M</th> <th>D</th> <th>D</th> <th>M</th> <th>D</th> <th>D</th> </tr> </thead> <tbody> <tr> <td>Sand</td> <td>10</td> <td>70</td> <td>25</td> <td>5</td> <td>—</td> <td>10</td> <td>—</td> </tr> <tr> <td>Silt</td> <td>40</td> <td>10</td> <td>10</td> <td>25</td> <td>80</td> <td>20</td> <td>20</td> </tr> <tr> <td>Clay</td> <td>50</td> <td>20</td> <td>65</td> <td>70</td> <td>20</td> <td>70</td> <td>80</td> </tr> </tbody> </table> <p>TEXTURE:</p> <table border="1"> <thead> <tr> <th></th> <th>1, 80</th> <th>2, 27</th> <th>3, 20</th> <th>5, 80</th> <th>5, 105</th> <th>7, 40</th> <th>7, 86</th> </tr> </thead> <tbody> <tr> <td>Quartz</td> <td>—</td> <td>—</td> <td>10</td> <td>—</td> <td>—</td> <td>—</td> <td>—</td> </tr> <tr> <td>Clay</td> <td>45</td> <td>15</td> <td>65</td> <td>55</td> <td>20</td> <td>38</td> <td>5</td> </tr> <tr> <td>Volcanic glass</td> <td>10</td> <td>70</td> <td>15</td> <td>5</td> <td>75</td> <td>5</td> <td>—</td> </tr> <tr> <td>Foraminifers</td> <td>—</td> <td>—</td> <td>—</td> <td>—</td> <td>—</td> <td>1</td> <td>Tr</td> </tr> <tr> <td>Nannofossils</td> <td>—</td> <td>—</td> <td>—</td> <td>5</td> <td>—</td> <td>30</td> <td>70</td> </tr> <tr> <td>Diatoms</td> <td>15</td> <td>5</td> <td>Tr</td> <td>25</td> <td>Tr</td> <td>5</td> <td>15</td> </tr> <tr> <td>Radiolarians</td> <td>5</td> <td>1</td> <td>—</td> <td>Tr</td> <td>—</td> <td>5</td> <td>—</td> </tr> <tr> <td>Sponge spicules</td> <td>25</td> <td>10</td> <td>10</td> <td>10</td> <td>5</td> <td>15</td> <td>10</td> </tr> <tr> <td>Silicoflagellates</td> <td>—</td> <td>—</td> <td>Tr</td> <td>Tr</td> <td>—</td> <td>—</td> <td>—</td> </tr> </tbody> </table> <p>COMPOSITION:</p> <table border="1"> <thead> <tr> <th></th> <th>1, 80</th> <th>2, 27</th> <th>3, 20</th> <th>5, 80</th> <th>5, 105</th> <th>7, 40</th> <th>7, 86</th> </tr> </thead> <tbody> <tr> <td>Quartz</td> <td>—</td> <td>—</td> <td>10</td> <td>—</td> <td>—</td> <td>—</td> <td>—</td> </tr> <tr> <td>Clay</td> <td>45</td> <td>15</td> <td>65</td> <td>55</td> <td>20</td> <td>38</td> <td>5</td> </tr> <tr> <td>Volcanic glass</td> <td>10</td> <td>70</td> <td>15</td> <td>5</td> <td>75</td> <td>5</td> <td>—</td> </tr> <tr> <td>Foraminifers</td> <td>—</td> <td>—</td> <td>—</td> <td>—</td> <td>—</td> <td>1</td> <td>Tr</td> </tr> <tr> <td>Nannofossils</td> <td>—</td> <td>—</td> <td>—</td> <td>5</td> <td>—</td> <td>30</td> <td>70</td> </tr> <tr> <td>Diatoms</td> <td>15</td> <td>5</td> <td>Tr</td> <td>25</td> <td>Tr</td> <td>5</td> <td>15</td> </tr> <tr> <td>Radiolarians</td> <td>5</td> <td>1</td> <td>—</td> <td>Tr</td> <td>—</td> <td>5</td> <td>—</td> </tr> <tr> <td>Sponge spicules</td> <td>25</td> <td>10</td> <td>10</td> <td>10</td> <td>5</td> <td>15</td> <td>10</td> </tr> <tr> <td>Silicoflagellates</td> <td>—</td> <td>—</td> <td>Tr</td> <td>Tr</td> <td>—</td> <td>—</td> <td>—</td> </tr> </tbody> </table>																			1, 80	2, 27	3, 20	5, 80	5, 105	7, 40	7, 86		D	M	D	D	M	D	D	Sand	10	70	25	5	—	10	—	Silt	40	10	10	25	80	20	20	Clay	50	20	65	70	20	70	80		1, 80	2, 27	3, 20	5, 80	5, 105	7, 40	7, 86	Quartz	—	—	10	—	—	—	—	Clay	45	15	65	55	20	38	5	Volcanic glass	10	70	15	5	75	5	—	Foraminifers	—	—	—	—	—	1	Tr	Nannofossils	—	—	—	5	—	30	70	Diatoms	15	5	Tr	25	Tr	5	15	Radiolarians	5	1	—	Tr	—	5	—	Sponge spicules	25	10	10	10	5	15	10	Silicoflagellates	—	—	Tr	Tr	—	—	—		1, 80	2, 27	3, 20	5, 80	5, 105	7, 40	7, 86	Quartz	—	—	10	—	—	—	—	Clay	45	15	65	55	20	38	5	Volcanic glass	10	70	15	5	75	5	—	Foraminifers	—	—	—	—	—	1	Tr	Nannofossils	—	—	—	5	—	30	70	Diatoms	15	5	Tr	25	Tr	5	15	Radiolarians	5	1	—	Tr	—	5	—	Sponge spicules	25	10	10	10	5	15	10	Silicoflagellates	—	—	Tr	Tr	—	—	—
	1, 80	2, 27	3, 20	5, 80	5, 105	7, 40	7, 86																																																																																																																																																																																																																		
	D	M	D	D	M	D	D																																																																																																																																																																																																																		
Sand	10	70	25	5	—	10	—																																																																																																																																																																																																																		
Silt	40	10	10	25	80	20	20																																																																																																																																																																																																																		
Clay	50	20	65	70	20	70	80																																																																																																																																																																																																																		
	1, 80	2, 27	3, 20	5, 80	5, 105	7, 40	7, 86																																																																																																																																																																																																																		
Quartz	—	—	10	—	—	—	—																																																																																																																																																																																																																		
Clay	45	15	65	55	20	38	5																																																																																																																																																																																																																		
Volcanic glass	10	70	15	5	75	5	—																																																																																																																																																																																																																		
Foraminifers	—	—	—	—	—	1	Tr																																																																																																																																																																																																																		
Nannofossils	—	—	—	5	—	30	70																																																																																																																																																																																																																		
Diatoms	15	5	Tr	25	Tr	5	15																																																																																																																																																																																																																		
Radiolarians	5	1	—	Tr	—	5	—																																																																																																																																																																																																																		
Sponge spicules	25	10	10	10	5	15	10																																																																																																																																																																																																																		
Silicoflagellates	—	—	Tr	Tr	—	—	—																																																																																																																																																																																																																		
	1, 80	2, 27	3, 20	5, 80	5, 105	7, 40	7, 86																																																																																																																																																																																																																		
Quartz	—	—	10	—	—	—	—																																																																																																																																																																																																																		
Clay	45	15	65	55	20	38	5																																																																																																																																																																																																																		
Volcanic glass	10	70	15	5	75	5	—																																																																																																																																																																																																																		
Foraminifers	—	—	—	—	—	1	Tr																																																																																																																																																																																																																		
Nannofossils	—	—	—	5	—	30	70																																																																																																																																																																																																																		
Diatoms	15	5	Tr	25	Tr	5	15																																																																																																																																																																																																																		
Radiolarians	5	1	—	Tr	—	5	—																																																																																																																																																																																																																		
Sponge spicules	25	10	10	10	5	15	10																																																																																																																																																																																																																		
Silicoflagellates	—	—	Tr	Tr	—	—	—																																																																																																																																																																																																																		



TIME-ROCK UNIT	BIOSTRAT. ZONE/ FOSSIL CHARACTER					PHYS. PROPERTIES	CHEMISTRY	SECTION	METERS	GRAPHIC LITHOLOGY	DRILLING DISTURB.	SED. STRUCTURES	SAMPLES	LITHOLOGIC DESCRIPTION																																																																								
	FORAMINIFERS	NANNOFOSSILS	RADIOLARIANS	DIATOMS	SILICOS PALYMONORPHS										PALEOMAGNETICS																																																																							
MIDDLE MIOCENE	F/M F/M	NSPF3/ Benthic Zone B							0.5 1.0					<p>NANNOFOSSIL-SILICEOUS OOZE</p> <p>Entire core is undeformed.</p> <p>Major lithology: Nanno-siliceous ooze, dark gray (5Y 4/1), olive gray (5Y 5/2) to greenish gray (5GY 5/1) and grayish green (5G 5/2), heavily bioturbated. Rare faint laminations, burrows, and <i>Zooophycos</i> trace fossils.</p> <p>Minor lithology: Volcanic ash. Sandy ash pocket at Section 4, 25-26 cm. Ash layer with sharp base and gradational top at Section 5, 54-57 cm.</p> <p>SMEAR SLIDE SUMMARY (%):</p> <table border="1" style="margin-left: auto; margin-right: auto;"> <tr> <td></td> <td>1, 100</td> <td>3, 80</td> <td>5, 15</td> <td>5, 55</td> <td>7, 20</td> </tr> <tr> <td></td> <td>D</td> <td>D</td> <td>D</td> <td>M</td> <td>D</td> </tr> </table> <p>TEXTURE:</p> <table border="1" style="margin-left: auto; margin-right: auto;"> <tr> <td>Sand</td> <td>—</td> <td>—</td> <td>—</td> <td>95</td> <td>—</td> </tr> <tr> <td>Silt</td> <td>40</td> <td>50</td> <td>60</td> <td>5</td> <td>60</td> </tr> <tr> <td>Clay</td> <td>60</td> <td>50</td> <td>40</td> <td>—</td> <td>40</td> </tr> </table> <p>COMPOSITION:</p> <table border="1" style="margin-left: auto; margin-right: auto;"> <tr> <td>Quartz</td> <td>—</td> <td>—</td> <td>1</td> <td>—</td> <td>—</td> </tr> <tr> <td>Clay</td> <td>5</td> <td>20</td> <td>10</td> <td>97</td> <td>25</td> </tr> <tr> <td>Nannofossils</td> <td>55</td> <td>35</td> <td>25</td> <td>—</td> <td>15</td> </tr> <tr> <td>Diatoms</td> <td>15</td> <td>20</td> <td>35</td> <td>1</td> <td>35</td> </tr> <tr> <td>Radiolarians</td> <td>—</td> <td>—</td> <td>2</td> <td>—</td> <td>—</td> </tr> <tr> <td>Sponge spicules</td> <td>25</td> <td>25</td> <td>25</td> <td>2</td> <td>25</td> </tr> <tr> <td>Silicoflagellates</td> <td>—</td> <td>—</td> <td>2</td> <td>—</td> <td>Tr</td> </tr> </table>		1, 100	3, 80	5, 15	5, 55	7, 20		D	D	D	M	D	Sand	—	—	—	95	—	Silt	40	50	60	5	60	Clay	60	50	40	—	40	Quartz	—	—	1	—	—	Clay	5	20	10	97	25	Nannofossils	55	35	25	—	15	Diatoms	15	20	35	1	35	Radiolarians	—	—	2	—	—	Sponge spicules	25	25	25	2	25	Silicoflagellates	—	—	2	—	Tr
	1, 100	3, 80	5, 15	5, 55	7, 20																																																																																	
	D	D	D	M	D																																																																																	
Sand	—	—	—	95	—																																																																																	
Silt	40	50	60	5	60																																																																																	
Clay	60	50	40	—	40																																																																																	
Quartz	—	—	1	—	—																																																																																	
Clay	5	20	10	97	25																																																																																	
Nannofossils	55	35	25	—	15																																																																																	
Diatoms	15	20	35	1	35																																																																																	
Radiolarians	—	—	2	—	—																																																																																	
Sponge spicules	25	25	25	2	25																																																																																	
Silicoflagellates	—	—	2	—	Tr																																																																																	
	C/P	NN 15-7																																																																																				
	R/M	NSR8																																																																																				
	A/M	<i>Denticulopsis hustedtii</i> - <i>D.lauta</i> Zone (NNPD5), subzone B																																																																																				
	C/G A/G	<i>Nematosphaeropsis aquaeducta</i> Zone PM4 <i>Mesocena circulus</i> Zone																																																																																				

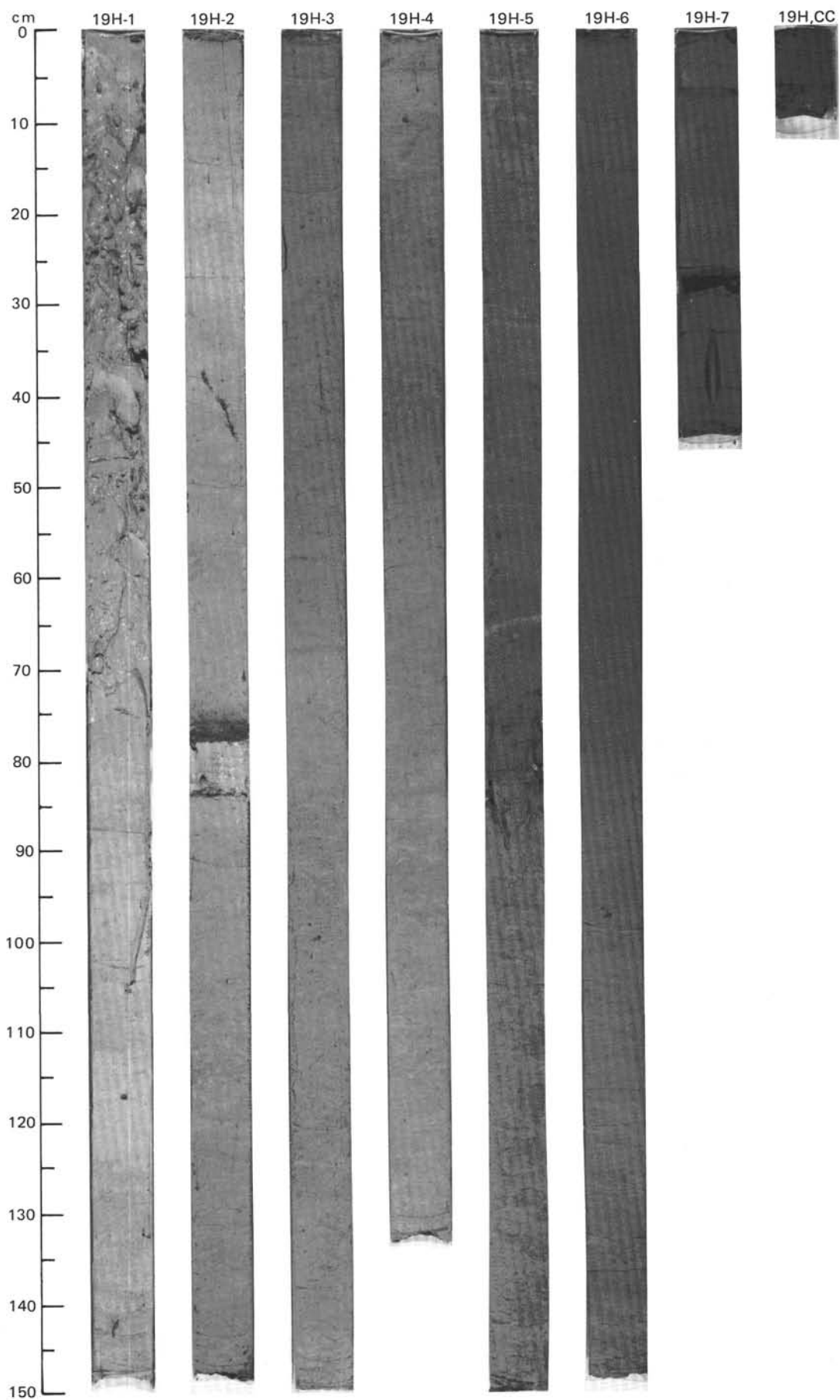


TIME-ROCK UNIT		BIOSTRAT. ZONE/ FOSSIL CHARACTER	PHYS. PROPERTIES	CHEMISTRY	SECTION	METERS	GRAPHIC LITHOLOGY	DRILLING DISTURB.	SED. STRUCTURES	SAMPLES	LITHOLOGIC DESCRIPTION																																																												
MIDDLE MIOCENE											<p>SILICEOUS MUD and SILICEOUS NANNOFOSSIL OOZE</p> <p>Entire core is undisturbed.</p> <p>Major lithology: Siliceous mud and siliceous nannofossil ooze, greenish gray (5GY 5/1) to gray (5Y 5/1), interbedded with gradational and indistinct boundaries. Moderately to heavily bioturbated and mottled. Rare faint color laminations, especially of grayish green.</p> <p>Minor lithology: Siliceous mud, possibly rich in altered basaltic glass. Occurs in lenses; Section 3, 81-83 and 142-145 cm; Section 4, 94-98 cm.</p> <p>SMEAR SLIDE SUMMARY (%):</p> <table border="1"> <tr> <td></td> <td>1, 75</td> <td>3, 82</td> <td>4, 50</td> <td>6, 100</td> </tr> <tr> <td></td> <td>D</td> <td>M</td> <td>D</td> <td>D</td> </tr> </table> <p>TEXTURE:</p> <table border="1"> <tr> <td>Sand</td> <td>—</td> <td>20</td> <td>—</td> <td>—</td> </tr> <tr> <td>Silt</td> <td>40</td> <td>50</td> <td>40</td> <td>30</td> </tr> <tr> <td>Clay</td> <td>60</td> <td>30</td> <td>60</td> <td>70</td> </tr> </table> <p>COMPOSITION:</p> <table border="1"> <tr> <td>Clay</td> <td>55</td> <td>30</td> <td>20</td> <td>30</td> </tr> <tr> <td>Volcanic glass</td> <td>—</td> <td>15</td> <td>—</td> <td>—</td> </tr> <tr> <td>Nannofossils</td> <td>15</td> <td>10</td> <td>45</td> <td>45</td> </tr> <tr> <td>Diatoms</td> <td>10</td> <td>20</td> <td>15</td> <td>10</td> </tr> <tr> <td>Radiolarians</td> <td>Tr</td> <td>—</td> <td>—</td> <td>—</td> </tr> <tr> <td>Sponge spicules</td> <td>20</td> <td>25</td> <td>20</td> <td>15</td> </tr> <tr> <td>Silicoflagellates</td> <td>Tr</td> <td>—</td> <td>Tr</td> <td>—</td> </tr> </table>		1, 75	3, 82	4, 50	6, 100		D	M	D	D	Sand	—	20	—	—	Silt	40	50	40	30	Clay	60	30	60	70	Clay	55	30	20	30	Volcanic glass	—	15	—	—	Nannofossils	15	10	45	45	Diatoms	10	20	15	10	Radiolarians	Tr	—	—	—	Sponge spicules	20	25	20	15	Silicoflagellates	Tr	—	Tr	—
	1, 75	3, 82	4, 50	6, 100																																																																			
	D	M	D	D																																																																			
Sand	—	20	—	—																																																																			
Silt	40	50	40	30																																																																			
Clay	60	30	60	70																																																																			
Clay	55	30	20	30																																																																			
Volcanic glass	—	15	—	—																																																																			
Nannofossils	15	10	45	45																																																																			
Diatoms	10	20	15	10																																																																			
Radiolarians	Tr	—	—	—																																																																			
Sponge spicules	20	25	20	15																																																																			
Silicoflagellates	Tr	—	Tr	—																																																																			
F/M F/M	NSPF3/ Benthic Zone B		● $\gamma = 1.49$ $\phi = 72$	● 9 %	1	0.5				*																																																													
C/M	NN 6-1					1.0																																																																	
R/M	NSR8																																																																						
A/M	<i>Denticulopsis hustedtii</i> - <i>D.lauta</i> Zone (NNPD5), subzone A				2																																																																		
C/G C/G	<i>Batiacasphaera baculata</i> ZonePM5 <i>Mesocena circulus</i> Zone		● $\gamma = 1.47$ $\phi = 74$	● 17 %	3					*																																																													
					4					*																																																													
					5					*																																																													
					6					*																																																													
					7					*																																																													



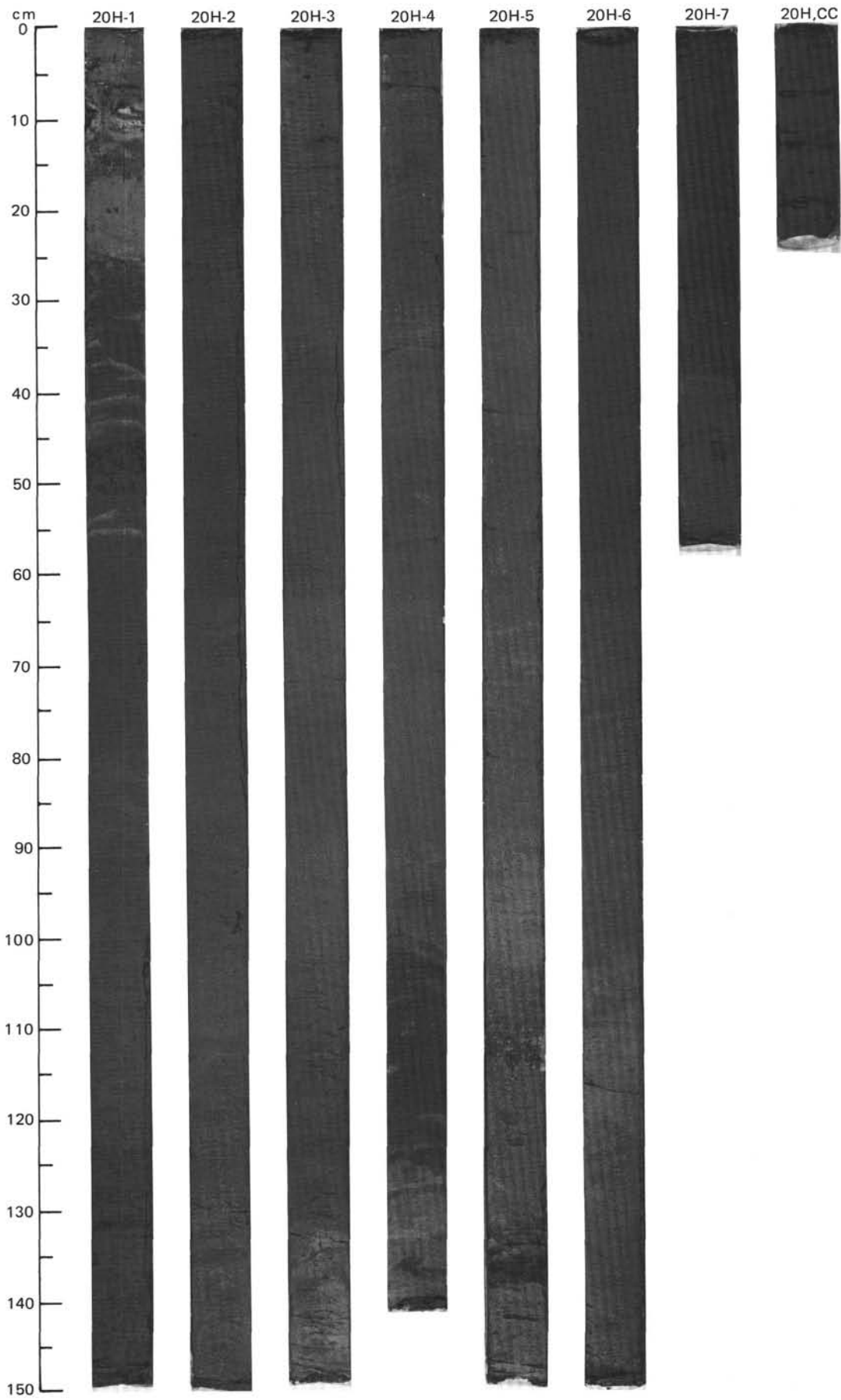
SITE 642 HOLE B CORE 19H CORED INTERVAL 1443.7-1453.4 mbsf; 157.70-167.40 mbsf

TIME-ROCK UNIT		BIOSTRAT. ZONE/ FOSSIL CHARACTER	PALEOMAGNETICS	PHYS. PROPERTIES	CHEMISTRY	SECTION	METERS	GRAPHIC LITHOLOGY	DRILLING DISTURB.	SED. STRUCTURES	SAMPLES	LITHOLOGIC DESCRIPTION																																																																	
FORAMINIFERS	NANNOFOSSILS	RADIOLARIANS	DIATOMS	SILICOS	SECTION	METERS																																																																							
MIDDLE MIOCENE		Benthic Zone C1										<p>SILICEOUS MUD</p> <p>Entire core is undeformed.</p> <p>Major lithology: Siliceous mud, very dark gray (5Y 3/1), dark gray (5Y 4/1), and greenish gray (5GY 5/1), bioturbated and mottled. Rare identifiable <i>Zoophycos</i>.</p> <p>Minor lithology: Ash, very dark gray (5Y 3/1). Section 2, 75-79 cm.</p> <p>SMEAR SLIDE SUMMARY (%):</p> <table border="1"> <tr> <td></td> <td>1, 140</td> <td>2, 76</td> <td>3, 100</td> <td>6, 100</td> </tr> <tr> <td></td> <td>D</td> <td>M</td> <td>D</td> <td>D</td> </tr> </table> <p>TEXTURE:</p> <table border="1"> <tr> <td>Sand</td> <td>—</td> <td>95</td> <td>5</td> <td>—</td> </tr> <tr> <td>Silt</td> <td>50</td> <td>5</td> <td>25</td> <td>40</td> </tr> <tr> <td>Clay</td> <td>50</td> <td>—</td> <td>70</td> <td>60</td> </tr> </table> <p>COMPOSITION:</p> <table border="1"> <tr> <td>Quartz</td> <td>—</td> <td>—</td> <td>5</td> <td>5</td> </tr> <tr> <td>Clay</td> <td>50</td> <td>—</td> <td>45</td> <td>60</td> </tr> <tr> <td>Volcanic glass</td> <td>—</td> <td>95</td> <td>—</td> <td>—</td> </tr> <tr> <td>Nannofossils</td> <td>15</td> <td>—</td> <td>—</td> <td>—</td> </tr> <tr> <td>Diatoms</td> <td>15</td> <td>2</td> <td>35</td> <td>10</td> </tr> <tr> <td>Radiolarians</td> <td>—</td> <td>—</td> <td>Tr</td> <td>—</td> </tr> <tr> <td>Sponge spicules</td> <td>20</td> <td>3</td> <td>15</td> <td>—</td> </tr> <tr> <td>Silicoflagellates</td> <td>—</td> <td>—</td> <td>—</td> <td>25</td> </tr> </table>		1, 140	2, 76	3, 100	6, 100		D	M	D	D	Sand	—	95	5	—	Silt	50	5	25	40	Clay	50	—	70	60	Quartz	—	—	5	5	Clay	50	—	45	60	Volcanic glass	—	95	—	—	Nannofossils	15	—	—	—	Diatoms	15	2	35	10	Radiolarians	—	—	Tr	—	Sponge spicules	20	3	15	—	Silicoflagellates	—	—	—	25
	1, 140	2, 76	3, 100	6, 100																																																																									
	D	M	D	D																																																																									
Sand	—	95	5	—																																																																									
Silt	50	5	25	40																																																																									
Clay	50	—	70	60																																																																									
Quartz	—	—	5	5																																																																									
Clay	50	—	45	60																																																																									
Volcanic glass	—	95	—	—																																																																									
Nannofossils	15	—	—	—																																																																									
Diatoms	15	2	35	10																																																																									
Radiolarians	—	—	Tr	—																																																																									
Sponge spicules	20	3	15	—																																																																									
Silicoflagellates	—	—	—	25																																																																									
R/P B		NSR8																																																																											
F/P		NN 6-1																																																																											
F/M		NSR7																																																																											
A/M		basal <i>Denticulopsis hustedii</i> <i>D.lauta</i> Zone (NNPD5), subzone A																																																																											
F/G		No zonal designation																																																																											
				● $\gamma=1.50$ $\phi=74$	● 0 %																																																																								
				● $\gamma=1.47$ $\phi=74$	● 0 %																																																																								

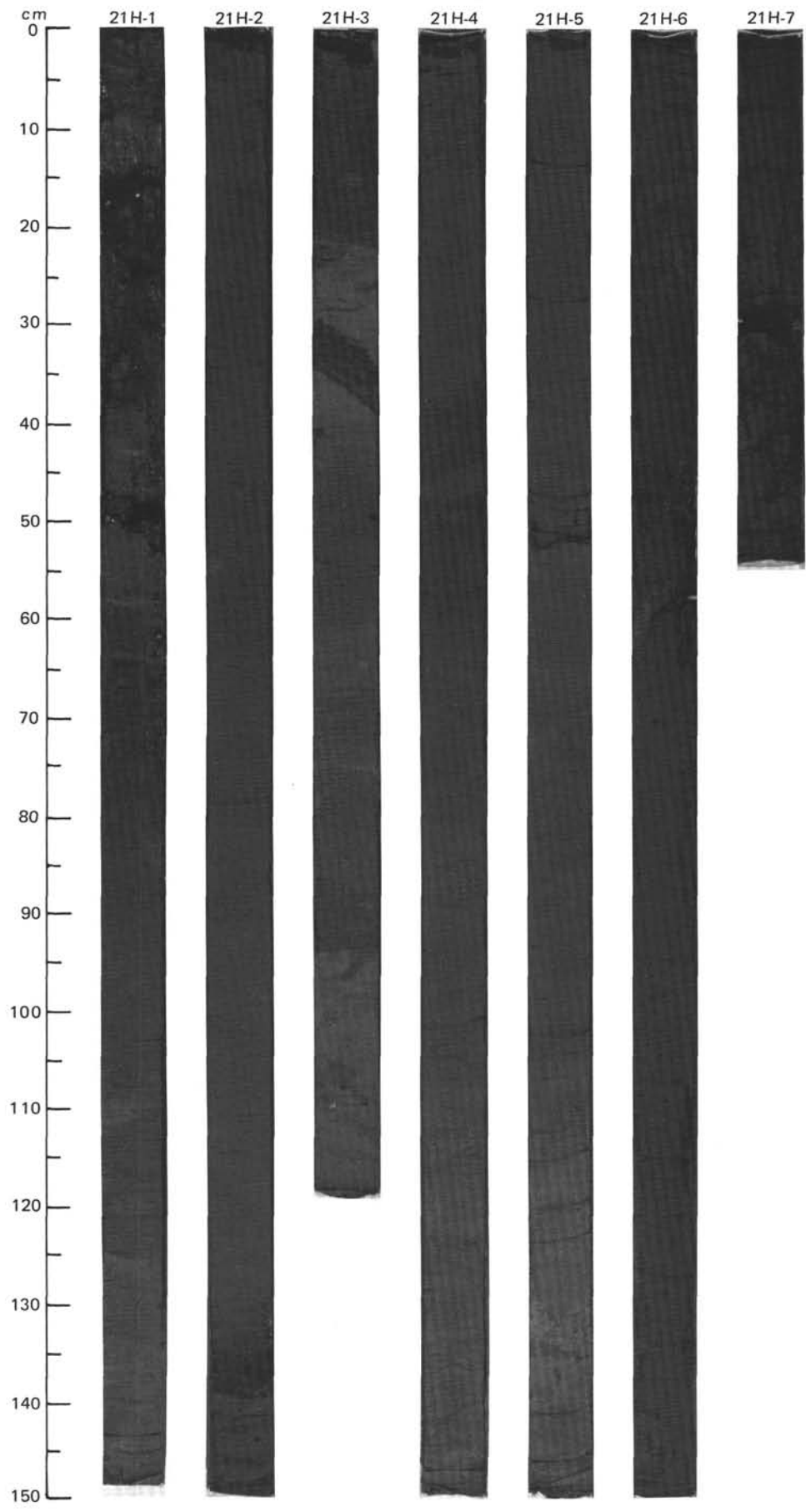


SITE 642 HOLE B CORE 20H CORED INTERVAL 1453.4-1463.1 mbsl; 167.40-177.10 mbsf

TIME-ROCK UNIT		BIOSTRAT. ZONE/ FOSSIL CHARACTER	SECTION	METERS	GRAPHIC LITHOLOGY	DRILLING DISTURB.	SED. STRUCTURES	SAMPLES	LITHOLOGIC DESCRIPTION																																																																																																
R/M B	B	FORAMINIFERS NANNOFOSSILS RADIOLARIANS DIATOMS SILICOS PALYMONORPHS																																																																																																							
MIDDLE MIOCENE	Benthic Zone C1								<p>SILICEOUS MUD</p> <p>Entire core is undeformed.</p> <p>Major lithology: Siliceous mud, very dark gray (5Y 3/1), gray (5Y 4/1), and greenish gray (5GY 5/1), mottled. Faint laminations in Section 6, 30-60 cm.</p> <p>Minor lithologies:</p> <p>a. Volcanic ash, very dark gray (5Y 3/1), with sharp base and gradational top. Section 1, 46-51 cm; Section 5, 110-114 and 135-138 cm.</p> <p>b. Siliceous mud, possibly enriched in altered basaltic glass. Section 2, 57 and 62 cm.</p> <p>SMEAR SLIDE SUMMARY (%):</p> <table border="1"> <tr> <td></td> <td>1, 20</td> <td>1, 46</td> <td>2, 72</td> <td>2, 100</td> <td>5, 100</td> <td>5, 113</td> <td>7, 35</td> </tr> <tr> <td></td> <td>D</td> <td>M</td> <td>M</td> <td>D</td> <td>D</td> <td>M</td> <td>M</td> </tr> </table> <p>TEXTURE:</p> <table border="1"> <tr> <td>Sand</td> <td>10</td> <td>60</td> <td>20</td> <td>15</td> <td>—</td> <td>—</td> <td>10</td> </tr> <tr> <td>Silt</td> <td>30</td> <td>20</td> <td>30</td> <td>30</td> <td>50</td> <td>50</td> <td>35</td> </tr> <tr> <td>Clay</td> <td>60</td> <td>20</td> <td>50</td> <td>55</td> <td>50</td> <td>50</td> <td>55</td> </tr> </table> <p>COMPOSITION:</p> <table border="1"> <tr> <td>Quartz</td> <td>5</td> <td>—</td> <td>—</td> <td>—</td> <td>3</td> <td>—</td> <td>—</td> </tr> <tr> <td>Clay</td> <td>50</td> <td>20</td> <td>50</td> <td>55</td> <td>50</td> <td>10</td> <td>55</td> </tr> <tr> <td>Volcanic glass</td> <td>10</td> <td>60</td> <td>20</td> <td>15</td> <td>2</td> <td>90</td> <td>10</td> </tr> <tr> <td>Diatoms</td> <td>10</td> <td>5</td> <td>10</td> <td>10</td> <td>25</td> <td>—</td> <td>15</td> </tr> <tr> <td>Radiolarians</td> <td>—</td> <td>Tr</td> <td>Tr</td> <td>Tr</td> <td>Tr</td> <td>—</td> <td>—</td> </tr> <tr> <td>Sponge spicules</td> <td>25</td> <td>15</td> <td>20</td> <td>20</td> <td>20</td> <td>—</td> <td>20</td> </tr> <tr> <td>Silicoflagellates</td> <td>—</td> <td>—</td> <td>—</td> <td>—</td> <td>1</td> <td>—</td> <td>—</td> </tr> </table>		1, 20	1, 46	2, 72	2, 100	5, 100	5, 113	7, 35		D	M	M	D	D	M	M	Sand	10	60	20	15	—	—	10	Silt	30	20	30	30	50	50	35	Clay	60	20	50	55	50	50	55	Quartz	5	—	—	—	3	—	—	Clay	50	20	50	55	50	10	55	Volcanic glass	10	60	20	15	2	90	10	Diatoms	10	5	10	10	25	—	15	Radiolarians	—	Tr	Tr	Tr	Tr	—	—	Sponge spicules	25	15	20	20	20	—	20	Silicoflagellates	—	—	—	—	1	—	—
	1, 20	1, 46	2, 72	2, 100	5, 100	5, 113	7, 35																																																																																																		
	D	M	M	D	D	M	M																																																																																																		
Sand	10	60	20	15	—	—	10																																																																																																		
Silt	30	20	30	30	50	50	35																																																																																																		
Clay	60	20	50	55	50	50	55																																																																																																		
Quartz	5	—	—	—	3	—	—																																																																																																		
Clay	50	20	50	55	50	10	55																																																																																																		
Volcanic glass	10	60	20	15	2	90	10																																																																																																		
Diatoms	10	5	10	10	25	—	15																																																																																																		
Radiolarians	—	Tr	Tr	Tr	Tr	—	—																																																																																																		
Sponge spicules	25	15	20	20	20	—	20																																																																																																		
Silicoflagellates	—	—	—	—	1	—	—																																																																																																		
	NSR7		1	0.5			*																																																																																																		
			2	1.0			*																																																																																																		
			3				*																																																																																																		
			4				*																																																																																																		
			5				*																																																																																																		
			6				*																																																																																																		
			7				*																																																																																																		
			8				*																																																																																																		



TIME-ROCK UNIT		BIOSTRAT. ZONE/ FOSSIL CHARACTER	PHYS. PROPERTIES	CHEMISTRY	SECTION	METERS	GRAPHIC LITHOLOGY	DRILLING DISTURB.	SED. STRUCTURES	SAMPLES	LITHOLOGIC DESCRIPTION																																												
FORAMINIFERS	FORAMINIFERS																																																						
MIDDLE MIOCENE											<p>SILICEOUS MUD</p> <p>Entire core is undeformed.</p> <p>Major lithology: Siliceous mud, very dark gray (5Y 3/1), slightly to moderately bioturbated and extensively mottled. Minor well-defined burrows.</p> <p>Minor lithology: Volcanic ash, very dark gray (5Y 3/1), with sharp base and gradational top. Section 2, 132-140 cm.</p> <p>SMEAR SLIDE SUMMARY (%):</p> <table border="1"> <tr> <td></td> <td>2, 145</td> <td>5, 60</td> <td>7, 20</td> </tr> <tr> <td>D</td> <td>D</td> <td>D</td> <td>D</td> </tr> </table> <p>TEXTURE:</p> <table border="1"> <tr> <td>Sand</td> <td>5</td> <td>—</td> <td>—</td> </tr> <tr> <td>Silt</td> <td>35</td> <td>40</td> <td>50</td> </tr> <tr> <td>Clay</td> <td>60</td> <td>60</td> <td>50</td> </tr> </table> <p>COMPOSITION:</p> <table border="1"> <tr> <td>Quartz</td> <td>—</td> <td>1</td> <td>Tr</td> </tr> <tr> <td>Clay</td> <td>60</td> <td>59</td> <td>50</td> </tr> <tr> <td>Volcanic glass</td> <td>5</td> <td>—</td> <td>Tr</td> </tr> <tr> <td>Diatoms</td> <td>10</td> <td>25</td> <td>30</td> </tr> <tr> <td>Radiolarians</td> <td>—</td> <td>Tr</td> <td>—</td> </tr> <tr> <td>Sponge spicules</td> <td>25</td> <td>15</td> <td>20</td> </tr> </table>		2, 145	5, 60	7, 20	D	D	D	D	Sand	5	—	—	Silt	35	40	50	Clay	60	60	50	Quartz	—	1	Tr	Clay	60	59	50	Volcanic glass	5	—	Tr	Diatoms	10	25	30	Radiolarians	—	Tr	—	Sponge spicules	25	15	20
	2, 145	5, 60	7, 20																																																				
D	D	D	D																																																				
Sand	5	—	—																																																				
Silt	35	40	50																																																				
Clay	60	60	50																																																				
Quartz	—	1	Tr																																																				
Clay	60	59	50																																																				
Volcanic glass	5	—	Tr																																																				
Diatoms	10	25	30																																																				
Radiolarians	—	Tr	—																																																				
Sponge spicules	25	15	20																																																				
BB	Benthic Zone C2		$\gamma = 1.41$ $\phi = 78$	6 %	1	0.5																																																	
B						1.0																																																	
C/G	NSR7				2																																																		
A/M	<i>Denticulopsis lauta</i> Zone (NNPD4), subzone A				3																																																		
F/M	no zonal designation				4																																																		
			$\gamma = 1.42$ $\phi = 76$	9 %	5																																																		
					6																																																		
					7																																																		



TIME-ROCK UNIT	BIOSTRAT. ZONE/ FOSSIL CHARACTER					PHYS. PROPERTIES	CHEMISTRY	SECTION	METERS	GRAPHIC LITHOLOGY	DRILLING DISTURB.	SED. STRUCTURES	SAMPLES	LITHOLOGIC DESCRIPTION
	FORAMINIFERS	NANNOFOSSILS	RADIOLARIANS	DIATOMS	SILICOS PALYMONORPHS									
LOWER MIOCENE														
B	Benthic Zone C2													
B B														
C/G		NSR6												
C/M		<i>Actinocyclus ingens</i> Zone (NNPD3), <i>Rhizosolenia bulbosa</i> Zone												
F/G C/G		<i>Batiacaphaera baculata</i> Zone PM5 <i>Corbisea triacantha</i> Zone												
						● $\gamma = 1.39$ $\phi = 78$								
						● 0 %								
								1	0.5					
								2	1.0					
								3						
								4						
								5						
								6						
						● $\gamma = 1.54$ $\phi = 80$		7						
						● 0 %								

SILICEOUS MUD

Entire core is undeformed.

Major lithology: Siliceous mud, dark olive gray (5Y 3/2), dark gray (5Y 4/1), and greenish gray (5GY 5/1). Moderately to heavily bioturbated, with mottling and discrete burrows.

Minor lithologies:

a. Volcanic ash, dark olive gray (5Y 3/2). Section 1, 138-143 cm. Lens of volcanic ash, Section 1, 76 cm.

b. Possibly disseminated, altered basaltic ash. Section 4, 117-123 cm; Section 6, 54-66, 98, 102-105, and 140-145 cm.

SMEAR SLIDE SUMMARY (%):

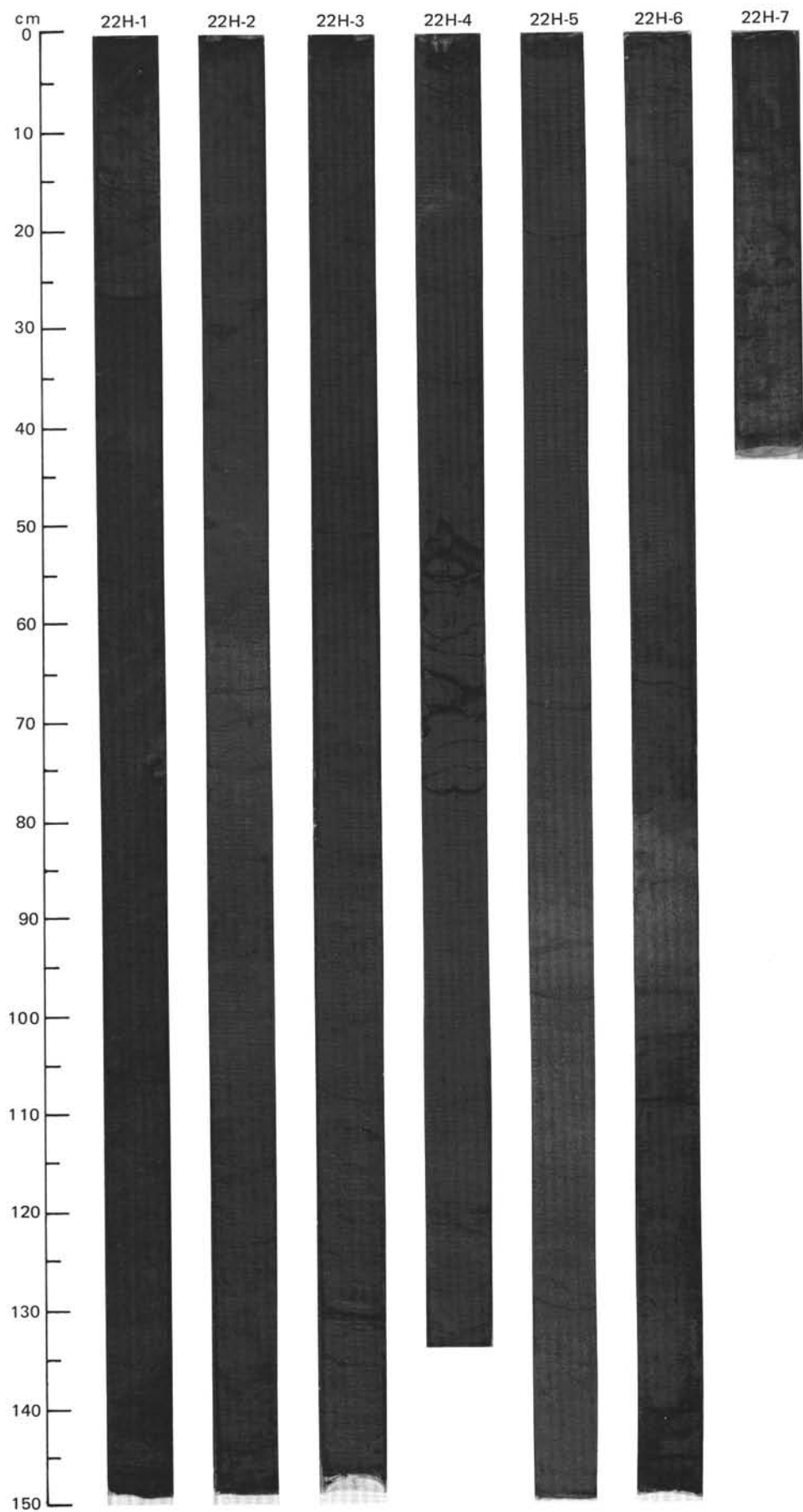
	2, 59	2, 70	4, 109	6, 64	CC, 27
	D	D	D	D	D

TEXTURE:

Sand	—	—	—	—	10
Silt	40	40	30	35	30
Clay	60	60	70	65	60

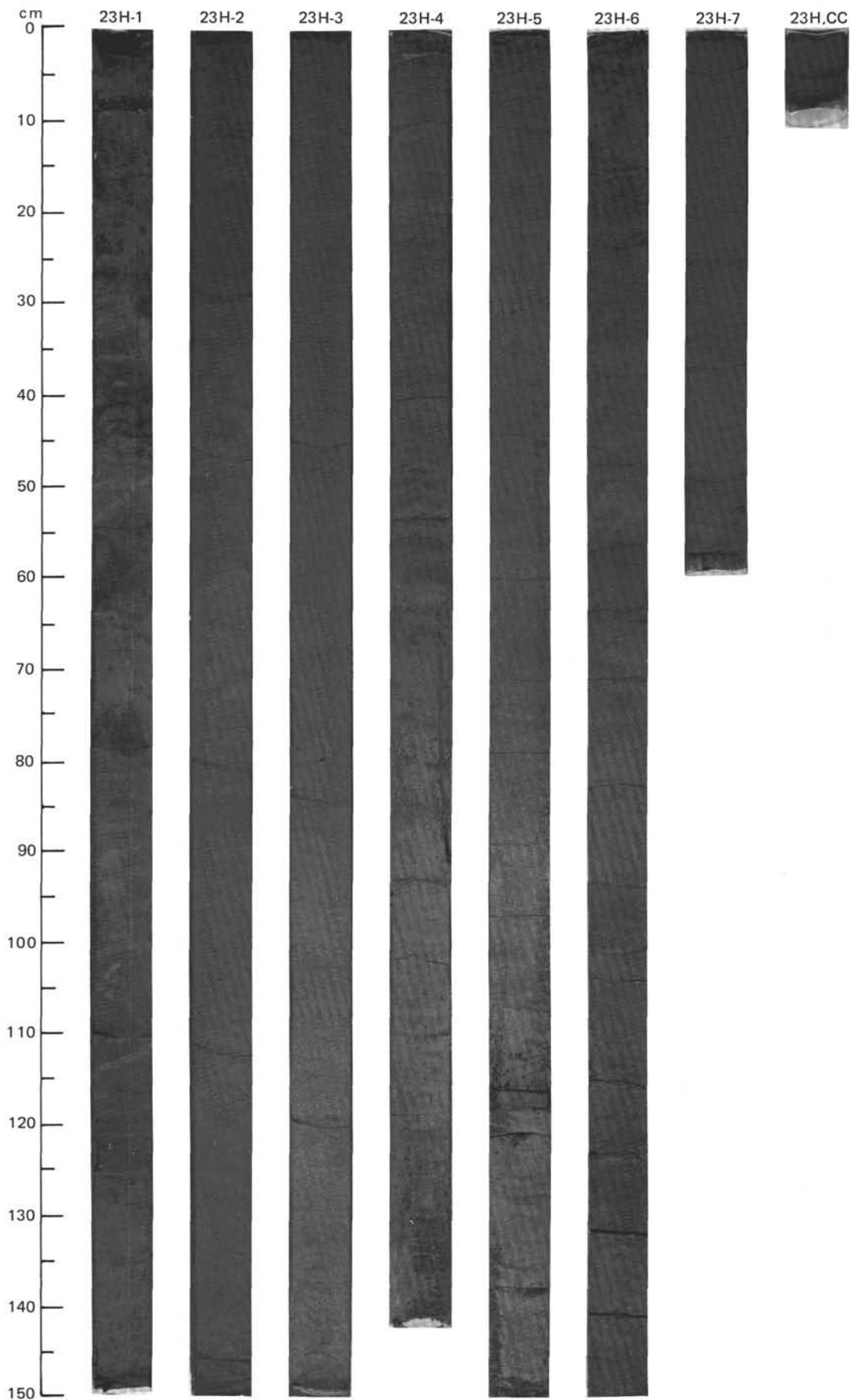
COMPOSITION:

Quartz	—	Tr	—	—	—
Clay	57	54	63	58	58
Volcanic glass	—	—	—	—	1
Accessory minerals:					
Glauconite	—	—	—	—	10
Nannofossils	—	—	—	5	—
Diatoms	25	20	25	20	20
Radiolarians	2	—	1	1	1
Sponge spicules	15	25	10	15	10
Silicoflagellates	1	1	1	1	—

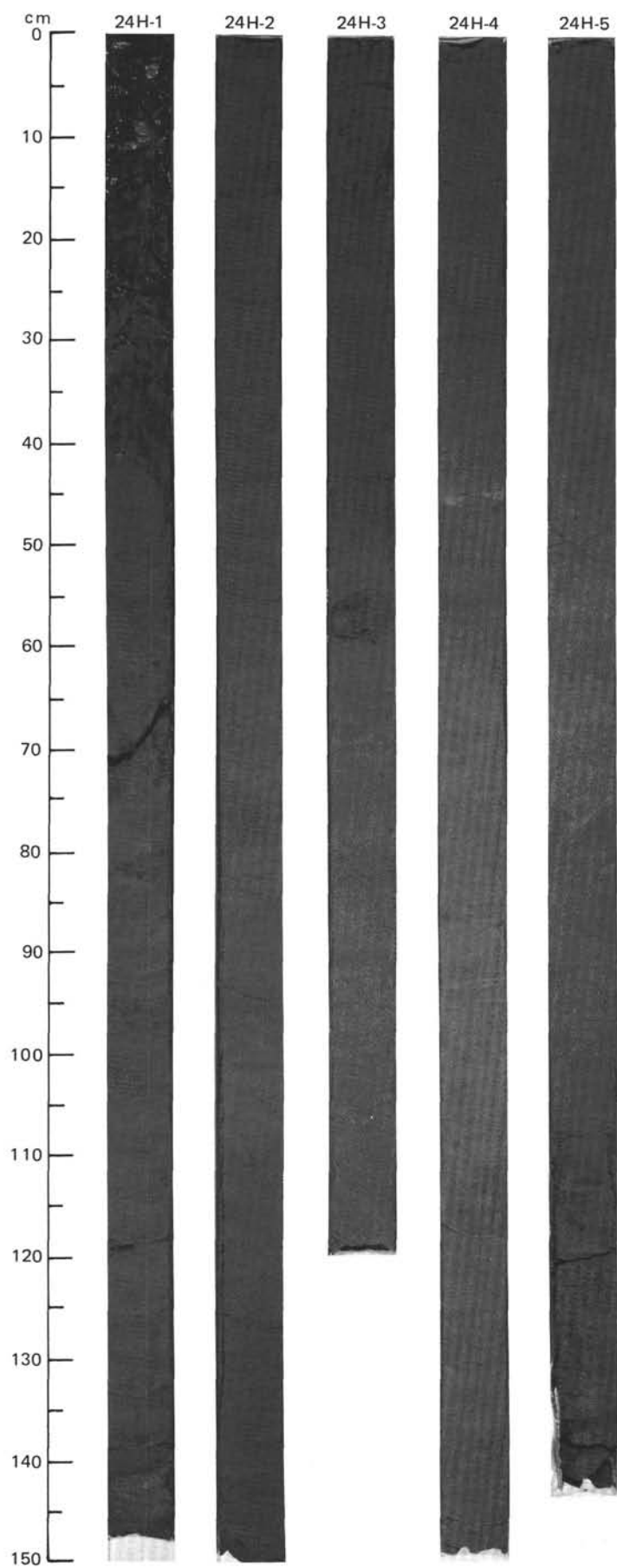


SITE 642 HOLE B CORE 23H CORED INTERVAL 1482.0-1491.6 mbsl; 196.00-205.60 mbsf

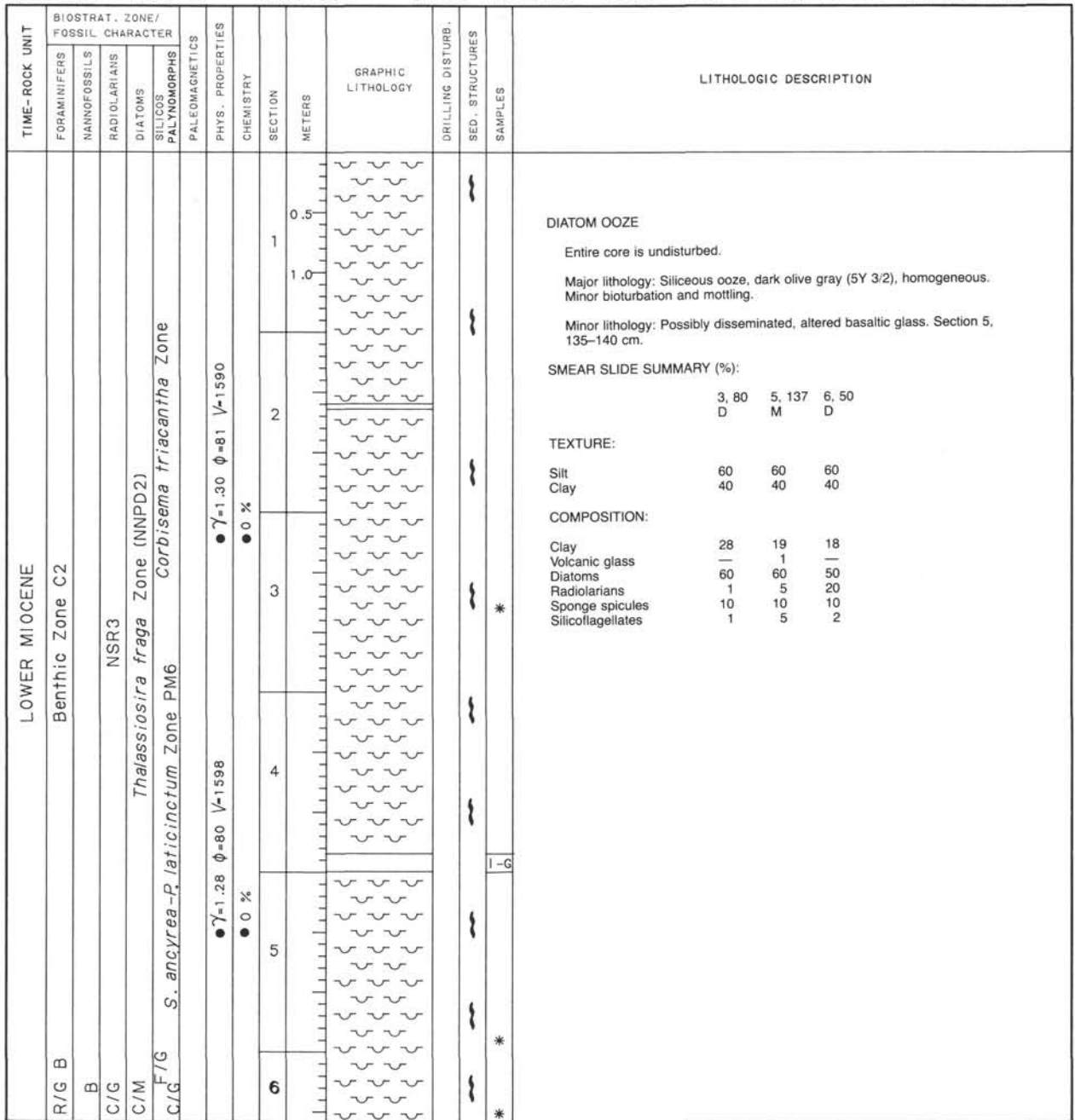
TIME-ROCK UNIT		BIOSTRAT. ZONE/ FOSSIL CHARACTER	PHYS. PROPERTIES	CHEMISTRY	SECTION	METERS	GRAPHIC LITHOLOGY	DRILLING DISTURB.	SED. STRUCTURES	SAMPLES	LITHOLOGIC DESCRIPTION												
R/P B	LOWER MIOCENE	FORAMINIFERS NANNOFOSSILS RADIOLARIANS DIATOMS SILICOS PALYMONORPHS PALEOMAGNETICS																					
C/G	Benthic Zone C2	NSR6 <i>Actinocyclus ingens</i> Zone (NPPD3), <i>Rhizosolenia Bulbosa</i> Zone <i>S.ancyrea-p.laticinctum</i> Zone PM6 <i>Corbisea triacantha</i> Zone	● $\gamma = 1.40$ $\phi = 76$ ● 6 %		1	0.5 1.0					DIATOMACEOUS MUD Entire core is undisturbed. Major lithology: Diatomaceous mud, dark olive gray (5Y 3/2). Heavily bioturbated, with burrows (2-3 mm wide) commonly visible. <i>Zoophycos</i> well developed in Section 1. Minor lithology: Possibly disseminated, altered basaltic ash. Section 1, 43, 62-63, 63-64, and 78-79 cm. SMEAR SLIDE SUMMARY (%): <table border="1"> <tr> <td></td> <td>1, 9</td> <td>1, 43</td> <td>1, 79</td> <td>3, 80</td> <td>6, 55</td> </tr> <tr> <td></td> <td>D</td> <td>M</td> <td>M</td> <td>D</td> <td>D</td> </tr> </table> TEXTURE: Sand 10 80 — — — Silt 30 20 20 40 50 Clay 70 — 80 60 50 COMPOSITION: Clay 66 — — 58 39 Volcanic glass — 100 80 — — Accessory minerals: Glauconite 1 — — — — Diatoms 20 — 19 30 50 Radiolarians 1 — — 1 — Sponge spicules 10 — — 10 10 Silicoflagellates 2 — 1 1 1		1, 9	1, 43	1, 79	3, 80	6, 55		D	M	M	D	D
	1, 9	1, 43	1, 79	3, 80	6, 55																		
	D	M	M	D	D																		
		NSR 5	● $\gamma = 1.33$ $\phi = 78$ ● 0 %		2																		
					3																		
					4																		
					5																		
					6																		
					7																		

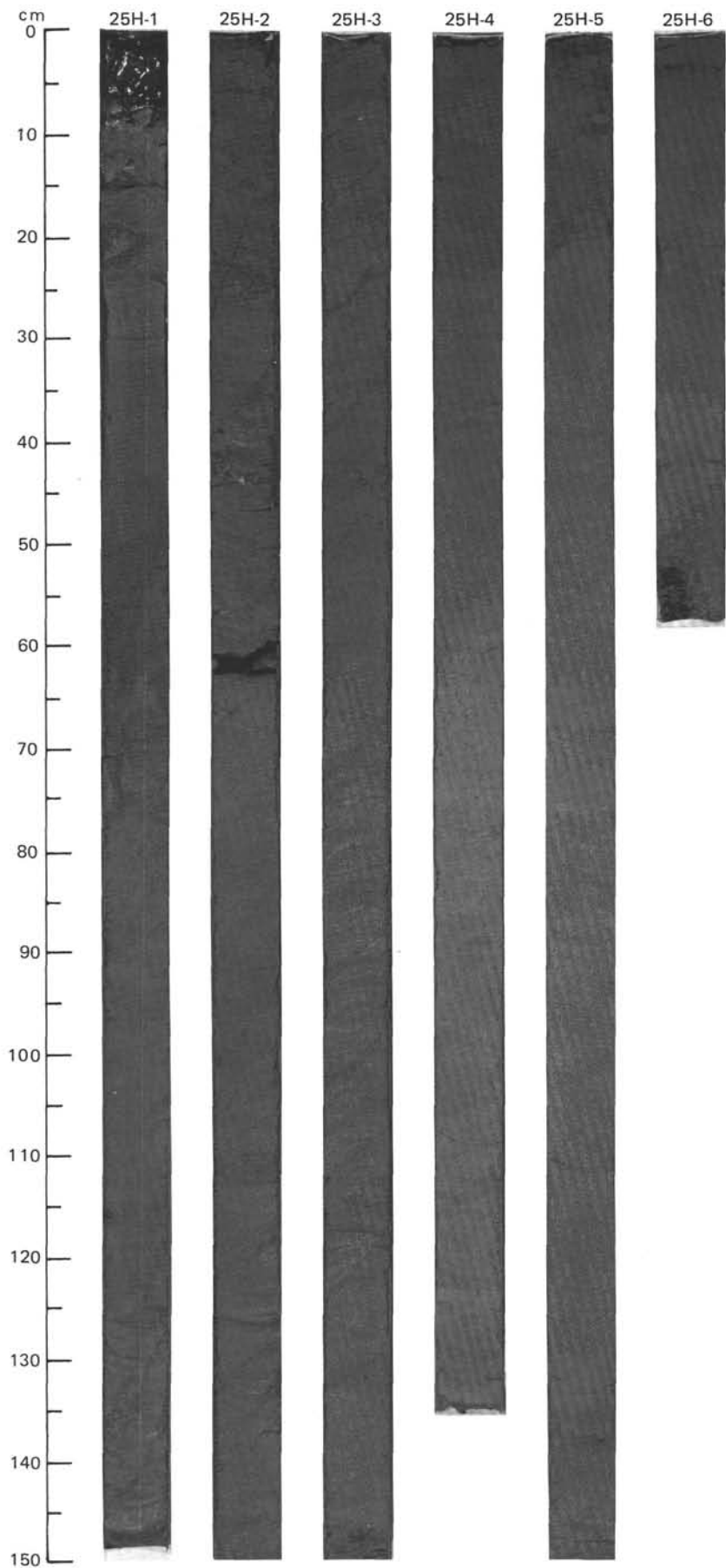


TIME-ROCK UNIT		BIOSTRAT. ZONE/ FOSSIL CHARACTER		PALEOMAGNETICS	PHYS. PROPERTIES	CHEMISTRY	SECTION	METERS	GRAPHIC LITHOLOGY	DRILLING DISTURB.	SED. STRUCTURES	SAMPLES	LITHOLOGIC DESCRIPTION																																												
FORAMINIFERS	NANNOFOSSILS	RADIOLARIANS	DIATOMS																																																						
LOWER MIOCENE													<p>DIATOMACEOUS MUD and DIATOM OOZE</p> <p>Entire core is undisturbed.</p> <p>Major lithology: Diatomaceous mud and diatom ooze, dark olive gray (5Y 3/2), homogeneous. Lithified to mudstone in minor intervals. Minor bioturbation and fine-scale mottling.</p> <p>SMEAR SLIDE SUMMARY (%):</p> <table border="1"> <tr> <td></td> <td>1, 20</td> <td>2, 80</td> <td>5, 70</td> </tr> <tr> <td>D</td> <td></td> <td>D</td> <td>D</td> </tr> </table> <p>TEXTURE:</p> <table border="1"> <tr> <td>Sand</td> <td>30</td> <td>20</td> <td>30</td> </tr> <tr> <td>Clay</td> <td>70</td> <td>80</td> <td>70</td> </tr> </table> <p>COMPOSITION:</p> <table border="1"> <tr> <td>Quartz</td> <td>—</td> <td>—</td> <td>1</td> </tr> <tr> <td>Clay</td> <td>62</td> <td>23</td> <td>27</td> </tr> <tr> <td>Volcanic glass</td> <td>1</td> <td>1</td> <td>—</td> </tr> <tr> <td>Diatoms</td> <td>30</td> <td>60</td> <td>60</td> </tr> <tr> <td>Radiolarians</td> <td>1</td> <td>10</td> <td>1</td> </tr> <tr> <td>Sponge spicules</td> <td>5</td> <td>5</td> <td>10</td> </tr> <tr> <td>Silicoflagellates</td> <td>1</td> <td>1</td> <td>1</td> </tr> </table>		1, 20	2, 80	5, 70	D		D	D	Sand	30	20	30	Clay	70	80	70	Quartz	—	—	1	Clay	62	23	27	Volcanic glass	1	1	—	Diatoms	30	60	60	Radiolarians	1	10	1	Sponge spicules	5	5	10	Silicoflagellates	1	1	1
	1, 20	2, 80	5, 70																																																						
D		D	D																																																						
Sand	30	20	30																																																						
Clay	70	80	70																																																						
Quartz	—	—	1																																																						
Clay	62	23	27																																																						
Volcanic glass	1	1	—																																																						
Diatoms	30	60	60																																																						
Radiolarians	1	10	1																																																						
Sponge spicules	5	5	10																																																						
Silicoflagellates	1	1	1																																																						
B B	Benthic Zone C2						1	0.5			*																																														
F/P	NSR3	NSR5					2	1.0			*																																														
A/M	<i>Thalassiosira fraga</i> Zone (NNPD2)						3																																																		
F/G C/G	S.ancyrea-P.lactitintum Zone PM6 <i>Corbisea triacantha</i> Zone						4																																																		
					• 1.36 $\phi=77$ $V=1537$		5					*																																													

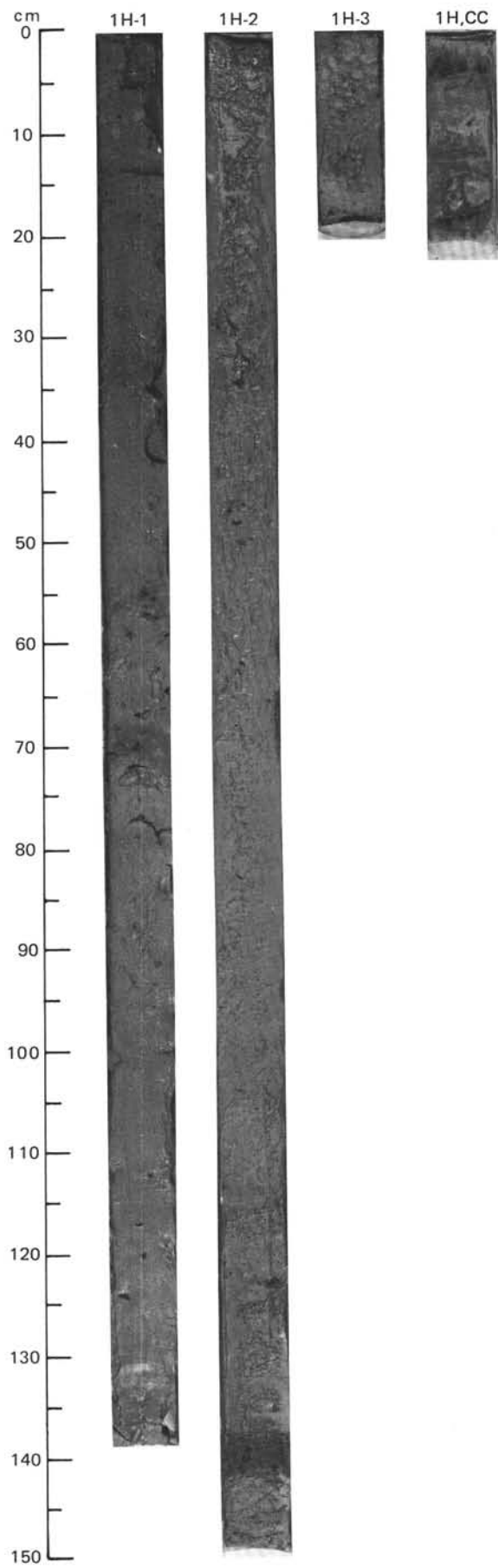


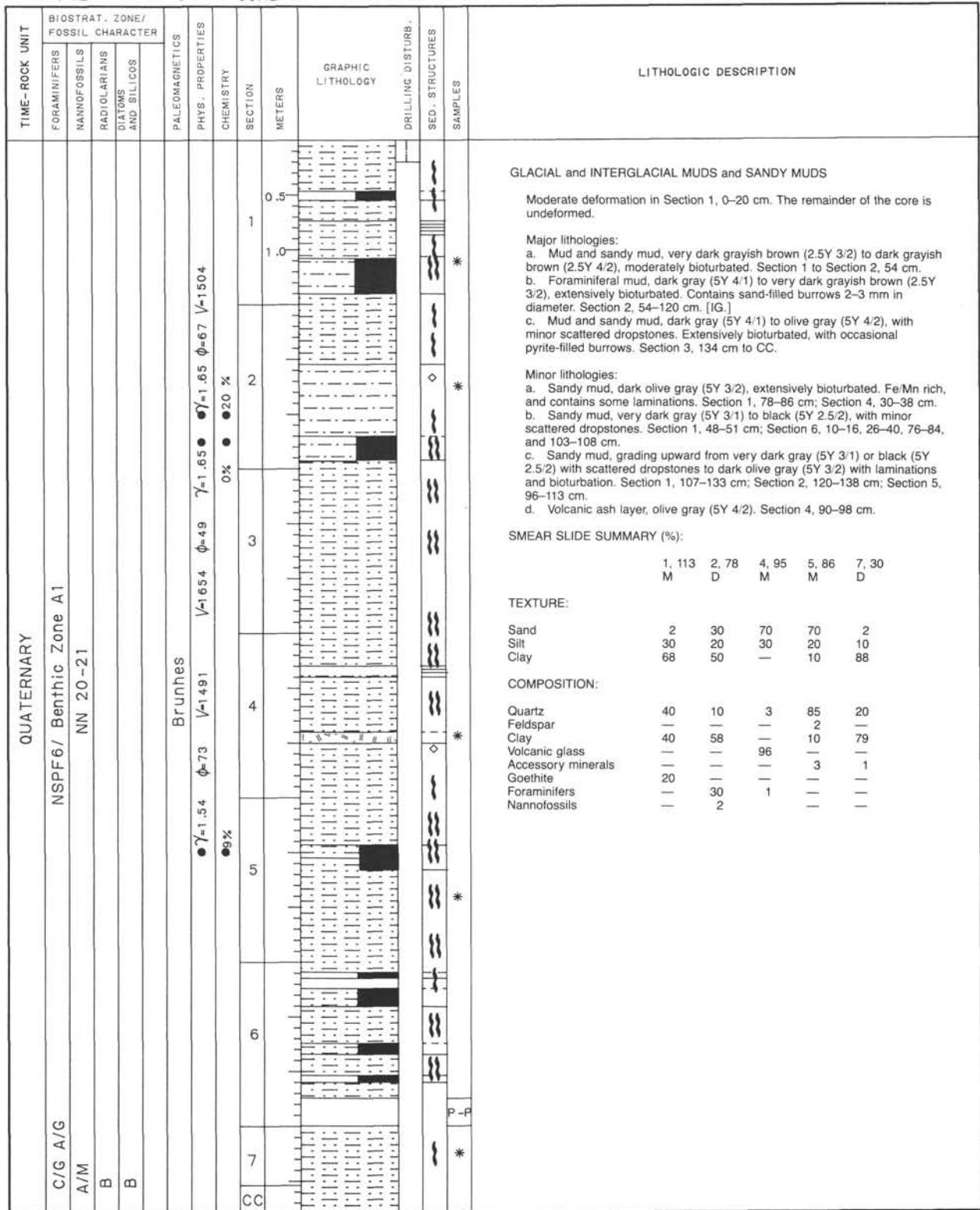
SITE 642 HOLE B CORE 25H CORED INTERVAL 1499.1-1507.1 mbsf; 213.10-221.10 mbsf

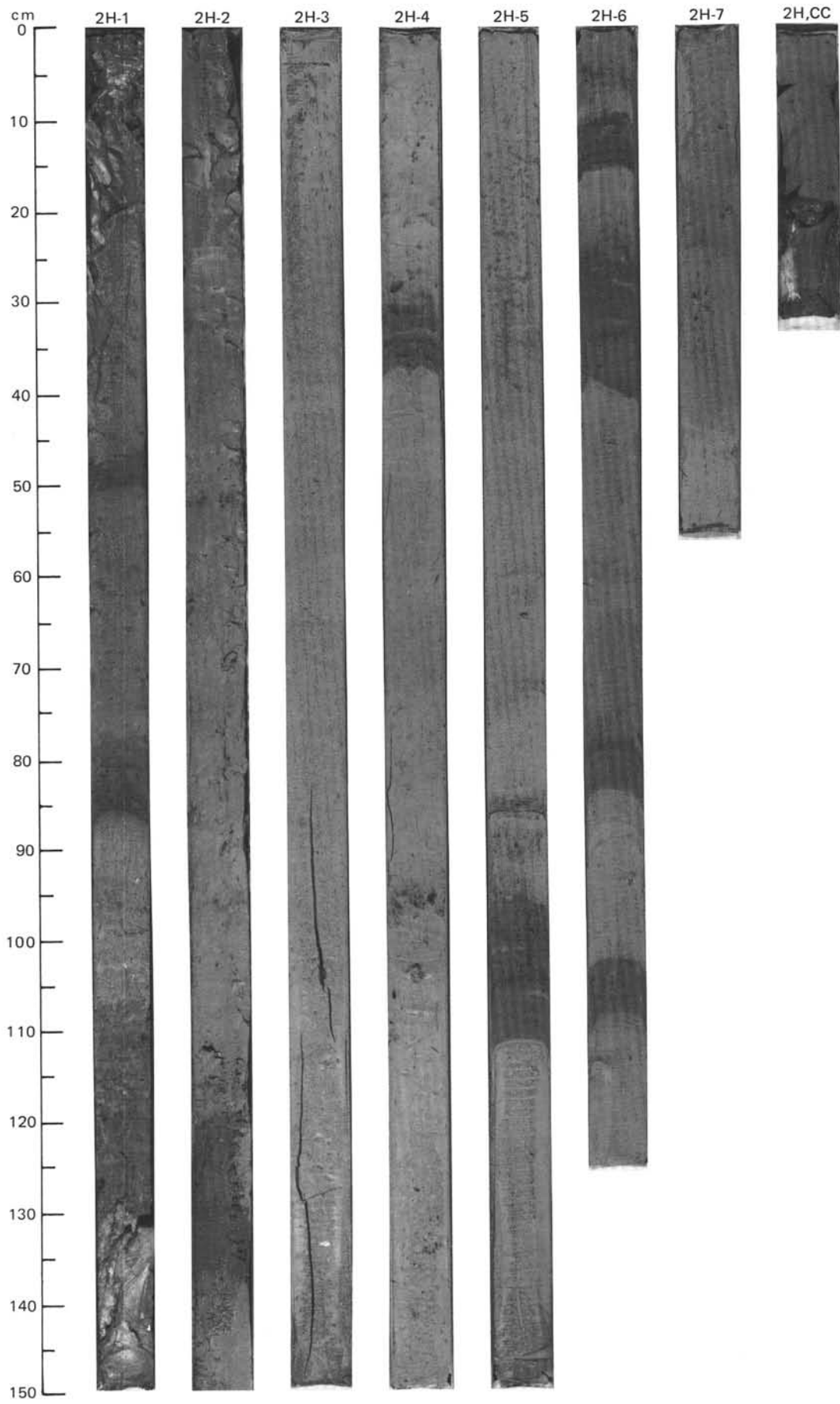




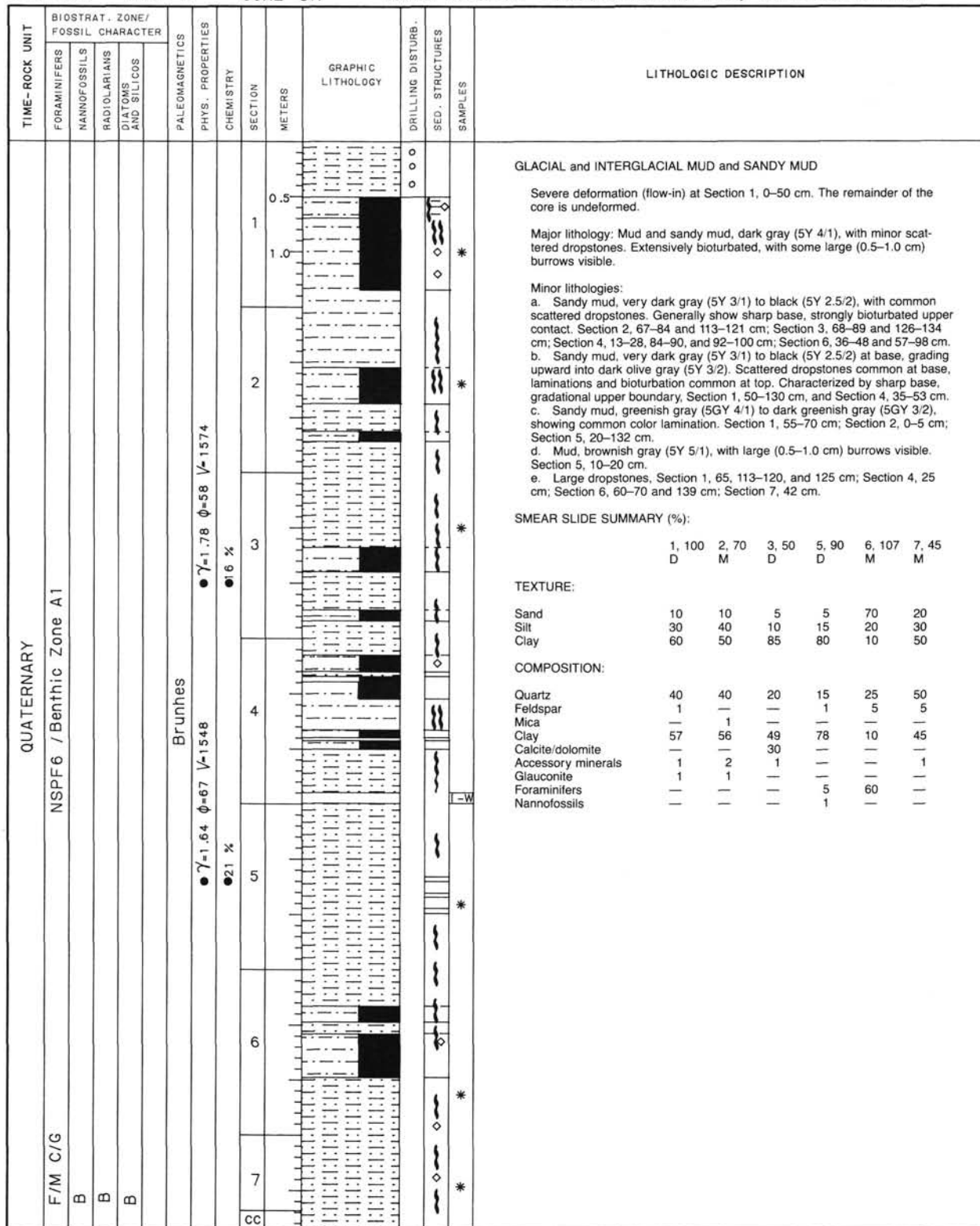
TIME-ROCK UNIT		BIOSTRAT. ZONE/ FOSSIL CHARACTER					SECTION	METERS	GRAPHIC LITHOLOGY	DRILLING DISTURB.	SED. STRUCTURES	SAMPLES	LITHOLOGIC DESCRIPTION																																																											
FORAMINIFERS	NANNOFOSSILS	RADIOLARIANS	DIATOMS-SILICOS	PALYNOMORPHS	PALEOMAGNETICS	PHYS. PROPERTIES								CHEMISTRY																																																										
QUATERNARY												<p>GLACIAL and INTERGLACIAL MUDS and SANDY MUDS</p> <p>Entire core is undeformed.</p> <p>Major lithologies:</p> <p>a. Foraminiferal mud, dark brown (10YR 3/3) to dark grayish brown (10YR 4/2), with scattered clay lumps. Slightly bioturbated. Section 1, 0-90 cm. [IG.]</p> <p>b. Mud and sandy mud, dark gray (5Y 4/1) to olive gray (5Y 4/2), with minor scattered mud dropstones. Mottled throughout interval. Section 1, 90 cm, to CC. [G.]</p> <p>Minor lithologies:</p> <p>a. Sandy mud, very dark gray (5Y 3/1) to black (5Y 2.5/2), with minor scattered dropstones. Section 1, 68-73 cm; Section 2, 139-144 cm; CC, 11-12 and 14-15 cm.</p> <p>b. Sandy mud, dark greenish gray (10Y 4/1). Section 1, 124-125 cm.</p> <p>c. Foraminiferal mud, olive gray (5Y 4/2) to dark grayish brown (2.5Y 4/2). Section 3, 0-18 cm.</p> <p>SMEAR SLIDE SUMMARY (%):</p> <table border="0"> <tr> <td></td> <td>1, 35</td> <td>2, 133</td> <td>3, 10</td> <td>CC, 3</td> </tr> <tr> <td></td> <td>D</td> <td>M</td> <td>D</td> <td>M</td> </tr> </table> <p>TEXTURE:</p> <table border="0"> <tr> <td>Sand</td> <td>10</td> <td>3</td> <td>2</td> <td>20</td> </tr> <tr> <td>Silt</td> <td>30</td> <td>30</td> <td>30</td> <td>30</td> </tr> <tr> <td>Clay</td> <td>60</td> <td>67</td> <td>68</td> <td>50</td> </tr> </table> <p>COMPOSITION:</p> <table border="0"> <tr> <td>Quartz</td> <td>30</td> <td>40</td> <td>20</td> <td>40</td> </tr> <tr> <td>Feldspar</td> <td>2</td> <td>5</td> <td>—</td> <td>5</td> </tr> <tr> <td>Clay</td> <td>66</td> <td>53</td> <td>60</td> <td>53</td> </tr> <tr> <td>Accessory minerals:</td> <td>1</td> <td>1</td> <td>1</td> <td>2</td> </tr> <tr> <td>Glauconite</td> <td>—</td> <td>1</td> <td>—</td> <td>—</td> </tr> <tr> <td>Foraminifers</td> <td>1</td> <td>—</td> <td>10</td> <td>—</td> </tr> <tr> <td>Nannofossils</td> <td>—</td> <td>—</td> <td>10</td> <td>—</td> </tr> </table>		1, 35	2, 133	3, 10	CC, 3		D	M	D	M	Sand	10	3	2	20	Silt	30	30	30	30	Clay	60	67	68	50	Quartz	30	40	20	40	Feldspar	2	5	—	5	Clay	66	53	60	53	Accessory minerals:	1	1	1	2	Glauconite	—	1	—	—	Foraminifers	1	—	10	—	Nannofossils	—	—	10	—
	1, 35	2, 133	3, 10	CC, 3																																																																				
	D	M	D	M																																																																				
Sand	10	3	2	20																																																																				
Silt	30	30	30	30																																																																				
Clay	60	67	68	50																																																																				
Quartz	30	40	20	40																																																																				
Feldspar	2	5	—	5																																																																				
Clay	66	53	60	53																																																																				
Accessory minerals:	1	1	1	2																																																																				
Glauconite	—	1	—	—																																																																				
Foraminifers	1	—	10	—																																																																				
Nannofossils	—	—	10	—																																																																				
C/G A/G	Benthic Zone	A1 / NSPF6					1				*	<p>1-W</p> <p>*</p> <p>*</p>																																																												
A/M		NN21?					0.5																																																																	
B							1.0																																																																	
T/P																																																																								
F/M																																																																								
Spiniferites elongatus Subzone/1a						N																																																																		
Brunhes																																																																								
							2																																																																	
							3																																																																	
							CC																																																																	

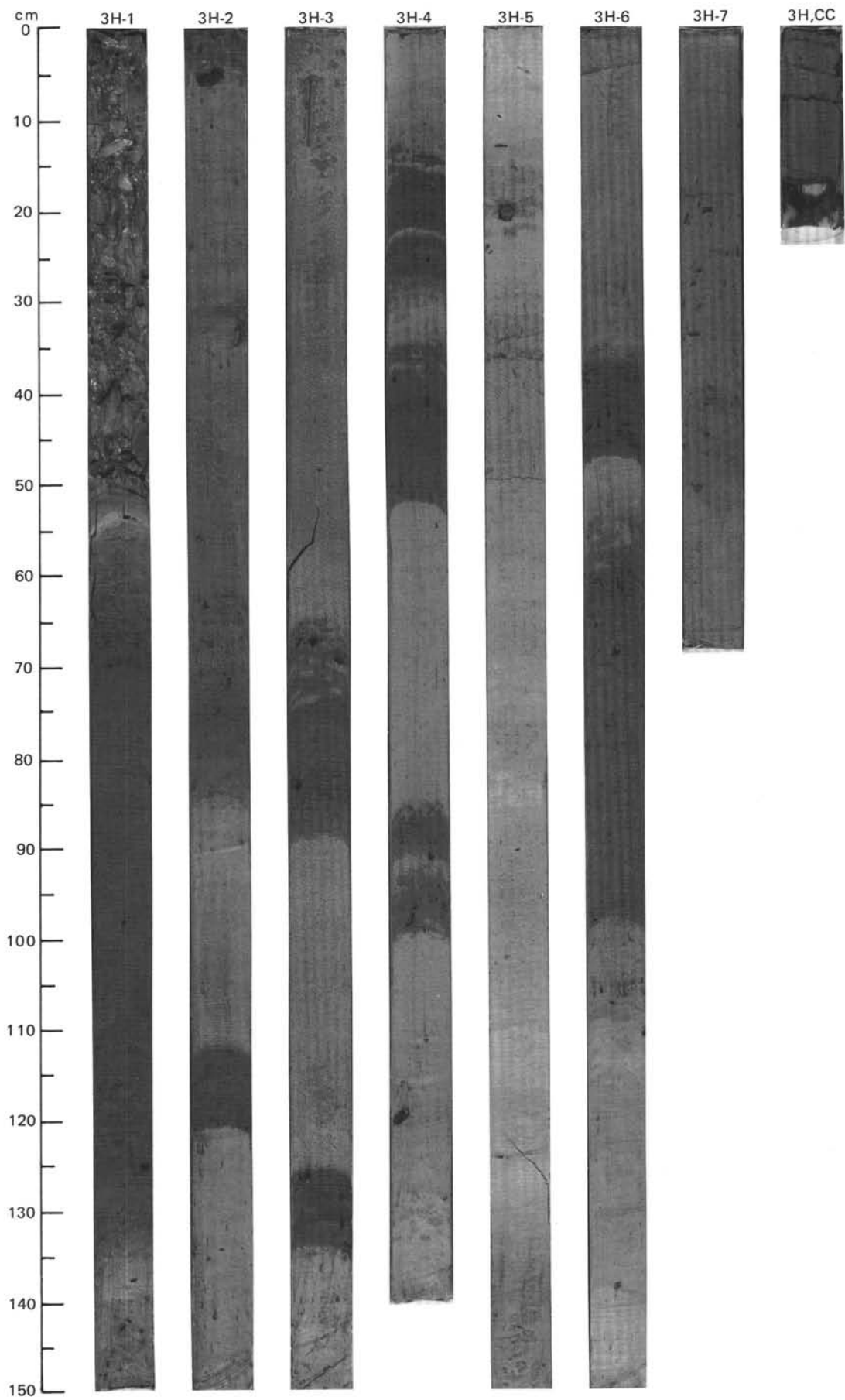


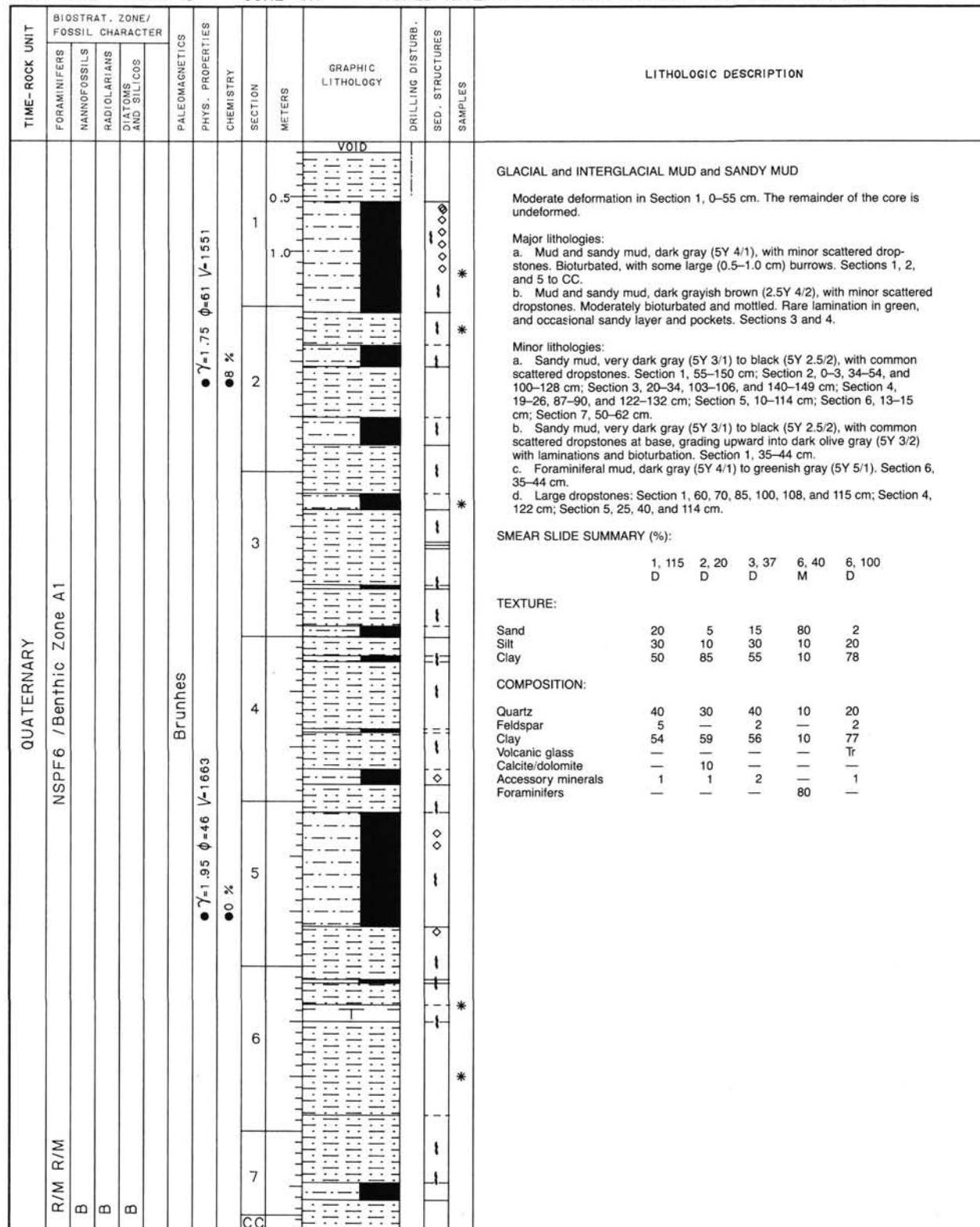


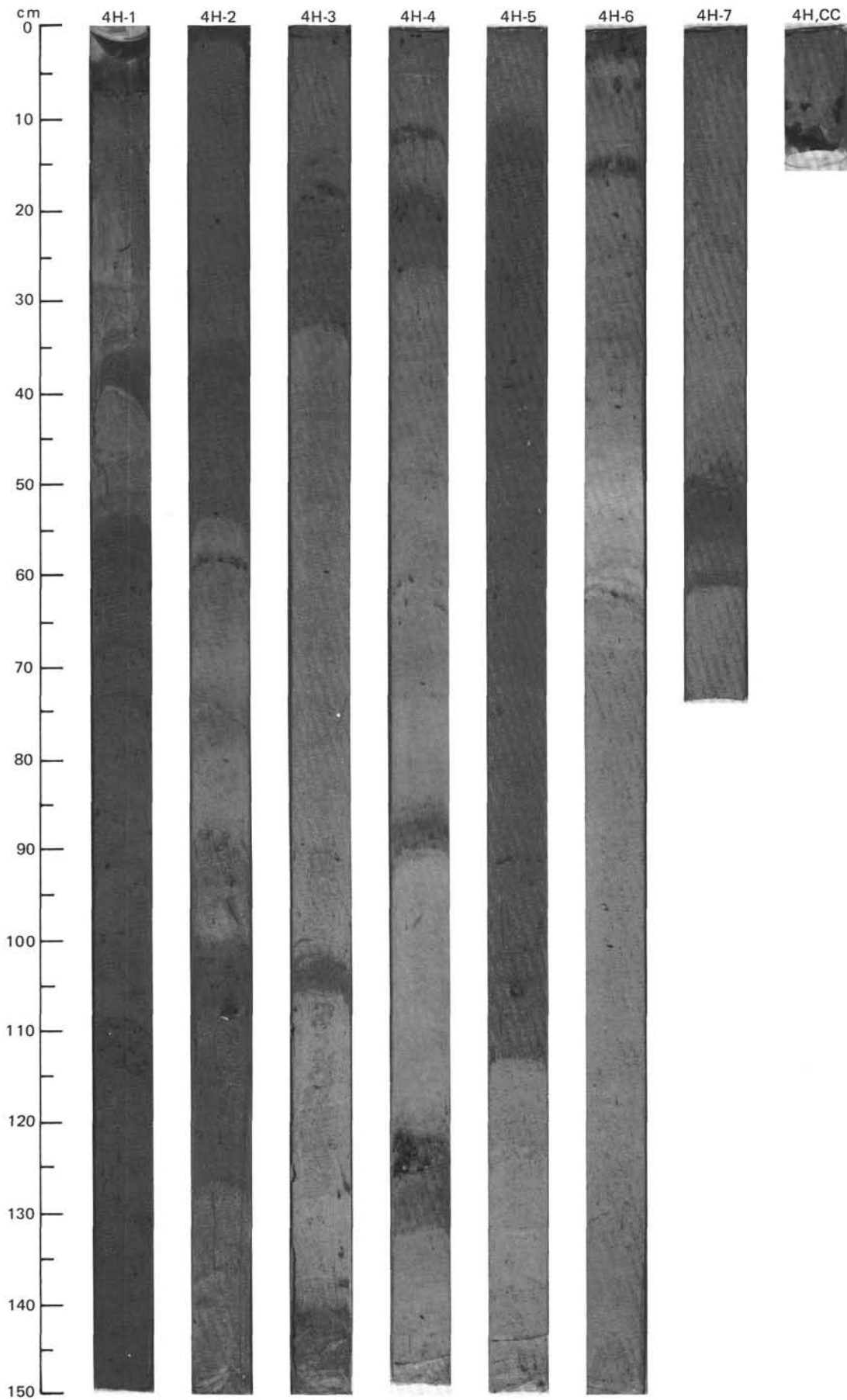


SITE 642 HOLE C CORE 3H CORED INTERVAL 1299.2-1309.1 mbsl; 13.20-23.10 mbsf

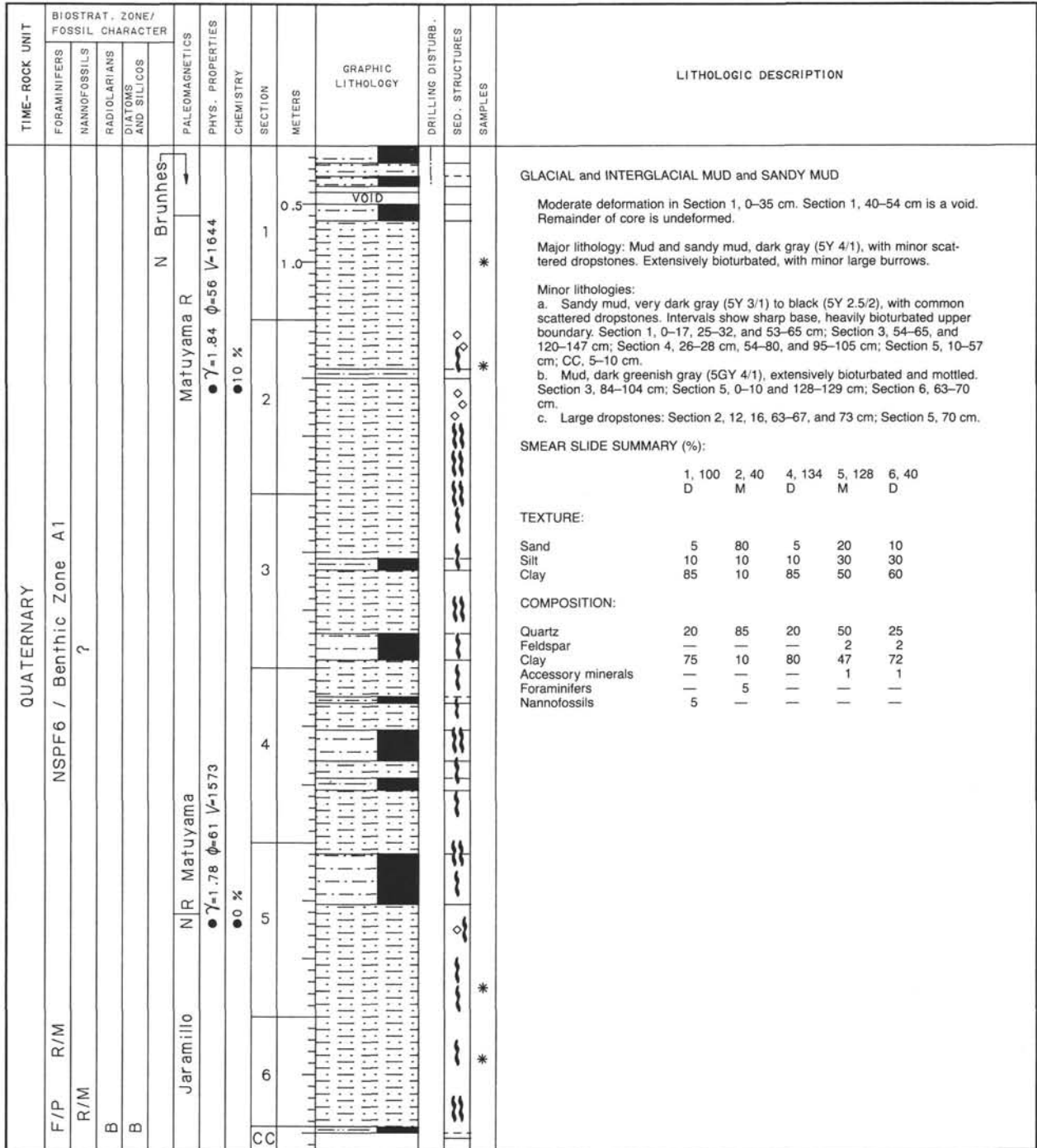


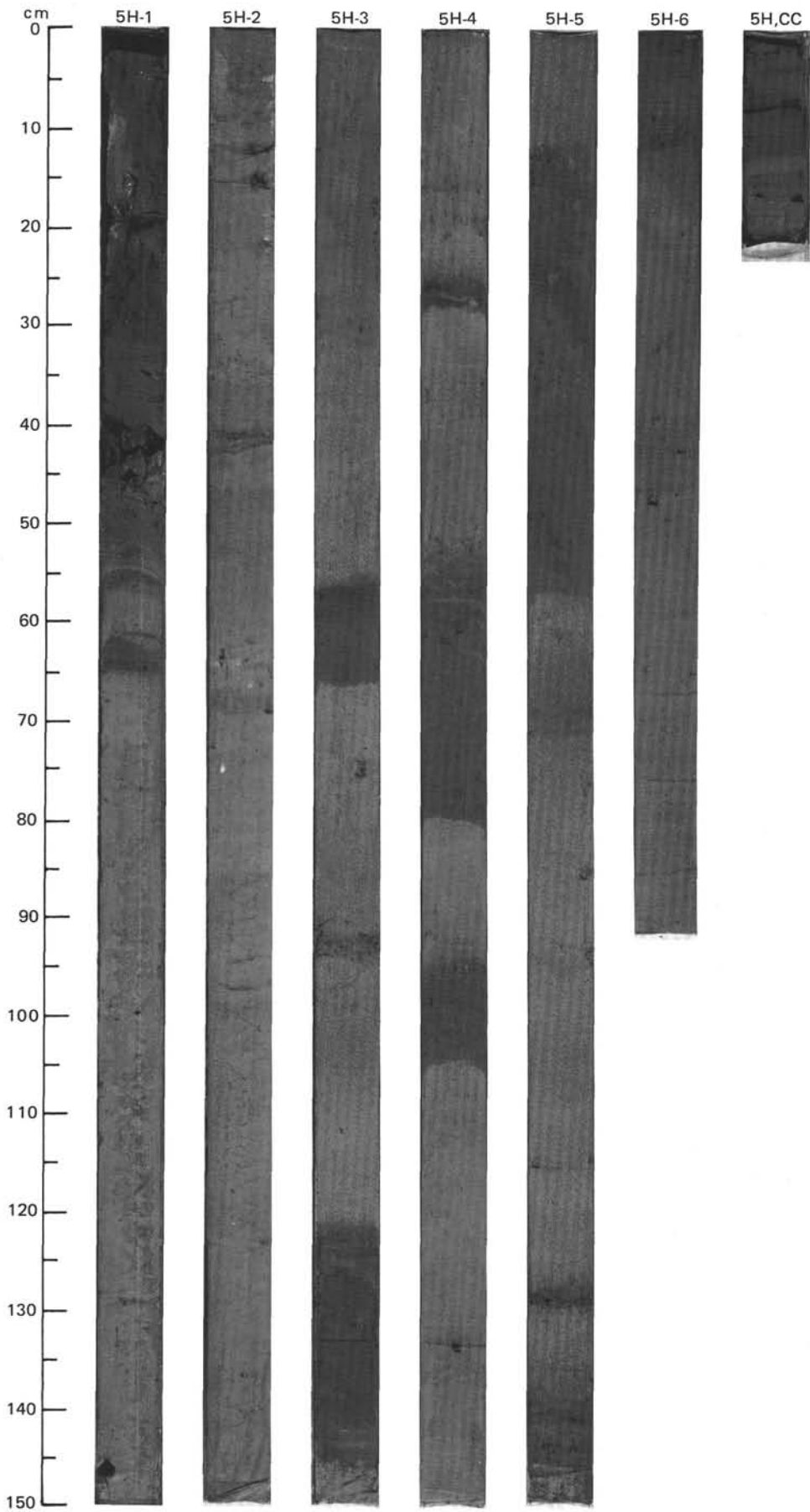




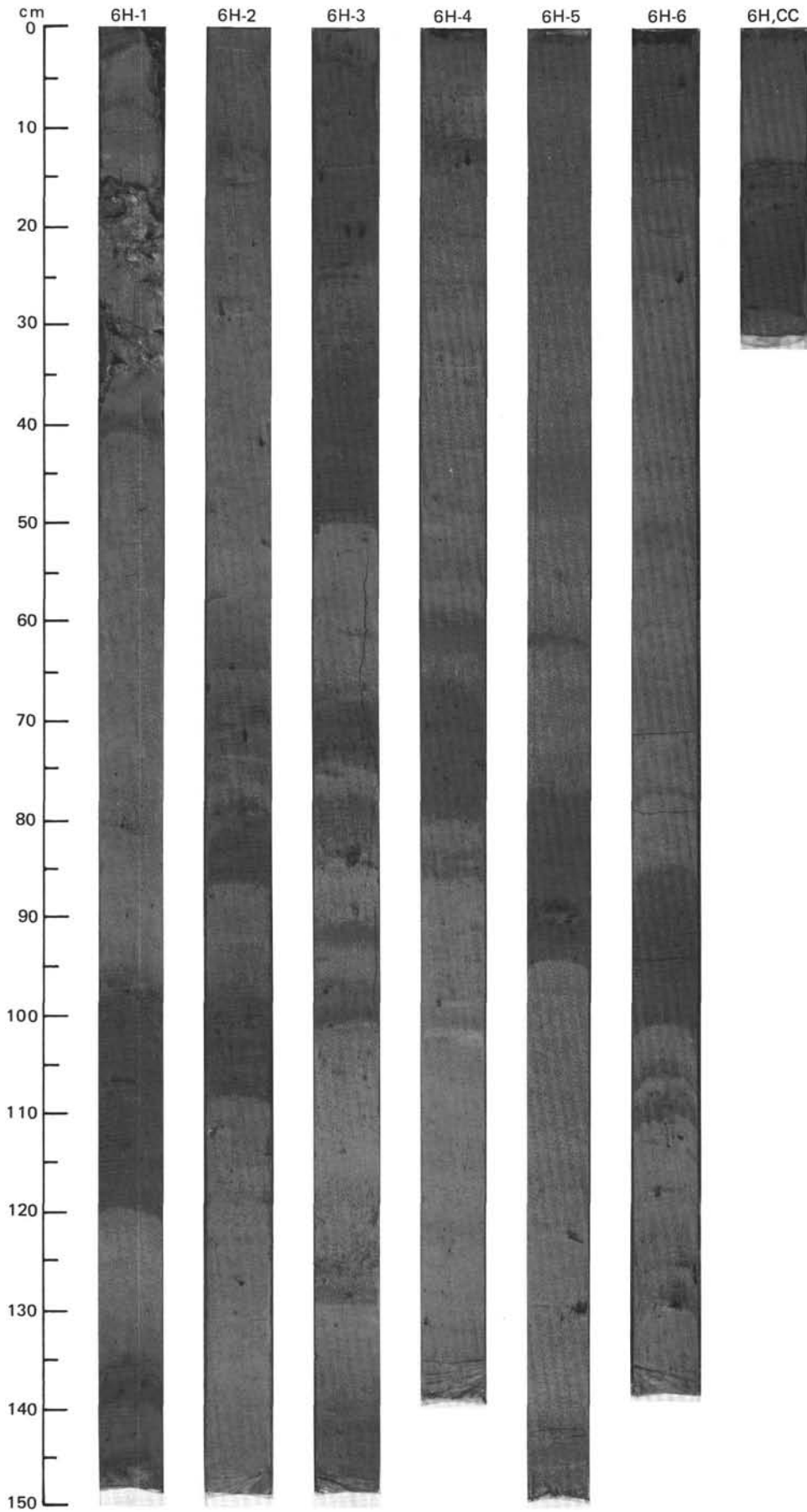


SITE 642 HOLE C CORE 5H CORED INTERVAL 1318.9-1327.4 mbsl; 32.90-41.40 mbsf

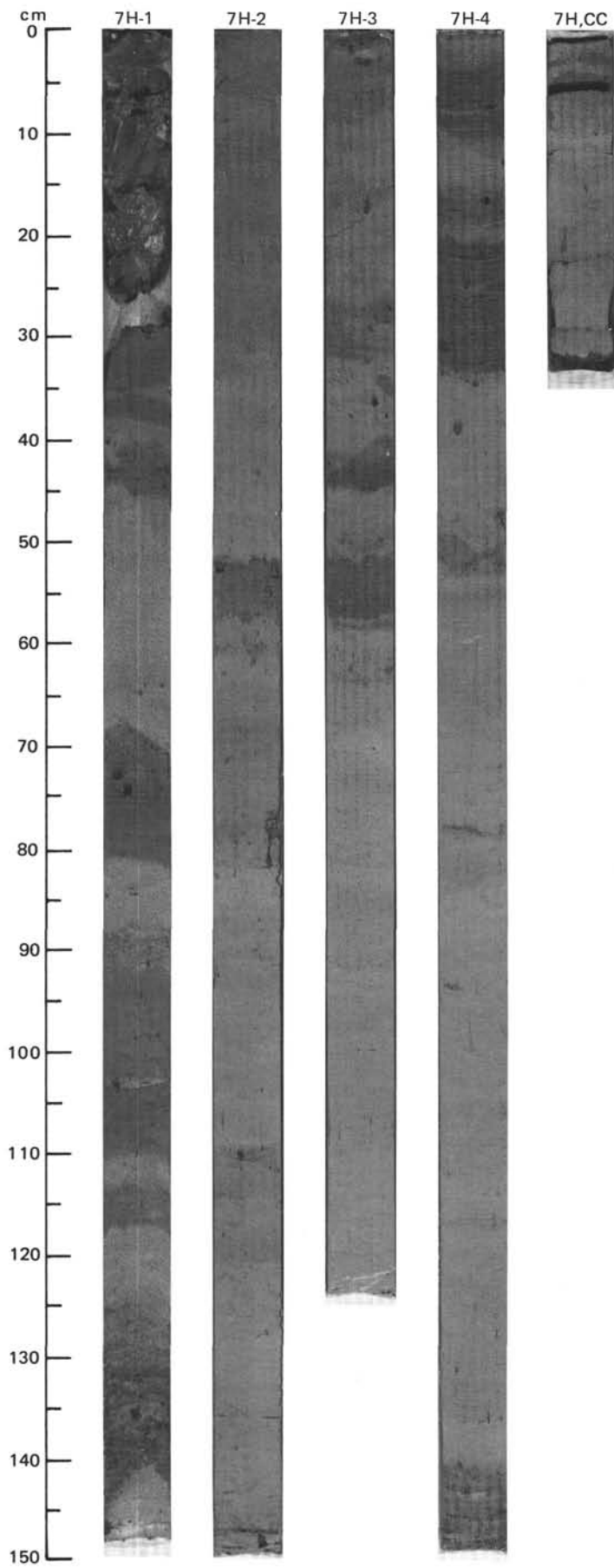




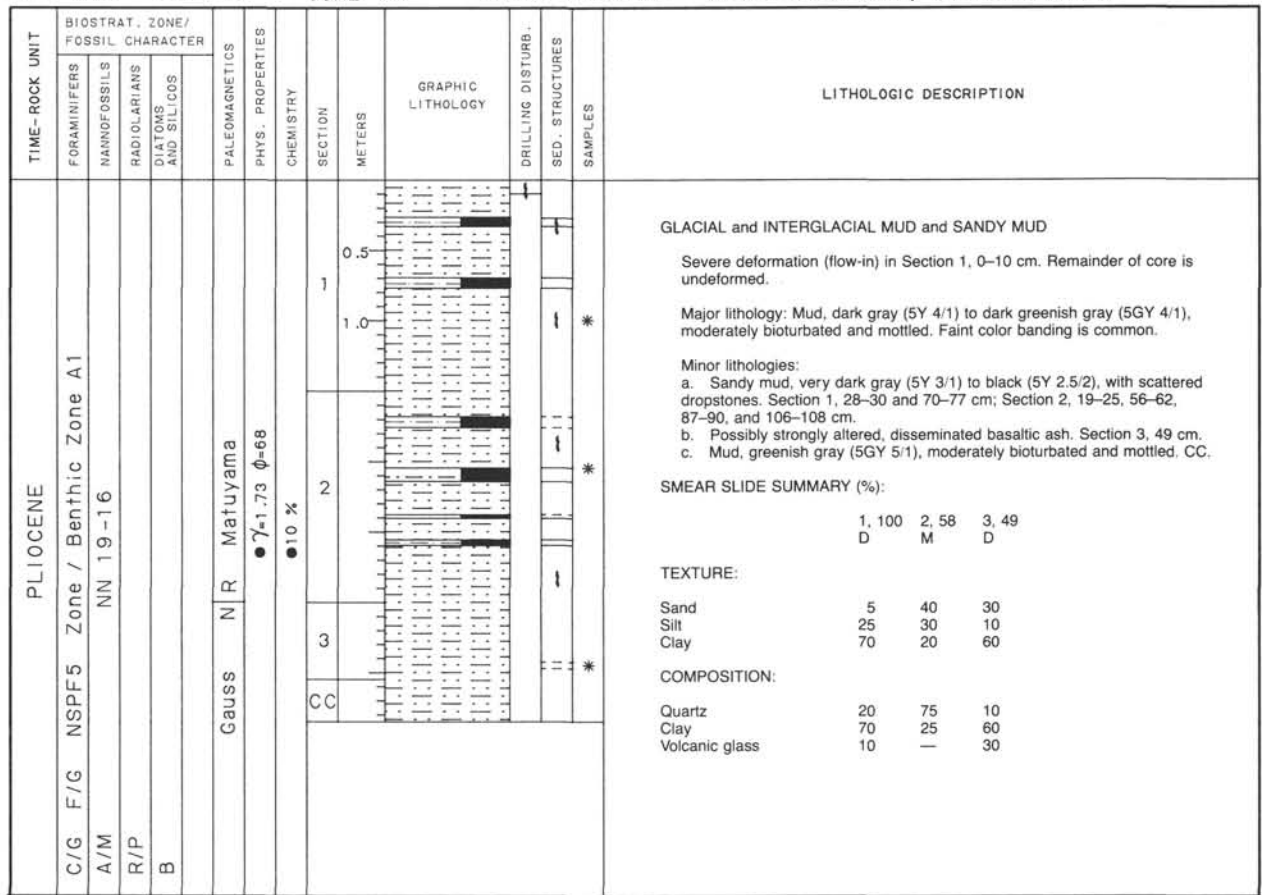
TIME-ROCK UNIT		BIOSTRAT. ZONE/ FOSSIL CHARACTER				PALEOMAGNETICS	PHYS. PROPERTIES	CHEMISTRY	SECTION	METERS	GRAPHIC LITHOLOGY	DRILLING DISTURB.	SED. STRUCTURES	SAMPLES	LITHOLOGIC DESCRIPTION																																																						
FORAMINIFERS	NANNOFOSSILS	RADIOLARIANS	DIATOMS AND SILICUS																																																																		
QUATERNARY																																																																					
NSPF6 /BENTHIC ZONE A1																																																																					
R/M	B					Matuyama R N Jaramillo	$\gamma_{1.78} \phi=60 \vee-1603$	$\bullet=7\%$	1	0.5					<p>GLACIAL and INTERGLACIAL MUD and SANDY MUD</p> <p>Entire core is undeformed.</p> <p>Major lithology: Mud, dark gray (5Y 4/1) to olive gray (5Y 4/2), with minor scattered dropstones and small lenses of sandy mud. Moderately bioturbated and mottled.</p> <p>Minor lithologies:</p> <p>a. Sandy mud, very dark gray (5Y 3/1) to black (5Y 2.5/2), with abundant scattered dropstones. Intervals show sharp base, extensively burrowed upper boundary. Section 1, 41-42, 90-121, and 137-142 cm; Section 2, 70-75, 80-88, and 100-110 cm; Section 3, 70-75, 79-83, 91-94, and 98-101 cm; Section 4, 67-81 cm; Section 5, 76-95 and 144-150 cm; Section 6, 0-16 and 86-102 cm; CC, 28-31 cm.</p> <p>b. Sandy mud, very dark gray (5Y 3/1) to black (5Y 2.5/2) at base, with abundant scattered dropstones, grading upward into dark olive gray (5Y 3/2) with laminations and bioturbation. Intervals show sharp bases and gradational tops. Section 3, 2-25, 28-31, and 116-130 cm; Section 4, 11-21 cm.</p> <p>c. Mud, greenish gray (10Y 5/1), moderately bioturbated and occasionally laminated. Section 2, 47-54, 60-70, and 75-78 cm; Section 3, 116-130 cm.</p> <p>d. Large dropstones: Section 1, 90 cm; Section 3, 86 and 100 cm; Section 6, 5 and 120 cm.</p> <p>SMEAR SLIDE SUMMARY (%):</p> <table border="1"> <tr> <td></td> <td>2, 80</td> <td>2, 130</td> <td>3, 130</td> <td>5, 42</td> <td>5, 90</td> </tr> <tr> <td></td> <td>D</td> <td>D</td> <td>M</td> <td>M</td> <td>D</td> </tr> </table> <p>TEXTURE:</p> <table border="1"> <tr> <td>Sand</td> <td>35</td> <td>20</td> <td>—</td> <td>5</td> <td>10</td> </tr> <tr> <td>Silt</td> <td>30</td> <td>15</td> <td>15</td> <td>55</td> <td>50</td> </tr> <tr> <td>Clay</td> <td>35</td> <td>65</td> <td>85</td> <td>40</td> <td>40</td> </tr> </table> <p>COMPOSITION:</p> <table border="1"> <tr> <td>Quartz</td> <td>60</td> <td>29</td> <td>15</td> <td>60</td> <td>60</td> </tr> <tr> <td>Feldspar</td> <td>5</td> <td>5</td> <td>—</td> <td>—</td> <td>—</td> </tr> <tr> <td>Clay</td> <td>35</td> <td>65</td> <td>85</td> <td>40</td> <td>40</td> </tr> <tr> <td>Accessory minerals</td> <td>Tr</td> <td>1</td> <td>—</td> <td>—</td> <td>—</td> </tr> </table>		2, 80	2, 130	3, 130	5, 42	5, 90		D	D	M	M	D	Sand	35	20	—	5	10	Silt	30	15	15	55	50	Clay	35	65	85	40	40	Quartz	60	29	15	60	60	Feldspar	5	5	—	—	—	Clay	35	65	85	40	40	Accessory minerals	Tr	1	—	—	—
	2, 80	2, 130	3, 130	5, 42	5, 90																																																																
	D	D	M	M	D																																																																
Sand	35	20	—	5	10																																																																
Silt	30	15	15	55	50																																																																
Clay	35	65	85	40	40																																																																
Quartz	60	29	15	60	60																																																																
Feldspar	5	5	—	—	—																																																																
Clay	35	65	85	40	40																																																																
Accessory minerals	Tr	1	—	—	—																																																																
B								2	1.0																																																												
B								3																																																													
B								4																																																													
								5																																																													
								6																																																													
CC																																																																					

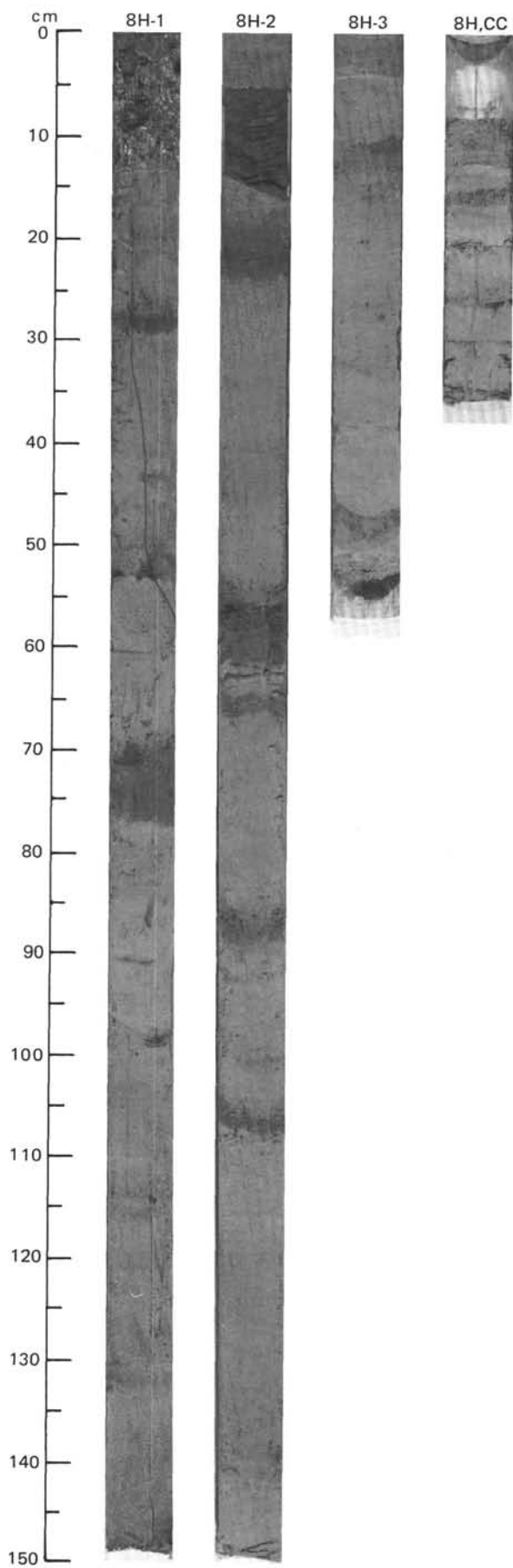


TIME-ROCK UNIT		BIOSTRAT. ZONE/ FOSSIL CHARACTER	PALEOMAGNETICS	PHYS. PROPERTIES	CHEMISTRY	SECTION	METERS	GRAPHIC LITHOLOGY	DRILLING DISTURB.	SED. STRUCTURES	SAMPLES	LITHOLOGIC DESCRIPTION																																																																						
QUATERNARY	FORAMINIFERS												NANNOFOSSILS	RADIOLARIANS	DIATOMS AND SILICOS																																																																			
B		<i>N. pachyderma</i> sin. ss / Benthic Zone A1	R N	Matuyama	• $\gamma = 1.72$ $\phi = 63$ $\psi = 1539$	1	0.5					<p>GLACIAL and INTERGLACIAL MUD and SANDY MUD</p> <p>Severe deformation (flow-in) at Section 1, 0-30 cm. The remainder of the core undeformed.</p> <p>Major lithologies:</p> <p>a. Mud, dark gray (5Y 4/1), with minor scattered dropstones and small lenses of sandy mud. Moderate bioturbation and mottling. Section 1; Section 2, 34-58 cm; Section 3, 0-53 and 125-150 cm; Section 4, 0-48 and 142-150 cm; Section 5 to CC.</p> <p>b. Mud, greenish gray to dark greenish gray (5GY 4/1), generally mottled, but with minor faint color banding and scattered small sand lenses (remainder).</p> <p>Minor lithologies:</p> <p>a. Sandy mud, very dark gray (5Y 3/1) to black (5Y 2.5/2), with abundant scattered dropstones. Intervals show sharp base, bioturbated top. Section 1, 30-38, 70-82, and 90-119 cm; Section 2, 52-58 cm; Section 3, 43-45 and 53-59 cm; Section 4, 4-10, 16-19, 20-33, and 142-150 cm; CC, 3-5 cm.</p> <p>b. Volcanic ash, thin disseminated layers. Section 1, 133-140 cm; Section 2, 148 cm.</p> <p>SMEAR SLIDE SUMMARY (%):</p> <table border="1"> <thead> <tr> <th></th> <th>1, 100</th> <th>2, 80</th> <th>3, 100</th> <th>4, 51</th> </tr> <tr> <th></th> <th>D</th> <th>M</th> <th>D</th> <th>M</th> </tr> </thead> <tbody> <tr> <td>Sand</td> <td>15</td> <td>10</td> <td>—</td> <td>80</td> </tr> <tr> <td>Silt</td> <td>30</td> <td>—</td> <td>20</td> <td>15</td> </tr> <tr> <td>Clay</td> <td>55</td> <td>90</td> <td>80</td> <td>5</td> </tr> </tbody> </table> <p>TEXTURE:</p> <table border="1"> <thead> <tr> <th></th> <th>1, 100</th> <th>2, 80</th> <th>3, 100</th> <th>4, 51</th> </tr> </thead> <tbody> <tr> <td>Sand</td> <td>15</td> <td>10</td> <td>—</td> <td>80</td> </tr> <tr> <td>Silt</td> <td>30</td> <td>—</td> <td>20</td> <td>15</td> </tr> <tr> <td>Clay</td> <td>55</td> <td>90</td> <td>80</td> <td>5</td> </tr> </tbody> </table> <p>COMPOSITION:</p> <table border="1"> <thead> <tr> <th></th> <th>1, 100</th> <th>2, 80</th> <th>3, 100</th> <th>4, 51</th> </tr> </thead> <tbody> <tr> <td>Quartz</td> <td>45</td> <td>—</td> <td>15</td> <td>55</td> </tr> <tr> <td>Clay</td> <td>55</td> <td>90</td> <td>80</td> <td>5</td> </tr> <tr> <td>Volcanic glass</td> <td>—</td> <td>10</td> <td>5</td> <td>40</td> </tr> <tr> <td>Accessory minerals</td> <td>Tr</td> <td>—</td> <td>—</td> <td>—</td> </tr> </tbody> </table>		1, 100	2, 80	3, 100	4, 51		D	M	D	M	Sand	15	10	—	80	Silt	30	—	20	15	Clay	55	90	80	5		1, 100	2, 80	3, 100	4, 51	Sand	15	10	—	80	Silt	30	—	20	15	Clay	55	90	80	5		1, 100	2, 80	3, 100	4, 51	Quartz	45	—	15	55	Clay	55	90	80	5	Volcanic glass	—	10	5	40	Accessory minerals	Tr	—	—	—
	1, 100	2, 80	3, 100	4, 51																																																																														
	D	M	D	M																																																																														
Sand	15	10	—	80																																																																														
Silt	30	—	20	15																																																																														
Clay	55	90	80	5																																																																														
	1, 100	2, 80	3, 100	4, 51																																																																														
Sand	15	10	—	80																																																																														
Silt	30	—	20	15																																																																														
Clay	55	90	80	5																																																																														
	1, 100	2, 80	3, 100	4, 51																																																																														
Quartz	45	—	15	55																																																																														
Clay	55	90	80	5																																																																														
Volcanic glass	—	10	5	40																																																																														
Accessory minerals	Tr	—	—	—																																																																														
B						2	1.0																																																																											
B						3																																																																												
B						4																																																																												
CC																																																																																		



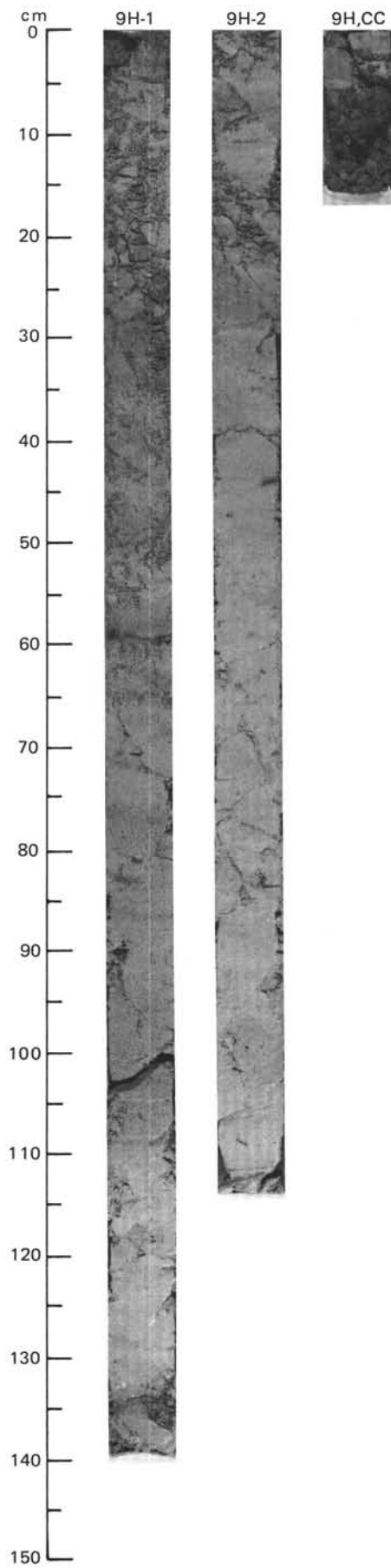
SITE 642 HOLE C CORE 8H CORED INTERVAL 1343.1-1346.7 mbsf; 57.10-60.70 mbsf





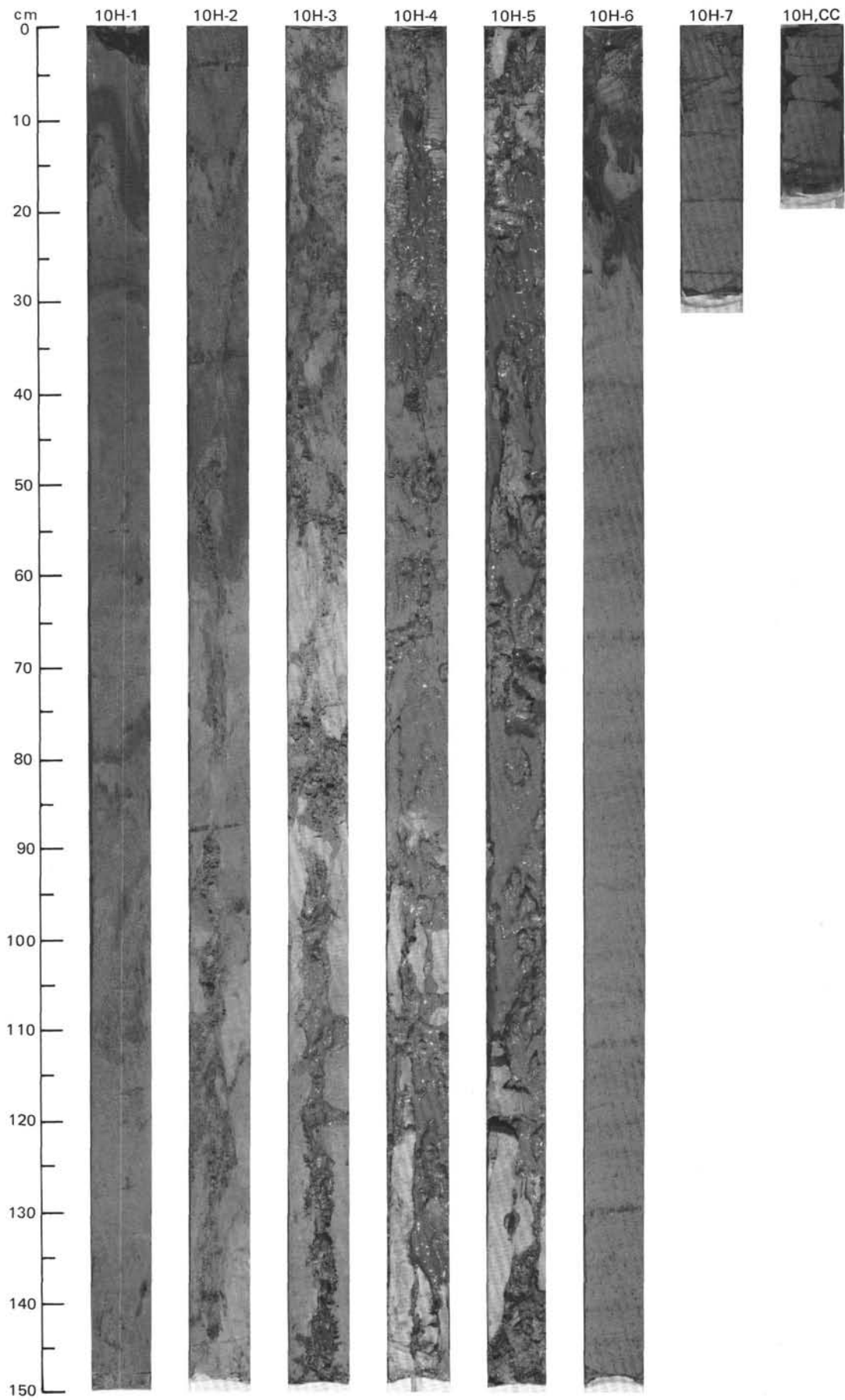
SITE 642 HOLE C CORE 9H CORED INTERVAL 1346.7-1349.5 mbsl; 60.70-63.50 mbsf

TIME-ROCK UNIT	BIOSTRAT. ZONE/ FOSSIL CHARACTER					PALEOMAGNETICS	PHYS. PROPERTIES	CHEMISTRY	SECTION	METERS	GRAPHIC LITHOLOGY	DRILLING DISTURB.	SED. STRUCTURES	SAMPLES	LITHOLOGIC DESCRIPTION
	FORAMINIFERS	NANNOFOSSILS	RADIOLARIANS	DIATOMS	SILICOS										
PLIOCENE	NSPF4 / Benthic Zone A2					● $\gamma = 1.47$ $\phi = 83$	● 47 %	CC	1	0.5 1.0				*	<p>NANNOFOSSIL OOZE</p> <p>Entire core was slightly disturbed during splitting.</p> <p>Major lithology: Nannofossil ooze, greenish gray (5GY 5/1), moderately bioturbated and mottled. Contains dark gray (5Y 4/2) and olive gray (5Y 4/2) faint, horizontal laminations.</p> <p>Minor lithology: Volcanic ash, disseminated. Composed of dark (altered basaltic glass?) and light shards. Section 1, 60 cm.</p> <p>SMEAR SLIDE SUMMARY (%):</p> <p style="text-align: right;">1, 70 D</p> <p>TEXTURE:</p> <p>Sand 5 Silt 25 Clay 70</p> <p>COMPOSITION:</p> <p>Clay 20 Volcanic glass 5 Nannofossils 50 Diatoms 5 Sponge spicules 20</p>
	F/P	NN19-16													
	R/M	NSR12													
	C/M	<i>Nitzschia touseae</i> Zone													
	F/G	<i>Distephanus boliviensis</i> Zone													



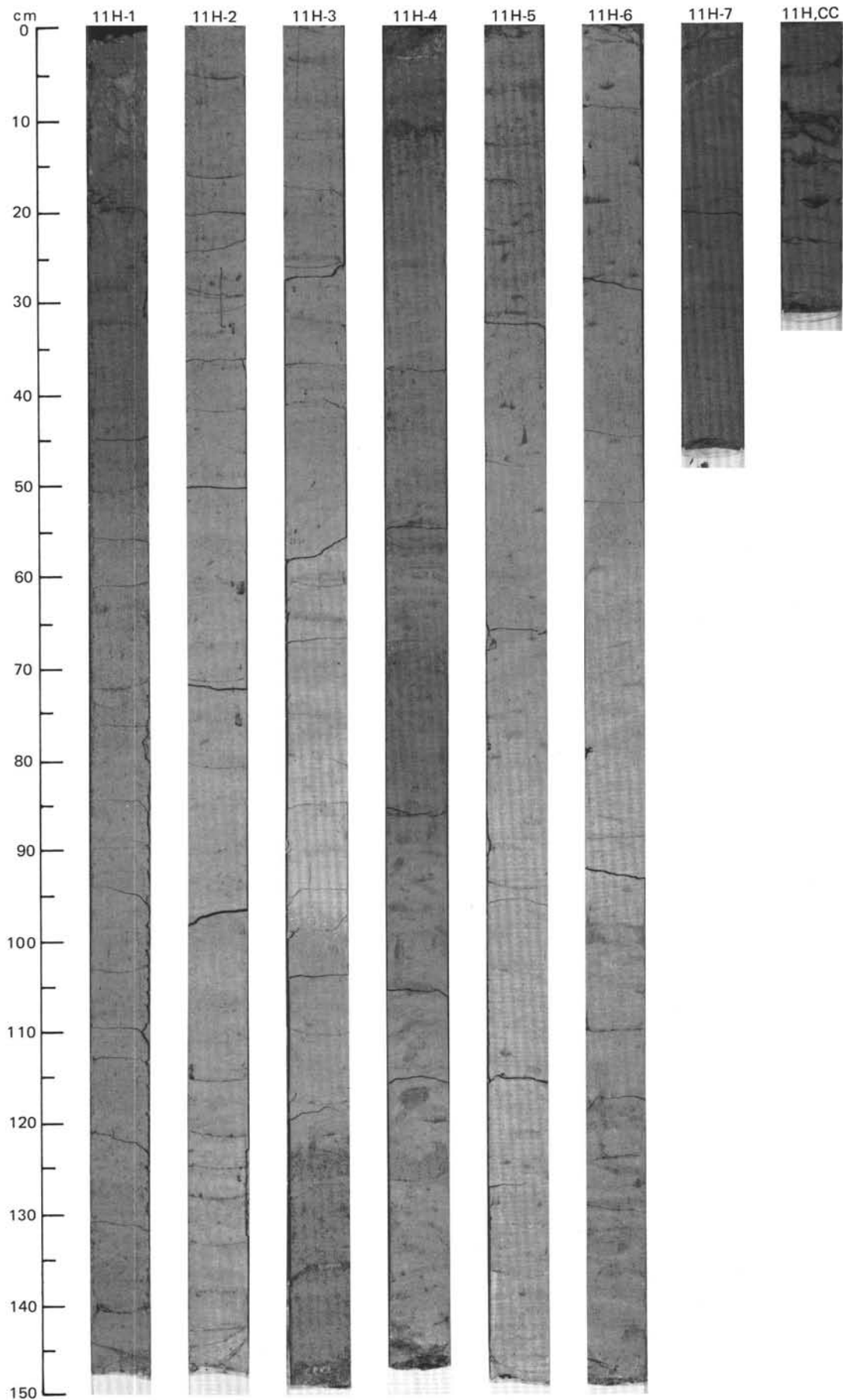
SITE 642 HOLE C CORE 10H CORED INTERVAL 1349.5-1359.0 mbsl; 63.50-73.00 mbsf

TIME-ROCK UNIT		FORAMINIFERS	NANNOFOSSILS	RADIOLARIANS	DIATOMS	SILICOS	PALEOMAGNETICS	PHYS. PROPERTIES	CHEMISTRY	SECTION	METERS	GRAPHIC LITHOLOGY	DRILLING DISTURB.	SED. STRUCTURES	SAMPLES	LITHOLOGIC DESCRIPTION																																																																
BIOSTRAT. ZONE/ FOSSIL CHARACTER																																																																																
PLIOCENE																																																																																
C/G	C/G	NSPF 4 /Benthic Zone A2																																																																														
C/M		NN 19-16																																																																														
C/G		NSR1 2																																																																														
F/P		<i>Nitzschia touseae</i> Zone																																																																														
F/G		<i>Distephanus boliviensis</i> Zone																																																																														
								● $\gamma=1.48$ $\phi=76$																																																																								
								● 18 %																																																																								
										1	0.5				*																																																																	
										2	1.0				*																																																																	
										3																																																																						
										4																																																																						
										5																																																																						
										6					*																																																																	
										7					*																																																																	
										CC																																																																						
<p>NANNOFOSSIL OOZE</p> <p>Severe disturbance (drilling slurry) in Section 1 to Section 6, 37 cm. Remainder of core is slightly deformed.</p> <p>Major lithology: Nannofossil ooze, greenish gray (5GY 5/1) to dark greenish gray (5GY 4/1). Weak bioturbation and mottling; contains thin, faint grayish green (5GY 4/2) horizontal laminations spaced 3-5 cm apart.</p> <p>Minor lithologies: a. Possibly altered basaltic ash. Section 2, 20 cm. b. Volcanic ash, dark gray, with light and brown shards. Section 6, 20 cm.</p> <p>SMEAR SLIDE SUMMARY (%):</p> <table border="1"> <thead> <tr> <th></th> <th>1, 56</th> <th>2, 21</th> <th>6, 20</th> <th>6, 70</th> </tr> </thead> <tbody> <tr> <td>D</td> <td></td> <td>M</td> <td>M</td> <td>D</td> </tr> </tbody> </table> <p>TEXTURE:</p> <table border="1"> <thead> <tr> <th></th> <th>5</th> <th>100</th> <th>90</th> <th>—</th> </tr> </thead> <tbody> <tr> <td>Sand</td> <td></td> <td></td> <td></td> <td></td> </tr> <tr> <td>Silt</td> <td>40</td> <td>—</td> <td>5</td> <td>20</td> </tr> <tr> <td>Clay</td> <td>55</td> <td>—</td> <td>5</td> <td>80</td> </tr> </tbody> </table> <p>COMPOSITION:</p> <table border="1"> <thead> <tr> <th></th> <th>45</th> <th>—</th> <th>—</th> <th>—</th> </tr> </thead> <tbody> <tr> <td>Quartz</td> <td></td> <td></td> <td></td> <td></td> </tr> <tr> <td>Clay</td> <td>55</td> <td>—</td> <td>4</td> <td>10</td> </tr> <tr> <td>Volcanic glass</td> <td>—</td> <td>100</td> <td>90</td> <td>—</td> </tr> <tr> <td>Nannofossils</td> <td>—</td> <td>—</td> <td>—</td> <td>70</td> </tr> <tr> <td>Diatoms</td> <td>—</td> <td>—</td> <td>1</td> <td>5</td> </tr> <tr> <td>Sponge spicules</td> <td>—</td> <td>—</td> <td>5</td> <td>15</td> </tr> </tbody> </table>																	1, 56	2, 21	6, 20	6, 70	D		M	M	D		5	100	90	—	Sand					Silt	40	—	5	20	Clay	55	—	5	80		45	—	—	—	Quartz					Clay	55	—	4	10	Volcanic glass	—	100	90	—	Nannofossils	—	—	—	70	Diatoms	—	—	1	5	Sponge spicules	—	—	5	15
	1, 56	2, 21	6, 20	6, 70																																																																												
D		M	M	D																																																																												
	5	100	90	—																																																																												
Sand																																																																																
Silt	40	—	5	20																																																																												
Clay	55	—	5	80																																																																												
	45	—	—	—																																																																												
Quartz																																																																																
Clay	55	—	4	10																																																																												
Volcanic glass	—	100	90	—																																																																												
Nannofossils	—	—	—	70																																																																												
Diatoms	—	—	1	5																																																																												
Sponge spicules	—	—	5	15																																																																												

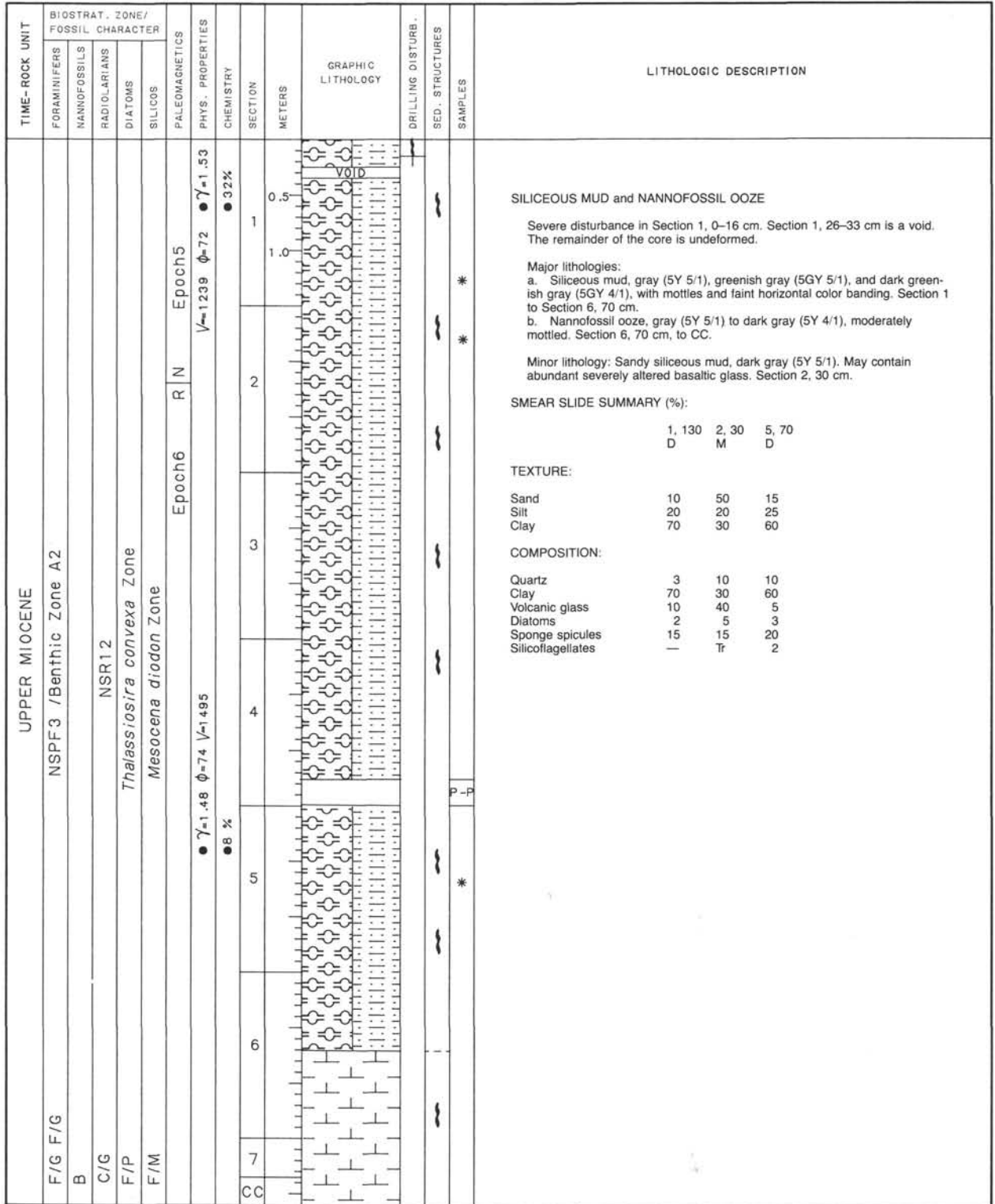


SITE 642 HOLE C CORE 11H CORED INTERVAL 1359.0-1368.5 mbsl; 73.00-82.50 mbsf

TIME-ROCK UNIT		BIOSTRAT. ZONE/ FOSSIL CHARACTER	PALEOMAGNETICS	PHYS. PROPERTIES	CHEMISTRY	SECTION	METERS	GRAPHIC LITHOLOGY	DRILLING DISTURB.	SED. STRUCTURES	SAMPLES	LITHOLOGIC DESCRIPTION																																																																																																		
FORAMINIFERS	NANNOFOSSILS																																																																																																													
PLIOCENE																																																																																																														
C/G	C/G	NSPF4 /Benthic Zone A2				1	0.5 1.0					<p>NANNOFOSSIL OOZE</p> <p>Entire core is undeformed.</p> <p>Major lithology: Nannofossil ooze, gray (5Y 5/1), moderately mottled. Contains thin, faint grayish green (5GY 4/2) horizontal laminations spaced 3-5 cm apart.</p> <p>Minor lithologies:</p> <p>a. Siliceous mud, greenish gray (5GY 5/1), containing well-developed grayish green (5GY 4/2) laminations. Laminations may contain severely altered basaltic glass. Section 3, 100 cm, to Section 4, 83 cm.</p> <p>b. Siliceous mud, dark gray (5Y 4/1), with abundant small-scale and scattered large-scale mottling. Section 7 to CC.</p> <p>SMEAR SLIDE SUMMARY (%):</p> <table border="1"> <tr> <td></td> <td>2, 75</td> <td>4, 11</td> <td>4, 40</td> <td>4, 83</td> <td>6, 60</td> <td>7, 39</td> </tr> <tr> <td></td> <td>D</td> <td>M</td> <td>D</td> <td>D</td> <td>D</td> <td>D</td> </tr> </table> <p>TEXTURE:</p> <table border="1"> <tr> <td>Sand</td> <td>—</td> <td>100</td> <td>55</td> <td>50</td> <td>—</td> <td>—</td> </tr> <tr> <td>Silt</td> <td>5</td> <td>—</td> <td>10</td> <td>20</td> <td>15</td> <td>35</td> </tr> <tr> <td>Clay</td> <td>95</td> <td>—</td> <td>35</td> <td>30</td> <td>85</td> <td>65</td> </tr> </table> <p>COMPOSITION:</p> <table border="1"> <tr> <td>Quartz</td> <td>—</td> <td>—</td> <td>15</td> <td>20</td> <td>—</td> <td>20</td> </tr> <tr> <td>Clay</td> <td>5</td> <td>—</td> <td>35</td> <td>30</td> <td>5</td> <td>60</td> </tr> <tr> <td>Volcanic glass</td> <td>—</td> <td>100</td> <td>40</td> <td>30</td> <td>—</td> <td>—</td> </tr> <tr> <td>Accessory minerals</td> <td>—</td> <td>Tr</td> <td>—</td> <td>—</td> <td>—</td> <td>—</td> </tr> <tr> <td>Foraminifers</td> <td>—</td> <td>—</td> <td>—</td> <td>1</td> <td>—</td> <td>—</td> </tr> <tr> <td>Nannofossils</td> <td>90</td> <td>—</td> <td>—</td> <td>—</td> <td>80</td> <td>5</td> </tr> <tr> <td>Diatoms</td> <td>—</td> <td>—</td> <td>—</td> <td>3</td> <td>5</td> <td>5</td> </tr> <tr> <td>Sponge spicules</td> <td>5</td> <td>—</td> <td>10</td> <td>15</td> <td>10</td> <td>10</td> </tr> <tr> <td>Silicoflagellates</td> <td>—</td> <td>—</td> <td>—</td> <td>1</td> <td>—</td> <td>—</td> </tr> </table>		2, 75	4, 11	4, 40	4, 83	6, 60	7, 39		D	M	D	D	D	D	Sand	—	100	55	50	—	—	Silt	5	—	10	20	15	35	Clay	95	—	35	30	85	65	Quartz	—	—	15	20	—	20	Clay	5	—	35	30	5	60	Volcanic glass	—	100	40	30	—	—	Accessory minerals	—	Tr	—	—	—	—	Foraminifers	—	—	—	1	—	—	Nannofossils	90	—	—	—	80	5	Diatoms	—	—	—	3	5	5	Sponge spicules	5	—	10	15	10	10	Silicoflagellates	—	—	—	1	—	—
	2, 75	4, 11	4, 40	4, 83	6, 60	7, 39																																																																																																								
	D	M	D	D	D	D																																																																																																								
Sand	—	100	55	50	—	—																																																																																																								
Silt	5	—	10	20	15	35																																																																																																								
Clay	95	—	35	30	85	65																																																																																																								
Quartz	—	—	15	20	—	20																																																																																																								
Clay	5	—	35	30	5	60																																																																																																								
Volcanic glass	—	100	40	30	—	—																																																																																																								
Accessory minerals	—	Tr	—	—	—	—																																																																																																								
Foraminifers	—	—	—	1	—	—																																																																																																								
Nannofossils	90	—	—	—	80	5																																																																																																								
Diatoms	—	—	—	3	5	5																																																																																																								
Sponge spicules	5	—	10	15	10	10																																																																																																								
Silicoflagellates	—	—	—	1	—	—																																																																																																								
		NN 15-7				2				*																																																																																																				
		NSR12				3																																																																																																								
		<i>Thalassiosira convexa</i> Zone				4				*																																																																																																				
		<i>Distephanus boliviensis</i> Zone				5				*																																																																																																				
		Epoch5 N R Gilbert				6				*																																																																																																				
						7				*																																																																																																				
						CC				*																																																																																																				



SITE 642 HOLE C CORE 12H CORED INTERVAL 1368.5-1378.0 mbsl; 82.50-92.00 mbsf



SILICEOUS MUD and NANNOFOSSIL OOZE

Severe disturbance in Section 1, 0-16 cm. Section 1, 26-33 cm is a void. The remainder of the core is undeformed.

Major lithologies:

a. Siliceous mud, gray (5Y 5/1), greenish gray (5GY 5/1), and dark greenish gray (5GY 4/1), with mottles and faint horizontal color banding. Section 1 to Section 6, 70 cm.

b. Nannofossil ooze, gray (5Y 5/1) to dark gray (5Y 4/1), moderately mottled. Section 6, 70 cm, to CC.

Minor lithology: Sandy siliceous mud, dark gray (5Y 5/1). May contain abundant severely altered basaltic glass. Section 2, 30 cm.

SMEAR SLIDE SUMMARY (%):

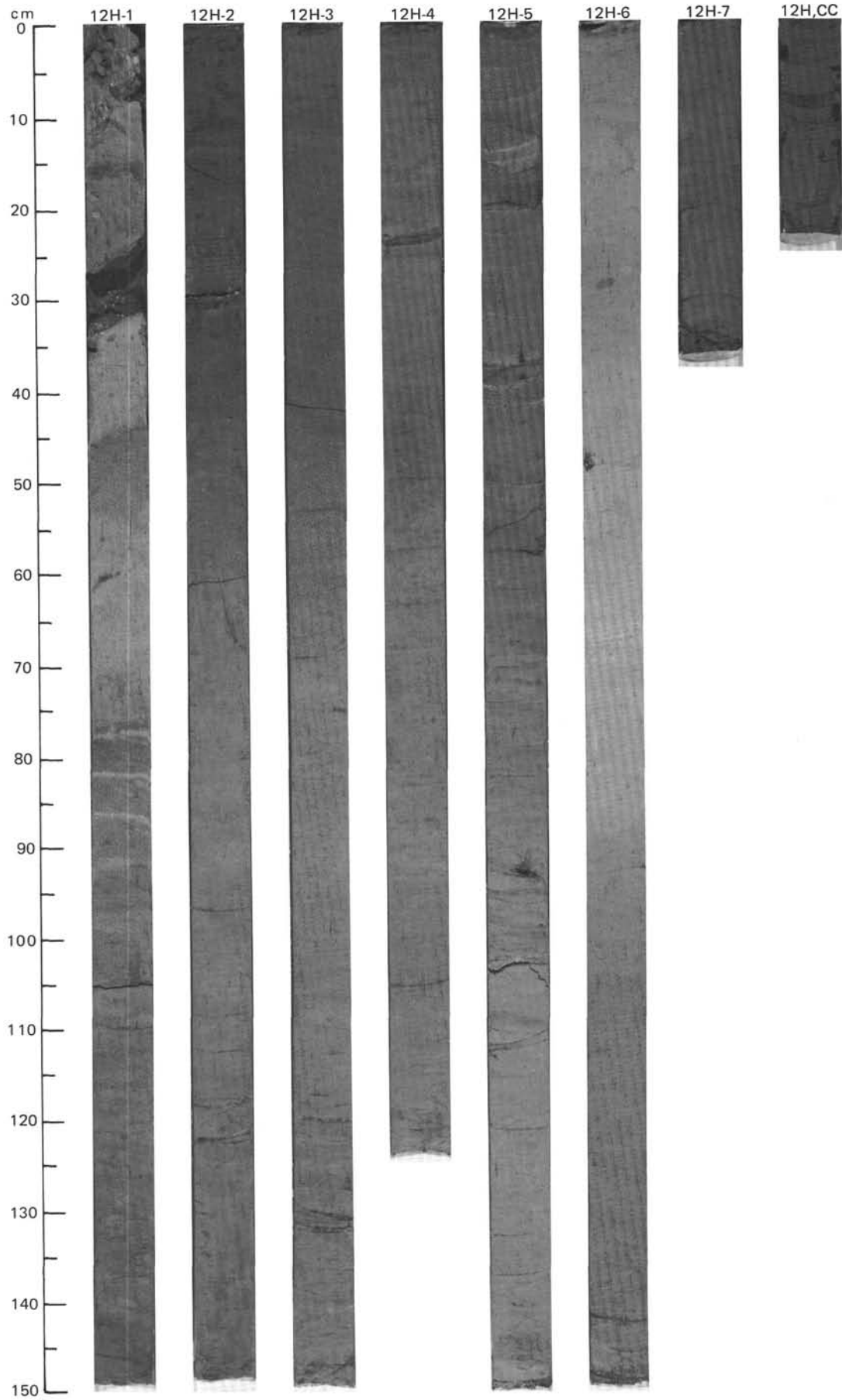
	1, 130	2, 30	5, 70
	D	M	D

TEXTURE:

Sand	10	50	15
Silt	20	20	25
Clay	70	30	60

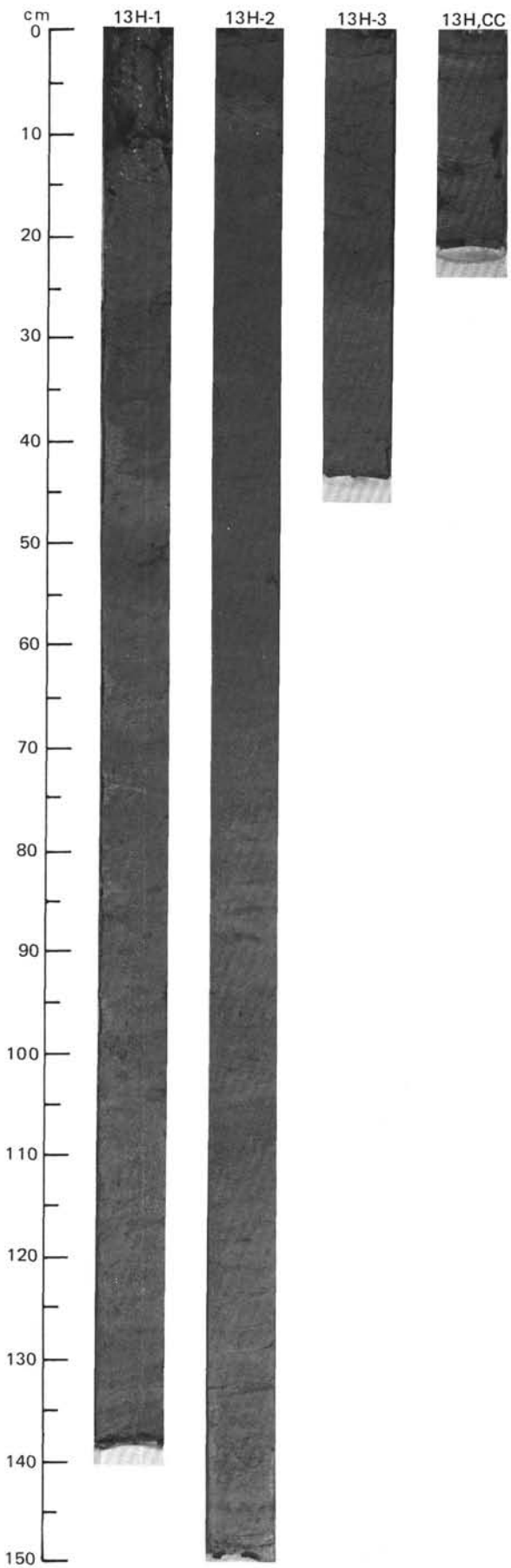
COMPOSITION:

Quartz	3	10	10
Clay	70	30	60
Volcanic glass	10	40	5
Diatoms	2	5	3
Sponge spicules	15	15	20
Silicoflagellates	—	Tr	2

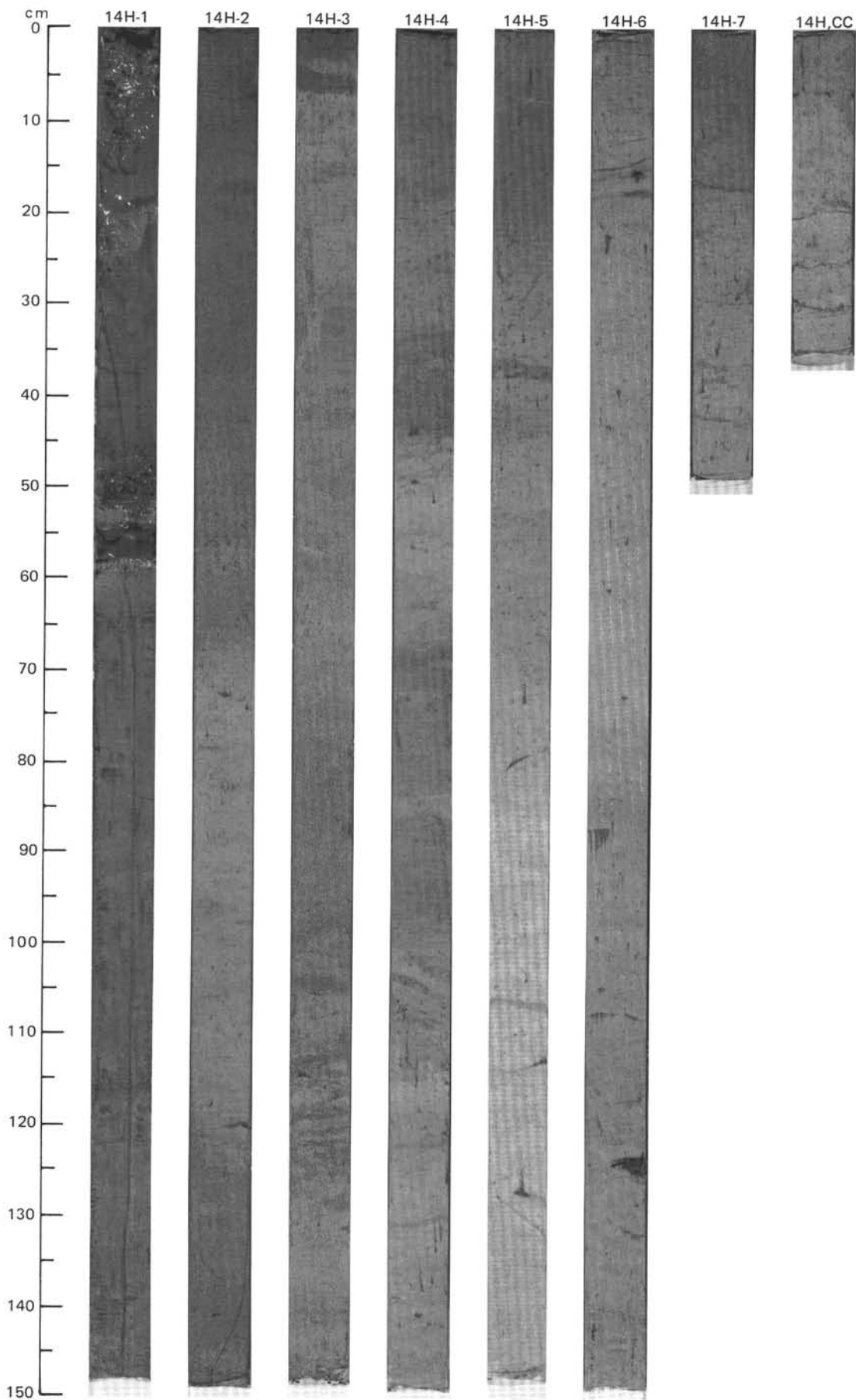


SITE 642 HOLE C CORE 13H CORED INTERVAL 1378.0-1387.5 mbsf; 92.00-101.50 mbsf

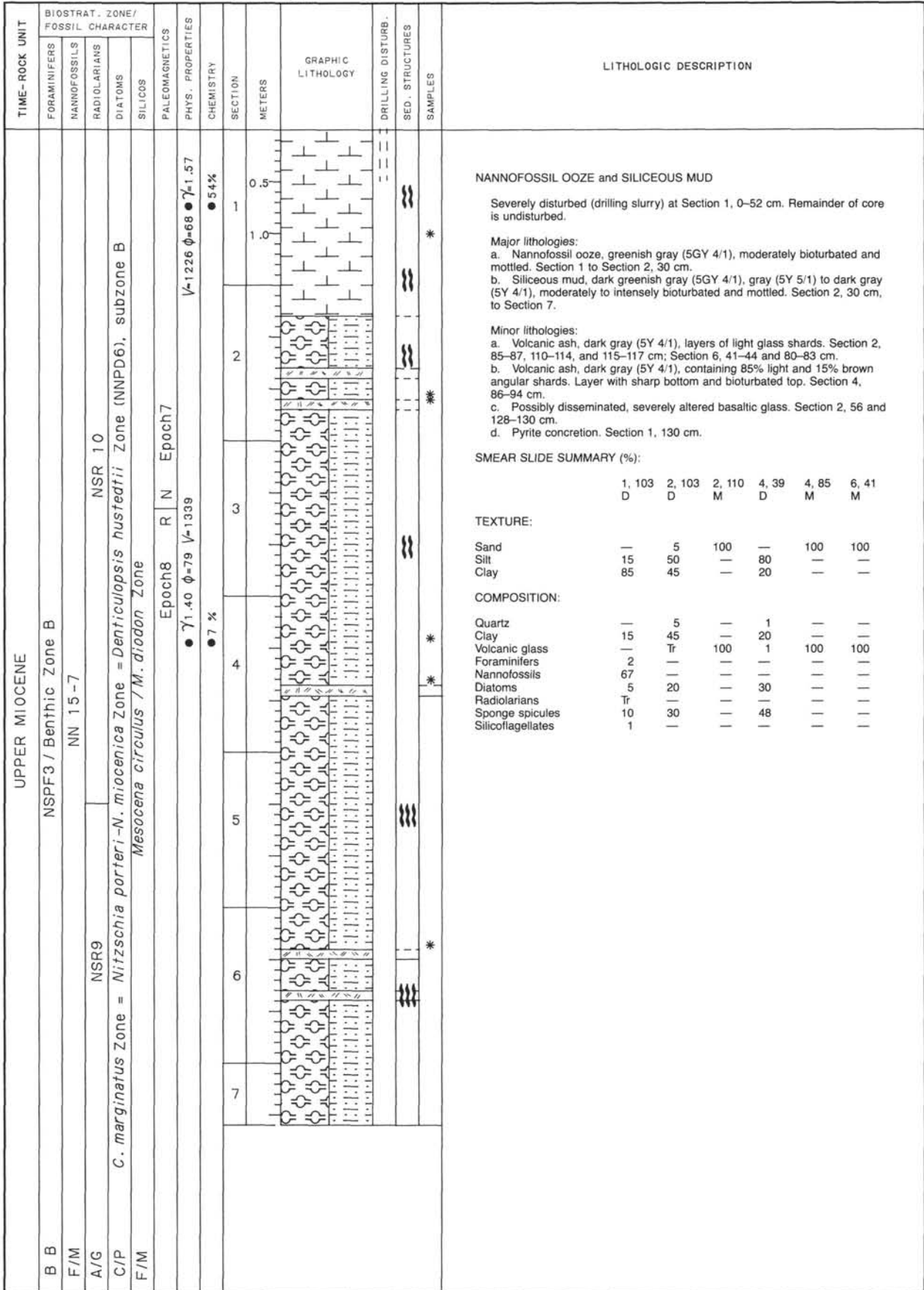
TIME-ROCK UNIT		BIOSTRAT. ZONE/ FOSSIL CHARACTER				PALEOMAGNETICS	PHYS. PROPERTIES	CHEMISTRY	SECTION	METERS	GRAPHIC LITHOLOGY	DRILLING DISTURB.	SED. STRUCTURES	SAMPLES	LITHOLOGIC DESCRIPTION																																																																						
FORAMINIFERS	NANNOFOSSILS	RADIOLARIANS	DIATOMS	SILICOS																																																																																	
UPPER MIOCENE																																																																																					
BB	NSPF3 / Benthic Zone A2								1	0.5					<p>SILICEOUS MUD</p> <p>Severe disturbance (drilling slurry) at Section 1, 0-14 cm. Moderate disturbance at Section 1, 14-27 cm. Remainder of core is undeformed.</p> <p>Major lithology: Siliceous mud, dark greenish gray (5GY 4/1), extensively bioturbated and mottled. Contains moderate faint color banding. Several zones may contain severely altered basaltic glass.</p> <p>Minor lithology: Volcanic ash, sandy lens. Section 1, 53 cm.</p> <p>SMEAR SLIDE SUMMARY (%):</p> <table border="1"> <thead> <tr> <th></th> <th>1, 53</th> <th>1, 117</th> <th>2, 96</th> <th>3, 22</th> </tr> </thead> <tbody> <tr> <td>M</td> <td></td> <td>M</td> <td>D</td> <td>D</td> </tr> </tbody> </table> <p>TEXTURE:</p> <table border="1"> <thead> <tr> <th></th> <th>1, 53</th> <th>1, 117</th> <th>2, 96</th> <th>3, 22</th> </tr> </thead> <tbody> <tr> <td>Sand</td> <td>35</td> <td>90</td> <td>10</td> <td>5</td> </tr> <tr> <td>Silt</td> <td>35</td> <td>5</td> <td>15</td> <td>40</td> </tr> <tr> <td>Clay</td> <td>30</td> <td>5</td> <td>75</td> <td>55</td> </tr> </tbody> </table> <p>COMPOSITION:</p> <table border="1"> <tbody> <tr> <td>Quartz</td> <td>5</td> <td>—</td> <td>3</td> <td>5</td> </tr> <tr> <td>Mica</td> <td>—</td> <td>—</td> <td>1</td> <td>—</td> </tr> <tr> <td>Clay</td> <td>30</td> <td>—</td> <td>75</td> <td>40</td> </tr> <tr> <td>Volcanic glass</td> <td>30</td> <td>95</td> <td>5</td> <td>—</td> </tr> <tr> <td>Diatoms</td> <td>15</td> <td>—</td> <td>5</td> <td>20</td> </tr> <tr> <td>Radiolarians</td> <td>—</td> <td>—</td> <td>1</td> <td>5</td> </tr> <tr> <td>Sponge spicules</td> <td>20</td> <td>5</td> <td>10</td> <td>30</td> </tr> <tr> <td>Silicoflagellates</td> <td>Tr</td> <td>—</td> <td>—</td> <td>—</td> </tr> </tbody> </table>		1, 53	1, 117	2, 96	3, 22	M		M	D	D		1, 53	1, 117	2, 96	3, 22	Sand	35	90	10	5	Silt	35	5	15	40	Clay	30	5	75	55	Quartz	5	—	3	5	Mica	—	—	1	—	Clay	30	—	75	40	Volcanic glass	30	95	5	—	Diatoms	15	—	5	20	Radiolarians	—	—	1	5	Sponge spicules	20	5	10	30	Silicoflagellates	Tr	—	—	—
	1, 53	1, 117	2, 96	3, 22																																																																																	
M		M	D	D																																																																																	
	1, 53	1, 117	2, 96	3, 22																																																																																	
Sand	35	90	10	5																																																																																	
Silt	35	5	15	40																																																																																	
Clay	30	5	75	55																																																																																	
Quartz	5	—	3	5																																																																																	
Mica	—	—	1	—																																																																																	
Clay	30	—	75	40																																																																																	
Volcanic glass	30	95	5	—																																																																																	
Diatoms	15	—	5	20																																																																																	
Radiolarians	—	—	1	5																																																																																	
Sponge spicules	20	5	10	30																																																																																	
Silicoflagellates	Tr	—	—	—																																																																																	
B								2	1.0																																																																												
A/G		NSR11	NSR12						3																																																																												
C/P	Thalassiosira convexa Zone = <i>Denticulopsis hustedtii</i> Zone (NNPD6), Subzone B								CC																																																																												
C/G	Mesocena diodon Zone																																																																																				
	Epoch 7 N R Epoch 6																																																																																				

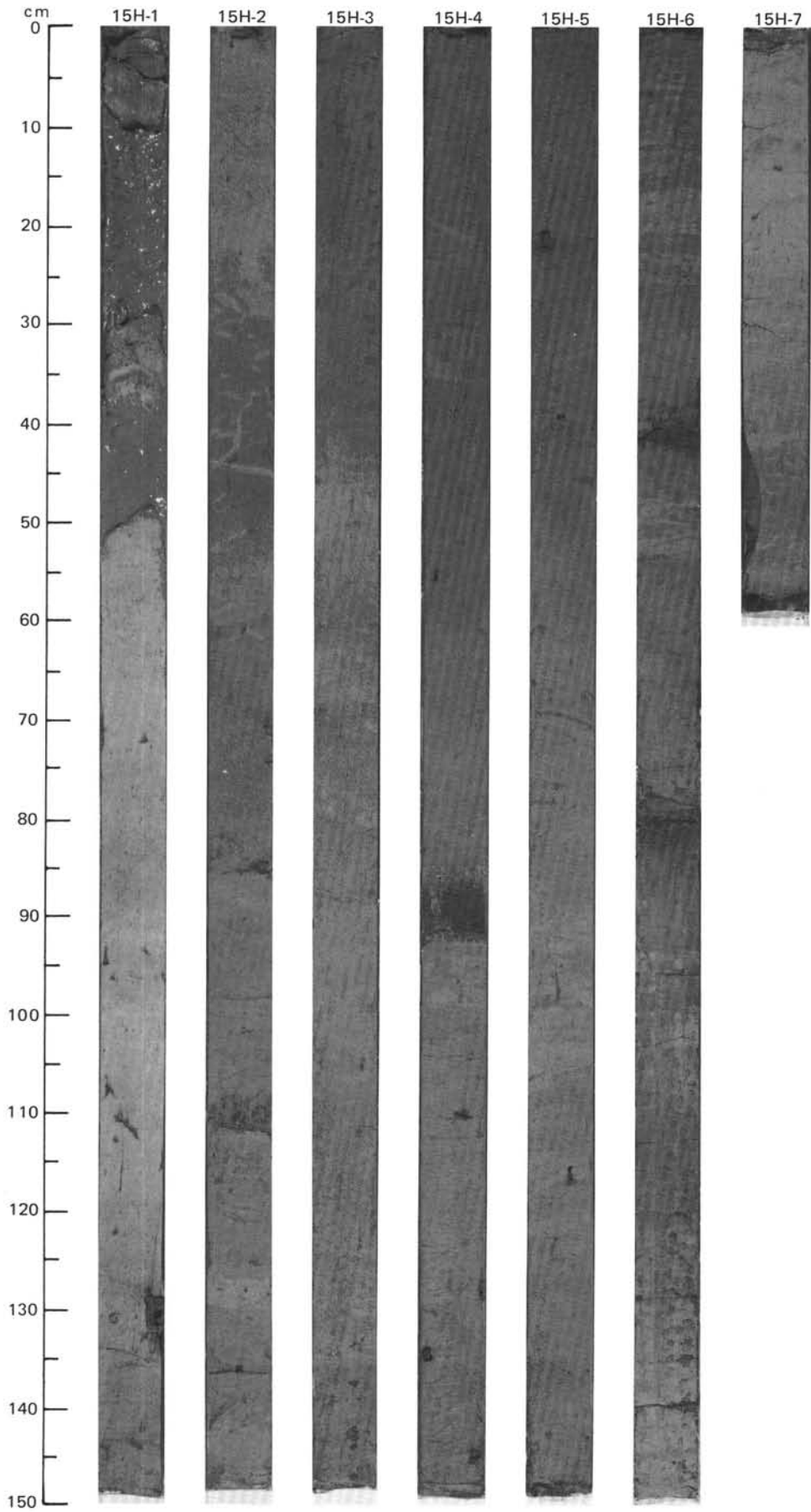


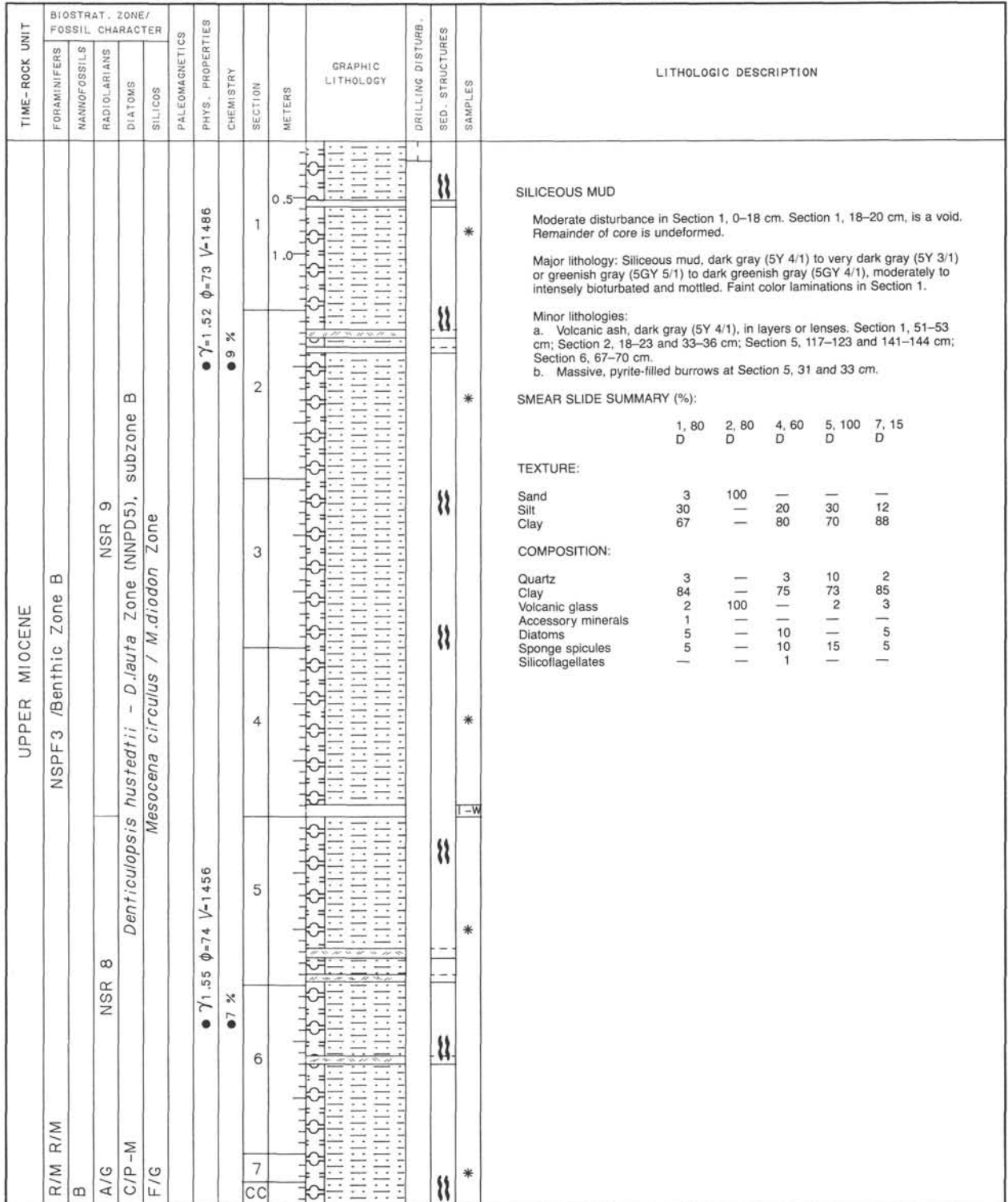
TIME-ROCK UNIT	BIOSTRAT. ZONE/ FOSSIL CHARACTER					PALEOMAGNETICS	PHYS. PROPERTIES	CHEMISTRY	SECTION	METERS	GRAPHIC LITHOLOGY	DRILLING DISTURB.	SED. STRUCTURES	SAMPLES	LITHOLOGIC DESCRIPTION																																																																	
	FORAMINIFERS	NANNOFOSSILS	RADIOLARIANS	DIATOMS	SILICOS																																																																											
UPPER MIOCENE																																																																																
C/G C/G	NSPF3 /Benthic Zone A2														<p>SILICEOUS MUD and NANNOFOSSIL OOZE</p> <p>Severe disturbance (drilling slurry) at Section 1, 10-20 cm. Section 1, 53-59 cm is a void. Remainder of core is undeformed.</p> <p>Major lithologies: a. Siliceous mud, gray (5Y 5/1) to dark greenish gray (5GY 4/1), extensively mottled and bioturbated, with scattered <i>Zoophycus</i>. Section 1 to Section 4. b. Nannofossil ooze, dark greenish gray (5GY 4/1), extensively bioturbated and mottled. Section 5 to Section 7.</p> <p>Minor lithology: Very dark gray ash, gradational top and sharp bottom contacts. Section 1, 46-53 cm.</p> <p>SMEAR SLIDE SUMMARY (%):</p> <table border="1"> <tr> <td></td> <td>2, 140</td> <td>3, 148</td> <td>5, 111</td> <td>7, 46</td> </tr> <tr> <td>D</td> <td>D</td> <td>D</td> <td>D</td> <td>D</td> </tr> </table> <p>TEXTURE:</p> <table border="1"> <tr> <td>Sand</td> <td>10</td> <td>25</td> <td>5</td> <td>—</td> </tr> <tr> <td>Silt</td> <td>40</td> <td>5</td> <td>15</td> <td>20</td> </tr> <tr> <td>Clay</td> <td>50</td> <td>70</td> <td>80</td> <td>80</td> </tr> </table> <p>COMPOSITION:</p> <table border="1"> <tr> <td>Quartz</td> <td>5</td> <td>5</td> <td>—</td> <td>—</td> </tr> <tr> <td>Clay</td> <td>50</td> <td>70</td> <td>20</td> <td>40</td> </tr> <tr> <td>Volcanic glass</td> <td>5</td> <td>20</td> <td>5</td> <td>—</td> </tr> <tr> <td>Accessory minerals</td> <td>Tr</td> <td>—</td> <td>—</td> <td>—</td> </tr> <tr> <td>Nannofossils</td> <td>—</td> <td>—</td> <td>60</td> <td>45</td> </tr> <tr> <td>Diatoms</td> <td>10</td> <td>—</td> <td>5</td> <td>5</td> </tr> <tr> <td>Radiolarians</td> <td>5</td> <td>—</td> <td>—</td> <td>—</td> </tr> <tr> <td>Sponge spicules</td> <td>25</td> <td>5</td> <td>10</td> <td>10</td> </tr> </table>		2, 140	3, 148	5, 111	7, 46	D	D	D	D	D	Sand	10	25	5	—	Silt	40	5	15	20	Clay	50	70	80	80	Quartz	5	5	—	—	Clay	50	70	20	40	Volcanic glass	5	20	5	—	Accessory minerals	Tr	—	—	—	Nannofossils	—	—	60	45	Diatoms	10	—	5	5	Radiolarians	5	—	—	—	Sponge spicules	25	5	10	10
	2, 140	3, 148	5, 111	7, 46																																																																												
D	D	D	D	D																																																																												
Sand	10	25	5	—																																																																												
Silt	40	5	15	20																																																																												
Clay	50	70	80	80																																																																												
Quartz	5	5	—	—																																																																												
Clay	50	70	20	40																																																																												
Volcanic glass	5	20	5	—																																																																												
Accessory minerals	Tr	—	—	—																																																																												
Nannofossils	—	—	60	45																																																																												
Diatoms	10	—	5	5																																																																												
Radiolarians	5	—	—	—																																																																												
Sponge spicules	25	5	10	10																																																																												
A/M	NN 15-7																																																																															
C/G	NSR10																																																																															
C/PCoscinodiscus marginatus Zone=basal	NSR 11																																																																															
R/G	<i>Thalassiosira convexa</i> Zone= <i>Denticulopsis hustedtii</i> Zone (NNPD6), subzone B																																																																															
	<i>Mesocena diodon</i> Zone																																																																															
	Epoch 7 N																																																																															
							● $\gamma = 1.46$ $\phi = 75$ $V = 1449$																																																																									
							● 0 %																																																																									
									1	0.5																																																																						
									2	1.0																																																																						
									3																																																																							
									4																																																																							
									5																																																																							
									6																																																																							
									7																																																																							
									CC																																																																							



SITE 642 HOLE C CORE 15H CORED INTERVAL 1397.0-1406.5 mbsl; 111.00-120.50 mbsf







SILICEOUS MUD

Moderate disturbance in Section 1, 0-18 cm. Section 1, 18-20 cm, is a void. Remainder of core is undeformed.

Major lithology: Siliceous mud, dark gray (5Y 4/1) to very dark gray (5Y 3/1) or greenish gray (5GY 5/1) to dark greenish gray (5GY 4/1), moderately to intensely bioturbated and mottled. Faint color laminations in Section 1.

Minor lithologies:

- a. Volcanic ash, dark gray (5Y 4/1), in layers or lenses. Section 1, 51-53 cm; Section 2, 18-23 and 33-36 cm; Section 5, 117-123 and 141-144 cm; Section 6, 67-70 cm.
- b. Massive, pyrite-filled burrows at Section 5, 31 and 33 cm.

SMEAR SLIDE SUMMARY (%):

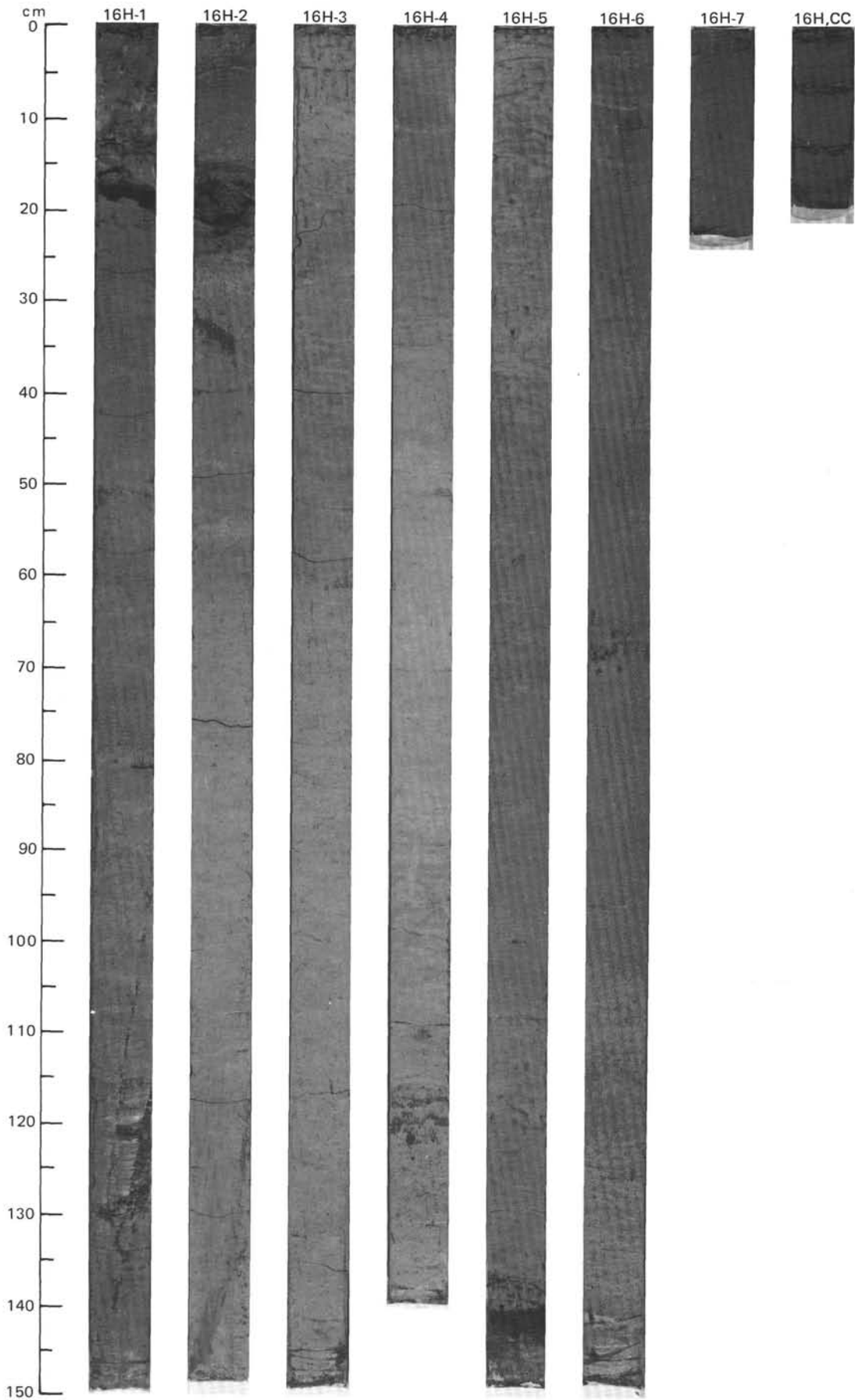
D	1, 80	2, 80	4, 60	5, 100	7, 15

TEXTURE:

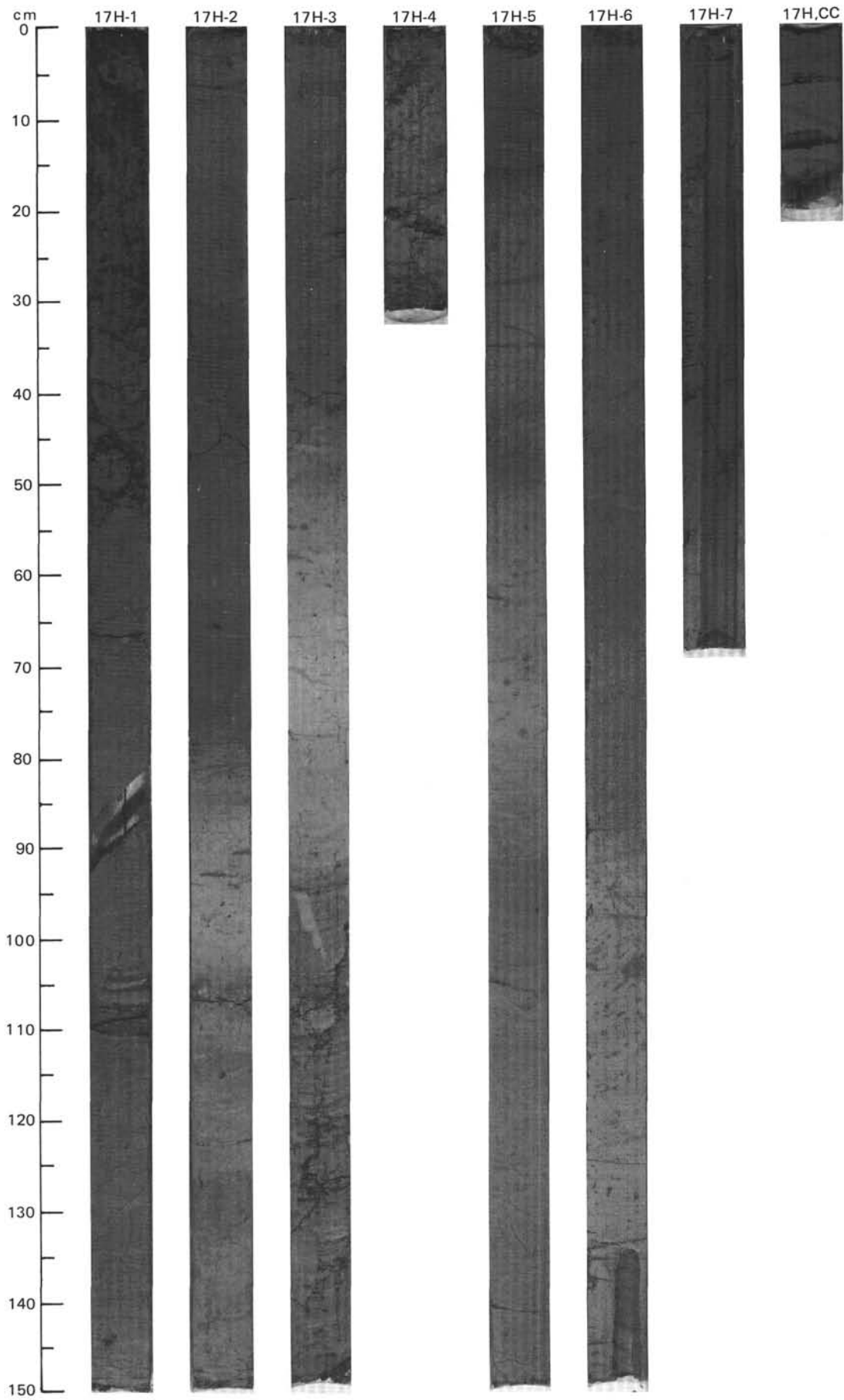
	3	100	20	30	12
Sand	3	100	20	30	12
Silt	30		80	70	88
Clay	67				

COMPOSITION:

	3	100	20	30	12
Quartz	3		3	10	2
Clay	84		75	73	85
Volcanic glass	2	100		2	3
Accessory minerals	1				
Diatoms	5		10		5
Sponge spicules	5		10	15	5
Silicoflagellates	1		1		1

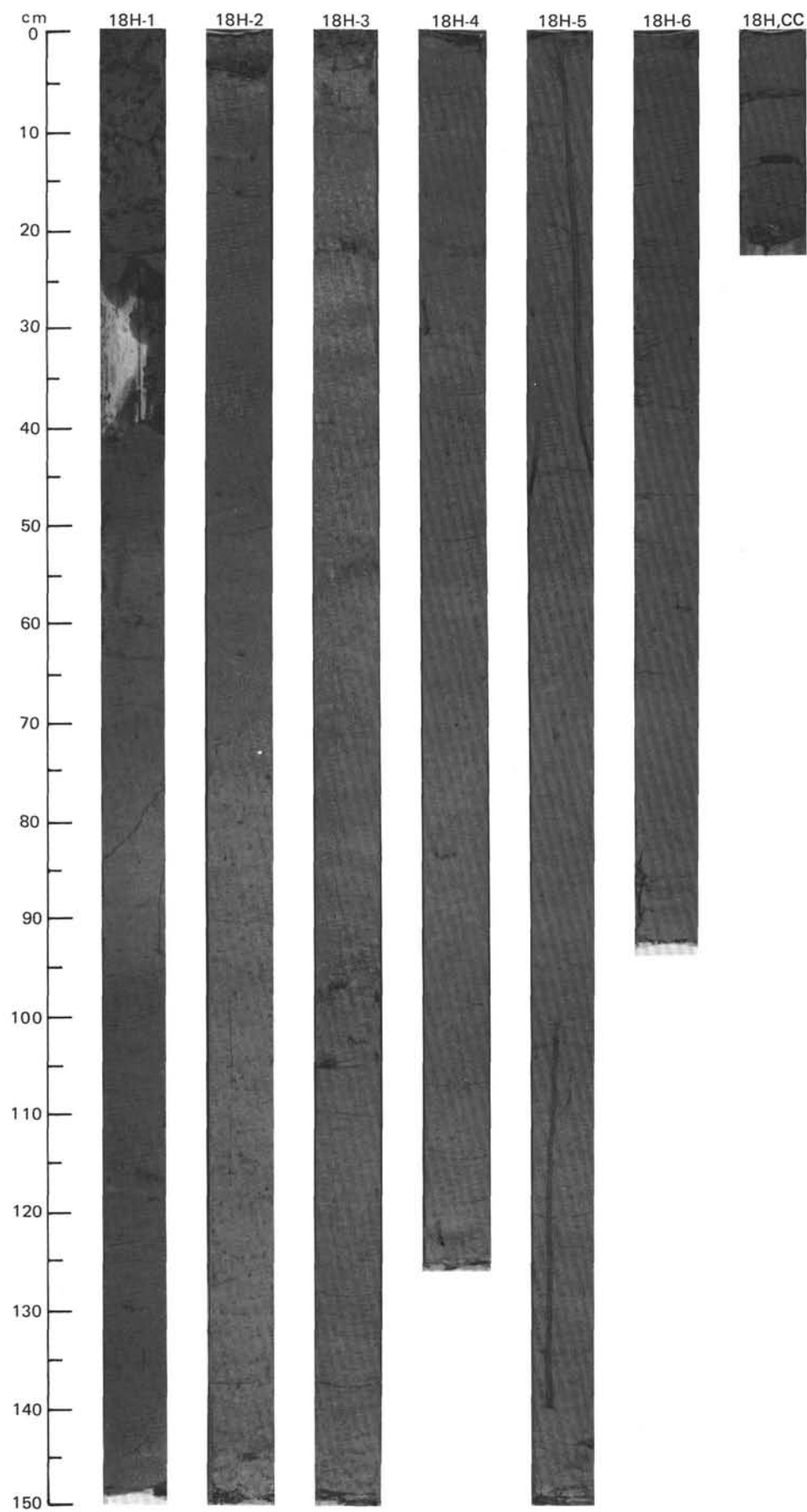


TIME-ROCK UNIT	BIOSTRAT. ZONE/ FOSSIL CHARACTER					PALEOMAGNETICS	PHYS. PROPERTIES	CHEMISTRY	SECTION	METERS	GRAPHIC LITHOLOGY	DRILLING DISTURB.	SED. STRUCTURES	SAMPLES	LITHOLOGIC DESCRIPTION																																																																																																																							
	FORAMINIFERS	NANNOFOSSILS	RADIOLARIANS	DIATOMS	PALYMONORPHS																																																																																																																																	
MIDDLE MIOCENE															<p>SILICEOUS MUD and DIATOMACEOUS NANNOFOSSIL OOZE</p> <p>Section 1, 83-90 cm, is a void. Severe disturbance at Section 6, 137 cm, to Section 7, 70 cm. Section 1, 90 cm, to Section 6, 137 cm, is undisturbed.</p> <p>Major lithologies:</p> <p>a. Siliceous mud, dark gray (5Y 4/1) to very dark gray (5Y 3/1), extensively bioturbated and mottled. Section 1 to Section 4; Section 5, 3-20, 46-52, and 84-110 cm; Section 6, 3-18 and 47-90 cm.</p> <p>b. Diatomaceous nannofossil ooze, light greenish gray (10Y 5/1) to olive gray (5Y 4/2), extensively bioturbated. Section 1, 91-105 cm; Section 2, 80-108 cm; Section 4, 0-31 cm; Sections 5 and 6.</p> <p>Bioturbation in these lithologies is of four types: faint tubes, small tubes (3-5 mm wide), large tubes (0.5-1.0 cm wide), and well-developed <i>Zoophycos</i>.</p> <p>Minor lithology: volcanic ash, dark gray (5Y 5/1) and disseminated. Possibly altered basaltic ash. Section 2, 105-108 cm; Section 3, 105-108 cm.</p> <p>SMEAR SLIDE SUMMARY (%):</p> <table border="1" style="width: 100%; text-align: center;"> <tr> <td></td> <td>1, 13 D</td> <td>1, 146 D</td> <td>2, 66 D</td> <td>2, 98 M</td> <td>2, 108 M</td> <td>5, 75 D</td> </tr> <tr> <td>Silt</td> <td>15</td> <td>15</td> <td>15</td> <td>30</td> <td>—</td> <td>20</td> </tr> <tr> <td>Clay</td> <td>85</td> <td>85</td> <td>85</td> <td>70</td> <td>—</td> <td>80</td> </tr> </table> <p>TEXTURE:</p> <table border="1" style="width: 100%; text-align: center;"> <tr> <td></td> <td>1, 13 D</td> <td>1, 146 D</td> <td>2, 66 D</td> <td>2, 98 M</td> <td>2, 108 M</td> <td>5, 75 D</td> </tr> <tr> <td>Silt</td> <td>15</td> <td>15</td> <td>15</td> <td>30</td> <td>—</td> <td>20</td> </tr> <tr> <td>Clay</td> <td>85</td> <td>85</td> <td>85</td> <td>70</td> <td>—</td> <td>80</td> </tr> </table> <p>COMPOSITION:</p> <table border="1" style="width: 100%; text-align: center;"> <tr> <td>Quartz</td> <td>3</td> <td>2</td> <td>2</td> <td>—</td> <td>—</td> <td>—</td> </tr> <tr> <td>Clay</td> <td>82</td> <td>67</td> <td>80</td> <td>—</td> <td>—</td> <td>—</td> </tr> <tr> <td>Volcanic glass</td> <td>5</td> <td>1</td> <td>2</td> <td>—</td> <td>69</td> <td>—</td> </tr> <tr> <td>Accessory minerals</td> <td>1</td> <td>—</td> <td>—</td> <td>—</td> <td>—</td> <td>—</td> </tr> <tr> <td>Pyrite</td> <td>—</td> <td>5</td> <td>—</td> <td>—</td> <td>—</td> <td>1</td> </tr> <tr> <td>Foraminifers</td> <td>—</td> <td>—</td> <td>—</td> <td>1</td> <td>—</td> <td>1</td> </tr> <tr> <td>Nannofossils</td> <td>—</td> <td>5</td> <td>—</td> <td>68</td> <td>20</td> <td>73</td> </tr> <tr> <td>Diatoms</td> <td>2</td> <td>10</td> <td>5</td> <td>20</td> <td>—</td> <td>15</td> </tr> <tr> <td>Radiolarians</td> <td>1</td> <td>—</td> <td>1</td> <td>1</td> <td>1</td> <td>—</td> </tr> <tr> <td>Sponge spicules</td> <td>5</td> <td>10</td> <td>10</td> <td>10</td> <td>10</td> <td>10</td> </tr> <tr> <td>Silicoflagellates</td> <td>1</td> <td>—</td> <td>—</td> <td>—</td> <td>—</td> <td>1</td> </tr> </table>		1, 13 D	1, 146 D	2, 66 D	2, 98 M	2, 108 M	5, 75 D	Silt	15	15	15	30	—	20	Clay	85	85	85	70	—	80		1, 13 D	1, 146 D	2, 66 D	2, 98 M	2, 108 M	5, 75 D	Silt	15	15	15	30	—	20	Clay	85	85	85	70	—	80	Quartz	3	2	2	—	—	—	Clay	82	67	80	—	—	—	Volcanic glass	5	1	2	—	69	—	Accessory minerals	1	—	—	—	—	—	Pyrite	—	5	—	—	—	1	Foraminifers	—	—	—	1	—	1	Nannofossils	—	5	—	68	20	73	Diatoms	2	10	5	20	—	15	Radiolarians	1	—	1	1	1	—	Sponge spicules	5	10	10	10	10	10	Silicoflagellates	1	—	—	—	—	1
	1, 13 D	1, 146 D	2, 66 D	2, 98 M	2, 108 M	5, 75 D																																																																																																																																
Silt	15	15	15	30	—	20																																																																																																																																
Clay	85	85	85	70	—	80																																																																																																																																
	1, 13 D	1, 146 D	2, 66 D	2, 98 M	2, 108 M	5, 75 D																																																																																																																																
Silt	15	15	15	30	—	20																																																																																																																																
Clay	85	85	85	70	—	80																																																																																																																																
Quartz	3	2	2	—	—	—																																																																																																																																
Clay	82	67	80	—	—	—																																																																																																																																
Volcanic glass	5	1	2	—	69	—																																																																																																																																
Accessory minerals	1	—	—	—	—	—																																																																																																																																
Pyrite	—	5	—	—	—	1																																																																																																																																
Foraminifers	—	—	—	1	—	1																																																																																																																																
Nannofossils	—	5	—	68	20	73																																																																																																																																
Diatoms	2	10	5	20	—	15																																																																																																																																
Radiolarians	1	—	1	1	1	—																																																																																																																																
Sponge spicules	5	10	10	10	10	10																																																																																																																																
Silicoflagellates	1	—	—	—	—	1																																																																																																																																
C/M F/M	NSPF3 /Benthic Zone B																																																																																																																																					
A/P	NN 15-7																																																																																																																																					
R/M	NSR8																																																																																																																																					
C/M	<i>Denticulopsis hustedtii</i> - <i>Denticulopsis lauta</i> Zone (NNPD5), subzone B																																																																																																																																					
F/G	<i>N.aquaeducta</i> Zone PM4 <i>Mesocena circulus</i> Zone																																																																																																																																					
	● $\gamma_1 .45$ $\phi=75$ $V=1444$																																																																																																																																					
	● 28 %																																																																																																																																					
						1			0.5				*																																																																																																																									
						2			1.0		VOID		*																																																																																																																									
						3							**																																																																																																																									
						4					VOID		**																																																																																																																									
						5							*																																																																																																																									
						6																																																																																																																																
						7																																																																																																																																
CC																																																																																																																																						

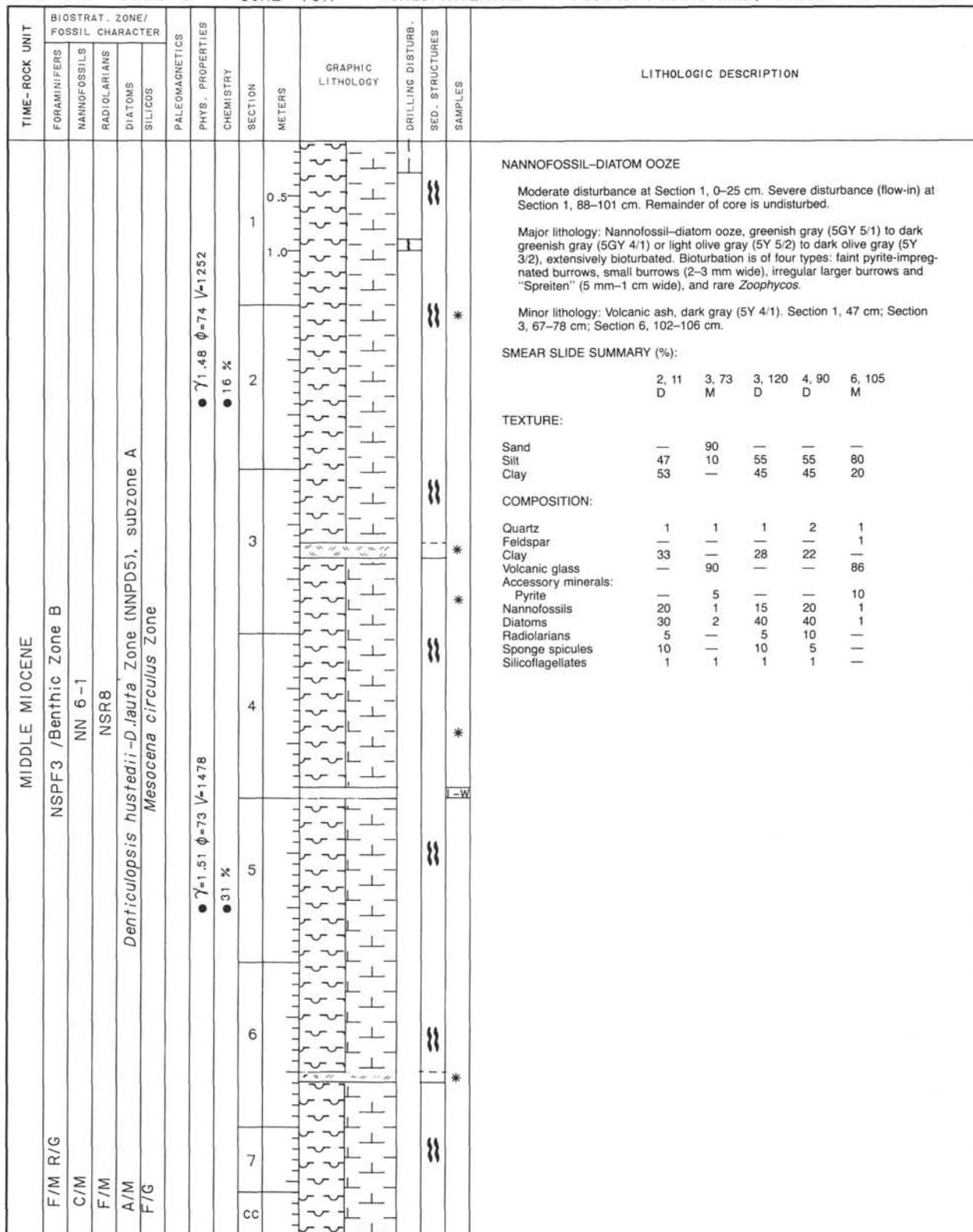


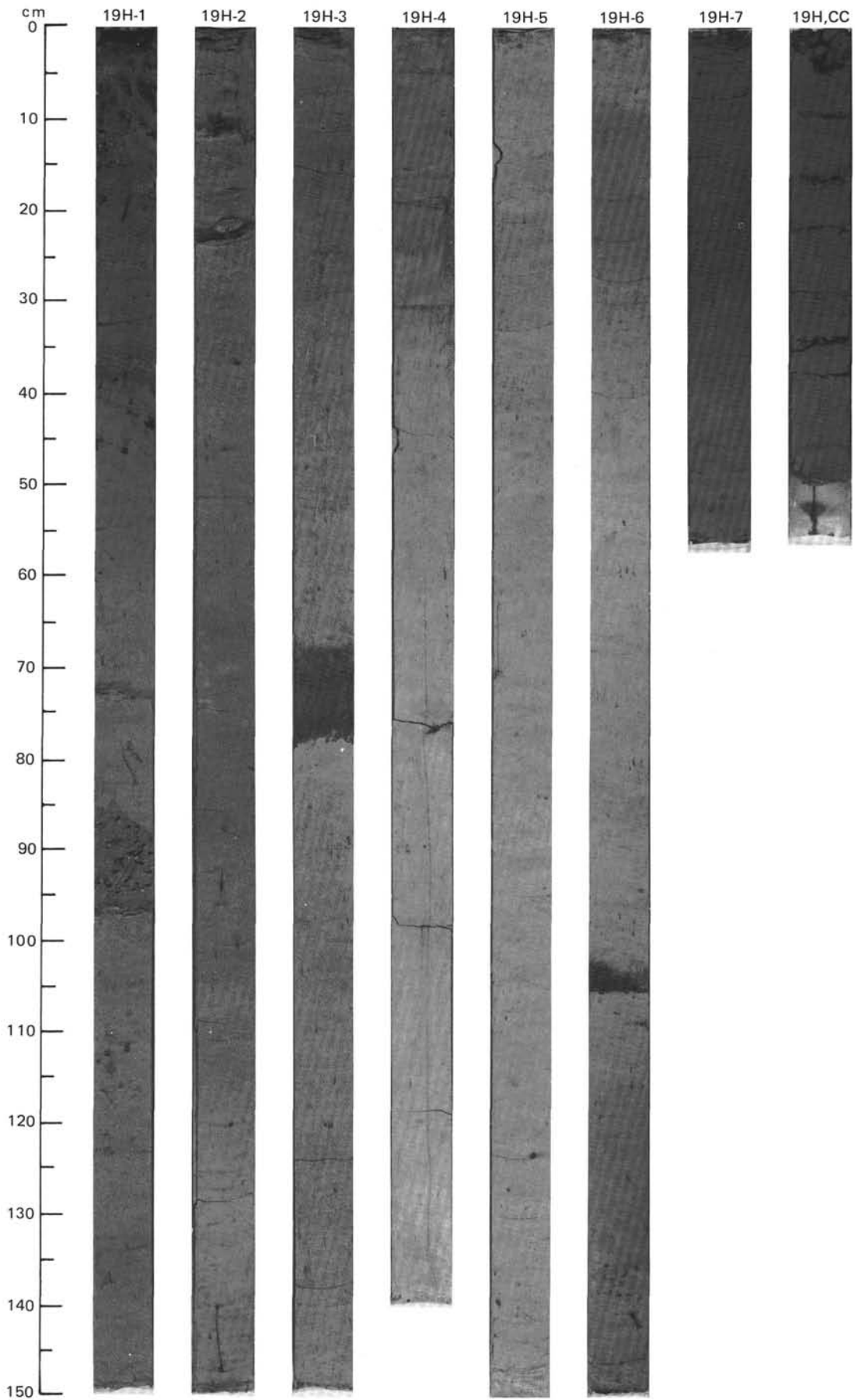
SITE 642 HOLE C CORE 18H CORED INTERVAL 1425.5-1435.0 mbsf; 139.50-149.00 mbsf

TIME-ROCK UNIT		BIOSTRAT. ZONE/ FOSSIL CHARACTER		PHYS. PROPERTIES	CHEMISTRY	SECTION	METERS	GRAPHIC LITHOLOGY	DRILLING DISTURB.	SED. STRUCTURES	SAMPLES	LITHOLOGIC DESCRIPTION																																																																											
FORAMINIFERS	MANNOFOSSILS	RADIOLARIANS	DIATOMS																																																																																				
MIDDLE MIOCENE																																																																																							
A/M	F/G	NSPF3 / Benthic Zone B																																																																																					
C/M		NN15-17																																																																																					
R/G		NSR8																																																																																					
A/M		<i>Denticulopsis hustedii</i> - <i>D. lauta</i> Zone (NNPD5), Subzone B																																																																																					
C/G		B. baculata Zone PM5 <i>Mesocena circulus</i>																																																																																					
				● $\gamma=1.45$ $\phi=77$ $\vee-1339$	● 10 %																																																																																		
				● $\gamma=1.48$ $\phi=75$ $\vee-1340$	● 13 %																																																																																		
						1	0.5	VOID				<p>SILICEOUS MUD and DIATOMACEOUS MUD</p> <p>Moderate disturbance in Section 1, 0-23 cm. Section 1, 23-42 cm, is a void. Remainder of core is undeformed.</p> <p>Major lithologies: a. Siliceous mud, dark gray (5Y 4/1), extensively bioturbated, with pyritized burrows common. Faint color lamination common. Section 1, 0-95 cm; Section 1, 100 cm, to Section 3, 70 cm; Section 3, 100 cm, to Section 7. b. Diatomaceous mud, dark olive gray (5Y 3/2) to very dark gray (5Y 3/1), extensively bioturbated, with pyritized burrows common. Section 1, 95-100 cm; Section 3, 70-100 cm.</p> <p>Minor lithologies: a. Volcanic ash, light gray (5Y 6/1) layer. Section 3, 21-22 cm. b. Possibly disseminated, altered basaltic ash. Section 2, 0-4 cm.</p> <p>SMEAR SLIDE SUMMARY (%):</p> <table border="1"> <tr> <td></td> <td>2, 2</td> <td>2, 80</td> <td>3, 97</td> <td>4, 70</td> </tr> <tr> <td></td> <td>M</td> <td>D</td> <td>M</td> <td>D</td> </tr> </table> <p>TEXTURE:</p> <table border="1"> <tr> <td>Sand</td> <td>90</td> <td>2</td> <td>10</td> <td>—</td> </tr> <tr> <td>Silt</td> <td>10</td> <td>28</td> <td>50</td> <td>50</td> </tr> <tr> <td>Clay</td> <td>—</td> <td>70</td> <td>40</td> <td>50</td> </tr> </table> <p>COMPOSITION:</p> <table border="1"> <tr> <td>Quartz</td> <td>1</td> <td>1</td> <td>—</td> <td>2</td> </tr> <tr> <td>Clay</td> <td>2</td> <td>60</td> <td>29</td> <td>52</td> </tr> <tr> <td>Volcanic glass</td> <td>97</td> <td>1</td> <td>20</td> <td>—</td> </tr> <tr> <td>Accessory minerals:</td> <td></td> <td></td> <td></td> <td></td> </tr> <tr> <td> Pyrite</td> <td>—</td> <td>—</td> <td>20</td> <td>—</td> </tr> <tr> <td> Nannofossils</td> <td>—</td> <td>10</td> <td>—</td> <td>2</td> </tr> <tr> <td> Diatoms</td> <td>Tr</td> <td>20</td> <td>20</td> <td>30</td> </tr> <tr> <td> Radiolarians</td> <td>—</td> <td>2</td> <td>5</td> <td>2</td> </tr> <tr> <td> Sponge spicules</td> <td>—</td> <td>5</td> <td>5</td> <td>10</td> </tr> <tr> <td> Silicoflagellates</td> <td>—</td> <td>1</td> <td>1</td> <td>1</td> </tr> </table>		2, 2	2, 80	3, 97	4, 70		M	D	M	D	Sand	90	2	10	—	Silt	10	28	50	50	Clay	—	70	40	50	Quartz	1	1	—	2	Clay	2	60	29	52	Volcanic glass	97	1	20	—	Accessory minerals:					Pyrite	—	—	20	—	Nannofossils	—	10	—	2	Diatoms	Tr	20	20	30	Radiolarians	—	2	5	2	Sponge spicules	—	5	5	10	Silicoflagellates	—	1	1	1
	2, 2	2, 80	3, 97	4, 70																																																																																			
	M	D	M	D																																																																																			
Sand	90	2	10	—																																																																																			
Silt	10	28	50	50																																																																																			
Clay	—	70	40	50																																																																																			
Quartz	1	1	—	2																																																																																			
Clay	2	60	29	52																																																																																			
Volcanic glass	97	1	20	—																																																																																			
Accessory minerals:																																																																																							
Pyrite	—	—	20	—																																																																																			
Nannofossils	—	10	—	2																																																																																			
Diatoms	Tr	20	20	30																																																																																			
Radiolarians	—	2	5	2																																																																																			
Sponge spicules	—	5	5	10																																																																																			
Silicoflagellates	—	1	1	1																																																																																			
						2				*																																																																													
						3				*																																																																													
						4				*																																																																													
						5																																																																																	
						6																																																																																	
CC																																																																																							

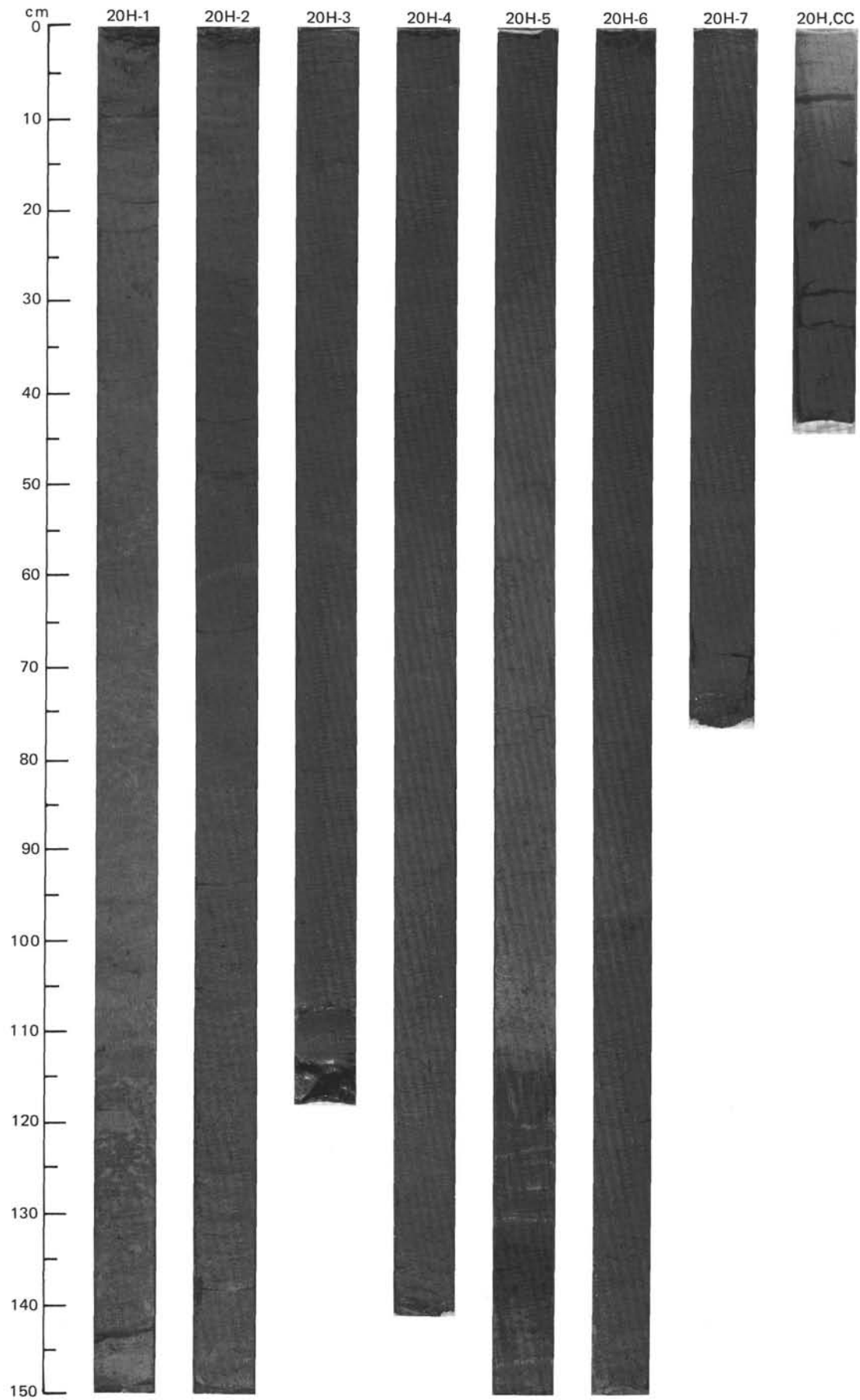


SITE 642 HOLE C CORE 19H CORED INTERVAL 1435.0-1444.5 mbsl; 149.00-158.50 mbsf





TIME-ROCK UNIT		BIOSTRAT. ZONE/ FOSSIL CHARACTER				CHEMISTRY	SECTION	METERS	GRAPHIC LITHOLOGY	DRILLING DISTURB.	SED. STRUCTURES	SAMPLES	LITHOLOGIC DESCRIPTION																																																																																																																								
R/P B	F/P	FORAMINIFERS	NANNOFOSSILS	RADIOLARIANS	DIATOMS PALYMONOPHS									PALEOMAGNETICS	PHYS. PROPERTIES																																																																																																																						
MIDDLE MIOCENE													<p>DIATOM OOZE and SILICEOUS MUD</p> <p>Entire core is undeformed.</p> <p>Major lithologies:</p> <p>a. Siliceous mud and diatom ooze, dark olive gray (5Y 3/2), extensively bioturbated. Section 1, Section 5, 23-113 cm.</p> <p>b. Diatom ooze and siliceous mud, very dark olive gray to black (5Y 2.5/2), extensively bioturbated. Section 2 to Section 5, 23 cm; Section 5, 113 cm, to CC.</p> <p>Minor lithology: Volcanic ash, dark gray (5Y 4/1). Section 5, 134-140 cm; Section 6, 98 cm (pyritized ash).</p> <p>SMEAR SLIDE SUMMARY (%):</p> <table border="1"> <thead> <tr> <th></th> <th>1, 30 D</th> <th>1, 130 D</th> <th>2, 100 D</th> <th>4, 80 D</th> <th>5, 105 D</th> <th>6, 68 D</th> <th>6, 98 M</th> </tr> </thead> <tbody> <tr> <td>Sand</td> <td>10</td> <td>—</td> <td>—</td> <td>—</td> <td>—</td> <td>—</td> <td>70</td> </tr> <tr> <td>Silt</td> <td>50</td> <td>40</td> <td>40</td> <td>20</td> <td>25</td> <td>20</td> <td>20</td> </tr> <tr> <td>Clay</td> <td>40</td> <td>60</td> <td>60</td> <td>80</td> <td>75</td> <td>80</td> <td>10</td> </tr> </tbody> </table> <p>TEXTURE:</p> <p>COMPOSITION:</p> <table border="1"> <tbody> <tr> <td>Quartz</td> <td>1</td> <td>5</td> <td>20</td> <td>5</td> <td>5</td> <td>2</td> <td>2</td> </tr> <tr> <td>Feldspar</td> <td>—</td> <td>—</td> <td>1</td> <td>1</td> <td>1</td> <td>—</td> <td>—</td> </tr> <tr> <td>Clay</td> <td>21</td> <td>64</td> <td>53</td> <td>78</td> <td>71</td> <td>80</td> <td>10</td> </tr> <tr> <td>Volcanic glass</td> <td>1</td> <td>Tr</td> <td>1</td> <td>Tr</td> <td>1</td> <td>—</td> <td>70</td> </tr> <tr> <td>Accessory minerals:</td> <td></td> <td></td> <td></td> <td></td> <td></td> <td></td> <td></td> </tr> <tr> <td> Pyrite</td> <td>—</td> <td>—</td> <td>—</td> <td>—</td> <td>—</td> <td>—</td> <td>10</td> </tr> <tr> <td> Nannofossils</td> <td>10</td> <td>—</td> <td>—</td> <td>—</td> <td>—</td> <td>—</td> <td>—</td> </tr> <tr> <td> Diatoms</td> <td>40</td> <td>20</td> <td>20</td> <td>10</td> <td>10</td> <td>10</td> <td>5</td> </tr> <tr> <td> Radiolarians</td> <td>5</td> <td>—</td> <td>—</td> <td>—</td> <td>1</td> <td>2</td> <td>1</td> </tr> <tr> <td> Sponge spicules</td> <td>20</td> <td>10</td> <td>5</td> <td>5</td> <td>10</td> <td>5</td> <td>1</td> </tr> <tr> <td> Silicoflagellates</td> <td>2</td> <td>1</td> <td>—</td> <td>1</td> <td>1</td> <td>1</td> <td>1</td> </tr> </tbody> </table>		1, 30 D	1, 130 D	2, 100 D	4, 80 D	5, 105 D	6, 68 D	6, 98 M	Sand	10	—	—	—	—	—	70	Silt	50	40	40	20	25	20	20	Clay	40	60	60	80	75	80	10	Quartz	1	5	20	5	5	2	2	Feldspar	—	—	1	1	1	—	—	Clay	21	64	53	78	71	80	10	Volcanic glass	1	Tr	1	Tr	1	—	70	Accessory minerals:								Pyrite	—	—	—	—	—	—	10	Nannofossils	10	—	—	—	—	—	—	Diatoms	40	20	20	10	10	10	5	Radiolarians	5	—	—	—	1	2	1	Sponge spicules	20	10	5	5	10	5	1	Silicoflagellates	2	1	—	1	1	1	1
	1, 30 D	1, 130 D	2, 100 D	4, 80 D	5, 105 D	6, 68 D	6, 98 M																																																																																																																														
Sand	10	—	—	—	—	—	70																																																																																																																														
Silt	50	40	40	20	25	20	20																																																																																																																														
Clay	40	60	60	80	75	80	10																																																																																																																														
Quartz	1	5	20	5	5	2	2																																																																																																																														
Feldspar	—	—	1	1	1	—	—																																																																																																																														
Clay	21	64	53	78	71	80	10																																																																																																																														
Volcanic glass	1	Tr	1	Tr	1	—	70																																																																																																																														
Accessory minerals:																																																																																																																																					
Pyrite	—	—	—	—	—	—	10																																																																																																																														
Nannofossils	10	—	—	—	—	—	—																																																																																																																														
Diatoms	40	20	20	10	10	10	5																																																																																																																														
Radiolarians	5	—	—	—	1	2	1																																																																																																																														
Sponge spicules	20	10	5	5	10	5	1																																																																																																																														
Silicoflagellates	2	1	—	1	1	1	1																																																																																																																														



SITE 642 HOLE C CORE 21H CORED INTERVAL 1454.0-1463.5 mbsf; 168.00-177.50 mbsf

TIME-ROCK UNIT		BIOSTRAT. ZONE/ FOSSIL CHARACTER		PALEOMAGNETICS	PHYS. PROPERTIES	CHEMISTRY	SECTION	METERS	GRAPHIC LITHOLOGY	DRILLING DISTURB.	SED. STRUCTURES	SAMPLES	LITHOLOGIC DESCRIPTION
FORAMINIFERS	NANNOFOSSILS	RADIOLARIANS	DIATOMS										
MIDDLE MIOCENE													
R/P B	Benthic Zone C1												
B													
C/M	NSR7												
A/M	<i>Denticulopsis lauta</i> Zone (NNPD4), subzone B												
F/M	no zonal designation												
				● $\gamma=1.41$ $\phi=77$ V-1515			1	0.5					
				● 0 %			2	1.0					
				● $\gamma=1.42$ $\phi=78$ V-1518			3						
				● 0 %			4						
				● $\gamma=1.36$ $\phi=78$			5						
				● 0.4 %			6						
							7						
CC													

SILICEOUS MUD

Moderate deformation at Section 1, 0-15 cm. Remainder of core is undeformed.

Major lithology: Siliceous mud, very dark olive gray (5Y 3/2) to black (5Y 2.5/2), extensively bioturbated. Well-developed *Zoophycos* common. Section 3, 100 cm, to Section 4, 40 cm, and Section 5, 5-50 cm, rich in large radiolarians.

Minor lithology: Volcanic ash, dark gray (5Y 4/1). Section 3, 123-126 cm (possibly severely altered basaltic ash); Section 4, 3-5 cm; Section 6, 2-10 cm.

SMEAR SLIDE SUMMARY (%):

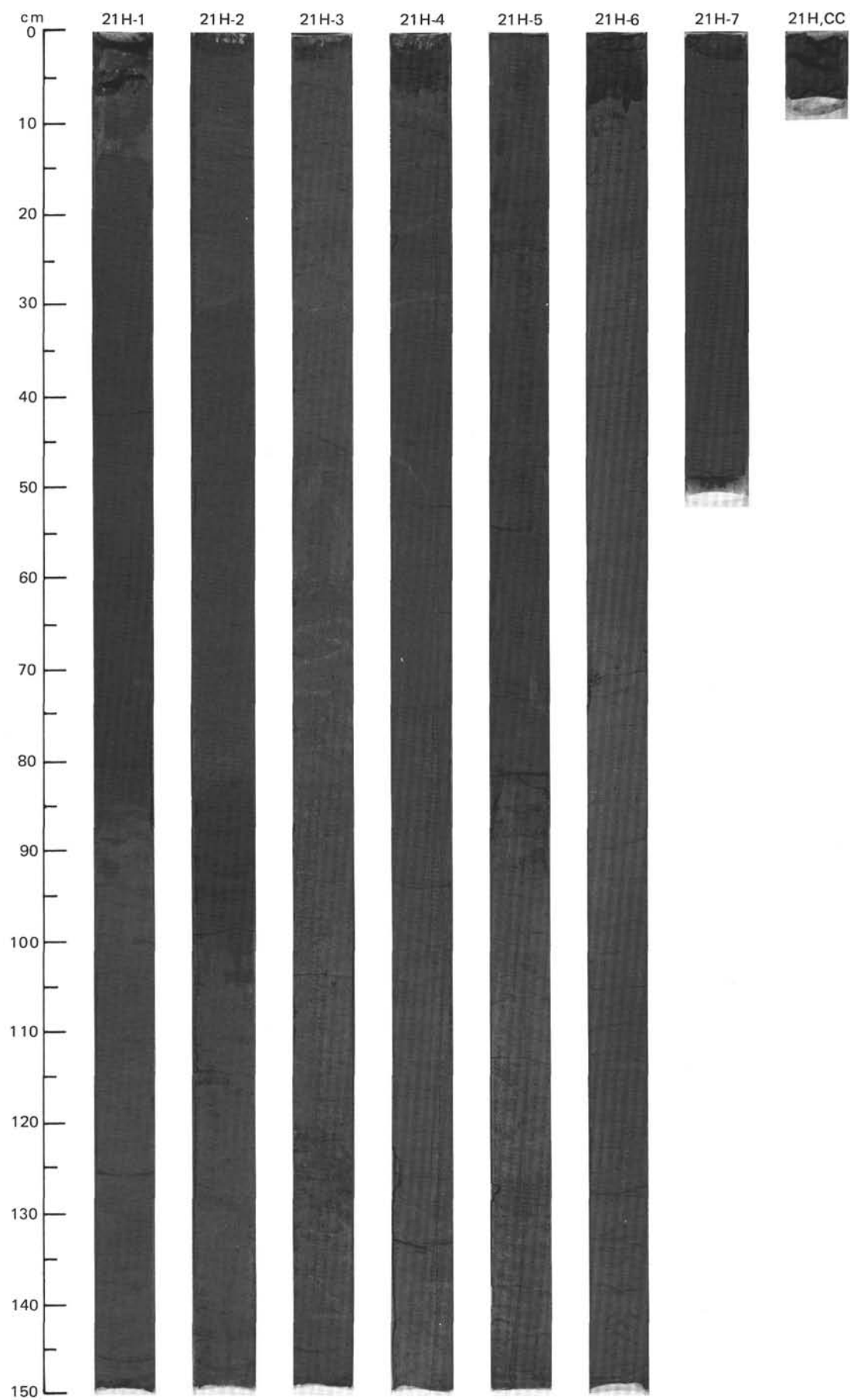
	1, 75	3, 104	3, 125	4, 6	6, 70
	D	D	M	M	D

TEXTURE:

Sand	—	5	80	40	—
Silt	20	35	20	40	25
Clay	80	60	—	20	75

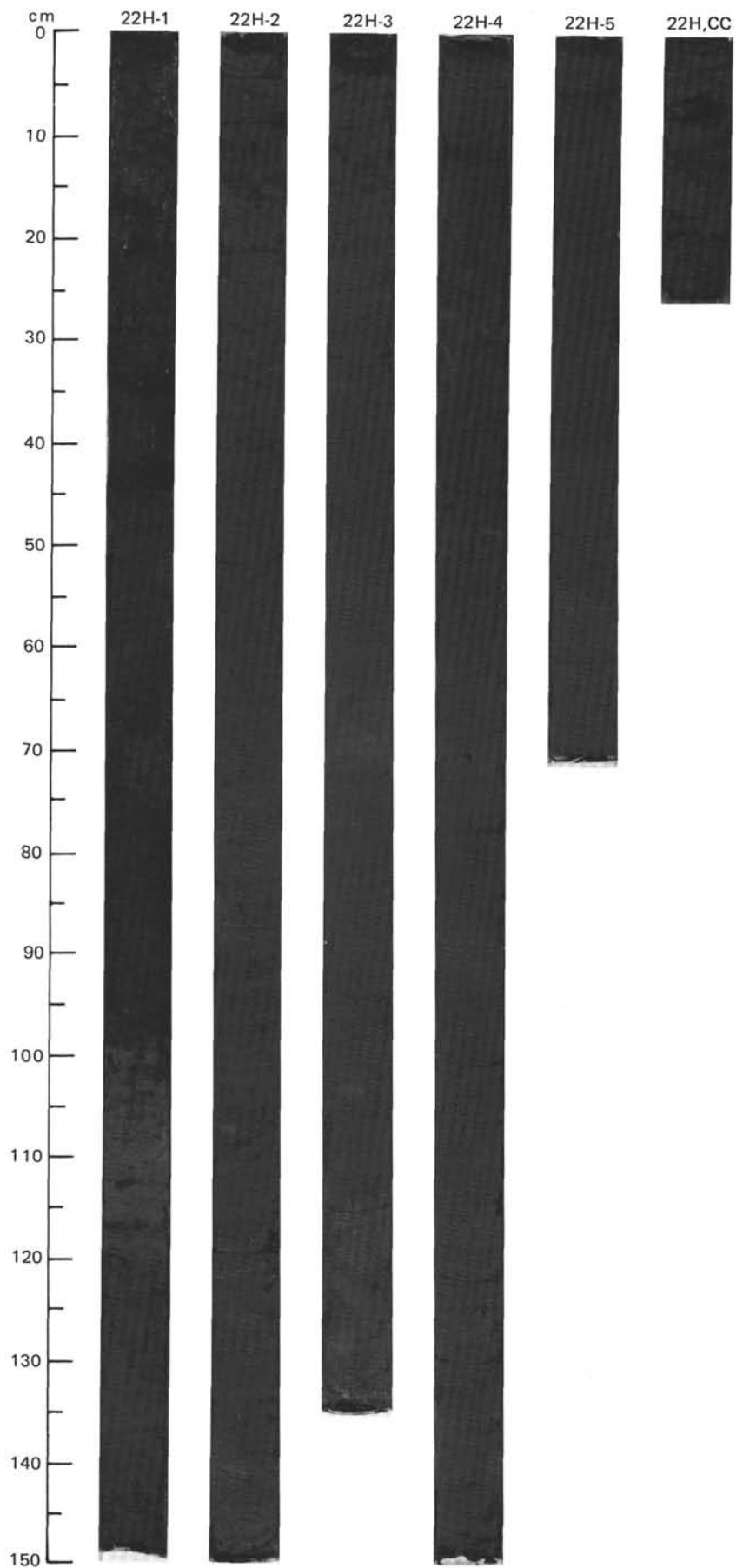
COMPOSITION:

Quartz	1	5	2	—	1
Clay	66	50	10	10	63
Volcanic glass	1	—	86	40	—
Accessory minerals:					
Goethite	10	—	—	—	—
Diatoms	10	20	1	30	20
Radiolarians	1	20	—	10	10
Sponge spicules	10	5	1	10	5
Silicoflagellates	1	—	—	—	1



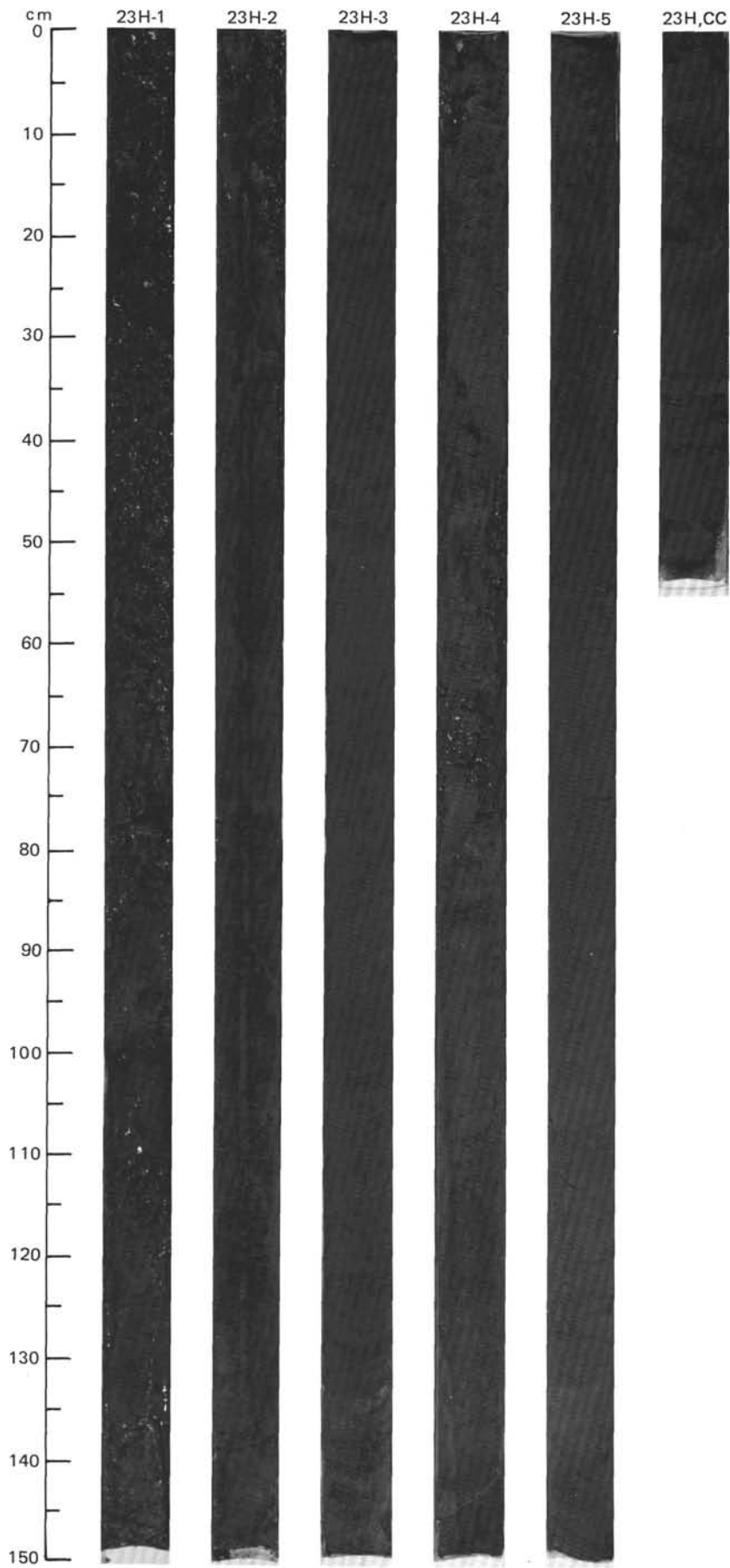
SITE 642 HOLE C CORE 22H CORED INTERVAL 1463.5-1470.3 mbsl; 177.50-184.30 mbsf

TIME-ROCK UNIT		BIOSTRAT. ZONE/ FOSSIL CHARACTER		PALEOMAGNETICS	PHYS. PROPERTIES	CHEMISTRY	SECTION	METERS	GRAPHIC LITHOLOGY	DRILLING DISTURB.	SED. STRUCTURES	SAMPLES	LITHOLOGIC DESCRIPTION																																																				
FORAMINIFERS	NANNOFOSSILS	RADIOLARIANS	DIATOMS											SILICOS																																																			
LOWER MIOCENE													<p>RADIOLARIAN-DIATOM OOZE and SILICEOUS MUD</p> <p>Section 1, 33-46 cm, is a void. Remainder of core is undeformed.</p> <p>Major lithology: Radiolarian-diatom ooze and siliceous mud, very dark olive gray (5Y 3/2) to black (5Y 2.5/2), moderately bioturbated. Section 3 is rich in large radiolarians.</p> <p>Minor lithology: Volcanic ash, dark gray (5Y 4/1). Section 1, 64-69 cm. Disseminated ash lens(?), Section 1, 15-17 cm.</p> <p>SMEAR SLIDE SUMMARY (%):</p> <table border="1"> <tr> <td></td> <td>1, 17</td> <td>1, 111</td> <td>4, 70</td> </tr> <tr> <td></td> <td>D</td> <td>D</td> <td>D</td> </tr> </table> <p>TEXTURE:</p> <table border="1"> <tr> <td>Sand</td> <td>70</td> <td>10</td> <td>—</td> </tr> <tr> <td>Silt</td> <td>20</td> <td>40</td> <td>20</td> </tr> <tr> <td>Clay</td> <td>10</td> <td>50</td> <td>80</td> </tr> </table> <p>COMPOSITION:</p> <table border="1"> <tr> <td>Quartz</td> <td>—</td> <td>1</td> <td>3</td> </tr> <tr> <td>Feldspar</td> <td>—</td> <td>1</td> <td>—</td> </tr> <tr> <td>Clay</td> <td>10</td> <td>45</td> <td>29</td> </tr> <tr> <td>Volcanic glass</td> <td>30</td> <td>1</td> <td>1</td> </tr> <tr> <td>Diatoms</td> <td>5</td> <td>20</td> <td>30</td> </tr> <tr> <td>Radiolarians</td> <td>49</td> <td>30</td> <td>30</td> </tr> <tr> <td>Sponge spicules</td> <td>5</td> <td>—</td> <td>5</td> </tr> <tr> <td>Silicoflagellates</td> <td>1</td> <td>2</td> <td>2</td> </tr> </table>		1, 17	1, 111	4, 70		D	D	D	Sand	70	10	—	Silt	20	40	20	Clay	10	50	80	Quartz	—	1	3	Feldspar	—	1	—	Clay	10	45	29	Volcanic glass	30	1	1	Diatoms	5	20	30	Radiolarians	49	30	30	Sponge spicules	5	—	5	Silicoflagellates	1	2	2
	1, 17	1, 111	4, 70																																																														
	D	D	D																																																														
Sand	70	10	—																																																														
Silt	20	40	20																																																														
Clay	10	50	80																																																														
Quartz	—	1	3																																																														
Feldspar	—	1	—																																																														
Clay	10	45	29																																																														
Volcanic glass	30	1	1																																																														
Diatoms	5	20	30																																																														
Radiolarians	49	30	30																																																														
Sponge spicules	5	—	5																																																														
Silicoflagellates	1	2	2																																																														
R/P B	Benthic Zone C1						1	0.5			*	VOID																																																					
B							2	1.0			*																																																						
C/G	NSR 7						3																																																										
A/M-P	<i>Denticulopsis lauta</i> (NNPD4) subzone A						4																																																										
R/M	no zonal designation						5																																																										
				● $\gamma=1.37$	● $\phi=79$	● $V=1550$	CC																																																										
				● 0.2%																																																													



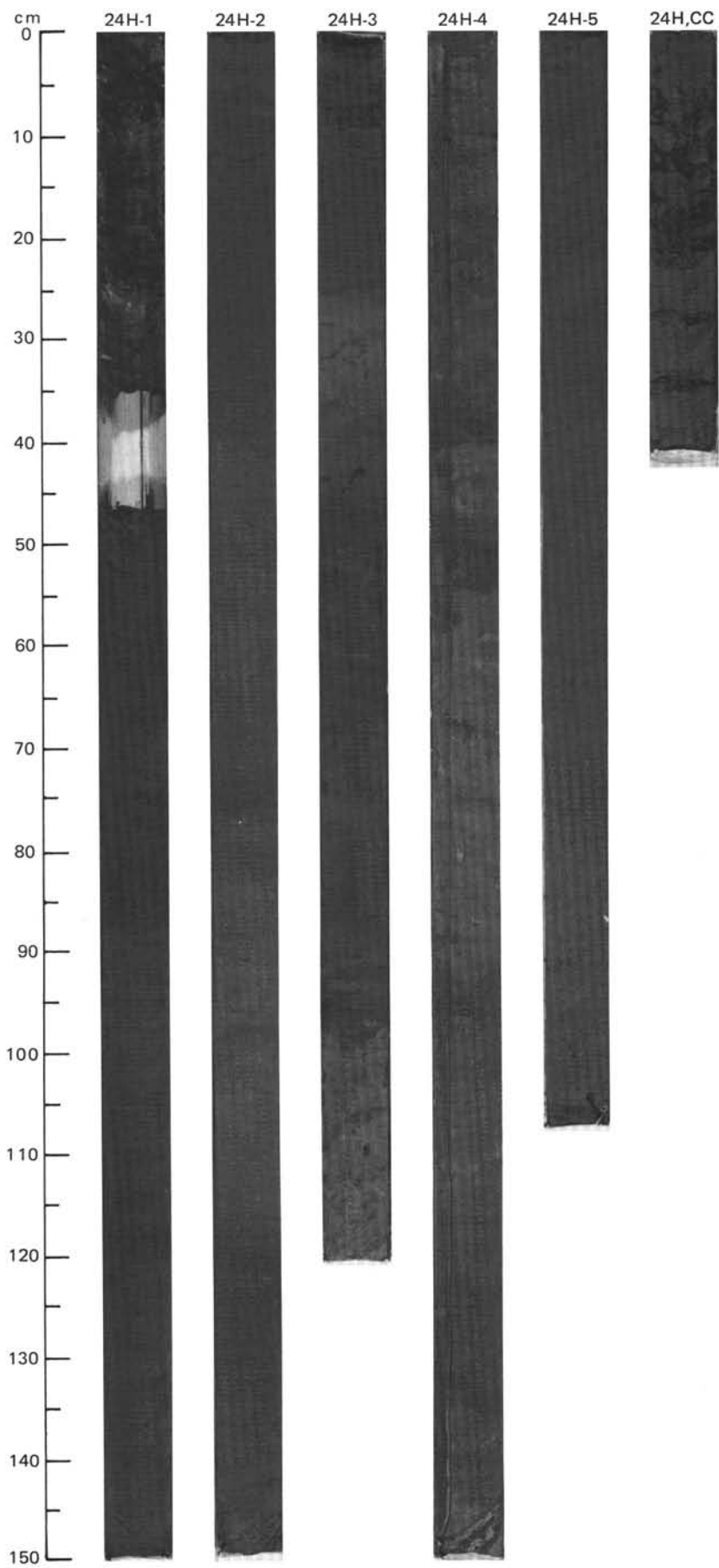
SITE 642 HOLE C CORE 23H CORED INTERVAL - 1470.3-1478.4 mbsf; 184.30-192.40 mbsf

TIME-ROCK UNIT		BIOSTRAT. ZONE/ FOSSIL CHARACTER		SECTION	METERS	GRAPHIC LITHOLOGY	DRILLING DISTURB.	SED. STRUCTURES	SAMPLES	LITHOLOGIC DESCRIPTION																																																				
FORAMINIFERS	NANNOFOSSILS	RADIOLARIANS	DIATOMS																																																											
PALEOMAGNETICS																																																														
PHYS. PROPERTIES	CHEMISTRY																																																													
LOWER MIOCENE																																																														
R/P B	Benthic Zone C1			1	0.5 1.0		---	---	---	<p>SILICEOUS MUD and RADIOLARIAN-DIATOM OOZE</p> <p>Severe disturbance (drilling slurry) in Section 1, flow-in in Section 4, 65-75 cm. Moderate disturbance at Section 5, 0-80 cm. Remainder of core is undisturbed.</p> <p>Major lithology: Siliceous mud and radiolarian-diatom ooze, very dark olive gray (SY 3/2), moderately bioturbated.</p> <p>Minor lithology: Possibly disseminated, severely altered basaltic ash. Section 2, 40 cm.</p> <p>SMEAR SLIDE SUMMARY (%):</p> <table style="margin-left: 40px;"> <tr> <td></td> <td>2, 40</td> <td>2, 91</td> <td>4, 110</td> </tr> <tr> <td></td> <td>M</td> <td>D</td> <td>D</td> </tr> </table> <p>TEXTURE:</p> <table style="margin-left: 40px;"> <tr> <td>Sand</td> <td>90</td> <td>30</td> <td>—</td> </tr> <tr> <td>Silt</td> <td>10</td> <td>40</td> <td>50</td> </tr> <tr> <td>Clay</td> <td>—</td> <td>30</td> <td>50</td> </tr> </table> <p>COMPOSITION:</p> <table style="margin-left: 40px;"> <tr> <td>Quartz</td> <td>1</td> <td>—</td> <td>1</td> </tr> <tr> <td>Feldspar</td> <td>1</td> <td>—</td> <td>—</td> </tr> <tr> <td>Clay</td> <td>—</td> <td>20</td> <td>41</td> </tr> <tr> <td>Volcanic glass</td> <td>94</td> <td>—</td> <td>1</td> </tr> <tr> <td>Diatoms</td> <td>1</td> <td>20</td> <td>30</td> </tr> <tr> <td>Radiolarians</td> <td>1</td> <td>40</td> <td>20</td> </tr> <tr> <td>Sponge spicules</td> <td>1</td> <td>20</td> <td>5</td> </tr> <tr> <td>Silicoflagellates</td> <td>1</td> <td>—</td> <td>2</td> </tr> </table>		2, 40	2, 91	4, 110		M	D	D	Sand	90	30	—	Silt	10	40	50	Clay	—	30	50	Quartz	1	—	1	Feldspar	1	—	—	Clay	—	20	41	Volcanic glass	94	—	1	Diatoms	1	20	30	Radiolarians	1	40	20	Sponge spicules	1	20	5	Silicoflagellates	1	—	2
	2, 40	2, 91	4, 110																																																											
	M	D	D																																																											
Sand	90	30	—																																																											
Silt	10	40	50																																																											
Clay	—	30	50																																																											
Quartz	1	—	1																																																											
Feldspar	1	—	—																																																											
Clay	—	20	41																																																											
Volcanic glass	94	—	1																																																											
Diatoms	1	20	30																																																											
Radiolarians	1	40	20																																																											
Sponge spicules	1	20	5																																																											
Silicoflagellates	1	—	2																																																											
B				2			*																																																							
C/G	NSR6	C/G	NSR7	3																																																										
A/M	<i>Actinocyclus ingens</i> Zone (NNPD3) = <i>Rhizosolenia bulbosa</i> Zone			4																																																										
F/M	C/G	<i>S.ancyrea-P.jaficinctum</i> Zone PM6 no zonal designation			5			*																																																						
				C																																																										



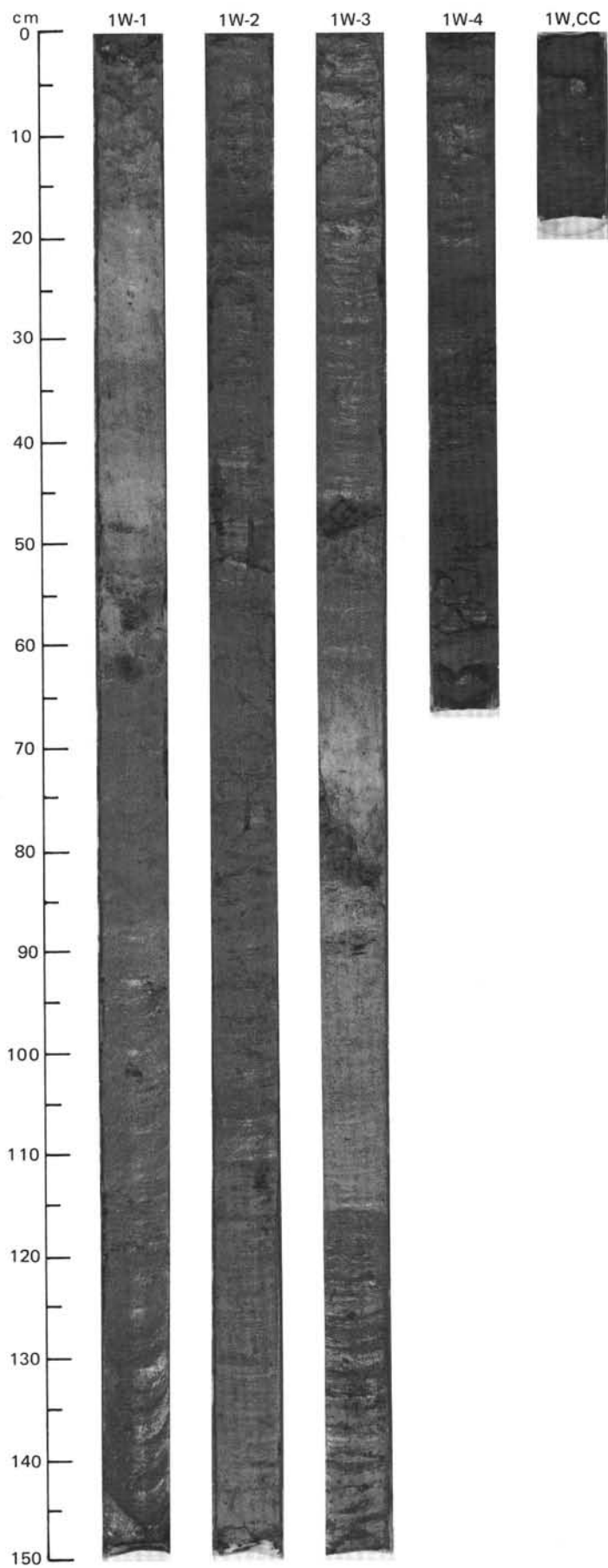
SITE 642 HOLE C CORE 24H CORED INTERVAL 1478.4-1485.6 mbsl; 192.40-199.60 mbsf

TIME-ROCK UNIT		BIOSTRAT. ZONE/ FOSSIL CHARACTER		CHEMISTRY		SECTION METERS	GRAPHIC LITHOLOGY	DRILLING DISTURB.	SED. STRUCTURES	SAMPLES	LITHOLOGIC DESCRIPTION																																																																																																																
FORAMINIFERS	NANNOFOSSILS	RADIOLARIANS	DIATOMS	SILICOS PALYMONORPHS	PALEOMAGNETICS							PHYS. PROPERTIES																																																																																																															
LOWER MIOCENE																																																																																																																											
R/G B	Benthic Zone C1																																																																																																																										
B																																																																																																																											
C/M	R/M	NSR5	R/M	NSR6	C/G																																																																																																																						
A/P	C/G		Actinocyclus ingens Zone (NNPD3)																																																																																																																								
F/G	C/G	S.ancyrea-P.laticinctum	Zone PM6 no zonal designation																																																																																																																								
				● $\gamma=1.35$ $\phi=78$ $V=1767$																																																																																																																							
				● 0.4 %																																																																																																																							
						1																																																																																																																					
						2				*																																																																																																																	
						3				*																																																																																																																	
						4				CG																																																																																																																	
						5				*																																																																																																																	
						6				*																																																																																																																	
						6C				*																																																																																																																	
<p>SILICEOUS MUD</p> <p>Section 1, 34-36 cm, is a void. The remainder of the core is undisturbed.</p> <p>Major lithology: Siliceous mud, dusky yellow green (5G 3/2) or very dark olive gray (5Y 3/2) to black (5Y 2.5/2), extensively bioturbated.</p> <p>Minor lithologies:</p> <p>a. Volcanic ash, dark gray (5Y 4/1). Section 3, 6-10 cm; Section 4, 37-41 and 48-55 cm.</p> <p>b. Possibly disseminated, severely altered basaltic ash. Section 3, 48 cm.</p> <p>c. Massive pyrite filling of burrow. Section 2, 79 and 85 cm.</p> <p>SMEAR SLIDE SUMMARY (%):</p> <table border="1"> <thead> <tr> <th></th> <th>2, 90 D</th> <th>3, 48 M</th> <th>3, 106 M</th> <th>4, 39 M</th> <th>4, 96 D</th> <th>5, 100 D</th> </tr> </thead> <tbody> <tr> <td>Sand</td> <td>—</td> <td>12</td> <td>—</td> <td>20</td> <td>—</td> <td>—</td> </tr> <tr> <td>Silt</td> <td>50</td> <td>38</td> <td>50</td> <td>40</td> <td>50</td> <td>57</td> </tr> <tr> <td>Clay</td> <td>50</td> <td>50</td> <td>50</td> <td>40</td> <td>50</td> <td>43</td> </tr> </tbody> </table> <p>TEXTURE:</p> <p>COMPOSITION:</p> <table border="1"> <thead> <tr> <th></th> <th>1</th> <th>1</th> <th>1</th> <th>—</th> <th>3</th> <th>2</th> </tr> </thead> <tbody> <tr> <td>Quartz</td> <td>—</td> <td>—</td> <td>—</td> <td>—</td> <td>—</td> <td>—</td> </tr> <tr> <td>Clay</td> <td>33</td> <td>33</td> <td>42</td> <td>30</td> <td>34</td> <td>43</td> </tr> <tr> <td>Volcanic glass</td> <td>—</td> <td>10</td> <td>—</td> <td>20</td> <td>3</td> <td>—</td> </tr> <tr> <td>Accessory minerals:</td> <td></td> <td></td> <td></td> <td></td> <td></td> <td></td> </tr> <tr> <td> Glauconite</td> <td>—</td> <td>1</td> <td>—</td> <td>—</td> <td>—</td> <td>—</td> </tr> <tr> <td> Pyrite</td> <td>—</td> <td>—</td> <td>—</td> <td>10</td> <td>—</td> <td>—</td> </tr> <tr> <td>Nannofossils</td> <td>1</td> <td>—</td> <td>—</td> <td>—</td> <td>—</td> <td>—</td> </tr> <tr> <td>Diatoms</td> <td>40</td> <td>30</td> <td>20</td> <td>30</td> <td>30</td> <td>30</td> </tr> <tr> <td>Radiolarians</td> <td>20</td> <td>20</td> <td>30</td> <td>10</td> <td>20</td> <td>15</td> </tr> <tr> <td>Sponge spicules</td> <td>5</td> <td>5</td> <td>5</td> <td>—</td> <td>10</td> <td>10</td> </tr> <tr> <td>Silicoflagellates</td> <td>—</td> <td>—</td> <td>2</td> <td>—</td> <td>—</td> <td>—</td> </tr> </tbody> </table>													2, 90 D	3, 48 M	3, 106 M	4, 39 M	4, 96 D	5, 100 D	Sand	—	12	—	20	—	—	Silt	50	38	50	40	50	57	Clay	50	50	50	40	50	43		1	1	1	—	3	2	Quartz	—	—	—	—	—	—	Clay	33	33	42	30	34	43	Volcanic glass	—	10	—	20	3	—	Accessory minerals:							Glauconite	—	1	—	—	—	—	Pyrite	—	—	—	10	—	—	Nannofossils	1	—	—	—	—	—	Diatoms	40	30	20	30	30	30	Radiolarians	20	20	30	10	20	15	Sponge spicules	5	5	5	—	10	10	Silicoflagellates	—	—	2	—	—	—
	2, 90 D	3, 48 M	3, 106 M	4, 39 M	4, 96 D	5, 100 D																																																																																																																					
Sand	—	12	—	20	—	—																																																																																																																					
Silt	50	38	50	40	50	57																																																																																																																					
Clay	50	50	50	40	50	43																																																																																																																					
	1	1	1	—	3	2																																																																																																																					
Quartz	—	—	—	—	—	—																																																																																																																					
Clay	33	33	42	30	34	43																																																																																																																					
Volcanic glass	—	10	—	20	3	—																																																																																																																					
Accessory minerals:																																																																																																																											
Glauconite	—	1	—	—	—	—																																																																																																																					
Pyrite	—	—	—	10	—	—																																																																																																																					
Nannofossils	1	—	—	—	—	—																																																																																																																					
Diatoms	40	30	20	30	30	30																																																																																																																					
Radiolarians	20	20	30	10	20	15																																																																																																																					
Sponge spicules	5	5	5	—	10	10																																																																																																																					
Silicoflagellates	—	—	2	—	—	—																																																																																																																					

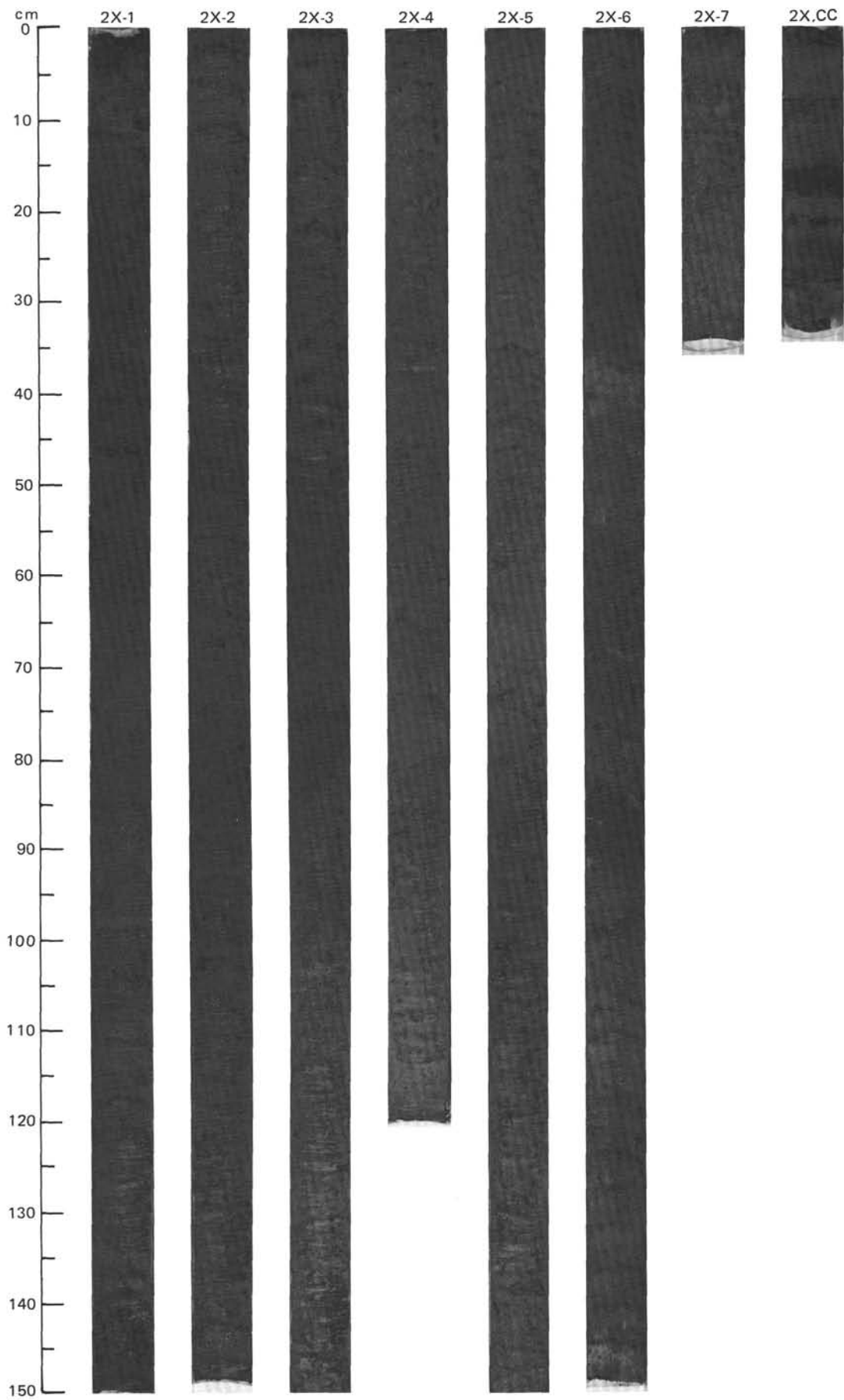


SITE 642 HOLE D CORE 1W CORED INTERVAL 1286.0-1475.9 mbsl; 0.00-189.90 mbsf

TIME-ROCK UNIT	BIOSTRAT. ZONE/ FOSSIL CHARACTER				PALEOMAGNETICS	PHYS. PROPERTIES	CHEMISTRY	SECTION	METERS	GRAPHIC LITHOLOGY	DRILLING DISTURB.	SED. STRUCTURES	SAMPLES	LITHOLOGIC DESCRIPTION																																																																														
	FORAMINIFERS	NANNOFOSSILS	RADIOLARIANS	DIATOMS																																																																																								
LOWER MIOCENE														<p>MUDDY DIATOM OOZE and DIATOMACEOUS MUD</p> <p>Major lithology: Muddy diatom ooze and diatomaceous mud, dusky yellow green (10GY 3/2), grayish olive green (5GY 3/2), light greenish gray (10Y 5/1), and very dark gray (5Y 3/1), interbedded with gradational and indistinct contacts. Minor bioturbation, showing faint burrows with pyrite impregnation.</p> <p>Minor lithologies: a. Volcanic ash, dark gray (5Y 4/1). Section 2, 16-20 cm; Section 3, 46-48 cm. b. Possibly disseminated, severely altered basaltic ash. Section 1, 62-63 cm; Section 3, 85-86 cm.</p> <p>SMEAR SLIDE SUMMARY (%):</p> <table border="1"> <thead> <tr> <th></th> <th>2, 18</th> <th>2, 86</th> <th>3, 47</th> <th>3, 86</th> <th>3, 126</th> </tr> <tr> <th></th> <th>M</th> <th>D</th> <th>M</th> <th>M</th> <th>D</th> </tr> </thead> <tbody> <tr> <td>Sand</td> <td>90</td> <td>10</td> <td>100</td> <td>20</td> <td>5</td> </tr> <tr> <td>Silt</td> <td>10</td> <td>40</td> <td>—</td> <td>60</td> <td>35</td> </tr> <tr> <td>Clay</td> <td>—</td> <td>50</td> <td>—</td> <td>20</td> <td>60</td> </tr> </tbody> </table> <p>TEXTURE:</p> <p>COMPOSITION:</p> <table border="1"> <tbody> <tr> <td>Quartz</td> <td>5</td> <td>30</td> <td>—</td> <td>—</td> <td>30</td> </tr> <tr> <td>Clay</td> <td>—</td> <td>14</td> <td>—</td> <td>20</td> <td>20</td> </tr> <tr> <td>Volcanic glass</td> <td>80</td> <td>Tr</td> <td>100</td> <td>20</td> <td>Tr</td> </tr> <tr> <td>Accessory minerals</td> <td>—</td> <td>Tr</td> <td>Tr</td> <td>—</td> <td>2</td> </tr> <tr> <td>Diatoms</td> <td>5</td> <td>50</td> <td>—</td> <td>40</td> <td>40</td> </tr> <tr> <td>Radiolarians</td> <td>10</td> <td>Tr</td> <td>—</td> <td>—</td> <td>—</td> </tr> <tr> <td>Sponge spicules</td> <td>—</td> <td>3</td> <td>—</td> <td>20</td> <td>5</td> </tr> <tr> <td>Silicoflagellates</td> <td>—</td> <td>3</td> <td>—</td> <td>—</td> <td>3</td> </tr> </tbody> </table>		2, 18	2, 86	3, 47	3, 86	3, 126		M	D	M	M	D	Sand	90	10	100	20	5	Silt	10	40	—	60	35	Clay	—	50	—	20	60	Quartz	5	30	—	—	30	Clay	—	14	—	20	20	Volcanic glass	80	Tr	100	20	Tr	Accessory minerals	—	Tr	Tr	—	2	Diatoms	5	50	—	40	40	Radiolarians	10	Tr	—	—	—	Sponge spicules	—	3	—	20	5	Silicoflagellates	—	3	—	—	3
	2, 18	2, 86	3, 47	3, 86	3, 126																																																																																							
	M	D	M	M	D																																																																																							
Sand	90	10	100	20	5																																																																																							
Silt	10	40	—	60	35																																																																																							
Clay	—	50	—	20	60																																																																																							
Quartz	5	30	—	—	30																																																																																							
Clay	—	14	—	20	20																																																																																							
Volcanic glass	80	Tr	100	20	Tr																																																																																							
Accessory minerals	—	Tr	Tr	—	2																																																																																							
Diatoms	5	50	—	40	40																																																																																							
Radiolarians	10	Tr	—	—	—																																																																																							
Sponge spicules	—	3	—	20	5																																																																																							
Silicoflagellates	—	3	—	—	3																																																																																							
F/M	B				● $\gamma_{n1} .46 \phi = 75$ V-1356	● 0 %	1	0.5																																																																																				
	B						2	1.0				*																																																																																
							3					*																																																																																
					● $\gamma_{n1} .44 \phi = 78$	● 0 %	4					*																																																																																
							CC																																																																																					

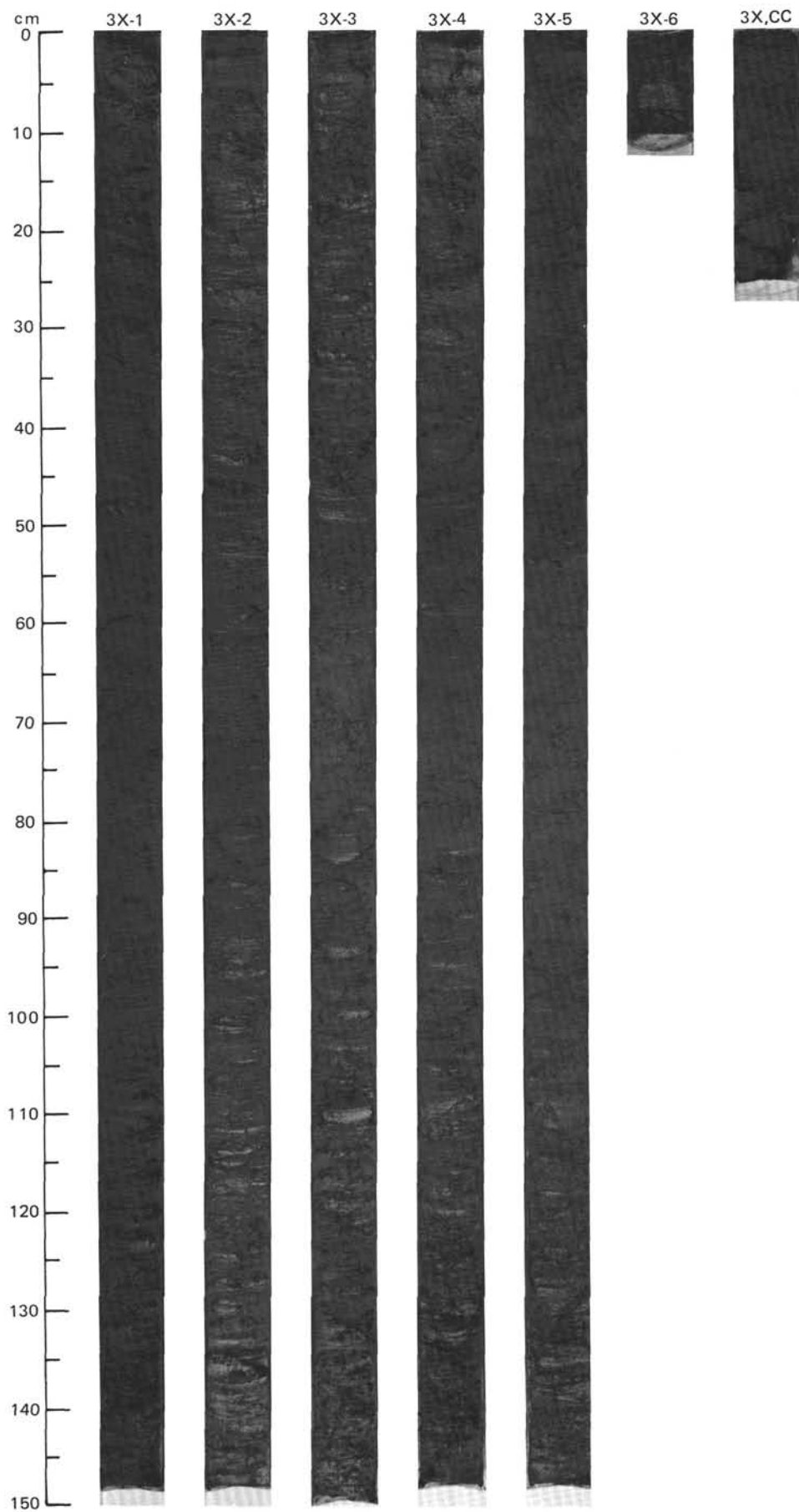


TIME-ROCK UNIT		BIOSTRAT. ZONE/ FOSSIL CHARACTER	SECTION		METERS	GRAPHIC LITHOLOGY	DRILLING DISTURB.	SED. STRUCTURES	SAMPLES	LITHOLOGIC DESCRIPTION																																																																																				
FORAMINIFERS	NANNOFOSSILS	RADIOLARIANS	DIATOMS	SILICIOS PALYMNORPHS							PALEOMAGNETICS	PHYS. PROPERTIES	CHEMISTRY																																																																																	
LOWER MIOCENE																																																																																														
R/M B	Benthic Zone C2				1		}	}	}	DIATOMACEOUS MUD Entire core is undeformed. Major lithology: Siliceous mud, dark olive gray (5Y 3/2) or very dark brown (10YR 3/2), homogeneous, slightly bioturbated and mottled. Minor lithologies: a. Volcanic ash, very dark gray (5Y 3/1), sandy layer. CC, 16-19 cm. b. Possibly disseminated, severely altered basaltic ash. Section 7, 30-33 cm; CC, 22-26 cm. SMEAR SLIDE SUMMARY (%): <table border="1" style="margin-left: 20px;"> <tr> <td></td> <td>2, 59</td> <td>5, 59</td> <td>7, 31</td> <td>CC, 3</td> <td>CC, 15</td> </tr> <tr> <td></td> <td>D</td> <td>D</td> <td>M</td> <td>D</td> <td>M</td> </tr> </table> TEXTURE: <table border="1" style="margin-left: 20px;"> <tr> <td>Sand</td> <td>5</td> <td>5</td> <td>35</td> <td>5</td> <td>100</td> </tr> <tr> <td>Silt</td> <td>55</td> <td>70</td> <td>35</td> <td>70</td> <td>—</td> </tr> <tr> <td>Clay</td> <td>40</td> <td>25</td> <td>30</td> <td>25</td> <td>—</td> </tr> </table> COMPOSITION: <table border="1" style="margin-left: 20px;"> <tr> <td>Quartz</td> <td>5</td> <td>3</td> <td>—</td> <td>—</td> <td>—</td> </tr> <tr> <td>Clay</td> <td>40</td> <td>25</td> <td>30</td> <td>27</td> <td>—</td> </tr> <tr> <td>Volcanic glass</td> <td>Tr</td> <td>Tr</td> <td>30</td> <td>15</td> <td>100</td> </tr> <tr> <td>Accessory minerals</td> <td>—</td> <td>—</td> <td>5</td> <td>—</td> <td>—</td> </tr> <tr> <td>Glauconite</td> <td>—</td> <td>—</td> <td>—</td> <td>3</td> <td>—</td> </tr> <tr> <td>Diatoms</td> <td>35</td> <td>30</td> <td>25</td> <td>35</td> <td>35</td> </tr> <tr> <td>Radiolarians</td> <td>Tr</td> <td>1</td> <td>—</td> <td>—</td> <td>—</td> </tr> <tr> <td>Sponge spicules</td> <td>20</td> <td>40</td> <td>10</td> <td>20</td> <td>—</td> </tr> <tr> <td>Silicoflagellates</td> <td>—</td> <td>1</td> <td>—</td> <td>—</td> <td>—</td> </tr> </table>		2, 59	5, 59	7, 31	CC, 3	CC, 15		D	D	M	D	M	Sand	5	5	35	5	100	Silt	55	70	35	70	—	Clay	40	25	30	25	—	Quartz	5	3	—	—	—	Clay	40	25	30	27	—	Volcanic glass	Tr	Tr	30	15	100	Accessory minerals	—	—	5	—	—	Glauconite	—	—	—	3	—	Diatoms	35	30	25	35	35	Radiolarians	Tr	1	—	—	—	Sponge spicules	20	40	10	20	—	Silicoflagellates	—	1	—	—	—
	2, 59	5, 59	7, 31	CC, 3	CC, 15																																																																																									
	D	D	M	D	M																																																																																									
Sand	5	5	35	5	100																																																																																									
Silt	55	70	35	70	—																																																																																									
Clay	40	25	30	25	—																																																																																									
Quartz	5	3	—	—	—																																																																																									
Clay	40	25	30	27	—																																																																																									
Volcanic glass	Tr	Tr	30	15	100																																																																																									
Accessory minerals	—	—	5	—	—																																																																																									
Glauconite	—	—	—	3	—																																																																																									
Diatoms	35	30	25	35	35																																																																																									
Radiolarians	Tr	1	—	—	—																																																																																									
Sponge spicules	20	40	10	20	—																																																																																									
Silicoflagellates	—	1	—	—	—																																																																																									
B					2																																																																																									
A/G	NSR5	C/G	NSR6		3																																																																																									
A/M	<i>Rhizosolenia bulbosa</i> Zone = <i>Actinocyclus ingens</i> Zone (NNPD3)				4																																																																																									
C/G	<i>S.ancyrea-P.laticinctum</i> Zone PM6		<i>Corbisema triacantha</i> Zone		5																																																																																									
C/M					6																																																																																									
				● $\gamma = 1.37$ $\phi = 78$ $V = 1340$																																																																																										
				● 8%																																																																																										
C					7																																																																																									
				* 0-G																																																																																										
				*																																																																																										
				*																																																																																										



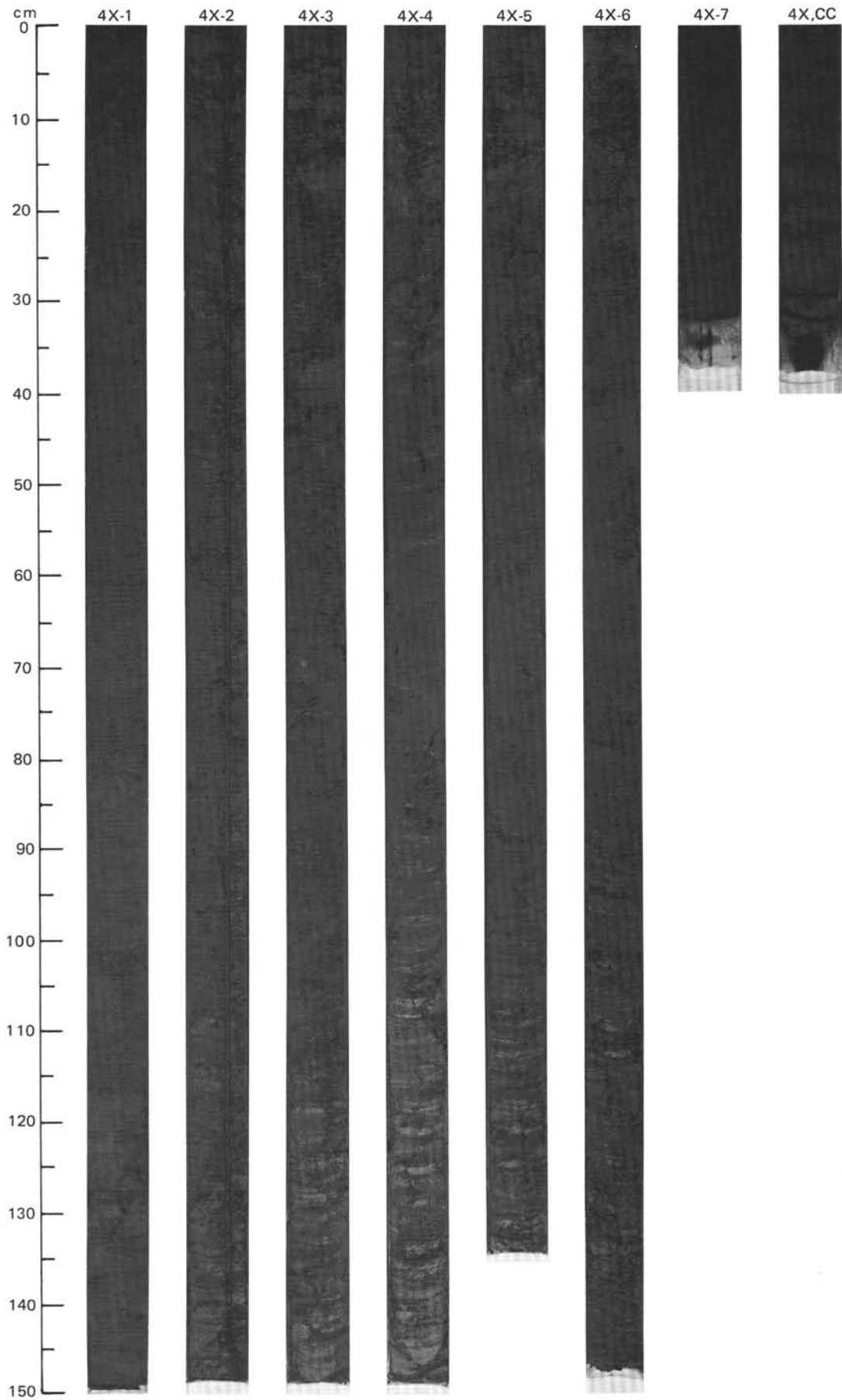
SITE 642 HOLE D CORE 3X CORED INTERVAL 1485.6-1495.2 mbsl; 199.60-209.20 mbsl

TIME-ROCK UNIT		BIOSTRAT. ZONE/ FOSSIL CHARACTER		PHYS. PROPERTIES	CHEMISTRY	SECTION	METERS	GRAPHIC LITHOLOGY	DRILLING DISTURB.	SED. STRUCTURES	SAMPLES	LITHOLOGIC DESCRIPTION																																	
FORAMINIFERS	MAMMIFOSILS	RADIOLARIANS	DIATOMS																																										
SILICOS	PALYMONOPHS	PALEOMAGNETICS																																											
		$\gamma = 1.32$	$\phi = 80$										V-1503																																
													● 12 %																																
LOWER MIOCENE												<p>SILICEOUS MUD and MUDDY SILICEOUS OOZE</p> <p>Entire core is undeformed.</p> <p>Major lithology: Siliceous mud and muddy siliceous ooze, olive gray (5Y 4/2) to dark olive gray (5Y 3/2), homogeneous to slightly mottled.</p> <p>SMEAR SLIDE SUMMARY (%):</p> <table style="margin-left: 20px;"> <tr> <td></td> <td>3, 100</td> <td>CC, 10</td> </tr> <tr> <td>D</td> <td>D</td> <td>D</td> </tr> </table> <p>TEXTURE:</p> <table style="margin-left: 20px;"> <tr> <td>Sand</td> <td>5</td> <td>5</td> </tr> <tr> <td>Silt</td> <td>45</td> <td>55</td> </tr> <tr> <td>Clay</td> <td>50</td> <td>40</td> </tr> </table> <p>COMPOSITION:</p> <table style="margin-left: 20px;"> <tr> <td>Quartz</td> <td>3</td> <td>4</td> </tr> <tr> <td>Clay</td> <td>50</td> <td>40</td> </tr> <tr> <td>Diatoms</td> <td>15</td> <td>25</td> </tr> <tr> <td>Radiolarians</td> <td>1</td> <td>Tr</td> </tr> <tr> <td>Sponge spicules</td> <td>30</td> <td>30</td> </tr> <tr> <td>Silicoflagellates</td> <td>1</td> <td>1</td> </tr> </table>		3, 100	CC, 10	D	D	D	Sand	5	5	Silt	45	55	Clay	50	40	Quartz	3	4	Clay	50	40	Diatoms	15	25	Radiolarians	1	Tr	Sponge spicules	30	30	Silicoflagellates	1	1
	3, 100	CC, 10																																											
D	D	D																																											
Sand	5	5																																											
Silt	45	55																																											
Clay	50	40																																											
Quartz	3	4																																											
Clay	50	40																																											
Diatoms	15	25																																											
Radiolarians	1	Tr																																											
Sponge spicules	30	30																																											
Silicoflagellates	1	1																																											
B B	Benthic Zone C2																																												
B			C/G																																										
A/G	F/G	NSR3																																											
A/P	Rhizosolenia bulbosa Zone = upper <i>Thalassiosira fraga</i> zone																																												
C/M	<i>Corbisema triacantha</i> Zone																																												
E/M	<i>S.ancyrea-P. laticinctum</i> Zone PM6																																												



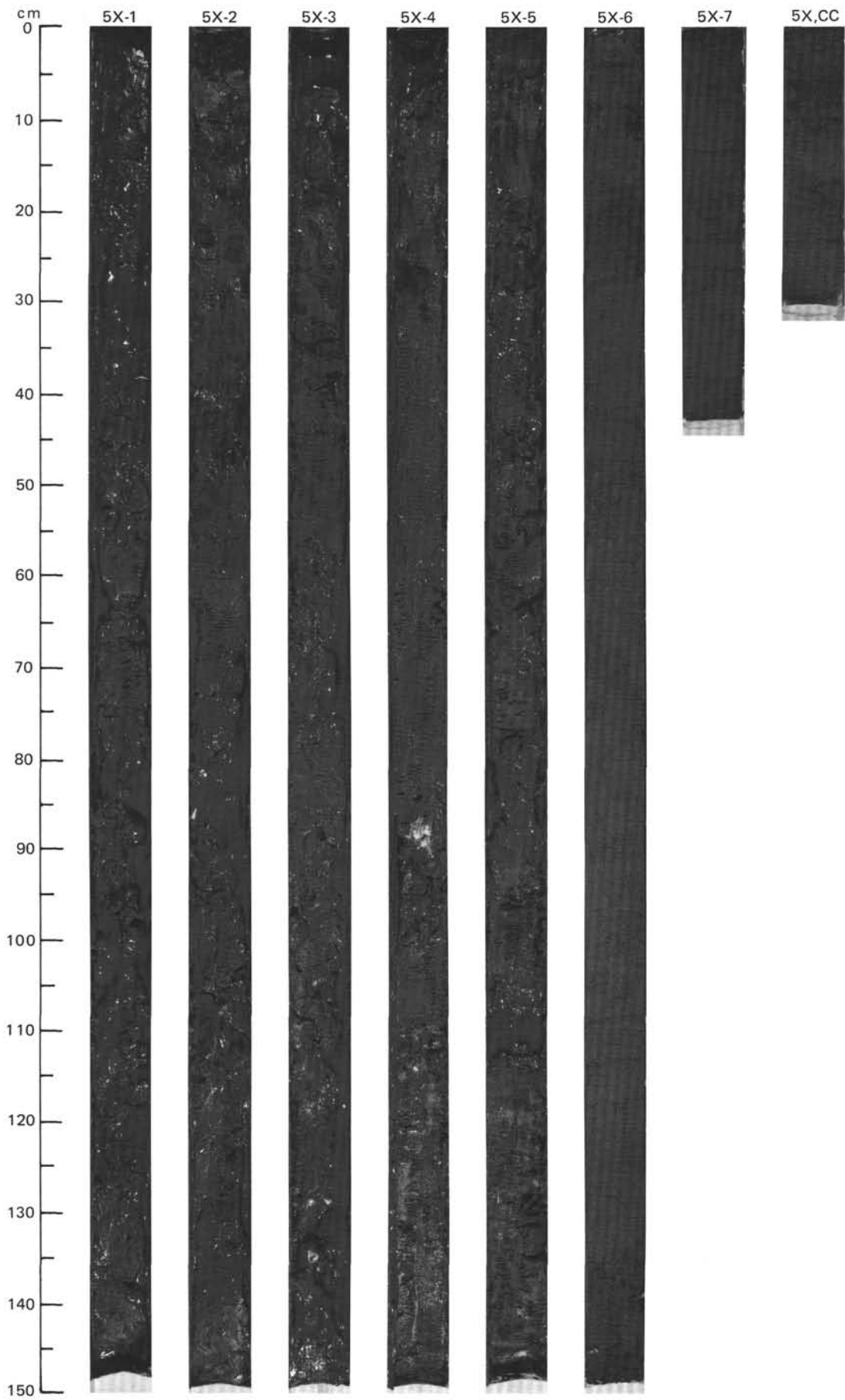
SITE 642 HOLE D CORE 4X CORED INTERVAL 1495.2-1504.9 mbsl; 209.20-218.90 mbsf

TIME-ROCK UNIT		BIOSTRAT. ZONE/ FOSSIL CHARACTER	SECTION	METERS	GRAPHIC LITHOLOGY	DRILLING DISTURB.	SED. STRUCTURES	SAMPLES	LITHOLOGIC DESCRIPTION						
LOWER MIOCENE															
B B		Benthic Zone C2													
B															
A/G		C/G													
A/M		NSR3													
F/G	C/G	<i>Thalassiosira fraga</i> Zone (NNPD2)													
		<i>Corbisema triacantha</i> Zone													
		<i>S. ancyrea-P. laticinctum</i> Zone PM6													
		● $\gamma=1.29$ $\phi=81$ $V=1630$													
		● 11 %													
			1	0.5					* MUDDY SILICEOUS OOZE and SILICEOUS OOZE Entire core is undeformed. Major lithology: Muddy siliceous ooze and siliceous ooze, olive gray (5Y 4/2), homogeneous to slightly mottled.						
			2	1.0					SMEAR SLIDE SUMMARY (%): <table border="1"><tr><td></td><td>1, 70</td><td>5, 70</td></tr><tr><td>D</td><td>D</td><td>D</td></tr></table>		1, 70	5, 70	D	D	D
	1, 70	5, 70													
D	D	D													
			3						TEXTURE: Sand 5 — Silt 50 80 Clay 45 20						
			4						COMPOSITION: Quartz 2 — Clay 45 20 Volcanic glass 1 — Foraminifers 1 — Diatoms 20 35 Radiolarians — 3 Sponge spicules 30 40 Silicoflagellates 1 2						
			5						* I-G						
			6												
			7												
			CC												

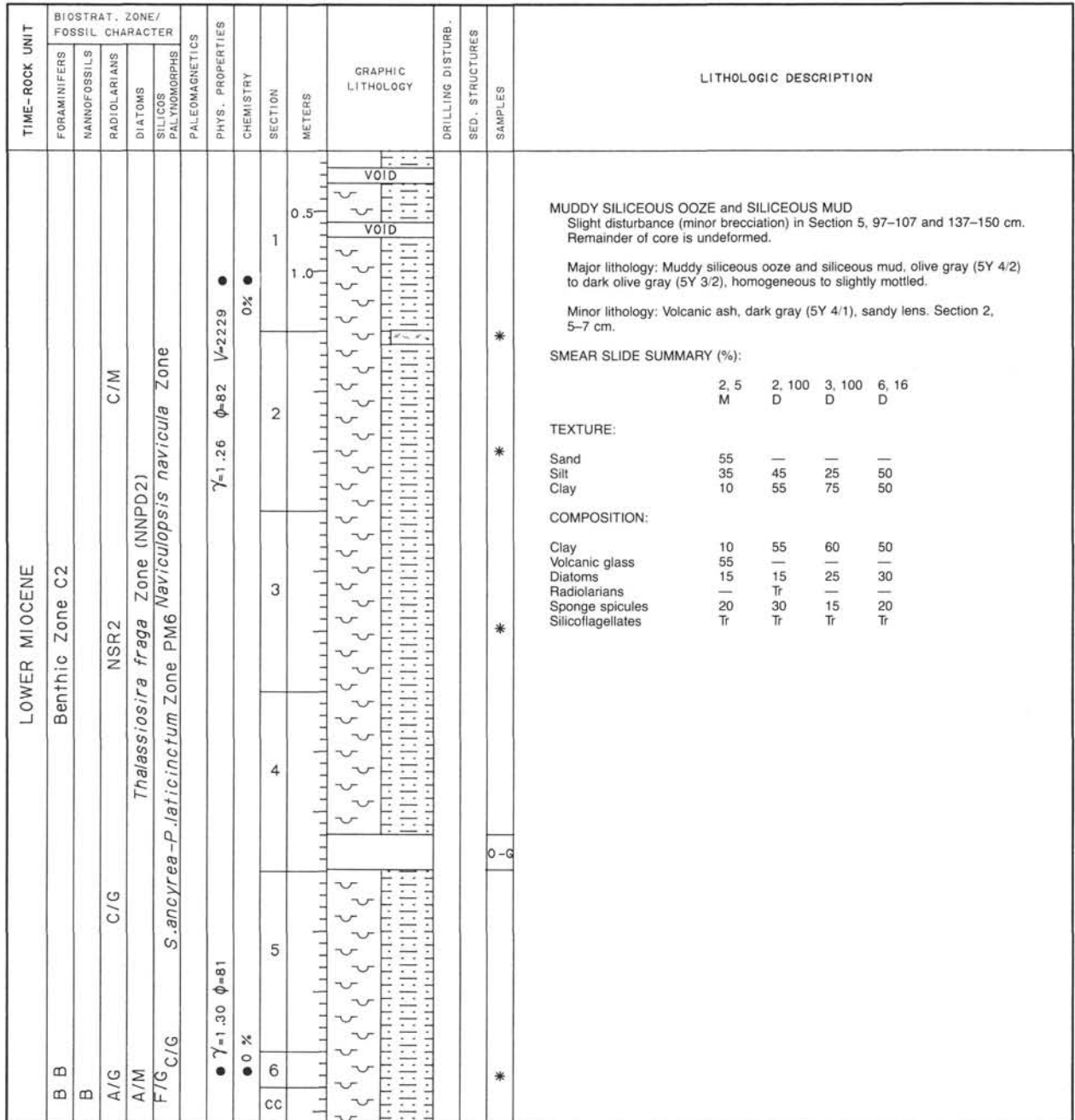


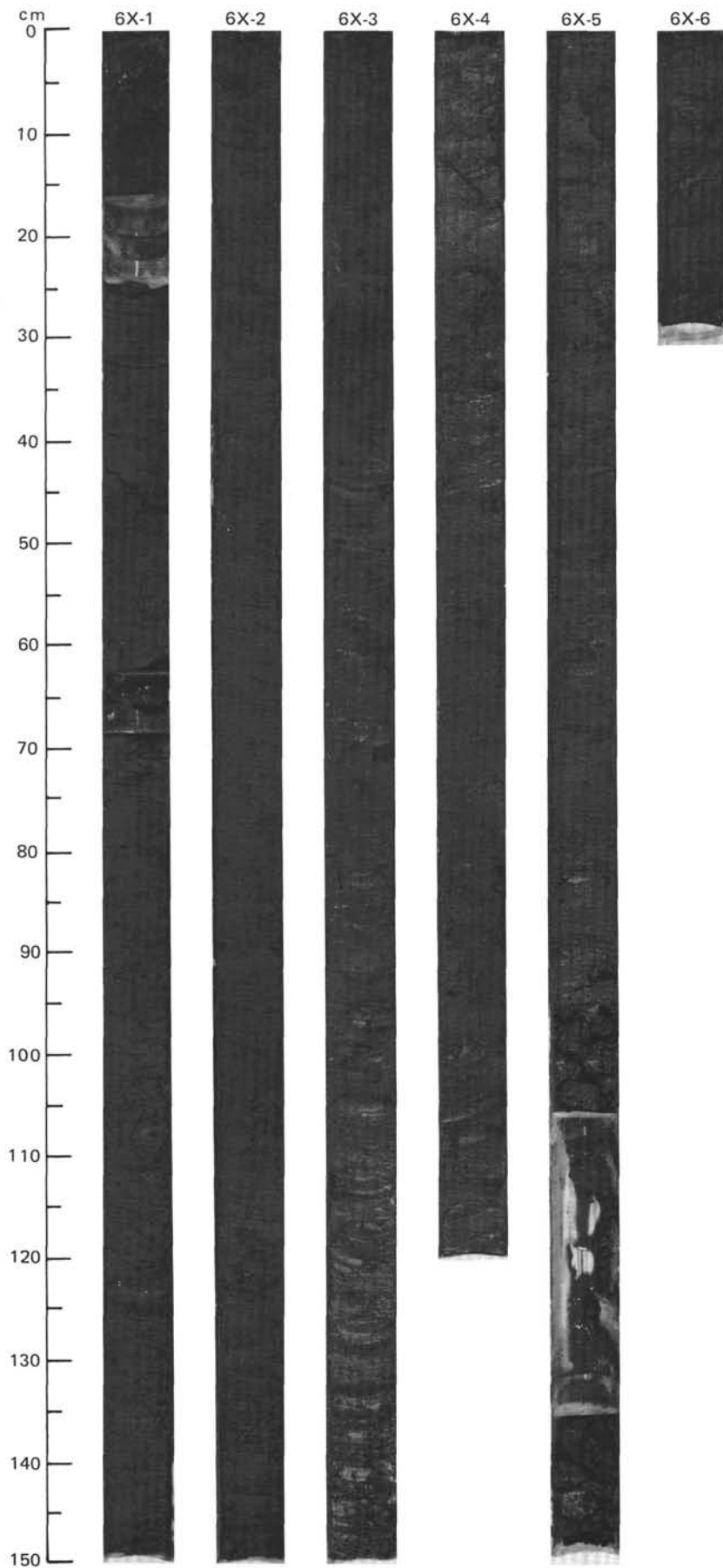
SITE 642 HOLE D CORE 5X CORED INTERVAL 1504.9-1514.5 mbsl; 218.90-228.50 mbsf

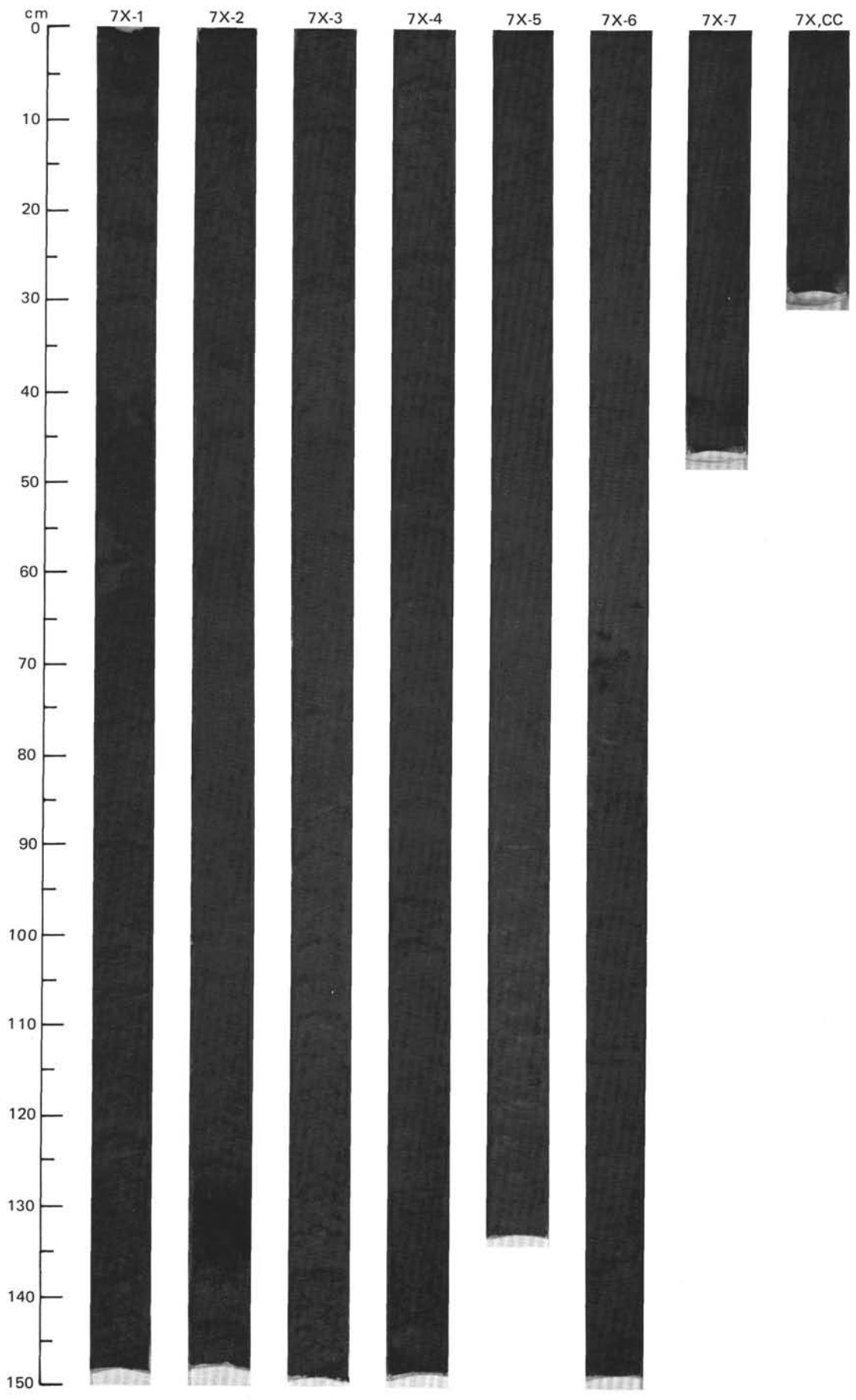
TIME-ROCK UNIT		BIOSTRAT. ZONE/ FOSSIL CHARACTER					SECTION	METERS	GRAPHIC LITHOLOGY	DRILLING DISTURB.	SED. STRUCTURES	SAMPLES	LITHOLOGIC DESCRIPTION																				
FORAMINIFERS	NANNOFOSSILS	RADIOLARIANS	DIATOMS	SILICOS PALYNOMORPHS	PALEOMAGNETICS																												
LOWER MIOCENE													<p>MUDDY DIATOM OOZE</p> <p>Moderate to severe disturbance from Section 1 to Section 6, 19 cm. Remainder of core is undisturbed.</p> <p>Major lithology: Muddy diatom ooze, olive gray (5Y 4/2), homogeneous to slightly mottled.</p> <p>SMEAR SLIDE SUMMARY (%):</p> <table style="margin-left: 20px;"> <tr><td></td><td>6, 60</td></tr> <tr><td>D</td><td></td></tr> </table> <p>TEXTURE:</p> <table style="margin-left: 20px;"> <tr><td>Silt</td><td>65</td></tr> <tr><td>Clay</td><td>35</td></tr> </table> <p>COMPOSITION:</p> <table style="margin-left: 20px;"> <tr><td>Quartz</td><td>1</td></tr> <tr><td>Clay</td><td>35</td></tr> <tr><td>Diatoms</td><td>35</td></tr> <tr><td>Radiolarians</td><td>1</td></tr> <tr><td>Sponge spicules</td><td>25</td></tr> <tr><td>Silicoflagellates</td><td>3</td></tr> </table>		6, 60	D		Silt	65	Clay	35	Quartz	1	Clay	35	Diatoms	35	Radiolarians	1	Sponge spicules	25	Silicoflagellates	3
	6, 60																																
D																																	
Silt	65																																
Clay	35																																
Quartz	1																																
Clay	35																																
Diatoms	35																																
Radiolarians	1																																
Sponge spicules	25																																
Silicoflagellates	3																																
R/P B	Benthic Zone C2					1	0.5																										
B						2	1.0																										
A/G	C/G	NSR2	C/G			3																											
A/M-P	<i>Thalassiosira fraga</i> Zone (NNPD2)					4																											
F/G	<i>S.ancyrea-P.laticinctum</i> Zone PM6 <i>Corbisema triacantha</i> Zone					5																											
A/G	<i>S.ancyrea-P.laticinctum</i> Zone PM6					6																											
CC	<p>● $\gamma=1.28$ $\phi=83$ $V=1838$</p> <p>● 0.2 %</p>					7																											



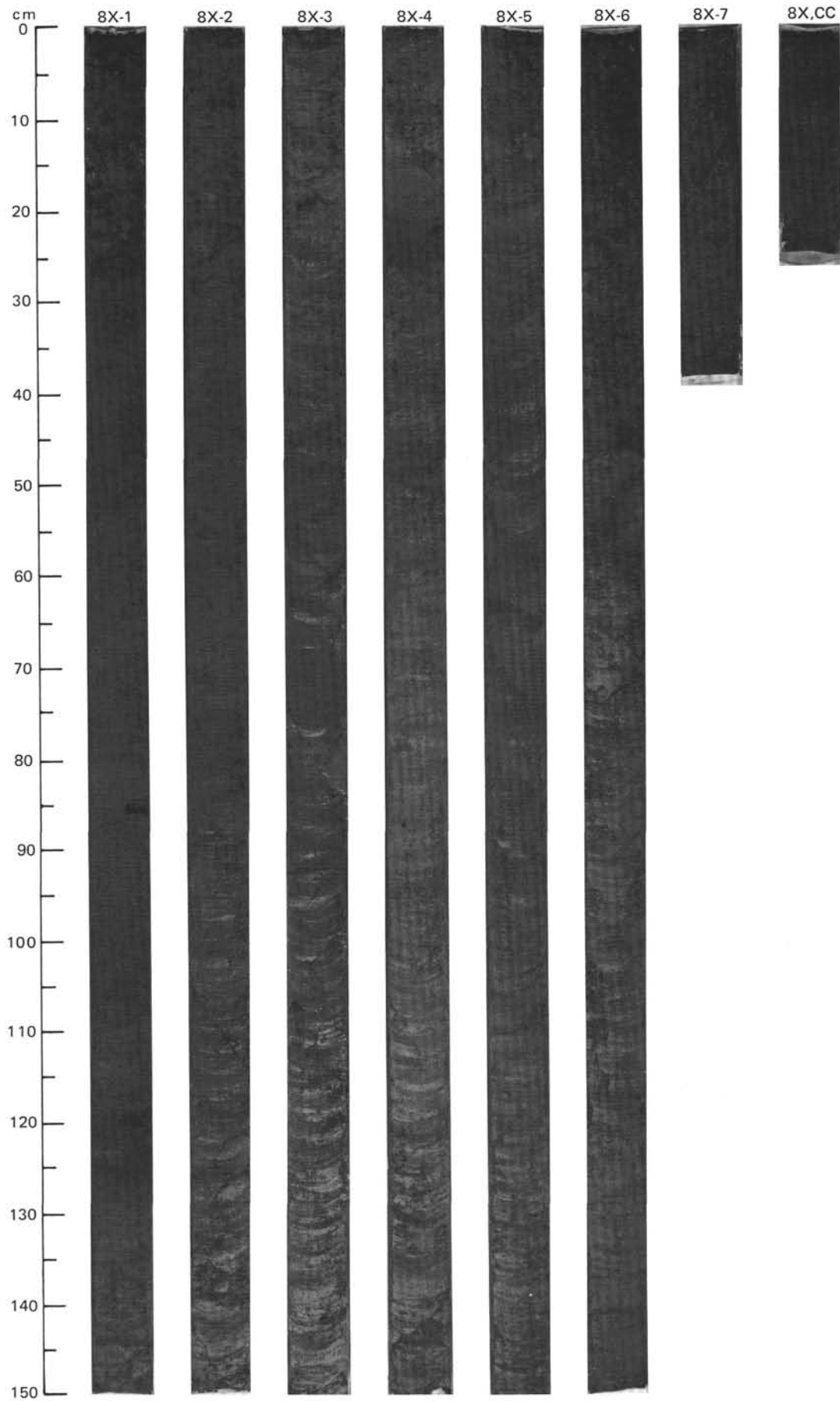
SITE 642 HOLE D CORE 6X CORED INTERVAL 1514.5-1524.2 mbsf; 228.50-238.20 mbsf





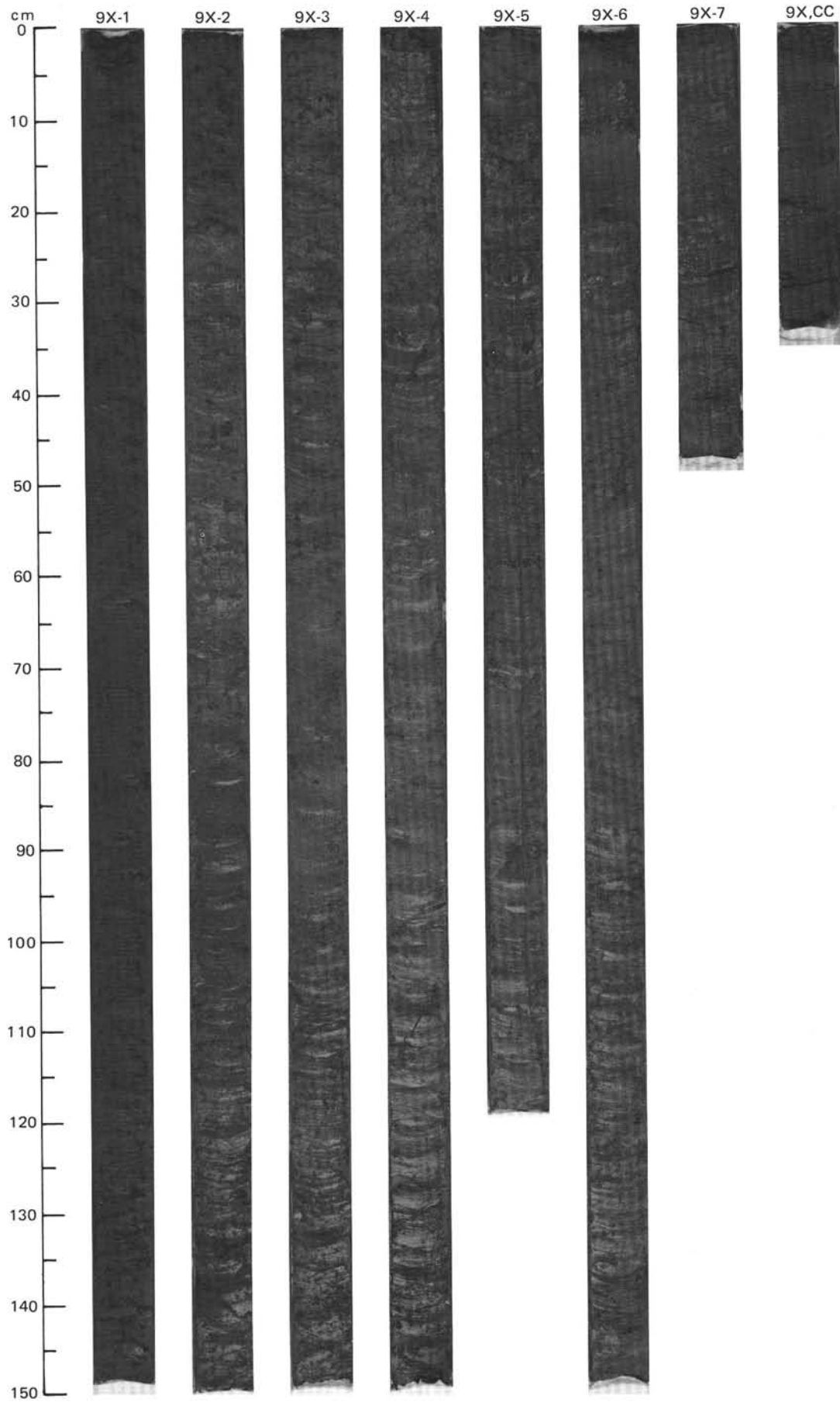


TIME-ROCK UNIT	BIOSTRAT. ZONE/ FOSSIL CHARACTER					PHYS. PROPERTIES	CHEMISTRY	SECTION	METERS	GRAPHIC LITHOLOGY	DRILLING DISTURB.	SED. STRUCTURES	SAMPLES	LITHOLOGIC DESCRIPTION																																																																																																												
	FORAMINIFERS	NANKOFOSSILS	RADIOLARIANS	DIATOMS	SILICOS PALYMONOPHS																																																																																																																					
LOWER MIOCENE																																																																																																																										
R/G	B				C/G			1	0.5					<p>MUDDY DIATOM OOZE, DIATOM OOZE, and SILICEOUS OOZE</p> <p>Entire core is undeformed.</p> <p>Major lithology: Muddy diatom ooze, diatom ooze, and siliceous ooze, olive gray (5Y 4/2), dark olive gray (5Y 3/2) to very dark grayish brown (2.5Y 3/2), interbedded with gradational and indistinct contacts. Homogeneous to slightly mottled.</p> <p>Minor lithologies:</p> <p>a. Volcanic ash, dark olive gray (5Y 3/2), sandy layer. Section 4, 20-25 cm. b. Glauconitic sandy lens. Section 1, 85-86 cm.</p> <p>SMEAR SLIDE SUMMARY (%):</p> <table border="1"> <thead> <tr> <th></th> <th>1, 86</th> <th>1, 100</th> <th>4, 22</th> <th>4, 85</th> <th>5, 85</th> </tr> <tr> <th></th> <th>M</th> <th>D</th> <th>M</th> <th>D</th> <th>M</th> </tr> </thead> <tbody> <tr> <td>Sand</td> <td>60</td> <td>—</td> <td>75</td> <td>—</td> <td>—</td> </tr> <tr> <td>Silt</td> <td>30</td> <td>70</td> <td>15</td> <td>80</td> <td>70</td> </tr> <tr> <td>Clay</td> <td>10</td> <td>30</td> <td>10</td> <td>20</td> <td>30</td> </tr> </tbody> </table> <p>TEXTURE:</p> <table border="1"> <thead> <tr> <th></th> <th>1, 86</th> <th>1, 100</th> <th>4, 22</th> <th>4, 85</th> <th>5, 85</th> </tr> </thead> <tbody> <tr> <td>Sand</td> <td>60</td> <td>—</td> <td>75</td> <td>—</td> <td>—</td> </tr> <tr> <td>Silt</td> <td>30</td> <td>70</td> <td>15</td> <td>80</td> <td>70</td> </tr> <tr> <td>Clay</td> <td>10</td> <td>30</td> <td>10</td> <td>20</td> <td>30</td> </tr> </tbody> </table> <p>COMPOSITION:</p> <table border="1"> <thead> <tr> <th></th> <th>1, 86</th> <th>1, 100</th> <th>4, 22</th> <th>4, 85</th> <th>5, 85</th> </tr> </thead> <tbody> <tr> <td>Clay</td> <td>10</td> <td>30</td> <td>10</td> <td>20</td> <td>30</td> </tr> <tr> <td>Volcanic glass</td> <td>—</td> <td>—</td> <td>75</td> <td>—</td> <td>—</td> </tr> <tr> <td>Accessory minerals:</td> <td></td> <td></td> <td></td> <td></td> <td></td> </tr> <tr> <td> Glauconite</td> <td>60</td> <td>—</td> <td>—</td> <td>—</td> <td>—</td> </tr> <tr> <td> Diatoms</td> <td>10</td> <td>40</td> <td>5</td> <td>35</td> <td>40</td> </tr> <tr> <td> Radiolarians</td> <td>—</td> <td>—</td> <td>—</td> <td>5</td> <td>Tr</td> </tr> <tr> <td> Sponge spicules</td> <td>20</td> <td>25</td> <td>10</td> <td>40</td> <td>30</td> </tr> <tr> <td> Silicoflagellates</td> <td>—</td> <td>5</td> <td>—</td> <td>—</td> <td>Tr</td> </tr> </tbody> </table>		1, 86	1, 100	4, 22	4, 85	5, 85		M	D	M	D	M	Sand	60	—	75	—	—	Silt	30	70	15	80	70	Clay	10	30	10	20	30		1, 86	1, 100	4, 22	4, 85	5, 85	Sand	60	—	75	—	—	Silt	30	70	15	80	70	Clay	10	30	10	20	30		1, 86	1, 100	4, 22	4, 85	5, 85	Clay	10	30	10	20	30	Volcanic glass	—	—	75	—	—	Accessory minerals:						Glauconite	60	—	—	—	—	Diatoms	10	40	5	35	40	Radiolarians	—	—	—	5	Tr	Sponge spicules	20	25	10	40	30	Silicoflagellates	—	5	—	—	Tr
	1, 86	1, 100	4, 22	4, 85	5, 85																																																																																																																					
	M	D	M	D	M																																																																																																																					
Sand	60	—	75	—	—																																																																																																																					
Silt	30	70	15	80	70																																																																																																																					
Clay	10	30	10	20	30																																																																																																																					
	1, 86	1, 100	4, 22	4, 85	5, 85																																																																																																																					
Sand	60	—	75	—	—																																																																																																																					
Silt	30	70	15	80	70																																																																																																																					
Clay	10	30	10	20	30																																																																																																																					
	1, 86	1, 100	4, 22	4, 85	5, 85																																																																																																																					
Clay	10	30	10	20	30																																																																																																																					
Volcanic glass	—	—	75	—	—																																																																																																																					
Accessory minerals:																																																																																																																										
Glauconite	60	—	—	—	—																																																																																																																					
Diatoms	10	40	5	35	40																																																																																																																					
Radiolarians	—	—	—	5	Tr																																																																																																																					
Sponge spicules	20	25	10	40	30																																																																																																																					
Silicoflagellates	—	5	—	—	Tr																																																																																																																					
							2	1.0																																																																																																																		
							3																																																																																																																			
							4																																																																																																																			
							5																																																																																																																			
							6																																																																																																																			
							7																																																																																																																			
							CC																																																																																																																			



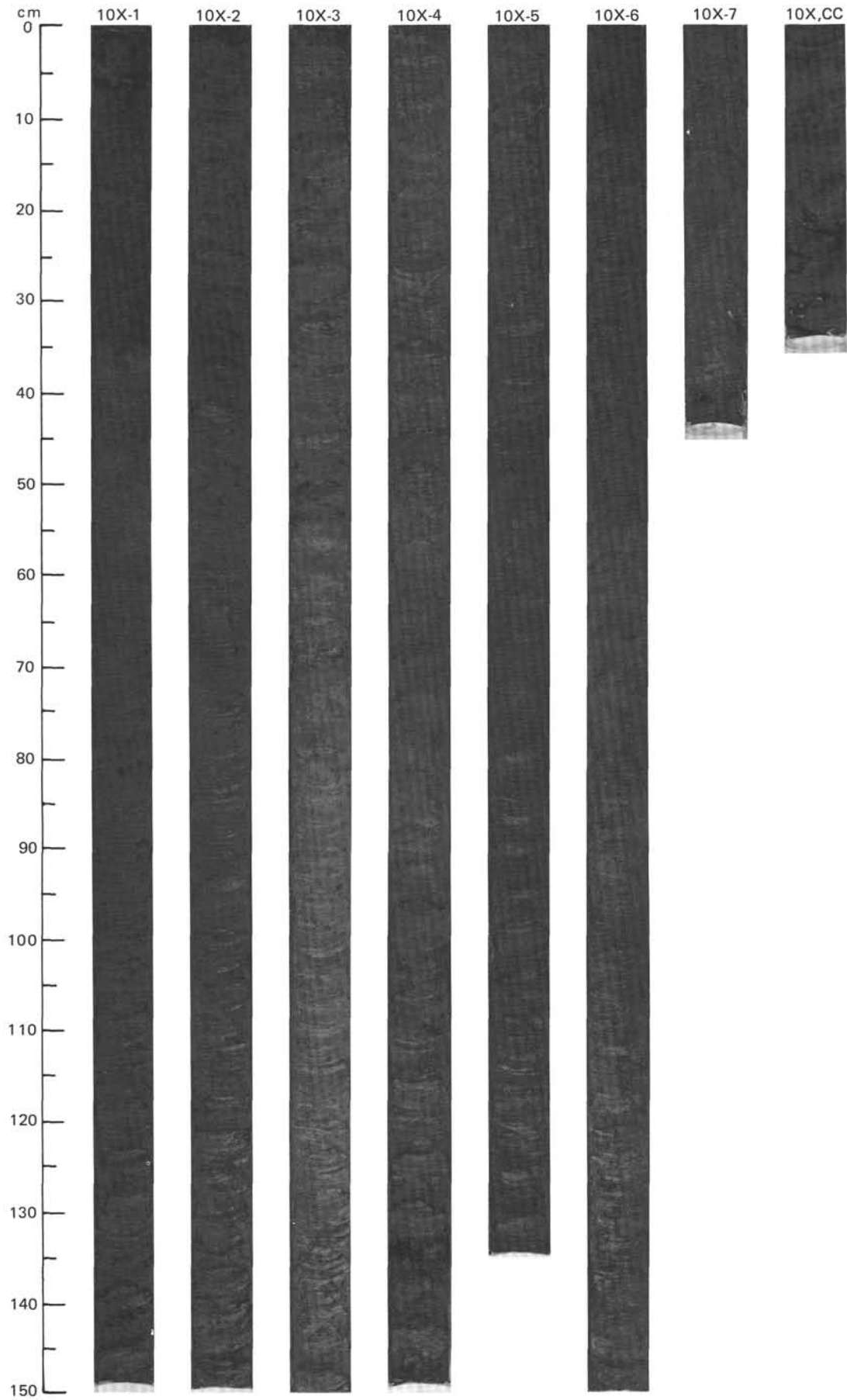
SITE 642 HOLE D CORE 9X CORED INTERVAL 1543.5-1553.1 mbsl; 257.50-267.10 mbsf

TIME-ROCK UNIT		BIOSTRAT. ZONE/ FOSSIL CHARACTER		PALEOMAGNETICS	PHYS. PROPERTIES	CHEMISTRY	SECTION	METERS	GRAPHIC LITHOLOGY	DRILLING DISTURB.	SED. STRUCTURES	SAMPLES	LITHOLOGIC DESCRIPTION																																																																				
FORAMINIFERS	NANNOFOSSILS	RADIOLARIANS	DIATOMS																																																																														
LOWER MIOCENE													<p>DIATOMACEOUS MUD</p> <p>Entire core is undisturbed.</p> <p>Major lithology: Diatomaceous mud, grayish olive green (10Y 4/2) to very dark grayish brown (2.5Y 3/2), homogeneous. Alternating faint color bands of greenish brown and brownish gray at Section 2, 22-67 and 117-138 cm; Section 3, 120-150 cm; Section 4, 0-33 cm; Section 6, 110-150 cm.</p> <p>Minor lithology: Volcanic ash, dark gray (5Y 4/1), sandy. Section 6, 18-22 cm.</p> <p>SMEAR SLIDE SUMMARY (%):</p> <table border="1"> <tr> <td></td> <td>3, 83</td> <td>6, 20</td> <td>6, 60</td> </tr> <tr> <td></td> <td>D</td> <td>M</td> <td>D</td> </tr> </table> <p>TEXTURE:</p> <table border="1"> <tr> <td>Sand</td> <td>—</td> <td>90</td> <td>—</td> </tr> <tr> <td>Silt</td> <td>50</td> <td>10</td> <td>40</td> </tr> <tr> <td>Clay</td> <td>50</td> <td>—</td> <td>60</td> </tr> </table> <p>COMPOSITION:</p> <table border="1"> <tr> <td>Quartz</td> <td>1</td> <td>—</td> <td>1</td> </tr> <tr> <td>Feldspar</td> <td>1</td> <td>1</td> <td>—</td> </tr> <tr> <td>Mica</td> <td>50</td> <td>—</td> <td>—</td> </tr> <tr> <td>Clay</td> <td>—</td> <td>—</td> <td>54</td> </tr> <tr> <td>Volcanic glass</td> <td>—</td> <td>94</td> <td>—</td> </tr> <tr> <td>Calcite/dolomite</td> <td>—</td> <td>Tr</td> <td>—</td> </tr> <tr> <td>Accessory minerals:</td> <td></td> <td></td> <td></td> </tr> <tr> <td> Pyrite</td> <td>3</td> <td>5</td> <td>—</td> </tr> <tr> <td> Nannofossils</td> <td>—</td> <td>—</td> <td>Tr</td> </tr> <tr> <td> Diatoms</td> <td>30</td> <td>—</td> <td>30</td> </tr> <tr> <td> Radiolarians</td> <td>5</td> <td>—</td> <td>10</td> </tr> <tr> <td> Sponge spicules</td> <td>10</td> <td>—</td> <td>5</td> </tr> </table>		3, 83	6, 20	6, 60		D	M	D	Sand	—	90	—	Silt	50	10	40	Clay	50	—	60	Quartz	1	—	1	Feldspar	1	1	—	Mica	50	—	—	Clay	—	—	54	Volcanic glass	—	94	—	Calcite/dolomite	—	Tr	—	Accessory minerals:				Pyrite	3	5	—	Nannofossils	—	—	Tr	Diatoms	30	—	30	Radiolarians	5	—	10	Sponge spicules	10	—	5
	3, 83	6, 20	6, 60																																																																														
	D	M	D																																																																														
Sand	—	90	—																																																																														
Silt	50	10	40																																																																														
Clay	50	—	60																																																																														
Quartz	1	—	1																																																																														
Feldspar	1	1	—																																																																														
Mica	50	—	—																																																																														
Clay	—	—	54																																																																														
Volcanic glass	—	94	—																																																																														
Calcite/dolomite	—	Tr	—																																																																														
Accessory minerals:																																																																																	
Pyrite	3	5	—																																																																														
Nannofossils	—	—	Tr																																																																														
Diatoms	30	—	30																																																																														
Radiolarians	5	—	10																																																																														
Sponge spicules	10	—	5																																																																														
R/G B	Benthic Zone C2						1	0.5					<p>● $\gamma = 1.34$ $\phi = 79$ V-1713</p> <p>● 0 %</p>																																																																				
B							2	1.0																																																																									
F/P	F/M	NSR2	C/M				3																																																																										
A/P	<i>Thalassiosira spinosa</i> Zone						4																																																																										
F/G	<i>S. ancyrea-P. laticinctum</i> Zone PM6						5																																																																										
C/G							6																																																																										
							7																																																																										
CC																																																																																	



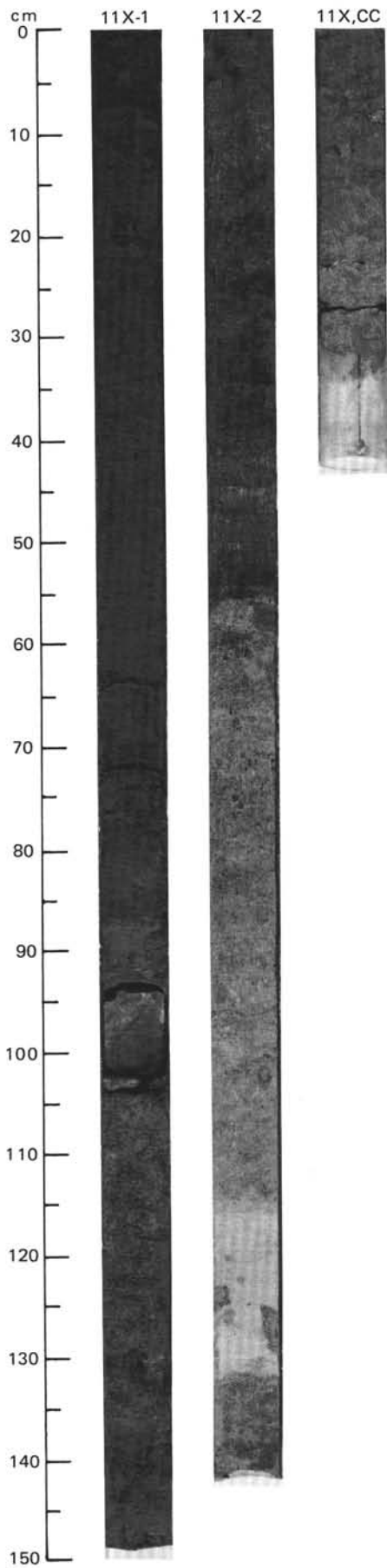
SITE 642 HOLE D CORE 10X CORED INTERVAL 1553.1-1562.8 mbsl; 267.10-276.80 mbsf

TIME-ROCK UNIT		BIOSTRAT. ZONE/ FOSSIL CHARACTER		C/M	SECTION	METERS	GRAPHIC LITHOLOGY	DRILLING DISTURB.	SED. STRUCTURES	SAMPLES	LITHOLOGIC DESCRIPTION																																																																																																																
FORAMINIFERS	MANNOFOSSILS	RADIOLARIANS	DIATOMS									SILICOS PALYNORRHIPS	PALEOMAGNETICS	PHYS. PROPERTIES	CHEMISTRY																																																																																																												
LOWER MIOCENE		Benthic Zone C2				0.5 1 1.0					<p>MUDDY DIATOM OOZE and MUDDY SILICEOUS OOZE</p> <p>Entire core is undeformed.</p> <p>Major lithology: Muddy diatom ooze and muddy siliceous ooze, grayish olive green (5GY 3/2) to dark olive gray (5Y 3/2), bioturbated and mottled, with pyritized burrows common throughout core.</p> <p>Minor lithology: Volcanic ash, gray (5Y 5/1), sandy and disseminated. Section 1, 5-8 cm; Section 4, 135-138 cm.</p> <p>SMEAR SLIDE SUMMARY (%):</p> <table border="1"> <tr> <td></td> <td>1, 7</td> <td>1, 85</td> <td>2, 80</td> <td>3, 100</td> <td>4, 137</td> <td>6, 110</td> </tr> <tr> <td></td> <td>M</td> <td>D</td> <td>D</td> <td>D</td> <td>M</td> <td>D</td> </tr> </table> <p>TEXTURE:</p> <table border="1"> <tr> <td>Sand</td> <td>50</td> <td>—</td> <td>—</td> <td>—</td> <td>70</td> <td>—</td> </tr> <tr> <td>Silt</td> <td>20</td> <td>55</td> <td>60</td> <td>50</td> <td>20</td> <td>50</td> </tr> <tr> <td>Clay</td> <td>30</td> <td>45</td> <td>40</td> <td>50</td> <td>10</td> <td>50</td> </tr> </table> <p>COMPOSITION:</p> <table border="1"> <tr> <td>Quartz</td> <td>—</td> <td>1</td> <td>—</td> <td>—</td> <td>1</td> <td>1</td> </tr> <tr> <td>Feldspar</td> <td>1</td> <td>—</td> <td>—</td> <td>—</td> <td>—</td> <td>1</td> </tr> <tr> <td>Clay</td> <td>28</td> <td>44</td> <td>34</td> <td>49</td> <td>10</td> <td>48</td> </tr> <tr> <td>Volcanic glass</td> <td>50</td> <td>—</td> <td>—</td> <td>—</td> <td>73</td> <td>—</td> </tr> <tr> <td>Accessory minerals</td> <td>—</td> <td>—</td> <td>Tr</td> <td>—</td> <td>—</td> <td>—</td> </tr> <tr> <td>Glauconite</td> <td>1</td> <td>—</td> <td>—</td> <td>—</td> <td>—</td> <td>—</td> </tr> <tr> <td>Pyrite</td> <td>—</td> <td>—</td> <td>—</td> <td>—</td> <td>10</td> <td>—</td> </tr> <tr> <td>Diatoms</td> <td>10</td> <td>40</td> <td>50</td> <td>25</td> <td>5</td> <td>30</td> </tr> <tr> <td>Radiolarians</td> <td>5</td> <td>10</td> <td>10</td> <td>10</td> <td>—</td> <td>10</td> </tr> <tr> <td>Sponge spicules</td> <td>5</td> <td>5</td> <td>5</td> <td>5</td> <td>1</td> <td>5</td> </tr> <tr> <td>Silicoflagellates</td> <td>—</td> <td>—</td> <td>1</td> <td>10</td> <td>—</td> <td>5</td> </tr> </table>		1, 7	1, 85	2, 80	3, 100	4, 137	6, 110		M	D	D	D	M	D	Sand	50	—	—	—	70	—	Silt	20	55	60	50	20	50	Clay	30	45	40	50	10	50	Quartz	—	1	—	—	1	1	Feldspar	1	—	—	—	—	1	Clay	28	44	34	49	10	48	Volcanic glass	50	—	—	—	73	—	Accessory minerals	—	—	Tr	—	—	—	Glauconite	1	—	—	—	—	—	Pyrite	—	—	—	—	10	—	Diatoms	10	40	50	25	5	30	Radiolarians	5	10	10	10	—	10	Sponge spicules	5	5	5	5	1	5	Silicoflagellates	—	—	1	10	—	5
	1, 7	1, 85	2, 80	3, 100	4, 137	6, 110																																																																																																																					
	M	D	D	D	M	D																																																																																																																					
Sand	50	—	—	—	70	—																																																																																																																					
Silt	20	55	60	50	20	50																																																																																																																					
Clay	30	45	40	50	10	50																																																																																																																					
Quartz	—	1	—	—	1	1																																																																																																																					
Feldspar	1	—	—	—	—	1																																																																																																																					
Clay	28	44	34	49	10	48																																																																																																																					
Volcanic glass	50	—	—	—	73	—																																																																																																																					
Accessory minerals	—	—	Tr	—	—	—																																																																																																																					
Glauconite	1	—	—	—	—	—																																																																																																																					
Pyrite	—	—	—	—	10	—																																																																																																																					
Diatoms	10	40	50	25	5	30																																																																																																																					
Radiolarians	5	10	10	10	—	10																																																																																																																					
Sponge spicules	5	5	5	5	1	5																																																																																																																					
Silicoflagellates	—	—	1	10	—	5																																																																																																																					
R/G B					$\gamma = 1.37 \phi = 79$ \downarrow -1764																																																																																																																						
B					\bullet 0%																																																																																																																						
R/P		NSR2			$\gamma = 1.37 \phi = 84$ \downarrow -1718																																																																																																																						
C/P					\bullet 0.1%																																																																																																																						
F/G/F/G					$\gamma = 1.37 \phi = 78$ \downarrow -1767																																																																																																																						
					\bullet 0.4%																																																																																																																						
CC																																																																																																																											

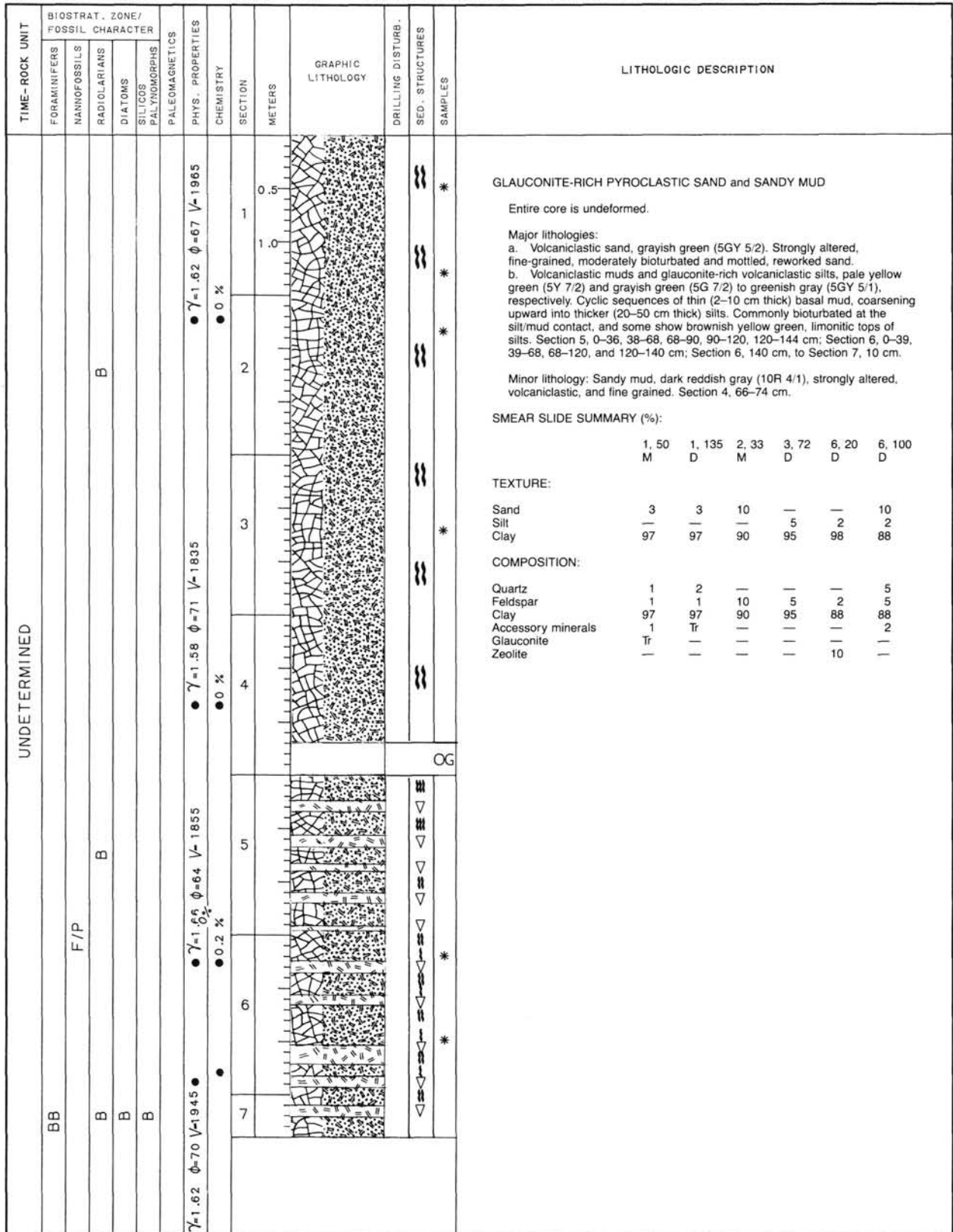


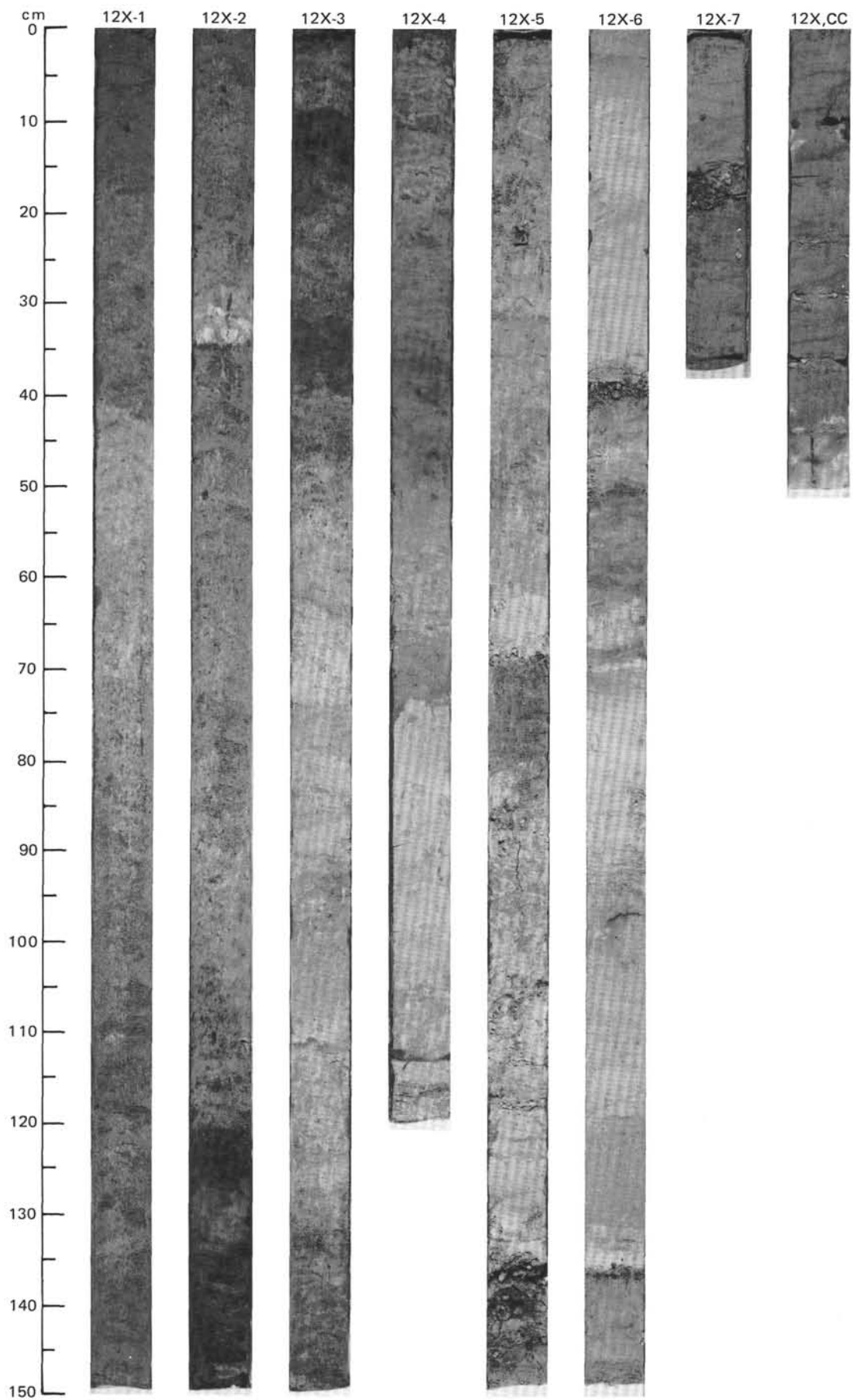
SITE 642 HOLE D CORE 11X CORED INTERVAL 1562.8-1572.5 mbsl; 276.80-286.50 mbsf

TIME-ROCK UNIT	BIOSTRAT. ZONE/ FOSSIL CHARACTER					CHEMISTRY	SECTION	METERS	GRAPHIC LITHOLOGY	DRILLING DISTURB.	SED. STRUCTURES	SAMPLES	LITHOLOGIC DESCRIPTION																																																																																			
	FORAMINIFERS	NANNOFOSSILS	RADIOLARIANS	DIATOMS	SILICOS PALYNOFORMPHS									PALEOMAGNETICS	PHYS. PROPERTIES																																																																																	
LOWER MIOCENE	BB						1 0.5 1.0 2 C					<p>SILICEOUS MUD and GLAUCONITE-RICH PYROCLASTIC SAND and SANDY MUD</p> <p>Entire core is undeformed.</p> <p>Major lithologies:</p> <p>a. Siliceous mud, dark olive gray (5Y 3/2), moderately bioturbated. Section 1, 0-78 and 87-88 cm.</p> <p>b. Glauconite-rich pyroclastic sandstone, black (5Y 2.5/1), well lithified, with horizontal and low-angle cross-stratification. Section 1, 94-104 cm.</p> <p>c. Glauconite-rich sand, olive gray (5Y 5/2), composed of reworked pyroclastics. Section 1, 104-136 cm.</p> <p>d. Glauconite-rich sand and sandy mud, dusky yellow green (5GY 3/2), composed of moderately bioturbated pyroclastics. Section 1, 136 cm, to Section 2, 128 cm. Sharp-based, upward-fining sequence above Section 2, 56 cm.</p> <p>A MAJOR UNCONFORMITY OCCURS AT SECTION 1, 94 CM.</p> <p>Minor lithologies:</p> <p>a. Volcanic ash, dark gray (5Y 4/1) to very dark gray (5Y 3/1). Section 1, 78-87 and 88-94 cm.</p> <p>b. Sandy mud, white (2.5Y 8/2), with gradational color change downcore. Section 2, 128-132 cm.</p> <p>c. Volcaniclastic sand, grayish green (5GY 5/2), moderately bioturbated and strongly altered. CC, 0-32 cm.</p> <p>SMEAR SLIDE SUMMARY (%):</p> <table border="1"> <tr> <td></td> <td>1, 43</td> <td>1, 85</td> <td>1, 92</td> <td>1, 107</td> <td>2, 127</td> </tr> <tr> <td></td> <td>D</td> <td>M</td> <td>M</td> <td>D</td> <td>M</td> </tr> </table> <p>TEXTURE:</p> <table border="1"> <tr> <td>Sand</td> <td>—</td> <td>80</td> <td>80</td> <td>20</td> <td>—</td> </tr> <tr> <td>Silt</td> <td>15</td> <td>20</td> <td>20</td> <td>20</td> <td>2</td> </tr> <tr> <td>Clay</td> <td>85</td> <td>—</td> <td>—</td> <td>60</td> <td>98</td> </tr> </table> <p>COMPOSITION:</p> <table border="1"> <tr> <td>Quartz</td> <td>—</td> <td>—</td> <td>—</td> <td>20</td> <td>1</td> </tr> <tr> <td>Feldspar</td> <td>—</td> <td>—</td> <td>1</td> <td>—</td> <td>—</td> </tr> <tr> <td>Clay</td> <td>85</td> <td>90</td> <td>94</td> <td>55</td> <td>98</td> </tr> <tr> <td>Accessory minerals</td> <td>—</td> <td>—</td> <td>—</td> <td>5</td> <td>1</td> </tr> <tr> <td>Pyrite</td> <td>—</td> <td>10</td> <td>5</td> <td>—</td> <td>—</td> </tr> <tr> <td>Goethite</td> <td>—</td> <td>—</td> <td>—</td> <td>20</td> <td>—</td> </tr> <tr> <td>Diatoms</td> <td>10</td> <td>Tr</td> <td>—</td> <td>—</td> <td>—</td> </tr> <tr> <td>Radiolarians</td> <td>2</td> <td>—</td> <td>—</td> <td>—</td> <td>—</td> </tr> <tr> <td>Sponge spicules</td> <td>3</td> <td>—</td> <td>—</td> <td>—</td> <td>—</td> </tr> </table>		1, 43	1, 85	1, 92	1, 107	2, 127		D	M	M	D	M	Sand	—	80	80	20	—	Silt	15	20	20	20	2	Clay	85	—	—	60	98	Quartz	—	—	—	20	1	Feldspar	—	—	1	—	—	Clay	85	90	94	55	98	Accessory minerals	—	—	—	5	1	Pyrite	—	10	5	—	—	Goethite	—	—	—	20	—	Diatoms	10	Tr	—	—	—	Radiolarians	2	—	—	—	—	Sponge spicules	3	—	—	—	—
		1, 43	1, 85	1, 92	1, 107	2, 127																																																																																										
		D	M	M	D	M																																																																																										
	Sand	—	80	80	20	—																																																																																										
Silt	15	20	20	20	2																																																																																											
Clay	85	—	—	60	98																																																																																											
Quartz	—	—	—	20	1																																																																																											
Feldspar	—	—	1	—	—																																																																																											
Clay	85	90	94	55	98																																																																																											
Accessory minerals	—	—	—	5	1																																																																																											
Pyrite	—	10	5	—	—																																																																																											
Goethite	—	—	—	20	—																																																																																											
Diatoms	10	Tr	—	—	—																																																																																											
Radiolarians	2	—	—	—	—																																																																																											
Sponge spicules	3	—	—	—	—																																																																																											



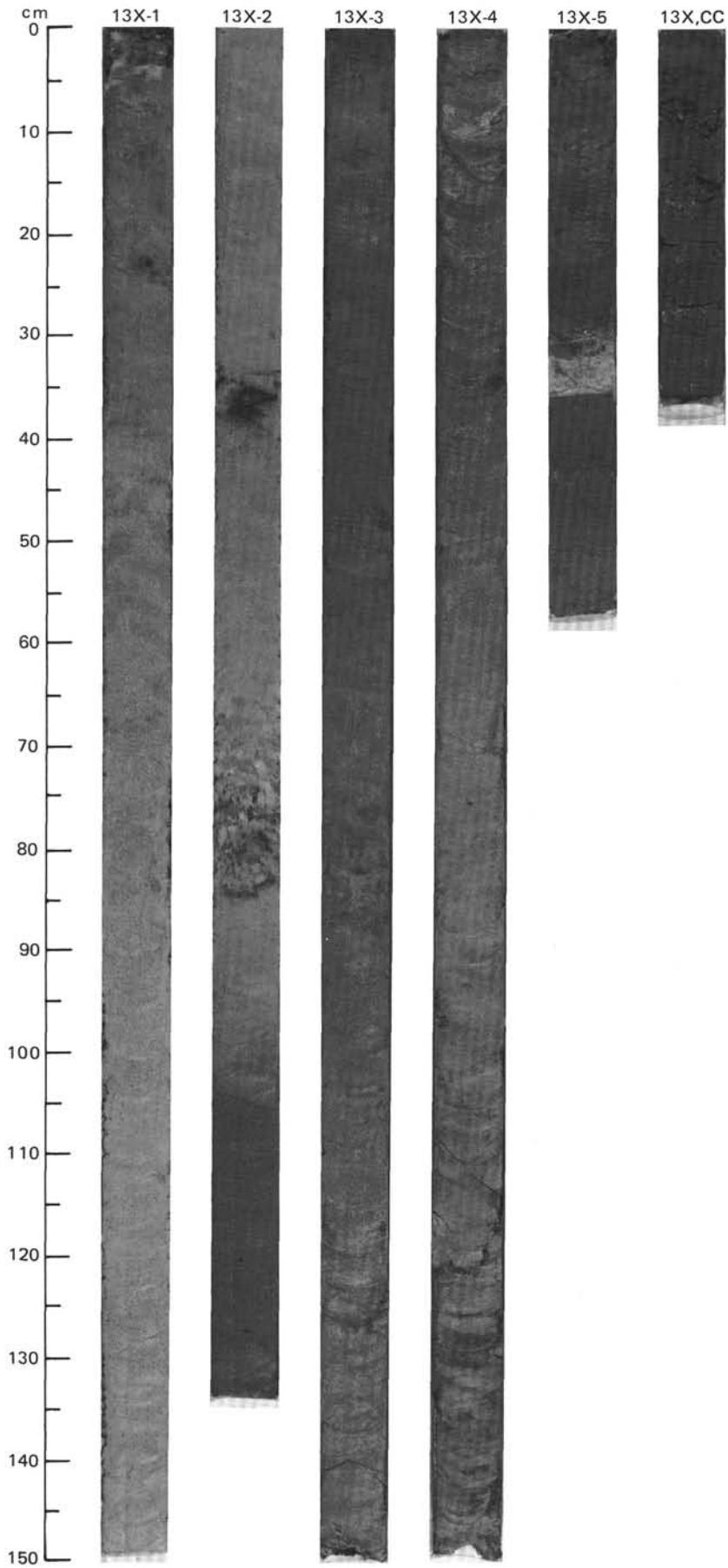
SITE 642 HOLE D CORE 12X CORED INTERVAL 1572.5-1582.2 mbsl; 286.50-296.20 mbsf





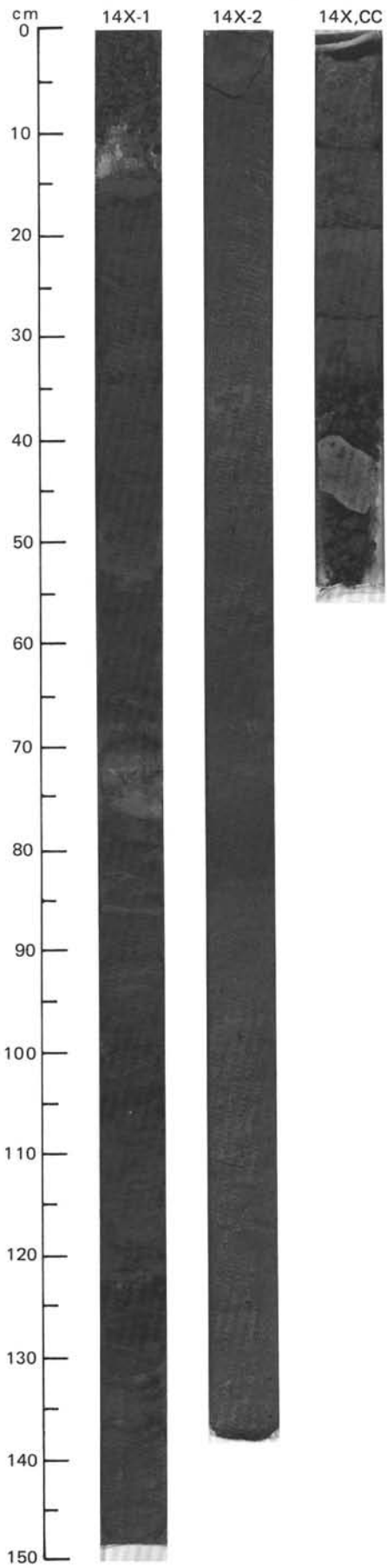
SITE 642 HOLE D CORE 13X CORED INTERVAL 1582.2-1591.8 mbsl; 296.20-305.80 mbsf

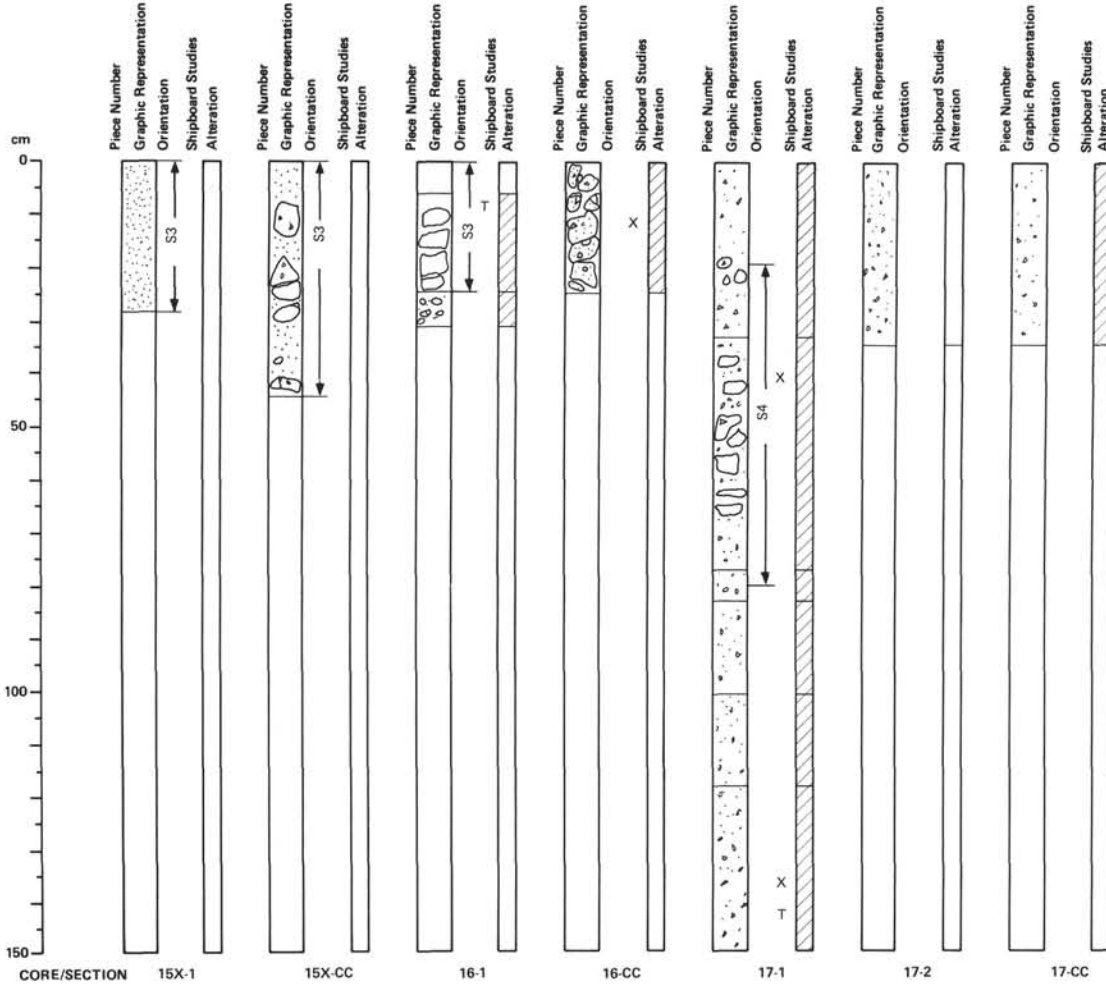
TIME-ROCK UNIT	BIOSTRAT. ZONE/ FOSSIL CHARACTER					PHYS. PROPERTIES	CHEMISTRY	SECTION	METERS	GRAPHIC LITHOLOGY	DRILLING DISTURB.	SED. STRUCTURES	SAMPLES	LITHOLOGIC DESCRIPTION																																															
	FORAMINIFERS	NANNOFOSSILS	RADIOLARIANS	DIATOMS	SILICCS PALYMONORPHS																																																								
UPPER EOCENE	BB					$\gamma = 1.55 \phi = 72 \quad V = 1737$ ● 0 %		1	0.5				<p>GLAUCONITE-RICH VOLCANICLASTIC SANDY MUD</p> <p>Entire core is undeformed.</p> <p>Major lithologies:</p> <p>a. Glauconite-rich volcaniclastic sandy mud, greenish gray (5GY 6/1), moderately bioturbated and mottled. Section 1 to Section 2, 105 cm.</p> <p>b. Glauconite-rich volcaniclastic sandy mud, very dark gray (5Y 4/1 to 5Y 3/1), with abundant small patches of zeolite. Section 2, 105 cm, to CC.</p> <p>Minor lithology: Volcanic ash, light gray (10YR 7/1) to gray (10YR 6/1), completely recrystallized to clay. Section 5, 32-36 cm.</p> <p>SMEAR SLIDE SUMMARY (%):</p> <table border="1"> <tr> <td></td> <td>2, 21</td> <td>2, 78</td> <td>2, 122</td> <td>4, 76</td> <td>5, 35</td> </tr> <tr> <td></td> <td>D</td> <td>M</td> <td>D</td> <td>D</td> <td>M</td> </tr> </table> <p>TEXTURE:</p> <table border="1"> <tr> <td>Sand</td> <td>1</td> <td>1</td> <td>—</td> <td>—</td> <td>—</td> </tr> <tr> <td>Silt</td> <td>10</td> <td>2</td> <td>12</td> <td>10</td> <td>6</td> </tr> <tr> <td>Clay</td> <td>89</td> <td>97</td> <td>88</td> <td>90</td> <td>94</td> </tr> </table> <p>COMPOSITION:</p> <table border="1"> <tr> <td>Feldspar</td> <td>11</td> <td>3</td> <td>2</td> <td>10</td> <td>1</td> </tr> <tr> <td>Clay</td> <td>89</td> <td>97</td> <td>88</td> <td>90</td> <td>94</td> </tr> </table> <p>Accessory minerals:</p> <table border="1"> <tr> <td>Zeolite</td> <td>—</td> <td>—</td> <td>10</td> <td>—</td> <td>5</td> </tr> </table>		2, 21	2, 78	2, 122	4, 76	5, 35		D	M	D	D	M	Sand	1	1	—	—	—	Silt	10	2	12	10	6	Clay	89	97	88	90	94	Feldspar	11	3	2	10	1	Clay	89	97	88	90	94	Zeolite	—	—	10	—	5
		2, 21	2, 78	2, 122	4, 76		5, 35																																																						
		D	M	D	D		M																																																						
	Sand	1	1	—	—		—																																																						
	Silt	10	2	12	10		6																																																						
Clay	89	97	88	90	94																																																								
Feldspar	11	3	2	10	1																																																								
Clay	89	97	88	90	94																																																								
Zeolite	—	—	10	—	5																																																								
B			B				2	1.0			*																																																		
B			B				3				*																																																		
B R/P			<i>C. dispersum</i>				4				*																																																		
			Zone				5				*																																																		
			PM7				CC																																																						



SITE 642 HOLE D CORE 14X CORED INTERVAL 1591.8-1601.4 mbsi; 305.80-315.40 mbsf

TIME-ROCK UNIT	BIOSTRAT. ZONE/ FOSSIL CHARACTER					PHYS. PROPERTIES	CHEMISTRY	SECTION	METERS	GRAPHIC LITHOLOGY	DRILLING DISTURB.	SED. STRUCTURES	SAMPLES	LITHOLOGIC DESCRIPTION																																																	
	FORAMINIFERS	MAMMOFOSILS	RADIOLARIANS	DIATOMS	SILICES PALYNOFORMS																																																										
UPPER EOCENE	B B	NN 6-1	R/P			<p>● $\gamma = 1.63$ $\phi = 68$ $V = 1.855$</p> <p>● 0.4 %</p>		1	0.5 1.0			*	<p>VOLCANICLASTIC SANDY MUD</p> <p>Moderate disturbance in Section 1, 0-15 cm. Remainder of core is undeformed.</p> <p>Major lithology: Volcaniclastic sandy mud, very dark gray (5Y 3/1), locally rich in glauconite, containing some clays and zeolites. Section 1 to CC, 33 cm.</p> <p>Minor lithologies:</p> <p>a. Basalt fragments, weathered and limonitic. Basalt is phenocryst-free, slightly vesicular (1-2%). CC, 33-40 cm.</p> <p>b. Basalt fragment, gray, vesicular, and strongly altered, with all mafic minerals replaced by smectites, some plagioclases replaced by zeolites. CC, 40-50 cm.</p> <p>SMEAR SLIDE SUMMARY (%):</p> <table border="1"> <tr> <td></td> <td>1, 25</td> <td>1, 73</td> <td>1, 127</td> <td>2, 100</td> </tr> <tr> <td></td> <td>D</td> <td>M</td> <td>M</td> <td>D</td> </tr> </table> <p>TEXTURE:</p> <table border="1"> <tr> <td>Sand</td> <td>—</td> <td>—</td> <td>—</td> <td>1</td> </tr> <tr> <td>Silt</td> <td>10</td> <td>5</td> <td>1</td> <td>20</td> </tr> <tr> <td>Clay</td> <td>90</td> <td>95</td> <td>99</td> <td>79</td> </tr> </table> <p>COMPOSITION:</p> <table border="1"> <tr> <td>Quartz</td> <td>—</td> <td>—</td> <td>—</td> <td>5</td> </tr> <tr> <td>Feldspar</td> <td>5</td> <td>5</td> <td>1</td> <td>15</td> </tr> <tr> <td>Clay</td> <td>88</td> <td>75</td> <td>99</td> <td>80</td> </tr> </table> <p>Accessory minerals:</p> <table border="1"> <tr> <td>Pyrite</td> <td>2</td> <td>—</td> <td>—</td> <td>—</td> </tr> <tr> <td>Zeolite</td> <td>5</td> <td>20</td> <td>—</td> <td>—</td> </tr> </table>		1, 25	1, 73	1, 127	2, 100		D	M	M	D	Sand	—	—	—	1	Silt	10	5	1	20	Clay	90	95	99	79	Quartz	—	—	—	5	Feldspar	5	5	1	15	Clay	88	75	99	80	Pyrite	2	—	—	—	Zeolite	5	20	—	—
	1, 25	1, 73	1, 127	2, 100																																																											
	D	M	M	D																																																											
Sand	—	—	—	1																																																											
Silt	10	5	1	20																																																											
Clay	90	95	99	79																																																											
Quartz	—	—	—	5																																																											
Feldspar	5	5	1	15																																																											
Clay	88	75	99	80																																																											
Pyrite	2	—	—	—																																																											
Zeolite	5	20	—	—																																																											
								2		BASALT		*																																																			





UNIT S3

~315.4~ 316.1 MBSF 642D-15X-1 (0 cm) TO 16X-1 (24 cm)

CONGLOMERATE, PARTLY OXIDIZED, SUBROUNDED TO ROUNDED PEBBLES. Pebbles are <30 cm in size. Components: vesicular, fine-grained basalt, aphyric, sparsely vesicular, phryic basalt; pale green coarse-grained basalt, fine-grained basalt with chilled margin and pockets filled by pale green tuff; carbonaceous tuff, light brown basaltic lapillistone; quartzofeldspathic biotite gneiss; slate, biotite rich; pyrite rich, fine-grained sediment.

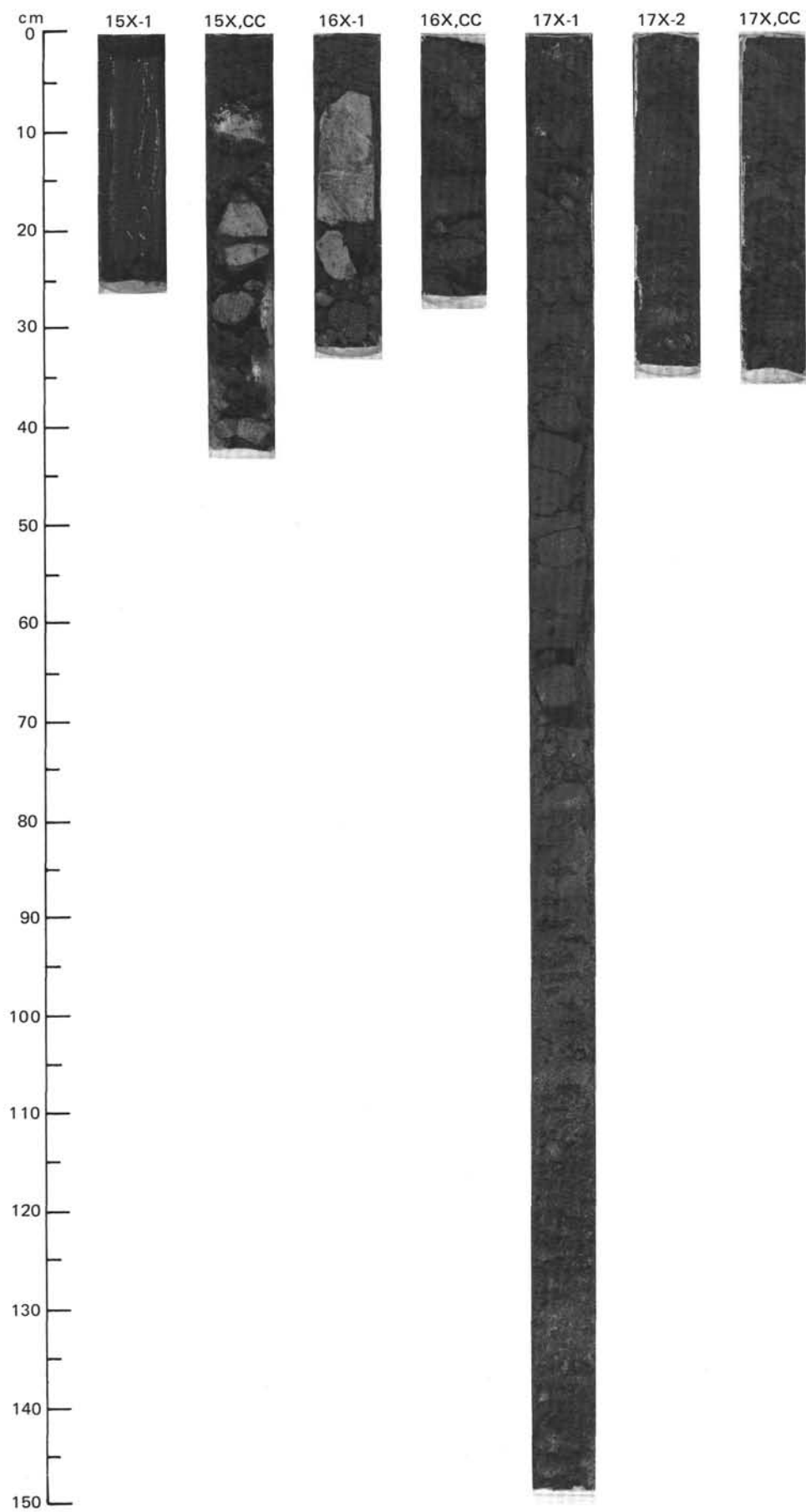
UNIT S4

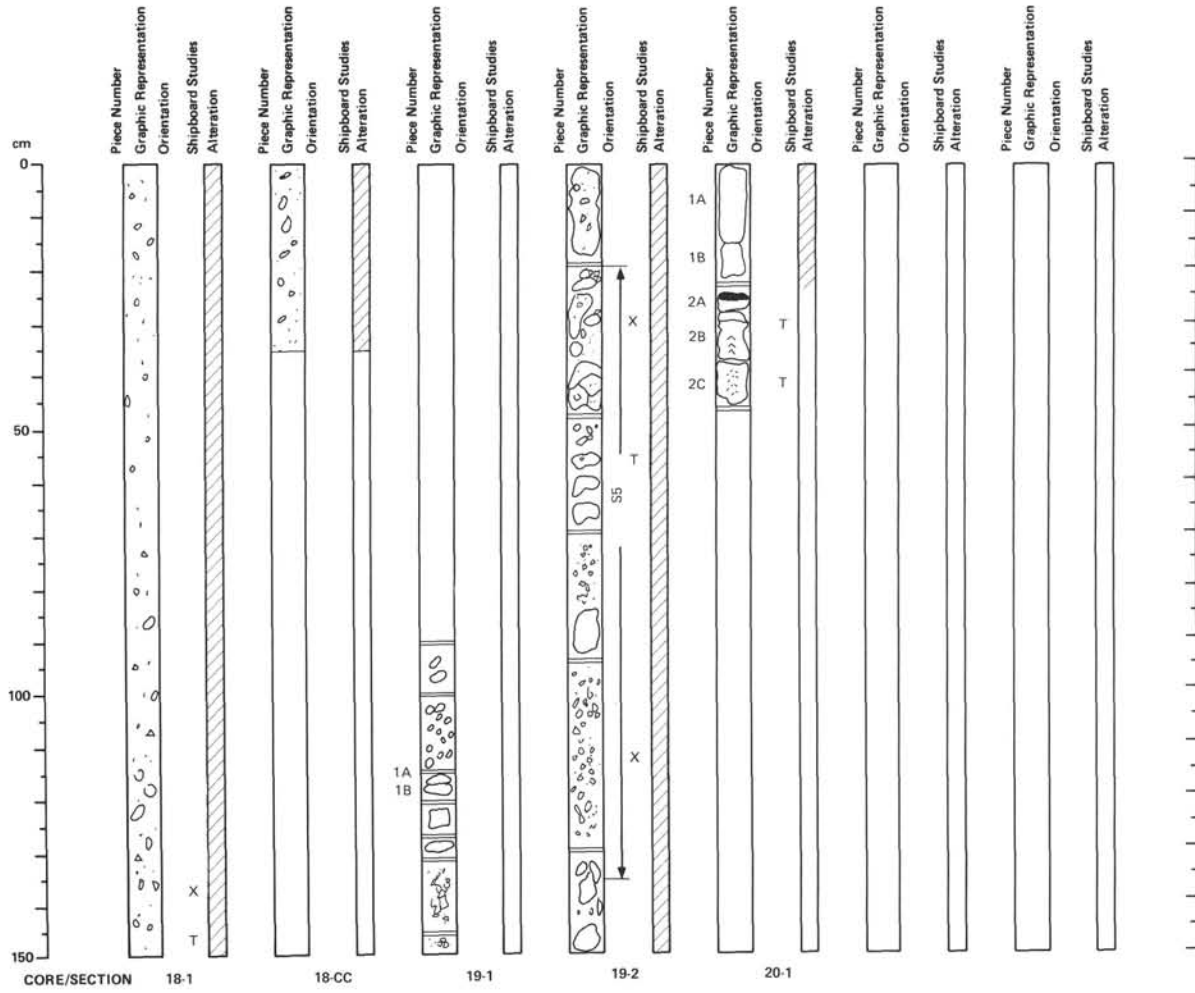
~316.5~ 317.1 MBSF 642D-17X-1 (20 cm) TO 17X-1 (80 cm)

TUFF, LAPILLI TUFF, AND LAPILLISTONE. Color is dark red to dark red brown, with basaltic scoria, red brown tuff, brownish yellow pumice, feldspar, coarse-grained basalt.

UNIDENTIFIED DRILLING RUBBLE

~317.1~ 328 MBSF 642D-17X-1 (80 cm) TO 19N-2 (25 cm)





UNIT S5(?)

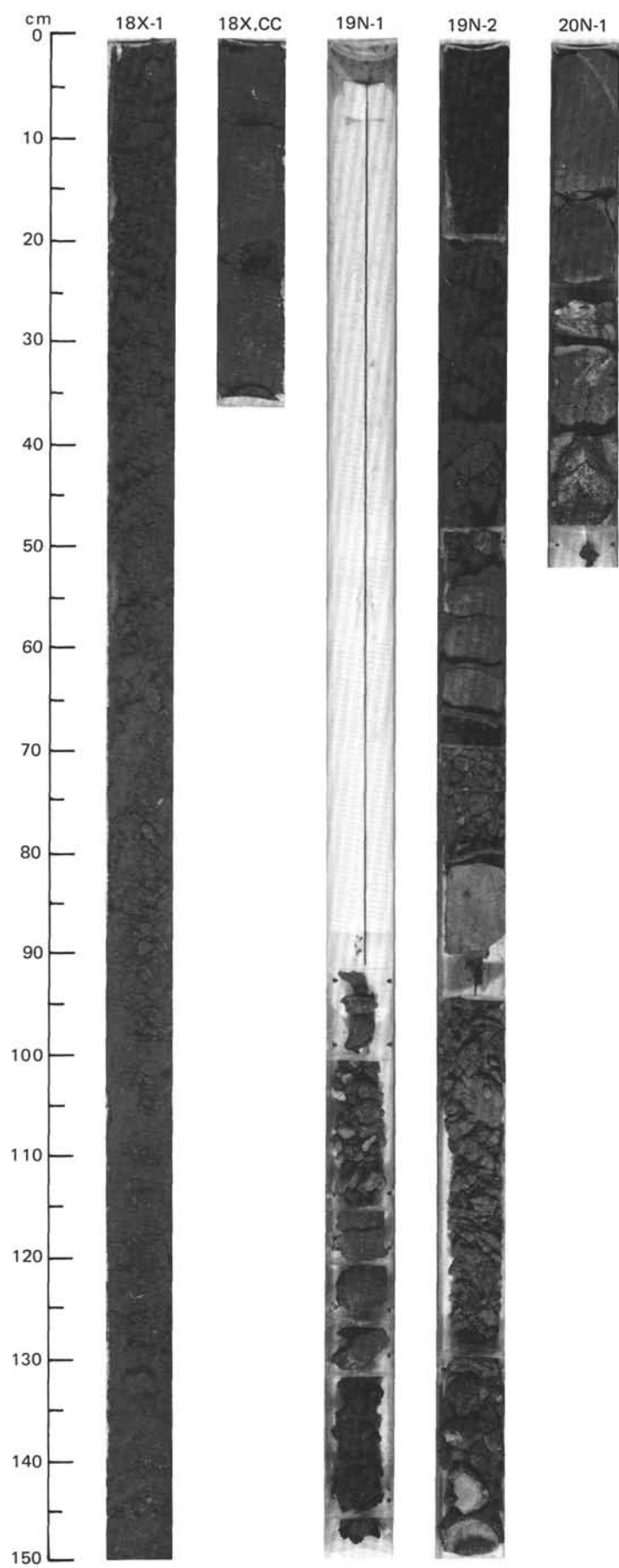
- 328-329 MBSF 642D-19N-2 (25 cm) TO 19N-2 (130 cm)

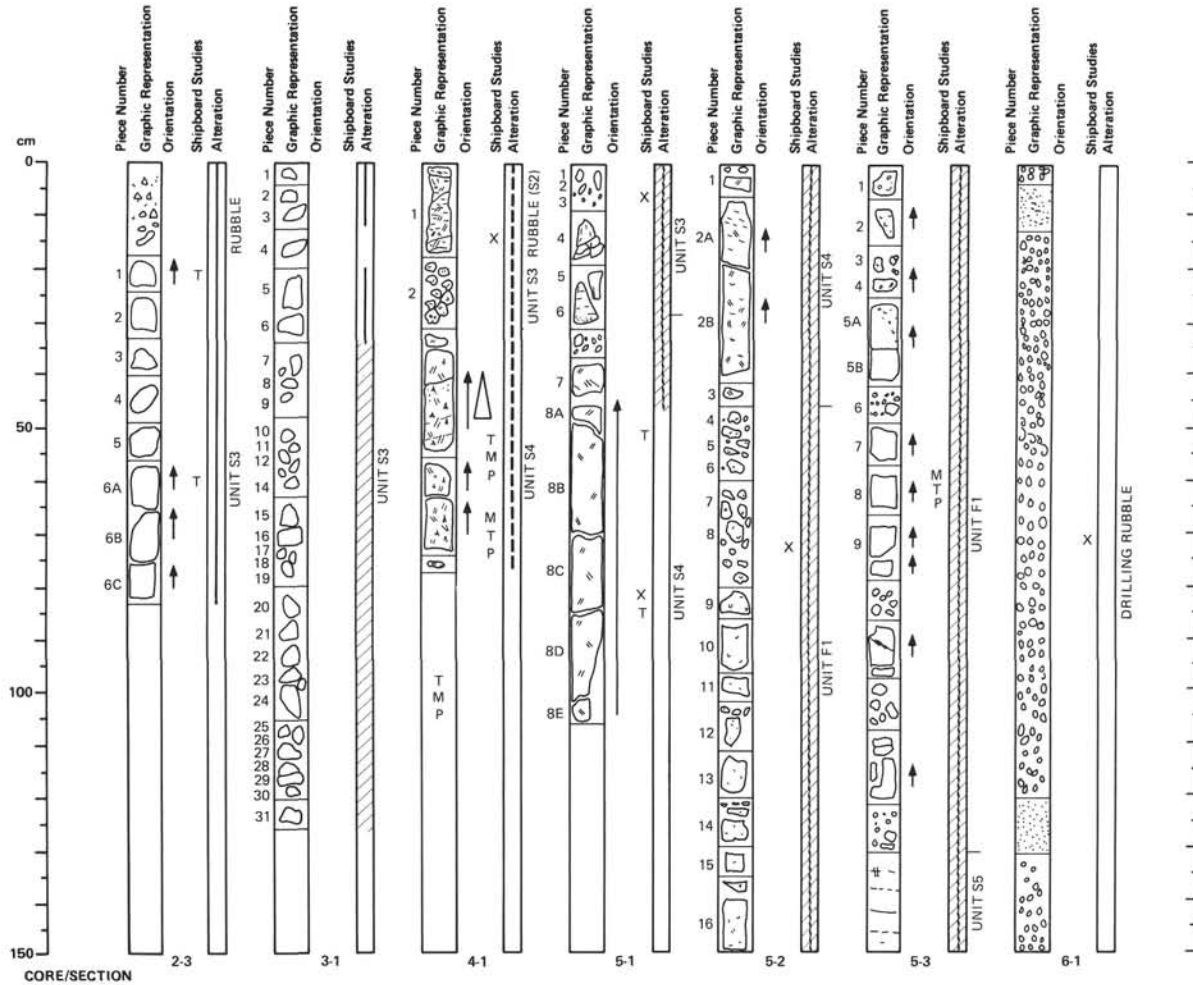
FINE-GRAINED BASALTIC VITRIC TUFF. Dark red brown to yellowish red brown fine-grained basaltic vitric tuff, median clast size <0.1 mm, containing angular to round fragments. Few subunits with gradational contacts, and horizontal bedding.

UNIDENTIFIED DRILLING RUBBLE

- 329- 329.9 MBSF 642D-19N-2 (130 cm) TO 20N-1 (47 cm)

PSEUDOTACHYLITE. Drilling induced alteration.





UNIT S3
 ~320.0--330.0 MBSF 642E-2W-3 (18 cm) TO 4R-1 (31 cm)
CONGLOMERATE, PARTLY OXIDIZED, SUBROUNDED TO ROUNDED PEBBLES. Pebbles are < 30 cm in size. Components: vesicular, fine-grained basalt, aphyric, sparsely vesicular, phyric basalt; pale green coarse-grained basalt, fine-grained basalt with chilled margin and pockets filled by pale green tuff; carbonaceous tuff, light brown basaltic lapillistone; quartzofeldspathic biotite gneiss; slate, biotite rich; pyrite rich, fine-grained sediment.

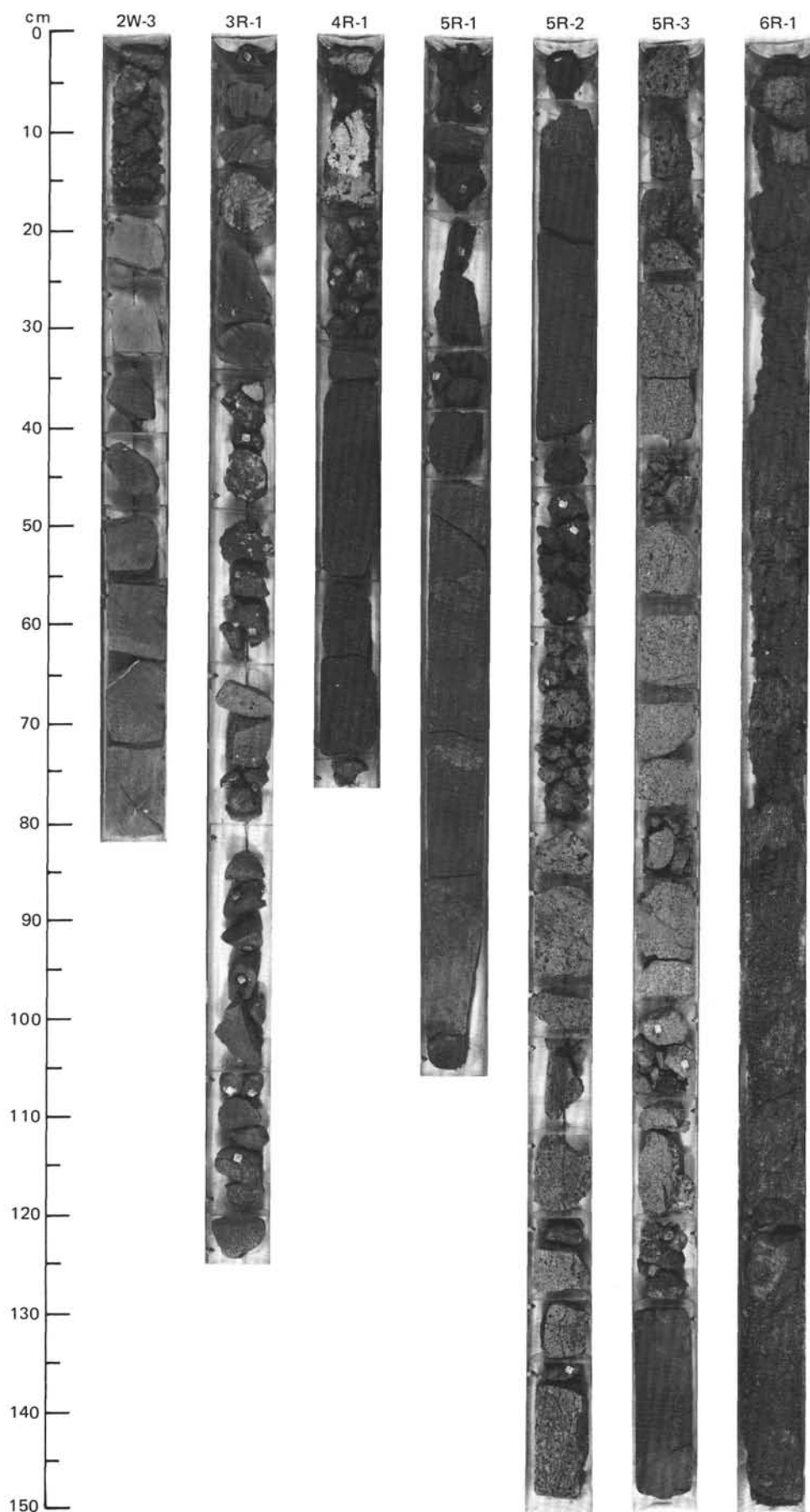
UNIT S4
 ~330.0-336.9 MBSF 642E-4R-1 (31 cm) TO 5R-2 (46 cm)
TUFF, LAPILLI TUFF, AND LAPILLISTONE. Color is dark red to dark red brown, with basaltic scoria, red brown tuff, brownish yellow pumice, feldspar, coarse-grained basalt.

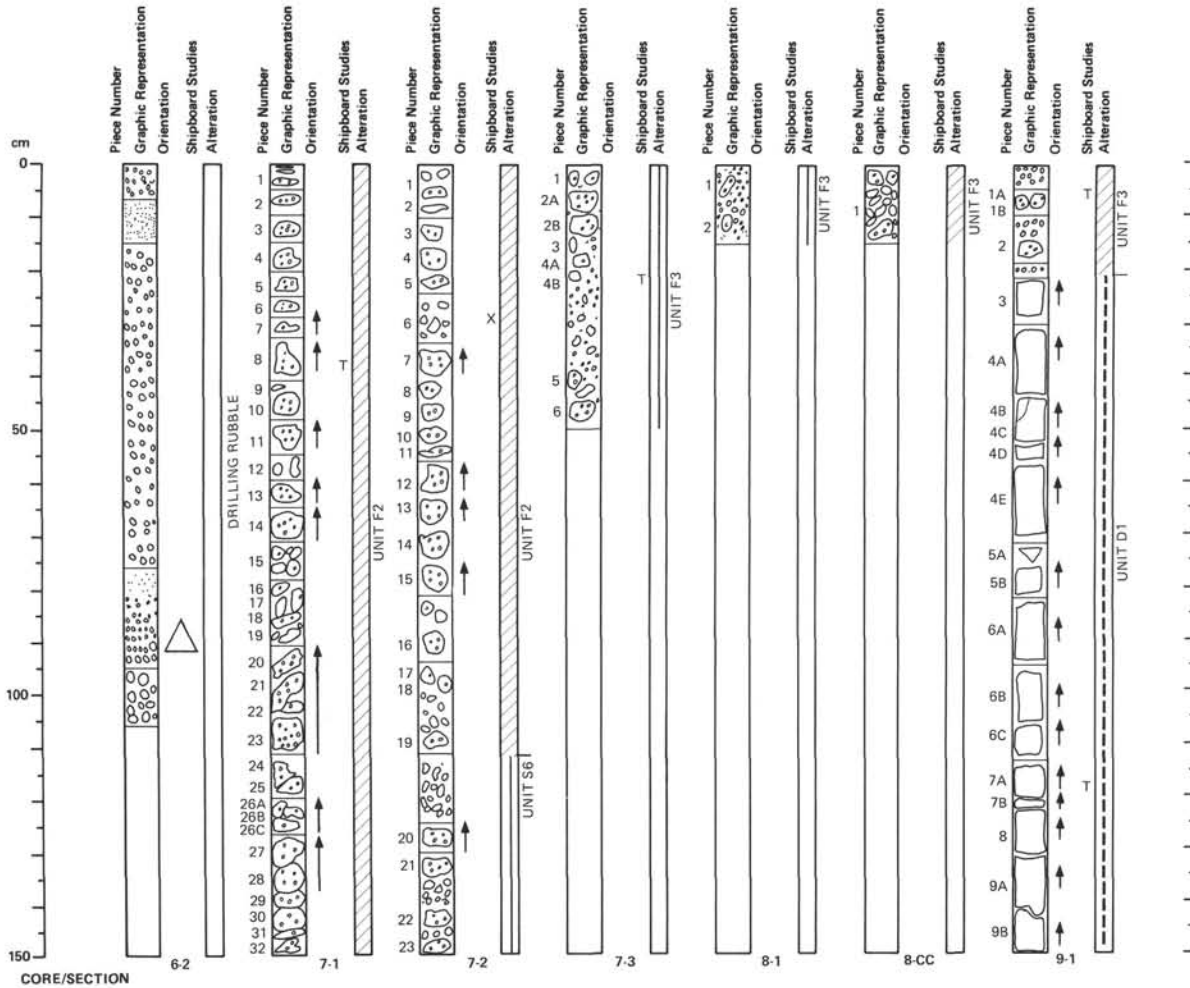
UNIT F1
 336.9-339.2 MBSF 642E-5R-2 (46 cm) TO 5R-3 (129 cm)
HIGHLY ALTERED, SPARSELY PLAGIOCLASE, PHYRIC GRAY GREEN BASALT FLOW. Moderately vesicular, but locally nonvesicular, coated with yellow limonite and filled with red clay. Hairline cracks throughout.

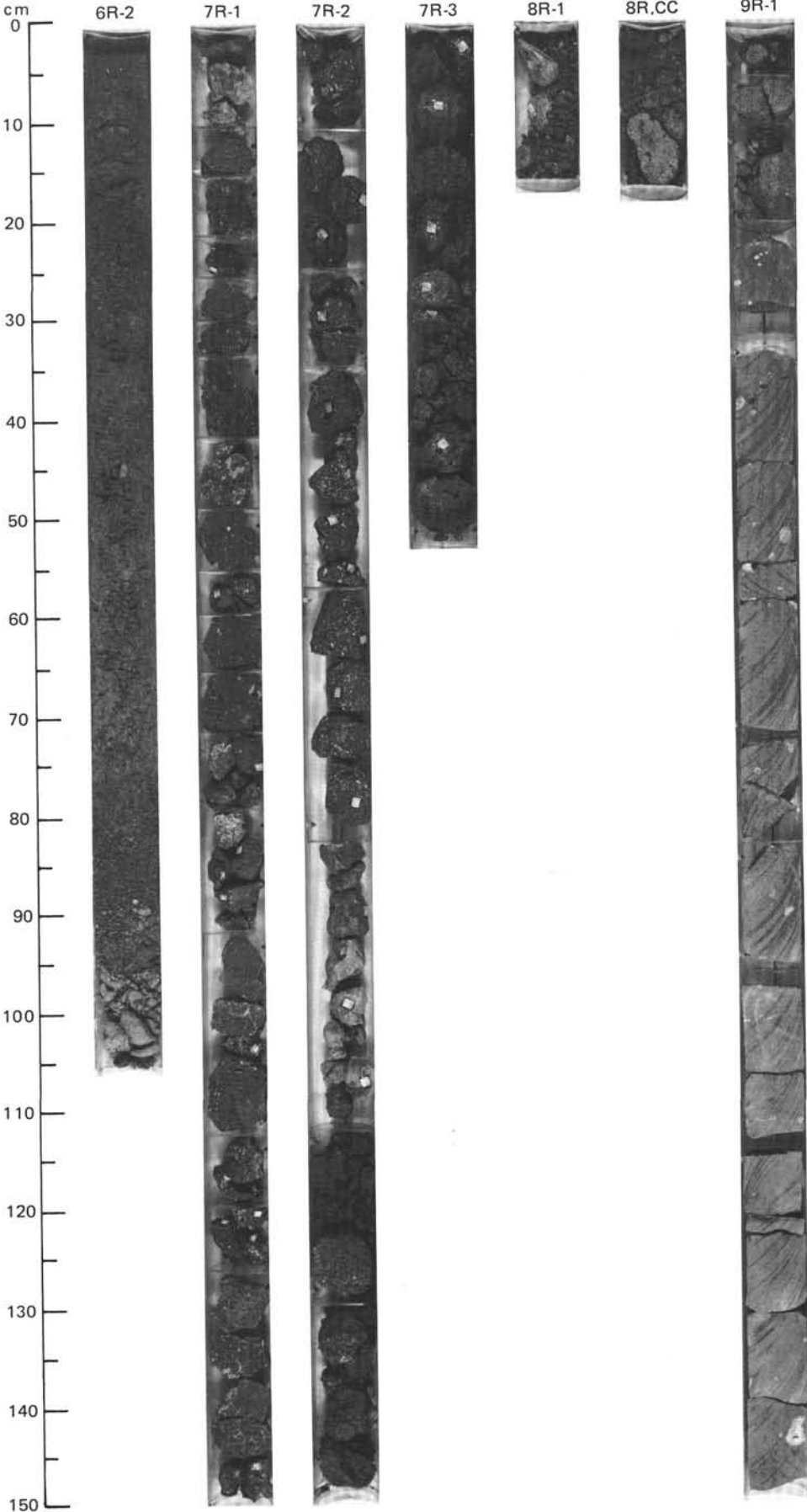
THIN SECTION DESCRIPTION
 642E-5R-3 (Piece 8, 61-63 cm): virtually completely altered to smectites and iddingsite; relict variolitic groundmass.

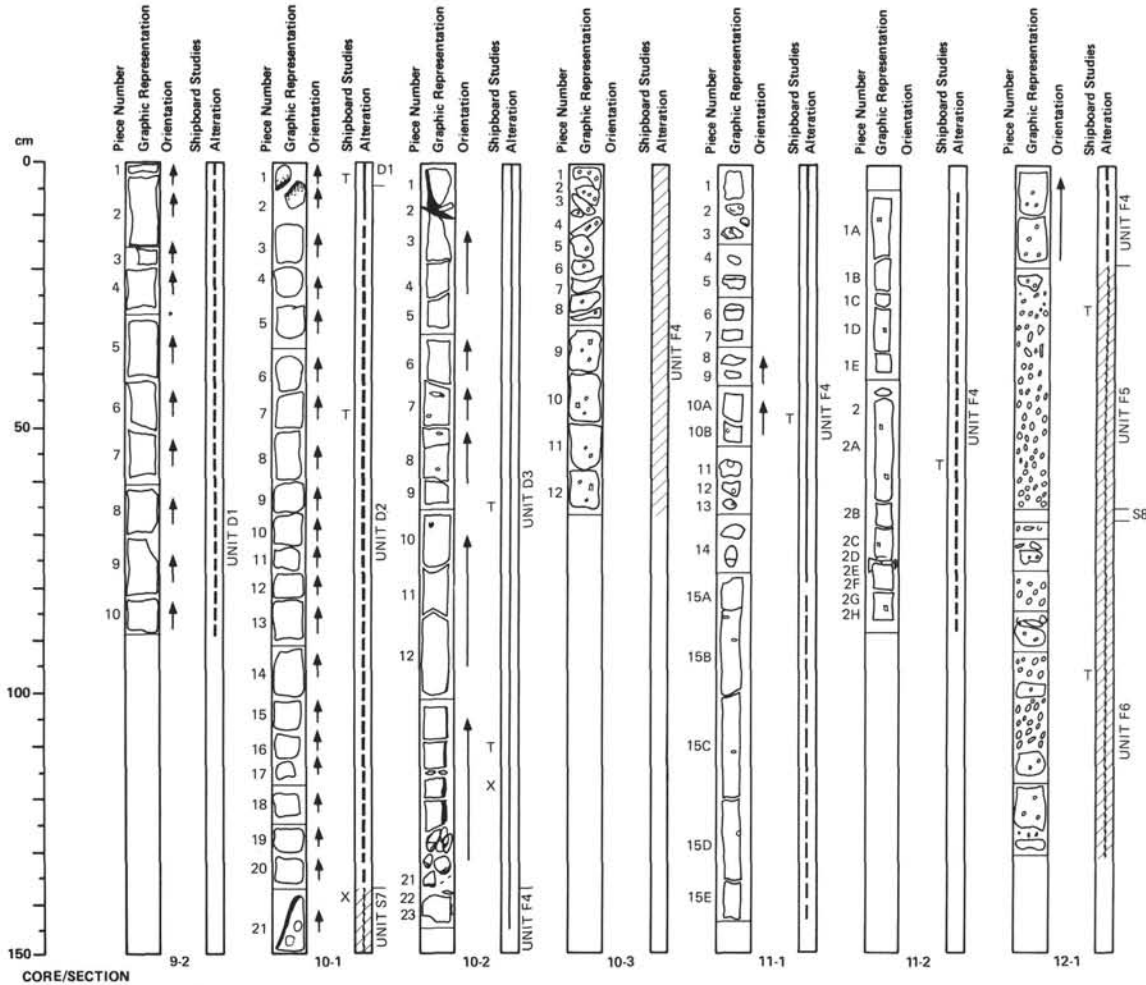
UNIT S5
 339.2-339.4 MBSF 642E-5R-3 (129 cm) TO 5R-3 (150 cm)
FINE-GRAINED BASALTIC VITRIC TUFF. Dark red brown to yellowish red brown fine-grained basaltic vitric tuff, median clast size < 0.1 mm, containing angular to round fragments. Few subunits with gradational contacts, and horizontal bedding.

UNIDENTIFIED DRILLING RUBBLE
 339.4-354.3 MBSF 642E-6R-1 (0 cm) TO 6R-2 (105 cm)









UNIT D1
366.0–375.4 MBSF 642E–9R–1 (22 cm) TO 10R–1 (4 cm)

FINE-GRAINED, SPARSELY PHYRIC, DARK GRAY BASALT. Moderately to sparsely vesicular. Vesicles filled with calcite and dark green smectite rims, or open. Some light gray green smectite and fine dark green smectite alteration in groundmass. Native copper present in 9R–1, Piece 5b. 10R–1, Piece 1, contains smectite-rich zone that may be a chilled margin or zone of tectonic shear.

UNIT D2
375.4–379.2 MBSF 642E–10R–1 (4 cm) TO 10R–1 (137 cm)

FINE-GRAINED, APHYRIC, DARK GRAY BASALT. Moderately vesicular, with vesicles filled by calcite, or rimmed by dark green or dark brown smectite. Iddingsite pseudomorphs after olivine locally glomeroporphyritic. 10R–1, Piece 2, contains smectite-rich zones that may be a chilled margin or zone of tectonic shear.

THIN SECTION DESCRIPTION

642E–10R–1 (Piece 7, 47–49 cm): 50% plagioclase, 15% clinopyroxene, 3% opaques, <5% altered olivine, 15% altered groundmass and glass. Intergranular, subophitic, variolitic.

UNIT S7
379.2–379.7 MBSF 642E–10R–1 (140 cm) TO 10R–1 (150 cm)
HIGHLY ALTERED, CRYSTAL-BEARING TUFF. Dark olive gray, possibly tectonic, at contact to overlying unit; pale brown, highly fragmented away from contact.

UNIT D3
379.7–381.0 MBSF 642E–10R–2 (0 cm) TO 10R–2 (137 cm)
FINE-GRAINED, SPARSELY OLIVINE PHYRIC BASALT. Very fine-grained smectite-rich zone at 8–10 cm, possibly an inclined chilled margin or tectonic shear zone. Sparsely vesicular, with green smectite and calcite fillings. Subparallel, dark streaking (flow fabric) throughout unit.

UNIT F4
381.0–386.6 MBSF 642E–10R–3 (0 cm) TO 12R–1 (20 cm)
FINE-GRAINED, APHYRIC TO SPARSELY PHYRIC GRAY BASALT FLOW. Highly to sparsely vesicular with vesicles filled with calcite and dark green smectite. Some alteration to smectite(?) along fractures. Native copper blebs within vesicle fillings. Some weak development of streaky lamination.

THIN SECTION DESCRIPTION

642E–11R–2 (Piece 2A, 55–57 cm): 45% plagioclase, 30% clinopyroxene, 1% iddingsite; 3–4% opaques; 20% intersertal smectite.

UNIT F5
386.6–392.2 MBSF 642E–12R–1 (20 cm) TO 12R–1 (68 cm)

VERY FINE-GRAINED, APHYRIC BLACK BASALT FLOW. Locally massive, but generally brecciated and highly altered to clay minerals.

THIN SECTION DESCRIPTION

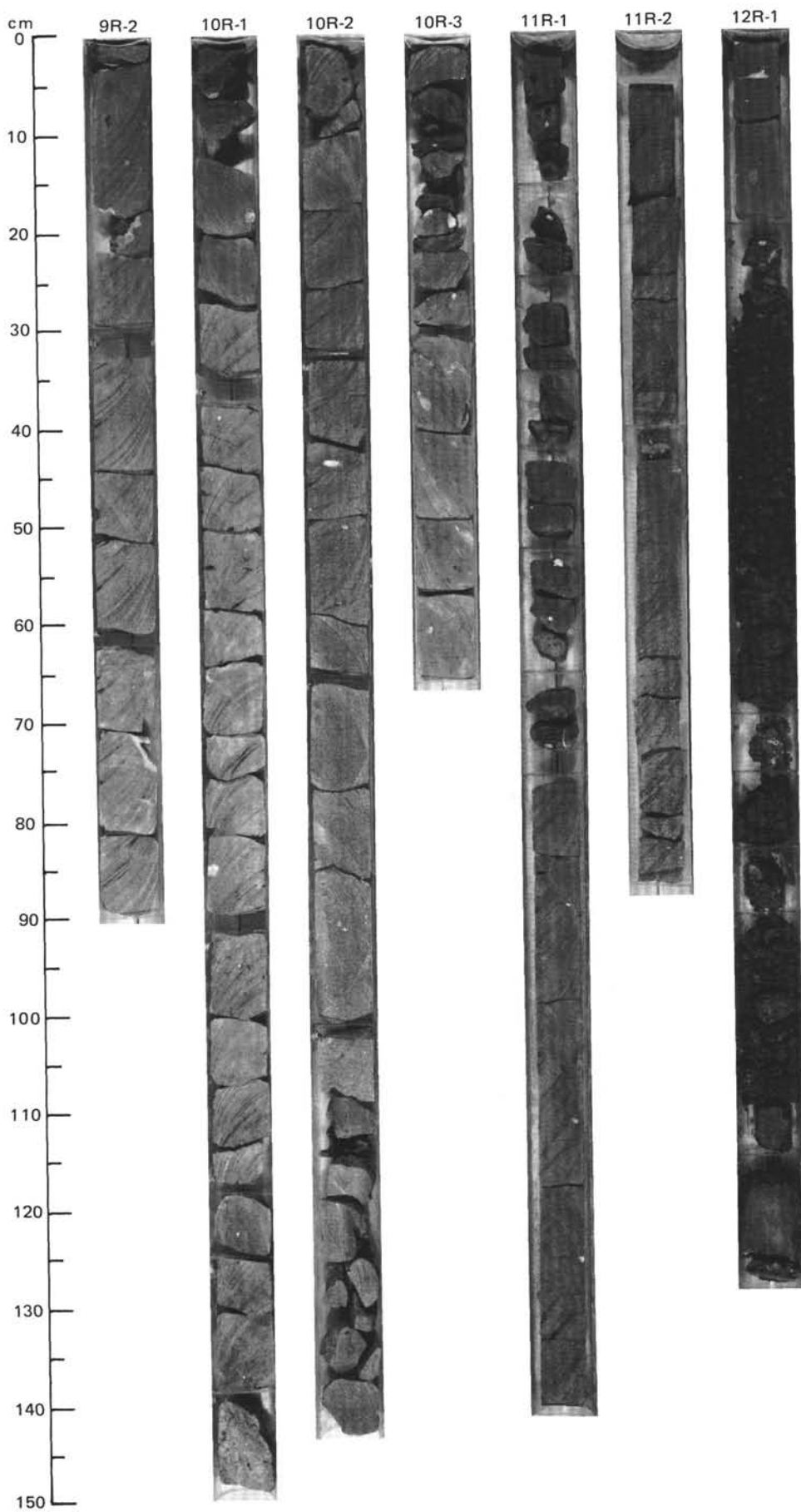
642E–12R–1 (29–30 cm): aphyric; 10% iddingsite, 40% smectite after plagioclase; 40% strongly altered clinopyroxene, 3% opaques, 7% intersertal smectite.

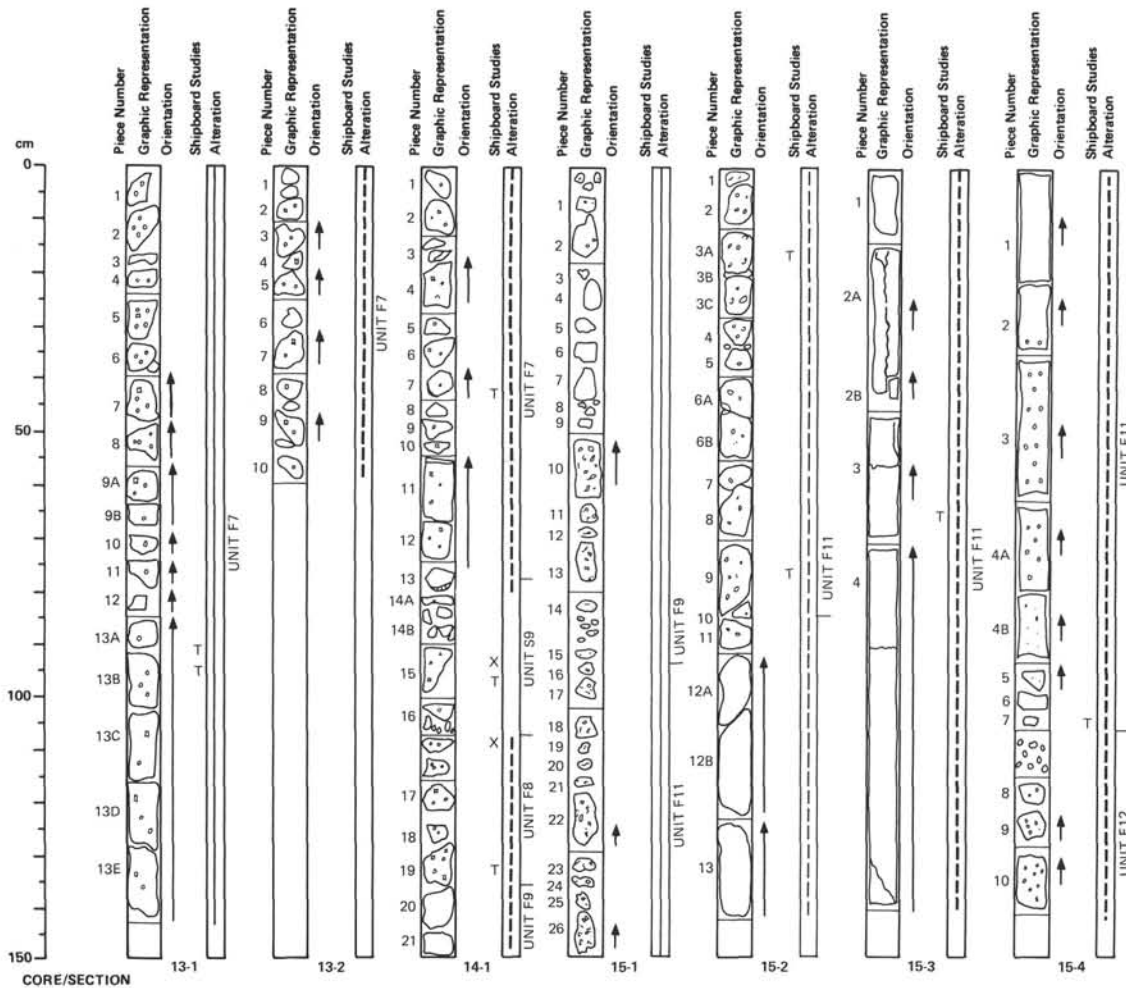
UNIT S8
392.2–392.4 MBSF 642E–12R–1 (68 cm) TO 12R–1 (69 cm)

DARK BROWN TUFF LAYER WITH POCKET FILLINGS OF VITRIC TUFFS IN THE UNDERLYING BRECCIA. Contains cuneiform shards replaced by pale to dark green secondary minerals.

UNIT F6
392.4–395.8 MBSF 642E–12R–1 (69 cm) TO 12R–1 (130 cm)

FINE-GRAINED, GLASSY, APHYRIC, BLACK BASALT FLOW. Moderately vesicular, filled with dark green smectite with subordinate calcite.





UNIT F7

395.8–401.5 MBSF

642E–13R–1 (0 cm) TO 14R–1 (80 cm)

FINE-GRAINED, APHYRIC TO SPARSELY PHYRIC, GRAY BASALT FLOW. Moderate vesicularity, vesicles filled with dark green smectite, some calcite, some coalescence of vesicles to irregular shapes. Euhedral plagioclase phenocrysts. Some local subhorizontal streaking (flow fabric) defined by smectite-rich bands.

THIN SECTION DESCRIPTIONS

642E–13R–1 (Piece 13B, 91–95 cm): 10% plag phenocrysts. Groundmass: 50% plag; 20% cpx; 5% opaques; <1% iddingsite; 10–12% interstitial smectite.

642E–13R–1 (94–97 cm): 5% plag phenocrysts. Groundmass: 45% plag, 25% cpx, 5% opaques, 20% interstitial smectite.

642E–14R–1 (Piece 7, 39–43 cm): 15% glomerophyric plag. Groundmass: 35% plag, 20% cpx, 3% opaques, 25% interstitial smectite. Intersertal.

UNIT S9

401.5–402.0 MBSF

642E–14R–1 (80 cm) TO 14R–1 (107 cm)

DUSKY GREEN TO BROWN VITRIC TUFF. Contains fresh and altered vesicular and pumiceous shards.

UNIT F8

402.0–403.3 MBSF

642E–14R–1 (107 cm) TO 14R–1 (136 cm)

FINE- TO MEDIUM-GRAINED, APHYRIC TO SPARSELY PHYRIC, GRAY, BASALT FLOW. As F7, except that the plagioclase phenocrysts become more common lower in the flow, along with an increase in grain size.

THIN SECTION DESCRIPTION

642E–14R–1 (Piece 19, 128–130 cm): 10% plag phenocrysts. Groundmass: 30% partly altered plag, <10% altered ol, 25% partly altered cpx, 3% opaques, 20% interstitial smectite. Intergranular-intersertal, subophitic.

UNIT F9

403.3–406.3 MBSF

642E–14R–1 (136 cm) TO 15R–1 (93 cm)

MEDIUM-GRAINED, SPARSELY PHYRIC, GRAY BASALT FLOW. Sparsely vesicular with smectite coatings and some calcite fills. Plagioclase and olivine phenocrysts form 1%–2% and are < 1.0 mm in diameter.

UNIT F11

406.3–411.4 MBSF

642E–15R–2 (93 cm) TO 15R–4 (106 cm)

MEDIUM-GRAINED, PLAGIOCLASE PHYRIC, GRAY BASALT FLOW. Nonvesicular and has light gray to white feldspar phenocrysts. Minor bleaching of groundmass, some fracturing filled with dark green smectite and calcite. Common dark green smectite patch alteration.

THIN SECTION DESCRIPTIONS

642E–15R–2 (Piece 3A, 15–18 cm): aphyric. 5% hematite after olivine; 40% partly altered plag, 40% partly altered cpx, 5% other opaques; 5% interstitial smectite. Intergranular, subophitic.

642E–15R–2 (Piece 9, 73–76 cm): 50% plag, 40% cpx, 5% opaques, 5% altered glass.

642E–15R–4 (103–106 cm): 2% plag phenocrysts. Groundmass: 30% plag, 20% cpx, 5% iddingsite, 2% opaques, 40% intergranular smectite.

UNIT F12

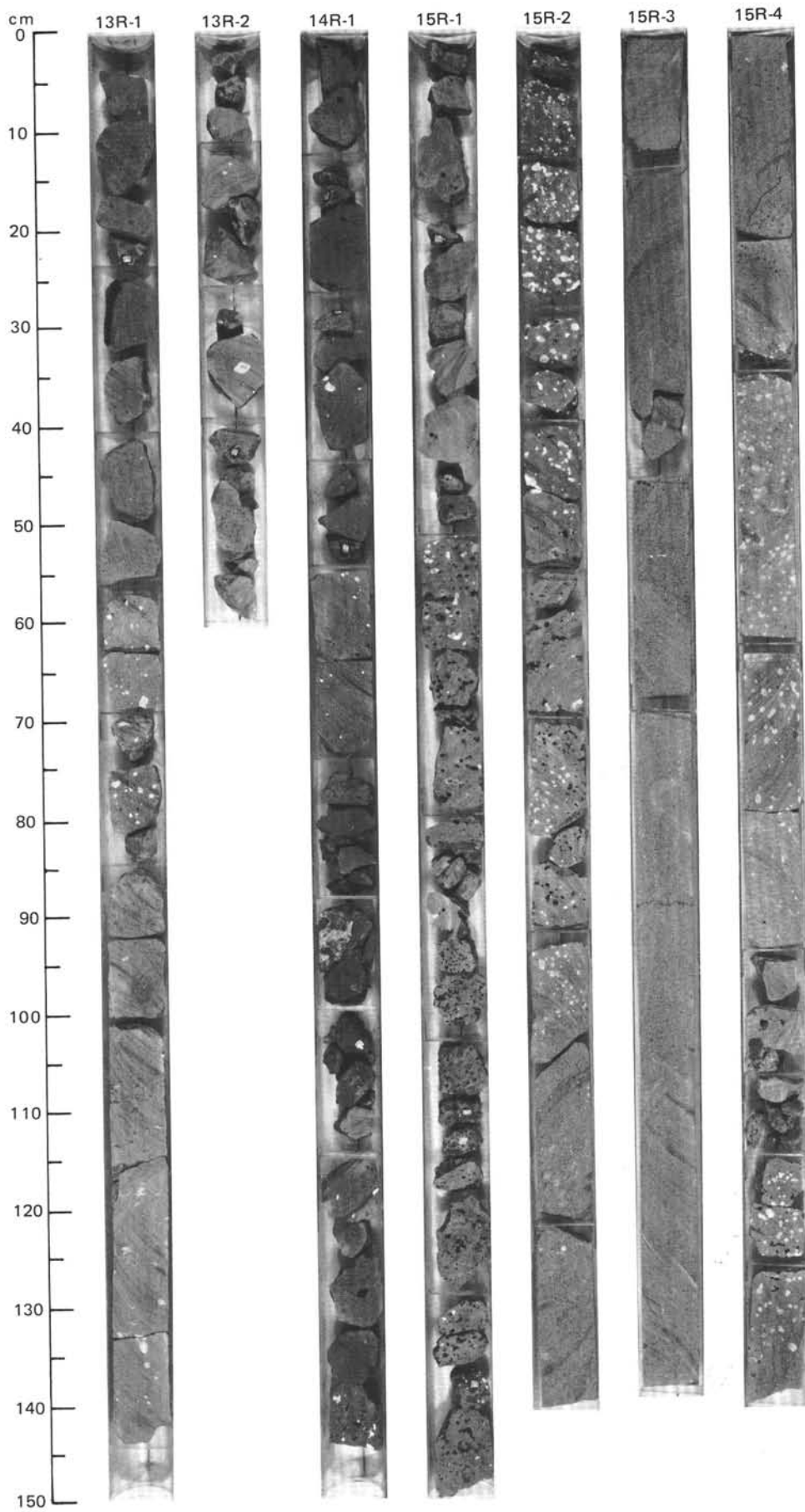
411.4–413.2 MBSF

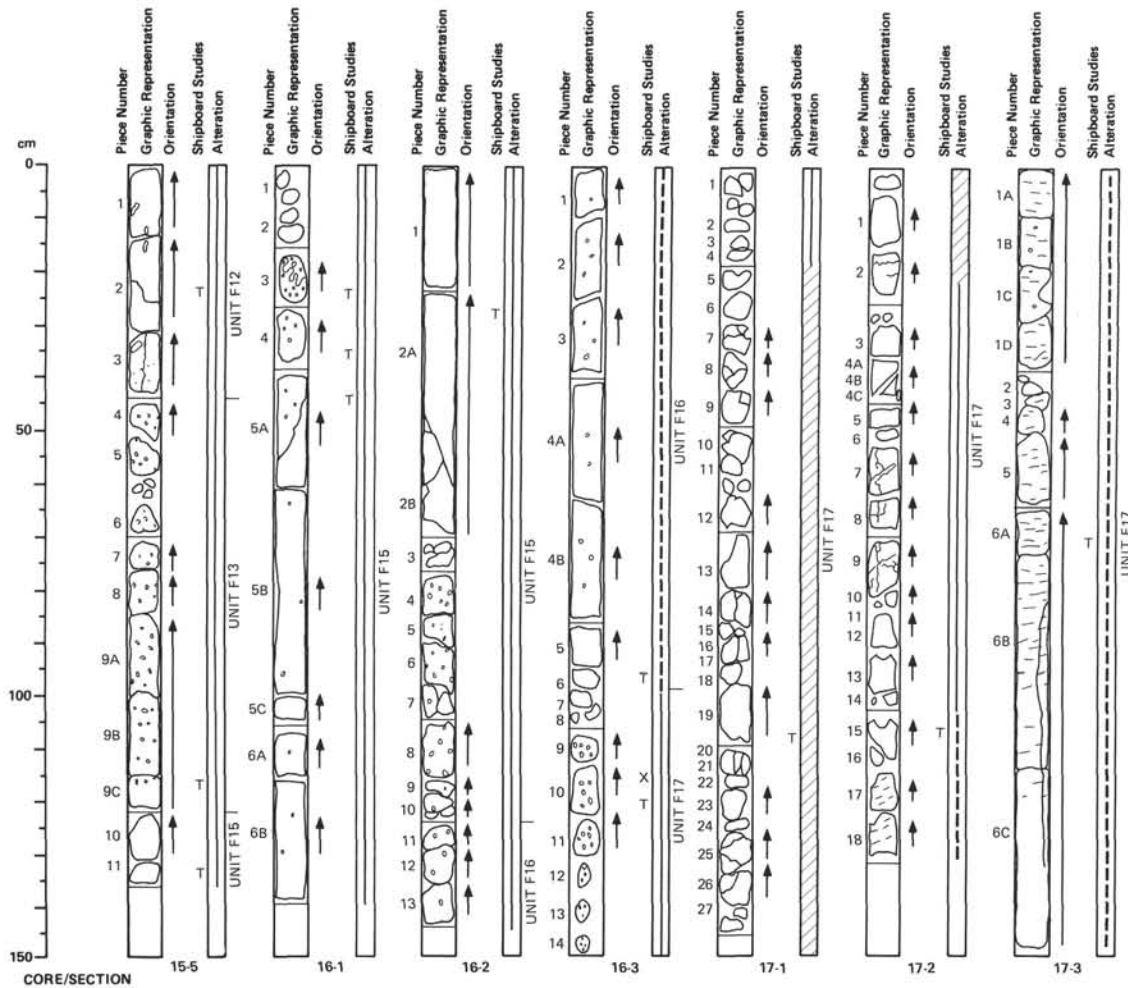
642E–15R–4 (106 cm) TO 15R–5 (45 cm)

MEDIUM-GRAINED, MODERATELY OLIVINE PHYRIC, GRAY BASALT FLOW. 0.5–0.75 mm diameter olivine phenocrysts, iddingsitized and smectite-rich. Highly vesicular at flow top breccia, with lower vesicles containing calcite and some green smectite. Smectite patch alteration throughout groundmass. Slightly more vesicular at flow base.

THIN SECTION DESCRIPTION

642E–15R–5 (Piece 1, 9–12 cm): <1% plag phenocrysts. Groundmass: 35% partly altered plag, 35% partly altered cpx, 7% iddingsite, 5% opaques. Smectite replacing mesostasis and crystals.





UNIT F13
413.2–414.0 MBSF 642E–15R–5 (45 cm) TO 15R–5 (122 cm)

MEDIUM- TO FINE-GRAINED, MODERATELY PLAGIOCLASE + OLIVINE PHYRIC BASALT FLOW. Vesicular throughout, almost all vesicles open but some are filled with calcite and thin dark green smectite rims.

THIN SECTION DESCRIPTION

642E–15R–5 (105–112 cm): 5% glomerophyric plag. Groundmass: 50% plag, 25% cpx, 7% altered ol, 5% opaques, 10% intergranular smectite.

UNIT F15
414.0–418.0 MBSF 642E–15R–5 (122 cm) TO 16R–2 (123 cm)

MEDIUM-GRAINED, APHYRIC, GRAY BASALT FLOW. Weakly reddened, highly vesicular near flow top, moderate to sparse below. Calcite, zeolite, green smectite fills in vesicles. Dark green smectite spotting or irregular patches throughout the groundmass.

Contacts at 16R-1, 17 to 16R-1, 23 and 16R-1, 44 to 16R-1, 56 mark contact between fine-grained basalt enclave within F15. Parts of Pieces #3 and #5 and all #4 are fine-grained. Upper contact shows intimate complex mixing zone. Mostly open highly vesicular basal 50 cm.

THIN SECTION DESCRIPTIONS

642E–15R–5 (Piece 10, 129–131 cm): Phenocrysts: <1% iddingsitized ol, <1% prismatic plag. Groundmass: 10% ol, 25% cpx, 35% plag, 2% opaques, all thoroughly altered; >20% intergranular smectite.

642E–16R–1 (22–24 cm): Medium-grained domains: 40% plag, 45% cpx, 5% opaques, 10% smectite. Fine-grained domains: 35% plag, 5% cpx, 5% opaques, 55% clays after mesostasis. Sharp boundaries between domains.

642E–16R–1 (Piece 4, 32–34 cm): Medium-grained domains: 35% plag, 20% cpx, 5% iddingsitized ol, 10% opaques, 30% clay. Fine-grained domains: 45% plag, 2% cpx, 8% opaques, 45% altered mesostasis. Sharp boundaries between domains.

642E–16R–1 (Piece 5A, 49–53 cm): Phenocrysts: 2% plag, 4% cpx. Groundmass: 40% partly altered plag, 40% partly altered cpx, 5% opaques, 10% altered mesostasis.

UNIT S9A

418.0–418.3 MBSF NOT RECOVERED

UNIT F16

418.3–420.7 MBSF 642E–16R–2 (123 cm) TO 16R–3 (100 cm)

FINE-GRAINED, MODERATELY OLIVINE-PLAGIOCLASE PHYRIC, GRAY BASALT FLOW. Plagioclase phenocrysts are up to 4.0 mm long and olivines up to 0.7 mm in diameter. Highly to moderately vesicular with calcite, dark green smectite and zeolite fills.

THIN SECTION DESCRIPTION

642E–16R–3 (Piece 5, 91–93 cm): <1% plag phenocrysts. Groundmass: 40% plag, 35% cpx, 5% opaques, 25% altered mesostasis and ol(?).

UNIT F17

420.7–439.2 MBSF 642E–16R–3 (100 cm) TO 18R–4 (150 cm)

FINE-GRAINED, APHYRIC, GRAY BASALT FLOW. Flow base not recovered. Thick (>2.0 m) reddened gray to brownish gray highly vesicular flow top, containing reddish iddingsitized olivines, and green smectite or calcite filled vesicles. Vesicularity decreases to moderate or sparsely vesicular downsection, predominantly dark green smectite fills. Development of subhorizontal laminar streaking (flow fabric) below 17R-2, 113 cm, seen as continuous and discontinuous smectite-rich laminae, some reddening from the iddingsitization of olivines. Some massive zones, e.g. 17R-4. Native copper disseminated throughout groundmass or within vesicles.

THIN SECTION DESCRIPTIONS

642E–16R–3 (Piece 10, 116–117 cm): <1% plag, <2% altered ol phenocrysts. Groundmass: 40% plag, 30% cpx, 4% opaques, <10% altered ol, >10% altered mesostasis.

642E–17R–1 (104–106 cm): 40% plag, 35% cpx, 5% opaques, 20% altered ol and mesostasis. Weakly pilotaxitic.

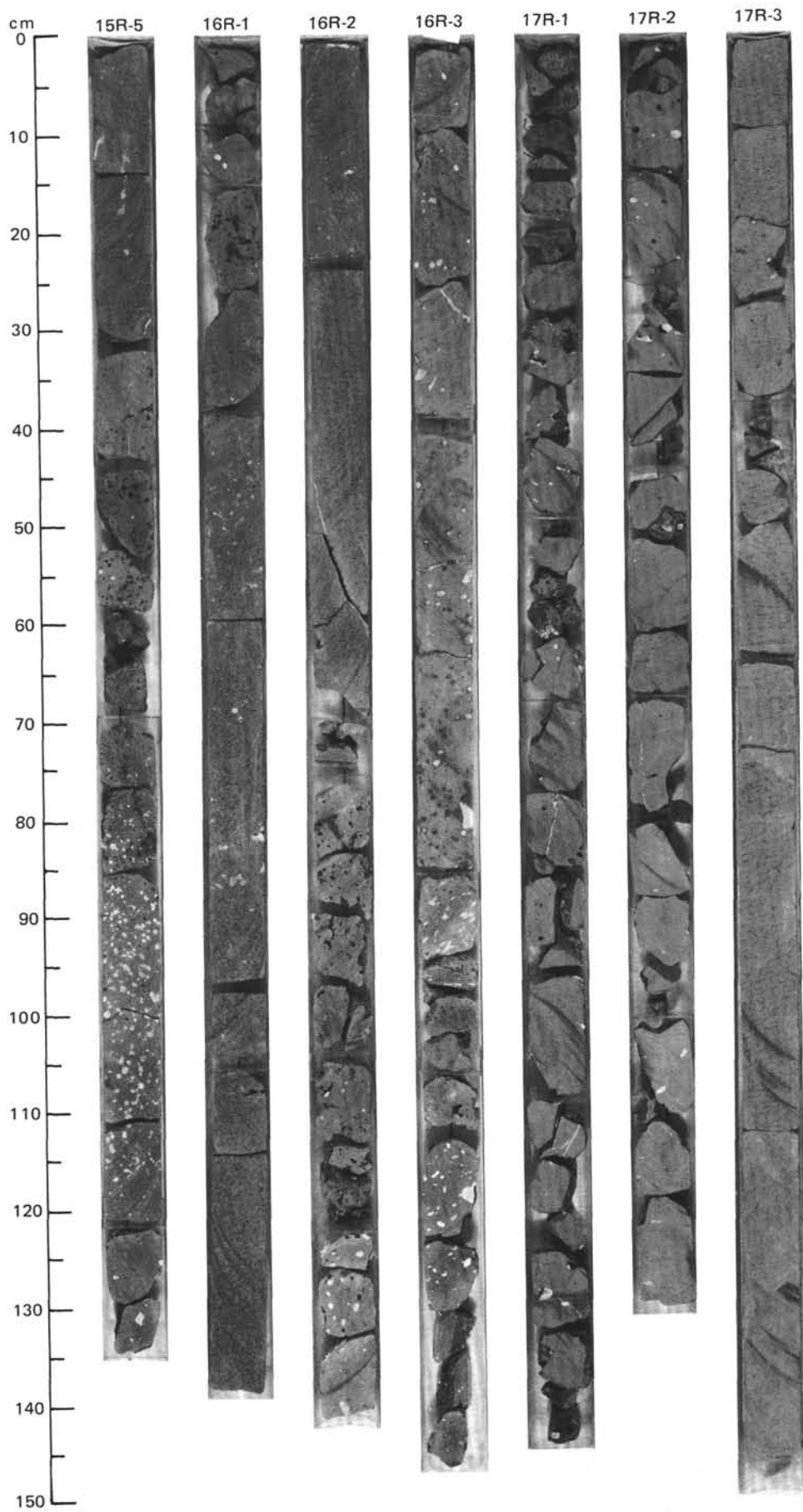
642E–17R–2 (Piece 15, 105–109 cm): 30% plag, 40% cpx, 5% altered ol, 7% opaques, >15% altered mesostasis.

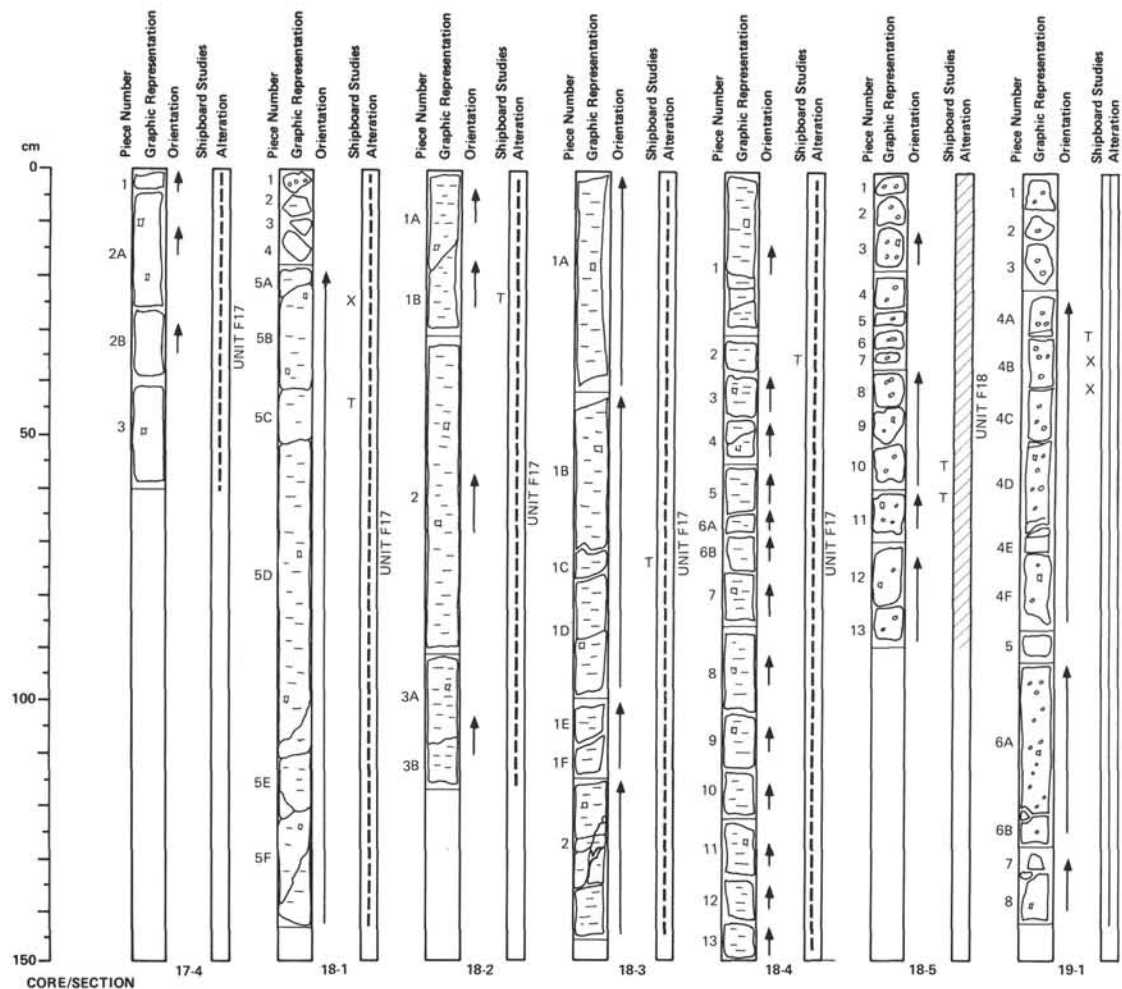
642E–17R–3 (Piece 6, 70–72 cm): <2% glomerophyric plag, 45% plag, 35% cpx, <5% opaques, <7% altered ol, <2% altered mesostasis.

642E–18R–2 (Piece 11B, 27–29 cm): 40% plag, 40% cpx, 5% altered ol, 5% opaques, 10% altered mesostasis.

642E–18R–3 (Piece 1B, 72–75 cm): <1% altered ol and <1% plag phenocrysts. 45% plag, 35% cpx, 8% ol, <10% altered mesostasis. Intergranular-intersertal. Subophitic.

642E–18R–4 (37–39 cm): 42% plag, 38% cpx, 12% altered ol, 8% opaques. Pilotaxitic.





CORE/SECTION

UNIT F17

420.7–439.2 MBSF 642E–16R–3 (100 cm) TO 18R–4 (150 cm)

FINE-GRAINED, APHYRIC, GRAY BASALT FLOW. Flow base not recovered. Thick (>2.0 m) reddened gray to brownish gray highly vesicular flow top, containing reddish iddingsitized olivines, and green smectite or calcite filled vesicles. Vesicularity decreases to moderate or sparsely vesicular downsection, predominantly dark green smectite fills. Development of subhorizontal laminar streaking (flow fabric) below 17R-2, 113 cm, seen as continuous and discontinuous smectite-rich laminae, some reddening from the iddingsitization of olivines. Some massive zones, e.g. 17R-4. Native copper disseminated throughout groundmass or within vesicles.

THIN SECTION DESCRIPTIONS

642E–16R–3 (Piece 10, 116–117 cm): <1% plag, <2% altered ol phenocrysts. Groundmass: 40% plag, 30% cpx, 4% opaques, <10% altered ol, >10% altered mesostasis.

642E–17R–1 (104–106 cm): 40% plag, 35% cpx, 5% opaques, 20% altered ol and mesostasis. Weakly pilotaxitic.

642E–17R–2 (Piece 15, 105–109 cm): 30% plag, 40% cpx, 5% altered ol, 7% opaques, >15% altered mesostasis.

642E–17R–3 (Piece 6, 70–72 cm): <2% glomerophytic plag, 45% plag, 35% cpx, <5% opaques, <7% altered ol, <2% altered mesostasis.

642E–18R–2 (Piece 11B, 27–29 cm): 40% plag, 40% cpx, 5% altered ol, 5% opaques, 10% altered mesostasis.

642E–18R–3 (Piece 1B, 72–75 cm): <1% altered ol and <1% plag phenocrysts. 45% plag, 35% cpx, 8% ol, <10% altered mesostasis. Intergranular-interstitial. Subophitic.

642E–18R–4 (37–39 cm): 42% plag, 38% cpx, 12% altered ol, 8% opaques. Pilotaxitic.

UNIT S9B

439.2–439.2 MBSF

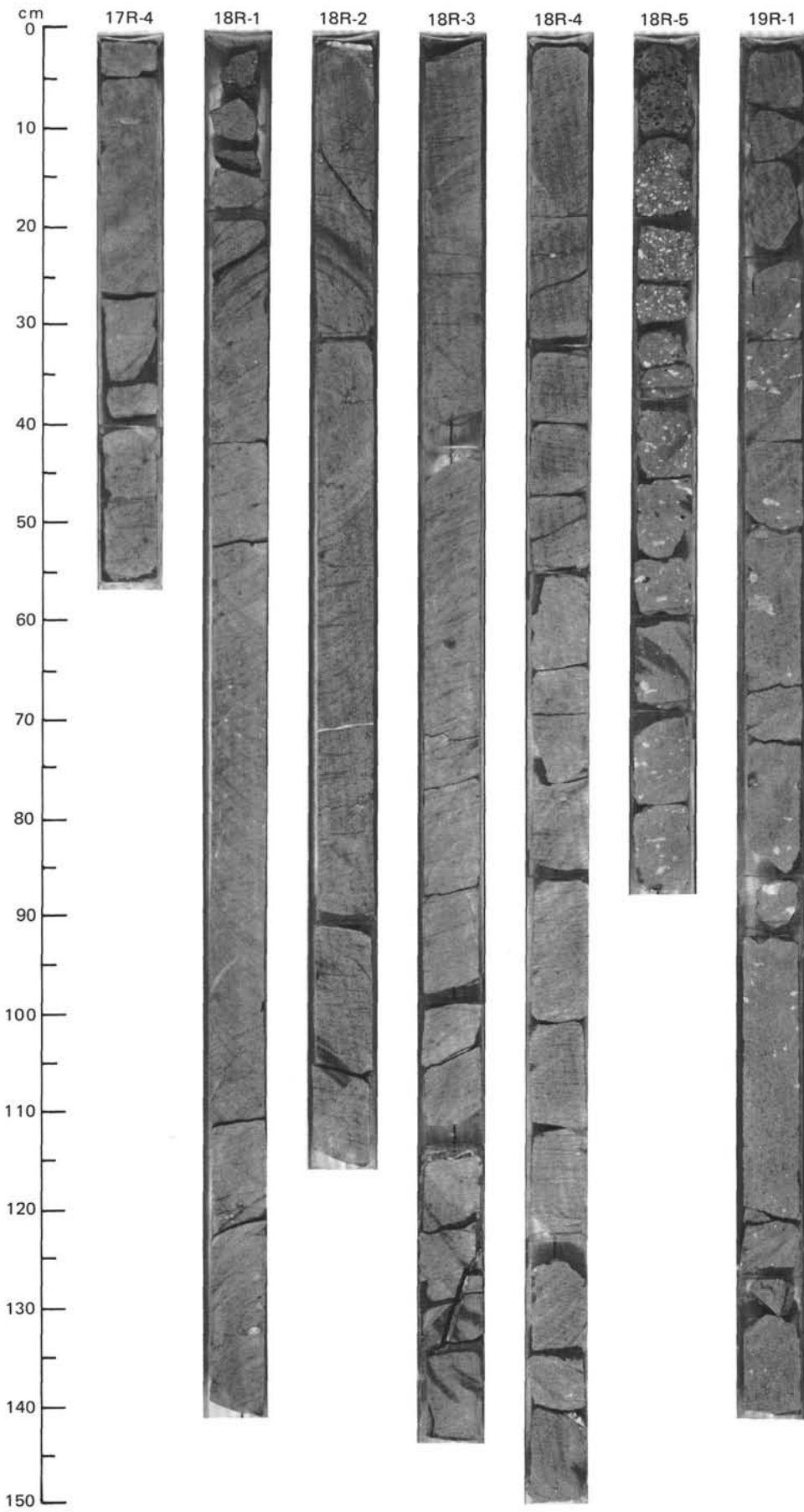
NOT RECOVERED

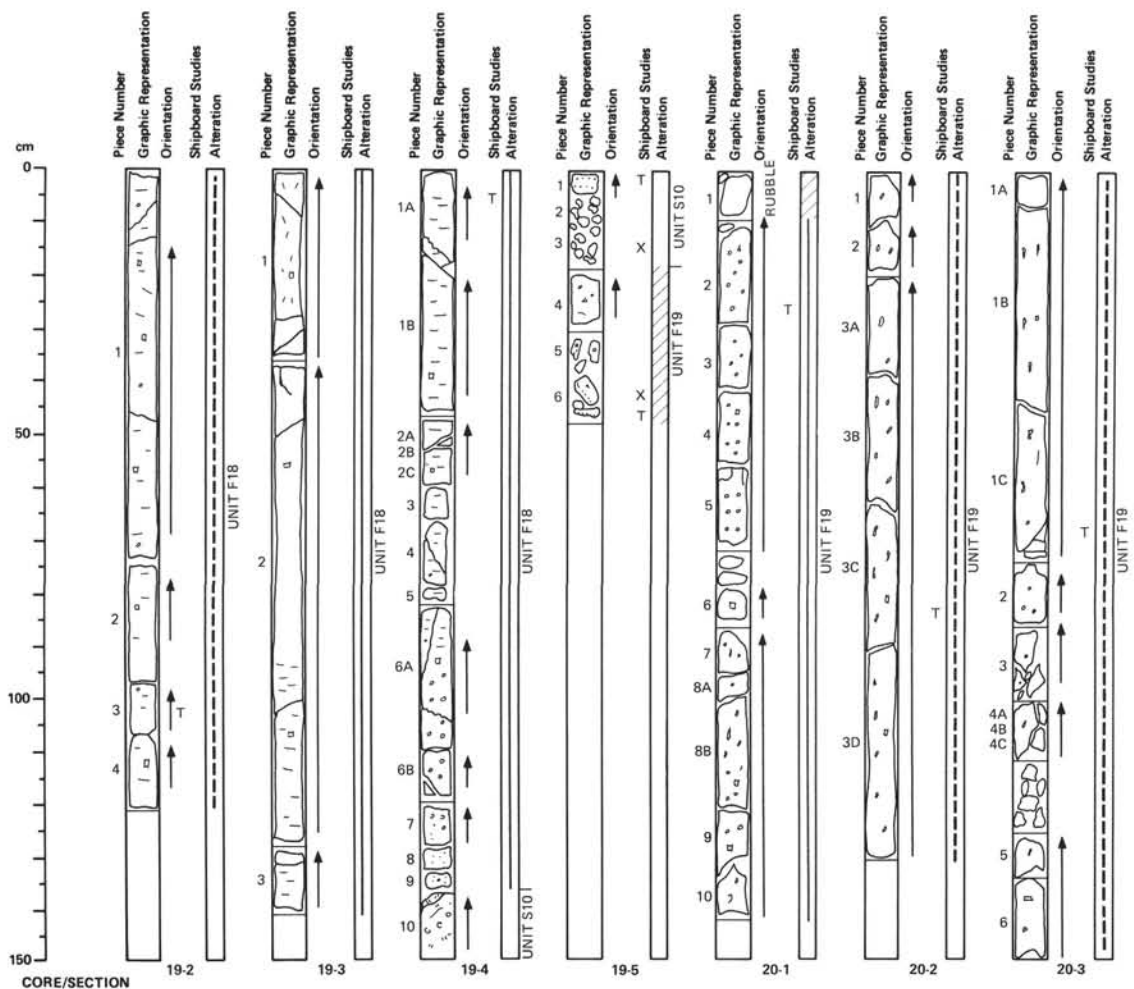
UNIT F18

439.2–447.0 MBSF

642E–18R–5 (0 cm) TO 19R–4 (137 cm)

FINE-GRAINED, APHYRIC, GRAY BASALT FLOW. Light reddish brown, highly vesicular flow top, grading to brownish gray and gray. As F17 with some subhorizontal fracturing < 1.0 mm wide filled with smectite. Generally weak streaking fabric in central flow. Disseminated copper present. Basal contact with S10 is irregular and quenched.





UNIT F18

439.2–447.0 MBSF 642E–18R–5 (0 cm) TO 19R–4 (137 cm)

FINE-GRAINED, APHYRIC, GRAY BASALT FLOW. Light reddish brown, highly vesicular flow top, grading to brownish gray and gray. As F17 with some subhorizontal fracturing < 1.0 mm wide filled with smectite. Generally weak streaking fabric in central flow. Disseminated copper present. Basal contact with S10 is irregular and quenched.

THIN SECTION DESCRIPTIONS

642E–19R–1 (Piece 4C, 42–44 cm): <2% plag phenocrysts. 35% plag, 35% cpx, 10% altered ol, <5% opaques, >10 altered mesostasis. Intergranular-intersertal. Subophitic.

642E–19R–2 (Piece 3, 99–102 cm): 1% glomerophytic plag, 40% plag, 40% cpx, <5% altered ol, 2% opaques, 10% altered mesostasis. Intersertal, subophitic.

642E–19R–4 (9–10 cm): >1% zoned plag phenocrysts. 40% plag, 40% cpx, 10% altered ol, 5% opaques, 5% smectite patches. Subophitic.

UNIT S10

447.0–450.1 MBSF 642E–19R–4 (137 cm) TO 19R–5 (20 cm)

DARK BROWN TO GRAY GREEN, WELL-SORTED VITRIC TUFF. Contains accretionary lapilli and rounded clasts of brown to fine red tuff. Pale green smectite present in pore spaces. Very few fresh shards. Pocket infilling of scoriaceous material, top to F19.

UNIT F19

450.1–457.4 MBSF 642E–19R–5 (20 cm) TO 20R–4 (104 cm)

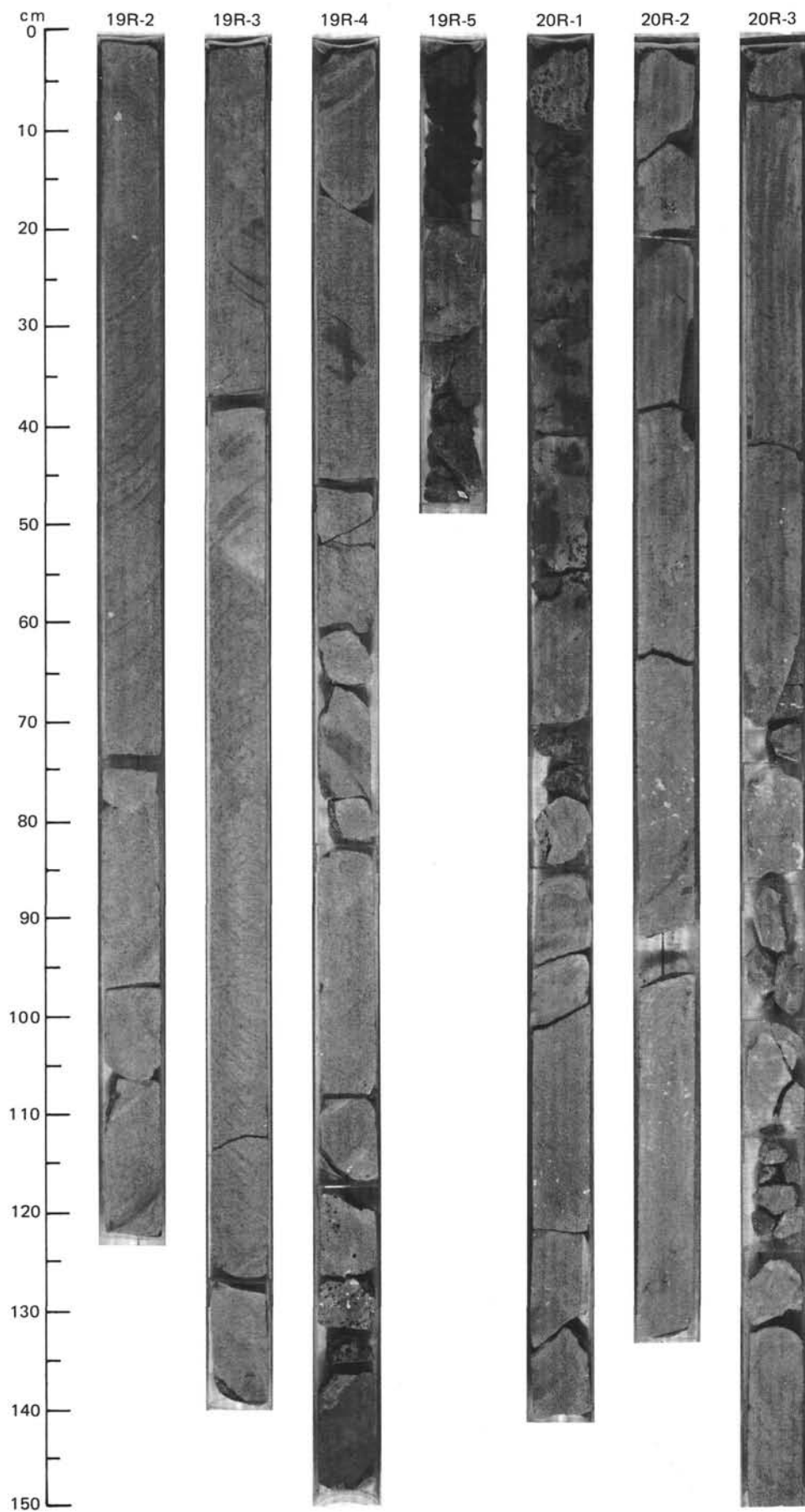
FINE-GRAINED, APHYRIC, DARK GRAY BASALT FLOW. Flow base not recovered. Highly vesicular at flow top, dark greenish gray from smectite alteration. Local coalescence of vesicles to up to 25% of rock volume, filled with dark green smectite. Toward base, from 20R–4, 30 cm down to base of recovery, streaky (flow fabric) laminations present, accompanied by elongate green smectite-filled vesicles. [Unrelated rubble at 642E–20R–1 (0–9 cm)]

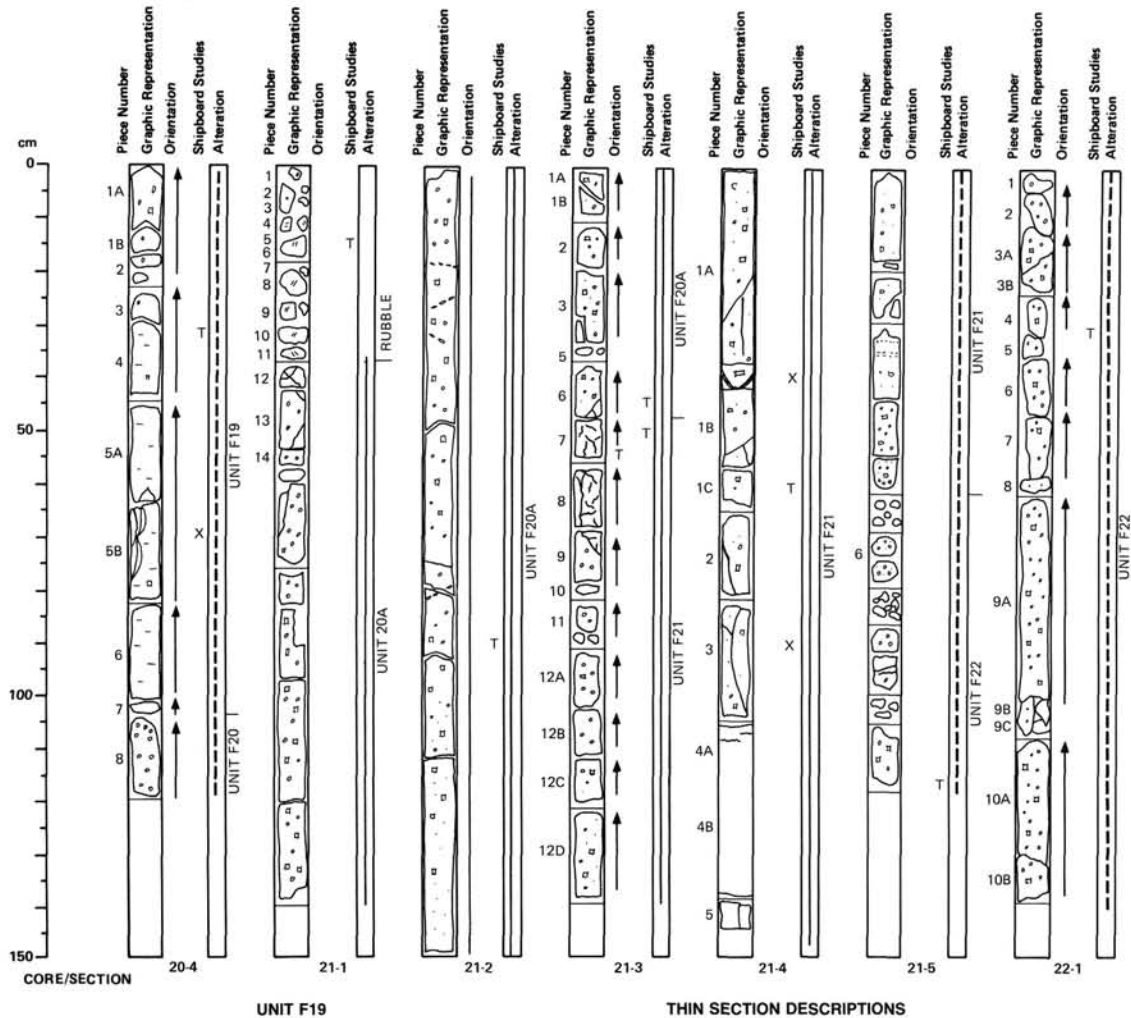
THIN SECTION DESCRIPTIONS

642E–19R–5 (45–48 cm): 40% plag, 30% cpx, <5% ol, 10% opaques, 10% mesostasis; all altered to variable extents. Brecciated.

642E–20R–2 (Piece 3C, 84–87 cm): 40% plag, 40% cpx, 5% opaques, 5% altered mesostasis. All minerals strongly altered.

642E–20R–3 (Piece 1C, 64–67 cm): 40% plag, 40% cpx, 5% opaques, 5% altered mesostasis; all strongly altered.





450.1–457.4 MBSF

642E–19R–5 (20 cm) TO 20R–4 (104 cm)

FINE-GRAINED, APHYRIC, DARK GRAY BASALT FLOW. Flow base not recovered. Highly vesicular at flow top, dark greenish gray from smectite alteration. Local coalescence of vesicles to up to 25% of rock volume, filled with dark green smectite. Toward base, from 20R–4, 30 cm down to base of recovery, streaky (flow fabric) laminations present, accompanied by elongate green smectite-filled vesicles. [Unrelated rubble at 642E–20R–1 (0–9 cm)]

THIN SECTION DESCRIPTIONS

642E–19R–5 (45–48 cm): 40% plag, 30% cpx, <5% ol, 10% opaques, 10% mesostasis; all altered to variable extents. Brecciated.

642E–20R–2 (Piece 3C, 84–87 cm): 40% plag, 40% cpx, 5% opaques, 5% altered mesostasis. All minerals strongly altered.

642E–20R–3 (Piece 1C, 64–67 cm): 40% plag, 40% cpx, 5% opaques, 5% altered mesostasis; all strongly altered.

UNIT S10A

457.4–458.2 MBSF

NOT RECOVERED

UNIT F20

458.2–463.0 MBSF

642E–20R–4 (104 cm) TO 20R–4 (120 cm)

MEDIUM-GRAINED MODERATELY PLAGIOCLASE-OLIVINE PHYRIC, GRAY TO DARK GRAY BASALT FLOW. Highly vesicular, mostly dark green smectite filled vesicles with minor calcite and zeolite, grading to sparsely vesicular in lower section. Dark green gray smectite filled hairline fracturing. Some inclination of vesicles streaming in center of flow.

UNIT F20A

463.0–466.2 MBSF

642E–21R–1 (38 cm) TO 21R–3 (48 cm)

AS F20. [Unrelated rubble of volcanoclastic sediment at 642E–21R–1 (0–38 cm)]

UNIT F21

466.2–468.9 MBSF

642E–21R–3 (48 cm) TO 21R–5 (61 cm)

MEDIUM-GRAINED, MODERATELY PHYRIC, DARK GRAY BASALT FLOW. Very dark gray to black highly vesicular flow top, red-veined and brecciated. Vesicles filled lower in flow by dark green smectite. 2.0–4.0 mm long plagioclase laths and < 3.0 mm olivines present. Predominantly subvertical or steeply inclined smectite filled veining.

UNIT F22

468.9–473.2 MBSF

642E–21R–5 (61 cm) TO 22R–3 (86 cm)

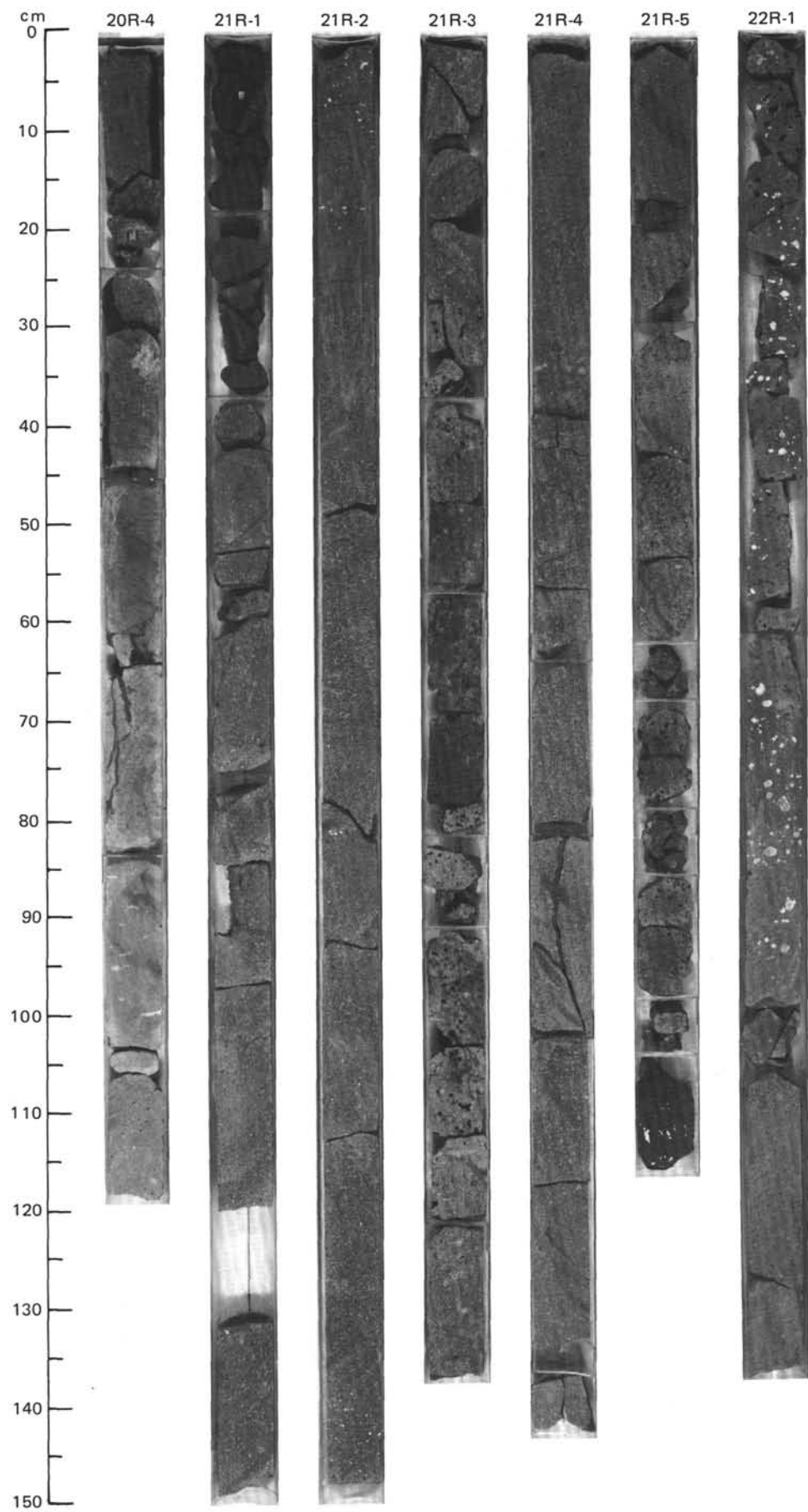
MEDIUM-GRAINED, SPARSELY TO MODERATELY OLIVINE-PLAGIOCLASE PHYRIC, GRAY BASALT FLOW. Euhedral olivines and plagioclase laths < 3.0 mm diameter. Moderately vesicular, filled with dark green smectite. Steeply inclined fracturing filled with smectite. Subhorizontal elliptical vesicles at 22R–2, 60 to 62 cm.

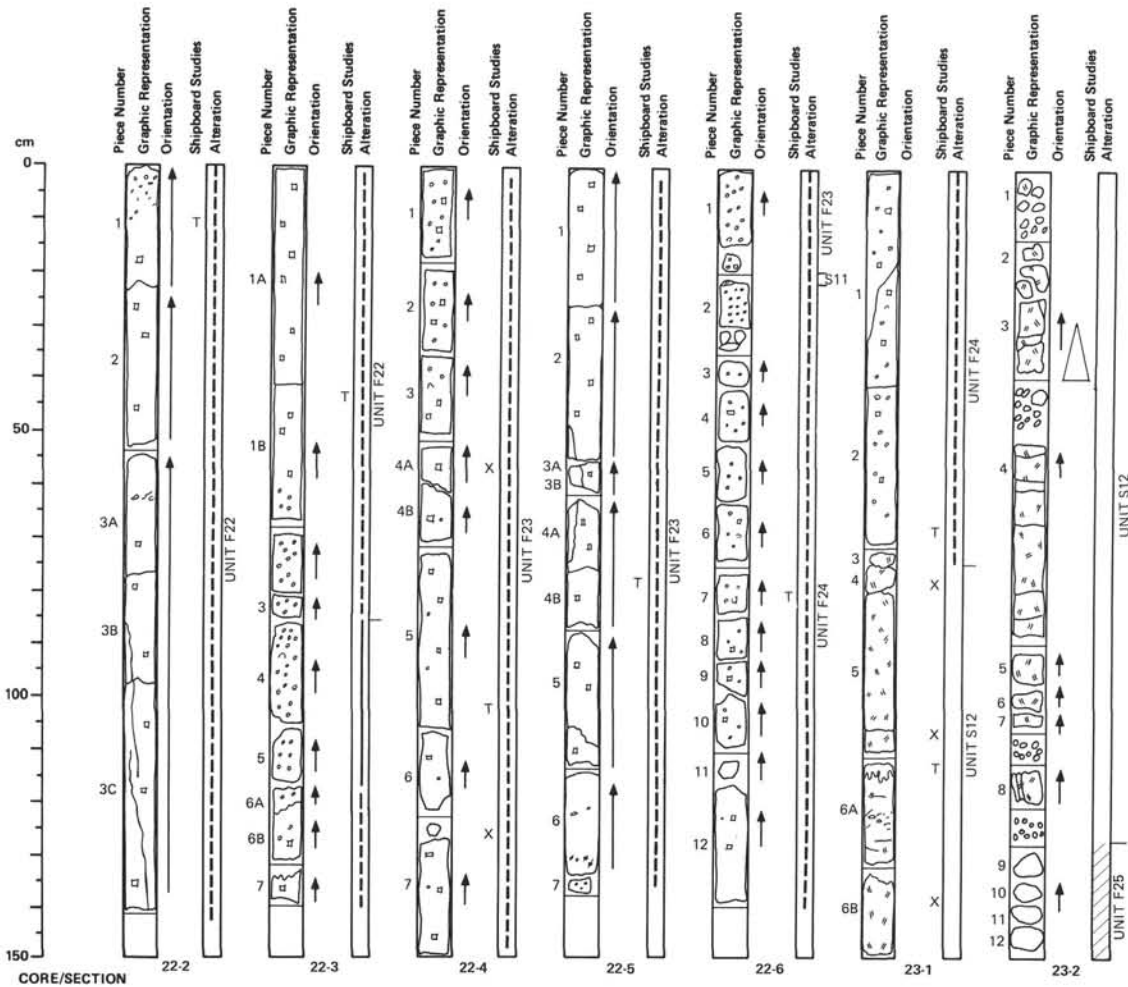
THIN SECTION DESCRIPTIONS

642E–22R–1 (Piece 4, 26–28 cm): 2% plag phenocrysts, 40% plag, 35% cpx, 10% opaques, 13% altered mesostasis.

642E–22R–2 (Piece 1, 9–10 cm): 10% plag phenocrysts. Groundmass: 40% plag, 25% cpx, 5% opaques, 20% altered mesostasis.

642E–22R–3 (Piece 1B, 44–45 cm): 10% plag phenocrysts. Groundmass: 40% plag, 30% cpx, 10% altered ol, 5% opaques, 5% altered mesostasis. Intergranular, subophitic.





UNIT F22

468.9–473.2 MBSF

642E–21R–5 (61 cm) TO 22R–3 (86 cm)

MEDIUM-GRAINED, SPARSELY TO MODERATELY OLIVINE-PLAGIOCLASE PHYRIC, GRAY BASALT FLOW. Euhedral olivines and plagioclase laths < 3.0 mm diameter. Moderately vesicular, filled with dark green smectite. Steeply inclined fracturing filled with smectite. Subhorizontal elliptical vesicles at 22R–2, 60 to 62 cm.

THIN SECTION DESCRIPTIONS

642E–22R–1 (Piece 4, 26–28 cm): 2% plag phenocrysts, 40% plag, 35% cpx, 10% opaques, 13% altered mesostasis.

642E–22R–2 (Piece 1, 9–10 cm): 10% plag phenocrysts. Groundmass: 40% plag, 25% cpx, 5% opaques, 20% altered mesostasis.

642E–22R–3 (Piece 1B, 44–45 cm): 10% plag phenocrysts. Groundmass: 40% plag, 30% cpx, 10% altered ol, 5% opaques, 5% altered mesostasis. Intergranular, subophitic.

UNIT F23

473.2–477.1 MBSF

642E–22R–3 (86 cm) TO 22R–6 (20 cm)

MEDIUM-GRAINED, SPARSELY OLIVINE PLAGIOCLASE PHYRIC, GRAY BASALT FLOW. Highly vesicular flow top, smectite rimmed or unfilled at top, decreasing to moderate or nonvesicular in lower flow. Euhedral iddingsitized olivines and tabular plagioclase 0.3–0.5 mm diameter. Vesicular base.

THIN SECTION DESCRIPTIONS

642E–22R–4 (Piece 6, 104–107 cm): 10% plag phenocrysts. Groundmass: 35% plag, 35% cpx, 10% opaques, 10% altered mesostasis. Equigranular.

642E–22R–5 (Piece 5, 79–81 cm): 10% plag phenocrysts. Groundmass: 35% plag, 35% cpx, >5% opaques, <15% altered mesostasis.

UNIT S11

477.1 MBSF

642E–22R–6 (20 cm) TO 22R–6 (21 cm)

DARK RED BROWN TUFF, basaltic vitric.

UNIT F24

477.1–480.5 MBSF

642E–22R–6 (21 cm) TO 23R–1 (73 cm)

MEDIUM-GRAINED OLIVINE PHYRIC, GRAY BASALT FLOW. Reddened brown gray highly vesicular flow top, iddingsitized olivines common. Vesicles filled with green smectite and some calcite. Some patch smectite alteration, steeply inclined 2.0 mm wide fracturing and brecciation at 23R–1, 17–34 cm.

THIN SECTION DESCRIPTIONS

642E–22R–6 (Piece 7, 77–88 cm): Phenocrysts: <5% altered ol, <10% plag. Groundmass: 40% plag, 30% cpx, <5% altered ol, >5% opaques, 5% altered mesostasis. Subophitic.

642E–23R–1 (Piece 2, 66–69 cm): 3% glomerophyric plag, 30% plag, 30% cpx, 7% opaques, 30% altered mesostasis.

UNIT S12

480.5–482.7 MBSF

642E–23R–1 (73 cm) TO 23R–2 (125 cm)

GREEN TO RED BROWN OR OLIVE BROWN TUFF. Median grain diameter of 0.15 mm, with some fragments of finer grained differentiated tuffs and some medium sorted basaltic tuffs. Irregular bedding features.

UNIT F25

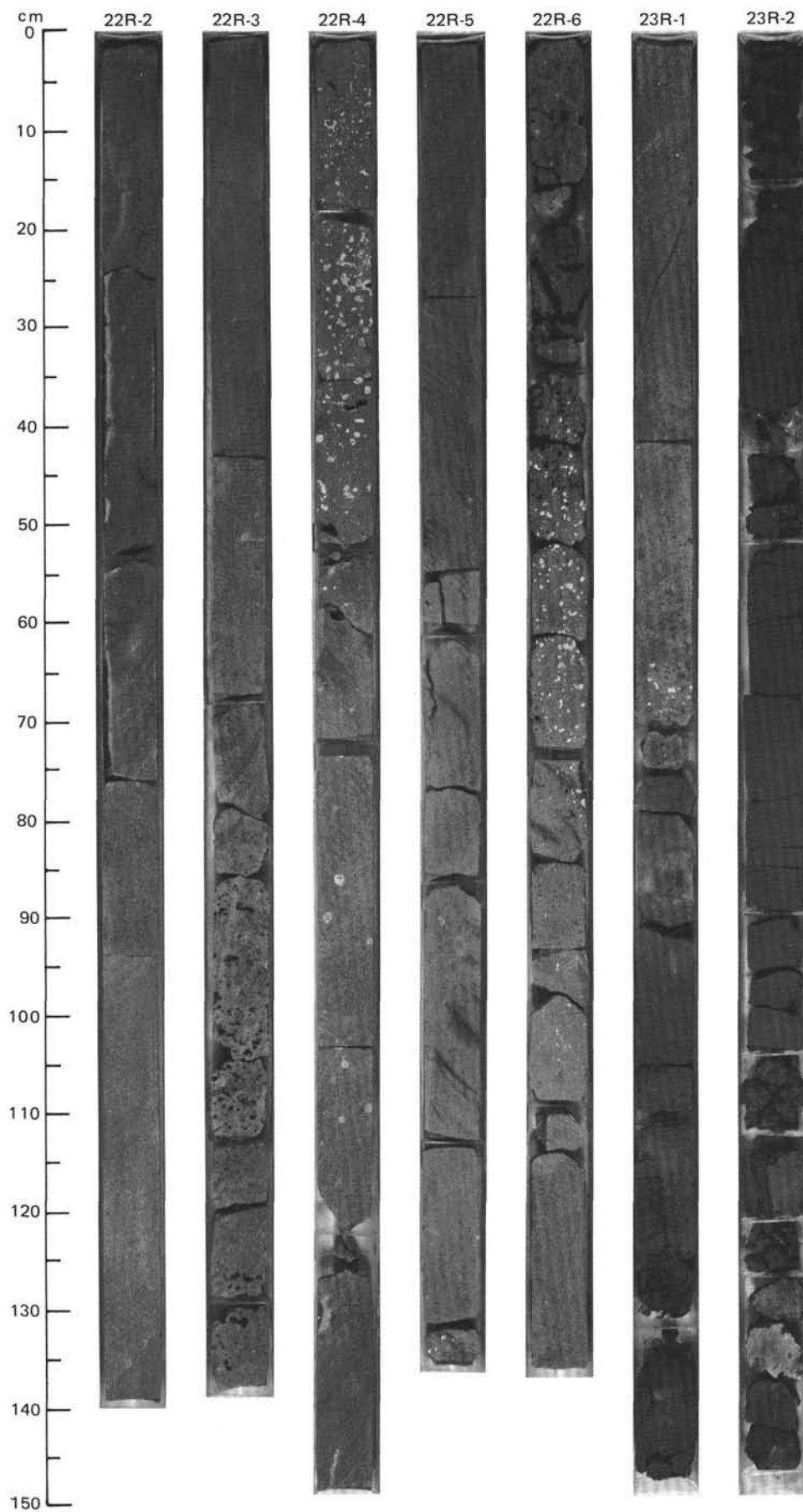
482.7–485.8 MBSF

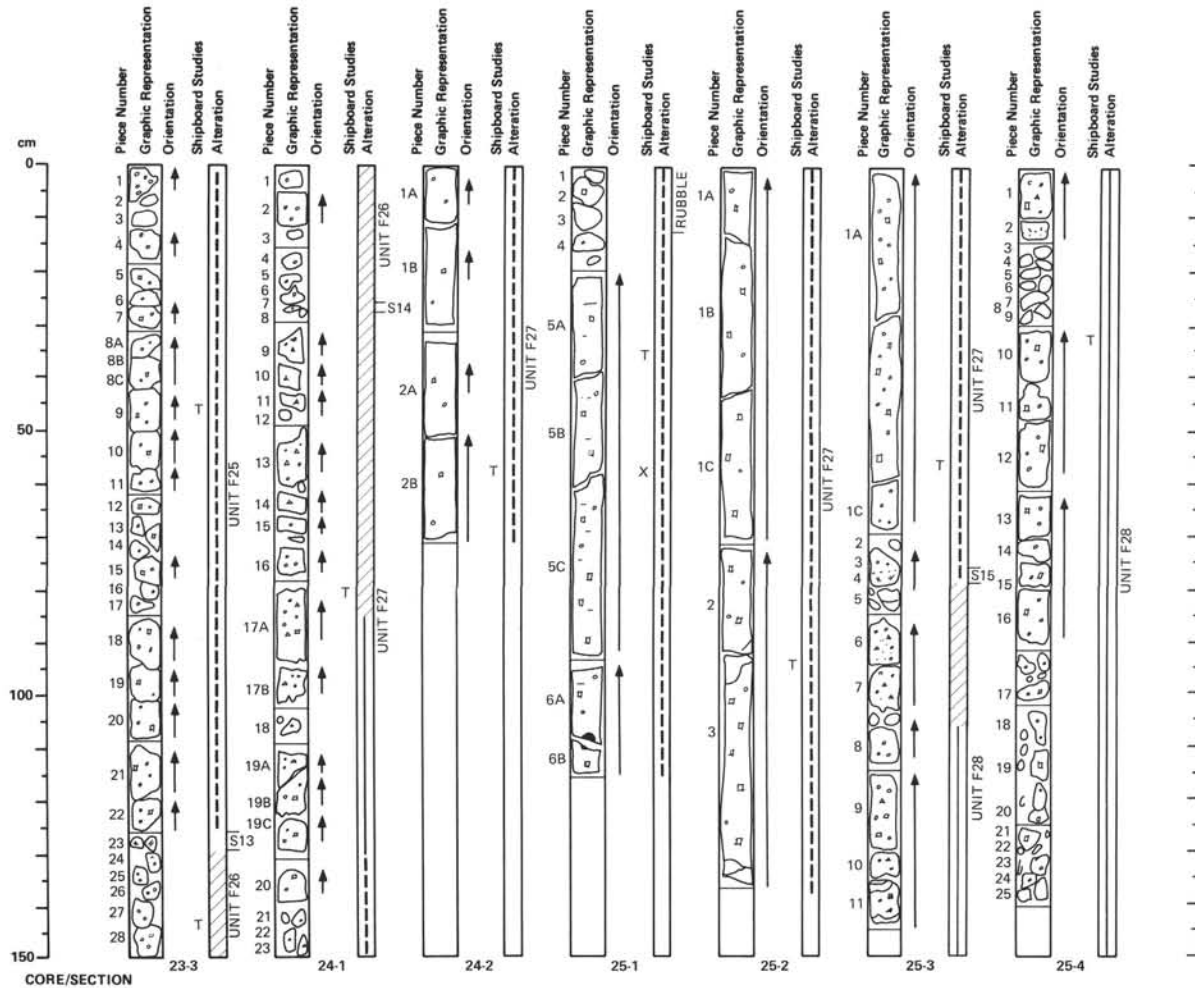
642E–23R–2 (125 cm) TO 23R–3 (126 cm)

FINE-GRAINED, APHYRIC TO MODERATELY OLIVINE-PLAGIOCLASE PHYRIC BASALT FLOW. Moderate vesicularity, but variable and locally highly vesicular, some breccia zones. Vesicles filled with dark green smectite, locally calcite.

THIN SECTION DESCRIPTION

642E–23R–3 (Piece 10, 47–49 cm): <2% plag phenocrysts. 40% plag, 30% cpx, >5% altered ol, 5% opaques, >10% altered mesostasis. Brecciated.





UNIT F25

482.7–485.8 MBSF 642E–23R–2 (125 cm) TO 23R–3 (126 cm)

FINE-GRAINED, APHYRIC TO MODERATELY OLIVINE-PLAGIOCLASE PHYRIC BASALT FLOW. Moderate vesicularity, but variable and locally highly vesicular, some breccia zones. Vesicles filled with dark green smectite, locally calcite.

THIN SECTION DESCRIPTION

642E–23R–3 (Piece 10, 47–49 cm): <2% plag phenocrysts. 40% plag, 30% cpx, >5% altered ol, 5% opaques, >10% altered mesostasis. Brecciated.

UNIT S13

485.8–486.3 MBSF 642E–23R–3 (126 cm) TO 23R–3 (127 cm)

DARK BROWN, FINE-GRAINED TUFF. Rounded lapilli of fine grained tuff. Contacts with adjacent units not recovered.

UNIT F26

486.3–489.6 MBSF 642E–23R–3 (127 cm) TO 24R–1 (27 cm)

MEDIUM-GRAINED, MODERATELY OLIVINE-PLAGIOCLASE PHYRIC BASALT FLOW. Moderate vesicularity, vesicles filled with dark green smectite.

UNIT S14

489.6 MBSF 642E–24R–1 (27 cm) TO 24R–1 (30 cm)

VERY DARK BROWN TUFF.

UNIT F27

489.6–495.2 MBSF 642E–24R–1 (30 cm) TO 25R–3 (79 cm)

FINE-GRAINED, APHYRIC GRAY BASALT FLOW. Locally micro-brecciated flow top, with some pale green smectite-filled fractures. Most vesicles are dark green smectite filled. Moderately vesicular toward center of flow. Some rare rounded cognate xenoliths of highly vesicular, fine-grained aphyric gray basalt present. Fine basal breccia at 25R–3, 76–79 cm. [Unrelated rubble at 642E–25R–1 (0–12 cm)]

THIN SECTION DESCRIPTIONS

642E–24R–2 (Piece 2B, 56–58 cm): Phenocrysts: 2% glomerophytic plag, 1% cpx. Groundmass: 35% plag, 10% cpx, 5% opaques, 47% altered mesostasis and cognate xenolith.

642E–25R–1 (Piece 5A, 35–37 cm): 4% oscillatory zoned plag phenocrysts, 40% plag, 40% cpx, both somewhat altered. 5% opaques, 11% altered mesostasis.

UNIT S15

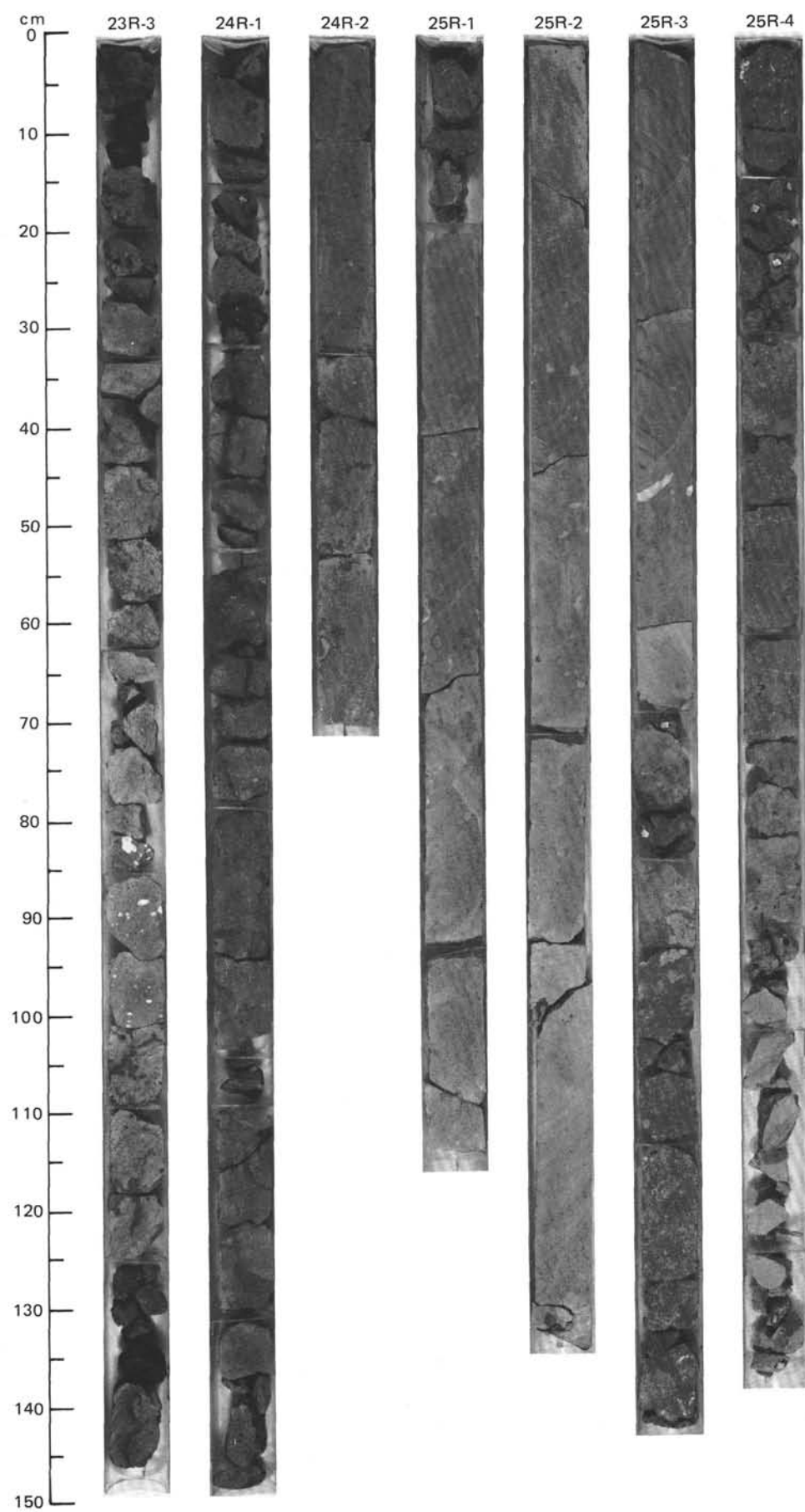
495.2–495.8 MBSF 642E–25R–3 (79 cm) TO 25R–3 (84 cm)

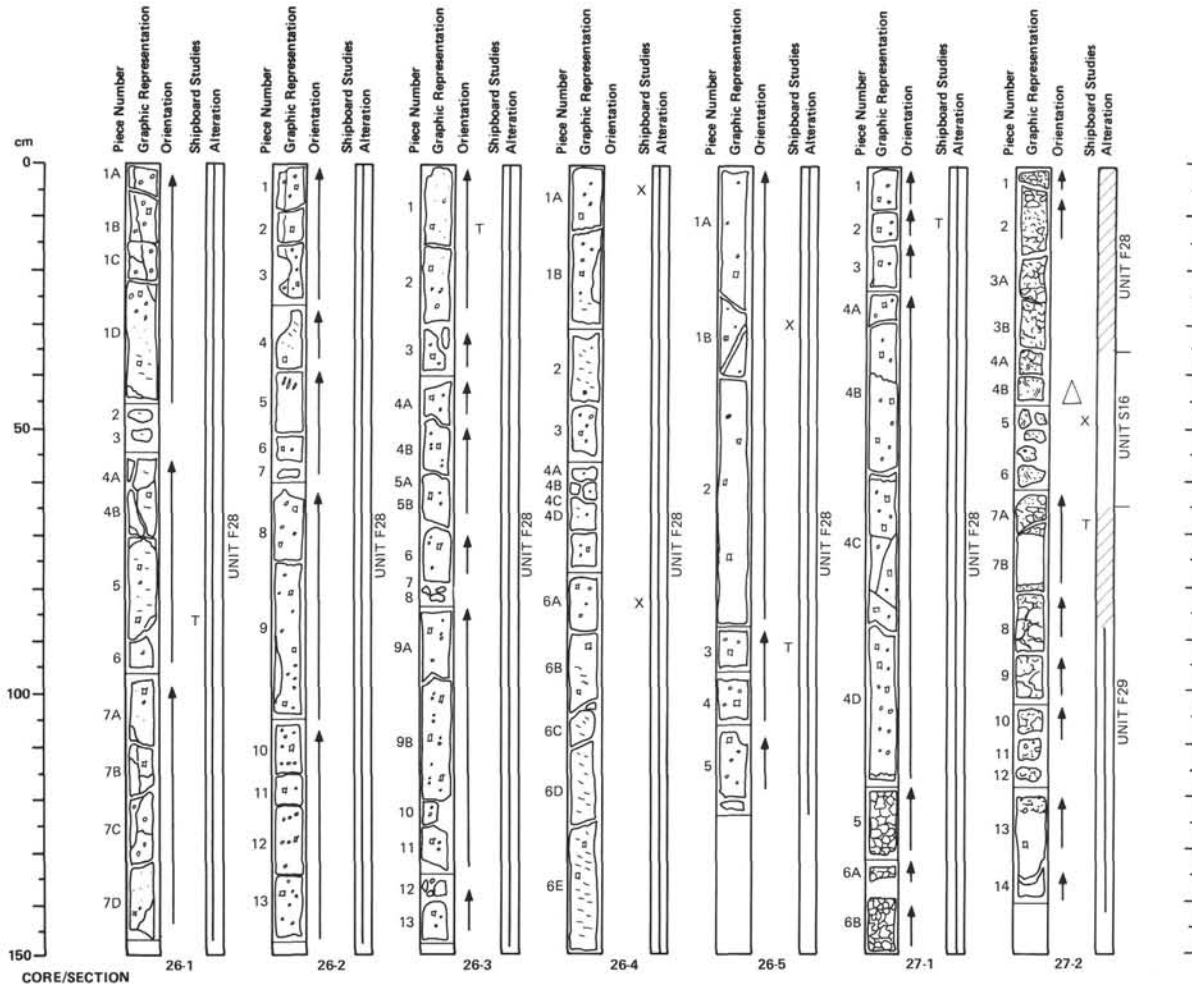
VERY DARK BROWN TUFF. Tuff has lithic fragments of overlying breccia. Some slightly altered shards, light green and more vesicular, black.

UNIT F28

495.8–511.0 MBSF 642E–25R–3 (79 cm) TO 27R–2 (35 cm)

FINE-GRAINED, PLAGIOCLASE PHYRIC GRAY BASALT FLOW. Moderately to highly vesicular at flow top, streamed and coalesced. Some fracturing, subvertical. Streaking (flow fabric) from 26R–4, 95 cm, downsection, locally inclined, mainly subhorizontal. Xenolithic. 70 cm thick dark gray to dark brownish gray basal breccia.





UNIT F28

495.8–511.0 MBSF 642E–25R–3 (79 cm) TO 27R–2 (35 cm)

FINE-GRAINED, PLAGIOCLASE PHYRIC GRAY BASALT FLOW. Moderately to highly vesicular at flow top, streamered and coalesced. Some fracturing, subvertical. Streaking (flow fabric) from 26R–4, 95 cm, downsection, locally inclined, mainly subhorizontal. Xenolithic. 70 cm thick dark gray to dark brownish gray basal breccia.

UNIT S16

511.0–511.5 MBSF 642E–27R–2 (35 cm) TO 27R–2 (64 cm)

DARK RED BROWN TO PURPLE TUFFS AND SANDY TUFFS. Subhorizontally layered. Contains pebbles of basaltic breccia, some zones with fresh glass.

UNIT F29

511.5–521.2 MBSF 642E–27R–2 (64 cm) TO 28R–3 (117 cm)

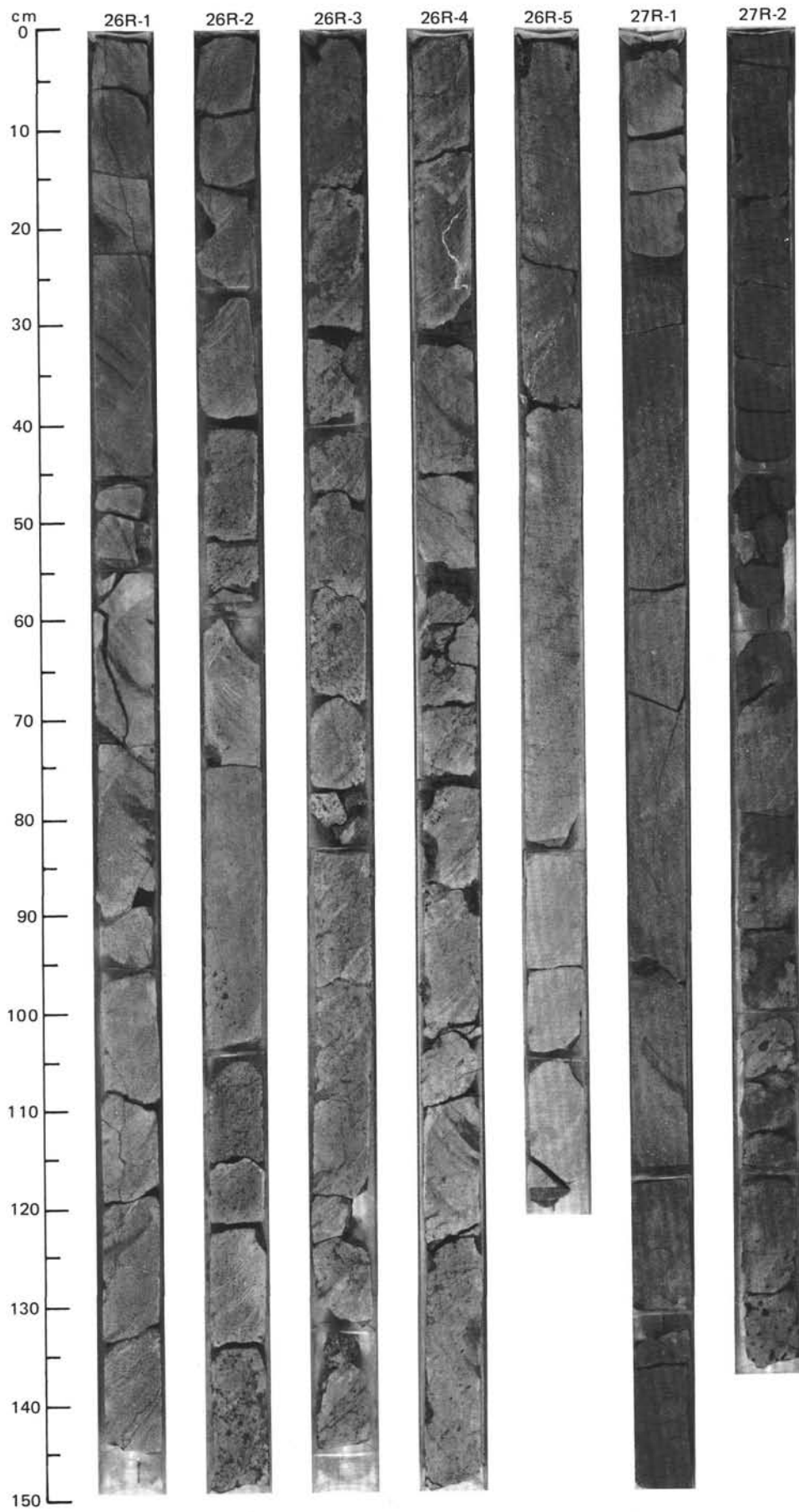
FINE GRAINED, MODERATELY PLAGIOCLASE PHYRIC, DARK GRAY BASALT FLOW. Reddened scoriaceous breccia flow top, with vesicularity decreasing downsection, some streaming and coalescence of dark green smectite filled vesicles. Well developed streaking (flow fabric) from 28R–1, 0 cm, downward. True inclination of fabric locally up to 45 degrees. Rare xenoliths, basal vesicular zone, breccia and contact with S17 well preserved.

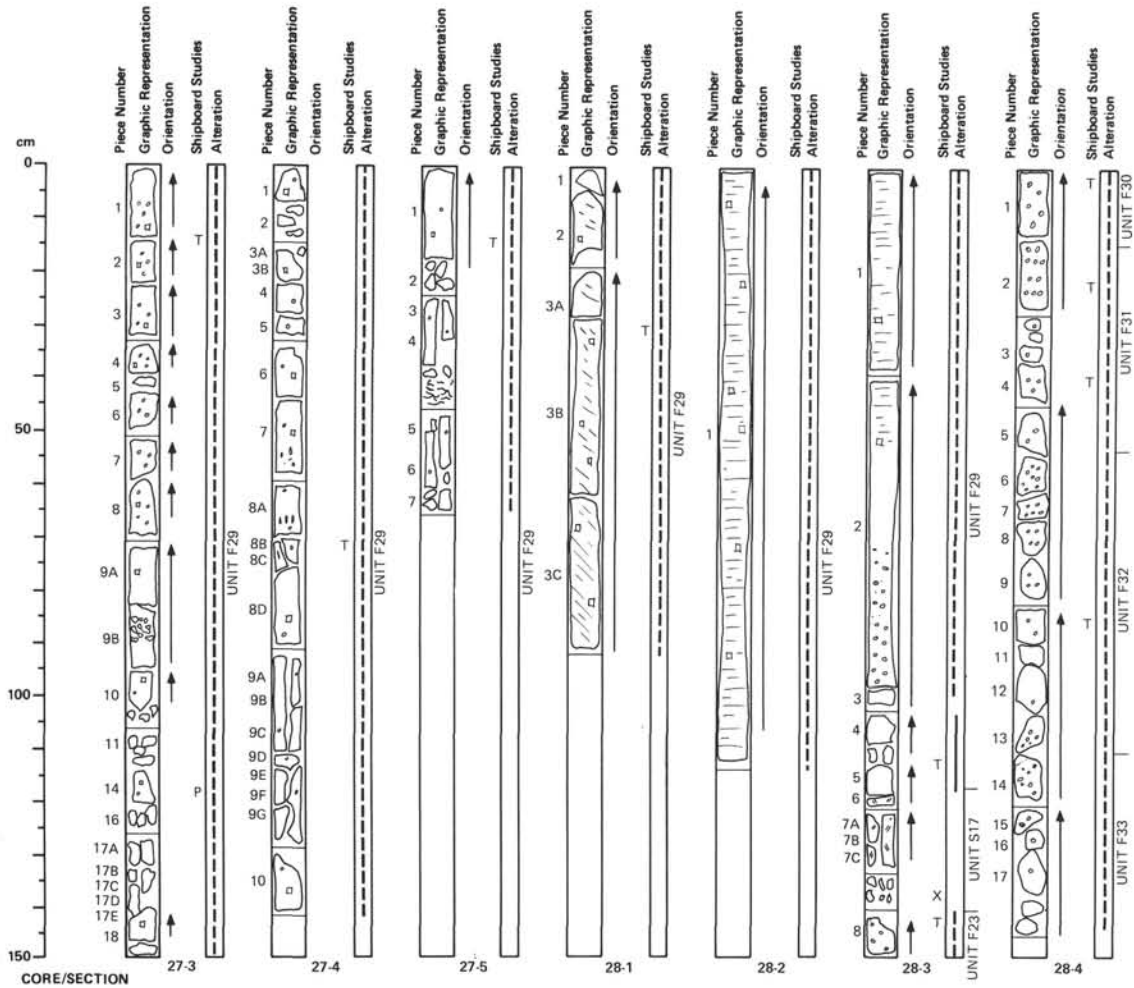
THIN SECTION DESCRIPTIONS

642E–27R–3 (Piece 14, 15–19 cm): 1% plag phenocrysts, 40% groundmass plag, 5% cpx, 14% altered mesostasis, 40% altered material of a cognate xenolith.

642E–27R–4 (Piece 8A, 66–68 cm): 10% plag phenocrysts. 35% plag, 5% cpx, 2% ol, 5% opaques in groundmass. 43% altered mesostasis. Intersertal.

642E–27R–5 (Piece 1, 11–15 cm): Phenocrysts: 12% plag, 2% cpx. Groundmass: 45% plag, 35% cpx, 3% opaques. 3% altered mesostasis. Intersertal to subophitic.





UNIT F29

511.5–521.2 MBSF 642E–27R–2 (64 cm) TO 28R–3 (117 cm)

FINE GRAINED, MODERATELY PLAGIOCLASE PHYRIC, DARK GRAY BASALT FLOW. Reddened scoriaceous breccia flow top, with vesicularity decreasing downsection, some streaming and coalescence of dark green smectite filled vesicles. Well developed streaking (flow fabric) from 28R–1, 0 cm, downward. True inclination of fabric locally up to 45 degrees. Rare xenoliths, basal vesicular zone, breccia and contact with S17 well preserved.

THIN SECTION DESCRIPTIONS

642E–27R–3 (Piece 14, 15–19 cm): 1% plag phenocrysts, 40% groundmass plag, 5% cpx, 14% altered mesostasis, 40% altered material of a cognate xenolith.

642E–27R–4 (Piece 8A, 66–68 cm): 10% plag phenocrysts, 35% plag, 5% cpx, 2% ol, 5% opaques in groundmass. 43% altered mesostasis. Intersertal.

642E–27R–5 (Piece 1, 11–15 cm): Phenocrysts: 12% plag, 2% cpx. Groundmass: 45% plag, 35% cpx, 3% opaques. 3% altered mesostasis. Intersertal to subophitic.

UNIT S17

521.2–522.7 MBSF 642E–28R–3 (117 cm) TO 28R–3 (140 cm)

DARK BROWN TO BROWN SANDY BASALTIC VITRIC TUFF. Pale green spotting. Uniform shards slightly vesicular.

UNIT F30

522.7–523.2 MBSF 642E–28R–3 (140 cm) TO 28R–4 (16 cm)

MEDIUM- TO FINE-GRAINED, APHYRIC BLACK BASALT. Fine grained and vesicular upper flow. Vesicles rimmed with green smectite, none filled. Crystallinity grades into medium grade lower in flow.

UNIT F31

523.3–524.2 MBSF 642E–28R–4 (16 cm) TO 28R–4 (53 cm)

MEDIUM-GRAINED APHYRIC, BLACK BASALT FLOW. Grades from glassy, highly vesicular flow top rapidly into medium-grain size. Open vesicles are coated with green smectite.

UNIT F32

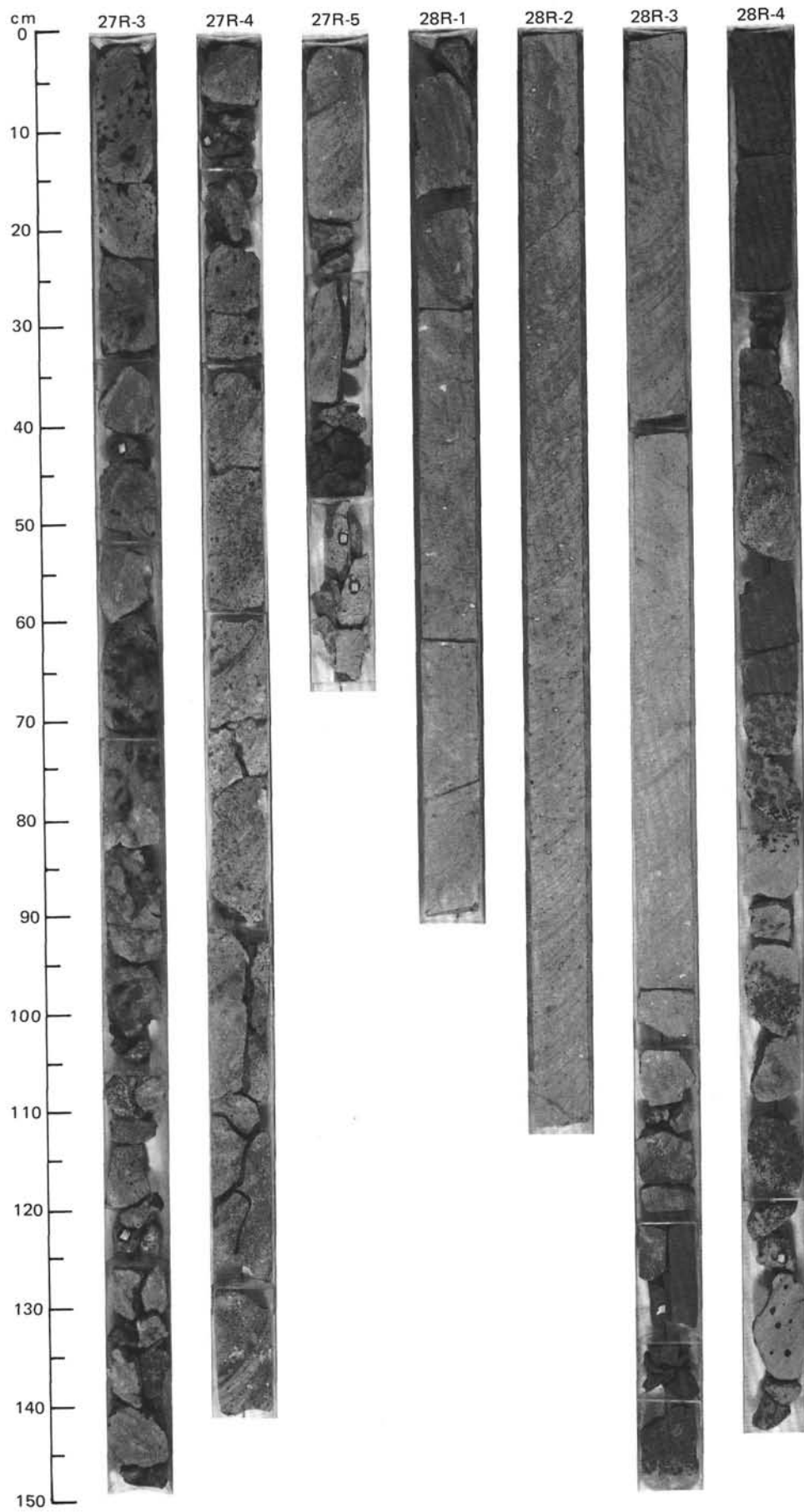
524.2–525.0 MBSF 642E–28R–4 (53 cm) TO 28R–4 (110 cm)

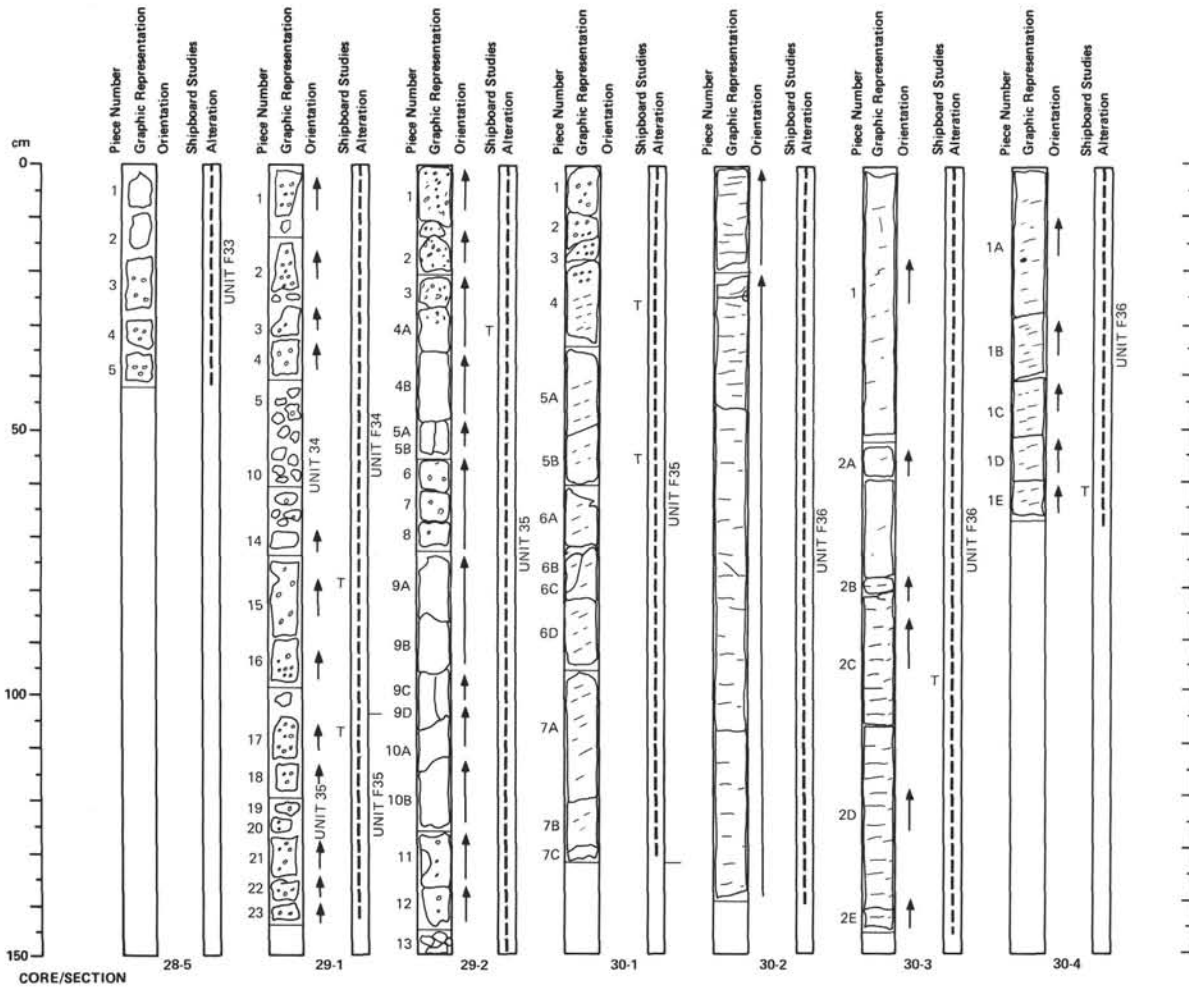
AS F31.

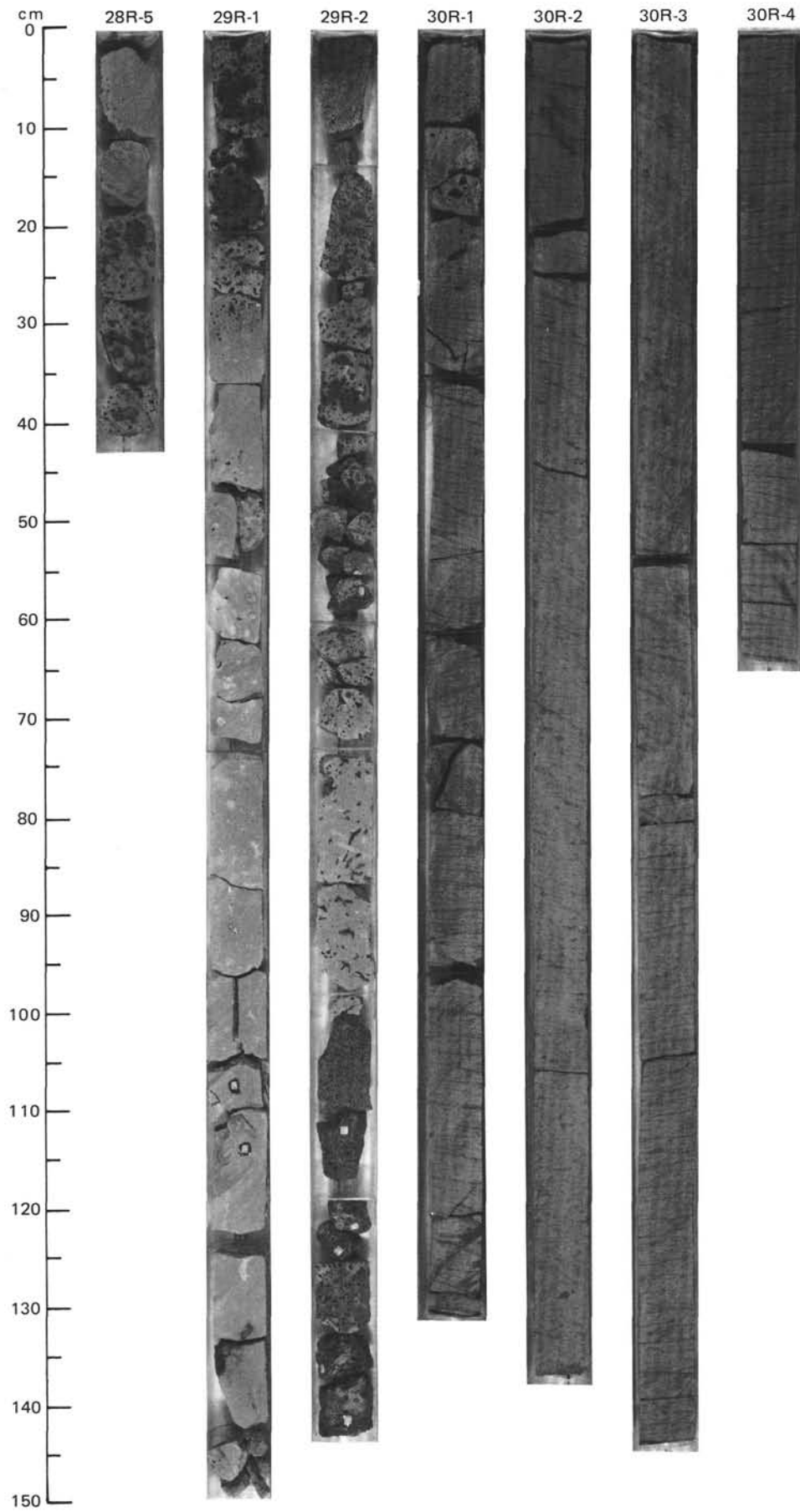
UNIT F33

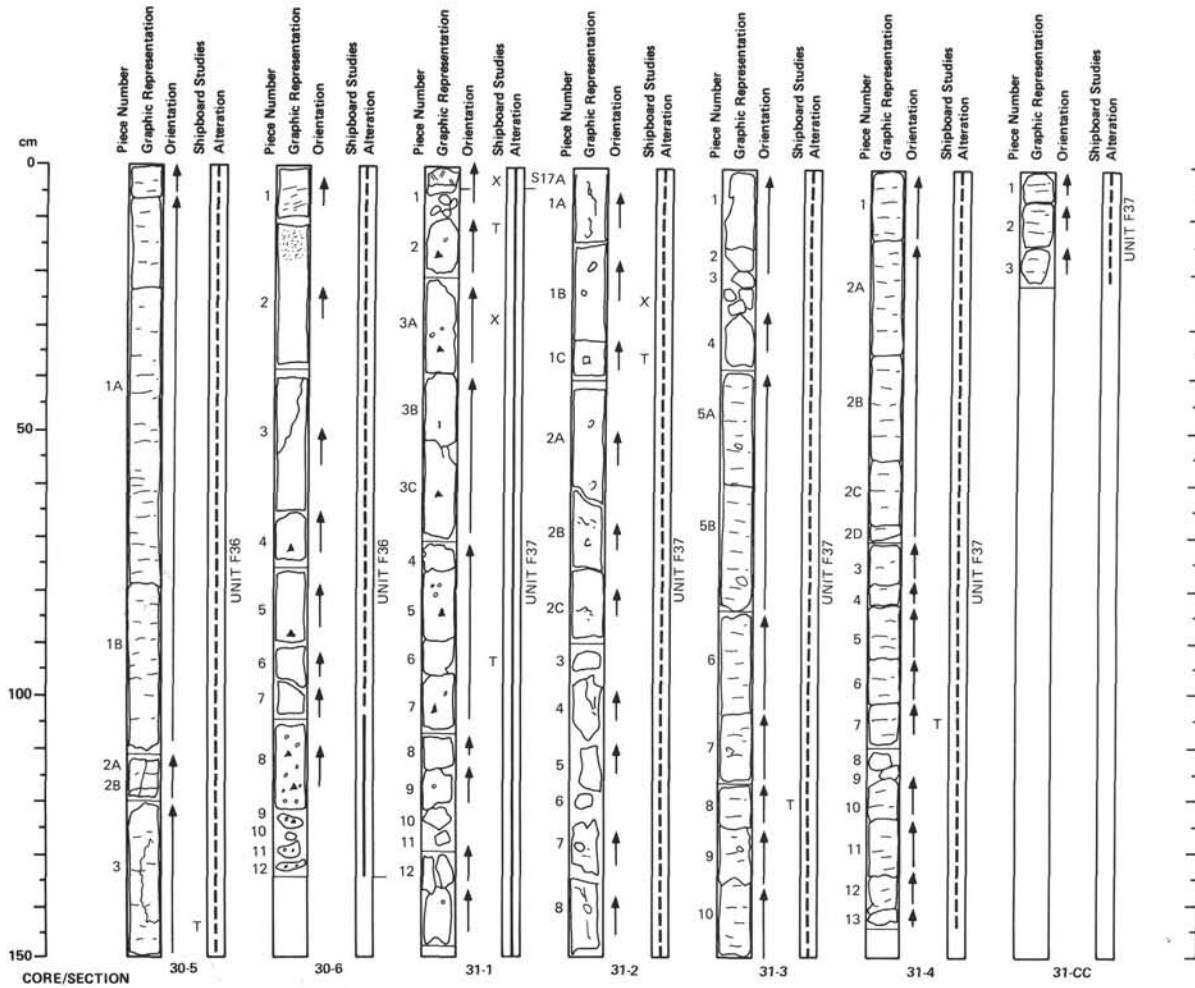
525.0–526.9 MBSF 642E–28R–4 (110 cm) TO 28R–5 (42 cm)

AS F31.









UNIT F36

533.7–546.3 MBSF

642E–30R–1 (0 cm) TO 30R–6 (135 cm)

FINE-GRAINED, APHYRIC, GRAY BASALT FLOW. Flow top not recovered. Locally highly vesicular at top of unit, but missing uppermost vesicular zone. Streamed vesicularity overlies thick streaky (flow laminated) section. Xenolithic and fractured with dark green smectite predominant in veins.

THIN SECTION DESCRIPTION

642E–30R–1 (24–26 cm): Phenocrysts: < 1% plag, trace cpx. Groundmass: 40% plag, 35% cpx, 5% opaques, 19% altered mesostasis.

UNIT S17A

546.3–546.4 MBSF

642E–31R–1 (0 cm) TO 31R–1 (4 cm)

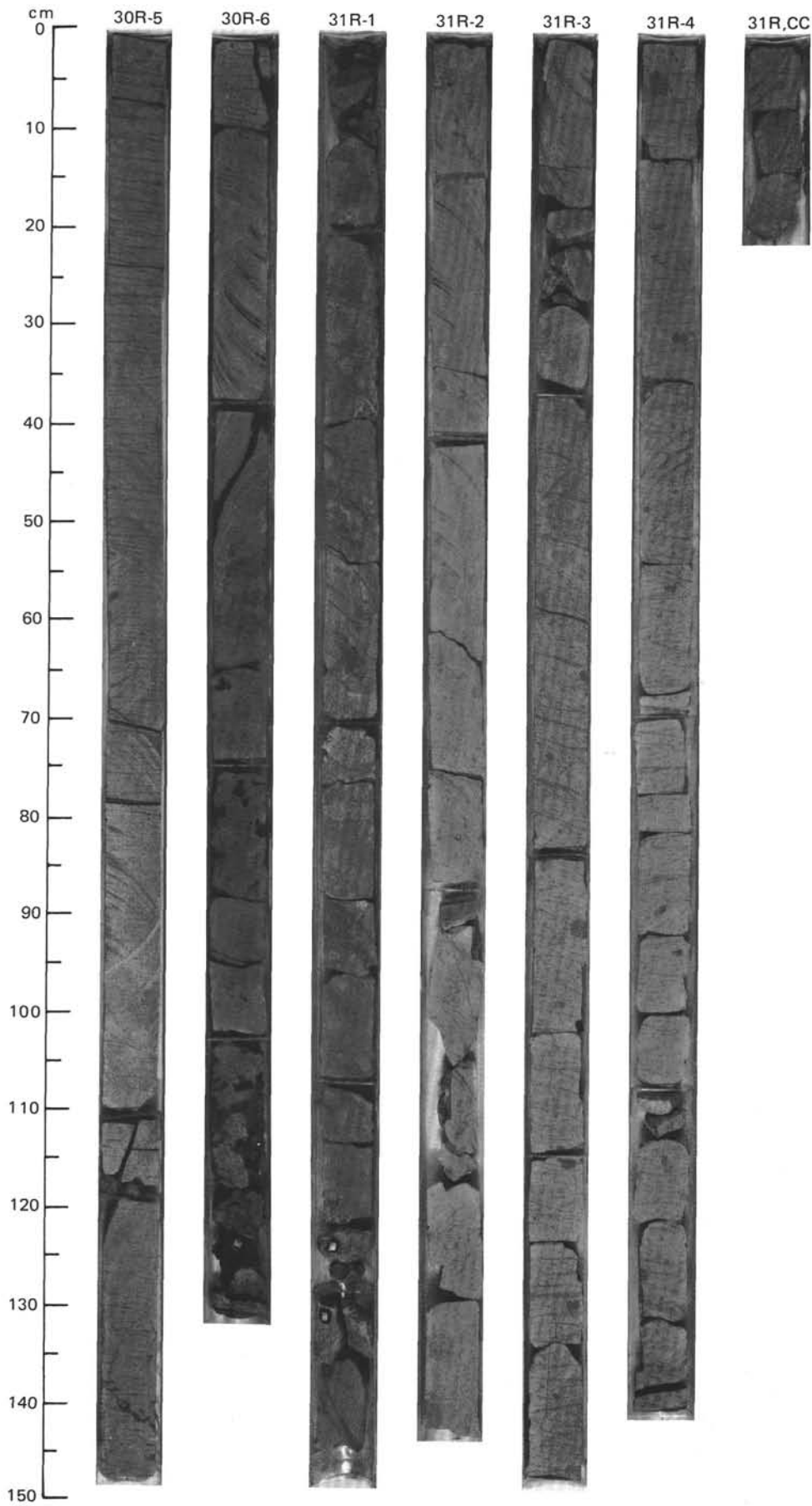
BASALTIC VITRIC TUFF IN PLACE AS RUBBLE. Forms top of flow unit F37.

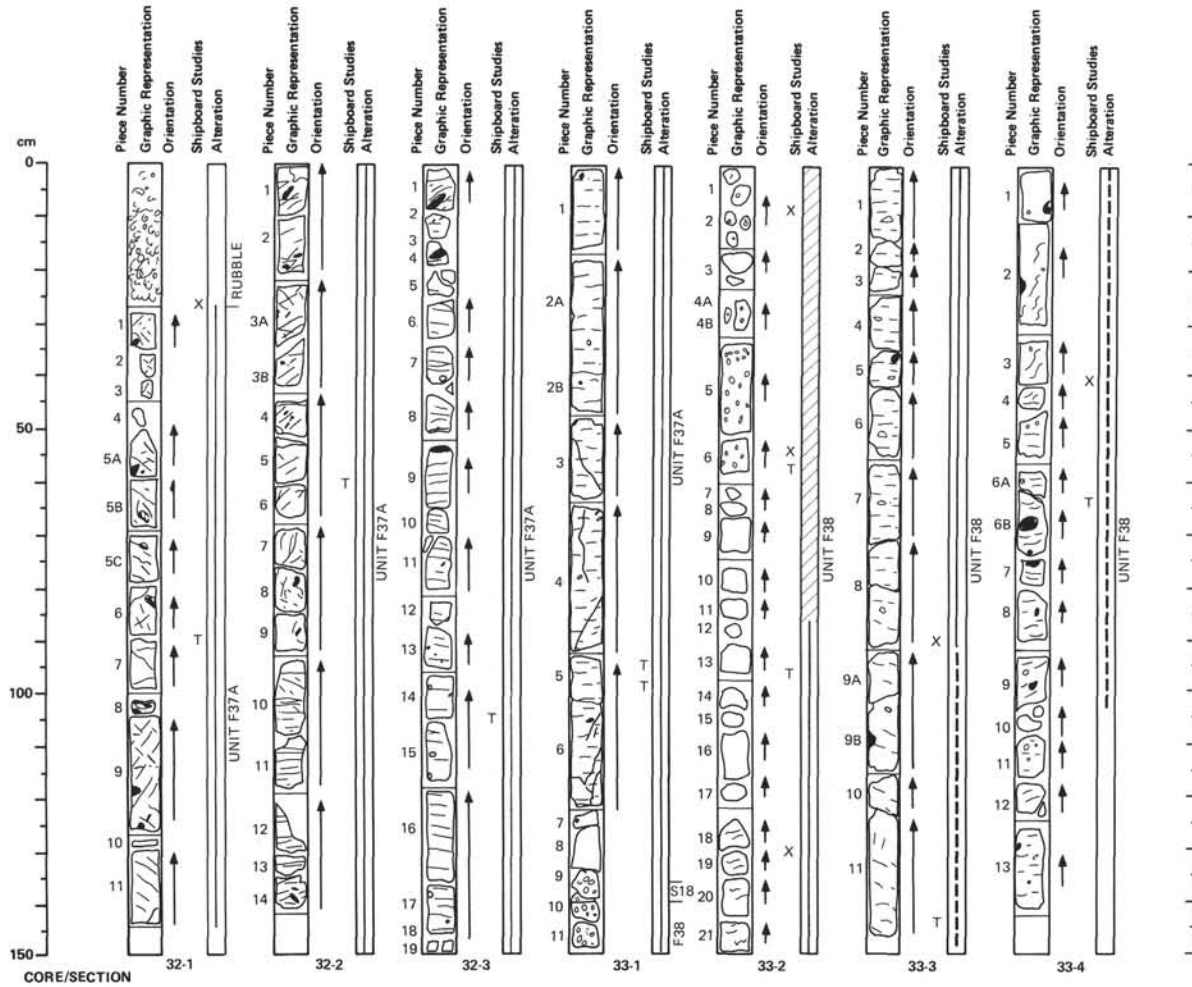
UNIT F37

546.4–556.0 MBSF

642E–31R–1 (4 cm) TO 31R–CC (22 cm)

FINE-GRAINED, APHYRIC, GRAY BASALT FLOW. Flow base not recovered. Reddened through upper section. As F36, with streaking fabric wrapping and deflected by abundant xenoliths.



**UNIT F37A**

556.0–565.6 MBSF 642E–32R–1 (27 cm) to 33R–1 (136 cm)

FINE-GRAINED, APHYRIC, GRAY BASALT FLOW. Flow base and flow top recovered. As F36 and F37, with streaking fabric wrapping and deflected by abundant xenoliths. Local cross-hatching of poorly developed fabric.

THIN SECTION DESCRIPTION

642E–32R–1 (89–91 cm): Phenocrysts: <1% plag, <1% cpx. Groundmass: 45% plag, 40% cpx, 5% opaques, 9% altered mesostasis.

UNIT S18

565.6–565.7 MBSF 642E–33R–1 (136 cm) TO 33R–1 (138 cm)

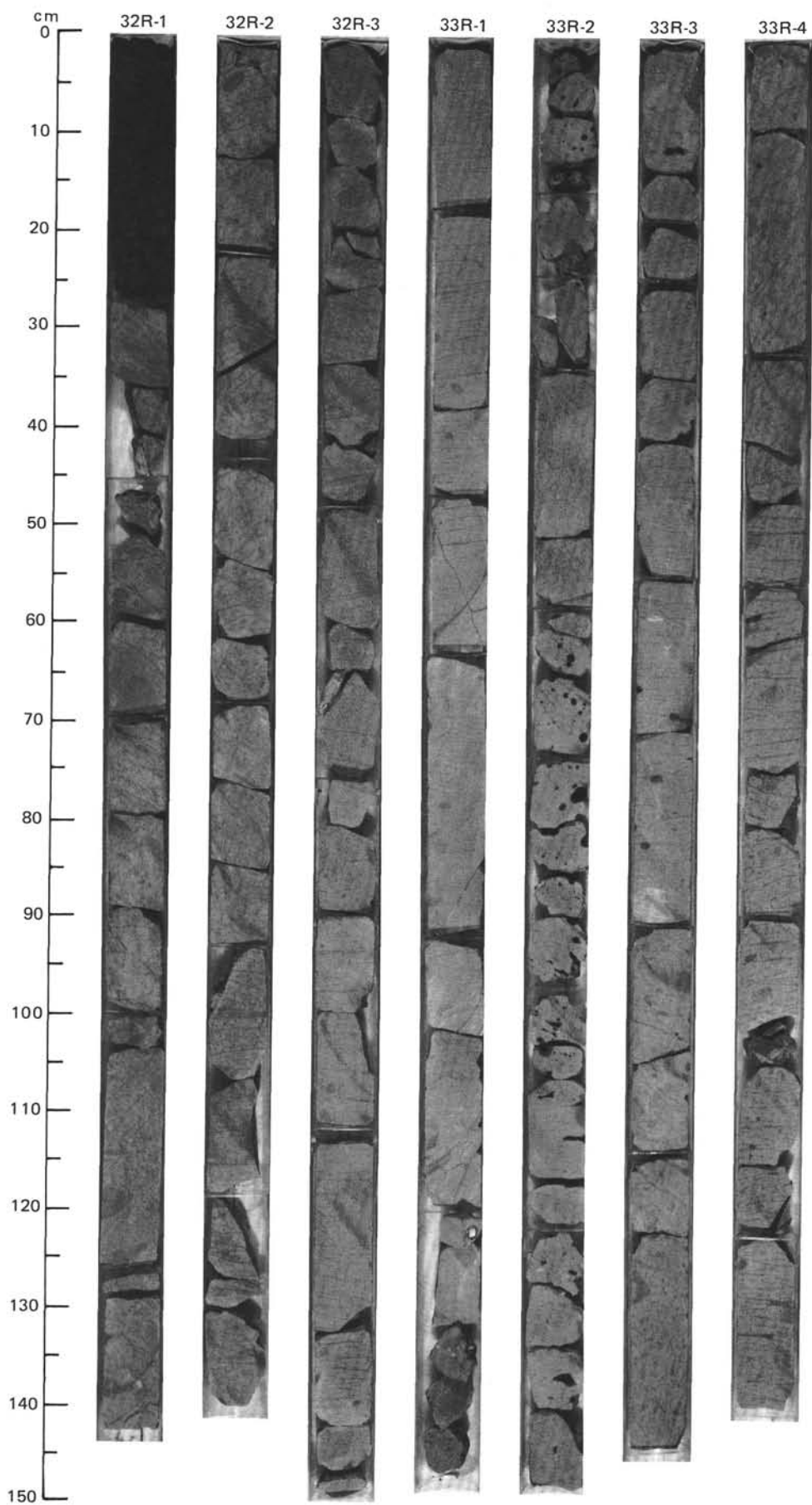
DARK RED BROWN TUFF.**UNIT F38**

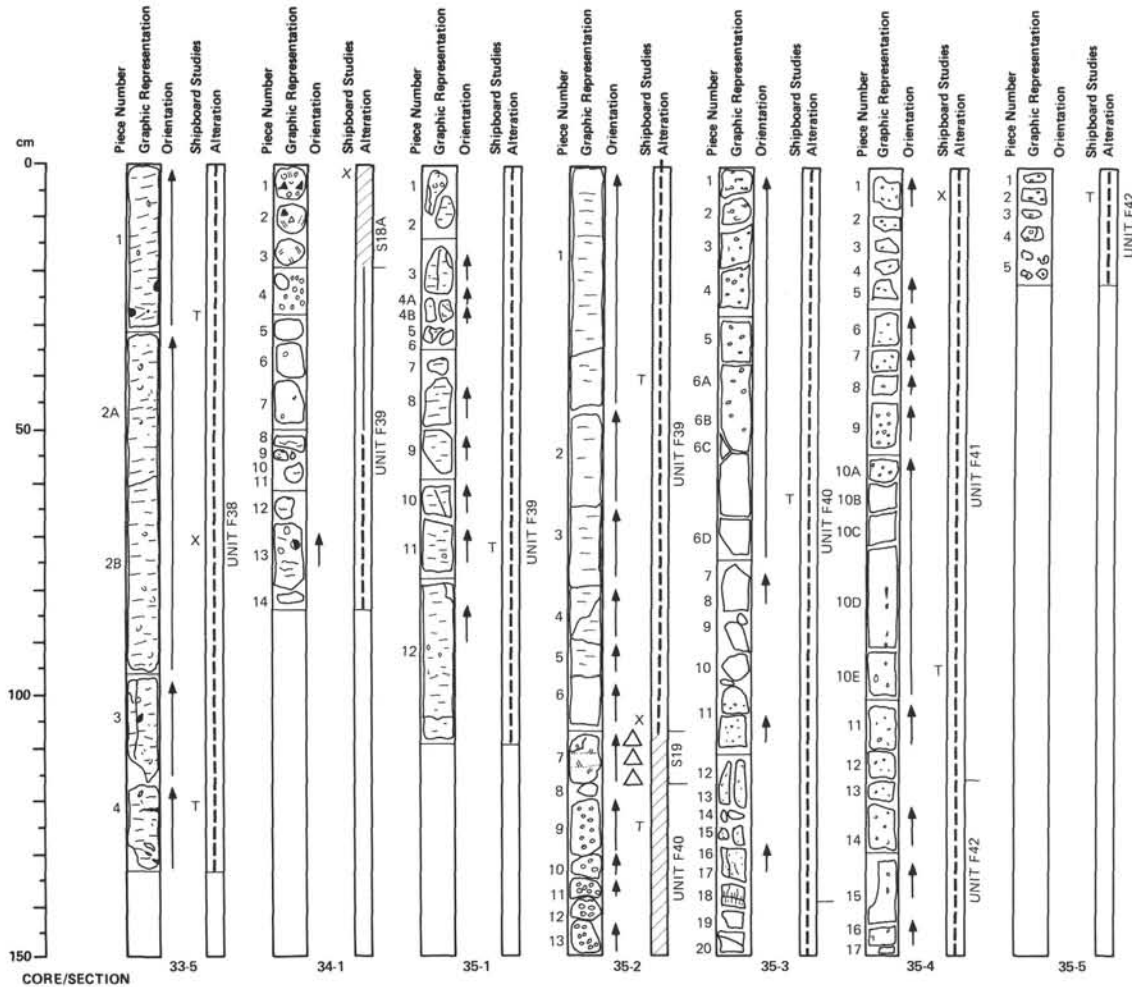
565.7–572.6 MBSF 642E–33R–1 (138 cm) TO 33R–5 (134 cm)

FINE-GRAINED, APHYRIC, GRAY BASALT FLOW. Flow base not recovered. Reddened vesicular flow top. Patch smectite alteration throughout groundmass, some blue green smectite (celadonite?) vesicle filling. Olivine iddingsitized throughout.

THIN SECTION DESCRIPTION

642E–33R–2 (Piece 6, 54–56 cm): 35% plag, 30% cpx, 5% opaques, 10% iddingsite, 20% altered variolitic mesostasis. Intergranular-intersertal, subophitic.





UNIT F38

565.7–572.6 MBSF 642E–33R–1 (138 cm) TO 33R–5 (134 cm)

FINE-GRAINED, APHYRIC, GRAY BASALT FLOW. Flow base not recovered. Reddened vesicular flow top. Patch smectite alteration throughout groundmass, some blue green smectite (celadonite?) vesicle filling. Olivine iddingsitized throughout.

THIN SECTION DESCRIPTION

642E–33R–2 (Piece 6, 54–56 cm): 35% plag, 30% cpx, 5% opaques, 10% iddingsite, 20% altered variolitic mesostasis. Intergranular-interstitial, subophitic.

UNIT S18A

572.6–573.2 MBSF 642E–34R–1 (0 cm) TO 34R–1 (18 cm)

BASALTIC VITRIC TUFF. As rubble in place.

UNIT F39

573.2–584.1 MBSF 642E–34R–1 (18 cm) TO 35R–2 (106 cm)

FINE-GRAINED, APHYRIC, GRAY BASALT. Flow base missing. Weakly reddened, highly vesicular upper section, locally brecciated. Streamed and coalesced vesicular zone. Subparallel, subhorizontal streaking (flow fabric) with tightening of fabric toward base of section. Iddingsitization gives reddish hue to streaks. Slight increase in vesicularity at base, highly vesicular base missing.

UNIT S19

584.1–584.3 MBSF 642E–35R–2 (106 cm) TO 35R–2 (114 cm)

BRICK RED BROWN, UPWARD-FINING TUFF SEQUENCES. Three cycles, fresh glass at base of middle sequence. Basaltic fragment at base.

UNIT F40

584.3–586.8 MBSF 642E–35R–2 (114 cm) TO 35R–3 (137 cm)

MEDIUM-GRAINED, MODERATELY PLAGIOCLASE PHYRIC BASALT. Reddish dark gray mottled with dark green smectitic alteration, moderately vesicular with some vesicles elongated or collapsed. Vertical openings into base of flow with smectite and breccia fillings.

THIN SECTION DESCRIPTION

642E–35R–2 (Piece 9, 125–128 cm): 35% plag, 30% cpx, 2% ol, 8% opaques, 20% altered variolitic mesostasis.

UNIT F41

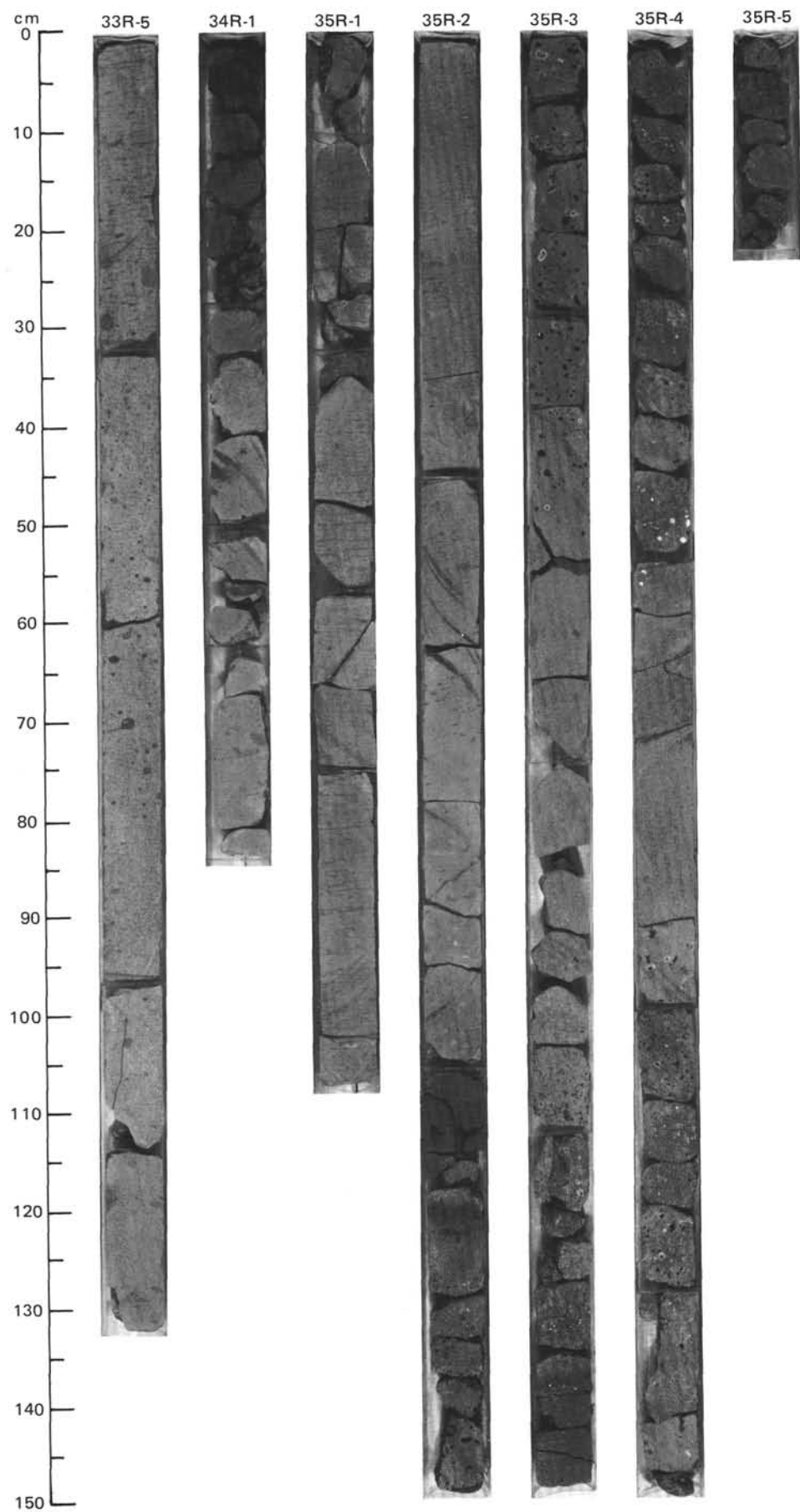
586.8–589.7 MBSF 642E–35R–3 (137 cm) TO 35R–4 (115 cm)

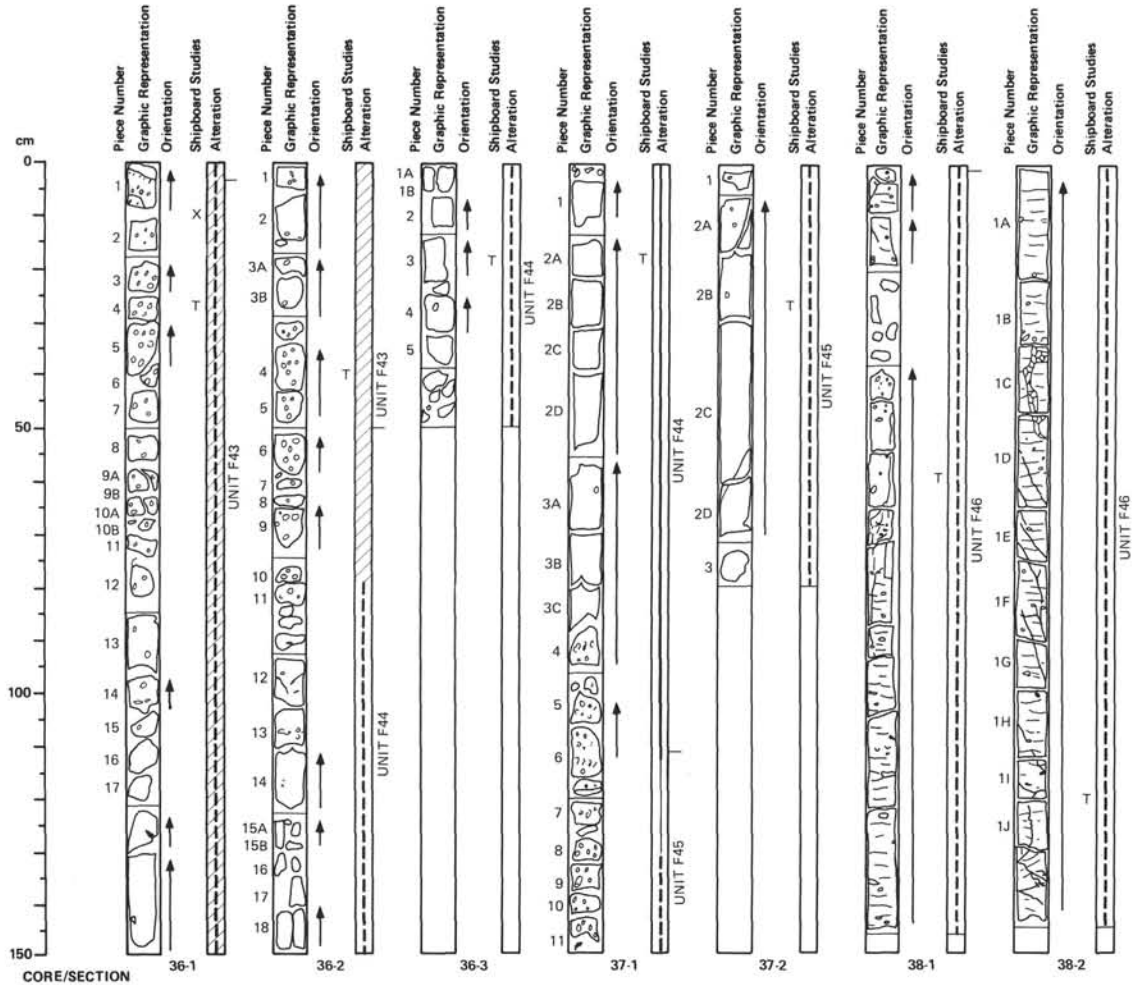
AS F40 with reddish gray groundmass color.

UNIT F42

589.7–591.4 MBSF 642E–35R–4 (115 cm) TO 36R–1 (4 cm)

AS F40, with reddish dark gray, fine-grained flow top.





UNIT F43

591.4–594.0 MBSF 642E–36R–1 (4 cm) TO 36R–2 (52 cm)

MEDIUM-GRAINED GRAY BASALT FLOW. Purplish gray vesicular flow top, with vesicularity up to 15%. Rare phenocrysts of plagioclase and olivine(?) completely altered to secondary minerals. Some vesicles filled with dark green smectite and/or pale green celadonite.

THIN SECTION DESCRIPTIONS

642E–36R–1 (28–30 cm): 35% plag, 35% cpx, 3% altered ol, 10% opaques, 17% altered mesostasis. Intergranular to intersertal.

642E–36R–2 (Piece 4, 38–40 cm): Phenocrysts: 15% plag, 3% cpx. Groundmass: 5% plag, 3% cpx, 6% ol, 15% cryptocrystalline, 35% Fe-oxide-stained altered mesostasis, 18% clays.

UNIT F44

594.0–601.6 MBSF 642E–36R–2 (52 cm) TO 37R–1 (112 cm)

AS F43. With black to purple basal vesicular zones. Contact preserved.

THIN SECTION DESCRIPTION

642E–36R–3 (16–18 cm): 48% plag, 22% cpx, 10% ol, 1% opaques, 19% altered mesostasis.

UNIT F45

601.6–607.4 MBSF 642E–37R–1 (112 cm) TO 37R–2 (82 cm)

MEDIUM-GRAINED, APHYRIC, GRAY BASALT FLOW. Vesicular, with vesicles filled with calcite and/or zeolite. Locally light green smectite (?celadonite).

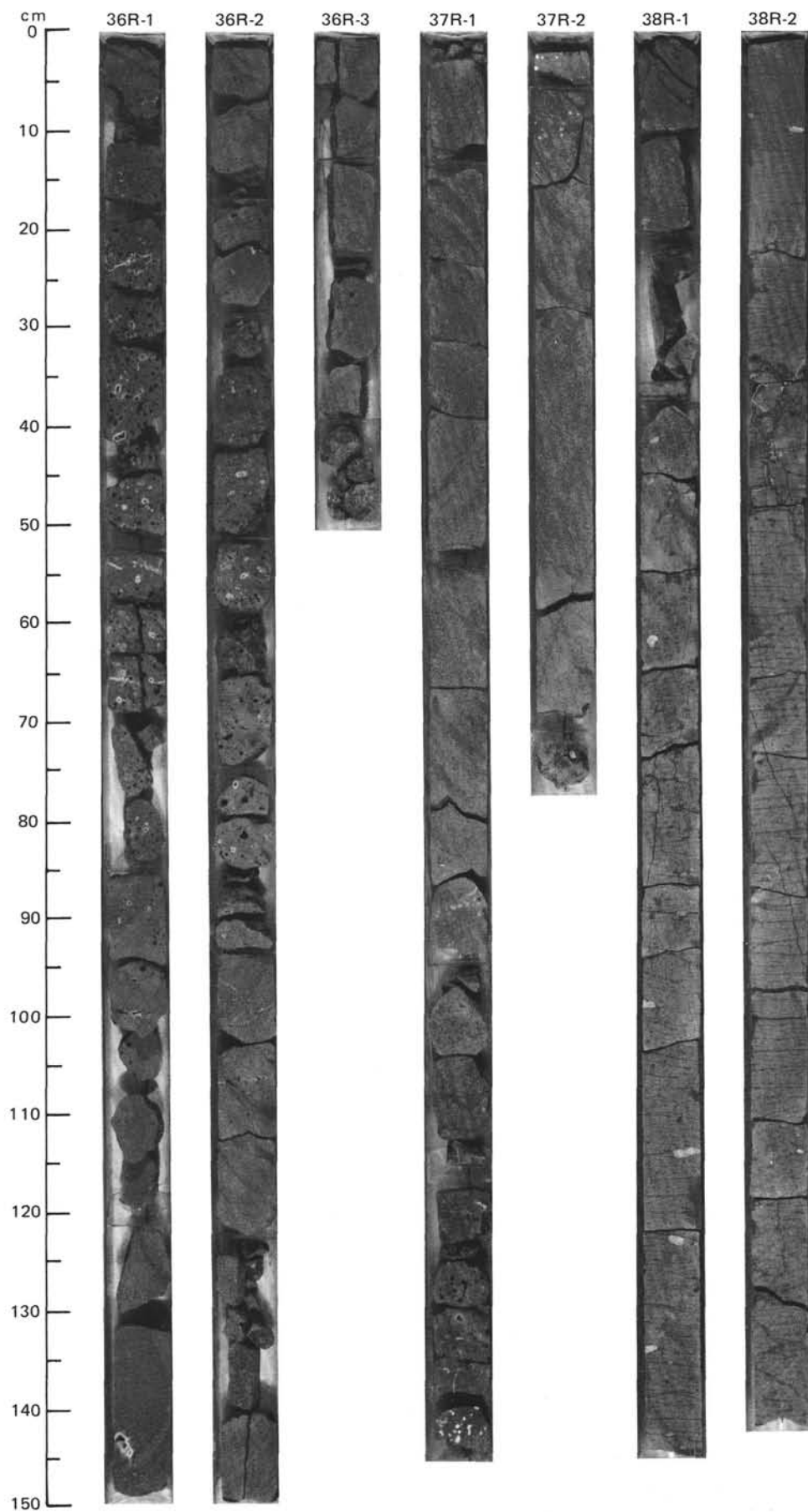
UNIT S19A

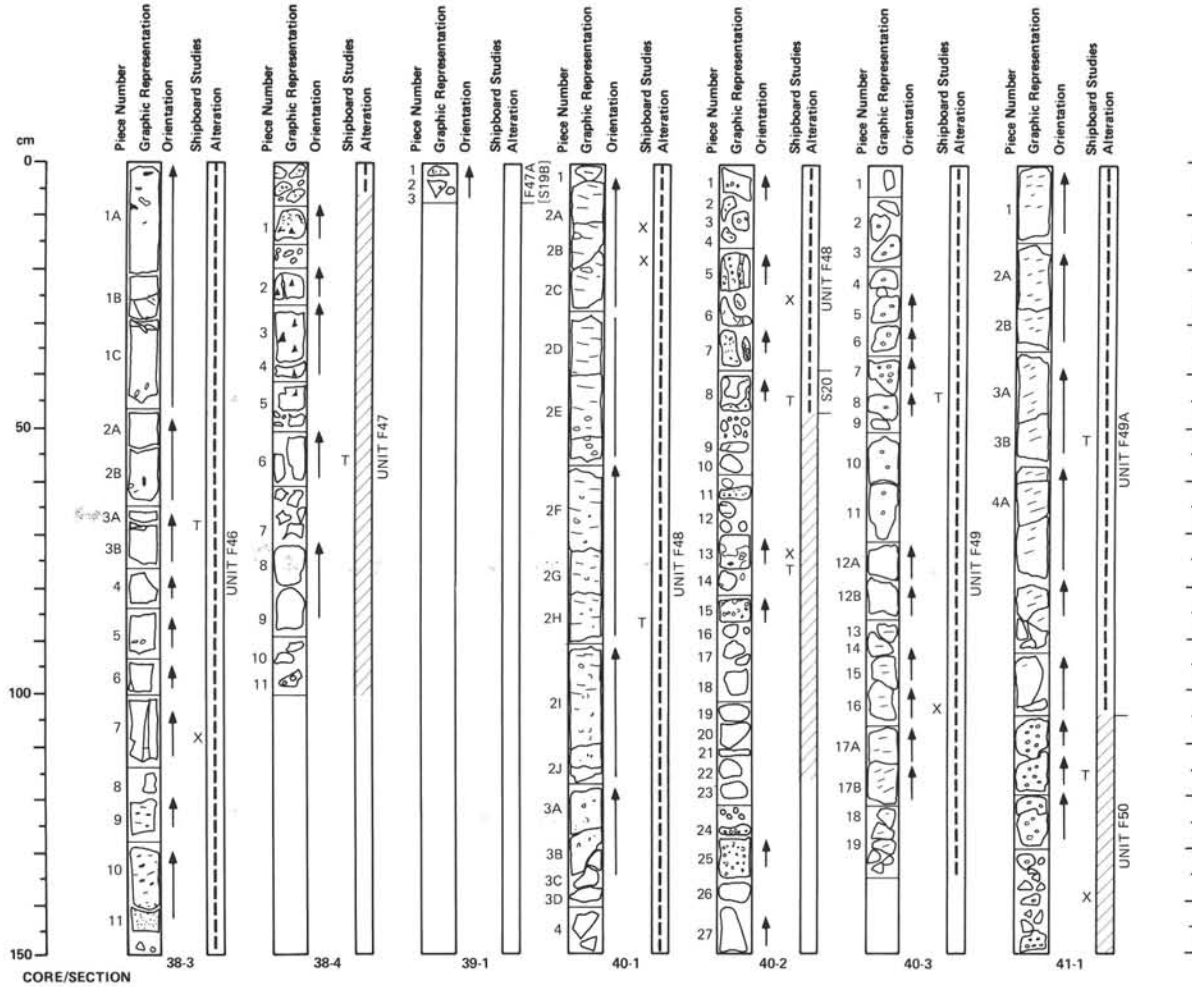
607.4–607.5 MBSF NOT RECOVERED

UNIT F46

607.5–614.6 MBSF 642E–38R–1 (0 cm) TO 38R–3 (150 cm)

FINE-GRAINED, APHYRIC, GRAY BASALT FLOW. Flow top not recovered. Sparsely vesicular throughout, except for highly vesicular flow base (38R–3, 140–145 cm). Vesicles filled with green smectite and/or calcite, subhorizontally elongated at 38R–3, 120–140 cm. Sub-horizontal spaced streaking (flow lamination) gives way to massive base below 38R–3, 90 cm. Rounded xenoliths of vesicular, gray, aphyric basalt throughout. Steeply inclined or vertical fine smectite filled veins, narrow breccia zone at 38R–2, 32–50 cm. Fresh plagioclase laths are locally aligned, accompanied by fresh anhedral clinopyroxene, and smectite/iddingsite pseudomorphs after olivine.





607.5–614.6 MBSF

FINE-GRAINED, APHYRIC, GRAY BASALT FLOW. Flow top not recovered. Sparsely vesicular throughout, except for highly vesicular flow base (38R-3, 140–145 cm). Vesicles filled with green smectite and/or calcite, subhorizontally elongated at 38R-3, 120–140 cm. Subhorizontal spaced streaking (flow lamination) gives way to massive base below 38R-3, 90 cm. Rounded xenoliths of vesicular, gray, aphyric basalt throughout. Steeply inclined or vertical fine smectite filled veins, narrow breccia zone at 38R-2, 32–50 cm. Fresh plagioclase laths are locally aligned, accompanied by fresh anhedral clinopyroxene, and smectite/iddingsite pseudomorphs after olivine.

UNIT F46

642E–38R-1 (0 cm) TO 38R-3 (150 cm)

614.6–617.7 MBSF

FINE-GRAINED, APHYRIC BASALT FLOW. Flow base and probably center not recovered. Upper part scoriaceous and brecciated, red to purplish gray, highly vesicular and gray below, vesicles rimmed or smectite filled. Olivine completely iddingsitized, abundant Fe oxides.

UNIT F47

642E–38R-4 (0 cm) TO 38R-4 (100 cm)

617.7–618.5 MBSF

UNIT S19B

NOT RECOVERED

618.5–625.6 MBSF

UNIT F47A

642E–39R-1 (0 cm) TO 39R-1 (5 cm)

AS F47.

UNIT S19C

625.6–625.9 MBSF

NOT RECOVERED

625.9–631.6 MBSF

UNIT F48

642E–40R-1 (0 cm) TO 40R-2 (40 cm)

FINE-GRAINED, APHYRIC, GRAY BASALT FLOW. Flow top not recovered. Moderately to sparsely vesicular throughout, with green smectite and/or calcite filling. Subhorizontal spaced streaking (flow fabric) down to 40R-1, 100 cm. Fine fracturing 75–90 cm, with calcite and smectite filled veins near base of flow.

UNIT S20

631.6–631.7 MBSF

642E–40R-2 (40 cm) TO 40R-2 (46 cm)

DARK RED BROWN TUFF. Contains irregular vesicular fragments from the underlying flow.

UNIT F49

631.7–636.6 MBSF

642E–40R-2 (46 cm) TO 40R-3 (134 cm)

FINE-GRAINED, APHYRIC, GRAY BASALT FLOW WITH REDDENED FLOW TOP. Flow base not recovered. Moderately to sparsely vesicular throughout with smectite and locally calcite filling; some vesicles flattened toward base. Horizontal spaced streaking (flow fabric) below 40R-3, 85 cm, locally chaotic. Some subvertical hairline fracturing is smectite filled, one example 4 mm at wide, 40R-3, 30–85 cm.

UNIT 49A

636.6–640.8 MBSF

642E–41R-1 (0 cm) TO 41R-1 (103 cm)

AS F49.

UNIT F50

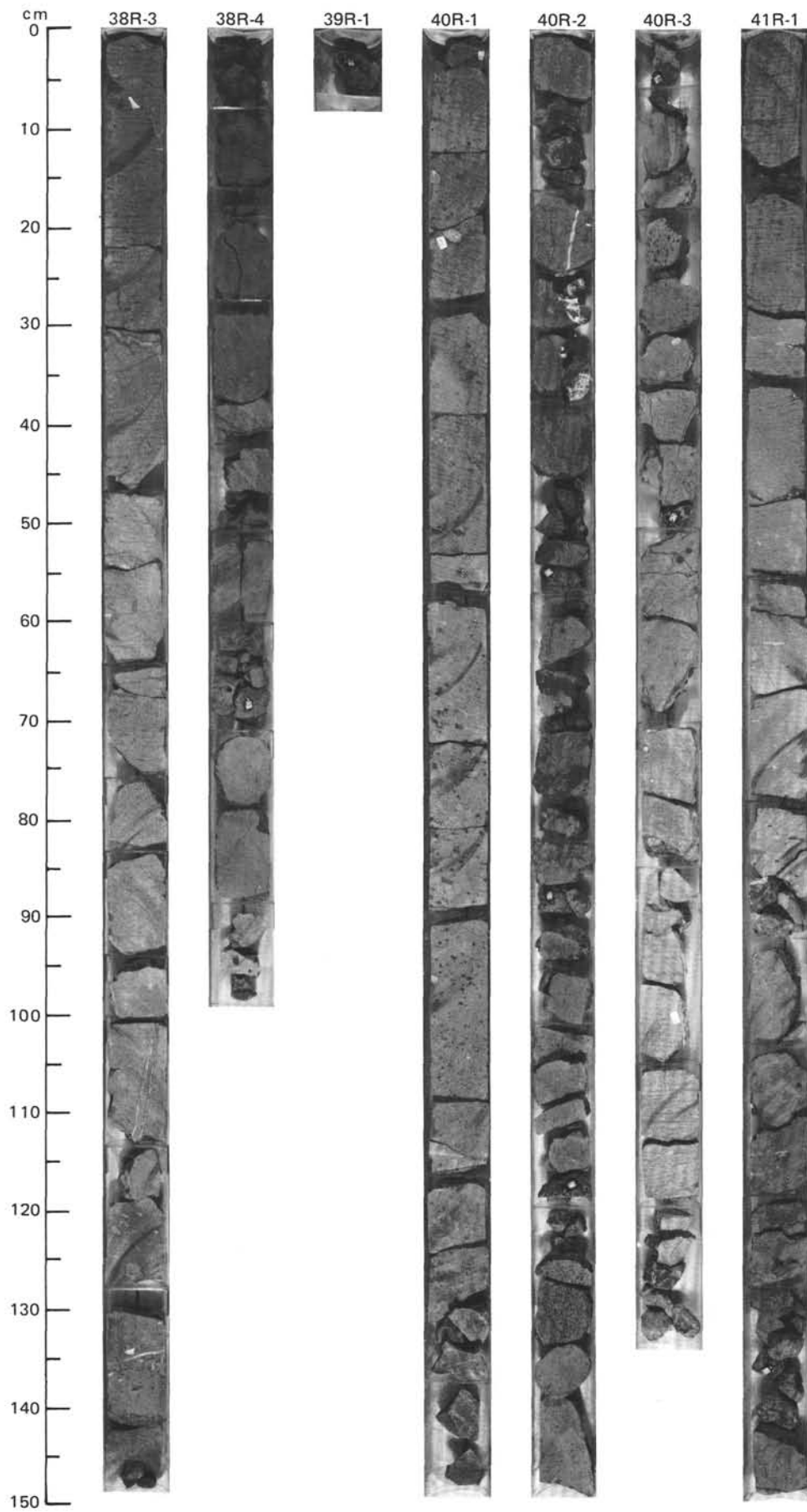
640.8–645.0 MBSF

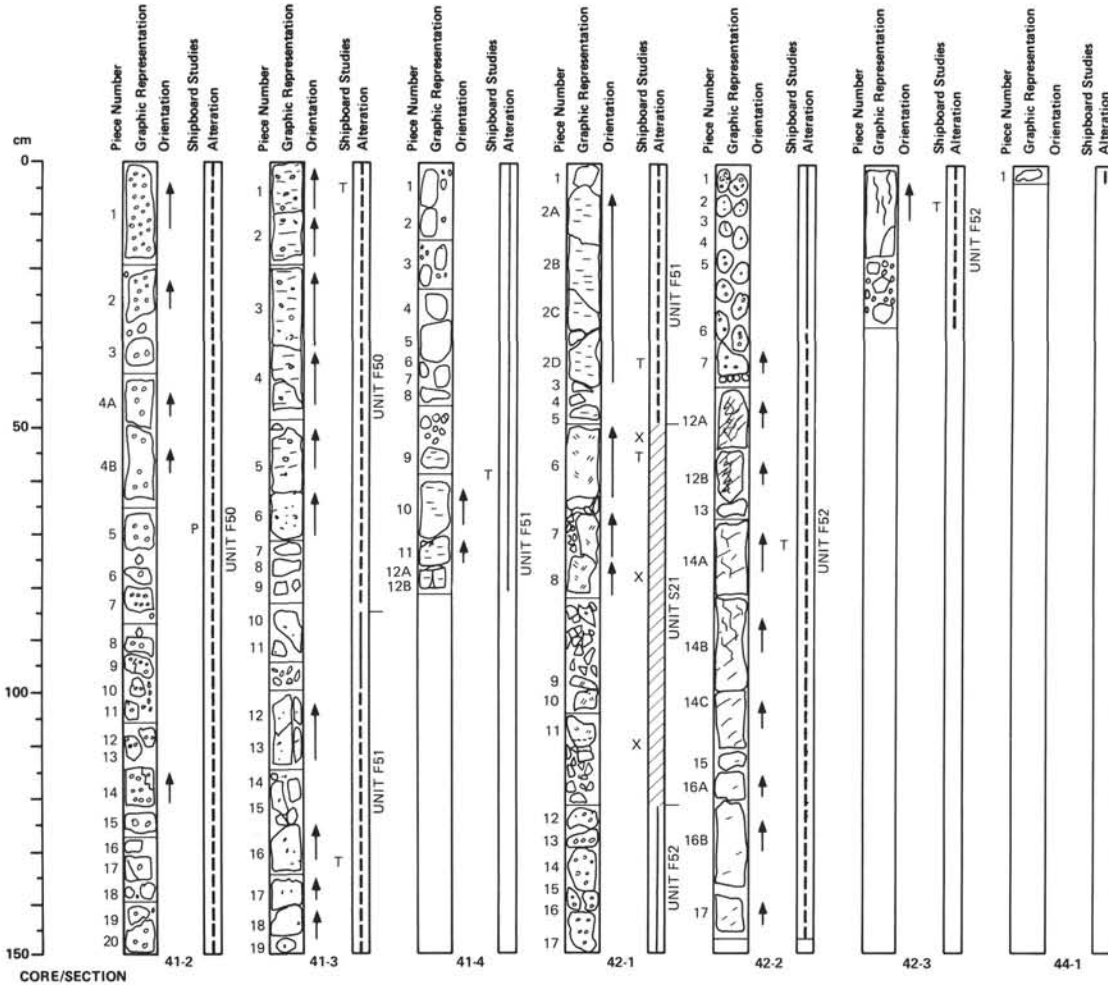
642E–41R-1 (103 cm) TO 41R-3 (85 cm)

FINE-GRAINED, SPARSELY PLAGIOCLASE PHYRIC, GRAY BASALT FLOW. Scoriaceous, highly vesicular reddened flow top, moderately vesicular to vesicular gray center and base. Dark green smectite filled vertical or irregularly "streamed" vesicle trains. Subhorizontal streaking (flow fabric) between 41R-3, 0–62 cm. Several subvertical or steeply inclined smectite filled fine fractures.

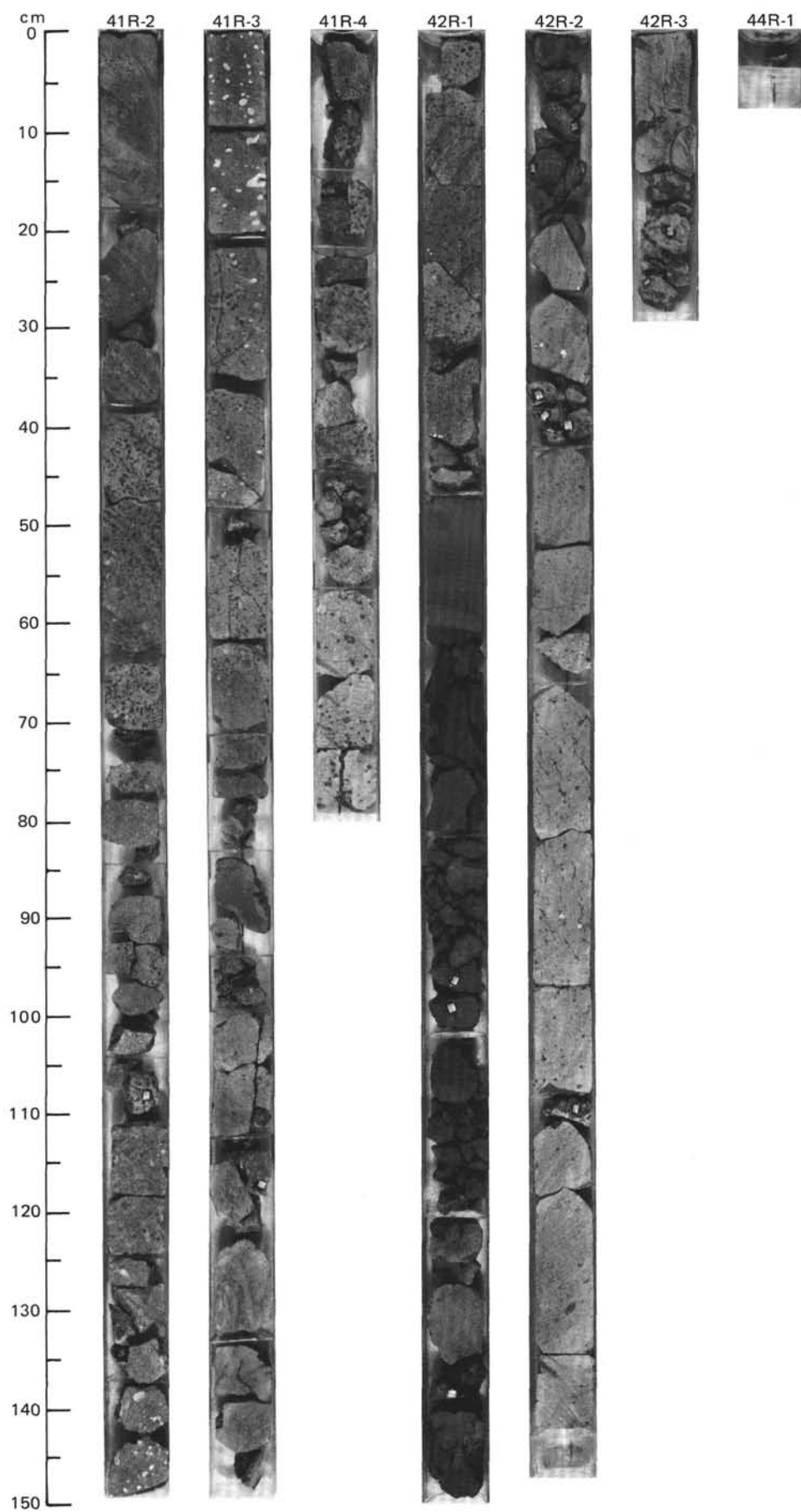
THIN SECTION DESCRIPTION

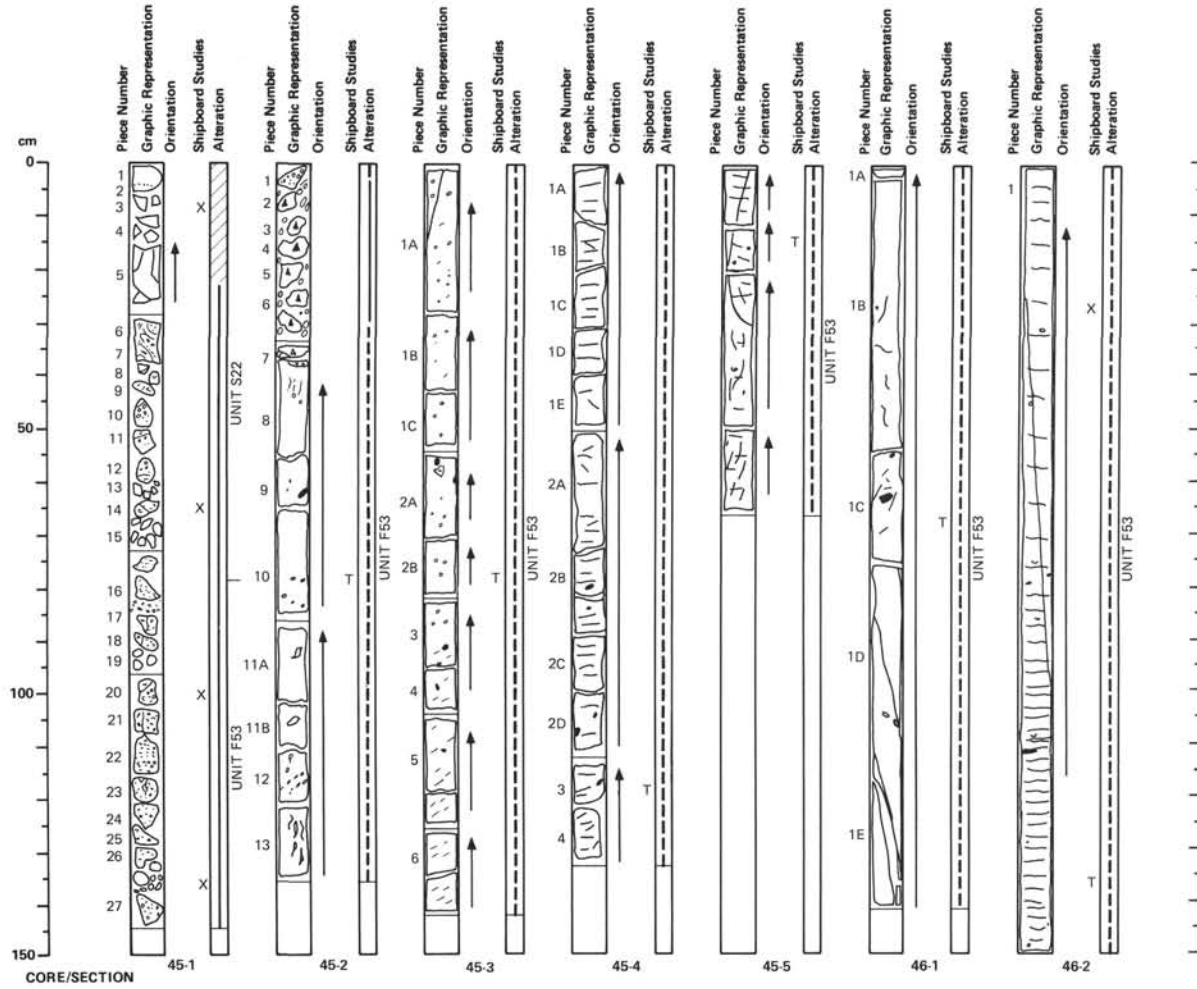
642E–41R-1 (Piece 8, 115–117 cm): <1% plag phenocrysts. 20% plag, 5% cpx, 15% opaques, 5% oi, 55% altered groundmass and mesostasis. Intergranular to intersertal.





	UNIT F50	
640.8–645.0 MBSF	642E–41R–1 (103 cm) TO 41R–3 (85 cm)	
FINE-GRAINED, SPARSELY PLAGIOCLASE PHYRIC, GRAY BASALT FLOW. Scoriaceous, highly vesicular reddened flow top, moderately vesicular to vesicular gray center and base. Dark green smectite filled vertical or irregularly "streamed" vesicle trains. Subhorizontal streaking (flow fabric) between 41R–3, 0–62 cm. Several subvertical or steeply inclined smectite filled fine fractures.		
THIN SECTION DESCRIPTION		
642E–41R–1 (Piece 8, 115–117 cm):	<1% plag phenocrysts. 20% plag, 5% cpx, 15% opaques, 5% ol, 55% altered groundmass and mesostasis. Intergranular to intersertal.	
	UNIT F51	
645.0–649.5 MBSF	642E–41R–3 (85 cm) TO 42R–1 (48 cm)	
FINE-GRAINED, SPARSELY PLAGIOCLASE PHYRIC, GRAY BASALT FLOW. Flow base not recovered. Sparsely vesicular to vesicular, green smectite and calcite filled vesicles. Subhorizontal streaking (flow fabric) between 41R–4, 55 cm, and 42R–1, 48 cm. Some fine (<1 mm) subvertical fracturing with smectite filling.		
	UNIT S21	
649.5–650.4 MBSF	642E–42R–1 (49 cm) TO 42R–1 (121 cm)	
BASALTIC VITRIC TUFF. Dark brown, dark gray brown, grayish red brown, brownish green, well sorted, upward-fining sequence at 42R–1, 49–62 cm; variable content of lapilli of differentiated composition: heterogeneous tuff, pale green vitric tuff, yellowish brown, crystal rich tuff, fragments of accretionary lapilli.		
	UNIT F52	
650.4–662.5 MBSF	642E–42R–1 (121 cm) TO 42R–3 (29 cm)	
FINE-GRAINED, APHYRIC, DARK GRAY BASALT FLOW. Flow base not recovered. Moderately to sparsely vesicular, upper section vesicles open or rimmed with pale green smectite, lower section filled with dark green smectite. Between 42R–2, 66–102 cm, steeply inclined sigmoidal tension gash arrays suggest shear motion approximately parallel to flow fabric.		
	UNIT S21A	
662.5–663.4 MBSF	NOT RECOVERED	
	UNIT F52A	
663.4–672.0 MBSF	NOT RECOVERED	
	UNIT S21B	
672.0–672.2 MBSF	NOT RECOVERED	
	UNIT F52B	
672.2–676.1 MBSF	NOT RECOVERED	





UNIT S22

676.1–677.1 MBSF

642E–45R–1 (0 cm) TO 45R–1 (78 cm)

THREE UPWARD-FINING SEQUENCES OF DARK BROWN TUFF.

Contains fresh black shards in the top sequence, and gray-green lapilli in the middle. 45R–1, 27–78 cm, dark brown tuff mixed with vesicular blocks of top of underlying flow.

UNIT F53

677.1–691.6 MBSF

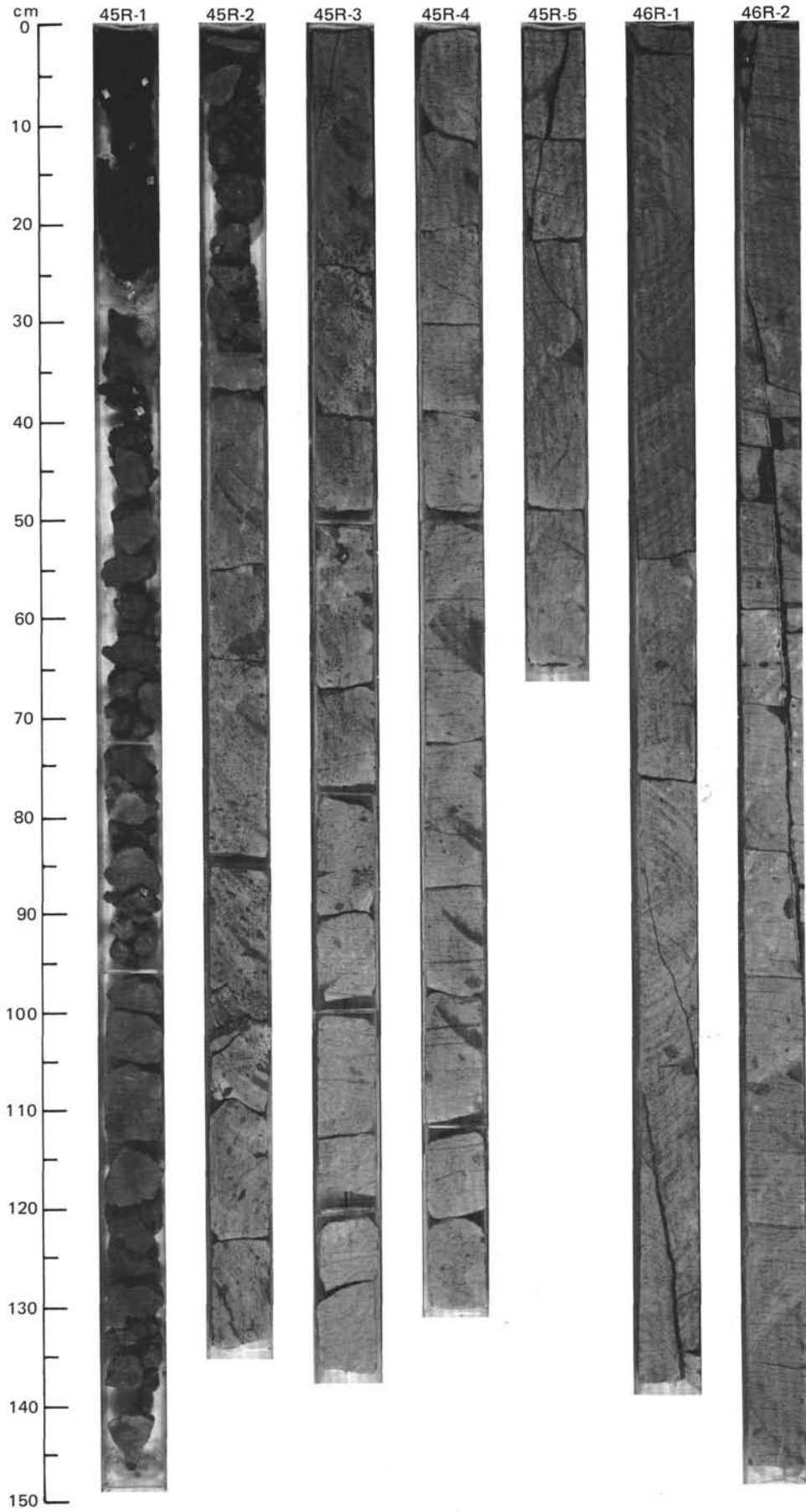
642E–45R–1 (78 cm) TO 46R–4 (48 cm)

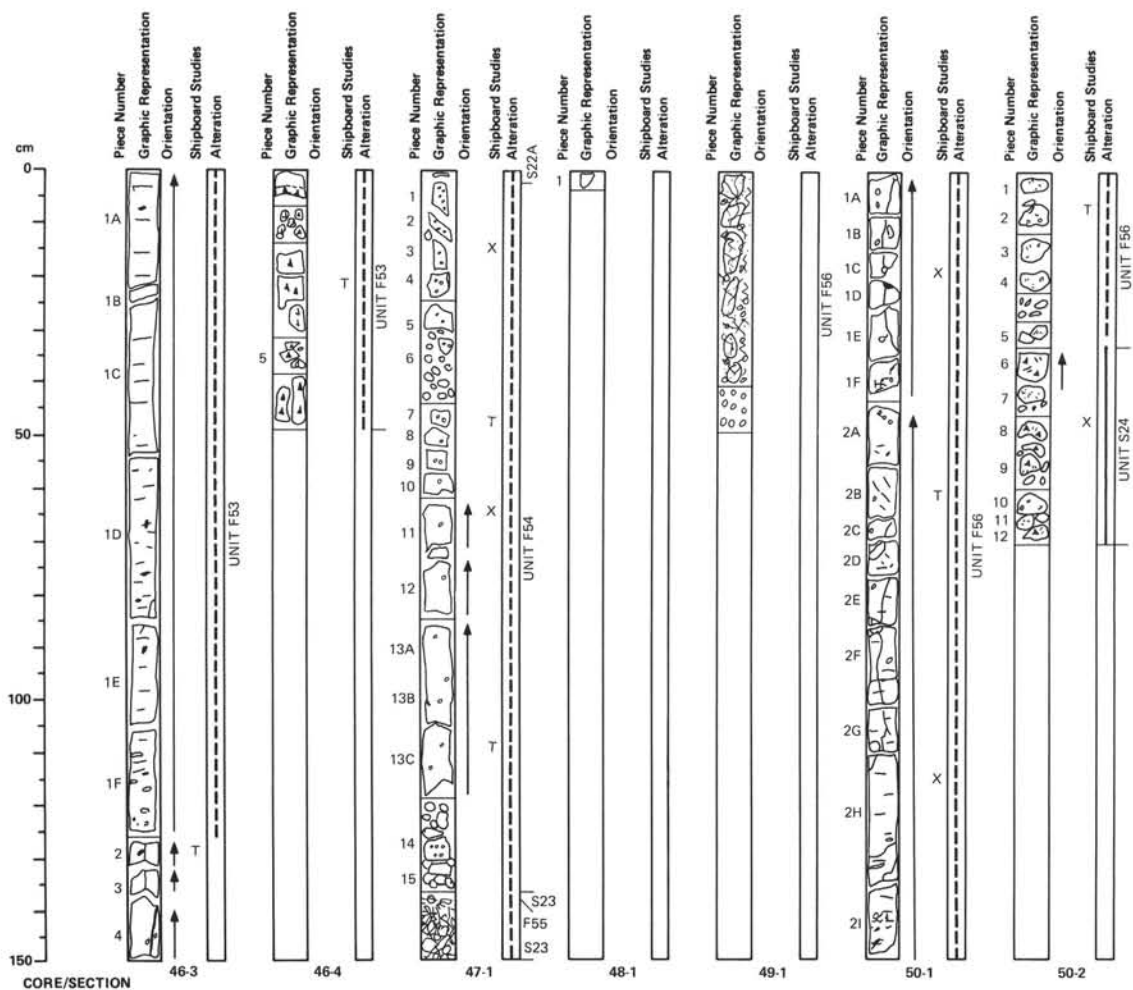
FINE-GRAINED, APHYRIC, GRAY BASALT FLOW. Dark gray scoriaceous flow top breccia with pale green coating of vesicles. Highly vesicular lower top, vesicles locally streamed and filled with dark green smectite. Thick central section streaky with well developed flow fabric, locally random with tightening of fabric toward base accompanied by some subhorizontal elongation of vesicles. Rounded xenoliths of vesicular basalt occur sporadically throughout the unit. Steeply inclined smectite and calcite filled fractures common. Gray to reddish gray basal breccia with reddish brown, fine-grained tuffaceous(?) matrix.

THIN SECTION DESCRIPTIONS

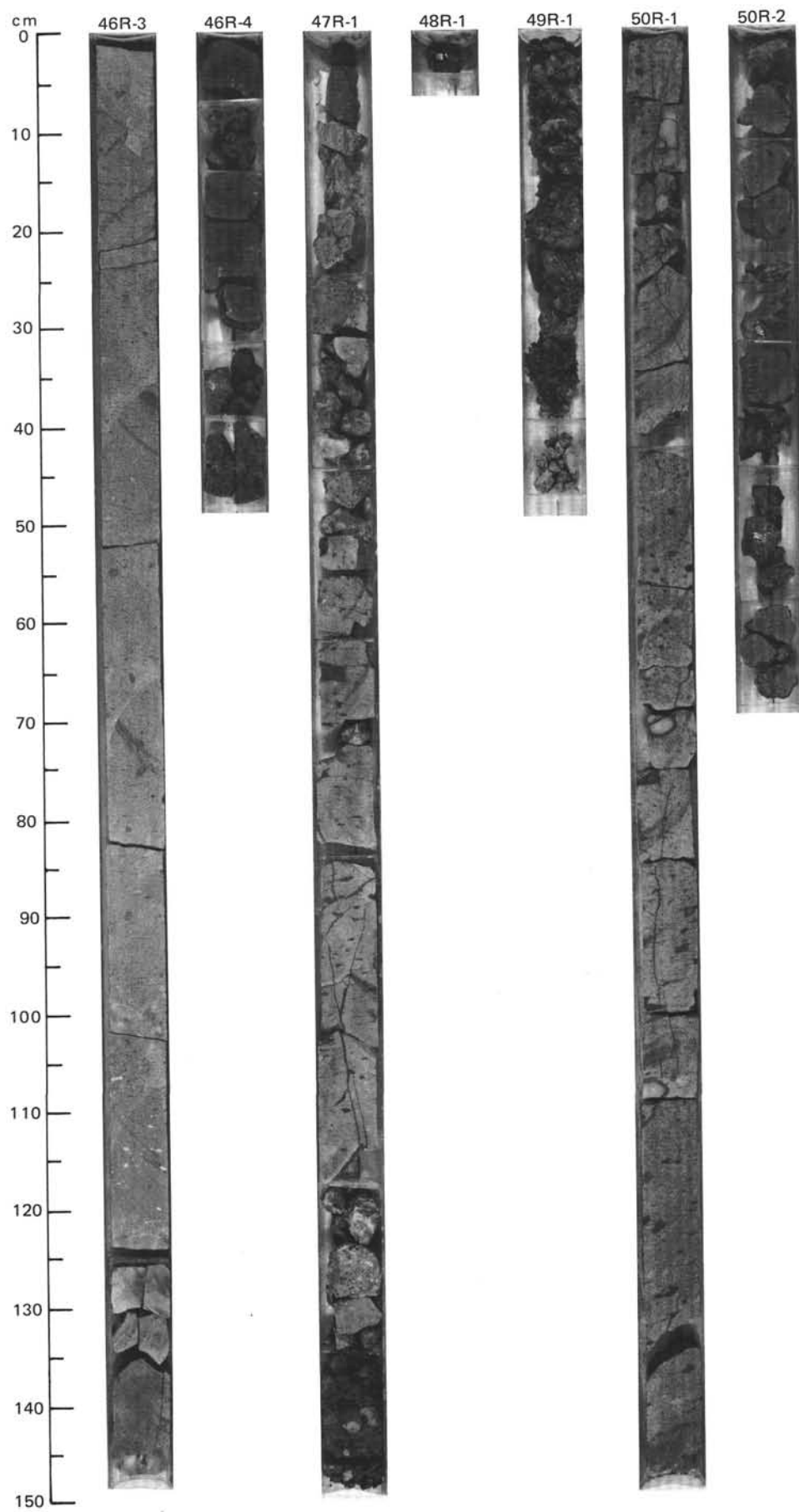
642E–45R–4 (Piece 3, 118–120 cm): 35% plag, 35% cpx, 10% altered ol, 10% opaques, 10% altered mesostasis. Intersertal to intergranular, subophitic.

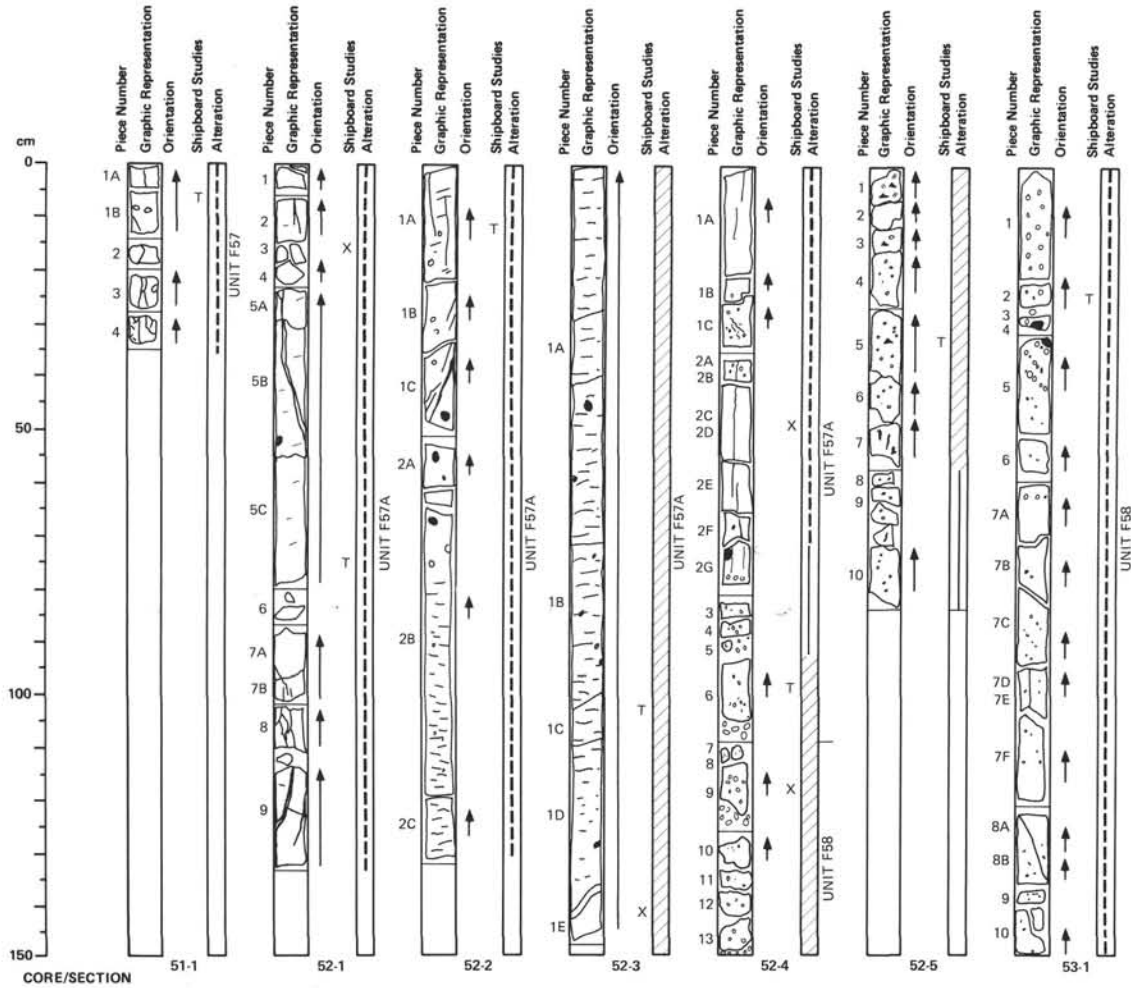
642E–45R–5 (Piece 1C, 15–17 cm): 45% plag, 35% cpx, <10% altered ol, 5% opaques, 5% altered mesostasis. Intersertal to intergranular, subophitic.





	UNIT F53
677.1–691.6 MBSF	642E–45R–1 (78 cm) TO 46R–4 (48 cm)
	FINE-GRAINED, APHYRIC, GRAY BASALT FLOW. Dark gray scoriaceous flow top breccia with pale green coating of vesicles. Highly vesicular lower top, vesicles locally streambed and filled with dark green smectite. Thick central section streaky with well developed flow fabric, locally random with tightening of fabric toward base accompanied by some subhorizontal elongation of vesicles. Rounded xenoliths of vesicular basalt occur sporadically throughout the unit. Steeply inclined smectite and calcite filled fractures common. Gray to reddish gray basal breccia with reddish brown, fine-grained tuffaceous(?) matrix.
	UNIT S22A
691.6–691.7 MBSF	642E–47R–1 (0 cm) TO 47R–1 (2 cm)
	DARK BROWN BASALTIC TUFF.
	UNIT F54
691.7–697.6 MBSF	642E–47R–1 (2 cm) TO 47R–1 (136 cm)
	FINE-GRAINED, APHYRIC, GRAY BASALTIC FLOW. Moderate vesicularity, decreasing in central section. Streaky flow fabric in the flow center. Drilling terminated with jammed bit.
	UNIT F55
697.6–703.9 MBSF	642E–47R–1 (137 cm) TO 47R–1 (149 cm)
	FRAGMENTS OF FINE-GRAINED, APHYRIC, GRAY BASALT FLOW.
	UNIT S23
703.9–704.0 MBSF	642E–47R–1 (136–137 cm) AND 47R–1 (149–150 cm)
	DARK BROWN TUFF.
	UNIT F56
704.0–712.9 MBSF	642E–48R–1 (0 cm) TO 50R–2 (32 cm)
	FINE-GRAINED, APHYRIC, GRAY BASALT FLOW. Vesicles are smectite filled, and elongate at base. Streaky flow fabric is chaotic in upper section, subhorizontal in lower. Subvertical fracturing. Some reddening of fragments at base of unit.
	UNIT S24
712.9–713.4 MBSF	642E–50R–2 (32 cm) TO 50R–2 (70 cm)
	DARK BROWN VITRIC, BASALTIC TUFF. Contains platy, vesicular, glass shards, some fresh, as well as clinopyroxene and feldspar; median shard diameter 0.2 mm.





UNIT F57

713.4–717.4 MBSF

642E–51R–1 (0 cm) TO 51R–1 (35 cm)

FINE-GRAINED, APHYRIC, GRAY BASALT FLOW. Massive, sparsely vesicular. Vertical to subvertical fracture set.

UNIT F57A

717.4–726.3 MBSF

642E–52R–1 (0 cm) TO 52R–4 (109 cm)

FINE-GRAINED, APHYRIC, GRAY BASALT FLOW. Reddened vesicular flow top breccia, with moderate to highly vesicular basal section, but mostly nonvesicular or sparsely vesicular, filled with dark green smectite or rare calcite. Streaky flow fabric well developed below 52R–2, 80 cm. Local fine subvertical fracturing. A series of continuous, subvertical arcuate veins, maximum width 4 mm with smectite filling between 52R–1, 0 cm, and 52R–2, 50 cm. Rounded vesicular xenoliths, 0.5–1.5 cm diameter, occur sporadically throughout unit, and are locally wrapped by flow fabric.

UNIT S25

726.3–726.5 MBSF

642E–52R–4 (109 cm)

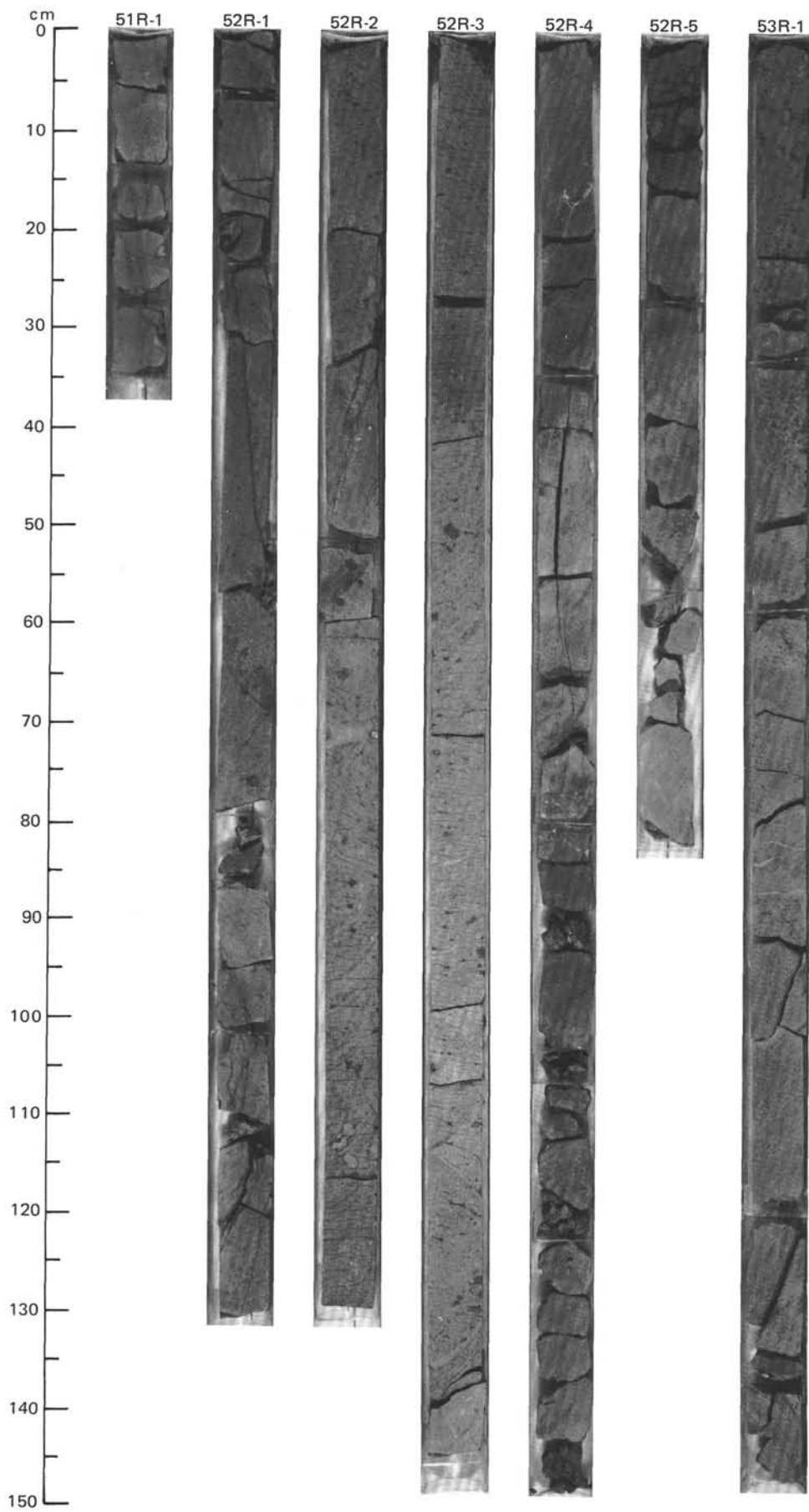
DARK RED BROWN, HOMOGENEOUS, BASALTIC, VITRIC TUFF. Present only as matrix between breccia clasts in flow top and base.

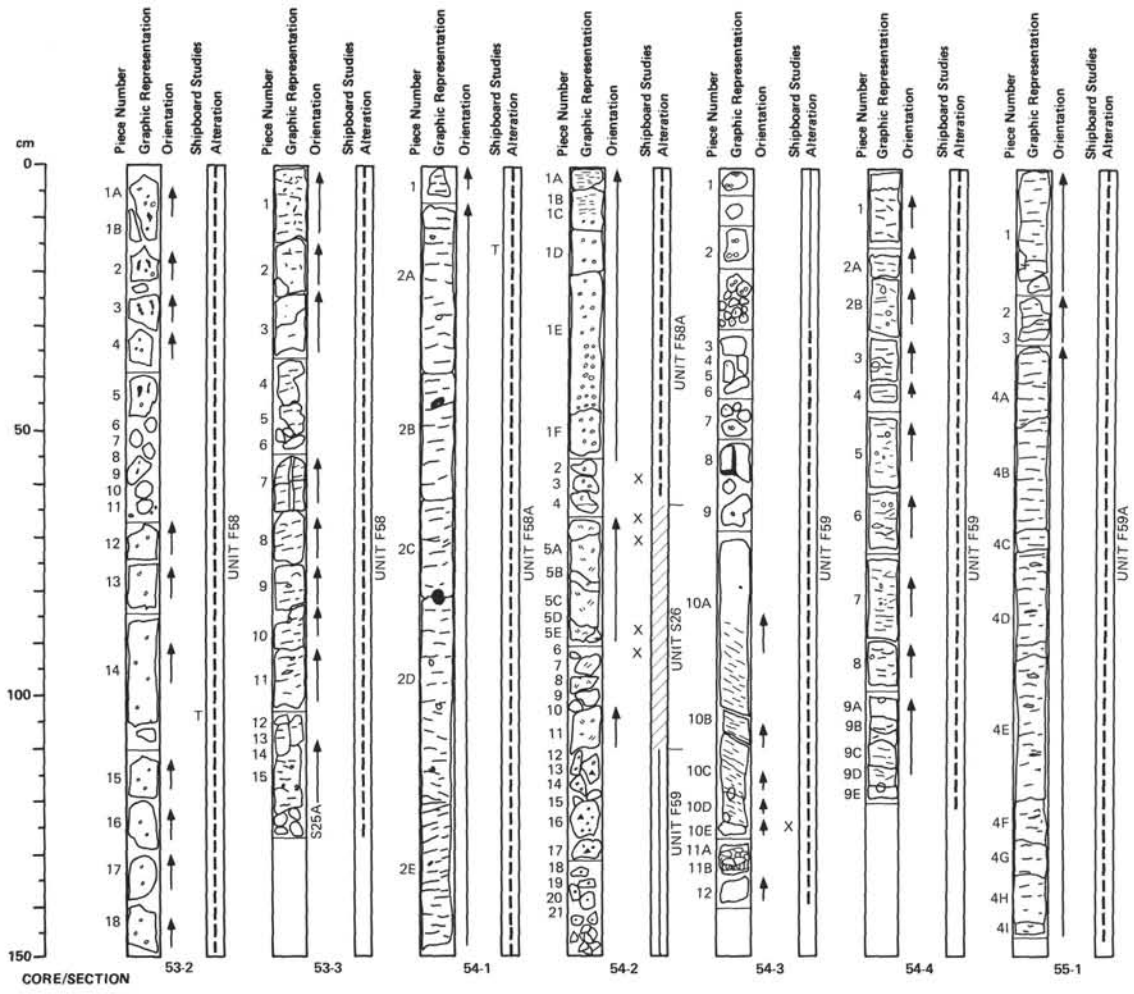
UNIT F58

726.5–732.3 MBSF

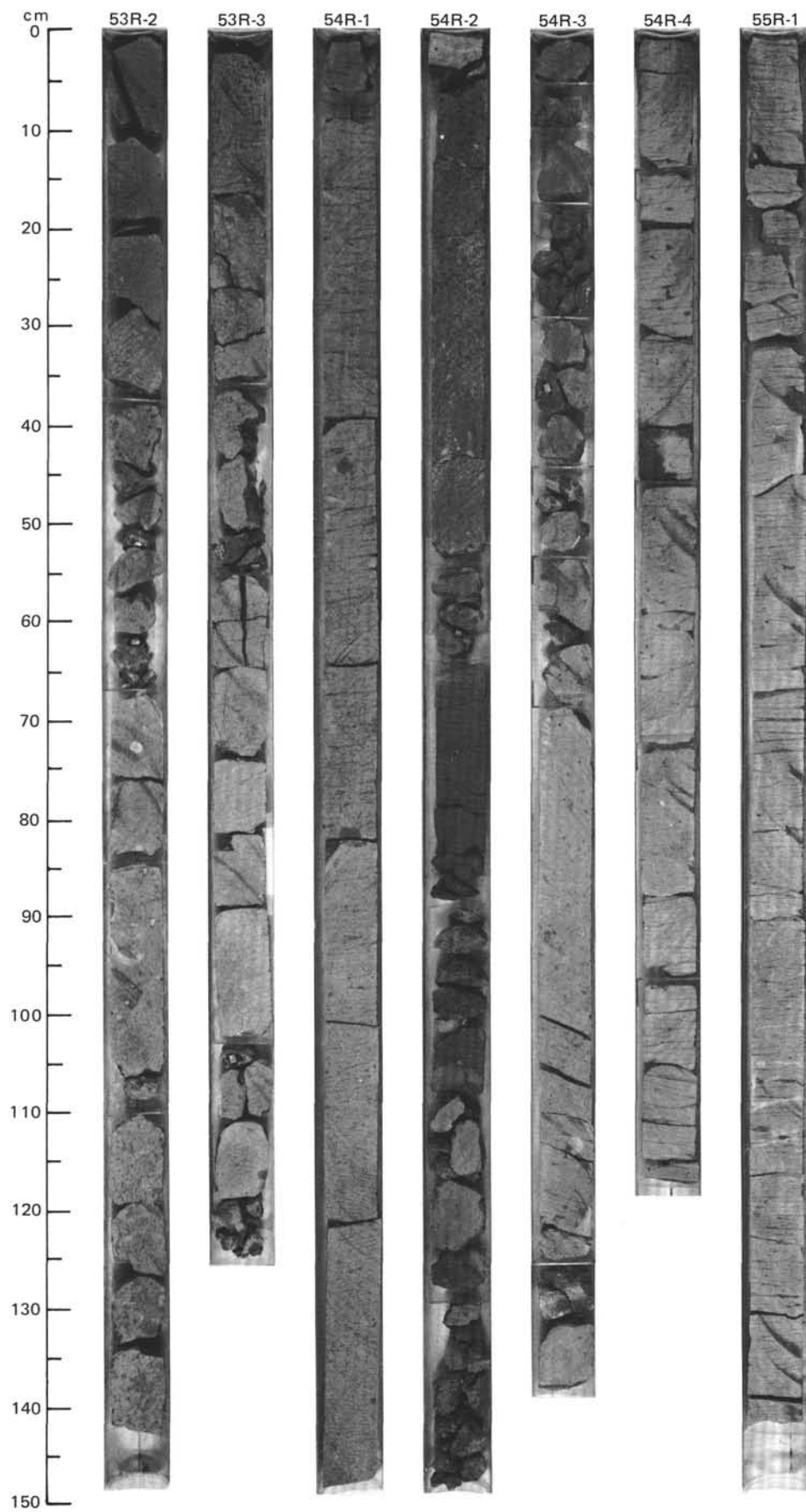
642E–52R–4 (109 cm) TO 53R–3 (128 cm)

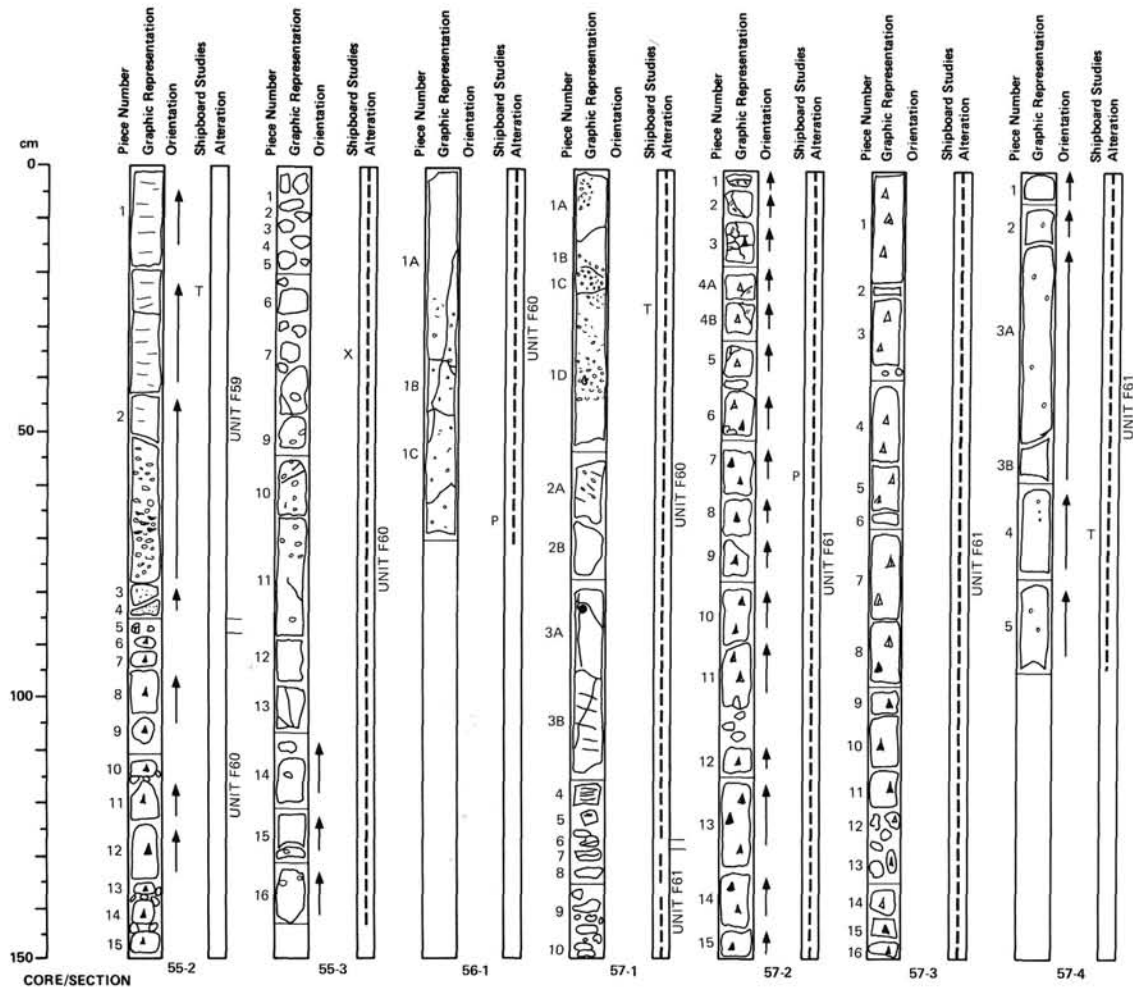
FINE-GRAINED, APHYRIC, GRAY BASALT FLOW. Reddened, highly vesicular basalt breccia with fine tuff matrix overlying thick (2.0 m) highly vesicular streamered and coalesced zone, vesicles with dark green smectite fillings. 2.8 m thick recovery of subhorizontally streaked (flow fabric) central zone, carrying few elongate vesicles subparallel to fabric. Rare, rounded, vesicular, aphyric, gray basalt xenoliths throughout unit, vertical fracturing and smectite veining occupies partings up to 1.0 mm wide, some subparallel to flow fabric.



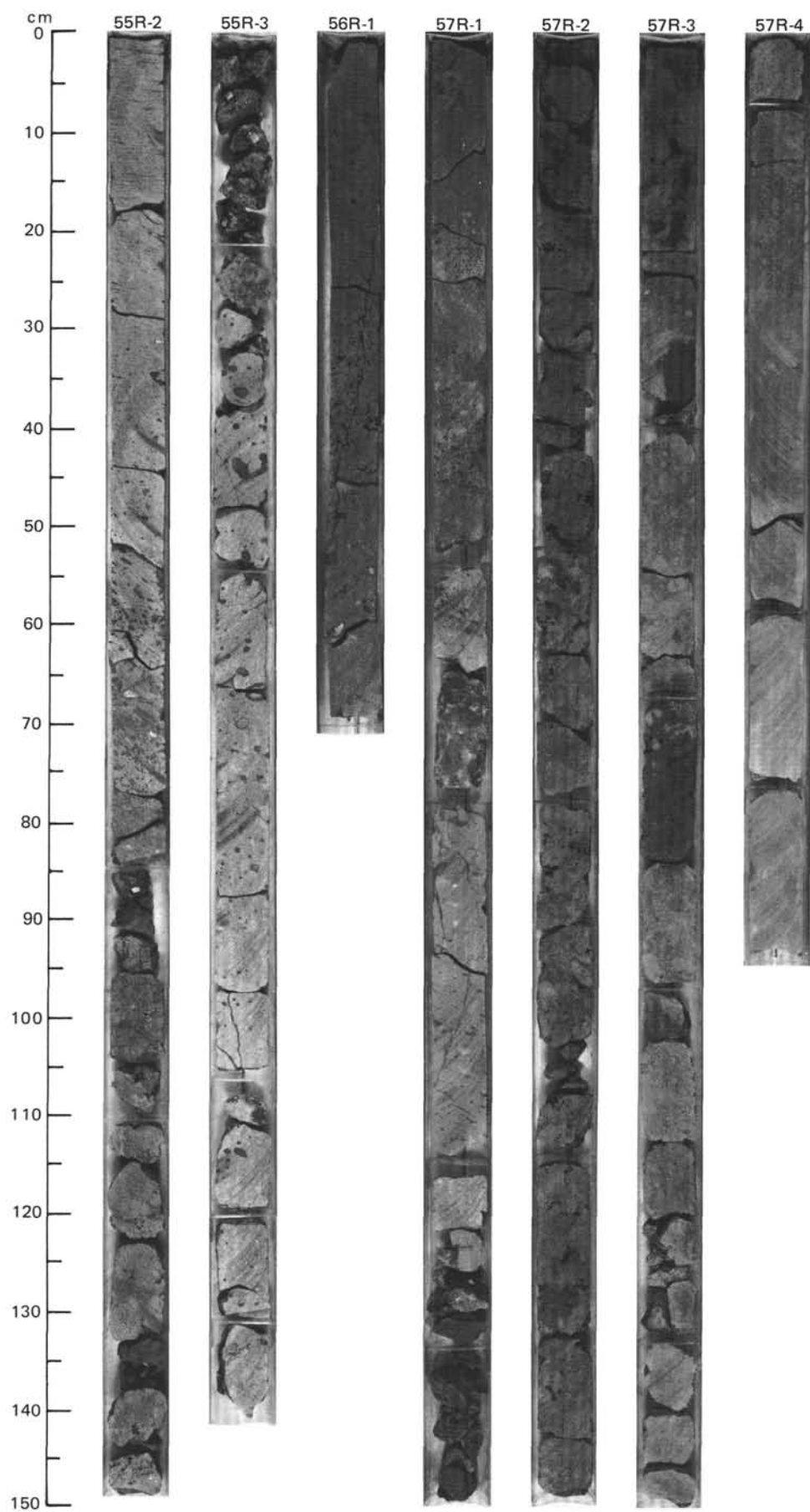


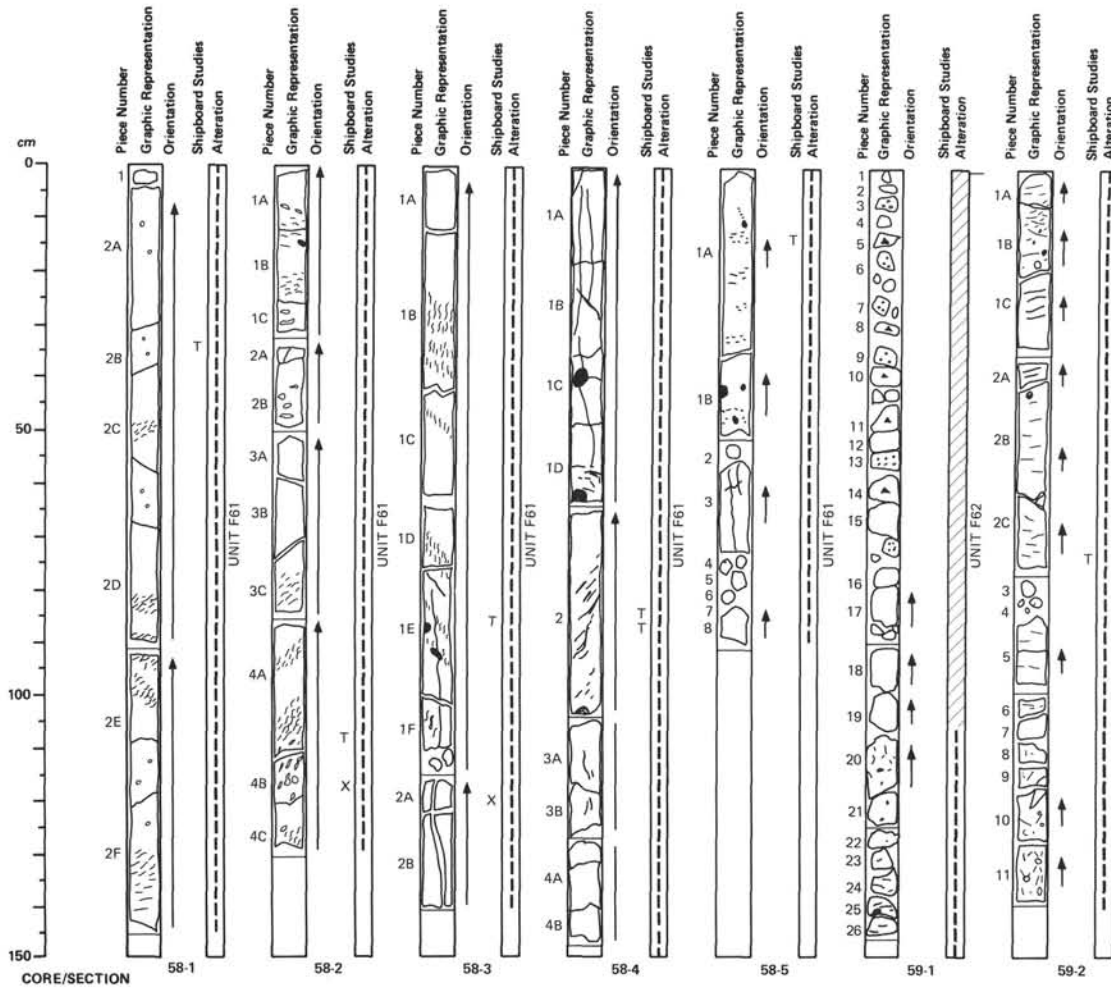
	UNIT F58
726.5–732.3 MBSF	642E–52R–4 (109 cm) TO 53R–3 (128 cm)
<p>FINE-GRAINED, APHYRIC, GRAY BASALT FLOW. Reddened, highly vesicular basalt breccia with fine tuff matrix overlying thick (2.0 m) highly vesicular streamered and coalesced zone, vesicles with dark green smectite fillings. 2.8 m thick recovery of subhorizontally streaked (flow fabric) central zone, carrying few elongate vesicles subparallel to fabric. Rare, rounded, vesicular, aphyric, gray basalt xenoliths throughout unit, vertical fracturing and smectite veining occupies partings up to 1.0 mm wide, some subparallel to flow fabric.</p>	
	UNIT S25A
732.3–732.5 MBSF	NOT RECOVERED
	UNIT F58A
732.5–739.0 MBSF	642E–54R–1 (0 cm) TO 54R–2 (62 cm)
AS F58.	
	UNIT S26
739.0–739.5 MBSF	642E–54R–2 (62 cm) TO 54R–2 (110 cm)
<p>RED-BROWN, BASALTIC, VITRIC TUFF. Subhorizontal bedding common, with at least one upward-fining sequence (54R–2, 67–74 cm). Sandy interval overlies zone of lapilli-sized clasts and basal breccia. Some pocket infilling of underlying basalt flow top.</p>	
	UNIT F59
739.5–748.2 MBSF	642E–54R–2 (110 cm) TO 54R–4 (120 cm)
<p>FINE-GRAINED, APHYRIC, GRAY BASALT FLOW. Reddened flow top breccia with highly vesicular "streamed" upper zone, overlying moderately to sparsely vesicular unit. Most vesicles filled by dark green smectite, rare calcite, and some zeolite, especially Pieces 11A and B. Shallowly inclined (20 degrees) or subhorizontal streaky flow fabric through central and basal section except for highly vesicular base. Weak flattening/truncation of vesicles by fabric. Rare rounded, highly vesicular basalt xenoliths.</p>	
	UNIT 59A
748.2–753.3 MBSF	642E–55R–1 (0 cm) TO 55R–2 (85 cm)
AS F59.	





	UNIT 59A
748.2–753.3 MBSF	642E–55R–1 (0 cm) TO 55R–2 (85 cm)
AS F59.	
	UNIT S27
753.3–753.4 MBSF	642E–55R–2 (85 cm) TO 55R–2 (88 cm)
BASALTIC VITRIC TUFF. Uniformly dark red brown, pocket fillings of underlying flow top to 55R–2, 143 cm.	
	UNIT F60
753.4–758.7 MBSF	642E–55R–2 (88 cm) TO 57R–1 (128 cm)
FINE-GRAINED, APHYRIC, GRAY BASALT FLOWS. Central section possibly not recovered. Reddened and scoriaceous flow top breccia overlying moderately vesicular zone with dark green smectite fillings. Some entrainment of vesicles into inclined zones in lower sections. No streaked flow fabric recognized, but suspect from drilling logs that much of the central zone may be missing. Rare xenoliths are present, along with a few fine smectite filled fractures.	
	UNIT S28
758.7–758.8 MBSF	642E–57R–1 (128 cm) TO 57R–1 (130 cm)
DARK RED BROWN BASALTIC, VITRIC TUFF. Uniformly grained. Extends down to pocket fillings of underlying flow at 57R–2, 50 cm.	
	UNIT F61
758.8–771.3 MBSF	642E–57R–1 (130 cm) TO 58R–5 (90 cm)
FINE-GRAINED, APHYRIC, GRAY BASALT FLOW. A 2.0 m thick red scoriaceous and highly vesicular breccia flow top containing some vesicles with smectite fills. Moderately vesicular for most of the unit, with local collapsed and/or filled vesicles deformed into sigmoidal shapes, aligned into <i>en echelon</i> arrays. Toward the base are several steeply inclined to vertical smectite-filled fractures along with some complex braided partings. Rounded and subrounded, vesicular, aphyric xenoliths occur locally.	





UNIT F61

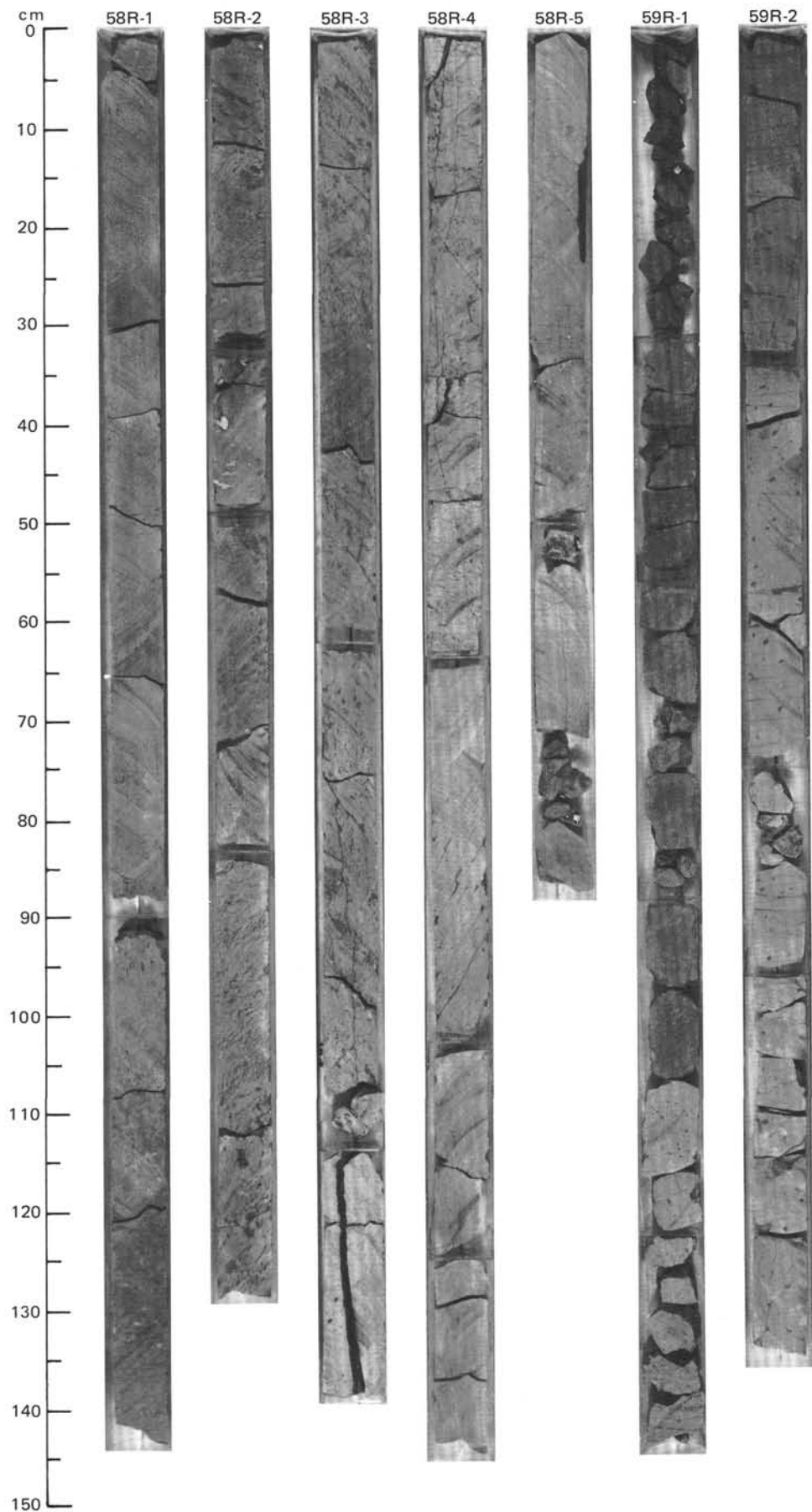
758.8-771.3 MBSF 642E-57R-1 (130 cm) TO 58R-5 (90 cm)

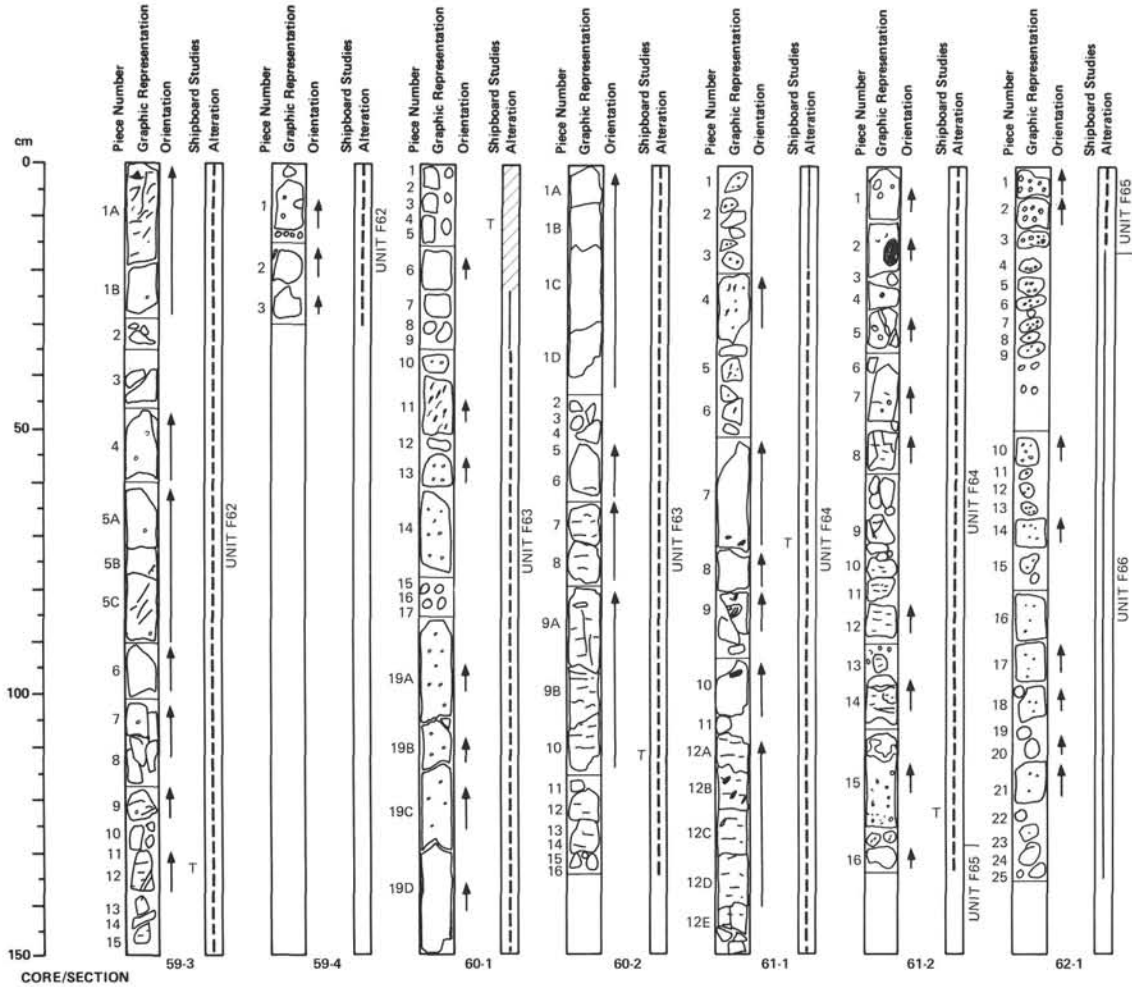
FINE-GRAINED, APHYRIC, GRAY BASALT FLOW. A 2.0 m thick red scoriaceous and highly vesicular breccia flow top containing some vesicles with smectite fills. Moderately vesicular for most of the unit, with local collapsed and/or filled vesicles deformed into sigmoidal shapes, aligned into *en echelon* arrays. Toward the base are several steeply inclined to vertical smectite-filled fractures along with some complex braided partings. Rounded and subrounded, vesicular, aphyric xenoliths occur locally.

UNIT F62

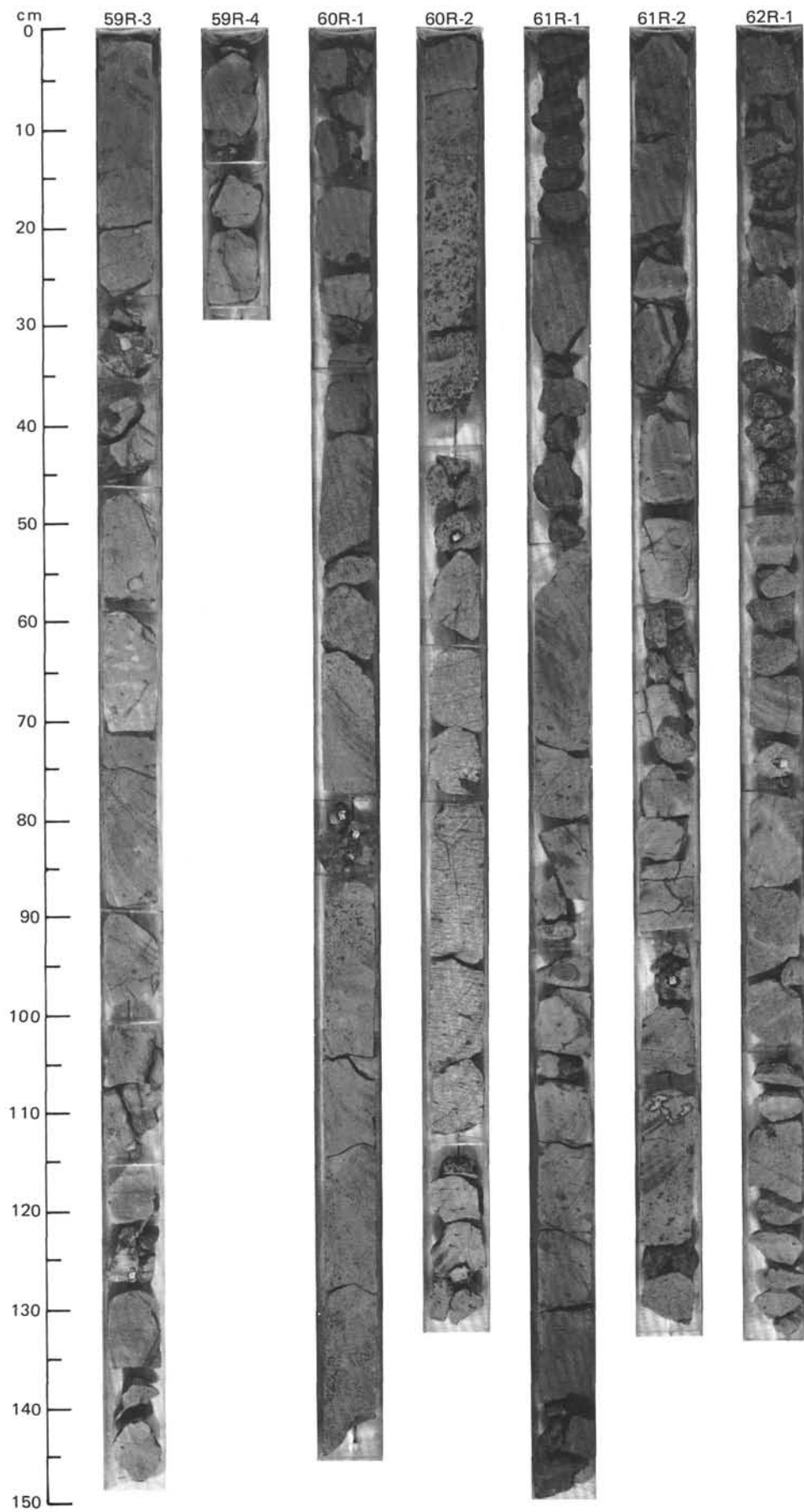
771.3-782.1 MBSF 642E-59R-1 (0 cm) TO 59R-4 (30 cm)

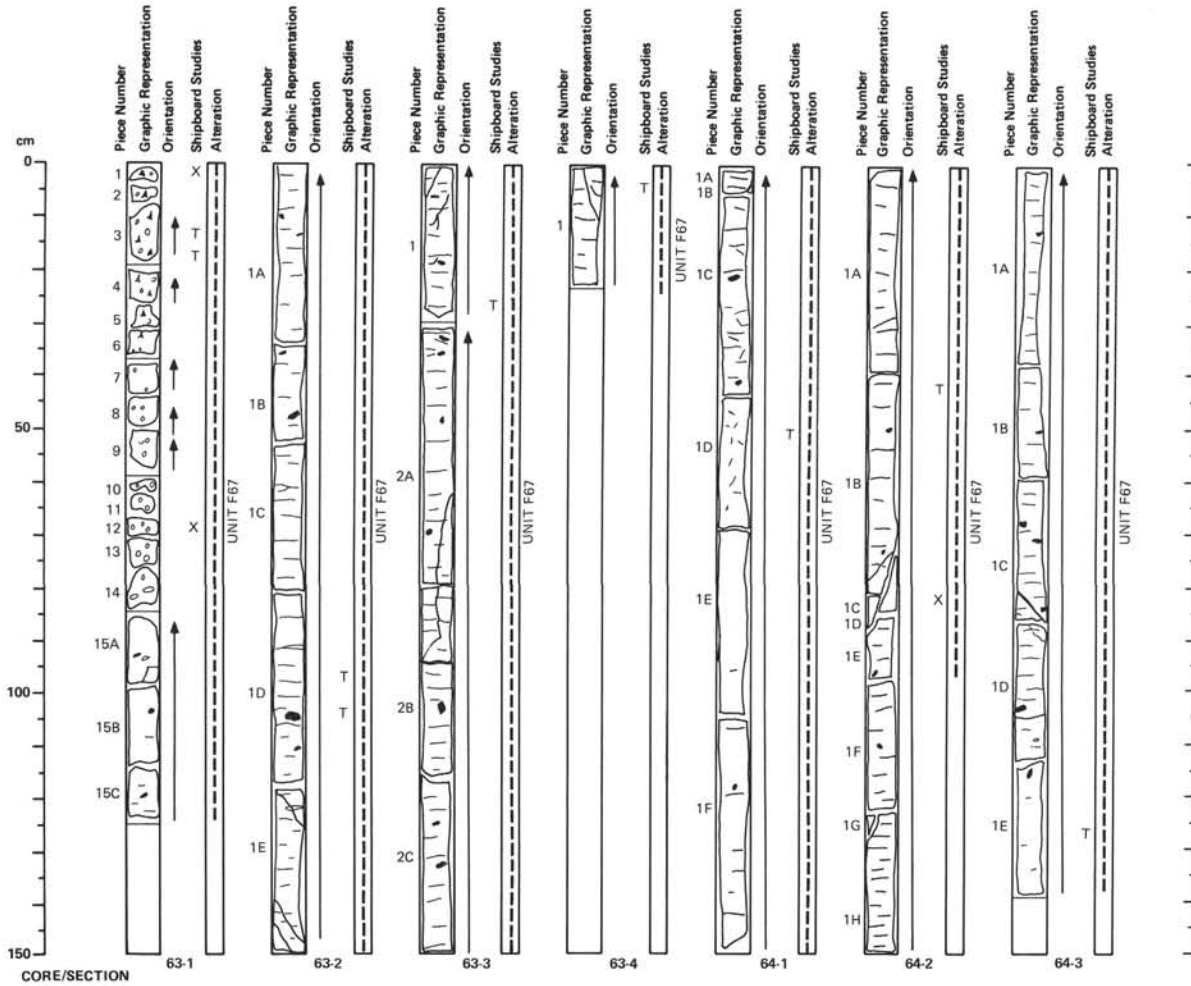
FINE-GRAINED, APHYRIC, BASALT FLOW. Flow base not recovered. Reddened flow top breccia, carrying vesicular fragments up to 5 cm in diameter, overlying sparsely vesicular unit, with vesicles filled with green smectite. Upper streaky flow fabric subhorizontal but locally chaotic toward lowest recovered section. Rare xenoliths. Much fracturing and subvertical partings toward base with dark green smectite and celadonite(?) fillings.





Depth (MBSF)	Unit	Description
782.1–785.4	UNIT F63	642E–60R–1 (0 cm) TO 60R–2 (133 cm)
		FINE-GRAINED, APHYRIC BASALT FLOW. Flow top and base not recovered. Weakly red gray at top of unit over moderately vesicular zone, displaying coalescence of vesicles, alignment and preservation of interconnecting channels in locally intensely vesicular zones. Well-developed streaking fabric 60R–2, 60–120 cm. Some vertical fracturing in Piece 9A.
785.4–789.9	UNIT F63A	NOT RECOVERED
789.9–790.0	UNIT S28A	NOT RECOVERED
790.0–798.5	UNIT F64	642E–61R–1 (0 cm) TO 61R–2 (128 cm)
		FINE-GRAINED, APHYRIC BASALT FLOW. Gray and dark gray highly vesicular flow top breccia, with some pale green smectite alteration. Moderately to highly vesicular, dark green smectite-filled "streamed" upper section, sparsely vesicular below 61R–1, 110 cm. Subparallel to flattened vesicles. Abundant highly vesicular, aphyric basalt xenoliths present, especially at 61R–1, 70–100 cm.
798.5–798.6	UNIT S28B	NOT RECOVERED
798.6–801.5	UNIT F65	642E–61R–2 (128 cm) TO 61R–2 (132 cm)
		MEDIUM-GRAINED, APHYRIC, DARK GRAY BASALT FLOW. Vesicular, with average grain sizes ranging between 2.0 and 8.0 mm in diameter; vesicles mostly dark green smectite filled, some with pale green cores.
801.5–803.5	UNIT F65A	NOT RECOVERED
803.5–805.5	UNIT F65B	NOT RECOVERED
805.5–807.5	UNIT F66	642E–62R–1 (0 cm) TO 62R–1 (17 cm)
		FINE-GRAINED, APHYRIC, GRAY BASALT FLOW. Weakly reddened to gray unit, highly vesicular, ranging from upper zones of green smectite rims to complete fills in lower zones. No streaky flow fabric recognized, but some local mixed turbulent(?) zones in Pieces 14, 17, and 18.





UNIT F67

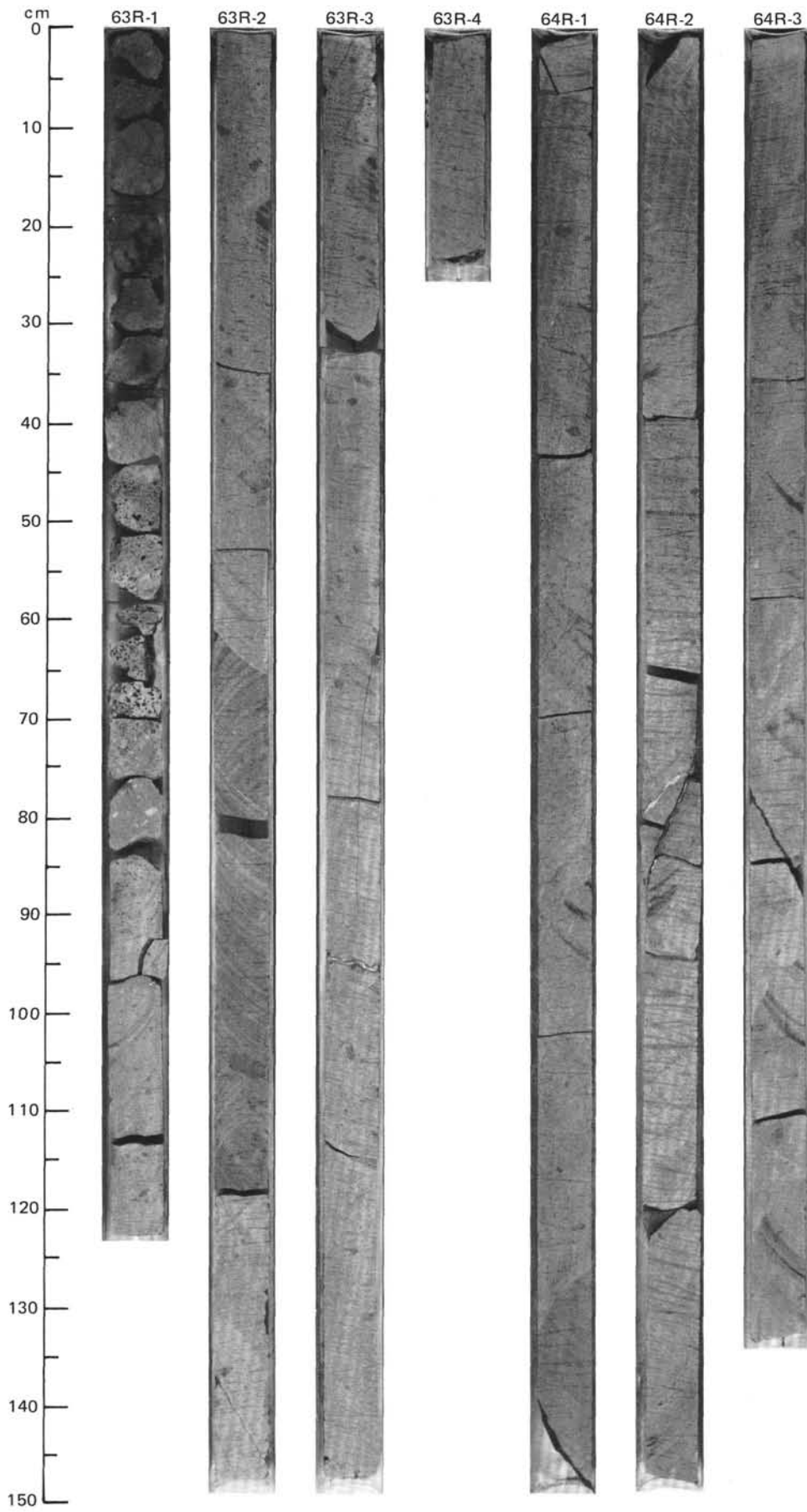
807.5–818.0 MBSF

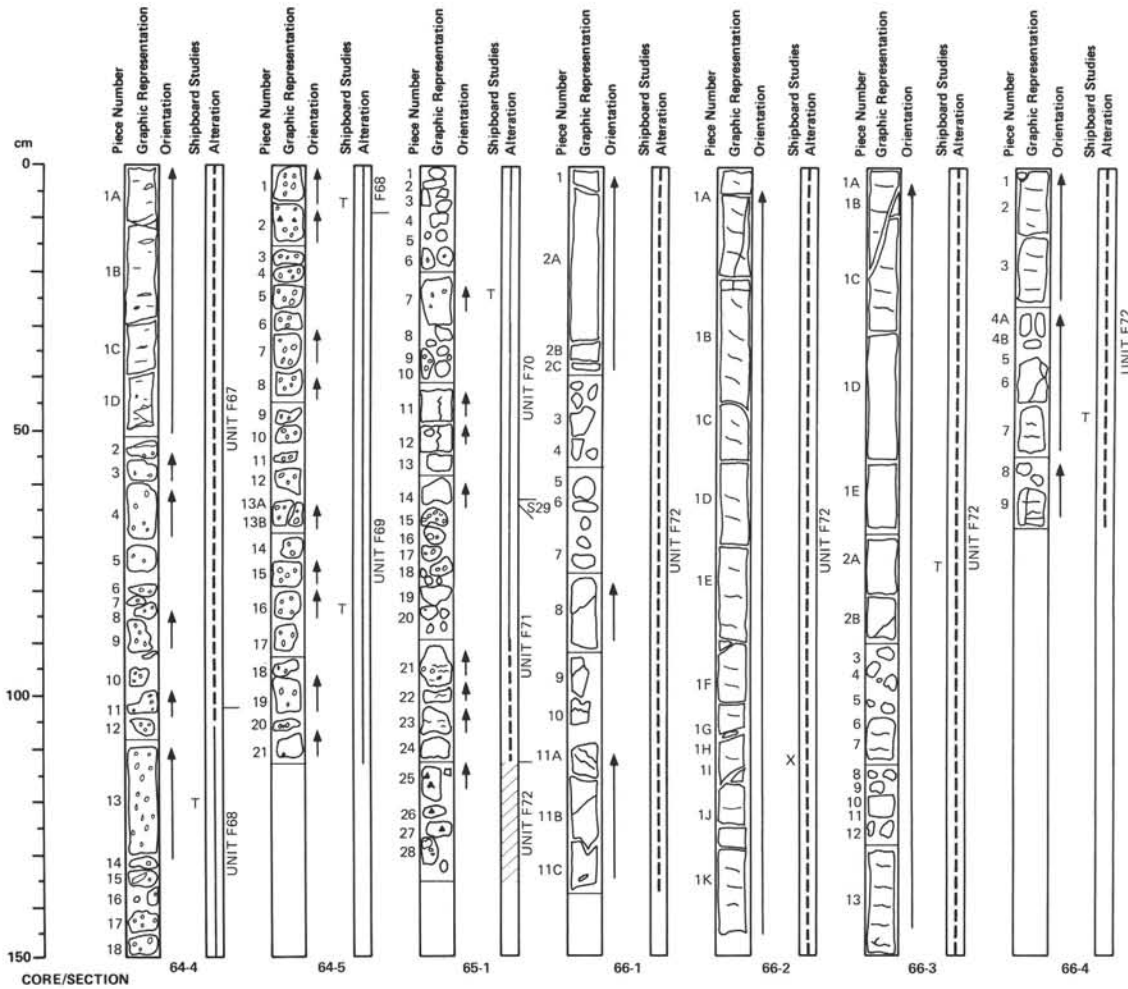
642E–63R–1 (0 cm) TO 64R–4 (103 cm)

FINE-GRAINED, APHYRIC, GRAY BASALT FLOW. Reddened vesicular breccia flow top overlying sparsely vesicular unit. Narrow vesicular base, carrying flattened vesicles in several bands, 64R–4, 53 to 103 cm. Well recovered streaky flow fabric section, with a zone of randomly orientated fabric at 64R–1, 25–54 cm. Several subvertical fractures filled with green smectite with some calcite, locally offsetting flow fabric. Native copper as disseminated blebs in groundmass and in lower veins, along with trace of unidentified metallic mineral.

THIN SECTION DESCRIPTION

642E–63R–2 (Piece 1C, 102–103 cm): 4% plag phenocrysts. 40% plag, 40% cpx, 5% altered ol, 5% altered mesostasis, 10% opaques. Intersertal to intergranular, subophitic.





UNIT F68

818.0–820.8 MBSF 642E–64R–4 (103 cm) TO 64R–5 (10 cm)

FINE-GRAINED, APHYRIC, GRAY BASALT FLOW. Reddened, highly vesicular unit, underlying fine breccia top (3 cm thick), with unfilled vesicles, or with partly filled vesicles containing green smectite and/or calcite. Size of vesicles decreases toward base. Sharp basal contact with F69.

THIN SECTION DESCRIPTION

642E–64R–4 (Piece 1B, 117–119 cm): 40% plag, 35% cpx, 5% altered ol, 5% opaques, 10% altered variolitic mesostasis. Strongly altered. Intersertal to subophitic.

UNIT F69

820.8–822.7 MBSF 642E–64R–5 (10 cm) TO 65R–1 (0 cm)

FINE-GRAINED, APHYRIC, GRAY BASALT FLOW. Reddened and vesicular top. As F68, except for well defined alternating zones of varying vesicle size. Vesicles in breccia zone are pale green and smectite filled.

UNIT F70

822.7–826.6 MBSF 642E–65R–1 (0 cm) TO 65R–1 (64 cm)

FINE-GRAINED, APHYRIC, GRAY BASALT FLOW. Flow base not recovered. Highly vesicular toward top, ranging down to sparsely vesicular in bottom section. Pale gray green smectite filled with some Fe oxide staining around vesicles and subvertical fine fracturing. Narrow streaky flow fabric zone at 65R–1, 46–64 cm.

UNIT S29

826.6 MBSF 642E–65R–1 (64 cm)

FINE-GRAINED, DARK RED BROWN TUFF. Coating on vesicular top of F71.

UNIT F71

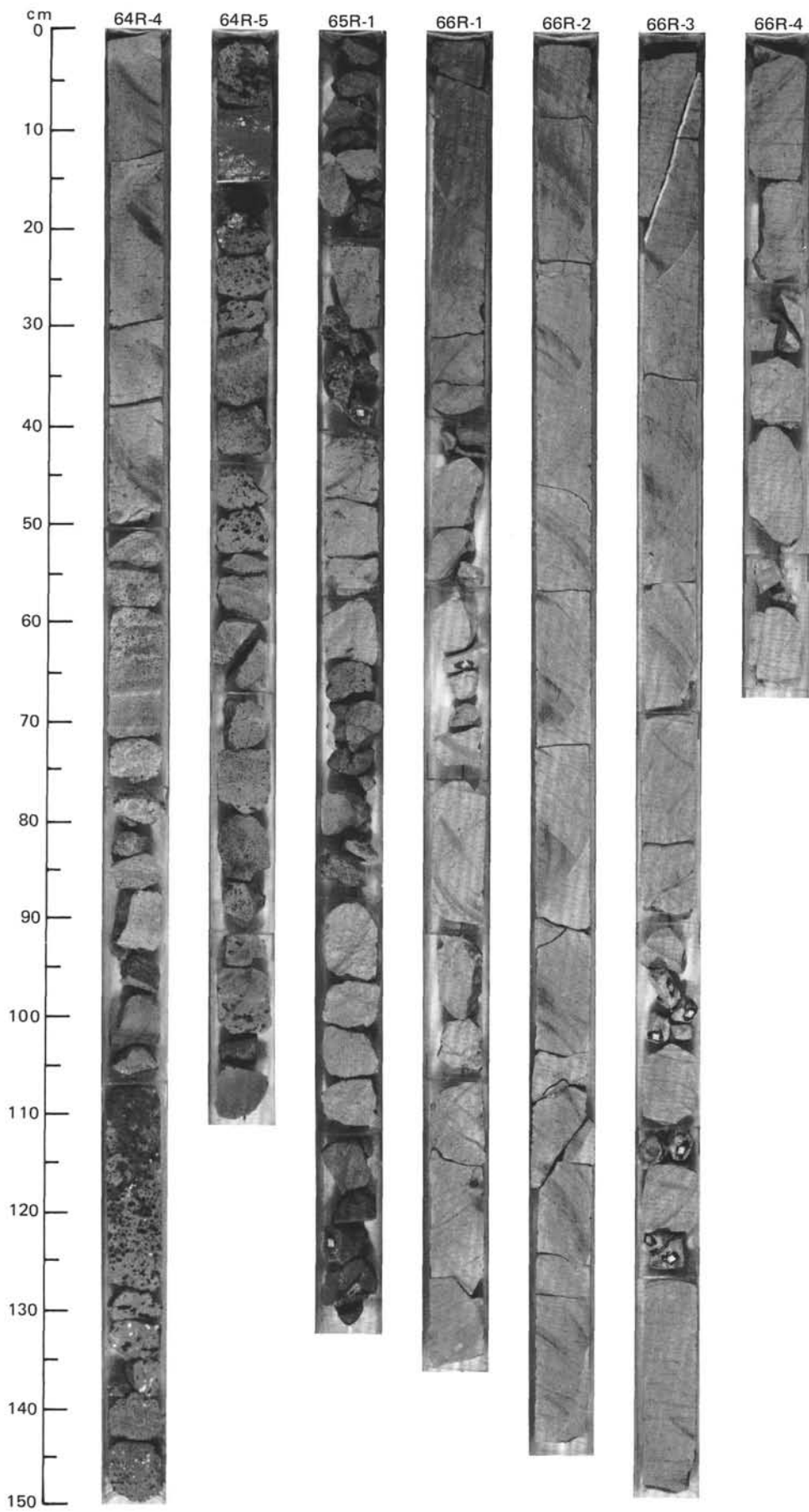
826.6–829.2 MBSF 642E–65R–1 (64 cm) TO 65R–1 (112 cm)

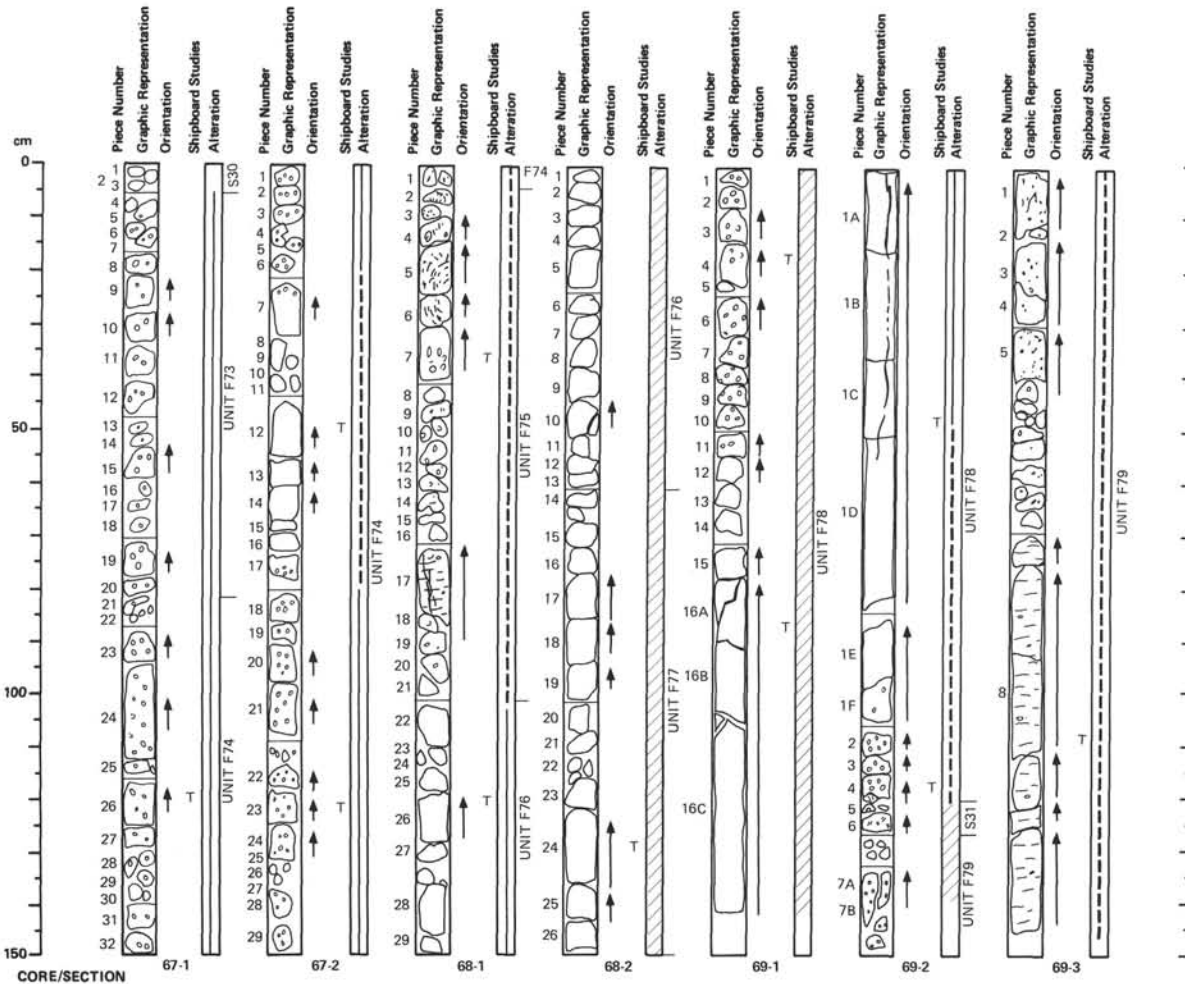
FINE-GRAINED, APHYRIC, GRAY BASALT. Flow base possibly not fully recovered. Highly vesicular, brown gray breccia pebbles at top with moderate vesicularity toward center and base. Some vesicle coalescence into streaks.

UNIT F72

829.2–840.5 MBSF 642E–65R–1 (112 cm) TO 66R–4 (67 cm)

FINE-GRAINED, SPARSELY PLAGIOCLASE PHYRIC, GRAY BASALT. Brown to purplish gray vesicular flow top breccia (<1.0 m thick), vesicles showing pale green smectite rims. Moderately to sparsely vesicular below. Plagioclase phenocrysts 1.0–2.0 mm in diameter throughout. Well developed streaky flow fabric between 66R–1, 75 cm, and 66R–4, 67 cm, except for massive zone at 66R–3, 30–90 cm. Fracturing common, celadonite(?) forms part of vein fill in 66R–4, Piece 6. Copper in vein at 66R–2, 23 cm.





UNIT S30
840.5–840.6 MBSF 642E–67R–1 (0 cm) TO 67R–1 (5 cm)

DARK RED BROWN LITHIC TUFF. Contains some vesicular basaltic clasts, ≤ 2 mm diameter, without vitric clasts. Contains clasts of quartz, mica and clinopyroxene.

UNIT F73
840.6–844.0 MBSF 642E–67R–1 (5 cm) TO 67R–1 (81 cm)

MEDIUM-GRAINED, APHYRIC, DARK GRAY BASALT FLOW. Weakly reddened to dark gray, vesicular throughout, and locally coalesced. Vesicles unfilled or with green smectite rims.

UNIT F74
844.0–847.9 MBSF 642E–67R–1 (81 cm) TO 68R–1 (6 cm)

MEDIUM-GRAINED, APHYRIC, DARK GRAY BASALT FLOW. As F73, except for moderate vesicularity at 67R–2, 25–75 cm, and celadonite(?) filling in vesicles at 67R–2, 25 cm.

THIN SECTION DESCRIPTIONS

642E–67R–1 (Piece 26, 121–123 cm): 45% plag, 35% cpx, 5% altered ol, 5% opaques, 10% altered mesostasis. Strongly altered. Intersertal to subophitic.

642E–67R–2 (Piece 12, 52–54 cm): 40% plag, 25% cpx, 2% altered ol, 3% opaques, 30% altered mesostasis. Intersertal.

UNIT F75
847.9–851.0 MBSF 642E–68R–1 (6 cm) TO 68R–1 (100 cm)

FINE-GRAINED, APHYRIC, GRAY BASALT FLOW. Flow top and flow base not recovered. Vesicularity ranges from highly vesicular in top half of section to moderate from 68R–1, 42 cm, downward. Some coalescence and streaming in upper section, dark green smectite fills throughout. Complex subvertical fracturing in Piece 17. Weak, diffuse streaking (flow fabric) developing below 68R–1, 42 cm.

UNIT F76
851.0–856.6 MBSF 642E–68R–1 (100 cm) TO 68R–2 (60 cm)

MEDIUM-GRAINED, APHYRIC BASALT FLOW. Red gray throughout, except for gray at very base. Moderate to highly vesicular, either rimmed or filled with dark green smectite, some smectite patch alteration, which does not exceed 5%. Iddingsitized olivine.

UNIT F77
856.6–864.1 MBSF 642E–68R–2 (60 cm) TO 68R–2 (150 cm)

MEDIUM-GRAINED, APHYRIC BASALT FLOW. Purplish gray at top, grading down to gray at base. Moderately vesicular throughout. Vesicles mostly unfilled, but rimmed with green smectite, locally blue-green celadonite.

UNIT F78
864.1–870.6 MBSF 642E–69R–1 (0 cm) TO 69R–2 (120 cm)

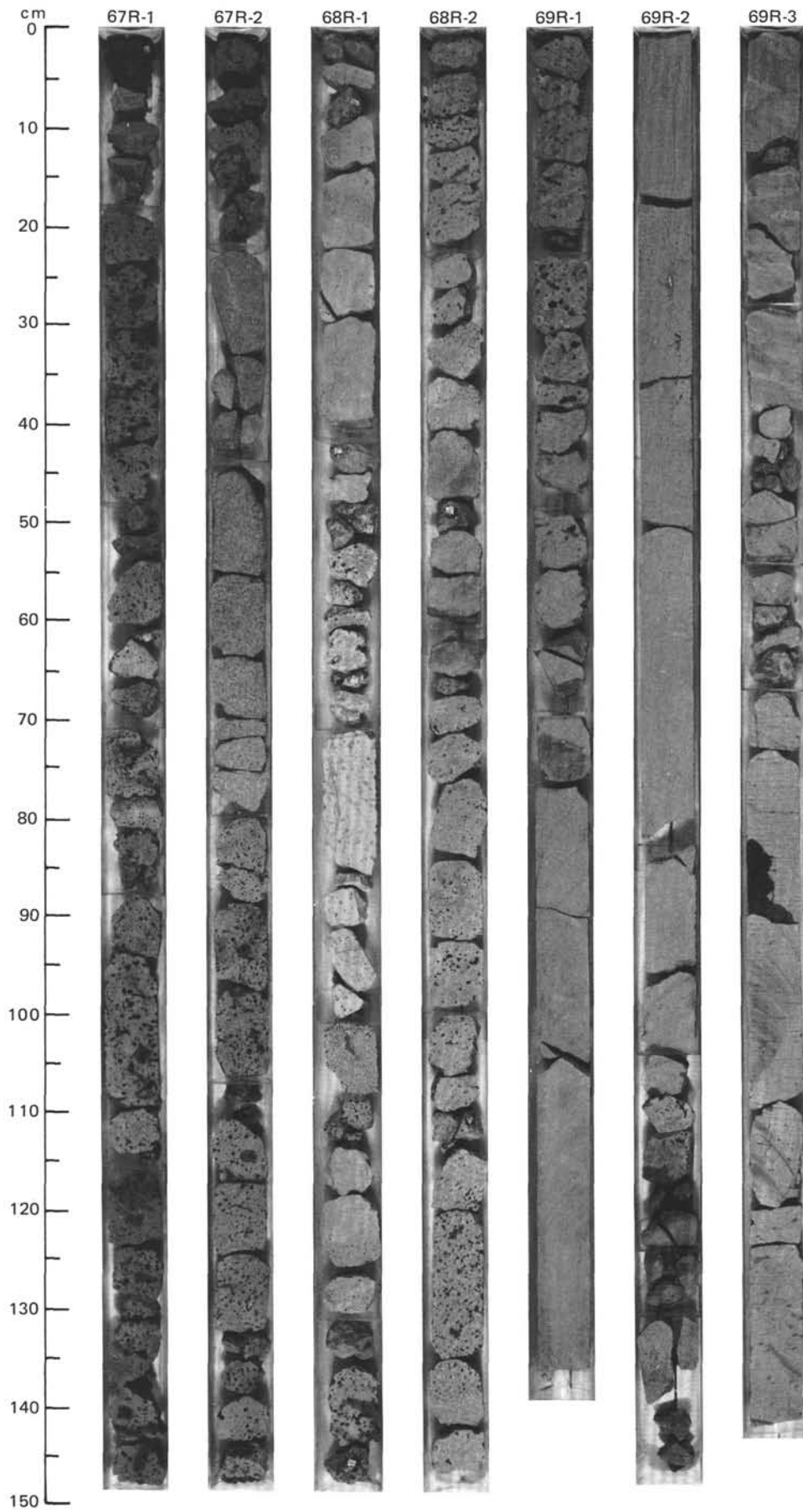
MEDIUM-GRAINED, APHYRIC BASALT FLOW. Reddened through top of section, moderately vesicular, with smectite rimmed vesicles in upper 78 cm. Nonvesicular central zone. Lower 120 cm is moderately vesicular and has dark green smectite fillings. Iddingsitization of olivines extensive, smectitic patchy alterations. Copper disseminated through groundmass, or concentrated as blebs in smectite veins in subvertical partings. Sharp basal contact of flow between highly vesicular basalt and tuff S31.

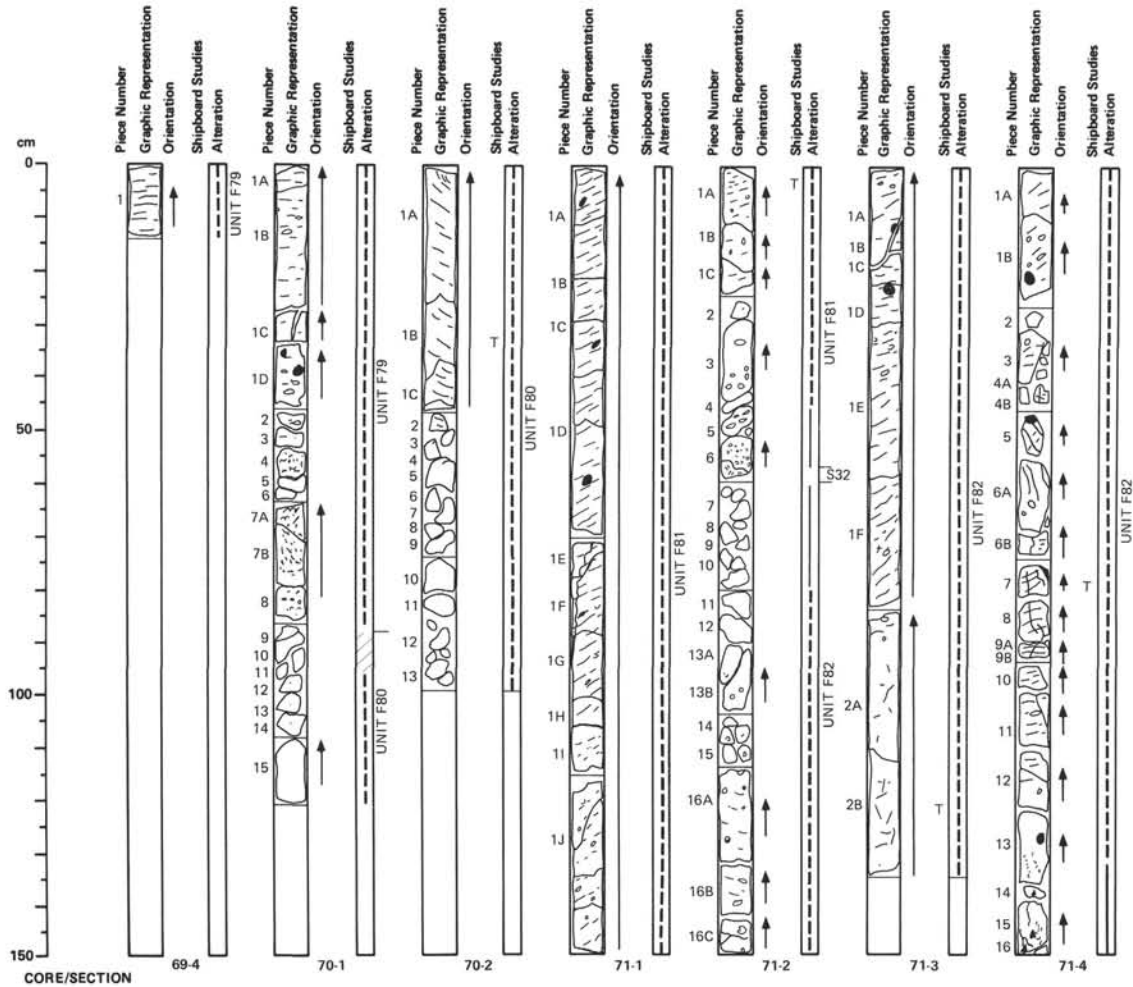
UNIT S31
870.6–871.6 MBSF 642E–69R–2 (120 cm) TO 69R–2 (125 cm)

DARK RED BROWN TUFF. Crystal, lithic, vitric tuff, containing aegirine-augite feldspar crystals, mica, and quartz. Contacts with F78 and F79 recovered.

UNIT F79
871.2–874.3 MBSF 642E–69R–2 (125 cm) TO 70R–1 (88 cm)

FINE-GRAINED, APHYRIC, GRAY BASALT FLOW. Highly vesicular gray flow top of collapsed vesicles with green smectite matrix. Moderately vesicular coalesced and streamed vesicle zone, filled with dark green smectite. Single example of zeolite fill at 69R–3, 126 cm, and vesicle flattening between 70R–1, 40 and 50 cm. Basal increase in vesicularity, some streaming and irregular flow pattern. Streaky flow fabric well developed in central zone, tightly spaced toward base.





UNIT F79

871.6–874.3 MBSF 642E–69R–2 (125 cm) TO 70R–1 (88 cm)

FINE-GRAINED, APHYRIC, GRAY BASALT FLOW. Highly vesicular gray flow top of collapsed vesicles with green smectite matrix. Moderately vesicular coalesced and streamed vesicle zone, filled with dark green smectite. Single example of zeolite fill at 69R–3, 126 cm, and vesicle flattening between 70R–1, 40 and 50 cm. Basal increase in vesicularity, some streaming and irregular flow pattern. Streaky flow fabric well developed in central zone, tightly spaced toward base.

UNIT F80

874.3–880.3 MBSF 642E–70R–1 (88 cm) TO 70R–2 (99 cm)

FINE-GRAINED, APHYRIC, GRAY BASALT FLOW. Possibly missing center and base. Reddened vesicular flow top, with streamed, coalesced, collapsed vesicles containing dark green smectite fill. Low-angle, inclined streaking (flow fabric) dies out to massive section form at base of recovery.

UNIT F81

880.3–886.2 MBSF 642E–71R–1 (0 cm) TO 71R–2 (56 cm)

FINE-GRAINED, APHYRIC, GRAY BASALT FLOW. Top and central flow not recovered. Sparsely vesicular except for lowest 50 cm, moderately to highly vesicular, filled with green smectite throughout. Flattened vesicles subparallel to fabric at 71R–2, 47–50 cm. Streaky flow fabric well developed from top of recovery almost to base, generally shallowly inclined. Basal contact with S32 shows slight purplish-gray alteration.

UNIT S32

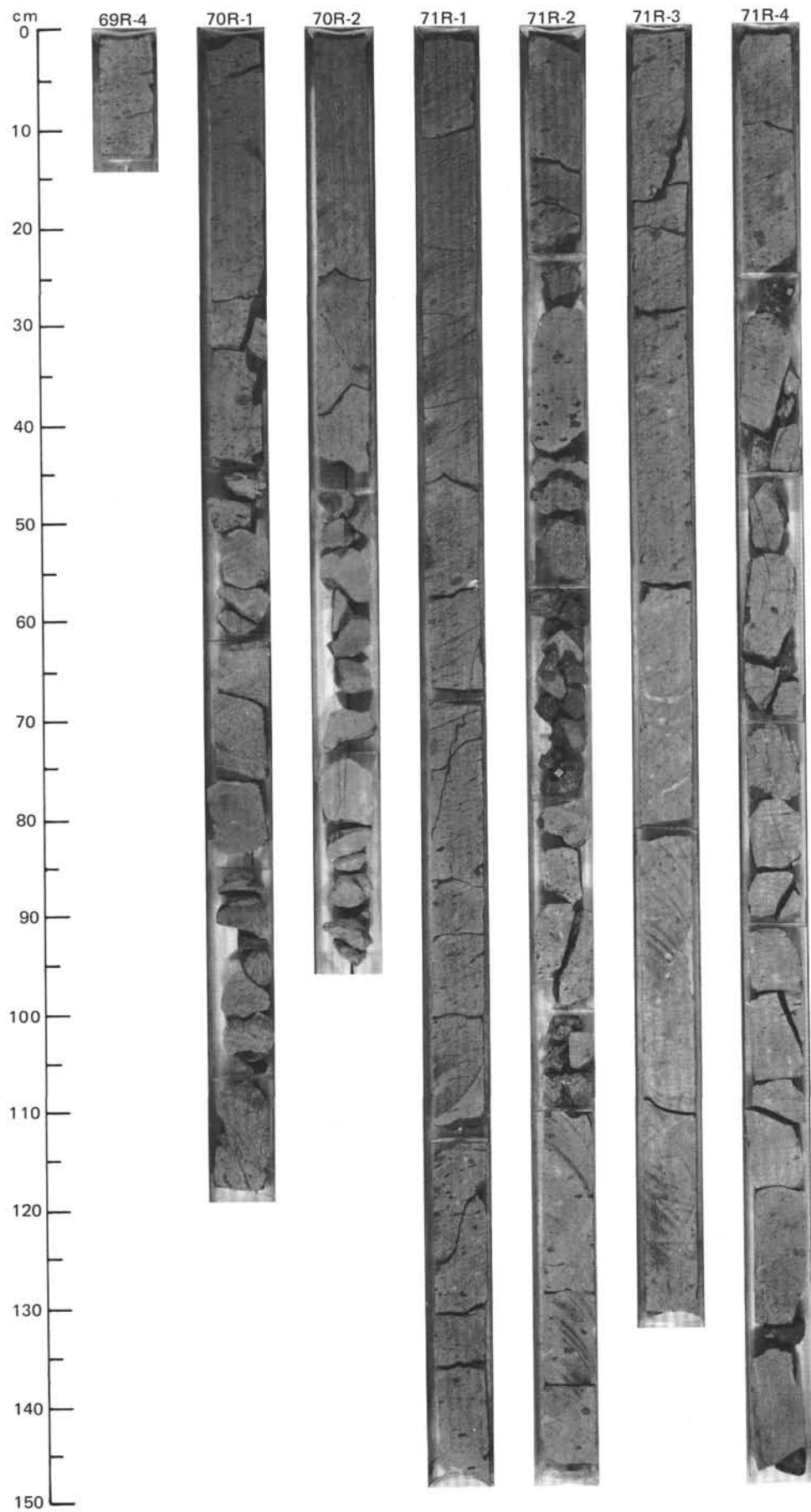
886.2 MBSF 642E–71R–2 (56 cm) TO 71R–2 (58 cm)

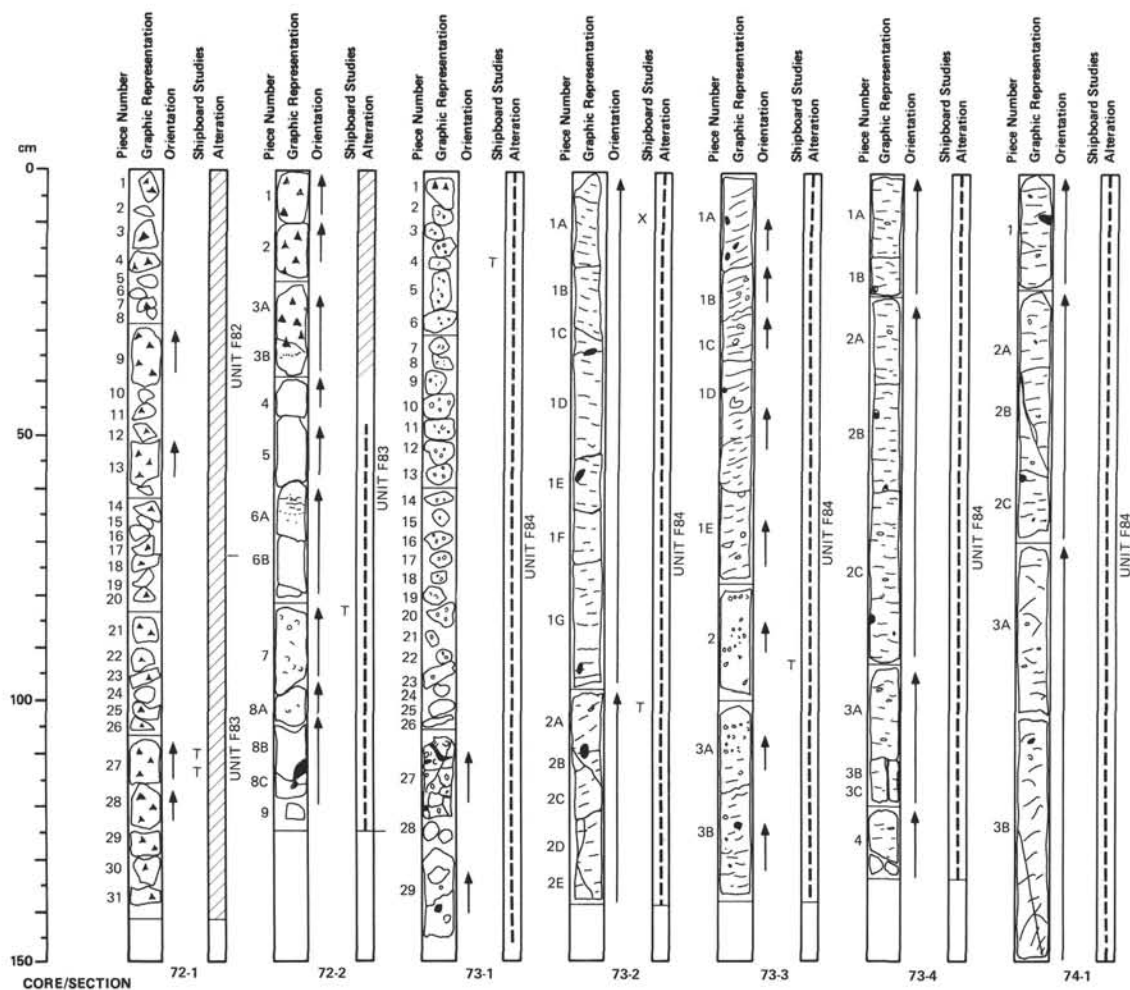
RED BROWN, VITRIC, BASALTIC TUFF. Contains vesicular, coniform shards, including 10% palagonitic black glass. <5% lithic fragments comprised of basaltic clasts from the underlying flow, as well as 2% feldspar and traces of quartz grains.

UNIT F82

886.2–891.2 MBSF 642E–71R–2 (58 cm) TO 72R–1 (71 cm)

FINE-GRAINED, APHYRIC, BASALT FLOW. Isolated purple coloration at top of unit. Vesicular smectite filled zone, becoming sparse and not streamed with depth. In lowest 90 cm of flow, increasing vesicularity, then development of polymictic breccia of vesicular fragments of mixed base and underlying flow top. Streaking (flow fabric) well developed, sub-horizontally inclined for much of unit, with discrete chaotic zone. Several subrounded vesicular, aphyric basalt xenoliths present. Local vertical/subvertical fracture sets toward base of flow.





UNIT F82

886.2-891.2 MBSF 642E-71R-2 (58 cm) TO 72R-1 (71 cm)

FINE-GRAINED, APHYRIC, BASALT FLOW. Isolated purple coloration at top of unit. Vesicular smectite filled zone, becoming sparse and not streamed with depth. In lowest 90 cm of flow, increasing vesicularity, then development of polymictic breccia of vesicular fragments of mixed base and underlying flow top. Streaking (flow fabric) well developed, sub-horizontally inclined for much of unit, with discrete chaotic zone. Several subrounded vesicular, aphyric basalt xenoliths present. Local vertical/subvertical fracture sets toward base of flow.

UNIT F83

891.2-894.0 MBSF 642E-72R-1 (71 cm) TO 72R-2 (124 cm)

FINE-GRAINED, APHYRIC, GRAY BASALT FLOW. Flow base not recovered. Slightly reddened flow top breccia, with dark green smectite matrix, to highly vesicular blocks. Moderately vesicular and gray at base of unit, some local streaming of green smectite filled vesicles. Few xenoliths, iddingsitized olivine.

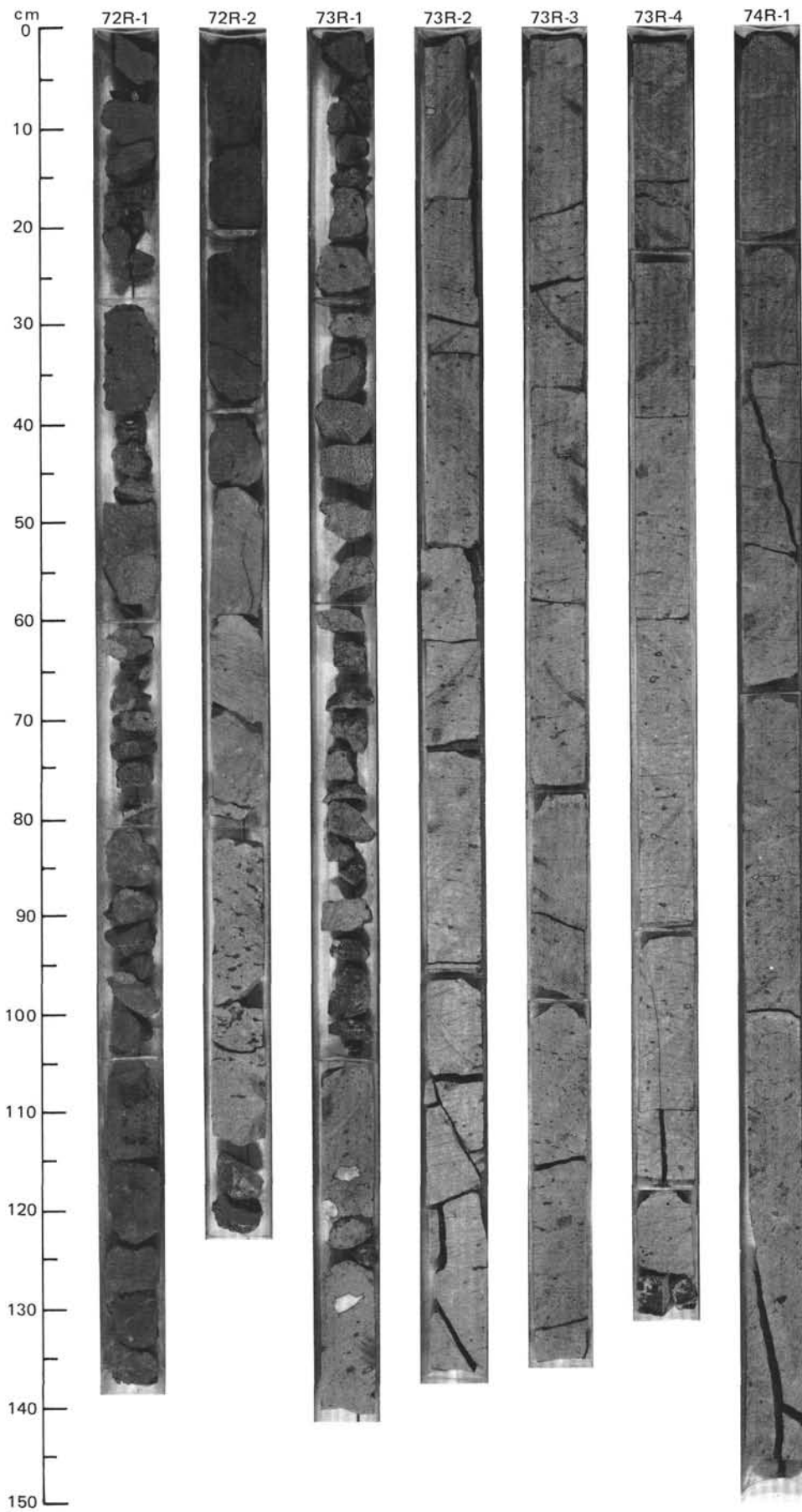
UNIT F84

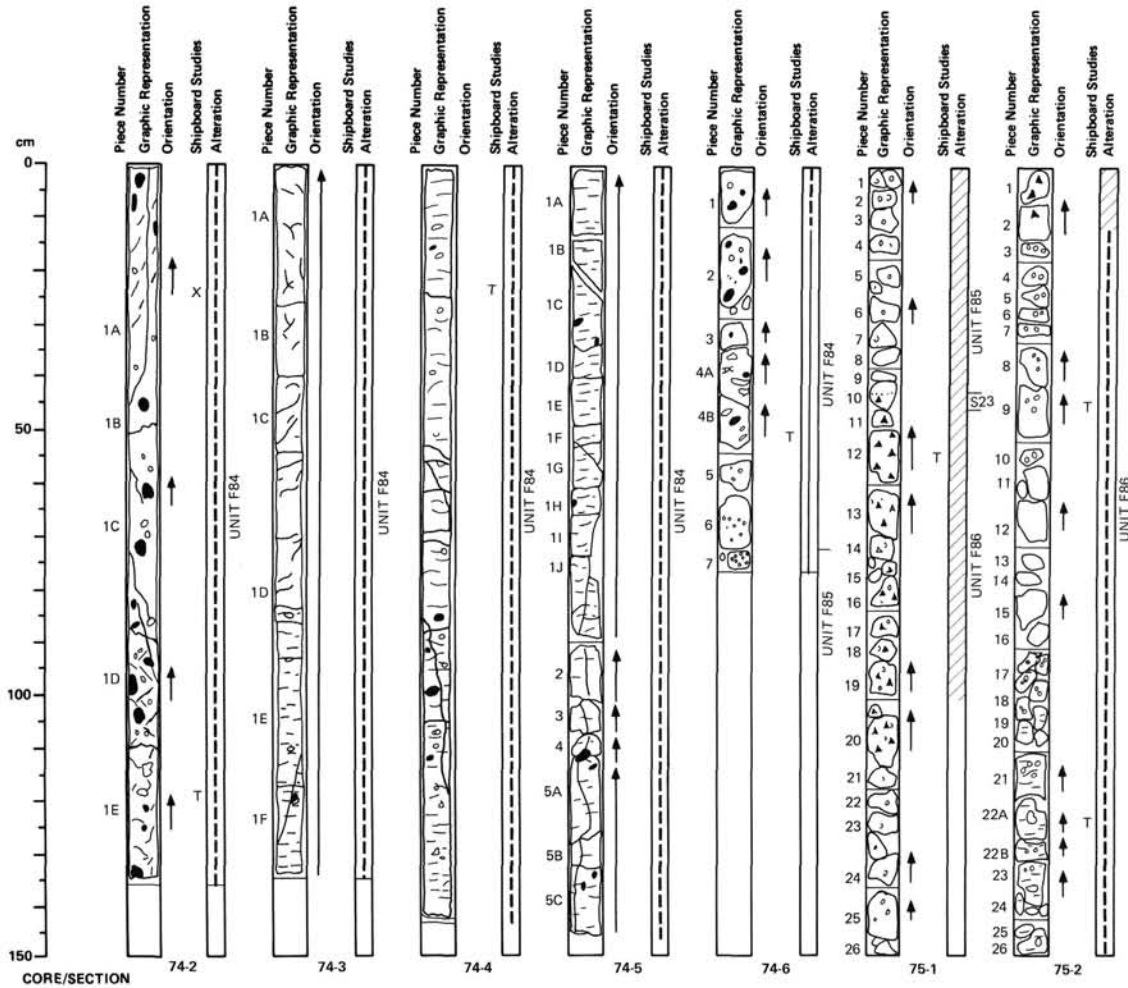
894.0-908.2 MBSF 642E-73R-1 (0 cm) TO 74R-6 (72 cm)

FINE-GRAINED, APHYRIC, GRAY BASALT FLOW. Base not recovered. Highly vesicular and brecciated top, with slight purple coloration. Vesicles with predominantly dark green smectite and subordinate calcite fillings. Zone of calcite veining and cavity fill in 73R-1, 107-135 cm. Excellent section of streaky flow fabric, including chaotic zone, 74R-1, 75 cm to 74R-3, 85 cm. Lowest 70 cm of unit unstreamed and increasingly vesicular and xenolith rich. Xenoliths common throughout flow, abundant in chaotic fabric zone.

THIN SECTION DESCRIPTION

642E-73R-2 (Piece 7, 103-105 cm): 2% plag phenocrysts. 40% plag, 40% cpx, 5% altered ol, 5% opaques, 10% altered mesostasis. Intersertal-intergranular, subophitic.





UNIT F84

894.0-908.2 MBSF

642E-73R-1 (0 cm) TO 74R-6 (72 cm)

FINE-GRAINED, APHYRIC, GRAY BASALT FLOW. Base not recovered. Highly vesicular and brecciated top, with slight purple coloration. Vesicles with predominantly dark green smectite and subordinate calcite fillings. Zone of calcite veining and cavity fill in 73R-1, 107-135 cm. Excellent section of streaky flow fabric, including chaotic zone, 74R-1, 75 cm to 74R-3, 85 cm. Lowest 70 cm of unit unstrained and increasingly vesicular and xenolith rich. Xenoliths common throughout flow, abundant in chaotic fabric zone.

THIN SECTION DESCRIPTION

642E-73R-2 (Piece 7, 103-105 cm): 2% plag phenocrysts, 40% plag, 40% cpx, 5% altered ol, 5% opaques, 10% altered mesostasis. Intersertal-intergranular, subophitic.

UNIT F85

908.2-911.2 MBSF

642E-74R-6 (72 cm) TO 75R-1 (38 cm)

FINE-GRAINED, MODERATELY PLAGIOCLASE PHYRIC, GRAY BASALT FLOW. Reddened and vesicular rubbly basalt fragments throughout. Most vesicles filled with dark green smectite, few zeolites, some coalesced toward base(?). Plagioclase laths 0.6-0.8 mm in length, locally clustered and fresh.

UNIT S33

911.2 MBSF

642E-75R-1 (38 cm) TO 75R-1 (45 cm)

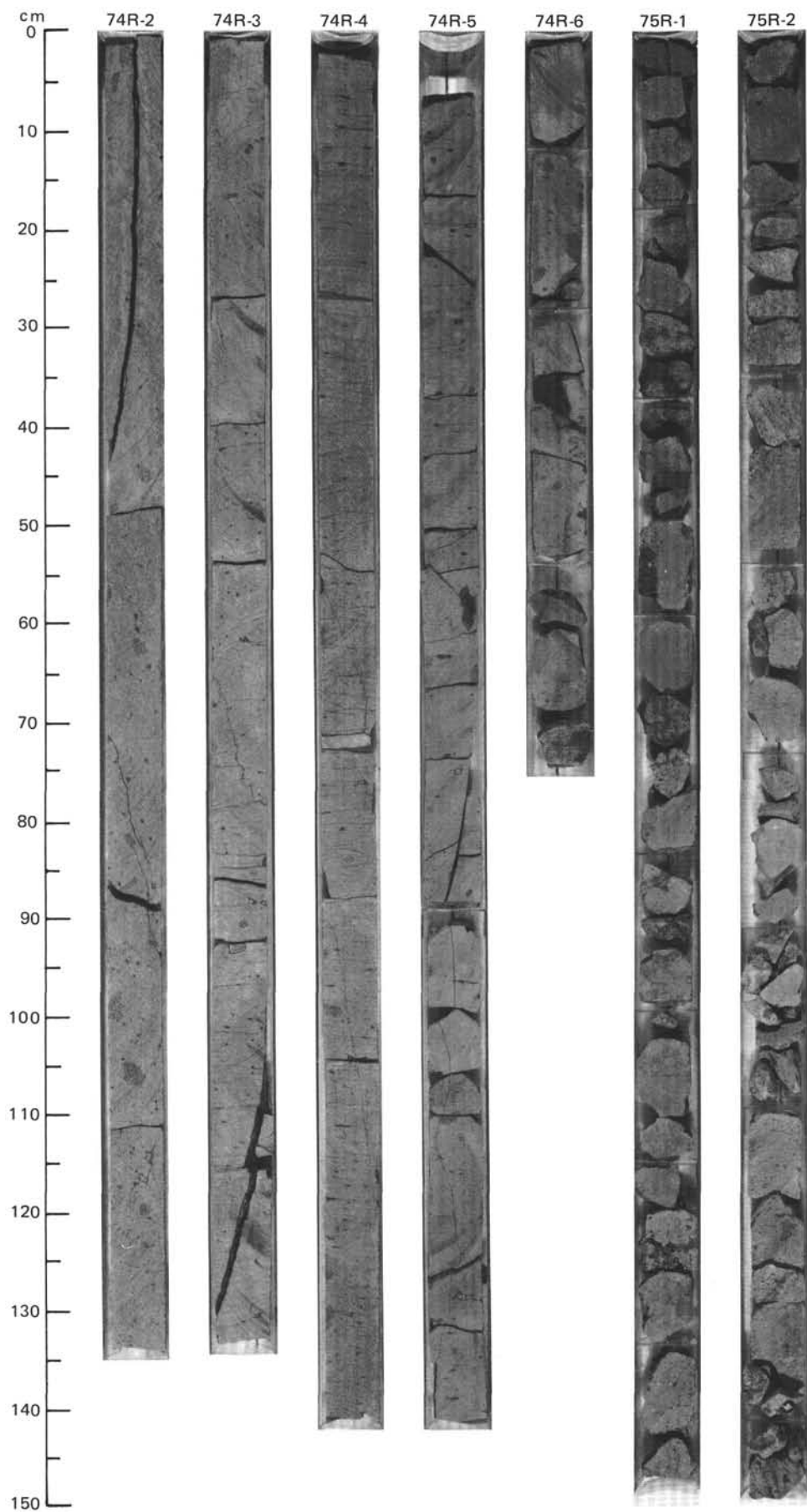
VERY DARK BROWN TUFF. Contains white feldspar specks, containing lithics (basaltic), laminated redeposited(?) tuffs, quartz, feldspar, and possibly micas. Contact with F85 missing, with F86 recovered. Pocket infilling down to 75R-1, 107 cm.

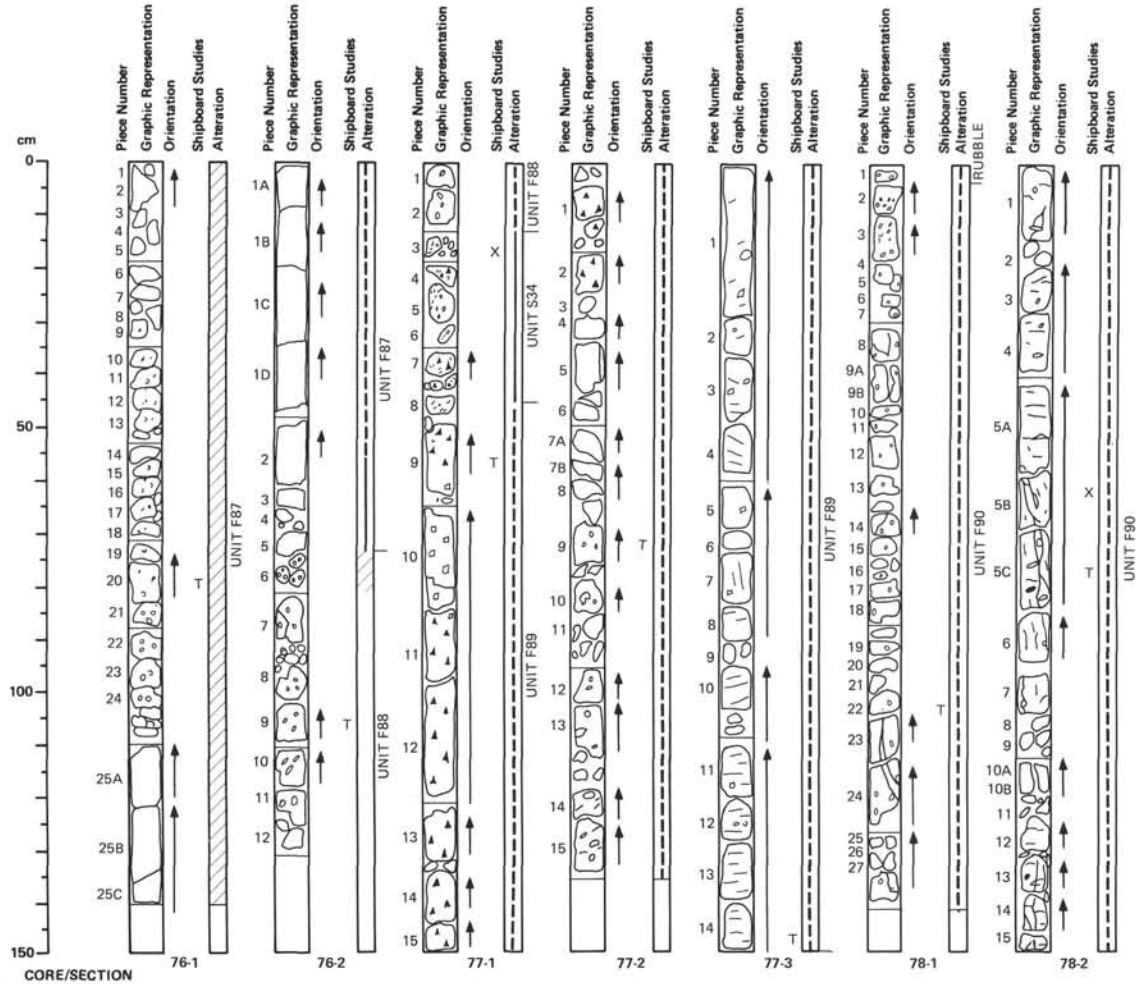
UNIT F86

911.2-918.2 MBSF

642E-75R-1 (45 cm) TO 75R-2 (150 cm)

FINE-GRAINED, SPARSELY PLAGIOCLASE PHYRIC, GRAY BASALT FLOW. Base (and center?) not recovered. Reddish brown gray top breccia containing scoriaceous and highly vesicular fragments with tuff matrix and fill. 1% plagioclase phenocrysts \leq 2 mm diameter. Moderate to highly vesicular throughout, all dark green smectite filled. Weakly developed streaky flow fabric.





UNIT F87

918.2–923.5 MBSF 642E–76R–1 (0 cm) TO 76R–2 (75 cm)

MEDIUM-GRAINED, APHYRIC, GRAY BASALT FLOW. Weakly reddened throughout, highly vesicular between 76R–1, 10 cm, and 76R–1, 110 cm. Olivines iddingsitized.

THIN SECTION DESCRIPTION

642E–76R–1 (76–78 cm): 21% plag, 3% cpx, 1% ol, 64% cryptocrystalline, 11% altered mesostasis.

UNIT F88

923.5–927.6 MBSF 642E–76R–2 (75 cm) TO 77R–1 (13 cm)

MEDIUM-GRAINED, APHYRIC, GRAY BASALT FLOW. Slight reddening at top with iddingsitized olivines. Moderately vesicular with vesicles mostly filled or rimmed as above, elongated in 76R–2, Piece 10. Minor fracturing.

UNIT S34

927.6–928.1 MBSF 642E–77R–1 (13 cm) TO 77R–1 (47 cm)

DARK BROWN VITRIC TUFF. Mostly containing coarse ash particles, with larger clasts vitric and vesicular, black to pale green in color. Subhorizontal orientation of clasts, some collapsed pumice fragments. Contact with F89 recovered.

UNIT F89

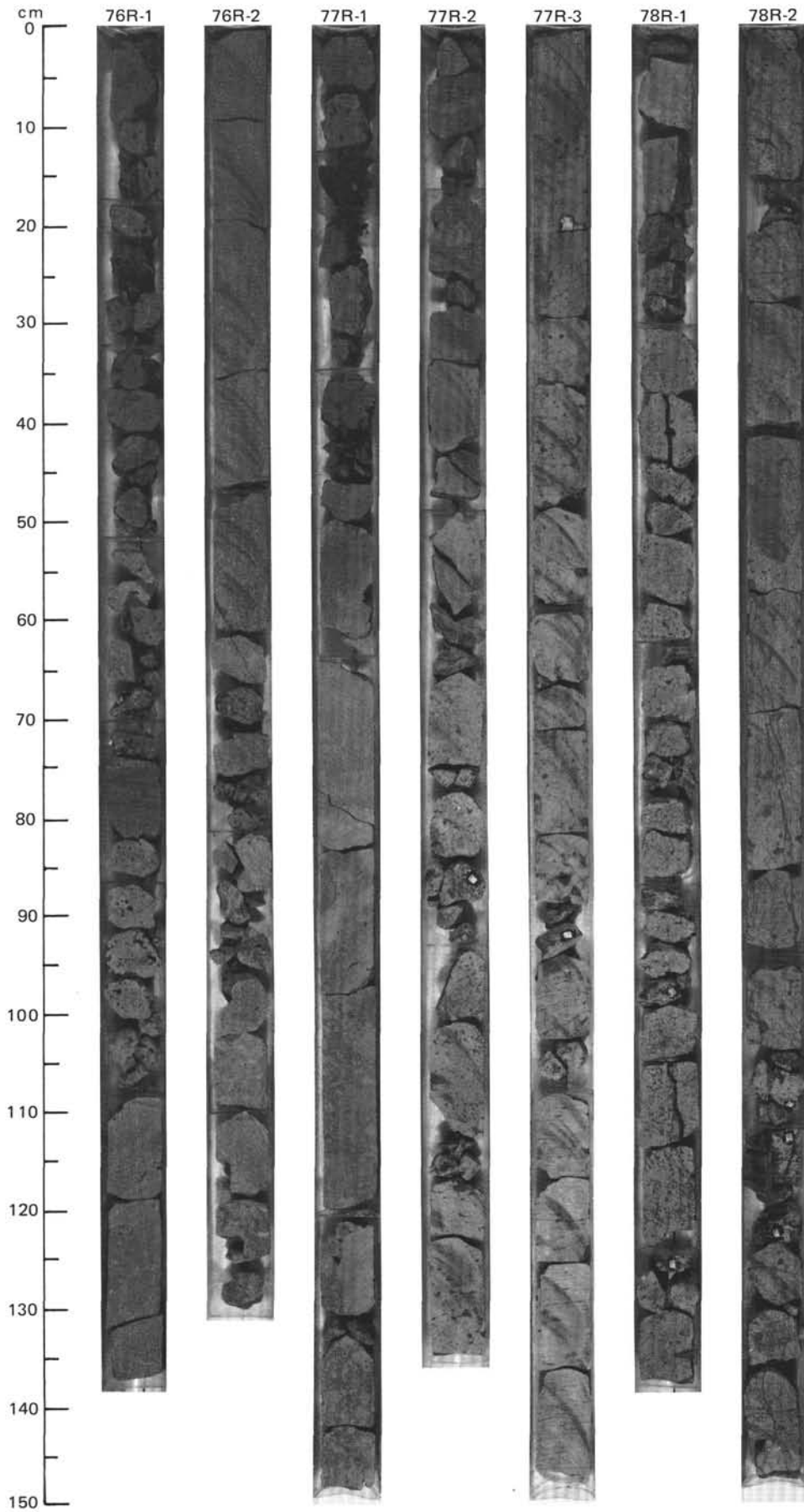
928.1–935.9 MBSF 642E–77R–1 (47 cm) TO 77R–3 (150 cm)

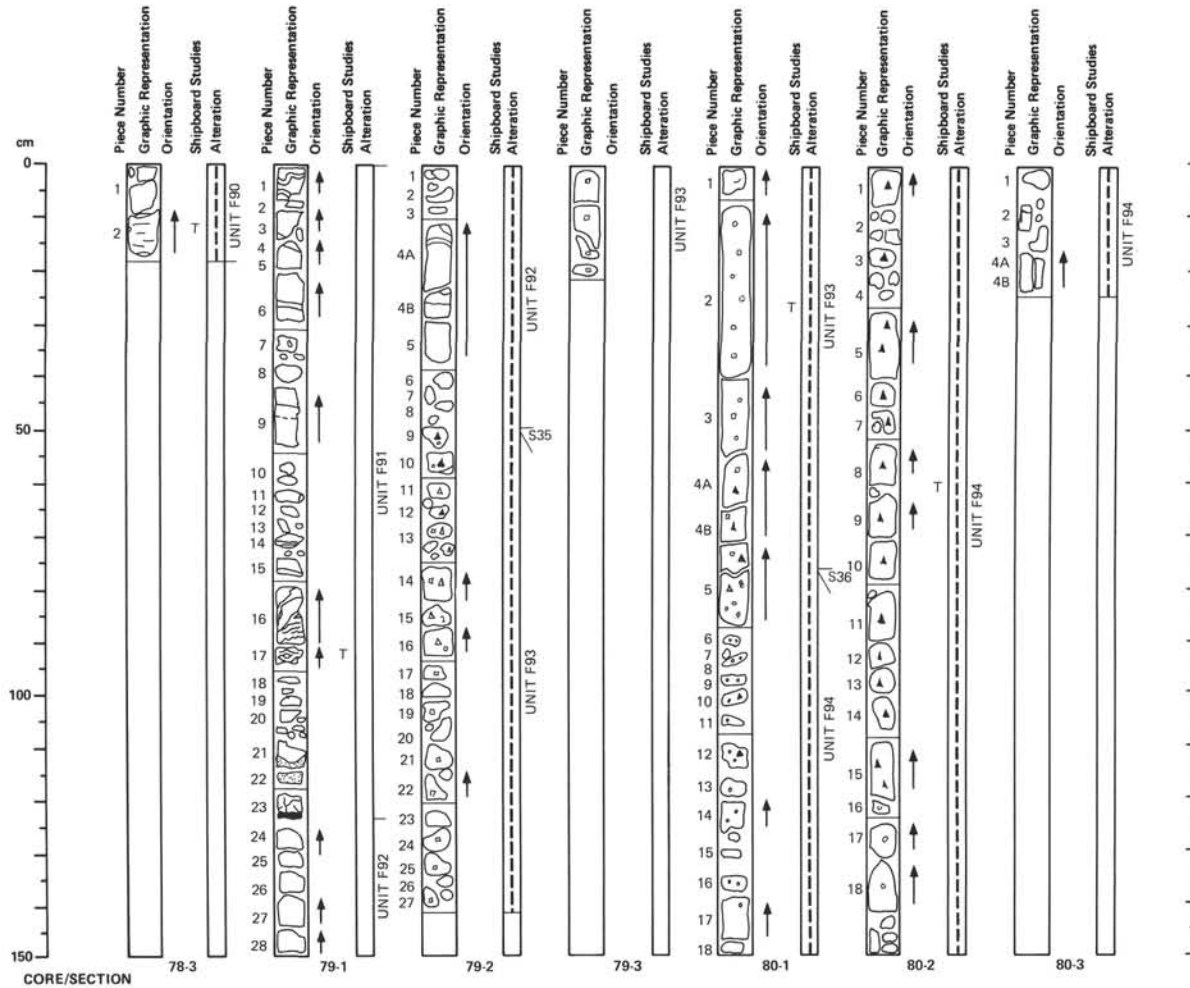
FINE-GRAINED, APHYRIC TO SPARSELY PYROXENE–PLAGIOCLASE PHYRIC BASALT FLOW. Flow base and probably much of the center missing. Locally reddish brown flow top breccia of subrounded vesicular fragments, vesicles filled with light green and medium green smectites: celadonite(?)/saponite. Sparsely vesicular lower section, with weak streaky flow fabric. Plagioclase phenocrysts tending to glomeroporphyritic.

UNIT F90

935.9–944.0 MBSF 642E–78R–1 (3 cm) TO 78R–3 (18 cm)

FINE-GRAINED, SPARSELY PYROXENE–PLAGIOCLASE PHYRIC BASALT FLOW. Base and possibly much of center not recovered. Highly vesicular upper section, decreasing downward. Some irregular shaped and streamed vertically and collapsed, filled or partly filled with dark green smectite. Phenocrysts as in F89. Flow fabric streaking poorly developed but subhorizontal to base of recovery. Some rounded vesicular xenoliths, subvertical fracturing with green smectite filling.





935.9–944.0 MBSF

FINE-GRAINED, SPARSELY PYROXENE–PLAGIOCLASE PHYRIC BASALT FLOW. Base and possibly much of center not recovered. Highly vesicular upper section, decreasing downward. Some irregular shaped and streamed vertically and collapsed, filled or partly filled with dark green smectite. Phenocrysts as in F89. Flow fabric streaking poorly developed but subhorizontal to base of recovery. Some rounded vesicular xenoliths, subvertical fracturing with green smectite filling.

UNIT F90

642E–78R–1 (3 cm) TO 78R–3 (18 cm)

944.0–952.2 MBSF

MIXED FINE-GRAINED AND MEDIUM-GRAINED, APHYRIC, GRAY BASALT FLOW. Top probably not recovered. Fine-grained and medium-grained basalt layers disposed in sharply defined bands, contrasting grain size and vesicularity: 20–40% in mediums, 3–10% in fines. Vesicles locally show strong elongation in fine bands and close to basal contact. Dark green smectite filling throughout. Base is dark gray to dark reddened gray, highly vesicular to pumiceous 1 cm of glass.

THIN SECTION DESCRIPTION

642E–79R–1 (Piece 17, 90–92 cm): 40% plag, 35% cpx, 10% ol, 3% opaques, 10% variolitic groundmass, all slightly to thoroughly altered. Intersertal to intergranular.

UNIT F91

642E–79R–1 (0 cm) TO 79R–1 (124 cm)

UNIT F92

952.2–957.2 MBSF 642E–79R–1 (124 cm) TO 79R–2 (49 cm)

MIXED FINE-GRAINED AND MEDIUM-GRAINED, APHYRIC, GRAY BASALT FLOW. Slightly reddened gray, internally layered/banded fine (lighter gray) and medium (darker gray) basalts of 1.0–22.0 cm width. Smaller vesicles in finer bands, some hairline veins cutting banding.

UNIT S35

957.2 MBSF 642E–79R–2 (49 cm) TO 79R–2 (50 cm)

DARK RED BROWN, BASALTIC, VITRIC TUFF. Rather coarse, median diameter 0.5 mm. Spotted with dark shards of fresh glass.

UNIT F93

957.2–964.8 MBSF 642E–79R–2 (51 cm) TO 80R–1 (76 cm)

MEDIUM-GRAINED, SPARSELY PLAGIOCLASE PHYRIC TO APHYRIC, GRAY BASALT FLOW. Purplish gray top to vesicular flow top breccia. Plagioclase phenocrysts \leq 2.0 mm. Trace pyroxene phenocrysts \leq 1.0 mm. Slightly vesicular center flow, vesicles filled with smectite. Dark gray basal breccia preserved.

UNIT S36

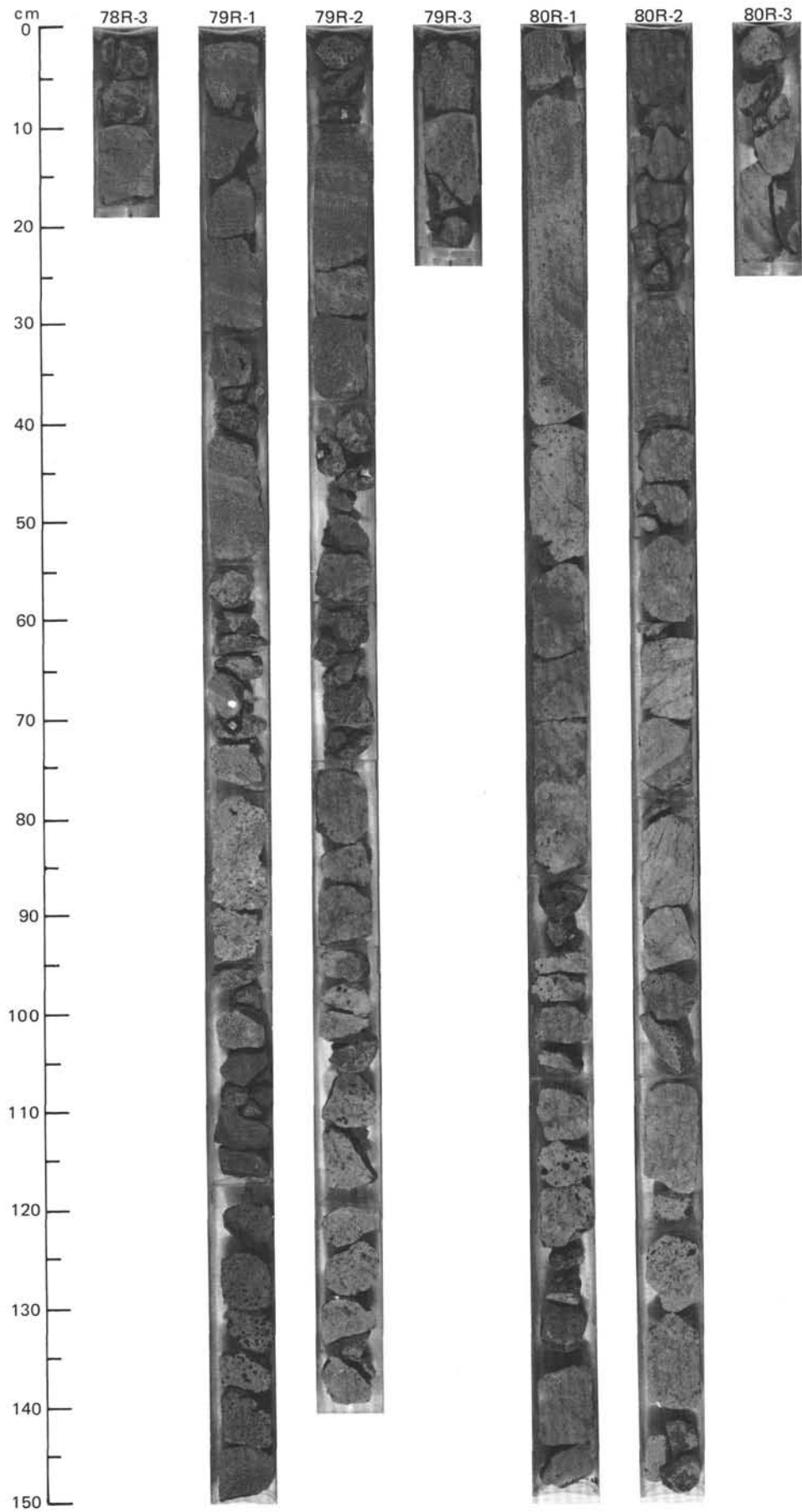
964.8 MBSF 642E–80R–1 (76 cm) TO 80R–1 (77 cm)

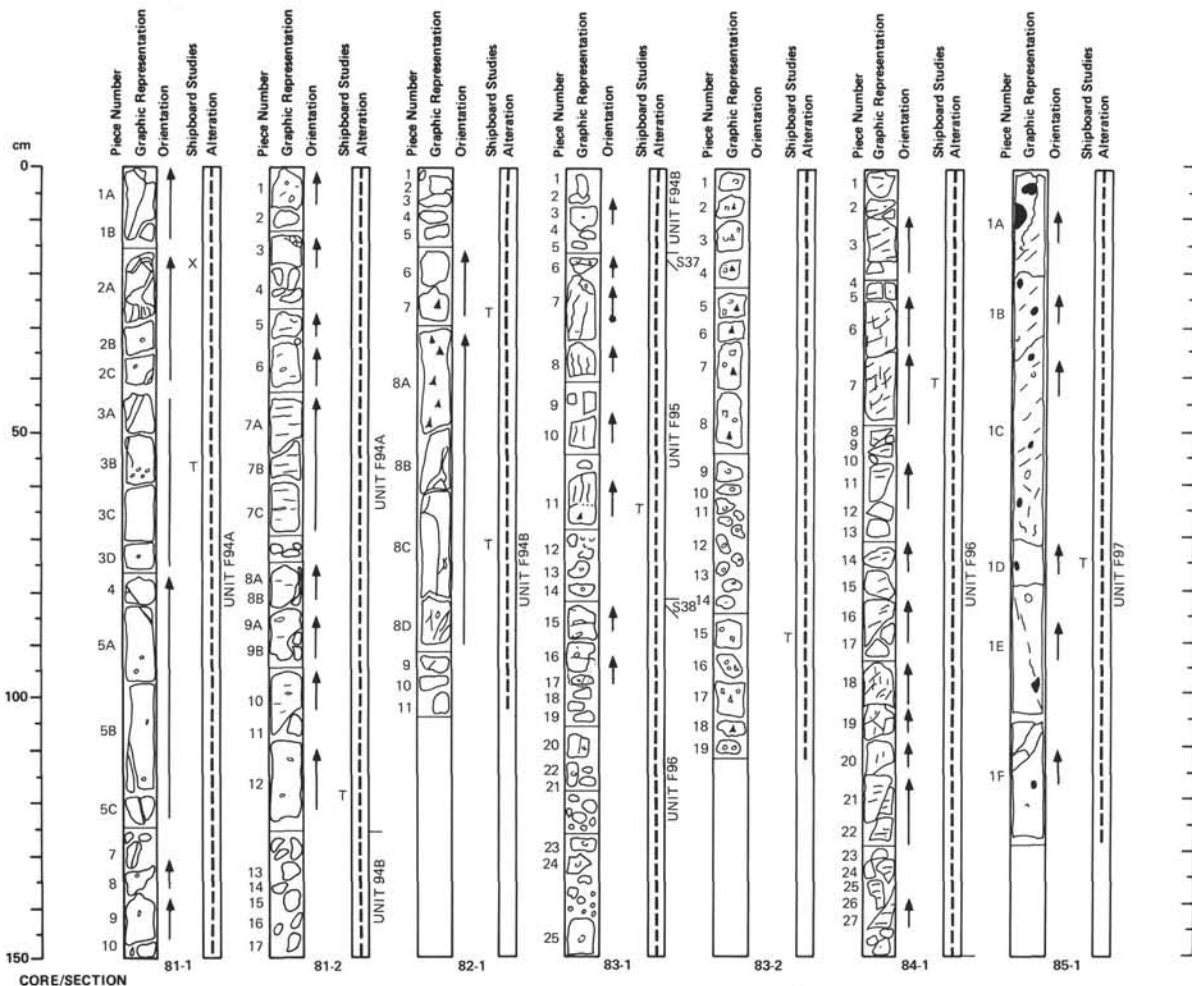
DARK RED BROWN TUFF. Clast median diameter of 0.02 mm, much unrecovered.

UNIT F94

964.8–970.4 MBSF 642E–80R–1 (77 cm) TO 80R–3 (24 cm)

FINE-GRAINED, APHYRIC, GRAY BASALT FLOW. Base not recovered. Good flow top breccia down to 80R–2, 120 cm. Vesicular to moderately vesicular.





970.4–974.5 MBSF

UNIT F94A

642E–80R–3 (24 cm) TO 81R–2 (125 cm)

FINE-GRAINED, APHYRIC TO SPARSELY PLAGIOCLASE–CLINOPYROXENE PHYRIC, GRAY BASALT FLOW. Top and base not recovered. Vesicles and steeply inclined fractures filled by saponite.

THIN SECTION DESCRIPTION

642E–81R–1 (Piece 3B, 60–62 cm): Phenocrysts: <1% plag, <1% cpx. Groundmass: 40% plag, 35% cpx, 5% ol, 5% opaques, variably altered. 10% altered mesostasis.

974.5–978.9 MBSF

UNIT F94B

642E–81R–2 (125 cm) TO 83R–1 (16 cm)

FINE-GRAINED, SPARSELY PLAGIOCLASE–CLINOPYROXENE PHYRIC, GRAY BASALT FLOW. Top and base not recovered. Vesicular to sparsely vesicular, with locally complex zones of streaming and interconnecting veins. Dark green and light green celadonite (?) and smectite fillings, intra-unit breccia cemented by dark green smectite 82R–1, 24–50 cm. Some propagation of fractures from vesicles. Streaking (flow fabric) laminations toward lowest sections.

978.9 MBSF

UNIT S37

642E–83R–1 (16 cm) TO 83R–1 (18 cm)

RED BROWN BASALTIC, VITRIC TUFF. Subhorizontal orientation of clasts, 90% nonvesicular shards, 10% lithics of underlying basalt. Sparse plagioclase, clinopyroxene crystals, quartz grains. Erosional contact with F95 recovered.

978.9–986.2 MBSF

UNIT F95

642E–83R–1 (18 cm) TO 83R–1 (82 cm)

MEDIUM-GRAINED, SPARSELY PHYRIC, GRAY BASALT. Purplish gray, strongly vertically veined and moderately vesicular. Plagioclase phenocrysts up to 2.0 mm in diameter, plus iddingsitized olivines < 0.5 mm.

986.2 MBSF

UNIT S38

642E–83R–1 (82 cm)

DARK BROWN, LITHIC, VITRIC TUFF. Contains green patches and white feldspar(?) spotting. Arcuate and vesicular dark gray shards, few underlying basaltic lithic fragments, plagioclase crystals approximately 0.6 mm in diameter.

986.2–997.6 MBSF

UNIT F96

642E–83R–1 (82 cm) TO 84R–1 (150 cm)

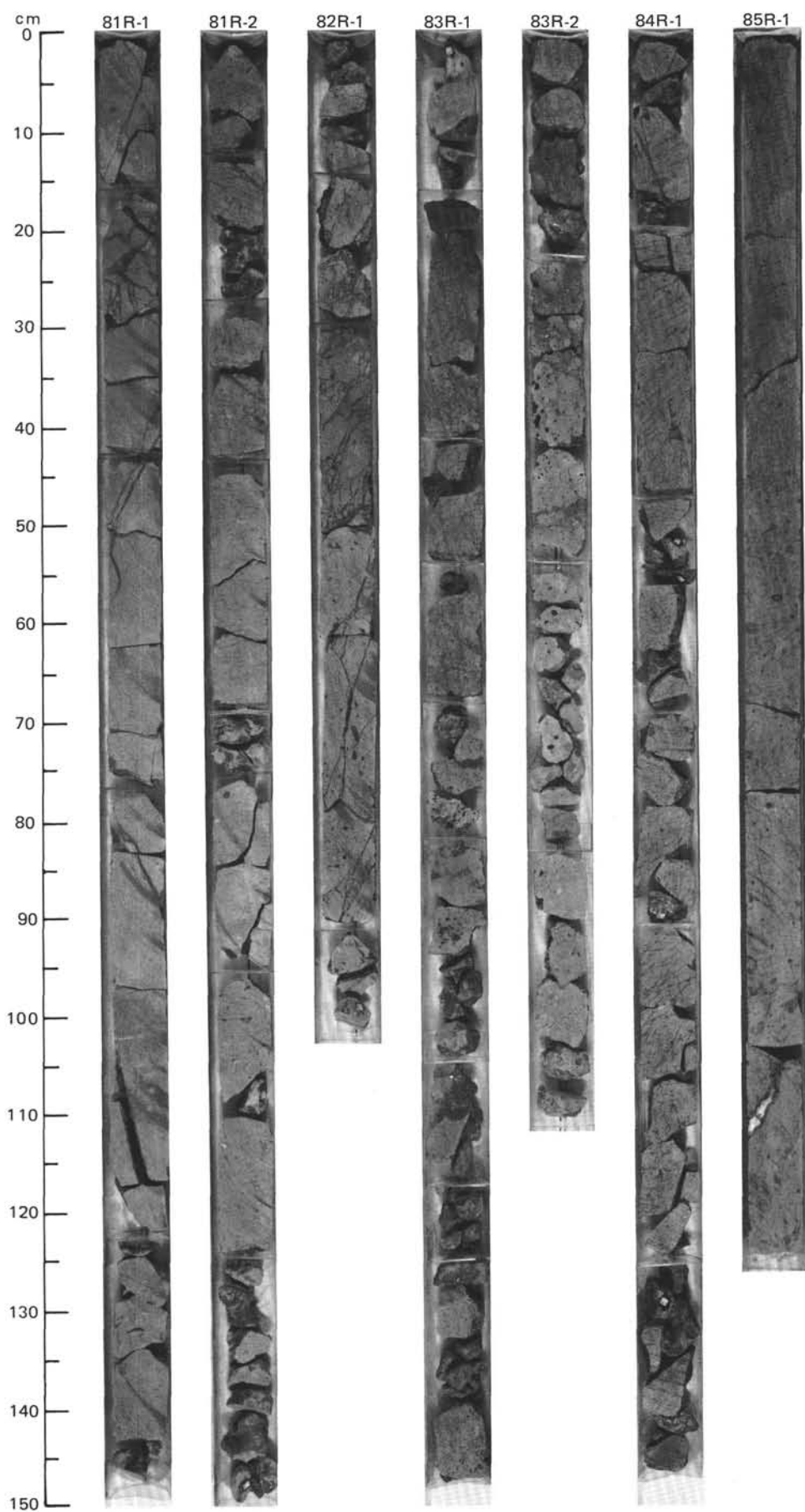
FINE-GRAINED, SPARSELY PHYRIC, GRAY BASALT FLOW. Base not recovered. Moderately vesicular, purplish gray to gray brecciated basalt top, < 1% plagioclase and clinopyroxene, locally glomeroporphyritic. Central/lower sections nonvesicular and streaked (flow fabric) within well-developed random orientation zone.

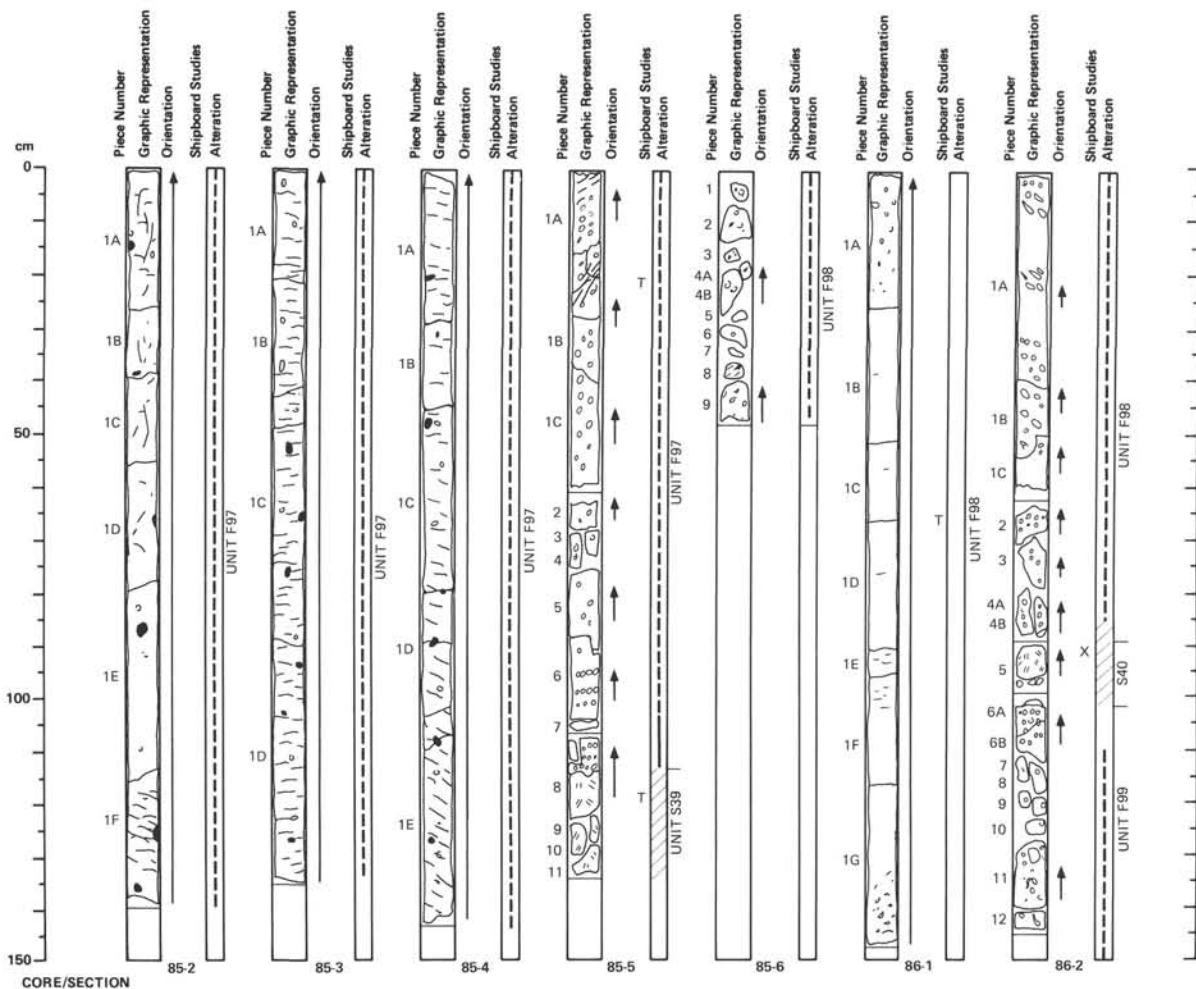
997.6–1011.3 MBSF

UNIT F97

642E–85R–1 (0 cm) TO 85R–5 (113 cm)

FINE-GRAINED, APHYRIC, GRAY BASALT FLOW. Top and upper center flow not recovered. Recovery commences in chaotic laminar zone, abundantly xenolithic, cut by subvertical, *en echelon*, hairline fractures, and giving way to regular subhorizontal fabric. Disseminated copper blebs throughout groundmass and concentrated in vesicles. 2–5% xenolithic with highly vesicular, aphyric gray basalt. Highly vesicular base, up to 35% vesicles at contact, streaking (flow fabric) becomes more diffuse and mottled from 85R–5, 0 cm, downward.





UNIT F97

997.6–1011.3 MBSF 642E–85R–1 (0 cm) TO 85R–5 (113 cm)

FINE-GRAINED, APHYRIC, GRAY BASALT FLOW. Top and upper center flow not recovered. Recovery commences in chaotic laminar zone, abundantly xenolithic, cut by subvertical, *en echelon*, hairline fractures, and giving way to regular subhorizontal fabric. Disseminated copper blebs throughout groundmass and concentrated in vesicles. 2–5% xenolithic with highly vesicular, aphyric gray basalt. Highly vesicular base, up to 35% vesicles at contact, streaking (flow fabric) becomes more diffuse and mottled from 85R–5, 0 cm, downward.

UNIT S39

1011.3–1011.6 MBSF 642E–85R–5 (113 cm) TO 85R–5 (134 cm)

DARK RED BROWN, WELL SORTED, VITRIC, LITHIC TUFF. 10–15% lapilli-sized basalt fragments, tachylitic, quenched and microcrystalline. Vitrics are vesicular angular or arcuate shards. Contact with F97 recovered, with F98 not recovered, quartz grains are present. Shards replaced by analcite.

UNIT F98

1011.6–1016.4 MBSF 642E–85R–6 (0 cm) TO 86R–2 (85 cm)

MEDIUM-GRAINED, MODERATELY PLAGIOCLASE PHYRIC, GRAY BASALT FLOW. Vesicular to highly vesicular flow top, with coalesced vesicles and mixed green smectite-rich top. Smectite-rich alteration patches show weak subhorizontal alignment, especially between 86R–1, 90 and 105 cm. Toward base, vesicles are larger and elongate at shallow angle to horizontal. Glassy base with plagioclase microlites, slightly reddened near base.

UNIT S40

1016.4–1016.7 MBSF 642E–86R–2 (85 cm) TO 86R–2 (101 cm)

DARK RED (TOP) TO GRAY BROWN (BASE), VITRIC, LITHIC LAPILLI TUFF. Normally graded. Fragments are highly vesicular and show a continuous range from vitric to microcrystalline. Monolithologic. Shards are zeolitized.

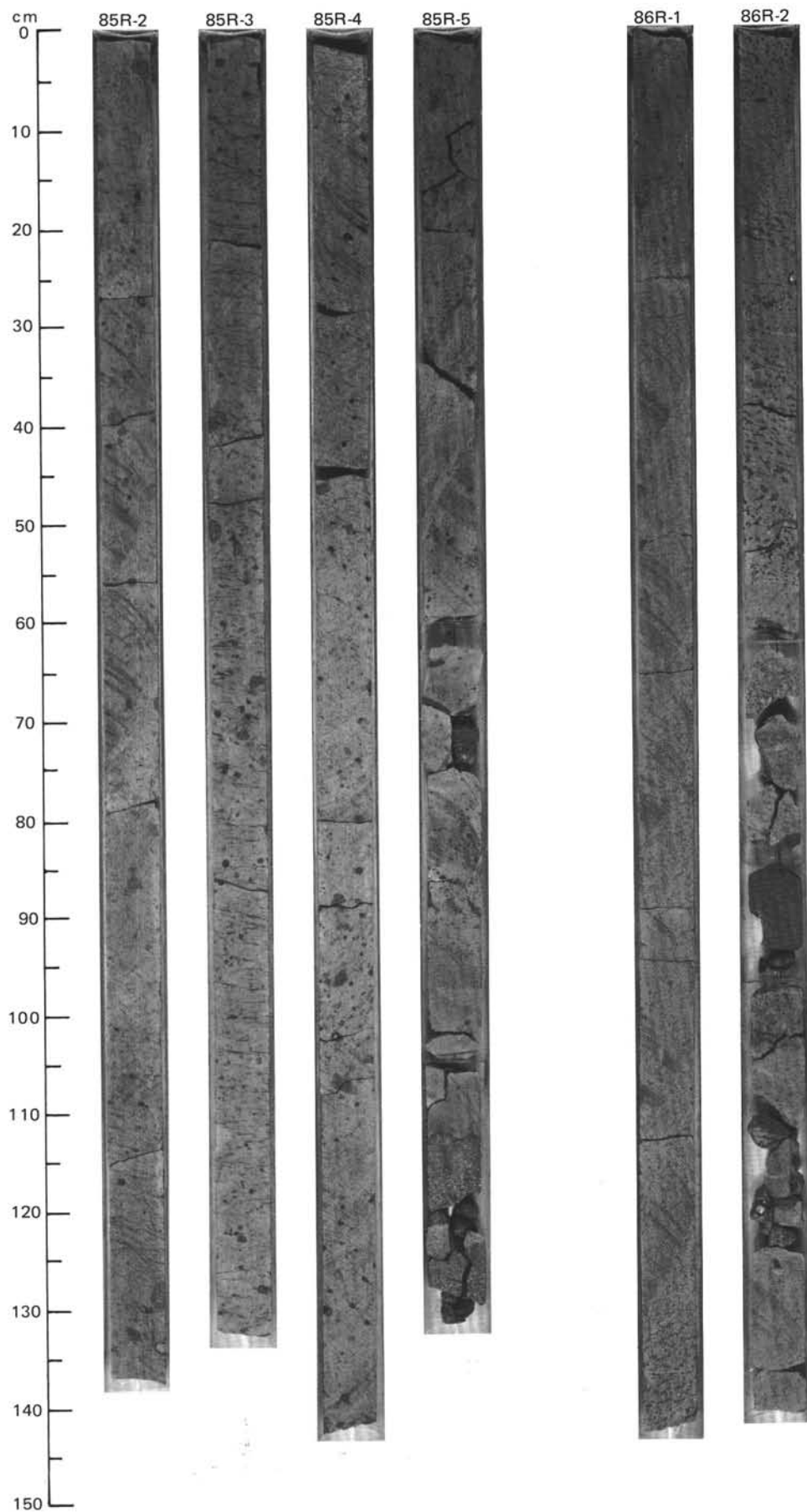
UNIT F99

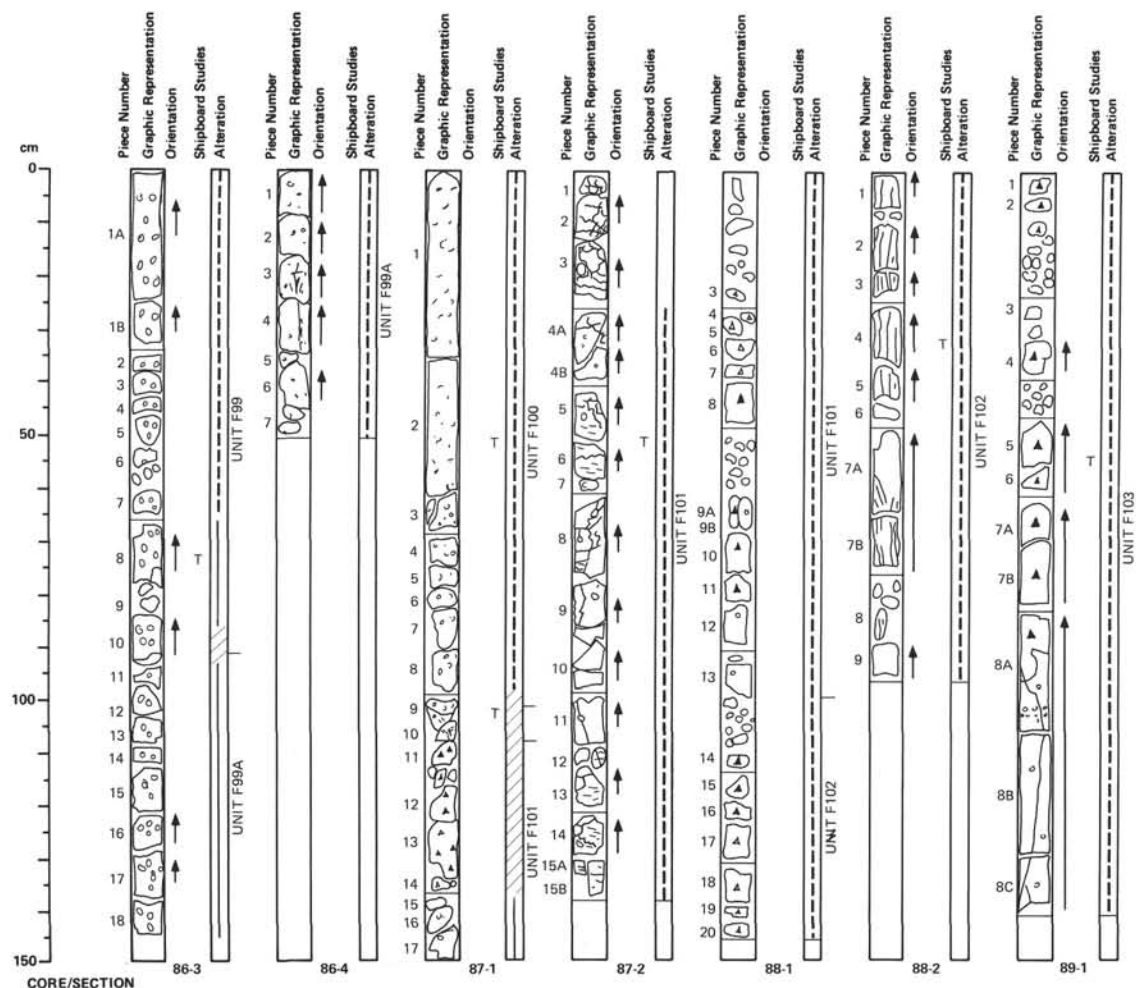
1016.7–1021.4 MBSF 642E–86R–2 (101 cm) TO 86R–3 (92 cm)

MIXED MEDIUM-GRAINED AND FINE-GRAINED, SPARSELY PHYRIC, DARK GRAY BASALT FLOW. Very fine-grained within top 10 cm, with brown smectite-lined vesicles. Central section is alternately banded medium-fine-grained basalts up to 3 cm wide. 2% volume plagioclase phenocrysts < 3.0 mm diameter. Fine network breccia veining at 86R–3, 5–20 cm.

THIN SECTION DESCRIPTION

642E–86R–3 (Piece 8, 73–75 cm): 40% plag, 30% cpx, 2% ol, 2% opaques, strongly altered. 26% altered variolitic mesostasis. Intergranular-intersertal, subophitic.





UNIT F99

1016.7–1021.4 MBSF 642E–86R–2 (101 cm) TO 86R–3 (92 cm)

MIXED MEDIUM-GRAINED AND FINE-GRAINED, SPARSELY PHYRIC, DARK GRAY BASALT FLOW. Very fine-grained within top 10 cm, with brown smectite-lined vesicles. Central section is alternately banded medium-fine-grained basalts up to 3 cm wide. 2% volume plagioclase phenocrysts < 3.0 mm diameter. Fine network breccia veining at 86R–3, 5–20 cm.

THIN SECTION DESCRIPTION

642E–86R–3 (Piece 8, 73–75 cm): 40% plag, 30% cpx, 2% ol, 2% opaques, strongly altered. 26% altered variolitic mesostasis. Intergranular-interstitial, subophitic.

UNIT F99A

1021.4–1024.5 MBSF 642E–86R–3 (92 cm) TO 86R–4 (51 cm)

MIXED MEDIUM-GRAINED AND FINE-GRAINED, APHYRIC GRAY BASALT. Quenched top with plagioclase microlites < 0.25 mm. Identical banding of basalt grain-size variations to those F99, grading into wholly medium-grained in upper 50 cm.

UNIT F100

1024.5–1028.7 MBSF 642E–87R–1 (0 cm) TO 87R–1 (100 cm)

MEDIUM-GRAINED, APHYRIC GRAY BASALT. Glassy base with plagioclase microlites < 0.20 mm. Moderate vesicularity, increasing toward base. Locally glomeroporphyritic plagioclase. Local intra-unit brecciation in intensively vesicular zones 87R–1, 60–65 cm.

UNIT S41

1028.7–1028.8 MBSF 642E–87R–1 (100 cm) TO 87R–1 (108 cm)

DARK RED BROWN BASALTIC, LITHIC, VITRIC TUFF. Ash clasts (95%) are arcuate vitric shards, some pumice(?). 5% lithic tuff fragments. Some feldspar crystals. Terrigenous clinopyroxene and quartz fragments.

UNIT F101

1028.8–1035.0 MBSF 642E–87R–1 (108 cm) TO 88R–1 (99 cm)

FINE-GRAINED, APHYRIC, GRAY BASALT FLOW. Reddened vesicular and fragmented basalt with pocket infills of red brown tuff in upper section. Sparse vesicles filled with dark green smectite. Some weak streaking (flow fabric), discontinuous and closely spaced. Basal breccia 88R–1, 20–96 cm, without volcanoclastics.

UNIT F102

1035.0–1044.1 MBSF 642E–88R–1 (99 cm) TO 88R–2 (96 cm)

FINE-GRAINED, APHYRIC, GRAY BASALT FLOW. Base not recovered. Purplish, moderately vesicular breccia flow top overlies subvertically streamed vesicular zone. Smectite filled vesicles with surrounding red oxidation and along hairline fractures.

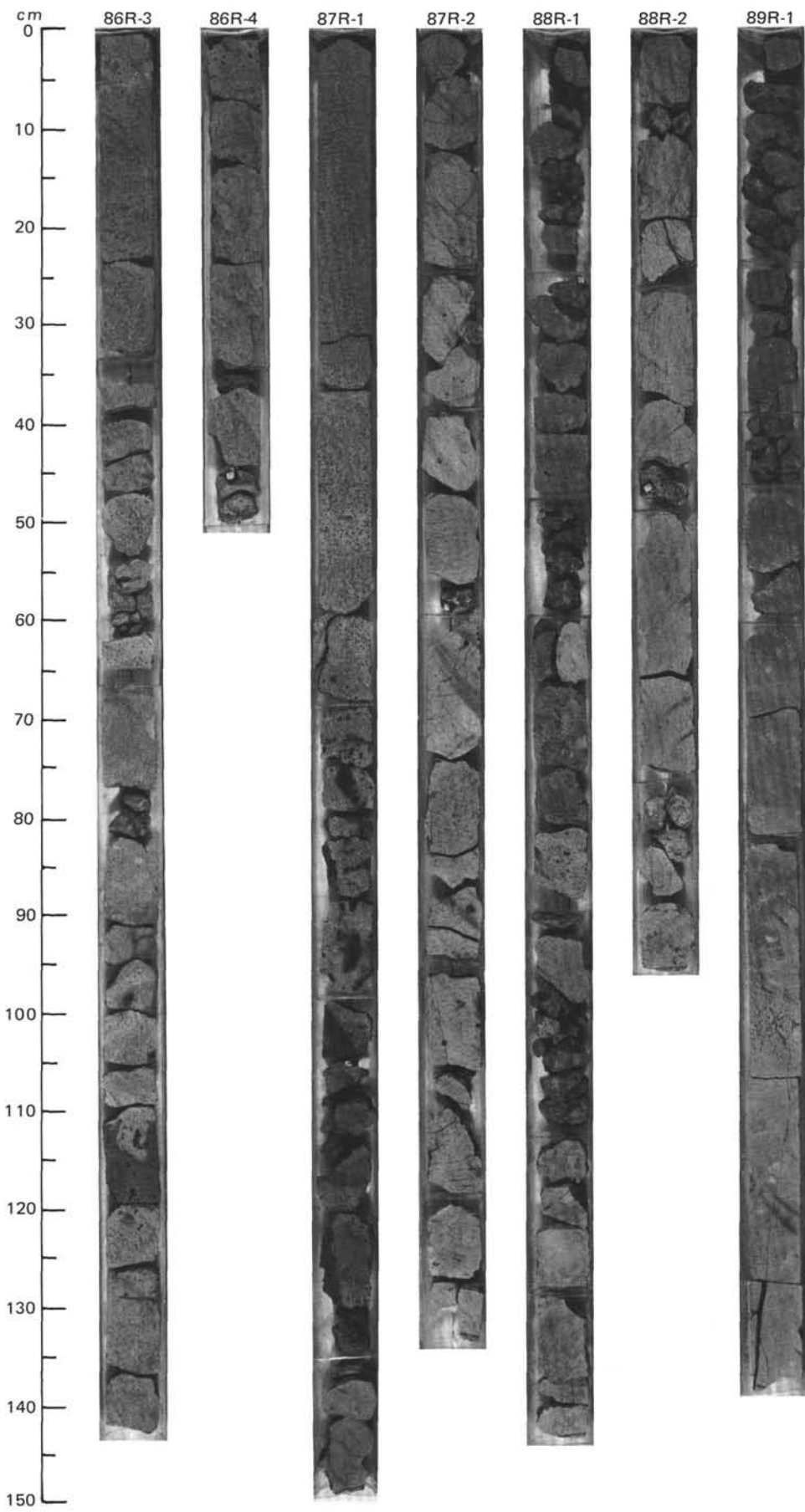
UNIT F103

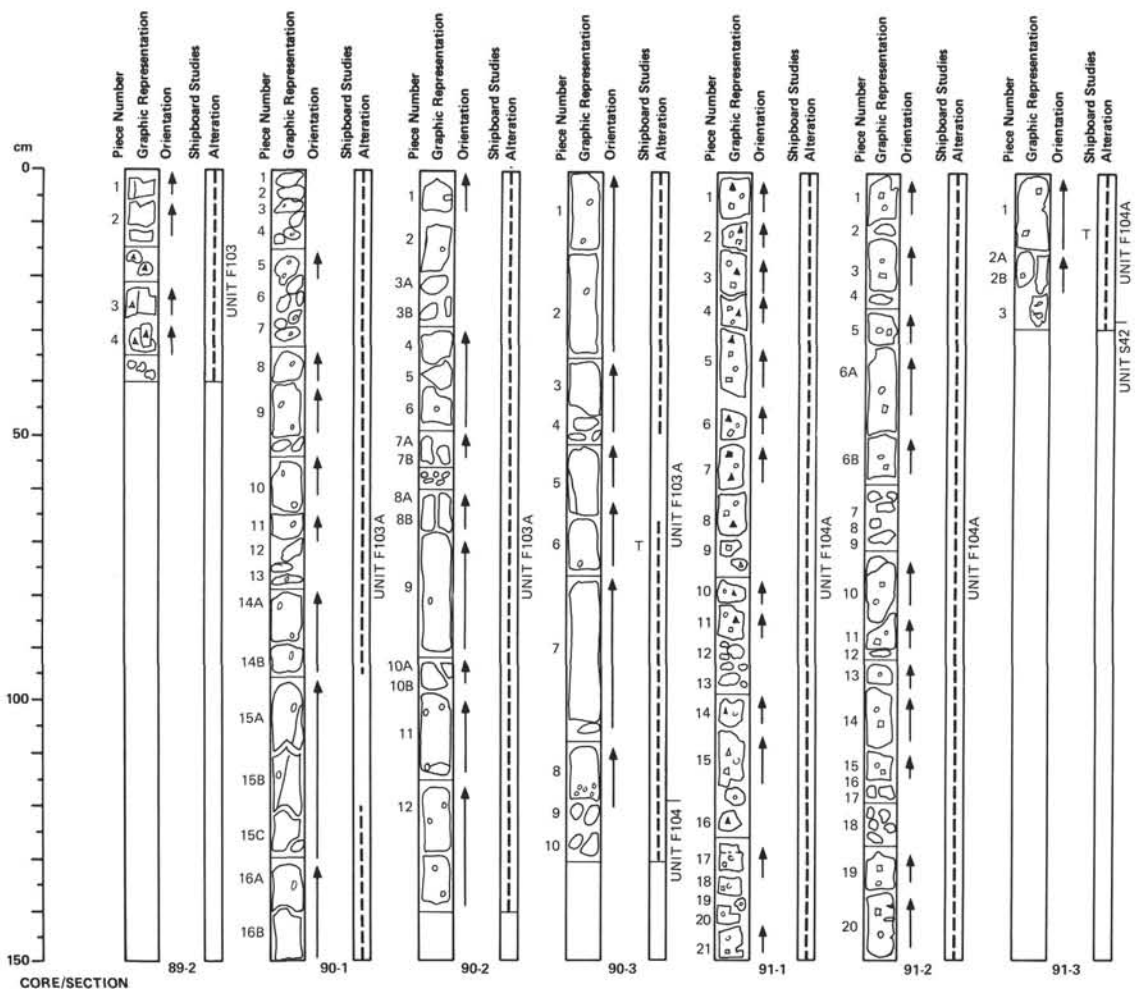
1044.1–1049.1 MBSF 642E–89R–1 (0 cm) TO 89R–2 (42 cm)

FINE-GRAINED, GRAY BASALT FLOW. Aphyric to sparsely plagioclase phyric. Purplish gray flow top breccia, moderately vesicular, dark gray brown matrix without tuff. Zones of yellowish to orange red discoloration around vesicles and veins indicate hydrothermal(?) alteration. Plagioclase and olivine(?) phenocrysts in locally glomeroporphyritic clusters. Some filling of vesicles by smectite, but calcite and quartz common. A weak streaky (flow fabric) lamination develops toward the base of the unit. Vesicular base of flow.

THIN SECTION DESCRIPTION

642E–89R–1 (Piece 5, 50–52 cm): 40% plag, 40% cpx, 5% ol, 5% opaques, variably altered. 10% altered variolitic mesostasis. Intersertal.





UNIT F103

1044.1–1049.1 MBSF 642E–89R–1 (0 cm) TO 89R–2 (42 cm)

FINE-GRAINED, GRAY BASALT FLOW. Aphyric to sparsely plagioclase phyric. Purplish gray flow top breccia, moderately vesicular, dark gray brown matrix without tuff. Zones of yellowish to orange red discoloration around vesicles and veins indicate hydrothermal(?) alteration. Plagioclase and olivine(?) phenocrysts in locally glomeroporphyritic clusters. Some filling of vesicles by smectite, but calcite and quartz common. A weak streaky (flow fabric) lamination develops toward the base of the unit. Vesicular base of flow.

THIN SECTION DESCRIPTION

642E–89R–1 (Piece 5, 50–52 cm): 40% plag, 40% cpx, 5% ol, 5% opaques, variably altered. 10% altered variolitic mesostasis. Intersertal.

UNIT F103A

1049.1–1057.2 MBSF 642E–90R–1 (0 cm) TO 90R–3 (119 cm)

AS F103.

UNIT F104

1057.2–1062.0 MBSF 642E–90R–3 (119 cm) TO 90R–3 (125 cm)

FINE-GRAINED, MODERATELY PLAGIOCLASE–CLINOPYROXENE PHYRIC, GRAY BASALT. Purplish gray breccia flow top, vesicular. Vesicles coated with blue green celadonite. Plagioclase is locally glomeroporphyritic. Some reddening along fractures and adjacent to vesicles.

UNIT F104A

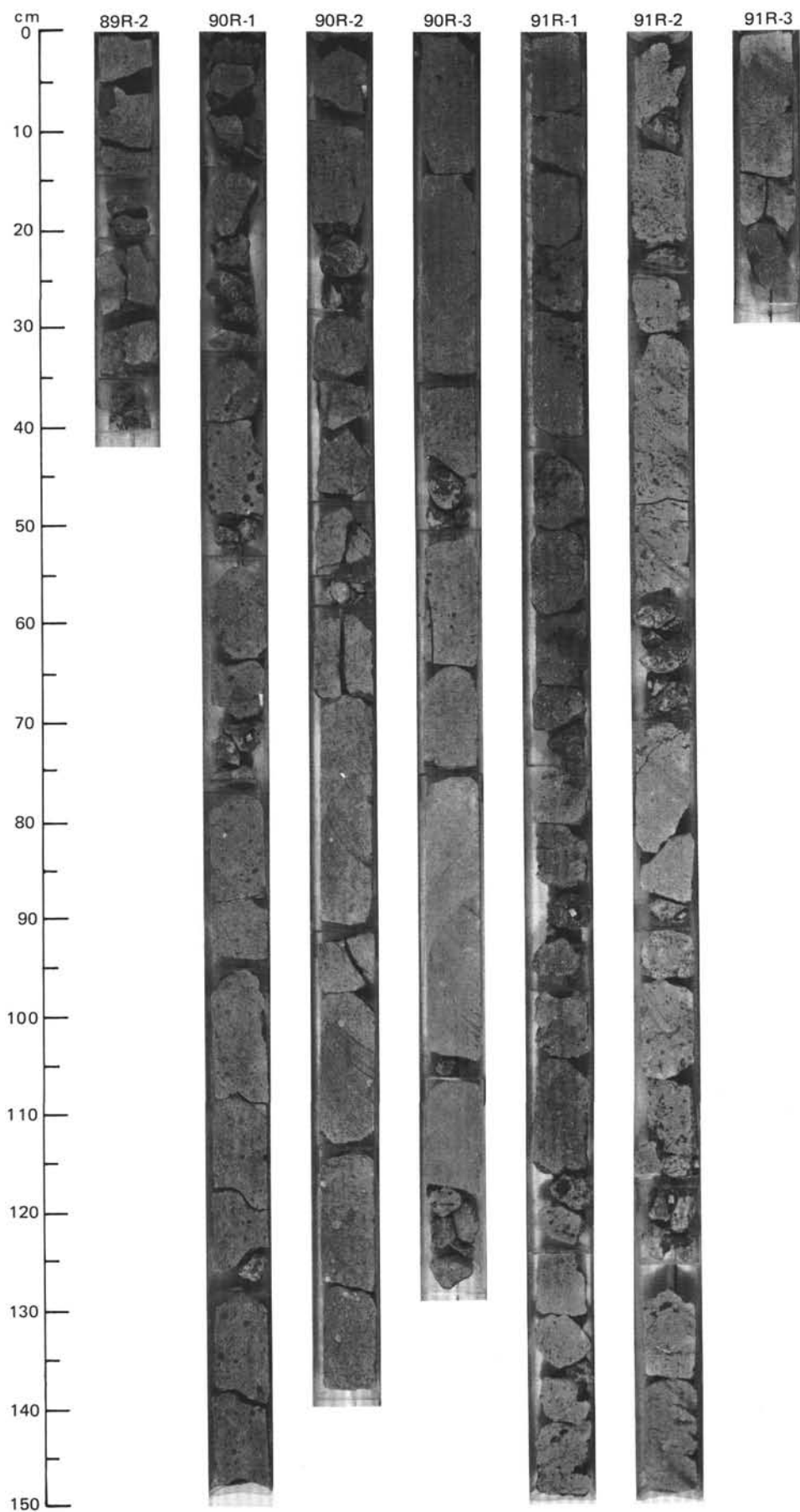
1062.0–1068.1 MBSF 642E–91R–1 (0 cm) TO 91R–3 (27 cm)

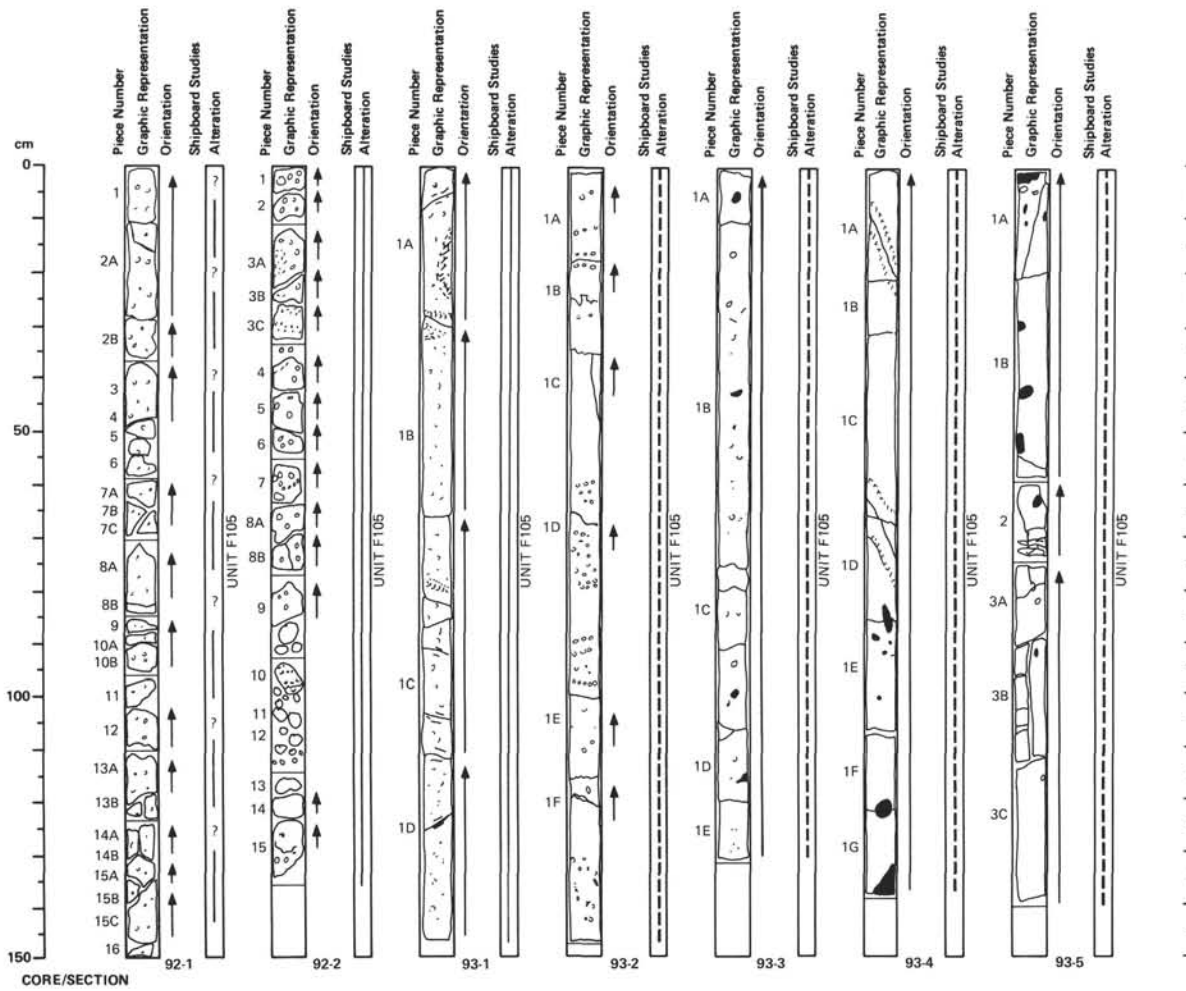
FINE-GRAINED, MODERATELY PLAGIOCLASE–CLINOPYROXENE PHYRIC, GRAY BASALT. Vesicles coated with blue green celadonite. Plagioclase is locally glomeroporphyritic. Flow center moderately vesicular. Some reddening along fractures and adjacent to vesicles, intense below 91R–2, 137 cm. Base of recovery extensively stained.

UNIT S42

1068.1 MBSF 642E–91R–3 (27 cm) TO 91R–3 (30 cm)

LITHIC, VITRIC TUFF. Red brown or red clasts in green matrix, median grain size 0.4 mm, matrix unsupported, well sorted, comagmatic; (>70%) vesicular shards, some fresh, arcuate to scoriaceous lithics (<30%); vitric tuff, rounded, crystalline basalt.



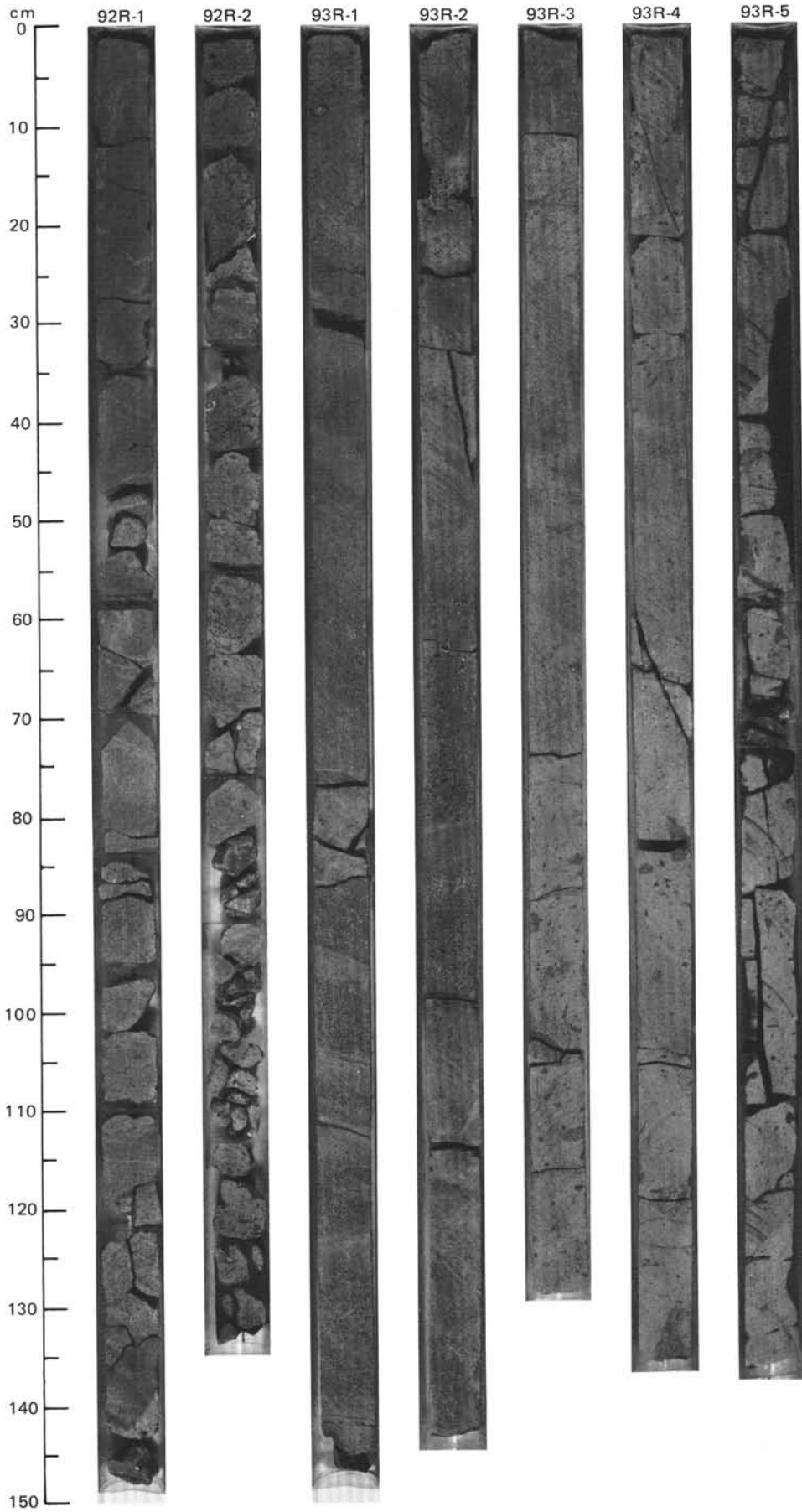


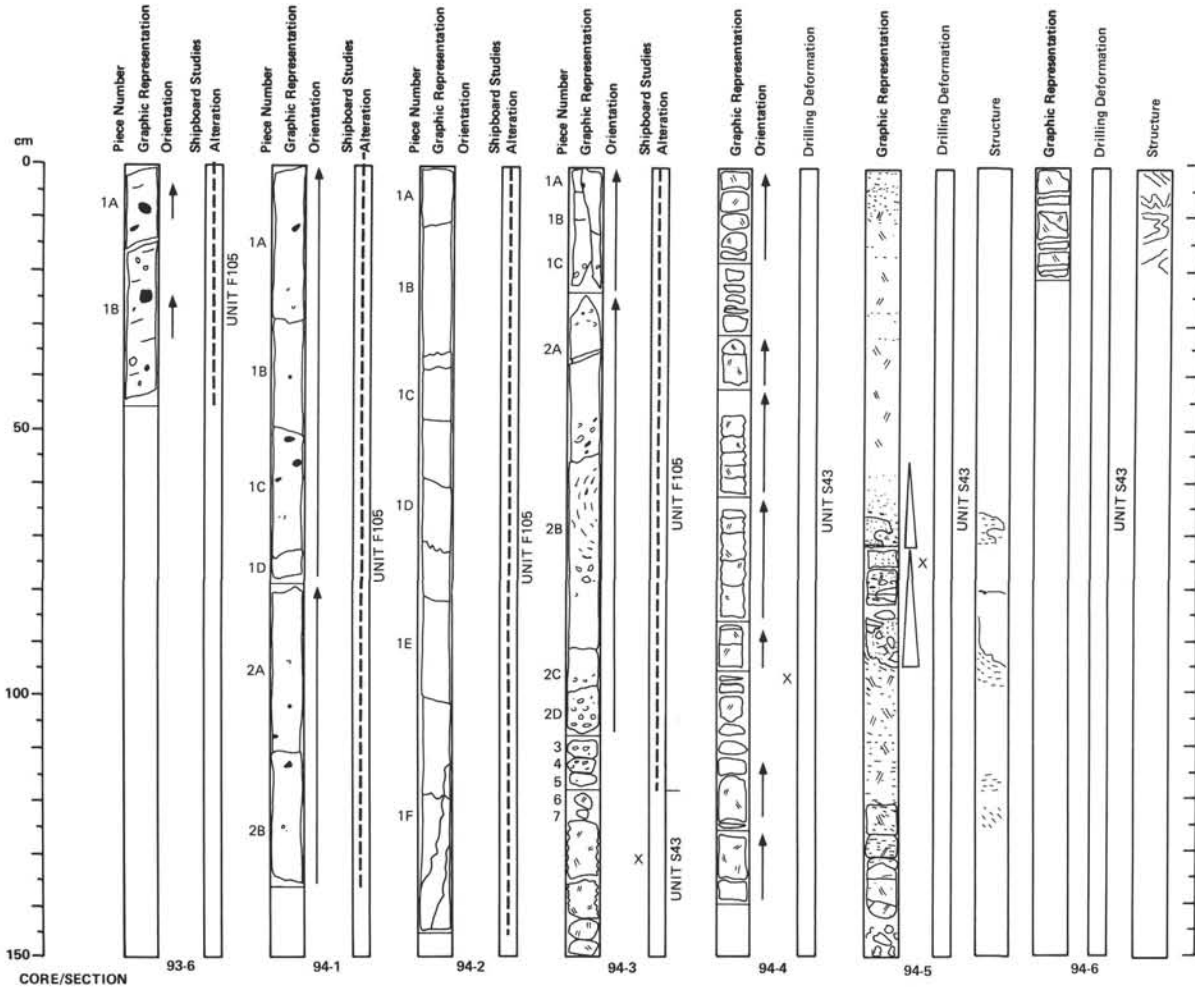
UNIT F105

1068.1-1086.8 MBSF

642E-92R-1 (0 cm) TO 94R-3 (117 cm)

"MIXED" MEDIUM- AND FINE-GRAINED, APHYRIC BASALT FLOW.
 Flow base not recovered. Reddened, variably vesicular unit, locally subhorizontally mixed/banded, with either alternations in grain size or streaming. Toward center and base, unit becomes fine-grained, local development of streaky (flow fabric) texture. Coarse, moderately to highly vesicular at upper section, with calcite, dark green smectite, and red brown zeolite fillings. Some copper blebs in vesicles and along veins. Common alteration by red staining of groundmass around fractures and vesicles. Highly vesicular xenolith-rich zones, vesicles locally flattened and streamed, some development of sigmoidal shear-induced structures (94R-1, 127-130 cm). Base of flow is highly vesicular, calcite and/or green smectite filled vesicles. Sharp contact with S43 recovered.





UNIT F105

1068.1–1086.8 MBSF

642E–92R–1 (0 cm) TO 94R–3 (117 cm)

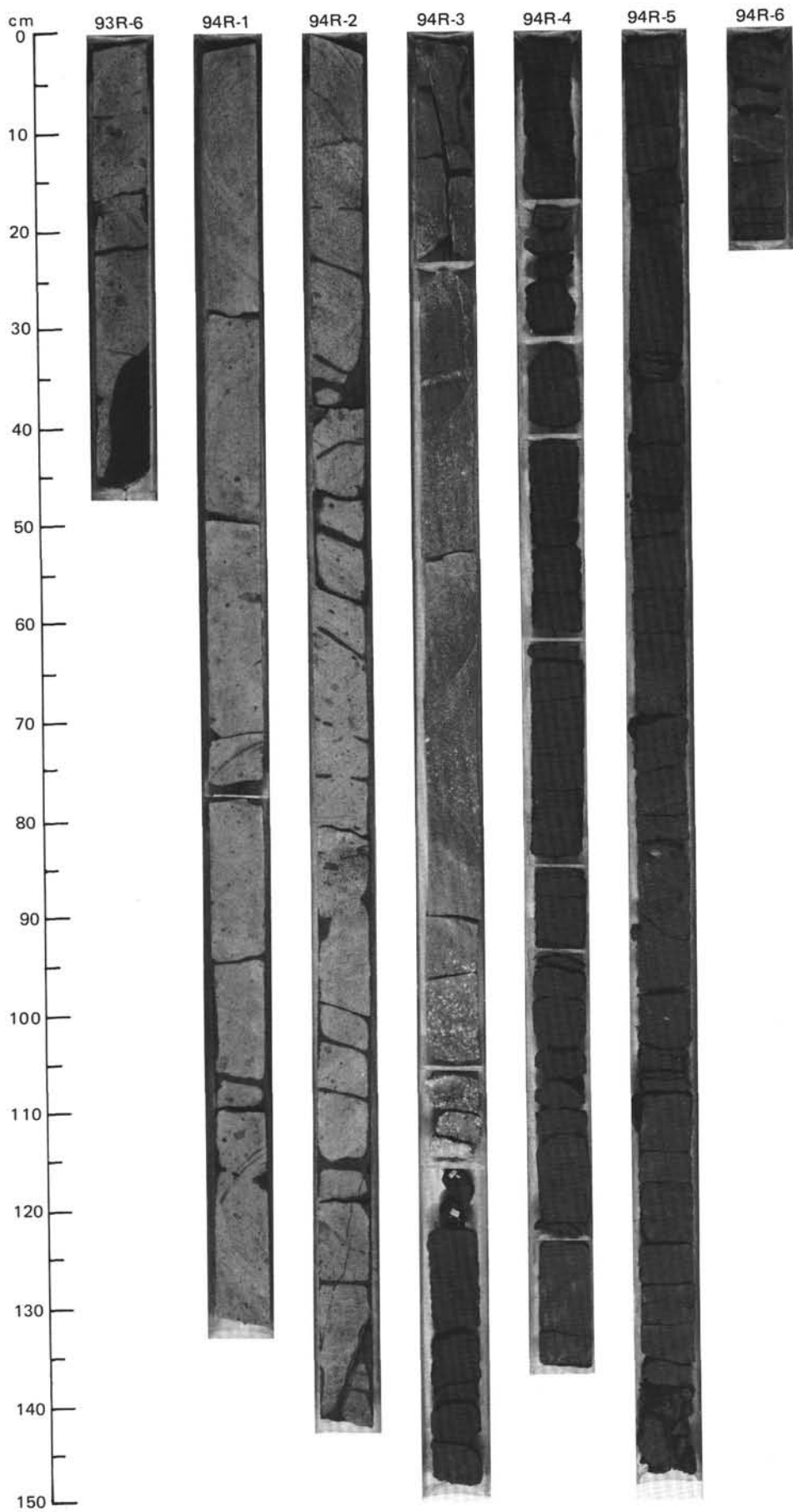
"MIXED" MEDIUM- AND FINE-GRAINED, APHYRIC BASALT FLOW.
Flow base not recovered. Reddened, variably vesicular unit, locally subhorizontally mixed/banded, with either alternations in grain size or streaming. Toward center and base, unit becomes fine-grained, local development of streaky (flow fabric) texture. Coarse, moderately to highly vesicular at upper section, with calcite, dark green smectite, and red brown zeolite fillings. Some copper blebs in vesicles and along veins. Common alteration by red staining of groundmass around fractures and vesicles. Highly vesicular xenolith-rich zones, vesicles locally flattened and streamed, some development of sigmoidal shear-induced structures (94R–1, 127–130 cm). Base of flow is highly vesicular, calcite and/or green smectite filled vesicles. Sharp contact with S43 recovered.

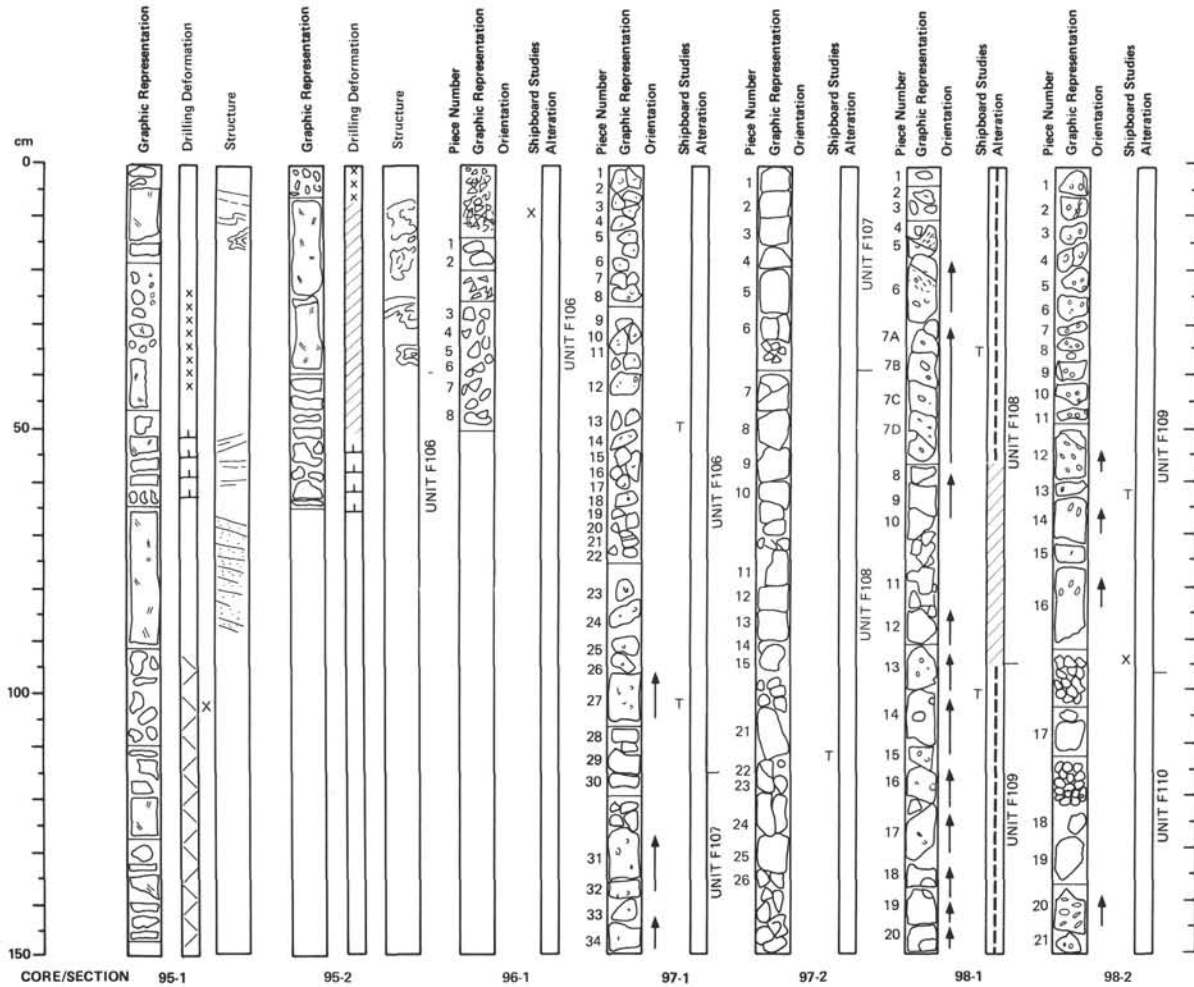
UNIT S43

1086.8–1100.0 MBSF

642E–94R–3 (117 cm) TO 95R–2 (36 cm)

DARK GREEN TO DARK GRAYISH BROWN, CRYSTAL VITRIC TUFF.
Contains gradational contacts into quartz–mica–sandstone at 94R–4, 12–26 cm; upward-fining sequences 94R–5, 72–95 cm, with conglomeratic erosional base, 94R–5, 55–72 cm. 94R–3, 127 cm, to 94R–4, 140 cm, pumice altered but not collapsed. 94R–5, 95 cm, to 95R–2, 38 cm; extremely variable in color from yellow brown to dusky red to purple to very dark gray; volcaniclastic, slightly sandy mudstone, finely laminated to complexly turbulently mixed, pumice abundant, collapsed; red quartz mica sandstone with gradational upper and lower boundaries at 95R–1, 110–140 cm.





UNIT S43
1086.8–1100.0 MBSF 642E–94R–3 (117 cm) TO 95R–2 (36 cm)

DARK GREEN TO DARK GRAYISH BROWN, CRYSTAL VITRIC TUFF. Contains gradational contacts into quartz–mica–sandstone at 94R–4, 12–26 cm; upward-fining sequences 94R–5, 72–95 cm, with conglomeratic erosional base, 94R–5, 55–72 cm, 94R–3, 127 cm, to 94R–4, 140 cm, pumice altered but not collapsed. 94R–5, 95 cm, to 95R–2, 38 cm; extremely variable in color from yellow brown to dusky red to purple to very dark gray; volcanoclastic, slightly sandy mudstone, finely laminated to complexly turbulently mixed, pumice abundant, collapsed; red quartz mica sandstone with gradational upper and lower boundaries at 95R–1, 110–140 cm.

UNIT F106
1100.0–1111.0 MBSF 642E–95R–2 (36 cm) TO 97R–1 (115 cm)

MIXED FRAGMENTS OF ALTERED GRAY GREEN GLASS AND FINE-GRAINED SPARSELY VESICULAR GRAY FLOW. Gray rock is rarely plagioclase phyric, moderately vesicular, with quartz and calcite fills, or open with pale green celadonite rims. Fine pyrite cores to smectite-rich zones.

THIN SECTION DESCRIPTIONS

642E–97R–1 (Piece 17, 54–56 cm): 2% plag microphenocrysts, 7% swallowtailed plag. 91% altered quenched microlites and mesostasis. Thoroughly altered.

642E–97R–1 (100–102 cm): 2% glomerophyric plag in 98% perlitic glass.

UNIT F107
1111.0–1114.0 MBSF 642E–97R–1 (115 cm) TO 97R–2 (38 cm)

GLASSY, PURPLISH GRAY FLOW. Beautifully well developed perlitic texture. Deep purple, altered, glassy quenched margins with pale to dark green smectite-rich alteration zones throughout. Vesicles are smectite filled and disaggregated along smectitic fractures, locally tending to hyaloclastic.

UNIT F108
1114.0–1117.5 MBSF 642E–97R–2 (38 cm) TO 98R–1 (96 cm)

GLASSY TO CRYPTOCRYSTALLINE FLOW. Aphyric. Glassy purple to green altered flow top and flow base margins, and smectite-rich patch alteration. Moderately vesicular, with calcite and/or smectite fills plus silica phase. Most streaked into prolate forms, rounded below 97R–2, 114 cm, away from the flow margin. Rare blue rims to some open vesicles. Hyaloclastic base.

UNIT F109
1117.5–1119.0 MBSF 642E–98R–1 (96 cm) TO 98R–2 (97 cm)

PARTLY DEVITRIFIED GLASSY FLOW. As F108, with precise flow boundaries difficult to identify within glassy marginal zone. Moderately vesicular, with weak attenuation into prolate shaped fabrics. Some vesicular geopetal structures (quartz over smectite) 98R–1, 113–127 cm. Base of unit is black glassy rind. Perlitic texture throughout.

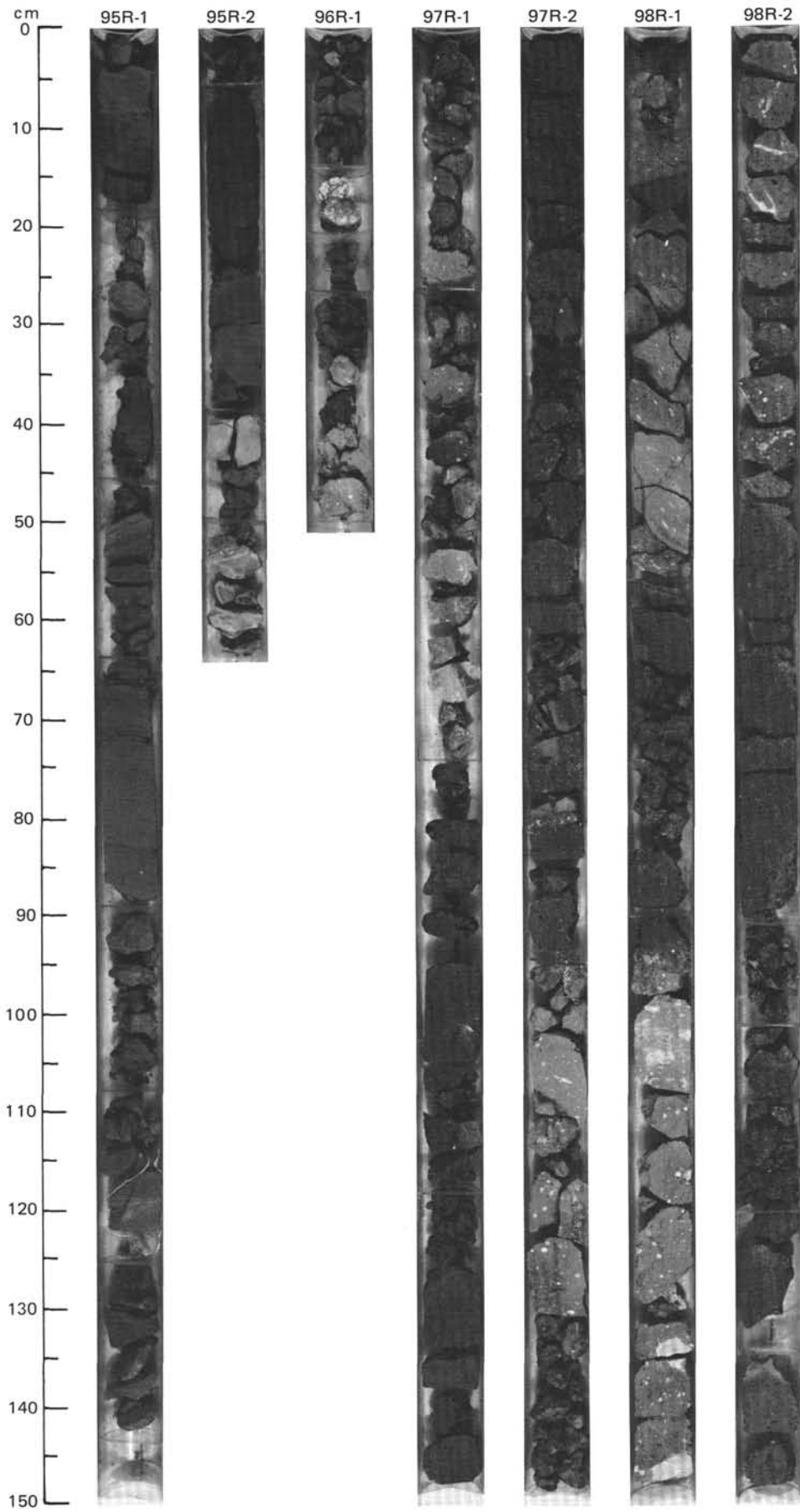
THIN SECTION DESCRIPTIONS

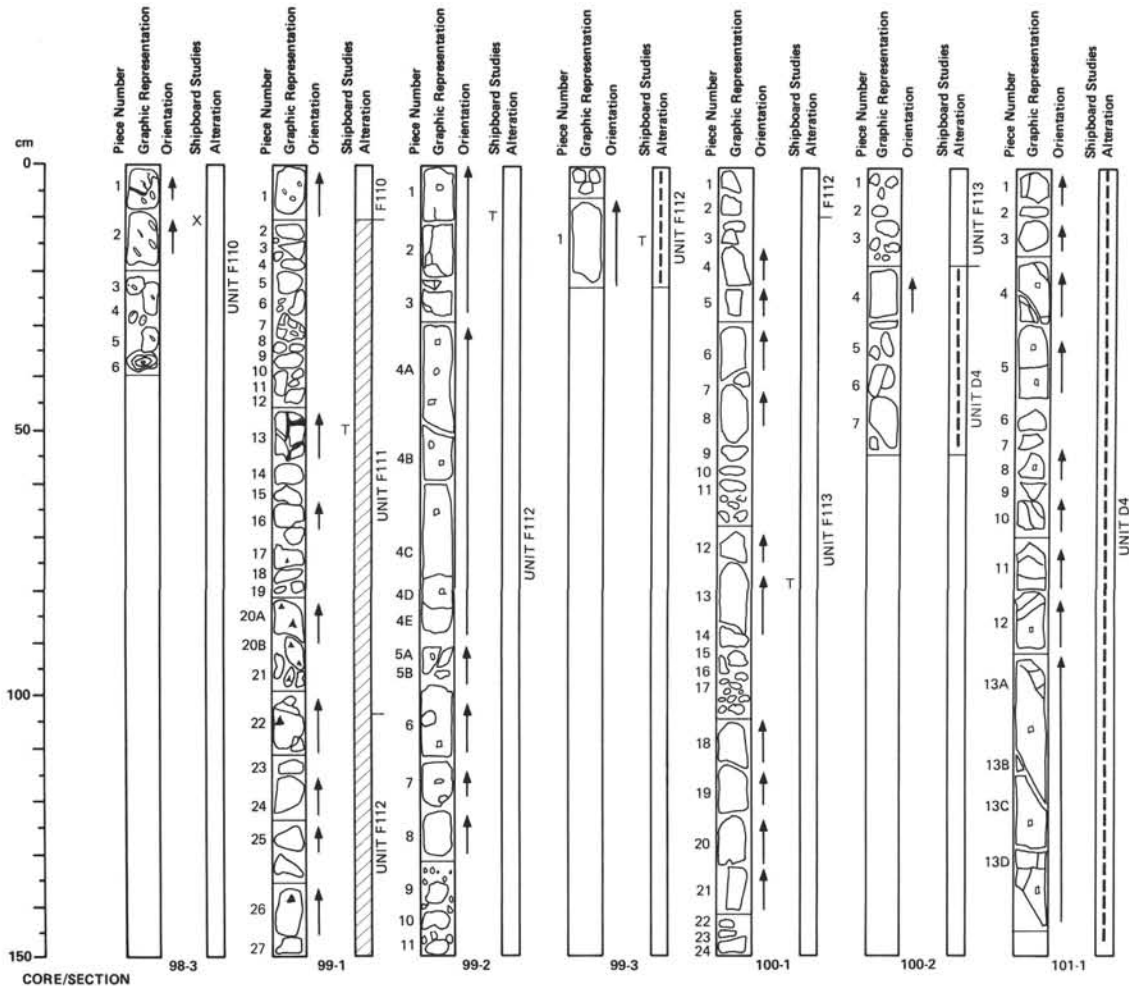
642E–98R–1 (Piece 14, 106–108 cm): <1% plag phenocrysts. 10% swallowtailed plag, 90% quenched groundmass. Strongly altered.

642E–98R–2 (Piece 13, 62–64 cm): 2% glomerophyric plag, 98% light purplish brown perlite.

UNIT F110
1119.9–1122.0 MBSF 642E–98R–2 (97 cm) TO 99R–1 (10 cm)

FRAGMENTS OF PURPLE BLACK, GLASSY BASALT FLOW. Perlitic texture throughout, altered green smectite-rich glass. Vesicular, with green halos around fractures and vesicles.





UNIT F110

1119.9–1122.0 MBSF 642E–98R–2 (97 cm) TO 99R–1 (10 cm)

FRAGMENTS OF PURPLE BLACK, GLASSY BASALT FLOW.

Perlitic texture throughout, altered green smectite-rich glass. Vesicular, with green halos around fractures and vesicles.

UNIT F111

1122.0–1126.0 MBSF 642E–99R–1 (10 cm) TO 99R–1 (101 cm)

PARTLY DEVITRIFIED GLASSY FLOW. Pale green. Intensely veined and fractured, sparsely vesicular, with vesicles locally rimmed with pale blue silica phase. Perlitic fracturing throughout, quench texture (swallowtail plagioclase) in thin section, brecciation toward base tending to hyaloclastite.**THIN SECTION DESCRIPTION****642E–99R–1 (50–51 cm):** 3% plag phenocrysts, 25% aligned plag microlites, 72% altered microlites and glass.

UNIT F112

1126.0–1129.5 MBSF 642E–99R–1 (101 cm) TO 100R–1 (10 cm)

PARTLY DEVITRIFIED GLASSY FLOW. Pale green, sparsely phyrlic. Highly altered, devitrified and locally brecciated, groundmass containing altered plagioclase needles. Altered phenocrysts of plagioclase, locally glomeroporphyritic, fresh clinopyroxene (possibly aegirine-augite). Vesicles are calcite filled or coated with light blue silica phase; siderite(?) present along fractures and around some vesicles. Base of flow exhibits increasing preferred alignment of quenched acicular minerals.**THIN SECTION DESCRIPTIONS****642E–99R–2 (Piece 2, 20–22 cm):** 3% plag phenocrysts. 20% plag microlites, 5% "trellis" opaques, 75% altered microlites and glass.**642E–99R–3 (Piece 1, 13–15 cm):** 15% swallowtail and skeletal plag, 15% acicular pyroxene, 70% altered, devitrified mesostasis. Quench textures.

UNIT F113

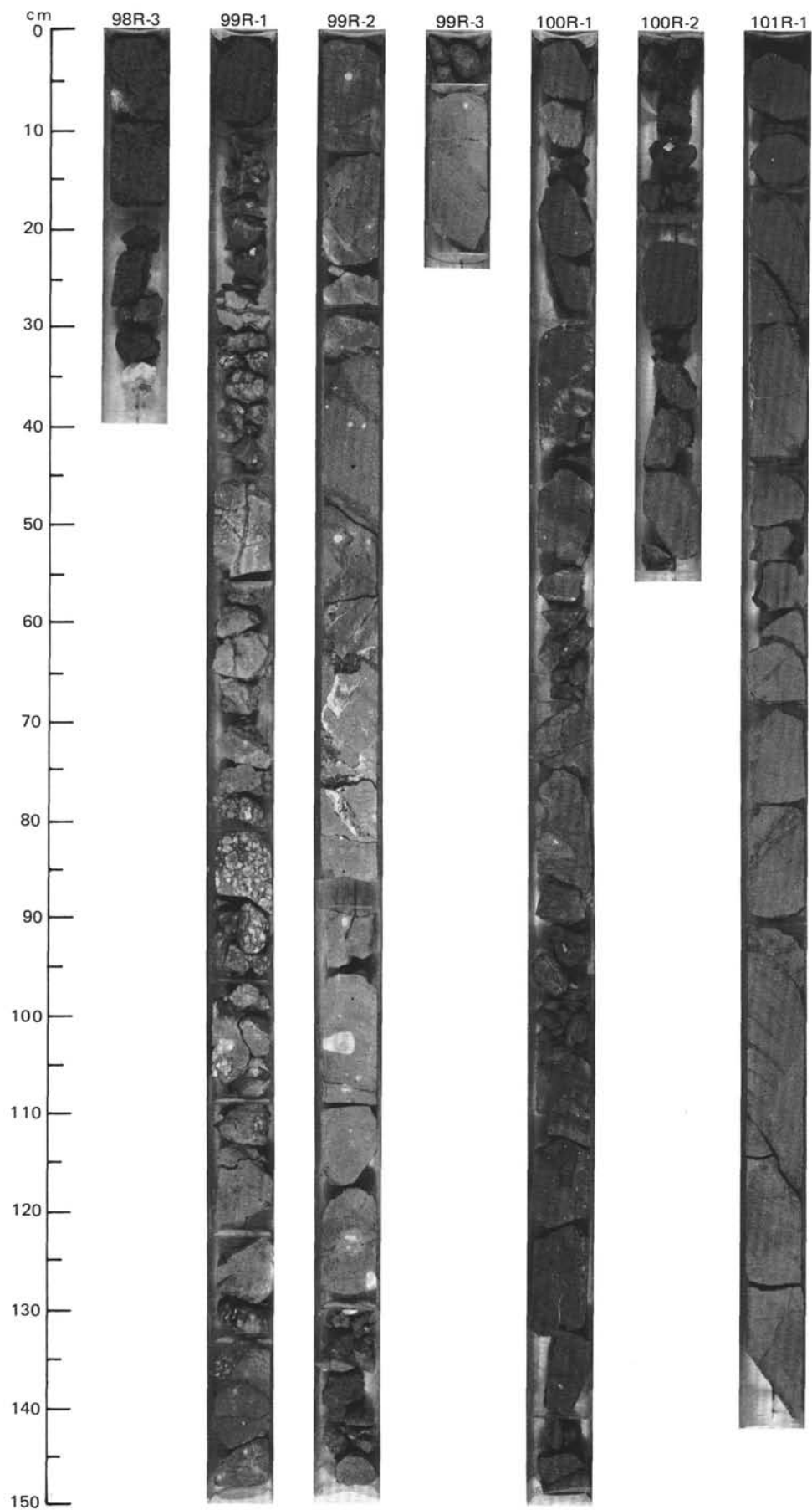
1129.5–1132.7 MBSF 642E–100R–1 (10 cm) TO 100R–2 (18 cm)

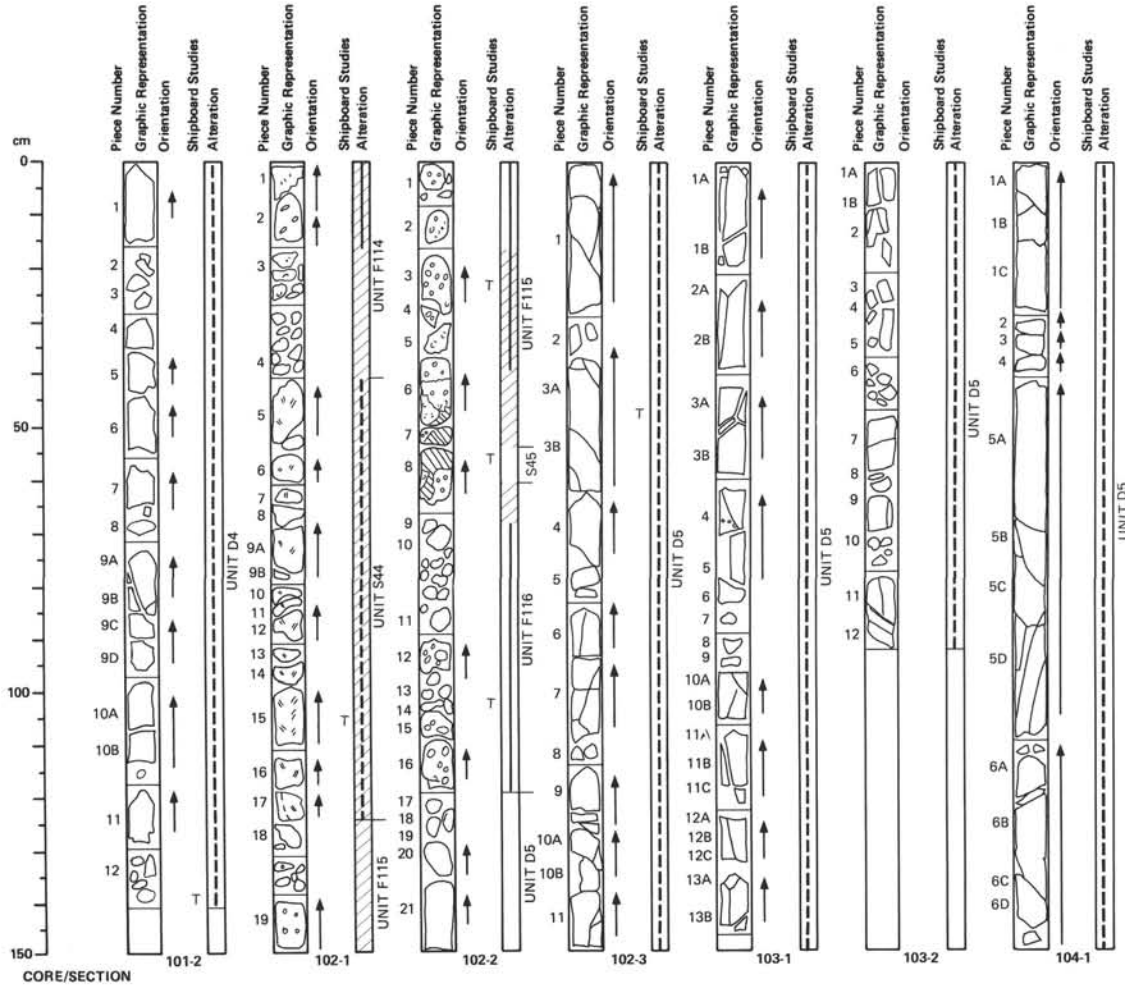
DEVITRIFIED GLASSY FLOW. Sparsely plagioclase phyrlic, gray to greenish gray. Sparsely to moderately vesicular, vesicles filled with dark green smectite, calcite, or coated with blueish silica phase. Plagioclase, olivine and clinopyroxene phenocrysts variously replaced by smectite. Local alignment of elongated minerals in groundmass. Intensely veined and locally brecciated.**THIN SECTION DESCRIPTION****642E–100R–1 (80–81 cm):** 40% acicular plag, 3% acicular pyroxene, 7% skeletal and very fine microlites, 50% altered groundmass.

UNIT D4

1132.7–1153.5 MBSF 642E–100R–2 (18 cm) TO 101R–2 (141 cm)

FINE-GRAINED, SPARSELY TO MODERATELY PHYRIC, GRAY VOLCANIC ROCK. Fresh phenocrysts of plagioclase, some olivines, set in plagioclase-rich intersertal groundmass exhibiting locally good crystal alignment. Rare vesicles filled with smectite and pyrite. Veining (generally subvertical) with smectite, calcite, siderite and pyrite, possibly quartz in centers.





UNIT D4

1132.7–1153.5 MBSF 642E–100R–2 (18 cm) TO 101R–2 (141 cm)

FINE-GRAINED, SPARSELY TO MODERATELY PHYRIC, GRAY VOLCANIC ROCK. Fresh phenocrysts of plagioclase, some olivines, set in plagioclase-rich intersertal groundmass exhibiting locally good crystal alignment. Rare vesicles filled with smectite and pyrite. Veining (generally subvertical) with smectite, calcite, siderite and pyrite, possibly quartz in centers.

UNIT F114

1153.5–1155.0 MBSF 642E–102R–1 (0 cm) TO 102R–1 (42 cm)

DEVITRIFIED GLASSY FLOW. Very pale green to green. Highly altered, hydrothermally leached quenched unit. Altered glass throughout with relict perlitic texture, sparse phenocrysts, vesicles lined or filled with dark green smectite, pyrite, brown smectite, locally elongate and inclined.

UNIT S44

1155.0–1156.8 MBSF 642E–102R–1 (42 cm) TO 102R–1 (123 cm)

UNIFORMLY FINE-GRAINED, GRAY CRYSTAL VITRIC TUFF (SANDY SANDSTONE). Median diameter, 20 microns; strongly altered to smectite–illite–chlorite–zeolite–pyrite; fine illitic smectite thought to have been vitric. Xenoliths as quartz, light mica, brown mica, spherulitic glass, sphene, zircon.

UNIT F115

1156.8–1158.8 MBSF 642E–102R–1 (123 cm) TO 102R–2 (57 cm)

PARTLY DEVITRIFIED GLASSY FLOW. Green, sparsely glomeroporphyritic. Vesicular, hydrated glass flow, with perlitic fracture texture. Alteration colors locally varying between dark green/black to pale gray green. Vesicles filled with calcite and/or siderite near flow top, dark green smectite below. Siderite/calcite veining.

THIN SECTION DESCRIPTION

642E–102R–2 (Piece 7, 26–28 cm): 5% glomerophytic plag, <<1% skeletal pyrite, 95% cryptocrystalline. Basalt has been "bleached" white.

UNIT S45

1158.8–1158.9 MBSF 642E–102R–2 (57 cm) TO 102R–2 (62 cm)

FINE-GRAINED, VERY DARK GRAY, CRYSTAL VITRIC TUFF (SANDY MUDSTONE). Strongly cemented, pumice, quartz, mica; alteration to clinoptilolite, illite, smectite, chlorite, pyrite.

UNIT F116

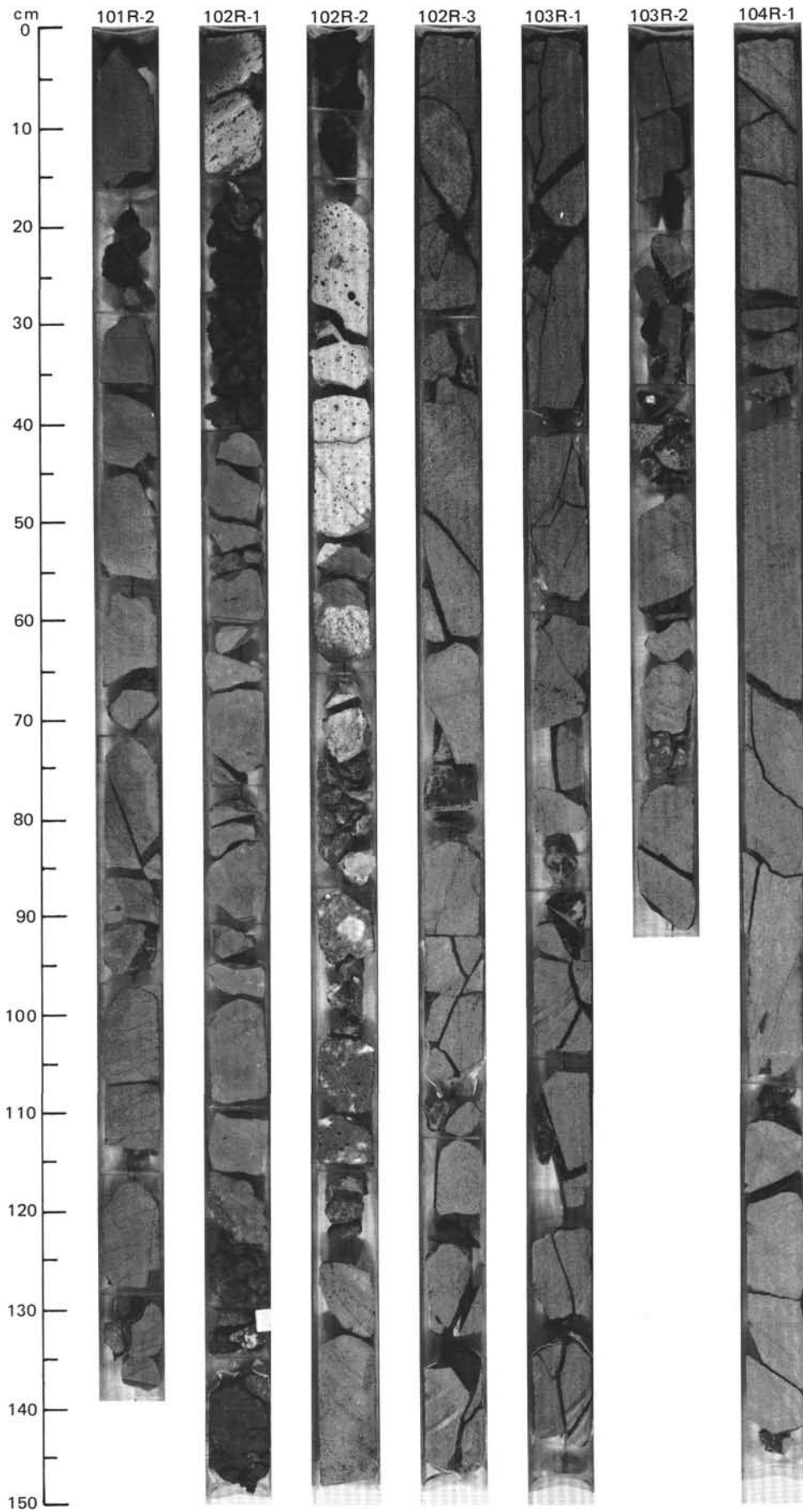
1158.9–1161.5 MBSF 642E–102R–2 (62 cm) TO 102R–2 (117 cm)

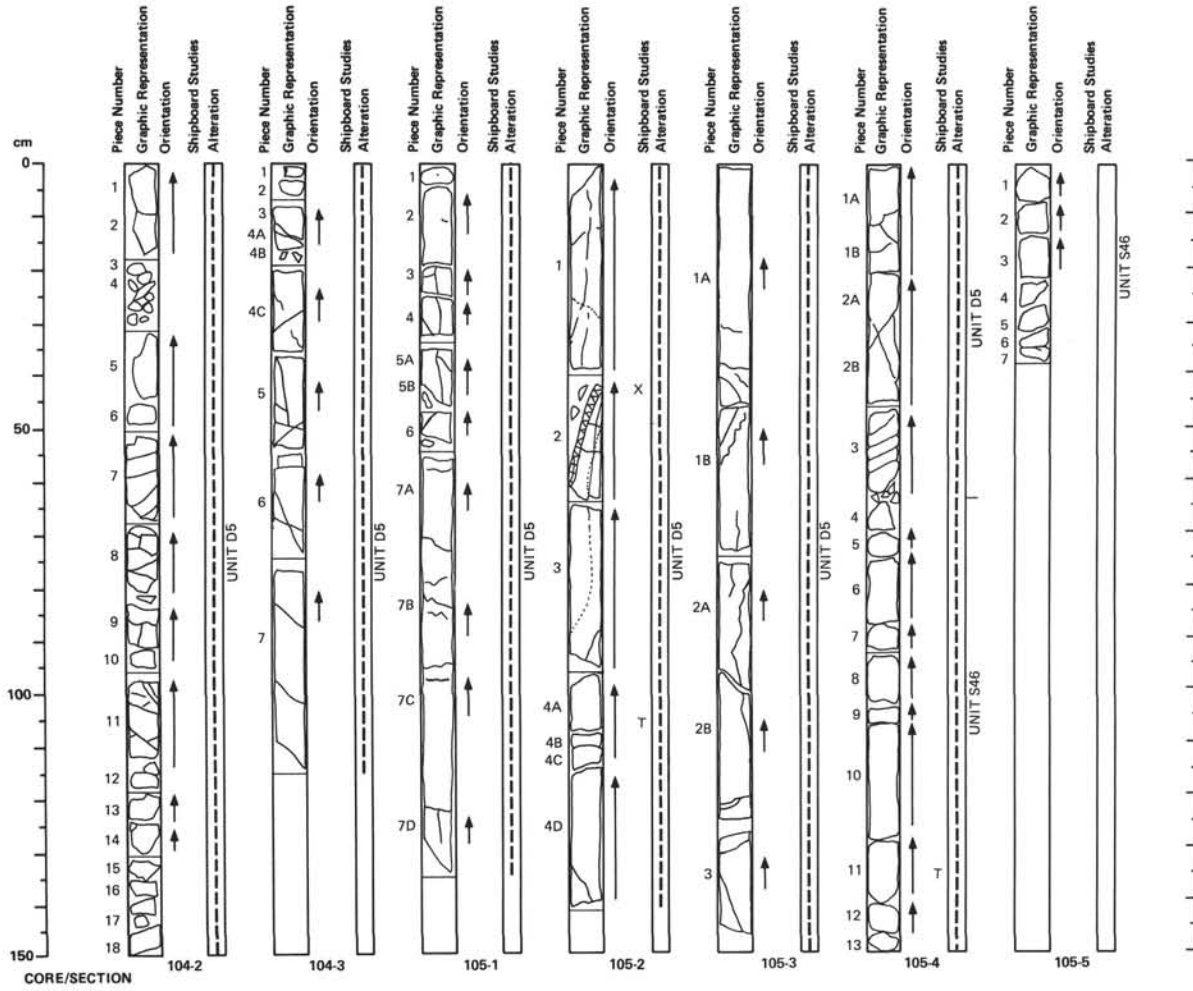
CRYPTOCRYSTALLINE FLOW. Aphyric, gray to dark gray. Base is purple, glassy, with local alignment of plagioclase microlites. Moderately vesicular, with some fillings of opaline quartz and dark green smectite, other vesicles with smectite rims. Some pyrite in fractures and vesicles, and at basal contact.

UNIT D5

1161.5–1179.5 MBSF 642E–102R–2 (117 cm) TO 105R–4 (63 cm)

MEDIUM-GRAINED, APHYRIC, GRAY BASALT. Uniform gray with rare plagioclase phenocrysts, some dark green smectitic patch alteration. Strongly fractured throughout, subvertical and steeply inclined, locally curvilinear and *en echelon*, with smectite, calcite, and pyrite common fillings. Hydrothermal veining at 105R–2, 40–60 cm, with adjacent pyrite concentration zone. Contacts with F116 and S46 pyritized.





UNIT D5

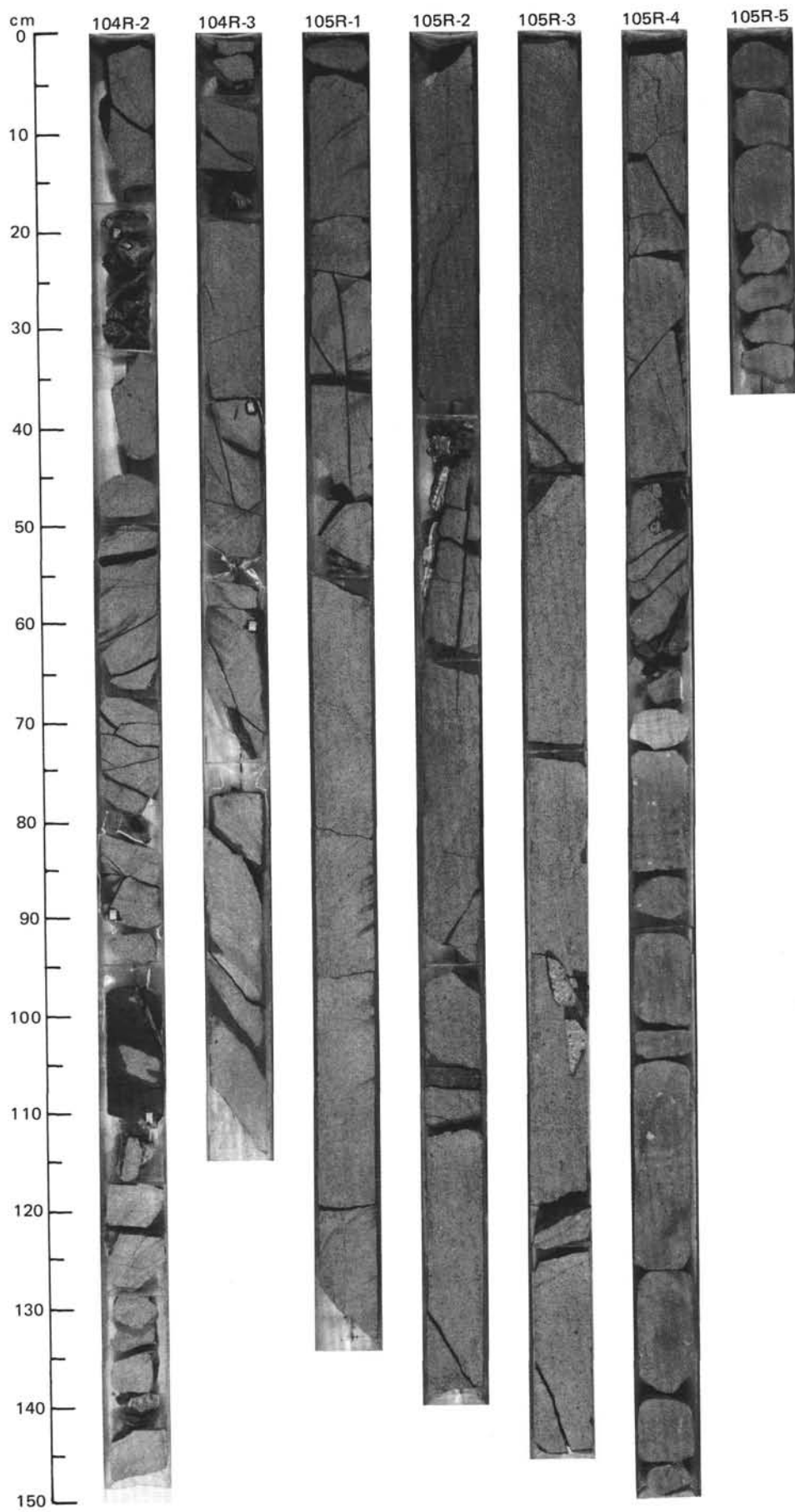
1161.5–1179.5 MBSF 642E–102R–2 (117 cm) TO 105R–4 (63 cm)

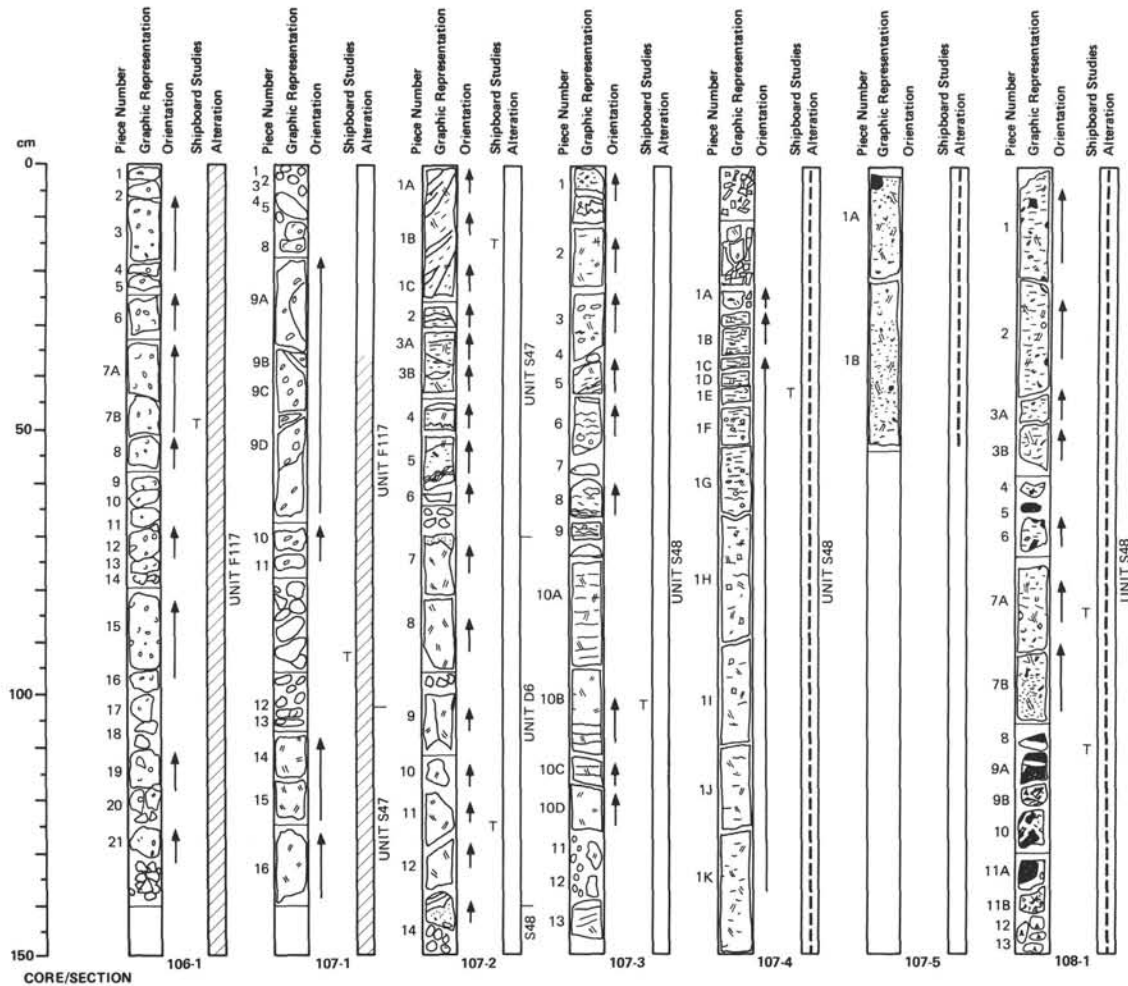
MEDIUM-GRAINED, APHYRIC, GRAY BASALT. Uniform gray with rare plagioclase phenocrysts, some dark green smectitic patch alteration. Strongly fractured throughout, subvertical and steeply inclined, locally curvilinear and *en echelon*, with smectite, calcite, and pyrite common fillings. Hydrothermal veining at 105R–2, 40–60 cm, with adjacent pyrite concentration zone. Contacts with F116 and S46 pyritized.

UNIT S46

1179.5–1182.3 MBSF 642E–105R–4 (63 cm) TO 105R–5 (38 cm)

FINE-GRAINED, DARK GRAY VOLCANICLASTIC SEDIMENT.
Lithologically identical to S45.





UNIT F117

1182.3–1194.0 MBSF 642E–106R–1 (0 cm) TO 107R–1 (102 cm)

GLASSY, PURPLISH GRAY BASALTIC FLOW. Moderately phyrlic. Altered, moderately to highly vesicular cryptocrystalline unit, displaying aligned microclites and locally clustered plagioclase phenocrysts. Vesicles filled with opaline silica or zeolites, and weakly attenuated into prolate shaped fabrics, some as geopetals. Color alteration to gray and pale gray accompanies disaggregation of basalt. Pyrite in pockets, with smectite in vein fills. Glassy base at 107R–1, 78–102 cm.

UNIT S47

1194.0–1196.6 MBSF 642E–107R–1 (102 cm) TO 107R–2 (67 cm)

LIGHT TO DARK GRAY VOLCANICLASTIC MUDSTONE. Laminated, wispy to thinly bedded, with pinch and swell, lateral pinch outs. Lamination dips at 10–30 degrees, grain size up to coarse silts. Some carbonate veining, with some pyrite surface coatings on largest ash clasts. Extensive alteration at recovered contact with D6. Lithologically, upper part of ignimbrite unit S48.

UNIT D6

1196.6–1198.0 MBSF 642E–107R–2 (67 cm) TO 107R–2 (137 cm)

FINE-GRAINED SUBOPHITIC, GRAY, NONVESICULAR BASALT.**THIN SECTION DESCRIPTION**

642E–107R–2 (Piece 11, 124–126 cm): <1% plag, 40% cpx, 5% pyrite and magnetite, 55% tachylite and altered glass. Hyalocrystalline.

UNIT S48

IGNIMBRITE FLOW UNIT

1198.0–1203.0 MBSF 642E–107R–2 (137 cm) TO 108R–2 (47 cm)

642E–107R–2 (137 cm) TO 107R–3 (70 cm)

LIGHT GRAY TO MEDIUM GRAY VOLCANICLASTIC MUDSTONE. Lithologically identical to S45–S47; leucocratic gneiss with ragged edges at 107R–2, 143 cm.

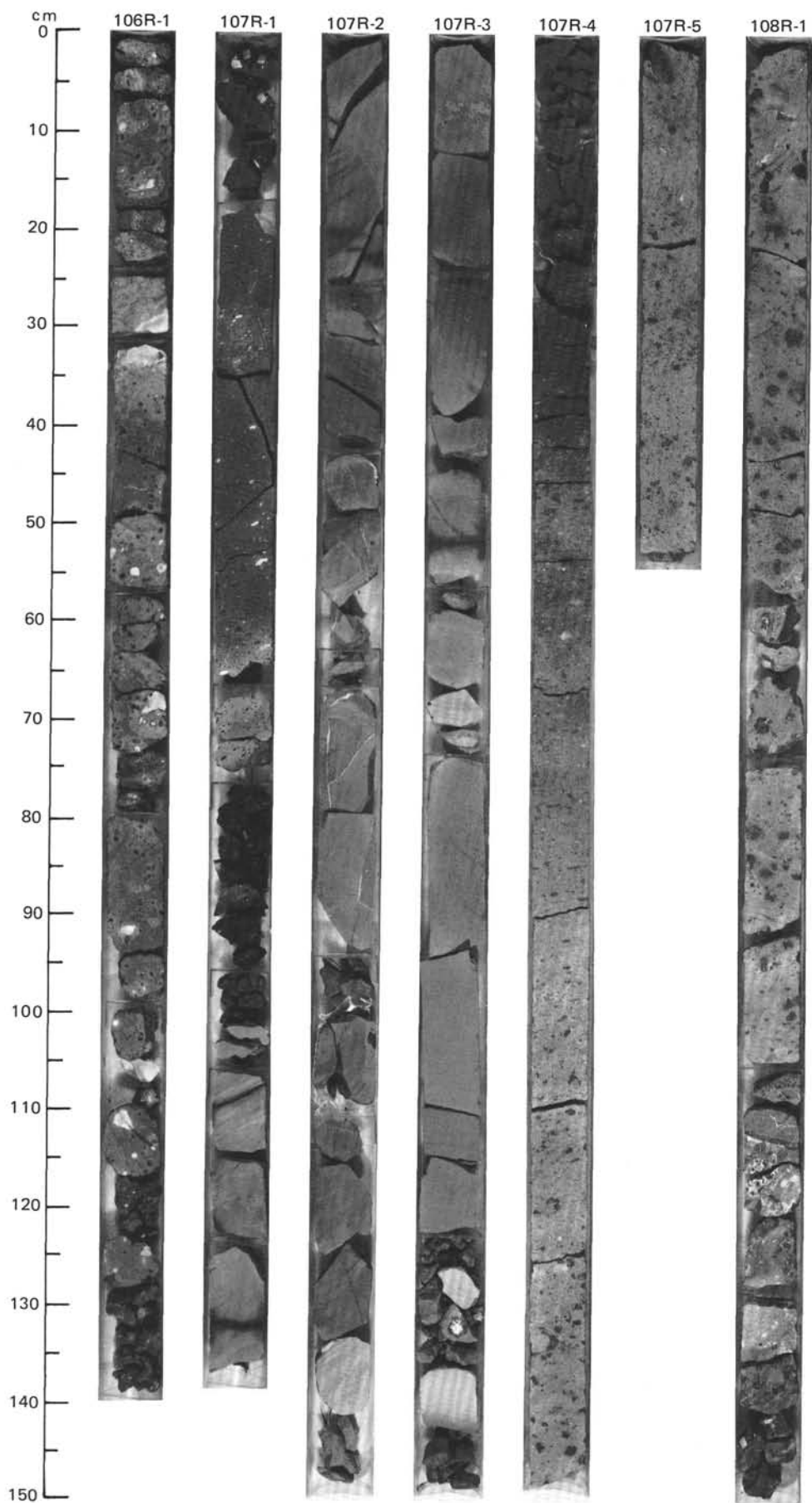
642E–107R–3 (70 cm) TO 107R–3 (138 cm)

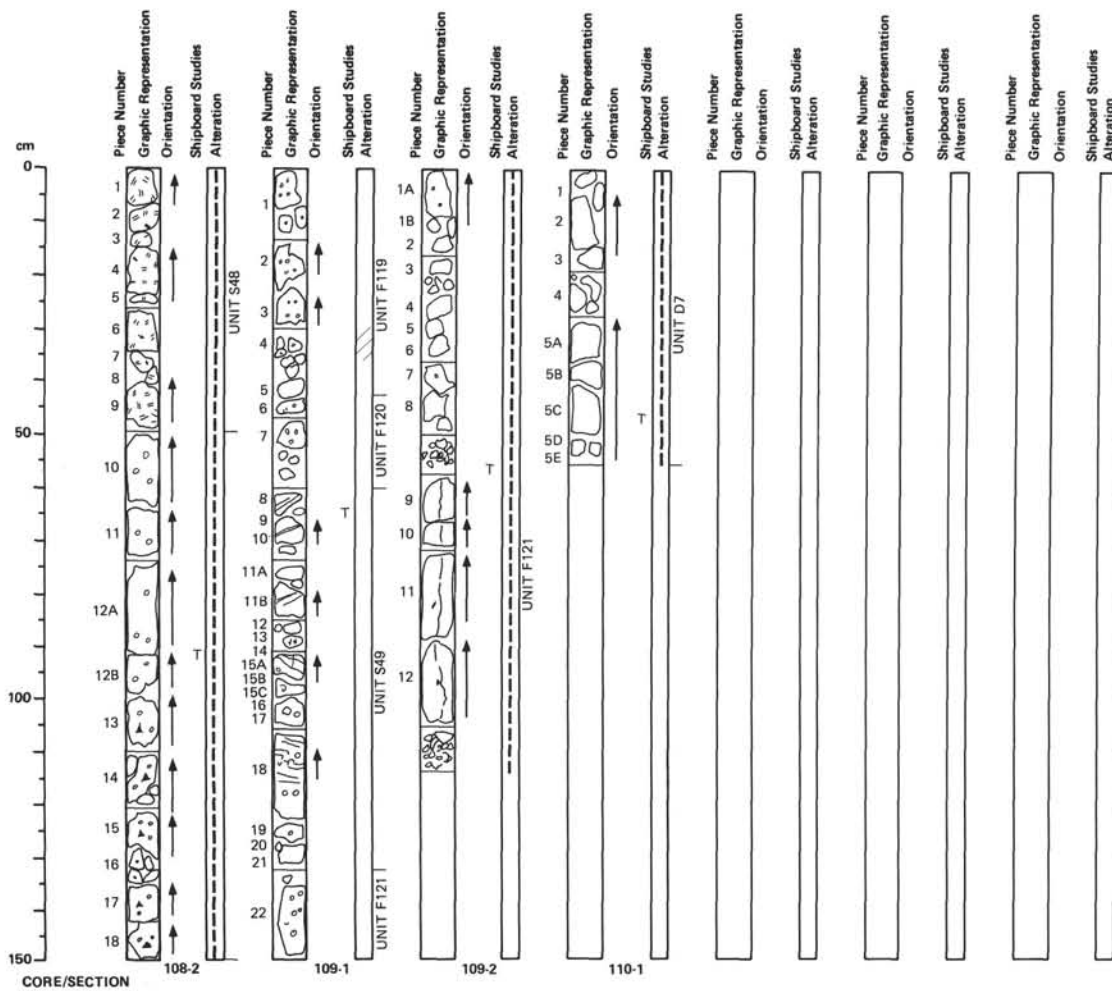
WELL SORTED, GRAY TO WHITE VITRIC TUFF.

642E–107R–3 (138 cm) TO 108R–2 (50 cm)

MASSIVE IGNIMBRITE UNIT, PUMICE AND XENOLITHS IN CRYSTAL-POOR ASH MATRIX. Pumice lapilli increase in abundance and size upward from 1 to 10% and from 1 to 20 mm respectively; xenoliths decrease in size (from 100 to 5 mm) and abundance (from 50 to 3 vol.%) upward. Zonation of ignimbrite:

- 5.8 cm fine-grained vitric ash at base
 - 90 cm of lithic breccia
 - 10 cm strongly eutaxitic, lithic-poor vitric tuff
 - 510 cm central zone, lithic-vitric tuff, eutaxitic texture
 - 70 cm crystal-vitric tuff, rich in strongly compacted, very dark gray pumice lapilli (primary welding?)
 - 20 cm fine-grained vitric ash
- Xenoliths: 70% perlitic lapilli, angular; 25% aphanitic lapilli and blocks; 5% crystalline felsic lapilli, quartz, and light mica; 1% volcaniclastic sediments.
- Alteration: smectite, clinoptilolite, phillipsite, silica-phases, illite, calcite, pyrite.





CORE/SECTION

UNIT S48

1198.0–1203.0 MBSF 642E–107R–2 (137 cm) TO 108R–2 (47 cm)
 642E–107R–2 (137 cm) TO 107R–3 (70 cm)

LIGHT GRAY TO MEDIUM GRAY VOLCANICLASTIC MUDSTONE.
 Lithologically identical to S45–S47; leucocratic gneiss with ragged edges at 107R–2, 143 cm.

642E–107R–3 (70 cm) TO 107R–3 (138 cm)

WELL SORTED, GRAY TO WHITE VITRIC TUFF.

642E–107R–3 (138 cm) TO 108R–2 (50 cm)

MASSIVE IGNI MBRITE UNIT, PUMICE AND XENOLITHS IN CRYSTAL-POOR ASH MATRIX. Pumice lapilli increase in abundance and size upward from 1 to 10% and from 1 to 20 mm respectively; xenoliths decrease in size (from 100 to 5 mm) and abundance (from 50 to 3 vol.%) upward. Zonation of ignimbrite:

5.8 cm fine-grained vitric ash at base
 90 cm of lithic breccia
 10 cm strongly eutaxitic, lithic-poor vitric tuff
 510 cm central zone, lithic-vitric tuff, eutaxitic texture
 70 cm crystal-vitric tuff, rich in strongly compacted, very dark gray pumice lapilli (primary welding?)
 20 cm fine-grained vitric ash
 Xenoliths: 70% perlitic lapilli, angular; 25% aphanitic lapilli and blocks; 5% crystalline felsic lapilli, quartz, and light mica; 1% volcaniclastic sediments.
 Alteration: smectite, clinoptilolite, phillipsite, silica-phases, illite, calcite, pyrite.

UNIT F118

1203.0–1209.5 MBSF 642E–108R–2 (47 cm) TO 108R–2 (150 cm)

FINE-GRAINED, GRAY BASALT. Aphyric to sparsely porphyritic, phryc, brecciated. Subordinate amounts of glassy perlitic pore space between clasts partly filled by tuff of overlying ignimbrite unit. Calcite abundant as vesicle or vein filling.

THIN SECTION DESCRIPTION

642E–108R–2 (Piece 12B, 95–97 cm): <1% plagioclase (cordierite?) phenocrysts, 40% acicular plagioclase, 5% opaques, 55% altered microlites and glass.

UNIT F119

1209.5–1212.0 MBSF 642E–109R–1 (0 cm) TO 109R–1 (43 cm)

FINE-GRAINED, GRAY BASALT. Sparsely plagioclase glomeroporphyritic, vesicular (15%); becomes light gray, perlitic, toward base.

UNIT F120

1212.0–1214.2 MBSF 642E–109R–1 (43 cm) TO 109R–1 (60 cm)

AS F119. Vesicles filled with calcite.

UNIT S49

1214.2–1216.0 MBSF 642E–109R–1 (60 cm) TO 109R–1 (132 cm)

LIGHT TO MEDIUM GRAY VOLCANICLASTIC MUDSTONE. Identical to S45–S47. No flame, bedding on 0.1 mm scale, some isoclinal slump folds.

UNIT F121

1216.0–1219.0 MBSF 642E–109R–1 (132 cm) TO 109R–2 (112 cm)

FINE-GRAINED TO CRYSTOCRYSTALLINE BASALT. Glomerophytic vesicles. Vesicular to sparsely vesicular; vesicles filled by dark green smectite; calcite; veins; pyrite disseminated but concentrated at vesicles.

UNIT D7

1219.0–? MBSF 642E–110R–1 (0 cm) TO 110R–1 (55 cm)

END OF HOLE. GRAY, SUBOPHITIC, FINE-GRAINED BASALT. Nonvesicular, locally enriched in pyrite (5–7%). Elongated vesicles, subvertical, calcite-pyrite filled.

